Development of platforms for detection of single nucleotide polymorphisms: applications on pathogens, genetic diseases, and beyond

Nuttada Panpradist

A dissertation submitted in partial fulfillment of
the requirements for the degree of

Doctor of Philosophy

University of Washington
2021

Reading Committee:
Barry Lutz, Chair
Paul Drain
Jr-Iuan Lai

Program Authorized to Offer Degree:
Bioengineering

© Copyright 2021
Nuttada Panpradist

University of Washington

Abstract

Development of platforms for detection of single nucleotide polymorphisms: applications on pathogens, genetic diseases, and beyond

Nuttada Panpradist

Chair of the Supervisory Committee: Barry Lutz

Department of Bioengineering

HIV was once a pandemic, but development of drugs has allowed people to live long healthy lives despite infection with HIV. Unfortunately, HIV has developed resistance to many drugs, and threatens to become a pandemic again. In 2019, 1 out of 4 infected people had HIV with mutations that render first-line drugs ineffective. The situation was much worse among infants born to HIV-infected mothers, of whom 3 out of 4 had drug-resistant HIV. In response to this pressing issue, the WHO recommends that countries switch their first-line treatments to dolutegravir-based regimens. For countries that continue to use the old first-line drugs, WHO recommends testing individuals for HIV drug resistance (**HIVDR**). HIVDR test results can guide clinicians to select the most effective treatment. Unfortunately, HIVDR tests are typically only available in advanced centralized laboratories, and a whole country our continent may be served by a single WHO-certified testing site. The primary aim of this thesis was to address this urgent unmet need improving speed, cost, and affordability of an existing HIVDR testing method.

© Copyright 2021 | N Panpradist

Single nucleotide polymorphisms (**SNPs**) are proven biomarkers for HIVDR. **Chapter 1 Introduction** provides the background on SNPs, their relationship with HIVDR, the magnitude of the HIVDR problem, and existing technologies to detect these HIVDR SNPs. Materials related to this chapter are included in the following publications.

> 1) Horacio A Duarte, **Nuttada Panpradist**, Ingrid A Beck, Barry Lutz, James Lai, Ruth M Kanthula, Rami Kantor, Anubhav Tripathi, Shanmugam Saravanan, Iain J MacLeod, Michael H Chung, Guoqing Zhang, Chunfu Yang, Lisa M Frenkel. "Current status of point-of-care testing for human immunodeficiency virus drug resistance" J Infect Dis. 2017;216(suppl_9): S824-S828. PMID: 29040621. DOI: 10.1093/infdis/jix413.
>
> 2) **Nuttada Panpradist**, James J Lai. "Point-of-care diagnostics" 2016. Biomaterials Nanoarchitectonics. 2016. DOI: 10.1016/B978-0-323-37127-8.00009-1.
>
> 3) Ross S. Milne, Ingrid A. Beck, Molly Levine, Isaac So, Nina Anderson, Wenjie Deng, Thomas R. Sibley, **Nuttada Panpradist**, James Kingoo, Catherine Kiptinness, Nelly Yatich, James N Kiarie, Samah R Sakr, Michael H Chung, Lisa M Frenkel. "Low-frequency pretreatment HIV drug-resistance effects on 2-year outcome of first-line efavirenz-based antiretroviral therapy" submitted to AIDS.

Chapters 2 – 5 describe how we simplified SNP detection based on the oligonucleotide ligation assay (OLA) pioneered by the Frenkel lab nearly 20 years ago. The OLA consists of four main modules: sample preparation, amplification, ligase

© Copyright 2021 | N Panpradist

detection reaction (LDR), and detection of the ligated probes, which indicates the presence or absence of a particular SNP. Specifically, **Chapter 2 Nucleic acid preparation** describes the significance of using DNA vs. RNA and how to prepare them for the HIVDR test. We developed non-proprietary RNA extraction kits and evaluated them on clinical specimens. **Chapter 3 Paper-based detection for HIVDR** showcases three generations of OLA detection that rely on the principles of paper microfluidics, nucleic acid thermodynamics, protein chemistries, and multi-target binding interactions. Herein I also discuss the comparisons of human visual classification and software analysis to improve signal-noise discrimination via linear discriminant analysis. **Chapter 4 Ready-to-use dry reagents** details the strategies for preparing lyophilized, ready-to-use reagents in different platforms, selecting appropriate excipients, characterization methods, additional considerations for complex molecular assays, and the potential use of Arrhenius's equation in accelerated long-term storage study. Combinations of this know-how in **Chapter 2 – Chapter 4** are the basis of developing "OLA-Simple 1.0 kits for HIVDR test" in **Chapter 5 OLA-Simple kit for HIVDR**. First, the OLA-Simple kit was made "universal" and used to validate an archived specimen panel of 168 specimens (672 SNPs tested) containing globally represented subtypes from Thailand (AE and B), South Africa (C), Peru (B), and Kenya (A, D, and AD). Next, the OLA-Simple kit was tailored for subtype-B specific HIV and tested on circulating variants in Mexico City in 60 specimens (300 SNPs tested); at that time, the country was not a part of the dolutegravir patent pool and would likely have benefitted from the OLA-Simple kits. Last, an interactive Aquarium software guide was developed through a new collaboration with the Klavins lab to enable the use of OLA-Simple kits with minimal

© Copyright 2021 | N Panpradist

or no training. This software guide, added to the OLA-Simple kits, resulted in successful demonstrations in the USA (41 participants) and Kenya (12 participants). My contributions in these areas led to the following publications. The complete lists are available in **Appendix 7 – Appendix 9**.

PUBLICATIONS

1) **Nuttada Panpradist**, Ingrid A Beck, Michael H Chung, James N Kiarie, Lisa M Frenkel, Barry R Lutz. "Simplified paper format for detecting HIV drug resistance in clinical specimens by oligonucleotide ligation." PLoS One. 2016. DOI: 10.1371/journal.pone.0145962

2) **Nuttada Panpradist**, Ingrid A Beck, Justin Vrana, Nikki Higa, David McIntyre, Parker S Ruth, Isaac So, Enos C Kline, Ruth Kanthula, Annie Wong-On-Wing, Jonathan Lim, Daisy Ko, Ross Milne, Theresa Rossouw, Ute D Feucht, Michael Chung, Gonzague Jourdain, Nicole Ngo-Giang-Huong, Laddawan Laomanit, Jaime Soria, James Lai, Eric D Klavins, Lisa M Frenkel, Barry R Lutz. "OLA-Simple: A software-guided HIV-1 drug resistance test for low-resource laboratories". EBiomedicine. 2019. DOI: 10.1016/j.ebiom.2019.11.002

3) **Nuttada Panpradist***, Ingrid A Beck*, Parker S Ruth, Santiago Avila-Rios, Claudia Garcia-Morales, Maribel Soto-Nava, Daniela Tapia-Trejo, Margarita Matias-Florentino, Hector E Paz-Juarez, Silvia Del Arenal-Sanchez, Gustovo Reyes-Teran, Barry R Lutz, Lisa M Frenkel. "Near point-of-care, point-mutation test to detect drug resistance in HIV-1: A validation study in a

© Copyright 2021 | N Panpradist

Mexican cohort." AIDS. 2020. PMID:32205723 DOI: 10.1097/QAD.0000000000002524 * **Authors with equal contributions.**

4) Justin D Vrana*, **Nuttada Panpradist***, Nikki Higa, Daisy Ko, Parker Ruth, Ruth Kanthula, James J Lai, Yaoyu Yang, Samar Rafie Sakr, Bhavna Chohan, Michael H Chung, Lisa M Frenkel, Barry R Lutz, Eric Klavins, Ingrid A Beck. "Implementation of an interactive mobile application to pilot a rapid assay to detect HIV drug resistance mutations in Kenya." medRxiv. DOI: 10.1101/2021.05.06.21256654 ***Authors with equal contributions**.

5) Gaurav Gulati*, **Nuttada Panpradist***, Samuel W A Stewart, Amy K Oreskovic, Santiago Avila, Gustavo Reyes-Terán, Peter D Han, Lea M Starita, Ingrid Beck, Lisa M Frenkel, Barry R Lutz, James J Lai. "Inexpensive workflow to enable simultaneous screening for Covid-19 and monitoring HIV viral load" medRXiv. PMID: 34462759 DOI: 10.1101/2021.08.18.21256786. * **Authors with equal contributions.**

PATENT APPLICATION

1) PCT Application WO 2019/222716 filed on 05/17/2019 Entitled: "Systems and Methods for ligation.

Chapter 6 Strategies to improve amplification and ligation for HIVDR proposes an effective workflow for a viral load test and reflexed HIVDR test, eliminating redundancies in sample collection and extraction and speeding up test turnaround time while reducing costs. I discuss our efforts to increase speed

© Copyright 2021 | N Panpradist

further, reduce complexity, and integrate the amplification and ligation module in the OLA-Simple. Five hours of sample-to-results time in OLA-Simple 1.0 could be reduced to as low as 1 hour. We used different techniques to enable isothermal molecular reactions, such as thermostable helicase-dependent amplification, recombinase polymerase amplification, and loop-mediated amplification. **Chapter 7 Fluorescence-based detection of LDR products** describes novel strategies to chemically integrate all steps into a single reaction tube using fluorescent-based detection approaches *via* reverse-molecular beacons robust to sequence polymorphisms in HIV. **Chapter 8 Integration of HIVDR OLA into a more simplified device** highlights different methods we applied to physically integrate OLA into a device, such as a 1-dimensional sequential delivery, a magnetic valve, a pull tab valve, and a wax-based encapsulation and release system. This work was reported in the following conference proceedings and manuscripts:

CONFERENCE PROCEEDINGS

1) **N Panpradist**, EC Kline, IA Beck, AK Oreskovic, I Hull, M Purfield, S Avila-Ríos, C García-Morales, G Reyes- Terán, LM Frenkel, BR Lutz. "Rapid semi-quantitative viral load assay and reflex drug resistance test for management of HIV antiretroviral therapy." 28th International Workshop on HIV Drug Resistance & Treatment Strategies. 2019. Johannesburg, South Africa. (Poster Presentation)

2) **N Panpradist**, D McIntyre, A Wong-On-Wing, A Sriram, I Beck, L Frenkel, B Lutz. "Development of a Near Equipment-free, Self-Contained HIV Drug Resistance Test." Biomedical Engineering Society Conference. 2017. Phoenix, Arizona, USA. (Oral Presentation)

© Copyright 2021 | N Panpradist

3) **N Panpradist**, A Wong-On-Wing, I Beck, J Lai, L Frenkel, B Lutz. "Progress towards Development of a Novel Isothermal Ligation Reaction for HIV Drug Resistance Testing." XXV International Workshop on HIV Drug Resistance. 2016. Boston, MA. (Poster Presentation)

4) **N Panpradist**, N Higa, A Wong-On-Wing, I Andrews, B Atkinson, I Beck, L Frenkel, B Lutz. "Novel Platform for Simple Lab-based Oligonucleotide Ligation Assay for Detection of HIV Drug Resistance in sub-Saharan Africans." XXV International Workshop on HIV Drug Resistance. Boston, MA. 2016 (Poster Presentation).

SUBMITTED MANUSCRIPT

1) Ian T. Hull, Enos C. Kline, Gaurav K. Gulati, Jack Henry Kotnik**,** **Nuttada Panpradist**, Kamal G. Shah, Qin Wang, Lisa Frenkel, James Lai, Joanne Stekler, and Barry R. Lutz. "Isothermal Amplification with a Target-Mimicking Internal Control and Quantitative Lateral Flow Readout for Rapid HIV Viral Load Testing in Low-Resource Settings" accepted to Analytical Chemistry.

MANUSCRIPT IN PREPARATION:

1) **Nuttada Panpradist***, Amy Oreskovic*, Enos Kline, Ian Hull, Parker Ruth, Ingrid A Beck, Santiago Avila-Rios, Michael Chung, Ute Feucht, Lisa Frenkel, Gonzhang Jourdain, Enos Kline, Jonathan Lim, Nicole Ngo-Niang-Ngo, Theresa Rossouw, Lisa M Frenkel, Barry R Lutz. "Hour-long assay for detection of drug resistance in HIV-1 cross subtypes using recombinase

© Copyright 2021 | N Panpradist

> polymerase amplification integrated into paper-based oligonucleotide ligation" * **Authors with equal contributions.**

The technologies developed for OLA for HIV are platforms that can be adapted to detect other diseases and conditions. **Chapter 9 HOLA: OLA to detect a human allele (HLA-B*57:01)** describes our adaptation of OLA-Simple technologies to detect human allele HLA-B*57:01, which confers Abacavir hypersensitivity. **Chapter 10 Technologies in response to SARS-CoV-2 pandemic** describes recent work on SARS-CoV-2 detection built upon the knowledge in **Chapters 2** - **4** and **6** and my prior work on swab characterization and transfer methods during my first-year rotation. The SARS-CoV-2 lyophilized RT-PCR assay was evaluated at Duke University, the University of Zimbabwe, and a pediatric clinic at Georgetown University. **Chapter 11 Fish-OLA – Species identification tool to regulate IUU** describes the development of Fish-OLA, which is an adaptation of the OLA-Simple chemistry to detect the presence of the two biomarker SNPs unique to codfish from the Bering Sea and the Aleutian Islands. We conducted a blind study to evaluate the Fish-OLA on >200 specimens. Such tools could contribute to the management of illegal, unreported, and unregulated (**IUU**) fishing. Below are the publications, upcoming manuscripts, and patent applications based on the work in this area:

PUBLICATIONS

> 1) Jackson J Wallner, Ingrid A Beck, **Nuttada Panpradist**, Santiago Avila-Ríos, Humberto Valenzuela-Ponce, Maribel Soto-Nava, Barry R Lutz, Lisa M Frenkel. "Rapid, Near Point-of-Care Assay for HLA-B*57:01

© Copyright 2021 | N Panpradist

Genotype Associated with Severe Hypersensitivity to Abacavir". AIDS Research and Human Retroviruses**.** DOI: 10.1089/aid.2021.0103

2) **Nuttada Panpradist**, Qin Wang, Parker S Ruth, Jack H Kotnik, Amy K Oreskovic, Abraham Miller, Samuel WA Stewart, Justin Vrana, Peter D Han, Ingrid A Beck, Lea M Starita, Lisa M Frenkel, Barry R Lutz. "Simpler and faster Covid-19 testing: Strategies to streamline SARS-CoV-2 molecular assays." EBiomedicine. 2021. PMID: 33582488. DOI: 10.1016/j.ebiom.2021.103236

3) **Nuttada Panpradist**, Robert Atkinson, Michael Roller, Enos Kline, Ian Hull, Qin Wang, Jack Henry Kotnik, Amy K Oreskovic, Crissa Bennett, Daniel Leon, Victoria Lyon, Peter D Han, Lea M Starita, Matthew Thompson, Barry R Lutz. "Harmony Covid-19: development and evaluation of ready-to-use reagents, hardware, and software package for point-of-care SARS-CoV-2 nucleic acid amplification test" Accepted to Science Advances 2021. DOI: 10.1101/2021.08.12.21261875.

4) Enos Kline, **Nuttada Panpradist**, Ian Hull, Qin Wang, Amy K Oreskovic, Peter D Han, Lea M Starita, Barry R Lutz. "Development of novel engineered polymerase and universal probe design to enable robust RT-LAMP for SARS-CoV-2 detection." medRxiv. PMID: 34462755. DOI: 10.1101/2021.08.13.21261995.

© Copyright 2021 | N Panpradist

5)Jason Hoffman, Matthew Hirano, **Nuttada Panpradist**, Joseph Bre da, Parker Ruth, Yuanyi Xu, Jonathan Lester, Bichlien Nguyen, Luis Ce ze, Shwetak N. Patel. "Passively Sensing SARS-CoV-2 RNA in Public Transit Buses. BioRXiv" https://doi.org/10.1101/2021.06.02.21258184

6) Andrew C. Hunt, James Brett Case, Young-Jun Park, Longxing Cao, Kejia Wu, Alexandra C. Walls, Zhuoming Liu, John E. Bowen, Hsien-Wei Yeh, Shally Saini, Louisa Helms, Yan Ting Zhao, Tien-Ying Hsiang, Tyler, N. Starr, Inna Goreshnik, Lisa Kozodoy, Lauren Carter, Rashmi Ravichandran, Lydia B. Green, Wadim L. Matochko, Christy A. Thomson, Bastain Vögeli, Antje Krüger-Gericke, Laura A. VanBlargan, Rita E. Chen, Baoling Ying, Adam L. Bailey, Natasha M. Kafai, Scott Boyken, Ajasja Ljubetič, Natasha Edman, George Ueda, Cameron Chow, Amin Addetia, **Nuttada Panpradist**, Michael Gale Jr, Benjamin S. Freedman, Barry R. Lutz, Jesse D. Bloom, Hannele Ruohola-Baker, Sean P. J. Whelan, Lance Stewart, Michael S. Diamond, David Veesler, Michael C. Jewett, David Baker. "Multivalent designed proteins protect against SARS-CoV-2 variants of concern" https://doi.org/10.1101/2021.07.07.451375

7) **Nuttada Panpradist**, Bhushan J Toley, Xiaohong Zhang, Samantha Byrnes, Joshua R Buser, Janet A Englund, Barry R Lutz. "Swab sample transfer for point-of-care diagnostics: characterization of swab types and manual agitation methods" 2014. PloS One. PMID: 25181250. DOI: 10.1371/journal.pone.0105786

© Copyright 2021 | N Panpradist

MANUSCRIPT IN PREPARATION

1) **Nuttada Panpradist**, Carolyn M Tarpey, Anita Wray, Parker S Ruth, Ingrid Spies, Barry R Lutz, Karl F Bohringer, Lorenz Hauser. "Fish-OLA: rapid and inexpensive population assignment for Pacific Cod (Gadus macrocephalus)"

PATENT APPLICATIONS

1) Provisional Patent Application 63/165,029 filed 3/23/2021 Entitled: "SYSTEMS AND METHODS FOR DETECTING SARS-COV-2 RNA."

2) Provisional Patent Application 63/049,941 filed 7/9/2020 Entitled: "Kit for Sample Collection and Preparation for Amplification."

3) Provisional Patent Application 63/049,758 filed 7/9/2020 Entitled: "Amplification Device."

Chapter 12 Summary of contributions and impact summarizes my contributions to the field and the impact of these works. In addition to the outcomes described in my thesis, I consulted other researchers on other projects, including diagnostics of cell-free DNA in urine samples and detection of TB drug metabolites. I was a visiting scholar at Stanford University and researched the dynamic host responses to pathogen infections *via* viral-inclusive single-cell RNASeq. Some of my contributions beyond thesis work are listed below. The complete list is available in **Appendix 7** and **Appendix 8**.

© Copyright 2021 | N Panpradist

1) Zhiyuan Yao, Fabio Zanini, Sathish Kumar, Marwah Karim, Sirle Saul, Nishank Bhalla, **Nuttada Panpradist**, Avery Muniz, Aarthi Narayanan, Stephen R Quake, Shirit Einav. "The transcriptional landscape of Venezuelan equine encephalitis virus infection" 2021. PLoS Neglected Diseases, DOI: 10.1371/journal.pntd.0009306

2) Amy Oreskovic, **Nuttada Panpradist,** Diana Marangu, M William Ngwane, Zanele P Magcaba, Sindiswa Ngcobo, Zinhle Ngcobo, David J Horne, Douglas PK Wilson, Adrienne E Shapiro, Paul K Drain, Barry R Lutz. "Diagnosing pulmonary tuberculosis using sequence-specific purification of urine cell-free DNA."2021. JCM. PMID: 33789959; DOI: 10.1128/JCM.00074-21

3) Sylvia M LaCourse, Daniel Leon, **Nuttada Panpradist**, Barbra A Richardson, Elizabeth Maleche-Obimbo, Jerphason Mecha, Daniel Matemo, Jaclyn N Escudero, John Kinuthia, Barry Lutz, Grace John-Stewart. "Urine Biomarker Assessment of Infant Adherence to Isoniazid Prophylaxis" Pediatr Infect Dis J. 2021 Jan;40(1):e43-e45. DOI: 10.1097/INF.0000000000002936

4) Amy Oreskovic, Norman D Brault, **Nuttada Panpradist**, James J Lai, Barry R Lutz. "Analytical comparison of methods for extraction of short cell-free DNA from urine" The Journal of Molecular Diagnostics. 2019. PMID: 31442674. DOI: 10.1016/j.jmoldx.2019.07.002

© Copyright 2021 | N Panpradist

Besides presenting conference proceedings, I have shared my expertise through other speaking platforms such as invited talks and lectures. Below are some highlights. The complete lists are available in **Appendix 5** and **Appendix 9.**

> 1) PHPT, Chiang Mai University, Thailand (**2020**)
>
> 2) Department of Medicine, University of Zimbabwe, Zimbabwe (**2019**)
>
> 3) KwaZulu-Natal Research Innovation and Sequencing Platform (KRISP), UKZN, Durban, South Africa (**2018)**
>
> 4) Michael Mayer Lab, University of Fribourg, Switzerland. (**2017**)
>
> 5) MEMS Research Unit, University of Mechanical Engineering, Chulalongkorn University, Bangkok, Thailand (**2015**)
>
> 6) PHPT, Chiang Mai University, Thailand (**2015**)
>
> 7) Department of Material Sciences, Silpakorn University, Thailand (**2015**)

© Copyright 2021 | N Panpradist

ACKNOWLEDGMENTS

For the past 8 years, I have been honored and grateful to be a part of the UW Bioengineering and Global Health community. Coming from a small town in Thailand, I would not have imagined being a part of these proud moments. I was officially and unofficially advised by supportive mentors and worked with multiple teams of talented and dedicated researchers. I was thrilled to be interviewed by a local news reporter about our research, to stand in front of hundreds of investors to pitch an idea and win money to support commercialization efforts, to be featured on the Seattle metro, to join the expert panels including at the OPEN2019 in Washington DC, to lecture both bioengineering and global health classes at the UW, and to travel the world to present at international meetings including the one arranged by the WHO in South Africa. All these would have been impossible without your support.

DR. BARRY LUTZ

I would like to thank my Ph.D. Advisor, **Dr. Barry Lutz**, for his continued support and guidance. Barry, thank you for the opportunities to pursue the path longer than a usual Ph.D. but satisfactory to my professional endeavors. Barry received several mentoring awards, and the strength of his mentorship is patience: patience to "questioning us to think rather than immediately giving us the

Dr. Barry Lutz at the 2018 Husky 100 award event.

© Copyright 2021 | N Panpradist

answers," patience to give students the time needed to explore and investigate rather than telling us exactly what to do, and patience and positive attitudes towards issues that arise. Altogether, Barry's mentorship helped shape me to become independent and academically confident. Barry is the golden example of resilience, and this encouraged me when facing failures. It was disappointing when I learned that none of my four fellowship applications were funded at the national level. Still, later I learned that one already accomplished the first step by putting oneself outside the comfort zone. The outside critiques are additional motivations to improve oneself, not a reflection of lifetime incompetency. Barry's humbleness is a reason many researchers want to collaborate with him. Barry often offered to remove himself from the last author to give more credits to other collaborators. Barry, despite being busy, would step in during the time his students needed help, such as carrying the light pole during the interview, showing us how to handle the BSL-2 waste properly, or donating his blood for research. Barry, I am grateful for your efforts in nominating me to various awards, especially those unrequested. Even though I did not always receive the awards, your kind words and recognitions inspired me to improve myself further.

Some behind-the-scene moments of Dr. Lutz

Assistant to the cameraman on the news interview day

Demonstrator on how to take care of BSL-2 wastes

Healthy volunteer for blood samples

© Copyright 2021 | N Panpradist

PH.D. ADVISORY COMMITTEE:
DR. JAMES LAI, DR. WENDY THOMAS, DR. PAUL DRAIN, DR. DANIEL CHIU, AND DR. JAY SHENDURE

Dr. James Lai and **Dr. Wendy Thomas**, thank you for serving on my committee since the Qualifying Examination. **Dr. James Lai** and **Dr. Paul Drain,** thank you for serving on my reading committee of this historically long thesis. **Dr. James Lai**, thank you for inviting me to co-write a book chapter, and most recently, for your advice on our HIV/SARS-CoV-2 extraction paper. Thank you for always taking the time to meet. I also thank your lab member, **Dr. Gaurav Gulati,** for his contributions to the RNA extraction work in the OLA-Simple project.

Dr. Wendy Thomas, you are one of my female role models. I felt honored to be in the same picture frame with you at the 2016 undergraduate student award event. Your mentorship, teaching, and contributions to make the department a more diverse community are exemplary. Thank you for including me in depart-mental events such as the Chair Search. I hope I can follow your path to contribute more to the UW community in the future. **Dr. Paul Drain**, I appreciate clinical insights on HIV, tuberculosis, and recently on SARS-CoV-2. I look forward to continuing to collaborate with you

Dr. Paul Drain

Dr. Daniel Chiu

Dr. James Lai

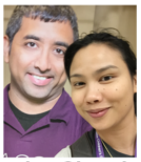
Dr. Jay Shendure's (elevator poster)

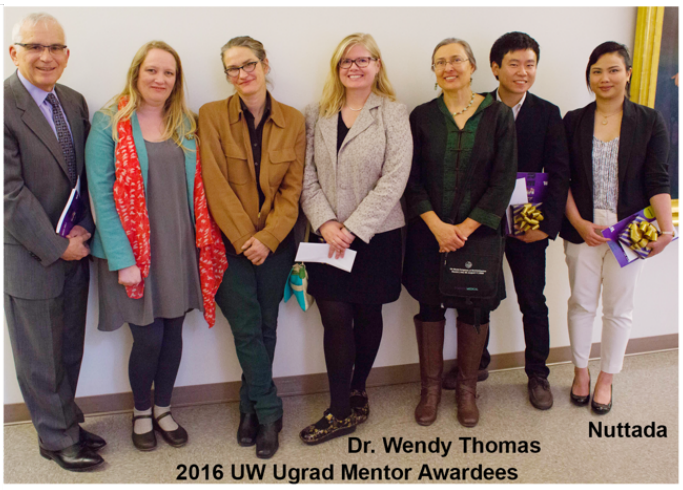

Dr. Wendy Thomas
2016 UW Ugrad Mentor Awardees

© Copyright 2021 | N Panpradist

through these ongoing projects. **Dr. Daniel Chiu,** I am grateful for your questions during the exams and committee meetings. Your questions were thoughtful and thought-provoking, from the K_a of antibodies I used in lateral flow strips to comparisons of different OLA-Simple platforms. I hope to learn more about your research in the future. **Dr. Jay Shendure**, I met you more often than Dr. Lutz – through your human-size photos at various locations in the Health and Science Building. I attended your talks and, even though I did not understand them much at first, your talks sparked my interest in single-cell RNA Seq. I later did a fellowship to learn more about it and now know what the t-SNE plots are. I am also grateful for all your support through the recent collaboration on the SARS-CoV-2 projects.

THE OLA-SIMPLE "*WUNDER*" (WONDERFUL + UNDER) GRADS.

Ian Andrews, **Nikki Higa**, **Annie Wong-On-Wing**, **David McIntyre**, **Annapurni Sriram**, and **Jonathan Lim** - you are all rock stars. You are an essential part of my graduate school experience. Your curiosity, hard work, and creativity kept me excited to come to work every day. The 2016 summer was a particularly productive and fun time. It was amazing that we, according to Dr. Lutz, collected the data that would have been equivalent for an R01 in three months. I was immensely proud to see your growth from starting in the lab to presenting your work at the group meetings and the local and international conferences throughout these years.

Thank, **Ian**, for your work on detection and toehold mediated strand displacement. Thank, **Nikki**, for your work on dry reagents, enzyme conjugation, and kit 1 dry reagent fabrication for Kenya. Your organizational skill and resilience are unmatched. We still use your excel sheets for the kit 1 production. Also, we still have not seen

© Copyright 2021 | N Panpradist

2016 UW Ugrad Research Symposium; L to R: Annie, Nuttada, Ian, and Nikki

2016 Jonathan

2016 Deriving Tm Eq. Annapurni

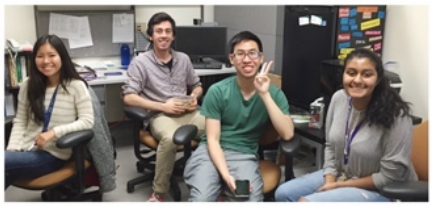
Lutz Lab Bunker (2016) L to R: Nikki David, Jonathan, Annapurni

2017 UW Ugrad Research Symposium L to R: Annie, Annapurni, Nuttada, Jonathan, and David

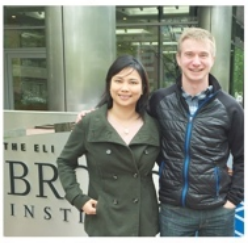
Ian at MIT (2017)

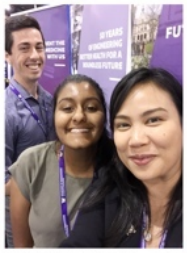
2018 BMES, AZ David, Annapurni, Nuttada

2016 HIVDR wksp Boston

2016 Lutz lab: Ian & Annie

2020 Reunion L to R: Jonathan, Annapurni, Isabella, Nuttada, Isaac

Business training (2018) L to R: David, Betty, Annapurni, Nuttada, Jonathan

2016 Lutz lab on the news

anyone's melt curve data look as good as yours. Thank, **Annie**, for your positive outlook in life and your hard work on antibody cross-reactivity work, helicase-dependent amplification and ligation, and real-time detection of ligase detection reaction. Thank you for stopping by the UW to volunteer for other studies even though you are already a Medical School student. **Nikki**, **Annie**, and **Ian** – We shared an unforgettable moment of overcoming the plate washer's cricket sound when we tested 36 combinations of the DNA barcodes. **David**, you never stopped impressing the people around you with your enthusiasm, dedication, and willingness to learn. These days, we still use the DNA binding kinetic data from your capstone project report. Before your capstone project, you had already contributed to the project in many ways, including 3D drawing/printing/testing of the pull-tab devices, zillions of

© Copyright 2021 | N Panpradist

ways to encapsulate DNA using the wax barrier, and amplicon-contained detection devices. **Annapurni**, you could master many research areas during your undergraduate school – working with Rahil on microfluidics and monitoring freezer alarm and then switched to working with us on the asymmetric amplification – all these while serving as the UW BMES President. **Jonathan**, Thank you a lot for your work on sequence-specific capture of HIV DNA. You conducted many experiments that led to interesting results. These results were challenging to troubleshoot, but you did not give up on them quickly.

Celebration with the traditional Thai pink soup.

Isaac So, you joined the pack as a post-bac when we needed help the most with the dry reagent study. You graduated from dental school and yet came back to volunteer for the feasibility of the COVID-19 test. **Isabella Spielmann**, I did not mentor you directly, but I find your hard work and fun spirit admirable. Thank you for your contributions to the OLA-Simple project on polymerase processivity. **Parker Ruth**, thank you for work on image analysis and the survey for visual detection on projects even after moving on from the Klavins lab and now at Stanford University. It has been a

© Copyright 2021 | N Panpradist

pleasure working with you. **Betty Yohannes**, Thank you for your contributions to the development of HIV RNA extraction methods.

LUTZ LAB MEMBERS

I would like to thank Lutz lab members for all the support and technical discussion: **past and current Lutz lab fellow graduate students**: Shivani Dharmaraja, Dr. Rahil Jain, Robert Atkinson, Dr. Amy Oreskovic, Ian Hull, Qin Wang, Shane Gilligan-Steinberg, Colin Eckhoff, and Josef Henthorn. **Past and current research engineers and scientists**: Enos Kline, Michael Roller, Daniel Leon, Samuel Stewart, Jack Henry Kotnik, Abraham Miller, Crissa Bennett, Jordan Campbell, Leila Ahmadiniaz, and Garima Kumar. I also thank Hunter Robbins and Jennifer Sprecher for their help on the administrative side.

Lutz lab (L to R, 2016): Annie, Daniel, Amy, Neona, Ian, Annapurni, Barry, Nuttada, David, Rahil, Doan, Isabella, Bob, and Nikki

Lutz lab (L to R, 2019): Nuttada, Qin, Barry, Rahil, Amy, Ian, Shivani

Shivani, thank you for the first introduction of the bioengineering research during my intern in 2012. Your training on aseptic techniques and micropipette use is still helpful for me today. **Rahil** and **Bob**, I am glad to have you joining the roller coaster ride with me – even more, happy to not have to move the lab to Michigan. **Rahil**, thank you for bringing in your expertise in microfluidic and electrical engineering. **Bob**, your endeavor to come back to graduate school after already having a

© Copyright 2021 | N Panpradist

successful career at Microsoft was inspirational. Thank you for bringing in your expertise in the computational design of nucleic acids. Your barcode DNA design was helpful for multiplexed OLA-Simple. **Rahil** and **Bob**, now that you both are busy running companies, I feel lucky I had a chance to share meaningful moments making/baking the Penguin cake with you.

Amy, thank you for your advice on sequence-specific capture work and the use of the engineered tag to bypass the issues from the endogenous sequence and for your work on RNA extraction of clinical samples. Most importantly, thank you for being there for me when I needed a second pair of eyes and ears. Also, I missed your desserts. **Ian** and **Qin** – thank you for your contributions to many projects we worked on together – HIV OLA and SARS-CoV-2 Harmony work – from protein/RNA generation to troubleshooting assays. **Qin, Jack Henry, Abe**, and **Sam**, thank you for joining the force to work on another SARS-CoV-2 project, lyophilized RT-PCR, and many related projects. It was the most productive time when we met daily from 8 – 8:30 AM, and I felt that we could contribute to the SARS-CoV-2 pandemic issue as a team. **Shane**, despite being relatively new to the lab, you have already contributed to so many projects! Thank you for your hard work on plotting all the real-time data in the Harmony manuscript, and I look forward to working with you more on future projects. **Colin**, thank you for your work on the heater for OLA-Simple.

Enos, thank you for being the resource for all of us graduate students. Just a brief conversation with you could give us many insights on how to troubleshoot our assay. Thank you for all your design work that led to the novel polymerase and probe design that we all get to use and your designed RPA RT primer and fast PCR primers. Most

© Copyright 2021 | N Panpradist

importantly, thank you for including other graduate students and me in working on your SARS-CoV-2 RT-LAMP assay. I learned LAMP inside out through my primary experience working with you on this project. **Mike**, thank you for being a brilliant and humble human. It was terrific to see generations of your inventions for heater/readers and microfluidic devices. I am honored that you decided to stay on to work on this SARS-CoV-2 typing project. Thank you also to you and **Kristen** for arranging special **Ellie** visit sessions during my tough times. **Daniel**, thank you so much for all your help around the lab, training many of us how to use lateral flow manufacturing machines, training me how to use 3D printing software, and your contributions to many projects such as dry reagent characterization and TB drug adherent test. I still remember the day when you had pain in your legs because of the cold weather, but you still helped me chip the ice off the freezer. **Sam**, thank you for your high-standard lab work and for training Leila and Jordan. **Jordan**, we are lucky to have you for the Kenya 2020-21 project. Thank you for all your work for the OLA-Simple project and for helping and always offering to help me with all the lab obligations to free up my time to finish my writing.

The 2014 award-winning Lutz Jingling Penguin Cake – "the story of Lutz lab."

> *Shivani Dharmaraja, Bob Atkinson, Rahil Jain, Nuttada Panpradist, Ian Andrews, Doan Dinh, Nikki Higa, David McIntyre, Annapurni Sriman, Isabella Spielmann, Annie Wong-on-Wing, Norman Brault, Ryan Gallagher, Enos Kline, Barry Lutz*

Why penguin cake? Short answer: "Penguins are super adorable!" If you haven't seen the movie, "March of the Penguins," you'd better take care of that during the weekends! But if you are one of the few 'penguinologists,' you probably know why

© Copyright 2021 | N Panpradist

they are fantastic: their bravery, persistence, and excellent communication among themselves.

BioE Holiday party 2014

We had more participatns but my hands were full of powder sugar, so I did not take the pictures.

Throughout winters, they travel many miles away from the food source to lay their eggs on the land. During the windy snowstorms, they make a group hug and shield their eggs. They take turns on the periphery so that everyone gets a chance to stay warm when inside. Together, they see themselves through the difficult times and stay positive and productive for the progeny of their species. Therefore, we select the penguins to represent all of us as in this Holiday Bake-off competition.

Throughout this year, the Lutz lab has been through an emotional rollercoaster ride. Dr. Lutz (the giant penguin with some hair poking towards Saturn) was promoted to a tenure-track position and now leads the evolving research team (the other penguins). We just moved into our own lab space (2 days ago), and new members are already popping (and some about-to-be hatched penguin eggs). We are very much like penguins ourselves. We take pride in our work. We are brave to work against complex, impactful problems to improve human lives. We stick together through communication and the bonds we share between us and others in the outstanding UW BIOE Department and the rest of the scientific community. Outside the lab, we have a fun time (as seen as penguins making snow angels, music-responsive dance lights) and spend time with family and friends (check out the penguin-lover couple from the back of the cake).

© Copyright 2021 | N Panpradist

Despite our busiest time (setting up the new lab, training new personnel, and taking final exams), we sought to start a tradition in the lab by participating in the bake-off event by ourselves! We got together, brainstormed, and started making this cake from scratch. We are excited to share the Lutz Lab Edition 1 cake with the UW BIOE family. Participating in this bake-off and being on the same platform as veteran bakers brought us even closer. The trophy will serve as an inspirational source to keep doing great science here in N209C."

TEAM MEMBERS AT THE UW HIC, BPC & NSF I-CORPs

This section would not be possible with **Dr. Rahil Jain,** who convinced me to explore this world of entrepreneurship, and **Dr. Josh Buser** for his expertise on heating and fluidic components of the device. Because of you both, we began the UW HIC competition. Thank you, **Qin Wang**, for being the lifesaver for the last minute of prop integration and even stepped in during the actual competition day. I am proud that we were able to get the 2nd prize. I thank my team members for the BPC competition at the Sweet-16 round: **Dr. Rahil Jain**, **Dr. Blythe Adamson**, **Annapurni Sriram**, and **David McIntyre**, and the Final competition: **Dr. Josh Buser**, **Dr. Justin Vrana**,

2018 UW HIC Competition, L to R: Qin, Josh, Nuttada, and Rahil

2018 UW BPC Competition, L to R: Annapurni, David, Nuttada, Blythe

L to R: Nuttada, Justin, Richard

Nuttada, Josh, Justin, Blythe

© Copyright 2021 | N Panpradist

Dr. Blythe Adamson. Last, I thank **Dr. Justin Vrana** and **Dr. Richard Lee** for joining me in the participation in the UW I-Corps program. Altogether, this experience has helped me understand the work area after product development in the lab and how one might transfer the technology to impact outside the lab.

Moreover, I owe many thanks to **Roi Eisenkot** from UW CoMotion, who spent hours listening and coaching me on entrepreneurship and many other professional aspects. Thank you for introducing me to many programs, from prototype seed funds to the UW NSF I-Corps program. I would also like to thank **Dr. Terri Butler** from HIC and WE-REACH for her advice and support throughout these years.

DR. LISA FRENKEL

Dr. Lisa Frenkel has been critical in my research. I am grateful to the Frenkel lab members for welcoming me to the lab and always being helpful: Ingrid Beck, Dr. Martha Bull, Dr. Ruth Kanthula, Dr. Harocio Duarte, Dr. Thor Wagner, Donald Birch, Steve Bii, Daisy Ko, Jeffrey Myers, Ceejay Boyce, Ross Milne, Hannah Huang, Corey Williams, Molly Levine, Isaac So, and Sheila Styrchak.

Lisa, thank you for being my unofficial mentor and teacher. You introduced me to the field of HIVDR, and I felt honored to be sitting by your side when participating at the annual WHO meetings and being introduced to scientists and clinicians around the world. Dr. Frenkel is knowledgeable about many subjects, and I often learned new concepts beyond science when attending the conference with Dr. Frenkel.

© Copyright 2021 | N Panpradist

Dr. Lisa Frenkel (2018) taught me about Mexican history.

Frenkel lab (2016) from left to right: Sheila, Corey, Martha, Nuttada, Ingrid, Molly, Ross, Thor, and Ruth.

Lisa and **Ingrid**, I am thankful for your hard work and efforts on all the manuscripts and conference proceedings. I am grateful for the personal support and care you have given me through these years. **Ingrid**, it has been a pleasure working with you. Thank you for teaching me about the original OLA, how to work with HIV-seropositive specimens, and your contributions to the OLA-Simple project. You gave me many pieces of advice in research and personal lives every step in a way over the past nine years. I could always turn to you when I faced problems. **Ruth**, thank you for being both my colleague and friend. Even though we live apart, I feel we are immediately connected anytime we meet again. Thank you for spearheading our recent collaboration on SARS-CoV-2 at the Georgetown University pediatric clinic. I am excited to be writing a manuscript with you.

© Copyright 2021 | N Panpradist

DR. ERIC KLAVINS

I would like to thank Dr. Eric Klavins and his lab: **Dr. Justin Vrana, Dr. Yaoyu Yang, Dr. Benjamin Keller, Cami Cordray** for collaborating with us on developing and feasibility testing of OLA-Simple kit 1.0. The interactive guidance was crucial for the implementation of the OLA-Simple kits. We also thank you for the opportunity to participate in the subsequent collaboration of the SARS-CoV-2 detection project led by **Dr. Devin Strickland** and **Cannon Mallory**.

VOLUNTEERS FOR FEASIBILITY TESTS

I thank all the volunteers for evaluating OLA-Simple both here at the UW and in Kenya in 2018. Additionally, I thank the healthcare worker volunteers who participated in the feasibility testing of the COVID-19 Harmony test in 2020. Your feedback was crucial for us to continue to improve the devices.

INBIOS INTERNATIONAL, INC.

I thank **Dr. Syamal Raychaudhuri** and his team for their in-kind assistance in producing the lateral flow strips used in the 2018 Kenya OLA-Simple study and the donation of the Smart Detect™ SARS-CoV-2 rRT-PCR kits in 2020.

© Copyright 2021 | N Panpradist

Syamal, I am grateful for all your helpful advice, discussion, and vision. I thank Dindo Reyes, Kim Polizzi, and Jessica Price for their efforts in producing high-quality lateral flow tests; and Dr. Aarthy Vallur and Kathryn Hjerrild for providing feedback OLA-Simple prototypes. For the SARS-CoV-2 project, I also thank Dr. Frances Chu and Dr. Gwong-Jen J. Chang for their stimulating discussion.

IEH LABORATORY AND CONSULTING GROUP

I thank **Dr. Mansour Samadpour** and his team for the collaboration and support on kit manufacturing for the 2020-21 Kenya Opt4mom/Opt4kids HIVDR studies and the 2021 Fish-OLA project. **Mansour**, thank you for sharing your academic and industrial perspectives and your motivations to do things for the global good. I thank Dr. Hao Geung, Dr. Xing Fei, and Ms. Hikari Akasaki for their work on kit production for the Optstudies. I also thank Dr. Youngsil Ha and Chris Chiu for their work on transitioning the Fish-OLA assay into the format compatible with lyophilized beads and Watson™ mini-cyclers, which the UW Fishery class will use in November 2021.

ADDITIONAL COLLABORATORS

I would like to also thank our clinical collaborators from the OLA-Simple HIV project from the US (**Dr. Rena Patel**, **Dr. Bhanva Cohan**, and **Dr. Paul Drain** from the UW, **Dr. Phyllis Kanki** and **Dr. Holly Rawizza** from Harvard University), Thailand (**Dr. Gonzague Jourdain** and **Dr. Nicole Ngo-Giang-Huong**), Mexico (**Dr. Santiago Ávila-Ríos**), Peru (**Dr. Jaime Soria**), South Africa (**Dr. Theresa Rossouw**), and Kenya (**Dr. Michael Chung** and **Dr. Leonard Kingwara**). I also thank **Dr. Janet Englund** for her advice on swab transfer work.

© Copyright 2021 | N Panpradist

For the SARS-CoV-2 project, I thank our collaborators here on the UW campus (**Dr. Lea Starita**, **Dr. Jay Shendure, Dr. Matthew Thompson, Dr. David Baker, Dr. Paul Yager, Dr. Eric Klavins,** and **Dr. Shwetak Patel**) and collaborators the Fred Hutch (**Dr. Keith Jerome** and **Dr. Pavitra Roychoudhury**), Georgetown University (**Dr. Ruth Kanthula**), Duke University (**Dr. Steve Haase**), Stanford University (**Dr. Benjamin Pinsky**), NIH (**Dr. Benjamin Chimukangara**), and other international collaborators from UK (**Dr. Anton Pozniak** and **Dr. Maria-Teresa Cutino-Moguel**), Brazil (**Dr. Ricardo Diaz**), Zimbabwe (**Dr. Justen Manasa** and **Dr. Vinie Kouamou**), and Mexico (**Dr. Santiago Ávila-Ríos**). Last, I thank our collaborators from the UW Fishery (**Dr. Lorenz Hauser**), UW EE (**Dr. Karl Böhringer**), and NOAA (**Dr. Ingrid Spies**) for the fish project. The complete lists of the collaborators and projects are in **Appendix 6**.

DR. PAUL YAGER, DR. ALBERT FOLCH, & DEAN ALISSA AGNELLO

Coming from a different discipline Petrochemical Engineering, I thought it would be impossible to join Bioengineering. I am grateful to these people who helped prove this wrong. My initial entry to the UW Bioengineering as an intern was made possible because Dean **Alissa Agnello** at North Seattle College introduced me to **Dr. Albert Folch.** I was then referred to **Dr. Paul Yager,** who helped introduced me to his lab members, and eventually, Dr. Lutz offered me an intern position.

After getting accepted to grad school, I began my Ph.D. in the Lutz lab, when the space was shared with Dr. Paul Yager's group. I joined the MAD NAAT project that

© Copyright 2021 | N Panpradist

helped prepare me for the rest of my Ph.D. years. That period was one of the steepest learning curves. Dr. Yager, Dr. Lutz, and other investigators on the project would exchange their ideas from chemistry, physics, and device integrations. Participating in these dynamic meetings and discussion were eye-opening. I would like to thank Dr. Yager and his lab members during the year of 2013 – 2014 who helped me get started in the lab and provided helpful feedback: Dr. Samantha Byrnes, Dr. Josh Bishop, Dr. Joshua Buser, Dr. Lisa LaFleur, Mallory Monahan, Dr. Carly Holstein, Dr. Gina Fridley, Peter Kauffmann, Dr. Bushan Toley, Dr. Mel Li, Dr. Juan Pablo Esquivel, Dr. Xiaohong Zhang, Dr. Erin Heiniger, Dr. Paula Laad, Ryan Gallagher, Max Weller, and Sujatha Ramachandra. I thank recent members for the technical discussion: Dr. Caitlin Anderson and Dr. Kamal Shah. **Dr. Yager**, thank you for your continued support throughout these years. Your advice and feedback on the design of microfluidic devices were helpful for the SARS-CoV-2 typing projects.

GLOBAL WACH & GLOBAL HEALTH COMMUNITY

GH 511 class (2019)

Global WACh 2019 event presentation

As a Global WACh graduate certificate student, I am grateful to be a part of the school of public health. I had an opportunity to learn from my classmates from all around

© Copyright 2021 | N Panpradist

the world and the faculty members who have experience working in different global health settings. I thank **Dr. Judith Wasserheit**, Chair of UW Global Health, and **Dr. Grace John-Stewart**, Director of Global WACh, for their continued support through writing letters of recommendation. Additionally, I thank **Dr. Diana Marangu** for co-developing the proposal idea for detecting tuberculosis in urine samples. I thank **Dr. Brandon Guthrie** and **Dr. Patricia Pavlinac** for giving me opportunities to lecture in their classes. I thank **Dr. Sylvia LaCourse** for collaborating with our lab on the TB drug adherence project. I thank **Dr. Melissa Mugambi** for inviting me to join the expert panel at the OPEN2019 in Washington DC.

DR. SHIRIT EINAV AND DR. STEPHEN QUAKE

I thank **Dr. Shirit Einav** at the School of Medicine at Stanford University and **Dr. Stephen Quake** at the Department of Biophysics at Stanford University for their support and training during my 6-month fellowship to learn about dynamic host responses to infectious diseases using single-cell RNA Seq. This experience was a pivotal part of my Ph.D. **Shirit**, I appreciate your willingness to host me after a cold email and a phone call. You are always responsive to all emails. Thank you for all your valuable career advice. Last year, I was able to apply the knowledge I

Dr. Quake, Nuttada, Dr. Zazini, and Bob

Dr. Einav, Nuttada

Dr. Einav lab (2018)

© Copyright 2021 | N Panpradist

received from this training to help advise other researchers who worked on a SARS-CoV-2 project. I hope I have an opportunity to collaborate/work with you again. Last, I particularly thank **Dr. Fabio Zanini** for his day-to-day supervision and for introducing me to extensive data analysis and rock climbing. I still need further improvements on these skills. Nevertheless, being able to perform basic python coding was practical when I analyzed large datasets in my Ph.D. research.

BIOENGINEERING DEPARTMENT

I am grateful for the support from many people in the Bioengineering Department. I thank the former Chair, **Dr. Cecilia Giachelli**, and Assistant to Chair: **Shirley Nollette** for their help preparing letters of recommendation. **Dr. Giachelli**, thank you for teaching us the professional development class. I still practice my first few sentences to get over my nerves before each talk. I thank former and current UWBioE Academic Counselors: **Dorian Taylor**, **Dr**. **Marta Scatena**, **Dr. Peggy Sharp**, and **Kalei Combs** – for their advice and help prepare letters to apply for the visa and other documents frequently needed to satisfy international F-1 visa. I thank **Chelsea Musick, Elizabeth Mounce, Elisha Hamilton**, and **Norbert Berger,** who helped with countless orderings. **Buzzy**, during the SARS-CoV-2 pandemic, you were very helpful in helping us find alternative supplies so that we could continue research activities in the lab. I thank **Andy Nicastro** for all his help answering questions about international student logistics for every transition: intern to tech, tech to a student, and now a student to a postdoc. I thank **Ruth Woods** for her advice in hiring and training new Lutz lab personnel. I thank **Colleen Irvin** for her help with autoclave training and other logistics. Most importantly, **Colleen**, I will never forget that snack

© Copyright 2021 | N Panpradist

bar you gave me when I was starving. Last, I thank **Laura Wright,** who always shouted out for our successes, big or small. On difficult days, your writing helped cheer me up by reminding me of why I am here.

FUNDING AGENCIES

I thank the APF Student Technology Award for Primary Healthcare for funding my research in 2017-2018. I thank the UW Medicine Bud Tribble and Susan Barnes Graduate Discovery Fellowship for their financial support of my 6-month fellowship at Stanford University in 2018. I thank the 2018 UW Holloman Health Innovation Challenge and Business Plan Competition awards, Lutz's Pilcher Faculty Fellowship, and Office of Science-Industry Partnerships at Seattle Children's Research Institute for their support in the feasibility study OLA-Simple in the USA. I thank Mary Gates undergraduate fellowships that supported all the undergraduate student mentees from 2014 to 2016. OLA-Simple HIV Drug Resistance test development was funded by the 2012 Global WACh-Coulter seed grant and NIH R01 (2013 – 2018: Frenkel AI110375). V-OLA was supported by an NIH R01 (2019 – 2024: Lutz AI145486). The NSF funded codfish species identification (NSF ECCS-183847). SARS-CoV-2 RT-PCR detection project was partly financed by NIH R01 (Lutz AI145486), and the DARPA was funded through the ECE Klavins lab. SARS-CoV-2 LAMP detection project was funded by the US (Lutz AI145486) and UW WE-REACH (U01HL152401).

FAMILY AND FRIENDS

My route to and through the Ph.D. bioengineering program at the UW was non-traditional. It started with my parents, who believed in the power of education. Thank

© Copyright 2021 | N Panpradist

you, Dad and Mom, for being an inspiration and for the sacrifices you have made to fight for your own and our education. My family had a lot of patience while I followed my professional dream so far away from home since 2009. Homesickness was significantly mitigated by my cousins and her co-workers, who fed me many delicious meals.

Before starting grad school at the UW in 2013, I faced financial hardship and had to win the scholarships quarter by quarter to continue my education in the USA. **Dana Brolley** (and her husband **Wolfgang**) helped guide me to secure scholarships and supported me since 2012. While working as an admin at North Seattle College, I received support from **Susan Shanahan**, **Tam Nguyen**, and **Fleetwood Wilson**.

Quynh Ho fed me many meals and drove me to take the GRE far from Seattle on a rainy day. **Fleetwood** helped me apply for the residential tuition fee adjustment and

© Copyright 2021 | N Panpradist

allowed me to stay in school from my own savings. I thank **Greg and his family** for all the support throughout these years. I am grateful for my family and long-term friends in Thailand and new friends in Seattle and many places, all of whom have shared laughter and tears with me throughout this long journey. You know who you are in the photos.

© Copyright 2021 | N Panpradist

TABLE OF CONTENTS

ABSTRACT iii

ACKNOWLEDGMENTS xvi

CHAPTER 1: INTRODUCTION

1.1 Single nucleotide polymorphisms 1
1.2 HIV and HIV drug resistance 2
1.3 Magnitudes of HIVDR and significance of HIVDR testing 7
1.4 Genotypic approaches to detect HIVDR 12
1.5 Oligonucleotide ligation assay for HIVDR detection 22

CHAPTER 2: NUCLEIC ACID PREPARATION

2.1 Viral RNA and DNA as a target for HIVDR test 42
2.2 DNA preparation methods for HIVDR OLA 43
2.3 RNA preparation methods for HIVDR OLA 48
2.4 Future directions 78
2.5 Supplementary information for Chapter 2 94

CHAPTER 3: PAPER-BASED DETECTION FOR HIVDR OLA

3.1 Detection step in the original HIVDR OLA (2002) 103
3.2 Generation 1: Dipstick paper-based detection 104
3.3 Generation 2: Bi-plex paper-based detection 125
3.4 Generation 3: Single-step, sequential delivery paper-based detection 143
3.5 Alternative capture molecules to enable multiplexed detection of HIVDR 160
3.6 Human visual classifications 166
3.7 Analysis software of paper-based detection 167
3.8 Supplementary information for Chapter 3 178

CHAPTER 4: READY-TO-USE DRY REAGENTS

4.1 Excipient formulations 214
4.2 Fabrication platforms of lyophilized reagents 225
4.3 Long-term storage analysis of lyophilized reagents 230
4.4 Other considerations for lyophilizing molecular reactions 234
4.5 Future directions 239
4.6 Supplementary information for Chapter 4 241

CHAPTER 5: OLA-SIMPLE 1.0 KIT FOR HIVDR

5.1 Background 248
5.2 Clinical validation of OLA-Simple 1.0 kits 251
5.3 Usability of OLA-Simple 1.0 kits at UW Klavins laboratory 259
5.4 Piloting OLA-Simple 1.0 to detect HIVDR in Kenya 264
5.5 Adaptation of OLA-Simple 1.0 kit for HIVDR detection in a Mexican cohort 277
5.6 Future directions 292
5.7 Supplementary information for Chapter 5 295

CHAPTER 6: STRATEGIES TO IMPROVE AMPLIFICATION AND LIGATION FOR HIVDR OLA

6.1 Fast PCR 339
6.2 Isothermal nucleic acid amplification technologies 340
6.2.1 iSDA 342
6.2.2 tHDA 343
6.2.3 RPA 346
6.2.4 LAMP 352
6.3. Investigation of ligation 355
6.3.1 Low ligation yield and the possible causes 355
6.3.2 Variable ligation yield across mutations 357
6.3.3 Factors impacting the ligation yield, sensitivity, and specificity 358
6.4 Strategies for isothermal ligation (iLDR) 368
6.5 V-OLA 1.0 (Fast semi-quantitative PCR, iLDR) 370
6.6 V-OLA 2.0 (Single-tube quantitative tHDA and iLDR) 373

6.7 OLA-Simple 2.0 | Fast RT-RPA and 5-cycle ligation 377
6.8 VL test with low-cost equipment and analysis 378
6.9 Supplementary information for Chapter 6 385

CHAPTER 7: FLUORESCENCE-BASED DETECTION OF LDR PRODUCTS
7.1 Molecular beacons and their use in SNP detection 416
7.2 Overcoming polymorphism using reverse MB 420
7.3 Novel Thai elephant probe – an efficient turn-on rMB 426

CHAPTER 8: INTEGRATION OF HIVDR OLA INTO A MORE SIMPLIFIED DEVICE
8.1. Wax-based barriers 429
8.2 Self-contained system for paper-based detection 433
8.3 Pull-tab as a control tool for sequential delivery 435
8.4 Integrated OLA device (version 1) 437
8.5 Solid-phase iNAAT and iLDR 442
8.6 Integrated OLA-Simple version 2 (crossroad design) 443

CHAPTER 9: HOLA: OLA TO DETECT A HUMAN ALLELE (HLA-B*57:01)
9.1 H-OLA for HLA-B*57:01 detection 456
9.2 RPA assay and fast ligation to speed up assay time 464

CHAPTER 10: TECHNOLOGIES IN RESPONSE TO SARS-COV-2 PANDEMIC
10.1 Sample characterization & engineering of swab transfer methods 481
10.2 Simpler & faster RT-qPCR for SARS-CoV-2 detection 517
10.3 Harmony Point-of-Care SARS-CoV-2 detection 549
10.4 Ongoing work 595
10.4.1 A feasibility study of simplified, low-cost covid-19 assay in Zimbabwe 595
10.4.2 In-clinic feasibility testing 604
10.4.3 Use of human-in-the-loop automation to enable SARS-CoV-2 detection 608
10.4.4 SARS-CoV-2 typing assay 611
10.5 Supplementary information for Chapter 10 617

CHAPTER 11: FISH-OLA - SPECIES IDENTIFICATION TOOL TO REGULATE IUU ___ 714

CHAPTER 12: SUMMARY OF CONTRIBUTIONS AND IMPACT 736

APPENDIX 1: FIGURE LIST xxvii

APPENDIX 2: TABLE LIST xxxvi

APPENDIX 3: ABBREVIATIONS xxxix

APPENDIX 4: AWARDS & RECOGNITION xlii

APPENDIX 5: TEACHING & MENTORING xlvii

APPENDIX 6: COLLABORATORS & PROJECTS l

APPENDIX 7: PUBLICATIONS AND MANUSCRIPTS liii

APPENDIX 8: PATENT APPLICATIONS lix

APPENDIX 9: PRESENTATIONS lx

CHAPTER 1: INTRODUCTION

1.1 SINGLE NUCLEOTIDE POLYMORPHISMS

Single nucleotide polymorphisms (**SNPs,** pronounced "snip") are mutations that involve a single nucleotide change (**Figure 1.1**) in the genome. The presence of these SNPs could lead to no translation (nonsense mutation), encoding of the same amino acid as in the wild-type strain (silent mutation), or encoding of different amino acids (missense mutation) from the wild-type strain. Some missense mutations lead to the differences in charge and/or polarity of the encoded amino acids, which can drastically alter protein folding or interaction with other proteins or other surrounding molecules. SNPs are reportedly associated with diseases such as sickle cell anemia[1], Alzheimer's, type-1 diabetes, Crohn's disease, and rheumatoid arthritis[1-3]. SNPs are associated with resistance to treatment for pathogens such as HIV[4], *M tuberculosis*[5], *Bacillus anthracis*[6], *Yersinia pestis*[7], and *Francisella tularensis*[8]. Moreover, SNPs are biomarkers for species or strain identifications[9, 10].

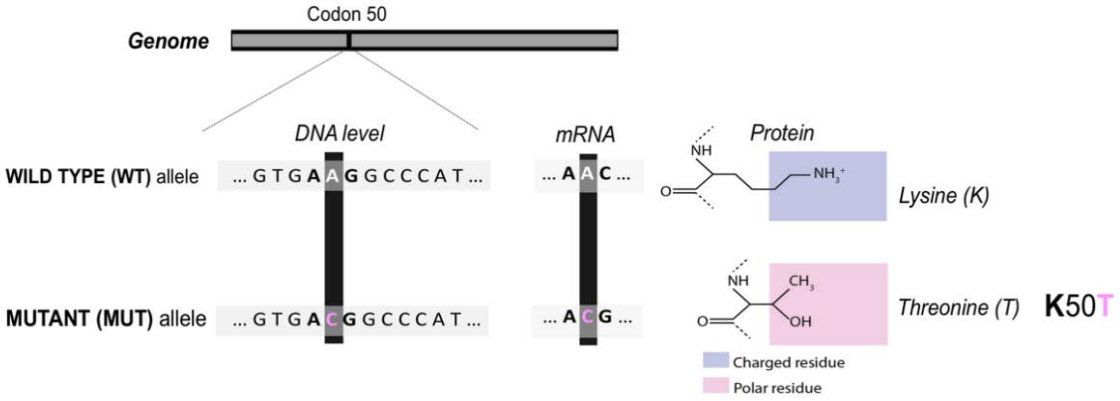

Figure 1.1 | Example of SNP in the genome (K50T).

A base at codon 50 was changed from A in WT to C in the MUT allele. This SNP change can lead to a shift of lysine to threonine.

© Copyright 2021 | N Panpradist

1.2 HIV AND HIV DRUG RESISTANCE

1.2.1 STRUCTURE AND LIFE CYCLE OF HIV

Each HIV virion has an envelope covering a capsid that contains two strands of RNA and three enzymes essential for its replication – reverse transcriptase, integrase, and protease[11]. HIV virion targets white blood cells in the human immune system, such as CD4 helper T cells[12] (**Figure 1.2**). HIV envelope proteins bind to the chemokine receptors on the surface of CD4 cells, causing membrane fusion. This process releases viral RNA strands and the three enzymes into the host cells. The reverse transcriptase enzyme of HIV then uses host resources to generate viral DNA. The integrase enzyme of HIV then inserts the viral DNA into the human genome. Through a routine process of human genome replication and transcription, HIV polyprotein and RNA are regenerated. The HIV polyprotein and viral RNA are then packaged and budded out of the CD4 cells. Next, the protease enzyme of HIV cleaves the polyproteins into three functional enzymes. If unsuppressed, this cycle of HIV replication continues and further attacks the human immune system.

1.2.2 ANTIRETROVIRAL DRUGS DISRUPT THE HIV REPLICATION CYCLE.

To date, there are six classes of antiretroviral drugs (**ARVs**) designed to target different steps in HIV replication (**Figure 1.3**) – Nucleoside reverse transcriptase inhibitors (**NRTIs**), Non-nucleoside reverse transcriptase inhibitors (**NNRTIs**), Protease inhibitors (**PIs**), Integrase inhibitors (**INSTIs**), Fusion inhibitors (**FIs**), and Chemokine receptor antagonists (**CCR5 antagonists**).

© Copyright 2021 | N Panpradist

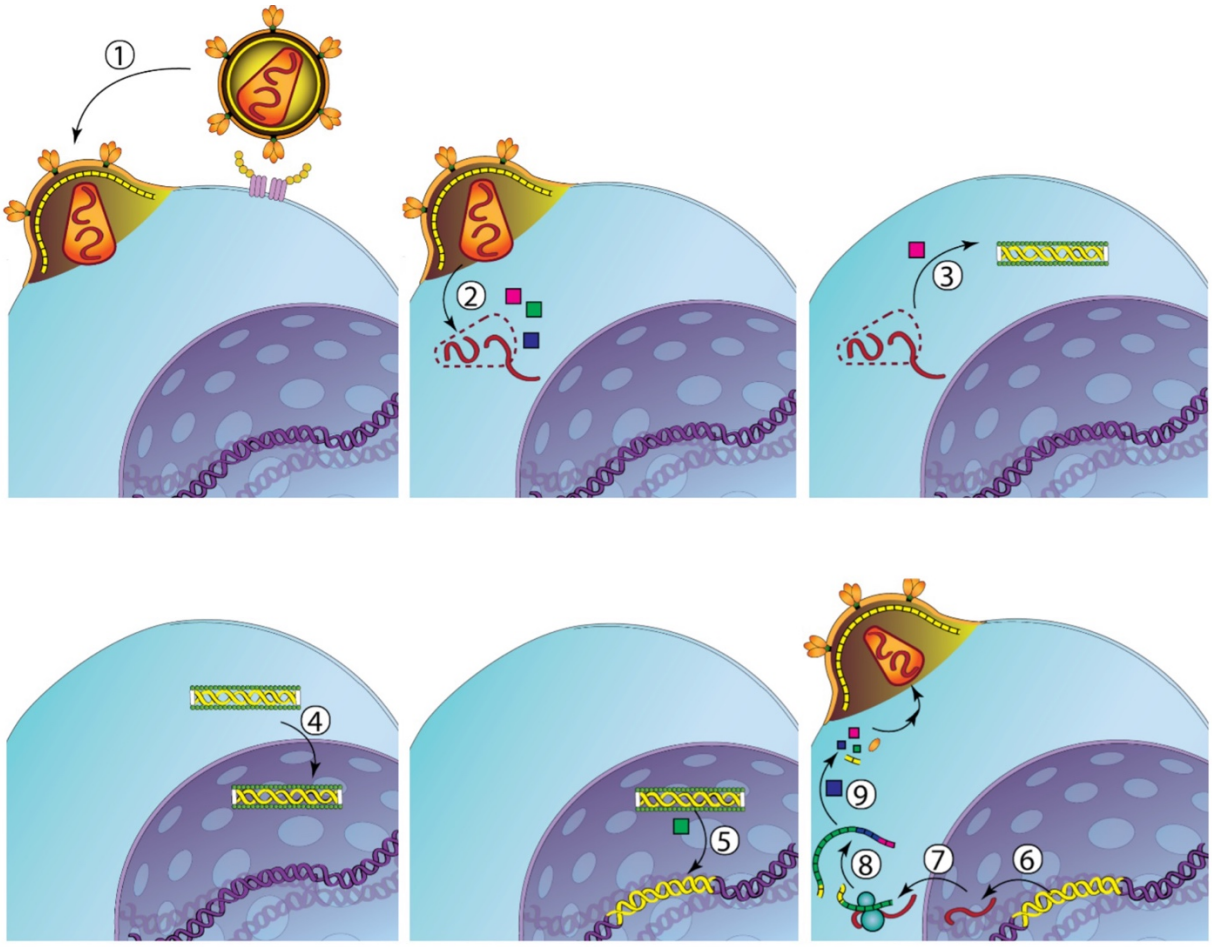

Figure 1.2 | Schema of HIV integration into human genomic DNA.

(**1**) HIV enters host T-cells by attaching its *gp120* domain to the human CD4 receptor. (**2**) Nucleocapsid is uncoated, releasing HIV RNA and HIV enzymes: reverse transcriptase (pink), integrase (green), and protease (blue). (**3**) HIV reverse transcriptase (RT) enzyme generates complementary DNA (cDNA) strand of the HIV RNA. (**4**) Unintegrated HIV DNA travels through nucleopores into the nucleus. (**5**) HIV DNA is incorporated into the human genome as proviral DNA. Via human machinery, **(6) – (9)** proviral DNA was transcribed into the RNA, later translated into HIV polyprotein. All component of HIV virion is then packaged and budded outside the CD4 of the host. HIV protease converts polyproteins into functional proteins in mature HIV virions.

© Copyright 2021 | N Panpradist

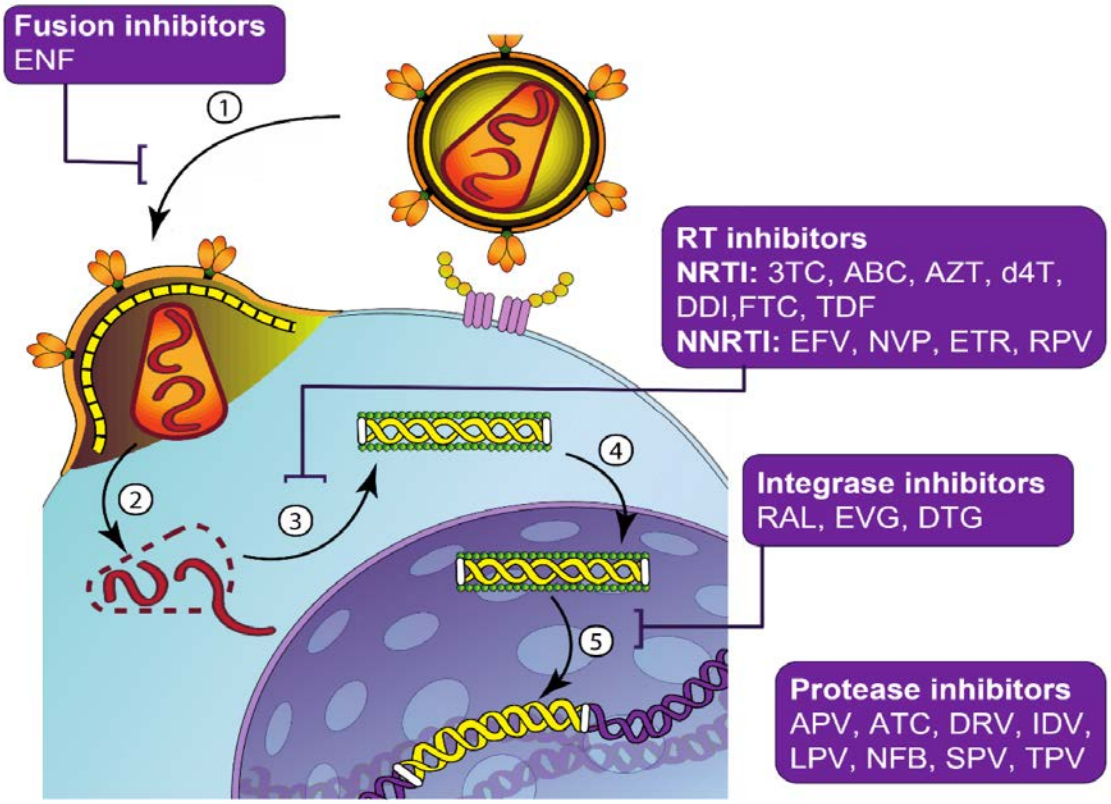

Figure 1.3 | HIV antiretroviral treatments disrupt different steps of HIV replication.

Treatment regimens contain a combination of these ARVs. In the USA and resource-rich communities, HIV-infected individuals have access to multiple ART regimens throughout their lifetime. On the other hand, those in LMICs typically have limited access to only a few standard regimens, referred to as first-line and second-line ART. In the past decade, the WHO has launched different guidelines for treatment options (**Table 1.1**). The median price of the 1st-line ART is reduced over time, and more people are on ART. In many low-income countries, the current first-line is made of two NRTIs (**TDF**/**3TC**) and dolutegravir (**DTG**)[13]. However, some medium-income countries not a part of the DTG patent pool waiver still do not have access to DTG, and the first-line ART is still made of two NTRI or one NNRTIs (*e.g.*, tenofovir + lamivudine or emtricitabine). For the pediatric

© Copyright 2021 | N Panpradist

population, DTG containing formulation may not be applicable for all ages and weights (**Table 1.2**).

Table 1.1 | Landscape of adult global HIV treatment over the past 10 years.

Parameters	2010	2013	2017	2021
People living with HIV (PLHIV)	33M	35M	37M	38M
PLHIV on ART	7M	10M	21M	28M
New HIV infections/year	2.6M	2.1M	1.8M	1.5M
AIDS deaths	1.8M	1.6M	1M	0.7M
Global treatment policy/strategy	Treatment 2.0	15 by 15	Treat all	End AIDS by 2030 (95-95-95)
Most used 1st line regimen in LMICs	AZT/3TC/NVP (d4T phase out)	TDF/XTC/EFV (consolidation)	TDF/XTC/EFV (Transition to DTG)	TDF/3TC/DTG (consolidation)
Median price 1st line regimen in LMICs per person per year (in $US)	160	120	85	65

Table 1.2| WHO 2019 Pediatric ART recommendations

Parameters	Neonates	Children
Preferred	AZT+3TC+RAL	ABC+3TC+DTG[1]
Alternatives	AZT+3TC+NVP	ABX+3TC+LPV/r ABC+3TC+RAL[2] TAF[3]+3TC+(or FTC) + DTG
Special circumstances[4]	AZT + 3TC+LPV/r	ABC + 3TC+NVP ABC+3TC+EFV AZT+3TC+EFV AZT+3TC+RAL AZT+3TC+LPV/r AZT+3TC+NVP

1. For age and weight groups with approved DTG dosing (50mg adult tablet form 20kg, TLD can be used in adolescents weighing more than 30kg). 2. RAL should only be used as an alternative regimen only if

© Copyright 2021 | N Panpradist

LPV/r solid formulations are not available. 3. For age and wright groups with approved TAF dosing (adult dose of TAF can be used in children weighing 25kg or more) 4. In cases where no other alternatives are available.

1.2.3 REVERSE TRANSCRIPTASE INHIBITORS

NRTIs and NNRTI are the most used ARVS. They disrupt HIV reverse transcriptase functions using different mechanisms. NRTIs are chain terminations. Once activated via intracellular phosphorylation to have three phosphate groups, they mimic the structure of the human nucleoside structures and compete with the human nucleosides during the cDNA generation step. Except these phosphorylated NRTIs do not have 3' hydroxyl, hence if they are incorporated during cDNA generation step, the HIV RT would not add the next nucleotide. In contrast, the NNRTIs bind directly to the p66 subunit of HIV RT[14], leading to a conformational change in its polymerase domain and halt the DNA polymerization step.

1.2.4 HIV RAPIDLY MUTATES TO BECOME RESISTANT TO ART

During replication, the error-prone HIV RT introduces mutations at a high rate[15]. For each cycle of replication, 5-10 SNPs can occur[16]. In an unsuppressed individual, new 10^{11} virion can be reproduced daily[17], and thus theoretically, 180-360 SNPs can arise. Missense SNP, altering amino acid sequences near drug-targeting sites (**Figure 1.4**), causes these mutant strains to become resistant to specific drugs across the 1st-line NRTI/NNRTI regimen[18].

© Copyright 2021 | N Panpradist

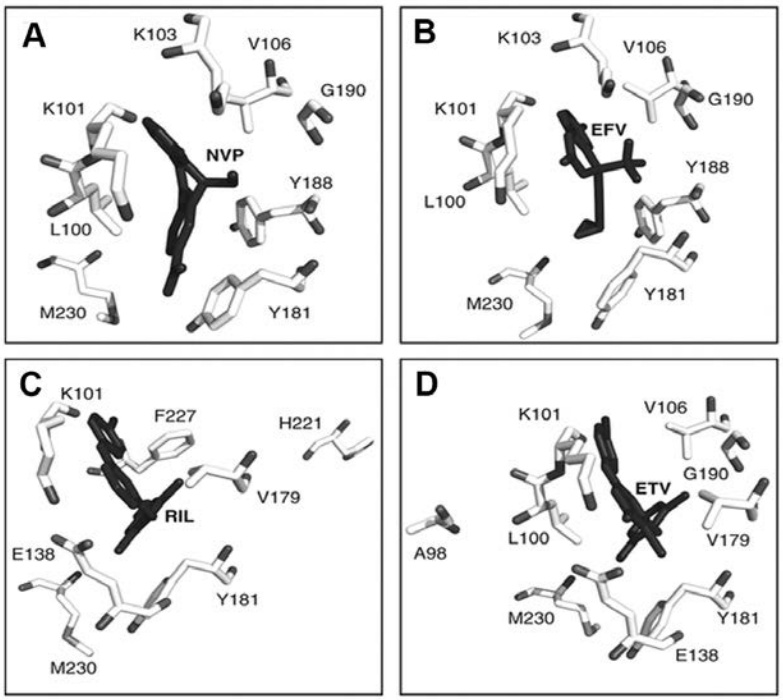

Figure 1.4 | Amino acid residues near the binding pockets of RT inhibitors

(**A**) Nevirapine (NVP), (**B**) Efavirenz (EFV), (**C**) Rilpirivine (RIL), and (**D**) Etravirine. The image was obtained from the Handbook of Antimicrobial resistance[19].

1.3 MAGNITUDES OF HIVDR AND SIGNIFICANCE OF HIVDR TESTING

In LMICs, HIV treatment programs rely on the public health approach of "treating all with the 1st-line therapy," which can be ineffective due to the selection of drug-resistant HIV (**Figure 1.5A**). Specifically, individuals infected with drug-resistant HIV are more likely to fail therapy[20], which in turn can lead to transmission of HIVDR, increased morbidity and mortality, and higher healthcare costs. Rising pre-therapy HIVDR occurred as the ART scaled up globally[21], with a pre-treatment HIVDR (**PDR**) prevalence of 5–20% and 50–90% in people failing ART[22]. In women and children with previous exposure to

© Copyright 2021 | N Panpradist

antiretroviral drugs for prevention of mother-to-child transmission (**MTCT**) of HIV, PDR to nucleoside reverse transcriptase inhibitors (**NRTIs**) and non-nucleoside reverse transcriptase inhibitors (**NNRTIs**) can be up to 30 and 75%, respectively[23]. In addition, a study in Uganda reported 98% of children failing an NNRTI first-line regimen had dual-class HIVDR, with thymidine analog mutations in 50%[24], which can undermine the effectiveness of the second-line and third-line regimens.

In response to the high prevalence of PDR to NNRTI, the WHO recommends countries with more than 10% PDR start all people living with HIV on a preferred first-line regimen containing dolutegravir/NRTIs[25], which has demonstrated a high barrier to resistance in multiple clinical trials[26, 27]. However, NNRTI-based regimens are still the preferred first-line option in many communities that recognize drug patents due to the high cost of DTG-based regimens[28], and in populations with fixed-dose combinations containing dolutegravir are not recommended such as persons co-infected with tuberculosis or young infants. In countries with more than 10% PDR where using an integrase inhibitor-based regimen is not feasible, the WHO recommends testing for PDR to guide selecting an effective regimen[25]. In addition, in populations switching to DTG-based regimens where HIVDR to NRTIs is prevalent, HIVDR testing could aid in selecting effective NRTI combinations to prevent the possibility of functional dolutegravir monotherapy, as increased virologic failure has been associated with dolutegravir monotherapy[29].

© Copyright 2021 | N Panpradist

Based on these findings, we highlight the importance of guiding ART choice by HIVDR testing as is done in the USA, as this could maximize the efficacy of ART and improve survival and rates of suppression of HIV replication (**Figure 1.5B**).

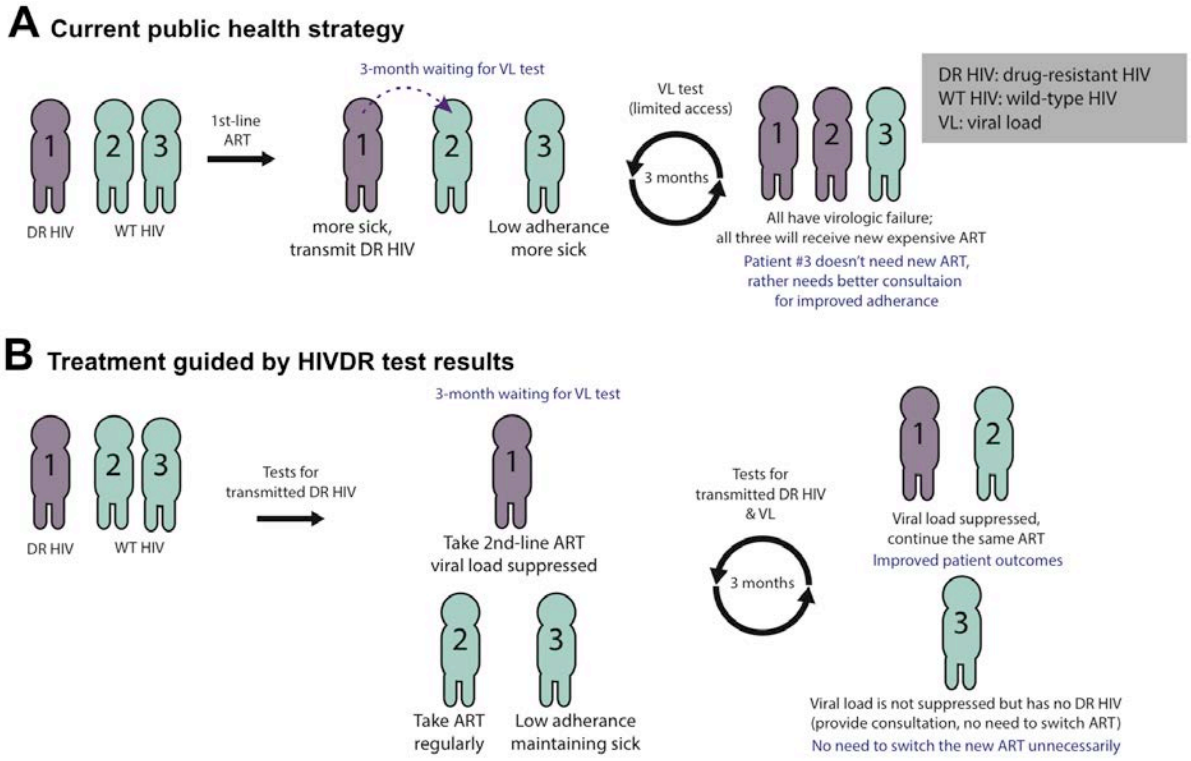

Figure 1.5 | Comparison of HIV treatment strategies.

(A) Public health strategy: treatment of PIH based on 1st-line ART in a trial-and-error fashion. During the wait time for the VL (>3 months), patients infected with drug-resistant HIV continue to infect non-HIV-infected individuals or re-infect HIV-infected individuals with drug-resistant HIV. Additionally, a VL test cannot differentiate between virologic failure due to HIVDR or poor adherence (patient not taking the drugs), resulting in an unnecessary switch to a more expensive ART regimen. (**B**) Patient-guided strategy. PIH is treated based on the HIV variants and VL status. HIVDR testing can detect transmitted HIVDR before ART initiation to ensure an effective outcome. Effective treatment will reduce cases of virologic failure in patients taking their ART regularly. Patients with low adherence will still have a virologic failure, but with access to HIVDR technology, the clinicians will know that they are not taking their

© Copyright 2021 | N Panpradist

drugs. Instead of switching to new ART, these patients need a consultation to improve adherence. HIVDR testing in primary care settings will improve patient outcomes, reduce HIV transmission, and prevent wasted resources.

Compared to the case of patients receiving the same ART without HIVDR testing, it has been shown that using the gold standard consensus sequence as a tool to enable patient-guided therapy before ART initiation is cost-effective despite its high cost (>$200-$700/specimen)[30, 31]. Treating patients with proper ART will improve patient outcomes and preserve a more expensive second-line ART for those who have already developed HIVDR. For post-ART HIV-infected individuals, the WHO recommends using a viral load test to evaluate the drug's performance six months after ART initiation (whereas in the USA, it is recommended 2-4 weeks)[32]. Compared to switching the ART without the VL results, it was shown that using a viral load test as a treatment-monitoring tool is cost-effective despite its high cost (>$200/specimen)[33, 34]. Patients failing treatment will be switched to the new regimens, potentially improving patient outcomes and reducing HIV transmission. However, virologic failures can be caused due to low adherence (patients not taking the drugs) or HIVDR. If the cause is due to low adherence, patients should not be switched to the new ART regimen, but rather need adherence counseling to improve the reliability of drug intake.

In 2015 the WHO authorized the use of oral PrEP (Pre-exposure prophylaxis) that is the blend of NNRTIs in populations with a high risk of HIV infection. If HIVDR could be an issue in this population when (i) PrEP is initiated during undiagnosed acute HIV infection, (ii) unrecognized HIV infections exposed to PrEP for longer

© Copyright 2021 | N Panpradist

periods, or (iii) a person infected with transmitted HIVDR. Thus, HIVDR testing prior to or after breakthrough infections is crucial in countries scaling up PrEP.

SUMMARY OF POTENTIAL USE CASES FOR HIVDR TEST BASED ON THE WHO 2019 GUIDELINE

In adult populations, including pregnant women

a. If they are PrEP users, NNRTI/NRTI HIVDR testing should be performed as a pre-treatment HIVDR test to enable proper 1st-line treatment initiation.
b. If they are not PrEP users when switching the 2nd line to 3rd line treatment, HIVDR testing on mutations associated with NRTI, PI, or NNRTI is recommended

In children populations

c. For pre-treatment populations or populations switching to 2nd-line treatment, HIVDR testing on mutations associated with INSTI/NRTI is recommended.
d. For 2nd-line switching to 3rd-line treatment, HIVDR testing on mutations associated with PI, NRTI, NNRTI is recommended.

CHALLENGES IN THE DEVELOPMENT OF HIVDR TEST FOR LOW-RESOURCE SETTINGS

To date, there exist several molecular tools for specific detection of SNPs conferring HIVDR, but these technologies may not be suitable for HIV. First, the HIV genome is polymorphic. Hence, appropriate SNP detection technologies for HIV must tolerate genetic variations. Second, low proportions of HIV drug-resistant SNPs (*e.g.,* <10%) are associated with treatment failures[35]. Thus, such technologies should be sensitive enough to detect clinically relevant proportions of drug-resistant SNPs. Third and importantly, HIV is most prevalent in low-resource

© Copyright 2021 | N Panpradist

settings such as Sub-Saharan Africa and Southeast Asia. As a result, ideal SNP detection technologies for HIV should be affordable and easy to use.

1.4 GENOTYPIC APPROACHES TO DETECT HIVDR

Two main categories of SNP detection technologies are consensus sequencing and allele-specific discrimination. Below we describe the principles used in these SNP detection methods and their potential as tools for detecting HIVDR.

1.4.1 SEQUENCING

These sequencing methods are not specific to HIV. Instead of looking at specific sets of SNPs, it provides the sequence information of a region **(Figure 1.6A**) or the whole genome. Based on this feature, all HIVDR SNPs can be screened at once. However, consensus sequencing such as the Sanger method cannot detect low levels of drug-resistant HIV (~10%-25% of total virus)[36, 37]. It is unsuitable for use in poor regions because it is expensive ($200-$700/specimen) and requires training and sophisticated laboratory facilities[30, 31]. ViroSeq™ was the first platform for HIV genotyping approved by FDA/EU, but it is currently being discontinued. A next-generation sequencing (**NGS**) based HIVDR test, "VELA Diagnostics," has recently been authorized by the US FDA for clinical use. The system is fully automated and validated in several laboratories in UK[38], US[39,40], and other countries[41, 42]. Vela Sentosa™ diagnostics detected down to 1-5% frequencies of quasispecies[38, 43] in PR, RT, and IN regions of HIV. ABL DeepChek also offers FDAEU-approved HIV genotyping assays using both Sanger and NGS platforms. The US CDC also developed research use only kits for PR and RT regions anis d currently made available via

© Copyright 2021 | N Panpradist

ThermoFisher. Due to its high cost and requirement of sophisticated laboratory facilities, these sequencing-based technologies will likely be limited within centralized, national laboratories.

Several portable platforms of sequencing technologies are being developed. A palm-sized sequencer "MinION" by Oxford Nanopore Technologies can be connected to a computer's USB port currently commercialized with a $1000 installation cost. Previously, the capability of MinION in detecting SNPs was limited due to a high miscalling error rate of 15-20% [44], but improved algorithms have been demonstrated to reduce the error rate. Analysis of HIV amplicon using MinION showed 95% concordance to Sanger sequencing[45].

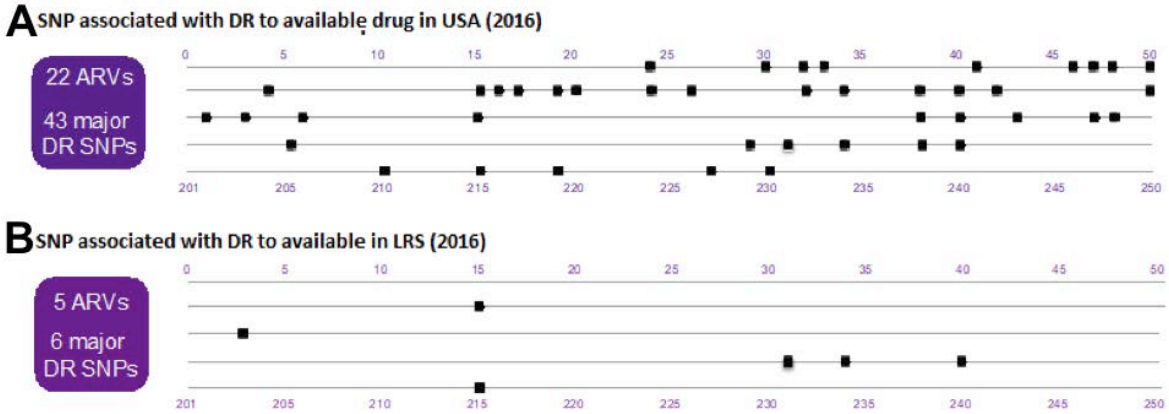

Figure 1.6 | SNPs associated with ART failures.

(**A**) SNPs associated with 22 antiretroviral drugs (**ARVs**) available in the USA in 2016 – all are screened before treatment initiation. PIH's blood is tested for the presence of these SNPs in the HIV RT region using sequencing-based genotyping. (**B**) In low-resource settings (**LRS**), only a few ART regimens are available. The NNRTI-based 1st-line regimen has only six associated HIVDR SNPs. The position on the lines is the codons in the HIV RT from 1 – 250.

© Copyright 2021 | N Panpradist

1.4.2 ALLELE DISCRIMINATION

One set of oligonucleotide probes or primers is designed to detect only a single SNP using one or more of the following principles: hybridization, nucleotide incorporation (extension), nucleotide ligation, and nucleotide cleavage. These technologies could be beneficial in LRS where available ART regimens are limited, and the HIVDR test only needs to detect these few known SNPs (**Figure 1.6B**).

1.4.2.1 HYBRIDIZATION-BASED SNP DETECTION

An allele-specific probe is used to discriminate a mutant template with the SNP of interest from a wild-type template (**Figure 1.7A**). A single-base mismatch sufficiently destabilizes the duplex of probe and template. Only when there is a perfect match at the SNP of interest, probe and template hybridization occurs. The presence of probe and template duplexes can be detected. For example, two ends of an allele-specific probe (loop) can each be conjugated to each other through a complementary oligonucleotide pair (stem) region to become a molecular beacon probe (**Figure 1.7B**). Hybridization of the loop region to the template opens the stem region, separating the quencher from the fluorophore. This state creates a signal. When there is no hybridization of the loop region, the stem region stays bound and keeps the quencher and fluorophore molecule in proximity. This state does not create a signal.

© Copyright 2021 | N Panpradist

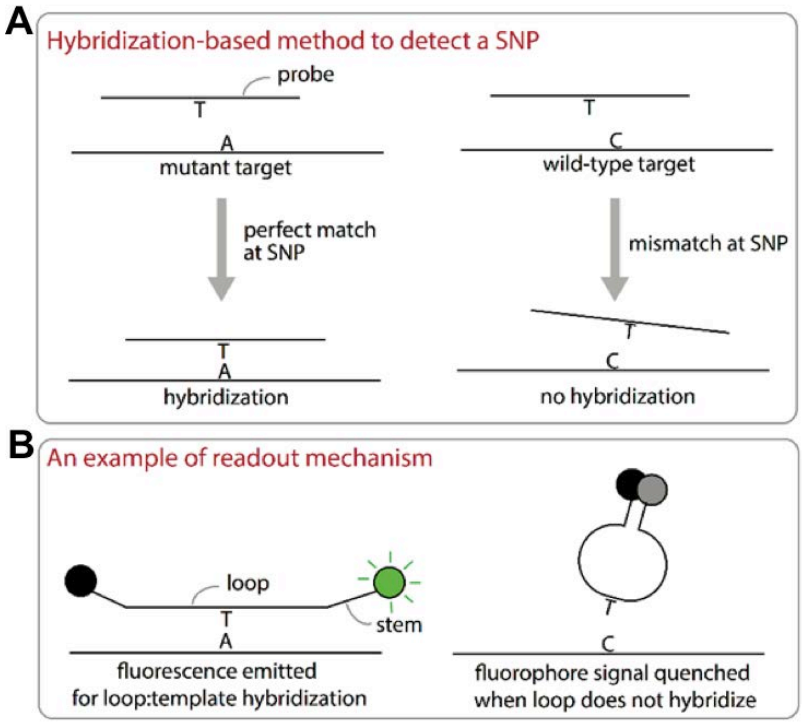

Figure 1.7 | Hybridization-based SNP detection.

Because the HIV genome is highly variable, standard hybridization-based approaches do not apply to HIV targets (**Figure 1.8A**). Dr. Shafer's group at Stanford University exploited the differences in affinity between the matched and mismatched sequences to detect different HIVDR variants via multiplexed melt curve analysis. The microscopy-based prototype could detect ≥10% K103N[46]. Dr. Essex's group at Harvard University developed **PANDAA**[47] (Pan Degenerate Adaptation and Amplification), PANDAA probes wipe out these polymorphisms around the targeting SNPs. During the amplification step, forward and reverse primers are designed to include degenerate bases to account for HIV polymorphisms upstream and downstream of the probe hybridization region (**Figure 1.8B**).

© Copyright 2021 | N Panpradist

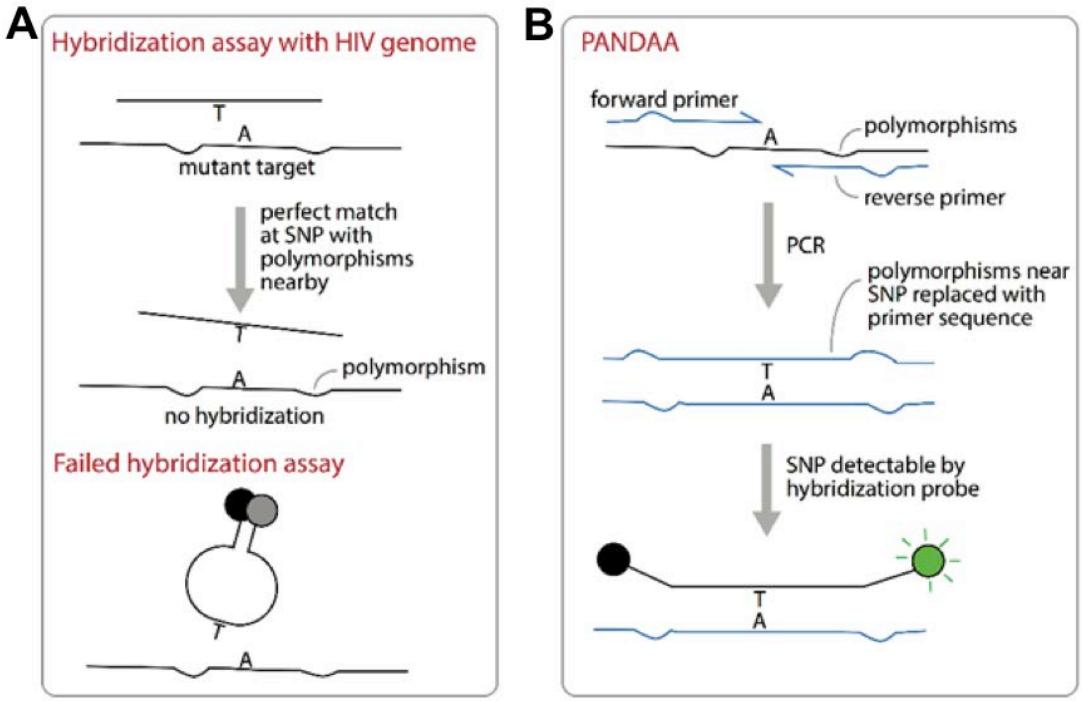

Figure 1.8 | **Hybridization-based SNP detection in a highly-polymorphemic genome.**

(**A**) Issues in traditional hybridization probe on HIV genome. (**B**) How PANDAA overcomes the issue.

The sequences of the primers in this region remain conserved to the HIV consensus sequence. During the amplification step of PANDAA, only one nucleotide at the SNP is extended from the 3' end of primers[48]. This process removes genomic variation of HIV near the SNP of interest and allows for successful probe hybridization. The PANDAA has been shown to reliably detect six SNPs associated with HIVDR with a sensitivity of ≥5% mutation[47] with 2 hours to results (after nucleic acid extraction step). Compared to NGS, PANDAA shows 96.9% sensitivity and 97.5% specificity. However, the specificity was reportedly lower in a study in Zimbabwe with 76% specificity in NNTRI DR detection versus Sanger, and the majority of these were proven falsely detected MUT by NGS[49]. Employment of PANDAA outside the centralized laboratories presents

© Copyright 2021 | N Panpradist

challenges. First, robust one-base discrimination in a hybridization-based detection method requires a stringent condition. Variation of salt concentrations during the manual PCR setup can impact the assay's sensitivity and necessitate the need for trained personnel. Second, PANDAA relies solely on PCR amplification. Formation of non-template amplification, such as amplification of primer-dimers, can create false-positive results or impact assay specificity. Third, PANDAA requires a costly thermal cycler machine (~$30k) with a capacity to measure multiple fluorescence signals to track the presence of HIVDR and WT.

1.4.2.2 NUCLEOTIDE-INCORPORATING SNP DETECTION

Nucleotide-incorporating SNP detection is also known as allele-specific PCR (**AS-PCR**). The specificity of this method relies on an allele-specific probe and a highly selective polymerase. An allele-specific primer is designed to include the SNP of interest at 3'end. A polymerase selectively extends the 3' end only when the base at the 3' end is perfectly complementary to the template (**Figure 1.9**). Extended products (amplicon) inferring the presence of the SNP can be detected in real-time using molecular beacon probes or at the end using electrophoresis. Several research groups have successfully designed singleplex and multiplexed nucleotide-incorporating assays to detect HIVDR as low as 2-5% mutation [50-52]. AS-PCR also has been transferred to the isothermal AS-LAMP (allele-specific loop-mediate isothermal amplification) assay to detect SNPs in the mosquito genome [53, 54]. This platform eliminates the need for a thermal cycler and is more suitable for low-resource settings. However, the *Bst* 2.0 polymerase used in AS-LAMP has not yet been tested to tolerate genetic variations of the HIV genome.

© Copyright 2021 | N Panpradist

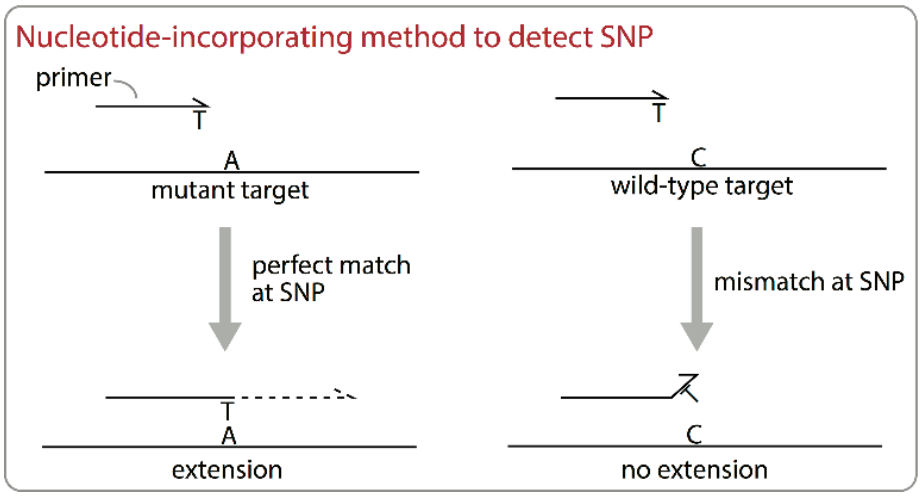

Figure 1.9 | Nucleotide-incorporating SNP detection.

1.4.2.3 NUCLEOTIDE CLEAVAGE DETECTION

Nucleotide cleavage detection is also known as the invader assay or invasive assay. The specificity of this method relies on two allele-specific probes and one structure-specific flap endonuclease (**FEN**) (**Figure 1.10A**). An invader probe is complementary to the template except for the 3' end, which has a non-matching base at the SNP of interest. Another probe is complementary to the template with a 5' matching base at the SNP and an extended flap region that does not complement the template. FEN recognizes this structure of probes and templates and cleaves the flap region, including the SNP. If the probe with the flap contains a quencher and a fluorophore (**Figure 1.10B**), the cleavage can be detected from the emission of the fluorophore that is no longer in proximity with the quencher. The probe design is very crucial for the specificity of the invader assay. The 3' end of the invader probe determines the cleaving position of FEN. Thus, it must be on the SNP location. One base shift can lead to a false positive or negative signal[55]. The invader assay has not been used to detect

© Copyright 2021 | N Panpradist

drug-resistant HIV. To date, it has also not yet been reported how well FEN tolerates polymorphisms near the SNP.

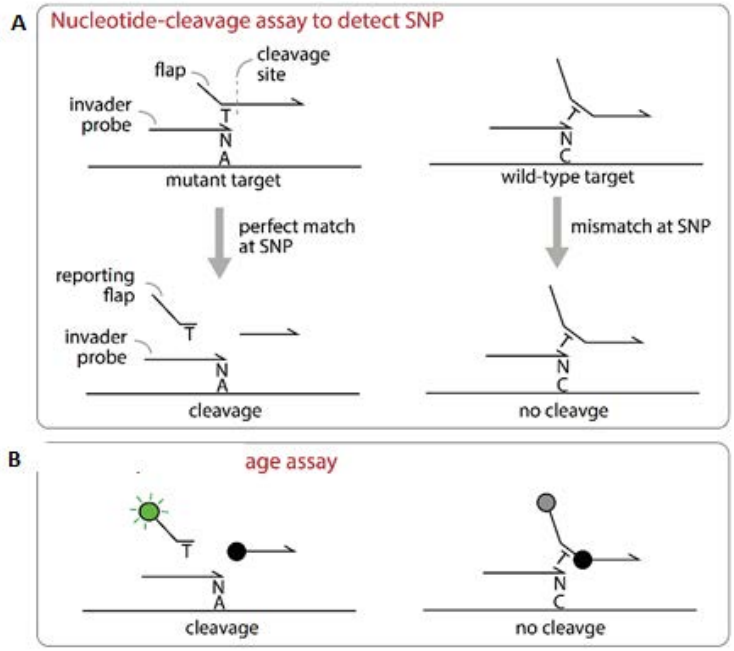

Figure 1.10 | Nucleotide-cleave assay to detect SNPs.

1.4.2.4 CRISPR/CAS-BASED SNP DETECTION

Clustered regularly interspaced short palindromic repeats (**CRISPR**), DNA sequences found in ≥50% of prokaryotic genomes, are derived through previous phage infections to defend the prokaryotes from future phage infections. The enzyme CRISPR-associated proteins (**Cas**) uses these CRISPR DNA sequences to guide the sequence-specific cleavage. CRISPR/Cas gene-editing systems have been utilized as research tools both therapeutic[56, 57] and diagnostic proposes[58, 59]. Each CRISPR/Cas system is slightly different in terms of the size of Cas proteins, nucleic acid (dsDNA, ssDNA, or RNA) that it cuts, and dependency of protospacer adjacent motifs (**PAMs**). CRISPR/Cas9 was first used in diagnostics of Zika virus[60],

© Copyright 2021 | N Panpradist

and later CRISPR/Cas12, CRISPR/Cas13, and CRISPR/Cas14 are discovered and also used in diagnostic applications (**Table 1.3**)[61] including SNP detection. Detection of SNPs associated with genetic diseases in dsDNA human DNA targets present at a relatively high concentration can be done directly without amplification using a CRISPR/Cas9 system[59]. SHERLOCK technologies used CRISPR/Cas12a and CRISPR/Cas14 systems to discriminate one SNP. These systems target dsDNA or ssDNA; thus, to detect SNP in viral RNA, reverse transcription (optionally with amplification) is performed before SNP discrimination. Fluorescence-based detection of SNP after RNA extraction and RT-RPA (reverse transcription, recombinase polymerase amplification) has been developed to detect SNPs in SARS-CoV-2 with 95% specificity and 96% sensitivity[62]. In the context of HIV cure, a CRISPR/Cas9 system was used to *in-vitro* edit HIV-1 *tat* and *rev* genes, demonstrating highly suppressed p24 levels. CRISPR/Cas13 system was used as part of an on-chip droplet microscopy platform for multiplex detection (splitting reactions in tiny droplets) of the 6 SNPs associated with HIVDR, with an aM ($6x10^{12}$ copies/μL) sensitivity range. Compared to other standard methods, this system has 90-93% clinical sensitivity versus Sanger and 86-93% versus NGS (n=22, from multiple subtypes)[63]. It is worth noting that a few mismatches in the target region could drastically drop the performance of this approach. Still, the performance can be gained by altering the base at the mismatched locations. Given that this system has flexibility in assigning multiple droplets to detect a single HIVDR SNP, the system is likely tunable to detect a low copy number of HIV. However, its specificity to discriminate minority variants in a single patient must be further tested in the larger population.

© Copyright 2021 | N Panpradist

Table 1.3 | Properties of CRISPR/Cas systems commonly used in diagnostics[61].

Protein Family	Cas12a	Cas13	Cas14
Rough protein length (amino acids)	~1,300	~1,400	~400 - 700
Single guide molecule size (nucleotides, nt)	42-44 nt	~64 nt	~140 nt
Targeted nucleic Acids (DNA or RNA)	DNA (ss or ds)	RNA (ss)	DNA (ss or ds)
Non-specifically cut nucleic acids (DNA or RNA)	DNA (ss)	RNA (ss)	DNA (ss)
Targeting restrictions	dsDNA targets must be near TTTN	Weak requirements dependent upon family member. Activity is also constrained by RNA secondary structure	None for ssDNA. dsDNA targets must be near T-rich sequences like TTTA
Accuracy	Effectively discriminates between targets off by one bp (dsDNA)	Difficulty discriminating between targets off by one bp	Effectively discriminates between targets off by one bp (ssDNA)

1.4.2.5 LIGATION-BASED SNP DETECTION

The ligation-based SNP detection reaction involves two allele-specific probes and one template-dependent ligase (**Figure 1.11**). One of the complementary probes must be phosphorylated at the 3' end, while the 5' of the other complementary probes must also include the base at the SNP. If the bases at the juncture of the two probes are perfectly complementary to those of the template, the two probes are covalently linked (ligated). Ligation-based SNP detection such as **LCR** (Ligase Chain Reaction)[64] can directly detect SNPs without amplification. It can also be coupled with pre-amplification or post-amplification steps such as **LRA** (Ligation RNA Amplification)[65], **OLA** (Oligonucleotide Ligation Assay)[66, 67], and **MIPA** (Molecular Inversion Probe Assay)[68]. LRA has been used to detect as low as 0.01%

© Copyright 2021 | N Panpradist

K103N mutation when using $2.5x10^5$ RNA copies[65]. Like, PANDAA, LRA still relies on an expensive thermal cycler with a capacity to measure fluorescence.

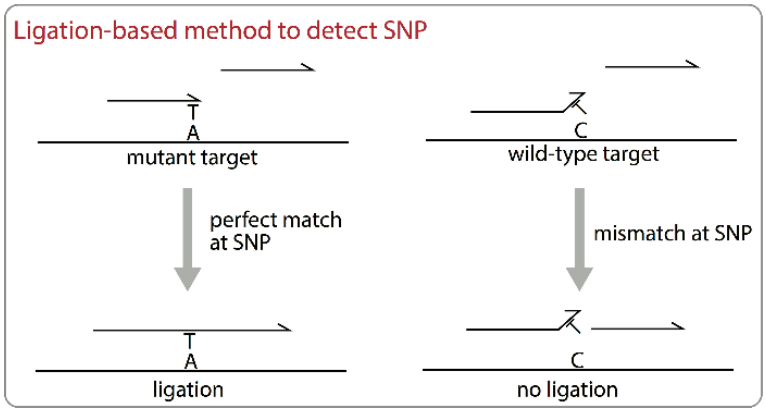

Figure 1.11 | Ligation-based SNP detection.

1.5 OLIGONUCLEOTIDE LIGATION ASSAY FOR HIVDR DETECTION

In 1988, the oligonucleotide ligation assay (**OLA**) was first developed to diagnose mutations associated with sickle-cell anemia[69]. The Frenkel lab at Seattle Children's Research Institute was then adapted to detect HIVDR mutations[70]. To detect HIVDR, it is essential to include the WT allele detection as a control to differentiate truly WT from failed ligation reaction (i.e., indeterminate results). The Frenkel lab validated the assay for detection of HIVDR associated with protease and reverse transcriptase inhibitors[67, 71], and the lab has been CLIA-certified to perform this assay for clinical diagnosis of HIVDR. This CLIA OLA is highly sensitive for detecting minority mutant variants (2–5% of an individual's HIV population)[72, 73] and is tolerant of genetic polymorphisms in clinical specimens[71], and can be adapted to regional variants[74]. The OLA has been used outside the USA to study HIVDR in various clinical scenarios in Thailand[75] and Africa[76, 77].

© Copyright 2021 | N Panpradist

OLA takes advantage of probe hybridization and absolute specificity of ligation to identify a specific base mutation (**Figure 1.12**). Two DNA probes hybridize adjacent to one another, with the 3'-end of the upstream probe annealing to the site of the mutation of interest. The probes are then covalently linked by a thermostable ligase only when perfect complementation with the template at the mutation site and adjacent 1–3 bases. Performing the ligation at a relatively low temperature (37 °C) minimizes the effects of polymorphisms within the target sequence while maintaining the specificity at the site of interest.

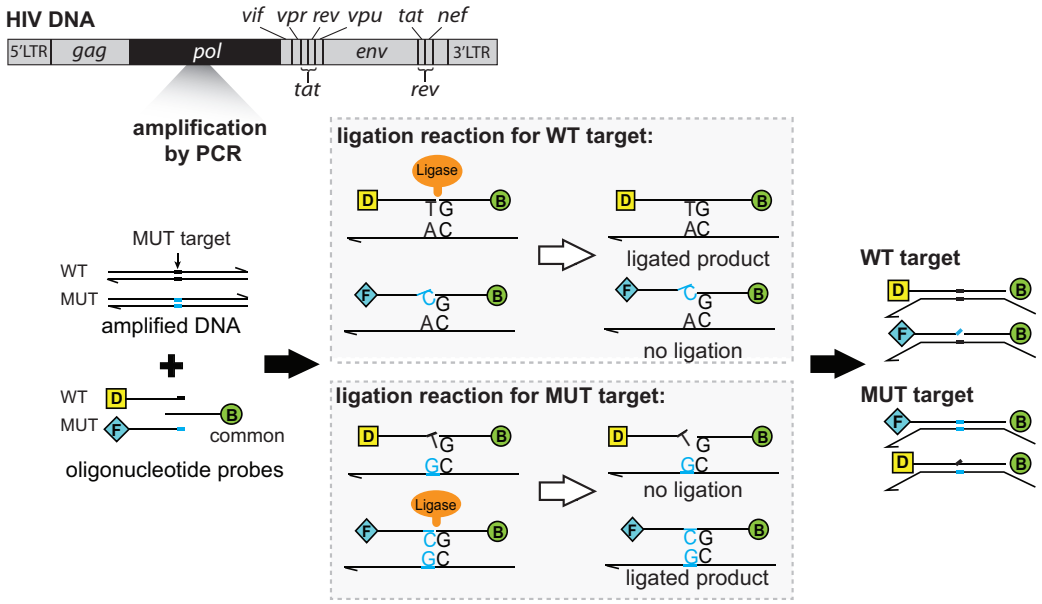

Figure 1.12 | Schematic of enzyme-mediated ligation in OLA for HIVDR test.

Nested PCR amplifies the pol gene of HIV DNA. Note that the HIV DNA gene map is not to scale positions. A portion of the amplicon is mixed with three oligonucleotide probes: (**1**) 5' fluorescein-conjugated mutant (MUT)-specific HIV probe; (**2**) 5' digoxigenin-conjugated wild-type (WT)-specific probe; and (**3**) a 5' phosphorylated, 3' biotinylated common probe. When specific probes are complementary at the mutation site, they are ligated to the common probe to create a DNA strand with labels at both

© Copyright 2021 | N Panpradist

ends. The image was obtained from N Panpradist et al. 2016 (https://doi.org/10.1371/journal.pone.0145962)

Processed a batch of 40 samples on six plates (1 plate/mutation), CLIA-OLA costs $5/mutation site. However, OLA requires full microbiology facilities and a >9-hour procedure (**Figure 1.13**) with multiple manual steps for nucleic acid extraction (e.g., viral RNA or viral DNA), HIV amplification, single-base mutation detection via probe ligation, and an enzyme-linked immunoassay (**ELISA**) to quantify the percentage of HIVDR. Despite its substantially reduced cost and high sensitivity compared to Sanger sequencing, the OLA is ill-suited for low resource laboratories due to its complex, labor-intensive procedures that require trained personnel and moderately expensive instruments (e.g., ~$2k thermal cycler, ~$3k plate reader, and ~$3k plate washer).

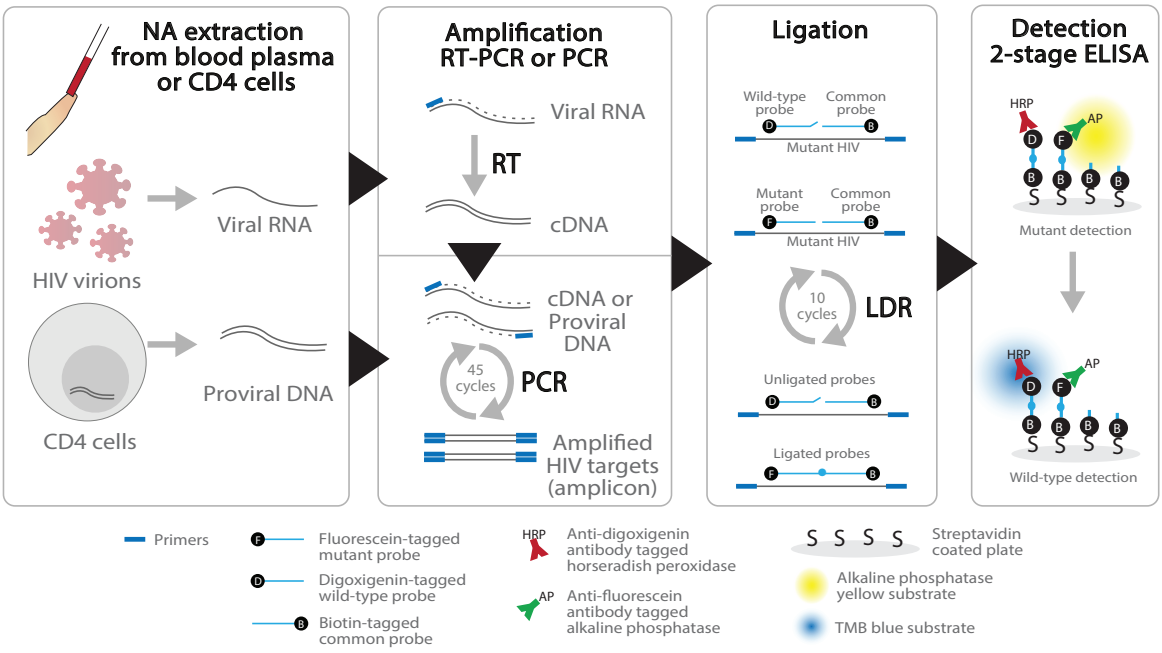

Figure 1.13 | Workflow of CLIA-OLA (Frenkel lab 2002).

© Copyright 2021 | N Panpradist

Viral RNA from HIV virion particles or proviral DNA in CD4 cells is first extracted from the blood sample. HIV pol region is then amplified using RT-PCR for RNA targets or PCR for DNA targets. Ligase detection reaction (LDR) is conducted. Here wild-type probes or mutant probes are ligated in the presence of wild-type targets or mutant targets, respectively. The ligated probes are then detected using ELISA.

© Copyright 2021 | N Panpradist

CHAPTER 1 REFERENCESS

1. Sebastiani, P.; Solovieff, N.; Hartley, S. W.; Milton, J. N.; Riva, A.; Dworkis, D. A.; Melista, E.; Klings, E. S.; Garrett, M. E.; Telen, M. J.; Ashley-Koch, A.; Baldwin, C. T.; Steinberg, M. H., Genetic modifiers of the severity of sickle cell anemia identified through a genome-wide association study. *American journal of hematology* **2010,** *85* (1), 29-35.

2. Poduslo, S. E.; Huang, R.; Huang, J.; Smith, S., Genome screen of late-onset Alzheimer's extended pedigrees identifies TRPC4AP by haplotype analysis. *American journal of medical genetics. Part B, Neuropsychiatric genetics : the official publication of the International Society of Psychiatric Genetics* **2009,** *150b* (1), 50-5.

3. Castellanos-Rubio, A.; Ghosh, S., Disease-Associated SNPs in Inflammation-Related lncRNAs. *Front Immunol* **2019,** *10*, 420.

4. Akinsete, O.; Hirigoyen, D.; Cartwright, C.; Schut, R.; Kantor, R.; Henry, K., K103N Mutation in Antiretroviral Therapy—Naive African Patients Infected with HIV Type 1. *Clinical Infectious Diseases* **2004,** *39* (4), 575-578.

5. Rachkov, A.; Patskovsky, S.; Soldatkin, A.; Meunier, M., Discrimination of single base mismatched oligonucleotides related to the rpoB gene of Mycobacterium tuberculosis using a surface plasmon resonance biosensor. *Biotechnology and applied biochemistry* **2013,** *60* (4), 453-8.

© Copyright 2021 | N Panpradist

6. Price, L. B.; Vogler, A.; Pearson, T.; Busch, J. D.; Schupp, J. M.; Keim, P., In vitro selection and characterization of Bacillus anthracis mutants with high-level resistance to ciprofloxacin. *Antimicrobial agents and chemotherapy* **2003,** *47* (7), 2362-5.

7. Eppinger, M.; Radnedge, L.; Andersen, G.; Vietri, N.; Severson, G.; Mou, S.; Ravel, J.; Worsham, P. L., Novel plasmids and resistance phenotypes in Yersinia pestis: unique plasmid inventory of strain Java 9 mediates high levels of arsenic resistance. *PLoS One* **2012,** *7* (3), e32911.

8. Gunnell, M. K.; Adams, B. J.; Robison, R. A., The Genetic Diversity and Evolution of Francisella tularensis with Comments on Detection by PCR. *Current Issues in Molecular Biology* **2016,** *18* (1), 79-92.

9. Baltas, I.; Boshier, F. A. T.; Williams, C. A.; Bayzid, N.; Cotic, M.; Guerra-Assunção, J. A.; Irish-Tavares, D.; Haque, T.; Hart, J.; Roy, S.; Williams, R.; Breuer, J.; Mahungu, T. W., Post-vaccination COVID-19: A case-control study and genomic analysis of 119 breakthrough infections in partially vaccinated individuals. *Clin Infect Dis* **2021**.

10. Taher, I.; Almaeen, A.; Ghazy, A.; Abu-Farha, M.; Mohamed Channanath, A.; Elsa John, S.; Hebbar, P.; Arefanian, H.; Abubaker, J.; Al-Mulla, F.; Alphonse Thanaraj, T., Relevance Between COVID-19 and Host Genetics of Immune Response. *Saudi J Biol Sci* **2021**.

11. Menéndez-Arias, L., Special issue: retroviral enzymes. *Viruses* **2010,** *2* (5), 1181-4.

© Copyright 2021 | N Panpradist

12. Walker, B.; McMichael, A., The T-cell response to HIV. *Cold Spring Harb Perspect Med* **2012,** *2* (11).

13. World Health Organization In *Updated recommendations on HIV prevention, infant diagnosis, antiretroviral initiation and monitoring*, 2021.

14. Schauer, G.; Leuba, S.; Sluis-Cremer, N., Biophysical Insights into the Inhibitory Mechanism of Non-Nucleoside HIV-1 Reverse Transcriptase Inhibitors. *Biomolecules* **2013,** *3* (4), 889-904.

15. Roberts, J. D.; Bebenek, K.; Kunkel, T. A., The accuracy of reverse transcriptase from HIV-1. *Science (New York, N.Y.)* **1988,** *242* (4882), 1171-3.

16. Oude Essink, B. B.; Berkhout, B., The fidelity of reverse transcription differs in reactions primed with RNA versus DNA primers. *J Biomed Sci* **1999,** *6* (2), 121-32.

17. Coffin, J.; Swanstrom, R., HIV pathogenesis: dynamics and genetics of viral populations and infected cells. *Cold Spring Harb Perspect Med* **2013,** *3* (1), a012526.

18. Rhee, S. Y.; Blanco, J. L.; Jordan, M. R.; Taylor, J.; Lemey, P.; Varghese, V.; Hamers, R. L.; Bertagnolio, S.; Rinke de Wit, T. F.; Aghokeng, A. F.; Albert, J.; Avi, R.; Avila-Rios, S.; Bessong, P. O.; Brooks, J. I.; Boucher, C. A.; Brumme, Z. L.; Busch, M. P.; Bussmann, H.; Chaix, M. L.; Chin, B. S.; D'Aquin, T. T.; De Gascun, C. F.; Derache, A.; Descamps, D.; Deshpande, A. K.; Djoko, C. F.; Eshleman, S. H.; Fleury, H.; Frange, P.; Fujisaki, S.;

© Copyright 2021 | N Panpradist

Harrigan, P. R.; Hattori, J.; Holguin, A.; Hunt, G. M.; Ichimura, H.; Kaleebu, P.; Katzenstein, D.; Kiertiburanakul, S.; Kim, J. H.; Kim, S. S.; Li, Y.; Lutsar, I.; Morris, L.; Ndembi, N.; Ng, K. P.; Paranjape, R. S.; Peeters, M.; Poljak, M.; Price, M. A.; Ragonnet-Cronin, M. L.; Reyes-Terán, G.; Rolland, M.; Sirivichayakul, S.; Smith, D. M.; Soares, M. A.; Soriano, V. V.; Ssemwanga, D.; Stanojevic, M.; Stefani, M. A.; Sugiura, W.; Sungkanuparph, S.; Tanuri, A.; Tee, K. K.; Truong, H. M.; van de Vijver, D. A.; Vidal, N.; Yang, C.; Yang, R.; Yebra, G.; Ioannidis, J. P.; Vandamme, A. M.; Shafer, R. W., Geographic and temporal trends in the molecular epidemiology and genetic mechanisms of transmitted HIV-1 drug resistance: an individual-patient- and sequence-level meta-analysis. *PLoS medicine* **2015,** *12* (4), e1001810.

19. Schauer, G.; Sluis-Cremer, N., HIV-1 Resistance to Reverse Transcriptase Inhibitors. In *Handbook of Antimicrobial Resistance*, Berghuis, A.; Matlashewski, G.; Wainberg, M. A.; Sheppard, D.; Gotte, M., Eds. Springer New York: New York, NY, 2017; pp 523-542.

20. Koigi, P.; Ngayo, M. O.; Khamadi, S.; Ngugi, C.; Nyamache, A. K., HIV type 1 drug resistance patterns among patients failing first and second line antiretroviral therapy in Nairobi, Kenya. *BMC research notes* **2014,** *7*, 890.

21. Kouamou, V.; Mavetera, J.; Manasa, J.; Ndhlovu, C. E.; Katzenstein, D.; McGregor, A. M., Pretreatment HIV Drug Resistance Among Adults Initiating or Re-Initiating First-Line Antiretroviral Therapy in Zimbabwe: Fast-Tracking

© Copyright 2021 | N Panpradist

the Transition to Dolutegravir-Based First-Line Regimens? *AIDS research and human retroviruses* **2021**.

22. World Health Organization *HIV Drug Resistance Report 2017*; 2017.

23. World Health Organization *HIV Drug Resistance Report 2019*; July 2019, 2019.

24. Sigaloff, K. C.; Kayiwa, J.; Musiime, V.; Calis, J. C.; Kaudha, E.; Mukuye, A.; Matama, C.; Nankya, I.; Nakatudde, L.; Dekker, J. T.; Hamers, R. L.; Mugyenyi, P.; Rinke De Wit, T. F.; Kityo, C., Short communication: high rates of thymidine analogue mutations and dual-class resistance among HIV-infected Ugandan children failing first-line antiretroviral therapy. *AIDS research and human retroviruses* **2013,** *29* (6), 925-30.

25. World Health Organization *Guidelines on the public health response to pre-treatment HIV drug resistance July 2017*; 978-92-4-155005-5; 2017.

26. Dow, D. E.; Bartlett, J. A., Dolutegravir, the second-generation of Integrase Strand Transfer Inhibitors (INSTIs) for the treatment of HIV. *Infect Dis Ther* **2014,** *3*, 83-102.

27. Christopher E Kandel; Walmsley, S. L., Dolutegravir – a review of the pharmacology, efficacy, and safety in the treatment of HIV. *Drug Des Devel Ther.* **2015,** *9*, 3547–3555.

28. Sim, J.; Hill, A., Is pricing of dolutegravir equitable? A comparative analysis of price and country income level in 52 countries. *Journal of Virus Eradication* **2018,** (4), 230-237.

© Copyright 2021 | N Panpradist

29. Hocqueloux, L.; Raffi, F.; Prazuck, T.; Bernard, L.; Sunder, S.; Esnault, J. L.; Rey, D.; Le Moal, G.; Roncato-Saberan, M.; Andre, M.; Billaud, E.; Valery, A.; Avettand-Fenoel, V.; Parienti, J. J.; Allavena, C.; group, M. s., Dolutegravir Monotherapy Versus Dolutegravir/Abacavir/Lamivudine for Virologically Suppressed People Living With Chronic Human Immunodeficiency Virus Infection: The Randomized Noninferiority MONotherapy of TiviCAY Trial. *Clin Infect Dis* **2019,** *69* (9), 1498-1505.

30. Crona, J.; Verdugo, A. D.; Granberg, D.; Welin, S.; Stålberg, P.; Hellman, P.; Björklund, P., Next-generation sequencing in the clinical genetic screening of patients with pheochromocytoma and paraganglioma. *Endocrine connections* **2013,** *2* (2), 104-11.

31. Levison, J. H.; Wood, R.; Scott, C. A.; Ciaranello, A. L.; Martinson, N. A.; Rusu, C.; Losina, E.; Freedberg, K. A.; Walensky, R. P., The clinical and economic impact of genotype testing at first-line antiretroviral therapy failure for HIV-infected patients in South Africa. *Clin Infect Dis* **2013,** *56* (4), 587-97.

32. DHHS Panel on Antiretroviral Guidelines for Adults and Adolescents Guidelines for the Use of Antiretroviral

Agents in Adults and Adolescents with HIV. https://clinicalinfo.hiv.gov/sites/default/files/guidelines/documents/AdultandAdolescentGL.pdf (accessed 26 August).

33. Kimmel, A. D.; Resch, S. C.; Anglaret, X.; Daniels, N.; Goldie, S. J.; Danel, C.; Wong, A. Y.; Freedberg, K. A.; Weinstein, M. C., Patient- and population-

© Copyright 2021 | N Panpradist

level health consequences of discontinuing antiretroviral therapy in settings with inadequate HIV treatment availability. *Cost effectiveness and resource allocation : C/E* **2012,** *10* (1), 12.

34. Bendavid, E.; Young, S. D.; Katzenstein, D. A.; Bayoumi, A. M.; Sanders, G. D.; Owens, D. K., Cost-effectiveness of HIV Monitoring Strategies in Resource-Limited Settings: A Southern African Analysis. *Archives of Internal Medicine* **2008,** *168* (17), 1910-1918.

35. Milne, R. S.; Silverman, R. A.; Beck, I. A.; McKernan-Mullin, J.; Deng, W.; Sibley, T. R.; Dross, S.; Kiarie, J. N.; Sakr, S. R.; Coombs, R. W.; Chung, M. H.; Frenkel, L. M., Minority and majority pre-treatment HIV-1 drug resistance associated with failure of first-line nonnucleoside reverse-transcriptase inhibitor antiretroviral therapy in Kenyan women. *AIDS (London, England)* **2019,** *33* (6), 941-951.

36. Palmer, S.; Kearney, M.; Maldarelli, F.; Halvas, E. K.; Bixby, C. J.; Bazmi, H.; Rock, D.; Falloon, J.; Davey, R. T., Jr.; Dewar, R. L.; Metcalf, J. A.; Hammer, S.; Mellors, J. W.; Coffin, J. M., Multiple, linked human immunodeficiency virus type 1 drug resistance mutations in treatment-experienced patients are missed by standard genotype analysis. *Journal of clinical microbiology* **2005,** *43* (1), 406-13.

37. Günthard, H. F.; Wong, J. K.; Ignacio, C. C.; Havlir, D. V.; Richman, D. D., Comparative performance of high-density oligonucleotide sequencing and

© Copyright 2021 | N Panpradist

dideoxynucleotide sequencing of HIV type 1 pol from clinical samples. *AIDS research and human retroviruses* **1998,** *14* (10), 869-76.

38. May, S.; Adamska, E.; Tang, J., Evaluation of Vela Diagnostics HIV-1 genotyping assay on an automated next generation sequencing platform. *J Clin Virol* **2020,** *127*, 104376.

39. Weber, J.; Volkova, I.; Sahoo, M. K.; Tzou, P. L.; Shafer, R. W.; Pinsky, B. A., Prospective Evaluation of the Vela Diagnostics Next-Generation Sequencing Platform for HIV-1 Genotypic Resistance Testing. *The Journal of Molecular Diagnostics* **2019,** *21* (6), 961-970.

40. Tzou, P. L.; Ariyaratne, P.; Varghese, V.; Lee, C.; Rakhmanaliev, E.; Villy, C.; Yee, M.; Tan, K.; Michel, G.; Pinsky, B. A.; Shafer, R. W.; Caliendo, A. M., Comparison of an In Vitro Diagnostic Next-Generation Sequencing Assay with Sanger Sequencing for HIV-1 Genotypic Resistance Testing. *Journal of clinical microbiology* **2018,** *56* (6), e00105-18.

41. Gholami, M.; Rouzbahani, N.; Samiee, S.; Tayeri, K.; Ghorban, K.; Dehkharghani, A. D.; Gholami, A. A.; Moshiri, F.; Sattari, A.; Dadmanesh, M.; Mohraz, M., HIV-1 drug resistance mutations detection and HIV-1 subtype G report by using next-generation sequencing platform. *Microb Pathog* **2020,** *146*, 104221.

42. Raymond, S.; Nicot, F.; Carcenac, R.; Lefebvre, C.; Jeanne, N.; Saune, K.; Delobel, P.; Izopet, J., HIV-1 genotypic resistance testing using the Vela

© Copyright 2021 | N Panpradist

automated next-generation sequencing platform. *J Antimicrob Chemother* **2018,** *73* (5), 1152-1157.

43. Raymond, S.; Nicot, F.; Abravanel, F.; Minier, L.; Carcenac, R.; Lefebvre, C.; Harter, A.; Martin-Blondel, G.; Delobel, P.; Izopet, J., Performance evaluation of the Vela Dx Sentosa next-generation sequencing system for HIV-1 DNA genotypic resistance. *J Clin Virol* **2020,** *122*, 104229.

44. Brookes, K. J.; Patel, T.; Zapata-Erazo, G.; Barber, I.; Braae, A.; Guetta-Baranes, T.; Clement, N. S.; Medway, C.; Chappell, S.; Morgan, K. In *P2-065: Identifying Polymorphisms in The Alzheimer's Related APP Gene Using The Oxford Nanopore Minion Sequencer*, Alzheimer's Association International Conference (AAIC): P2, Monday, July 25, 2016; 2016.

45. Gonzalez, C.; Gondola, J.; Ortiz, A. Y.; Castillo, J. M.; Pascale, J. M.; Martinez, A. A., Barcoding analysis of HIV drug resistance mutations using Oxford Nanopore MinION (ONT) sequencing. *bioRxiv* **2018**, 240077.

46. Clutter, D. S.; Mazarei, G.; Sinha, R.; Manasa, J.; Nouhin, J.; LaPrade, E.; Bolouki, S.; Tzou, P. L.; Hannita-Hui, J.; Sahoo, M. K.; Kuimelis, P.; Kuimelis, R. G.; Pinsky, B. A.; Schoolnik, G. K.; Hassibi, A.; Shafer, R. W., Multiplex Solid-Phase Melt Curve Analysis for the Point-of-Care Detection of HIV-1 Drug Resistance. *J Mol Diagn* **2019,** *21* (4), 580-592.

47. MacLeod, I. J.; Rowley, C. F.; Essex, M., PANDAA intentionally violates conventional qPCR design to enable durable, mismatch-agnostic detection of highly polymorphic pathogens. *Communications biology* **2021,** *4* (1), 227.

© Copyright 2021 | N Panpradist

48. Duarte, H. A.; Panpradist, N.; Beck, I. A.; Lutz, B.; Lai, J.; Kanthula, R. M.; Kantor, R.; Tripathi, A.; Saravanan, S.; MacLeod, I. J.; Chung, M. H.; Zhang, G.; Yang, C.; Frenkel, L. M., Current Status of Point-of-Care Testing for Human Immunodeficiency Virus Drug Resistance. *The Journal of Infectious Diseases* **2017,** *216* (suppl_9), S824-S828.

49. Kouamou, V.; Manasa, J.; Katzenstein, D.; McGregor, A. M.; Ndhlovu, C. E.; Makadzange, T., Diagnostic Accuracy of Pan-Degenerate Amplification and Adaptation Assay for HIV-1 Drug Resistance Mutation Analysis in Low- and Middle-Income Countries. *Journal of clinical microbiology* **2020,** *58* (9).

50. Zhang, G.; Cai, F.; Zhou, Z.; DeVos, J.; Wagar, N.; Diallo, K.; Zulu, I.; Wadonda-Kabondo, N.; Stringer, J. S.; Weidle, P. J.; Ndongmo, C. B.; Sikazwe, I.; Sarr, A.; Kagoli, M.; Nkengasong, J.; Gao, F.; Yang, C., Simultaneous detection of major drug resistance mutations in the protease and reverse transcriptase genes for HIV-1 subtype C by use of a multiplex allele-specific assay. *Journal of clinical microbiology* **2013,** *51* (11), 3666-74.

51. Rowley, C. F.; Boutwell, C. L.; Lee, E. J.; MacLeod, I. J.; Ribaudo, H. J.; Essex, M.; Lockman, S., Ultrasensitive detection of minor drug-resistant variants for HIV after nevirapine exposure using allele-specific PCR: clinical significance. *AIDS research and human retroviruses* **2010,** *26* (3), 293-300.

52. Nishizawa, M.; Hattori, J.; Shiino, T.; Matano, T.; Heneine, W.; Johnson, J. A.; Sugiura, W., Highly-sensitive allele-specific PCR testing identifies a greater

© Copyright 2021 | N Panpradist

prevalence of transmitted HIV drug resistance in Japan. *PLoS One* **2013,** *8* (12), e83150.

53. Badolo, A.; Okado, K.; Guelbeogo, W. M.; Aonuma, H.; Bando, H.; Fukumoto, S.; Sagnon, N.; Kanuka, H., Development of an allele-specific, loop-mediated, isothermal amplification method (AS-LAMP) to detect the L1014F kdr-w mutation in Anopheles gambiae s. l. *Malaria journal* **2012,** *11*, 227.

54. Yongkiettrakul, S.; Kampeera, J.; Chareanchim, W.; Rattanajak, R.; Pornthanakasem, W.; Kiatpathomchai, W.; Kongkasuriyachai, D., Simple detection of single nucleotide polymorphism in Plasmodium falciparum by SNP-LAMP assay combined with lateral flow dipstick. *Parasitology international* **2017,** *66* (1), 964-971.

55. Olivier, M., The Invader assay for SNP genotyping. *Mutation research* **2005,** *573* (1-2), 103-10.

56. Akram, F.; Ikram Ul, H.; Ahmed, Z.; Khan, H.; Ali, M. S., CRISPR-Cas9, A Promising Therapeutic Tool for Cancer Therapy: A Review. *Protein Pept Lett* **2020,** *27* (10), 931-944.

57. Pattabhi, S.; Lotti, S. N.; Berger, M. P.; Singh, S.; Lux, C. T.; Jacoby, K.; Lee, C.; Negre, O.; Scharenberg, A. M.; Rawlings, D. J., In Vivo Outcome of Homology-Directed Repair at the HBB Gene in HSC Using Alternative Donor Template Delivery Methods. *Mol Ther Nucleic Acids* **2019,** *17*, 277-288.

© Copyright 2021 | N Panpradist

58. Chen, Y.; Mei, Y.; Jiang, X., Universal and high-fidelity DNA single nucleotide polymorphism detection based on a CRISPR/Cas12a biochip. *Chemical Science* **2021,** *12* (12), 4455-4462.

59. Balderston, S.; Taulbee, J. J.; Celaya, E.; Fung, K.; Jiao, A.; Smith, K.; Hajian, R.; Gasiunas, G.; Kutanovas, S.; Kim, D.; Parkinson, J.; Dickerson, K.; Ripoll, J.-J.; Peytavi, R.; Lu, H.-W.; Barron, F.; Goldsmith, B. R.; Collins, P. G.; Conboy, I. M.; Siksnys, V.; Aran, K., Discrimination of single-point mutations in unamplified genomic DNA via Cas9 immobilized on a graphene field-effect transistor. *Nature Biomedical Engineering* **2021,** *5* (7), 713-725.

60. Xiang, X.; Qian, K.; Zhang, Z.; Lin, F.; Xie, Y.; Liu, Y.; Yang, Z., CRISPR-cas systems based molecular diagnostic tool for infectious diseases and emerging 2019 novel coronavirus (COVID-19) pneumonia. *J Drug Target* **2020,** *28* (7-8), 727-731.

61. Ford, T. The Cas proteins behind CRISPR diagnostics. https://mammoth.bio/2019/06/10/the-cas-proteins-behind-crispr-diagnostics/.

62. de Puig, H.; Lee, R. A.; Najjar, D.; Tan, X.; Soekensen, L. R.; Angenent-Mari, N. M.; Donghia, N. M.; Weckman, N. E.; Ory, A.; Ng, C. F.; Nguyen, P. Q.; Mao, A. S.; Ferrante, T. C.; Lansberry, G.; Sallum, H.; Niemi, J.; Collins, J. J., Minimally instrumented SHERLOCK (miSHERLOCK) for CRISPR-based point-of-care diagnosis of SARS-CoV-2 and emerging variants. *Sci Adv* **2021,** *7* (32).

© Copyright 2021 | N Panpradist

63. Ackerman, C. M.; Myhrvold, C.; Thakku, S. G.; Freije, C. A.; Metsky, H. C.; Yang, D. K.; Ye, S. H.; Boehm, C. K.; Kosoko-Thoroddsen, T.-S. F.; Kehe, J.; Nguyen, T. G.; Carter, A.; Kulesa, A.; Barnes, J. R.; Dugan, V. G.; Hung, D. T.; Blainey, P. C.; Sabeti, P. C., Massively multiplexed nucleic acid detection with Cas13. *Nature* **2020,** *582* (7811), 277-282.

64. Zhou, Q. Y.; Zhong, X. Y.; Zhao, L. L.; Wang, L. J.; Zhou, Y. L.; Zhang, X. X., High-throughput ultra-sensitive discrimination of single nucleotide polymorphism via click chemical ligation. *The Analyst* **2019,** *145* (1), 172-176.

65. Zhang, L.; Wang, J.; Coetzer, M.; Angione, S.; Kantor, R.; Tripathi, A., One-Step Ligation on RNA Amplification for the Detection of Point Mutations. *J Mol Diagn* **2015,** *17* (6), 679-88.

66. Chung, M. H.; Beck, I. A.; Dross, S.; Tapia, K.; Kiarie, J. N.; Richardson, B. A.; Overbaugh, J.; Sakr, S. R.; John-Stewart, G. C.; Frenkel, L. M., Oligonucleotide Ligation Assay Detects HIV Drug Resistance Associated with Virologic Failure among Antiretroviral-Naïve Adults in Kenya. *Journal of Acquired Immune Deficiency Syndromes* **2014,** *67* (3), 246-253.

67. Beck, I. A.; Mahalanabis, M.; Pepper, G.; Wright, A.; Hamilton, S.; Langston, E.; Frenkel, L. M., Rapid and sensitive oligonucleotide ligation assay for detection of mutations in human immunodeficiency virus type 1 associated with high-level resistance to protease inhibitors. *Journal of clinical microbiology* **2002,** *40* (4), 1413-9.

© Copyright 2021 | N Panpradist

68. Hardenbol, P.; Yu, F.; Belmont, J.; Mackenzie, J.; Bruckner, C.; Brundage, T.; Boudreau, A.; Chow, S.; Eberle, J.; Erbilgin, A.; Falkowski, M.; Fitzgerald, R.; Ghose, S.; Iartchouk, O.; Jain, M.; Karlin-Neumann, G.; Lu, X.; Miao, X.; Moore, B.; Moorhead, M.; Namsaraev, E.; Pasternak, S.; Prakash, E.; Tran, K.; Wang, Z.; Jones, H. B.; Davis, R. W.; Willis, T. D.; Gibbs, R. A., Highly multiplexed molecular inversion probe genotyping: over 10,000 targeted SNPs genotyped in a single tube assay. *Genome research* **2005,** *15* (2), 269-75.

69. Landegren, U.; Kaiser, R.; Sanders, J.; Hood, L., A ligase-mediated gene detection technique. *Science (New York, N.Y.)* **1988,** *241* (4869), 1077-80.

70. Herzog, V.; Fahimi, H. D., A new sensitive colorimetric assay for peroxidase using 3,3'-diaminobenzidine as hydrogen donor. *Analytical biochemistry* **1973,** *55* (2), 554-62.

71. Beck, I. A.; Crowell, C.; Kittoe, R.; Bredell, H.; Machaba, M.; Willamson, C.; Janssens, W.; Jallow, S.; van der Groen, G.; Shao, Y.; Jacob, M.; Samuel, N. M.; de Rivera, I. L.; Ngo-Giang-Huong, N.; Cassol, S.; Alemnji, G.; Frenkel, L. M., Optimization of the oligonucleotide ligation assay, a rapid and inexpensive test for detection of HIV-1 drug resistance mutations, for non-North American variants. *Journal of acquired immune deficiency syndromes (1999)* **2008,** *48* (4), 418-27.

72. Beck, I. A.; Deng, W.; Payant, R.; Hall, R.; Bumgarner, R. E.; Mullins, J. I.; Frenkel, L. M., Validation of an oligonucleotide ligation assay for

© Copyright 2021 | N Panpradist

quantification of human immunodeficiency virus type 1 drug-resistant mutants by use of massively parallel sequencing. *Journal of clinical microbiology* **2014,** *52* (7), 2320-7.

73. Ellis, G. M.; Mahalanabis, M.; Beck, I. A.; Pepper, G.; Wright, A.; Hamilton, S.; Holte, S.; Naugler, W. E.; Pawluk, D. M.; Li, C. C.; Frenkel, L. M., Comparison of oligonucleotide ligation assay and consensus sequencing for detection of drug-resistant mutants of human immunodeficiency virus type 1 in peripheral blood mononuclear cells and plasma. *Journal of clinical microbiology* **2004,** *42* (8), 3670-4.

74. Mutsvangwa, J.; Beck, I. A.; Gwanzura, L.; Manhanzva, M. T.; Stranix-Chibanda, L.; Chipato, T.; Frenkel, L. M., Optimization of the oligonucleotide ligation assay for the detection of nevirapine resistance mutations in Zimbabwean Human Immunodeficiency Virus type-1 subtype C. *Journal of virological methods* **2014,** *210C*, 36-39.

75. Jourdain, G.; Wagner, T. A.; Ngo-Giang-Huong, N.; Sirirungsi, W.; Klinbuayaem, V.; Fregonese, F.; Nantasen, I.; Techapornroong, M.; Halue, G.; Nilmanat, A.; Wittayapraparat, P.; Chalermpolprapa, V.; Pathipvanich, P.; Yuthavisuthi, P.; Frenkel, L. M.; Lallemant, M., Association between detection of HIV-1 DNA resistance mutations by a sensitive assay at initiation of antiretroviral therapy and virologic failure. *Clin Infect Dis* **2010,** *50* (10), 1397-404.

© Copyright 2021 | N Panpradist

76. Chung, M. H.; Beck, I. A.; Dross, S.; Tapia, K.; Kiarie, J. N.; Richardson, B. A.; Overbaugh, J.; Sakr, S. R.; John-Stewart, G. C.; Frenkel, L. M., Oligonucleotide ligation assay detects HIV drug resistance associated with virologic failure among antiretroviral-naive adults in Kenya. *Journal of acquired immune deficiency syndromes (1999)* **2014,** *67* (3), 246-53.

77. Chung, M. H.; McGrath, C. J.; Beck, I. A.; Levine, M.; Milne, R. S.; So, I.; Andersen, N.; Dross, S.; Coombs, R. W.; Chohan, B.; Yatich, N.; Kiptinness, C.; Sakr, S. R.; Kiarie, J. N.; Frenkel, L. M., Evaluation of the management of pre-treatment HIV drug resistance by oligonucleotide ligation assay: a randomised controlled trial. *The lancet. HIV* **2020,** *7* (2), e104-e112.

© Copyright 2021 | N Panpradist

CHAPTER 2: NUCLEIC ACID PREPARATION

PREFACE

Whole blood or plasma are specimens commonly used for HIVDR testing and require nucleic acid purification step. Nucleic acid purification is one of the most challenging steps in molecular assays. A typical workflow involves multiple washing steps and relies on a high-speed centrifuge. First, we discuss the pros and cons of using RNA or DNA as a target for the HIVDR test in section **2.1**. Section **2.2** describes different DNA preparation methods and a new method to enrich CD4+ cells to improve sensitivity and specificity of HIV nucleic acid amplification. Section **2.3** discusses the development of the non-proprietary RNA extraction method and its evaluation on HIV plasma specimens. Considering the SARS-CoV-2 pandemic, we also proposed an efficient workflow to test for HIV VL and simultaneously screen for SARS-CoV-2 infection. In section **2.4**, I discuss ongoing development for sequence-specific capture of HIV DNA and RNA.

PREVIOUS PUBLICATIONS

Some text and images in this section were published under

1) N Panpradist *et al.* 2019 (https://doi.org/10.1016/j.ebiom.2019.11.002),
2) G Gulati *et al.* 2021 (https://doi.org/10.1101/2021.08.18.21256786)
3) A patent application (17/055,966).

© Copyright 2021 | N Panpradist

2.1 VIRAL RNA AND DNA AS A TARGET FOR HIVDR TEST

HIV is a retrovirus and incorporates its genome into the human host (HIV proviral DNA). To detect HIVDR, we can target either viral RNA or DNA. Viral DNA is a more stable target than RNA and potentially a more suitable target to work within low-resource settings to guide treatment initiation. In the pre-therapy population, HIVDR mutations found in proviral DNA reportedly correlate with those in viral RNA[1]. Using the DNA as the target for HIVDR testing offers several advantages over RNA, such as cost savings from reverse transcriptase enzyme and easier handling and processing (no need for RNAse-free reagents and plastic/glassware). HIV proviral DNA is present as a small fraction of total DNA from leukocytes. One copy of HIV proviral DNA is present in every 1200 leukocytes[2]. In 1µL whole blood, there are 4000 – 11,000 leukocytes and thus approximately 3-9 copies of HIV proviral DNA. However, in terms of mass concentration, HIV proviral DNA is present at a ratio of 1 to $4x10^8$ human genomic DNA (1 copy of 10^4 bp HIV proviral DNA versus 1200 copies of $3.3x10^9$ bp human genome). Amplification or detection of HIV proviral DNA is challenging in the overwhelming presence of human genomic DNA (see **Chapter 2.4**).

On the other hand, targeting viral RNA has an advantage since this allows for detecting HIVDR both before ART initiation and after virologic failure. HIV RNA can be extracted from plasma in nearly cell-free conditions; thus, amplification or detection of HIV RNA is not in competition with HIV genomic DNA. Additionally, amplification of RNA can potentially address the need for viral load testing. Coupling HIVDR and VL tests will enable clinicians to identify the

© Copyright 2021 | N Panpradist

cause of virologic failure, either from drug resistance or from low adherence, and prevent an unnecessary ART switch.

2.2 DNA PREPARATION METHODS FOR HIVDR OLA

CONTRIBUTORS*:* Daisy Ko, Ingrid Beck, Nuttada Panpradist, Nikki Higa, James Lai, Lisa Frenkel, Justin Vrana, Barry Lutz. ***Contributions:*** DK and IB optimized the CD4 negative selection protocol. NH and JL developed in-house magnetic separation used in the CD4 negative selection protocol. JV developed an interactive software guide for the CD4 negative protocol. NP evaluated multiple approaches for DNA extraction for OLA use. LF and BR oversaw the study.

MATERIALS AND METHODS

FTA dried blood spots (DBS). Briefly, 125µL blood was collected on Whatman FTA paper (GE Healthcare Life Sciences). A 3mm-diameter disk was excised from each DBS specimen and washed following the manufacturer's instructions. The HIV viral DNA copy number on each DBS punch was quantified using a nested, real-time HIV *gag* PCR assay[3].

DNA extraction from PBMC. PBMC separation from whole anti-coagulated blood was performed using Ficoll medium. Washed PMBC pellets were either lysed with an in-house lysis buffer or lysis buffer provided by 5 Prime DNA purification kits (Fisher Scientific).

© Copyright 2021 | N Panpradist

DBS collected on Whatman 903 cards were prepared as previously described using Chelex Solution[4].

***In-house CD4 enrichment approach*.** As illustrated in **Figure 2.1**, 500µL anti-coagulated whole blood diluted wiDulbecco'sbecco's PBS without Ca^{2+} and Mg^{2+} was mixed with 25µL EasySep Direct RapidSpheres and EasySep Isolation Cocktail (STEMCELL Technologies) and separated following the manufacturer's protocol using an in-house manufactured magnetic. The final cell suspension was pelleted, resuspended in 1mL RBC lysis buffer (150mM NH_4Cl, 10mM $NaHCO_3$, 1mM EDTA), re-pelleted, and washed with Dulbecco's PBS. PBMC separation from whole anti-coagulated blood was performed using Ficoll medium. Washed pellets were either lysed with an in-house lysis buffer or lysis buffer provided by 5 Prime DNA purification kit

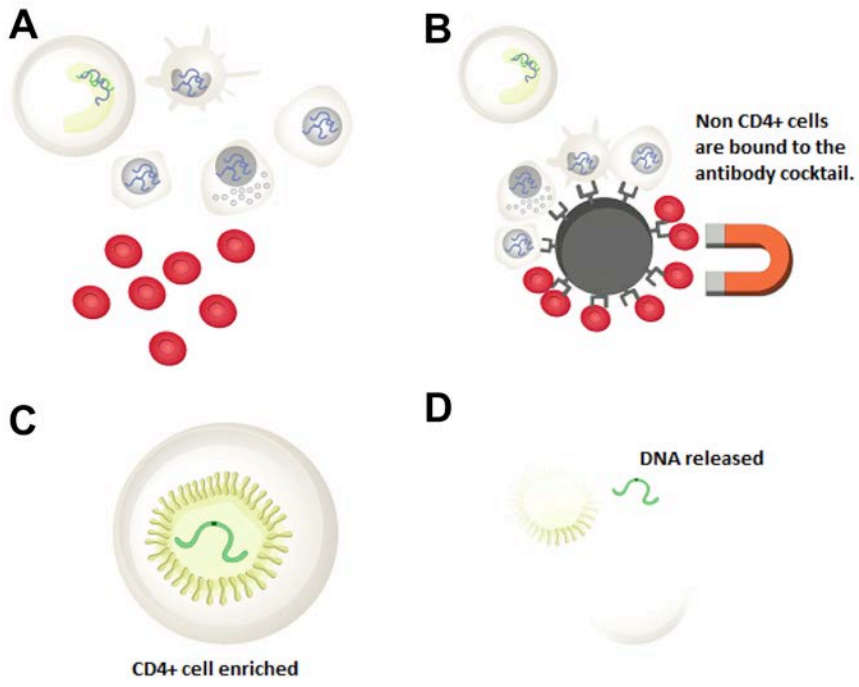

Figure 2.1 | Schema of in-house CD4+ cell enrichment chemistry.

© Copyright 2021 | N Panpradist

(**A**) HIV DNA (green) harboring cells are found primarily on CD4+ cells, while many other leukocytes contain human genomic DNA without HIV DNA (cells without green DNA). (**B**) EasySep antibody cocktails bind to non-CD4+ cells, and the complexes are removed from the solution using a magnet. (**C**) The supernatant now has concentrated CD4+ cells. (**D**) The CD4+ cells are pellet and subjected to in-house lysis protocol. The lysate is added to the PCR reaction directly without additional purification.

Preparation of CD4 or PBMC lysate*:* The remaining cell pellet after CD4-cell depletion containing CD4+ cell or PBMC pellet was lysed in 30µl in-house white blood cell (WBC) lysis buffer (10mM Tris pH 8.3, 50mM KCl, 0.45% Tween-20, 0.45% Nonidet-40, 0.5 mg/ml proteinase K) at 56°C for 10 minutes, followed by deactivation de-activation at 95°C for 5 minutes. 10µL room-temperature lysate was added to 50µLPCR reaction or frozen at -20°C. As an alternative method for processing freshly drawn whole blood, we developed this in-house approach using a customized 3D-printed magnetic bar ($1-2) to deplete CD4-negative cells and lysis buffer compatible with downstream PCR. This method also addresses PCR inhibition caused by using >2µg human background DNA by pre-enriching HIV targets to increase the HIV copy/total DNA ratio.

2.2.1 DNA EXTRACTION METHODS WERE TESTED IN COMPARISON WITH IN-HOUSE CD4 ENRICHMENT

We first evaluated the OLA-Simple's performance across specimen types using synthetic HIV DNA template at 10% MUT or 0% MUT (pure WT) spiked into nucleic acids from uninfected blood, including DNA extracted from peripheral blood mononuclear cells (**PBMC**), PBMC cell lysate, CD4 cell lysate, eluate from

© Copyright 2021 | N Panpradist

903 dried blood spots (**DBS**) and washed FTA DBS. FTA DBS slightly impaired assay performance. Regardless, all specimen types were able to differentiate the 10% MUT sample from the 0% MUT (pure WT) sample ($P < 0.05$, 0% vs. 10% for each specimen type) (**Figure 2.2**). CD4 enrichment sample preparation method yielded the highest MUT to WT signal difference, comparable to PBMC lysate and most used 903 DBS lysate.

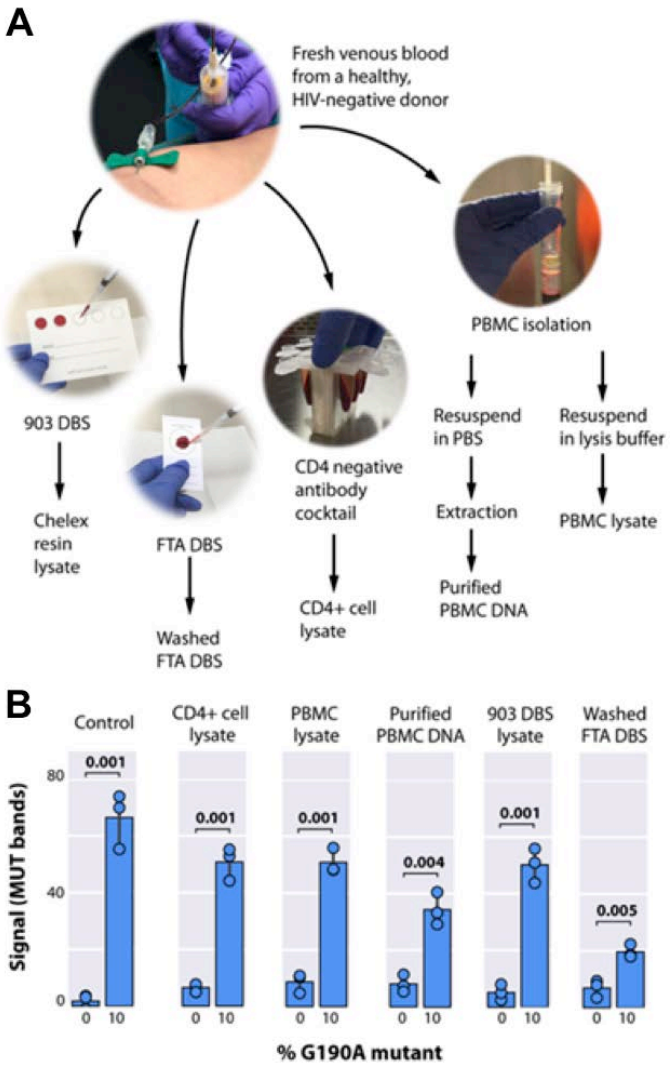

Figure 2.2 | Impact of carryover inhibitors from different blood specimen types.

© Copyright 2021 | N Panpradist

(**A**) Mock specimen panels were generated from a healthy donor. The OLA-Simple kit was used to analyze a plasmid mixture of 10% G190A in WT plasmid, or pure WT plasmid (2000 copies input) spiked into 10µL eluate from each processed specimen compared to plasmid alone (Control). (**B**) Signal (means ± SD, n=3) of the MUT and WT bands of samples with WT plasmid versus 10% G190A in 90% WT plasmid were plotted. MUT signals from 0% and 10% G190A samples were compared using a two-tailed t-test with Holm-Bonferroni correction. The image was obtained from N Panpradist *et al.* 2019 (https://doi.org/10.1016/j.ebiom.2019.11.002).

2.2.2 USE OF CD4 ENRICHMENT PROTOCOL PERFORMED BY TECHNOLOGIES IN KENYA

The in-house protocol (**Figure 2.3**) was converted to an interactive instruction "Aquarium" (i.e., OLA Automation) with embedded pictorial graphics. 12 Kenyan technologists processed two different whole blood specimens, and results were comparable to those performed by trained personnel in the US (**Table 2.1**). See **section 5.4** for full detail.

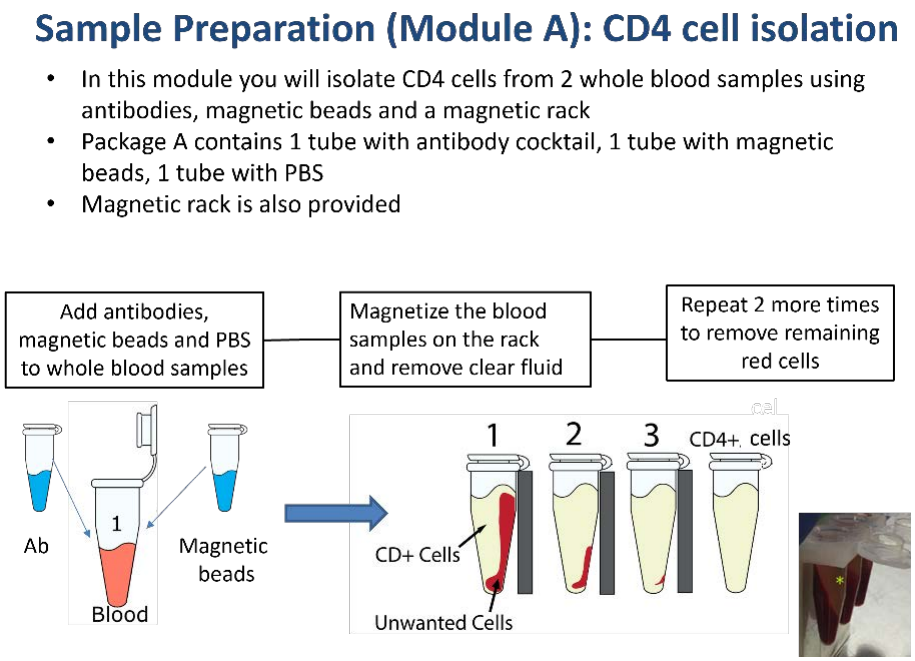

Figure 2.3 | Protocol for CD4 cell enrichment protocol from fresh whole blood.

Figure courtesy: Justin Vrana and Ingrid Beck

© Copyright 2021 | N Panpradist

Table 2.1 | Quantification of human DNA yield from the sample preparation steps.

Sample #	Sample	copies/5ul		average copies/5ul	SD	total cells	Avg/tech	SD/tech	Avg/blood sample	SD/blood sample
1	1AK1 IB	70,290	86,350	78,300	11,400	469,800	441,000	40,729	526,500	101,607
2	1AK2 IB	64,120	73,310	68,700	6,500	412,200				
3	2AK1 IB	98,490	102,600	101,000	2,870	606,000	612,000	8,485		
4	2AK2 IB	107,300	99,230	103,000	5,720	618,000				
5	3AK1 VG	55,600	48,140	51,900	5,280	311,400	264,000	67,034	261,975	32,151
6	3AK2 VG	34,140	38,040	36,100	2,750	216,600				
7	4AK1 VG	48,090	45,480	46,800	1,850	280,800	280,200	849		
8	4AK2 VG	43,200	49,940	46,600	4,760	279,600				
9	5AK1 VG	46,160	46,350	46,300	137	277,800	257,100	29,274		
10	5AK2 VG	35,140	43,750	39,400	6,090	236,400				
11	6AK1 VG	43,080	45,250	44,200	1,540	265,200	246,600	26,304		
12	6AK2 VG	35,820	40,110	38,000	3,040	228,000				
13	7AK1 BC	73,600	74,630	74,100	728	444,600	417,900	37,760	357,171	80,209
14	7AK2 BC	65,320	65,130	65,200	136	391,200				
15	8AK1 BC*	31,640	31,290	31,500	248	189,000	297,600	153,584		
16	8AK2 BC	74,500	60,830	67,700	9,670	406,200				
17	9AK1 BC	62,240	62,160	62,200	54	373,200	384,900	16,546		
18	9AK2 BC	67,580	64,700	66,100	2,040	396,600				
19	10AK1 BC	42,260	40,990	41,600	895	249,600	244,200	7,637		
20	10AK2 BC	39,090	40,460	39,800	967	238,800				
21	11AK1 D	68,570	74,090	71,300	3,900	427,800	316,500	157,402	336,600	115,191
22	11AK2 D	35,190	33,170	34,200	1,430	205,200				
23	12AK1 D	72,290	73,840	73,100	1,090	438,600	356,700	115,824		
24	12AK2 D	43,960	47,540	45,800	2,540	274,800				
25	5AK1 PL	35,250	38,490	36,900	2,300	221,400	254,700	47,093		
26	5AK2 PL	45,130	50,860	48,000	4,050	288,000				

IB is the trained Seattle team member. All CD4 separations were performed from 0.5mL blood, and cells were lysed in 30ul of LB/PK. 25 and 26: This blood sample did not separate and lysed well and had a brown lysate. Table 2. was published as J Vrana and N Panpradist et al., DOI: https://doi.org/10.1101/2021.05.06.21256654.

2.3 RNA PREPARATION METHODS FOR HIVDR OLA

IN-HOUSE RNA EXTRACTION METHODS FOR HIV AND/OR SARS-COV-2 DETECTION

CONTRIBUTORS: Gaurav K Gulati, Nuttada Panpradist, Samuel W A Stewart, Ingrid A Beck, Ceejay Boyce, Amy K Oreskovic, Claudia García-Morales, Santiago Avila-Ríos, Peter D. Han, Gustavo Reyes-Terán, Lea M. Starita, Lisa M Frenkel, Barry R Lutz, James J Lai. **CONTRIBUTIONS**: NP envisioned the integrated workflow for HIV viral load testing and COVID-19 screening. GG, NP, SWAS, AKO, IB, and CB conducted the experiments. GG and NP performed data analysis. SA, PDH, GRT, and LS

© Copyright 2021 | N Panpradist

characterized and provided specimens used in this evaluation. IB and LF provided technical insights on the discussion. BRL and JJL oversaw the study. All authors contributed to writing this manuscript and approved the final version for submission.

CONTEXT. COVID-19 pandemic interrupted routine care for individuals living with HIV, putting them at risk of becoming virologically unsuppressed and ill. Often, they are at high risk for exposure to SARS-CoV-2 infection and severe disease once infected. For this population, it is urgent to closely monitor HIV VL and screen for SARS-COV-2 infection.

DELIVERABLES. First, we have developed a non-proprietary method to isolate RNA from plasma, NS, or both. HIV, SARS-CoV-2, and human RP targets in extracted RNA are then RT-qPCR to estimate the VL and classify HIV/SARS-CoV-2 status (*i.e.,* HIV as VL failure or suppressed; SARS-CoV-2 as positive, presumptive positive, negative, or indeterminate). Second, we evaluated this workflow on 133 clinical specimens: 40 plasma specimens (30 HIV-seropositive), 67 NS specimens (31 SARS-CoV-2-positive), and 26 pooled plasma/NS specimens (26 HIV-positive with 10 SARS-CoV-2-positive), and compared the results obtained using the in-house extraction to those using a commercial extraction kit. In-house extraction had a detection limit of 200-copies/mL for HIV and 100-copies/mL for SARS-CoV-2. In-house and commercial methods yielded positively correlated HIV VL (R^2: 0.98 for contrived samples; 0.81 for seropositive plasma). SARS-CoV-2 detection had 100% concordant classifications in contrived samples, and

© Copyright 2021 | N Panpradist

in clinical NS extracted by in-house method, excluding indeterminate results, was 95% concordant (25 positives, six presumptive positives, and 31 negatives) to those using the commercial method. The pooled plasma/NS analysis showed R^2 of 0.91 (contrived samples) and 0.71 (clinical specimens) for HIV VL correlations obtained by both extraction methods, while SARS-CoV-2 detection showed 100% concordance in contrived and clinical specimens.

INTERPRETATION. Our low-cost workflow for molecular testing of HIV and SARS-CoV-2 could serve as an alternative to current standard assays for laboratories in low-resource settings

MATERIALS AND METHODS

Generation and characterization of in-vitro transcribed RNA standards. DNA fragments (GenBlock, Integrated DNA Technology, Coralville, IA) containing the amplification regions for HIV LTR assay (base position: 544-621 HXB2; GenBank: K03455.1) or N1/N2 assay (base position: 28,307-28,334 and 29,184-29,212 SARS-CoV-2 respectively; GenBank: NC_045512.2) with upstream T7 RNA promoter sequence was used as starting DNA construct for RNA generation. 100ng DNA construct was converted to RNA using T7 RNA polymerase (M0251; New England Biolabs (NEB), Ipswich, MA) and after digestion with DNAse I (M0303, NEB) was purified (T2040, NEB) according to the manufacturer's protocols[5, 6]. Product fragment lengths were confirmed using TapeStation Agilent 2200 (5067-5578), Agilent, Santa Clara, CA).

© Copyright 2021 | N Panpradist

Finally, Crystal digital PCR (**cdPCR**) was used to quantify the in-vitro transcribed RNA standard (**Figure S2.17**).

Contrived specimens for assay optimization. For HIV testing, contrived samples were prepared by adding *in-vitro* transcribed HIV RNA (for positive samples) or water (for negative samples) to negative pooled plasma specimens (IPLAWBK2E100ML, Innovative Research, Novi, MI) mixed with lysis buffer after a 10–15-minute incubation. For COVID-19 testing, negative Viral Transport Media (**VTM**) (220220, Becton Dickenson, Franklin Lakes, NJ) was spiked with 1ng/µL human genomic DNA (3041, Promega, Madison, WI), lysed similarly as contrived HIV samples, and then spiked with *in-vitro* transcribed SARS-CoV-2 RNA (for positive samples) or water (for negative samples).

The panel of clinical specimens. We used a total of 113 specimens to evaluate the proposed workflows. These remnant NS and plasma specimens went through several freeze-thawing cycles and therefore were suboptimal to directly compare the original results by the certified laboratories to results obtained by the in-house workflow. Thus, in this study, we extracted the specimens using the commercial RNA extraction kit (referred to as standard extraction kit) and in-house extraction kit (referred to as in-house extraction kit). The extracted RNA was subsequently analyzed using the same RT-qPCR, and results were compared. Discordant results were ruled out using the original results previously reported by the certified laboratories. We calculated that we would need at least 30 SARS-CoV-2 positive specimens to estimate 95%CI of 90%-100%, should all the analysis be accurate (Binomial Exact Proportion Estimation). For OPTION 1 workflow, remnant NS in **VTM** that were positive

© Copyright 2021 | N Panpradist

for SARS-CoV-2 (*n = 31*) and negative for SARS-CoV-2 (*n = 36*) but positive for other respiratory pathogens (*e.g.,* influenza, seasonal coronavirus, adenovirus, parainfluenza virus, metapneumovirus, enterovirus, bocavirus, and pneumonia were used[7]. These specimens were either nasopharyngeal specimens collected by health personnel or observed self-collected nasal swabs from individuals presenting respiratory symptoms as part of the Seattle Flu Study in 2020. The swabs were suspended in 3mL VTM and previously tested in a CLIA-certified laboratory[7]. Aliquots of these specimens were de-identified before testing in the UW Lutz laboratory and Seattle Children's Research Institute Frenkel laboratory as part of this study.

Remnant HIV-seropositive plasma (*n = 30*) was used to evaluate the performance of the HIV viral load tests using the in-house extraction method compared to the standard extraction method. The HIV- seropositive plasma specimens were obtained from the CIENI/INER (WHO HIV certified lab) plasma bank in Mexico City in 2018, as described[8]. HIV VL was measured in all the selected samples using the Abbott m2000 system (Chicago, IL) and known to contain near or above 1000 copies/mL HIV RNA. We randomly selected at least 30 specimens to allow estimation of VL. As a negative control for the HIV VL test, we included ten negative plasma specimens. All samples were de-identified before shipment to and testing in the Seattle Children Research Institute Frenkel laboratory. We also analyzed HIV-seronegative (*n = 10*, screened by the vendor Innovative Research, Inc, MI, USA) plasma as a negative control.

© Copyright 2021 | N Panpradist

To test the OPTION 2 workflow, a subset of specimens (*n = 26*) remaining from the OPTION 1 workflow experiments were mixed with NS to create 26 HIV-seropositive specimens. Ten were SARS-CoV-2 positive, and 16 were SARS-CoV-2-negative specimens.

Ethics statement. The remnant respiratory specimens were collected as part of the Seattle Flu Study in 2020 (IRB#: STUDY0006181). Informed consent was obtained from adult participants and parents or permanent legal guardians of participant children. Archived specimens were randomly chosen for use in the current study. Participants from CIENI/INER gave written consent to use remnant plasma samples, approved by the Institutional Review Board of the National Institute of Respiratory Diseases (Project code: E02-17).

In-house RNA extraction kit*.* Lysis buffer was freshly prepared from mixing the buffer (4M guanidine thiocyanate, 10mM MES pH 5.5) with 6% (v/v) 1mg/mL tRNA (AM7119, ThermoFisher, Waltham, MA), 2% (v/v) 2M DTT (P1771, Promega, Madison, WI). VTM (50µL), plasma (140µL), or pooled VTM (50µL)/plasma (140µL) was mixed with 4x volume of lysis buffer and incubated at room temperature for 15 minutes. The 630µL mixture was then added to the silica column (Epoch Life Sciences, 1920-250) and centrifuged at 6000g for 1 minute. Flow-through fluid was decanted, and the remaining mixture underwent repeated centrifugation until all the lysed sample was captured by silica. After the last spin of the lysed sample, a new collection tube was placed, 800µL wash buffer 1 (1M guanidinium thiocyanate, 10mM Tris-HCl pH 7.4) was added. The tube and column were centrifuged at 6000g for 1 minute. Flow-through was discarded, and a new collection tube was placed. 800µL wash

© Copyright 2021 | N Panpradist

buffer 2 (80% ethanol; 20% 10mM Tris-HCl pH 7.4) was added, and the tube was centrifuged at 20,000g for 3 minutes. Flow-through was discarded, and the tube was centrifuged at 21,000g for an additional 1 minute to remove any residual wash buffer completely. The spin-column was then transferred to a clean 1.5mL tube (Lo-bind DNA, Eppendorf), and 0.04% (w/v) sodium azide in water was added to elute the RNA (60µL for either plasma or NS; and 80µL for co-extracted specimens to have sufficient samples for all the RT-qPCR experiments. After 1-min incubation at room temperature and 1-minute 6000g centrifugation, the resultant RNA was collected and stored at -80°C until tested by RT-qPCR. All samples underwent only a single freeze-thawing cycle to avoid significant RNA degradation.

***Commercial RNA extraction method (referred to as standard method**).* The QIAamp viral RNA kits (52904, Qiagen, Hilden, Germany) was used as a standard method to compare the performance of the in-house RNA extraction protocol using the same input volume of specimens described above. All samples were processed according to the manufacturer's protocol[9].

***RT-qPCR assays for HIV viral load and SARS-CoV-2 detection**.* We adopted clinically validated primer and probe sets for the detection of HIV[10] and SARS-CoV-2[11]. We selected this LTR assay as its probe and primers have melting temperatures similar to those used in the US CDC SARS-CoV-2 N1, N2 assays. Using the same temperature cycling profile, we reliably amplified the *in-vitro* transcribed HIV and SARS-CoV-2 RNA down to 10 copies/reaction when running for 40 cycles (**Figure S2.18**).

© Copyright 2021 | N Panpradist

Four separate RT-qPCR reactions targeting HIV long terminal repeat (**LTR**), SARS-CoV-2 nucleocapsid gene regions N1 and N2, and human ribonuclease P (**RP**) were set up for each sample. Each 20µL RT-PCR reaction contained 1x TaqPath master mix (A15299, ThermoFisher, Waltham, MA), HIV, SARS-CoV-2, or human RP primers/probes (**Table S2.3**) and 5µL extracted RNA or RNA standards at 0 - 10^7 copies/reaction. The reaction mixtures were run on a real-time thermal cycler (CFX96, Biorad) using 2 min at 25°C for primer annealing and UNG digestion; 15 min at 50°C for reverse transcription; 2 min at 95°C for reverse transcriptase deactivation and initial denaturing, and 50 cycles of 3 sec at 95°C, 30 sec at 55°C. At the end of 30 sec at 55°C, the fluorescence was read using the FAM channel. Sample copies per reaction were calculated using the RNA standard curve included in each run and used to calculate RNA copies/mL of the original specimen. The number of RT-qPCR replicates provided in the caption of each experiment. RT-qPCR data were analyzed using CFX Maestro (Biorad). Data were normalized using cycles 5-10, and samples were determined positive when the normalized signals were above 200 RFU. The Cq values of samples were interpolated based on the linear fit to the Cq values and log10 of input concentration of the RNA standards from 0-10^7 copies/reaction.

Interpretation of measured VL results and statistical analysis. In contrived specimens, the measured VL from RNA extracted by both methods were plot against the spiked-in RNA input concentration to demonstrate the performance of each extraction method.

© Copyright 2021 | N Panpradist

The measured VL were classified as correct if they fell within the upper and lower bounds of precise measurements defined as ±0.3log10(RNA copies/mL)[12]. For HIV-seropositive specimens, VL values from the RNA extracted by in-house vs. standard methods were assessed for their correlation. R^2 values from a linear regression fit of scattered plots and p-values from the Wilcoxon Signed-Rank test (two-tailed) were reported. Next, we used the US NIH VF cutoff[13] or the WHO VF cutoff[14] to classify specimens as VL suppressed "**VLS**" (VL <200 or VL <1000 copies/mL, respectively) or virologic failure "**VF"** (VL≥200 or VL≥1000 copies/mL, respectively). % Concordance of the HIV VL classifications from RNA extracted by the in-house vs. the standard RNA extraction method was calculated from the concordant VL classifications (*i.e.,* VLS vs. VF)/ number of seropositive samples tested. Similarly, for SARS-CoV-2 specimens, measured VL values from the RNA extracted by in-house vs. standard methods were assessed for the correlation using a linear regression fit and for its statistical difference using the Wilcoxon Signed-Rank test (two-tailed). Next, we classified results as "negative," "positive," or "presumptive positive," based on the results of N1, N2, and RP assays. Positive samples have detection of N1 and N2 regardless of the results from the RP assay. Presumptive samples have detection of either N1 or N2 regardless of the results from the RP assay. Negative samples are negative for both N1 and N2 but are positive for RP. If samples are not detected of N1, N2, and RP, they are classified as indeterminate results. % Concordance of the SARS-CoV-2 results by the in-house vs. standard RNA extraction method was

© Copyright 2021 | N Panpradist

calculated from the # of samples with concordant results (*i.e.,* negative, positive, presumptive positive, and indeterminate)/ # of samples tested.

RESULTS

2.3.1 INTEGRATED WORKFLOW FOR HIV VL TEST & SARS-COV-2 SCREENING

SARS-CoV-2 RNA has been detected in both plasma and respiratory specimens, and thus, we have envisioned two options for screening SARS-CoV-2 infection while performing routine HIV viral load tests (**Figure 2.4A**). OPTION 1 utilizes plasma specimens as the sole sample source for HIV RNA load test and SARS-CoV-2 screening. The extracted RNA is subjected to four RT-qPCR reactions; two non-overlapping regions in the SARS-CoV-2 nucleocapsid gene (**N1** and **N2**), HIV long terminal repeat (**LTR**) gene, and human ribonuclease P (**RP**) gene. If samples test negative for all assays, this suggests procedural errors, and re-testing and/or re-collecting samples is recommended (**Figure 2.4B**). RT-qPCR results report HIV VL and SARS-CoV-2 infection status (**Figure 2.4C**). Individuals present different levels of risks to develop poor health outcomes. Because SARS-CoV-2 viral loads in respiratory specimens are generally higher than in plasma, we propose an alternative workflow (OPTION 2) to increase the sensitivity of SARS-CoV-2 detection by combining the extraction of plasma/NS for detection. RNA extraction in OPTION 1 and 2 workflows is performed using an in the Boom's method. Analysis of contrived plasma and contrived pooled plasma/NS samples confirmed detection of 200 copies/mL of HIV and SARS-CoV-2 RNA (**Figure 2.4D** and **Figure 2.4E**). Based on the definition of virologic failure

© Copyright 2021 | N Panpradist

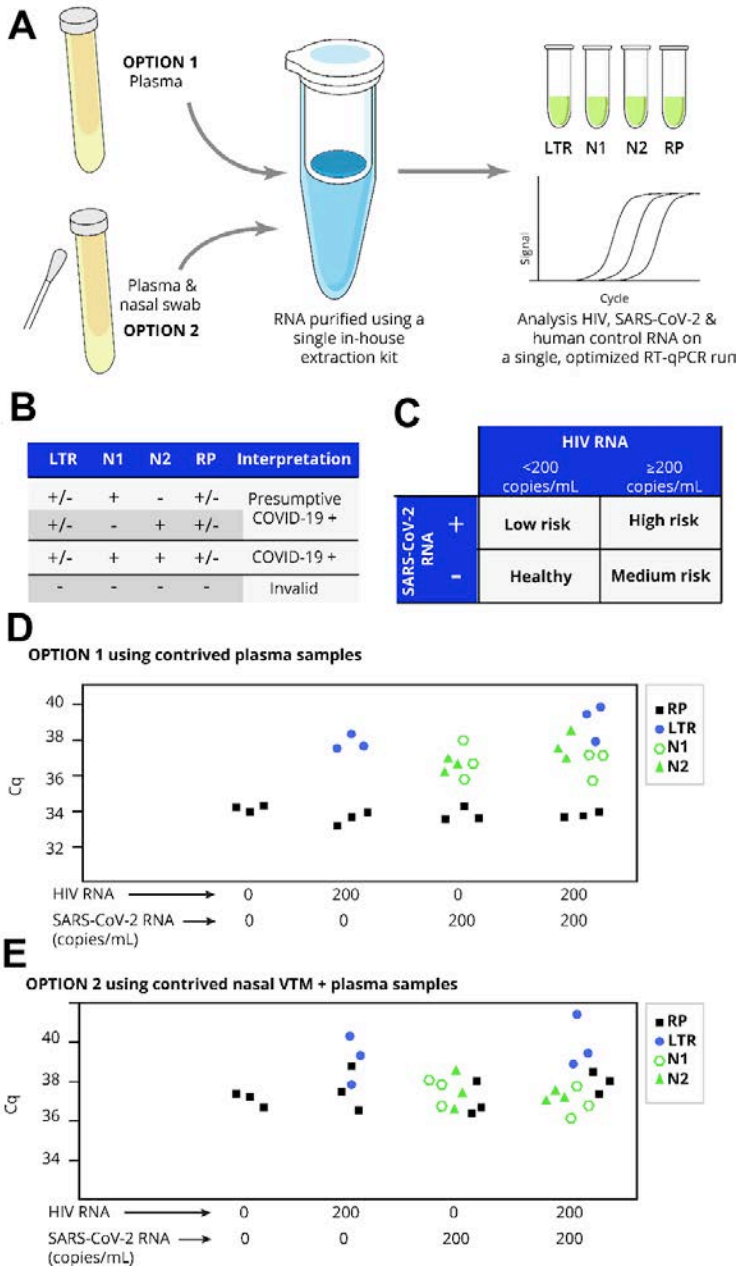

Figure 2.4 | Workflows for SARS-CoV-2 screening and HIV VL testing.

(**A**) Schema of the workflows for the analysis of only plasma specimens or the mixtures of plasma and respiratory specimens. Specimens are extracted using our low-cost, in-house extraction method and analyzed using RT-qPCR assays, which target the HIV LTR gene, SARS-CoV-2 N gene (N1, N2), and human RP gene (RP). (**B**) Assay interpretation of the results based on HIV and SARS-CoV-2 RT-qPCR results (**C**) Clinical interpretation based on the status of HIV viral load and SARS-CoV-2 infection. (**D**) Analysis of HIV and SARS-CoV-2 RNA spiked in lysed negative plasma at 0 or 200 copies/mL (**E**) Analysis

© Copyright 2021 | N Panpradist

of HIV, and SARS-CoV-2 RNA spiked in lysed pooled NS and plasma at 0 or 200 copies/mL. Individual Cq values of three technical replicates (individually extracted and RT-qPCR assayed) are plotted. The image was published: DOI: https://doi.org/10.1101/2021.08.18.21256786.

(**VF**) by the US National Institutes of Health[13], this limit of detection (**LoD**) of HIV assay at 200 copies/mL would allow differentiation of samples collected from PLH with VF (>200 copies/mL, as these, would be detected) vs. viral load suppressed (**VLS**, undetected). For the SARS-CoV-2 RNA, the 200 copies/mL is lower than the reported LoD of the US CDC SARS-CoV-2 assay[15]. We appropriately detected the human RP gene control (**Figure 2.4D** and **Figure 2.4E**) in all contrived samples.

2.3.2 DEVELOPMENT OF RNA EXTRACTION PROTOCOL

The in-house RNA extraction protocol is based on Boom's Boom's method[16], wherein RNA is bound to a silica column, followed by washing steps to remove PCR inhibitors and then eluted out in a low salt buffer. Herein, a lysis buffer comprised of 4M guanidinium thiocyanate (**GuSCN**), a potent chaotropic salt, was used to lyse virus and deactivate RNases, as well as serve as a salt bridge between negatively-charged RNA and negatively-charged silica, although 2M GuSCN was previously shown to be sufficient[17]. In addition to GuSCN in the lysis buffer, we used a combination of a reducing agent (Dithiothreitol, DTT) to deactivate RNases via reduction of disulfide bonds and sacrificial non-HIV RNA molecules (tRNA) in a relatively low pH buffer (MES, pH 5). RNA phosphodiester bonds are less prone to hydrolysis at pH 4-5[18]. tRNA and DTT are prone to oxidation and unstable in the liquid form at room temperature, so

© Copyright 2021 | N Panpradist

we stored them at -20 ºC and mixed them with GuSCN and MES lysis buffer just before the extraction experiments. A more stable reducing agent, β mercaptoethanol, has been successfully used in lysis buffer for RNA extraction[19], but DTT is less toxic[20] and less pungent than β mercaptoethanol. The optimal concentration of 20-40mM DTT **(Figure 2.5**) showed a 30% recovery of spiked HIV RNA compared to the standard RNA extraction kit. We hypothesized that the rate of viral lysis might be faster than the RNAse deactivation, allowing RNases to remain active and digest HIV RNA released from the viral particle. An addition of tRNA as sacrificial molecules with DTT improved the yield of HIV RNA. We found amplifiable HIV RNA yields were comparable to the standard RNA extraction kit when 22.4-33.6µg non-target tRNA was added to the lysis mixture (**Figure 2.6**). It is important to note that the addition of tRNA beyond 6µg in the lysis buffer did not protect HIV RNA. The silica column we used (

© Copyright 2021 | N Panpradist

Table S2.2) has a high capacity to capture up to 40µg and should accommodate absorption of both tRNA and HIV RNA targets, but the tRNA eluted along with the target HIV RNA could compete during the RT-PCR amplification step (**Figure 2.7**). We observed inefficient target amplification when non-target DNA is present at more than 2 ng/µL depending on the PCR reaction conditions[21, 22]. To wash loosely bound charged molecules from the silica membrane and further purify the RNA, we used two wash buffers starting from a high salt wash buffer: 1M GuSCN, 10mM Tris-HCl pH 7.4; and followed by a low-salt wash buffer: 10mM Tris-HCl pH 7.4 with 80% ethanol. A high ethanol concentration can solubilize residual salts but not RNA from the silica membrane when GuSCN is absent to serve as a salt bridge.

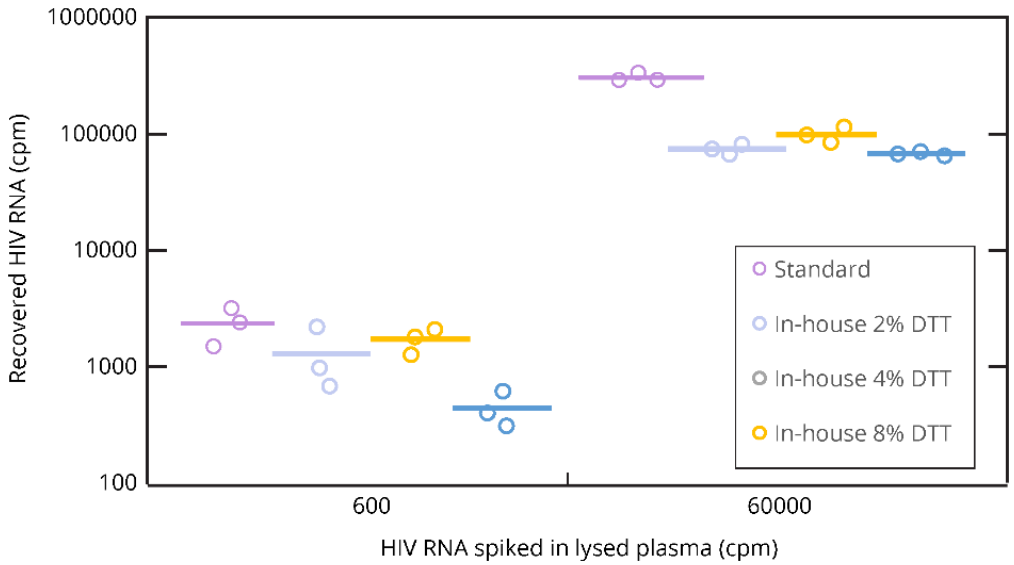

Figure 2.5 | Effect of DTT concentrations in in-house lysis buffer.

The in-house RNA lysis buffer containing 2 - 8% (v/v) DTT (2M) in 4M GuSCN, 10mM MES pH 5.5, or the standard lysis buffer (Qiagen ViralAmp kit) was used to lyse HIV negative human plasma. After 10min (Qiagen protocol) and 15min (in-house protocol) incubation, HIV RNA was spiked into the samples either at 0, 600, or 60000 copies/mL. The samples were then proceeded with the rest of the extraction

© Copyright 2021 | N Panpradist

protocol and analyzed using RT-qPCR. The Cq values from each condition were converted to recovered copies and plotted (mean ± SE, *n* = *3*).

The image was published: DOI: https://doi.org/10.1101/2021.08.18.21256786.

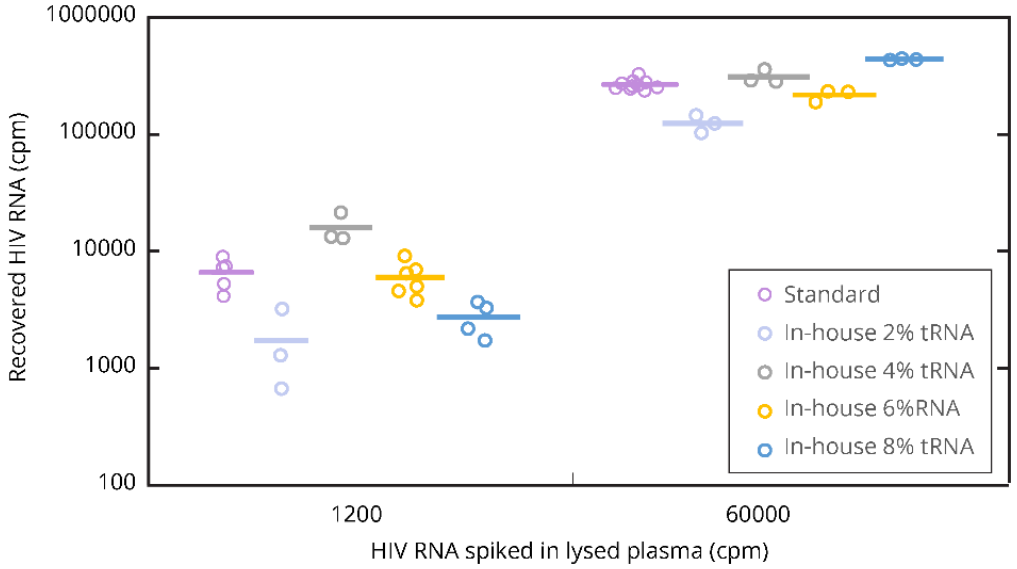

Figure 2.6 | Effect of carrier RNA in in-house lysis buffer.

The in-house RNA lysis buffer (4M GuSCN, 10mM MES pH 5.5, 4% DTT) containing 2 - 8% (v/v) 1mg/mL tRNA or the standard lysis buffer (Qiagen ViralAmp kit) was used to lyse HIV negative human plasma. After 10min (Qiagen protocol) and 15min (in-house protocol) incubation, HIV RNA was spiked into the samples either at 0, 1200, or 60000 copies/mL. The samples proceeded with the rest of the extraction protocol and were analyzed using RT-qPCR. The Cq values from each condition were converted to recovered copies and plotted (mean ± SE, *n* = *3*).

The image was published: DOI: https://doi.org/10.1101/2021.08.18.21256786.

© Copyright 2021 | N Panpradist

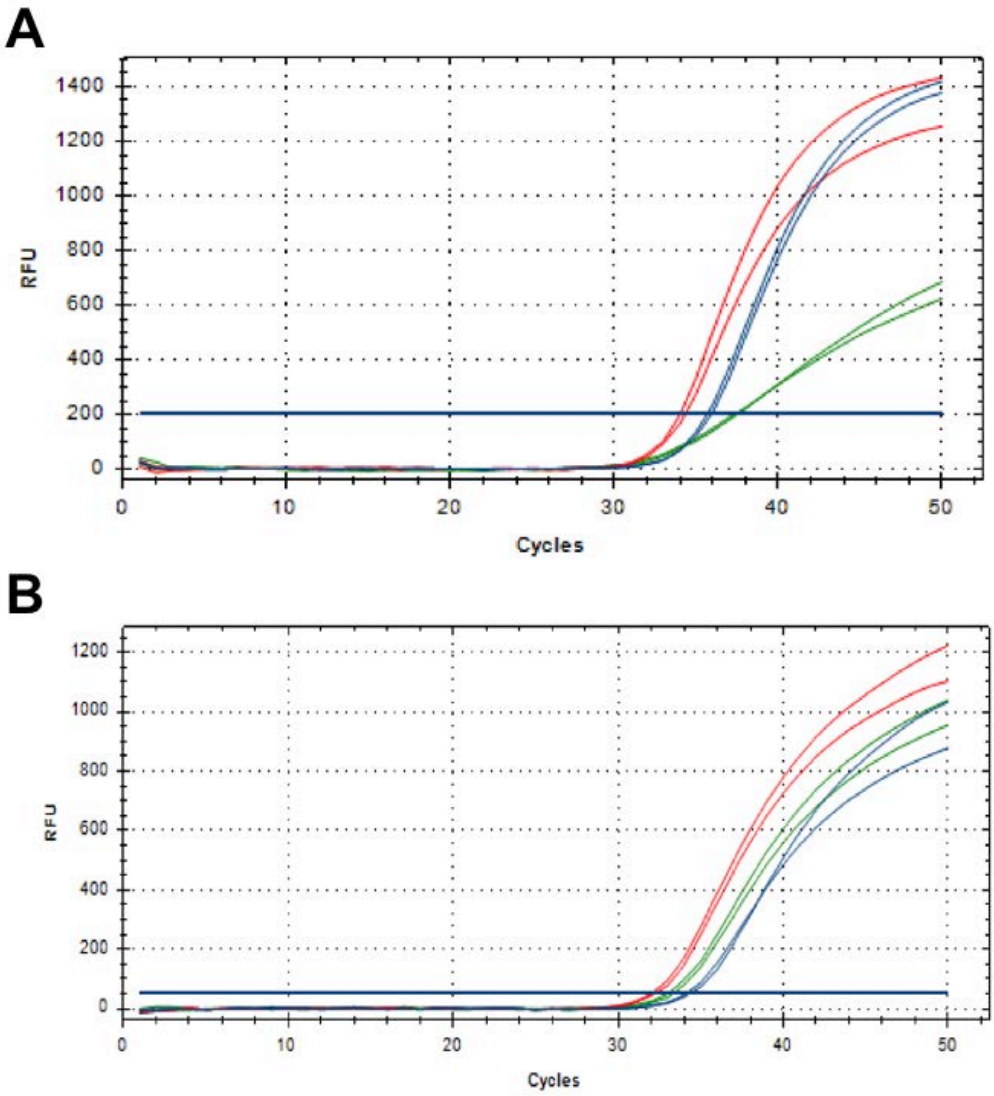

Figure 2.7 | Impact of carrier tRNA concentration on RT-qPCR.

(**A**) Amplification curves of 5µL extracted RNA (**B**) Amplification curves of 2µL extracted RNA from HIV RNA 1000copies/mL using either standard protocol (red lines), standard tRNA condition (1%) in in-house buffer (blue lines), or 8% tRNA in in-house buffer (green lines). Each condition was performed in duplicates and individually plotted. The image was published as G Gulati* and N Panpradist* et al. (DOI: https://doi.org/10.1101/2021.08.18.21256786).

2.3.3 ANALYTICAL SENSITIVITY IN CONTRIVED SPECIMENS

The analytical sensitivity of OPTION 1 and OPTION 2 workflows using the in-house extraction method was assessed and compared to the standard

© Copyright 2021 | N Panpradist

extraction method. We analyzed single-target contrived samples for the OPTION 1 workflow (*i.e.,* either HIV or SARS-CoV-2 RNA spiked in lysed human plasma). **Figure 2.8A** and **Figure 2.8B** show scatter plots of the input VL spiked in contrived samples and measured VL from the RNA extracted by in-house or standard methods. Across the concentrations from the LoD to 60K copies/mL, the in-house extraction method has a 1.09 ± 0.5 (mean ± SD) efficiency (slopes of fitted linear regression, **Figure 2.8A** - **Figure 2.8B**), compared to 0.94 ± 0.1 efficiencies of the standard method. Regardless of the extraction methods used, classifications as positive (detectable VL) and negative (undetectable VL) revealed RNA from the in-house extracted method was successfully detected in 100% (12/12) positive samples spiked with ≥200 copies/mL HIV RNA and undetected in 3/3 negative samples. Analysis of RNA from contrived SARS-CoV-2 samples, using in-house versus standard extraction methods, showed 100% agreement for the positive (detectable VL) and negative (undetectable VL) classifications (**Figure 2.8B**), with an LoD of 100 copies/mL in positive samples. For the OPTION 2 workflow (pooled plasma/NS), the in-house extraction method yielded LoDs identical to those obtained from the OPTION 1 workflow (*i.e.*, 200 copies/mL for HIV; 100 copies/mL for SARS-CoV-2, Figure S2.19). HIV VL measured in the RNA obtained from both extraction methods are in close agreement (linear regression fit R^2: 0.98 for measured VL correlation between the two different extraction methods from plasma (y-axes in both plots in **Figure 2.8A**); 0.92 for measured VL correlation between the two extraction methods from pooled plasma/NS samples (y-axes in both plots in **Figure S2.19B**). The yields of HIV

© Copyright 2021 | N Panpradist

RNA from both extraction methods were found to be more variable in ≤200copies/mL samples (**Figure 2.8A** – **Figure 2.8B**, black diamonds are samples with measured VL significantly deviated from the theoretical yield). This observation is expected because the theoretical RNA concentration per RT-qPCR reaction is very low (i.e., <7 copies/reaction for the starting 140µL of samples with <600 copies/mL). The variations of measured VL in <600copies/mL samples are also observed in pooled plasma/NS (Figure S2.19). We used a 50-cycle RT-qPCR (while 40-cycle RT-qPCR is common) to increase the opportunity to detect low-concentration RNA in 100-200 copies/mL samples. However, the limit of quantification (**LOQ**) of HIV VL in contrived plasma or plasma/NS is 600 copies/mL, higher than the LoD. **Figure 2.8C** and **Figure 2.8D** summarize the performance of both OPTION 1 and OPTION 2 workflows on SARS-CoV-2 RNA detection (*i.e.,* positive vs. negative) and HIV VL classifications (*i.e.,* VLS vs. VD) based on the US NIH VF threshold.

© Copyright 2021 | N Panpradist

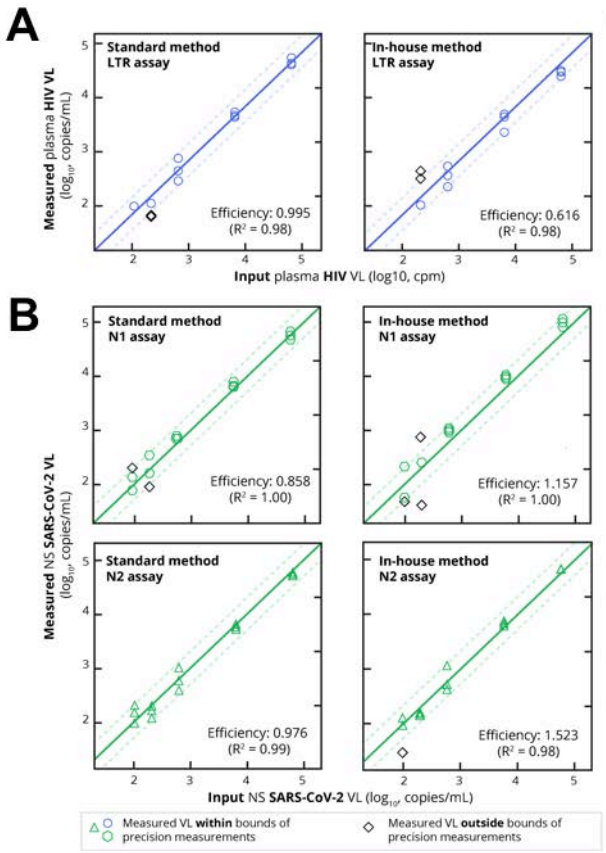

C

Single-target analysis (OPTION 1)

RNA concentration (copies/mL)	HIV status	# HIV VL with correct classification		SARS-CoV-2 status	Correct SARS-CoV-2 detection	
		Standard	In-house		Standard	In-house
0	Negative	3	3	Negative	3	3
100	VLS	3	3		3	3
200	VF	1	3	Positive	3	3
600		3	3		3	3
6,000		3	3		3	3
60,000		3	3		3	3
% Accuracy		94%	100%		100%	100%

(3 replicates of contrived samples were independently extracted and amplified)

D

Multi-target analysis (OPTION 2)

RNA concentration (copies/mL)	HIV status	# HIV VL with correct classification		SARS-CoV-2 status	Correct SARS-CoV-2 detection	
		Standard	In-house		Standard	In-house
0	Negative	2	2	Negative	2	2
100	VLS	2	2		2	2
200	VF	2	2	Positive	2	2
600		2	2		2	2
6,000		2	2		2	2
60,000		2	2		2	2
% Accuracy		100%	100%		100%	100%

(Duplicates of contrived samples were independently extracted and amplified)

Figure 2.8 | Quantitation and classification of HIV and SARS-CoV-2.

Scatter plots of (**A**) measured HIV VL (*n = 3*) vs. input RNA in contrived plasma samples (lysed plasma and spiked with synthetic HIV RNA at 0, 100, 200, 600, 6K, or 60K copies/mL), and (**B**) measured SARS-Cov-2 VL (*n = 3*) v.s input RNA in contrived NS (lysed and spiked with synthetic SARS-CoV-2 RNA at 0, 100, 200, 600, 6K, or 60K copies/mL). Diagonal lines represent 100% theoretical RNA recovery from the extraction method based on the spiked-in RNA input. Dashed diagonal lines indicate the bound for precise measurement (*i.e.,* measured VL within ±0.3 $\log_{10}$(VL, copies/mL of input)). The efficiency of each extraction method for each assay is the slope of the linear regression fit, reported along with its R^2. Summary of HIV VL classification and SARS-CoV-2 detection using both extraction methods using (C) OPTION 1 workflow to analyze either NS or plasma, and (d) OPTION 2 workflow to analyze pooled plasma/NS samples. For HIV samples, we classified results as VLS or VF. For SARS-CoV-2, we classified results as positive or negative based on whether they were detected or not detected by both N1 and N2 assays. The image was published: DOI: https://doi.org/10.1101/2021.08.18.21256786.

© Copyright 2021 | N Panpradist

2.3.4 CLINICAL EVALUATION OF HIV IN PLASMA SPECIMENS

Figure 2.9A shows our experimental design to compare the performance of standard versus in-house extraction methods. RNA extracted using the in-house method (**Figure 2.9B**) was detected in 100% (30/30; 95%CI: 88-100) of HIV-seropositive plasma (median VL: 30,604 copies/mL; IQR: 6,503 - 96,626 copies/mL) and not falsely detected in HIV-seronegative plasma (10/10). Human RP genes were detectable in all negative specimens, confirming a functioning assay. However, human RP levels in HIV-seronegative plasma were significantly higher (lower Cq values) than those of HIV-seropositive plasma (**Figure 2.9B** and **Figure S2.20**). Measured HIV VL levels in the RNA extracted by in-house and standard methods were positively correlated (**Figure 2.9C**, linear regression fit, R^2: 0.81) but were statistically different ($p<0.05$, Wilcoxon Signed-Rank test, two-tailed). Compared to the standard method (**Figure 2.9C**), 20/30 measured VL values of RNA extracted by the in-house method were within the precise measurement bound. Still, RNA extracted by the in-house method led to 7 overestimated VL values and 3 underestimated VL values (black diamonds). Regardless, classifications (*i.e.,* VLS vs. VF) of measured VL results (**Figure 2.9D**) from RNA obtained by both extraction methods, either at ≥200 copies/mL for VF threshold (US NIH guideline[13]) or ≥1000copies/mL for VF (WHO guideline[14]), had 100% concordance (30/30; 95% CI: 90-100).

© Copyright 2021 | N Panpradist

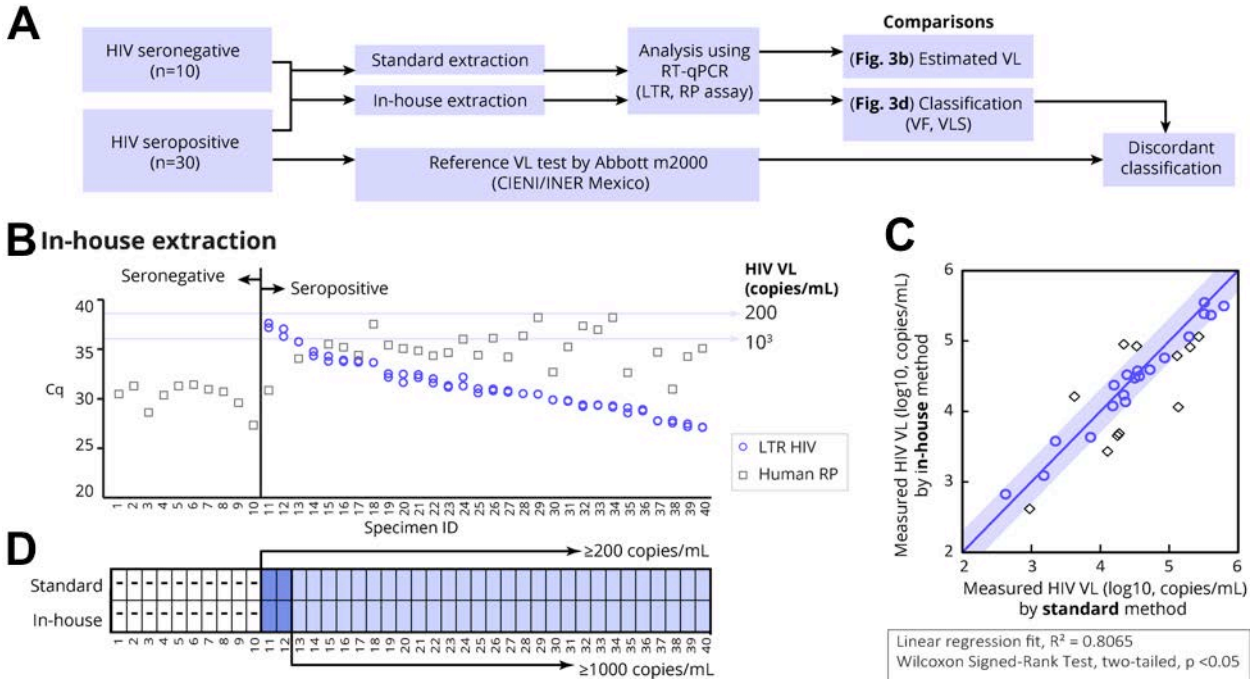

Figure 2.9 | Quantitation and classification of HIV RNA in clinical plasma specimens.

(**A**) Schema of experimental design to compare the performance of standard vs. in-house extraction methods. Plasma RNA extracted by standard or in-house extraction was evaluated using RT-qPCR. The RT-qPCR results were compared in terms of measured viral load and classifications. All HIV seropositive specimens had VL ≥1000 copies/mL when tested by the reference lab using Abbott m2000. (**B**) Cq values of the HIV long-terminal repeat (LTR) assay and human ribonuclease P (RP) assay (control for negative specimens) from the plasma RNA extracted by the in-house method. Extracted RNA from HIV-seropositive specimens were analyzed by LTR and RP RT-qPCR assays in duplicate. HIV-seronegative specimens (as tested by the vendor) were each extracted twice, and each extracted RNA aliquot was analyzed by LTR and RP RT-qPCR assays. The average RP Cq values are plotted. (**C**) Scatter plot of measured HIV VL in specimens extracted by standard vs. in-house methods. The diagonal line represents a theoretical 100% correlation of HIV VL measured in RNA extracted from both extraction methods. The shaded boxes around the diagonal lines indicate precise measurement bound (±0.3 $\log_{10}$(VL measured in RNA extracted by the standard method, copies/mL)). Diamonds are samples with measured VL outside precise measurement bound. (**D**) Classifications correspond to VL results. Negative results are labeled as "-" in white boxes. Virologic failure results were classified using 200 copies/mL (dark purple boxes) and 1000 copies/mL (light purple boxes) thresholds. RNA extracted by both methods

© Copyright 2021 | N Panpradist

was collected by one assay operator and analyzed by RT-qPCR by another assay operator. The image was published: DOI: https://doi.org/10.1101/2021.08.18.21256786.

2.3.5 CLINICAL EVALUATION OF SARS-COV-2 IN NS SPECIMENS

Figure 2.10A shows our experimental design to compare the performance of standard versus in-house extraction methods. NS was previously tested in a CLIA-certified laboratory, as 31 positive and 36 negative NS specimens for SARS-CoV-2. In this study, due to the limited volume of specimens available, we extracted 50µL specimens instead of 140µL (as was done in the above contrived sample experiment). Of 31 specimens previously tested positive for SARS-CoV-2 (**Figure 2.10B** and **Figure 2.10C**), the in-house method detected 25 (81%) as positive (detected by the N1 and N2 assay; median VL: 4180 copies/mL; IQR:3912-176168 copies/mL) and 6 (19%) as presumptive positive (detected by either the N1 or N2 assay; median VL: 84 copies/mL; IQR: 39–203 copies/mL). Two SARS-CoV-2 specimens (VL: 162 and 268 copies/mL) detected by the in-house method (confirmed true positive by the certified lab results) were falsely negative and presumptive positive by the standard method. Measured concentrations of the SARS-CoV-2 RNA obtained by in-house versus standard extraction methods revealed high correlations (R^2: 0.95 for N1 in **Figure 2.10D**; 0.99 for N2 in **Figure 2.10E**) and had no significant difference ($p>0.05$; Wilcoxon Signed-Rank test, two-tailed). Comparing the measured VL from the RNA obtained from the in-house and standard extraction methods, we found a few measured VL values in the N1 assay outside the precise measurement bound (**Figure 2.10D**). Still, the

© Copyright 2021 | N Panpradist

measured VL values from the same specimens were within acceptable variation in the N2 assay (**Figure 2.10E**). Possibly, this is due to the reportedly lower sensitivity of the N1 assay[11]. Thus the N1 assay could not detect low concentrations of the SARS-CoV-2 RNA in these specimens (VL: <500 copies/mL from the 50µL sample, equivalent to <178 copies/mL from a 140µL sample, which is around the LoD we observed from the contrived specimens).

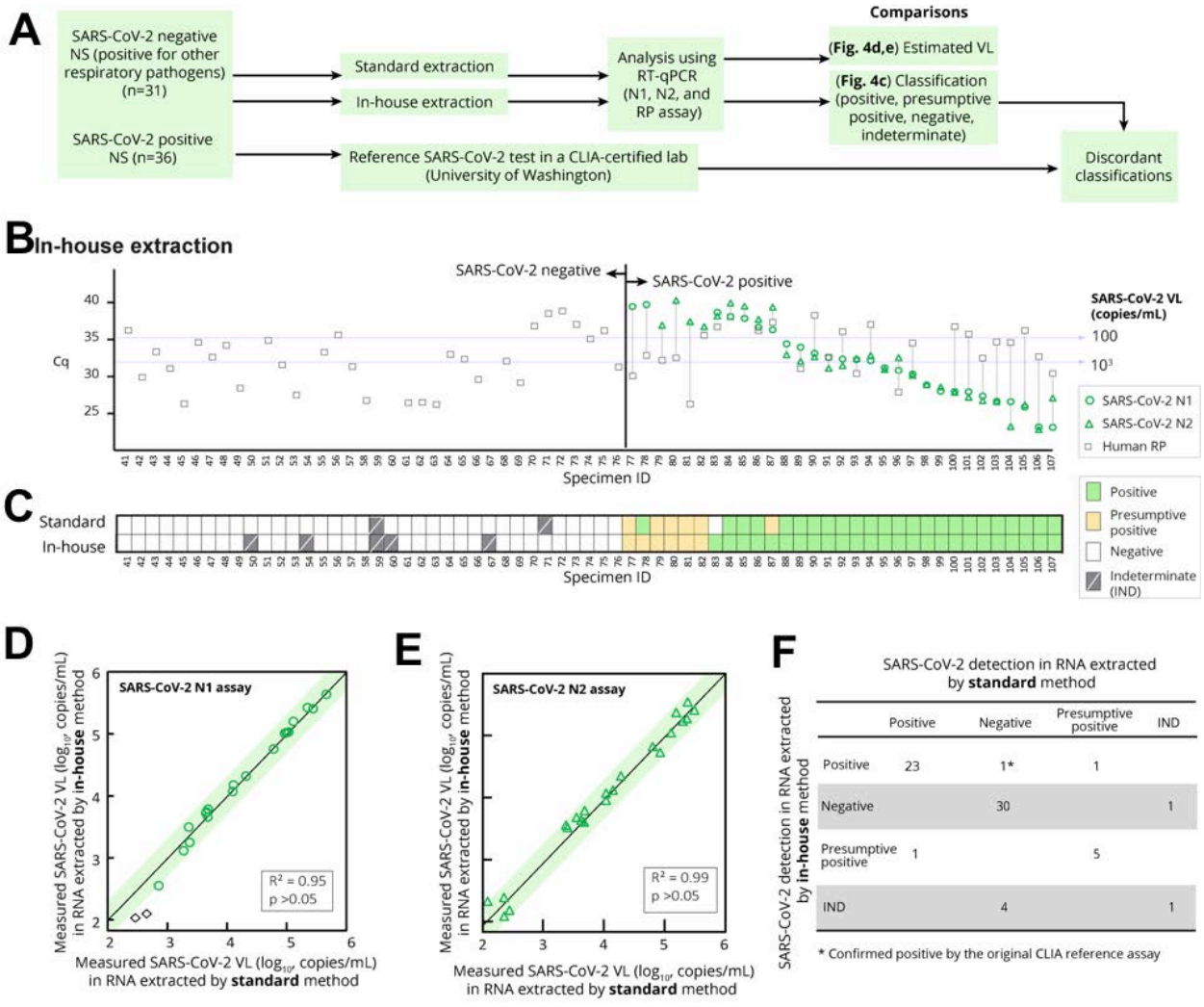

Figure 2.10 | Quantification and detection of SARS-CoV-2 RNA in clinical NS.

(**A**) Schema of experimental design to compare the performance of standard vs. in-house extraction methods. NS RNA obtained from standard or in-house extraction was evaluated using RT-qPCR. The RT-

© Copyright 2021 | N Panpradist

qPCR results were compared in terms of measured viral load and classifications. Discordant classifications were ruled out based on previous results from the CLIA-certified lab. (**B**) Cq values of the SARS-CoV-2 N1, N2, and human RP assay (control for negative specimens) from the in-house method. Each specimen was extracted, followed by RT-qPCR, and represented as individual data points. (**C**) Classifications of specimens based on the results from the two extraction methods. Specimens detected by N1 and N2 (regardless of RP detection) are classified as positive; specimens detected by either N1 or N2 assays are classified as presumptive positive; specimens not detected by N1 and N2 but detected by RP assay are classified as negative; specimens not detected by any assays are classified as indeterminate (IND). Scatter plot of measured SARS-CoV-2 in specimens extracted by standard vs. in-house methods in (**D**) N1 assay (e) N2 assay. The diagonal lines represent a theoretical 100% correlation of SARS-CoV-2 VL measured in RNA extracted from both extraction methods. Dashed lines indicate RT-qPCR precise measurement bound (*i.e.,* ±0.3log10(VL measured in RNA extracted from the standard method, copies/mL). Diamonds are samples with measured VL that significantly deviates from those obtained via standard extraction. (F) Summary table for classifications by the two methods. Two assay operators collected data.

The image was published: DOI: https://doi.org/10.1101/2021.08.18.21256786.

Similarly, the RP assay had 4, and 2 indeterminate (**IND**) results in the workflow using RNA obtained from the in-house and standard methods, respectively. These specimens contained <250 copies/mL human RP, thus, this discordance is likely due to variations of RT-qPCR near the LoD. **Figure 2.10F** summarizes the SARS-CoV-2 detection results from the RNA obtained by standard and in-house extraction methods.

2.3.6 CLINICAL EVALUATION OF HIV AND SARS-COV-2 IN POOLED CLINICAL PLASMA AND NS

© Copyright 2021 | N Panpradist

We tested the OPTION 2 co-extraction workflow on a subset of available remnant NS and plasma specimens (**Figure 2.11A**) previously tested in the CLIA-certified and reference labs, respectively. Here, each HIV-seropositive

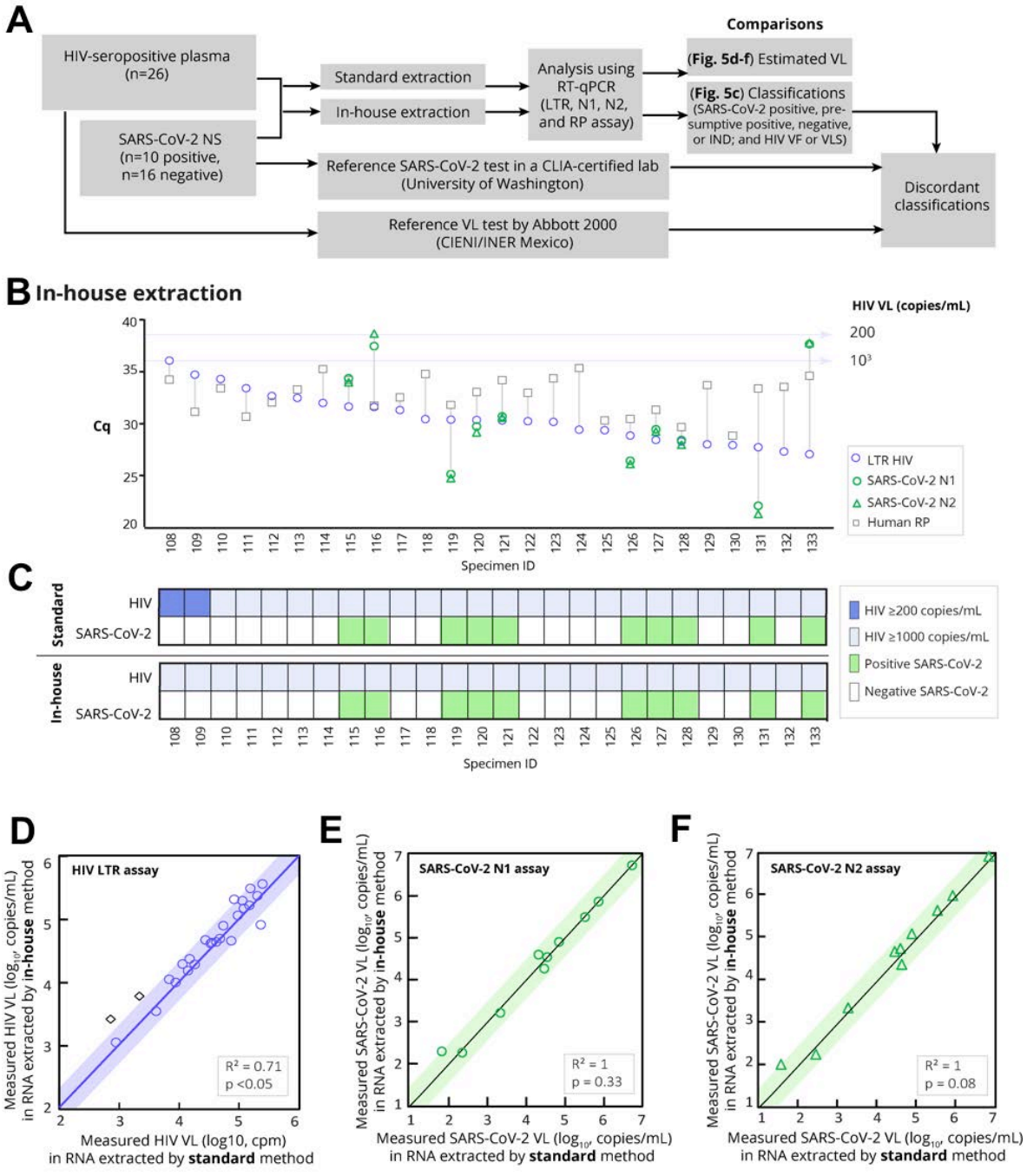

Figure 2.11 | HIV LTR and SARS-CoV-2 Cq values from RNA co-extracted from NS/plasma specimens.

© Copyright 2021 | N Panpradist

(**A**) Schema of experimental design to compare the performance of standard vs. in-house extraction methods. NS/plasma RNA extracted by standard or in-house extraction were evaluated using RT-qPCR. The RT-qPCR results were compared in terms of measured VL and classifications. (**B**) Cq values of the SARS-CoV-2 LTR, N1, N2, and human RP assay (control for negative specimens) from the in-house method. Each specimen was extracted, followed by RT-qPCR, and represented as individual data points. (**C**) Classifications of specimens based on the results from the two extraction methods. Scatter plot of measured SARS-CoV-2 in specimens extracted by standard vs. in-house methods in (**D**) LTR (**E**) N1 (**F**) N2 assay. The diagonal lines represent a theoretical 100% correlation of VL measured in RNA extracted from both methods. Dashed lines indicate precise measurement bound. Diamonds are samples with measured VL that significantly deviates from those obtained via standard extraction. The image was published: DOI: https://doi.org/10.1101/2021.08.18.21256786.

plasma specimen (*n = 26*) was randomly assigned to mix with either positive (*n = 10*) or negative SARS-CoV-2 specimens (*n = 16*). Each plasma/nasal specimen pool was then extracted using the in-house method and the standard method. **Figure 2.11B** shows the Cq values of SARS-CoV-2 N1 and N2, HIV LTR, and human RP assays from the samples extracted by the in-house method. Using the US NIH 200copies/mL cutoff for HIV VF (**Figure 2.11C**), there was a 100% (26/26) concordance with the standard method. Detection of SARS-CoV-2 was also 100% (26/26) concordant. **Figure 2.11D** – **Figure 2.11F** show high correlations of measured VL of HIV LTR, SARS-CoV-2 N1, and SARS-CoV-2 N2 targets, respectively. Interesting, the measured HIV VL values in these specimens from RNA obtained by the in-house method were significantly higher than those by the standard method ($p<0.05$, Wilcoxon Signed-Ranked test, two-tailed); but the measured VL of SARS-CoV-2 are similar between the two groups.

DISCUSSION

© Copyright 2021 | N Panpradist

We developed a new workflow with an optimized in-house RNA extraction method to enable simultaneous quantification of HIV VL and detection of SARS-CoV-2 in a single RT-qPCR run. The workflow can be tailored to different clinical use by isolating target RNA from plasma or plasma pooled with NS via a single extraction kit.

In contrived specimens, both OPTION 1 and OPTION 2 workflows can detect low concentrations of the HIV RNA (200 copies/mL) and SARS-CoV-2 RNA (100 copies/mL). We anticipate that this highly sensitive SARS-CoV-2 assay would be able to detect most SARS-CoV-2 positive clinical specimens, as the LoD of 100 copies/mL is lower than the reported medians of SARS-CoV-2 VL in blood in the first two weeks and ~50-fold lower than the medians of SARS-CoV-2 viral loads in respiratory samples during the first 6 weeks[23]. When testing clinical NS, we found that the in-house method had positive results for all SARS-CoV-2 respiratory specimens with ≥1000 copies/mL but only around 50% positive and 50% presumptive positive results in 100-1000 copies/mL specimens. Due to the limited availability of specimens, we only used 50µL specimens from 1mL swab eluate. Processing a larger volume of specimens (i.e., 140µL per extraction like the case of HIV specimens or contrived SARS-CoV-2 samples) would likely improve detection of specimens with <1000 copies/mL by increasing the RNA input in the final RT-PCR reaction. Measured HIV VL in contrived specimens by OPTION 1 and OPTION 2 also showed near 100% correlations. In clinical plasma specimens, the in-house method also accurately classified HIV VF compared to the standard method. The new workflow can potentially streamline HIV management and SARS-CoV-2 detection by determining if a PLH has detectable

© Copyright 2021 | N Panpradist

viremia as well as SARS-CoV-2 infection by extracting RNA from plasma alone or pooled plasma/NS using a single in-house method. Combining the detection of these two viruses can help address the challenges associated with the overlay of the COVID-19 pandemic on the existing HIV epidemic.

Our workflow utilizes an internal control based on the detection of the human RP gene, which is also used for many clinical assays[24-26]. In addition to reporting proper assay function, detection of the RP gene can confirm whether the samples were properly collected, especially for the self-collection of NS for SARS-CoV-2. As an alternative to human genes, MS2 bacteriophage can be spiked into the sample as the control[27, 28]. For this approach, the level of MS2 will not reflect proper sample collection or release. Rather, the MS2 bacteriophage can be used as an engineering tool to measure how well the extraction and amplification are performed accurately.

The workflow also helps to circumvent the issues associated with the availability of commercial RNA extraction kits and reduces the cost of RT-qPCR. Because of the high demand for COVID-19 tests, procuring RNA extraction kits has been difficult, limiting routine HIV testing. RNA extraction kits have contributed to high reagent costs for most RT-qPCR workflows (approximately $6/kit). Our in-house method uses low-cost alternatives that can be obtained as off-the-shelf reagents (

© Copyright 2021 | N Panpradist

Table S2.2), which allows laboratories to assemble their own low-cost RNA extraction kits ($1.85/kit). Using the proposed workflow to analyze the plasma/NS with a single in-house kit would require $1.85, 5-times less expensive for consumables than a traditional workflow requiring two commercial kits ($12) for each specimen.

Our workflow detects HIV, SARS-CoV-2, and human RNA via separate RT-qPCR reactions to maximize sensitivity. Co-amplification of SARS-CoV-2 and human RNA was performed but reportedly had reduced sensitivity compared to single-target amplification[29]. To improve the detection of the co-amplification, sequence-specific extraction of RNA from HIV or SARS-CoV-2[21, 30-32] could be useful by increasing the target concentrations. Although single-target RT-PCR amplification using FAM can be expensive, it is possible to eliminate the need for the thermal cycler. End-point analysis of single-channel fluorescence such as FAM can be analyzed via cell phone images and has been shown to have a high correlation with the Cq values[7]. Using multiplexed amplification may require a higher cost RT-qPCR than a $5000 single-channel qPCR machine, but the overall cost may be offset by higher throughput. Still, it could reduce per-test cost since one sample can be analyzed in a single RT-qPCR reaction per sample instead of four RT-qPCR reactions per sample.

Overall, the utility of such effective workflows for PLH is not limited to SARS-CoV-2 but should be explored for other common HIV comorbidities (*e.g.,* tuberculosis, hepatitis B, hepatitis C), or other AIDS-defining opportunistic infections still causing high disease burden in low- and middle-income countries (*e.g., Pneumocystis jirovecii* pneumonia, histoplasmosis, toxoplasmosis, cryptococcal

© Copyright 2021 | N Panpradist

meningitis, and mycobacteriosis). This allows the pre-scheduled VL tests to screen for other diseases that could worsen the health of PLH, reducing diagnosis costs and time.

ACKNOWLEDGMENTS. We thank Dr. Lucia Vojtech for training and access to the equipment needed for the cdPCR experiment. The Naica cdPCR system from Stilla Inc. was funded by the NIH-funded Centers for AIDS Research (P30 AI027757 and P30 AI064518). We thank other Lutz Lab members: Ian Hull, Qin Wang, and Jordan Campbell, for their technical support. We thank the Seattle Flu Study and the Seattle Coronavirus Assessment Network (SCAN) teams led by Principal Investigators: Helen Y. Chu, MD, MPH, Michael Boeckh, MD, Ph.D., Janet A. Englund, MD, Michael Famulare, Ph.D., Barry R. Lutz, Ph.D., Deborah A. Nickerson, Ph.D., Mark J. Rieder, Ph.D., Lea M. Starita, Ph.D., Matthew Thompson, MD, MPH, DPhil, Jay Shendure, MD, Ph.D. and Trevor Bedford, Ph.D. for providing specimens for testing.

2.4 FUTURE DIRECTIONS

> **Contributors**: Nuttada Panpradist, Amy Oreskovic, Jonathan Lim (undergraduate student co-mentored with Amy Oreskovic).

2.4.1 ISSUES WITH TRADITIONAL EXTRACTION METHODS

Conventional nucleic acid extraction methods collect both HIV and non-HIV nucleic acids. The non-HIV nucleic acids will compete for resources such as salts, enzymes, and primers and, as a result, inhibit nucleic acid amplification

© Copyright 2021 | N Panpradist

if present at a high concentration in the reaction (**Figure 2.12**). To avoid this issue, it is a common practice to dilute the extracted nucleic acid to a proper concentration for successful amplification. Not only does this step require an instrument (such as a Nanodrop) to measure the nucleic acid concentration, diluting the amount of total nucleic acid also reduces the amount of HIV targets that go into amplification, which in turn reduces the sensitivity of the assay. Often, specimens with low viral loads and detection of low frequencies (e.g., <10%) of HIVDR quasispecies can be missed. This stresses the need for a method that discards non-HIV targets while retaining HIV targets.

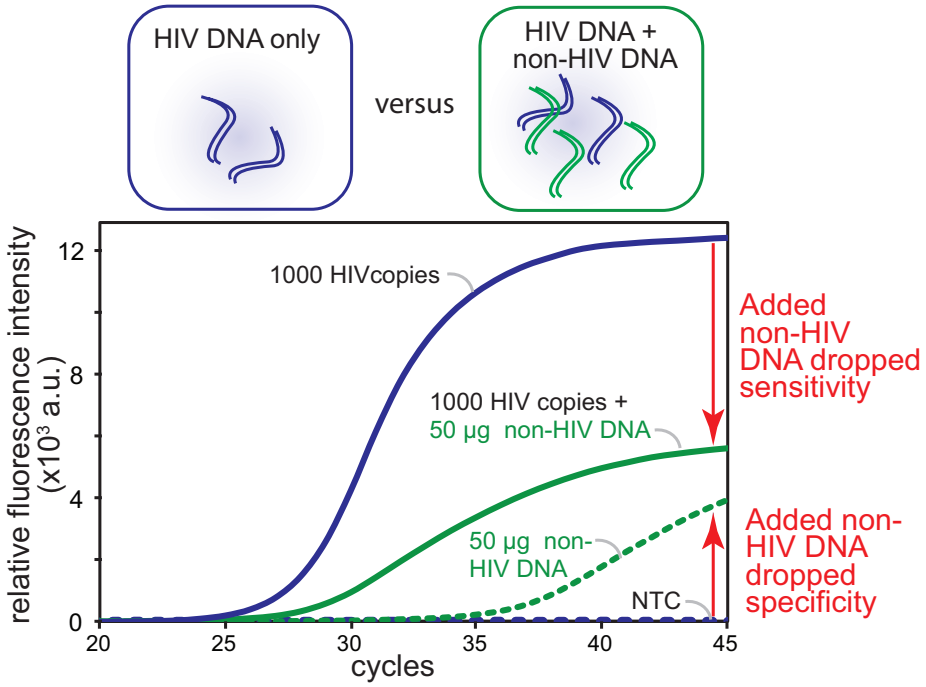

Figure 2.12 | Non-target DNA harms sensitivity and specificity of amplification.

qPCR amplification of patient-driven HIV plasmids using a clinically validated HIV *pol* primer. The presence of 50µg non-HIV DNA reduced half of the amplified products in 10^3 HIV copies samples. **NTC** (no HIV template control) with added 50 µg of non-HIV DNA showed high non-specific amplification.

© Copyright 2021 | N Panpradist

2.4.2 WE CAPTURED HIV NUCLEIC ACID SPECIFICALLY AS IT FLOWS IN PAPER.

A key advantage for using a lateral flow membrane aside from being equipment-free is that its flow rate can be fine-tuned by engineering geometry and membrane materials to favor nucleic acid hybridization. For initial testing, we anchored the HIV-specific capture oligonucleotide probe on the nitrocellulose membrane. The mock targets, 10^{12} copies of fluorescein tagged 80-bp HIV *pol* gene were introduced and wicked past the capture probe zone. The captured HIV sequence was detected using a labeling enzyme and substrate that creates visible colored bands. HIV sequences were successfully captured as they flowed through paper, and our capture system was affected by the presence of human plasma and/or 25 µg of spiked non-HIV DNA (**Figure 2.13**).

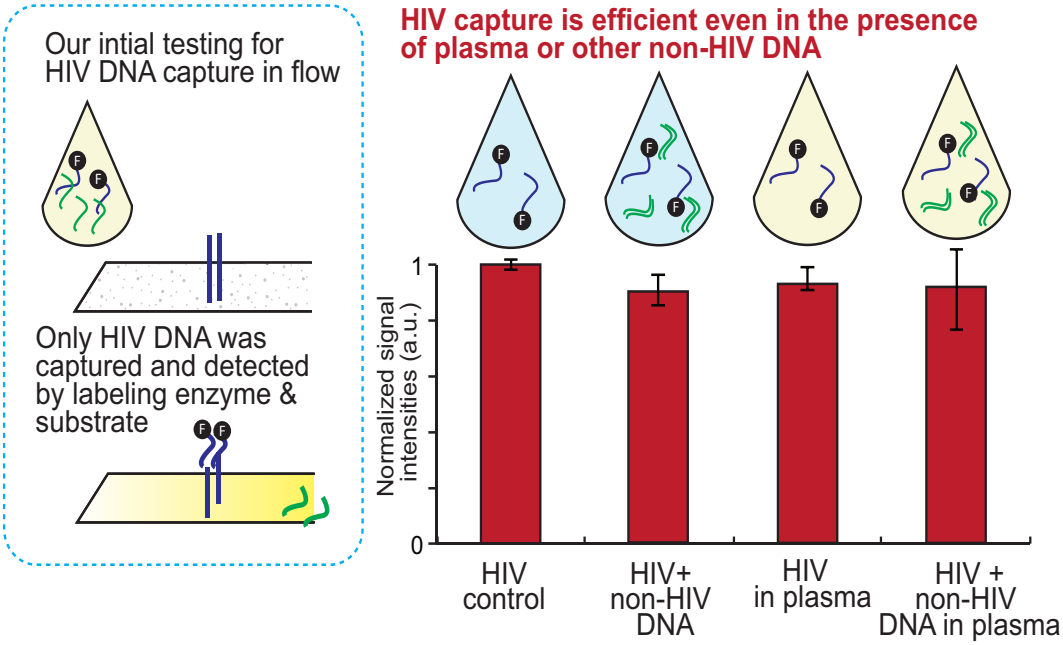

Figure 2.13 | HIV DNA captured specifically in the presence of non-HIV DNA and/or plasma. 10^{12} copies of HIV-tagged fluorescein targets were captured on the membrane and detected by anti-fluorescein antibody tagged alkaline phosphatase/ purple substrate. The capture efficiencies indicated

© Copyright 2021 | N Panpradist

by the color intensities were normalized to the control case of HIV without the human plasma and spiked non-HIV DNA. The capture efficiencies did not depend on non-HIV DNA and plasma.

2.4.3 OUR CAPTURE METHOD IS COMPATIBLE WITH DOWNSTREAM AMPLIFICATION.

Our capture method was further tested using a low (pre-amplification) level concentration of synthetic 80-base HIV *pol* gene (10^4 copies). Three samples – (1) HIV DNA without plasma, (2) HIV DNA spiked in plasma, and (3) negative plasma – were wicked in paper past the capture zone containing the immobilized probes that recognize HIV. The capture zone was then excised for subsequent PCR and gel electrophoresis. As mentioned above, non-specific amplification is caused by the presence of non-HIV DNA (**Figure 2.12**). Our specific-capture system effectively removed non-HIV nucleic acids in plasma, as indicated by the disappearance of non-specific amplification in plasma samples (**Figure 2.14, lane 3 vs. 6**). We anticipate a marked increase in sensitivity will be observed when applying our system in lysates of HIV-infected specimens with more cell-free nucleic acid in plasma[33].

© Copyright 2021 | N Panpradist

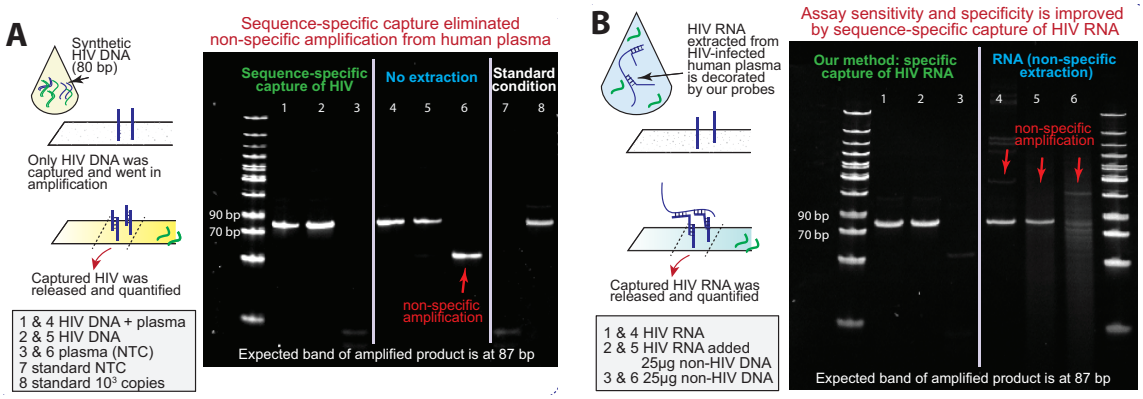

Figure 2.14 | Sequence-specific capture of synthetic HIV DNA & genomic clinical HIV RNA. (**A**) Non-specific amplification from plasma was eliminated: lane 3 vs. 6 (**B**) RNA from HIV-infected patients can be specifically captured using our method (lane 1 vs. 4, 2 vs. 5, and 3 vs. 6).

2.4.4 FOR ALL-IN-ONE DRUG RESISTANCE AND VIRAL LOAD TEST, RNA IN PLASMA IS THE CLINICALLY ACCEPTED SPECIMEN; AND OUR CAPTURE SYSTEM IS ALSO APPLICABLE FOR HIV RNA.

Since we have not yet developed a viral lysis buffer, our RNA model target (10^4) is from HIV-infected plasma extracted by a commercial RNA extraction kit. The model RNA target contains both HIV and non-HIV nucleic acids that are fragmented to <10 kb from centrifugation, so it should flow through the paper membrane. To ensure efficient capturing of a whole HIV *pol* gene, we used multiple nucleotide probes to bind to different *pol* regions. The probes have a common engineered nucleotide barcode region that allows the RNA-probe duplex to be captured by its complementary barcode immobilized on the membrane. After the RNA-probe duplex wicked past the capture zone, the capture zone was excised for subsequent RT-PCR and gel electrophoresis. Our preliminary data showed that our capture method improved assay specificity and sensitivity by eliminating non-specific amplification contributed from both

© Copyright 2021 | N Panpradist

non-HIV RNA present in plasma (from the non-specific RNA extraction kit) and added 20µg of non-HIV DNA (**Figure 2.14B**).

2.4.3 VISION FOR INTEGRATED SAMPLE COLLECTION AND PREPARATION FOR SMALL SAMPLE VOLUME

We have designed a workflow for lysis and plasma filtration that is rapid, simple, and reduces the risk of infection for healthcare workers (**Figure 2.15A**). The lysed plasma can then be added to the sample port of the device where only HIV RNA will be captured, and other nucleic acids will be wicked away (**Figure 2.15B**).

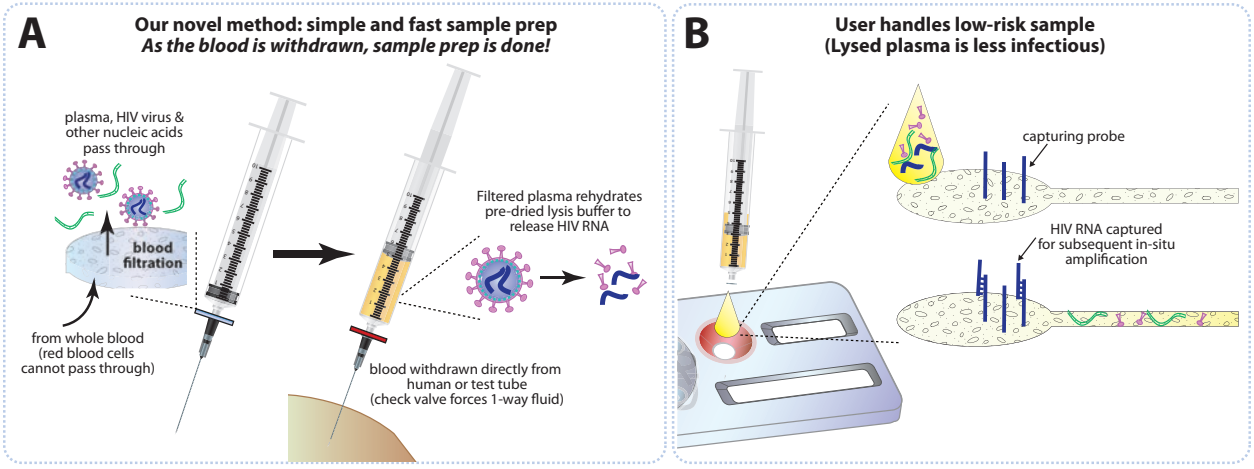

Figure 2.15 | Vision of our novel simple and fast sample preparation method.

(**A**) All-in-one sample collection and preparation method. Between the tip and collecting tube, a blood filter membrane layer will be installed to filter out the cells in the blood and let plasma containing HIV viral particles and other nucleic acids pass through to the collecting column. We also will install a check valve between the tip and the filter to force one-way flow. This will allow the syringe to be pulled but not pushed. The filtered plasma entering the column will rehydrate the pre-dried viral lysis buffer that will release HIV RNA. RNAse inhibitors will be added as part of the dried mixture to prevent RNA degradation. Our previous work has shown rehydration, mixing, and lysis steps are very fast (altogether ~ 2 minutes)[34]. This workflow will require no user training; the user will be collecting blood as is done

© Copyright 2021 | N Panpradist

regularly. Additionally, users will handle lysed plasma, which is less infectious than whole blood. (**B**) The lysed plasma will be added into the device where fluid is forced to pass through the zone where HIV-capturing probes are immobilized. Only HIV RNA will be captured, followed by in-situ amplification.

2.4.4 SEQUENCE-SPECIFIC CAPTURE OF HIV RNA FROM LARGE-VOLUME SAMPLES.

Previously Amy Oreskovic *et al.* developed a sequence-specific capture method to extract diluted, short cell-free tuberculosis (**MTB**) DNA fragments[35, 36] in human urine. Streptavidin magnetic beads decorated with 1-2 biotinylated TB-specific DNA capture probes hybridize respectively to sense or both antisense/sense strands of MTB cell-free DNA. The captured MTB DNA was then released from the DNA probes using sodium hydroxide. The resultant DNA was then pH neutralized prior to analysis using PCR.

HIV RNA is nearly 10kb nucleotides, much longer than MTB cell-free DNA. Thus, capture efficiency would likely be improved using multiple capture probes. Stronger total hybridization forces from probe/RNA duplexes could reduce the effect of shearing during multiple washing steps. Additionally, RNA has been known to be prone to degradation, especially in a high-pH condition, so releasing the captured RNA using sodium hydroxide would not be compatible. We hypothesize that the following modifications would increase the RNA capture yields: (*i*) increase the length of the HIV capture probe to 120 nt. (*ii*) increase the number of probes from one to five across HIVDR RT region (1300 bases) covering 46% of HIV RNA segment, and (*iii*) Use strand displacement to release the target strand and digest the leftover capture probes with add DNAse to avoid probe interfering with amplification.

© Copyright 2021 | N Panpradist

In multiple sequencing applications, viral RNA is captured using multiple probes[37-39]. A set of 161 120-nucleotide biotinylated DNA probes was used to capture HIV RNA[38], and the NGS results reveal high sequence coverage across genomes, but this probe capture design is exhaustive (2x redundant, overlapping regions of the whole HIV genome). For cost-saving in initial testing, we used only five probes across segments of the HIV RT region (1300 bases). Additionally, this protocol requires a 4h 65 °C incubation. We plan to reduce the incubation time by reversing the order of hybridization. We first will incubate the five different HIV probes (**Table S2.4**) with the HIV RNA for 10 minutes at 65°C in solution (**Figure 2.16A**). Separately, the streptavidin bead construct will be prepared by mixing the streptavidin magnetic bead and the universal probes (**Figure 2.16B**). Then, HIV RNA: probe duplexes are captured onto the streptavidin bead construct (**Figure 2.16C**). After washing away HIV-RNA-free components from the sample, the [HIV RNA: capture probe] is released via toehold-mediated strand displacement (see **Chapter 3.4**). Lastly, DNA probes are digested by DNAse prior to downstream detection of HIV RNA.

© Copyright 2021 | N Panpradist

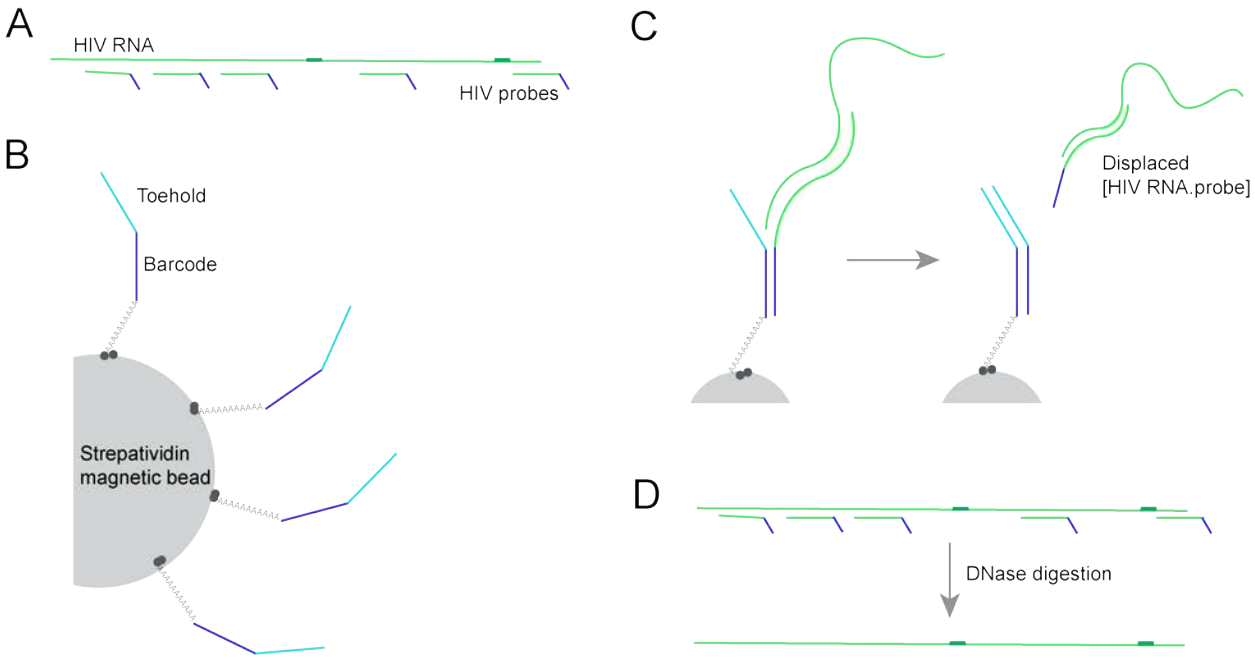

Figure 2.16 | Schema of HIV RNA capture in large volume specimens.

(**A**) HIV RNA is hybridized to multiple HIV 120-nucleotide DNA probes (green) tagged with a complementary sequence of the engineered barcode (blue). (**B**) Streptavidin bead construct is the streptavidin-coated magnetic nanoparticles bound to the biotinylated universal probes. Universal probe sequences contain a region of engineered barcode and poly(A)40 tag to reduce steric hindrance. (**C**) RNA: probe complexes are mixed with the streptavidin bead construct. Inhibitors are washed away before the elution of HIV RNA: probe complex via strand displacement. (**D**) DNA probes are digested via DNase prior to the detection of RNA.

© Copyright 2021 | N Panpradist

CHAPTER 2 REFERENCES

1. Boukli, N.; Boyd, A.; Collot, M.; Meynard, J. L.; Girard, P. M.; Morand-Joubert, L., Utility of HIV-1 DNA genotype in determining antiretroviral resistance in patients with low or undetectable HIV RNA viral loads. *The Journal of antimicrobial chemotherapy* **2018,** *73* (11), 3129-3136.
2. Spear, G. T.; Ou, C. Y.; Kessler, H. A.; Moore, J. L.; Schochetman, G.; Landay, A. L., Analysis of lymphocytes, monocytes, and neutrophils from human immunodeficiency virus (HIV)-infected persons for HIV DNA. *The Journal of infectious diseases* **1990,** *162* (6), 1239-44.
3. Micek, Mark A.; Blanco, Ana J.; Beck, Ingrid A.; Dross, S.; Matunha, L.; Montoya, P.; Seidel, K.; Gantt, S.; Matediane, E.; Jamisse, L.; Gloyd, S.; Frenkel, Lisa M., Nevirapine Resistance by Timing of HIV Type 1 Infection in Infants Treated with Single-Dose Nevirapine. *Clinical Infectious Diseases* **2010,** *50* (10), 1405-1414.
4. Mutsvangwa, J.; Beck, I. A.; Gwanzura, L.; Manhanzva, M. T.; Stranix-Chibanda, L.; Chipato, T.; Frenkel, L. M., Optimization of the oligonucleotide ligation assay for the detection of nevirapine resistance mutations in Zimbabwean Human Immunodeficiency Virus type-1 subtype C. *J Virol Methods* **2014,** *210C*, 36-39.
5. New England Biolabs, I. Protocol for Standard RNA Synthesis 2021. https://www.neb.com/protocols/2015/03/09/protocol-for-standard-rna-synthesis.

© Copyright 2021 | N Panpradist

6. New England Biolabs, I. Monarch® RNA Cleanup Kit (50 µg) 2021. https://www.neb.com/products/t2040-monarch-rna-cleanup-kit-50-ug#Product%20Information.

7. Panpradist, N.; Wang, Q.; Ruth, P. S.; Kotnik, J. H.; Oreskovic, A. K.; Miller, A.; Stewart, S. W. A.; Vrana, J.; Han, P. D.; Beck, I. A.; Starita, L. M.; Frenkel, L. M.; Lutz, B. R., Simpler and faster Covid-19 testing: Strategies to streamline SARS-CoV-2 molecular assays. *EBioMedicine* **2021,** *64*.

8. Panpradist, N.; Beck, I. A.; Ruth, P. S.; Ávila-Ríos, S.; García-Morales, C.; Soto-Nava, M.; Tapia-Trejo, D.; Matías-Florentino, M.; Paz-Juarez, H. E.; del Arenal-Sanchez, S.; Reyes-Terán, G.; Lutz, B. R.; Frenkel, L. M., Near point-of-care, point-mutation test to detect drug resistance in HIV-1: a validation study in a Mexican cohort. *AIDS* **2020,** *34* (9).

9. QIAGEN QIAamp® Viral RNA Mini Handbook. https://www.qiagen.com/us/resources/download.aspx?id=c80685c0-4103-49ea-aa72-8989420e3018&lang=en.

10. Arvold, N. D.; Ngo-Giang-Huong, N.; McIntosh, K.; Suraseranivong, V.; Warachit, B.; Piyaworawong, S.; Changchit, T.; Lallemant, M.; Jourdain, G., Maternal HIV-1 DNA load and mother-to-child transmission. *AIDS Patient Care STDS* **2007,** *21* (9), 638-43.

11. U.S. Centers for Disease Control and Prevention. CDC 2019-Novel Coronavirus (2019-nCoV) Real-Time RT-PCR Diagnostic Panel (Instructions for Use) 2020. https://www.fda.gov/media/134922/download.

© Copyright 2021 | N Panpradist

12. Drain, P. K.; Dorward, J.; Bender, A.; Lillis, L.; Marinucci, F.; Sacks, J.; Bershteyn, A.; Boyle, D. S.; Posner, J. D.; Garrett, N., Point-of-Care HIV Viral Load Testing: an Essential Tool for a Sustainable Global HIV/AIDS Response. *Clin Microbiol Rev* **2019,** *32* (3).
13. U.S. National Institute of Health GLOSSARY of HIV/AIDS-Related Terms. https://clinicalinfo.hiv.gov/sites/default/files/glossary/Glossary-English_HIVinfo.pdf.
14. World Health Organization, *Consolidated guidelines on the use of antiretroviral drugs for treating and preventing HIV infection: recommendations for a public health approach*. 2nd ed ed.; World Health Organization: Geneva, 2016.
15. U.S. Centers for Disease Control and Prevention CDC 2019-Novel Coronavirus (2019-nCoV) Real-Time RT-PCR Diagnostic Panel. https://www.fda.gov/media/134922/download (accessed 9th August).
16. Boom, R.; Sol, C. J.; Salimans, M. M.; Jansen, C. L.; Wertheim-van Dillen, P. M.; van der Noordaa, J., Rapid and simple method for purification of nucleic acids. *Journal of Clinical Microbiology* **1990,** *28* (3), 495-503.
17. Padhye, V. V.; York, C.; Burkiewicz, A. Nucleic acid purification using silica gel and glass particles. https://patents.google.com/patent/US5808041A/en.
18. Bernhardt, H. S.; Tate, W. P., Primordial soup or vinaigrette: did the RNA world evolve at acidic pH? *Biol Direct* **2012,** *7*, 4.
19. Escobar, M. D.; Hunt, J. L., A cost-effective RNA extraction technique from animal cells and tissue using silica columns. *Journal of biological methods* **2017,** *4* (2), e72.

© Copyright 2021 | N Panpradist

20. Mommaerts, K.; Sanchez, I.; Betsou, F.; Mathieson, W., Replacing β-mercaptoethanol in RNA extractions. *Analytical Biochemistry* **2015,** *479*, 51-53.

21. Oreskovic, A.; Brault, N. D.; Panpradist, N.; Lai, J. J.; Lutz, B. R., Analytical Comparison of Methods for Extraction of Short Cell-Free DNA from Urine. *The Journal of Molecular Diagnostics* **2019,** *21* (6), 1067-1078.

22. Panpradist, N.; Beck, I. A.; Vrana, J.; Higa, N.; McIntyre, D.; Ruth, P. S.; So, I.; Kline, E. C.; Kanthula, R.; Wong-On-Wing, A.; Lim, J.; Ko, D.; Milne, R.; Rossouw, T.; Feucht, U. D.; Chung, M.; Jourdain, G.; Ngo-Giang-Huong, N.; Laomanit, L.; Soria, J.; Lai, J.; Klavins, E. D.; Frenkel, L. M.; Lutz, B. R., OLA-Simple: A software-guided HIV-1 drug resistance test for low-resource laboratories. *EBioMedicine* **2019,** *50*, 34-44.

23. Colagrossi, L.; Antonello, M.; Renica, S.; Merli, M.; Matarazzo, E.; Travi, G.; Vecchi, M.; Colombo, J.; Muscatello, A.; Grasselli, G.; Molteni, S. N.; Scaravilli, V.; Cattaneo, E.; Fanti, D.; Vismara, C.; Bandera, A.; Gori, A.; Puoti, M.; Cento, V.; Alteri, C.; Perno, C. F., SARS-CoV-2 RNA in plasma samples of COVID-19 affected individuals: a cross-sectional proof-of-concept study. *BMC Infectious Diseases* **2021,** *21* (1), 184.

24. World Health Organization WHO in-house assay. https://www.who.int/docs/default-source/coronaviruse/whoinhouseassays.pdf.

25. Pau, C. P.; Wells, S. K.; Rudolph, D. L.; Owen, S. M.; Granade, T. C., A rapid real-time PCR assay for the detection of HIV-1 proviral DNA using double-stranded primer. *J Virol Methods* **2010,** *164* (1-2), 55-62.

© Copyright 2021 | N Panpradist

26. U.S. Centers for Disease Control and Prevention. CDC 2019-Novel Coronavirus (2019-nCoV) Real-Time RT-PCR Diagnostic Panel For Emergency Use Only 2020. https://www.fda.gov/media/134922/download (accessed December 1st, 2020).

27. Oscorbin, I. P.; Shevelev, G. Y.; Pronyaeva, K. A.; Stepanov, A. A.; Shamovskaya, D. V.; Mishukova, O. V.; Pyshnyi, D. V.; Filipenko, M. L., Detection of SARS-CoV-2 RNA by a Multiplex Reverse-Transcription Loop-Mediated Isothermal Amplification Coupled with Melting Curves Analysis. *Int J Mol Sci* **2021,** *22* (11).

28. Mikel, P.; Vasickova, P.; Kralik, P., Methods for Preparation of MS2 Phage-Like Particles and Their Utilization as Process Control Viruses in RT-PCR and qRT-PCR Detection of RNA Viruses From Food Matrices and Clinical Specimens. *Food Environ Virol* **2015,** *7* (2), 96-111.

29. Byrnes, S. A.; Gallagher, R.; Steadman, A.; Bennett, C.; Rivera, R.; Ortega, C.; Motley, S. T.; Jain, P.; Weigl, B. H.; Connelly, J. T., Multiplexed and Extraction-Free Amplification for Simplified SARS-CoV-2 RT-PCR Tests. *Analytical chemistry* **2021,** *93* (9), 4160-4165.

30. Oreskovic, A.; Panpradist, N.; Marangu, D.; Ngwane, M. W.; Magcaba, Z. P.; Ngcobo, S.; Ngcobo, Z.; Horne, D. J.; Wilson, D. P. K.; Shapiro, A. E.; Drain, P. K.; Lutz, B. R., Diagnosing pulmonary tuberculosis using sequence-specific purification of urine cell-free DNA. *J Clin Microbiol* **2021**.

31. Zhao, Z.; Cui, H.; Song, W.; Ru, X.; Zhou, W.; Yu, X., A simple magnetic nanoparticles-based viral RNA extraction method for efficient detection of SARS-CoV-2. *bioRxiv* **2020**, 2020.02.22.961268.

© Copyright 2021 | N Panpradist

32. Iwase, S. C.; Miyazato, P.; Katsuya, H.; Islam, S.; Yang, B. T. J.; Ito, J.; Matsuo, M.; Takeuchi, H.; Ishida, T.; Matsuda, K.; Maeda, K.; Satou, Y., HIV-1 DNA-capture-seq is a useful tool for the comprehensive characterization of HIV-1 provirus. *Scientific Reports* **2019,** *9* (1), 12326.

33. Giacona, M. B.; Ruben, G. C.; Iczkowski, K. A.; Roos, T. B.; Porter, D. M.; Sorenson, G. D., Cell-free DNA in human blood plasma: length measurements in patients with pancreatic cancer and healthy controls. *Pancreas* **1998,** *17* (1), 89-97.

34. Panpradist, N.; Toley, B. J.; Zhang, X.; Byrnes, S.; Buser, J. R.; Englund, J. A.; Lutz, B. R., Swab sample transfer for point-of-care diagnostics: characterization of swab types and manual agitation methods. *PLoS One* **2014,** *9* (9), e105786.

35. Oreskovic, A.; Brault, N. D.; Panpradist, N.; Lai, J. J.; Lutz, B. R., Analytical Comparison of Methods for Extraction of Short Cell-Free DNA from Urine. *J Mol Diagn* **2019,** *21* (6), 1067-1078.

36. Oreskovic, A. K.; Brault, N. D.; Lutz, B. R., Analytical comparison of methods for extraction of short cell-free DNA from urine. *Submitted for peer review*.

37. Yao, Z.; Zanini, F.; Kumar, S.; Karim, M.; Saul, S.; Bhalla, N.; Panpradist, N.; Muniz, A.; Narayanan, A.; Quake, S. R.; Einav, S., The transcriptional landscape of Venezuelan equine encephalitis virus (TC-83) infection. *PLoS neglected tropical diseases* **2021,** *15* (3), e0009306.

38. Miyazato, P.; Katsuya, H.; Fukuda, A.; Uchiyama, Y.; Matsuo, M.; Tokunaga, M.; Hino, S.; Nakao, M.; Satou, Y., Application of targeted

© Copyright 2021 | N Panpradist

enrichment to next-generation sequencing of retroviruses integrated into the host human genome. *Scientific reports* **2016,** *6*, 28324.

39. Zanini, F.; Robinson, M. L.; Croote, D.; Sahoo, M. K.; Sanz, A. M.; Ortiz-Lasso, E.; Albornoz, L. L.; Rosso, F.; Montoya, J. G.; Goo, L.; Pinsky, B. A.; Quake, S. R.; Einav, S., Virus-inclusive single-cell RNA sequencing reveals the molecular signature of progression to severe dengue. *Proceedings of the National Academy of Sciences* **2018,** *115* (52), E12363.

© Copyright 2021 | N Panpradist

2.5 SUPPLEMENTARY INFORMATION FOR CHAPTER 2

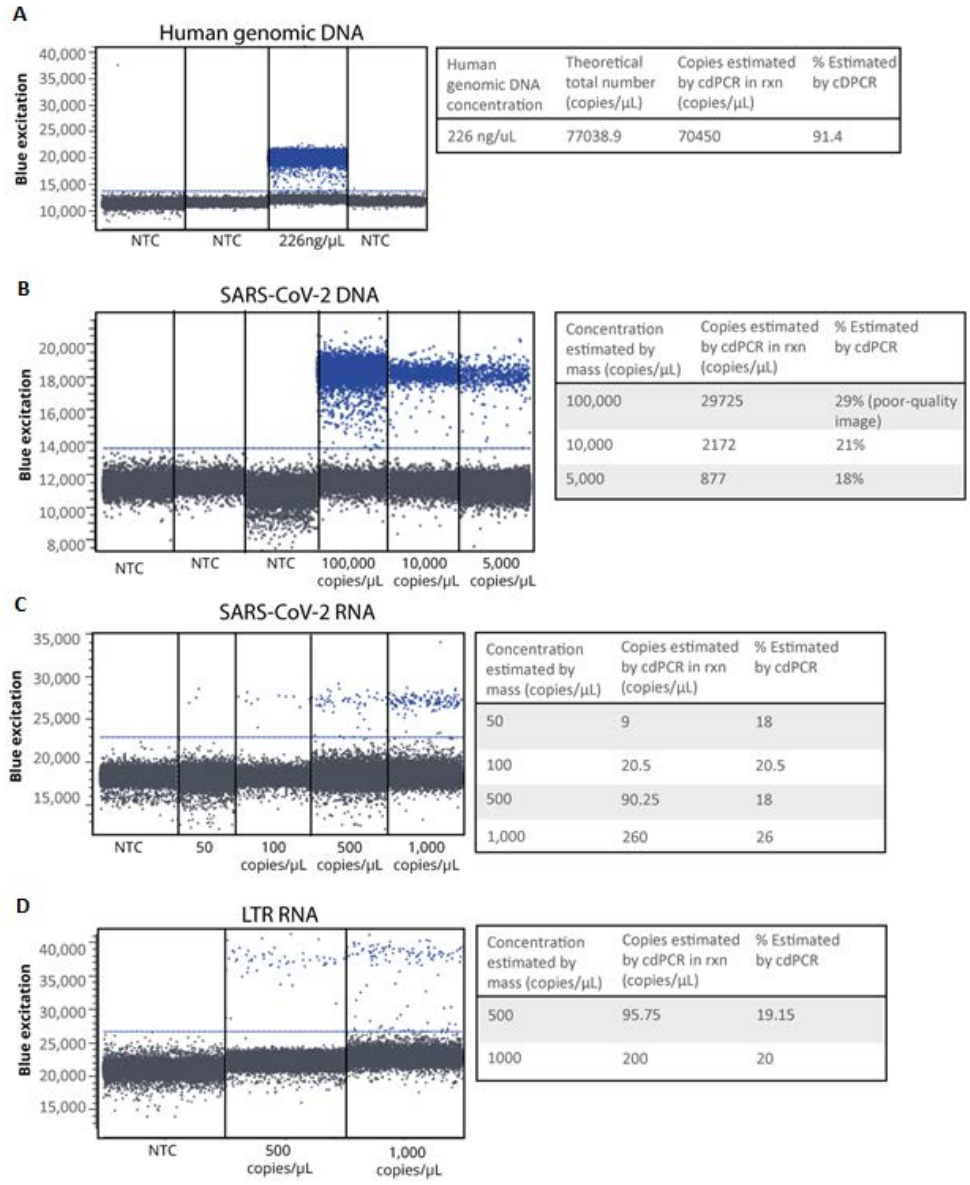

Human genomic DNA concentration	Theoretical total number (copies/µL)	Copies estimated by cdPCR in rxn (copies/µL)	% Estimated by cDPCR
226 ng/uL	77038.9	70450	91.4

Concentration estimated by mass (copies/µL)	Copies estimated by cdPCR in rxn (copies/µL)	% Estimated by cdPCR
100,000	29725	29% (poor-quality image)
10,000	2172	21%
5,000	877	18%

Concentration estimated by mass (copies/µL)	Copies estimated by cdPCR in rxn (copies/µL)	% Estimated by cdPCR
50	9	18
100	20.5	20.5
500	90.25	18
1,000	260	26

Concentration estimated by mass (copies/µL)	Copies estimated by cdPCR in rxn (copies/µL)	% Estimated by cdPCR
500	95.75	19.15
1000	200	20

Figure S2.17 | Characterization of in vitro transcribed RNA standards using Crystal digital PCR (cdPCR).

(**A**) Quantification of human genomic DNA with a known concentration (226ng/µl, Promega) shows accurate estimation of concentration by cdPCR (**B**) Estimation of HIV RNA concentration by cdPCR shows ~20% of concentration measured by mass using Nanodrop instrument (ThermoFisher Scientific, US) (**C**) The measured concentrations based on the total mass of in vitro transcribed HIV RNA and COVID RNA was verified using cdPCR. We found that estimation of COVID RNA concentrations by cdPCR using

© Copyright 2021 | N Panpradist

N2 assay shows ~20% of concentration, and thus, we have corrected the concentration of the RNA stocks based on this cdPCR. The Naica Geode (cdPCR) was programmed to perform PCR thermal cycling program: 95 °C for 10minutes, followed by 55 cycles of 95 °C for 30 seconds and 60 °C for 30 seconds. Image acquisition was performed using the Naica Prism3 reader in the blue channel (excitation range 415-480 nm and emission range 495-520 nm) at an exposure time of 100 ms. Droplet counts were enabled by the detection of reference dye FITC in the blue channel and were performed by the Crystal Reader software. Extracted fluorescence value for each droplet was analyzed by Crystal Miner software. The blue threshold line was adjusted manually above the negative droplets of the NTC sample in the Crystal Miner software.

© Copyright 2021 | N Panpradist

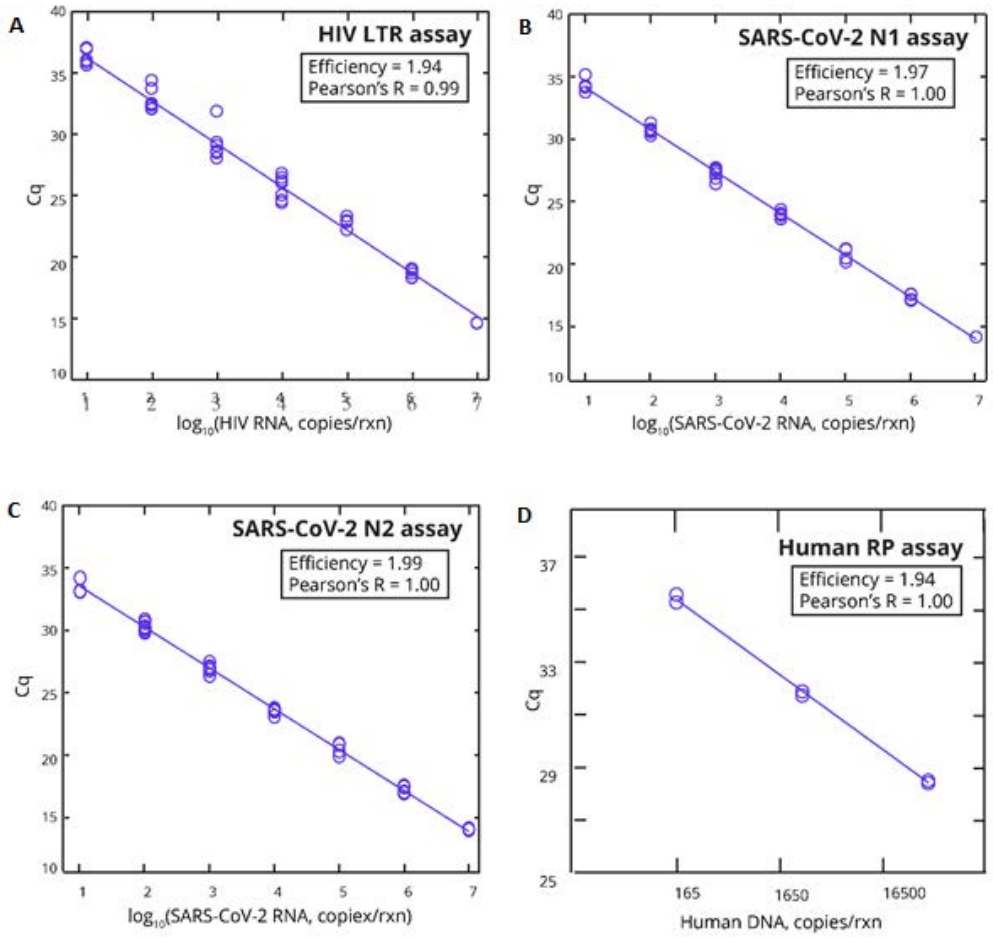

Figure S2.18 | Standard curves of RT-qPCR assays.

(**A**) HIV LTR assay (**B**) SARS-CoV-2 N1 assay (**C**) SARS-CoV-2 N2 (D) human genomic DNA For (**A**), (**B**), and (**C**), single-use stock of the standard RNA templates quantified by cdPCR (**Figure S2.17**) were diluted in nuclease-free water down to 2 - 2,000,000 copies/uL. 5µL of each RNA standard or water was added to 15µL of the qPCR master mix and subjected to RT-qPCR cycling as described in the methods section. Two replicate reactions were performed on each plate, and data were pooled from four experiments on different days, accounting for a total of eight replicates. For human controls (**D**), two replicates/concentrations were run in RT-qPCR. The concentrations were based on the reported values from the manufacturer (Promega). Note that to allow comparison across plates, we normalized the data of cycles 5-10 and used a fixed threshold of 200 RFU to determine the Cq values. All replicates were

© Copyright 2021 | N Panpradist

plotted along with the fitted linear regression. CorrespPearson'sarson's R values were reported along with the RT-PCR efficiency.

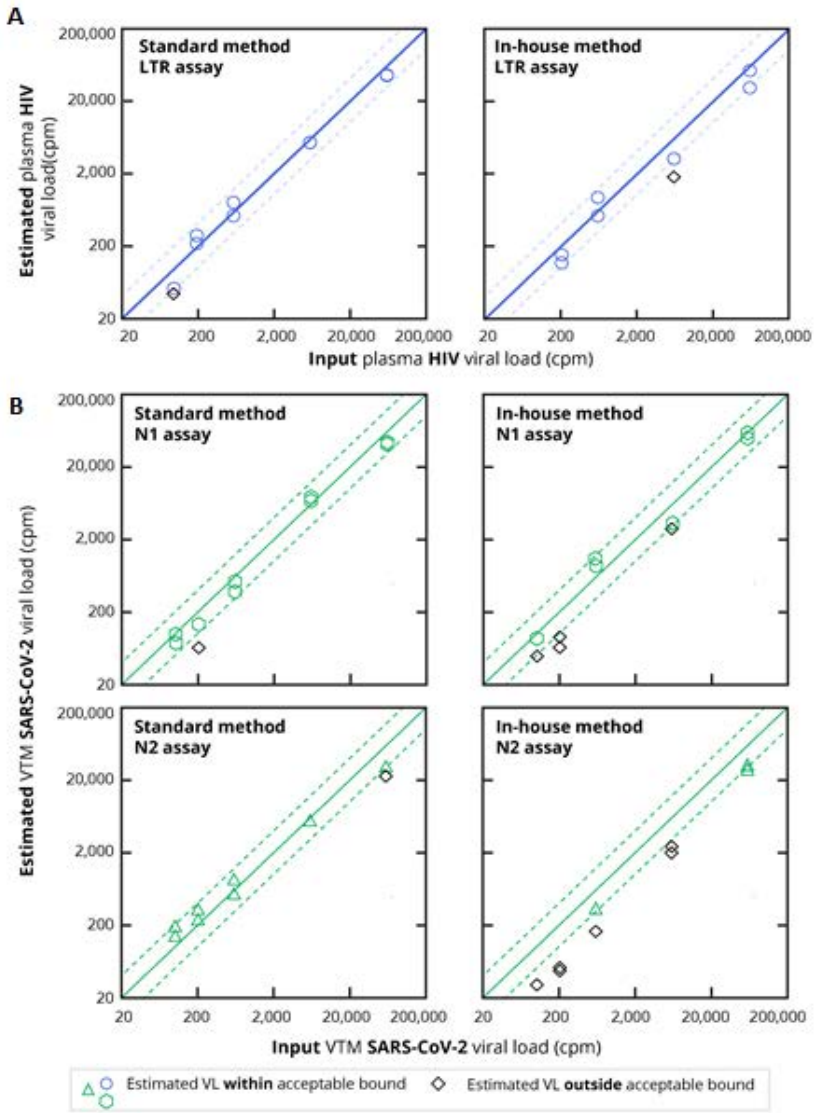

Figure S2.19 | Correlation plots of measured VL from co-extraction of contrived plasma/NS. Measured VL of (**A**) HIV and (**B**) SARS-CoV-2 targets in contrived plasma samples (lysed plasma and spiked with synthetic HIV RNA and SARS-CoV-2 RNA at 0, 100, 200, 600, 6000, or 60000 copies/mL). All individual data are plotted. Diagonal lines represent 100% recovery, with the dash lines indicating precise measurement bound of ±0.3 log10 (VL input, copies/mL).

© Copyright 2021 | N Panpradist

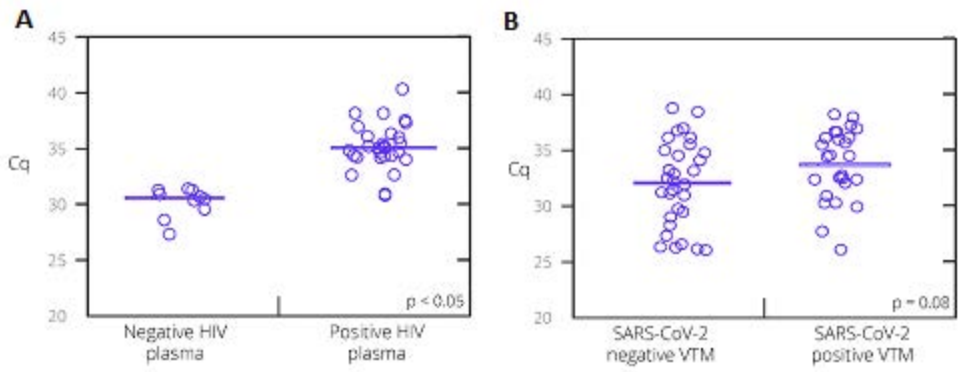

Figure S2.20 | Levels of RP gene of clinical specimens.

(**A**) Plasma. HIV-seronegative plasma was purchased from Innovative Research, Inc, MI, USA. HIV-seropositive plasma was collected from treatment-naive individuals in Mexico City. (**B**) NS both SARS-CoV-2 positives and negatives were collected from individuals in the US with respiratory symptoms in US. All specimens were stored at –80 °C until the test. Averages of the positive and negative groups were assessed for statistical differenceStudent'sudent's t-test (two-tailed). The image was published: DOI: https://doi.org/10.1101/2021.08.18.21256786.

© Copyright 2021 | N Panpradist

Table S2.2 | List of items used in non-proprietary RNA extraction kit.

The table was published at DOI: https://doi.org/10.1101/2021.08.18.21256786.

Consumables/reagents	**Source**	**Unit**	**Cost**
GuSCN	VWR, 97061-524	500g	$252.96
MES buffer	Sigma, 76039	1M, 0.5L	$116
Tris-HCl buffer	Fisher, 15568025	1M, 1L	$95.25
DTT	Promega, C4H10O2S2	5g	$139.10
Collection tubes	Qiagen, 19201	1000 tubes	$166
Spin column tubes	Epoch Life Science, 1920	250 tubes	$100
tRNA	Fisher, AM7119	5mg	$95.25
Buffer (50mL stock)			
Lysis buffer	4M GuSCN, 10mM MES	50mL	$13.66
Wash buffer 1	1M GuSCN, 10mM Tris-HCl	50mL	$3.18
Wash buffer 2	10mM Tris-HCl	50mL	$0.05
Cost/kit (140µL sample)			
Epoch column			$0.40
Collection tubes			$0.51 (3 x $0.17)
Lysis buffer			$0.15
tRNA			$0.64
DTT			$0.10
Wash buffer 1			$0.05
Wash buffer 2			negligible
Total cost			**$1.85**

© Copyright 2021 | N Panpradist

Table S2.3 | Primers and probe sequences.

nCoV-N control: severe acute respiratory syndrome coronavirus 2 isolate Wuhan-Hu-1, complete genome (GenBank: NC_045512.2). The table was published at DOI: https://doi.org/10.1101/2021.08.18.21256786.

Name	Sequence (’’ to 3’)	Base positions mapped to reference sequences	Final concentration in RT-qPCR mixture
2019-nCoV_N1-F (N1 forward primer)	GAC CCC AAA ATC AGC GAA AT	28287 - 28306 nCoV-2	500 nM
2019-nCoV _N1-R (N1 reverse primer)	TCT GGT TAC TGC CAG TTG AAT CTG	28335 - 28358 nCoV-2	500 nM
2019-nCoV_N1-P (N1 probe)	FAM-ACC CCG CAT /ZEN/ TAC GTT TGG TGG ACC-3IABkFQ	28309 - 28332 nCoV-2	125 nM
2019-nCoV_N2-F (N2 forward primer)	TTA CAA ACA TTG GCC GCA AA	29164 - 29183 nCoV-2	500 nM
2019-nCoV_N2-R (N2 Reverse primer)	GCG CGA CAT TCC GAA GAA	29213 - 29230 nCoV-2	500 nM
2019-nCoV_N2-P (N2 probe)	FAM-ACA ATT TGC /ZEN/ CCC CAG CGC TTC AG-3IABkF	29188 - 29210 nCoV-2	125 nM
LTR Forward primer	GCCTCAATAAAGCTTGCCTTGA	522 - 543 HXB2	250 nM
LTR Reverse primer	GGCGCCACTGCTAGAGATTTT	622- 642 HXB2	250 nM
LTR Probe	/56-FAM/CTGGTAACTAGAGATCCCT/3MGBEC/	581- 599 HXB2	250 nM
RP-F (RP forward primer)	AGA TTT GGA CCT GCG AGC G	28 - 46 Human RP gene (NM_006413.5)	500 nM
RP-R (RP reverse primer)	GAG CGG CTG TCT CCA CAA GT	73 - 92 Human RP gene	500 nM
RP-P (RP probe)	FAM-TTC TGA CCT /ZEN/ GAA GGC TCT GCG CG-3IABkFQ	49 - 71 Human RP gene	125 nM

© Copyright 2021 | N Panpradist

Table S2.4 | Probe sequences for HIV RNA capture.

Below is the mapping of sequences relative to HXB2 coordinates.

Italic text is an engineered barcode sequence. SpC3 is three units of carbon spacers to prevent extension.

Name	Sequence '5' ' 3')
5' barcode	*T TTT ACT ACT TTT CTT ACA ATA GAA CCT C'C CA*
5' displacing strand	*GTG CGA CCT TTT ACT ACT TTT CTT ACA ATA GAA CCT CAC CA*/3SpC3/
Bead capture:	/52-Bio/AAAAAAAAAAAAAAAAAAAA AAAAAAAAAAAAAAAAAAAA*TGG TGA GGT TCT ATT GTA AGA AAA GTA GTA AAA GGT CGC AC* /3SpC3/
2124_2244 (reversed)	*T TTT ACT ACT TTT CTT ACA ATA GAA CCT CAC CA* AGGATACAGT TCCTTGTCTA TCGGCTCCTG CTTCTGAGGG GGAGTTGTTG TCTCTACCCC AGACCTGAAG CTCTCTTCTG GTGGGGCTGT TGGCTCTGGT CTGCTCTGAA GAAAATTCCC /3SpC3/
2301_2421 (reversed)	*T TTT ACT ACT TTT CTT ACA ATA GAA CCT CAC CA* TTACTTTGAT AAAACCTCCA ATTCCCCCTA TCATTTTTGG TTTCCATCTT CCTGGCAAACTCATTTCTTC TAATACTGTA TCATCTGCTC CTGTATCTAA TAGAGCTTCC TTTAGTTGCC /3SpC3/
2478_2598 (reversed)	*T TTT ACT ACT TTT CTT ACA ATA GAA CCT CAC CA* CCATTCCTGG CTTTAATTTT ACTGGTACAG TCTCAATAGG GCTAATGGGA AAATTTAAAGTGCAACCAAT CTGAGTCAAC AGATTTCTTC CAATTATGTT GACAGGTGTA GGTCCTACTA /3SpC3/
2950 _ 3070 (reversed)	*T TTT ACT ACT TTT CTT ACA ATA GAA CCT CAC CA* TGTTTTCTAA AAGGCTCTAA GATTTTTGTC ATGCTACTTT GGAATATTGC TGGTGATCCTTTCCATCCCT GTGGAAGCAC ATTGTACTGA TATCTAATCC CTGGTGTCTC ATTGTTTATA /3SpC3/
3245_3365 (reversed)	*T TTT ACT ACT TTT CTT ACA ATA GAA CCT CAC CA* TGGGTAAATC TGACTTGCCC AATTCAATTT CCCCACTAAC TTCTGTATGT CATTGACAGTCCAGCTGTCT TTTTCTGGCA GCACTATAGG CTGTACTGTC CATTTATCAG GATGGAGTTC /3SpC3/

© Copyright 2021 | N Panpradist

CHAPTER 3:
PAPER-BASED DETECTION FOR HIVDR OLA

SIGNIFICANCE. Based on the previous implementation experience of our collaborator Dr. Frenkel who pioneered and validated the traditional HIVDR OLA in LMICs (*i.e.,* Kenya, Peru, Thailand, and China), the complex detection workflow is the key obstacle for OLA adoption in low-resource settings. As the first step toward simplifying HIVDR OLA (Frenkel lab 2002), we first focused on the most complex part of the workflow, the detection step.

DELIVERABLES. Several generations of paper-based detection (akin to a pregnancy test) for OLA were developed. They are simple-to-use and provide visual readout (e.g., yes/no drug-resistant HIV), eliminating the need for equipment used in the original plate-based HIVDR OLA protocol (*e.g.,* a plate washer and a plate reader).

PREVIOUS PUBLICATIONS

Some texts and images used in this chapter were published as:

1) N Panpradist *et al.* 2016 (DOI: https://DOI.org/10.1371/journal.pone.0145962)
2) N Panpradist *et al.* 2019 (DOI: https://DOI.org/10.1016/j.ebiom.2019.11.002)
3) N Panpradist *et al.* 2020 (DOI: 10.1097/QAD.0000000000002524)
4) J Vrana *et al.* 2021 (DOI: https://DOI.org/10.1101/2021.05.06.21256654)

© Copyright 2021 | N Panpradist

3.1 DETECTION STEP IN THE ORIGINAL HIVDR OLA (2002)

Following the ligation step, the ligated probes are detected via surface **c**apture, **d**enaturation of oligonucleotide from DNA, and plate-based enzyme-linked immunoassay (**ELISA**) **d**etection (**Figure 3.1A,** short for **CDD**). Ligation and detection are performed after PCR amplification and can target either HIV DNA or viral RNA. Probe sets specific for the wild-type (**WT**) and the mutant (**MUT**) genotypes estimate their relative proportion.

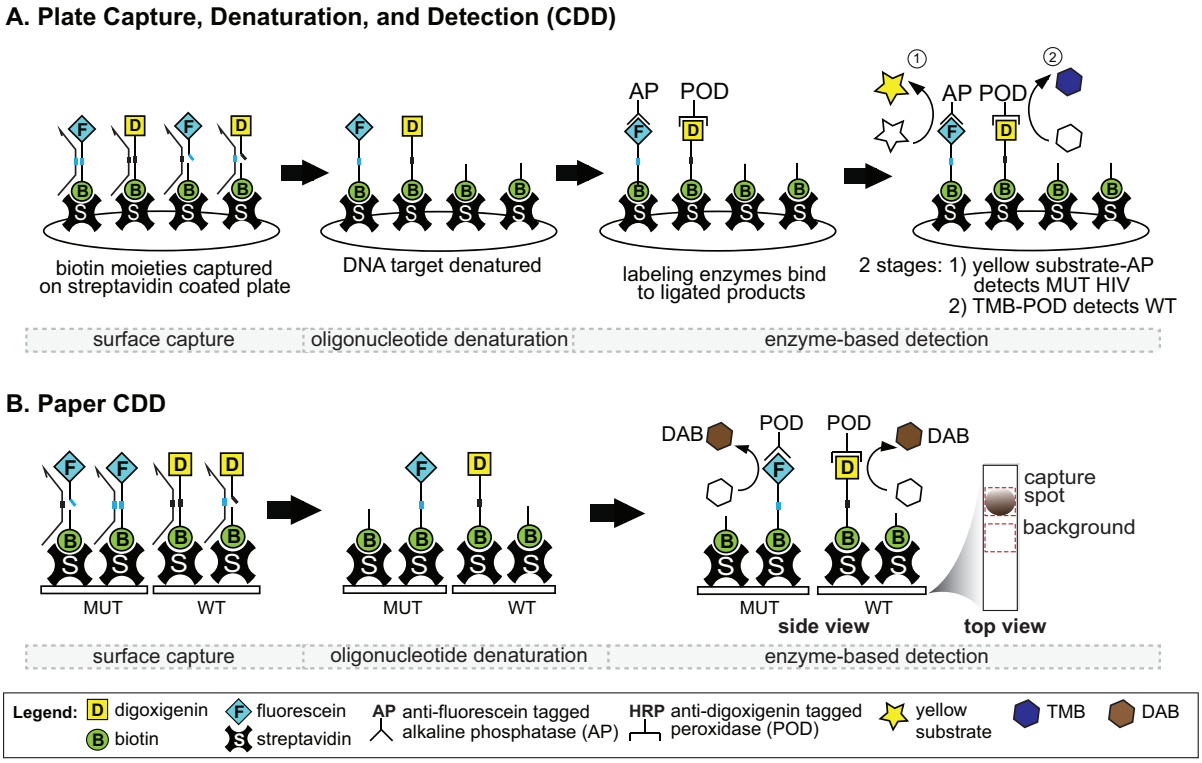

Figure 3.1 | Comparison of the plate and 1st-generation paper OLA detection.

(A) The plate format includes steps for surface capture, oligonucleotide denaturation, and enzyme-based detection (CDD). Products from ligation (both ligated and non-ligated products) are captured on a streptavidin-coated plate. Non-ligated probes are released during oligonucleotide denaturing. Ligated probes are then detected in sequential enzyme-based immunoassays (labeling by two detection antibodies, alkaline phosphatase yellow substrate development, optical density reading at 405nm, wash

© Copyright 2021 | N Panpradist

steps, tetramethylbenzidine (TMB) development, stop solution, and optical density reading at 450nm. (**B**) Paper format CDD. Products from ligation (both ligated and non-ligated products) were captured on strips by immobilized streptavidin. Non-ligated probes were released during oligonucleotide denaturing, and ligated probes were labeled by horseradish peroxidase (POD) conjugated to antibodies targeting end labels on the mutant (MUT) or wild-type (WT) probes. POD converted 3,3 diazoamino benzidine substrate (DAB) into brown precipitates. The signal can be observed by eye or a camera or flatbed scanner and analysis software. Reported signals represent capture spot intensity minus a background region from the strip. The image was obtained from N Panpradist et al. 2016 (**https://DOI.org/10.1371/journal.pone.0145962**)

3.2 GENERATION 1: DIPSTICK PAPER-BASED DETECTION

Lateral flow detection technologies have been used to replace ELISAs, including rapid HIV antibody and antigen detection. Here we reformatted a multistep plate-based ELISA to a paper-based detection with sequential delivery. This modification drastically speeds up the detection time from the original 2.5 hours to 45 minutes and eliminates the need for a plate reader and plate washer. Last, 1st-generation dipstick paper-based detection was then used to blindly analyze the 26 blood DNA specimens compared to the plate-based OLA detection.

MATERIALS AND METHODS

Study design and specimens. Blood specimens from HIV-infected Kenyans enrolled in a prospective observational study of transmitted HIVDR were collected as approved by Human Subjects Protection Committees at the UW and Kenyatta National Hospital. Written informed consent to perform viral testing was signed by all participants; this was approved by the UW and Kenyatta

© Copyright 2021 | N Panpradist

National Hospital. The data were analyzed anonymously. Specimens collected during virologic failure of first-line ART were chosen to include mutations at four codons (K103N, Y181C, G190A, and M184V) spanning a wide range of frequencies in each subjects' HIV population. The 1st-generation dipstick was compared to ELISA (i.e., plate-based detection) in original OLA by testing the same set of PCR amplicons from participant specimens and plasmid standards containing the mutations of interest. The Probe hybridization and ligation step were performed separately and at different times for the plate and paper detection using the same protocol and reagents. Laboratory personnel was "blinded" to the mutational content of each specimen during testing of the paper detection.

Extraction and amplification of HIV pol on participant specimens. To extract DNA, the first participant's PBMCs were isolated from whole blood by gradient centrifugation in Histopaque (Sigma, 1077, St. Louis, MO). 2 µg of genomic DNA was then extracted from frozen c.a. 3x106 PBMC pellets using a DNA Archive Pure DNA Purification System (5 PRIME, Inc., Gaithersburg, MD) similar to previous OLA work (Beck 2014). Nested PCR amplified a 1009 bp region of the pol gene. Two µg of each DNA were added to a 50µl reaction mixture containing 400nM of forward (CCT ACA CCT GTC AAC ATA ATT GG) and reverse primers (AAC TTC TGT ATA TCA TTG ACA GTC CA), 200µM dNTPs, 3mM MgCl2, and 2.5U of MyTaqTM DNA polymerase (Bioline USA, Inc., Taunton, MA). Cycling conditions included a denaturation cycle of 5 minutes at 94°C and 35 cycles of 30 seconds at 94°C, 30 seconds at 55°C, and 1 minute at 72°C, followed by an extension step of 7 minutes at 72°C. Nested PCR was

© Copyright 2021 | N Panpradist

performed by adding 2µl of the first-round amplicon to a 50µl reaction mixture containing 400nM of inner forward primer (CAA ATC ACT CTT TGG CAR CGA CC) and inner reverse primer (CAY TTG TCA GGA TGG AGT TCA TA), 200µM dNTPs, 3mM MgCl2, and 2.5U of MyTaq DNA polymerase. Second round cycling conditions were the same as the first round, except the extension time was reduced to 30 seconds. Second-round PCR products were visualized by agarose gel electrophoresis.

Plasmid DNA standards. Plasmid DNA containing HIV *pol* sequences with mutations at codons of interest served as standards. Plasmid standards for each of the four codons tested were prepared by mixing mutant (**MUT**) plasmid with wild-type (**WT**) plasmid (concentrations of 0%, 5%, and 50% MUT). Plasmid standards (0.1ng) were amplified in a 50µl reaction mixture containing forward and reverse M13 primers using the same reagents and conditions as the second round PCR used for participants. PCR products were visualized by agarose gel electrophoresis.

Ligation. Ligation reactions were carried out in separate wells for each codon to avoid competition between overlapping probes. DNA amplicons were diluted 1:4 in nuclease-free water (Promega, P1193, Madison, WI). Two µl of diluted DNA were added to 20µl reaction mixture containing: 0.67U of thermostable Ampligase ligase (Epicentre Technology, A3210K, Madison, WI), 12.5mM KCl, 1mM NAD (Sigma, 7004, St. Louis, MO), 1X ligase buffer (20mM Tris pH 8.0, 10mM $MgCl_2$, 1mM DDT), 0.1075% Triton-X 100, and the oligonucleotide probes (**Table S3.2**) specific for each mutation tested (Integrated DNA Technology DNA oligo HPLC purified, Coralville, IA). The mixture was subjected to

© Copyright 2021 | N Panpradist

10 cycles of 94°C for 30 seconds, followed by 37°C for 4 minutes, followed by inactivation of the ligase enzyme by addition of 10µl of 100mM EDTA/0.1% Triton X-100.

Plate-based ELISA. The ligation step (32µL) product was transferred to a streptavidin-coated plate (Roche/BM 1734776, Indianapolis, IN) and incubated at room temperature in the dark without being shaken for a minimum of one hour. The plate was then washed twice with 1X denaturing buffer (0.01N sodium hydroxide, 0.05% Tween-20) followed by two washes with 1X neutralization buffer (100mM Tris pH 7.5, 150mM sodium chloride, 0.05% Tween-20). Fifty µl of an antibody mixture (37.5mU anti-fluorescein-alkaline phosphatase (**AP**) Fab fragments (Roche, 11426338910, Indianapolis, IN) and 7.5mU anti-digoxigenin-peroxidase (**POD**) Fab fragments (Roche, 11207733910, Indianapolis, IN) in 1X Phosphate Buffered Saline (1X **PBS**) with 0.5% Bovine Serum Albumin (Sigma, A6793, St. Louis, MO) was added to each well and incubated for 30 minutes at room temperature in the dark. The plate was then washed six times with 1X neutralization buffer. Subsequently, 100µl of alkaline phosphate yellow liquid substrate (Sigma, P7998, St. Louis, MO) were added and incubated until the yellow color developed fully (20 to 35 minutes, depending on the mutation tested). The optical density (**OD**) was read at 405nm (SpectraMax 190, Molecular Devices, Sunnyvale, CA) to measure the MUT signal level. The plate was then washed six times with 300µl of 1X neutralization buffer and 50µl of tetramethylbenzidine (**TMB**). One Solution (Promega, G7431, Madison, WI) was added to each well. After 3-5 minutes at room

© Copyright 2021 | N Panpradist

temperature, 50µl of 0.3M H_2SO_4 was added to each well to stop the reaction. The OD was read at 450nm to measure the WT signal level.

1ST-generation dipstick paper-based detection. A Mylar-backed nitrocellulose membrane (EMD Millipore, High-Flow Plus 13504XSS, Billerica, MA) was cut into 3mm x 25mm strips using a CO2 laser cutter (Universal Laser Systems, Scottsdale, AZ) at 5% speed, 5% power, and 1000 pulses per inch (S2A Fig.). The strips were hand-spotted with 1µl of 1mg/ml streptavidin (Sigma, S-0677, St. Louis, MO) in 1X PBS (Corning, 21-040-CV, Manassas, VA), incubated 2 hours at 37°C (Thermo Forma Water Jacketed CO2 incubator), and kept dry in a desiccator (Bel-Art 42073100, Wayne, NJ) at 20% humidity, 22–25°C. A cellulose absorbent pad (EMD Millipore, CF22300, Billerica, MA) was attached to the nitrocellulose strips via an adhesive plastic backing (10 mil Melinex with adhesive on one side, Fraylock, San Carlos, CA). The paper dipsticks (**Figure 3.2**) can be assembled as two-legged strips to either WT or MUT in one sample or multiple samples (set of 8 samples on two sets of strips for WT and MUT detection).

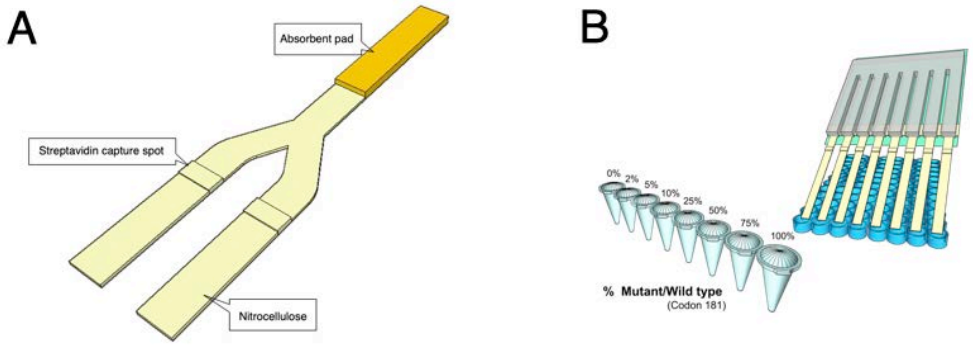

Figure 3.2 | Different assembly for the 1st-generation paper dipstick.

© Copyright 2021 | N Panpradist

(**A**) Two-legged paper dipstick for one sample detection, either WT or MUT. (**B**) Eight-legged paper dipstick to detect WT or MUT signal from 8 samples. To perform the detection, the dipsticks were moved across the wells containing different reagents.

Reagents as well as ligation product species (

Figure 3.3) were wicked through the series of reagents to allow for detection: **(1)** 25µL blocking agent 1% BSA/PBS **(2)** 27.5µl ligated products, **(3)** 25µl 10X denaturing solution (0.1N sodium hydroxide with 0.05% Tween-20), **(4)** 25µl 1X neutralizing buffer, **(5)** 25µl of labeling antibodies (3.75U of anti-digoxigenin-POD (Roche, 11207733910, Indianapolis, IN) for WT detection or anti-fluorescein-POD (Roche, 11426346910, Indianapolis, IN) for MUT detection), **(6)** 25µl of 1X PBS with 0.05% Tween-20 (**PBST**), **(7)** 40µl of signal amplification reagent (250µg/ml 3,3'-diaminobenzidine (**DAB**), KPL, 710008, Gaithersburg, MD) with 250µg/ml w/v sodium percarbonate (Sigma, 371432, St. Louis, MO) in 1X PBST, and **(8)** 25µl of 1X PBST. Mechanisms of how WT and MUT signals were detected are shown in **Figure 3.4**. Wet strips were then scanned using a flatbed scanner (Epson V700, Long Beach, CA) and SilverFast software (LaserSoft Imaging, Sarasota, FL). The humidity and temperature during the experiments were not controlled but were measured (45-50% humidity and 22-25°C). The OD (range: 0-4 a.u.) reported for each specimen was calculated from the raw OD of the specimen minus the average OD of the blank wells (enzyme substrates only). The OD data of all plate experiments were summarized in **Table S3.3**. The signal from the paper experiments was summarized in **Table S3.4**.

© Copyright 2021 | N Panpradist

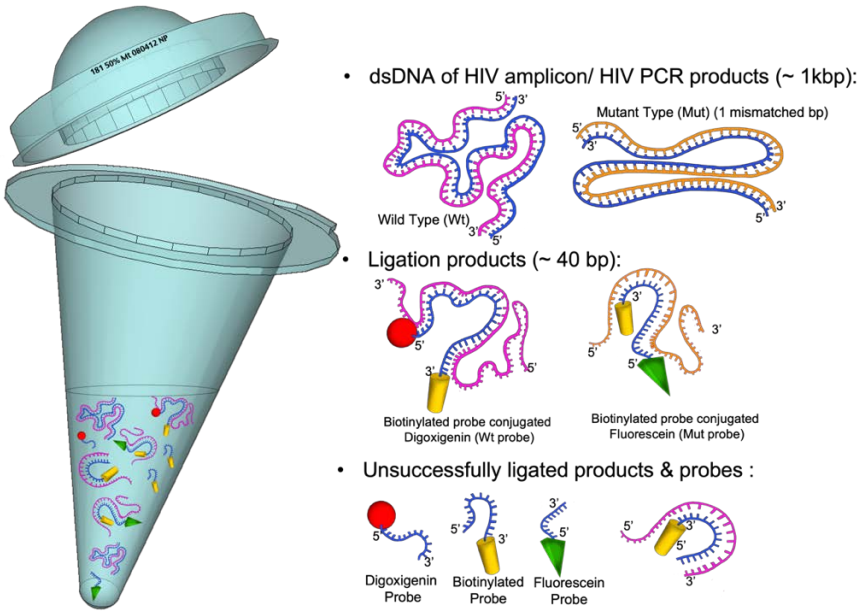

Figure 3.3 | Species present in the reaction at the end of the ligation step.

Amplicon template can anneal to its complementary strand to form dsDNA (double-stranded amplicon). Ligated probes are annealed to the complementary template strand. Mismatched unsuccessfully ligated probes can also anneal to the complementary strand.

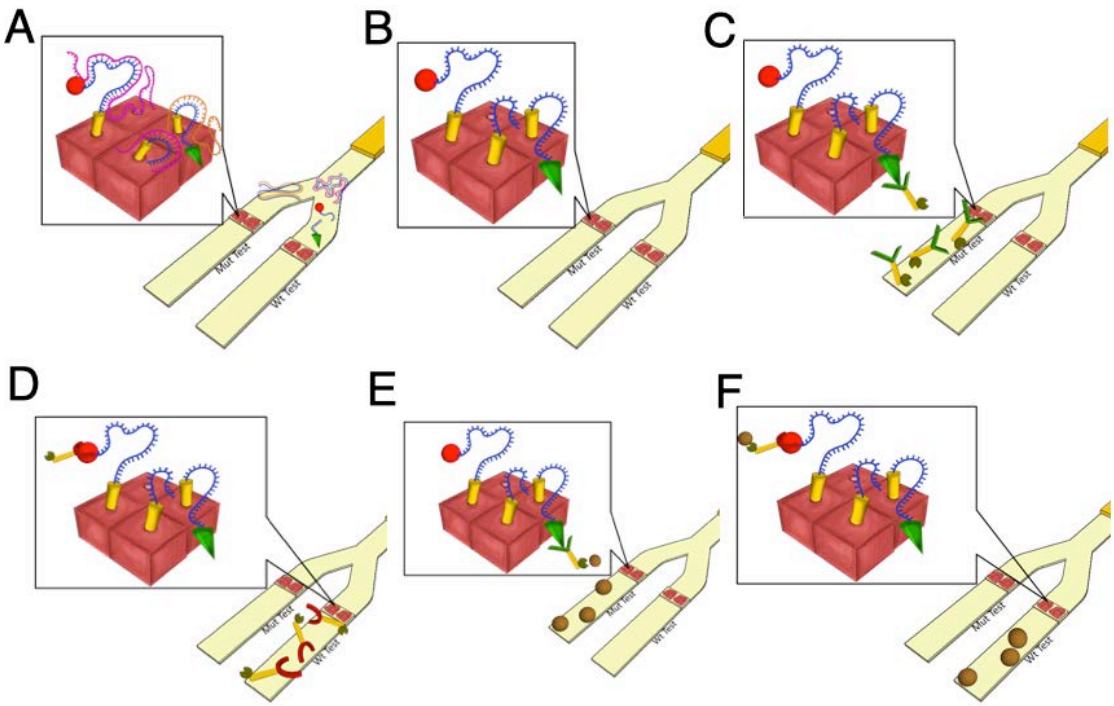

Figure 3.4 | Schema of detection mechanisms in the 1st-generation paper dipstick.

© Copyright 2021 | N Panpradist

(**A**) Streptavidin (brown tetramer blocks, zoomed) at the capture areas bind to biotin moieties, both ligated and unligated products. (**B**) NaOH wash denatures the DNA duplexes, getting rid of the unligated probes at the capture areas. After adding neutralizing buffer, (**C**) anti-FAM POD antibody or (**D**) anti-digoxigenin POD antibody is added to bind to FAM or digoxigenin moieties for MUT or WT detection, respectively. Lastly, (**E**) MUT and (**F**) WT signals are visible as DAB substrate converted into brown precipitate in the presence of the POD enzyme.

RESULTS AND DISCUSSION

3.2.1 KEY MODIFICATIONS USED IN 1ST-GENERATION PAPER DETECTION

To test the feasibility of the lateral flow test, we directly transfer the chemistry from the plate-based OLA detection to paper-based lateral flow strips. The key distinctions here (**Figure 3.1B**) are the type of substrate used to immobilize the capturing molecules and the type of labeling molecules. Here, streptavidin capturing molecules are immobilized onto the nitrocellulose membrane instead of being coated onto the polystyrene plate. A high surface-to-volume ratio of porous nitrocellulose enables fast molecular capture without the need for incubation. The products of the ligation step can be introduced and captured at the area where streptavidin is immobilized through passive wicking toward the negative-pressure end of the strip connected to the absorbent pad.

Additionally, both antibodies are labeled with horseradish peroxidase (HRP) to permit visual readouts, which turns DAB into a brown precipitate. The signal is highly concentrated at the capture lines and enables visual readout. These modifications reduced the number of steps and total assay time and allowed visual detection of results using an office scanner.

© Copyright 2021 | N Panpradist

3.2.2 FIRST GENERATION PAPER DETECTION HAD COMPARABLE SENSITIVITY TO PLATE DETECTION

In the plate ELISA (**CDD** – capture, denaturation, and detection), conditions for the MUT assay were chosen to give sensitive responses to samples with low % MUT. Conditions for the WT assay were selected to give saturated signals in the range of low % MUT to serve as a positive control for successful ligation and detection. To investigate the analytical response of the paper detection, a plasmid dilution series for the Y181C codon (0, 2, 5, 10, 25, 50, 75, 100% MUT) was tested for MUT and WT responses (**Figure 3.5**). The paper detection showed a strong MUT signal for 2% MUT, but its signal saturated at a lower % MUT than plate detection (**Figure 3.5A**). The paper detection showed strong WT signals across the full dilution series, as plate detection (**Figure 3.5B**). Correlation plots of WT from data in **Figure 3.5A**, MUT from data in **Figure 3.5B**, and MUT Ratios (MUT/(MUT+WT)) from the plate and paper detection were shown in **Figure S3.52**.

© Copyright 2021 | N Panpradist

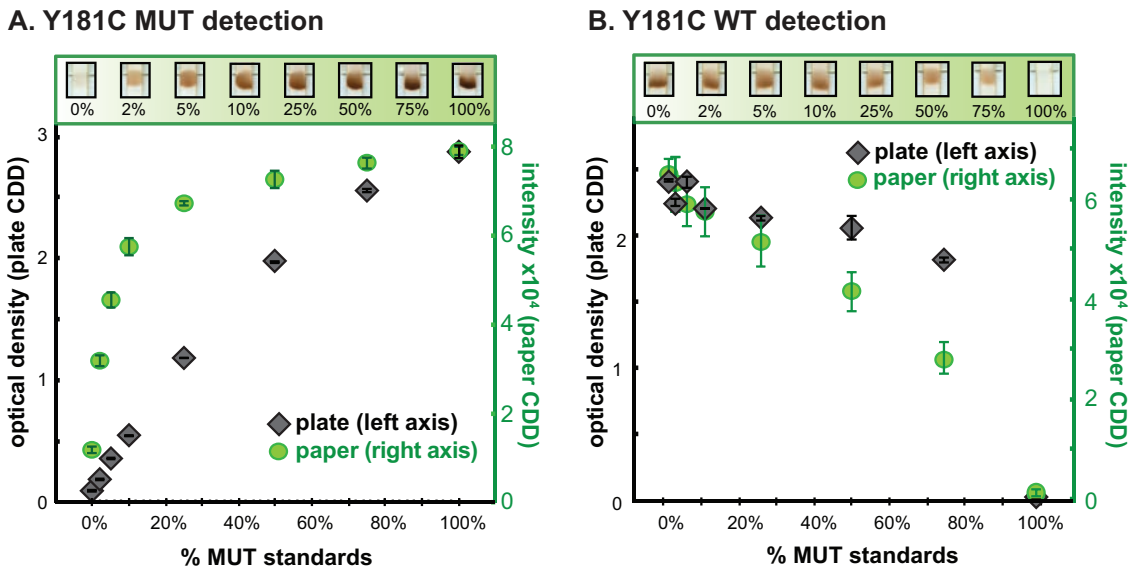

Figure 3.5 | Comparison of plate vs. 1st-generation paper detection for analysis of Y181C plasmid standards.

(**A**) Mutant (MUT) detection (**B**) wild-type (WT) detection. Left axes: Specimen optical density (OD) minus negative control OD analyzed in duplicate by plate detection (mean ± SE). Right axes: Specimen capture intensity minus background intensity analyzed in triplicate by paper detection (mean ± SE). Scanned images of the paper detection strip are shown below each specimen. The ratio of mean signal intensities for 2% MUT and 0% MUT was 2.00 for plate DETECTION and 2.74 for paper DETECTION. The image was obtained from N Panpradist et al. 2016 (**https://DOI.org/10.1371/journal.pone.0145962**)

3.2.3 1ST-GENERATION DIPSTICK SENSITIVELY DETECTED HIVDR IN PATIENT-DERIVED DNA SPECIMENS

Analysis of mutations for HIVDR codons (K103N, Y181C, M184V, and G190A) in 26 blood specimens showed a strong MUT signal ratio correlation between the paper and the plate detection.

Participant specimens and plasmid standards at 0, 5, and 50% MUT were tested for HIVDR mutations at four HIV codons (K103N, Y181C, M184V, and

© Copyright 2021 | N Panpradist

G190A, N total =104) by paper and plate detection (**Figure 3.6A-D, Figure 3.7A-D**). The MUT assay showed a linear correlation between both detection formats for specimens with low % MUT. In contrast, signal saturation in the paper detection resulted in non-linear correlation at high % MUT (**Figure 3.6E&G, Figure 3.7E&G**). The 5% MUT plasmid standard (used below as a threshold standard) fell within the linear correlation range. The WT assay showed strong responses for most specimens and plasmid standards in both formats (**Figure 3.6F&G, Figure 3.7F&G**). For all codons combined, the MUT Ratios for paper and plate detection correlate strongly across participants' data (**Figure 3.8**).

3.2.4 PAPER DETECTION REQUIRES STRINGENT DENATURATION THAN PLATE DETECTION.

The plate detection uses streptavidin-coated well plates to capture ligation probes and a denaturing buffer to remove un-ligated probes from template DNA. In the paper OLA, streptavidin was immobilized onto nitrocellulose strips via spotting and drying. We found that a more stringent denaturing buffer (10X compared to plate detection) was needed to achieve low background **(Figure 3.9**). The 10X denaturing buffer did not strip streptavidin from the nitrocellulose (One-Way ANOVA, α=0.05) and had little impact on its ability to capture a biotinylated target (**Figure 3.10**, statistically significant but small effect).

© Copyright 2021 | N Panpradist

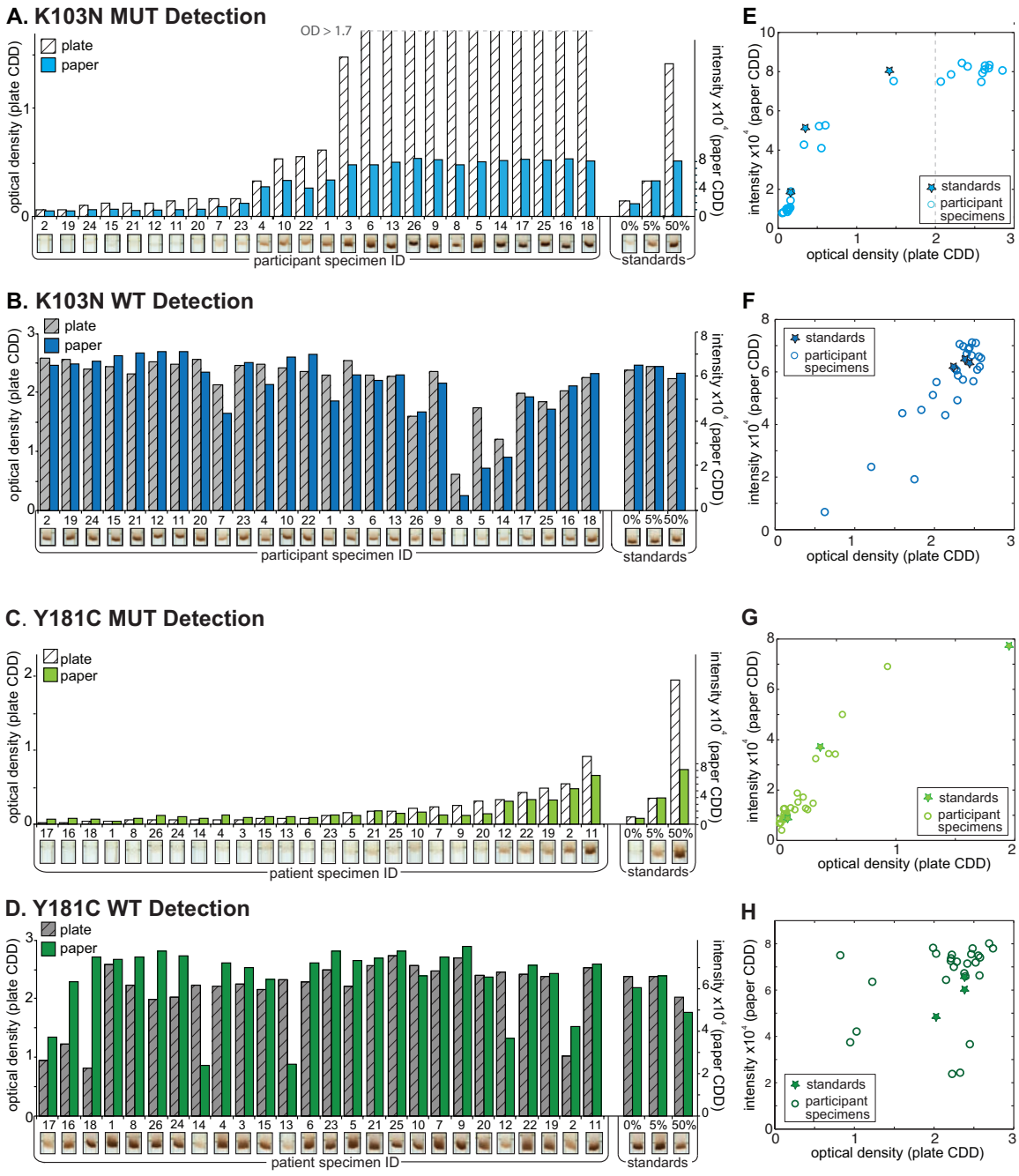

Figure 3.6 | Analysis of clinical specimens by 1st-generation detection for K103A & Y181C.

Panel A and C shows mutant (MUT) detection, and Panel B and D show wild-type (WT) detection. Specimen optical density (OD) minus negative control OD (left y-axis) for each participant's specimen is shown in white/gray by rank along the x-axis, from the lowest OD of MUT, followed by the plasmid standards (0%, 5%, 50% MUT) performed in duplicate. Spot intensity minus background intensity (right y-axis) for each participant's specimen is shown in pink/purple, followed by the plasmid

© Copyright 2021 | N Panpradist

standards (0%, 5%, 50% MUT) performed in triplicate. Scanned images of the paper detection strip are shown below each specimen. Panels E - H show a correlation between paper CDD and plate detection for the data of A - D, respectively. Participant specimens are shown as open circles, and plasmid standards (0%, 5%, 50% MUT) are shown as stars. The image was published, N Panpradist et al. 2016 (**https://DOI.org/10.1371/journal.pone.0145962**)

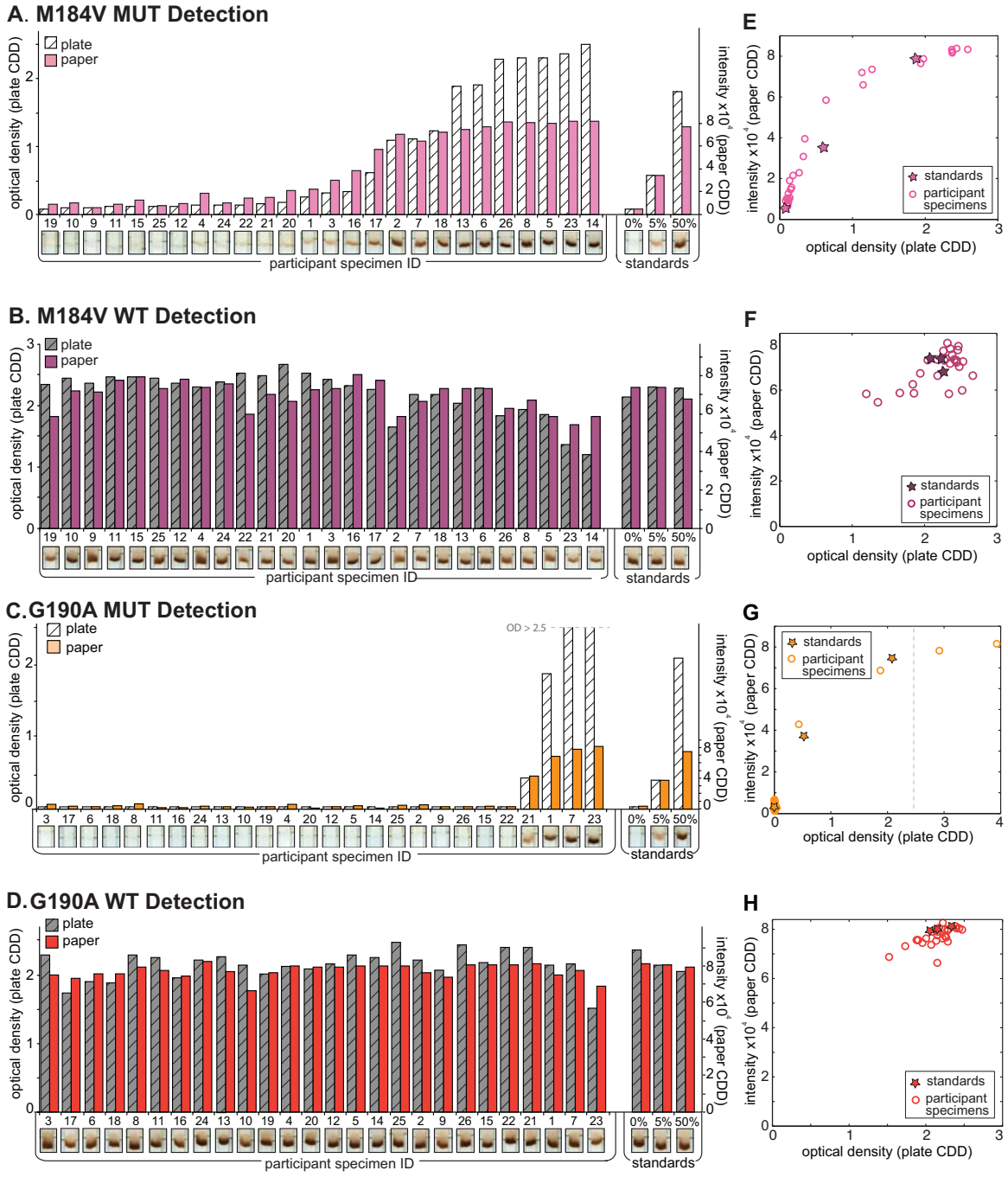

Figure 3.7 | Analysis of clinical specimens by 1st-generation detection for M184V & G190A.

© Copyright 2021 | N Panpradist

Panel A and C shows mutant (MUT) detection, and Panel B and D show wild-type (WT) detection. Specimen optical density (OD) minus negative control OD (left y-axis) for each participant's specimen is shown in white/gray by rank along the x-axis, from the lowest OD of MUT, followed by the plasmid standards (0%, 5%, 50% MUT) performed in duplicate. Spot intensity minus background intensity (right y-axis) for each participant's specimen is shown in pink/purple, followed by the plasmid standards (0%, 5%, 50% MUT) performed in triplicate. Scanned images of the paper detection strip are shown below each specimen. Panels E - H show a correlation between paper DETECTION and plate CDD for the data of A - D, respectively. Participant specimens are shown as open circles, and plasmid standards (0%, 5%, 50% MUT) are shown as stars. The image was obtained from N Panpradist et al. 2016 (**https://DOI.org/10.1371/journal.pone.0145962**)

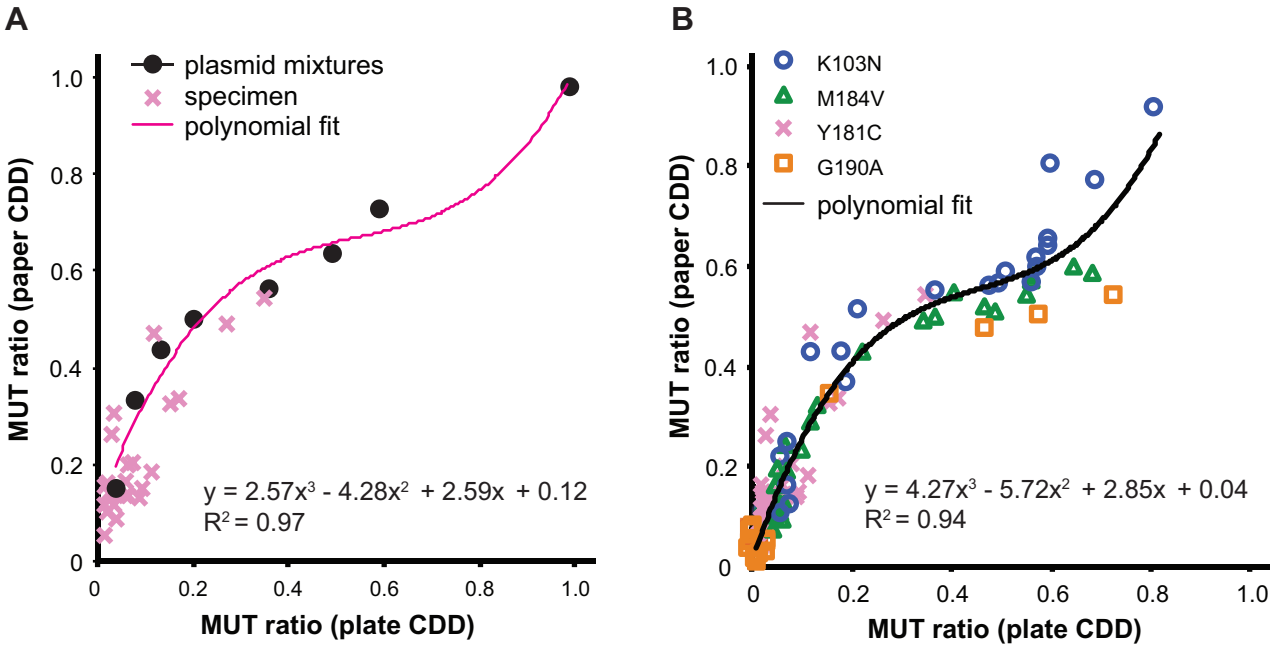

Figure 3.8 | Correlation plots of the signal ratio by plate vs. 1st-generation paper detection. **(A)** Y181C Mutant (MUT) Ratios for 26 subjects' HIV DNA compared to the plasmid mixtures (0% - 100% Y181C MUT) and specimen. The polynomial fit was used to report the R^2 based on the overturn behavior found in specimens with a high %MUT. (**B**) MUT Ratios for all four HIVDR codons determined by paper capture, denaturation, and detection CDD versus plate CDD. The polynomial fit was used to fit the high % MUT data points, which are expected to create an overturn behavior. The image was obtained from N Panpradist et al. 2016 (https://DOI.org/10.1371/journal.pone.0145962)

© Copyright 2021 | N Panpradist

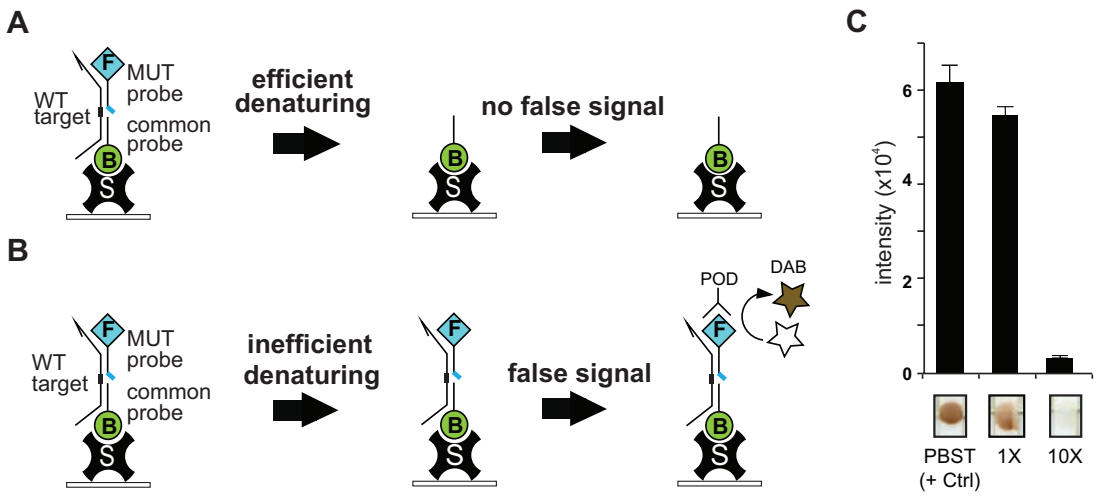

Figure 3.9 | Denaturing of non-ligated probes to remove the background using NaOH.

(**A**) Schematic of efficient oligonucleotide denaturing. DNA target is completely dissociated from probes, and the false signal is not detected. (**B**) Schematic of inefficient oligonucleotide denaturing. Non-ligated probes bound to target template DNA can be detected, contributing to false signals. (**C**) Comparison of denaturing methods. 1X and 10Xconcentrationsn of denaturing buffer were tested for their ability to denature non-ligated probes from target template DNA compared to a 1X PBST control. To generate complete non-ligated probes, a 0% mutant (MUT) plasmid standard of Y181C was mixed with probes and subjected to 10-cycle ligation without ligase enzyme. 1X denaturing buffer was ineffective at reducing background (11% reduction), but the 10x denaturing buffer was effective (94% reduction). The image was obtained from N Panpradist et al. 2016 (https://DOI.org/10.1371/journal.pone.0145962).

© Copyright 2021 | N Panpradist

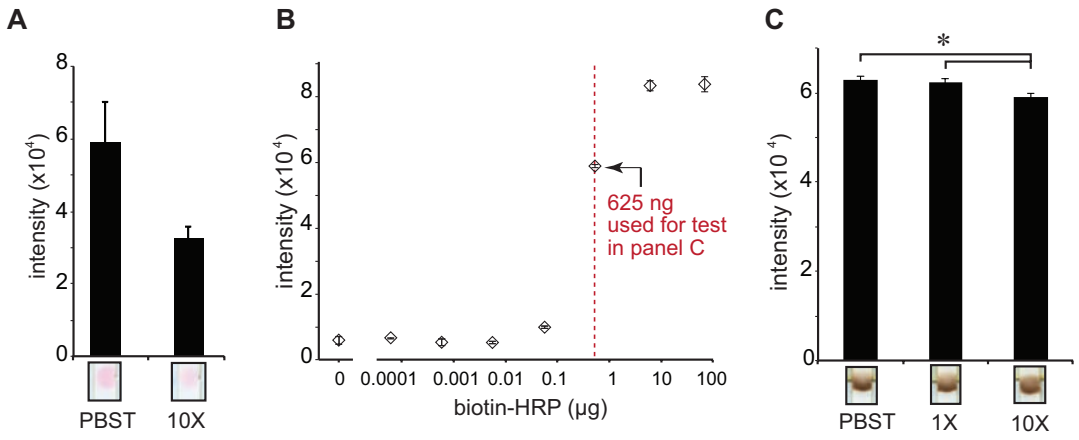

Figure 3.10 | On-paper oligonucleotide capture by immobilized streptavidin.

(**A**) Streptavidin presence on the membrane after 1X PBST or 10X denaturing buffer wash. The presence of streptavidin immobilized nitrocellulose was visualized by Ponceau S solutions (10 minutes in Ponceau S solution and 5 minutes in distilled water). The wet strips were scanned and analyzed. The plot represents the signal intensity of stained streptavidin in each case (mean ±SE; n=4). There was no significant difference between means (one-way ANOVA, p = 0.07) (B) Determination of linearity of biotin-conjugated-POD (biotin-POD) concentrations captured by on-paper streptavidin. Biotin-POD was used as a model analyte to quantify capture performance. 25µL of 10-fold serial dilutions of biotin-POD/ PBST (6.25pg to 62.5µg) was used as a model analyte (n=4). The strips were dipped in a timed sequence (5 minutes each) in polystyrene wells containing the following reagents: (1) 25µL of biotin–POD, (2) 25µL of PBST wash, (3) 40µL of DAB substrate, and (4) 25µL of PBST wash. Wet strips were scanned and analyzed. The plot represents signal intensity (mean ± SE, n=4). The linear range was estimated as 0.1-10µg of biotin-POD, and 625ng of biotin-POD was chosen for the experiment in C (such that an effect, if present, would be observed by a change in signal intensity). (C) Effect of denaturing buffer on the ability of immobilized streptavidin to capture biotin-POD. The strips were dipped in a timed sequence (5 minutes each) in a series of polystyrene wells containing the following reagents: (1) 25µL of 1X PBST, 1X denaturing buffer, or 10X denaturing buffer, (2) 25µL of neutralizing buffer (twice), (3) 25µL of 625ng of biotin-POD (within the responsive range from panel B), (4) 25µL of PBST, (5) 40µL of DAB substrate, and (6) 25µL of PBST. On-paper streptavidin after 10X denaturing buffer yielded significantly lower signal intensity than those treated with PBST or 1X denaturing buffer (One-way ANOVA, Post-hoc

© Copyright 2021 | N Panpradist

comparison (Tukey Kramer test, α = 0.05). The image was obtained from N Panpradist et al. 2016 (https://DOI.org/10.1371/journal.pone.0145962)

DISCUSSION

THE PAPER STRIP FORMAT REDUCED THE TIME NEEDED TO PERFORM THE ASSAY.

Typical plate assays require long incubation steps for target capture and labeling, primarily due to the slow diffusion of probes and other reagents to the plate capture surface. In contrast, delivery by flow in the paper provides intimate contact of reagents with the detection surface, as targets and labels diffuse rapidly across the tiny pores (mean of 2.8μm[1]). As a result, capture and labeling of ligated products could be completed within 5 minutes each in the paper CDD, compared to long incubations (1-hour and 30-minute incubations, respectively) in the plate CDD.

THE USE OF THE POD ENZYMATIC SYSTEM SPEEDED UP MUT DETECTION BUT RESULTED IN A MORE SATURATED SIGNAL FOR HIGH %MUT.

In the plate CDD, the POD system produces detectable signals much faster (5 minutes) than the AP system (15–45 minutes), and the two detection steps for MUT and WT are performed sequentially in a single well. To improve the speed of detection in the paper format, a single enzyme system (*i.e.,* POD) was used to label MUT, and WT probes in parallel strips run simultaneously using the same procedure. TMB is the most common substrate for POD-based plate assays, but it requires the addition of H_2SO_4 to stop the reaction before reading[2], and the soluble

© Copyright 2021 | N Panpradist

TMB product [3] would be washed away in the paper CDD. DAB is extensively used to measure peroxidase activity in tissues[4]; it has only one oxidation state (does not require post-treatment to fix the color) and forms visible brown precipitate at the detection spots on the paper strip. The replacement of AP by POD for MUT detection and the use of DAB substrate likely caused the differences between the plate and paper signal saturation seen with all specimens and standards. The oligonucleotide probe concentrations had been optimized in the plate CDD for the slower AP-yellow substrate system, and probe concentrations were not adjusted in the paper CDD. However, a linear correlation can likely be achieved in the paper CDD by altering the concentrations of oligonucleotide probes. If detecting low MUT HIV levels is needed to predict treatment failure, tuning CDD for a strong low-level response may be desirable. The relatively large SD values on the standard control samples were greater for codons 103 and 181 than 184 and 190. The small number of standard control samples (triplicate) was sensitive to variation. The variability in these experiments was likely due to manual spotting of the paper strips instead of controlled strip preparation. Controlled strip preparation (e.g., lateral flow striper) is expected to reduce the variability. Overall, the paper CDD showed analytical sensitivity comparable to the plate CDD for a plasmid mixture series (Y181C, **Figure 3.5** & **Figure S3.53I**), and results for clinical specimens showed strong concordance across four relevant DR codons (**Figure 3.8** & **Figure S3.53J**).

While we did not attempt to evaluate % MUT quantification here, our results suggest a quantitative correlation with plate CDD, which correlates strongly with proportions of mutant in the HIV population as measured by Roche's 454

© Copyright 2021 | N Panpradist

pyrosequencing[5]. In addition, drug resistance surveillance and treatment monitoring require a test that targets all DR mutations prevalent in the patient population. Here, we tested three common nevirapine- and one lamivudine-resistance mutation currently prevalent in Kenya[6]. With the availability of new drug choices for first-line ART, additional DR mutations such as K65R will likely be needed to assess transmitted and selected HIVDR. More comprehensively. The clinical utility of the test will require evaluation based on available treatment options. Notably, the paper CDD is expected to translate well to new DR mutations since the capture and detection chemistries are not target-dependent. OLA can be performed on amplicon derived from either plasma viral RNA or cellular DNA (PBMC, whole blood, dried blood spots)[5, 7-9]. This study used PBMC DNA as the HIV DR target because DNA-based assays offer several advantages over RNA, including cost savings from reverse transcriptase enzyme and easier handling and processing (no need for RNAse-free reagents and plastic/glassware). In addition, DNA is adequate for pre-ART testing of DR and can detect archived resistance mutations no longer detectable in plasma[10, 11]. However, testing for DR in plasma RNA may be more sensitive in patients with early rebound viremia. The existing plate CDD measures WT and MUT in sequential reactions within a single well. In the paper CDD, we separated the WT and MUT detection into two strips run in parallel to reduce the protocol time and complexity. However, a procedural control may be needed to ensure the validity of each strip.

The modifications developed here simplified the CDD steps and reduced the total time (**Figure 3.11**). Both plate and paper CDDs share the upstream processes (DNA extraction, amplification, and ligation), which take 420min. Paper CDD

© Copyright 2021 | N Panpradist

reduced the total OLA time from 420min plus 150min/ 1 DR codon to 420 min plus 45 min/ 1 DR codon. The costs for the complete OLA processes with plate and paper CDDs are comparable (~ $5/codon, **Table S3.5**). Note that the costs reported representing batching of 36 and 9 samples for plate and paper CDDs, respectively. More simplifications on paper CDD can be done. For example, the CDD reagents could be stored dry without refrigeration and supplied in wells, as reagent pads integrated into strips similar to conventional lateral flow tests or printed directly onto the strip[12]. Long-term storage of some CDD reagents has been demonstrated: DAB substrate[13], POD-conjugated antibodies[14, 15]. While the paper CDD presented here requires manually moving the paper strips between wells every 5 minutes, there is potential to automate the timed steps needed for the CDD protocol. Paper-microfluidic tools such as dissolvable sugar time delays[16], shunt time delay valves[17], and capillary-based paper networks[18, 19] could automate the protocol presented here. Increasing the simplicity of the paper CDD through dry reagents and automation of the protocol is the subject of current work.

© Copyright 2021 | N Panpradist

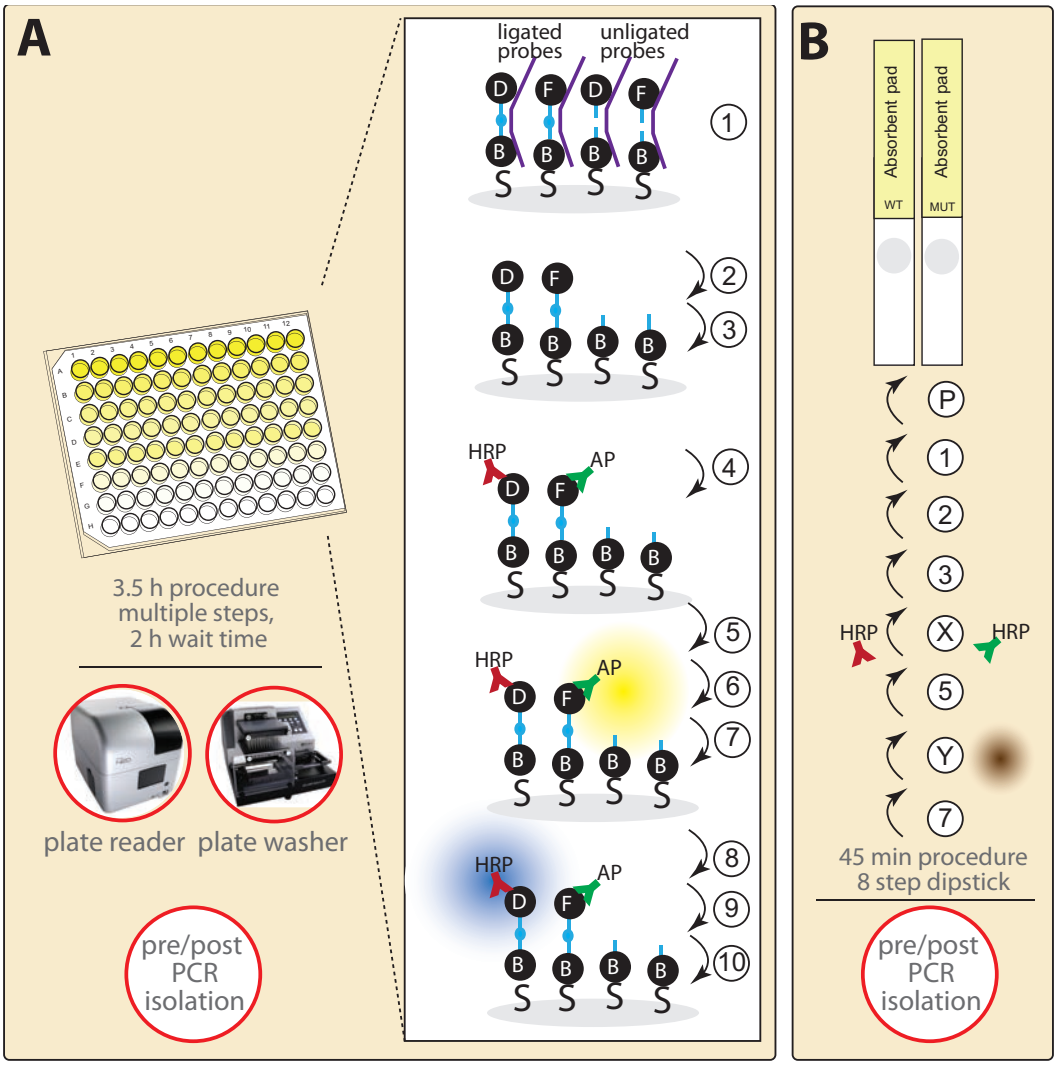

Figure 3.11 | Traditional plate-based ELISA versus Generation 1 dipstick paper-based detection (CDD).

(A) In traditional OLA ELISA, a streptavidin-coated plate was used to capture the ligated product in step 1 during a 1.5h incubation. A series of fluids was added and decanted as follows. Sodium hydroxide (NaOH) wash was introduced to eliminate the duplex of un-ligated probes and amplicon before neutralization in steps 2&3. Antibodies mix (anti-fluorescein tagged alkaline phosphatase (AP) and anti-digoxigenin tagged horse-radish peroxidase (HRP)was added to label the ligated products and incubate for 0.5 h in step 4. Excess antibodies are washed away in step 5. AP substrate was added and read at 405nm after 20-45 minutes in ssteps6 and 7. Another wash was added, followed by the addition of HRP substrate and sulfuric acid addition in steps 8-10. (**B)** In paper-based OLA ELISA, different fluids were

© Copyright 2021 | N Panpradist

wicked past the immobilized streptavidin. Every reagent was identical to plate-plate ELISA, except step P (blocking reagent added), step X either anti-fluorescein-HRP or anti-digoxigenin-HRP added for mutant and wild-type detection, and step Y DAB solution is added to create brown precipitates for visual readout.

3.3 GENERATION 2: BIPLEX PAPER-BASED DETECTION

Next, we further simplified the 1st-generation dipstick to a lateral flow device. Our first-generation detection involved manually moving the dipsticks through a series of reagents and required two strips to detect each set of MUT or WT HIV (*i.e.,* 12 strips for six mutation sites). In the 2nd-generation paper detection, both WT and MUT are detected on a single strip using different chemistries (**Figure 3.12**).

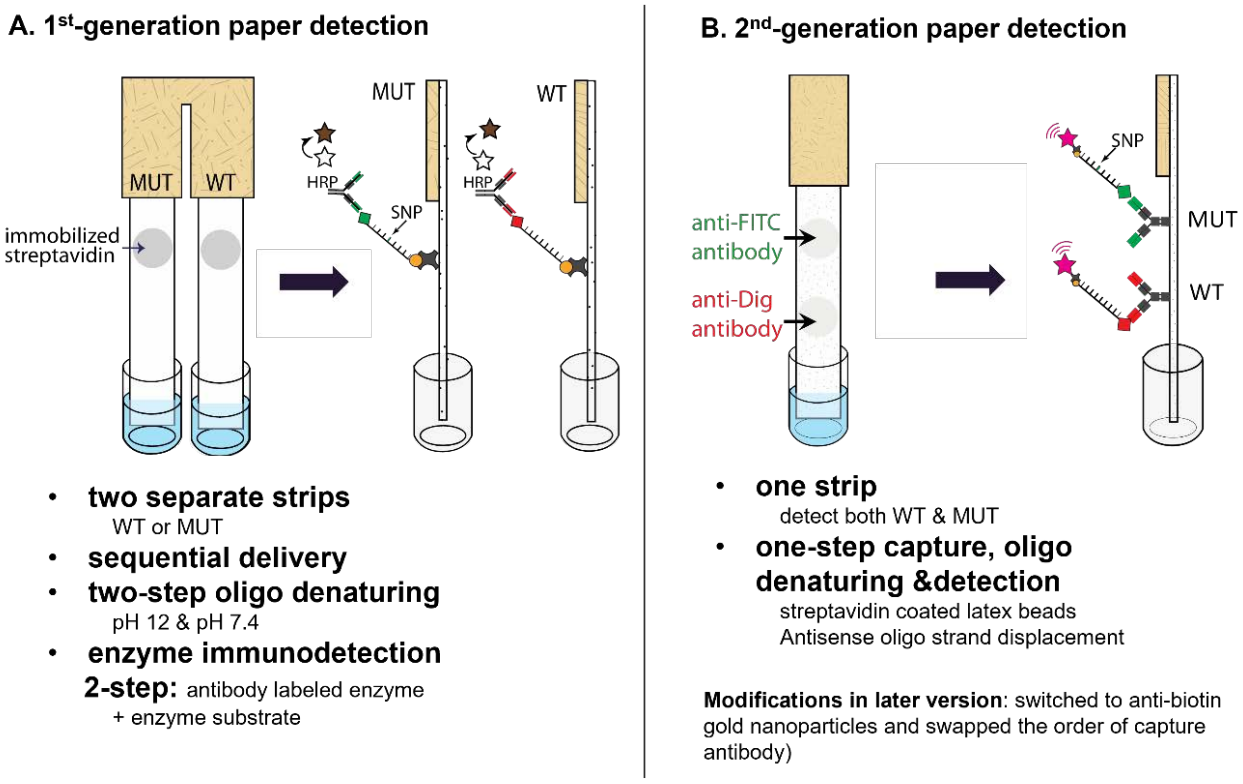

Figure 3.12 | Comparison of 1st and 2nd generation paper detection.

© Copyright 2021 | N Panpradist

MATERIALS AND METHODS

Bead buffer optimization.1µL biotin-conjugated BSA (Sigma A8549-10MG, lot# SLBC7388V) diluted in 1xPBS to achieve at 0, 0.2, 0.5, 1, 2.5, 5, 7.5 10 mg/mL) was hand-spotted on Millipore HF135 nitrocellulose ester membrane and left dried (1 hour at 37 °C and kept at desiccator until tested). Polystyrene conjugated dyed microsphere Cabo blue (Bang's lab CP01B, lot# 10620) in 0.09% sodium azide stock was diluted 100-fold in different candidate buffers. 50 µL of diluted blue beads in candidate buffers were wicked through the membrane (N=3 in each case). Candidate buffers tested were: (1) Storage buffer from the manufacture (Bang's lab) (2) Lateral flow buffer (Epoch Biosciences).

Lateral flow strip fabrication. 0.5 µg anti-FAM antibodies (Southern Biotech), anti-digoxigenin antibodies (Novus Biologicals), and biotinylated BSA (Sigma) was striped onto each nitrocellulose sheet (EMD Millipore) adhered onto a PVC backing card and dried overnight in the desiccator. Two ends of the nitrocellulose were then assembled to the glass fiber (EMD Millipore) and absorbent pads (GE Healthcare). The assembled sheet was cut into 3.5 mm × 6 mm strips and placed into plastic cartridges (DCN Diagnostics). Assembled devices were stored in foil pouches with a desiccant at four °C until use.

RESULTS

3.3.1 THE 2ND-GENERATION LATERAL FLOW TEST

The 2nd generation detection test was designed for rapid lateral flow detection that simultaneously detects WT and MUT ligated probes (**Figure 3.13A**), using:

© Copyright 2021 | N Panpradist

multiplexed capture by immobilized antibodies, denaturation of un-ligated probes using “competing oligo,” and a shared gold nanoparticle label for both WT and MUT ligated products. In the following sections, we describe different rationale optimization steps we took to achieve these results.

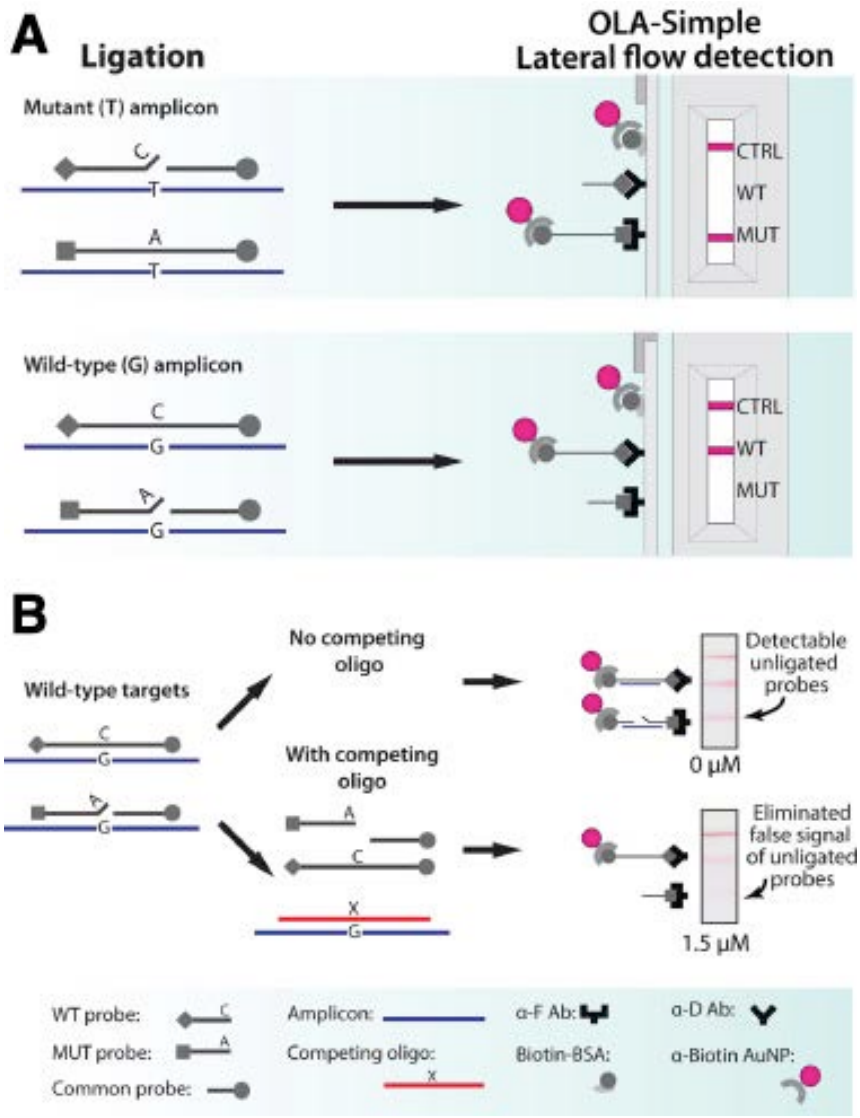

Figure 3.13 | Detection of single-base mutations in 2nd generation paper detection.

(**A**) 5′-digoxigenin-labeled wild-type (WT) and 5′-FAM-labeled mutant (MUT) probes are ligated to the 3′-biotinylated, 5′-phosphorylated common probes when these anneal to WT and MUT HIV amplicon templates, respectively. A mismatched probe: template complex precludes ligation due to ligase specificity for complementary bases at the ligation site. MUT and WT ligated products are captured on the

© Copyright 2021 | N Panpradist

strip by immobilized anti-FAM antibody (α-F Ab) and anti-digoxigenin antibody (α-D Ab), respectively. Anti-biotin antibody-coated gold nanoparticles in the chase buffer bind to the ligated products as well as the biotin-conjugated BSA (Biotin-BSA) control line (CTRL), all labeled by an anti-biotin antibody conjugated gold nanoparticle (α- Biotin AuNP). (**B**) Effects of competing oligo concentrations. Examples of scanned lateral flow strips analyzing WT HIV ligation products after treating with 0 or 1.5 μM competing oligo concentrations are shown.

3.3.2 MULTIPLEXED CAPTURE WAS ENABLED BY USING IGG/ANTIGEN PAIRS.

Inverting the detection stack (**Figure 3.12**), we had antibodies as capture molecules instead of labeling molecules. Testing cross-reactivity between different IgG/antigen pairs, we used OLA plate ELISA to quantitatively assess the performance of eight commercially available molecular binding pairs and found three pairs (*e.g.,* anti-digoxigenin, anti-FAM, and anti-Texas red IgG) bound without cross-reactivity and maintained high specificity when immobilized onto nitrocellulose test strips (**Figure 3.14**). Based on these results, we can estimate the affinity of these hapten/IgG binding pairs. In OLA detection, the hapten/IgG antibodies' binding had a lower affinity than the streptavidin/biotin binding, with a K_D (dissociation constant) of 50pM vs. 0.13 pM of streptavidin/biotin interaction. The stronger binding would detect low concentrations of biotinylated probes. In OLA, biotinylated probes are present in the nM range; thus, even with a higher K_D of these antibodies, these hapten/IgG pairs are sufficient for our need in the OLA detection.

© Copyright 2021 | N Panpradist

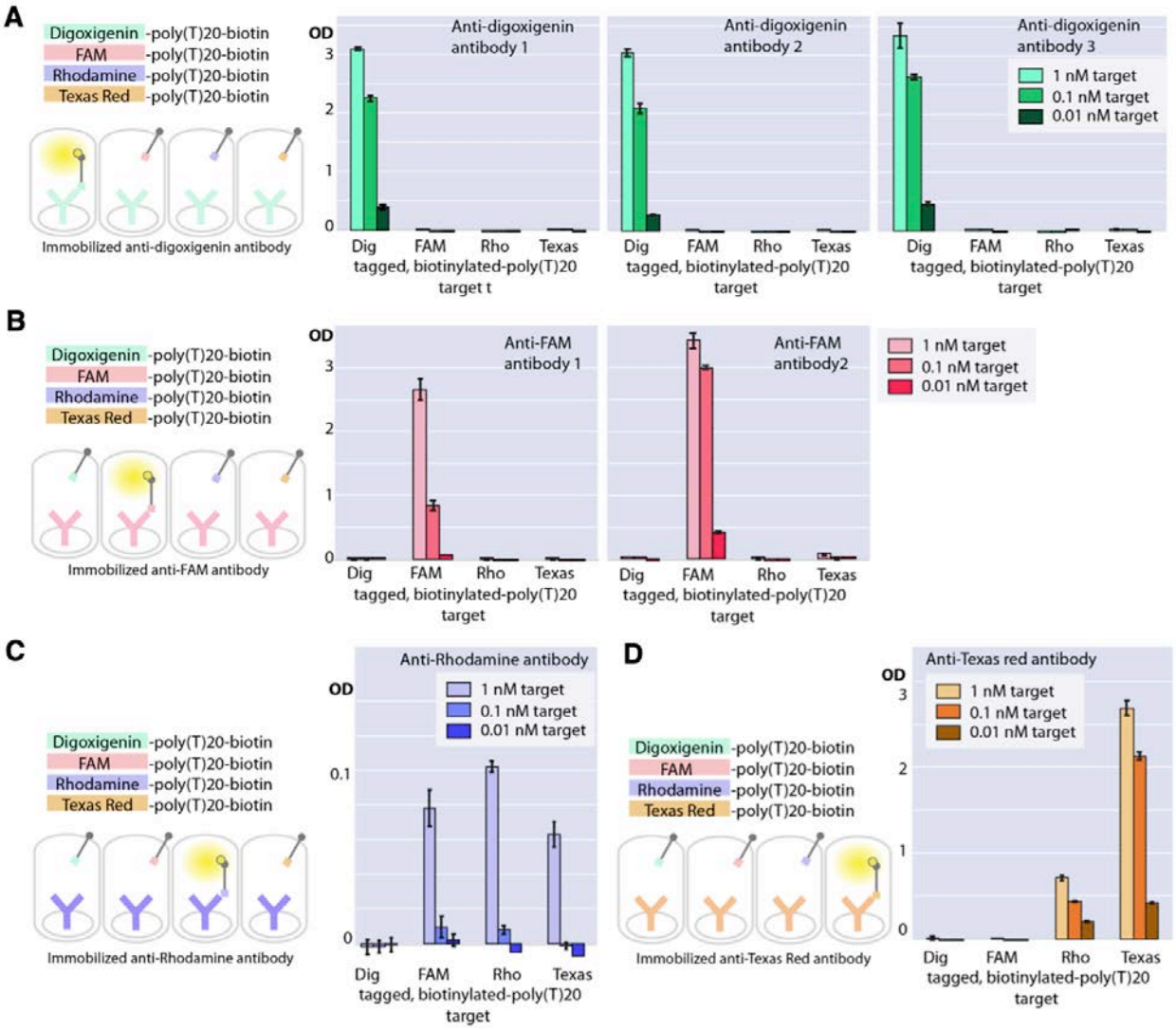

Figure 3.14 | Characterization of antibody capture cross-reactivity.

Commercially available small molecules and antibody pairs were tested for their specificity and sensitivity using ELISA. Synthetic ligated products: 3'-biotinylated poly(T)$_{20}$ with 5'-end tagged with digoxigenin (Dig), FAM, rhodamine (Rho), Texas Red (Texas) diluted in ligation buffer at 0.01-1 nM was added to the immobilized capture antibody. Optical densities (OD) (means ± SD, n=6) were plotted for TMB substrate reaction with streptavidin-conjugated horseradish peroxidase that bound to biotinylated synthetic ligated product captured by immobilized antibody: (**A**) anti-digoxigenin antibody (**B**) anti-FAM antibody) (**C**) the anti-rhodamine antibody, and (**D**) anti-Texas Red antibody. Anti-Rhodamine and anti-Texas Red showed cross-reactivity. Three antibody pairs – anti-FAM, anti-digoxigenin,

© Copyright 2021 | N Panpradist

and anti-Texas Red can be used for multiplexed detection. For OLA-Simple, only two combinations are needed, so we selected economical options (anti-digoxigenin type 2 and anti-FAM type 2).

3.3.3 IGG WHOLE ANTIBODIES VS. FAB FRAGMENTS OF ANTI-FAM ANTIBODIES

Instead of using Fab fragments of antibodies as done in the 1st-generation dipstick format, we used the whole IgG. As protein physisorption onto nitrocellulose membranes relies on the strength of dipole and hydrophobic interactions[20], we anticipated that higher molecular weight IgG antibodies (~150 KDa) would adhere to nitrocellulose better than lower molecular weight Fab fragments (~50 KDa). Surprisingly, we found that Fab fragments stuck to the membranes and detected the ligation products down to 2% MUT (**Figure 3.15**). Regardless, we initiatively selected IgG capture as the capture molecules moving forward. We used 1µg IgG (6 pmol, 12 pmol binding capacity) when hand-spotting the IgG onto the nitrocellulose and 0.5µg IgG (3 pmol, 6 pmol binding capacity). We hypothesize that some IgG binding sites may not be accessible after physisorption, so we ensure that we have at least a 1:2 molar ratio of FAM probe in a ligation reaction: anti-FAM antibody and at least 1:8 molar ratio of Dig probe in a ligation reaction: anti-DIG antibody.

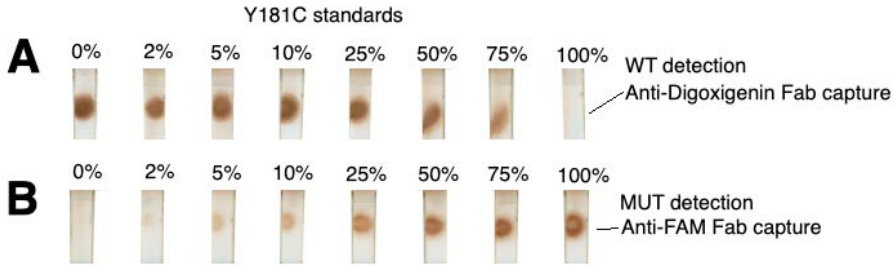

Figure 3.15 | Use of Fab fragment tagged AP antibodies as capture molecules.

1:1000 from the stock concentration of labeling antibodies were used as the capture molecules. The mass concentration is unknown as the attention was reported based on the enzymatic activity unit.

© Copyright 2021 | N Panpradist

Thus, the same concentration used in the 1st-generation dipstick was applied here. The same condition of nested PCR and 10-cycle ligation was also used. However, competing oligo and heat were used as the method for denaturation of non-ligated probes from the amplicon instead of NaOH (discussed later in this chapter).

3.3.4 BUFFER COMPONENTS AFFECTED ANTIBODY FUNCTIONALITY.

Buffer components affected antibody functionality.

During the initial screening of immobilized antibodies, all antibodies were diluted in 1xPBS. However, salts in the buffer could significantly impact the physisorption of antibodies to bind to nitrocellulose via physisorption and their functionality[21]. We found buffers used as the diluent during the immobilization affected its stability when challenged with the wash buffer and its functionality (**Figure 3.16**).

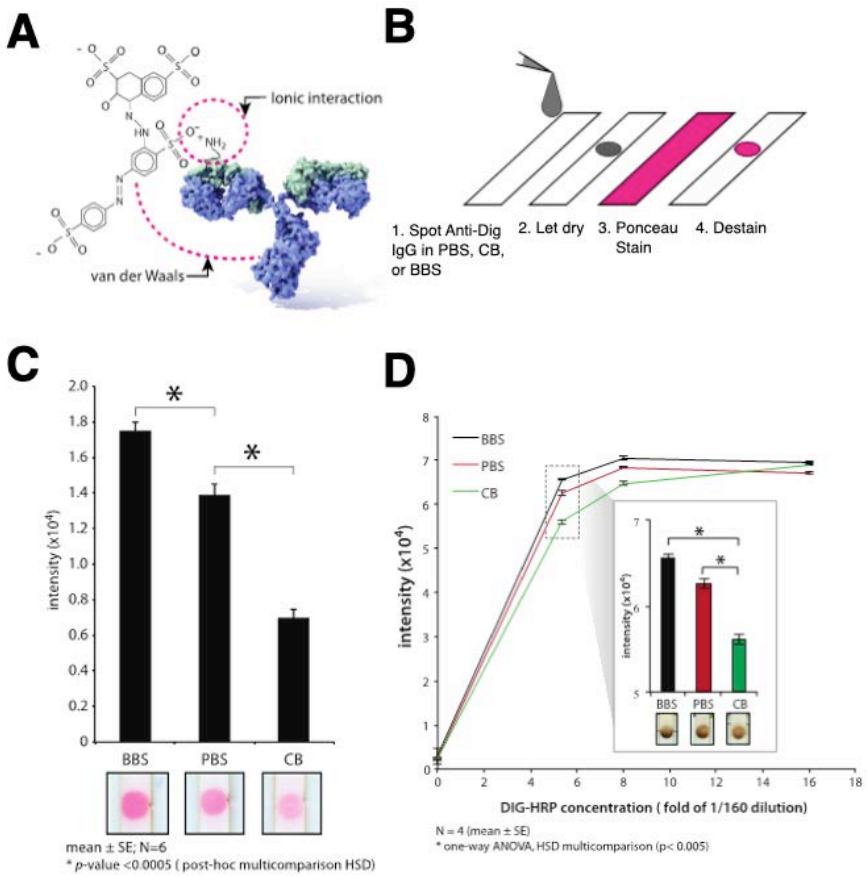

Figure 3.16 | Effect of buffer pH and salts on immobilized IgG.

© Copyright 2021 | N Panpradist

(**A**) Ponceau stain (with its chemical structure) binds to the protein via van der Waals force and through its primary amine via ionic interaction. (**B**) Protocol for protein visualization after being challenged with the detection buffer. (**C**) Presence of immobilized anti-digoxigenin IgG in different buffers detected by ponceau stain. Borate buffered saline (BBS) is 10mM sodium borate, 150mM sodium chloride (pH 8.2). Phosphate buffered saline (PBS) is 10mM phosphate ions, 137mM sodium chloride, and 2.7mM potassium chloride (pH 7.4), and carbonate buffer (CB) is 10mM sodium carbonate, 90mM sodium bicarbonate (pH 9.2). (**D**) The functionality of immobilized IgG based on a signal generated from interaction with Digoxigenin tagged horse-radish peroxidase (DIG-HRP).

3.3.5 ALTERNATIVE DENATURATION METHODS TO NAOH

Next, we investigated denaturation methods to remove unlighted probe: template complexes that can cause false signals. 1st-generation paper detection uses alkaline denaturing buffer, but this denaturation method or heat near 95C previously used in plate-based OLA successfully[22] are incompatible with immobilized antibodies on nitrocellulose as antibodies are stripped away from the capture line (**Figure 3.17**). Here, we used antisense "competing oligonucleotides" (13 bases longer than the unlighted probes) which can form more thermodynamically stable duplexes to the sense strands of amplified targets and can spontaneously displace the unligated probes (**Figure 3.18A**). This process, when properly working, can eliminate signals from the duplexes of unligated probes/amplified targets (**Figure 3.18B**), and the results are more consistent when a brief denaturation and re-annealing of ligation product was done in the presence of these competing oligos in the OLA-Simple kit (**Chapter 5**). **Section 3.4** discusses the approach to bypass the heat denaturing step.

© Copyright 2021 | N Panpradist

Heat-assisted competing oligo in conjunction with the Inverted assay stack (antibody captures instead of labels) permits detection of both wild-type and drug-resistant HIV in a single strip (**Figure 3.18C**).

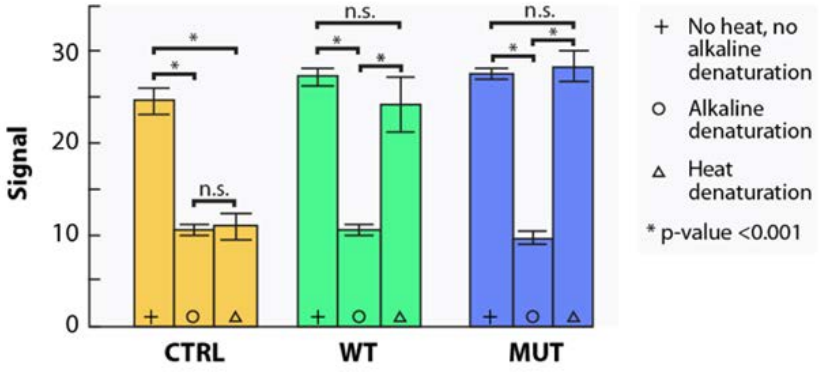

Figure 3.17 | Effect of different denaturation methods on the immobilized antibody.

Strips treated with 1x PBS (control), pH 11 buffer (alkaline denaturation), or 95°C for 5 minutes (heat denaturation) were stained with Ponceau dye. The signals from WT, MUT, and CTRL lines (means ± SD, n=5) were compared (t-test, Holm-Bonferroni correction).

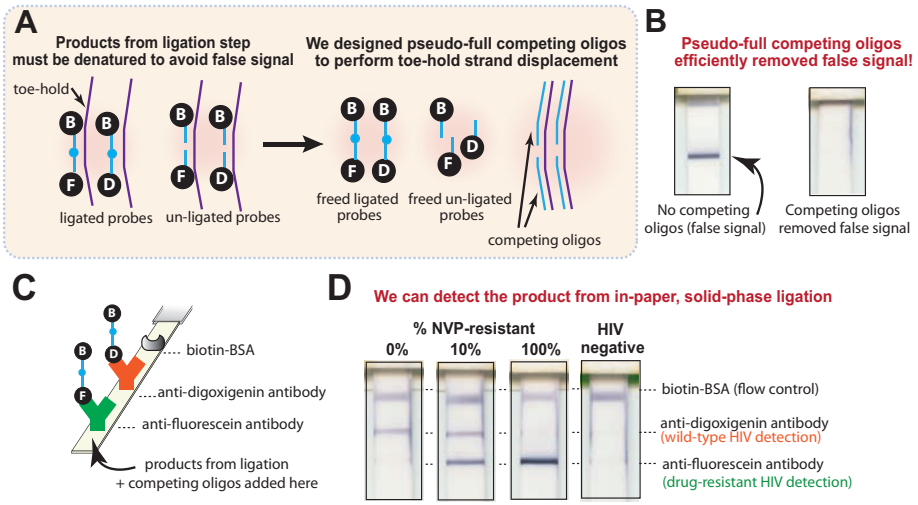

Figure 3.18 | Detection of HIVDR on a single strip using AP/Purple substrate system.

(**A**) False signal from the duplex of un-ligated probes and target must be eliminated. We designed pseudo-full competing oligonucleotides that can anneal to toehold regions of the target and displace both ligated and un-ligated probes. (**B**) This approach is efficient as the false signal was completely knocked down. (**C**) Immobilized antibodies are used to capture the ligated probes and detected by the

© Copyright 2021 | N Panpradist

reaction of streptavidin-alkaline phosphatase/substrate that creates purple bands. (**D**) Example of HIVDR test from in-paper isothermal ligation.

Combined this competing oligo denaturation method with the POD detection approach used in 1st-generation detection (**Figure 3.19**), we could sensitively detect MUT in a 2% Y181C sample after a 1-cycle ligation product (instead of traditional 10-cycle ligation). Alternative to POD, phosphatase (**AP**) with its substrate (**Figure 3.18D**) can be used to visualize the presence of ligated products.

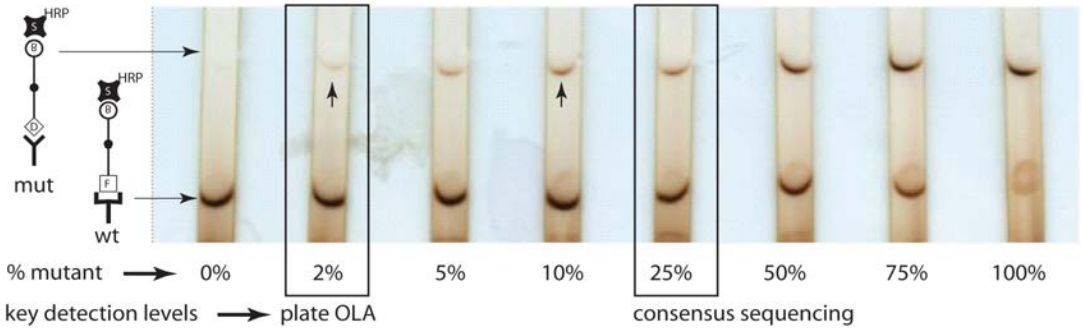

Figure 3.19 | Detection of HIVDR on a single strip using POD/DAB system.

Although AP and POD labeling systems provided a sensitive detection, the protocol involves three steps to detect the ligated probes (*i.e.,* adding the enzyme, wash, and substrate, respectively). To further simplify the detection step, we investigated the possibility of using nanoparticles or dyed microspheres.

3.3.6 BSA-BLOCKED NANOPARTICLE/MICROSPHERES COULD FLOW ON LATERAL FLOW STRIPS WHEN DILUTED IN AN APPROPRIATE BUFFER.

© Copyright 2021 | N Panpradist

We compared the detection of streptavidin-coated colored microspheres when diluted in different buffers. Beads diluted in the bead storing buffer were stuck at the bottom of the nitrocellulose membrane strips (**Figure 3.20**) while moving to the capture areas and binding to the positive control (Biotin-BSA at many concentrations) and not binding to the negative control strip (BSA), (**Figure 3.20**). Similar phenomena were found when in anti-biotin gold nanoparticles. We tested this labeling system with the IgG/hapten pairs proven to have no cross-reactivity by ELISA (**Figure 3.14**). Anti-Digoxigenin IgG and anti-FAM IgG antibodies had a high signal when tested in the OLA ligation and detection when labeled with gold nanoparticles (**Figure 3.21**). Therefore, we selected these two antibodies for OLA detection moving forward.

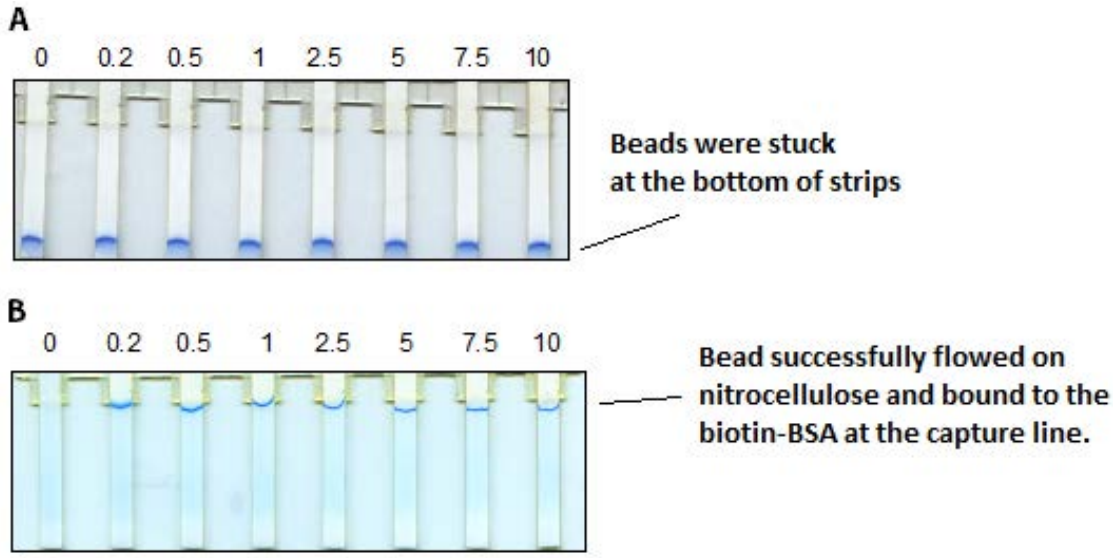

Figure 3.20 | Effect of buffer on lateral flow detection with streptavidin polystyrene beads.

The dried spot of different concentrations of BSA-biotin from left to right :0, 0.2, 0.5, 1, 2.5, 5, 7.5 10 mg/mL as labeled on top of each strip. Strips were scanned after being dipped into the blue bead solution diluted in (**A**) storage buffer from Bang's lab (**B**) lateral flow buffer by Epoch Biosciences. Images were scanned after 10 minutes after the bead solutions were introduced.

© Copyright 2021 | N Panpradist

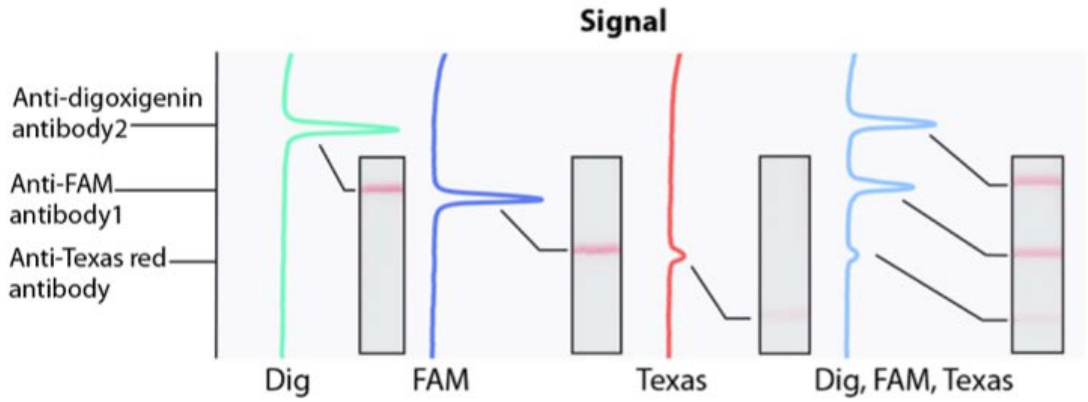

Figure 3.21 | Specific antibody pairs tested on the lateral flow detection.

Immobilized anti-D, Anti-F, and anti-Texas Red antibodies (Anti-T) were used to detect each or a mixture of synthetic ligated products (0.6μM Syn-D, Syn-F, and Syn-T) pre-mixed with gold nanoparticles coated with anti-biotin antibodies.

The result highlights the significance of buffer. For the successful flow of dyed streptavidin-coated microsphere, an optimized lateral flow buffer must be used. The component of the lateral flow buffer was listed along with the rationales for its roles in lateral flow buffer (**Table S3.6**). Streptavidin-coated microsphere (diameter ≤ 0.3 μm) has a very high surface-to-volume ratio. Hence, they are prone to aggregation. It is useful to sonicate the suspension before using it. Based on the conversation with Bang's bead company, the company also recommended washing the beads before use to remove the stabilizer or further dilute in the optimized buffer. This supports the idea of diluting the stock bead into the lateral flow buffer.

3.3.7 PREMIXING OF GOLD NANOPARTICLES AND THE PRODUCT FROM THE LIGATION STEP.

© Copyright 2021 | N Panpradist

Premixing streptavidin (detection molecules) to biotin moieties can lead to inaccurate results. This is because streptavidin has four binding sites. One molecule can bind to biotin moieties present in both wild-type and mutant ligated products, dropping assay accuracy depending on the location of the capture antibody on the strips (**Figure 3.22**).

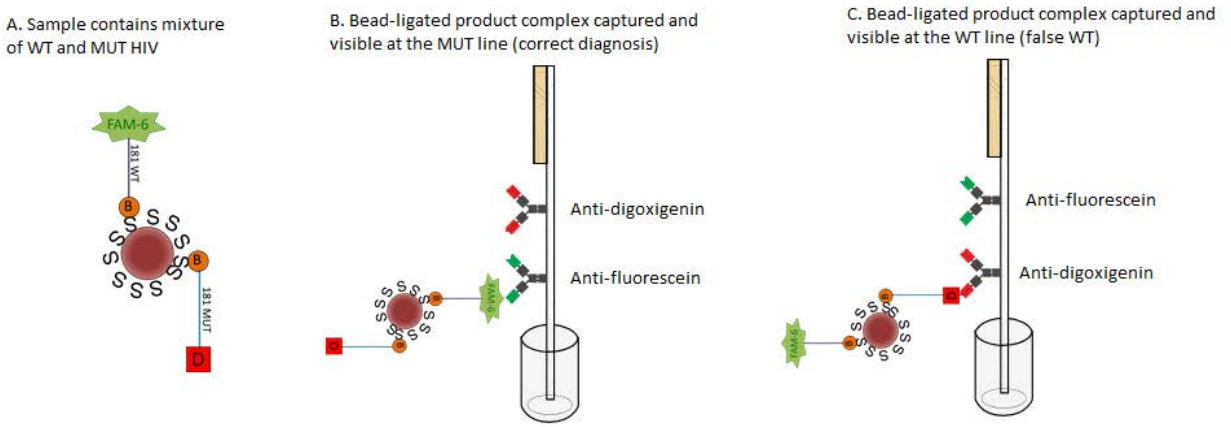

Figure 3.22 | Streptavidin-limited detection can cause false results.

(**A**) Schema of a 50% MUT and 50% WT sample, and in a streptavidin concentration-limited regime, two biotin moieties from WT and MUT ligated probes can bind to a single streptavidin bead. Depending on the location of the immobilized antibody, the bead will be captured at the first line and report the result as (**B**) MUT and (**C**) WT. Both are inaccurate reports of 50% samples, but only (**B**) would lead to the correct diagnosis.

We applied computational analysis to help calculate the amount of streptavidin labeling molecules to ensure each streptavidin binds to single biotin (**see Supplementary Information for MATLAB code**). Specifically, Monte Carlo's method was used to calculate the probability of each outcome assuming random binding of biotin to streptavidin in the determining system with 5,000 iterations (assuming no cooperative binding). The mean of each outcome of all iterations is reported in **Figure 3.23A**. We tested this model in a simple design

© Copyright 2021 | N Panpradist

with a free streptavidin model using ELISA set up (**Figure 3.23B**) to depict the only signal generated from WT and MUT ligated products bound to a single streptavidin molecule. We observed the trend matching our model; 100 streptavidin: biotin ratio led to nearly zero false signal compared to the case of 0.1 ratios (**Figure 3.23C**). Unfortunately, when we translated this model to streptavidin beads, we found inconclusive results across experiments.

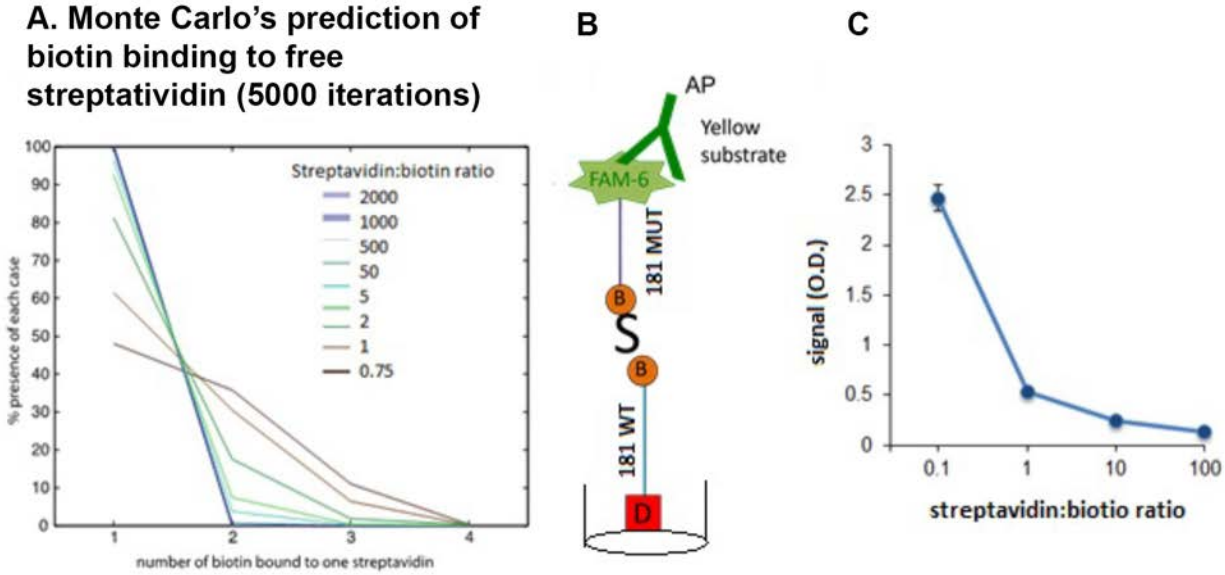

Figure 3.23 | Effect of streptavidin: biotin ratio on false MUT detection.

(**A**) Prediction of the proportion of single biotin bound to one streptavidin when using different streptavidin: biotin ratio. (**B**) Experimental design to detect multiple biotins bound to single streptavidin molecules. Only when ligated WT probe (181 WT) and MUT probes (181 MUT) bound to the same streptavidin, the signal is detected via ELISA. (**C**) Signal of a single molecule of streptavidin bound WT and MUT probes using different ratios of streptavidin: biotin (average of n=2).

We hypothesized that the variable results could be due to limited diffusion. If there was low mixing when the bead solution was introduced to the ligation reaction, one bead could still bind to multiple ligated products (**Figure 3.24A** and **Figure 3.24B**). To reduce this effect, we partially prefill the streptavidin

© Copyright 2021 | N Panpradist

binding sites on beads with biotinylated moieties before mixing with ligated products (**Figure 3.24C**). As the concentration of BSA-biotin to pre-block the streptavidin beads increased, we observed the correct signal distribution of WT and MUT ligated probes (**Figure 3.24D** and **Figure 3.24E**). The MUT/(MUT+WT) ratio of the case of streptavidin bead pre-blocked with 1mg biotin-BSA nearly matched the results from the 1st generation dipstick (**Figure 3.24F**).

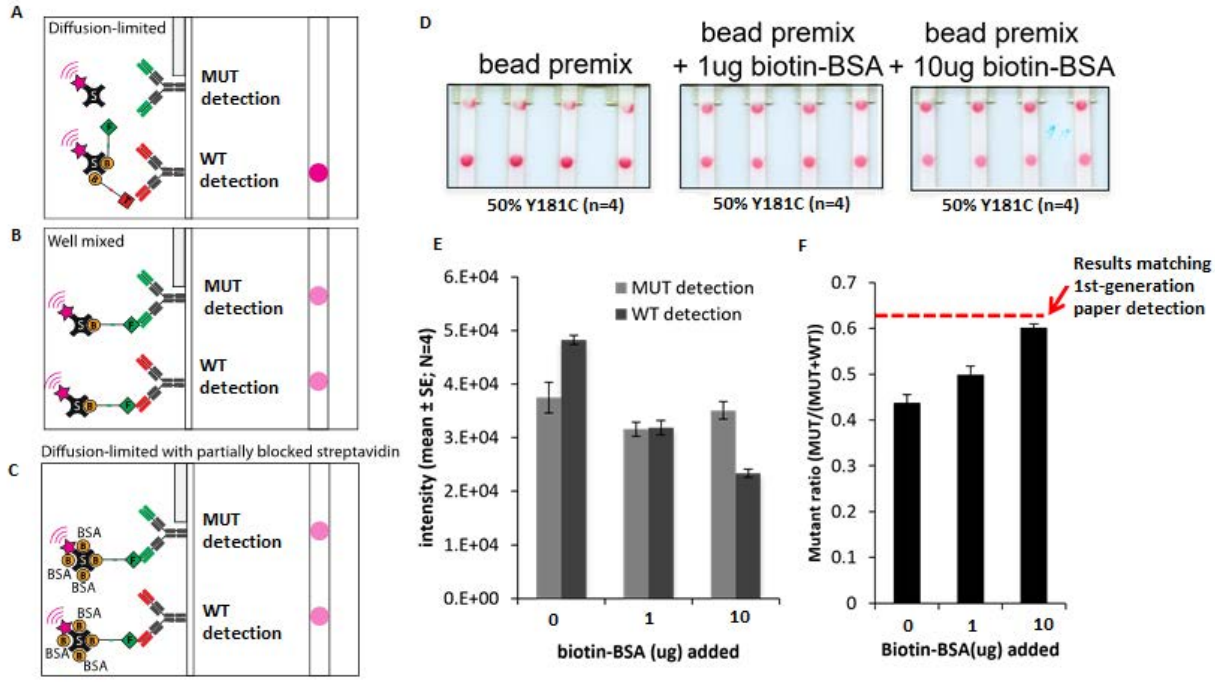

Figure 3.24 | Partially filled streptavidin reduced the effect of diffusion limit during the pre-mixing step.

(**A**) Expected results when diffusion is limited. (**B**) Expected results when diffusion is not limited, biotin molecules are well distributed across all streptavidin beads. (**C**) Expected results when the diffusion is limited, but streptavidin has a reduced binding capacity (prefilled with biotin-BSA). (**D**) Scanned results from all the cases. (**E**) Quantified MUT and WT signals. (**F**) Ratio of MUT / (MUT + WT).

© Copyright 2021 | N Panpradist

We applied this partially pre-filled streptavidin bead approach and competing oligo to detect 1-cycle and 10-cycle ligation products. However, we still observed a high WT background signal in the 100% MUT sample (**Figure 3.25**). This was not due to the inefficiency of completing oligo for strand displacement since we observed a similar signal for (**Figure 3.25C** and **Figure 3.25D**). By design, WT probes are present at a lower concentration than the MUT probes to boost the sensitivity for MUT detection. The inefficient toehold-mediated strand displacement would lead to a false MUT signal rather than a false WT signal. We suspect that this could be due to some cross-reactivity of the streptavidin beads, which tend to adhere to themselves, and insufficient vortexing/sonicating can lead to aggregation and possibly impaired performance.

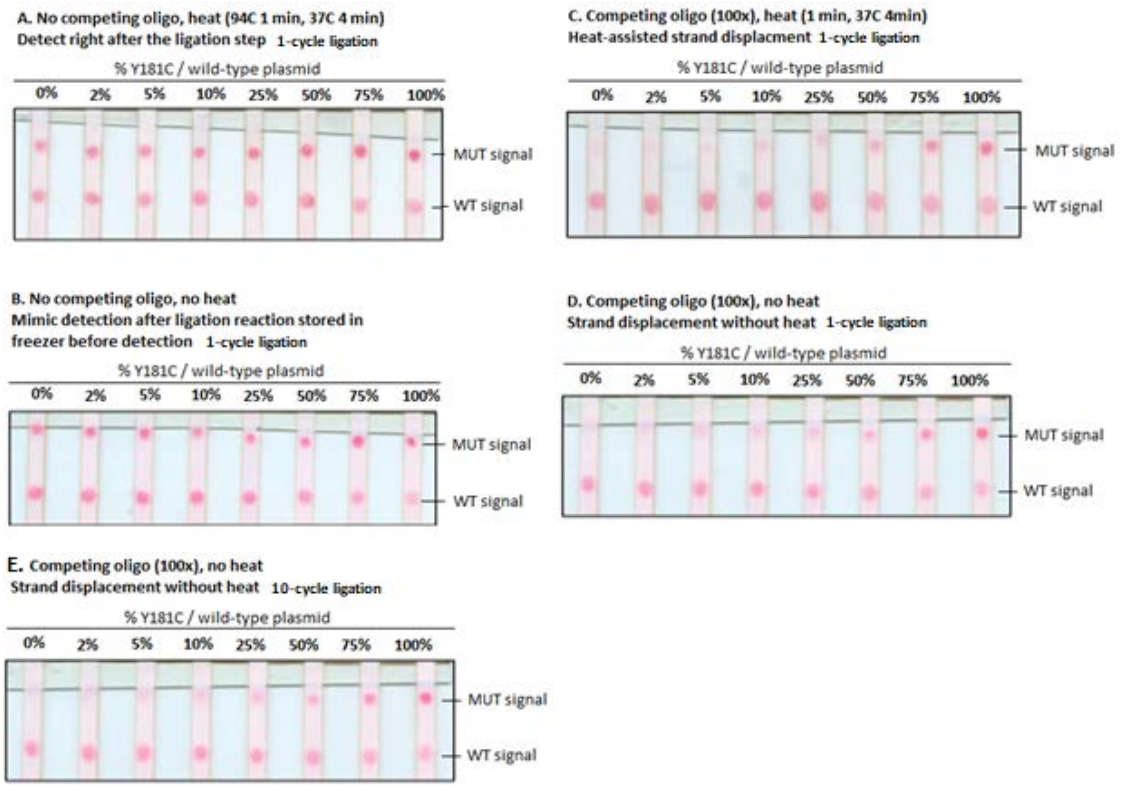

Figure 3.25 | Detection of ligation products with 1µg-BSA prefilled streptavidin microsphere beads.

© Copyright 2021 | N Panpradist

Pre-mixed of prefilled streptavidin microsphere beads with 1-cycle ligation product from Y181C standards (**A**) without competing oligo and with heat denaturing (**B**) without competing oligo and without heat denaturing (**C**) Competing oligo with heat denaturing and (**D**) with competing oligo without heat denaturing. (**E**) Pre-mixed pre-filled streptavidin microsphere beads with 10-cycle ligation product from Y181C standards.

3.3.8 THE FINAL VERSION OF 2ND-GENERATION PAPER DETECTION

We overcame diffusion-limited during the pre-mixing of gold nanoparticles (i) using anti-biotin gold with lower binding capacity per bead, (ii) using sequential delivery, and (iii) switching the anti-FAM antibody to the lower position. First, we used monoclonal anti-biotin antibody conjugated gold nanoparticles (~10^9 particles/μL 10OD stock with a binding capacity of ~11 biotin/particle or 1.1x10^{10} biotin-binding capacity/μL 10OD stock). Each 22μL ligation mixture has a maximum of 7.9 x 10^{11} copies of biotinylated probes. Still, we quantify that found that only 2% of the biotinylated probes were converted to ligated probes (1.7 x 10^{10} biotinylated probes) for a 100% mutant sample. For the sequential delivery method, the ligation product is added and then chased by the gold buffer. Only ligated probes are biotinylated, and we would need only 1.7 x 10^{10} biotinylated probes. At 1.1 biotinylated probes/binding capacity, we will need 1.5μL of 10OD stock (1.7 x 10^{10} ligated products/1.1x10^{10} biotin binding capacity/μL). To be conservative and have enough for the flow control line, 3μL 10OD stock was used.

Additionally, the multi-probe binding to the beads would cause the reduced sensitivity for the detection of whichever assay of which capture line appeared later in the flow (**Figure 3.22**). To avoid any possibility of the MUT signal being

© Copyright 2021 | N Panpradist

compromised due to any premixing of the gold solution to the tail end of the ligation fluid, we switched the position of the capture antibodies. These approaches were used in the final 2nd generation paper-based detection and resulted in sensitive and specific detection. The 2nd-generation paper detection was used as part of the OLA-Simple 1.0 kit (see **Chapter 5**).

Current Paper-Based Detection Can Detect Amplification Products To Verify Hiv Infections in replacement of gel electrophoresis and potentially can be used as a method to detect viral loads from RNA samples, which will be further discussed in **Chapter 6**. **Figure 3.26** shows an example of our detection of HIV amplicon on paper detection.

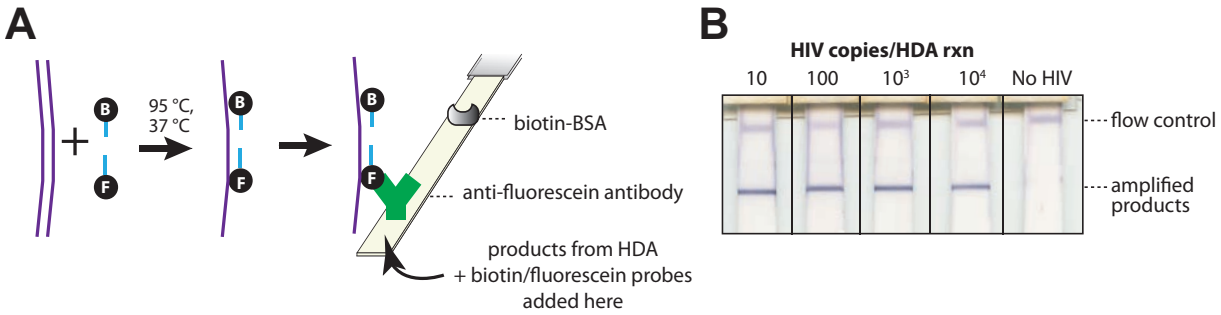

Figure 3.26 | Paper-based detection for amplification products.

(**A**) To detect the amplified HIV target, we used the hybridization of tagged probes. Biotinylated and fluorescein probes complementary to the reverse strand were mixed with the template and added to the membrane. The captured duplexes with biotin moieties were then labeled from streptavidin-conjugated alkaline phosphatase and purple substrate to create visual bands. (**B**) All amplification products at various HIV input copies can be detected using our method.

© Copyright 2021 | N Panpradist

3.4 GENERATION 3: SINGLE-STEP, SEQUENTIAL DELIVERY PAPER-BASED DETECTION

Variable performance of toehold-mediated strand displacement across ligation products of different codons was observed when the strand displacement underwent 5-minute incubation at room temperature before the detection. Thus, in the 2nd generation reaction, we used heat denaturing (95 °C 1 minute) and hybridization (37 °C 4 minutes) to speed up the displacement step and ensure reliable detection outcome (**Figure 3.18E**).

We investigated the effects of multiple variables on strand displacement rates and developed a new approach to overcome poor strand displacement reactions.

3.4.1 INVESTIGATION OF TOEHOLD STRAND DISPLACEMENT RATES IN OLA BUFFER WITH EXCIPIENTS.

Toehold-mediated strand displacement in the solution can take more than 20-30 minutes to achieve 100% completion[23]. However, the rates can be impacted by different variables, including salts and pH. Thus, we designed an experiment to measure the rate of toehold-mediated strand displacement in the buffer condition used in OLA. We designed the target HIV strand that has regions (a and b) complementary to the ligated G190A probe region (a' and b') and toehold region (c) downstream of the G190A probe, which can be hybridized to the invading strand (*i.e.*, competing oligo) to initiate strand displacement. If the invading strand successfully displaced the ligated probe, the BHQ1

© Copyright 2021 | N Panpradist

quencher of the target would be apart from the FAM of the ligated probe, emitting the signal (**Figure 3.27**).

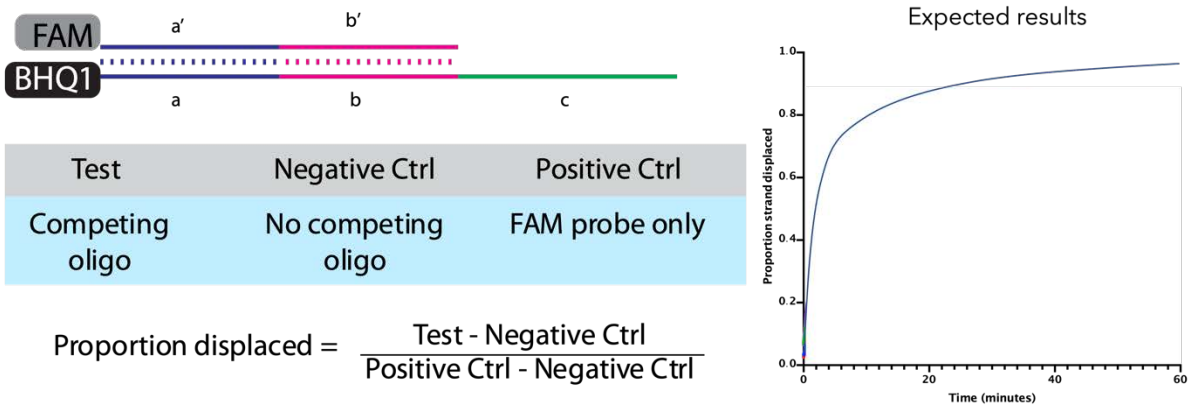

Figure 3.27 | Experimental design to investigate toehold-mediated strand displacement in OLA buffer.

Duplex of mock target strand with 3' BHQ1 quencher is hybridized to the mock ligated probes with 5' FAM. Without strand displacement (negative control), FAM is in proximity with BHQ1, and the BHQ1 quencher absorbs the emitted signal from FAM. In the test case, the competing oligo is added, and if displacement occurs, the mock ligated probes with 5' FAM are released, and the signal from FAM is emitted. Only the mock ligated probe was added in the positive control case, so the FAM signal is always on. The reaction was measured during the one h incubation period at room temperature. The expected results of the test case are shown in the right graph.

Effect of toehold lengths. 6-8 nucleotide toehold length was reportedly yielded the maximum rate of toehold-mediated strand displacement[24]. We observed similar findings in the OLA buffer system (**Figure 3.28**). Longer toehold sequences do not necessarily increase the displacement rate and yield as the overhang region might form a secondary structure.

© Copyright 2021 | N Panpradist

Effect of competing oligo concentrations. We used 6-nucleotide long toehold competing oligo in this experiment. 4-fold competing oligo concentration higher than ligation probe concentration increased the displacement rate from 1-fold to 2-fold of competing oligo concentrations were used (**Figure 3.29**). Competing oligo concentration at 10-fold concentration did not seem to improve the speed. The maximum yield was ~70% displacement in 30 minutes.

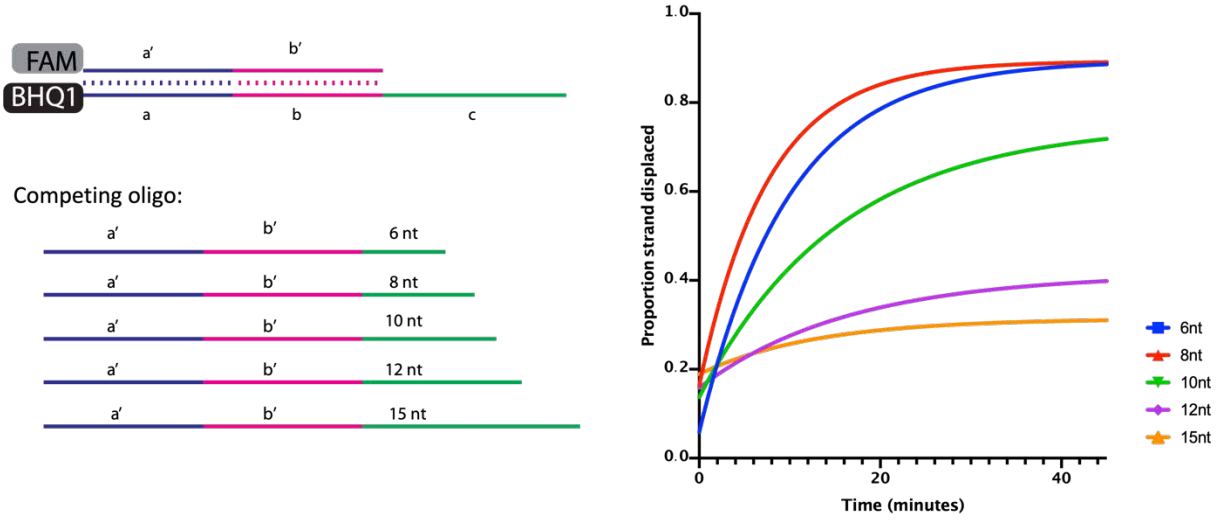

Figure 3.28 | Effect of toehold length on strand displacement in OLA buffer.

800nM 6-, 8-, 10-, 12-, and 15-nucleotide toehold competing oligo was added to the reaction containing 200nM each mock ligated probes (5'FAM-a'-b') and mock target (3' BHQ1 a-b-c) and read FAM channel for 1 hour at room temperature. The exponential fit of the proportion strand displaced vs. time was plotted. The exponential fit was performed by Prism.

© Copyright 2021 | N Panpradist

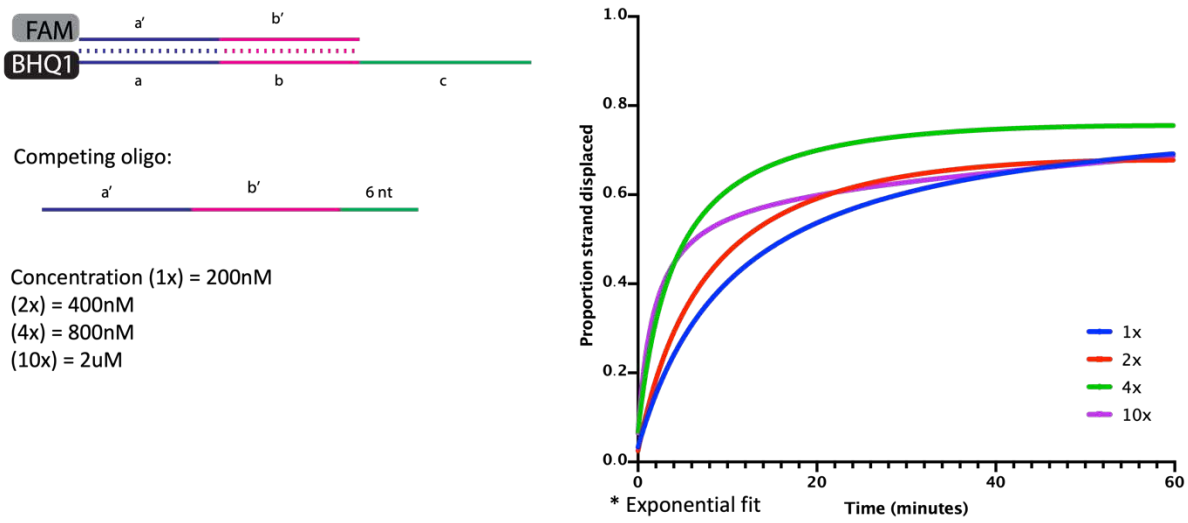

Figure 3.29 | Effect of competing oligo concentrations on toehold-mediated strand displacement.

200nM, 400nM, 800nM, or 2μM 6-nt toehold competing oligo was added to the reaction containing 200nM each mock ligated probes (5′FAM-a′-b′) and mock target (3′ BHQ1 a-b-c) and read FAM channel for 1 hour at room temperature. The exponential fit of the proportions strand displaced versus time was plotted. The exponential fit was performed by Prism.

Effect of polymorphisms in toehold regions. Mismatched sequences in the toehold regions could drastically impact the rate of toehold-mediated strand displacement [25]. Here we varied the sequences in the competing oligo strand to contain different polymorphisms in the HIV genome [26]. A mismatched nucleotide (indicated as "x") outside the toehold region did not significantly impact the displacement rate (**Figure 3.30**). However, we observed a drastic drop in the displacement yield from 70% to 50% when a mismatched nucleotide was introduced in the toehold region. Two to three mismatches in the toehold region resulted in only 10-20% displacement yield. For the case of two mismatched in toehold, we further investigate the use of SuperT (5-hydroxybutynyl-2′-deoxyuridine) and SuperG (8-aza-7-deazaguanosine). SuperT can stabilize the duplex and increase its melting

© Copyright 2021 | N Panpradist

temperature. SuperG can reduce naturally occurring secondary structures found in guanine-rich sequences[27]. We found that the use of SuperT and SuperG can reverse the impact of polymorphisms in the toehold region, yielding the rate and yield comparable to the case without polymorphisms in the toehold region (**Figure 3.31**).

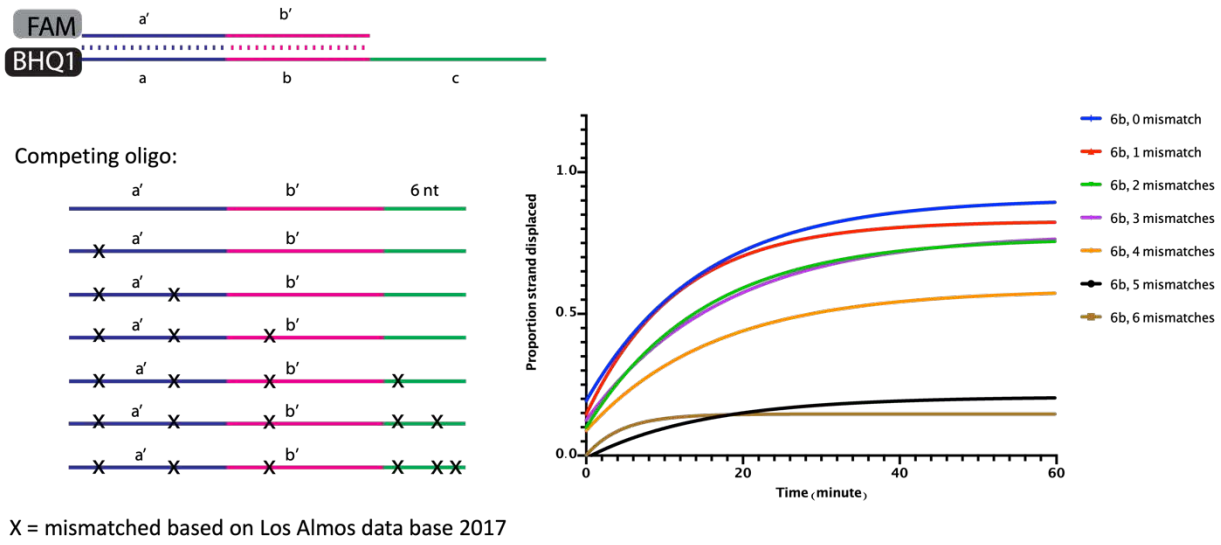

Figure 3.30 | Effect of polymorphisms on toehold-mediated strand displacement.

"x" mismatched nucleotide found in the HIV genome was added at a different location in the competing oligonucleotide. 800nM of each competing oligo was added to the reaction containing 200nM each mock ligated probes (5'FAM-a'-b') and mock target (3' BHQ1 a-b-c) and read FAM channel for 1 hour at room temperature. The exponential fit of the proportions strand displaced versus time was plotted. Exponential fit was performed by Prism.

© Copyright 2021 | N Panpradist

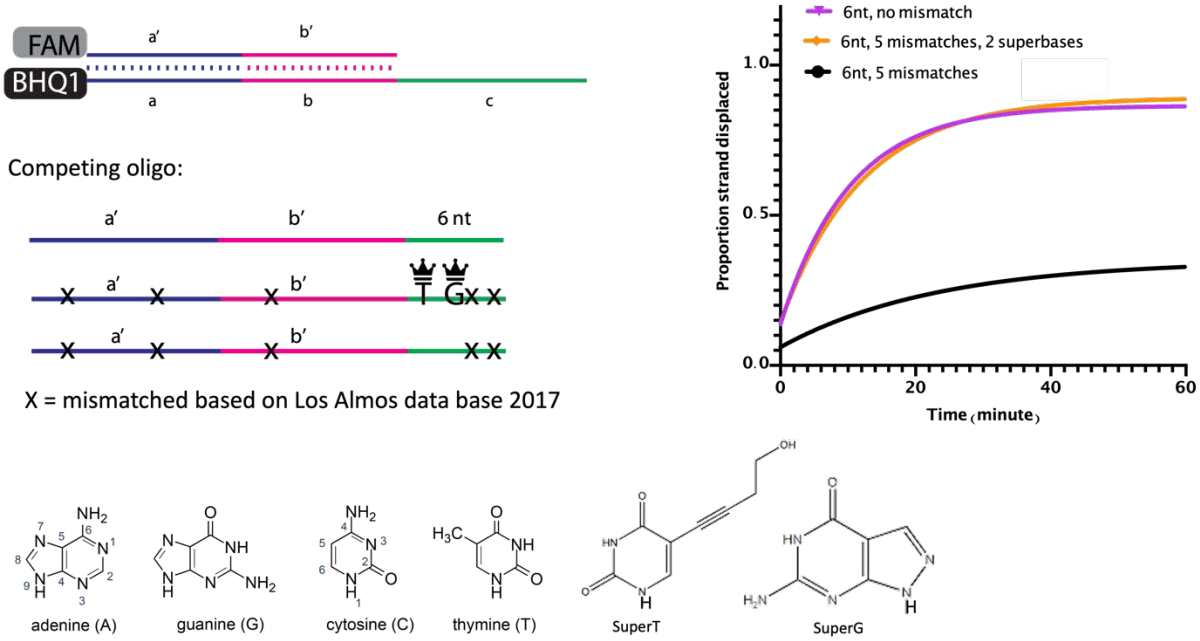

Figure 3.31 | Effect of modified bases (SuperT and SuperG) on improving polymorphisms. The displacement rates using 800nM competing oligo without and without 2 mismatched nucleotides in toehold regions were compared to the competing oligo with 2 mismatched nucleotides, 1 SuperT, and 1 SuperG substitution. The competing oligo was mixed with 200nM each mock ligated probes (5'FAM-a'-b') and mock target (3' BHQ1 a-b-c), and the mixture was read FAM channel for 1 hour at room temperature. The exponential fit of the proportions strand displaced versus times were plotted. The exponential fit was performed by Prism.

Effect of displaced length in toehold regions. Only non-ligated probe: amplicon duplex can lead to false WT or MUT signal. As a result, the displacement of the full-length ligated products is not necessarily. A non-ligated 25-nucleotide probe can be displaced 100% within 8-10 minutes with 6-nt competing oligo (**Figure 3.32**). Thus, using two competing oligos to displace the non-ligated probes would improve the speed in strand displacement at room temperature.

© Copyright 2021 | N Panpradist

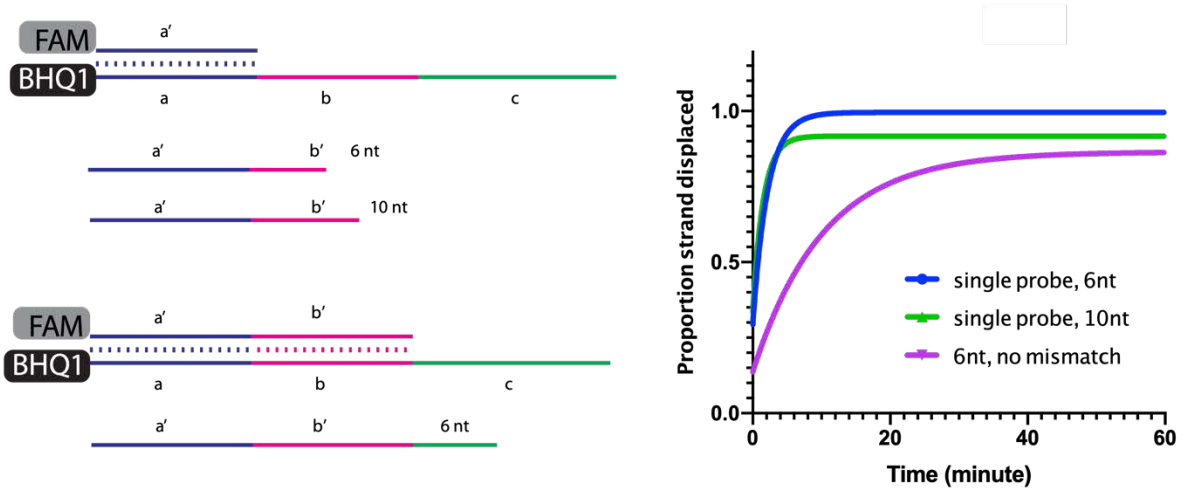

Figure 3.32 | Effect of displaced length on toehold-mediated strand displacement.

800nM 6-nt or 10-nt toehold competing oligo was added to the reaction containing 200nM mock ligated probes (5'FAM-a'-b') or mock unligated probes (5'FAM-a') with 200nM mock target (3' BHQ1 a-b-c) and read FAM channel for 1 hour at room temperature. The exponential fit of the proportions strand displaced versus times were plotted. Exponential fit was performed by Prism.

Summary. Depending on regions in the genome, toehold regions should have less secondary structure and are more accessible for invading strands. 4x competing oligo (invading strand) faster than 1x, but 10x did not improve speed. Polymorphisms in toehold regions drastically reduce rates and yields but incorporating Superbase™ in toehold region improves displacement rate in highly polymorphic toeholds. Lastly, Single-probe (25nt) displacement is ~4 times faster than two-probe (50nt) displacement.

3.4.2 TOEHOLDS NEAR HIV LIGATION PROBES HAVE DIFFERENT LEVELS OF SECONDARY STRUCTURES

© Copyright 2021 | N Panpradist

Secondary structures in HIV genomes and/or polymorphism have been shown to inhibit reliable strand displacement[28]. We predicted secondary structures of the DNA in and near the probe regions during the ligation reaction. G190A probe region has a much more accessible toehold compared to K65R, and this would make strand displacement of K65R probes much slower and possibly a lot less yield (**Figure 3.33**).

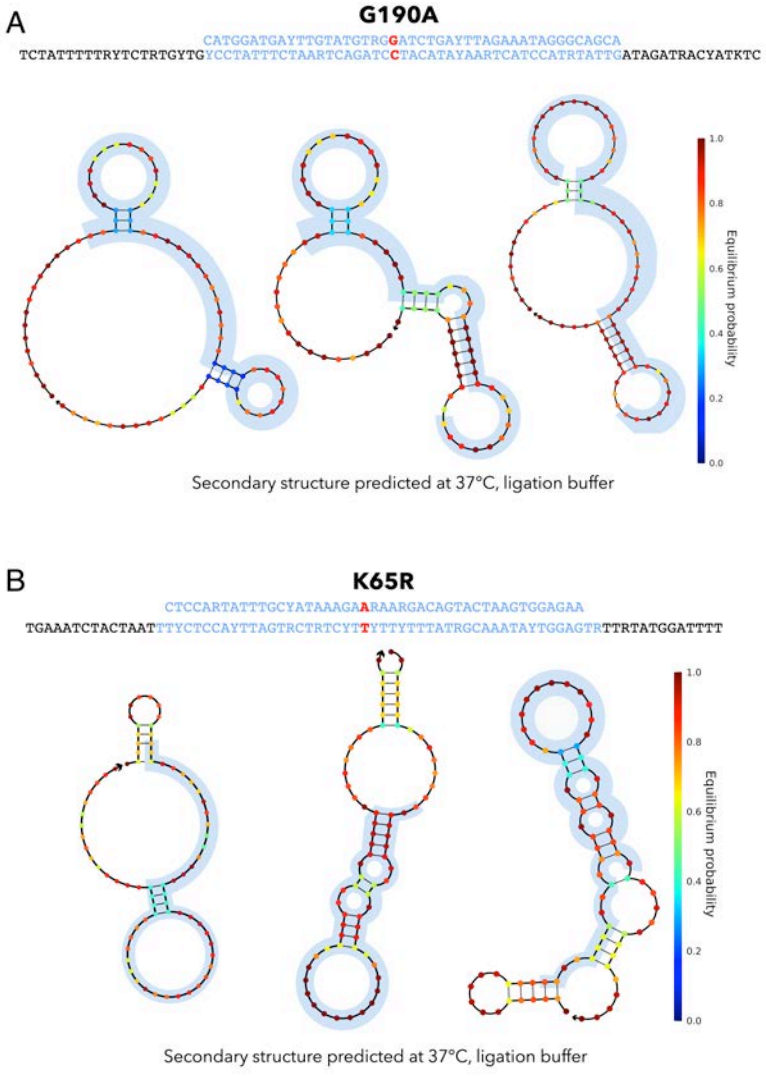

Figure 3.33 | Secondary structures of single-stranded HIV DNA near and within the probe regions.

© Copyright 2021 | N Panpradist

Secondary structures of the DNA probe sequences (highlighted in blue shadow) and the region that would have been the toehold after DNA: probe hybridization occurs. (**A**) G190A probe (**B**) K65R probe. Secondary structures were predicted under the salt and temperature concentrations using NUPACK.

3.4.2 OVERCOMING SECONDARY STRUCTURES IN TOEHOLD REGIONS OF ENDOGENOUS HIV SEQUENCE

Figure 3.34A shows the new probe design to include the adapter regions at the 3’ and 5’ ends for specific probes (WT or MUT) and common probes, respectively. Adapter regions can serve as the toehold that allows two competing oligos to displace, making the initiation of toehold-mediated strand displacement fully controllable by design. Additionally, the displacement occurred within five minutes, and

© Copyright 2021 | N Panpradist

its speed was not impacted by background human genomic DNA up to 2µg in the reaction (**Figure 3.35**).

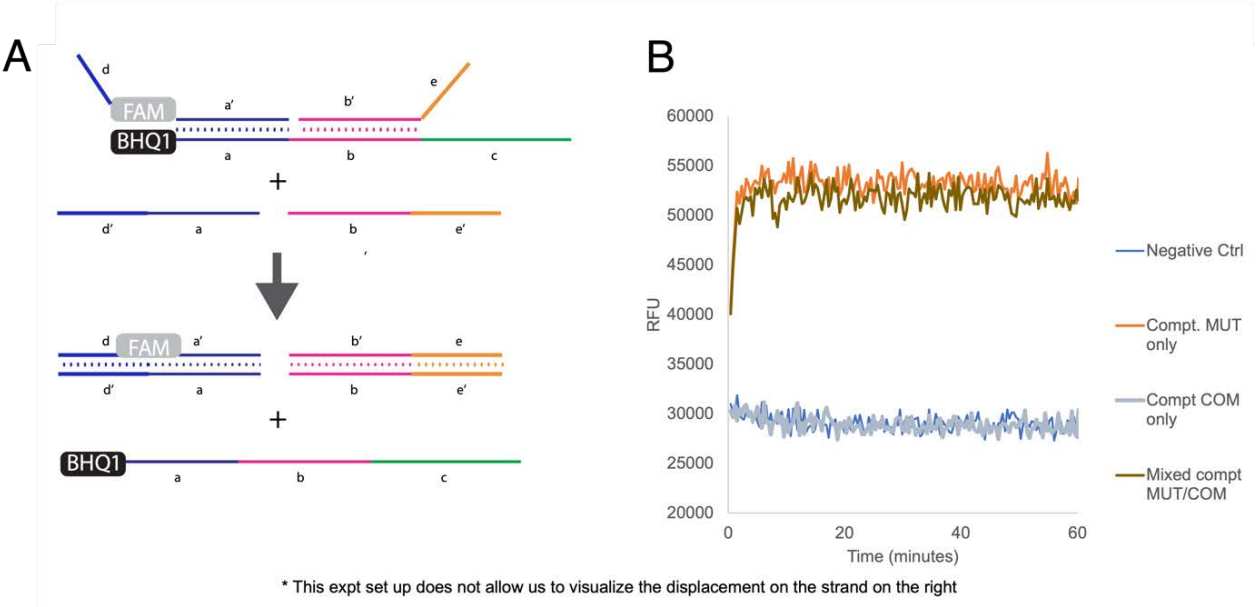

Figure 3.34 | Novel design of the ligation probe adapter to overcome issues with endogenous HIV sequence.

(**A**) Adapter regions (d and e) are added to each mock non-ligated probe. Two competing oligos bind to the toeholds, the engineered adapters, and start toehold-mediated strand displacement. (**B**) FAM signal measured during 1h-incubation at room temperature from the reaction containing 800µM competing oligos, 200µM each of mock target (BHQ1-a-b-c), unligated probes (d-FAM-a') and (b'-e). Amy Oreskovic suggested the idea from the adapter probe.

© Copyright 2021 | N Panpradist

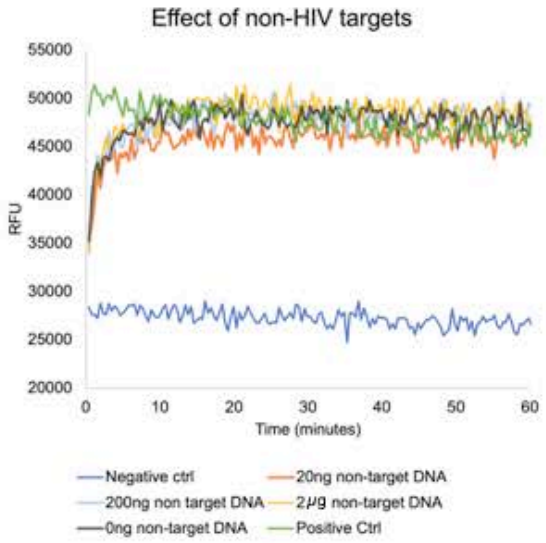

Figure 3.35 | Effect of human genomic DNA on engineered toehold-mediated strand displacement.

FAM signal measured during 1h-incubation at room temperature from the reaction containing 800μM competing oligos, 200μM each of mock target and unligated probes in the presence of 0 – 2μg human genomic DNA.

3.4.3 ON-PAPER STRAND DISPLACEMENT

MATERIALS AND METHODS.

Experimental setup. All DNA oligonucleotides used were conjugated to a Texas Red fluorophore (IDT). Fluorescence measurements were made in the "glow box" (**Figure 3.36**) by exciting the fluorophore with 470 nm green light (470 nm). The Signal was captured by an iPhone 8 camera (Apple Inc.) covered with a 650 nm filter (Thor Lapse). Time-lapse images were taken through the Lapse-it application with exposure settings of 1/9.0 aperture speed and 536 ISO speed. To investigate the speed of strand displacement on paper, we either add liquid competing oligo to the pad or lyophilized competing oligo the glass fiber pad to test the on-paper

© Copyright 2021 | N Panpradist

strand displacement. Then, we introduced the (mock target: mock ligated probe) duplex to the glass fiber pad with (test case) or without competing oligo (negative control). For the positive control, we only load the mock ligated probe on the glass fiber pad without competing oligo.

***Computational analysis tool for fluorescent detection*.** This analysis tool was adapted from one of the LDA unit vectors (discussed later in this chapter). David McIntyre altered the unit vector to measure the Texas-red fluorophore and automating measurement across each frame in the time-lapse. MATLAB algorithms can be found in Supplementary Information[29].

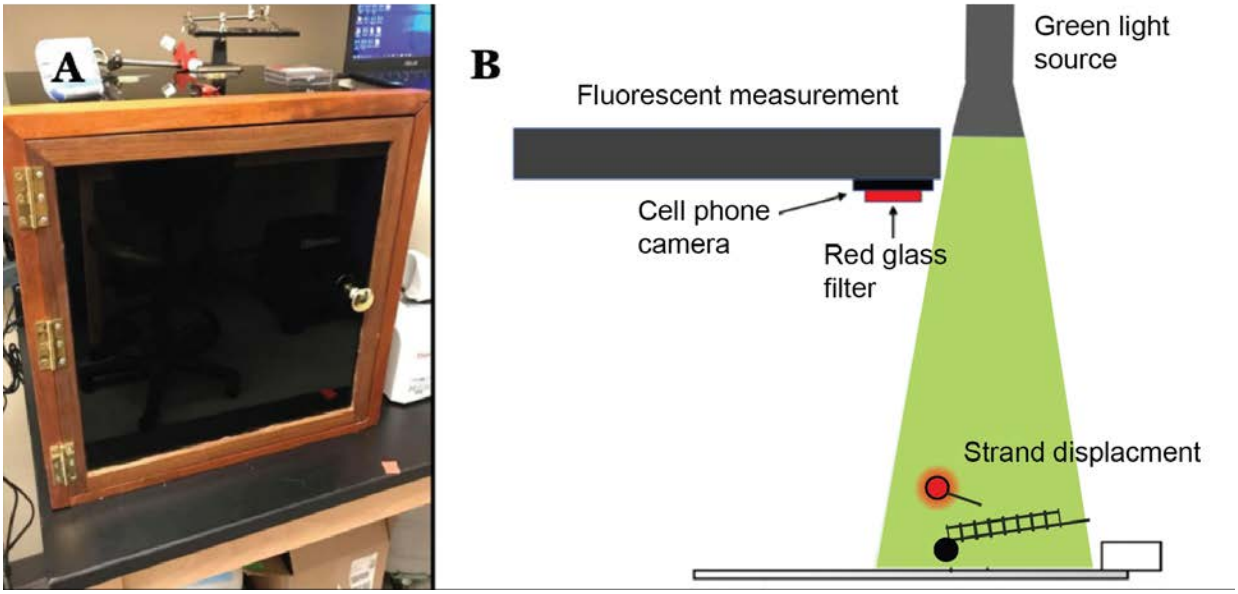

Figure 3.36 | **Schematic of the fluorescence measurement system.**

(**A**) All measurements are made inside of a closed "glow-box" to prevent exposure to external light developed by the Yager lab. (**B**) Quantification of fluorescence signal. The image was adapted from David McIntyre's capstone report[29].

Results. We observed 70% of toehold strand displacement after 18 minutes when the two pads: (i) the competing oligo pad and (ii) the (mock target with quencher:

© Copyright 2021 | N Panpradist

mock ligated probes with Texas Red) mixture, were brought in contact (

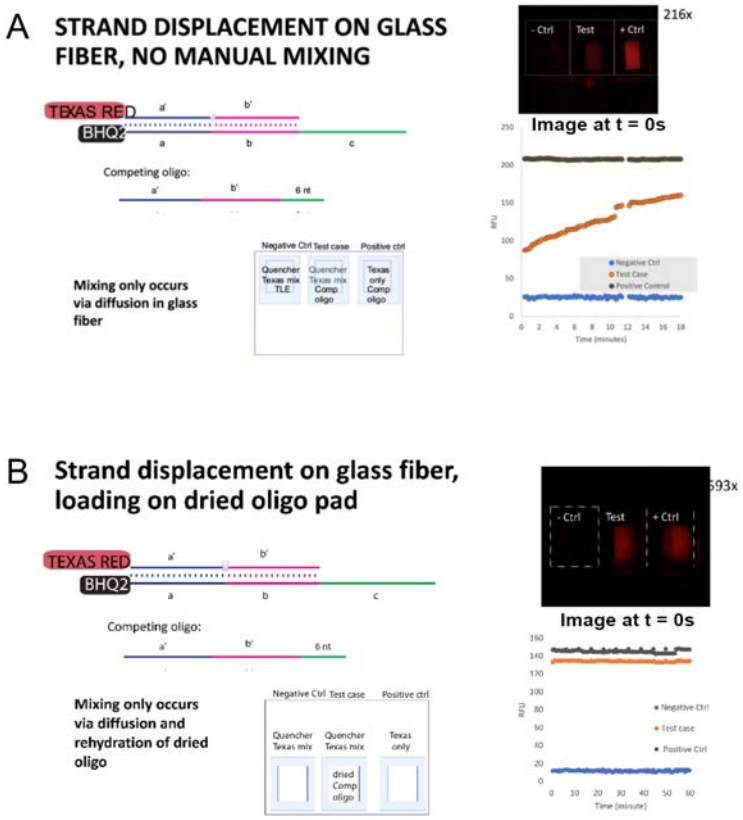

Figure 3.37**A**). The displacement here occurred at speed similar to the reaction in the solution phase (**Figure 3.28**). In contrast, we observed the displacement

© Copyright 2021 | N Panpradist

occurred in the first few minutes (

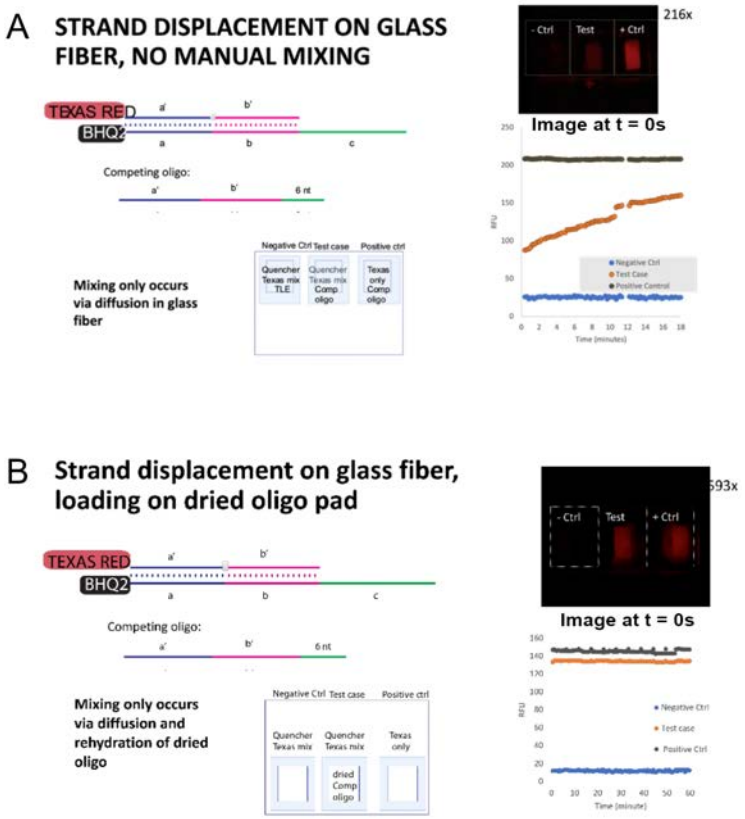

Figure 3.37**B**) when adding the mixture of the mock target with a quencher and mock ligated probes with Texas Red to rehydrate the lyophilized competing oligo on the pad. This was because the mixture fluid was forced to enter the tortuous

© Copyright 2021 | N Panpradist

pores of the dry pad and interacted with the competing oligo. In contrast, in

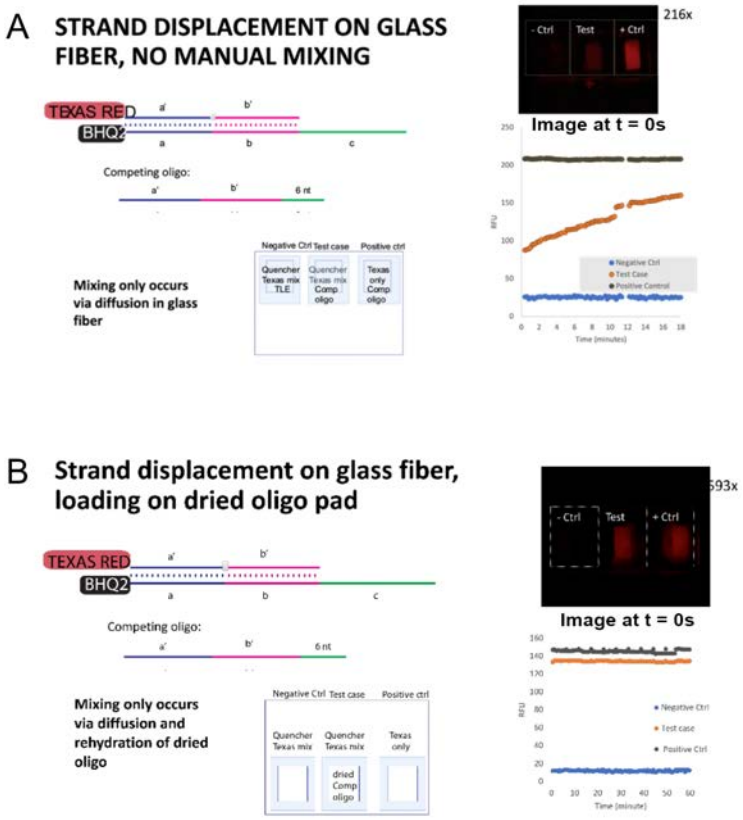

Figure 3.37**A**, the two pads were full, and mixtures only interacted via passive diffusion.

© Copyright 2021 | N Panpradist

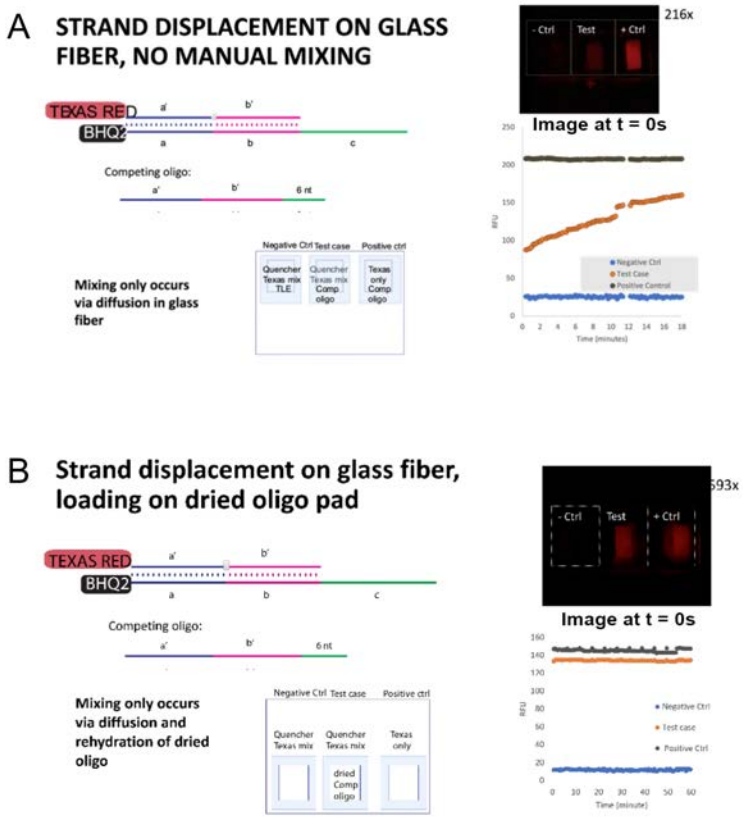

Figure 3.37 | Toehold-mediated strand displacement on paper.

(**A**) 800μM competing oligo solution (a'-b'-6nt complementary to c region) was added to a pad for the test case. For the negative and positive control, TLE buffer was added to the pad instead. This set of pads was brought in contact with another set of pads preloaded with the mixture of mock target and mock ligation probes for the negative and test cases. A pad preloaded with mock ligation probes only for positive cases. Texas signal was extracted from the regions of the pad across 16min-incubation time. (**B**) 800μM dried competing oligo (a'-b'-6nt complementary to c region) was rehydrated with the mixture of the mock target (BHQ2-a-b-c) and mock non-ligated probes (Texas red-a'-b' and b'). Texas signal was extracted from the regions of the pad across 1h-incubation time.

3.4.4 INTEGRATED SYSTEM FOR DETECTION IN A SINGLE STEP.

Our lab demonstrated an autonomous sequential delivery using pseudo **2DPN** (two-dimensional paper network). Here the fluid (green, red, and yellow) was preloaded in multiple capillary tube sources and contacted the paper [30]. The source exposed to the negative pressure of the paper drained first. The rest of the fluid

© Copyright 2021 | N Panpradist

sources remained in the capillary tubes due to no pressure difference (**Figure 3.38**). After the first tube drained, the second would start draining and so forth. This microfluidic principle will allow us to program the fluid in the paper network to release in a controlled spatial and temporal sequence without any external pump.

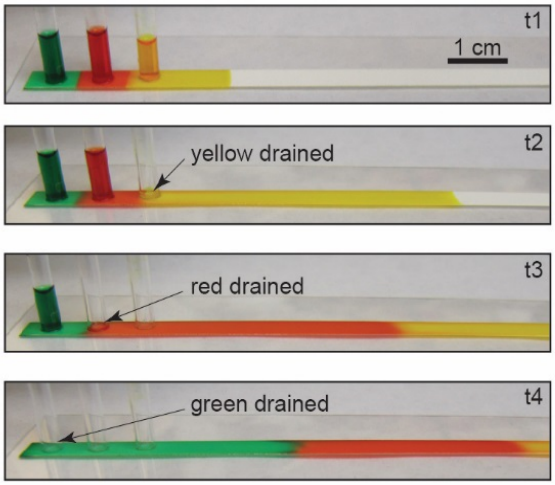

Figure 3.38 | Autonomous pseudo 1DPN sequential fluid delivery [30].

We used a folding card, which adapted the 1DPN model by using glass fiber pads as fluid reservoirs instead of capillary tubes (**Figure 3.39**). We tested the effect of sequential delivery of ligation product, competing oligo using the new adapter probe design, and the gold solution. **Figure 3.40** showed successful in-flow strand displacement false signal from the ligation reaction without ligase was eliminated.

© Copyright 2021 | N Panpradist

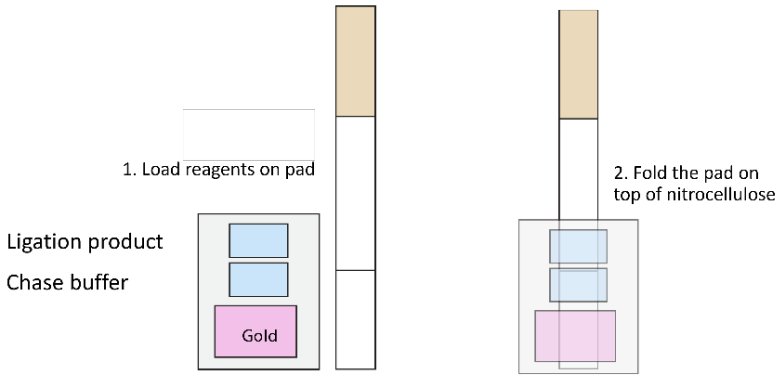

Figure 3.39 | Set up for sequential delivery for 3rd generation paper-based detection.

Left: A plastic sheet was loaded with a series of glass fiber pads with the capacity of 25µL, 25µL, and 60µL from top to bottom, respectively. Reagents can be loaded on the pad from top to bottom: ligation product, competing oligo, and gold solution. The plastic card with the pads was folded on top of the nitrocellulose dipstick to initiate the detection.

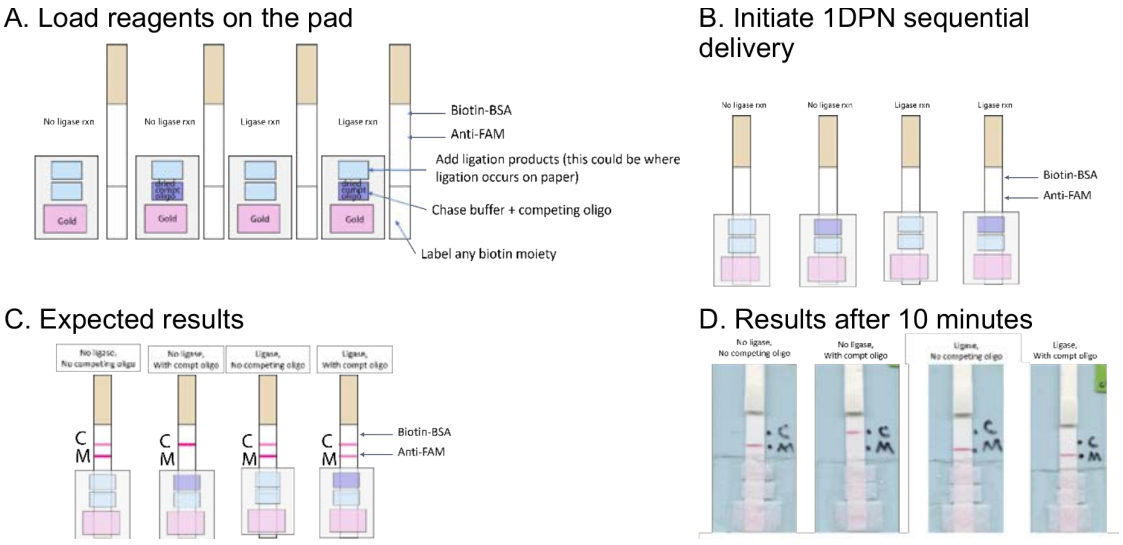

Figure 3.40 | 3rd-generation paper detection of HIVDR ligation reaction.

3.5 ALTERNATIVE CAPTURE MOLECULES TO ENABLE MULTIPLEXED DETECTION OF HIVDR

© Copyright 2021 | N Panpradist

Contributors: Nuttada Panpradist, Robert G Atkinson, Annie Wong-On-Wing, Nikki Higa, Ian Andrews, and David McIntyre. **Contributions**: RGA designed engineered barcodes. NP, AW, NH, IA, and DW performed experiments. NP analyzed the data.

MATERIALS AND METHODS

Anchoring barcode DNA via UV-crosslinked thymine residues. Strips were prepared as previously described[29]. Sartorius UniSart CF95 nitrocellulose membrane (25 x 300 mm) was to the middle section of the DCN backing card (DCN Diagnostics MIBA-020; 60 x 300 mm). All capture molecules were loaded and dispensed 30 mm from the bottom of the sheet with a reagent striper (Biodot ZX1010 Frontline HR) at a rate of 1 µL/cm for 1 mg/mL proteins or 0.4 µL/cm for 400µM nucleic acids. Poly-thymine tail-containing DNA oligonucleotides were then subject to 10-min UV irradiation (Fisher Scientific UV Crosslinker FB-UVXL-1000). After overnight drying in a desiccator, membranes were attached to a conjugate pad (Millipore GFCP 203000; 23 x 300 mm), cut into 4.5 mm strips (Kinbio Tech Co. ZQ2000) and an absorbent pad (Whatman CF7; 22 x 17.5 mm). Strips were stored at 4℃ until use.

3.5.1 FOR MULTIPLEXED DETECTION, WE DEVELOPED HIGHLY SPECIFIC COMPUTATIONALLY DESIGNED NUCLEIC ACID BARCODE PAIRS.

We aim to combine all 6 SNPs in one strip, which requires six unique binding pairs. Initially, we tested commercially available hapten-antigen pairs. We found only three pairs bound specifically to their intended partners: anti-

© Copyright 2021 | N Panpradist

fluorescein antibody/fluorescein, anti-digoxigenin antibody/digoxigenin, and anti-texas red antibody/ texas red. As a result, we need an alternative for molecular binding pairs. To address this issue, we are collaborating with another Ph.D. student in our lab (a former software engineer at Microsoft) to design non-natural DNA barcode pairs. These are normal DNA, but the sequence is chosen so that they do not cross-react with other pairs and do not cross-react with known organisms in the sample. We evaluated the specificity of these engineered DNA barcodes (**Figure 3.41**). At room temperature, in the presence of 10^{11} HIV DNA copies, these barcodes are only bound to their matching pairs. This is a significant success because the barcodes have a melting temperature at ~60 C. Normally, at the temperature well below the melting temperature, DNA binding is expected to be non-specific, but we observed nearly zero non-specific interactions here. This feature makes our engineered barcodes robust to temperature changes for use at point-of-care.

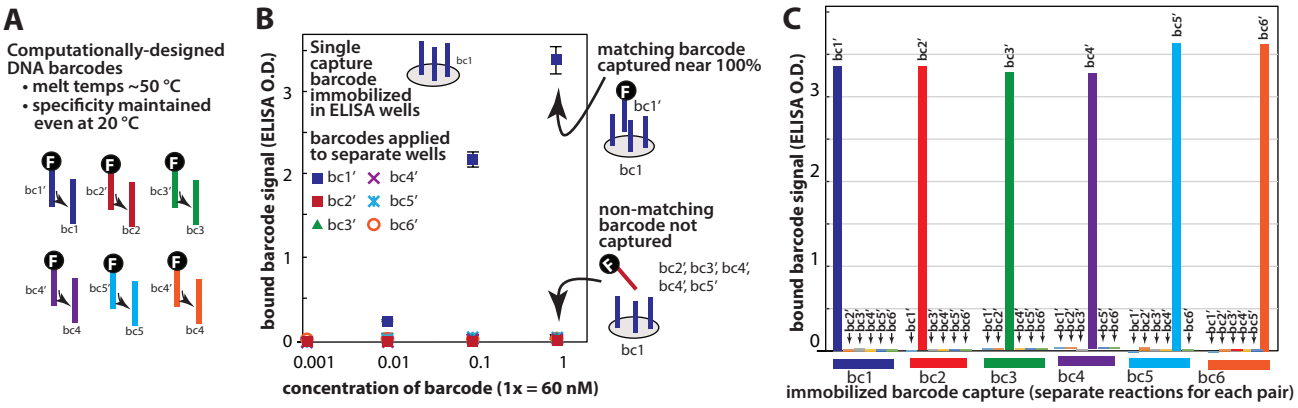

Figure 3.41 | Our high specific computationally designed DNA barcodes.

(A) Six pairs of engineered DNA codes were designed to have non-natural sequences. Each barcode has a melting temperature at of ~50 °C. **(B)** Each barcode was tested for its specificity using ELISA. A single

© Copyright 2021 | N Panpradist

barcode sequence was immobilized onto ELISA well, and all complementary barcode pairs were introduced to a bind to an immobilized barcode. Matching barcode pairs were found to have near 100% binding sensitivity. **(C)** All six barcodes were found to only bind to their own matching pairs.

Another challenge for using a DNA-DNA barcode system to replace antibody-hapten pairs is that the DNA-DNA hybridization may not be fast enough. Not all ligated products will be captured as they flow in the paper if this is the case. As a fallback approach for DNA-DNA barcodes, we also tested commercially available nucleotide analogs that have been shown to have faster hybridization than DNA barcode pairs in our buffer system. Locked nucleic acid (**LNA**) has modified bases to allow for closer base stacking.[27,28] Peptide nucleic acid (**PNA**) has a charge-neutral peptide backbone to allow for a more favorable PNA-DNA pair binding than DNA-DNA pairs with repulsive, negatively charged phosphate backbones.[29] Our preliminary data showed a slight improvement and decreased sensitivity compared to DNA-DNA pairs when using LNA-LNA and PNA-DNA barcodes, respectively **(Figure 3.42**).

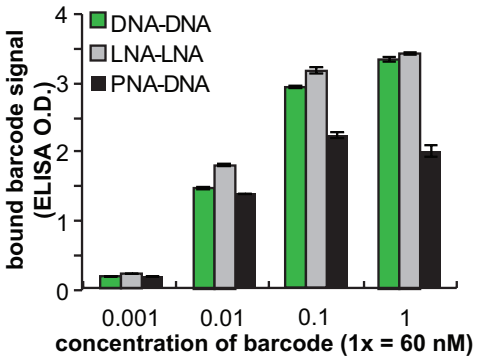

Figure 3.42 | Sensitivity of DNA derivative barcodes.

The sensitivity of our DNA-DNA barcodes is comparable and better than LNA and PNA systems, respectively. A single matching barcode pair was tested for the sensitivity in DNA-DNA, LNA-LNA, and PNA-DNA systems using ELISA similarly to **Figure 3.41**.

© Copyright 2021 | N Panpradist

3.5.2 PAPER-BASED MULTIPLEXED DETECTION USING SPECIFIC BAR-CODE NUCLEIC ACID PAIRS.

We considered different approaches to anchor the DNA barcodes onto the paper membranes (see Supplementary information on other options). Thymine-20 (T20) and Cytosine-20 (C20) have been used as adapters to DNA probes to aid immobilization on glass slide[31]. To transfer the engineered DNA barcode detection system from plate-ELISA format into a paper-based format, we added a poly(thymine)$_{20}$ tail (T20) to the 5' end of the oligonucleotide barcode - probe, the sequence can be immobilized to nitrocellulose membrane via UV-crosslinking. To test the barcodes' sensitivity and specificity on paper, we striped one membrane with four barcodes. Our preliminary data (**Figure 3.43**) showed excellent specificity and sensitivity at 10% HIVDR (~0.6 nM ligated probes). However, we observe unequal intensities of lines from different barcodes. We suspected that this could be the DNA barcodes' sequence-dependent behavior that responds differently to UV crosslinking. As part of the UWBioE Capstone project, David McIntyre led the investigation of kinetic binding of these DNA barcodes and the impact of UV-crosslinking on the thymine-containing and/or cytosine-containing sequences. Barcodes with thymine and/or cytosine had lower binding capacities than the barcodes without thymine or cytosine (**Figure 3.44**). This suggested that UV-crosslink also impacts the sequences of the barcode adapter and might also explain the variation in signal observed in (**Figure 3.43**). We conclude that it is essential that the future designs of the DNA barcode exclude the thymine and cytosine.

© Copyright 2021 | N Panpradist

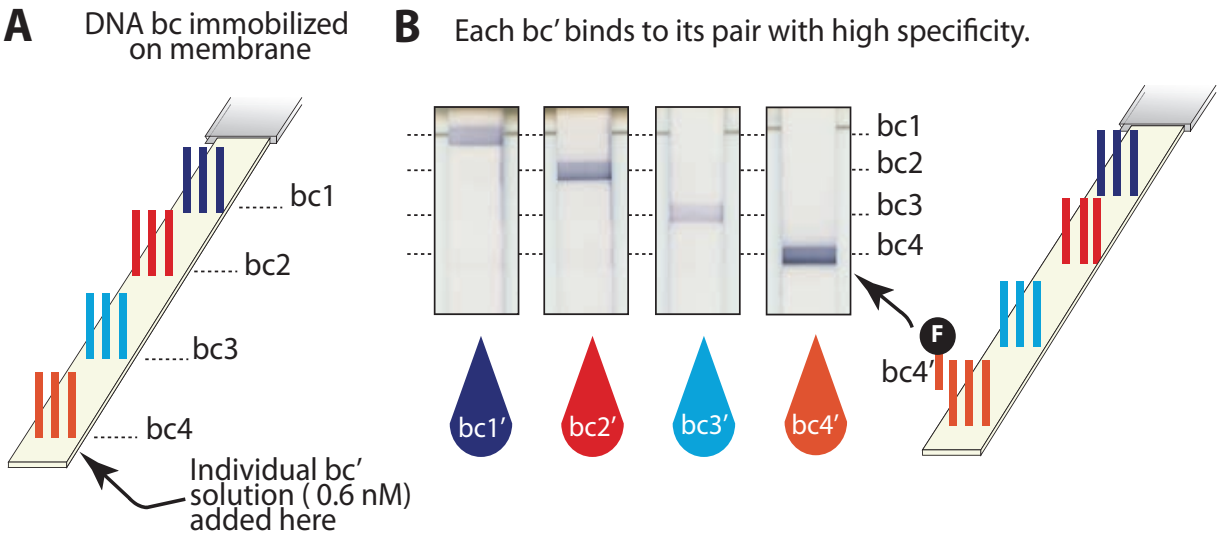

Figure 3.43 | Our on-paper multiplexed detection using DNA barcodes.

(**A**) Engineered DNA barcodes are conjugated to poly(T)20, which can be UV-crosslinked onto nitrocellulose paper membrane. (**B**) Each 0.6 nM fluorescein (F)-tagged barcode complement (bc') in ligation buffer was mixed with anti-fluorescein antibody tagged alkaline phosphatase before adding the strip. Purple AP substrate was then used to chase the flow and create a signal, indicating the barcode being captured. These engineered barcode DNA sequences are computationally engineered by Robert Atkinson.

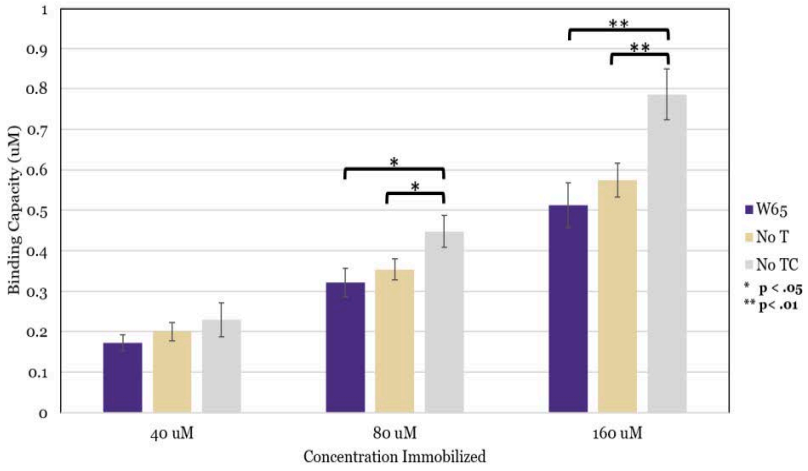

Figure 3.44 | Effect of UV-crosslinking on barcode sequences.

W65 barcode contains both thymines and cytosines. No T barcode contains A, G, and C sequences. No T barcode contains A, G. The barcode sequences were designed to have minimal secondary structure. As the immobilized barcode concentration increased, significant differences in DNA/DNA binding capacity

© Copyright 2021 | N Panpradist

were significantly different between barcode designs. The image was obtained from David McIntyre's capstone report[29].

3.6 HUMAN VISUAL CLASSIFICATIONS

CONTRIBUTORS: Parker S Ruth, Nuttada Panpradist, and Justin Vrana

To evaluate the consistency and accuracy of human interpretation of test strips results, 72 participants were recruited to fill out an online survey. The participants included 48 undergraduate students and 19 graduate students. None of the participants had prior knowledge of our assay chemistry and completed the survey on their personal computers.

Each participant was presented with 20 strips drawn randomly from a collection of 100 images and asked to make calls using a legend depicting the possible band patterns. We found that batch size did not significantly affect the number of images with >80% concordant scores (Chi-square analysis, P=0.741). Most of the participants achieved the accuracy of 90-100% visual classification compared to the ground truth (i.e., genotyping results).

© Copyright 2021 | N Panpradist

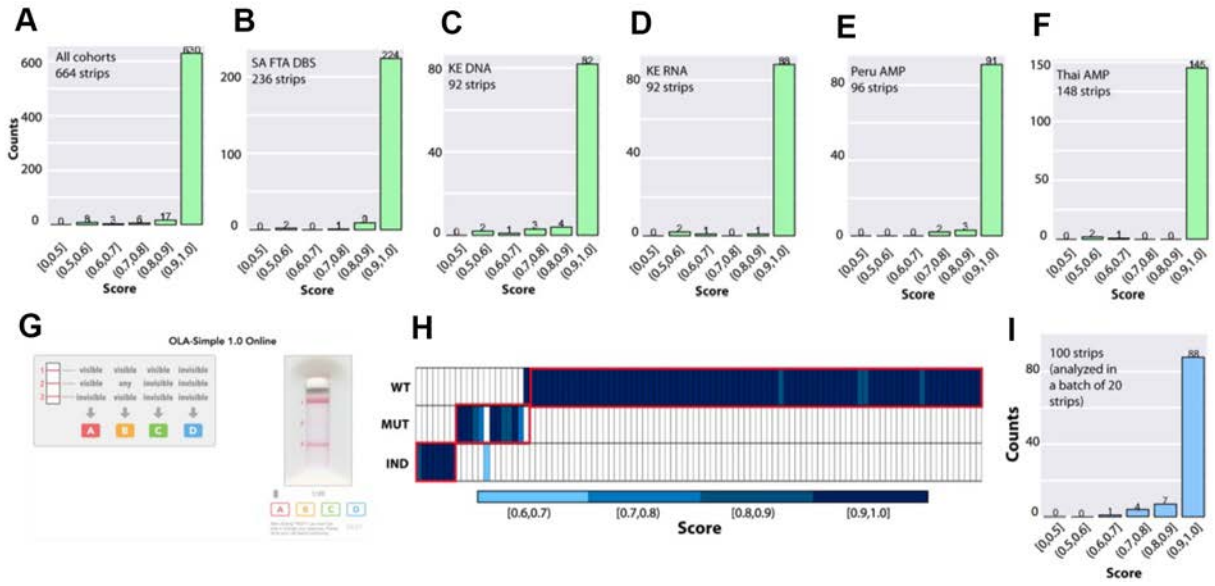

Figure 3.45 | Analysis of OLA-Simple by human visual calls from scanned images.

(**A**) Human mode call scores from all cohorts combined. (**B**)-(**F**) Human mode call scores based on multiple evaluators (n=11 for B-E; n=13 for F) analyzing the strip images in batch sizes of 236, 92, 92, 96, and 148, respectively. (**G**) Visual calls from online participants. Any participants did not select option D (no bands visible). (**H**) Heatmap of concordance scores from online participant calls on the 100 images are represented, columns are images, rows show calls, with the key for the number of calls below. Red boxes surround the human mode calls for each image. (**I**) Human mode call scores for all 100 images when evaluators analyzed 20 strips at a time.

3.7 ANALYSIS SOFTWARE OF PAPER-BASED DETECTION

CONTRIBUTORS: Nuttada Panpradist and Parker S Ruth

3.7.1 LINEAR DISCRIMINANT ANALYSIS IMPROVED THE SENSITIVITY OF LATERAL FLOW IMMUNOASSAY

Lateral flow immunoassays utilize color development to indicate the presence of the target analyte. The sensitivity of immunoassays directly relies on the

© Copyright 2021 | N Panpradist

ability to discriminate the color signal from the background. Additionally, an improved ability to distinguish the gradation of the color signal can enhance assay dynamic range. Here we present linear discriminant analysis (**LDA**) as an alternative method that can be specifically developed and applied to differentiate signal from background and color within levels of gradation of the commonly used detection molecules: blue polystyrene beads, gold nanoparticles, and enzymatic systems such as horse-radish peroxidase/ substrate.

The relationship of intensity value and RGB values

The intensity of the region of interest (**ROI**) in a digital image can be calculated by projecting the pixel distribution in RGB space onto a unit vector: [r g b] ^{T}. This operation can be stated as shown in **Figure 3.46A** (given ROI of 50 x 50 pixels, **Figure 3.46B**) where each row of the matrix corresponds to one pixel.

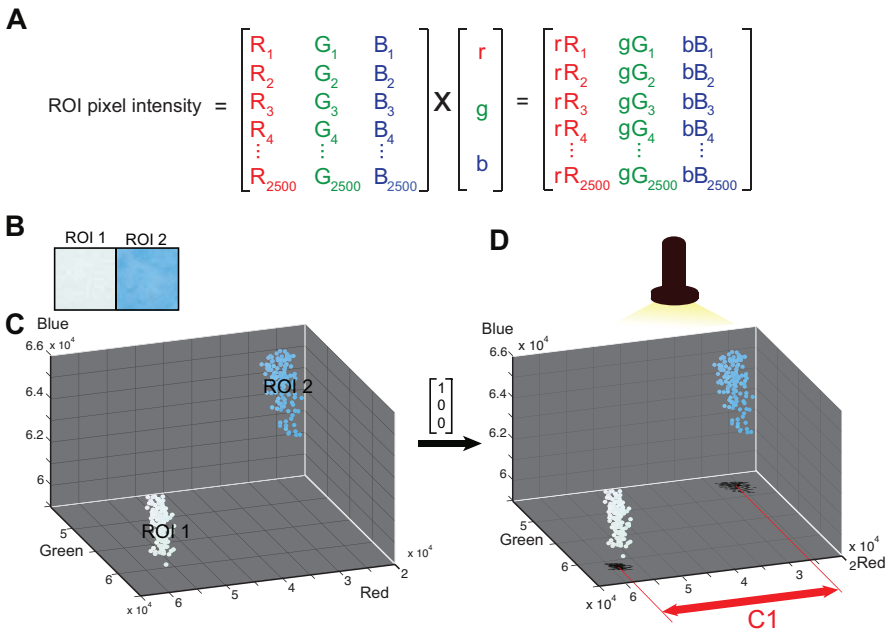

Figure 3.46 | Intensity and RGB values.

© Copyright 2021 | N Panpradist

(**A**) Demonstration of how intensity can be calculated from RGB values (B) 50x50 pixel scanned image of two concentrations of blue beads directly spotted membrane (ROI 1: 1000 ng/mL and ROI 2: 7300 ng/mL) (B) Sample distributions of ROI 1 and ROI 2 in 3D RGB space. (**B**) When being projected onto a plane, ROI 1 and ROI 2 distributions are in 2D shadows. When being projected onto a unit vector, the mean difference of ROI 1 and RO2 are 1D lines. (**C**) demonstrates the projections of ROI 1 and ROI 2 onto the green-red plane, and (C1) is the mean difference of projected ROI1 and ROI2 onto the unit vector $[1\ 0\ 0]^T$ or Red Channel.

Table 3.1 | Examples of unit vectors that can be used to discriminate two distributions.

A. Monochromatic channels unit vector	
A1 Red Channel	$[1\ 0\ 0\ ]^T$
A2 Green Channel	$[0\ 1\ 0]^T$
A3 Blue Channel	$[0\ 0\ 1]^T$
B. Multichannel unit vector	
B1 Unweighted sum	$[1/3\ 1/3\ 1/3]^T$
B2 Additive channels (not unit vector)	$[1\ 1\ 1]^T$
B3 Weighted (human eye)	$[0.299\ 0.587\ 0.114]^T$

The first group of commonly used unit vectors is monochromatic channels unit vectors (**Figure 3.46A**); a single red, green, or blue component is extracted. To illustrate, for red channel extraction, [1 0 0] would be used as the unit vector onto which the pixel distributions (**Figure 3.46B**) would be projected (**Figure 3.46C**). Despite the popularity of using a monochromatic channel as a unit vector, this can reduce assay limit of detection (LoD) and/or narrow dynamic range, especially when the signal intensity does not align with any monochromatic channel. On the other hand, a multiple-channel unit vector (**Figure 3.46B**) can be derived by various methods to discriminate signal and

© Copyright 2021 | N Panpradist

background distributions. Two examples of common multichannel unit vectors are the unweighted sum (**Figure 3.46B**, **B1**) used in ImageJ (newer than version 1.31) and the weighted human eye (**Figure 3.46B**, **B3**) used in ImageJ (version 1.31 and earlier) and Matlab (function RGB2gray). One method used to develop a multichannel unit vector discussed here is LDA (Linear Discriminant Analysis).

An LDA unit vector can be derived (**Figure 3.47**) under the assumption that the covariance structure of background and signal distribution is the same. Once the LDA unit vector has been derived, the ROI of the RGB image can be projected onto it using Equation1, similarly to other unit vectors. This LDA unit vector can be computed from one data set and used for any other data set if they use the same labeling molecule, and the image of the sample and calibration curve is analyzed under the same conditions and tools

$$\text{LDA unit vector} = \begin{bmatrix} \text{Var}_{(R)} & \text{Cov}_{(R,G)} & \text{Cov}_{(R,B)} \\ \text{Cov}_{(G,R)} & \text{Var}_{(G)} & \text{Cov}_{(G,B)} \\ \text{Cov}_{(B,R)} & \text{Cov}_{(B,G)} & \text{Var}_{(B)} \end{bmatrix}^{-1} \times \begin{bmatrix} \text{Mean R}_{\text{background}} - \text{Mean R}_{\text{signal}} \\ \text{Mean G}_{\text{background}} - \text{Mean G}_{\text{signal}} \\ \text{Mean B}_{\text{background}} - \text{Mean B}_{\text{signal}} \end{bmatrix} = \begin{bmatrix} r \\ g \\ b \end{bmatrix}$$

Figure 3.47 | Linear Discriminant Analysis (LDA) unit vector.

Mean RGB is the average R, G, or B values of pixels in ROI. It is crucial to ensure that number of pixels for background and signal areas are equal. The inverse of the covariance matrix is used to correct the variances in background and signal distributions, resulting in the final LDA vector that maximizes the separation between background and signal distributions. Note that the covariance matrix will be close to the identity matrix (times a constant) if the pixel clouds are symmetric.

MATERIAL AND METHODS

© Copyright 2021 | N Panpradist

DEVELOPING THE STANDARD CURVE OF DIFFERENT DETECTION MOLECULES

Blue bead solution (100-10000 ng/µL, Bangs Lab) was spotted onto the lateral flow (FF-80) and scanned immediately (16bit RGB, 600 Dpi, Tif). DAB signal, previous results from the two concentrations at 25% and 50% MUT of Y181C standard curves from the **Chapter 3.2** were included for demonstration. The intensity of each pixel from the capture spot (specimen) and a region upstream of the capture spot (background) was extracted from two regions of interest (ROIs) of equal size (55 x 40 pixels, 2.32mm x 1.70mm). The reported signal intensity was calculated as the 95th percentile of the intensity in the ROI capture spot minus the 95th percentile of ROI background. MATLAB code for analysis is enclosed in **Supplementary Information Chapter 3**.

Red, green, and blue pixels of the image were first projected onto an L-2 vector [0.684 0.1705 0.792], which was developed by linear discriminate analysis to best separate the color of the DAB signal from its background on nitrocellulose, and signals were reported as intensity (range: 0 – $3^{0.5}$ x 2^{16}A.U., **Equation 3.1**). The reported signal intensity is calculated using **Equation 3.2**.

Equation 3.1:

$$[Intensity]_{(55x40x1)} = [ROI\ pixel\ intensity]_{(55x40x3)} \times [L-2\ unit\ vector]_{(3x1)}$$

Equation 3.2:

signal intensity = 95th percentile of $[\text{intensity}]_{\text{background}}$ – 95th percentile of $[\text{intensity}]_{\text{signal}}$

© Copyright 2021 | N Panpradist

COMPARISON OF UNIT VECTORS' ABILITY TO DISCRIMINATE TWO DISTRIBUTIONS

A unit vector that best discriminates two distributions should have two desirable qualities: 1) the most significant difference between signal and background mean intensity and 2) the smallest deviation from the mean of both distributions. **Figure 3.48** shows projections of two-pixel distributions onto two hypothetical vectors (A and B). While the projection onto vector A or vector B provides the same Mean1 – Mean2, the projection with lower variance (**Figure 3.4B**) yields better discrimination. Therefore, to better compare the ability of the unit vector in discriminating signal and background distributions, the ratio of the mean difference to combined deviation should be reached; the best unit vector should provide the highest ratio. This method will normalize for the length of the vector onto which the data are projected. In other words, $[1\ 1\ 1]^T$ and $[1/3\ 1/3\ 1/3]^T$ should result in the same ratio.

© Copyright 2021 | N Panpradist

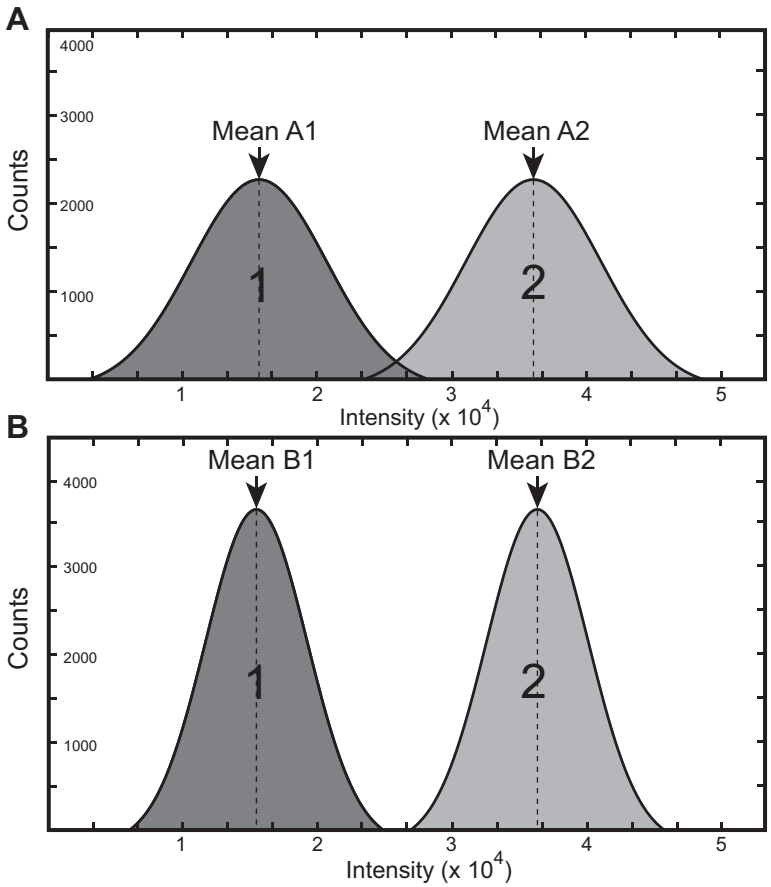

Figure 3.48 | Justification for a method to determine the best differentiation.

Histogram of two hypothetical distributions (1 and 2) after projecting onto two theoretical unit vectors (A and B). The mean difference of two distributions after projecting onto vector A (A) and onto vector B (B) are identical. In other words, (mean A1 – mean A2) is equal to (mean B1 – mean B2). However, the variance of A1 and A2 is greater than the variance of B1 and B2. This suggested that comparing mean differences is insufficient to select the best vector to discriminate between the two distributions.

Results

© Copyright 2021 | N Panpradist

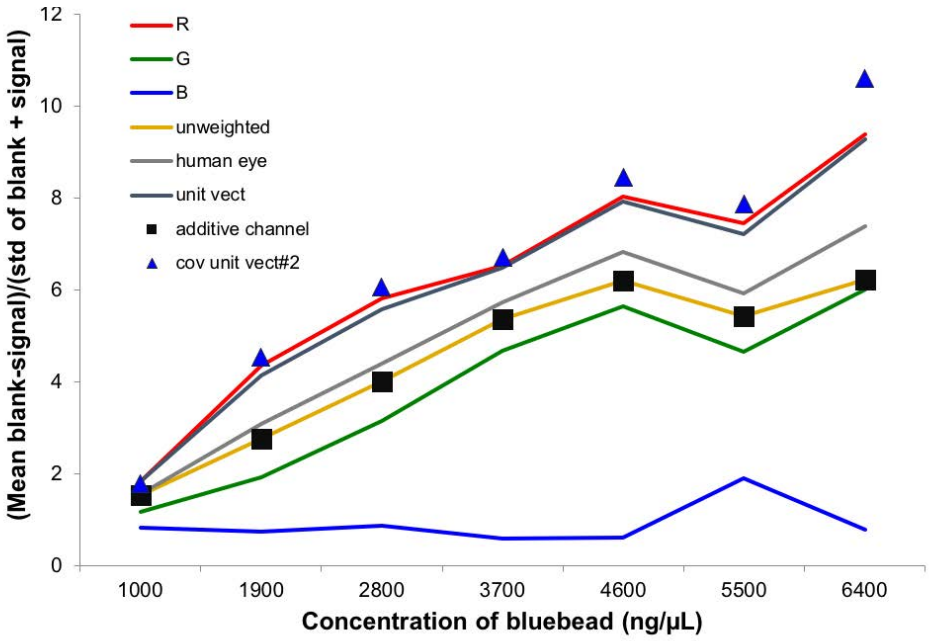

Figure 3.49 | Discriminations of blue bead signal by different unit vectors.

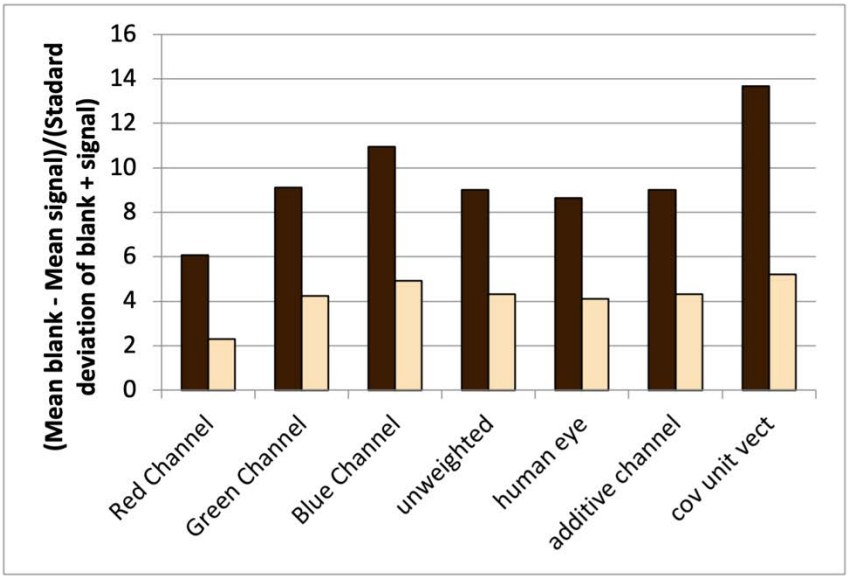

Figure 3.50 | Discriminations of DAB/HRP signal by different unit vectors.

The maximum intensity value from the projection of distribution to LDA is greater than that of another L-1 unit vector. Additional analysis can be performed to determine a reported intensity value. Note that there is some limitation in using this method in ImageJ; an LDA vector is considered an L-2 unit vector ($r^2 + g^2 + b^2 = 1$) while ImageJ only recognize the projection of L-1 unit

© Copyright 2021 | N Panpradist

vector (|r| + |g| + |b| = 1). Specifically, ImageJ can read intensity values up to 2^{bit} (2^8 and 2^{16} for 8-bit and 16-bit images, respectively) while the maximum intensity value calculated from an LDA unit vector can be as high as $\sqrt{3} \times 2^{bit.}$ The user would encounter an error if attempting to use a macro for measuring RGB, such as the following:

```
setRGBWeights(r, g, b);   run("Measure");

setResult("Label", nResults-1, "LDA Unit Vector");

updateResults();
```

To resolve this problem, a user can turn an LDA unit vector into an L-1 unit vector by dividing each component by |r| + |g| + |b|. This change would not affect the reported OD, defined as log(intensity $_{background}$ / intensity $_{signal}$), because the term |r| + |g| + |b| in background and signal intensity would cancel each other. However, if the reported value is not OD but intensity, the number calculated by ImageJ must be converted back to full-scale intensity value by multiplying by the |r| + |g| + |b| term. The value of LDA is developed after an assay was done. In other words, the standard color of a specific labeling molecule must be analyzed with the sample.

Conclusions: Red, Green, Blue channels are not the only unit vectors. Depending on the labeling types, a specific unit vector can improve signal and background discrimination.

© Copyright 2021 | N Panpradist

Acknowledgments: This work was supported by the DARPA MAD NAAT project. The author thanks Bhushan Toley, Josh Buser, and Greg Horwitz for assistance in blue beads experiments and intellectual discussion.

PYTHON-BASED TOOL TO REPORT T-STATISTIC BETWEEN THE SIGNAL AND RESULTS

Based on the training data set, the threshold for the MUT band was selected as the average of the lowest normalized t-statistic of MUT data and the highest normalized t-statistic of WT data. The threshold for the WT band was selected as the average of the lowest normalized t-statistic of WT data and the highest normalized t-statistic of IND data. The algorithm was used to classify strips based on these thresholds. The algorithm reports a MUT sample if the MUT band t-statistic is above the MUT band threshold. Next, the algorithm reports a WT sample if the WT band t-statistic is above the WT band threshold. If the WT band t-statistic is below the WT band, the algorithm reports an IND sample. This algorithm was used to evaluate 160 test images (unknowns) and achieved 99% concordance with a single call different from the human mode call but concordant with the sensitive comparator assay result. The MUT signal of this sample fell right between the lowest training MUT and the highest training WT and missed the threshold by just 0.2% of the overall pixel intensity range.

© Copyright 2021 | N Panpradist

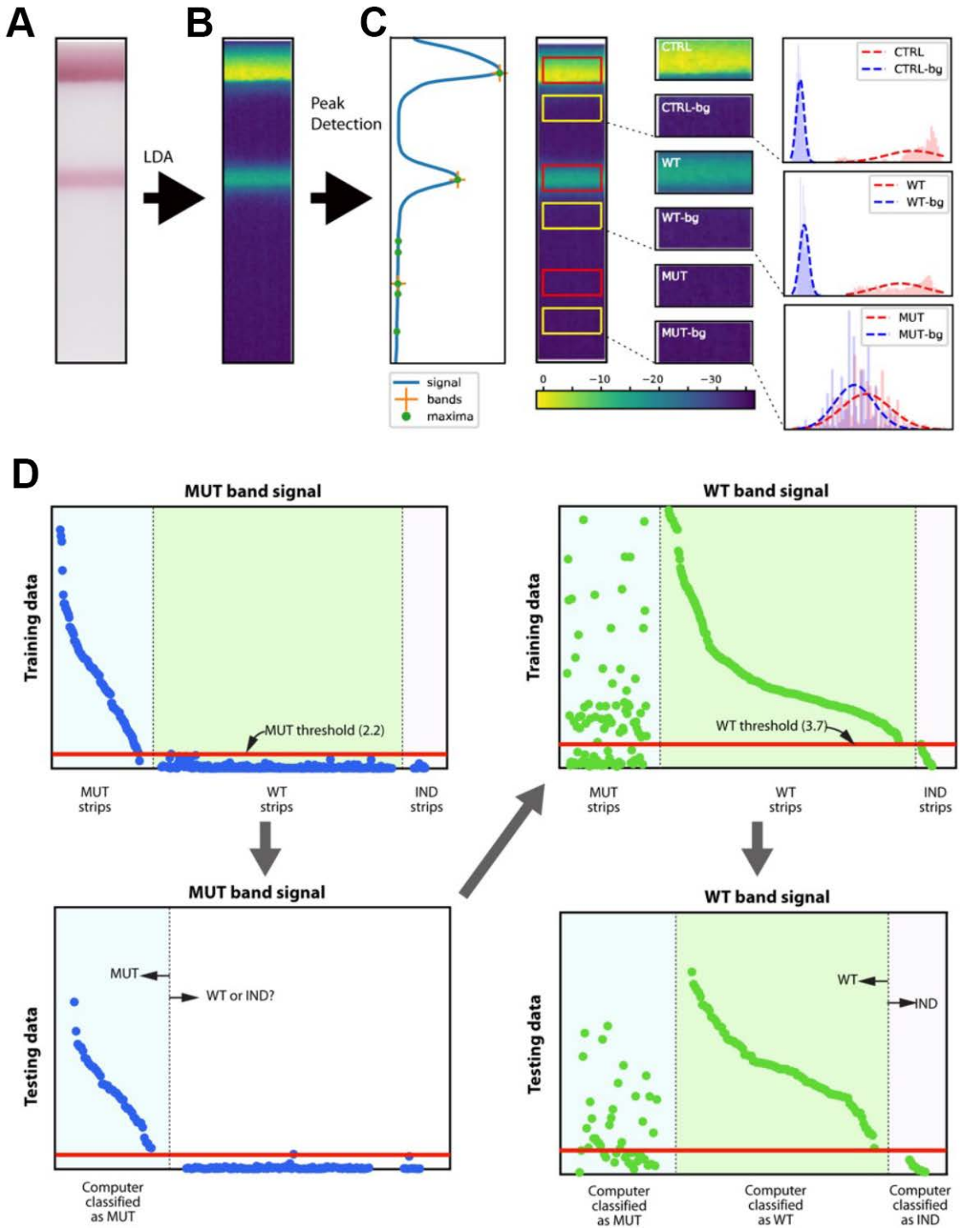

Figure 3.51 | Software Image Processing using t-statistics.

(**A**) – (**C**) Image processing for signal quantification. The image processing algorithm takes as input a full-color image from a flatbed scanner. The array of OLA-Simple strips is detected in the image, rotated to alignment, and cropped. The five paper strips for each codon are then cropped separately. To convert

© Copyright 2021 | N Panpradist

each strip image (**A**) into a single-channel image, the three-color channels are linearly combined with weights chosen using linear discriminant analysis (LDA) to differentiate bands from background pixels (**B**). The locations of the three bands are identified on each strip by a combination of peak detection and windowed search heuristics (**C**). Paired rectangular sample regions are selected on and adjacent to each of the three bands. The independent two-sample t-statistics are calculated for the means of the paired sample regions. The t-statistics for each band are normalized by dividing by the square root of the number of pixels in the sample region to account for differences in image resolution. (**D**) Image processing training and testing. The thresholds for the algorithm were assigned and evaluated using a clinical image data set, classified as WT, MUT, or IND by human mode calls from 13 evaluators (Thai cohort) and 11 evaluators (the other cohorts). Total 594 images were divided into training data set (434 images) and testing data set (160 images).

3.8 SUPPLEMENTARY INFORMATION FOR CHAPTER 3

Table S3.2 | Oligonucleotide probe sequences and concentration in OLA ligation (version 2016)

The table was published, N Panpradist et al. 2016 (https://DOI.org/10.1371/journal.pone.0145962).

SNP locus	oligonucleotide probe sequences (5' to 3')	concn (nM)
K103N	D ACACCCAGCA GGGTTAAAAA AGAAR	3.8
	F ACACCCAGCA GGGTTAAAAA AGAAY	15.1
	p AAATCAGTRA CAGTACTRGA TGTGGG B	15.1
Y181C	D CACAAAAYCC AGAMATAGTC ATYTA	15.1
	F CACAAAAYCC AGAMATAGTC ATYTG	50
	p YCAATATATG GATGACTTGT ATGTA B	50
M184V	D CCAGAAATAG TYATCTATCA ATAYA	15.1
	F CCAGAAATAG TYATCTATCA ATAYG	50
	p TGGATGACTT GTATGTAGGA TC B	50
G190A	D TATGGATGAC TTGTATGTAG G	3.8
	F TATGGATGAC TTGTATGTAG C	15.1
	p ATCTGAYTTA GAAATAGGGC AA B	15.1

Legend D: digoxigenin F: fluorescein
B: biotin *p* : phosphorylated
R : mixed A,G **Y** : mixed C,T **M** : mixed A,C

© Copyright 2021 | N Panpradist

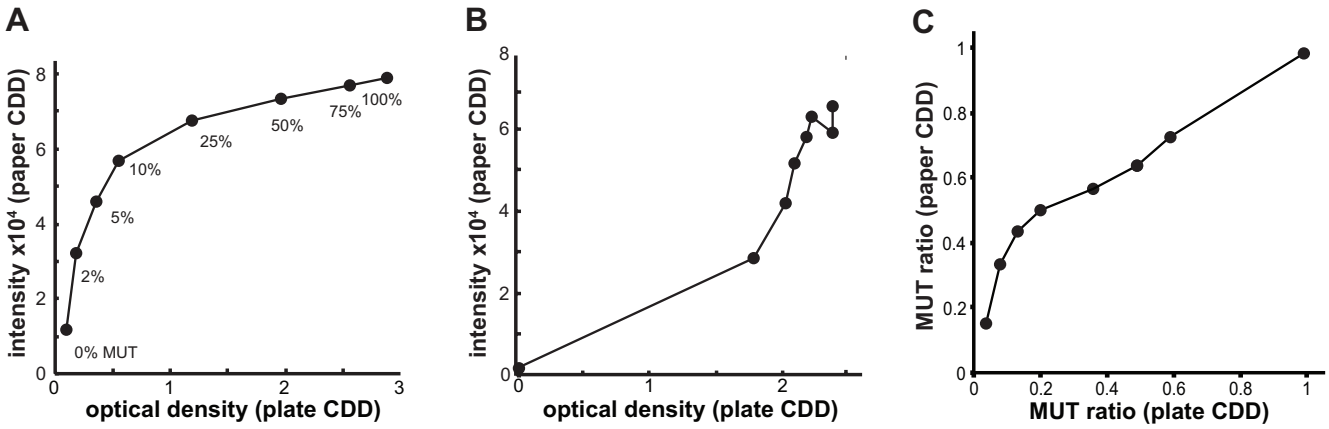

Figure S3.52 | Correlation plots of OD and MUT OD ratios by plate CLIA-OLA vs. intensities and MUT intensity ratio by 1st generation paper-based detection.

(**A**) Optical density (OD) of MUT detection from plate detection versus intensity of MUT detection from paper detection (**B**) OD of WT detection from plate DETECTION versus intensity of WT detection from paper CDD (**C**) MUT ratio: OD MUT/(OD WT + OD MUT) from plate CDD versus MUT ratio: intensity MUT/(intensity MUT + intensity WT) from paper detection. Image was obtained from N Panpradist et al. 2016 (**https://DOI.org/10.1371/journal.pone.0145962**)

© Copyright 2021 | N Panpradist

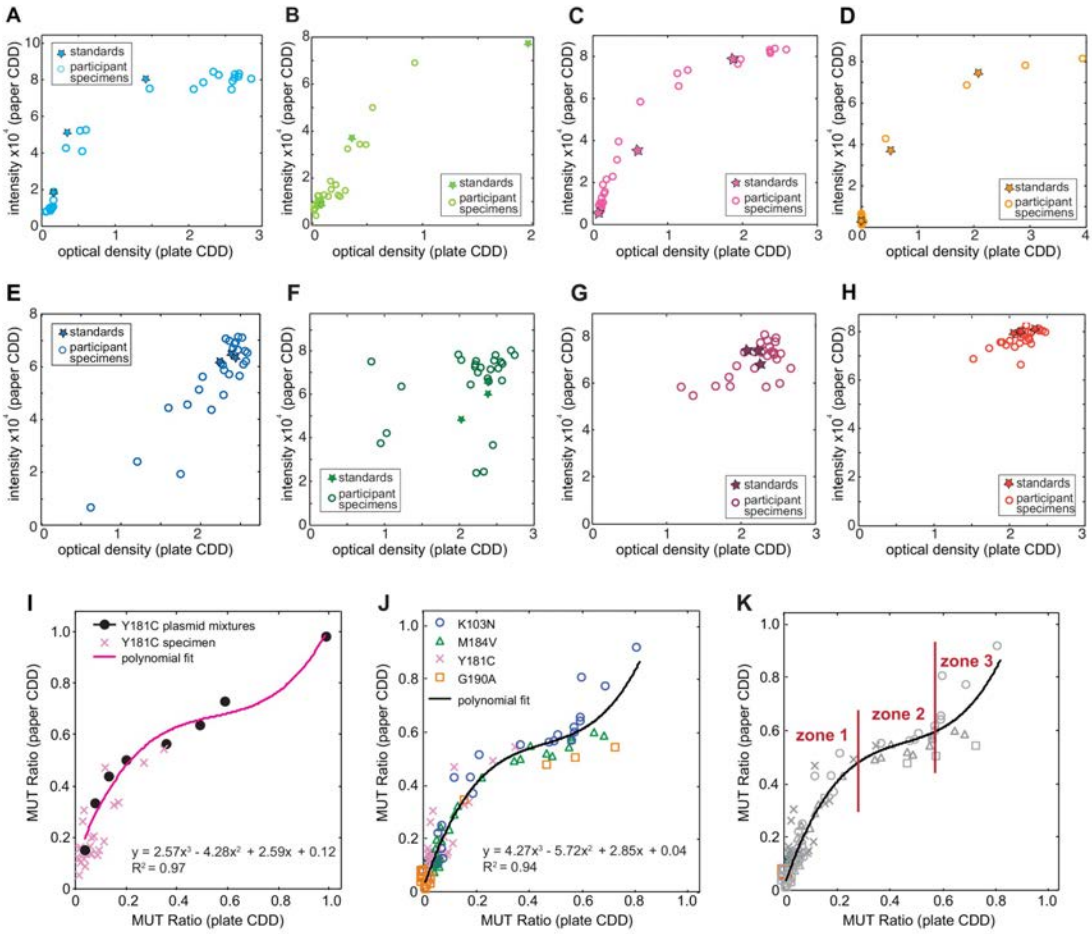

Figure S3.53 | Correlation plots of MUT ratio by 1st-generation paper detection vs. CLIA-OLA.

(**A**)-(**D**) MUT signal between paper CDD and plate CDD for the data in Figs **Figure 3.6A** & **Figure 3.5C** and **Figure 3.7A** & **Figure 3.7C**, respectively. (**E**)-(**H**) WT signal between paper CDD and plate CDD for the data in Figs **Figure 3.6B** & **Figure 3.6D** and **Figure 3.7B** & **Figure 3.7D**, respectively. (**I**) Correlation plot of Y181C Mutant (MUT) Ratios for 26 subjects' HIV DNA compared to the plasmid mixtures (0%–100% Y181C MUT) and specimen. (**J**) Correlation plot of MUT Ratios for all four HIV-drug-resistance codons determined by paper capture, denaturation, and detection (CDD) versus plate CDD as presented in **Figure 3.8**. In both plots, a polynomial fit was used to report R^2 values for the correlations. (K) Explanation of the non-linear curve in B. For samples containing low % mutant (zone 1), the MUT signals dominated the MUT Ratios because the WT signals were saturated in both plate and paper CDDs. Paper CDD is more sensitive at low % mutant than the plate CDD, resulting in a slope >1. The MUT signal of paper CDD reached saturation earlier than the plate CDD, which causes a

© Copyright 2021 | N Panpradist

plateau-like zone. WT signals were less saturated in samples with high % mutant as the slope increased (zone 3).

Table S3.3 | Signal ratios of samples evaluated by CLIA-OLA.

The table was obtained from N Panpradist et al. 2016 (https://DOI.org/10.1371/journal.pone.0145962)

Codon	K103N	Y181C	M184V	G190A
Plasmid standard	signal ratio (MUT OD/(MUT OD + WT OD), mean ± SD, n=2)			
5% MUT	0.120 ± 0.001	0.131 ± 0.001	0.207 ± 0.001	0.157 ± 0.005
50% MUT	0.387 ± 0.002	0.492 ± 0.005	0.449 ± 0.001	0.506 ± 0.002
Specimen ID				
1	0.209	0.015	0.096	0.468
2	0.020	0.349	0.405	0.004
3	0.367	0.029	0.118	0.001
4	0.117	0.028	0.055	0.002
5	0.598	0.064	0.561	0.002
6	0.474	0.036	0.465	0.001
7	0.071	0.089	0.345	0.576
8	0.806	0.022	0.550	0.001
9	0.506	0.088	0.043	0.006
10	0.178	0.079	0.038	0.002
11	0.054	0.269	0.045	0.001
12	0.050	0.117	0.049	0.002
13	0.491	0.034	0.486	0.002
14	0.685	0.027	0.683	0.003
15	0.047	0.035	0.045	0.013
16	0.570	0.019	0.129	0.001
17	0.571	0.022	0.219	0.001
18	0.559	0.039	0.368	0.001
19	0.026	0.171	0.033	0.002
20	0.058	0.113	0.064	0.002
21	0.050	0.063	0.061	0.153
22	0.189	0.152	0.055	0.018
23	0.063	0.044	0.642	0.721
24	0.042	0.029	0.054	0.002
25	0.593	0.061	0.046	0.004
26	0.594	0.028	0.562	0.007

© Copyright 2021 | N Panpradist

Table S3.4 | Signal ratios of samples evaluated by 1st-generation paper detection.

Codon	K103N	Y181C	M184V	G190A
Plasmid standard	signal ratio (MUT intensity/(MUT intensity + WT intensity), mean ± SD, n=3)			
5% MUT	0.446 ± 0.032	0.363 ± 0.034	0.323 ± 0.011	0.318 ± 0.013
(min-max)	0.403 - 0.498	0.321 - 0.409	0.309 - 0.343	0.298 - 0.337
50% MUT	0.567 ± 0.029	0.623 ± 0.083	0.537 ± 0.012	0.485 ± 0.012
(min-max)	0.534 ± 0.605	0.506 - 0.716	0.517 - 0.555	0.464 - 0.501
Specimen ID				
1	0.517	0.053	0.239	0.477
2	0.108	0.543	0.551	0.068
3	0.553	0.119	0.295	0.077
4	0.431	0.149	0.204	0.073
5	0.805	0.143	0.582	0.052
6	0.561	0.118	0.519	0.040
7	0.247	0.145	0.498	0.502
8	0.919	0.101	0.549	0.077
9	0.591	0.133	0.083	0.040
10	0.432	0.206	0.125	0.033
11	0.124	0.490	0.108	0.025
12	0.117	0.470	0.110	0.039
13	0.564	0.305	0.511	0.040
14	0.773	0.260	0.588	0.017
15	0.129	0.141	0.138	0.041
16	0.597	0.118	0.329	0.025
17	0.619	0.155	0.430	0.049
18	0.568	0.085	0.500	0.051
19	0.110	0.337	0.135	0.036
20	0.146	0.183	0.245	0.015
21	0.109	0.201	0.182	0.346
22	0.370	0.325	0.196	0.034
23	0.221	0.143	0.605	0.543
24	0.128	0.121	0.122	0.042
25	0.642	0.164	0.101	0.057
26	0.656	0.138	0.571	0.033

The table was obtained from N Panpradist et al. 2016 (https://DOI.org/10.1371/journal.pone.0145962)

© Copyright 2021 | N Panpradist

Table S3.5 | Comparison of 1st-generation paper-based detection and CLIA-OLA.

Time, cost, and instrument requirements for plate and paper CDDs and the other steps in OLA. The table was obtained from N Panpradist et al. 2016 (https://DOI.org/10.1371/journal.pone.0145962)

step	time		cost (reagents and materials)		required equipment / level of training	
DNA extraction	90 min		$1.51 (5 Primer DNA purification kit)		centrifuge	
amplification	270 min		$1.36 (nested PCR + agarose gel)		thermal cycler electrophoresis kit power supply	
ligation	60 min		$0.44 (96-well plate: 36 samples, controls, and standard controls in duplicate)		thermal cycler	
CDD for a codon	plate	paper	plate	paper	plate	paper
	150 min	45 min	non-labor cost: $1.65/codon	*membrane spotted streptavidin:* $0.18 for two strips *adhesive Mylar backing:* $0.375 *cellulose pad:* $0.008 *labeling antibodies and DAB* $0.95 for two strips non-labor cost: $1.52/test $2.03/codon (set of 9 samples + controls)	plate washer, plate reader extensive training	flatbed office scanner or phone camera minimal or no training
total OLA	420 min + 150 min/ CDD	420 min + 45 min/ CDD	$2.87 + $2.09/codon	$2.87 + $2.47/codon		

Table S3.6 | Compositions and anticipated functions in candidate buffers.

1) Storage buffer from the manufacture (Bang's lab) 100 mM MES(2-(*N*-morpholino) ethanesulfonic acid) +0.05% Tween + 0.1% BSA + 10mM EDTA pH 4.5	
MES 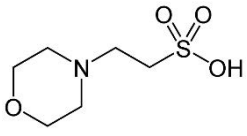	**2-(*N*-morpholino)ethanesulfonic acid** - MES does not generate any form of radicals[32]. This may be the reason why it is good for the long-term stability of beads. - Effective pH of MES alone = 5.5-6.7 - Another possible reason that beads are stored at acidic MES is that the reaction of carbodiimides (EDC and DCC) cross-linker that couples' carboxylates (-COOH) to primary amines (-NH_2). Bang's lab said the "polystyrene beads are negatively

© Copyright 2021 | N Panpradist

	charged" (Personal conversation with Juliana Isiar Bang's lab, March 11th, 2014). Negatively charged can be referred to as (1) endogenous charge aromatic ring or (2) chemically modified to have carboxylic groups on the surface. The carboxylic groups will later couple with primary amine groups in streptavidin. Acidic MES is the most effective condition for this to happen[33].
Tween-20 (MW 1228 Da) 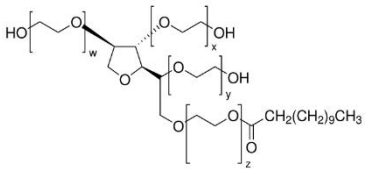	**Polyoxyethylene (20) sorbitan monolaurate** • Polysorbate 20 surfactant– oily liquids derived from PEG-ylate bitan esterified with fatty acids • Use in ELISA – washing, and blocker 1) As washing reagents – make TBST, PBST at 0.05% to 0.5% 2) As blocker - to saturate binding sites on the surface – use BSA • Has low CMC (0.06 mM), considered gentle surfactant- thus c affect protein function. In this solution 0.05% v/v tween = 0. tween (beyond CMC). At the detergent concentration higher t the CMC, the detergent will not solubilize the protein structur
EDTA 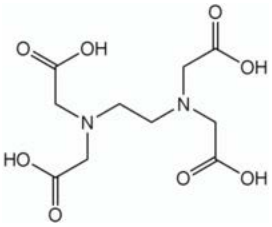	**Ethylene-diamine-tetraacetic acid** - Considered a synthetic amino acid - Chelates divalent cations – has a high affinity for calcium than for magnesium. - Most enzymes that involve NA synthesis and modification are magnesium ion-dependent. So EDTA helps these reactions.

2) Lateral flow buffer (optimized by Epoch)	
15 mM HEPES, 1% Triton-X100 + 0.5% w/v BSA, 0.4 M NaCl pH 7.1	
HEPES 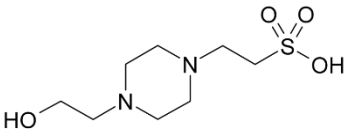	**2-[4-(2-hydroxyethyl)piperazin-1-yl]ethanesulfonic acid** - pH range 6.8-8.2 - generates hydrogen peroxide in the presence of light {Lepe-Zuniga JL et al., 1987; Zigler JS et al., 1985}. Presumably, this is the reason why it is not suitable for the long-term storage of blue beads. Lepe-Zuniga JL, Zigler JS, Gery I (October 1987). "Toxicity of light-exposed Hepes . *J. Immunol. Methods* 103 (1): 145.

© Copyright 2021 | N Panpradist

	Zigler JS, Lepe-Zuniga JL, Vistica B, Gery I (May 1985). "Analysis of the cytotoxic effects of light-exposed HEPES-containing culture medium." *In Vitro Cell. Dev. Biol.* 21 (5): 282–7.
TritonX-100 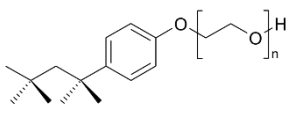	**polyethylene glycol p-(1,1,3,3-tetramethyl butyl)-phenyl ether** - Nonionic surfactant with a hydrophilic ethylene oxide chain and an aromatic hydrocarbon lipophilic (or hydrophobic group) - Main uses in biology: 1) part of lysis buffer – 5% in alkaline lysis buffer in DNA extraction 2) immunostaining to reduce surface tension – 0.1-0.5% in TBS and PBS 3) used as blocking buffer for immunohistochemistry [34] - CMC is 0.2-0.9 mM, which is higher than tween-20. 1% v/v Triton-X 100 =17 mM, which is very high. - Triton X-100 is mild. It is used to dissolve primary antibodies for immunocytochemistry [35]
NaCl	**Sodium Chloride** • NaCl can help drop the CMC of SDS down from 8 mM to 0.5 m • {Mary J. 2013} • pDNA capture hybridization requires an additional 400 mM NaC • Mary J. Detergents: Triton X-100, Tween-20, and More. Mater ods. 2013;3:163.

MATLAB algorithms for Monte Carlo method for estimate binding events

```
% Nuttada Panpradist
% 2014/03/06
% Monte Carlo method to preduct the proportion of single biotin bound to streptativin.
k = 1000; % no. of biotin
x = 0.75 % ratio of streptavidin:biotin
n = x*k; % no of streptavidin
M = sparse(n,4);
data = [];
```

© Copyright 2021 | N Panpradist

```
nitter = 5000;
% Use Monte Carlo method
for i = 1:nitter
    i
    temp = unidrnd(numel(M),10*k,1); % a randomized 1-k in random order
    B = unique(temp);
    C = 1:length(B);
    D = randperm(length(C));
    boundsites = B(D(1:k));
    M_2 = reshape(M,numel(M),1);
    M_2(boundsites(:)) = 1;
    M_2 = reshape(M_2,n,4);
    num_b2s = sum(M_2,2);
    b2s_0 = sum(num_b2s == 0);
    b2s_1 = sum(num_b2s == 1);
    b2s_2 = sum(num_b2s == 2);
    b2s_3 = sum(num_b2s == 3);
    b2s_4 = sum(num_b2s == 4);
    p_b2s_0 = b2s_0;
    p_b2s_1 = b2s_1;
    p_b2s_2 = b2s_2;
    p_b2s_3 = b2s_3;
    p_b2s_4 = b2s_4;

    data(:,i) = [ p_b2s_0  p_b2s_1  p_b2s_2  p_b2s_3  p_b2s_4];
end

mean_p = mean(data,2);
mean_p2 = mean_p(2:5)*100/sum(mean_p(2:5));
figure
plot([1,2,3,4],mean_p2,'.-','color',[0.4 0.35 0.95])
xlabel('number of biotin bound to a streptavidin')
ylabel('% biotin bound (1=4) to streptavidin')
ylim([0,100])
set(gca,'Xlim',[0.5,4.5],'XTick',[1 2 3 4],'XTicklabel',['1'; '2'; '3'; '4'])
legend (['streptavidin:biotin =', num2str(x)])
title('Marte Carlos method with 5000 interations')
```

Considering different methods to anchor nucleic acid on papers

The specific oligonucleotide probes can be immobilized onto membranes. Previous studies demonstrated the feasibility of in-situ ligation/detection on the glass slide to detect SNP mutations in TB[36]. We envisioned ligation and detection could occur sequentially on the membrane at each location where the specific probes are immobilized. To achieve

© Copyright 2021 | N Panpradist

this, the first step is to develop a method to immobilize specific probes onto the membrane wherein probe adherence to the membrane is robust and functionality for ligation is maintained.

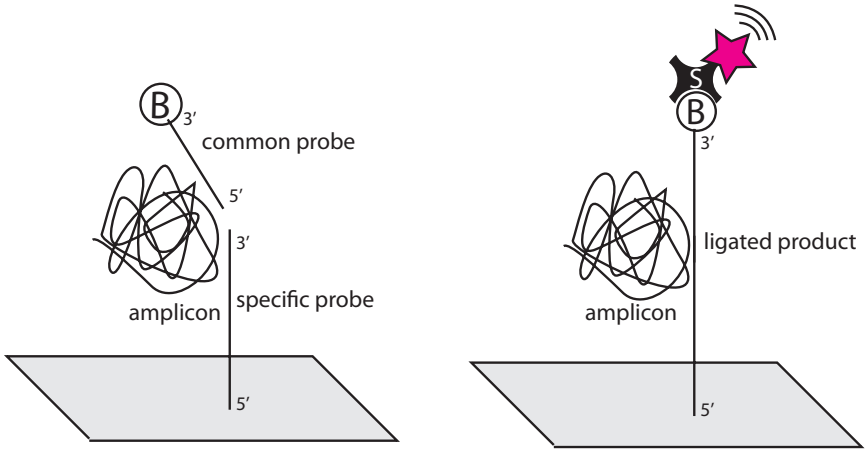

Figure S3.54 | Schematic of Chemistry of Ligation and Detection System in OLA on Membrane

Specific oligonucleotide probes can be immobilized onto membranes via physisorption and chemisorption. To achieve improved physisorption (great adherence), oligonucleotide probes are often either extended with polythymine (polyT) or conjugated to proteins such as streptavidin (tetramer, ~65 kDa). In the current format of OLA (Figure 3.1), anchoring oligonucleotide onto membrane via streptavidin is not compatible. This is because biotinylated common oligonucleotide probes can bind with available units of immobilized streptavidin and would not be available to bind to streptavidin labeling molecules unless they are completely blocked. Below are lists of potential methods based on my

© Copyright 2021 | N Panpradist

brainstorming with Dr. Barry Lutz and Dr. James Lai. These may be used to immobilize the specific probes as follows.

1. Physisorption

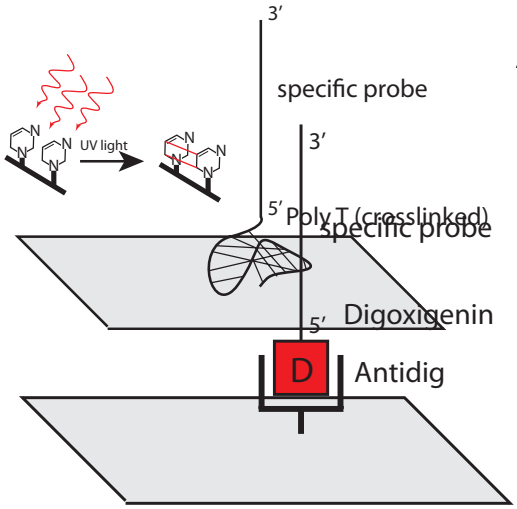

1.1 Bind hapten/anti-body to increase MW and enhance physisorption.

Mixed probe labeled antigen with its antibody to increase the MW. This process can be done by (1) premixing the probe labeled antigen with the antibody and then spot, or (2) spot antibody first and then spot the antigen-tagged probe on top of it. The antibody has a molecular weight of ~ 160 kDa. It is important to pay attention to antibodies purchased, whether it is Fab fragment or whole antibodies (monoclonal versus polyclonal). Briefly, polyclonal antibodies recognize more than one epitope on any one antigen (mainly made up of IgG subclass).

Advantages: 1) this approach can help amplify signals from target proteins with low expression levels, as the target protein will bind more than one Ab molecule on the multiple epitopes. 2) More tolerant of minor changes in the antigen (polymorphism, heterogeneity, or slight denaturation).

© Copyright 2021 | N Panpradist

Disadvantages: Prone to batch-to-batch variation; likely giving background signal in some applications. Multiple epitopes would make it important to check for any cross-reactivity.

1.2 Extend the probe with (polyT)$_{20}$ at 5'end to allow for crosslinking of thymines

To ensure that the enzyme ligase can still function, polyT tails (T20, which is 20 repeating units of thymines) can be attached. Thymine can be crosslinked under UV light and improve the immobilization of DNA onto the membrane. UV can, however, damage the target base at SNP as well.

Some studies used T10 and C10 tails to extend DNA probes to aid immobilization on glass slide[31]. The protocol they used (UV treatment) showed no effect on DNA mutation (still able to detect SNPs). This study also mentioned that UV crosslinking effect depends on the substrate used and the design of the probes. Thomas Schüler et. Al. Reported that UV-crosslinking (254 nm) of DNA probe (~24 bases) without any modification was effective, based on by flow test of the complementary probes and the signal was observed. However, it is noteworthy that this finding mentioned that the amino-modified probe on the epoxy surface gave a higher binding rate (LoD = 5 pM)[37].

© Copyright 2021 | N Panpradist

1.3 conjugate 5'end with bovine serum albumin

Alternatively, we can modify the 5'end of specific probes with BSA (66.5 kDa, 583 aa), improving DNA immobilization while reducing non-specific binding. The main difference of this method from

The price offered by biosynthesis company (Lewisville, TX | Heidi Feb 25th, 2014) is $1200 per micromole. Alternatively, Trilinksolulink (San Diego, CA) offers the protein-oligonucleotide conjugation kit. The kit requires three steps: (1) conjugate HyNic group to protein, (2) conjugate S-4FB to hydrazine group modified DNA, and (3) mix components prepared in steps (1) and (2). The solution with pH 6.0 solution and bis-acrylhydrazone group will be created. These bonds can be quantified by measuring the lambda max at 354 nm, epsilon 29000. Some studies have shown the use of this method in DNA chip technology [38]. Another possibility is the use of a 5' NHS-activated group + PEG spacer to conjugate with BSA.

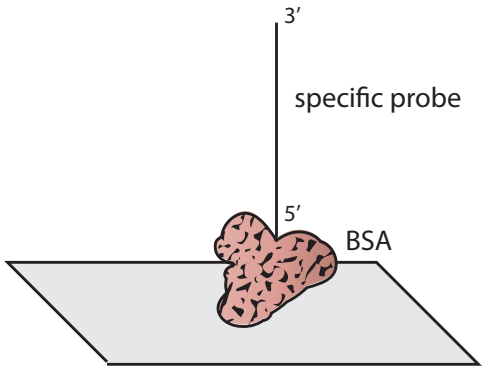

© Copyright 2021 | N Panpradist

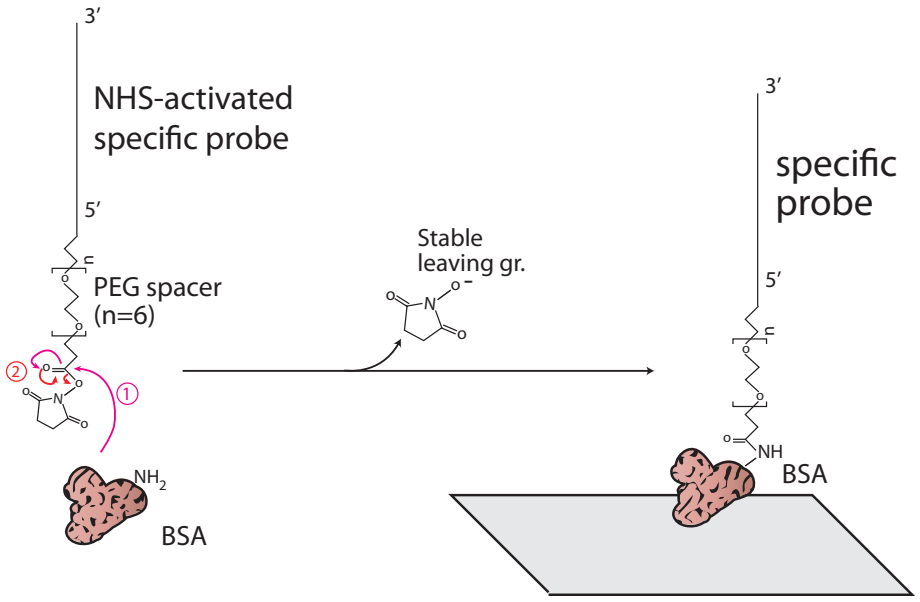

2. Chemisorption

2.1) 5’ NHS activated with PEG spacer, spotted on Nylon membrane with hydroxyl moieties

Pall Corporation (Port Washington, NY) sells Loprodyne®LP (Nylon membrane with hydroxyl moieties) membrane. This membrane can be an excellent source to create the covalent bonding between NHS-activated DNA probes via trans-esterification. Additionally, AL Golden et al.. demonstrated the conjugation of this membrane to polymer with 5’ carboxylated [39].

© Copyright 2021 | N Panpradist

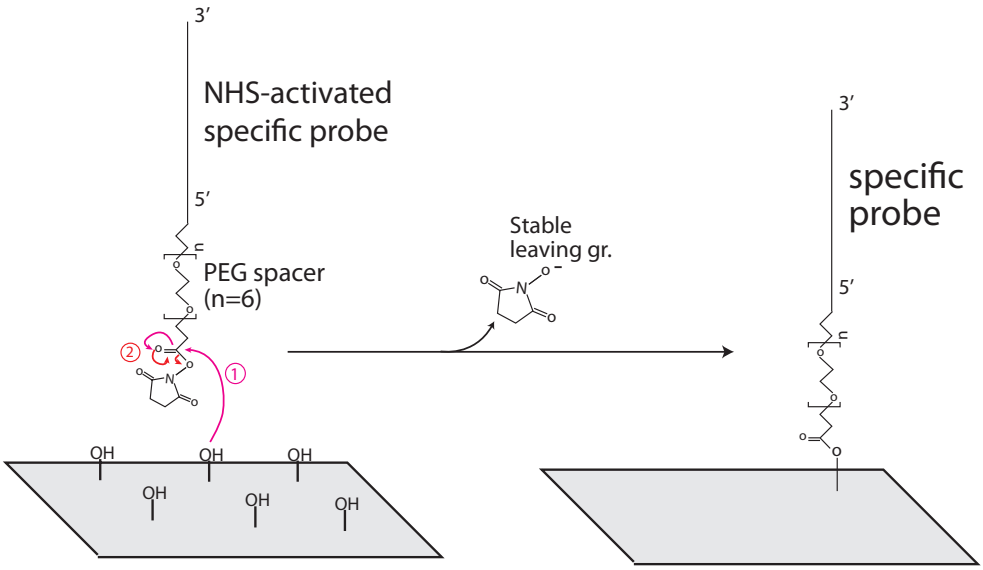

A disadvantage for this method may be that ester linkage that is not as robust as the amide group. In other words, ester linkage can be can hydrolyzed by acid and base easily. I contacted three companies (IDT, Biolink, and Thermo Fisher), but they do not have the free-end NHS activation.

2.2) 5’ amino-C6 spacer, conjugated onto Nylon membrane with carboxylate moieties

A study demonstrated the use of C6-amino-linker on the 5’end of the oligo to conjugate onto Biodyne C nylon membrane (Pall Corporation) activated by EDAC. C6 served as a spacer, while the amine group (NH_2) served as the active group to conjugate to carboxylate moieties on the membrane (in the presence of EDAC or EDC). This amine coupling can

© Copyright 2021 | N Panpradist

also create many side reactions, which can be the disadvantage of this method. The mechanism is demonstrated below[40].

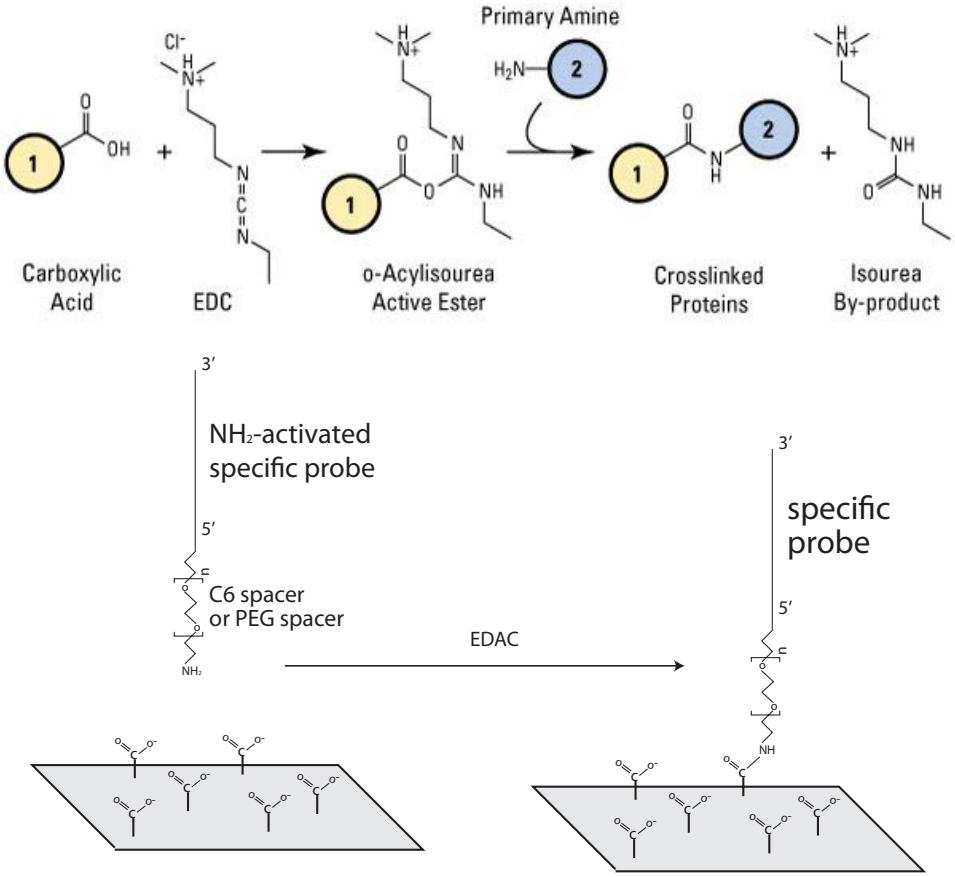

Alternatively, crosslinking of carboxylic and amine can occur using glutaraldehyde. This method has been used for decades to fixate samples for microscope or to immobilize cells and enzymes.

In alkaline aqueous solutions, glutaraldehyde undergoes polymerization via Aldol condensation, generating the mixtures of polymer chains (-CH=C(CHO)- groups. During the crosslinking process, the polymerization products can also react with other protein surface (for example,

© Copyright 2021 | N Panpradist

amines, thiols, phenols, and imidazole), dominated by the reactions with the side chain of lysine residues (primary amine) [41].

A protocol: Crosslinking should occur in amine-free buffers (so do not use Tris-HCl) such as phosphate buffers (pH 7.5-8.0) and HEPES buffers. Reaction mix with 50-100 µL of proteins in 20 mM HEPES (pH 7.5) in 100 µL total volume are treated with 5µL of 2.3% freshly prepared gluteraldehyde for 2-5 minutes at 37°C. The reaction is later terminated by adding 10µL of 1M Tris-HCl (pH 8.0) [42].

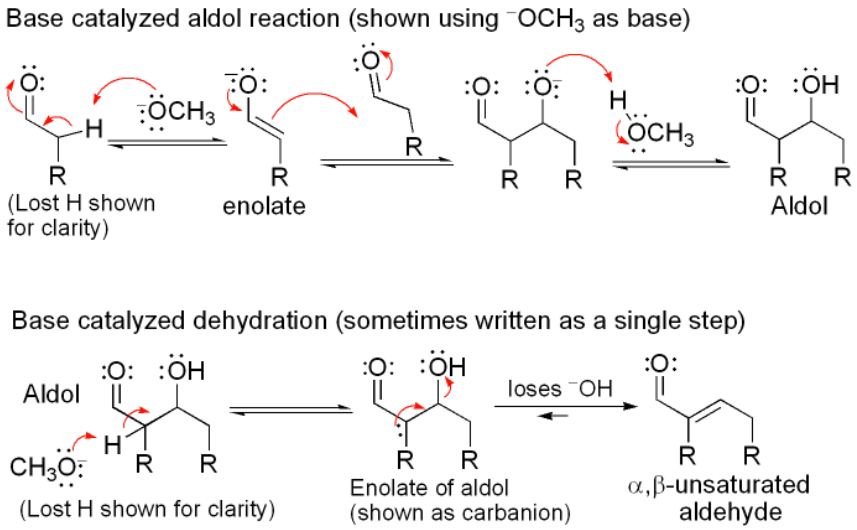

M. Walker. Base-catalysed mechanism for the aldol reaction (including aldol condensation) via enolate. 2006

2.3) Possibility of increasing the functionality of probe binding to membranes:

© Copyright 2021 | N Panpradist

Functionalized membrane can be first conjugated to polylysine, which can further conjugate to oligonucleotide strand. The potential pitfall of this method is that poly(L)lysine is positively charged, and this can form electrostatic complex with negatively charged oligo nucleotides.

MATLAB code for analysis of lateral flow strips

Part 1: Determine the LDA unit vector

```
A = imread('Positive_Color.tif'); figure; %imshow(A);
B = imread('Blank_Color.tif'); figure; %imshow(B);
Ared = A(:,:,1);
Agreen = A(:,:,2);
Ablue = A(:,:,3);
Bred = B(:,:,1);
Bgreen = B(:,:,2);
Bblue = B(:,:,3);

meanR = abs(mean(mean(Ared))-mean(mean(Bred)));
meanG = abs(mean(mean(Agreen))-mean(mean(Bgreen)));
meanB = abs(mean(mean(Ablue))-mean(mean(Bblue)));
mean_combine = [meanR meanG meanB]
longAred = reshape(Ared,(numel(Ared)),1);
longAgreen = reshape(Agreen,(numel(Agreen)),1);
longAblue = reshape(Ablue,(numel(Ablue)),1);

longBred = reshape(Bred,(numel(Bred)),1);
longBgreen = reshape(Bgreen,(numel(Bgreen)),1);
longBblue = reshape(Bblue,(numel(Bblue)),1);

A2 = [longAred(:) longAgreen(:) longAblue(:)];
B2 = [longBred(:) longBgreen(:) longBblue(:)];

covA = cov(double(A2))
covB = cov(double(B2))

cov_combined = covA + covB
invert_cov = inv(cov_combined)

LDA = mean_combine*invert_cov
```

© Copyright 2021 | N Panpradist

Part 2: Analysis of signal on strips

```
% Nuttada Panpradist
% 2016/10/07
bins = [0:65535];

a = imread('IMAGEfilename.tif');

imshow(a);
%[x,y] = getpts;
%hold on
%plot(x(:), y(:), 'r*','markersize',12);
%xdistance = abs(x(1,1)-x(2,1));
%ydistance = y(2,1)-y(1,1);
%angle = atan(ydistance./xdistance);
% --- Degugging ----
angle = 0;
% ------------------
b1 = imrotate(a,angle*180/pi);

keep_signal = [];
keep_blank = [];

%cropboxpos = [80 180 100 100];
imshow(b1);

XAXIS = [ 0, 2, 5, 10, 25, 50, 75, 100];
NO_STRIP = 8;
PERCENT_CUTOFF = 0.95;
y_value2 = 5;

% Get the crop area for strips - crop top and bottom for all strips
keep_cropboxpos = [];
%old cropboxpos = [40 144 25 20];
cropboxpos = [60 44 100 20];
for i = 1:NO_STRIP
for j = 1:2
   h = imrect(gca, cropboxpos);
   addNewPositionCallback(h,@(p) set(gcf,'UserData',p));
   wait(h);
   get(gcf,'UserData')
   keep_cropboxpos(:,j,i) = get(gcf,'UserData');
   %delete(h);
end
end

% Extracting the cropped parts of the image
% and storing them in "keep_signal" and "keep_blank"
keep_signal = [];
keep_blank = [];
hold on;
```

© Copyright 2021 | N Panpradist

```
for i = 1: NO_STRIP
% format of rect = [x,y,w,h]
   [c,rect1] = imcrop(b1,keep_cropboxpos(:,1,i));
   [d,rect2] = imcrop(b1,keep_cropboxpos(:,2,i));

   % Crop rectangle for capture area
   x = [rect1(1), rect1(1)+rect1(3), rect1(1)+rect1(3), rect1(1), rect1(1)];
   y = [rect1(2), rect1(2), rect1(2)+rect1(4), rect1(2)+rect1(4), rect1(2)];
   plot(x,y,'r-');

   % Crop rectangle for blank
   x = [rect2(1), rect2(1)+rect2(3), rect2(1)+rect2(3), rect2(1), rect2(1)];
   y = [rect2(2), rect2(2), rect2(2)+rect2(4), rect2(2)+rect2(4), rect2(2)];
   plot(x,y,'b-');


   keep_signal(:,:,:,i) = c;
   keep_blank(:,:,:,i) = d;
end

% %plot 3d of signal and blank
% figure;
% for i = 1:NO_STRIP
%     plot3(keep_signal(:,:,1),keep_signal(:,:,2), keep_signal(:,:,3),'r.')
%     hold on;
%     plot3(keep_blank(:,:,1), keep_blank(:,:,2), keep_blank (:,:,2), 'b.')
%     hold on;
%     plot3(684, 1705, 7092,'g']
%     xlabel('Red'); ylabel('Green'); zlabel('Blue');
%     %xlim([0 2^16]); ylim([0 2^16]); zlim([0 2^16]);
% end

% Reducing the data in "keep_signal" and "keep_blank" to
% a single color dimension by projecting onto the RGB2GRAYVECTOR
RGB2GRAYVECTOR = [2.7478    3.4663    0.8025]
graysignal = [];
grayblank = [];
for i = 1:NO_STRIP
   graysignal(:,:,i)= keep_signal(:,:,1,i)*RGB2GRAYVECTOR(1)+...
      keep_signal(:,:,2,i)*RGB2GRAYVECTOR(2)+...
      keep_signal(:,:,3,i)*RGB2GRAYVECTOR(3);

   grayblank(:,:,i)= keep_blank(:,:,1,i)*RGB2GRAYVECTOR(1)+...
      keep_blank(:,:,2,i)*RGB2GRAYVECTOR(2)+...
      keep_blank(:,:,3,i)*RGB2GRAYVECTOR(3);
end
% Getting the 5th percentile of each of the blanks
% Remember, small numbers mean greater signal
BLANK_PERCENT_CUTOFF = zeros(NO_STRIP,1);
for i=1:NO_STRIP
   tmp = grayblank(:,:,i);
```

© Copyright 2021 | N Panpradist

```
    BLANK_PERCENT_CUTOFF(i) = prctile(tmp(:),5);
end

% Getting the 5th percentile of each of the signal crops
% after removing all of the signal pixels that are below the
% BLANK_PERCENT_CUTOFF
SIG_PERCENTILE = zeros(NO_STRIP,1);
for i=1:NO_STRIP
    tmp = graysignal(:,:,i);
    SIG_PERCENTILE(i) = prctile(tmp(:),5);
end
figure;
for i=1:NO_STRIP
    tmp = graysignal(:,:,i);
    subplot(1,NO_STRIP,i);
    hist(tmp(:),[0:500:2^16*sqrt(3)]);
    set(gca,'Xlim',[0 2^16*sqrt(3)]);
   % tmp(tmp>BLANK_PERCENT_CUTOFF(i)) = [];
   % Uncomment the line above to cut the signal distn before calculating
   % the 95% (really 5th) percentiiile.
    SIG_PERCENTILE(i) = prctile(tmp(:),5);
end
figure;

for i=1:NO_STRIP
    tmp2 = grayblank(:,:,i);
    subplot(1,NO_STRIP,i);
    hist(tmp2(:),[0:500:2^16*sqrt(3)]);
    set(gca,'Xlim',[0 2^16*sqrt(3)]);
   % tmp(tmp>BLANK_PERCENT_CUTOFF(i)) = [];
   % Uncomment the line above to cut the signal distn before calculating
   % the 95% (really 5th) percentiiile.
    BLANK_PERCENT_CUTOFF(i) = prctile(tmp2(:),5);
end
% plotting the standard curve
figure;
plot(BLANK_PERCENT_CUTOFF-SIG_PERCENTILE,'k-o');
set(gca,'XTick',[1:NO_STRIP],'Xticklabel',num2str(XAXIS'))
BLANK_PERCENT_CUTOFF
SIG_PERCENTILE
```

MATLAB code for analysis of data from glow box (adapted the above code to analyze on-paper toehold mediated strand displacement experiment – the code was adapted by David McIntyre)

```
% David McIntyre
% June 1st, 2018
% This data analysis program extracts time-series fluorescence data of
%   Texas red fluorophores. This is intended to be used for measurement
%   of binding capacity and kinetics of DNA hybridization.
```

© Copyright 2021 | N Panpradist

```
% Adapted from Nuttada Panpradist

close all; clc
%% Get data and define region of analysis
%Request File info from user, reads 16 bit images
bins = 0:65535;
folderName = input('What is your image directory?  ','s');
srcFiles = dir(strcat(folderName, '\*.jpg'));
stackSize = length(srcFiles);
allOD = zeros(3, stackSize);

% Specifies area of analysis (capture line and background)
% User drags "crop box" to measure signal
fileBase = 'Image';
file = strcat(fileBase,'0',int2str(stackSize-1),'.jpg');
cropSet = imread(strcat(folderName, '\', srcFiles(length(srcFiles) - 25).name));
figure(1)
imshow(cropSet);

keep_cropboxpos = [];
NO_STRIP = 3; %Change if more strips are needed

for i = 1:NO_STRIP
    %Rectangle: xinit, yinit, width, height
    cropbox_size = [25 25 40 12];
    h = imrect(gca, cropbox_size);
    addNewPositionCallback(h,@(p) set(gcf,'UserData',p));
    wait(h);
    get(gcf,'UserData')
    keep_cropboxpos(:,1,i) = get(gcf,'UserData');
    signal_values = keep_cropboxpos(:,1,i);

    % automatically chooses background region (upstream of capture line)
    signal_values(2) = keep_cropboxpos(2,1,i) + 32;
    keep_cropboxpos(:,2,i) = signal_values;
end

%% Run analysis through the stack of images and save OD data

for k = 1: length(srcFiles)
    a = imread(strcat(folderName, '\', srcFiles(k).name));

    % rotate image if need be
    angle = 0;
    b1 = imrotate(a,0*180/pi); %why is this rotated

    % Extracting the cropped parts of the image
    % and storing them in "signal" and "backgrounds"
    signals = [];
    backgrounds = [];
```

© Copyright 2021 | N Panpradist

```
    for i = 1: NO_STRIP
        % format of rect = [x,y,w,h]
        %Retrieving the images of c and d at this time point
        [c,rect1] = imcrop(b1,keep_cropboxpos(:,1,i));
        [d,rect2] = imcrop(b1,keep_cropboxpos(:,2,i));

        signals(:,:,:,i) = c;
        backgrounds(:,:,:,i) = d;
    end

    RGB2GRAYVECTOR = [1.6052   0.8541   0.0409]; %LDA vector of Texas-Red
    gray_signal = [];
    gray_background = [];

    mean_background = zeros(NO_STRIP,1);
    for i = 1:NO_STRIP
        %Filter out nonspecific signal with LDA vector (determed with MATLAB)
        gray_signal(:,:,i)= signals(:,:,1,i)*RGB2GRAYVECTOR(1)+...
            signals(:,:,2,i)*RGB2GRAYVECTOR(2)+...
            signals(:,:,3,i)*RGB2GRAYVECTOR(3);
        mean_signal(i) = mean(mean(gray_signal(:,:,i)));

        gray_background(:,:,i)= backgrounds(:,:,1,i)*RGB2GRAYVECTOR(1)+...
            backgrounds(:,:,2,i)*RGB2GRAYVECTOR(2)+...
            backgrounds(:,:,3,i)*RGB2GRAYVECTOR(3);
        mean_background(i) = mean(mean(gray_background(:,:,i)));

    end

    % Save signal and background values at this specific time point
    allBackground(:,k+1) = mean_background;
    allSignal(:, k+1) = mean_signal;
end

%Calculate and plot background subtracted signal
subtracted =  allSignal - allBackground;
x = linspace(0, length(subtracted), length(subtracted));
figure(2)
title("Background Subtracted Fluorescence of Measured Strips")
plot(x, subtracted(1,:), 'ro'), hold on;
plot(x, subtracted(2,:), 'ko');
plot(x, subtracted(3,:), 'bo');
xlabel("Frame");
ylabel("Relative Fluorescence Units (RFU)");
hold off

%% Writing Data to MATLAB & Excel readable file
if input('Do you want to write this data to a file? (true or false):  ')
   signalName = input('Input requested signal file name:  ', 's');
   csvwrite(signalName, allSignal);
```

© Copyright 2021 | N Panpradist

```
    backgroundName = input('Input requested background file name:  ', 's');
    csvwrite(backgroundName, allBackground);

    subName = input('Input requested substracted data file name: ','s');
    csvwrite(subName, subtracted);
end
```

© Copyright 2021 | N Panpradist

Chapter 3 References

1. Fridley, G. E.; Holstein, C. A.; Oza, S. B.; Yager, P., The evolution of nitrocellulose as a material for bioassays. *MRS Bulletin* **2013,** *38* (4), 326-330.
2. Josephy, P. D.; Eling, T.; Mason, R. P., The horseradish peroxidase-catalyzed oxidation of 3,5,3',5'-tetramethylbenzidine. Free radical and charge-transfer complex intermediates. *J Biol Chem* **1982,** *257* (7), 3669-75.
3. Hiroshi Awano, O. I., Kazutaka Sawada, Hiroji Ohigashi, Highly dimerizable radical cation of 3,3’,5,5’-tetramethylbenzidine. *Berichte der Bunsengesellschaft für physikalische Chemie* **1996,** *100*, 1700–1705.
4. Herzog, V.; Fahimi, H. D., A new sensitive colorimetric assay for peroxidase using 3,3'-diaminobenzidine as hydrogen donor. *Analytical biochemistry* **1973,** *55* (2), 554-62.
5. Beck, I. A.; Deng, W.; Payant, R.; Hall, R.; Bumgarner, R. E.; Mullins, J. I.; Frenkel, L. M., Validation of an oligonucleotide ligation assay for quantification of human immunodeficiency virus type 1 drug-resistant mutants by use of massively parallel sequencing. *Journal of clinical microbiology* **2014,** *52* (7), 2320-7.
6. Chung, M. H.; Beck, I. A.; Dross, S.; Tapia, K.; Kiarie, J. N.; Richardson, B. A.; Overbaugh, J.; Sakr, S. R.; John-Stewart, G. C.; Frenkel, L. M., Oligonucleotide Ligation Assay Detects HIV Drug Resistance Associated with Virologic Failure among Antiretroviral-Naïve Adults in Kenya. *Journal of Acquired Immune Deficiency Syndromes* **2014,** *67* (3), 246-253.

© Copyright 2021 | N Panpradist

7. Beck, I. A.; Crowell, C.; Kittoe, R.; Bredell, H.; Machaba, M.; Willamson, C.; Janssens, W.; Jallow, S.; van der Groen, G.; Shao, Y.; Jacob, M.; Samuel, N. M.; de Rivera, I. L.; Ngo-Giang-Huong, N.; Cassol, S.; Alemnji, G.; Frenkel, L. M., Optimization of the oligonucleotide ligation assay, a rapid and inexpensive test for detection of HIV-1 drug resistance mutations, for non-North American variants. *J Acquir Immune Defic Syndr* **2008,** *48* (4), 418-27.

8. Edelstein, R. E.; Nickerson, D. A.; Tobe, V. O.; Manns-Arcuino, L. A.; Frenkel, L. M., Oligonucleotide ligation assay for detecting mutations in the human immunodeficiency virus type 1 pol gene that are associated with resistance to zidovudine, didanosine, and lamivudine. *J Clin Microbiol* **1998,** *36* (2), 569-72.

9. Beck, I. A.; Mahalanabis, M.; Pepper, G.; Wright, A.; Hamilton, S.; Langston, E.; Frenkel, L. M., Rapid and sensitive oligonucleotide ligation assay for detection of mutations in human immunodeficiency virus type 1 associated with high-level resistance to protease inhibitors. *J Clin Microbiol* **2002,** *40* (4), 1413-9.

10. Ellis, G. M.; Mahalanabis, M.; Beck, I. A.; Pepper, G.; Wright, A.; Hamilton, S.; Holte, S.; Naugler, W. E.; Pawluk, D. M.; Li, C. C.; Frenkel, L. M., Comparison of oligonucleotide ligation assay and consensus sequencing for detection of drug-resistant mutants of human immunodeficiency virus type 1 in peripheral blood mononuclear cells and plasma. *J Clin Microbiol* **2004,** *42* (8), 3670-4.

© Copyright 2021 | N Panpradist

11. Wagner, T. A.; Kress, C. M.; Beck, I.; Techapornroong, M.; Wittayapraparat, P.; Tansuphasawasdikul, S.; Jourdain, G.; Ngo-Giang-Huong, N.; Lallemant, M.; Frenkel, L. M., Detection of HIV-1 drug resistance in women following administration of a single dose of nevirapine: comparison of plasma RNA to cellular DNA by consensus sequencing and by oligonucleotide ligation assay. *J Clin Microbiol* **2010,** *48* (5), 1555-61.

12. Fridley, G. E.; Le, H. Q.; Fu, E.; Yager, P., Controlled release of dry reagents in porous media for tunable temporal and spatial distribution upon rehydration. *Lab Chip* **2012,** *12* (21), 4321-7.

13. Ramachandran, S.; Fu, E.; Lutz, B.; Yager, P., Long-term dry storage of an enzyme-based reagent system for ELISA in point-of-care devices. *Analyst* **2014,** *139* (6), 1456-62.

14. Montoya, A.; Castell, J. V., Long-term storage of peroxidase-labelled immunoglobulins for use in enzyme immunoassay. *J Immunol Methods* **1987,** *99* (1), 13-20.

15. Altikatoglu, M.; Basaran, Y., Additive effect of dextrans on the stability of horseradish peroxidase. *Protein J* **2011,** *30* (2), 84-90.

16. Lutz, B.; Liang, T.; Fu, E.; Ramachandran, S.; Kauffman, P.; Yager, P., Dissolvable fluidic time delays for programming multi-step assays in instrument-free paper diagnostics. *Lab Chip* **2013,** *13* (14), 2840-7.

17. Toley, B. J.; Wang, J. A.; Gupta, M.; Buser, J. R.; Lafleur, L. K.; Lutz, B. R.; Fu, E.; Yager, P., A versatile valving toolkit for automating fluidic operations in paper microfluidic devices. *Lab Chip* **2015,** *15* (6), 1432-44.

© Copyright 2021 | N Panpradist

18. Shivani, D.; Lisa, L.; Samantha, B.; Peter, K.; Josh, B.; Bhushan, T.; Elain, F.; Paul, Y.; Barry, L. In *Programming paper networks for point of care diagnostics*, Proc.SPIE, 2013.

19. Lutz, B. R.; Trinh, P.; Ball, C.; Fu, E.; Yager, P., Two-dimensional paper networks: programmable fluidic disconnects for multi-step processes in shaped paper. *Lab Chip* **2011,** *11* (24), 4274-8.

20. Kurien, B. T.; Dorri, Y.; Dillon, S.; Dsouza, A.; Scofield, R. H., An overview of Western blotting for determining antibody specificities for immunohistochemistry. *Methods in molecular biology (Clifton, N.J.)* **2011,** *717*, 55-67.

21. Holstein, C. Development of a Novel Paper-Based Flu Test for Improved Diagnosis at the Point of Care. https://digital.lib.washington.edu/researchworks/handle/1773/33583.

22. Black, W. C. t.; Gorrochotegui-Escalante, N.; Duteau, N. M., Heated oligonucleotide ligation assay (HOLA): an affordable single nucleotide polymorphism assay. *J Med Entomol* **2006,** *43* (2), 238-47.

23. Zhu, J.; Bošković, F.; Nguyen, B.-N. T.; Nitschke, J. R.; Keyser, U. F., Kinetics of Toehold-Mediated DNA Strand Displacement Depend on Fe(II)(4)L(4) Tetrahedron Concentration. *Nano letters* **2021,** *21* (3), 1368-1374.

24. Zhang, D. Y.; Winfree, E., Control of DNA Strand Displacement Kinetics Using Toehold Exchange. *Journal of the American Chemical Society* **2009,** *131* (47), 17303-17314.

© Copyright 2021 | N Panpradist

25. Broadwater, D. W. B., Jr.; Kim, H. D., The Effect of Basepair Mismatch on DNA Strand Displacement. *Biophys J* **2016,** *110* (7), 1476-1484.

26. Los Alamos National Laboratory HIV database. http://www.hiv.lanl.gov/.

27. Integrated DNA Technology Modified Bases Modifications. https://www.idtdna.com/site/Catalog/Modifications/Category/7.

28. Yu, W.; Tang, L.; Qiu, J.-H.; Zhang, Z.; Zhou, L.-L.; Li, J.-L.; Xie, G.-M., Systematic comparison between toehold exchange and toehold displacement: exploration for highly specific and sensitive DNA detection. *RSC Advances* **2017,** *7* (65), 40858-40865.

29. McIntyre, D. *Quantification of DNA Hybridization on Nitrocellulose Membranes*; Department of Bioengineering, University of Washington: 2018.

30. Dharmaraja, S.; Lafleur, L.; Byrnes, S.; Kauffman, P.; Buser, J.; Toley, B.; Fu, E.; Yager, P.; Lutz, B., *Programming paper networks for point of care diagnostics*. SPIE: 2013; Vol. 8615.

31. Gudnason, H.; Dufva, M.; Duong Bang, D.; Wolff, A., An inexpensive and simple method for thermally stable immobilization of DNA on an unmodified glass surface: UV linking of poly(T)10-poly(C)10-tagged DNA probes. *Biotechniques* **2008,** *45* (3), 261-71.

32. Grady, J. K.; Chasteen, N. D.; Harris, D. C., Radicals from "Good's" buffers. *Anal Biochem* **1988,** *173* (1), 111-5.

33. Douglas, H. Easy molecular binding crosslinking technology. https://tools.thermofisher.com/content/sfs/brochures/1602163-Crosslinking-Reagents-Handbook.pdf.

© Copyright 2021 | N Panpradist

34. Fang, S.; Wei, J.; Pentinmikko, N.; Leinonen, H.; Salven, P., Generation of functional blood vessels from a single c-kit+ adult vascular endothelial stem cell. *PLoS Biol* **2012,** *10* (10), e1001407.

35. Saito, H.; Dahlin, L. B., Expression of ATF3 and axonal outgrowth are impaired after delayed nerve repair. *BMC Neuroscience* **2008,** *9* (1), 88.

36. Deng, J. Y.; Zhang, X. E.; Mang, Y.; Zhang, Z. P.; Zhou, Y. F.; Liu, Q.; Lu, H. B.; Fu, Z. J., Oligonucleotide ligation assay-based DNA chip for multiplex detection of single nucleotide polymorphism. *Biosens Bioelectron* **2004,** *19* (10), 1277-83.

37. Schüler, T.; Nykytenko, A.; Csaki, A.; Möller, R.; Fritzsche, W.; Popp, J., UV cross-linking of unmodified DNA on glass surfaces. *Anal Bioanal Chem* **2009,** *395* (4), 1097-105.

38. Peyton, C. L.; Gravitt, P. E.; Hunt, W. C.; Hundley, R. S.; Zhao, M.; Apple, R. J.; Wheeler, C. M., Determinants of genital human papillomavirus detection in a US population. *J Infect Dis* **2001,** *183* (11), 1554-64.

39. Golden, A. L.; Battrell, C. F.; Pennell, S.; Hoffman, A. S.; Lai, J. J.; Stayton, P. S., Simple fluidic system for purifying and concentrating diagnostic biomarkers using stimuli-responsive antibody conjugates and membranes. *Bioconjug Chem* **2010,** *21* (10), 1820-6.

40. ThermoFisher Scientific Carbodiimide Crosslinker Chemistry. https://www.thermofisher.com/us/en/home/life-science/protein-biology/protein-biology-learning-center/protein-biology-resource-library/pierce-protein-methods/carbodiimide-crosslinker-chemistry.html#/legacy=www.piercenet.com.

© Copyright 2021 | N Panpradist

41. Wine, Y.; Cohen-Hadar, N.; Freeman, A.; Frolow, F., Elucidation of the mechanism and end products of glutaraldehyde crosslinking reaction by X-ray structure analysis. *Biotechnol Bioeng* **2007,** *98* (3), 711-8.

42. Kapoor, M. How to crosslink protein. http://www.fgsc.net/neurosporaprotocols/how%20to%20cross-link%20proteins.pdf.

© Copyright 2021 | N Panpradist

CHAPTER 4: READY-TO-USE DRY REAGENTS

CONTRIBUTORS. I collaborated with Nikki Higa (an undergraduate student mentee), Isaac So (a technician from Frenkel lab), and Daniel Leon (a researcher in the Lutz lab). We characterized key chemical properties of the excipient formulations: inhibitory effect (on specificity and sensitivity of LDR), lyoprotectant ability (ability to protect enzymes and DNA during freezing and drying), and stability after long-term storage. Additionally, the physical properties of the dried mixtures were also described and characterized. I collaborated with David McIntyre to develop the method for high-throughput bead production.

DELIVERABLES. We have developed and characterized formulations and fabrication platforms (e.g., in-tube, droplets, and in-tip) for dried reagents for the amplification, ligation, the detection steps in the OLA. Last, we discussed long-term storage analysis of lyophilized reagents and other considerations.

SIGNIFICANCE. This simplification significantly accelerated the preparation of PCR and ligation mixtures to less than a minute, with reduced chances for erroneous mixture preparation. Less manipulation of tubes potentially reduces opportunities for contamination. Near zero volume of dried mixtures permit more sample volume input which can increase sensitivity in low-concentration samples. Last, the stability of dried mixtures at room temperature can avoid -20°C storage for transportation and inventory. Developed approaches can be translated to other molecular assays that require PCR and ligation for any target organisms.

© Copyright 2021 | N Panpradist

Previous publications.

Several parts of texts and figures in this section are modified from publications:

1) N Panpradist et al. 2019 (https://doi.org/10.1016/j.ebiom.2019.11.002)

2) Patent application (17/055,966).

MATERIALS AND METHODS

Development of excipient formulations. One or multiple different excipients: trehalose from Life Science Advanced Technology, St. Petersburg, FL; dextran 500 kDa from Spectrum Chemical, New Brunswick, NJ; poly(vinyl alcohol) – PVA 89 kDa and poly(ethylene glycol) – PEG 35 kDa from Sigma-Aldrich, St. Louis, MO; mannitol and sucrose from OPS Diagnostics LLC, Lebanon, NJ – were spiked at the concentrations from 0.05-10%w/v into the standard ligation mixture previously described in **Chapter 3**. Briefly, the standard ligation mixture contained 1 mM NAD, 0.1%v/v Triton X-100, 20mM Tris hydrochloride pH 8.0, 10mM $MgCl_2$, 1mM DDT, 12mM KCl, 15 - 60 nM oligonucleotide probes and 0.67U of thermostable Ampligase ligase. For the inhibitory study experiment, a freshly prepared ligation mixture (24µL) was added with 2.4µL of 1:4 diluted amplicon containing the HIV *pol* gene. The ligation reaction mixtures underwent ten cycles of denaturation at 94°C for 30 seconds and annealing at 37°C for 4 minutes. Lastly, 12 µL of 100mM EDTA/ 0.1%v/v Triton X-100 was added to the reaction to inactivate the ligase enzyme. For the lyoprotectant study experiment, the ligation mixture was frozen in liquid nitrogen for 2 minutes and dried for 2 hours. Each dried ligation

© Copyright 2021 | N Panpradist

mixture was reconstituted with 24µL nuclease-free water and replaced with the freshly prepared ligation mixture described above.

Thermal stability study on a selected ligation mixture. Standard ligation mixtures with an addition of 1.5% PEG35K and 5% trehalose were frozen in liquid nitrogen and dried, as described in the lyoprotectant study experiments. After the drying process, the mixture was stored at room temperature (21-25 °C) under a <30% relative humidity for 3, 7, 21, 28, or 49 days before being subjected to ligation.

Quantitation of amplified HIV product. We quantified amplicon using two methods (i) quantitative Agarose gel electrophoresis (**Figure S4.17**) and (ii) mass quantitation of DNA after gel extraction (**Figure S4.18**).

Quantitation of ligated products by ELISA. 32µL ligation product was added to a streptavidin-coated 96-well plate for 1-hour incubation in the dark. The plate was washed twice with 0.01N sodium hydroxide and 0.05%v/v Tween-20, followed by two additional washes with Tris Wash (100mM Tris hydrochloride pH 7.5, 15mM sodium chloride, and 0.05%v/v Tween-20). 50µL of antibody mix containing 7.5mU anti-digoxigenin antibody tagged peroxidase, 7.5mU anti-fluorescein antibody labeled alkaline phosphatase in 0.5% bovine serum albumin in 1x phosphate buffer saline was added and incubated for 30 minutes. The plate was then washed six times with Tris Wash. Each well was then added 100µL of the yellow substrate. Kinetic reading of absorbance at 405nm was conducted every five minutes for one hour. The plate was then washed six times with Tris Wash. 50µL of TMB one solution was

© Copyright 2021 | N Panpradist

added, followed by 50µL of 0.3 M sulfuric acid before an absorbance reading at 450nm.

Tube-based platform. To prepare the tube-based platform, 24µL of the ligation mixture was aliquoted into 8-strip PCR tubes and frozen in a liquid nitrogen bath for at least 2 minutes. During the freeze-drying process, the caps remained open (Labconco Freeze Dry System / Freezone 4.5) at -40°C at 220 x 10^{-3} mbar for at least 2 hours. Mixtures were stored at room temperature (21-25 °C at a <30% relative humidity) before testing, otherwise indicated in figure caption.

Bead platform. To prepare this platform, a 24µL ligation mixture was added droplet-wise into a small bath of liquid nitrogen in 12-well plates (Sigma, CLS3512, St. Louis, MO). Only one droplet per well was added to prevent droplets from sticking to one another. After >2 minutes, the frozen" beads" were transferred to another 12-well plate, which was then covered with adhesive foil containing small holes to allow water to evaporate during the drying process. The plates were transferred to a freeze-drying flask and lyophilized for >2 hours. The beads were rehydrated in 8-strip PCR tubes with 24µL nuclease-free water and subjected to a vortexer to dissolve the dried reagents.

Pipette-based platform. To prepare this platform, the ligation mixture was aliquoted into 8-strip PCR tubes. A multichannel pipette was used to aspirate a 24µL reaction mixture plus 6µL liquid wax (Bio-Rad, CHO1401, Hercules, CA). The loaded pipette tips were frozen in a liquid nitrogen bath for >2

© Copyright 2021 | N Panpradist

minutes and transferred to a pipette tip rack. Once the rack was full, the tips were dipped in a thicker wax to form an external seal around the opening of the tips. The racks were transferred to a freeze-drying flask and lyophilized for >2 hours. Using a multichannel pipette, the tips were rehydrated by repeatedly aspirating and expelling 24µL nuclease-free water in 8-strip PCR tubes.

Full workflow of OLA using in-tip dried mixtures. Dried mixtures of standard PCR MyTaq polymerase with the addition of 5%w/v trehalose; and dried mixtures of standard ligation mixture with 5%w/v trehalose and 1.5% PEG were prepared in the pipette tip platform. The in-tip dried PCR reagent was mixed with a 25µL of 25pg plasmid containing the HIV *pol* gene, which corresponds to 200 copies of HIV (including 0%, 5%, and 100% nevirapine-resistant HIV) in 250 ng human genomic DNA. The mixture was then subjected to PCR. 2µL PCR product was taken out for gel electrophoresis while the rest of the PCR product was mixed with the dried ligation mixture preloaded in the pipette tip platform. Note that the ligation mixture was adjusted to be compatible with the full-volume PCR buffer by reducing salt to 20mM monovalent salts (instead of 33mM), 10 mM $MgCl_2$, and 75-300 nM ligation probes (instead of 15-60 nM ligation probes). The mixture was then subjected to LDR. After the completion of LDR, the product from the ligation step was analyzed using ELISA.

Lyoprotectant study and thermal stability of PCR mixtures. One or multiple different excipients: trehalose, dextran, PVA, PEG, mannitol, and sucrose, were spiked to the standard PCR mixture. The 25µL of standard PCR mixture (Bioline, Taunton, MA) contained 5mU MyTaq DNA polymerase or

© Copyright 2021 | N Panpradist

MyTaq HS DNA polymerase, 1x MyTaq reaction buffer (1mM dNTPs, 1.5 mM $MgCl_2$, proprietary stabilizers and enhancers at unknown concentrations) and 400nM forward primer (GRCCTACACCTGTCAACATAATTGG) and 400nM reverse primer (CAAAGRAATGGAGGTTCTTTCTGATG). The mixtures were frozen and dried, as described in lyoprotectant experiments. The dried mixtures were stored for 7 days before reconstitution with 22.5µL of water and 2.5µL of 0.01 ng/µL plasmid containing 0%, 5%, or 100% Y181C mutant/ wild-type HIV *pol* gene. The mixtures with MyTaq DNA polymerase were subjected to 35 cycles of 95°C for 3 minutes, 55°C for 30 seconds, and 72°C for 10 seconds. 5µL of 1:5 diluted amplicon, 1x blue juice tracking dye was added to each well of 1:10000 SYBR Safe stained 1% Agarose gel and ran at 90V for 45 minutes. The gel was imaged at a 1.2 second exposure time and analyzed using in-house MATLAB code. The intensity of each gel was then normalized to the intensity of the 2000 bp band of the low-range DNA ladder.

RESULTS

4.1 EXCIPIENT FORMULATIONS

Lyophilization or freeze-drying has been used to prepare dried mixtures in the presence of excipients to maintain the stability of pharmaceutical products[1]. During this process, a reagent mixture is frozen in liquid and dried via sublimation. For water as the only solvent, lyophilization must occur at temperatures and pressures lower than the triple point to enable sublimation (**Figure 4.1A**).

© Copyright 2021 | N Panpradist

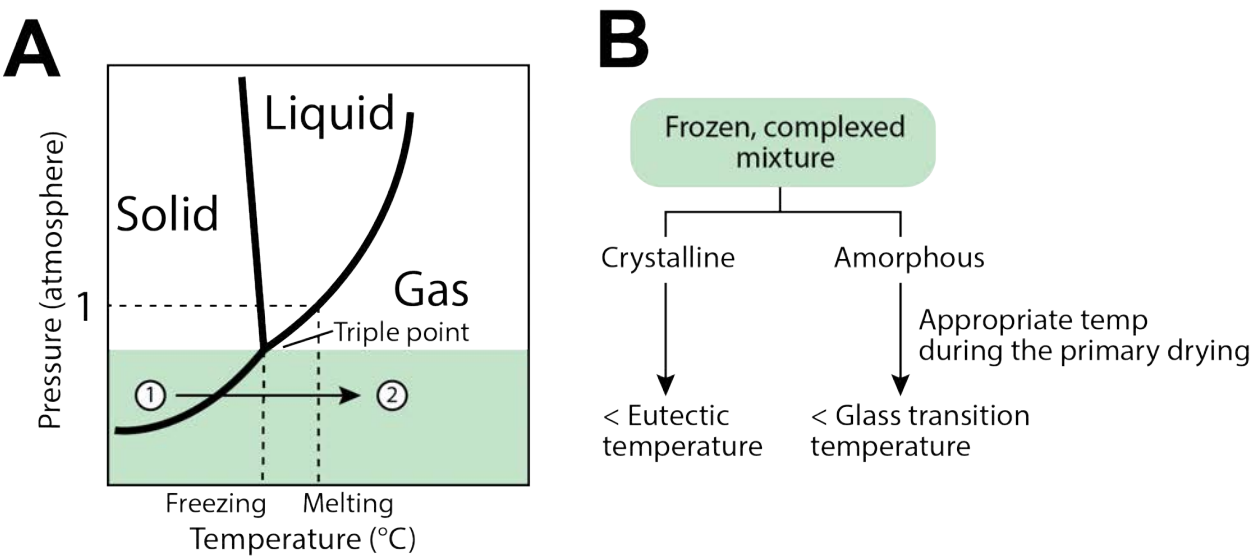

Figure 4.1 | Concept of lyophilization and critical temperatures.

(**A**) Phase diagram of water. The Lyophilization process involves the transition of solid (1) to gas (2). (**B**) The critical temperatures for the drying process depending on the types of substances.

However, lyophilization applications often involve a mixture that contains multiple components collectively called "excipient." Depending on the properties of the excipients, it is essential to set up the lyophilization under critical temperatures. Crystalline substances must be dried at lower than eutectic temperatures to avoid melting, while amorphous materials must be dried lower than the glass transition temperature to avoid collapsing (**Figure 4.1B**). In pharmaceutical industries, a set of excipients are commonly used to preserve the small molecules (*i.e.,* drugs) during the lyophilization process (**Figure 4.2**).

© Copyright 2021 | N Panpradist

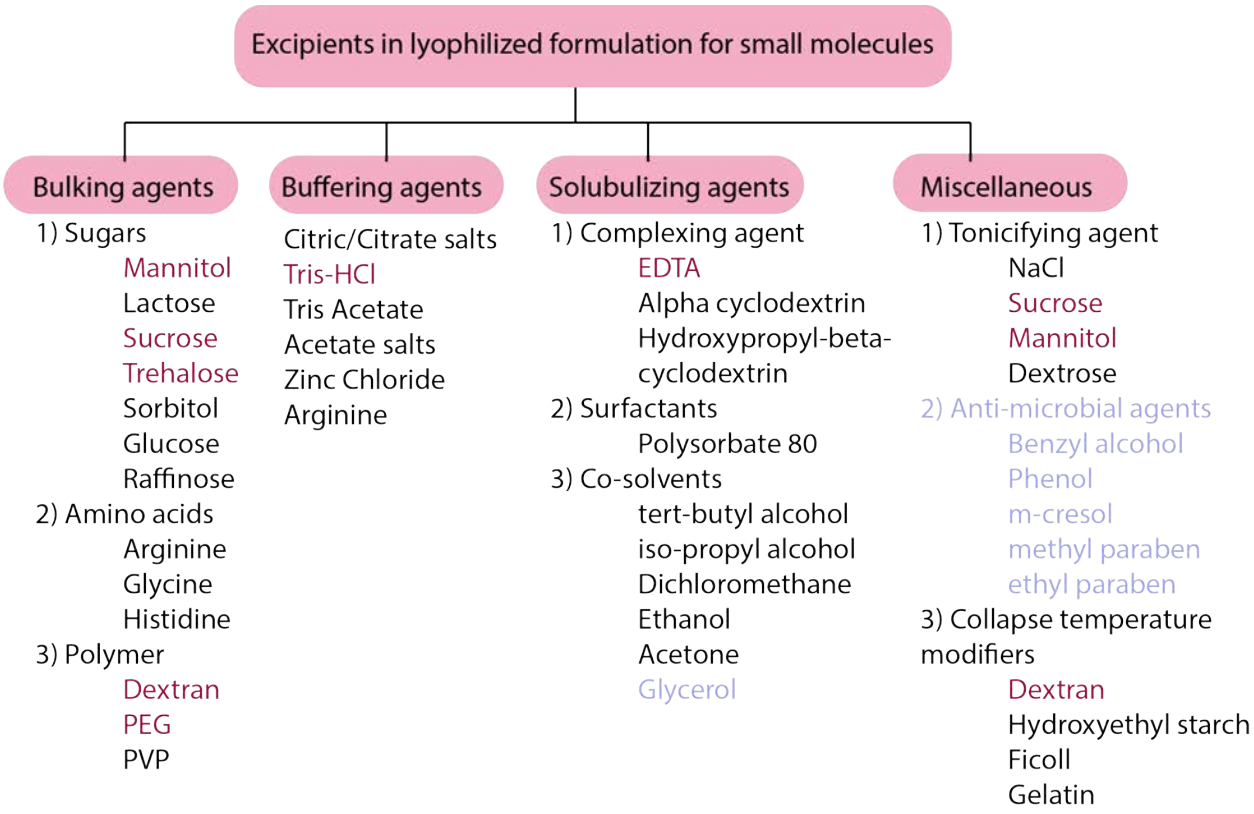

Figure 4.2 | Commonly used excipients for lyophilization of small molecules.

Red are the candidates we tested. Blue are the candidates theoretically incompatible with our assay. The list was modified from A Baheti et al[1]

These excipient formulations for lyophilizing small molecules are not readily translated to address specific functions required in molecular assays. Molecular assays involve nucleic acid and enzyme components, and thus the addition of certain excipients can impact assay performance. The addition of salts (e.g., Tris-HCl) and stabilizers (e.g., trehalose [2], polyols[3]) alters the melting temperatures of nucleic acid. Additionally, the ease of rehydration of dry reagents will also depend significantly on the formulations. Solubilizing agents (e.g., ethylenediamine tetra acetic acid (EDTA)) can improve the solubility of the mixture. Still, they can chelate magnesium ions required for polymerase

© Copyright 2021 | N Panpradist

and other enzymes to function properly in PCR. We included use of the bulking agents as they would be necessary for lyophilizing, in general, to provide the voids for vapor escape during the drying process. Based on the critical temperatures reported in **Table 4.1**[4-8], we set up our lyophilization temperature to be -55°C and the lowest pressure settings available on our machine (0.018 mbar) to ensure temperatures are lower than these critical temperatures.

Table 4.1 | Critical temperatures of excipient candidates (°C)

Excipient	Glass transition temperature	Collapse temperature
Sucrose	-32, -35	-34, -32
Trehalose	-27, -29	-29.5, -34
Mannitol	-35, -28	
Dextran	-10	-9, -10
PEG(4k)	-22.7	
PEG(6k)	-22.3	
PEG(20k)	-34.63	

4.1.1 EXCIPIENT FORMULATIONS COMPATIBLE WITH OLA

To develop the formulations for OLA-Simple dried reagents, we adopted the additive formulation 5% trehalose for lyophilization of *Taq* DNA polymerase[9], and developed new additive formulations for dry ligase enzyme and gold nanoparticles. We tested the preservative effects of bulky sugars and polyol additives previously used for dry enzymes and proteins: trehalose, dextran, mannitol, poly (ethylene glycol), and poly(vinyl alcohol). Sensitivity (**Figure 4.3A**) and specificity (**Figure 4.3B**) of probe ligation in the presence of these

© Copyright 2021 | N Panpradist

additives were compared to standard probe ligation with CLIA-OLA buffer. None of these additives strongly inhibited ligation, but some mixtures increased non-specific ligation. We chose a 5% trehalose and 1.5% poly (ethylene glycol) mixture for lyophilizing ligation reagents because it enhanced ligation yield without causing non-specific ligation. It was compatible with the 5% trehalose carried over from the PCR. Next, we tested the sensitivity and specificity of four commercial hot-start *Taq* polymerases in the presence of 5% trehalose with WT plasmid control and DNA extracted from six clinical specimens (**Figure 4.3, C-D**). Roche FastStart™ PCR in the presence of 5% trehalose yielded maximum target amplicon with minimal non-specific amplification signal. The ligation reaction using the product of this PCR mixture showed comparable results to CLIA-OLA (**Figure 4.3, E-F**). Hence, Roche FastStart™ PCR with 5% trehalose was selected. We also evaluated the long-term stability of the dry PCR and ligation reagents with the selected additive formulations.

© Copyright 2021 | N Panpradist

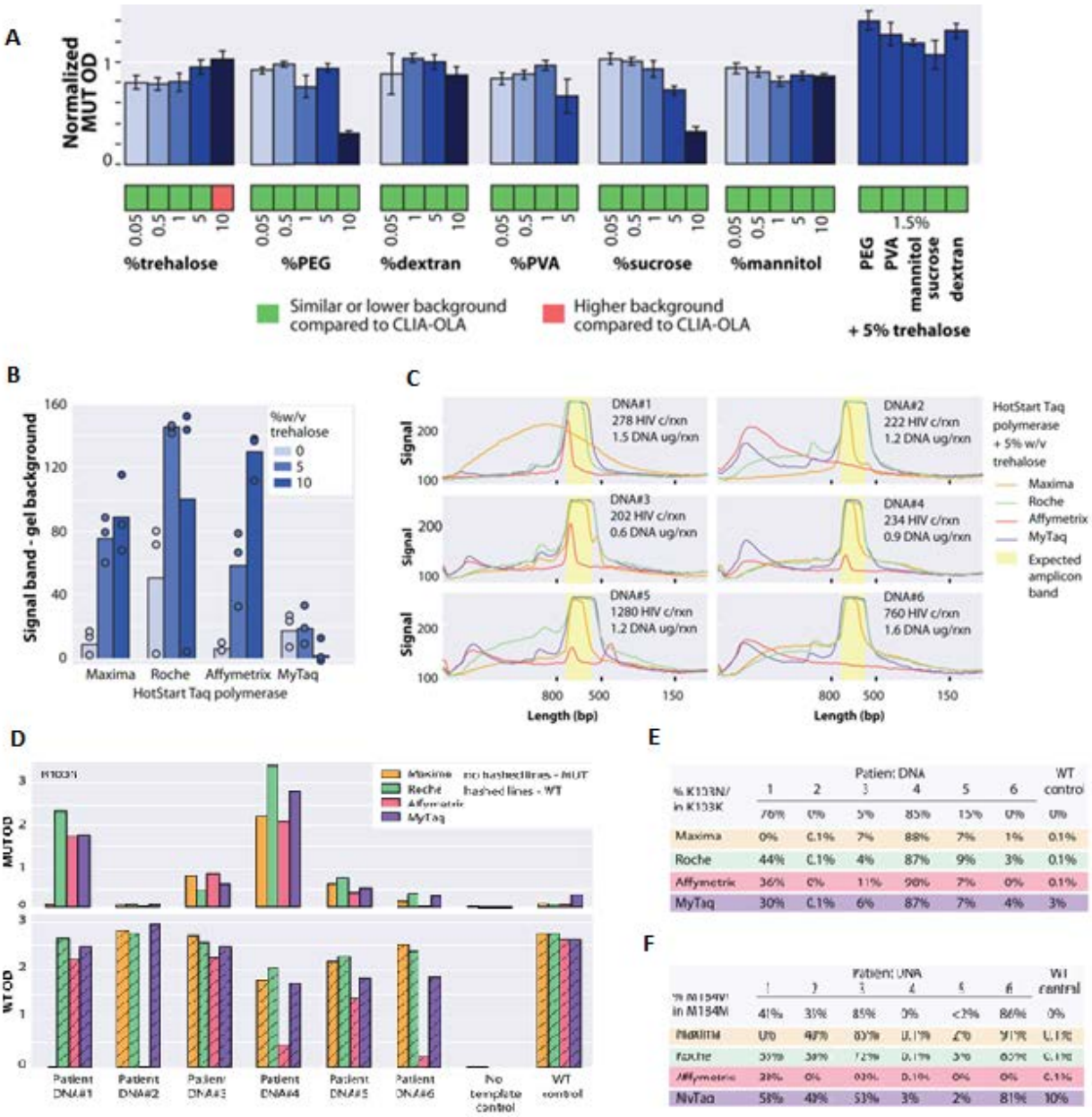

Figure 4.3 | Excipient formulations for OLA.

(**A**) Effect of additives on ligation yield. Ligation reactions spiked with 0.05% – 10% of a single additive (trehalose, dextran, poly (vinyl alcohol) (PVA), poly(ethylene glycol) (PEG), sucrose, or mannitol), or a combination of additives (5% trehalose mixed with 1.5% dextran, PEG, PVA, mannitol or sucrose) were mixed with a PCR-amplified 5% Y181C/Y181Y plasmid mixture. The vertical axis shows the MUT OD of the mixture spiked with additive(s) divided by the MUT OD by CLIA-OLA. Reported values are means ± SE of three to four replicates. (**B**) Effect of additives on the specificity of ligation. Similar experiments done in (**A**) were performed on PCR-amplified 0% MUT plasmid. Mixtures with a significantly higher

© Copyright 2021 | N Panpradist

background than the OD detected by CLIA-OLA are in red (P<0.05, t-test comparing the MUT OD of the mixture spiked with additive(s) and the MUT OD by CLIA-OLA). Reported values are means of three replicates. Note that 5%-10% *(w/v)* PVA were difficult to dissolve at room temperature and too viscous to flow in lateral flow detection. (C) Comparison of PCR-amplified products from 10 copies of WT plasmid from three replicates using commercially available Taq polymerases in the presence of 0%, 5%, and 10% *(w/v)* trehalose. The signal from each gel band (means, n=3) was calculated from the 95th percentile band intensity of expected band size minus 95th percentile band intensity of areas underneath the expected band size on 1% *(w/v)* Agarose stained with EtBr. All polymerases tested (Maxima^{TM} (Life Technology), FastStart^{TM} (Roche), HotStart-IT^{TM} (Affymetrix), and MyTaqHS (Bioline)) had increased amplification yield when adding 5% trehalose to the PCR mixture. FastStart polymerase had the highest and most reliable amplification of 10 HIV copy input. (D) Comparison of PCR-amplified products from six patient DNA specimens. Black and white images of 1% agarose gel stained with EtBr were rotated 90°, and the average signal across the distance that the amplification band migrated was plotted. The peak between 500-800 bp corresponded to the expected products. (E) The amplified products from (D) were subjected to CLIA-OLA ligation. MUT and WT OD are reported (means, n=2), respectively. (F) & (G) % mutant estimated from each PCR product compared to previously reported values by CLIA-OLA for K103N and M184V, respectively. MyTaq was associated with a false MUT signal in WT controls. Roche FastStart PCR yielded the most comparable results to original CLIA-OLA. Figure was modified from DOI: https://doi.org/10.1016/j.ebiom.2019.11.002.

4.1.2 OPTIMAL ENZYME CONCENTRATIONS IN LYOPHILIZED PCR AND LIGATION STEP

Lyophilized PCR using the manufacturer's recommended condition yielded 10-fold fewer amplicon concentrations compared to the nested PCR in the original OLA (10^{11} – 10^{12} copies/uL, **Figure 4.16** and **Figure S4.17**). We hypothesized that increasing the polymerase concentration and/or amplification cycles could increase the amplification yield. 55-cycle PCR had a higher yield than 45-cycle PCR only when doubled polymerase concentration was used (**Figure 4.4**). For

© Copyright 2021 | N Panpradist

the 45-cycle PCR, we observed a drastically increased amplification yield of low copy numbers (i.e., 20 copies). Next, we investigated how ligase concentration would impact the sensitivity and specificity of the OLA (**Figure 4.5**). Doubled ligase and polymerase concentration yielded the maximum MUT signal without sacrificing specificity. Thus, this condition was used in the final OLA-Simple 1.0 kit (discussed in **Chapter 5**).

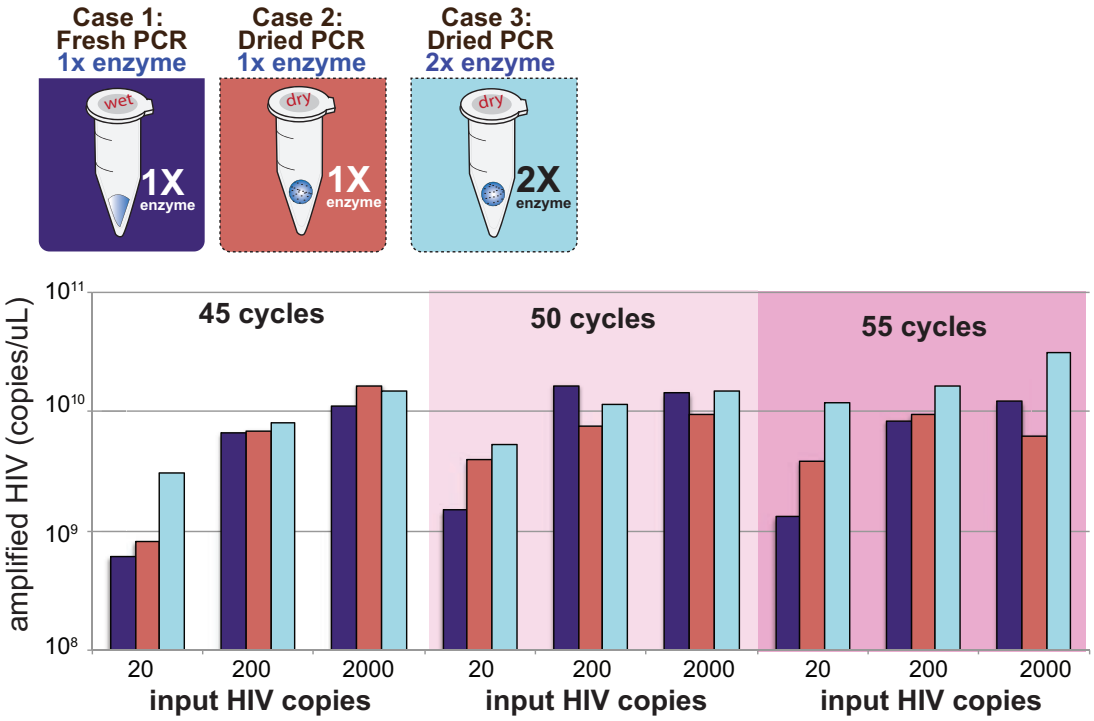

Figure 4.4 | Effect of polymerase concentrations on PCR.

© Copyright 2021 | N Panpradist

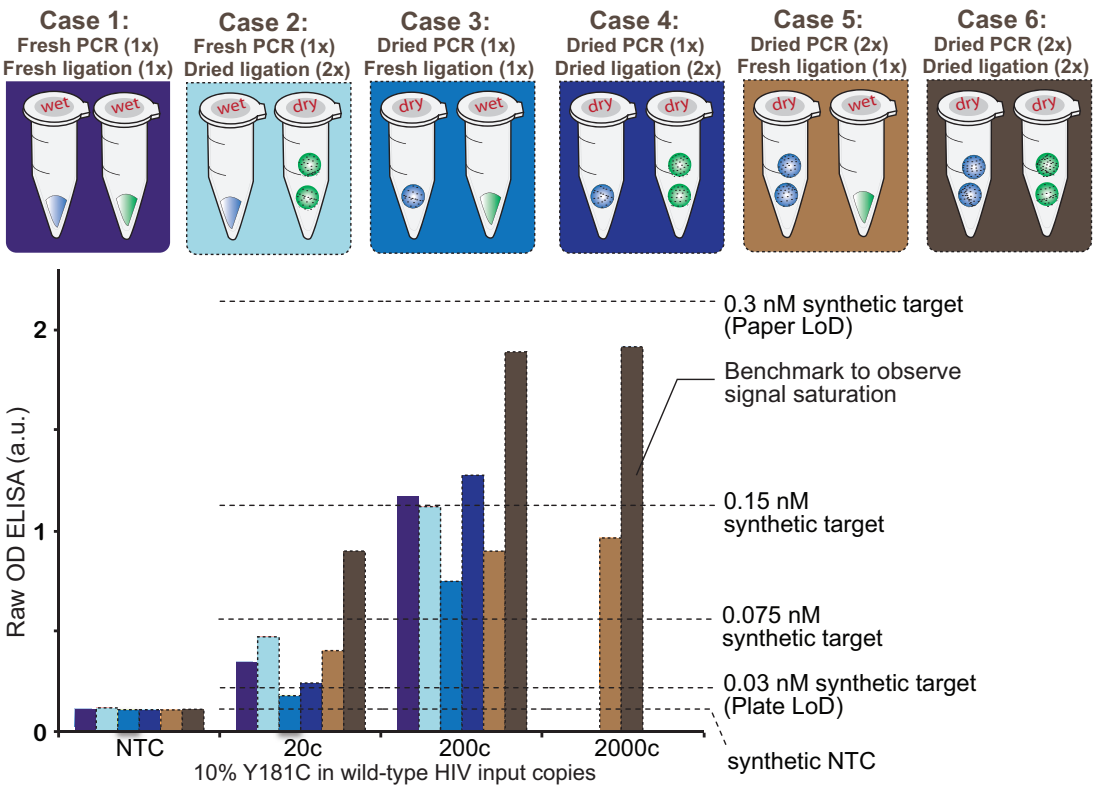

Figure 4.5 | Effect of ligase concentration on OLA.

4.1.3 THE PHYSICAL CHARACTERISTIC OF DRIED LIGATION MIXTURE.

Each mixture creates a different appearance of dried mixtures (**Figure 4.6**). PVA-containing ligation mixtures appear to shrink after lyophilization, whereas mannitol- or sucrose-containing ligation mixtures appear to expand after lyophilization. Interestingly, 5% trehalose mixture contributed to a high opaqueness, and that behavior was not altered in the presence of 1.5% PEG or PVA, while the trehalose mixtures became more transparent in the presence of 1.5% mannitol or sucrose.

© Copyright 2021 | N Panpradist

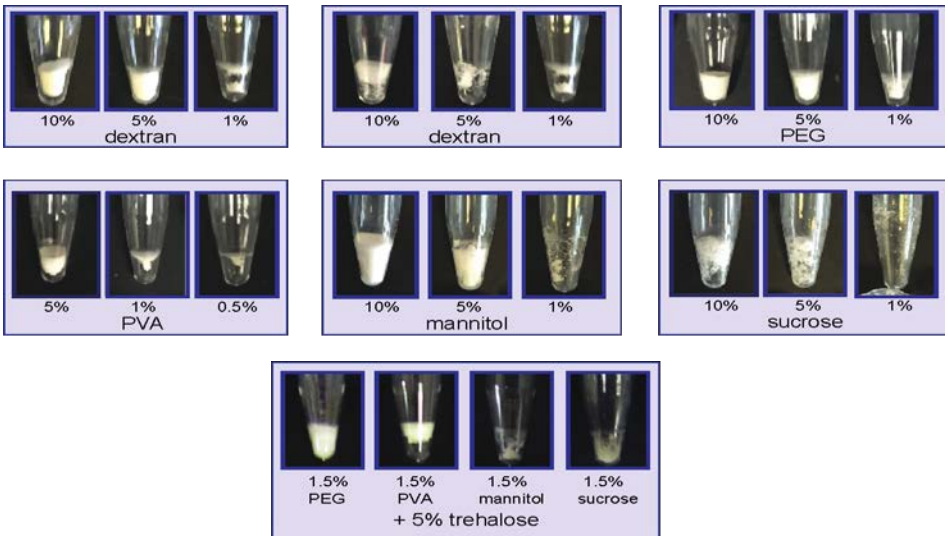

Figure 4.6 | **Physical appearance of dried ligation mix in the presence of excipients.**

Excipients were dextran 500 kDa, trehalose, poly (ethylene glycol) or PEG 35 kDa, poly(vinyl alcohol) or PVA 89 kDa, mannitol, and sucrose in the concentration range from 0.5% to 10% w/v.

4.1.4. PHYSICAL CHARACTERIZATION OF DRIED EXCIPIENTS USING XRAY DIFFRACTION

XRD has been used to determine % crystallinity of lyophilized component[11] and can verify the quality of the lyophilization process. A good lyophilization process involves rapid freezing, which disrupts the crystalline orientation of polymer and sugar molecules. The frozen mixtures are then subjected to a drying process under low pressure and temperature below the eutectic point of the mixtures. However, should freezing occur too slowly and water molecules have enough time to orient themselves, enzymes will be under stress. Should drying occur at such a high temperature that causes previously frozen mixture to melt, it will undergo evaporation instead of sublimation (**Figure 4.1B**), and enzymes will be under stress as they are in a high salt

© Copyright 2021 | N Panpradist

concentration solution. Such stress can damage enzyme function. In a good freezing and drying system, we expect to see broad XRD peaks of freeze-dried mixtures, and this pattern should be different from the crystalline forms of powered excipients from manufacturers. **Figure 4.7** demonstrates the XRD of matrices before and after our lyophilization process. Characteristic XRD peaks in manufactured trehalose and PEG disappear in lyophilized excipient formula, indicating fast freezing and good drying conditions.

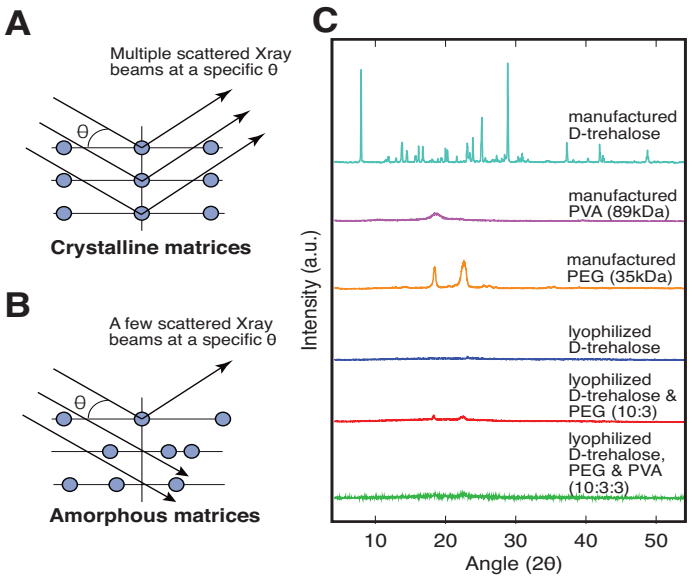

Figure 4.7 | X-ray Diffraction of matrices.

(**A**) Multiple X-ray beams are scattered at a particular incident X-ray angle (Theta) due to repeating patterns in crystalline matrices. (**B**) Only a few X-ray beams are scattered at a particular incident X-ray angle in amorphous matrices. (**C**) XRD of excipients before and after lyophilization. Daniel Leon collected data.

© Copyright 2021 | N Panpradist

4.2 FABRICATION PLATFORMS OF LYOPHILIZED REAGENTS

4.2.1 MULTIPLE PLATFORMS CAN BE USED TO STORE DRIED REAGENTS

The physical properties (density and viscosity) varied among excipient formulations. We use these properties as guidelines for selecting proper formulations used in the different platforms (**Figure 4.8**). In-tube[10 11, 12 13] and droplets[14, 15] (**Figure 4.9**) are the two existing dried reagent platforms. In-tube lyophilization applies to most excipient formulations. On the other hand, beads are prepared from freezing the droplets of reagents and may require a precise dispenser to create consistent sizes of the beads for consistency.

To maintain the integrity of the droplets after sublimation, the formulations must include a relatively high percentage of solid or high-molecular-weight polymers such as PEG or PVA. Beads with more dense structures can result in difficulties during the reconstitution require a more rigorous agitation by a vortex mixer or physically cracking by the pipette tip[16]. In addition to dried reagents in tubes and as beads, we developed a new platform for dry reagent storage for simple workflow and fast rehydration. The lyophilized reagents are stored within the pipette tips and covered with a removable wax-based external cap (**Figure 4.8C**). Users remove the wax cover and mix the dried reagent in the tip with the analyte through repeated fluid aspiration and release. This platform simplifies and speeds up the preparation step for molecular diagnostic assays.

© Copyright 2021 | N Panpradist

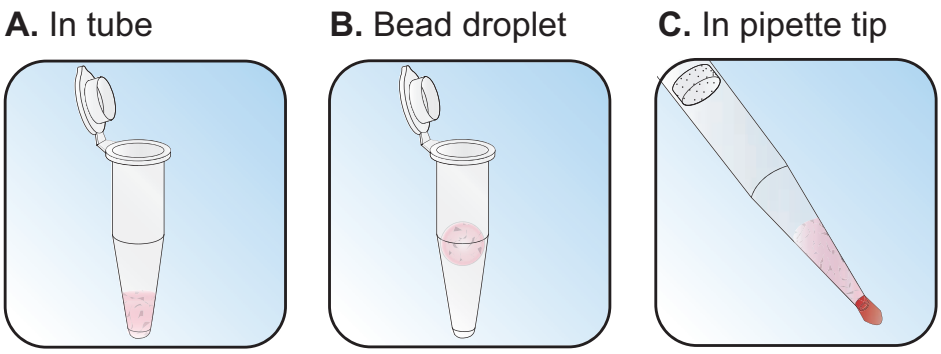

Figure 4.8 | Platforms for dried reagents.

(**A**) dried reagents in a tube, (**B**) bead droplets, and (**C**) in tips.

4.2.1 DEMONSTRATION OF SIMPLIFIED OLA WORKING USING IN-HOUSE BEAD DRY REAGENTS

We demonstrate the use of droplet dried PCR and ligation mixtures in the full OLA workflow. The droplet dried PCR reagent was mixed with a solution containing HIV plasmid (containing 200 copies of 0% - 100% nevirapine-resistant HIV) in 250ng human genomic DNA. The mixture was then subjected to 35 cycles of PCR. The PCR product in the original tube was mixed with another in-tip dried LDR mixture. The mixture was then subjected to 10-cycle ligation. After ligation, the product was analyzed using ELISA. The performance of in-tip dried reagents (3-day storage at room temperature) was comparable to the standard protocol, which involves fresh reagents and transferring of reagents across multiple tubes (**Figure 4.9B**).

© Copyright 2021 | N Panpradist

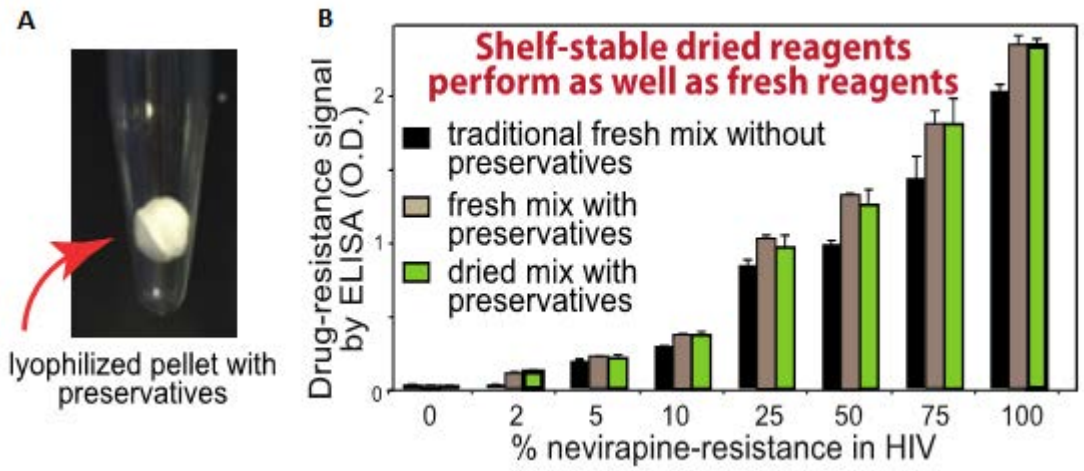

Figure 4.9 | Dry reagents in the bead format using 5% trehalose, 1.5% PEG, and 1.5% PVA. **(A)** Example of our dried ligation beads **(B)** Performance of our dried formulation compared to the traditional fresh mixture and fresh mixture with preservatives.

4.2.2 HIGH-THROUGHPUT BEAD FABRICATION

We have developed a new fabrication method to create dried reagent beads in a high-throughput fashion (**Figure 4.10**). We took advantage of the property of materials that changes due to cold stress to passively release the frozen beads from a mold. We first create mini reservoirs for the reagent droplets by pressing Parafilm to a mold (discarded pipette tip rack). We load the droplets of reagents with preservatives previously developed in 4.2.1 to the mini-reservoirs and then immerse the mold into liquid nitrogen. As the beads are frozen, the wax sheet cracks into pieces under cold stress and automatically releases the frozen reagent droplets. We can then retrieve the reagent beads after freezing. This approach can freeze 100 uniformed beads in minutes.

© Copyright 2021 | N Panpradist

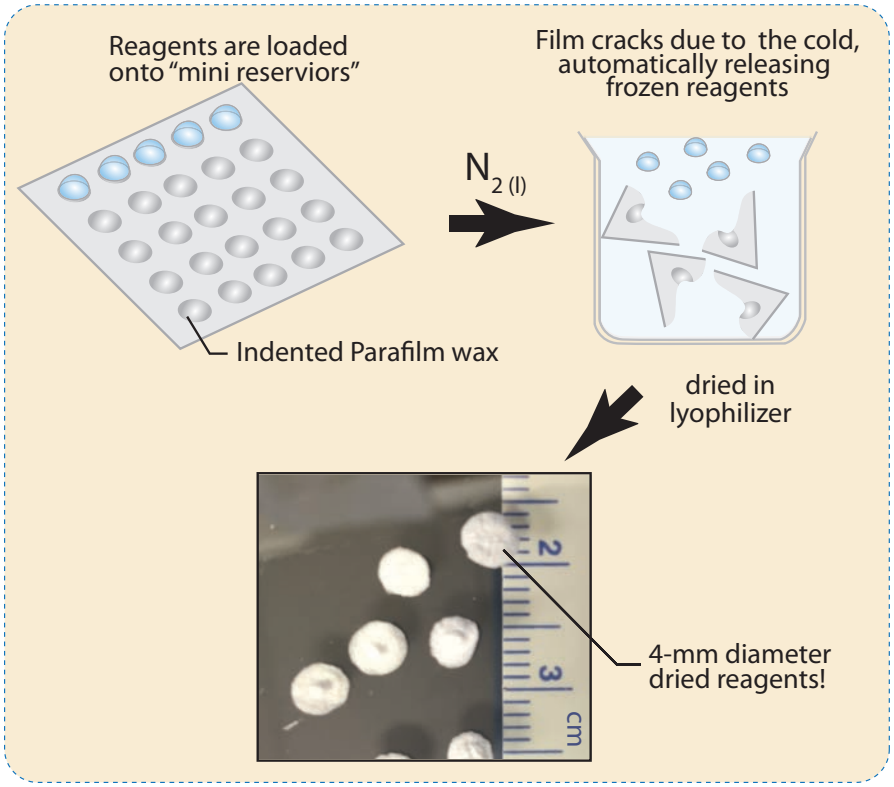

Figure 4.10 | Novel, high-throughput fabrication of dried reagent pellets.

We selected an inert, malleable Parafilm wax that can be indented into mini reservoirs. The fresh reagent mixtures in the presence of selected excipients are added to each well before introducing liquid nitrogen. As the droplet is being frozen, the Parafilm wax cannot tolerate high cold stress and cracks into pieces to release the frozen droplets. After drying, we obtain a large batch of dried reagents in a short period. This image was obtained from the patent application (**17/055,966).** David McIntyre collected data.

4.2.3 DEMONSTRATION OF SIMPLIFIED OLA WORKFLOW USING IN-TIP DRY REAGENTS

We demonstrate the use of in-tip dried PCR and ligation mixtures (**Figure 4.11A**) in the full OLA workflow (**Figure 4.11, B&C**). The in-tip dried PCR reagent was mixed with a solution containing HIV plasmid (containing 200 copies of 0%, 5%, and 100% nevirapine-resistant HIV) in 250ng human

© Copyright 2021 | N Panpradist

genomic DNA. The mixture was then subjected to 35 cycles of PCR. The PCR product in the original tube was mixed with another in-tip dried LDR mixture. The mixture was then subjected to 10-cycle ligation. After ligation, the product was analyzed using ELISA. The performance of in-tip dried reagents (3-day storage at room temperature) was comparable to the standard protocol, which involves fresh reagents and transferring of reagents across multiple tubes (**Figure 4.11C**).

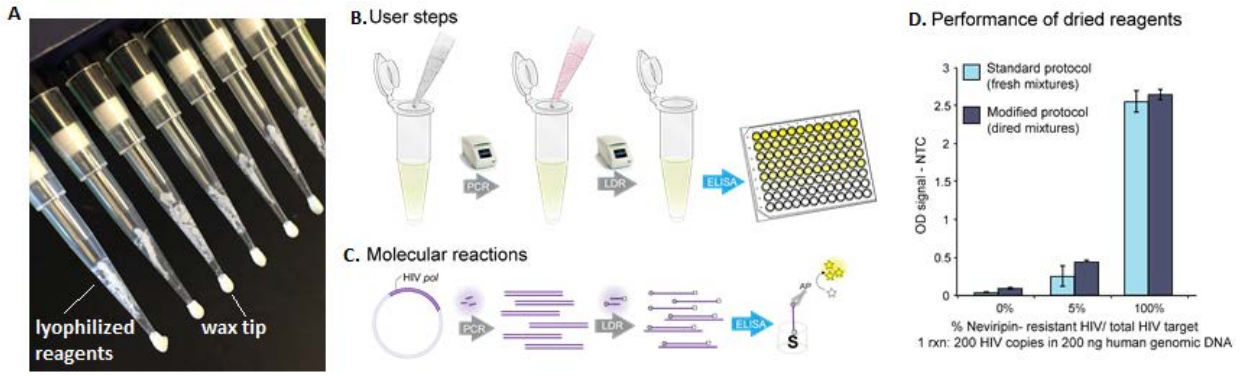

Figure 4.11 | Evaluation of in-tip dried reagent in OLA workflow.

(**A**) Photograph of lyophilized reagents in tips. (**B**) The user reconstituted the in-tip dried PCR mixtures in 200 copies HIV containing 5% Nevirapine-resistant HIV in 200ng human genomic NA solution. The mixture was then subjected to PCR. The product of PCR was then mixed with the in-tip dried ligation mixture. The original PCR tube then contained a ligation mixture, which was then subjected to 10-cycle ligation. The product of ligation was then evaluated using ELISA. (**B**) The molecular reactions where the plasmid containing HIV clones were amplified in PCR. The presence of Nevirapine-resistant HIV was probed using LDR. The product of LDR was then detected by ELISA. (**C**) The result of full OLA using in-tip dried PCR and ligation compared to the standard protocol. Nikki Higa collected data.

4.2.4 COMPARISONS ACROSS DRY REAGENT PLATFORMS

Tube-based is the easiest, most common way to prepare dried reagents. This platform is compatible with all formulations regardless of powdered or densely

© Copyright 2021 | N Panpradist

intact dried mixtures. However, the powdered mixture may require pre-centrifugation to pull down the dried mixtures before opening the tubes. Some mixtures that form a densely packed film on the surface of the tube may require vortexing or other methods of rigorous agitation to achieve homogeneous mixing. Bead droplets require developing an elegant cake of matrices that provides structural integrity that may require "cracking" to break up the dried mass into dissolvable pieces. This may be acceptable depending on the nature of the assay and can even be beneficial because none of the mixtures will stick to any surface of the tube or pipette. Last, drying reagents in pipette tips was mentioned in a patent of the filtered pipettes [20], but its practice has not been demonstrated. To our knowledge, we are the first who developed this platform for molecular assays. Using this platform, the mixing can occur as the release. This platform, however, may not be practical for highly viscous mixtures (e.g., >5% w/v PVA-containing mixtures).

4.3 Long-term storage analysis of lyophilized reagents

Three selected formulations: 5T, 5T1.5PEG, and 5T1.5PEG 1.5PVA, were lyophilized and dried in a tube as done in the lyoprotectant study. After the primary drying process, the mixture was stored at room temperature (20-25°C) or at 4 °C up to 8 weeks before ligation. **Figure 4.12** shows that all 4°C-stored mixtures at 1-week and 8-week storage had similar activities. However, in the 8-week, 20°C-storage condition, only 5% trehalose, 1.5% PEG, and 1.5% PVA consistently maintained high activity comparable to 1-week storage. Storage temperature impacted the stability of some

© Copyright 2021 | N Panpradist

formulations of dried reagents. While we continue to improve the formulations for long-term stability, dried PCR and LDR mixtures used in the OLA-Simple 1.0 will be stored at 4°C.

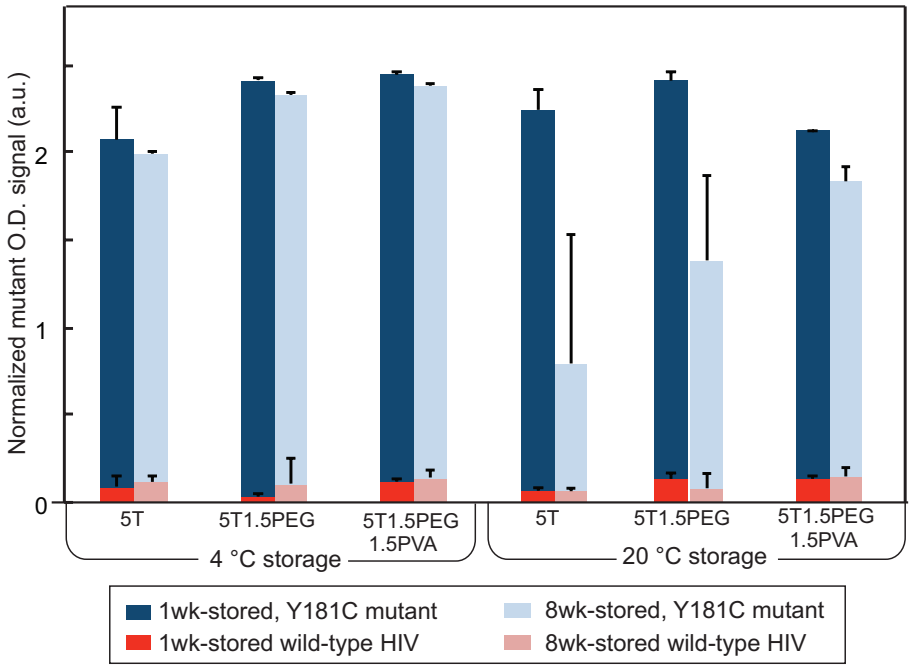

Figure 4.12 | Long-term stability of lyophilized LDR mixtures.

5T (5% trehalose), 5T1.5PEG (5% trehalose, 1.5% PEG), and 5T1.5PEG 1.5PVA (5% trehalose, 1.5PEG, and 1.5% PVA) were lyophilized and stored for one week and eight weeks either at four °C or 20 °C before subjected to LDR.

After 9-month storage at four °C, dry PCR reagents showed similar sensitivity to freshly prepared PCR reagents in the absence of additives (**Figure 4.13, A-B**). Similarly, after 4-month storage at four °C, dry ligase reagents retained activity and specificity to differentiate wild-type and mutant bases (**Figure 4.13, C-H**). Multiple additive formulations have been used to preserve dry nanoparticles [17]. For lateral flow detection, anti-biotin gold nanoparticles dry in buffer with 1% poly (ethylene glycol) and 1% sucrose performed similarly

© Copyright 2021 | N Panpradist

to the freshly prepared gold solution after 4-month storage at 4 °C (**Figure 4.13, I-J**).

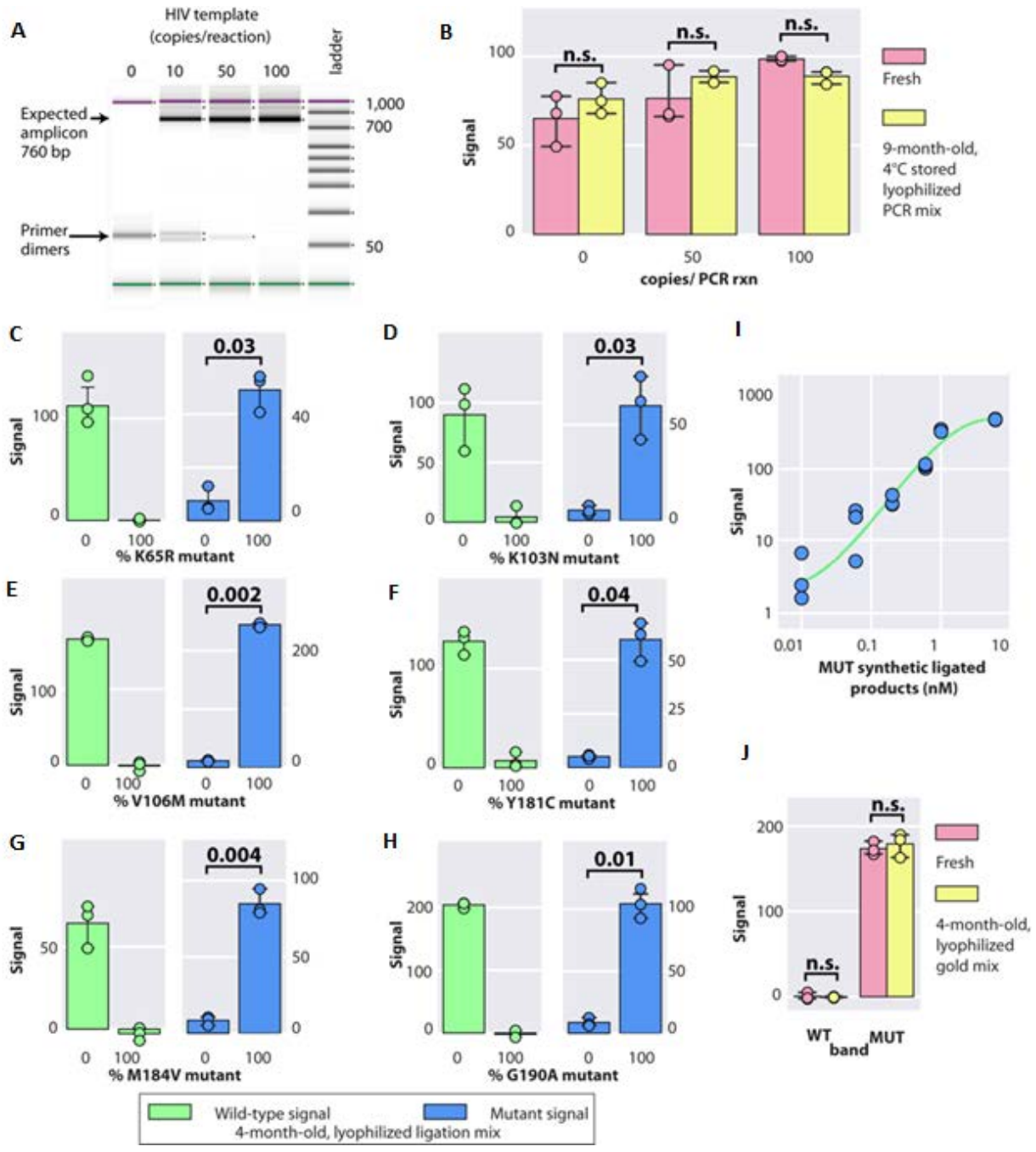

Figure 4.13 | Performance of OLA-Simple components after long-term storage.

(**A**)-(**B**) Dry PCR mixtures stored at 4°C for 9 months were compared to freshly prepared PCR without additives (means ± SD, n=3). (**A**) HIV DNA at 10, 50, or 100 copies were amplified in a 50µL PCR

© Copyright 2021 | N Panpradist

reaction. 1µL amplicon was run on a high-sensitivity TapeStation DNA chip. PCR was specific for HIV templates, showing primer dimers only at low input concentrations or no-template control. (**B**) PCR sensitivity was reported by integrating area under the curve for the 760 bp HIV band. The sensitivity of the freshly prepared versus dry PCR reagents was similar (P=0.64, 0.64, and 0.137 for 10, 50, and 100 copies, respectively, two-tailed t-test, Holm-Bonferroni correction). (**C**-**H**) Specificity of dried ligation mixture for detection of 100% MUT or 100% WT at K65R, K103N, V106M/I, Y181C, M184V, and G190A, respectively. Ligation products obtained from plasmid amplicons containing either WT or MUT bases at each target codon (means ± SD, n=3) were tested using OLA-Simple lateral flow strips. The signal of WT and MUT bands from scanned images was quantified by subtracting the 95th percentile of Linear Discriminant Analysis (LDA)-converted intensities in the area adjacent to the expected band position (background) from the 95th percentile LDA-converted intensities at the area of expected band position. (**I**) The dynamic range of OLA-Simple lateral flow detection using a synthetic MUT ligation product (5'-FAM, 3'-biotinylated poly(T)$_{20}$) at concentrations of 0, 0.01, 0.06, 0.2, 0.6, 1, and 6 nM in ligation buffer using the freshly prepared gold solution. (**J**) Stability of dried gold mixture. MUT ligation products at 0.3nM, a concentration within the dynamic range shown in (**I**), were spiked into the ligation reaction mixture and tested using >4-month-old lateral flow strips chased with either freshly prepared gold solution or 4-month-old gold solution. After 20 min, images were scanned, and the signal for WT and MUT bands was analyzed (means ±SD, n=3). We observed no significant difference in sensitivity (expected signal at MUT band) and specificity (false signal at WT band) between the 4-month-old and the freshly prepared dry gold (P=0.724 for WT band signal; P=0.594 for MUT band signal, two-tailed t-test).

Additionally, we tested trehalose's effect on the capture anti-digoxigenin IgG antibody stability after a long-term room temperature storage. After 1 day of post-immobilization, we noticed that the presence of IgG with 10% trehalose had a lower signal than the case of IgG without and with 5% trehalose (**Figure 4.14A**). Possibly this is because a high percentage of trehalose slows down the drying process. However, after the IgG capture was completely dried, we

© Copyright 2021 | N Panpradist

found that IgG conditions with 5% and 10% trehalose had higher signals than the IgG capture without trehalose (**Figure 4.14B**). 5% trehalose was ideal as it did not interfere with the drying process and helped stabilize the immobilized IgG to maintain stability even after 3 months.

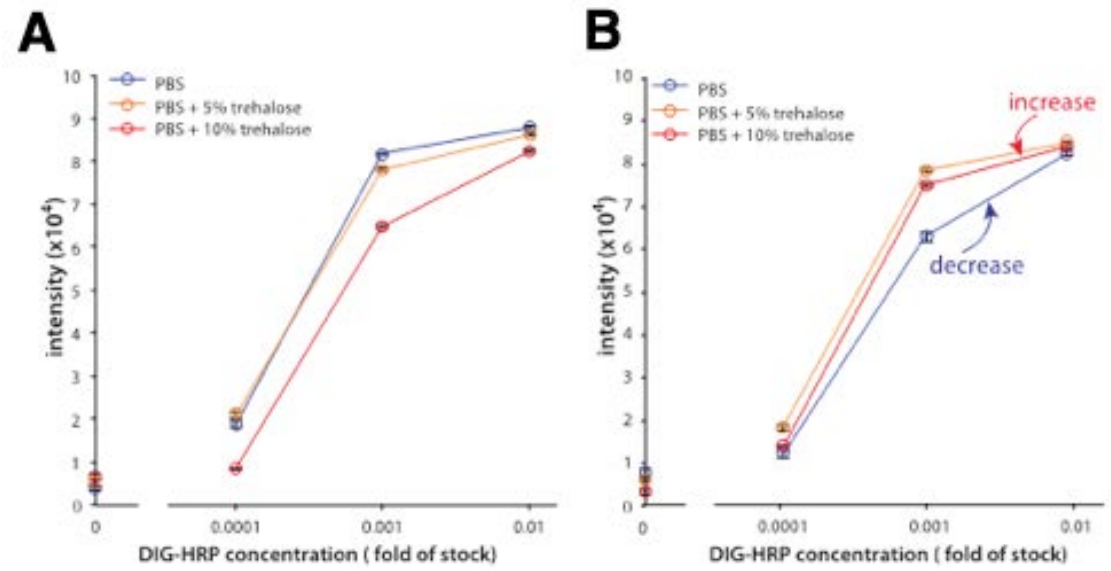

Figure 4.14 | Functionality of immobilized anti-digoxigenin IgG after 1 and 90 days.

Signal of DAB/Dig-HRP at 1:100, 1:1000, and 1:10000 of stock concentration after (**A**) one day and (**B**) 90 after immobilization.

4.4 OTHER CONSIDERATIONS FOR LYOPHILIZING MOLECULAR REACTIONS.

Glycerol. Enzymes are commonly stored in buffers containing glycerol while stored lower than 0 °C. At a concentration below 66.7% (w/w) of glycerol in water, the freezing points are reduced as glycerol concentrations increase[18]. 50% glycerol in water has a freezing point of -23 °C and remains liquid when

© Copyright 2021 | N Panpradist

stored at -20°C. Thus, this concentration is commonly used to store enzymes to avoid freeze-thawing.

Additionally, glycerol has been proven to play other roles in stabilizing enzymes by preventing protein unfolding[19]. During the prior development of excipient formulations for PCR and ligation reactions, we had access to very high enzyme concentrations of enzyme stocks. The final glycerol concentration in the lyophilized mix was ≤0.1%, and we did not observe a significant effect on lyophilization. However, as we switched to developing the lyophilization for RNA detection instead of DNA, multiple enzymes were used. Specifically, an RT-PCR reaction contains a reverse transcriptase, a polymerase, and an RNase inhibitor - all accumulated to relatively high glycerol concentrations (3.5 – 7%). In such high glycerol concentrations, we observed the collapse of lyophilized pellets and potentially impacted their long-term stability at ambient temperatures. It is recommended that glycerol in lyophilized reactions should be near or less than 0.1% in the final lyophilized reaction. Glycerol-free enzymes can be arranged directly to manufacturers, or buffer exchange can be performed to concentrate the enzymes before lyophilization. However, the latter may result in some loss as enzymes are bound to the Amicon membrane filter.

© Copyright 2021 | N Panpradist

Figure 4.15 | Lyophilized reactions with 10% glycerol.

Magnesium-free lyophilized reagents. The lyophilized reaction can be prepared magnesium-free, which prohibits any enzymatic activity before assay initiation. The lyophilized reaction is activated upon the addition of a sample that contains magnesium. This approach should be less prone to moisture degradation than magnesium-containing lyophilized reaction (see **Chapter 10.4** for more details).

Lyophilized reaction for isothermal amplification reactions. Hot- or Warm-start enzymes should be considered to ensure the assay is inactive at room temperature, prevent activities during the reaction set up, and eliminate the need for setting up the reaction on ice. Cold temperature can promote dimer and/or secondary structures of primers, which we observed as a negative impact on the assay sensitivity and speed. In fact, while setting up isothermal assays for lyophilization, primers and probes were heated and cooled down passively at room temperature to minimize secondary structures before mixing with the other components (see **Chapter 10.4** for more details).

© Copyright 2021 | N Panpradist

Use lower reaction volume during lyophilization. Water can be reduced by half of the reactions to double the excipient concentrations in the lyophilized pellet and shortens the lyophilization drying time. This approach allows the assay to suffer less impact of less concentrated excipients on the core assay function (see **Chapter 10.4** for more details).

Use of multiple temperatures and pressures during the drying process. In this study, we only investigated lyophilization with a fixed temperature and pressure condition during the drying process. This drying process can be performed as a multi-step process to increase the speed and quality of lyophilized reagents. During the primary drying, low temperature and pressure (lower than the critical temperatures) should be used to remove most of the water. Dry reagents could subsequently be subjected to secondary drying at a higher temperature (20°C for 45 minutes) to remove the last bit of tightly bound water molecules [20].

Packaging. Currently we used Mylar bag in a desiccant packet to prevent exposure to water content and light from outside environment. Another important step after lyophilization is packaging, as some excipients such as mannitol are highly hydroscopic. It is crucial to package lyophilized reagents in a low humidity environment such as in a glove box. Additionally, oxygen could introduce oxidative stress on the dry reagents, thus nitrogen gas can be used to flush out the air within the package before sealing. Use of desiccant packets filled with oxygen scavengers such as ferrous oxide might be beneficial [21].

© Copyright 2021 | N Panpradist

Accelerated study

Instead of real-time study for reagent stability, an accelerated study of lyophilized agents, especially in drug formulations, is commonly performed to predict stability and decide on the top excipient candidates to pursue real-time stability. Arrhenius (solid-state) approximation is commonly used:

$$k = A.\exp(-E_a/(RT)$$

where k = Rate of degradation

A = Collision frequency

E_a = Activation energy

R = Gas constant

T = Temperature in Kelvin

$$\ln(K) = \ln(A) - (E_a/R).(1/T)$$

By plotting a relationship of 1/T and ln(K), the degradation rate of lyophilized reagents can be interpolated from the rates at other temperatures. However, other factors in addition to temperatures, such as humidity, light, or oxygen level, can also accelerate the degradation of lyophilized reagents. Therefore, simple 0^{th} or 1^{st} order cures may be overly simplified [22]. Additionally, effects of humidity are not factored into the traditional Arrhenius equation [23], and humidity-corrected Arrhenius Equation was proposed:[24]

$$\ln(k) = \ln(A) - E_a/(R).(1/T) + B(\%\ \text{relative humidity})$$

© Copyright 2021 | N Panpradist

Initially, a few conditions of escalated temperature and %relative humidity can be set to obtain preliminary E_a and B after 14 days. These E_a and B values are then used to quantify the effects of %relative humidity and temperature.

4.5 FUTURE DIRECTIONS

4.5.1 PIPETTE-FREE DRY REAGENT SET-UP PLATFORM

To avoid the need for accurate pipetting, an easy set-up system was designed (**Figure 4.16A**). We envision users pop the dried reagent bead from a blister pack into a tube containing pre-measured diluent (e.g., water). The mixed fluid will be loaded onto the buffer ports that are connected to the paper network. Here bubbles should be avoided as they could block the flow of the fluid. Instead of using a costly and bubble-inducing vortex shaker, the mixing can be done effectively and economically using a piezoelectric buzzer. The piezoelectric buzzer generates the acoustic wave that vibrates fluid and facilitates mixing. This way of mixing could result in a bubble-free, well-mixed fluid. The user then will load the fluid into the buffer port. The bottom of the buffer port contains a loosely woven glass fiber layer (**Figure 4.16B**) to serve as a flow resistor that will slow down the fluid and mitigate the risk for bubble generation. Additionally, this glass fiber layer will also create capillary pressure that will stop the mid-air fluid in the channel from continuing to travel unless there is a consistent flow of fluid coming from the atop buffer port. This approach will ensure that the continuous flow of fluid is obtained.

© Copyright 2021 | N Panpradist

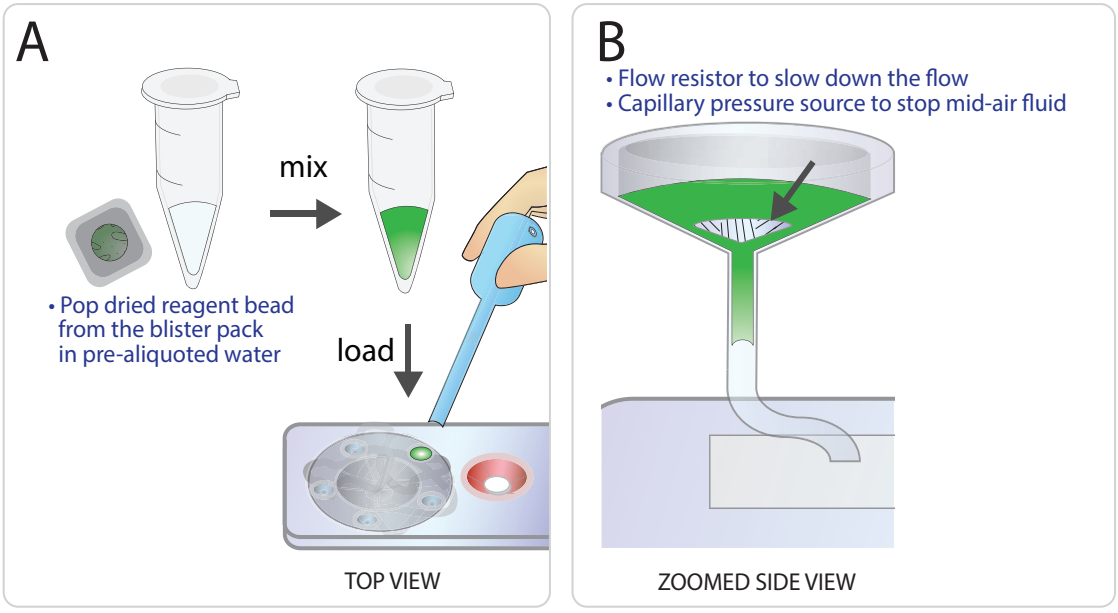

Figure 4.16 | Set up of reagent rehydration and buffer loading.

Acknowledgments. I thank our collaborators, Dr. James Lai, and Jeffrey Myers, for stimulating the discussion. I thank the members of Yager Group, Sujatha Dharmaraja, and Ryan Gallagher, for their technical support. We also thank Dr. Patrick Stayton and Robert H. Britschgi for providing access to the lyophilizer.

© Copyright 2021 | N Panpradist

4.6 SUPPLEMENTARY INFORMATION FOR CHAPTER 4

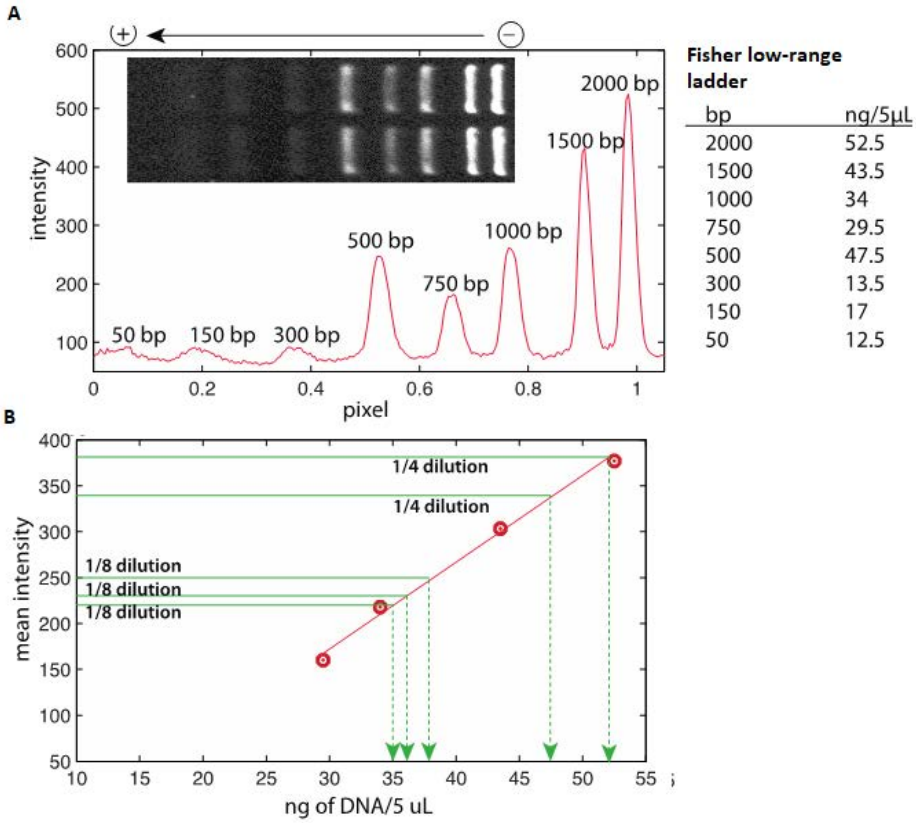

Figure S4.17 | Estimated amplicon concentration with quantitative gel electrophoresis.

Interpolated amplicon concentration = 51±4 x102 ng/µL

Amplicon (copies/µL) = (51 ± 4 ng/µL)/(1.89 x 10^5 g/mol)x (6.02x10^{23} copies/mol)

1.6 ± 0.1 x 10^{11} copies/µL (mean ±SE). Alternatively, this process can be done more conveniently using TapeStation.

© Copyright 2021 | N Panpradist

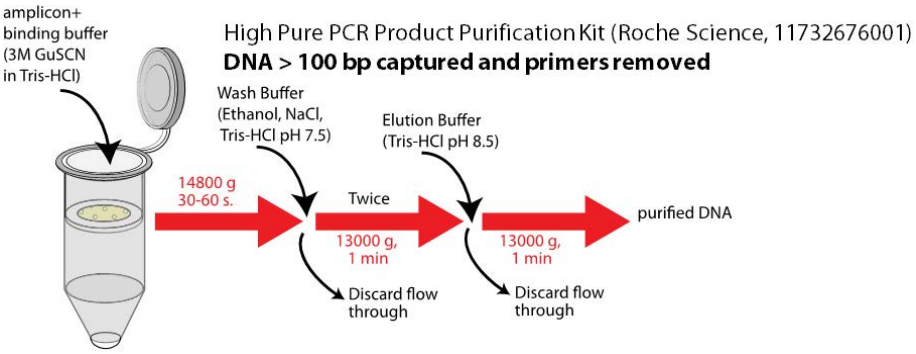

Figure S4.18 | Estimation of amplicon concentration based on purified DNA kit and mass measurement.

PCR purification kits has a cut off at 300 kb and helps remove the primer dimers. Amplicon concentration estimated by Nanodrop (N=3) = 66.5 ±0.4 ng/µL. Amplicon (copies/µL) = (66.5 ± 0.4 ng/µL)/ (1.89 x 10^5 g/mol) x (6.02x1023 copies/mol) = 2.1 ± 0.01 x 10^{11} copies/µL (mean ±SE).

© Copyright 2021 | N Panpradist

CHAPTER 4 REFERENCES

1. Baheti, A.; Kumar, L.; Bansal, A. K., Excipients used in lyophilization of small molecules. *Journal of Excipients and Food Chemicals* **2010,** (1), 41-54%V 1.
2. Spiess, A. N.; Mueller, N.; Ivell, R., Trehalose is a potent PCR enhancer: lowering of DNA melting temperature and thermal stabilization of taq polymerase by the disaccharide trehalose. *Clinical chemistry* **2004,** *50* (7), 1256-9.
3. Wang, C.; Altieri, F.; Ferraro, A.; Giartosio, A.; Turano, C., The effect of polyols on the stability of duplex DNA. *Physiol Chem Phys Med NMR* **1993,** *25* (4), 273-80.
4. Chang, B. S.; Randall, C. S., Use of subambient thermal analysis to optimize protein lyophilization. *Cryobiology* **1992,** *29* (5), 632-656.
5. MacKenzie, A. P., The physico-chemical basis for the freeze-drying process. *Dev Biol Stand* **1976,** *36*, 51-67.
6. Franks, F., Freeze-drying: from empiricism to predictability. The significance of glass transitions. *Dev Biol Stand* **1992,** *74*, 9-18; discussion 19.
7. Her, L. M.; Nail, S. L., Measurement of glass transition temperatures of freeze-concentrated solutes by differential scanning calorimetry. *Pharm Res* **1994,** *11* (1), 54-9.
8. PerkinElmer Tg and Melting Point of a Series of Polyethylene Glycols Using the Material Pocket. https://resources.perkinelmer.com/lab-solutions/resources/docs/APP_TgandMeltofPolyethylene.pdf.

© Copyright 2021 | N Panpradist

9. Klatser, P. R.; Kuijper, S.; Ingen, C. W. v.; Kolk, A. H. J., Stabilized, Freeze-Dried PCR Mix for Detection of Mycobacteria. *Journal of Clinical Microbiology* **1998,** *1998*, 1798-1800.

10. Moiana, A.; Turner, J.; Ventura, L.; Gramegna, M. Optimized room temprature stable, ready-to-use, one-step RT-PCR mix. https://www.sentineldiagnostics.com/en/wp-content/uploads/sites/2/scientific-area/105-1-PosterEuromedlab2.pdf.

11. Kamau, E.; Alemayehu, S.; Feghali, K. C.; Juma, D. W.; Blackstone, G. M.; Marion, W. R.; Obare, P.; Ogutu, B.; Ockenhouse, C. F., Sample-ready multiplex qPCR assay for detection of malaria. *Malaria journal* **2014,** *13* (1), 158.

12. Klatser, P. R.; Kuijper, S.; Ingen, C. W. v.; Kolk, A. H. J., Stabilized, Freeze-Dried PCR Mix for Detection of Mycobacteria. *Journal of clinical microbiology* **1998,** *36* (6), 1798-1800.

13. McHugh, M. P.; Gray, S. J.; Kaczmarski, E. B.; Guiver, M., Reduced turnaround time and improved diagnosis of invasive serogroup B Neisseria meningitidis and Streptococcus pneumoniae infections using a lyophilized quadruplex quantitative PCR. *Journal of Medical Microbiology* **2015,** *64* (11), 1321-1328.

14. Lucira Health. Lucira™ CHECK-IT COVID-19 Test Kit 2021. https://www.fda.gov/media/147494/download.

15. Evik Diagnostic Innovations Single assay beads: the modern way to create POC devices. https://www.evikdiagnostics.com/single-assay-beads.

© Copyright 2021 | N Panpradist

16. Crannell, Z. A.; Rohrman, B.; Richards-Kortum, R., Development of a quantitative recombinase polymerase amplification assay with an internal positive control. *J Vis Exp* **2015,** (97), 52620.

17. Abdelwahed, W.; Degobert, G.; Stainmesse, S.; Fessi, H., Freeze-drying of nanoparticles: Formulation, process and storage considerations☆. *Advanced Drug Delivery Reviews* **2006,** *58* (15), 1688-1713.

18. Lane, L. B., Freezing Points of Glycerol and Its Aqueous Solutions. *Industrial & Engineering Chemistry* **1925,** *17* (9), 924-924.

19. Vagenende, V.; Yap, M. G. S.; Trout, B. L., Mechanisms of Protein Stabilization and Prevention of Protein Aggregation by Glycerol. *Biochemistry* **2009,** *48* (46), 11084-11096.

20. Patel, A.; Burden, D. In Pursuit of a Ready-To-Use, Shelf-Stable qPCR Mix. https://opsdiagnostics.com/notes/lyoqpcrreagents.html.

21. Cichello, S. A., Oxygen absorbers in food preservation: a review. *J Food Sci Technol* **2015,** *52* (4), 1889-1895.

22. Waterman, K. C.; Carella, A. J.; Gumkowski, M. J.; Lukulay, P.; MacDonald, B. C.; Roy, M. C.; Shamblin, S. L., Improved protocol and data analysis for accelerated shelf-life estimation of solid dosage forms. *Pharm Res* **2007,** *24* (4), 780-790.

23. Jelić, D., Thermal Stability of Amorphous Solid Dispersions. *Molecules* **2021,** *26* (1).

24. Scrivens, G. Predicting the Long-Term Stability of Solid-State Pharmaceuticals. https://freethinktech.com/wp-content/uploads/2019/12/Garry-Scrivens_ASAP_London_March2015.pdf.

© Copyright 2021 | N Panpradist

CHAPTER 5: OLA-SIMPLE 1.0 KIT FOR HIVDR

SIGNIFICANCE: In 2017, the World Health Organization HIV Drug Resistance Network (HIVRESNET) reported that several point-mutation assays had been developed to detect HIV drug resistance, including the oligonucleotide ligation assay (University of Washington), PANDAA™ (Aldatu Biosciences), allele-specific primer extension (United States CDC), and multiplexed melt curve analysis (InSilixa). A more recent search on PubMed and Google Scholar using keywords such as "HIV drug resistance or "HIV genotyping," coupled with "point-of-care" up to August 30th, 2019, showed similar results. These point-mutation assays can be used in place of Sanger sequencing with a real-time thermal cycler or a standard thermal cycler and a plate reader with fluorescent or colorimetric sensing. Searching results indicate that none of these assays were implemented for routine clinical management. Evaluation of these assays using clinical specimens across various HIV subtypes and specimen types was not found. Furthermore, none of these assays were demonstrated for successful utility by non-experience users. Therefore, we concluded that HIVDR testing is still an unmet public health need in LRS.

DELIVERABLES: A low-cost, rapid point mutation assay (OLA-Simple) was developed to enable HIVDR detection in patient specimens across HIV-subtypes (A, B, C, D, and AE) from various specimen types (DBS, PMBC DNA, and plasma) using minimal equipment (a standard thermal cycler and pipettes). Comparative drug resistance detection between OLA-Simple and Sanger sequencing or higher sensitivity assays revealed highly concordant

© Copyright 2021 | N Panpradist

detection of mutations but a much shorter turnaround time (<4 h vs. 35–72 h by Sanger sequencing). Furthermore, OLA-Simple was designed to be easy to use. Dry reagents allowed fast and accurate assay setup, and lateral flow detection provided semi-quantitative results that can be analyzed by the unaided eye or the in-house software. The in-house software guided non-trained users and maintained the records of results and reagent stocks. Untrained, first-time users processed specimens using OLA-Simple with high accuracy.

INTERPRETATIONS: Our findings highlight the potential use of the OLA-Simple for HIVDR testing in a small laboratory in LRS that may lack sophisticated equipment and trained personnel. The entire reagent cost/ specimen is <$20 and requires < 10-min hands-on time from DNA or RNA. The critical equipment required in OLA-Simple is a standard thermal cycler (which is substantially more economical than a real-time thermal cycler or a sequencer) and an in-house software installed on a tablet. The rapid turnaround time of OLA-Simple could allow same-day guided ART selection in LRS.

PREVIOUS PUBLICATIONS:

Some texts and images used in this chapter were published as

1) N Panpradist *et al.* 2019 (https://DOI.org/10.1016/j.ebiom.2019.11.002)
2) N Panpradist *et al.* 2020 (DOI: 10.1097/QAD.0000000000002524)
3) J Vrana *et al.* 2021 (https://DOI.org/10.1101/2021.05.06.21256654).

© Copyright 2021 | N Panpradist

5.1 BACKGROUND

CONTRIBUTORS: Nuttada Panpradist, Ingrid A Beck, Nikki Higa, David McIntyre, Parker S Ruth, Isaac So, Enos C Kline, Ruth Kanthula, Annie Wong-On-Wing, Jonathan Lim, Daisy Ko, Ross Mline, Theresa Rossouw, Ute D Feucht, Chung Michael, Gonzague Jourdain, Nicole Ngo-Giang-Huong, Laddawan Laomanit, Jaime Soria, James Lai, Eric D Klavins, Lisa M Frenkel, Barry R Lutz.

CONTRIBUTIONS: NP led development and evaluation of OLA-Simple kit 1.0.

MATERIALS AND METHODS

Preparation of OLA-Simple kits. The kit includes lyophilized PCR and ligation reagents, gold mixture, and competing oligonucleotides. The 50 µL PCR was made from 5 U FastStart™ polymerase (Sigma), 0.5 mg/mL BSA, 0.2 nM dNTPs, 2 mM $MgCl_2$, and 0.4 µM of primers (forward primer: 5′ - GRC CTA CAC CTG TCA ACA TAA TTG G - 3′ and reverse primer: 5′ - CAA AGR AAT GGA GGT TCT TTC TGA TG - 3′) in water aliquoted before lyophilization. The 24 µL ligation reactions was made from 4–8 mU/µL thermostable Ampligase ligase (Epicentre Technology), 12.5 mM KCl, 1 mM NAD, 1× ligase buffer (20 mM Tris–HCl, 10 mM $MgCl_2$, 1 mM DDT), 0.1075% *(v/v)* Triton-× 100, 5% *(w/v)* trehalose, 1.5% *(w/v)* poly(ethylene glycol), and 3.75–60 nM probes for each DRM (**Table S5.6**) in 1×Tris-HCl pH 8.0, 0.1 mM EDTA, and water was aliquoted into 48 µL reactions prior to lyophilization. Anti-biotin antibody-coated gold nanoparticles (0.75 OD at 520 nm) were aliquoted into 860 µL reactions before lyophilization. The lyophilized reagents were packaged in heat-sealed foil pouches with desiccant packets and stored at 4 °C until use. For the user feasibility study, the

© Copyright 2021 | N Panpradist

lateral flow tests were prepared in-house. 0.5µg anti-FAM antibodies (Southern Biotech), anti-digoxigenin antibodies (Novus Biologicals), and biotin-conjugated BSA (Sigma) was striped onto each nitrocellulose sheet (EMD Millipore) adhered onto a PVC backing card and dried overnight in the desiccator. Two ends of the nitrocellulose were then assembled to the glass fiber (EMD Millipore) and absorbent pads (GE Healthcare). The assembled sheet was cut into 3.5 mm × 6 mm strips and placed into plastic cartridges (DCN Diagnostics). Assembled devices were stored in foil pouches with a desiccant at 4 °C until use. Lateral flow strips used in evaluating specimens were prepared using the same protocol by InBios International, Inc.

RESULTS

5.1.1 OLA-SIMPLE 1.0 KIT COMPONENTS

OLA-Simple (**Figure 5.1A**) was designed to reduce the complexity of the original OLA (referred to as CLIA-OLA), which contains four modules: sample preparation, polymerase chain reaction (PCR), enzyme-mediated probe ligation, and ELISA. In the OLA-Simple workflow, extracted nucleic acids from a specimen can be used to directly reconstitute the dry reagents, enabling fast set-up and accurate performance of the reactions. Visual readout of the lateral flow strips allows straightforward interpretation of results for the six DRMs with a total of <3.5-h wait-time (2-h PCR, 1-hour ligation, 20-min detection) and <10-min hands-on time (<1-min PCR, <3-min ligation, and ~6-min detection). The enzymes, co-factors, and buffers used in the OLA-Simple were also optimized to eliminate the need for purification between steps. The presented OLA-Simple kit

© Copyright 2021 | N Panpradist

detects key DRMs in HIV pol encoding reverse-transcriptase associated with resistance to the first-line NNRTIs (K103N, V106M/I, Y181C, G190A), tenofovir (K65R), and lamivudine (M184V). Primers used in PCR and probes used in ligation were designed to anneal to the most prevalent global HIV-1 subtypes by incorporating degenerate bases at variable positions in the Los Alamos HIV Database.

5.1.2 ANALYTICAL PERFORMANCE OF OLA-SIMPLE

Analytical performance at each DRM site was evaluated using synthetic DNA gene fragments containing 0%, 15%, and 25% mutant (MUT) in wild-type (WT) HIV sequences; the OLA-Simple kit discriminated MUT from WT HIV in samples containing 15% mutant HIV at the six DRMs tested (**Figure 5.1B**).

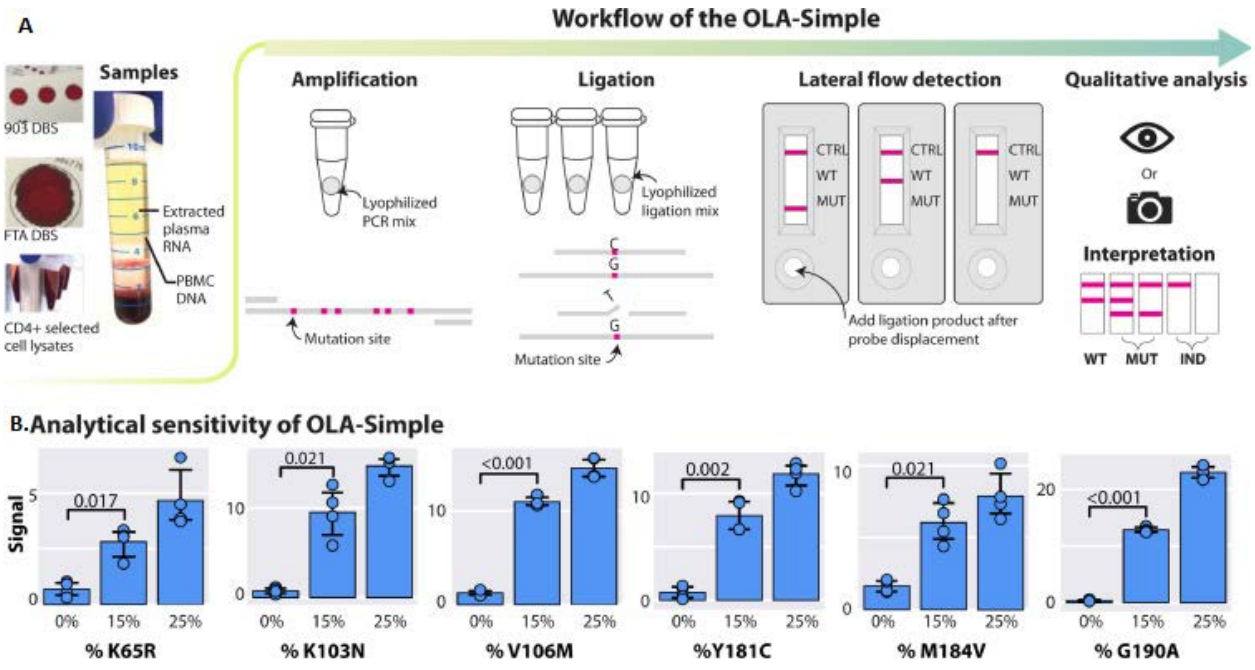

Figure 5.1 | Workflow and analytical performance of the OLA-Simple HIV genotyping assay. (**A**) Workflow of OLA-Simple. DNA obtained from dried blood spots (DBS), peripheral blood mononuclear cells (PBMC), cell lysates, or cDNA reverse-transcribed from plasma RNA are amplified using pre-

© Copyright 2021 | N Panpradist

measured, dry PCR reagents resuspended in a single buffer. Amplicons are then tested for the presence of mutations using dry ligation reagents. Probes complementary to the wild-type and the mutant bases are reacted simultaneously at each codon. The ligated products are detected using customized lateral flow test detection strips, which are then analyzed by eye or a scanner. The genotype is interpreted as mutant (MUT), wild type (WT), or indeterminate (IND, defined as the control line but no MUT or WT signal) by the presence or absence of lines on each strip. (**B**) Analytical performance of OLA-Simple. MUT signal (means ± SD, $n = 4$) quantified on the lateral flow test strips for K65R, M184V, G190A, K103N, V106M, and Y181C, respectively, from control mixtures containing 1000 copies of HIV DNA input with 0%, 15%, or 25% MUT. The vertical scale is linear. Signal was compared using *t*-test with Holm-Bonferroni adjustment.

5.2 CLINICAL VALIDATION OF OLA-SIMPLE 1.0 KITS

MATERIALS AND METHODS

Illumina MiSeq and Sanger sequencing. PCR amplicons derived from FTA DBS, PBMC DNA, RNA, and 1st-round amplicon were treated with ExoSAP-IT (Applied Biosystems, Foster City, CA) and submitted to Sanger sequencing or analyzed using HIV-1 ViroSeq™ kit (Abbott) (Thai cohort only). All mutations were confirmed by bi-directional sequencing. DRMs were identified by submitting FASTA files to the Stanford HIV Drug Resistance Database. GenBank accession numbers are KF544089-KF544288, MH509760-MH509936, MH935 645-MH935766, MK512771-MK513407, MH623786.1, MH623833.1, MH623884.1, MH623900.1, MH623907.1, MH623919.1, MH623924.1, MH623940.1, MH623950.1, MH623951.1, and pending release from GenBank for South African and Thailand cohort.

© Copyright 2021 | N Panpradist

CLIA-OLA procedure. PCR amplification used 2 µg of purified PBMC DNA as previously described [1] or 10 µL RNA eluates reverse-transcribed and amplified using Superscript IV (Invitrogen), followed by nested PCR. Amplicons from Peruvian [2] or Thai specimens were generated as previously described [3]. For ligation, 2µL 1:4 diluted PCR product was added to 20µL freshly prepared reactions containing probes specific for K103N, V106M/I, Y181C, G190A o,r V184M designed for HIV subtypes B, C, or A/D/C depending on the specimen's country of origin as previously described[4]. Products from the ligation step were detected by plate-based ELISAA[4] a, and optical densities were compared to standard curves of mutant and wild-type plasmid mixtures at 0%, 2%, 5%, 10%, 25%, 50%, 75%, and 100% mutant. The proportion of mutant variants in each specimen was quantified by comparing the MUT OD / (MUT OD + WT OD) to the standard curve (mean of $n = 2$). Samples with negative reactions for both MUT and WT were considered IND.

5.2.1 PERFORMANCE OF OLA-SIMPLE ON PATIENT-DERIVED DNA ACROSS SUBTYPES.

The robustness of OLA-Simple in analyzing DRMs in specimens across HIV-subtypes A, B, C, D, and AE was assessed using clinical specimens from multiple cohorts. A clinical panel with 168 specimens enriched for specimens with DRMs included: South African FTA DBS ($n = 60$), Kenyan PBMC ($n = 23$), Kenyan plasma ($n = 23$), and HIV *pol* PCR amplicon from Thailand ($n = 38$) and Peru ($n = 24$). Broken down by HIV subtypes, this specimen panel contained ($n = 25$), B ($n = 26$), C ($n = 62$), D ($n = 8$), AE ($n = 43$), AG ($n = 1$), G ($n = 1$), BC ($n = 1$),

© Copyright 2021 | N Panpradist

and CD ($n = 1$). OLA-Simple was performed by a trained operator "blinded" to prior genotypic testing of these specimens (**Figure 5.2A**).

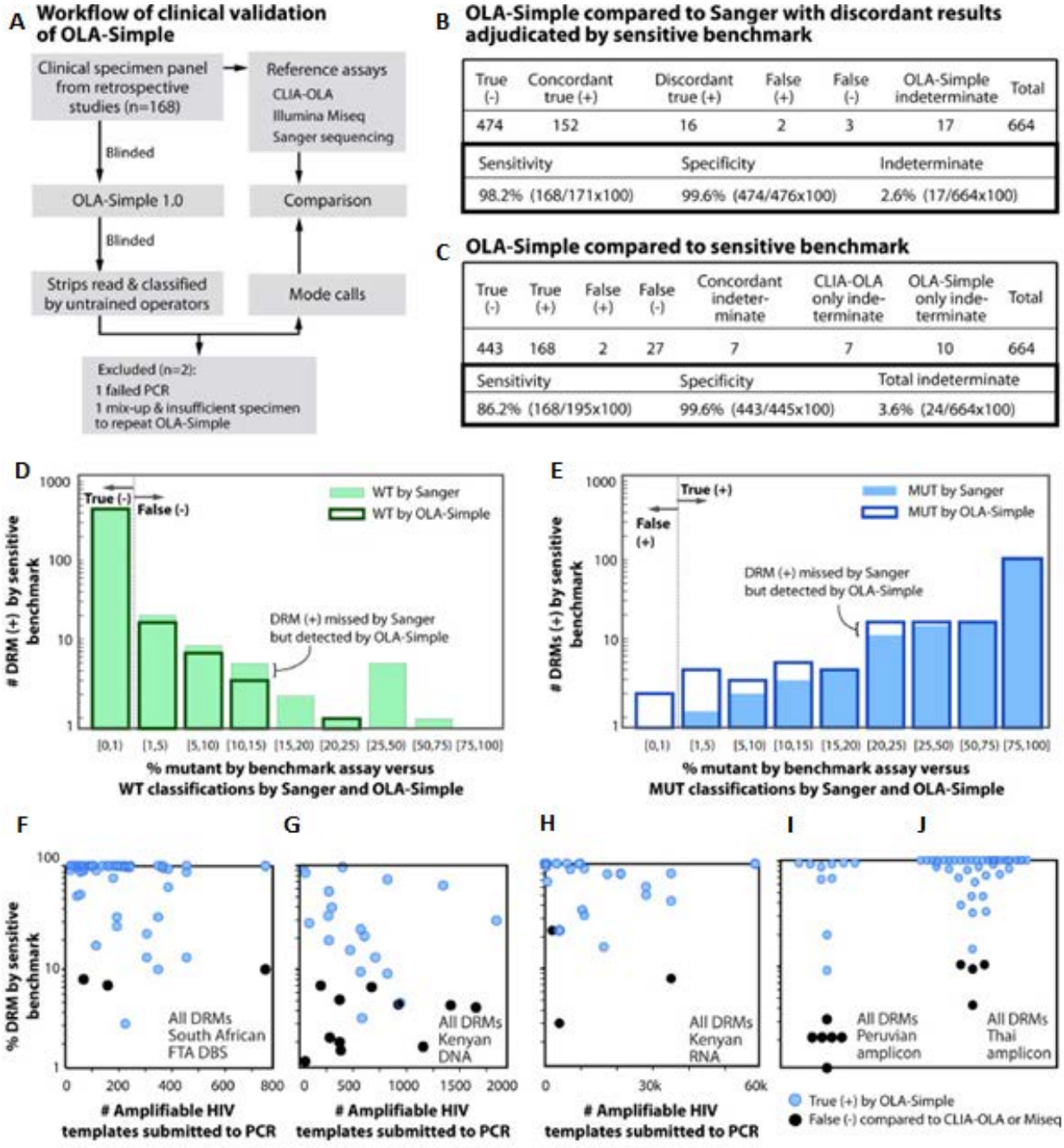

Figure 5.2 | Validations of the OLA-Simple on clinical specimens, compared to other comparator assays.

(A) Schema of OLA-Simple clinical specimen validation (n = 168, 672 codons). DNA, RNA, or amplicon (AMP) from specimens were re-labeled to blind the operator running the OLA-Simple test. The scanned

© Copyright 2021 | N Panpradist

images were sent to untrained volunteers for analysis (n = 13 for the Thai data set; n = 11 for other data sets). (B) Genotyping results of OLA-Simple compared to Sanger and (C) to a sensitive comparator assay. The comparator assay depended on the patient cohort and adjudicated discordant results between the OLA-Simple and Sanger sequencing. Indeterminates were excluded from sensitivity and specificity estimations. (E) histograms of MUT frequencies in specimens identified as having DRMs by a quantitative comparator assay (CLIA-OLA or MiSeq) versus (d) WT and (E) MUT classification by Sanger and OLA-Simple. Bin spacing was based on commonly used MUT thresholds at 1%, 5%, 10%, 15%, 20%, and 25% MUT frequencies. (F)–(J) MUT classifications of DNA samples from (f) South African FTA DBS, (g) Kenyan PBMC DNA, (H) Kenyan plasma RNA, (I) amplicon derived from Peruvian PBMC or plasma, and (J) Amplicon derived from Thai plasma. CLIA-OLA (F, H–J) or MiSeq (G) were used as the comparator assay.

The OLA-Simple PCR-amplified 167/168 (99%) specimens; one Thai amplicon had a failed PCR likely due to a defective dry PCR tube rather than a low copy number or the primer sequences. This was because CLIA-OLA using the same primers, successfully amplified this specimen. Following ligation, the OLA-Simple lateral flow detection strips were scanned and blindly classified as MUT, WT, or indeterminate (IND) by untrained evaluators ($n = 13$ for the Thai cohort or $n = 10$ for the other cohorts). Mode calls of the OLA-Simple strips were compared to classifications by Sanger sequencing and a sensitive comparator assay, MiSeq for Kenya PBMC specimens, and CLIA-OLA for the remaining specimens. Comparisons were made for K103N, V106M/I, Y181C, M184V, and G190A, with V106M/I tested only on specimens from South Africa, where HIV subtype C is most prevalent. One DBS sample was excluded from the comparison due to sample mix-up (identified due to highly discordant results to both CLIA-OLA and Sanger sequencing) and insufficient specimen to repeat OLA-Simple. **Figure 5.2B** summarizes the OLA-Simple genotyping results

© Copyright 2021 | N Panpradist

compared to Sanger sequencing and a sensitive comparator assay (CLIA-OLA or MiSeq).

Of the 664 codons analyzed, OLA-Simple had 17 indeterminate results (IND, 2.6%), not significantly different from 14 IND (2.1%) found in the same data set by CLIA-OLA (McNemar's test, $P = 0.63$). Of 24 IND results by CLIA-OLA and OLA-Simple combined: 7 were concordant, 7 were CLIA-OLA only, and 10 were OLA-Simple only. Four codons with IND results by OLA-Simple also had low WT signal in CLIA-OLA. The number of HIV templates submitted to OLA-Simple and/or CLIA-OLA from the 24 specimens with IND results (median = 271; interquartile range, IQR: 161–412 copies/reaction) did not differ significantly from the specimens categorized as WT (median = 270; IQR: 106–1821 copies/reaction, two-tailed Mann–Whitney U Test, $P = 0.70$) or MUT (median = 349; IQR: 139–1890 copies/reaction, two-tailed Mann–Whitney *U* Test, $P = 0.32$). Hence, IND results were not due to low HIV template concentrations in this study. IND results were distributed across the codons as follows: 11/166 (6.6%) at K103N, 1/59 (1.7%) at V106M/I, 3/166 (1.8%) at Y181C, 3/107 (2.8%) at M184V, and 6/166 (3.6%) at G190A. Sanger sequencing revealed that four IND codons had other mutant variants not detected by the current OLA-Simple probe sets (K103R, Y181I, and G190T). A total of 83% (20/24) IND specimens had sequence mismatches likely to have caused the assay to fail at one codon, including 12/24 (50%) IND having ≥1 polymorphic base within three bases of the ligation site and 8/24 (33%) IND having multiple (≥3) polymorphic bases within the span of the probes **Figure 5.3**.

© Copyright 2021 | N Panpradist

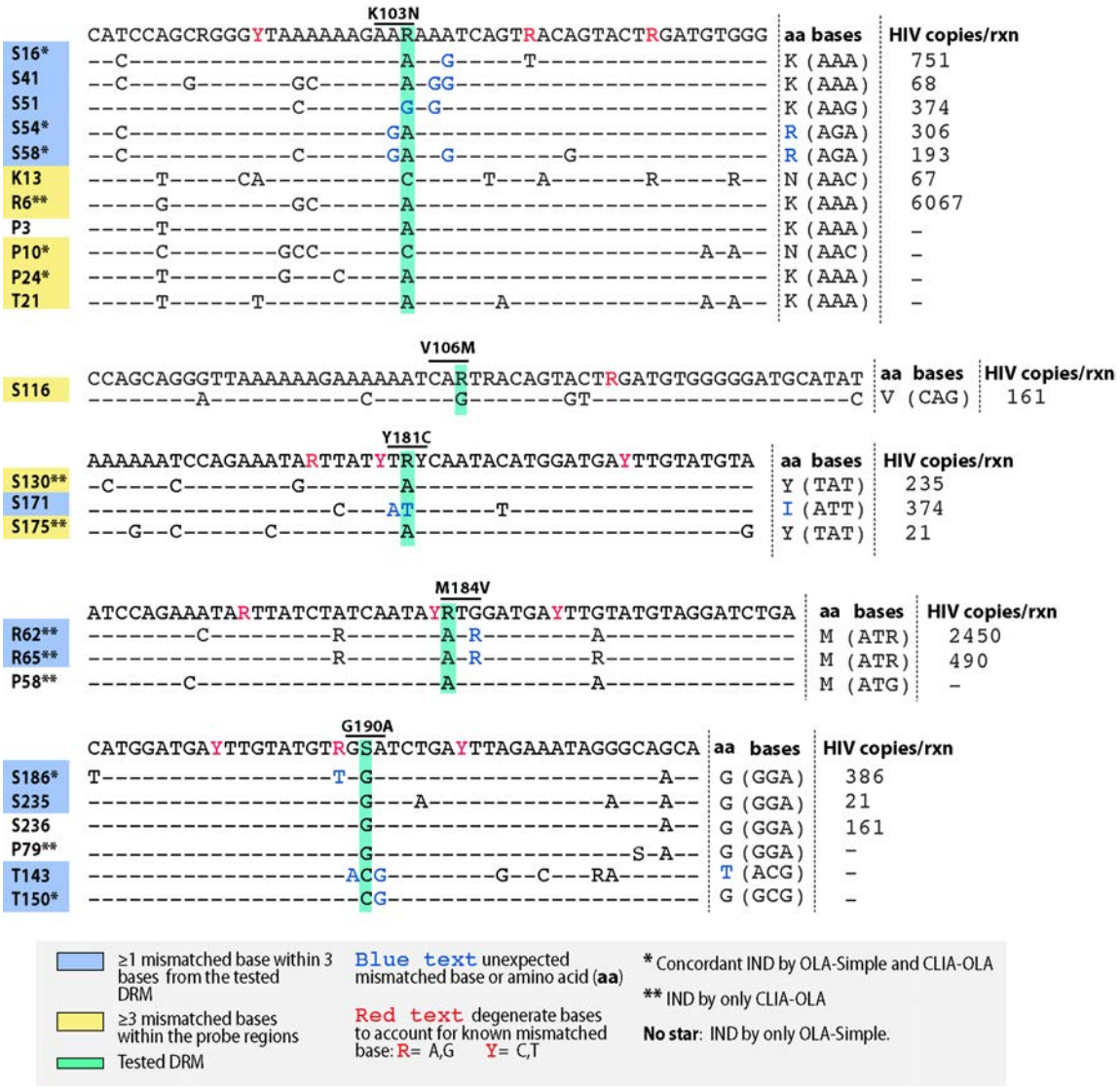

Figure 5.3 | Nucleotide sequences in the regions of the OLA-Simple's ligation probes for indeterminates identified by OLA-Simple and/or CLIA-OLA.

Sequences were obtained by Sanger sequencing. The letter in the specimen code indicated the country of specimen origin (S = South Africa, K = Kenya PBMC DNA, R = Kenya Plasma RNA, P = Peru, T = Thailand).

Compared to Sanger sequencing, OLA-Simple had 626 concordant and 21 discordant classifications (**Figure 5.2B** for combined DRM and

© Copyright 2021 | N Panpradist

Table S5.7 for each DRM). OLA-Simple detected 16 MUT missed by Sanger sequencing, with 10/16 having a MUT frequency ≤of 20%. Compared to Sanger sequencing, and excluding 17 IND cases, OLA-Simple had a combined specificity across codons of 100% (99%, 100%, 100%, 100%, and 99% for K103N, V106M/I, Y181C, M184V, and G190A, respectively), and a combined sensitivity across codons of 98% (97%, 100%, 98%, 100%, and 100% for K103N, V106M/I, Y181C, M184V, and G190A, respectively).

Comparing OLA-Simple to a sensitive genotyping method (either 2% MUT cutoff CLIA-OLA or 1% MUT cutoff MiSeq), 93% (617/664) results were concordant, including 168 MUT, 442 WT, and 7 IND (**Figure 5.2C** for combined DRM and **Table S5.10** for each DRM). Genotyping classifications by OLA-Simple and these methods were significantly different (McNemar's Test, $P<0.05$) but with an overall concordance of 95.5 ± 0.8% (SE). **Figure 5.2D** - **Figure 5.2E** shows the agreements and discrepancies of genotyping results across different MUT frequencies. OLA-Simple had 27 false negatives (MUT misclassified as WT) andtwo2 false positives (WT misclassified as MUT). All false negatives had ≤15% MUT except one with 23% MUT (**Figure 5.2F – Figure 5.2J**), while the input of HIV templates (median = 1498, IQR = 751–3710 HIV copies/reaction) of the false-negative group identified by OLA-Simple was not significantly different from the group of MUT concordant to sensitive methods (median = 349; IQR = 139–2450 HIV copies/reaction, two-tailed Mann–Whitney *U* Test, $P = 0.70$). Hence, false-negative results were not influenced by HIV template concentration in this study. Compared to the sensitive comparator assays and excluding 24 IND cases from both methods,

© Copyright 2021 | N Panpradist

OLA-Simple had a combined specificity of 100% (99%, 100%, 100%, 100%, and 99% for K103N, V106M/I, Y181C, M184V, and G190A, respectively); and a combined sensitivity of 86% (81%, 100%, 87%, 82%, and 97% for K103N, V106M/I, Y181C, M184V, and G190A, respectively). These sensitivities and specificities differ depending on pre-determined% mutant cutoffs. In this data set, OLA-Simple had a maximum combined concordance of 98 ± 1% compared to sensitive comparator assays with a cutoff of 12.5% MUT. The cutoffs with the maximum concordance for each DRM were different: 1% cutoff for G190A (99 ± 0.8% (SE)) and V106M/I (100%), 5% cutoff for M184V (99 ± 0.9%(SE)), 10% cutoff for K103N (96 ± 0.8% (SE)), and 12.5% for Y181C (99 ± 0.8% (SE)). Using results of sensitive methods as HIVDR outcomes, Receiver Operating Characteristic (ROC) curves of OLA-Simple and Sanger were compared (**Figure 5.4**). The ROC revealed that OLA-Simple was more sensitive than Sanger, but two false positives found in this study resulted in a similar area under the curve of 99.3%.

© Copyright 2021 | N Panpradist

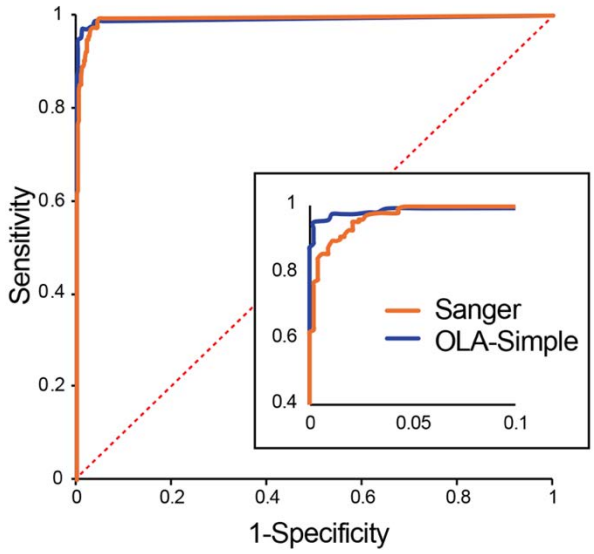

Figure 5.4 | ROC curves of OLA-Simple and Sanger sequencing.

Typical ROC curves set qualitative patient state outcomes as state outcomes and test a quantitative variable for its ability to predict the state outcomes. However, both OLA-Simple and Sanger sequencing results are qualitative. To plot ROC curves, we have set quantitative data from CLIA-OLA or NGS as a test variable and used nominal results by OLA-Simple and Sanger sequencing as the state outcomes. The area under the ROC curve of the OLA-Simple and Sanger sequence was both 0.993. SPSS was used to plot these ROC curves.

5.3 USABILITY OF OLA-SIMPLE 1.0 KITS AT UW KLAVINS LABORATORY

Usability is an overlooked aspect of implementing lab-based assays, particularly novel assays in low-resource settings. Esoteric instructions can lead to irreproducible test results and patient harm. In resource-rich communities, automation drastically improves the daily operation of clinical laboratories[5-7]. Patient samples can be quickly shipped to centralized laboratories for batch-processing and testing using highly efficient workflows that generate high-

© Copyright 2021 | N Panpradist

quality results while reducing costs and turnaround time[8, 9]. However, total automation is ill-suited for low-resource settings for many reasons. First, shipping samples to centralized laboratories can take ≥10 days[10], which undermines the benefits of fast turnaround results from an automated workflow. Second, in small communities, the demand for a clinical assay may be low, requiring a longer waiting period to receive enough samples to complete a full batch. Finally, automation is often used in conjunction with high-throughput robotic equipment that is cost-prohibitive for small laboratories. In low-resource settings, high-quality and fast laboratory results for complex assays will likely require unorthodox approaches to build on low-cost equipment and small batches of samples.

5.3.1 OLA Automation – an application to aid the implementation of OLA-Simple 1.0

OLA-Simple lab kit has greatly simplified the workflow of the original OLA, but it still contains several moving parts. To improve the implementation of the OLA-Simple, we are working with the Klavins lab (UW Electrical Engineering) to develop an application, **"OLA Automation."** The OLA Automation will better track patient specimens, a potential cause of contaminations and provide an interactive user manual (**Figure 5.5**). OLA Automation minimized user training and reduced day-to-day operational errors. I have collaborated with Justin Vrana (a Ph.D. Student) in the Klavins lab to develop the application protocol based on the provided written protocol and his hands-on experience on the

© Copyright 2021 | N Panpradist

provided OLA-Simple kit 1.0. The prototype of the OLA Automation was a part of the OLA-Simple 1.0 package for pilot testing in Kenya.

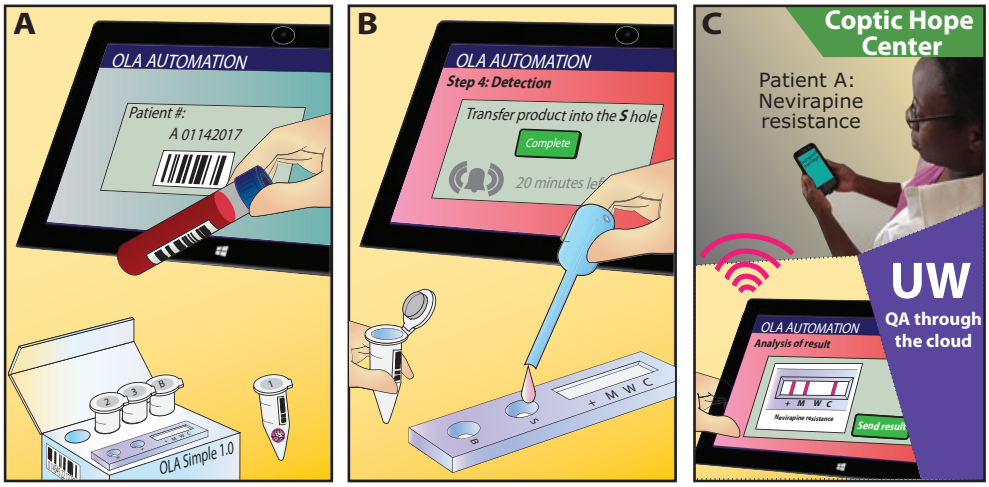

Figure 5.5 | Vision of the OLA Automation aquarium.

(**A**) Patient identification and the dried reagents used in each test are tracked via a barcode system. (**B**) Throughout the OLA-Simple procedure, technicians are guided through the process with step-by-step instructions. Alarm notifications are triggered at the end of all wait periods. (**C**) The results of paper-based tests are recorded by the tablet and automatically analyzed. The results are sent to the clinic managers designated in-clinic cell phone at the Coptic Hope Center through texting. Patients have the option to wait for their results, which improves the clinic's flow. The performance of the technicians is recorded and uploaded through the cloud. This helps facilitate quality assurance for the scientists and engineering teams located in the USA. The image was used as part of the 2016 Global WACh seed grant application.

5.3.2 OLA Automation Software-guided OLA-Simple workflow for first-time users

Next, we assessed if inexperienced users could successfully perform OLA-Simple. To provide detailed instructions for using OLA-Simple, we utilized a web-based human-in-the-loop laboratory automation application called "Aquarium." It

© Copyright 2021 | N Panpradist

integrates sample and inventory tracking, data collection, experimental protocols, and workflow management[11]. In this study, Aquarium was programmed to provide interactive protocol instruction and automatic data collection for OLA-Simple using a combination of on-screen elements that included text, checkboxes, and diagrams. Forty-one participants with no prior experience running OLA-Simple (**Figure 5.6A**) were provided information on the location of OLA-Simple reagents, pre-PCR bench, and post-PCR bench. Without additional training, the users were then instructed to perform OLA-Simple guided by the interactive Aquarium protocols to test two blinded DNA samples containing known DRMs at the six codons assessed by OLA-Simple (K65R, K103N, V106M/I, Y181C, M184V, and G190A) (**Figure 5.6B**) and (**Figure 5.6C**). Scanned images of the test results (**Figure 5.6D**) were visually classified by each user using guided interpretation by Aquarium and the in-house software as WT, MUT, and IND. Laboratory notebooks were not provided for data collection; instead, data such as test results, on-screen user selections, and images were automatically recorded in the Aquarium.

© Copyright 2021 | N Panpradist

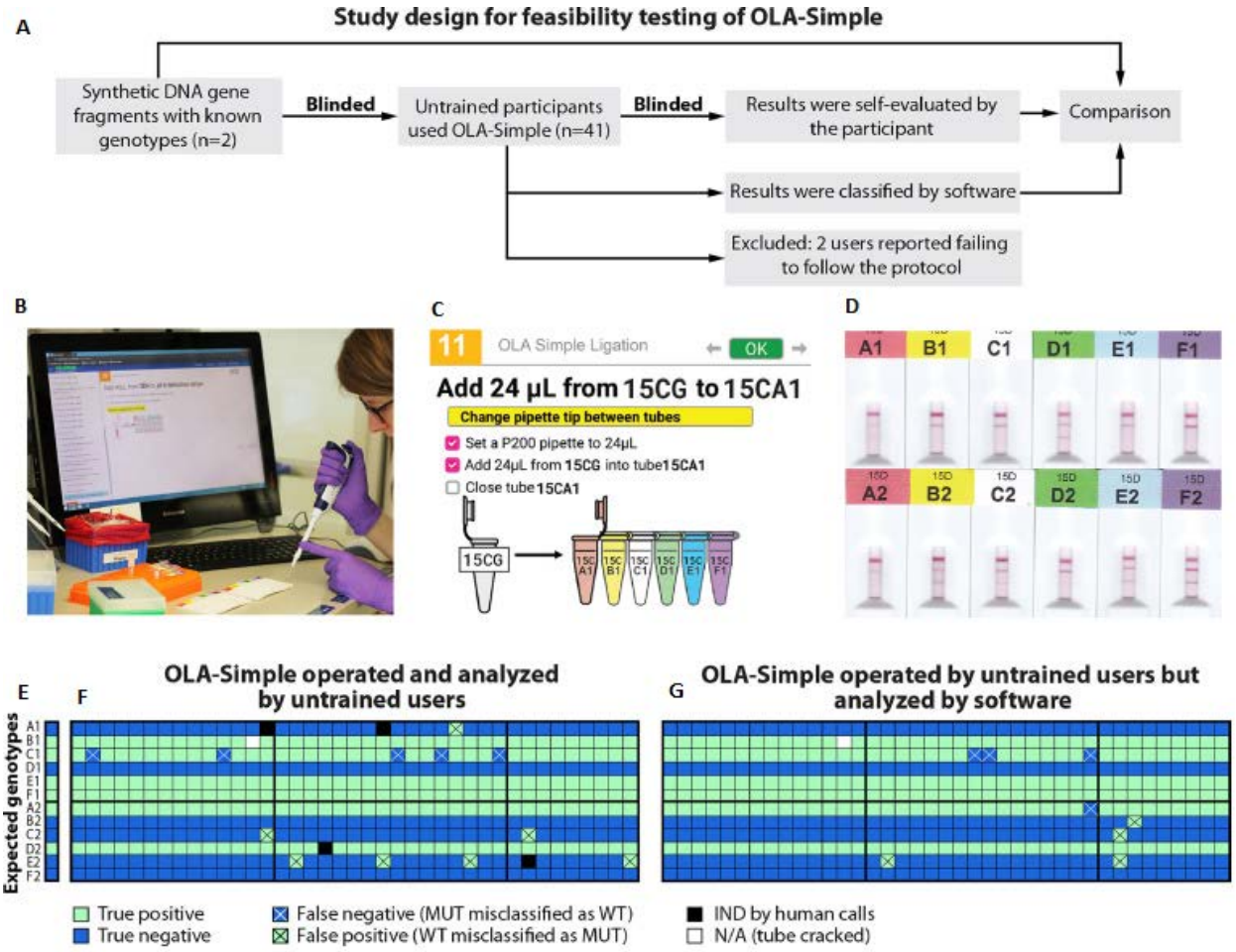

Figure 5.6 | Feasibility testing of OLA-Simple by inexperienced users guided by Aquarium software.

(**A**) Schema of feasibility testing. Forty-one untrained participants were recruited to each process two blinded samples made of synthetic DNA fragments software-guided guided protocol. The operators scanned the test strips, and the images were used to classify each DRM by visual inspection guided by Aquarium and a computer algorithm. The computer classification was then compared to calls made by each participant. (**B**) A user was performing OLA-Simple by following Aquarium. (**C**) Aquarium software guided users through the OLA-Simple protocol. Aquarium provided instructions as a series of interactive steps that included checkboxes, timers, selection boxes, tables, and images. Aquarium automatically generates unique identifiers and references to physical locations for all tubes and other items used in the protocols, which are then dynamically and automatically displayed in the tables, images, and text of the protocol steps shown on the computer or tablet. A permanent record is maintained for all steps, which mitigates the need for the user to record steps in a separate notebook. (**D**) Scanned lateral flow

© Copyright 2021 | N Panpradist

strip images at the end of the OLA-Simple workflow for the two samples tested (sample 1: MUT, WT, WT, MUT, WT, WT; sample 2: WT, MUT, MUT, WT, MUT, MUT for K65R, K103N, M106V, Y181C, M184V, G190A, respectively). Compared to the known genotypes (**E**), (**F**) and (**G**) are classifications by untrained users on their strips and by software, respectively. In one case (N/A), the ligation tube cracked during centrifugation, and the specimen was lost. Gold solutions were prepared from three different manufacturing batches, which resulted in differences in signal intensities. Batches are separated by thick vertical black lines. A thick horizontal line separates results from the two samples tested (A1–F1 and A2–F2). Reduced misclassifications of genotyping results by software classifications from scanned images of strips separated by kit batches. Note that we observed some variations between the signal of images from the low-cost USB-powered scanner used in this feasibility study and the office scanner used in the clinical study.

5.4 Piloting OLA-Simple 1.0 to detect HIVDR in Kenya

SIGNIFICANCE. This work presents the first use of human-in-the-loop automated tutorials of laboratory technicians to enable a resource-limited laboratory to operate an HIVDR test with minimal training. The custom mobile application based on Aquarium operating system describes procedures and workflows for the OLA-Simple kits. Here we show that Aquarium digital guidance allowed first-time users in a small laboratory in Kenya to perform the OLA-Simple kits accurately and derive HIVDR genotypes. We also present and discuss the technicians' feedback on their experience.

CONTRIBUTORS. Justin D. Vrana, Nuttada Panpradist, Nikki Higa, Daisy Ko, Parker Ruth, Ruth Kanthula, James J. Lai, Yaoyu Yang[5], Samar R. Sakr, Bhavna Chohan, Michael H. Chung, Lisa M. Frenkel, Barry R. Lutz, Eric Klavins, Ingrid A. Beck. Contributions: **CONTRIBUTORS.** NP, RK, and YY conceived the vision for Aquarium for OLA-Simple. NP, NH, DK, RK, IB, and JL developed and

© Copyright 2021 | N Panpradist

prepared the OLA-Simple kits. JDV, YY, and EK developed the software application for this work. JDV and IB traveled to Kenya to conduct this study. IB, NP, PR, and JDV analyzed the data. BRL, LMF, EK oversaw the overall study on the Seattle side. SRS, BC, and MHC oversaw the study design on the Kenya side and helped enrolled local technicians in Kenya.

METHODS

Study design. A Seattle traveled to Nairobi, Kenya set up a testing site at the Coptic Hope Center for Infectious Diseases, a large-scale antiretroviral treatment site[12], to evaluate the utility and performance of Aquarium in guiding first-time users to perform the OLA-Simple kits. We recruited 12 laboratory technicians from the Coptic Hospital clinical laboratories to perform OLA-Simple from April 4 – 13, 2018. We estimated that a sample size of 12 technicians, each testing ten HIVDR codons, was adequate to assess test feasibility and performance and to obtain representative feedback on the participants' perceptions related to the OLA-Simple kit and Aquarium digital instructions. This study was approved by the Institutional Ethics Review Committee (IERC) of the Aga Khan University in Kena and Seattle Children's Research Institute's IRB.

Laboratory setup. The laboratory's existing thermal cycler, biological safety hood, bench space, and refrigerator were utilized. The Seattle team brought the OLA-Simple kits, a minicentrifuge, micropipettes, scanner (CanoScan LiDE 300), tablets (Fire HD), foot controller, UPS battery backup and surge protector (APC 1500VA Compact), and server (Intel NUC7i3BNH Mini PC/HTPC) to set up and run Aquarium. The aquarium code is publicly available[13].

Evaluation of OLA-Simple. Two technicians worked with the Seattle team each day, with all 12 completing the project over six days. Each participating technician completed a demographic questionnaire and was given a 30-minute introduction to the principles and procedures used in the kit. Then each

© Copyright 2021 | N Panpradist

processed and tested two blinded blood samples. CD4+ cells were separated from 0.5 mL uninfected blood, lysed, and then spiked with mixtures of plasmids containing known HIVDR mutations. After PCR amplification of a region of HIV *pol*, mutation-specific probes were annealed, ligated, and then the ligated products were detected using lateral flow strips. The lateral flow strips were scanned, and the participants used the images displayed on the tablets to make visual calls and generate a report using Aquarium. Finally, the participants completed a questionnaire to give feedback on their experience with the kits and software.

Preparation of OLA-Simple kits. The OLA-Simple kit was prepared and assembled as previously described[14]. The EasySep CD4+ T-Cell isolation kit (STEMCELL Technologies, Vancouver, CA) was adapted to small blood volume processing, aliquote,d and packaged in foil pouches. Reagents for PCR, ligation for detecting five HIV major NNRTI/NRTI resistance codons (K65R, K103N, Y181C, M184, and G190A), and lateral flow strips to detect ligation products were packaged in foil pouches with desiccant. Each kit component was labeled with a unique identifier, matching the images illustrated in Aquarium instructions.

Post-analysis of samples in Seattle. The DNA yield in lysed cells obtained by Kenyan participants was assessed in Seattle by qPCR of human beta globin[15]. The lateral flow images and Aquarium reports generated by each participant were used to assess assay performance and interpretation of visual results. Test accuracy was determined by comparison to the expected genotype at each codon analyzed. Lateral flow strips images were re-analyzed using an in-house Python script[14] to determine if automated analyses improved test accuracy. 95% confidence intervals (CI) are reported for all proportions.

Participant characteristics. The 12 participating technicians were 83% male, median age 30 years old (range 26-42), had a median of 6 (range 3-10) years of experience as a laboratory technician, and all were conversant in English. Their education level ranged from secondary school with a certificate in Medical Laboratory Technology to a master’s degree in Laboratory Science,

© Copyright 2021 | N Panpradist

representative of most clinical laboratories in Kenya. They reported varying levels of experience working with HIV or molecular techniques (**Table 5.1**).

Table 5.1 | Demographics of participants

Variable	Value (N=12)
Age, median (range), years	30 (26-42)
Gender, N (%)	
Male	10 (83.3)
Female	2 (16.7)
Primary language, N (%)	
English	4 (33.3)
Swahili	1 (8.3)
English and Swahili	7 (58.3)
Highest education level, N (%)	
Masters	1 (8.3)
Bachelor	3 (25)
Technical/Vocational training	2 (16.7)
Secondary school diploma	6 (50)
Years of experience as a lab technologist/technician, median (range)	6 (3-10)
Hours/week worked for pay in current position, median (range)	45 (40-54)
Current position in laboratory, N	
Laboratory manager	2
Lab technologist†	4
Lab technician†	6
Ever performed lab procedures related to HIV, N (%)	10 (83.3)
Viral load tests	2
CD4 testing	3
ELISA test	2
Phlebotomy and blood separation	5
Ever performed DNA or RNA extraction, N (%)	5 (41.7)
Kit (Qiagen, COBAS Ampliprep and Taqman, Abbott M2000rt	3
Sputum lysis for GeneXpert	1
Cavidi technology	1
Ever used a thermocycler, N (%)	3 (25)
Ever set up PCR, N (%)	6 (50)

† Participants performed tests in one or several of the following areas: microbiology, hematology, biochemistry, parasitology, immunology sections, CD4/8, GeneXpert (TB), ELISA

© Copyright 2021 | N Panpradist

RESULTS AND DISCUSSION

5.4.1 Laboratory setup for Aquarium-assisted OLA-Simple training

The installation cost of OLA-Simple is low compared to automated sequencing platforms (> US$ 100,000) as it uses equipment that exists in most laboratories or is relatively inexpensive to acquire. Setting up the assay and software at the Coptic Hope Center laboratory required ~US$1,000 of additional equipment (scanner, microcentrifuge, vortexer, computer tablets, a server, and an uninterruptible power supply). For a laboratory without access to a thermal cycler, a battery-powered portable unit (~$500) can be used[16].

The laboratory was equipped with a Wi-Fi network to run Aquarium and coordinate assay steps across a pre-PCR and post-PCR room (**Figure 5.7A**). Participants worked in pairs follow the OLA-Simple workflow (**Figure 5.7B**): sample preparation and PCR set-up were carried out in the pre-PCR room, while PCR, ligation and detection were conducted in the post-PCR room to minimize the potential for amplicon-carryover contamination. Each participant processed two uninfected blood specimens and performed mutation testing on two contrived specimens with known HIV mutations following the interactive digital instructions provided by Aquarium.

To complete the workflow, it took the participants pairs an average of seven hours. This time included the introductory session, completion of surveys, and staggering some assay steps due to space and instrument constraints. The turnaround time would likely decrease to 4.5-5 hours once users become familiar with the software and the kits.

© Copyright 2021 | N Panpradist

The reported turnaround time for centralized HIVDR testing in resource-limited settings is 18 days[17] from sample collection, shipping to the laboratory, batching and testing samples, and transmitting results to the clinic. In this study, OLA-Simple was performed within the hospital grounds and thus could deliver test results within one day. Moreover, each kit tests two samples, a number suitable for the volume of weekly patient samples submitted for HIVDR testing in small laboratories in Kenya, eliminating the need to wait for an adequate number of specimens to batch for testing.

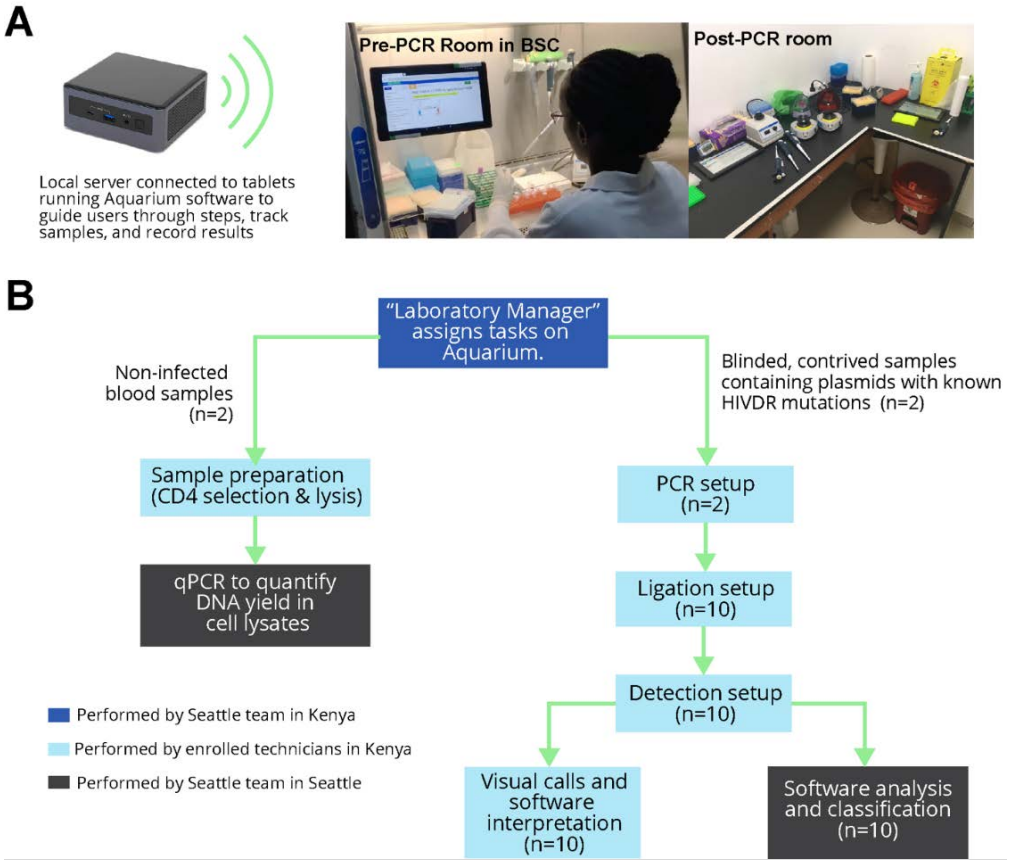

Figure 5.7 | OLA-Simple laboratory setup and workflow.

(A) Laboratory setup: Tablets were connected to a local server to run Aquarium software. The pre-PCR room had a refrigerator/freezer and a BSC where CD4+ separation and PCR reaction were set up. Technicians controlled the Aquarium-based software on the tablet with a foot pedal (not shown in the

© Copyright 2021 | N Panpradist

picture) while performing CD4+ preparation. The post-PCR room had two designated bench areas to set up ligation and detection separately. This room also contained a thermal cycler and a scanner. (B) Tasks assigned by Aquarium for Kenyan technicians to assess their performance using Aquarium-assisted OLA-Simple. The sample preparation module was separated from the amplification, ligation, detection, and interpretation module. Associated protocol code and examples of complete runs are publicly available (https://github.com/OLA-Simple/Papers-Vrana-Panpradist-et-al-2021).

5.4.2 PERFORMANCE OF PARTICIPANTS USING OLA-SIMPLE

All 12 participants successfully isolated CD4+ cells from whole blood collected from four donors with yields within the expected range (mean ± SD: 686,450 ± 216,500 CD4+ cells/mL) and completed genotyping of two samples using the OLA-Simple kits. The two blinded DNA samples tested by all participants included wild-type genotype only or mixtures of mutant and wild-type genotypes at each of five HIV reverse transcriptase codons, including K65R, K103N, Y181C, M184V, and G190A (total of 10 codons/participant) (**Figure 5.8A**). Participants correctly genotyped 70/72 (97.2%, 95% CI: 90-100%) mutant codons and 38/48 (79.2%, 95% CI: 65-90%) wild-type codons. The only two false negatives were due to Participant #6 erroneously testing Sample 1 twice and omitting testing of Sample 2. Of 10 false-positive results, 2 were due to testing Sample 1 in place of Sample 2 by Participant #6, 1 appeared to be contamination (light mutant signal at codon G190A likely from reusing a pipette tip contaminated with mutant ligation product), and 7 were due to light mutant background at codons K103N (n=6) and K65R (n=1). Analysis of the scanned images using our in-house image analysis software improved test accuracy to 97% (116/120, 95% CI: 92-99%) with 97% (70/72, 95% CI: 90-

© Copyright 2021 | N Panpradist

99%) mutant codons and 96% (46/48 95% CI: 86-99%) wild-type codons correctly genotyped (**Figure 5.8B**).

The image analysis software improved accuracy over the visual interpretation of results by establishing a threshold above the mutant background signal and thus eliminating false positives. The sample mix-up described above reduced the overall accuracy; this could be improved with changes in the kit labeling system to prevent this type of errors. Correcting for the sample that was added twice, the performance of the assay chemistry combined with software analysis yielded 100% accuracy (120/120, 95% CI: 97-100%).

© Copyright 2021 | N Panpradist

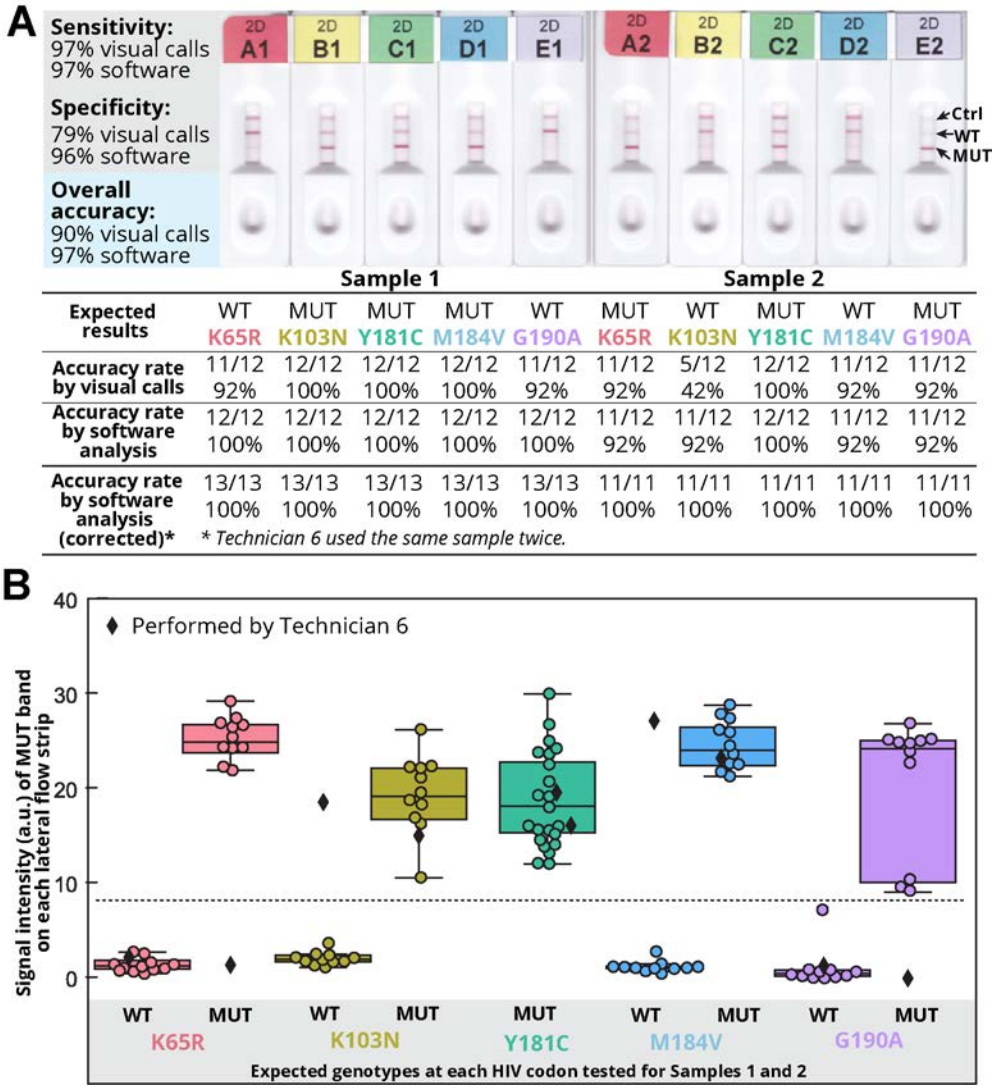

Expected results	WT K65R	MUT K103N	MUT Y181C	MUT M184V	WT G190A	MUT K65R	WT K103N	MUT Y181C	WT M184V	MUT G190A
Accuracy rate by visual calls	11/12 92%	12/12 100%	12/12 100%	12/12 100%	11/12 92%	11/12 92%	5/12 42%	12/12 100%	11/12 92%	11/12 92%
Accuracy rate by software analysis	12/12 100%	12/12 100%	12/12 100%	12/12 100%	12/12 100%	11/12 92%	11/12 92%	12/12 100%	11/12 92%	11/12 92%
Accuracy rate by software analysis (corrected)*	13/13 100%	13/13 100%	13/13 100%	13/13 100%	13/13 100%	11/11 100%	11/11 100%	11/11 100%	11/11 100%	11/11 100%

** Technician 6 used the same sample twice.*

Figure 5.8 | OLA-Simple HIVDR results and interpretations.

(**A**) Examples of scanned images of test strips for Samples 1 and 2 and test accuracy across each codon based on visual calls made by each participant and post-processing by the image analysis software. Sample1 and Sample 2 have different mutation profiles. (**B**) Mutant (MUT) signal intensity of each lateral flow strip. Middle lines on the box plot indicate medians. The top and bottom lines on the box plot indicate interquartile ranges. Dashed lines indicate the detection threshold for the MUT signal. Both Sample 1 and Sample 2 have mutant genotypes at codon Y181C. Diamonds correspond to signal from the strips of a Sample 1 that was erroneously tested in place of Sample 2.

© Copyright 2021 | N Panpradist

5.4.3 FEEDBACK FROM PARTICIPANTS

Overall, participants scored the use of software as helpful in learning to perform the assay and enjoyed the clear instructions and interpretability of the results using the tablets. They strongly agreed that they understood the meaning of the bands on the strips and that the Aquarium instructions were easy to follow. However, several participants felt the procedure was lengthy and involved too many steps

© Copyright 2021 | N Panpradist

Table 5.2 and **Table 5.3** summarize the survey responses). We have subsequently developed new chemistries to reduce assay time to 3.5 hours by replacing the 1.5-hour blood DNA preparation with a 30-minute plasma RNA extraction and the 2-hour PCR with 1-hour RT-PCR.

5.4.4 SURVEY RESPONSES FROM PARTICIPANTS REGARDING AQUARIUM & OLA-SIMPLE KIT.

Participants were asked to fill out a short survey immediately following the procedure, which included evaluating four statements on a 5-point Likert scale (strongly agree to disagree) (Error! Reference source not found.) and three open-ended qualitative questions (Error! Reference source not found.). For ordinal categorical values, modes are displayed for each statement. For open-ended questions, we present a summary of the responses describing the different points raised by all the participants.

© Copyright 2021 | N Panpradist

Table 5.2 | Response to the OLA-Simple user questionnaire
* Participants 11 and 12 answered NA to the PCR question, likely due to not performing PCR before this training. Rating scale: 1=strongly disagree, 2=disagree, 3=neutral, 4=agree, 5=strongly agree, and NA=not applicable.

Questionnaire statement	Mode
Specimen preparation: I was able to perform these steps in less time than my usual DNA extraction	4
PCR and Ligation: Using dried reagent is easier than setting up a traditional PCR reaction	4*
Detection: I understood the meaning of the bands in the strip	5
Kit instructions: Instructions were easy to follow	5

Table 5.3 | Summary of responses from OLA-Simple users

What did you like best about using this kit?	Which instruction(s) were not easy to follow? Please explain why.	What advice do you have for us to make the kit and instructions easier to use?
• The instructions were easy to follow • The protocol was easy to understand. • The examples in Aquarium were well labeled and made it easy to know where to add each reagent or sample • The kit is user-friendly and straightforward • The kit is easy to use compared to the plate-based OLA method • There was only one PCR step instead of the usual two for nested PCR • Aquarium simplified detection • Results are generated fast and are also portable • It is easy to read the bands and interpret the results: it clearly shows the control, the wild-type, and the mutant • A single sample can be easily processed without the need for batching	• The instructions and procedure were clear and easy to follow. • The instructions were Ok when following a step, but it was difficult to memorize the steps without a written protocol to follow • Some instructions did not include the specific vial or reagent in the heading, but it was in the pictorial • Sample preparation: - the multiple tubes and SOP instructions were not alphabetically arranged - includes many tubes, color coding would help to identify which to use first and avoid mix-ups - too many steps make it confusing - the process is long with many reagents, and waiting time • During the ligation/detection step had challenges remembering to add the reagent to the next strip • At times the tablet was not working, and we did not have a backup plan such as a written protocol with instructions.	• Enlarge the font under every heading. • Include the reagent vial ID on the headings for better clarity • The tube labels should match the SOP instruction labels. • Harmonize the sequence of adding reagents and closing of tubes to reduce multitasking and possible confusion. • Create a system for how to keep track of addition of reagents to tubes • State what to expect at the end of each step, e.g., maybe a clean supernatant /deposit so one can confidently move to the next step • Look for alternatives to replace the current sample preparation method • Make the incubation time shorter • Improve turn-around time for printouts of the protocols backup plan. • Make the kit commercially available with all the steps for laboratory technologists to follow.

© Copyright 2021 | N Panpradist

Our study shows it is feasible to use Aquarium to train local laboratory personnel with basic experience in lab work and onboard HIVDR tests. However, this pilot study was limited to the use of contrived specimens to establish analytical performance, and each participant was able to perform the OLA-Simple kit once. Thus, we were not able to assess the ability of each technician to maintain or improve their skills. A larger demonstration and evaluation study that includes HIV-infected clinical specimens and multiple OLA-Simple runs is ongoing in Kenya to assess the robustness of our HIVDR test.

The Aquarium software has valuable features for HIVDR testing, such as an automatic collection of operator interactions in the Aquarium's virtual laboratory notebook that can be useful for troubleshooting. Each kit item is labeled with a unique identifier that Aquarium instructions use in conjunction with corresponding pictures to avoid ambiguity and reduce the extent of in-person training needed. Uniquely labeled items also allow tracking stock consumption in real-time, which can be timesaving for laboratory management. Importantly, Aquarium could link test results to treatment algorithms to advise clinicians, and algorithms could be updated as clinical recommendations or policies change.

CONCLUSION. Aquarium-based software facilitated the deployment of the OLA-Simple in Kenya with minimal training, enabling local laboratory technicians to perform a HIVDR test. Human-in-the-loop automation could facilitate daily operations of laboratory-based assays and increase the performance and accuracy of diagnostic tests in small laboratories.

© Copyright 2021 | N Panpradist

ACKNOWLEDGMENTS. We are grateful to the Coptic Hospital and the Coptic Hope Center for their support and technologists from these institutions who participated in this study. We thank Syamal Raychaudhuri, Dindo Reyes, Kim Polizzi, and Jessica Price at InBios International, Inc. for producing the lateral flow strips used in the validation study; and Aarthy Vallur and Kathryn Hjerrild of InBios International, Inc. for providing feedback on OLA-Simple prototypes.

5.5 Adaptation of OLA-Simple 1.0 kit for HIVDR detection in a Mexican cohort

SIGNIFICANCE: In this study, we have further improved the OLA-Simple assay in two areas: validated probes for detection of K65R – a major resistance mutation to tenofovir, which is an NRTI widely used with NNRTIs or dolutegravir and exploited an in-house software program to quantify signal and classify results from lateral flow tests automatically. Additionally, we have adapted the OLA-Simple kit probe sequences to detect these NNRTI/NRTI mutations in a Mexican population and validated the improved kits by genotyping PDR in a cohort of adults initiating first-line NNRTI/NRTI regimens in Mexico City.

CONTRIBUTORS: Nuttada Panpradist*, Ingrid A. Beck*, Parker S. Ruth, Santiago Ávila-Ríos, Claudia García-Morales, Maribel Soto-Nava, Daniela Tapia-Trejo, Margarita Matías-Florentino, Hector E. Paz-Juarez, Silvia del Arenal-Sanchez, Gustavo Reyes-Terán, Barry R. Lutz, and Lisa M. Frenkel. * Equal contribution.

© Copyright 2021 | N Panpradist

METHODS

Study design for clinical validation. A database containing HIVDR profiles from 2412 individuals initiating first-line ART in Mexico City genotyped by MiSeq was used to select 60 plasma specimens enriched for mutations K65R, K103N/S, Y181C, M184V, and G190A. This set of mutations was selected due to their frequency in the Mexican cohort and their relevance for the preferred first-line regimens in use at the time of study design. All participants provided written informed consent before blood sample donation for HIV genotyping. The Institutional Review Board approved the study of the National Institute of Respiratory Diseases – the institution where HIV sequencing was performed (Project code: E02–17). De-identified specimens from treatment-naive adults were blindly tested by OLA-Simple, and the results compared to results from MiSeq sequencing. GenBank accession numbers are MT044195-MT044237; MT070765-MT070781.

Design of OLA-Simple probes for a Mexican population. OLA-Simple probes designed to detect K65R, K103N/S, Y181C, M184V, and G190A across multiple subtypes were modified to include polymorphisms observed frequently in *pol* sequences from individuals initiating an NNRTI/NRTI regimen in Mexico City between September 2017 and March 2018[18]. **Table S5.8** lists the probe sequences used for the Mexican cohort.

Preparation of OLA-Simple kits and sample testing. All kit components were manufactured and packaged in the Lutz lab at the University of Washington similarly to the original OLA-Simple 1.0, except the lyophilized

© Copyright 2021 | N Panpradist

reverse-transcription reagents (Takara Bio Inc., Shiga, Prefecture, Japan) and QIAamp viral RNA mini kit (Qiagen, Hilden, Germany). Briefly, PCR, ligation, and gold detection mixtures were lyophilized in the presence of additives to protect reaction components during the lyophilization and drying process. In this study, ligation mixtures included the newly designed oligonucleotide probes. Lateral flow strips were striped with anti-digoxigenin antibody, anti-fluorescein antibody, and biotin-bovine serum albumin. All kit components were stored at 4°C until use. Assay optimization was performed using HIV subtype B plasmids mixtures containing 0, 10, 25, and 100% mutant for all codons tested as previously described[19]. According to the manufacturer's instructions, plasma specimens were extracted using the Qiagen QIAamp Viral RNA kit (Qiagen, Hilden, Germany). Extracted RNA was reverse-transcribed in a rehydrated lyophilized reverse-transcription reaction. cDNA from plasma was then amplified in rehydrated lyophilized PCR reactions. Aliquots of amplicon were added to rehydrated lyophilized ligation mixtures for each mutation tested and subjected to ligation. Ligation products were then visualized by lateral flow detection using gold particles. Lateral flow detection strips were scanned after 15–20 min and analyzed using in-house software. To determine the threshold for IND results (i.e., negative for both mutant (MUT) and wild-type bands), 12 mock IND strips were generated using an HIV template-free ligation reaction.

Analysis of OLA-Simple results. The in-house python software was designed to automatically crop the region of interest (ROI) from the scanned images of lateral flow tests. The ROI was then converted to grayscale by

© Copyright 2021 | N Panpradist

linearly combining the Red-Green-Blue channels using coefficients selected by linear discriminant analysis to differentiate pixels in the band and paper background regions. The locations of the control, MUT, and wild-type bands were identified by a combination of peak detection and heuristic peak selection. The software calculated a t-statistic between rectangular pixel regions on and immediately adjacent to each band to compute the intensity. This normalized t-statistic is referred to as the 'signal' of the strip. The threshold for IND results was selected as six standard deviations (SDs) above the mean of the wild-type signal from mock indeterminate strips. A receiver-operating characteristic (ROC) curve was generated using SPSS Data Analysis Software (IBM, Armonk, New York, USA), setting the MUT signal from all OLA-Simple as the 'test variable' and the diagnostic wild-type or MUT classifications as the 'state variable.' The state variables were determined by MiSeq using 2, 5, 10, 15, 20, and 25% mutant frequency thresholds. At a 10% mutant diagnostic threshold, a MUT signal threshold was selected to maximize the concordance of OLA-Simple results and MiSeq data.

Analysis of HIVDR using MiSeq. Deep sequencing by MiSeq (Illumina, San Diego, California, USA) on near-full genome HIV amplicons was performed at the CIENI/INER laboratory in Mexico City as previously described[18, 20]. Briefly, DNA libraries were prepared using Nextera XT DNA Sample Preparation kit and Nextera XT Index Kits (Illumina), according to the manufacturer's protocol, and were run with 500-cycle MiSeq Reagent Kits v.2. Fastq files from the sequencing runs were aligned and assessed for HIVDR frequencies using HyDRA (National Microbiology Laboratory, Public Health Agency of Canada,

© Copyright 2021 | N Panpradist

Winnipeg, MB, Canada) [21]. Amino acid mutations were queried against the Stanford HIV Drug Resistance Database [22]. MiSeq has reported analytical sensitivities of less than 2% variants [23], but we chose a more conservative 2% threshold [24] as the lowest diagnostic threshold in this study.

Statistical analysis. The number of technical replicates in each experiment was reported in Figure 5. legends and provided in the 'Methods' section. Multiple comparisons of means across groups were calculated using the *t-test*, with alphas adjusted using the Holm-Bonferroni method. Concordance, sensitivity, specificity, and rates are reported with standard errors (SEs) of binomial proportion. The areas under the curve of ROC curves are reported with 95% confidence intervals (95% CI).

RESULTS

The workflow of the OLA-Simple kit includes four main steps: nucleic acid extraction (not shown), RT-PCR amplification, ligation, and detection (**Figure 5.9A**). These steps have been significantly simplified by premeasuring and lyophilizing reaction components to enable fast and accurate setup and increase stability without freezer storage. The lyophilized reaction mixtures include necessary enzymes, primers, and/or probes for HIVDR testing and can be activated by rehydration with water. OLA-Simple detection generates visible results on lateral flow strips, which can be read by the unaided eye, as previously reported[14]. We employed in-house software to quantify the signal and classify HIVDR results to enable consistent analysis and interpretation across users.

© Copyright 2021 | N Panpradist

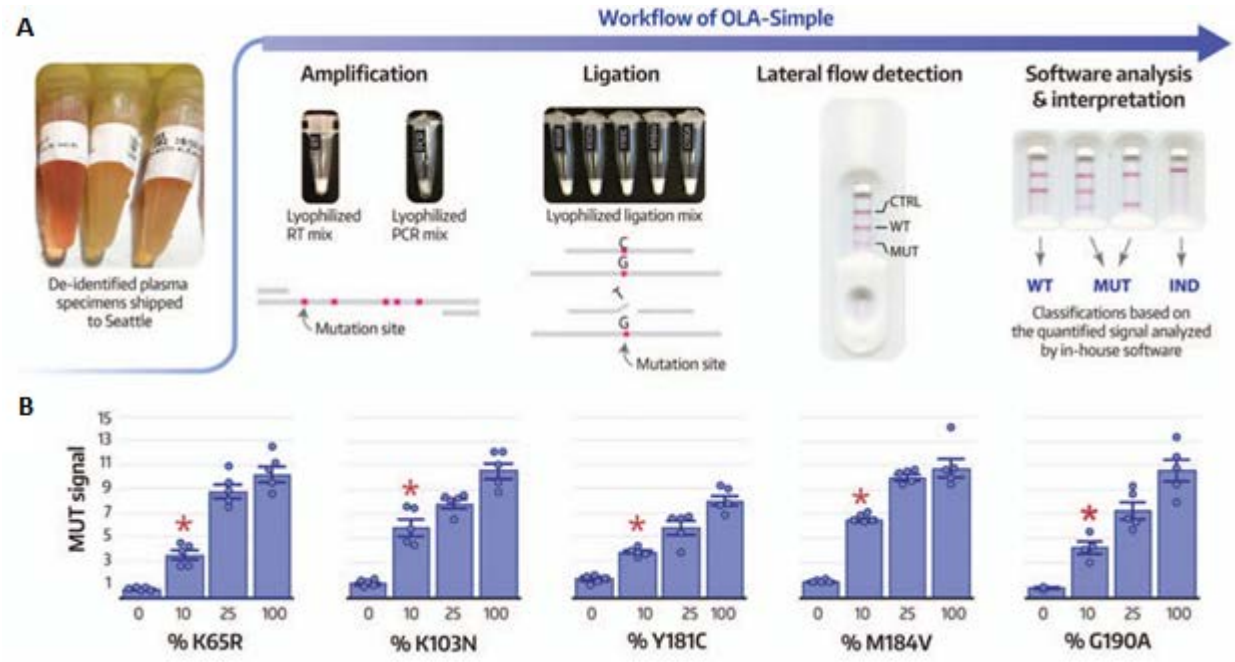

Figure 5.9 | Workflow and analytical sensitivity of the OLA-Simple kit using plasma.

(**A**) Workflow of OLA-Simple. Extracted RNA from plasma was directly added to rehydrate a lyophilized reverse transcription (RT) reaction mixture. The cDNA was then added to a rehydrated lyophilized PCR reaction mixture, and the PCR amplicon generated was subsequently added into the ligation reaction mixture for each mutation tested. The ligation products were visualized using lateral flow strips, which were scanned and analyzed using in-house software. Based on the signal of MUT and WT bands, OLA-Simple results were then classified as MUT, WT, or IND, as shown. (**B**) Analytical sensitivity of OLA-Simple. DNA standards containing plasmid mixtures with 0%, 10%, 25%, and 100% of MUT target (*n* = 5 each) were genotyped by OLA-Simple. Each circle represents the signal from one technical replicate (mean ± SE). *One technical replicate was excluded because the image of this strip had unusual color pixels in the background region of the lateral flow tests, causing artifacts in our software analysis. Means were compared by t-test corrected using the Holm-Bonferroni method. In all codons, the signal from the 0% mutant was significantly different from the 10% mutant ($P < 0.05$). Y-axes were shared across these graphs. IND, indeterminate; MUT, mutant; WT, wild type.

We adapted the ligation module of the OLA-Simple using probes optimized for the Mexican population. The concentrations of ligation probes and assay conditions were initially optimized and tested on HIV subtype B plasmid DNA

© Copyright 2021 | N Panpradist

standards (wild-type, mutant, or wild-type/mutant mixtures at the five codons tested). The updated OLA-Simple assay differentiated 0% (wild-type HIV) from 10% mutant across all codons (**Figure 5.9B**).

Clinical validation of this version of the OLA-Simple was conducted on 60 plasma specimens from a cohort in Mexico selected by collaborators at CIENI/INER to include a high proportion of specimens with PDR. Across these specimens, 98.3% (59/60) amplified by reverse transcription-polymerase chain reaction (RT-PCR) (median viral load: 103 586, range 176–10 000 000 copies/ml). The one specimen that failed amplification had a plasma HIV RNA load of 176 copies/ml, with an estimated 29 copies submitted to the RT-PCR reaction. The 59 specimens with successful amplification underwent ligation and detection for HIVDR testing on a total of 295 codons (five mutations each). OLA-Simple genotyping was indeterminate (IND) for 2.7% (8/295) of all codons tested (**Table 5.4**), with 8.5% (5/59) at K65R, 3.4% (2/59) at Y181C, and 1.7% (1/59) at G190A. There were no IND results at K103N/S and M184V.

Clinical validation of this version of the OLA-Simple was conducted on 60 plasma specimens from a cohort in Mexico selected by collaborators at CIENI/INER to include a high proportion of specimens with PDR. Across these specimens, 98.3% (59/60) amplified by reverse transcription, polymerase chain reaction (RT-PCR) (median viral load: 103 586, range 176–10 000 000 copies/ml). The one specimen that failed amplification had a plasma HIV RNA load of 176 copies/ml, with an estimated 29 copies submitted to the RT-PCR reaction. The 59 specimens with successful amplification underwent ligation and detection for HIVDR testing on a total of 295 codons (five mutations each).

© Copyright 2021 | N Panpradist

OLA-Simple genotyping was indeterminate (IND) for 2.7% (8/295) of all codons tested (**Table 5.4**), with 8.5% (5/59) at K65R, 3.4% (2/59) at Y181C, and 1.7% (1/59) at G190A. There were no IND results at K103N/S and M184V.

Table 5.4 | Genotyping results by OLA-Simple adapted for a Mexican cohort.

Codon tested	TP (MUT)	TN (WT)	FP	FN	IND	%Specificity	Sensitivity	%IND
K65R	1	53	0	0	5	100	100	8.5 ± 3.6
K103N/S	21	34	**0**	3	0	97.2 ± 2.2	87.0 ± 4.4	0
Y181C	10	47	0	0	2	100	100	3.4 ± 2.3
M184V	12	45	2	0	0	95.7 ± 2.6	100	0
G190A	10	44	3	1	1	93.6 ± 3.2	90.9 ± 3.7	1.7 ± 1.7
Overall	54	223	5	4	8	97.8 ± 0.9	93.1 ± 1.5	2.7 ± 0.9

Illumina MiSeq results were used as the sensitive reference assay; at least 10% mutant and less than 10% mutant results by MiSeq were classified as positive (mutant) or negative (wild-type), respectively, for the reference result. Percentage sensitivity, specificity, and IND are reported with standard errors. FN, false negative; FP, false-positive; IND, indeterminate; MUT, mutant; TN, true negative; TP, true-positive; WT, wild type.

Compared to MiSeq using 10% mutant frequency as the diagnostic threshold, OLA-Simple had five false-positive, four false-negative, and eight IND results. False-positive occurred at M184V (n = 2/59) and G190A (n = 3/59); all these false-positives by OLA-Simple were 100% WT by MiSeq. Of the four false-

© Copyright 2021 | N Panpradist

negative results, three were K103N/S (at 10.5, 11.9, and 22.4% mutant frequency) and one at G190A (at 20.59% mutant frequency). Based on these results, OLA-Simple had 93.1% sensitivity and 97.8% specificity across all codons. Genotyping data by OLA-Simple and MiSeq are available in **Table S5.9**. Percentage sensitivity and specificity at other diagnostic thresholds are shown in **Table S5.10**.

The accuracy of OLA-Simple genotyping results was estimated by comparison to MiSeq genotypes, excluding IND results (*n* = 287). ROC curves were generated using different diagnostic mutant frequency thresholds (**Figure 5.10**). The areas under the curve reflect the accuracy of the MUT signal from OLA-Simple for classifying HIVDR results compared to those determined by MiSeq. At 2, 5, 10, 15 (or 20%), and 25% mutant frequency thresholds, the accuracy of OLA-Simple was 93.2% (95% CI 89.0–97.5%), 96.3% (95% CI 93.0–99.6%), 97.2% (95% CI 94.1–100%), 97.4% (95% CI 94.4–100%), and 98.8% (95% CI 97.1–100%), respectively.

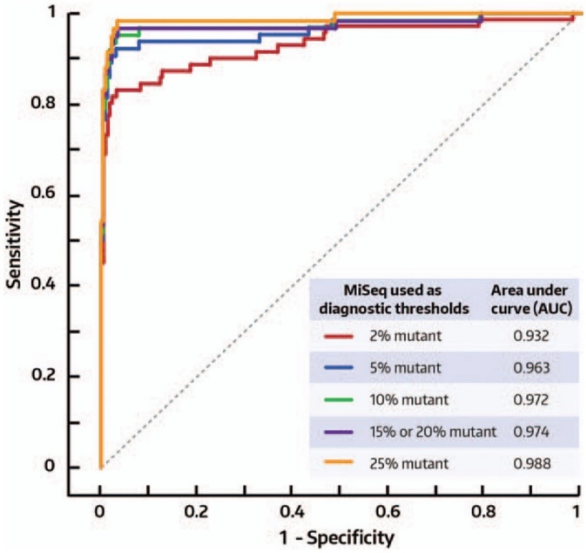

Figure 5.10 Receiver-operating characteristic (ROC) curves.

© Copyright 2021 | N Panpradist

The ROC curves show how well the mutant signal of OLA-Simple classifies HIVDR results (wild-type or mutant) determined by MiSeq using a 2, 5, 10, 15, 20, or 25% mutant frequency threshold. The dashed line is the reference line where sensitivity is equal to 1-specificity. Note that ROC curves for 15 and 20% are on top of each other. HIVDR, HIV-drug resistance.

DISCUSSION

We have adopted a low-cost, easy-to-use, rapid OLA-Simple HIVDR test for a Mexican population. Specifically, we have designed probes to detect major drug resistance mutations to NNRTIs (EFV/NVP) and NRTIs (3TC/TDF). The analytical sensitivity of OLA-Simple is 10% mutant among the HIV quasispecies, which is better than the reported sensitivities of 20–50% by Sanger sequencing[25, 26]. The OLA-Simple results were compared favorably to MiSeq results performed at CIENI/INER in Mexico City, which has met the WHO requirements for good laboratory practices and quality assurance in HIV genotyping.

In this study, OLA-Simple primers amplified all except one specimen with a viral load of 176 copies/ml (29 RNA copies/RT-PCR reaction), which is near the detection limit of the OLA-Simple PCR (10 copies of DNA/reaction)[14]. Amplification failure in this sample could be due to variations in the RNA extraction efficiency between the plasma aliquots used for viral load measurement and OLA-Simple, or lower efficiency during reverse transcription.

The IND results in OLA-Simple can occur due to mismatches of the probes to the target HIV sequence. The alignment of 2412 Mexican HIV *pol* sequences

© Copyright 2021 | N Panpradist

showed considerable variability in several OLA-Simple kit probes, which were designed as universal probes to test HIV subtypes A, B, C, D, and AE. To improve ligation efficiency in the Mexican cohort, where HIV subtype B accounts for nearly 99% of infections[27-30], we designed subtype B-specific probes that included mixtures of nucleotides at sites of frequent polymorphisms or mixtures of probes to accommodate variations at multiple sites close to the probes' ligation site. Probe design for K103N proved particularly challenging due to relatively frequent changes at this or adjacent codons 102 (K102Q/R), 103 (K103S, K103R), and 104 (K104R). K102Q/R, K103R, and K104R have not been associated with reduced susceptibility to NNRTIs[21] but can interfere with detection of K103N by OLA-Simple, as their presence could interfere with the DNA ligase requirement that the four nucleotides surrounding the ligation site have perfect complementarity with the target[31], causing an IND result.

In contrast, K103S confers high-level resistance to NVP and intermediate to EFV[32]. Therefore, probes detecting both K103N and K103S were tested simultaneously in this updated OLA-Simple kit by mixing four genotype-specific probes and one common probe, resulting in no IND results in K103N/S in this cohort. Universal probes for K65R in the OLA-Simple kit were slightly modified for the subtype B Mexican variants, and these had not been previously validated on clinical specimens. Despite modifications, these K65R probes had the highest rate of IND results (8.5%) mainly due to closely spaced nucleotide variations at codons 67, 68, and 69, including the polymorphic mutation S68G (**Table S5.10**). To reduce the IND rate for K65R, a mixture of

© Copyright 2021 | N Panpradist

common probes complementary to these polymorphisms/mutations may be necessary at this site. The subtype B-specific probes tested in this study reduced the combined IND rate at codons K103N/S, Y181C, M184V, and G190A to 1.3% (3/236) from a 2.7% IND rate observed when using probes designed to work 'universally' across multiple HIV-1 group M subtypes, and tested on specimens from Kenya, South Africa, Peru, and Thailand. Further reduction of the overall IND rate could be achieved by including probes for alternative variants at the codons tested, such as M184I and G190S, depending on the frequency of these mutations in the target population.

Quantitative comparison of OLA-Simple results and MiSeq was presented in ROC curves at different mutant frequency thresholds because a clinically relevant threshold has not yet been established[33]. The use of unique molecular indices (UMI) to quantify the actual number of HIV templates sequenced would likely allow a more accurate assessment of these thresholds. At 10% mutant threshold based on MiSeq, OLA-Simple's accuracy was higher than at 5% (97.2 vs. 96.3%) but gave 1.4% (4/295) false-negative and 1.7% (5/295) false-positive. Because the number of templates tested by each assay was unknown, the false-positive results could be true positives not detected by MiSeq. On the contrary, false positives could be due to faint background on the MUT band, which was classified as MUT by our software. In this study, we used a single signal threshold for MUT classification across all codons tested, but the OLA-Simple signals from different codons are not equal in their intensity. The signal threshold for software analysis can be further optimized for each codon once a larger dataset of OLA-Simple results is available to reduce the potential for

© Copyright 2021 | N Panpradist

false positives. Additionally, the present algorithm automatically selects the ROIs sensitive to image artifacts (e.g., visible stains, dirt, or defects on the strip) that can skew the means and variances of all pixels within the cropped region. Future versions of our software will be designed to be more robust to these artifacts by dynamically determining the shape of the band region based on the width of the p and raising unresolvable errors detected in the image to users for manual verification.

Setting up HIVDR testing using the approach presented here requires an RNA extraction step, which can be performed with commercially available kits in 20 min, and approximately 10 min of hands-on time for setting up RT/PCR amplification, ligation, and lateral flow detection. Lyophilized reagents drastically reduce assay setup time, eliminating the need to thaw reagents and precisely measure and mix different volumes of multiple reagents to prepare master mixes for each step (RT, PCR, and ligation). The total wait time includes 3-h RT/PCR amplification, 1-h ligation, and 20-min detection. See a detailed comparison of workflow, assay time, and cost between OLA-Simple and MiSeq sequencing in **Table S5.11** and **Table S5.12**. Recognizing that most of the wait-time comes from the amplification step, we have recently revamped this step to combine RT-PCR in a single tube and reduce the amplification time to 40 min. With this modification, the turnaround time can be reduced from approximately 4.5 h to less than 2.5 h.

The OLA-Simple is a platform technology that can be adapted to detect other point mutations. In the context of HIV, we have designed ligation probes to detect mutations associated with resistance to other drug classes. As new

© Copyright 2021 | N Panpradist

recommendations for first-line ART regimens are implemented globally, new formats of the OLA-Simple kit can be manufactured to detect relevant mutations associated with virologic failure of these ART.

The OLA-Simple kit has the potential to improve clinical management of HIV treatment in resource-limited settings by providing a less costly and complex workflow, simple data analysis, and faster turnaround time from sample to results compared to HIVDR testing by Sanger sequencing. Sequencing usually requires centralized testing due to the expensive and sophisticated equipment and technical expertise needed. In its present form, the OLA-Simple could be implemented in local clinics with laboratories of limited infrastructure as it only requires basic laboratory equipment such as micropipettes, a thermal cycler (~$500 miniPCR), a computer or tablet (~$50 Amazon Fire) to operate Aquarium software for guidance and analysis, and an office scanner (~$50Canonn CanoScan LiDE300) for acquiring the image of lateral flow tests. The lateral flow strips can be read visually or captured with a cell phone; however, we have used an office scanner to ensure even light exposure across images. In addition, digital images allow automated analysis using an in-house Python script, which decreases variation in interpretation of results when low-frequency mutations (minority variants) produce mutant bands of lower signal intensity. Settings in which access to electricity is intermittent, applications of OLA-Simple could use a utility power supply (e.g., ~$50 APC UPS BN450M). These simple equipment requirements and the relatively short OLA-Simple turnaround time could enable clinicians in low-resource settings to prescribe same-day guided antiretroviral treatment.

© Copyright 2021 | N Panpradist

Although the validation of the kit reagents and software on Mexican clinical specimens conducted in the Seattle laboratory showed high sensitivity and specificity to detect key HIV drug-resistance mutations, demonstration of the feasibility of on-site adoption and use of the current OLA-Simple kit is warranted. At the time of writing the present manuscript, Mexican ART guidelines were modified to include second-generation integrase inhibitor-based first-line ART regimens as the preferred option at the national level[34], making baseline HIVDR testing less relevant. Nevertheless, the need for rapid and economical HIVDR testing persists in several scenarios, including in infants born to ART-exposed mothers, persons failing first-line ART, persons switching to optimized ART regimens, and persons with medical conditions or drug availability issues need to start with efavirenz-based ART regimens. This OLA-Simple validation experience will be highly valuable for other countries with restricted access to HIV sequencing, which have shown high pretreatment HIVDR levels and that remain constrained in their ART regimen options.

CONCLUSIONS

Compared to MiSeq, the OLA-Simple detected HIVDR with high sensitivity and accuracy. Moreover, minor changes in probe design and refinement of the software analysis could further reduce indeterminate results and improve genotype classification accuracy. The use of OLA-Simple in RLS could improve access to affordable and rapid HIVDR testing, thus facilitating the appropriate choice of ART in populations using NNRTI-based regimens.

© Copyright 2021 | N Panpradist

ACKNOWLEDGMENTS

We thank our collaborators at the University of Washington: Dr. James Lai, Dr. Eric Klavins, and Justin Vrana, for their helpful technical discussion. We also thank Justin Vrana for his participation in the initial visit at the CIENI/INER along with N.P., B.R.L., and L.M.F. We thank other laboratory members: Colin Eckhoff for his generous technical support; Enos Kline, David McIntyre, Nikki Higa, Annie Wong-On-Wing, Jonathan Lim, Daisy Ko, and Ian Andrews for their technical contribution in the development of OLA-Simple that has led to this work. We thank our clinical collaborators who provided clinical insights in other related work: Drs Theresa Rossouw and Ute Feucht at the University of Pretoria, South Africa; Dr. Michael Chung at Coptic Hope Center, Kenya; Drs Gonzague Jourdain and Nicole Ngo-Giang-Huong at PHPT Thailand; and Dr. Jaime Soria at Hospital Nacional Dos de Mayo, Peru. Last, we thank Rahil Jain, Blythe Adamson, Joshua Buser, Qin Wang, Justin Vrana, and Richard Lee for collaborating with N.P. to acquire awards from UW Health Innovation Challenge and Business Plan Competition.

5.6 FUTURE DIRECTIONS

5.6.1 TECHNOLOGY TRANSFER TO INDUSTRIAL PARTNERS

Research scientists at InBios International Inc. visited our lab to learn the methods for preparation and testing the performance of the paper-based detection (**Figure 5.11**). InBios International, Inc. prepared the 2nd-generation paper device for in-house validation with freshly drawn blood specimens at the Frenkel lab and the on-site validation in Kenya.

© Copyright 2021 | N Panpradist

5.6.2 COLLABORATION WITH DR. RENA PANEL TEAM IN KENYA

Dr. Rena Patel and her team in Kenya aim to conduct a study using the OLA-Simple kit to test the clinical specimens in real-time this October (postponed from April 2020 due to the Covid-19 travel ban. I have been involved in the software guide upgrade, including generating graphic instructions for the RNA extraction module. I also initiated the new industrial contact, IEH, preparing lyophilized reagents and lateral flow tests. Additionally, I have reviewed the sequences from Kenya and suggested revision of the primers and probes, and performed sample size calculation (see **Supplementary Information Chapter 5**).

5.6.3 COLLABORATION WITH DR. HOLLY RAWIZZA TEAM IN NIGERIA

Dr. Holly Rawizza (Harvard University) and her team based in Nigeria planned to conduct a study using an OLA-Simple kit to test the clinical specimens. The project was initiated through the contact I met at the international HIV conference in 2017. For this project, I have revised and designed the probe sequences to detect 9 codons for subtype G/AG, which we have not investigated the performance of OLA-Simple (see **Supplementary Information Chapter 5**). I am collecting the data and prepare to submit this work post-graduation.

SUMMARY

The key advancement of OLA-Simple 1.0 from OLA is summarized in

© Copyright 2021 | N Panpradist

Table 5.5. OLA-Simple 1.0 significantly increases the speed and reduces cost and time in detecting HIVDR while remaining specificity and sensitivity needed to guide effective ART.

Table 5.5 | Summary improvement of OLA-Simple 1.0 from OLA 2002.

OLA-Simple HIVDR kit 1.0 – technical improvements

	OLA*	OLA-Simple 1.0
Developer-centered features		
Sensitivity	2% - 5% MUT	10% MUT (clinical relevance)
Specificity	100%	99.1%
Controls	Yes	Yes
Flexibility	HIV, HBV	HIV
User-centered features		
Speed	11 h dried blood spot (3h hands-on)	4h blood – 5h plasma (30min hands-on)*
Simplicity	No	Yes
Low cost	>$20,000	>$500 (thermal cycler)

*IA Beck 2002; 2008

© Copyright 2021 | N Panpradist

5.7 SUPPLEMENTARY INFORMATION FOR CHAPTER 5

Clinical validation of OLA-Simple 1.0 across subtypes

Table S5.6 | Sequences of OLA-Simple probes (2017).

K65R	**WT**	5′ - Digoxigenin - CTC CAR TAT TTG CYA TAA AGA A - 3
	MUT	FAM - CTC CAR TAT TTG CYA TAA AGA G - 3′
	COM1	5′ Phosphorylated - RAA RGA CAG TAC TAA GTG GAG AA - Biotin 3′
	COM2	Phosphorylated - AAA AGA YAG YAC TAA ATG GAG RA - Biotin 3′
	Competing oligo	5′ - CTC CAR TAT TTG CYA TAA AGA ARA ARG ACA GTA CTA AGT GGA GAA - 3′
K103N	**WT**	5′ - Digoxigenin - CAT CCA GCR GGG YTA AAA AAG AAR - 3′
	MUT	5′- FAM - CAT CCA GCR GGG YTA AAA AAG AAY - 3′
	COM	5′ Phosphorylated - AAA TCA GTR ACA GTA CTR GAT GTG GG - Biotin 3′
	Competing oligo	5′ - CAT CCA GCR GGG YTA AAA AAG AAR AAA TCA GTR ACA GTA CTR GAT GTG GG - 3′
V106M/I	**WT**	5′ - Digoxigenin - CCA GCA GGG TTA AAA AAG AAA AAA TCA G - 3′
	MUT	5′ - FAM - CCA GCA GGG TTA AAA AAG AAA AAA TCAA - 3′
	COM	5′ Phosphorylated - TRA CAG TAC TRG ATG TGG GGG ATG CAT AT - Biotin 3′
	Competing oligo	5′ - CCA GCA GGG TTA AAA AAG AAA AAA TCA GTR ACA GTA CTR GAT GTG GGG GAT GCA TAT - 3′
Y181C	**WT**	5′ - Digoxigenin - AAA AAA TCC AGA AAT ART TAT YTA - 3′
	MUT	5′ FAM - AAA AAA TCC AGA AAT ART TAT YTG - 3′
	COM	5′ Phosphorylated - YCA ATA CAT GGA TGA YTT GTA TGT A - Biotin 3′
	Competing oligo	5′ - AAA AAA TCC AGA AAT ART TAT YTA YCA ATA CAT GGA TGA YTT GTA TGT A - 3′,
M184V	**WT**	5′ - Digoxigenin - ATC CAG AAA TAR TTA TCT ATA ATA YA - 3′
	MUT	5′ FAM - ATC CAG AAA TAR TTA TCT ATC AAT AYG - 3′
	COM	5′ Phosphorylated - TGG ATG AYT TGT ATG TAG GAT CTG A Biotin 3′
	Competing oligo	5′ - ATC CAG AAA TAR TTA TCT ATC AAT AYA TGG ATG AYT TGT ATG TAG GAT CTG A - 3
G190A	**WT**	5′ Digoxigenin - CAT GGA TGA YTT GTA TGT RGG - 3′
	MUT	5′ FAM - CAT GGA TGA YTT GTA TGT RGC - 3′
	COM	5′ Phosphorylated - ATC TGA YTT AGA AAT AGG GCA GCA - Biotin 3′
	Competing oligo	5′ - CAT GGA TGA YTT GTA TGT RGG ATC TGA YTT AGA AAT AGG GCA GCA - 3

© Copyright 2021 | N Panpradist

Table S5.7 | Comparison of genotyping results by OLA-Simple to other comparator assays.

A. Green, blue, and black cells are codons classified as WT, MUT, and IND, respectively. Red wedges are codons with low WT OD; % MUT by CLIA-OLA may be overestimated as it was estimated from the ratio of MUT OD/(MUT OD + WT OD) and WT signals are typically near signal saturation in CLIA-OLA.

K103N

Index	Copies/ punch	OLA-Simple Evaluator 1 2 3 4 5 6 7 8 9 10 11	Score	OLA-Simple	CLIA-OLA	Sanger
S1	55		1.00			
S2	142		1.00			
S3	154		1.00			
S4	348		1.00		10%	K103NS
S5	270		1.00			
S6	386		1.00		62%	K103KN
S7	281		1.00			
S8	106		1.00			
S9	424		0.91			
S10	235		1.00			
S11	68		1.00			
S12	44		1.00		100%	K103N
S13	222		1.00			
S14	139		1.00			
S15	58		1.00			
S16	751		1.00			
S17	23		1.00		100%	K103KN
S18	20		1.00			
S19	98		1.00		100%	K103N
S20	34		1.00		100%	K103N
S21	86		1.00			
S22	121		1.00			
S23	61		1.00			
S24	240		1.00		99%	K103N
S25	87		1.00		100%	K103N
S26	366		1.00		100%	K103N
S27	78		1.00			
S28	67		1.00			
S29	140		1.00			
S30	150		1.00			
S31	68		1.00			
S32	189		0.91			
S33	349		1.00			
S34	455		1.00		100%	K103N
S35	179		1.00		100%	K103N
S36	57		1.00			
S37	178		1.00			
S38	66		1.00			
S39	244		1.00		100%	K103N
S40	677		1.00			
S41	208		0.91			
S42	302		0.64			
S43	2050		1.00			
S44	219		1.00			
S45	20		1.00		91%	K103N
S46	194		1.00			
S47	27		1.00			
S49	115		0.82			
S50	159		1.00			
S51	374		0.91			
S52	225		1.00		3%	
S53	42		1.00			
S54	306		1.00			
S55	21		1.00		100%	K103N
S56	161		1.00		100%	K103N
S57	104		1.00		100%	K103N
S58	193		1.00			
S59	199		1.00		100%	
S60	70		0.91			

V106M

Index	Copies/ punch	OLA-Simple Evaluator 1 2 3 4 5 6 7 8 9 10 11	Score	OLA-Simple	CLIA-OLA	Sanger
S61	55		1.00			
S62	142		1.00			
S63	154		1.00			
S64	348		1.00		32%	V106VM
S65	270		1.00			
S66	386		1.00			
S67	281		0.91			
S68	106		1.00			
S69	424		1.00			
S70	235		0.82			
S71	68		1.00			
S72	44		1.00		51%	V106VIM
S73	222		0.91			
S74	139		1.00			
S75	58		1.00			
S76	751		1.00		100%	V106M
S77	23		1.00			
S78	20		1.00			
S79	98		1.00			
S80	34		1.00			
S81	86		1.00			
S82	121		1.00			
S83	61		1.00			
S84	240		1.00			
S85	87		1.00			
S86	366		1.00			
S87	78		1.00			
S88	67		1.00			
S89	140		1.00			
S90	150		1.00			
S91	68		1.00			
S92	189		1.00			
S93	349		1.00			
S94	455		1.00		13%	V106VM
S95	179		1.00			
S96	57		1.00		89%	V106M
S97	178		1.00			
S98	66		1.00			
S99	244		1.00			
S100	677		1.00			
S101	208		1.00			
S102	302		1.00			
S103	2050		1.00			
S104	219		1.00			
S105	20		1.00			
S106	194		1.00		29%	V106I
S107	27		1.00			
S109	115		1.00			
S110	159		1.00		100%	V106M
S111	374		1.00			
S112	225		1.00			
S113	42		1.00		99%	V106M
S114	306		1.00			
S115	21		1.00			
S116	161		0.55			
S117	104		1.00			
S118	193		1.00			
S119	199		1.00			
S120	70		1.00			

© Copyright 2021 | N Panpradist

Y181C

Index	Copies/ punch	OLA-Simple evaluator 1 2 3 4 5 6 7 8 9 10 11	Score	OLA-Simple	CLIA-OLA	Sanger
S121	55		1.00		53%	Y181YC
S122	142		1.00			
S123	154		1.00			
S124	348		1.00			
S125	270		1.00			
S126	386		1.00		93%	Y181C
S127	281		1.00			
S128	106		1.00		100%	Y181C
S129	424		1.00			
S130	235		1.00			
S131	68		1.00			
S132	44		0.91			
S133	222		1.00		100%	Y181C
S134	139		1.00		100%	Y181C
S135	58		1.00			
S136	751		1.00		10%	
S137	23		1.00			
S138	20		1.00		100%	Y181C
S139	98		1.00			
S140	34		1.00			
S141	86		1.00		100%	Y181C
S142	121		1.00			
S143	61		1.00		100%	Y181C
S144	240		1.00		99%	Y181C
S145	87		1.00			
S146	366		1.00		95%	Y181YC
S147	78		1.00			
S148	67		1.00			
S149	140		1.00			
S150	150		1.00			
S151	68		1.00		8%	Y181C
S152	189		1.00			
S153	349		1.00		100%	Y181C
S154	455		1.00		87%	Y181C
S155	179		1.00		76%	Y181YC
S156	57		1.00			
S157	178		1.00			
S158	66		1.00		100%	Y181C
S159	244		1.00			
S160	677		1.00			
S161	208		1.00		99%	Y181C
S162	302		0.55			
S163	2050		1.00			
S164	219		1.00			
S165	20		1.00			
S166	194		1.00		32%	Y181C
S167	27		1.00			
S169	115		1.00		90%	Y181C
S170	159		1.00		7%	Y181C
S171	374		1.00		98%	
S172	225		1.00		97%	Y181C
S173	42		1.00			
S174	306		0.82		13%	Y181C
S175	21		1.00			
S176	161		1.00		99%	Y181C
S177	104		1.00			
S178	193		1.00		99%	Y181C
S179	199		1.00		100%	Y181C
S180	70		1.00		95%	Y181YC

G190A

Index	Copies/ punch	OLA-Simple evaluator 1 2 3 4 5 6 7 8 9 10 11	Score	OLA-Simple	CLIA-OLA	Sanger
S181	55		1.00			
S182	142		1.00			
S183	154		0.82			
S184	348		1.00			
S185	270		1.00			
S186	386		1.00			
S187	281		1.00			
S188	106		1.00			
S189	424		1.00			
S190	235		1.00			
S191	68		1.00			
S192	44		1.00			
S193	222		1.00			
S194	139		1.00			
S195	58		1.00		100%	G190A
S196	751		1.00		99%	G190A
S197	23		1.00			
S198	20		1.00			
S199	98		1.00			
S200	34		1.00			
S201	86		1.00			
S202	121		1.00			
S203	61		1.00		100%	G190A
S204	240		1.00			
S205	87		1.00			
S206	366		1.00			
S207	78		1.00			
S208	67		0.91			
S209	140		0.82		100%	G190A
S210	150		1.00			
S211	68		1.00		89%	G190A
S212	189		1.00			
S213	349		1.00			
S214	455		1.00			
S215	179		0.82			
S216	57		1.00		87%	G190A
S217	178		1.00			
S218	66		1.00			
S219	244		1.00			
S220	677		1.00			
S221	208		1.00			
S222	302		1.00			
S223	2050		1.00			
S224	219		1.00			
S225	20		1.00			
S226	194		1.00			
S227	27		1.00			
S229	115		1.00		17%	G190A
S230	159		1.00			
S231	374		1.00			
S232	225		1.00			
S233	42		1.00			
S234	306		1.00		22%	
S235	21		1.00			
S236	161		1.00			
S237	104		1.00			
S238	193		1.00		100%	G190A
S239	199		1.00			
S240	70		1.00			

S1, S54, S59, and S186 were IND by CLIA-OLA and OLA-Simple. S41, S51, S116, and S171 were IND by only OLA-Simple and had low WT signal by CLIA-OLA. S235 and S246 were IND by OLA-Simple and had normal WT signal by CLIA-OLA. S130, S150, S175, and S210 were only IND by CLIA-OLA.

© Copyright 2021 | N Panpradist

Kenyan adult PBMC DNA K103N, Y181C, M184V, and G190A

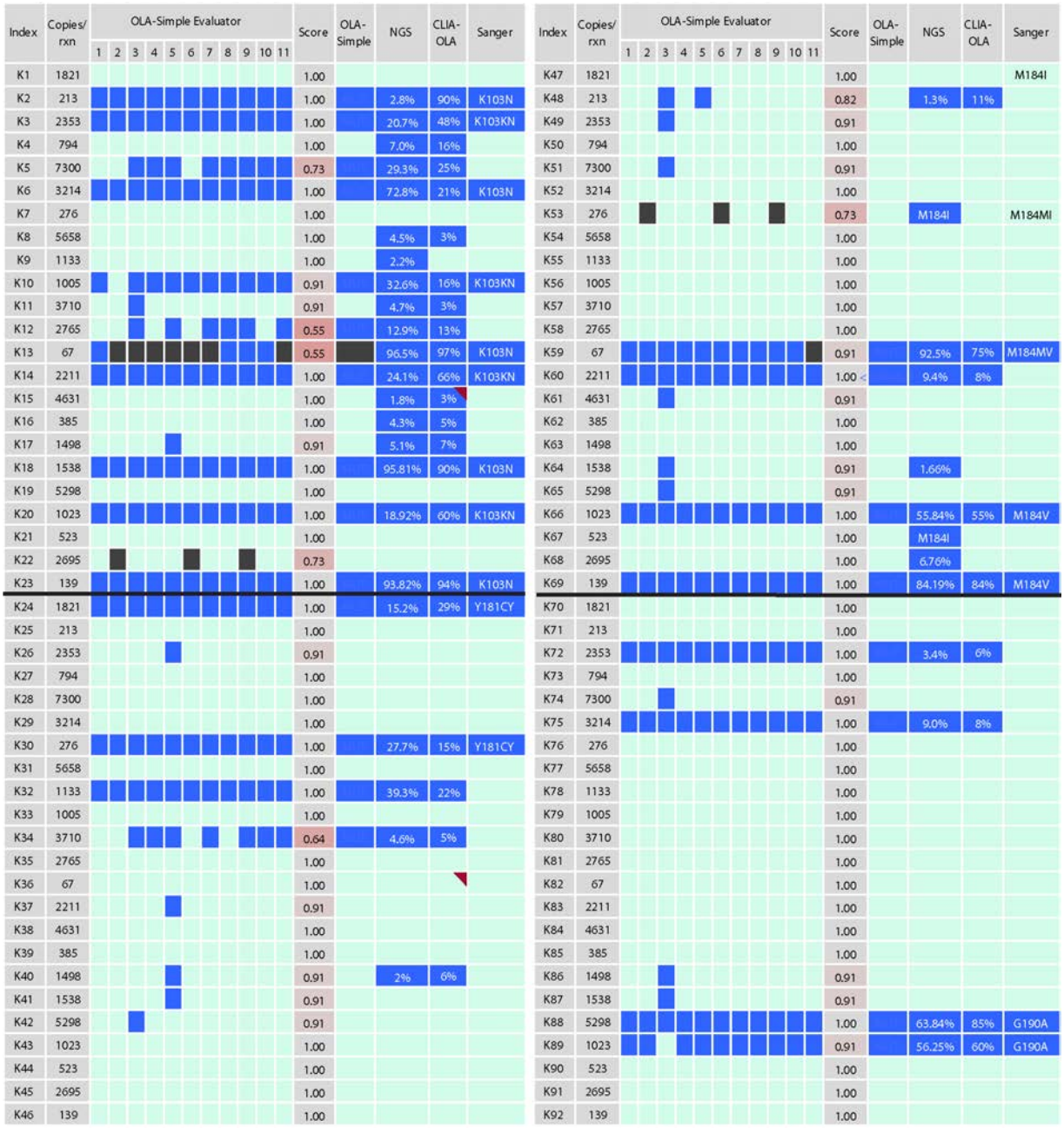

Index	Copies/rxn	OLA-Simple Evaluator 1	2	3	4	5	6	7	8	9	10	11	Score	OLA-Simple	NGS	CLIA-OLA	Sanger
K1	1821												1.00				M184I
K2	213												1.00		2.8%	90%	K103N
K3	2353												1.00		20.7%	48%	K103KN
K4	794												1.00		7.0%	16%	
K5	7300												0.73		29.3%	25%	
K6	3214												1.00		72.8%	21%	K103N
K7	276												1.00				
K8	5658												1.00		4.5%	3%	
K9	1133												1.00		2.2%		
K10	1005												0.91		32.6%	16%	K103KN
K11	3710												0.91		4.7%	3%	
K12	2765												0.55		12.9%	13%	
K13	67												0.55		96.5%	97%	K103N
K14	2211												1.00		24.1%	66%	K103KN
K15	4631												1.00		1.8%	3%	
K16	385												1.00		4.3%	5%	
K17	1498												0.91		5.1%	7%	
K18	1538												1.00		95.81%	90%	K103N
K19	5298												1.00				
K20	1023												1.00		18.92%	60%	K103KN
K21	523												1.00				
K22	2695												0.73				
K23	139												1.00		93.82%	94%	K103N
K24	1821												1.00		15.2%	29%	Y181CY
K25	213												1.00				
K26	2353												0.91				
K27	794												1.00				
K28	7300												1.00				
K29	3214												1.00				
K30	276												1.00		27.7%	15%	Y181CY
K31	5658												1.00				
K32	1133												1.00		39.3%	22%	
K33	1005												1.00				
K34	3710												0.64		4.6%	5%	
K35	2765												1.00				
K36	67												1.00				
K37	2211												0.91				
K38	4631												1.00				
K39	385												1.00				
K40	1498												0.91		2%	6%	
K41	1538												0.91				
K42	5298												0.91				
K43	1023												1.00				
K44	523												1.00				
K45	2695												1.00				
K46	139												1.00				

Index	Copies/rxn	OLA-Simple Evaluator 1	2	3	4	5	6	7	8	9	10	11	Score	OLA-Simple	NGS	CLIA-OLA	Sanger
K47	1821												1.00				
K48	213												0.82		1.3%	11%	
K49	2353												0.91				
K50	794												1.00				
K51	7300												0.91				
K52	3214												1.00				
K53	276												0.73		M184I		M184MI
K54	5658												1.00				
K55	1133												1.00				
K56	1005												1.00				
K57	3710												1.00				
K58	2765												1.00				
K59	67												0.91		92.5%	75%	M184MV
K60	2211												1.00		9.4%	8%	
K61	4631												0.91				
K62	385												1.00				
K63	1498												1.00				
K64	1538												0.91		1.66%		
K65	5298												0.91				
K66	1023												1.00		55.84%	55%	M184V
K67	523												1.00		M184I		
K68	2695												1.00		6.76%		
K69	139												1.00		84.19%	84%	M184V
K70	1821												1.00				
K71	213												1.00				
K72	2353												1.00		3.4%	6%	
K73	794												1.00				
K74	7300												0.91				
K75	3214												1.00		9.0%	8%	
K76	276												1.00				
K77	5658												1.00				
K78	1133												1.00				
K79	1005												1.00				
K80	3710												1.00				
K81	2765												1.00				
K82	67												1.00				
K83	2211												1.00				
K84	4631												1.00				
K85	385												1.00				
K86	1498												0.91				
K87	1538												0.91				
K88	5298												1.00		63.84%	85%	G190A
K89	1023												0.91		56.25%	60%	G190A
K90	523												1.00				
K91	2695												1.00				
K92	139												1.00				

K1-K23, K24-K46, K47-K68, and K69-K92 are genotyping results for K103N, Y181C, M184V, and G190A, respectively. K8-K9, K15-K17, K40, K48, K64, and K68 are FN by OLA-Simple. K13 is the only IND in this cohort. Green, blue, and black cells are codons classified as WT, MUT, and IND, respectively.

© Copyright 2021 | N Panpradist

Kenyan adult plasma RNA K103N,Y181C, M184V, and G190A

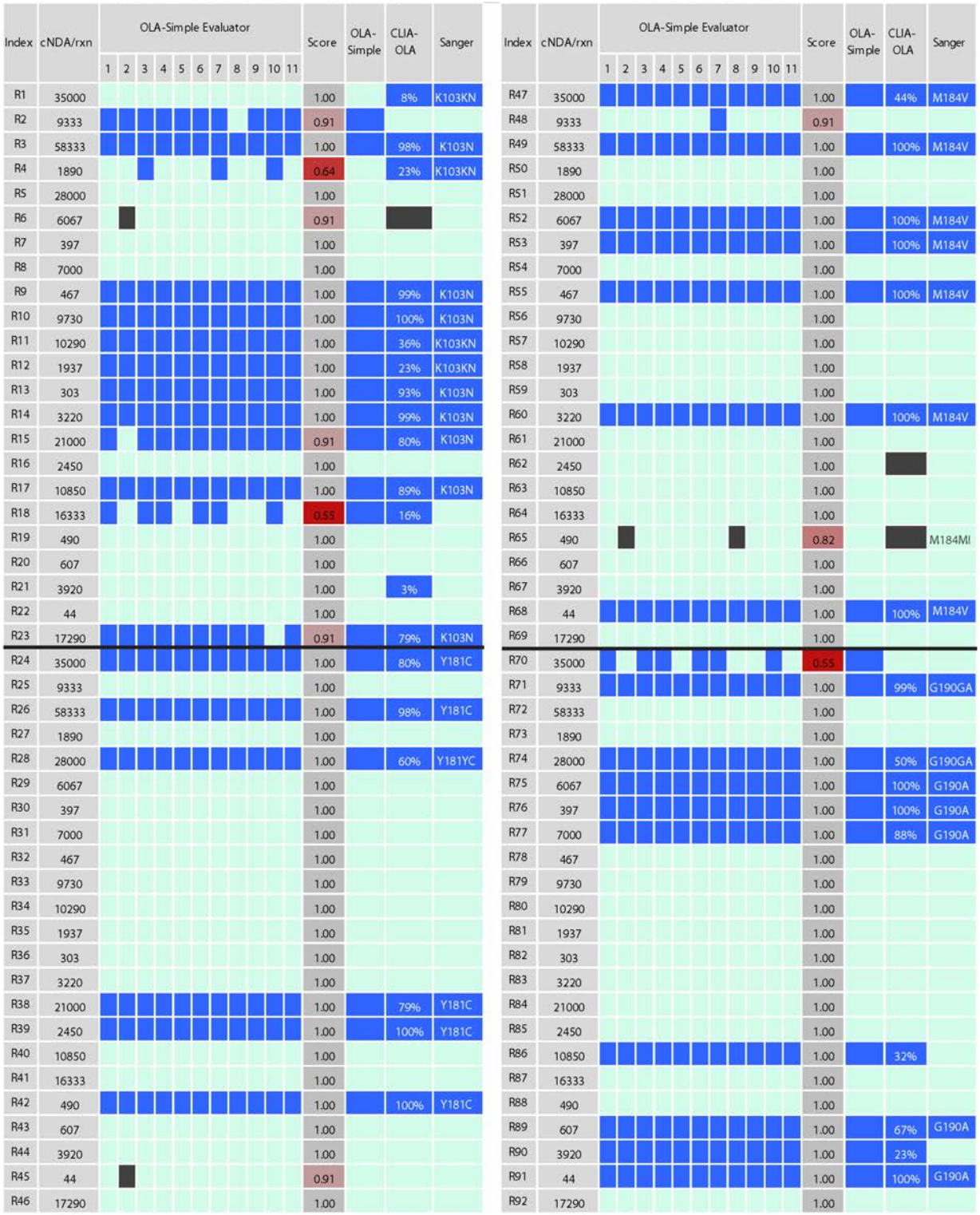

Index	cNDA/rxn	OLA-Simple Evaluator 1	2	3	4	5	6	7	8	9	10	11	Score	OLA-Simple	CLIA-OLA	Sanger
R1	35000												1.00		8%	K103KN
R2	9333												0.91			
R3	58333												1.00		98%	K103N
R4	1890												0.64		23%	K103KN
R5	28000												1.00			
R6	6067												0.91			
R7	397												1.00			
R8	7000												1.00			
R9	467												1.00		99%	K103N
R10	9730												1.00		100%	K103N
R11	10290												1.00		36%	K103KN
R12	1937												1.00		23%	K103KN
R13	303												1.00		93%	K103N
R14	3220												1.00		99%	K103N
R15	21000												0.91		80%	K103N
R16	2450												1.00			
R17	10850												1.00		89%	K103N
R18	16333												0.55		16%	
R19	490												1.00			
R20	607												1.00			
R21	3920												1.00		3%	
R22	44												1.00			
R23	17290												0.91		79%	K103N
R24	35000												1.00		80%	Y181C
R25	9333												1.00			
R26	58333												1.00		98%	Y181C
R27	1890												1.00			
R28	28000												1.00		60%	Y181YC
R29	6067												1.00			
R30	397												1.00			
R31	7000												1.00			
R32	467												1.00			
R33	9730												1.00			
R34	10290												1.00			
R35	1937												1.00			
R36	303												1.00			
R37	3220												1.00			
R38	21000												1.00		79%	Y181C
R39	2450												1.00		100%	Y181C
R40	10850												1.00			
R41	16333												1.00			
R42	490												1.00		100%	Y181C
R43	607												1.00			
R44	3920												1.00			
R45	44												0.91			
R46	17290												1.00			

Index	cNDA/rxn	OLA-Simple Evaluator 1	2	3	4	5	6	7	8	9	10	11	Score	OLA-Simple	CLIA-OLA	Sanger
R47	35000												1.00		44%	M184V
R48	9333												0.91			
R49	58333												1.00		100%	M184V
R50	1890												1.00			
R51	28000												1.00			
R52	6067												1.00		100%	M184V
R53	397												1.00		100%	M184V
R54	7000												1.00			
R55	467												1.00		100%	M184V
R56	9730												1.00			
R57	10290												1.00			
R58	1937												1.00			
R59	303												1.00			
R60	3220												1.00		100%	M184V
R61	21000												1.00			
R62	2450												1.00			
R63	10850												1.00			
R64	16333												1.00			
R65	490												0.82			M184MI
R66	607												1.00			
R67	3920												1.00			
R68	44												1.00		100%	M184V
R69	17290												1.00			
R70	35000												0.55			
R71	9333												1.00		99%	G190GA
R72	58333												1.00			
R73	1890												1.00			
R74	28000												1.00		50%	G190GA
R75	6067												1.00		100%	G190A
R76	397												1.00		100%	G190A
R77	7000												1.00		88%	G190A
R78	467												1.00			
R79	9730												1.00			
R80	10290												1.00			
R81	1937												1.00			
R82	303												1.00			
R83	3220												1.00			
R84	21000												1.00			
R85	2450												1.00			
R86	10850												1.00		32%	
R87	16333												1.00			
R88	490												1.00			
R89	607												1.00		67%	G190A
R90	3920												1.00		23%	
R91	44												1.00		100%	G190A
R92	17290												1.00			

R1-R23, R24-R46, R47-R68, and R69-R92 are genotyping results for K103N, Y181C, M184V, and G190A, respectively. CLIA-OLA had 3 IND: R6, R62, and R65. Although R65 for OLA-Simple was not classified as IND, it has lower concordant score than other samples. R70 classified as FP as the concordance score of 0.55 (6/5).

© Copyright 2021 | N Panpradist

Peruvian adult amplicon K103N,Y181C, M184V, and G190A

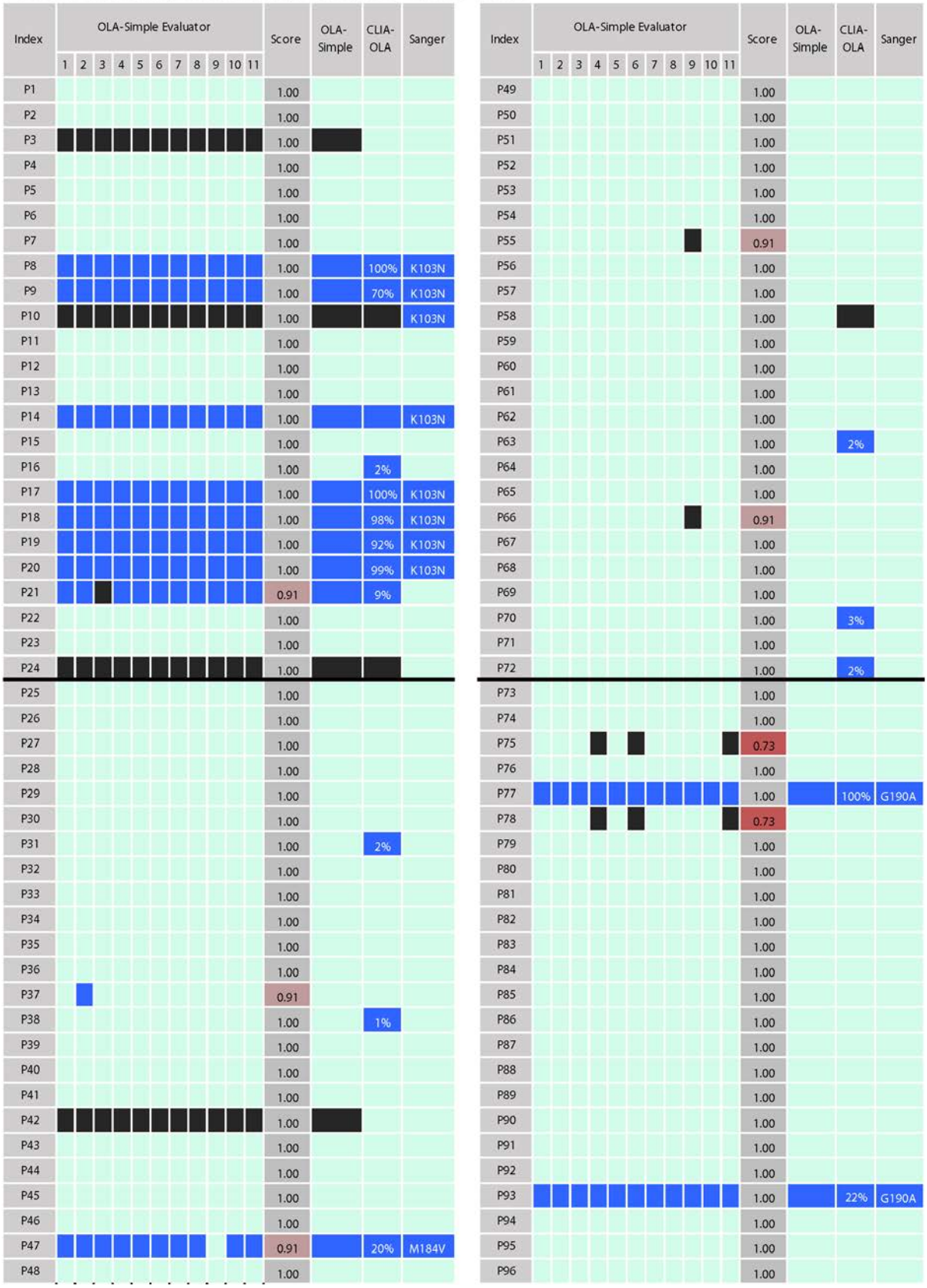

P1-P24, P25-P48, P49-P72, and P73-P96 are genotyping results for K103N, Y181C, M184V, and G190A, respectively. OLA-Simple had 2 concordant IND P10, P24; and 2 discordant IND P3, and P42.

© Copyright 2021 | N Panpradist

Thailand adult and child amplicon K103N,Y181C, M184V, and G190A

CLIA-OLA reports percentage of mutant in total DNA sequences. T1-P38, T39-T76, T77-T114, and T115-T152 are genotyping results for K103N, Y181C, M184V, and G190A, respectively. In the experiment that strips were blindly classified by computer, T26 was classified as MUT instead of WT. T26 is the only sample that the computer classified differently from human mode calls but the result improved accuracy of the test.

© Copyright 2021 | N Panpradist

B. Comparison of OLA-Simple for detection of DRMs in HIV-1 from multiple-cohort specimens to genotyping by Sanger sequencing.

Population	Sample type	n	DRM	Classifications by OLA-Simple compared to Sanger					
				True negative	True positive		False positive	False negative	IND
					Concordant	Discordant			
South African	FTA DBS	60*	K103N	36	17	1	0	0	5
			V106M	50	8	0	0	0	1
			Y181C	34	23	0	0	1	1
			G190A	47	8	1	0	0	3
			Percentage	***71%***	***25%***	***0%***	***0%***	***0%***	***4%***
Kenyan adults	PBMC DNA	23	K103N	12	8	2	0	0	1
			Y181C	19	2	2	0	0	0
			M184V	19	3	1	0	0	0
			G190A	19	2	2	0	0	0
			Percentage	***75%***	***16%***	***8%***	***0%***	***0%***	***1%***
Kenyan adults	Plasma RNA	23	K103N	9	10	1	1	2	0
			Y181C	17	6	0	0	0	0
			M184V	16	7	0	0	0	0
			G190A	13	7	2	1	0	0
			Percentage	***60%***	***33%***	***3%***	***2%***	***2%***	***0%***
Thai adults & children	AMP	38**	K103N	27	9	0	0	0	1
			Y181C	25	10	2	0	0	0
			M184V	21	16	0	0	0	0
			G190A	28	6	1	0	0	2
			Percentage	***68%***	***28%***	***2%***	***0%***	***0%***	***2%***
Peruvian adults	AMP	24	K103N	13	7	1	0	0	3
			Y181C	23	1	0	0	0	0
			M184V	24	0	0	0	0	0
			G190A	22	2	0	0	0	0
			Percentage	***85%***	***10%***	***1%***	***0%***	***0%***	***3%***
Total (n=168)				474	151	17	2	3	17

n = total samples tested, False negative means false mutant negative compared to Sanger sequencing, False positive means false mutant positive compared to CLIA-OLA or MiSeq, *One South African FTA DBS was excluded from the comparison due to possible specimen mix-up, and insufficient specimen to repeat CLIA-OLA, **One sample had failed PCR.

© Copyright 2021 | N Panpradist

C. Comparison of OLA-Simple for detection of DRMs in HIV-1 from multiple-cohort specimens to genotyping by sensitive comparator assays (NGS for Kenyan PBMC DNA and CLIA-OLA for all other cohorts.

Population	Specimen type	n	DRM	Classifications by OLA-Simple compared to CLIA OLA or NGS						
				True negative	True positive	False positive	False negative	Indeterminate		
								concordant	CLIA-OLA only	OLA-Simple only
South African	FTA DBS	60*	K103N	36	18	0	0	3	0	2
			V106M	50	8	0	0	0	0	1
			Y181C	30	23	0	3	0	2	1
			G190A	47	9	0	0	1	0	2
			Percentage	*69%*	*25%*	*0%*	*1%*	*2%*	*1%*	*3%*
Kenyan adults	PBMC DNA	23	K103N	5	10	0	7	0	0	1
			Y181C	18	4	0	1	0	0	0
			M184V	16	4	0	3	0	0	0
			G190A	19	4	0	0	0	0	0
			Percentage	*63%*	*24%*	*0%*	*12%*	*0%*	*0%*	*1%*
Kenyan adults	Plasma RNA	23	K103N	7	11	1	3	0	1	0
			Y181C	17	6	0	0	0	0	0
			M184V	14	7	0	0	0	2	0
			G190A	13	9	1	0	0	0	0
			Percentage	*55%*	*36%*	*2%*	*3%*	*0%*	*3%*	*0%*
	AMP	38**	K103N	25	9	0	2	0	0	1
			Y181C	24	12	0	1	0	0	0
			M184V	21	16	0	0	0	0	0
			G190A	27	7	0	1	1	0	1
			Percentage	*66%*	*30%*	*0%*	*3%*	*1%*	*0%*	*1%*
Peruvian adults	AMP	24	K103N	12	8	0	1	2	0	1
			Y181C	21	1	0	2	0	0	0
			M184V	20	0	0	3	0	1	0
			G190A	21	2	0	0	0	1	0
			Percentage	*77%*	*11%*	*0%*	*6%*	*2%*	*2%*	*1%*
Total (n=168)				443	168	2	27	7	7	10

n = total samples tested, False negative means false mutant negative compared to Sanger sequencing, False positive means false mutant positive compared to CLIA-OLA or MiSeq, *One South African FTA DBS was excluded from the comparison due to possible specimen mix-up, and insufficient specimen to repeat CLIA-OLA, **One sample had failed PCR.

© Copyright 2021 | N Panpradist

Clinical validation of OLA-Simple for a Mexican cohort.

Table S5.8 | Probe sequences for Mexican cohort (subtype B, 2020).

Codon	Probe	Sequence (5'→3')
K65R	WT	Digoxigenin – CTCCARTATTTGCYATAAAGAA
	MUT	FAM – CTCCARTATTTGCYATAAAGAG
	COM	Phosphorylated – RAARGACAGTACTAAATGGAGAA - Biotin
K103N/S	WT	Digoxigenin – CATCCYGCAGGRTTAAAAAAGAAR
	WT	Digoxigenin – CATCCYGCAGGRTTAAAAAAGAGR
	MUT	FAM – CATCCYGCAGGRTTAAAAAAGAAY
	MUT	FAM – CATCCYGCAGGRTTAAAAAAGAGC
	COM	Phosphorylated – ARATCAGTAACAGTACTRGATGTGGG - Biotin
Y181C	WT	Digoxigenin – ACAAAATCCAGAMATRGTTATYTA
	MUT	FAM – ACAAAATCCAGAMATRGTTATYTG
	COM	Phosphorylated – YCAATACATGGATGAYTTGTATGTA – Biotin
M184V	WT	Digoxigenin – ATCCAGAMATRGTTATCTATCAATAYA
	MUT	FAM – ATCCAGAMATRGTTATCTATCAATAYG
	COM	Phosphorylated – TGGATGAYTTGTATGTAGGATCTGA – Biotin
G190A	WT	Digoxigenin – CATGGATGAYTTGTATGTRGG
	MUT	FAM – CATGGATGAYTTGTATGTRGC
	COM	Phosphorylated – ATCTGAYTTAGAAATAGGRCAGCA – Biotin
	COM	Phosphorylated – STCTGACTTAGAAATAGGRCAGCA – Biotin

© Copyright 2021 | N Panpradist

Table S5.9 | Genotyping results by OLA-Simple and MiSeq.

ID	Viral load (copies/mL)	OLA-Simple results					MiSeq results (Entries are %mutant)					Comments regarding sequences in specimens classified as IND by OLA-Simple
		65	103	181	184	190	65	103	181	184	190	
1	3.75E+05	WT	MUT	WT	MUT	WT	WT	98.3 S	WT	99.00	WT	N/A
2	6.92E+04	WT	MUT	WT	MUT	WT	WT	98.5 N	WT	98.8	WT	**N/A**
3	3.56E+05	MUT	MUT	IND	WT	WT	78	82.2	83.5	79.8 I/ 2.2 V	WT	4 mutations on specific probes at 181
4	9.60E+04	IND	MUT	WT	MUT	FP	90.5	98	WT	91.8	WT	68G causing double mutations on common probes
5	2.29E+05	WT	MUT	MUT	MUT	MUT	WT	98.5	39.8	99.1	99.5	N/A
6	1.41E+05	WT	MUT	WT	MUT	WT	WT	98.30	WT	98.7	WT	N/A
7	5.55E+05	WT	WT	MUT	WT	WT	WT	WT	99.3	WT	WT (92 S)	N/A
8	4.41E+04	WT	WT	WT	MUT	WT	WT	WT	WT	99	WT	N/A
9	3.77E+05	WL	WT	MUT	WT	MUT	WT	WT	99.4	WT	99.5	N/A
10	2.24E+05	WT	WT	MUT	WT	WT	WT	WT	99.5	WT	WT	N/A
11	4.03E+05	WT	WT	MUT	WT	WT	WT	WT	99.2	WT	WT	N/A
12	8.51E+04	WT	WT	WT	WT	WT	4.82	WT	WT	WT	WT	N/A
13	2.44E+05	WT	WT	WT	WT	WT	WT	WT	WT	WT	WT	N/A
14	2.64E+05	WT	MUT	WT	WT	WT	WT	99.69	WT	WT	WT	N/A
15	7.24E+05	WT	MUT	WT	WT	WT	WT	99.48	WT	WT	WT	N/A
16	4.63E+04	WT	MUT	WT	WT	WT	WT	99.4	WT	WT	WT	N/A
17	1.82E+05	WT	MUT	WT	WT	WT	WT	99.34	WT	WT	WT	N/A
18	6.63E+06	IND	MUT	WT	WT	WT	WT	99.26	WT	WT	WT	3 mutations close together on 65 common probes
19	2.97E+04	WT	MUT	IND	WT	WT	WT	99.08	WT	WT	WT	Double mutations at 179
20	1.12E+06	WT	MUT	WT	WT	WT	WT	83.71	WT	WT	WT	N/A
21	3.33E+04	WT	MUT	WT	WT	WT	WT	69.16	WT	WT	WT	N/A
22	1.13E+06	WT	MUT	WT	WT	WT	WT	30.89	WT	WT	WT	N/A
23	9.03E+04	WT	MUT	WT	WT	WT	WT	30.64	WT	WT	WT	N/A
24	7.44E+04	WT	FN	WT	WT	WT	WT	22.4	WT	WT	WT	N/A
25	5.97E+04	WT	MUT	WT	WT	WT	WT	14.19	WT	WT	WT	N/A
26	7.69E+04	WT	FN	WT	FP	WT	WT	11.94	WT	WT	WT	N/A
27	6.99E+05	WT	FN	WT	WT	WT	WT	10.52	WT	WT	WT	N/A
28	6.17E+04	WT	MUT	MUT	WT	WT	WT	97.96	98.65	WT	WT	N/A
29	1.17E+05	WT	MUT	MUT	WT	WT	WT	98.82	98.46	WT	WT	N/A
30	1.28E+05	WT	WT	WT	WT	WT	WT	WT	4.57	WT	WT	N/A
31	2.05E+06	WT	WT	WT	MUT	FP	WT	WT	WT	98	WT	N/A
32	3.24E+04	WT	WT	WT	WT	WT	WT	WT	WT	7.85	WT	N/A
33	6.04E+05	IND	WT	WT	WT	WT	WT	WT	WT	5.74	WT	Double mutations at 65 common probe
34	8.24E+04	WT	WT	WT	WT	WT	WT	WT	WT	3.24	WT	N/A
35	4.75E+05	WT	WT	WT	WT	WT	WT	WT	WT	2.24	WT	N/A
36	N/A	WT	WT	WT	WT	MUT	WT	WT	WT	WT	99.4	N/A
37	1.52E+05	WT	WT	WT	WT	IND	WT	WT	WT	WT	99.36	1 mutation in common probe (4th base)
38	2.65E+06	WT	WT	WT	FP	MUT	WT	WT	WT	WT	99.16	N/A
39	5.81E+05	WT	WT	WT	WT	MUT	WT	WT	WT	WT	99.11	N/A
40	3.98E+05	WT	WT	WT	WT	MUT	WT	WT	WT	WT	99.11	N/A
41	1.00E+07	WT	WT	WT	WT	MUT	WT	WT	WT	WT	95.1	N/A
42	3.02E+04	WT	WT	WT	WT	MUT	WT	WT	WT	WT	70.23	N/A
43	2.80E+05	WT	WT	WT	WT	FN	WT	WT	WT	WT	20.59	N/A
44	N/A	WT	WT	WT	WT	WT	WT	WT	WT	WT	WT	N/A
45	N/A	WT	WT	WT	WT	WT	WT	WT	WT	WT	WT	N/A
46	1.80E+04	WT	MUT	WT	WT	WT	WT	99.25	WT	WT	WT	3 mutations on 103 specific probes
47	N/A	IND	MUT	MUT	WT	WT	WT	81.24	96.83	WT	WT	3 mutations on 65 common probe
48	1.84E+04	WT	WT	WT	WT	WT	WT	WT	3.73	WT	WT	N/A
49	N/A	WT	MUT	WT	MUT	WT	WT	98.28	WT	98.81	WT	N/A
50	N/A	WT	WT	WT	MUT	WT	WT	WT	WT	98.19	WT	N/A
51	1.96E+04	WT	WT	WT	MUT	WT	WT	WT	WT	16.33	WT	N/A
52	N/A	WT	WT	WT	WT	MUT	WT	WT	WT	WT	98.53	N/A
53	N/A	WT	WT	WT	WT	MUT	WT	WT	WT	WT	98.26	N/A
54	1.76E+02	PCR FAILURE					WT	WT	WT	WT	WT	N/A
55	1.81E+03	WT	WT	WT	MUT	WT	WT	WT	WT	98.06	WT	N/A
56	1.30E+03	IND	WT	WT	WT	WT	WT	WT	WT	3.81	WT	Double mutations on 65 common probe
57	1.32E+04	WT	WT	MUT	WT	WT	WT	WT	99.26	WT	WT	N/A
58	1.13E+04	WT	MUT	WT	MUT	FP	WT	98.7	WT	98.7/ 4.9 I	WT	N/A
59	7.05E+03	WT	WT	MUT	WT	WT	WT	WT	98.9	WT	WT	N/A
60	1.00E+03	WT	WT	IND	WT	WT	WT	WT	99.1	WT	WT	2 mutations on specific probes

MUT by OLA-Simple ≥10% mutant by MiSeq
WT by OLA-Simple <2% mutant by MiSeq
PCR failure by OLA-Simple
False negative (FN) by OLA-Simple
<10%,≥2% mutant by MiSeq
IND by OLA-Simple
False positive (FP) by OLA-Simple

© Copyright 2021 | N Panpradist

Table S5.10 | Specificity and sensitivity of the updated OLA-Simple kit at different diagnostic thresholds.

Diagnostic threshold	TP (MUT)	TN (WT)	FP	FN	%Sensitivity	%Specificity	% Mutant of codons missed by OLA-Simple
2% mutant	54	214	5	13	**80.6±2.3**	**97.7±0.9**	4.82 (K65R); 11.94, 10.52, and 22.4 (K103N/S); 3.73 and 4.57 (Y181C); 2.2, 2.24, 3.24, 3.81, 5.74, and 7.85 (M184V); 20.59(G190A)
5% mutant	54	221	5	6	**90.0±1.7**	**97.8±0.9**	11.94, 10.52, and 22.4 (K103N/S); 5.74 and 7.85 (M184V); 20.59(G190A)
10% mutant	54	223	5	4	**93.1±1.5**	**97.8±0.9**	11.94, 10.52, and 22.4 (K103N/S); 20.59(G190A)
15% or 20% mutant	54	225	5	2	**96.4±1.1**	**97.8±0.8**	22.4 (K103N/S); 20.59(G190A)
25% mutant	54	227	5	0	**100**	**97.8±0.8**	

MiSeq results were used as the sensitive reference assay; ≥ diagnostic threshold and <diagnostic threshold results by MiSeq were classified as positive (mutant) or negative (wild-type), respectively, for the reference result. TP = True positive, TN = True negative, FP = False positive, FN = FFalse-negative Percent sensitivity and specificity are reported with standard errors.

© Copyright 2021 | N Panpradist

Table S5.11 | Comparison of the workflows of OLA-Simple and MiSeq assays performed in this study.

	Key steps	Hands-on time	Wait time	Equipment requirement	Infrastructure
OLA-Simple workflow	Sample batching	No batching required	N/A	N/A	Refrigerator Stable electricity Economical computer operating software guidance and analysis Molecular Biology Laboratory with physical and materials/ personnel workflow to avoid molecular contamination
	RNA extraction	20 minutes (using commercial extraction kit)		Table-top centrifuge	
	RT-PCR	< 1 minute/ sample (thawing and reaction setup not required)	3 hours	Standard thermal cycler	
	Ligation	< 1 minute/ sample (thawing and reaction setup not required)	1 hour	Standard thermal cycler	
	Detection	< 2 minutes/ sample	10 minutes (denaturing) 15 minutes (signal development on lateral flow tests)	Standard thermal cycler, office scanner	
	Analysis	<1 minute/ sample	N/A	N/A	
MiSeq workflow	**Key steps**	**Hands-on time**	**Wait time**	**Equipment requirement**	**Infrastructure**
	Sample batching (96 specimens/ run)	Immediate to a few days (depending on demand)	N/A	N/A	80°C freezer 20°C freezer Refrigerator Molecular Biology Laboratory with physical and materials/ personnel workflow to avoid molecular contamination Internet access Computer server / cloud storage
	RNA extraction	1 hour for centrifugation 3 hours (per 96 sample batch using automated extraction instrument)	4 hours (per 96 sample batch, manually)	Biosafety Cabinet Table-top centrifuge Optional: Automated extraction instrument	
	RT -PCR	5 hours	1 hour	Standard thermal cycler	
	PCR visualization/ purification	40 minutes	1 hour	Electrophore-sis chamber	
	Library preparation	N/A	3 hours	Standard thermal cycler	
	Library quality control	40 minutes	10 minutes	Magnetic stand Tape station / Bioanalyzer	
	Library quantitation, normalization and pooling	N/A	2 hours	Fluorometer / qPCR machine	
	MiSeq run	36 hours	1 hour	MiSeq instrument	
	Data analysis	2 hours (using dedicated pipeline) plus time needed to upload files	30 minutes	Computer with Internet connection	

© Copyright 2021 | N Panpradist

Table S5.12 | Comparison of reagent costs, equipment costs, and assay times required in OLA-Simple and MiSeq.

	OLA-Simple	NGS (performed at CIENI)
Cost of reagents per sample	<$20	~$100
Hands-on time	<10 minutes	~12 hours
Wait time	2.5 or 4.5 hours	~46 hours
Minimum equipment cost	~$1,000	$128,000

Note the wait time does not include batching requirement in MiSeq workflow.

Figure 5.11 | Transition of technical knowledge and skills for OLA-Simple 1.0 to InBios International, Inc.

In 2018, Dr. Aarthy Vullar and Kathryn Hjerrild performed a blinded experiment using OLA-Simple 1.0 to detect drug resistance in patient-derived plasmid samples in March 2017.

OLA-Simple 1.0 still requires separation between pre and post-PCR. PCR chamber can be used to enable this separation within the same laboratory room. Below is an example that we could make an in-house PCR chamber at

© Copyright 2021 | N Panpradist

the cost of <$200 materials compared to the $5000 commercial unit on the left.

Figure S5.12 | Commercial and alternative PCR chamber.

Experimental modules in feasibility in Kenya

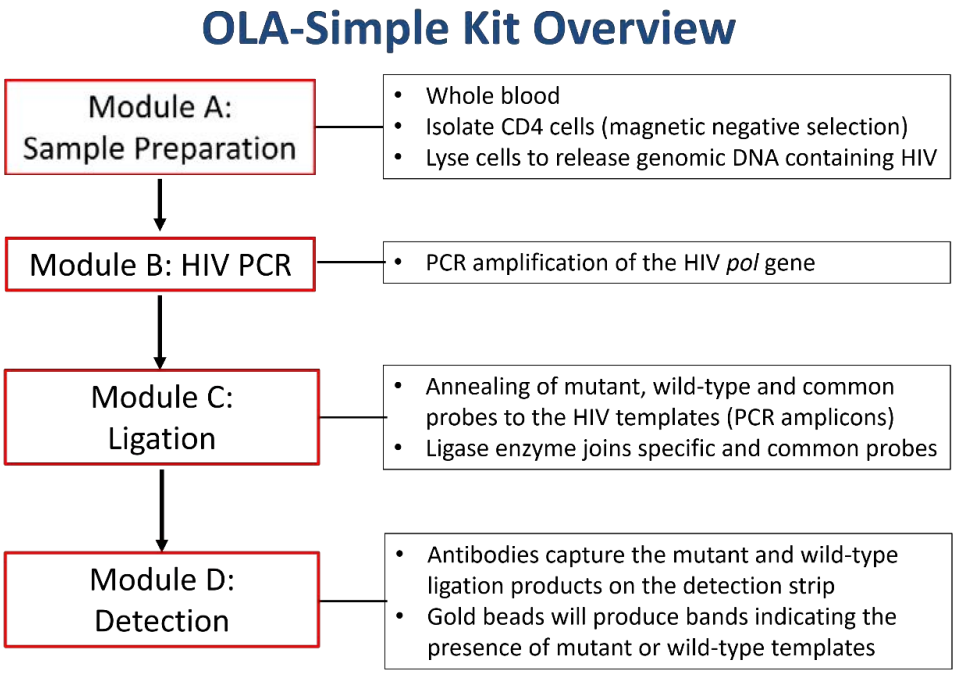

Figure S5.13 | Overall workflow of implementation study in Kenya

© Copyright 2021 | N Panpradist

Sample Preparation (Module A): CD4 cell isolation

- In this module you will isolate CD4 cells from 2 whole blood samples using antibodies, magnetic beads and a magnetic rack
- Package A contains 1 tube with antibody cocktail, 1 tube with magnetic beads, 1 tube with PBS
- Magnetic rack is also provided

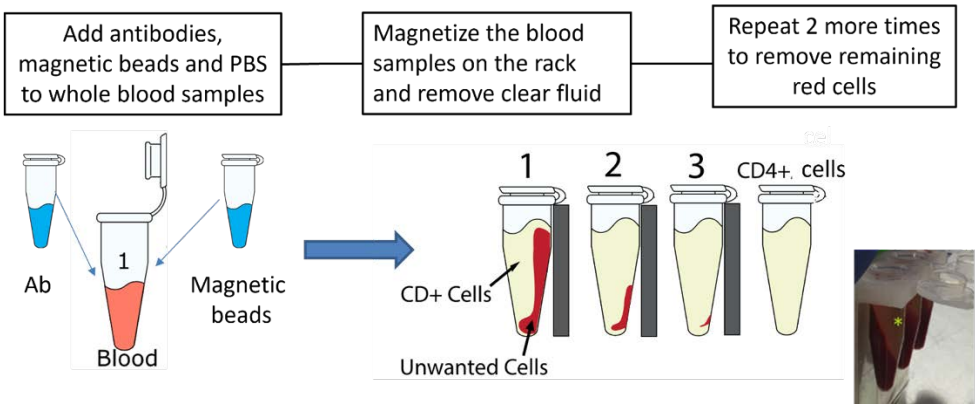

Figure S5.14 | HIVDR CD4 extraction module in Aquarium 2018.

Sample Preparation (Module A) : cell lysis

- You will wash and centrifuge the cells, and lyse with a detergent-based cell lysis buffer
- Package A contains 1 tube with red blood cell (RBC) lysis buffer, 1 tube with PBS, 1 tube with cell lysis buffer (proteinase K)

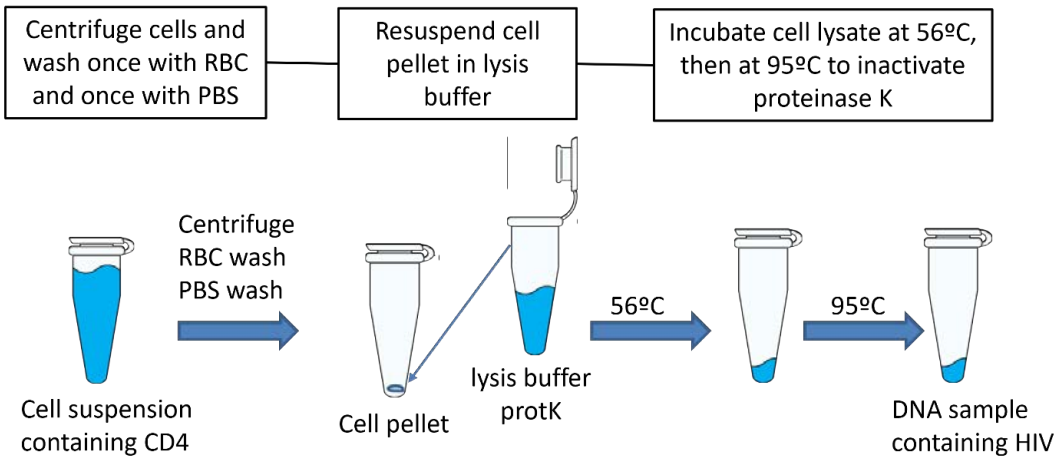

Figure S5.15 | HIVDR lysis module in Aquarium 2018.

© Copyright 2021 | N Panpradist

PCR (Module B)

- In this module you will use the two DNA samples to set up PCR
- Package B contains 1 tube with diluent and 2 PCR tubes with all the reagents necessary for PCR dried inside

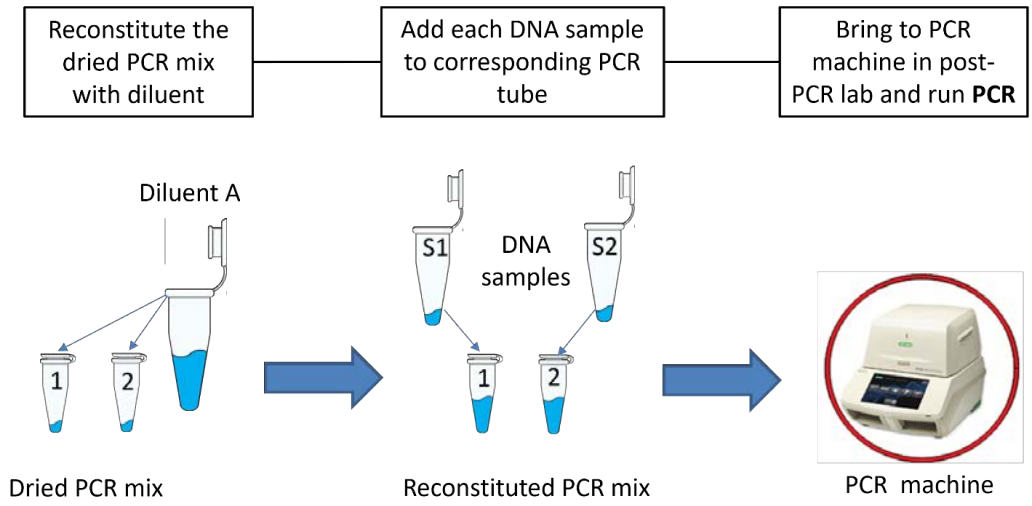

Figure S5.16 | HIVDR PCR module in Aquarium 2018.

Ligation (Module C)

- In this module you will use the amplicons generated by PCR to set-up ligation reactions
- Package C contains 1 tube with diluent, and two sets of 5 colored tubes containing dried ligation mix for each mutation to be tested (K65R, K103N, Y181C, M184V, G190A)

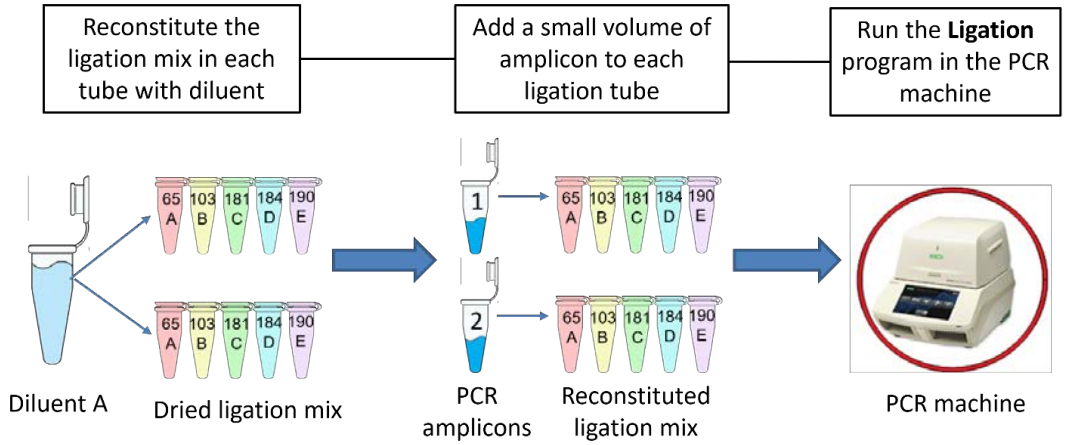

Figure S5.17 | HIVDR ligation module in Aquarium 2018.

© Copyright 2021 | N Panpradist

Detection (module D): part A

- In this module you will stop the ligation reaction and run a short program in the thermocycler
- Package D includes 1 tube with diluent, 1 tube with dried stop reagent, 1 tube with dried gold particles (for next step)

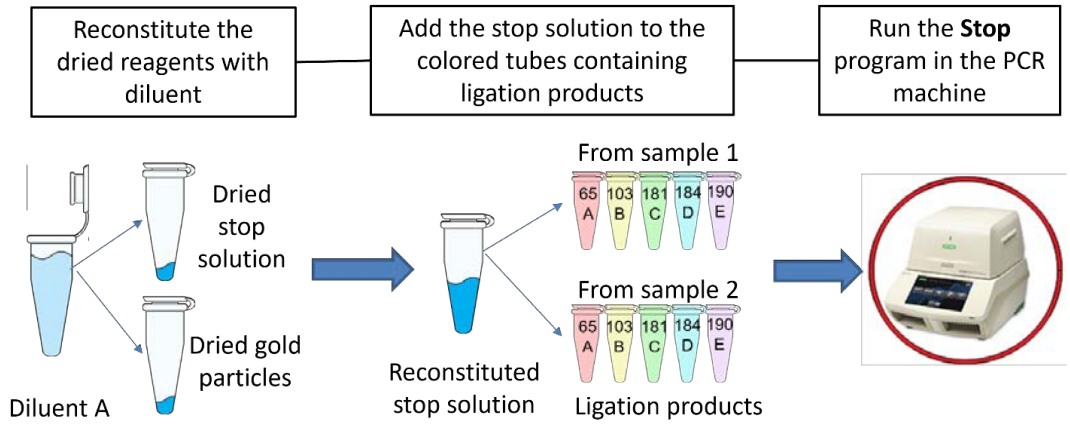

Figure S5.18 | HIVDR detection module in Aquarium 2018.

Detection (module D): part B

- In this module you will add ligated products to the detection strips, followed by gold detection beads

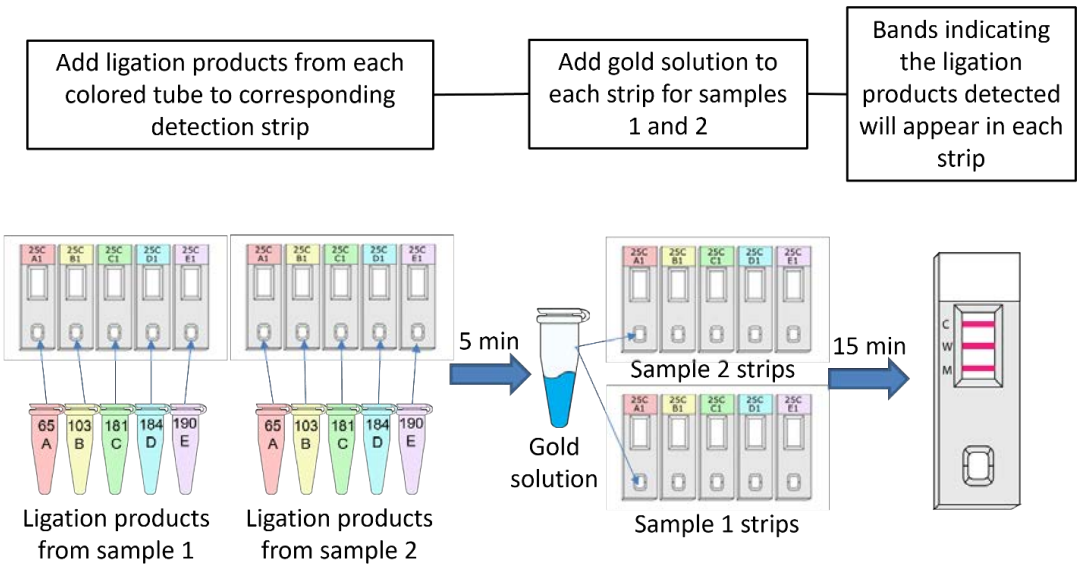

Figure S5.19 | HIVDR ligation module in Aquarium 2018.

© Copyright 2021 | N Panpradist

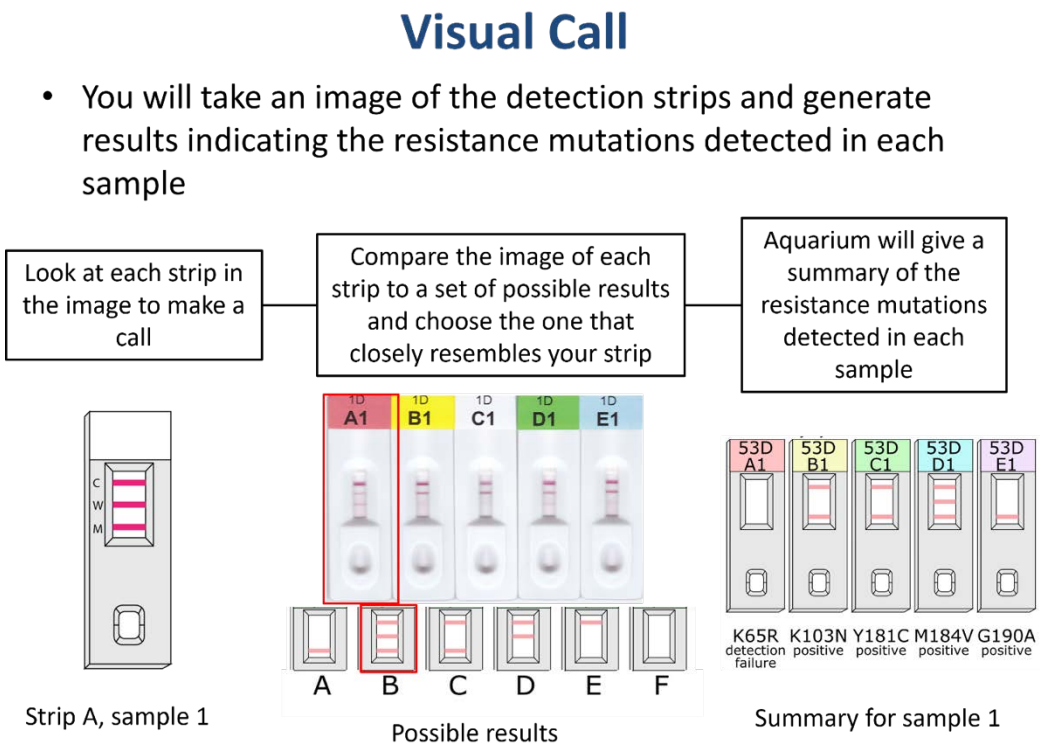

Figure S5.20 | HIVDR visual call module in Aquarium 2018.

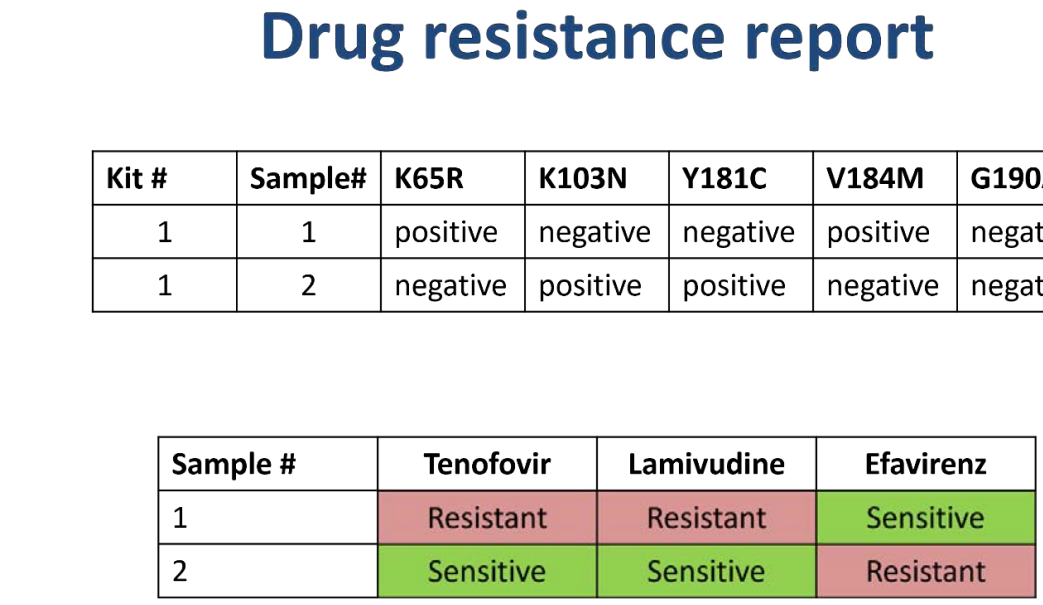

Kit #	Sample#	K65R	K103N	Y181C	V184M	G190A
1	1	positive	negative	negative	positive	negative
1	2	negative	positive	positive	negative	negative

Sample #	Tenofovir	Lamivudine	Efavirenz
1	Resistant	Resistant	Sensitive
2	Sensitive	Sensitive	Resistant

Figure S5.21 | HIVDR Interpretation module in Aquarium 2018

© Copyright 2021 | N Panpradist

Detailed technical protocol for OLA-Simple kit 1.0 production.

1) LIGATION MIXTURE COMPONENT

This reaction mixture has been adapted from SCRI's 2002 protocol by Ingrid Beck to include excipients that can stabilize dried mixtures. Below are the commercial sources for each required component.

Component (stock)	Sources
Molecular grade water	Molecular biology grade, USP sterile purified water, DNase-, RNase-, and Protease-free, Corning Cellgro, catalog# 46-000-CI Order link: here, Store at room temperature
Triton X-100™	Sigma, catalog # T8787 Order link: here, Store at room temperature
Tris-HCl pH 8.0	1M Tris-HCl pH 8.0 Affymetrix, catalog# 22638 Order link: here, Store at room temperature
Magnesium Chloride	2M $MgCl_2$ BioUltra molecular grade Sigma-Aldrich, catalog# 68475 Order link: here, Store at room temperature
Potassium Chloride	1M KCl, BioUltra molecular grade Sigma-Aldrich, catalog# 60142 Order link: here, Store at room temperature
1mM DTT	DTT 1,4 dithiothreitol Sigma-Aldrich, catalog# 10197777001 Order link: here, Store at -20 °C Add 8mL molecular grade to 2g of DTT from manufacture.
10x ligation buffer (200mM Tris pH 8.0, 100mM $MgCl_2$, 10mM DTT)	To make a 10mL stock: 2mL 1M Tris-HCl pH 8.0 stock 0.5mL 2M $MgCl_2$ 100µL 1M DTT Bring the final volume to 10mL by adding molecular grade water Store at -20 °C in 1mL aliquots
10mM NAD	Sigma-Aldrich, catalog # N7004-250mg Order link: here
20% w/v Polyethylene glycol (PEG) 35KDa	Bioultra, MW 35KDa Sigma-Aldrich, catalog# 94646 Order link: here
34% w/v trehalose dihydrate	Biomolecular grade Life Sciences Advanced Technologies Inc, catalog# TS1M-100 Order link: here Store at 4 °C
5U/µL Ampligase ligase	Epicenter, Catalog# A3210K Order link: here, Store at -20 °C
0.2mL PCR tubes	Genemate SnapStrip® 8-Strip 0.2 mL PCR tubes with individually attached dome caps, Bioexpress Order link: here Store at room temperature
Foil pouch	2"x4" white foil pouch DCN, Catalog # MFLP-120 Order link here, Store at room temperature

© Copyright 2021 | N Panpradist

Ligation mixture: 24uL reaction

Component (stock)	uL/rxn	Final concentration
0.1% v/v triton-X 100	15.25 – 15.79	Main diluent (~0.1% v/v triton-X100)
34% w/v Trehalose	3.53	5% w/v
20% w/v PEG 35kDa	1.80	1.5% w/v
10mM NAD	2.40	1 mM
10mM ligation buffer (200mM Tris-HCl pH 8.0, 100mM $MgCl_2$, 10mM DTT)	2.40	20mM Tris-HCl, 10mM $MgCl_2$, 1mM DTT
5uM ligation probe	0.18-0.72	3.75nM - 60nM (depending on the SNPs)
1M KCl	0.30	12.5 mM
5U/µL Ampligase ligase	0.40	8 mU/µL
Total ligation mixture	**24.00**	

PCR control mixture: 24uL reaction (optional)

Component (stock)	uL/rxn	Final concentration
0.1% v/v triton-X 100	15.65 – 16.19	Main diluent (~0.1% v/v triton-X100)
34% w/v Trehalose	3.53	5% w/v
20% w/v PEG 35kDa	1.80	1.5% w/v
10mM NAD	2.40	1 mM
10mM ligation buffer (200mM Tris-HCl pH 8.0, 100mM $MgCl_2$, 10mM DTT)	2.40	20mM Tris-HCl, 10mM $MgCl_2$, 1mM DTT
5uM ligation probe	1.44	120nM (K65R, K103N, G190A probe mixtures)
1M KCl	0.30	12.5 mM
Total	**24.00**	

These mixtures are currently prepared at 1.2x volume compared to Ingrid Beck's 2002 protocol to account for a higher chance for volume loss due to pipetting a relatively viscous mixture. The 24uL of ligation or detection mixture is then added to each 0.2mL. Tubes are closed and centrifuged down briefly. The caps are then re-opened during the 2-min submergence in liquid nitrogen. It is crucial not to press the tubes too

© Copyright 2021 | N Panpradist

tightly on the plastic rack as this can introduce physical stress during the freezing process, leading to cracked tubes. The frozen tubes are then transferred to the glass chamber while tubes are ensured not to be in direct contact with the glass chamber to avoid heat loss due to conduction. The glass chamber is also wrapped in aluminum foil to reduce heat loss through radiation. The frozen components undergo sublimation at -55°C, 0.014 mbar at least 2 hours. The dried mixtures are then transferred for packaging in a sealed foil pouch in the presence of desiccant packets. Unlike the ligation mixture, the PCR control mixture contains the probes from K65R, K103N, and G190A to occupy three regions of the HIV *pol* gene. The PCR mixture does not contain ligase, but the unligated probes hybridized to the amplicon template after running in the ligation protocol to generate the signal for PCR control.

Setting up ligation reaction and PCR detection mixtures

24uL diluent A (water) and the 2.4L amplicon (product after PCR amplification) are added to each ligation and PCR control mixture tube. The dried component should be readily dissolved. A gentle vortex mixing or finger tapping at the end is recommended but should be followed by pulse centrifugation to bring down all the fluid to the bottom of the tubes. The mixtures are subjected to 10-cycle ligation (94°C 3 minutes

© Copyright 2021 | N Panpradist

for initial denaturation followed by 10 cycles of 94°C for 30seconds and 37 °C for 4 minutes)

2) PREPARATION OF LIGATION SAMPLES BEFORE DOWNSTREAM PAPER-BASED DETECTION

After the 10-cycle ligation protocol is completed, 2.4uL of stop solution (8uM competing oligos in 10mM Tris, 100mM EDTA) is added to each ligation and PCR detection mixture, followed by a cycle of ligation. The mixture is now ready to be processed with a detection strip.)

This competing oligo mix contains 50-60 bp anti-sense competing strands at least 10x higher concentration (10^{12} copies/reaction) than typical amplicon concentration (10^{10} – 10^{11} copies/reaction) to make them kinetically favorable to compete with the anti-sense amplicon. These anti-sense oligos competitively anneal to the sense amplicon to free the unligated probes from re-annealing to the sense amplicon to create a false mutant signal. A single cycle of ligation speeds up the process of strand displacement and limit variations from different lab conditions.

It is essential for users not to add the stop solution for the PCR control reaction mixture because the competing oligo will displace the unligated probes.

3) DETECTION MIXTURE COMPONENT

© Copyright 2021 | N Panpradist

Component	Sources
Molecular grade water	Molecular biology grade, USP sterile purified water, DNase-, RNase-, and Protease-free, Corning Cellgro, catalog# 46-000-CI Order link: here, Store at room temperature
Triton X-100™	Molecular grade water Sigma, catalog # T8787 Order link: here, Store at room temperature
BSA	Protease-free, heat shock fraction, suitable for hybridization Sigma, catalog# B4287 Order link: here, Store at 4°C
Sodium Chloride	5M NaCl BioUltra molecular grade Sigma-Aldrich, catalog# 68475 Order link: here, Store at room temperature
HEPES buffer	1M, Gibco, catalog# 15630080 Order link: here, Store at room temperature
Poly(vinyl alcohol) or PVA (89kDa)	Sigma, catalog# 341584 Order link: here, Store at room temperature
Poly(ethylene glycol) or PEG (35kDa)	Sigma, catalog# 94646 Order link: here, Store at room temperature
Component	**Sources**
Sucrose	Sigma, catalog# 84097 Order link: here, Store at room temperature
OD10 monoclonal anti-biotin Ab (1.1 x 10^{10} biotin binding capacity/µL) gold np	40nm gold nanoparticles are passively coupled to citrate capped gold nanoparticles, blocked with BSA BBL, catalog # BA.MAB40, Order link: here

ddFLB buffer (chase buffer used to dilute and preserve anti-biotinylated gold nanoparticles during lyophilization)

Component (stock)	50mL stock	Final concentration
Triton-X 100	500 µL	1% v/v
1M HEPES buffer	750 µL	15mM
BSA	0.5 g	1% w/v
5M NaCl	4 mL	0.4 M
Sucrose	0.5 g	1% w/v
PEG (35KDa)	0.5 g	1% w/v
PVA (89KDa)	0.25 g	0.5% w/v
Add molecular grade water and adjust final pH to 7.4	**50 L total**	

© Copyright 2021 | N Panpradist

- **Monoclonal anti-biotin antibody conjugated gold nanoparticles**

To prepare a gold detection mixture, 3µL 10OD gold stock is mixed with 40µL of ddLFB buffer. The mixture is frozen in liquid nitrogen for at least 2 minutes before drying at -55°C, 0.014 mbar for at least 2 hours. Finally, the dried gold detection mixture is sealed in the foil pouch in the presence of the desiccant packets at 4°C. The targeted quantitative LoD for our paper-detection is desirable at < 0.3 nM ligated probes.

4) PREPARATION OF THE LATERAL FLOW DETECTION

Component	Sources
DCN Backing card – 0.010" thick 60mm x 300mm	DCN, catalog# MIBA-020 Order link: here, Store at room temperature
Nitrocellulose Cut to 30mmx300mm	Millipore Hi Flow Plus, Millipore, HF13504XSS Order link: here, Store at room temperature outside desiccator
Component	**Sources**
Glass fiber Cut to 17mmx254mm	Ahlstorm 8950 original dimension 8 inch x 10 inch Order via quotation, Store at room temperature outside desiccator
Absorbent pad Cut to 22mmx300mm	GE CF7 original dimension 22mm x 50m, catalog #8117-2250 Order via quotation, Store at room temperature outside desiccator
DCN 1-hole cassette	DCN, catalog# MICA-125 Order link: here, Store at room temperature
Anti-digoxigenin sheep IgG polyclonal diluted to 1mg/mL in 1xPBS	Stock 5mg/mL, 0.5mL, Novus Biologicals, Catalog # NB100-65495 Order link: here, Store at 4°C for short term and -20°C for long term (avoid freeze-thawing)
Anti-fluorescein sheep IgG stock is at 1mg/mL in 1xBBS pH 8.2	SouthernBiotech, catalog# 6400-01 Order link: here, Store at 2-8°C
Biotin-BSA diluted to 1mg/mL in 1x PBS	10mg (>8 mol biotin/mol BSA), 2% w/w biotin Sigma-Aldrich, catalog# A8549 Order: here, here, Store at 2-8 °C for short-term, and -20°C

© Copyright 2021 | N Panpradist

Integration of the lateral flow tests

The lateral flow tests are integrated using the backing card, precut nitrocellulose, glass fiber pad, and absorbent pad.

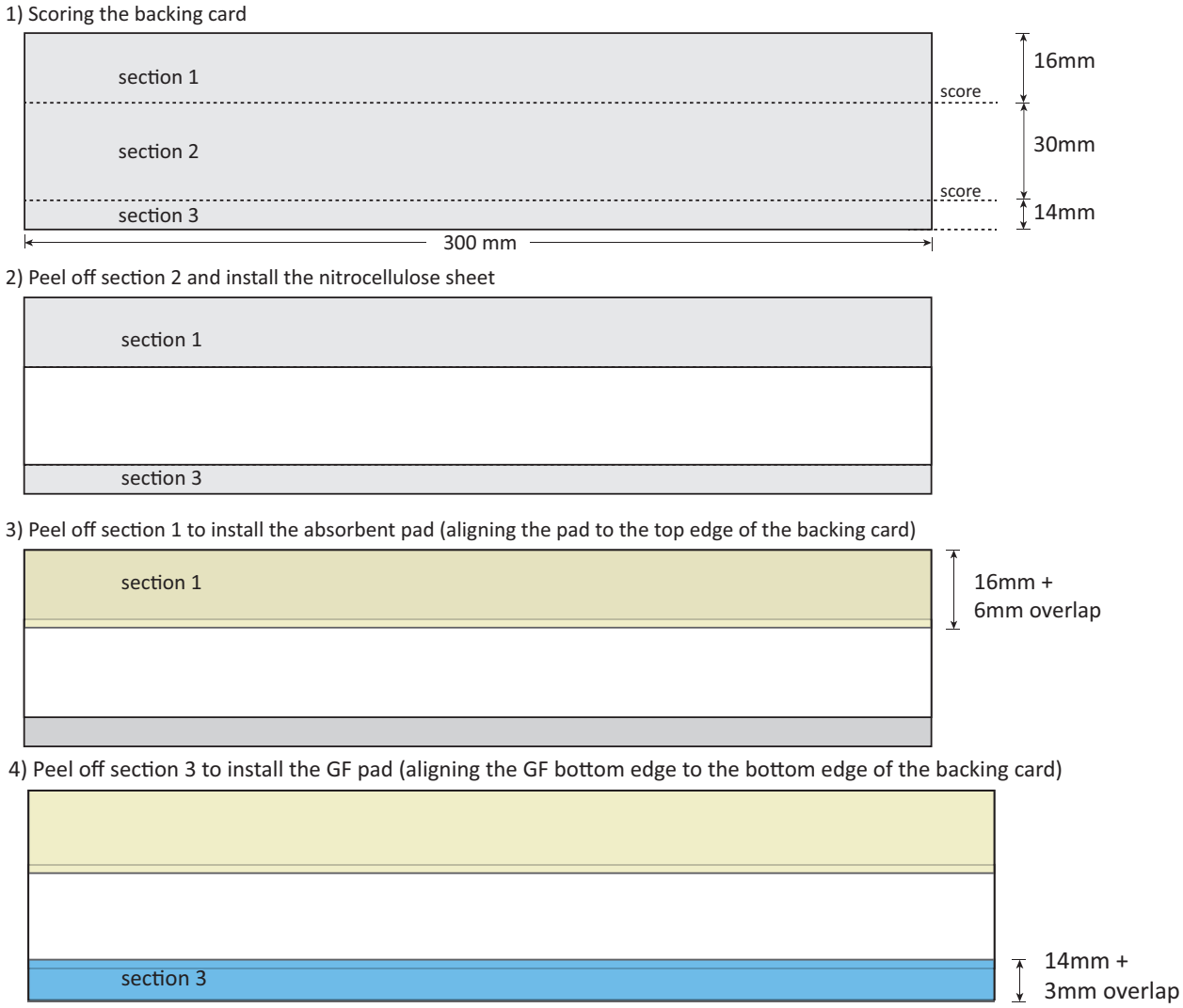

Patterning the capture lines on the integrated membrane

The position of each capture line is illustrated in the picture below. Before loading the capture reagents, the striping pathway is cleaned by 10 cycles of Biodot cleaning solution, 10 cycles of 100% ethanol, and 10 cycles of

© Copyright 2021 | N Panpradist

final rinse with molecular-grade water. In our current protocol, ~80µL reagent is fed from the tip, and as a result, the tips are submerged in the clean solution. The membrane that has been striped is incubated at 37 °C for 1.5 hours and dried overnight in the desiccator. The integrated membrane is then cut into 4.5mm x 60 mm strips. The strip is inserted in the DCN housing and packed 1 device in a foil pouch in the presence of desiccant packets.

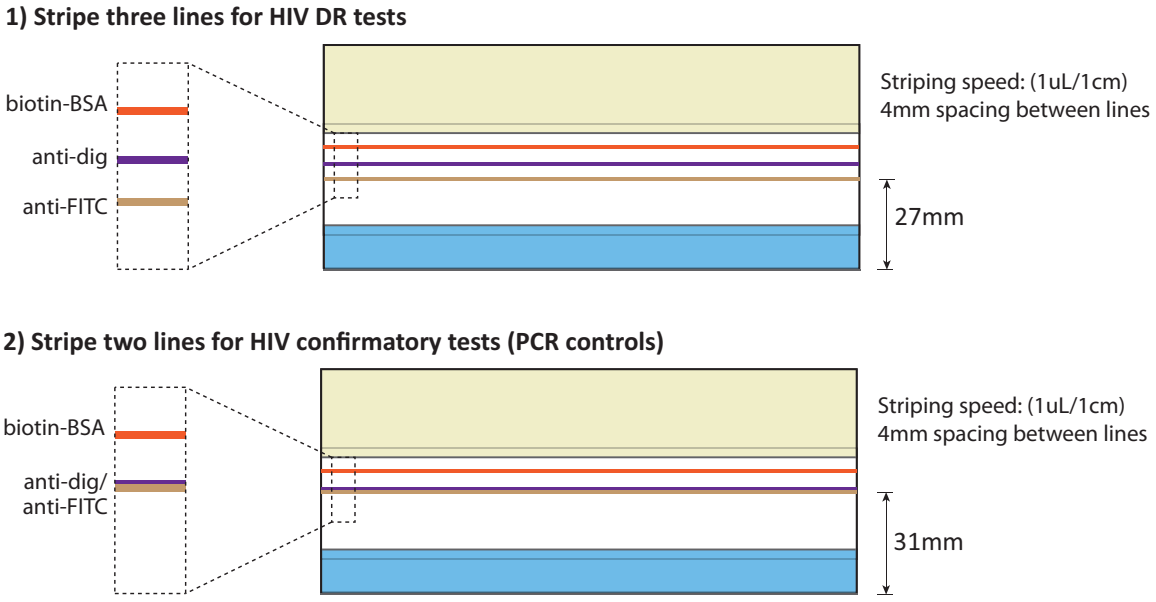

Setting up the detection system

24µL of the mixture (ligation mix, amplicon, and competing oligos) is added to the sample port. Up to 0.2x volume (6.6uL) of the mixture can be left in the tube, and this is intentional to make sure that at the end, there will be at least 24uL of samples going to each lateral flow test. 5 minutes after the initial addition, 40uL of rehydrated gold solution (up

© Copyright 2021 | N Panpradist

to 3µL gold mixture will remain) will be added to each lateral flow strip for the detection step.

Interpretation of the results:

The valid outcomes for drug resistance tests showed the different levels of the tested SNP: 0-<10% mutant, ≥10% mutant, and 100% mutant. For the Y181C and M184V, the threshold is currently at 25% mutant.

The indeterminate results can occur when no colors are in all lines, suggesting a failure in the detection step or when only the control (C) line shows up. This suggests a failure in ligation due to the reagents or high polymorphisms nearby the SNPs in this patient sample. The HIV infection confirmatory test has two outcomes (in addition to no line from detection failure). Two lines are expected in all patients tested for drug resistance, as this will confirm the infection of HIV in the samples. However, it may be possible that some patients might have been detected false positives from rapid antibody tests. In this case, the HIV infection test can show negative results, and only the control line shows up.

© Copyright 2021 | N Panpradist

Primers/probe for Kenya study 2020-2021

My analysis revealed the need to revise the K103N and G190A probes because several samples have common mutations within the two bases away from the target SNP and likely cause failed ligation. Based on these results, Ingrid Beck designed the new probes to include these mismatches.

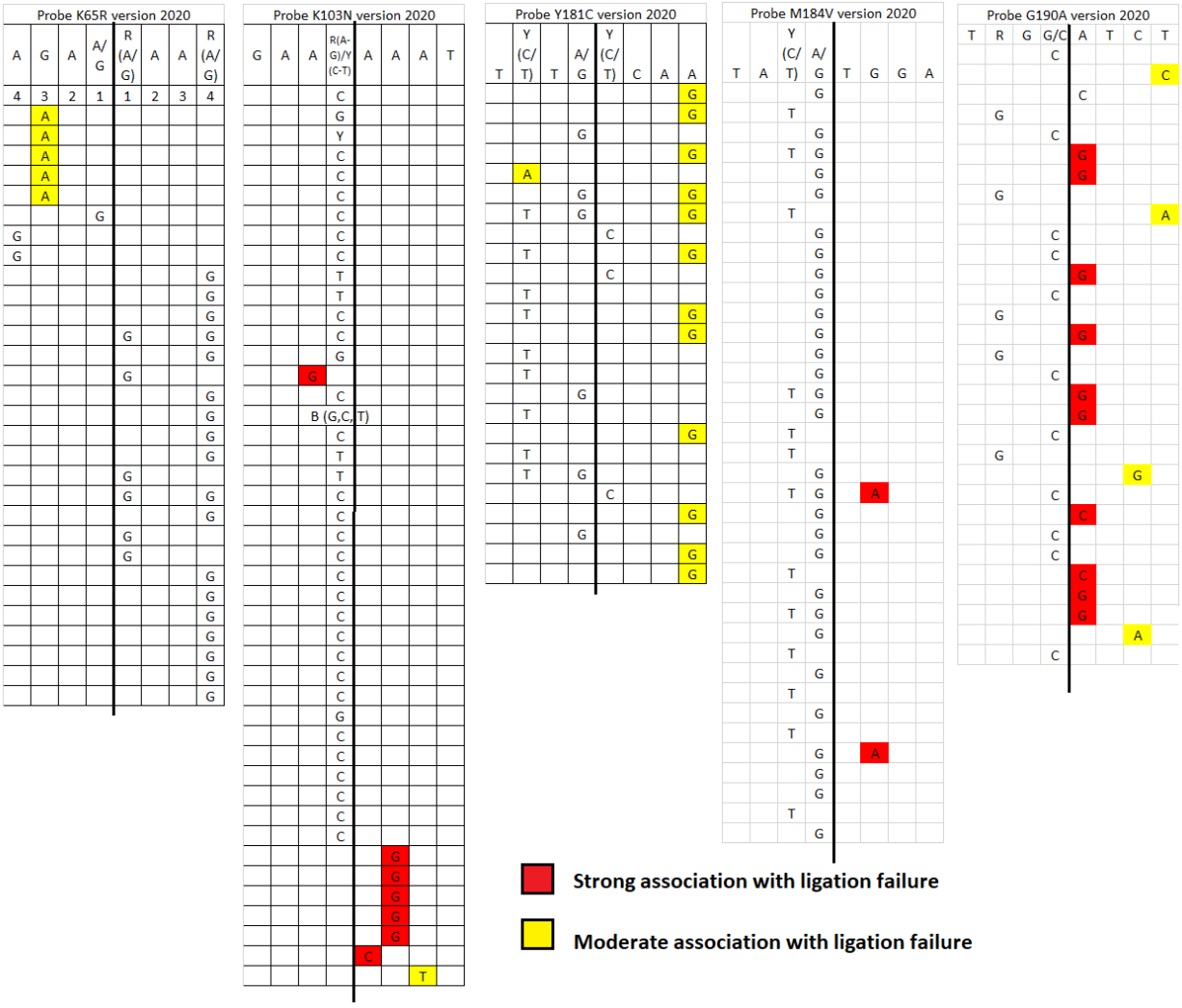

© Copyright 2021 | N Panpradist

Primers/probe for Nigeria study 2022

Codon M41L

The original probes were designed for subtype B contains multiple polymorphisms near the ligation site. Ingrid Beck developed the sequences in the Frenkel lab.

HIV-1 subtype B (2013) designed by Ingrid Beck.

M41 common: 5'-p-TGGAAAAGGAAGGRAAAATT-bio

MUT[C]: 5'-flu-CATTARTAGAAATTTGTACAGARC

MUT[L]: 5'-flu-CATTARTAGAAATTTGTACAGART

codon 41 wt: 5'-dig-CATTARTAGAAATTTGTACAGARA

Analysis of 380 sequences provided by Holly showed polymorphism in the specific probe at the second position from the ligation site (Y at 13.8% of the total sequences). This polymorphism likely causes ligation failure. To account for the additional " Y " polymorphisms, we add the mixture of v2 and v3 probes containing R and Y bases, respectively, to account for the additional “Y” polymorphisms.

WT41v2tag: /5DigN/ATGGGGGTGATTARGAGAAATTTGTACAGARA

WT41v3tag: /5DigN/ATGGGGGTGATTARGAGAAATTTGTACAGAYA

MUT41v3tag: /56-FAM/ATGGGGGTGATTARGAGAAATTTGTACAGAYY

MUT41v4tag: /56-FAM/ATGGGGGTGATTARGAGAAATTTGTACAGARY

COM41tag: /5Phos/TGGAAAAGGAAGGRAAAATTGGGGAAGG/3Bio/

M41vCompv1: RRT CTG TAC AAA TTT CTC YTA ATC ACC CCC AT

M41vCompv2: CCT TCC CCA ATT TTY CCT TCC TTT TCC A

K103N

HIV-1 subtype B (2013) designed by Ingrid Beck.

WT 103: /5DigN/CATCCAGCRGGGYTAAAAAAGAAR

MUT 103: /56-FAM/CATCCAGCRGGGYTAAAAAAGAAY

COM 103: /5Phos/AAATCAGTRACAGTACTRGATGTGGG/3Bio/

© Copyright 2021 | N Panpradist

My *in-silico* analysis showed polymorphisms near the ligation site unique to subtype G.

Specific probes:

0.78% sequence has G at the second position from the ligation site.

0.78% sequence has A/G at the second position from the ligation site.

Pure G will likely cause ligation failure. 0.78% failure is acceptable.

Common probes:

6.3% of sequences have G at the second position from the ligation site.

1.8% of sequences have A/G at the second position from the ligation site.

We will order the probe:

COM103v2: /5Phos/AGATCAGTRACAGTACTRGATGTGGG/3Bio/

The competing oligo will be the identical sequences. These do not have tags to make them consistent with the original probe version.

Y181C

HIV-1 subtype B (2013) designed by Ingrid Beck.

Y181C WT: /5DigN/AAAAAATCCAGAAATARTTATYTA

Y181C MUT: /56-FAM/AAAAAATCCAGAAATARTTATYTG

Y181C COM: /5Phos/YCAATACATGGATGAYTTGTATGTA/3Bio/

In-silico analysis showed polymorphisms near ligation sites unique to subtype G.

Specific probes at the 2nd position from the ligation site:

T	368
G	5
K (G/T)	3
A	3
C	2

© Copyright 2021 | N Panpradist

We will include the additional specific probes:

WT181v2: /5DigN/AAAAAATCCAGAAATARTTATYGA

MUT181v2: /56-FAM/AAAAAATCCAGAAATARTTATYGG

M184V

Ingrid Beck designed HIV-1 subtype B (2013).

M184V WT: /5DigN/ATCCAGAAATARTTATCTATCAATAYA

M184V MUT: /56-FAM/ATCCAGAAATARTTATCTATCAATAYG

M184V COM: /5Phos/TGGATGAYTTGTATGTAGGATCTGA /3Bio/

In-silico analysis showed polymorphisms near ligation sites unique to subtype G.

Common probes at the 2nd position from the ligation site. If we add "A" in the modified probe, we should recover 18.9% IND in this codon.

G	305	
A	65	18.9% IND
R	7	
T	4	1.05% IND

We will include:

COM184v2: /5Phos/TAGATGAYTTGTATGTAGGATCTGA /3Bio/

G190A

Ingrid Beck designed HIV-1 subtype B (2013).

WT 190: /5DigN/CATGGATGAYTTGTATGTRGG

MUT 190: /56-FAM/CATGGATGAYTTGTATGTRGC

COM 190: /5Phos/ATCTGAYTTAGAAATAGGGCAGCA/3Bio/In-silico analysis showed polymorphisms near ligation site unique to subtype G.

© Copyright 2021 | N Panpradist

Common probes at the 1st position from the ligation site. If we add "G" in the modified probe, we should recover 18.9% IND in this codon.

A	349	91.842
G	19	5.789
R	3	
C	8	2.632
T	2	

We will include:

COM190v2: /5Phos/GTCTGAYTTAGAAATAGGGCAGCA/3Bio

T215F/Y

Ingrid Beck designed HIV-1 subtype B (2013).

COM 215: 5'-p-CAC ACC AGA CAA AAA ACA TCA GAA-bio

MUT Y 215: 5'-flu-CAA CAT CTG TTG AGG TGG GGA TTT TA

MUT F 215: 5'-flu-CAA CAT CTG TTG AGG TGG GGA TTT TT

WT 215: 5'-dig-CAA CAT CTG TTG AGG TGG GGA TTT AC

Amino acid encoding:

T	ACA
	ACC
	ACG
	ACT
Y	TAT
	TAC
F	TTC
	TTT

Analysis of the WT or MUT probes at the 1st and 2nd position at the ligation site:

We will use the new probe design as follows:

© Copyright 2021 | N Panpradist

COM215v1tag: /5Phos/HACACCAGACAAAAAACATCAGAATCCCAACC/3Bio/

MUT215Ytag: /56-FAM/TTGTGATA CTAA ATCT G TTG AGG TGG GGA TTT TA

MUT215Ftag: /56-FAM/TTGTGATA CTAA AT CTG TTG AGG TGG GGA TTT TT

WT215tag: /5DigN/TTGTGATA CTA AAT CTG TTG AGG TGG GGA TTT AC

© Copyright 2021 | N Panpradist

CHAPTER 5 REFERENCES

1. Milne, R. S.; Silverman, R. A.; Beck, I. A.; McKernan-Mullin, J.; Deng, W.; Sibley, T. R.; Dross, S.; Kiarie, J. N.; Sakr, S. R.; Coombs, R. W.; Chung, M. H.; Frenkel, L. M., Minority and majority pretreatment HIV-1 drug resistance associated with failure of first-line nonnucleoside reverse-transcriptase inhibitor antiretroviral therapy in Kenyan women. *AIDS* **2019,** *33* (6).

2. Soria, J.; Mugruza, R.; Levine, M.; Leon, S. R.; Arevalo, J.; Ticona, E.; Beck, I. A.; Frenkel, L. M., Pretreatment HIV Drug Resistance and Virologic Outcomes to First-Line Antiretroviral Therapy in Peru. *AIDS Res Hum Retroviruses* **2019**.

3. Ngo-Giang-Huong, N.; Jourdain, G.; Amzal, B.; Sang-a-gad, P.; Lertkoonalak, R.; Eiamsirikit, N.; Tansuphasawasdikul, S.; Buranawanitchakorn, Y.; Yutthakasemsunt, N.; Mekviwattanawong, S.; McIntosh, K.; Lallemant, M.; Program for, H. I. V. P.; Treatment study, g., Resistance patterns selected by nevirapine vs. efavirenz in HIV-infected patients failing first-line antiretroviral treatment: a bayesian analysis. *PLoS One* **2011,** *6* (11), e27427.

4. Beck, I. A.; Deng, W.; Payant, R.; Hall, R.; Bumgarner, R. E.; Mullins, J. I.; Frenkel, L. M., Validation of an oligonucleotide ligation assay for quantification of human immunodeficiency virus type 1 drug-resistant

© Copyright 2021 | N Panpradist

mutants by use of massively parallel sequencing. *J Clin Microbiol* **2014,** *52* (7), 2320-7.

5. Sarkozi, L.; Simson, E.; Ramanathan, L., The effects of total laboratory automation on the management of a clinical chemistry laboratory. Retrospective analysis of 36 years. *Clin Chim Acta* **2003,** *329* (1-2), 89-94.

6. Holland, L. L.; Smith, L. L.; Blick, K. E., Total laboratory automation can help eliminate the laboratory as a factor in emergency department length of stay. *Am J Clin Pathol* **2006,** *125* (5), 765-70.

7. Da Rin, G.; Zoppelletto, M.; Lippi, G., Integration of Diagnostic Microbiology in a Model of Total Laboratory Automation. *Lab Med* **2016,** *47* (1), 73-82.

8. Miler, M.; Nikolac Gabaj, N.; Dukic, L.; Simundic, A. M., Key Performance Indicators to Measure Improvement After Implementation of Total Laboratory Automation Abbott Accelerator a3600. *J Med Syst* **2017,** *42* (2), 28.

9. Chung, H. J.; Song, Y. K.; Hwang, S. H.; Lee, D. H.; Sugiura, T., Experimental fusion of different versions of the total laboratory automation system and improvement of laboratory turnaround time. *J Clin Lab Anal* **2018,** *32* (5), e22400.

10. Bolduc, S. Sputum collection and transport in Africa: perspectives from Mozambique - part 1: Challenges. (accessed January 1st).

© Copyright 2021 | N Panpradist

11. Keller, B.; Vrana, J.; Miller, A.; Newman, G.; Klavins, E., Aquarium: The Laboratory Operating System (Version v2.5.0). *Zenodo.* *http://doi.org/10.5281/zenodo.2535715* **2019**.

12. Chung, M. H.; Drake, A. L.; Richardson, B. A.; Reddy, A.; Thiga, J.; Sakr, S. R.; Kiarie, J. N.; Yowakim, P.; John-Stewart, G. C., Impact of prior HAART use on clinical outcomes in a large Kenyan HIV treatment program. *Curr HIV Res* **2009,** *7* (4), 441-6.

13. Vrana, J. OLA Simple HIV Drug Resistance Test: An Aquarium Workflow. klavinslab.github.io/ola-simple/ (accessed January 2nd).

14. Panpradist, N.; Beck, I. A.; Vrana, J.; Higa, N.; McIntyre, D.; Ruth, P. S.; So, I.; Kline, E. C.; Kanthula, R.; Wong-On-Wing, A.; Lim, J.; Ko, D.; Milne, R.; Rossouw, T.; Ute D. Feucht, M. C., Gonzague Jourdain, Nicole Ngo-Giang-Huong, Laddawan Laomanit, Jaime Soria, James Lai, Eric E. Klavins, Lisa M. Frenkel, Barry R. Lutz OLA-Simple: a software-guided HIV-1 drug resistance test for low-resource laboratories. *EBiomedicine* **2019,** *In press*.

15. Zunt, J. R.; Montano, S. M.; Beck, I.; Alarcon, J. O.; Frenkel, L. M.; Bautista, C. T.; Price, R.; Longstreth, W. T., Human T-lymphotropic virus type 1-associated myelopathy/tropical spastic paraparesis: viral load and muscle tone are correlated. *J Neurovirol* **2006,** *12* (6), 466-71.

16. Panpradist, N.; Wang, Q.; Ruth, P. S.; Kotnik, J. H.; Oreskovic, A. K.; Miller, A.; Stewart, S. W. A.; Vrana, J.; Han, P. D.; Beck, I. A.; Starita, L. M.; Frenkel, L. M.; Lutz, B. R., Simpler and faster Covid-19 testing:

© Copyright 2021 | N Panpradist

Strategies to streamline SARS-CoV-2 molecular assays. *EBioMedicine* **2021,** *64*, 103236.

17. Lessells, R. J.; Avalos, A.; de Oliveira, T., Implementing HIV-1 genotypic resistance testing in antiretroviral therapy programs in Africa: needs, opportunities, and challenges. *AIDS Rev* **2013,** *15* (4), 221-9.

18. Matías-Florentino, M.; Chaillon, A.; Ávila-Ríos, S.; Mehta, S. R.; Paz-Juárez, H. E.; Becerril-Rodríguez, M. A.; Del Arenal-Sánchez, S. J.; Piñeirúa-Menéndez, A.; Ruiz, V.; Iracheta-Hernández, P.; Macías-González, I.; Tena-Sánchez, J.; Badial-Hernández, F.; González-Rodríguez, A.; Reyes-Terán, G., Pretreatment HIV drug resistance spread within transmission clusters in Mexico City. *J Antimicrob Chemother* **2020,** *75* (3), 656-667.

19. Beck, I. A.; Mahalanabis, M.; Pepper, G.; Wright, A.; Hamilton, S.; Langston, E.; Frenkel, L. M., Rapid and sensitive oligonucleotide ligation assay for detection of mutations in human immunodeficiency virus type 1 associated with high-level resistance to protease inhibitors. *J Clin Microbiol* **2002,** *40* (4), 1413-9.

20. Avila-Rios, S.; Sued, O.; Rhee, S. Y.; Shafer, R. W.; Reyes-Teran, G.; Ravasi, G., Surveillance of HIV Transmitted Drug Resistance in Latin America and the Caribbean: A Systematic Review and Meta-Analysis. *PLoS One* **2016,** *11* (6), e0158560.

21. Taylor, T.; Lee, E. R.; Nykoluk, M.; Enns, E.; Liang, B.; Capina, R.; Gauthier, M. K.; Domselaar, G. V.; Sandstrom, P.; Brooks, J.; Ji, H., A

© Copyright 2021 | N Panpradist

MiSeq-HyDRA platform for enhanced HIV drug resistance genotyping and surveillance. *Sci Rep* **2019,** *9* (1), 8970.

22. Shafer, R. W., Rationale and uses of a public HIV drug-resistance database. *J Infect Dis* **2006,** *194 Suppl 1*, S51-8.

23. Casadella, M.; Paredes, R., Deep sequencing for HIV-1 clinical management. *Virus Res* **2017,** *239*, 69-81.

24. Perrier, M.; Desire, N.; Storto, A.; Todesco, E.; Rodriguez, C.; Bertine, M.; Le Hingrat, Q.; Visseaux, B.; Calvez, V.; Descamps, D.; Marcelin, A. G.; Charpentier, C., Evaluation of different analysis pipelines for the detection of HIV-1 minority resistant variants. *PLoS One* **2018,** *13* (6), e0198334.

25. Gunthard, H. F.; Wong, J. K.; Ignacio, C. C.; Havlir, D. V.; Richman, D. D., Comparative performance of high-density oligonucleotide sequencing and dideoxynucleotide sequencing of HIV type 1 pol from clinical samples. *AIDS Res Hum Retroviruses* **1998,** *14* (10), 869-76.

26. Schuurman, R.; Demeter, L.; Reichelderfer, P.; Tijnagel, J.; de Groot, T.; Boucher, C., Worldwide evaluation of DNA sequencing approaches for identification of drug resistance mutations in the human immunodeficiency virus type 1 reverse transcriptase. *J Clin Microbiol* **1999,** *37* (7), 2291-6.

27. Avila-Rios, S.; Garcia-Morales, C.; Matias-Florentino, M.; Romero-Mora, K. A.; Tapia-Trejo, D.; Quiroz-Morales, V. S.; Reyes-Gopar, H.; Ji, H.; Sandstrom, P.; Casillas-Rodriguez, J.; Sierra-Madero, J.; Leon-Juarez, E. A.; Valenzuela-Lara, M.; Magis-Rodriguez, C.; Uribe-Zuniga, P.; Reyes-

© Copyright 2021 | N Panpradist

Teran, G.; Group, H. M., Pretreatment HIV-drug resistance in Mexico and its impact on the effectiveness of first-line antiretroviral therapy: a nationally representative 2015 WHO survey. *Lancet HIV* **2016,** *3* (12), e579-e591.

28. Avila-Rios, S.; Garcia-Morales, C.; Matias-Florentino, M.; Tapia-Trejo, D.; Hernandez-Alvarez, B. F.; Moreira-Lopez, S. E.; Quant-Duran, C. J.; Porras-Cortes, G.; Reyes-Teran, G., HIV Drug Resistance in Antiretroviral Treatment-Naive Individuals in the Largest Public Hospital in Nicaragua, 2011-2015. *PLoS One* **2016,** *11* (10), e0164156.

29. Avila-Rios, S.; Mejia-Villatoro, C. R.; Garcia-Morales, C.; Soto-Nava, M.; Escobar, I.; Mendizabal, R.; Giron, A.; Garcia, L.; Reyes-Teran, G., Prevalence and patterns of HIV transmitted drug resistance in Guatemala. *Rev Panam Salud Publica* **2011,** *30* (6), 641-8.

30. Avila-Rios, S.; Garcia-Morales, C.; Valenzuela-Lara, M.; Chaillon, A.; Tapia-Trejo, D.; Perez-Garcia, M.; Lopez-Sanchez, D. M.; Maza-Sanchez, L.; Del Arenal-Sanchez, S. J.; Paz-Juarez, H. E.; Quiroz-Morales, V. S.; Mehta, S. R.; Smith, D. M.; Leon-Juarez, E. A.; Magis-Rodriguez, C.; Reyes-Teran, G.; Group, H. M., HIV-1 drug resistance before initiation or re-initiation of first-line ART in eight regions of Mexico: a sub-nationally representative survey. *J Antimicrob Chemother* **2019,** *74* (4), 1044-1055.

31. Barany, F., Genetic disease detection and DNA amplification using cloned thermostable ligase. *PNAS* **1991,** *88*, 189-193.

© Copyright 2021 | N Panpradist

32. Stanford University HIV drug resistance database. https://hivdb.stanford.edu/.

33. Inzaule, S. C.; Hamers, R. L.; Noguera-Julian, M.; Casadella, M.; Parera, M.; Kityo, C.; Steegen, K.; Naniche, D.; Clotet, B.; Rinke de Wit, T. F.; Paredes, R.; PanAfrican Studies to Evaluate, R., Clinically relevant thresholds for ultrasensitive HIV drug resistance testing: a multi-country nested case-control study. *Lancet HIV* **2018,** *5* (11), e638-e646.

34. CENSIDA. Guía de Manejo Antirretroviral de las Personas con VIH. https://www.gob.mx/censida/documentos/guia-de-manejo-antirretroviral-de-las-personas-con-vih.

© Copyright 2021 | N Panpradist

CHAPTER 6: STRATEGIES TO IMPROVE AMPLIFICATION AND LIGATION FOR HIVDR OLA

OLA-SIMPLE 1.0 CAN BE FURTHER IMPROVED IN SEVERAL AREAS

First, OLA-Simple 1.0 relies on a thermal cycler to de-hybridize and re-hybridize HIV targets to the primers/probes (45 cycles for amplification, 10 cycles for ligation (**LDR**). Costs may not be the most challenging factor to procure a thermal cycler since, over the past decade, it has been drastically reduced to as low as $500 or lower. Instead, speed is the main challenge. The reaction speed is limited by the ability to heat up and cool down the heater of the thermal cycler, leading to a 2h PCR after 1h RT and 1h ligation.

IMPROVEMENT OF HIVDR INTEGRATION IN THE CLINICAL WORKFLOW

Implementation of OLA-Simple 1.0 in a clinical workflow is dependent on access to a VL test. The current HIVDR test is run separately from the VL test (**Figure 6.1A**). Only after consecutive VF test results, blood specimens are re-collected and tested for HIVDR.

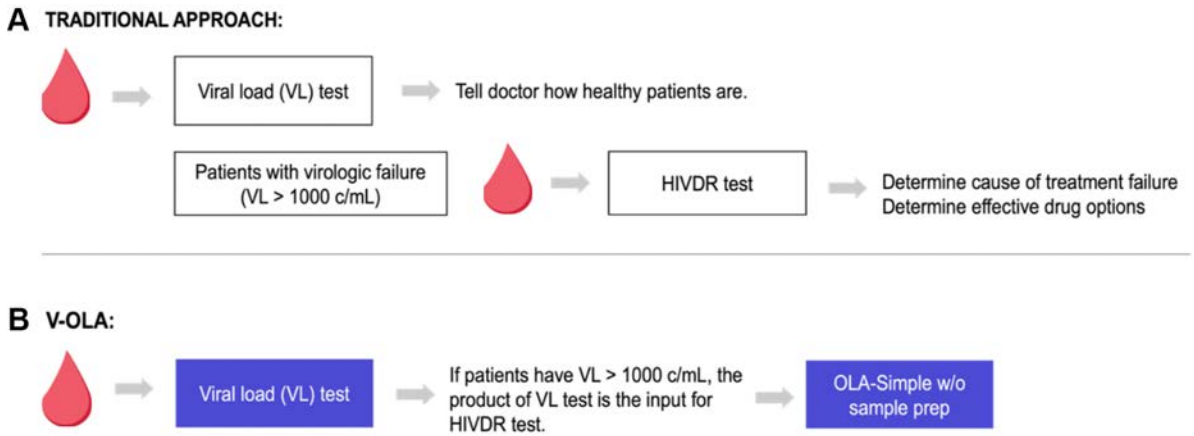

© Copyright 2021 | N Panpradist

Figure 6.1. | Traditional VL and HIVDR workflow versus V-OLA (HIV VL with reflexed OLA-Simple).

DELIVERABLES. In this section, we describe new development to improve speed and reduce the OLA-Simple assay cost. We investigated and developed HIV amplification assays using several isothermal amplification methods. We investigated the ligation yield and discussed different strategies to improve it. Last, we present our progress on "**V-OLA,**" which integrates the workflow of the VL test and reflexed HIVDR tests (**Figure 6.1B**). If a patient is tested VF, the reaction tube from the VL test can directly be used for HIVDR, eliminating the need for new sample collection and extraction.

MATERIALS AND METHODS

Fast PCR. Two assays were designed for fast PCR: one to amplify the region covering HIVDR against NNRTIs or NRTI, and the other to amplify the region covering HIVDR in HIV pol including PI and INSTI (**Table S6.6**). Each reaction tube contains 23µL master mix (1.5x FastStart buffer (Roche), 2mM $MgSO_4$, 10mM ea dNTPs, 0.2µM forward primer, 0.8µM reverse primer, 4.8% (v/v) trehalose, 1x Evagreen, 0.5µL RNASEin (Promega), 0.5µL One-Taq HotStart polymerase (NEB), and 0.5µL WarmStart RTx (NEB) in water) and 2µL RNA template or water. The mixture is set up at room temperature (not on ice). The reaction was subjected to a PCR run using CFX96 (Biorad) using an initial 8-minute incubation at 55°C for reverse transcription, 2 -minute incubation at 94°C to denature the RT enzyme and initiate the polymerase, followed by 2 cycles of 1 second at 94 °C, 30 seconds at 55 °C, and 30 seconds at 68 °C; and

© Copyright 2021 | N Panpradist

followed by 38 cycles of 1 second at 94 °C and 20 seconds at 66 °C before reading by FAM channel. Results are analyzed using CFX Maestro (Biorad).

Thermostable Helicase Dependent Amplification. The tHDA kit was purchased from NEB. Three sets of primers were designed against the HXB2 sequences: *(i)* amplified the region of K65R, *(ii)* amplified the region of K103N and V106M, and *(iii)* amplified the region of Y181C, M184V, and G190A (**Table S6.7**). Each reaction tube contains 20.5µL master mix (1x annealing buffer, 4mM $MgCl_2$, 40mM NaCl, 1.75µL IsoAmp® dNTP solution, 1x Evagreen, 5% (v/v) trehalose, and nuclease-free water), 2.5µL of template or water, and 2µL of primer mixture (1 part volume of 5µM forward primer and 4-part volume of 5µM reverse primer). The template and primer were added to the lid of the reaction tubes and mixed with the master mix right before subjecting the reaction tube to 65°C (heated lid set to 68°C) for 90 minutes. The enzymes were deactivated using a 15-minute incubation at 72°C before storage for downstream analyses such as electrophoresis. Salt concentrations are within the recommended range, but 80nM forward and 320nM reverse primers were beyond the recommended tittering range of 50-200nM[1].

Recombinase polymerase amplification. Lyophilized basic RPA mix (TwistDx) was rehydrated with 35µL of master mix (29.5µL rehydration buffer, 2.4µL of each 10µM forward and reverse primer (**Table S6.9**) in water) and mixed well. The reaction was then aliquoted into 5 of 7µL master mix. Each 7µL reaction was then added with a 2µL RNA/DNA template or water to the reaction. Then 1µL 140mM MgOAc was added to each reaction, mixed, and started immediately at 42°C (with

© Copyright 2021 | N Panpradist

lid off) for 30 minutes. The reaction was stopped at 85°C for 15 minutes unless proceeding to ligation immediately.

Loop-mediated isothermal amplification (LAMP). 10x LAMP primers[2] contained the mixture of 16μM FIP, 16μM BIP, 2μM F3, 2μM B3, 4μM Loop F, and 4μM Loop B in 1xTLE. 2μL template or water was mixed with 18μL master mix (0.5% TritonX-100, 5% trehalose, 1x isothermal amplification buffer (NEB), 1x Evagreen, 1x LAMP primer, 1.4mM dNTPs, 2mM $MgSO_4$ supplement to the 6mM MgSO4 in the isothermal amplification buffer, 7.5U RTxWarmStart (NEB), 0.24U TiPP (NEB), 40U RNASEin (Promega), and 1.2mg/mL in-house TFv1 polymerase. The reaction is mixed and subjected to 65°C for 40 minutes (FAM read every 30 seconds) before endpoint melt analysis.

Quantification of ligation yield. OLA ELISA was used to quantify the product along with the standard curves containing 0.06nM – 6nM synthetic MUT probes (5'biotin, 3'FAM, poly$(T)_{20}$) or synthetic WT probes (5'biotin, 3'digoxigenin, poly$(T)_{20}$). The probes were purchased from IDT, HPLC purified. The measured OD of the ligation was converted to the concentration of ligated WT probes or ligated MUT probes using the OD of the respective standard curves.

6.1 FAST PCR

Most conventional lab-based PCR protocols require a thermal cycler to cycle among three temperatures: 94°C to denature double-stranded DNA, 55°C to allow primers to anneal to the DNA target (5°C lower than the melting temperatures of primers), and 68-72°C to allow

© Copyright 2021 | N Panpradist

polymerization to occur at optimal operational temperature for polymerases. We developed a two-stage PCR to minimize the temperature gap between the annealing and denaturing temperatures to achieve a faster PCR. This approach was used in NGS library preparation to include the engineered adapter sequences without tube-opening after the amplification step[3]. Herein different 5' engineered adapters were added to forward and reverse primers. During the first few cycles, cycling would be proceeded like a typical PCR to incorporate the adapter sequence as part of the primer footprints. Subsequently, the annealing temperature can be increased to near or match the extension temperature. With refined optimization of primer and enzyme concentrations, we successfully developed a one-hour, single-tube RT-PCR that can sensitively amplify 100 copies of synthetic HIV RNA/reaction. We also used the mixture of Taq and Deep Vent polymerases to improve the fidelity of amplification compared to the Taq polymerase alone. See **section 6.4,** where we discussed our application of this technique to develop the V-OLA 1.0 workflow.

6.2 ISOTHERMAL NUCLEIC ACID AMPLIFICATION TECHNOLOGIES

Many attempts have been made to design alternative nucleic acid amplification techniques that operate at a fixed temperature (*i.e.,* isothermal amplification) to avoid the need for a thermal cycler. More than 25 variations of isothermal nucleic acid amplification technologies (**iNAATs**) have been reported[4, 5]. Examples are helicase-dependent amplification (**HDA**)[6-9], strand displacement amplification (**SDA**)[10], loop-mediated isothermal amplification (**LAMP**)[11], rolling circle amplification (**RCA**)[12], and recombinase polymerase amplification (**RPA**)[34, 13]. Some of these iNAATs were used for diagnostics for HIV[12,14, 15].

© Copyright 2021 | N Panpradist

However, it is less common for HIV NAAT to target the HIV *pol* gene for subsequent detection of the HIVDR. One key challenge is that the locations of the SNPs that confer HIVDR are spread across 670 bp within the HIV *RT* region (**Table 6.1**).

Table 6.1 | Key HIVDR mutations associated with NNRTI and NRTI resistance.

Blue boxes are the mutations we tested in OLA-Simple 1.0 (**2019**). The box with dashed was also considered for the future. In the version 2021-2022 Kenya, we dropped the M106V and added L74V/I and Y115F.

Major Non-Nucleoside RT Inhibitor (NNRTI) Resistance Mutations

HIV DR Stanford database 2020

Consensus	100 L	101 K	103 K	106 V	138 E	181 Y	188 Y	190 G	230 M
DOR	I	EP		AMI		CIV	LHC	SE	L
EFV	I	EP	NS	AM		CIV	LCH	ASE	L
ETR	I	EP			AGKQ	CIV	L	ASE	L
NVP	I	EP	NS	AM		CIV	LCH	ASE	L
RPV	I	EP			AGKQ	CIV	L	ASE	L

Major Nucleoside RT Inhibitor (NRTI) Resistance Mutations

	Discriminatory Mutations					Thymidine Analog Mutations (TAMs)						MDR Mutations	
Consensus	184 M	65 K	70 K	74 L	115 Y	41 M	67 D	70 K	210 L	215 T	219 K	69 T	151 Q
3TC	VI	R										Ins	M
FTC	VI	R										Ins	M
ABC	VI	R	E	VI	F	L			W	FY		Ins	M
DDI	VI	R	E	VI		L			W	FY		Ins	M
TDF	***	R	E		F	L		R	W	FY		Ins	M
D4T	***	R	E			L	N	R	W	FY	QE	Ins	M
ZDV	***	***	*	*		L	N	R	W	FY	QE	Ins	M

However, amplicon sizes generated by iNAATs are typically limited to 100 – 200 bp. This limitation may be caused by the fact that most isothermal amplification methods rely on run-on kinetics. Two or more enzymes are used to create the cycles consisting of three stages: enzymatic dehybridization or initiation, primer annealing, and extension. The orders of these stages are not

© Copyright 2021 | N Panpradist

as perfect in iNAATs, whereas in regular PCR, these three stages are entirely isolated from each other. For example, the polymerase extension may be disrupted by the dissociation of DNA by helicase in tHDA or primer insertion by recombinase enzyme in RPA. Among commercially available iNAATs, RPA reportedly amplified up to 1.5 kb[16], but the commercial proprietary formulation was optimized for shorter amplicon sizes (80-500 bp) [17].

Bacillus stearothermophilus (**Bst**) DNA polymerase, one of the most used polymerases in iNAATs, has a higher processivity (i.e., lower dissociation rate from the DNA template during the polymerization) than Taq polymerase used in PCR [18]. In the context of a genotyping assay, low-fidelity enzymes are more likely to incorporate incorrect bases and thus could impact the specificity of the assay. Bst polymerase reportedly has a 7-time higher fidelity than Taq typically used in PCR[18], so it should likely reduce the assay's chance to detect HIVDR falsely. We investigated four NAATs for the V-OLA and OLA-Simple applications: isothermal SDA, thermostable HDA, RPA, and LAMP.

6.2.1 iSDA

iSDA used to be one of the fastest isothermal amplification methods to date; it takes only 20 minutes to amplify 1,000 copies. Fortunately, we have a close relationship with Elitech Co., Ltd, which developed and owned this assay and allowed us to use their product. iSDA relies on a nicking enzyme and a polymerase to create a cycling mechanism (**Figure 6.2A**). They developed and tested an iSDA for HIV *pol*. iSDA assays successfully amplified one of the

© Copyright 2021 | N Panpradist

segments in *pol* containing 3 SNPs (Y181C, M184V, and G190A, **Figure 6.2B**), with a sensitivity of 400 HIV copies/reaction.

The iSDA operates at 49°C, a lower temperature than typical PCR annealing, and is prone to primer-dimer amplification. The amplification rate of primer-dimer (often shorter target size) is faster than the target amplification (100-200 bases), which could impact the sensitivity of iSDA [19]. The sensitivity of iSDA is also reduced by 5-fold in the presence of human genomic DNA and other inhibitors from nasal samples[19].

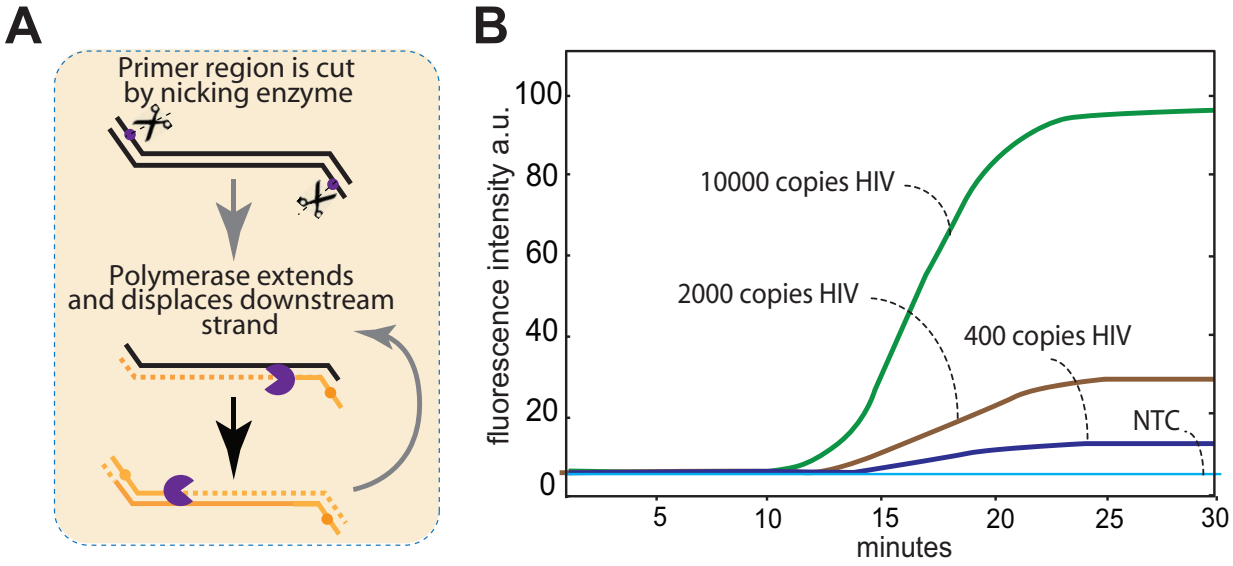

Figure 6.2. HIV isothermal strand displacement (iSDA) assay for HIV RT.

(**A**) Cycling mechanism. iSDA primers contain a nicking site. After initiation through breathing, the primers can get cleaved, which allows the polymerase to extend and displace the previous complementary strands. (**B**) Real-time iSDA of HIV *pol*. Data courtesy: Elitech.

6.2.2 tHDA

In tHDA, the helicase enzyme serves as a biological, thermal cycler to de-hybridize the template and allow primers to be annealed and extended by the

© Copyright 2021 | N Panpradist

polymerase[20]. The advantages of using tHDA are its relatively high reaction temperature at 65 °C and the requirement of only one pair of primers. Both advantages reduce opportunities for non-specific primer reactions. The enzymes used in tHDA operate at a high temperature (i.e., 65 °C) than RPA, iSDA, and a typical PCR annealing temperature. Thus, we anticipate these enzymes to have a longer shelf life in their dried format than enzymes used in other isothermal amplification methods.

I worked with Annie Wong-On-Wing (an undergraduate student mentee) to design and test primers with plasmids derived from patient HIV specimens, which contain genetic variants of HIV. tHDA provided exact salt concentrations, and we could use similar design tools to design the primers akin to PCR with adjustment to meet the requirements of tHDA reactions (see details in the **Supplementary information Chapter 6**).

We successfully identified a set of three primer pairs that can each amplify different regions of HIV *pol* containing HIVDR associated SNPs. **Figure 6.3** shows the sensitivity of the HDA using one of the three primer pairs that can detect as low as ten copies/25µL reaction. Unfortunately, the reaction time for HDA is longer than iSDA, but it is still faster than the PCR protocol used in the OLA-Simple 1.0. However, the amplification was highly specific, and we did not see any primer dimer as denaturing gel electrophoresis showed the two bands of the original forward and reverse primer length (less than 25 bases). tHDA reportedly can amplify up to 400 bases; it was posited that the helicase displaced Bst polymerase during base incorporation across the region of

© Copyright 2021 | N Panpradist

amplification[21]. The amplified targets from the three regions were tested for their compatibility with ligation. The amplicon generated by tHDA was correctly detected in the six HIVDR mutations (**Figure 6.4**).

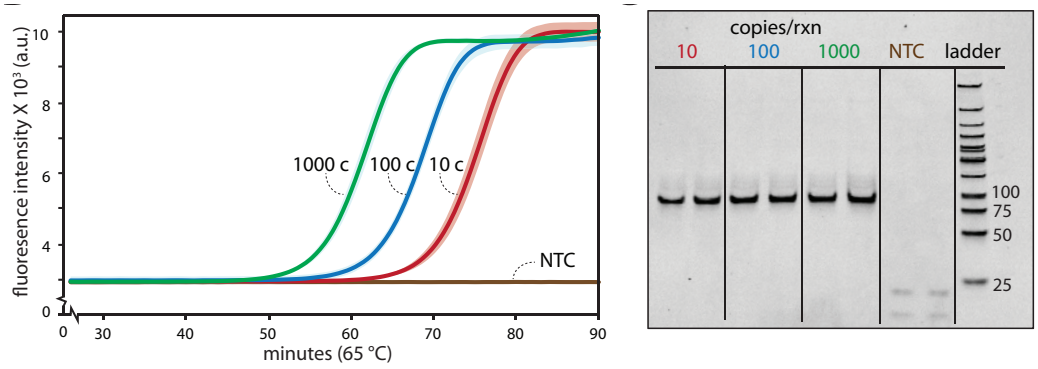

Figure 6.3 | tHDA real-time amplification and fragment analysis (denaturing gel).

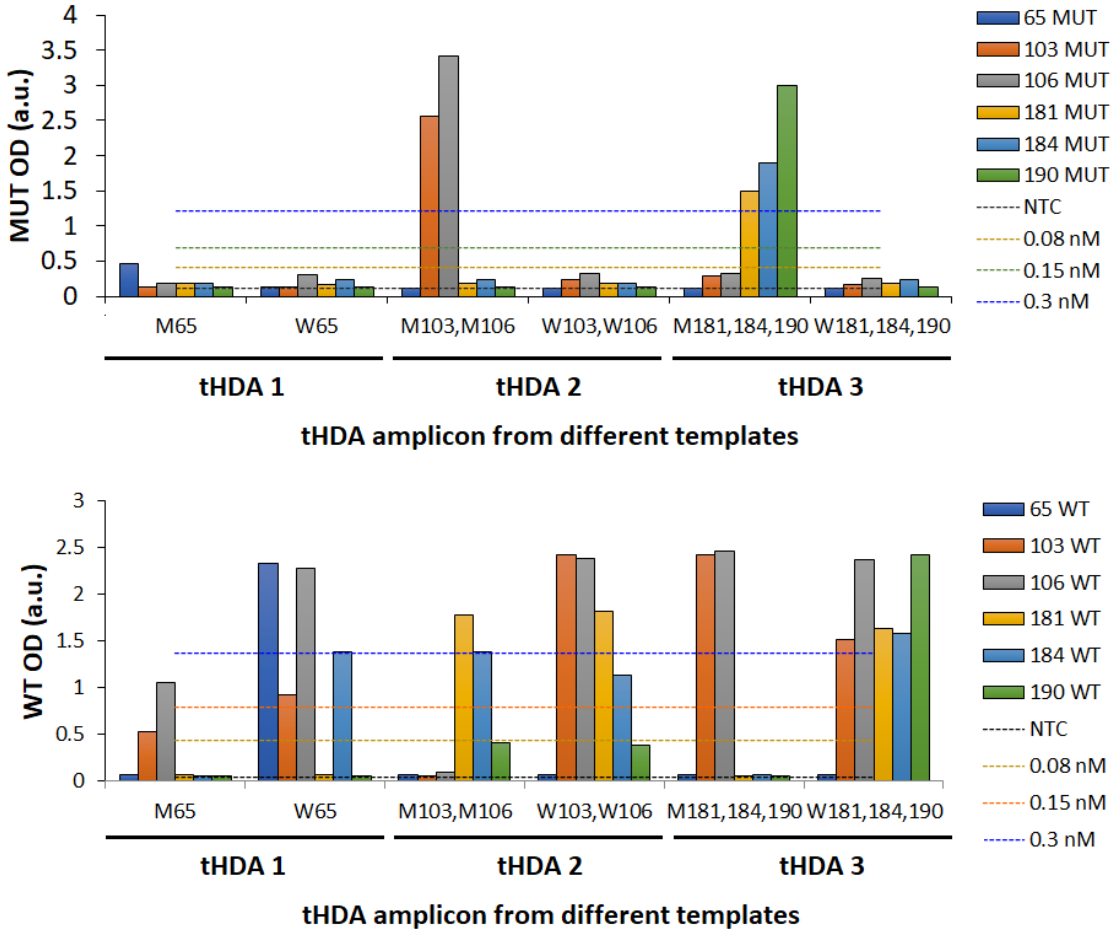

Figure 6.4 | OLA analysis of the product from tHDA to confirm the sequence accuracy.

© Copyright 2021 | N Panpradist

(**A**) MUT detection and (**B**) WT detection of the six templates: M65 contains K65R. W65 contains a wild-type sequence at the K65R codon. M103, M106 contains the K103N and V106M mutations, while W103, W106 contains wild-type sequences in these codons. M181, M184, M190 template contains the Y181C, M184V, and G190A mutations while W181, W184, W190 contain wild-type sequences in these codons. Annie Wong-On-Wing and Nuttada Panpradist collected data.

We found tHDA behaved very similarly to PCR and flexible to the primer concentrations in the reaction (see **Isothermal ligation section**).

6.2.3 RPA

RPA relies on enzyme-mediated initiation rather than DNA breathing like tHDA and iSDA. First, the recombinase protein binds to the primers (**Figure 6.5A**)[22]. Recombinase/primer complex scans for the homologous sequence, and once found, it inserts the primer in between the homologous dsDNA sequence. The displaced complementary DNA is bound to the single-stranded binding protein (i.e., gp32) to prevent re-annealing of the template. Bsu DNA polymerase then extends the 3’ end of the annealed primer to start the amplification process. The recombinase protein and the gp32 can bind to the primer, but the crowding agents (CarbowaxM20) in RPA shifted the equilibrium toward the recombinase/primer complex formation. **Table 6.2** summarizes the role of each component in the RPA[23].

© Copyright 2021 | N Panpradist

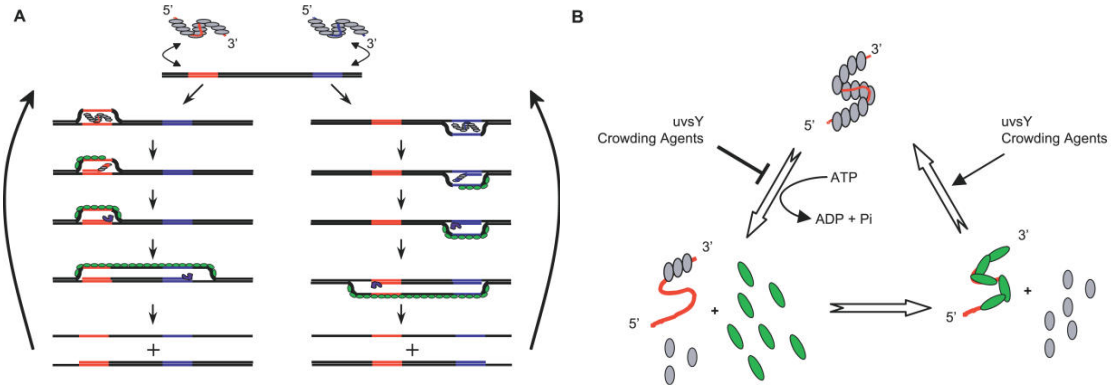

Figure 6.5 | Mechanisms of RPA[22]

(**A**) Recombinase/primer complex searches homologous sequences (red/blue) and inserts the primer between the dsDNA. The displaced DNA strand is bound by gp32 (green), followed by primers extension by Bsu polymerase (blue) to kick off the exponential amplification like PCR (**B**) uvsX (gray) binds to the primer (red). Via ATP hydrolysis, the nucleoprotein complex disassembles (left), and uvsX can be replaced by gp32 (green, right). The presence of uvsY and Carbowax20M shifts the equilibrium in favor of recombinase loading. This figure was obtained from O. Piepenburg et al. 2016[22].

Table 6.2 | Summary of RPA reaction components and their typical concentrations and functions[23]

Reaction components	Typical concentration	Functions
T4 UvsX protein	120 ng μL^{-1}	Recombinase possesses pairing and strand-transfer activity that is important in genetic recombination, DNA repair, and replication (or *E. coli* RecA; recombinase is a central component in the related processes of recombinational DNA repair homologous genetic recombination that is the ortholog of the UvsX protein).

© Copyright 2021 | N Panpradist

Reaction components	Typical concentration	Functions
T4 UvsY protein	60 ng μL^{-1}	Recombinase loading factor is classified as a recombination-mediator protein that stimulates the single-stranded DNA-dependent ATPase activity of T4 UvsX and lowers the critical concentration of T4 UvsX required for activity.
T4 gp32	600 ng μL^{-1}	Single-stranded binding (SSB) protein is involved in DNA replication, repair, and recombination and binds preferentially to single-stranded DNA. The T4 UvsX, T4 UvsY, and T4 gp32 proteins work co-operatively to initiate the RPA reaction *via* unwinding, D-loop formation, and stabilization of the DNA template.
Bacillus subtilis DNA polymerase I (*Bsu*) or *Staphylococcus aureus* polymerase (*Sau*)	*Bsu*: 30 ng μL^{-1}; *Sau*: 8.6 or 12.8 µg	DNA polymerase synthesizes new DNA templates homologous to the target nucleic acid by extending nucleotide building blocks from the bound primers, complementary to the original target nucleic acid sequence or "template."
Deoxynucleotide triphosphate (dNTP, N = A, T, C, G)	200 µM each	An equimolar solution of dATP, dCTP, dGTP and dTTP are building blocks used by the DNA polymerase to synthesize new templates.

© Copyright 2021 | N Panpradist

Reaction components	Typical concentration	Functions
Forward and reverse primers	Usually at 420 nM each, but can be varied in the concentration range of 150 nM to 600 nM	Primers are critical to directing the amplification event to the nucleic acid target of interest through homologous binding. After binding, the primers provide the essential 3′-OH for the polymerase to perform strand extension.
DNA template	—	The oligonucleotide that the primers bind to for the synthesis of exact new oligonucleotides
Carbowax20M (a high molecular weight polyethylene glycol (PEG))	PEG 35K (5%)	The crowding reagent is a good mimic of the real biomacromolecules condition *in vivo* and facilitates amplification, as the crowding agents can enhance the catalytic activity of the enzymes.
Dithiothreitol	Two mM	Stabilization of the enzymes by baring free sulfhydryl groups.
Phosphocreatine	50 mM	The three components form the energy-supply system for the activities of the recombinase and the DNA polymerase.
Creatine kinase	100 ng μL^{-1}	
Adenosine triphosphate (ATP)	Three mM	
Tris(hydroxymethyl)aminomethane (Tris)	50 mM (pH 7.9)	The two components serve to stabilize and solubilize the DNA in solution.
Potassium acetate	100 mM	
Magnesium acetate	14 mM	

© Copyright 2021 | N Panpradist

RPA is very fast and sensitive. Across several assays in our hands, 10 copies of DNA input with a 100-200 amplicon size can be amplified to the concentration detectable by gel electrophoresis in 5-10 minutes. However, designing the RPA primer is less straightforward, as it does not rely on the melting temperature. Rather, the primer should be in the length of 30-15 nucleotides so that the recombinase complex can recognize them. Primer screening was only performed experimentally via multiple iterations until achieving desirable speed and sensitivity.

Additionally, viscous CarbowaxM20 component and high concentrations of enzymes and associated proteins in RPA can interfere with downstream analysis. Previous use of RPA amplicon requires DNA purification/extraction before genotyping[15]. This post-amplification extraction step is cumbersome and highly prone to amplicon-carryover contamination.

Enos Kline (Research Scientist in the Lutz lab) designed RPA nested primer sets that amplified the full-length of HIVDR in the RT region (**Table 6.1**) to generate a 531 bp amplicon. I further optimized the sensitivity of 20 copies of DNA or RNA/10µL reaction in 20 minutes (**Figure 6.6**). One of the primers was designed to be slightly shorter than the recommended length to bases near 3’ end to be on the highly polymorphemic region in HIV and reduce the overall possibility for primer/dimer amplification. I also successfully designed two primer sets to amplify HIVDR mutations in PI and INT regions (see **Supplementary Information Chapter 6**).

© Copyright 2021 | N Panpradist

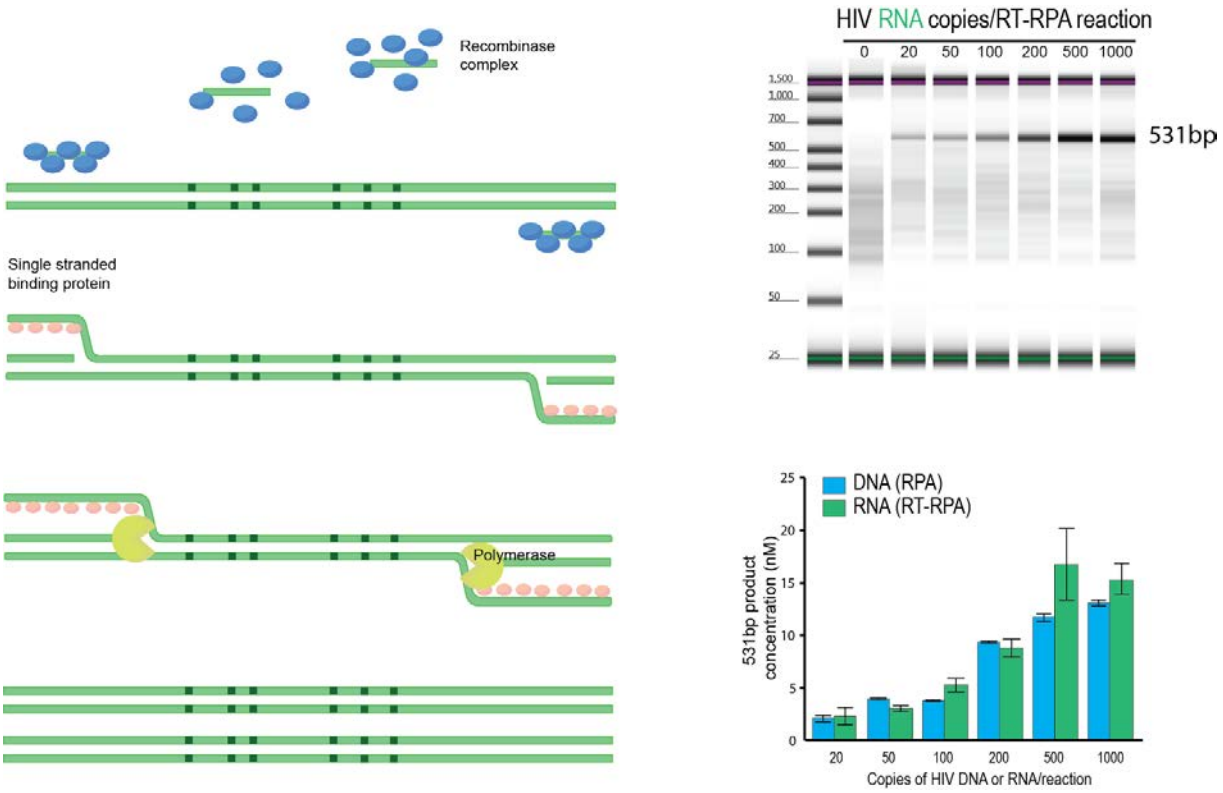

Figure 6.6 | RPA amplification of the whole HIVDR region in HIV RT.

The primer amplified the region covering the key 6 HIVDR mutations in RT, generating the 531bp amplicon confirmed by gel electrophoresis and at least 2.5 nM concentration of DNA template available for downstream ligation step.

RPA assays are tolerant to mismatched primer regions[24]. Our assay amplified 2000 copies/reaction of DNA derived from patient specimens across subtypes and showed 100% (78/78) successful amplification. Sequencing analysis of these specimens is in progress, but the preliminary results show that RPA is robust against multiple mismatched in the primer regions (**Figure 6.7**). One of the downsides of RPA is that it is highly susceptible to non-target DNA and primer concentrations.

© Copyright 2021 | N Panpradist

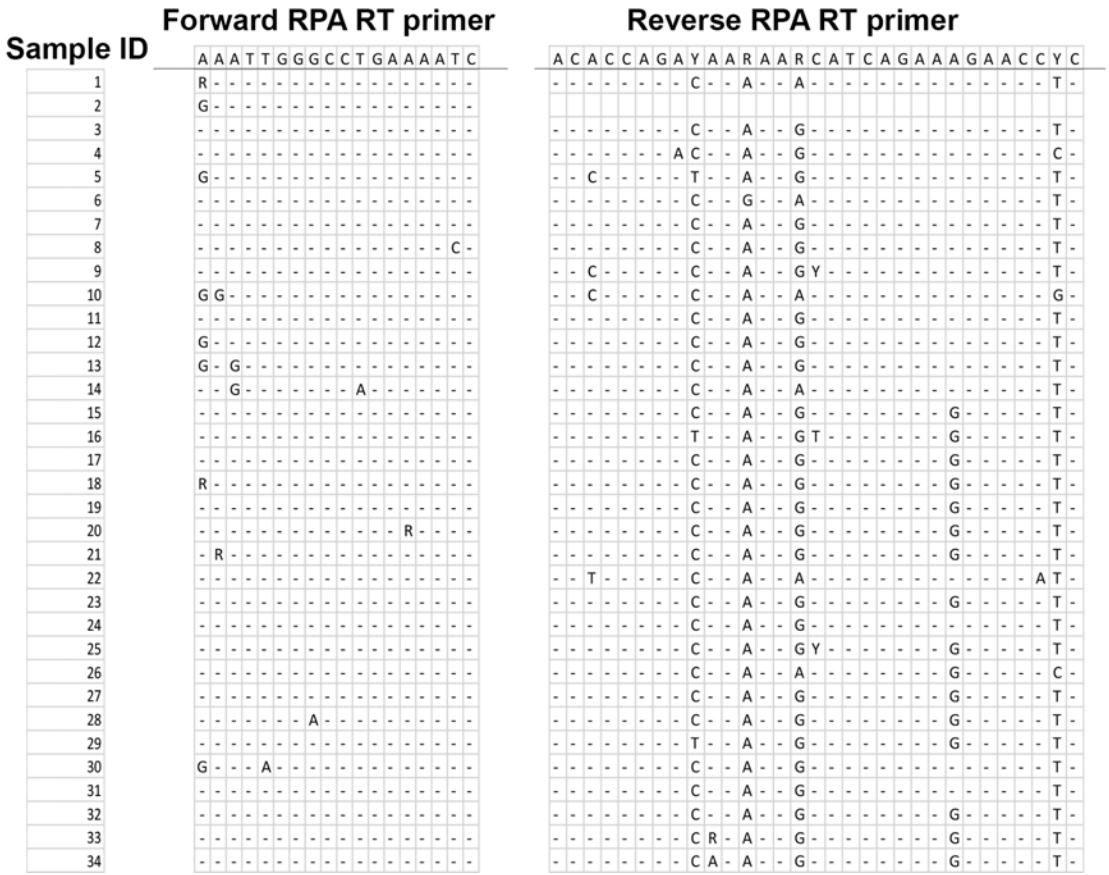

Figure 6.7 | Examples of the sequences of patient specimens in the RPA primer regions.

The empty cells are the sample that we did not have good quality sequences in the reverse primer region.

6.2.4 LAMP

LAMP involves essential four primers (FIP, BIP, F3, and B3), but additional two primers (loop forward and loop reverse) could significantly improve the speed[25] (**Figure 6.8**). Like iSDA and tHDA, LAMP is initiated by the breathing of the dsDNA template or cDNA. Primer transiently exchanges the strand with the template, and the annealed primer gets 3’ extended by the polymerase enzyme. In contrast to iSDA or tHDA, the FIP and BIP primers in LAMP have adapters that complement the other regions in the amplicon. After both FIP and BIP primers are incorporated

© Copyright 2021 | N Panpradist

into the amplicon, the amplicon will form a stable dumbbell structure that drastically increases the melting temperature of the primer region (switching from the intermolecular reaction to intramolecular binding). This helps make the LAMP assay faster and more sensitive than iSDA. However, LAMP can amplify up to 280 bases[26].

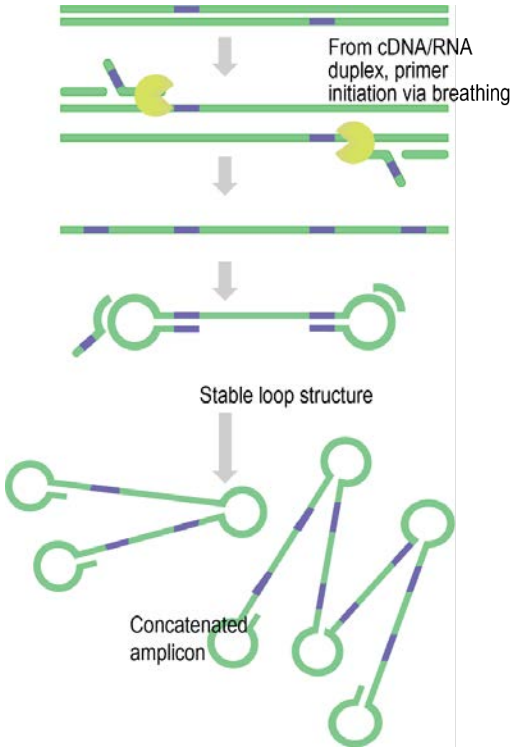

Figure 6.8 | Schematic of LAMP mechanisms

Enos Kline developed the TFv1 DNA polymerase, which is stable up to 95°C and thus allows the LAMP reaction to operate at a higher temperature. Running the reaction at a higher temperature would likely reduce non-target amplification. I have applied this polymerase in the existing HIV RT-LAMP assay[2] that targets the integrase region of HIV. I demonstrated sensitivity of 50 purified synthetic HIV RNA copies/20µL reaction. The formulation contains 0.5% Triton-X 100 in

© Copyright 2021 | N Panpradist

combination with heat during the RT-LAMP reaction could lyse the viral particle and release the RNA that immediately gets converted to the cDNA and subsequently amplified by LAMP. This modification enables the detection of down to 10 copies of HIV viral particles/20µL reaction. This development could be helpful for rapid, point-of-care VL detection. However, unlike the tHDA, RPA, and iSDA assay, the amplicon generated here cannot be used for HIVDR directly. See **Chapter 10.4** for more details about the TFv1 enzyme and direction to amplification via RT-LAMP.

Table 6.3 summarizes the advantages of presented amplification approaches to improve speed and cost. In addition to HIV, we also applied these isothermal amplification assays on human DNA (**Chapter 9**), SARS-CoV-2 (**Chapter 10**), and fish species (**Chapter 11**).

Table 6.3 | Summary of improvement in the OLA amplification step

Techniques		Advantages				Fish DNA	Human DNA	SARS-CoV-2 RNA	HIV RNA
		Speed	Cost	Quantification	No thermal cycler				
5' overhang adapter		✓				55 min	-	-	60 min[1]
End-point VL test		✓	✓	✓		-	-	Yes[2]	Yes
Isothermal amplification	Helicase Dependent Amplification (**HDA**)		✓	✓	✓	-	-	-	90 min[3]
	Recombinase Polymerase Amplification (**RPA/RT-RPA**)	✓	✓		✓	15 min	5 min	20 min	10-25 min (3 regions of HIV drug resistance) [4]
	Loop-mediated Isothermal Amplification (**LAMP/RT-LAMP**)	✓	✓	✓	✓	25 min	30 min	45 min[5]	35 min[6]

Other contributors: 1 E Kline; I Hull 2 Q Wang, PS Ruth (UW CSE) 3 A Wong-On-Wing; A Sriram 4 E Kline; I Hull 5 E Kline; 6 Adapted from N Hosaka et al 2009

© Copyright 2021 | N Panpradist

6.3 INVESTIGATION OF LIGATION.

6.3.1 LOW LIGATION YIELD AND THE POSSIBLE CAUSES

Ligation in OLA is a linear amplification process. Two matched probes at the SNP can be converted into one ligated probe (**Figure 6.9A**). Probes are used in excess (~4-fold higher concentration than the target), and the ligation yield is driven by the starting target concentration. Therefore, the maximum of the theoretical ligated probe would be the number of ligation cycle times the input target concentration. We designed an experiment to quantify the ligated plate via ELISA using synthetic ligated WT and MUT probes as standards. For the Y181C codon, we found a maximum of 8% ligation yield corresponding to 2% probes ligated after 10-cycle ligation. For the 100% MUT sample, there was no signal gain after 6-cycle ligation (**Figure 6.9B**). This level of MUT signal was still in the dynamic of the ELISA, so this observation of plateau signal post six cycle was not due to signal saturation in our measurement. For the 5% MUT sample, we observed linear signal amplification until the 10th cycle, but the OD of 0.5 at the 6-cycle ligation is detectable by the 3rd generation paper-based detection.

© Copyright 2021 | N Panpradist

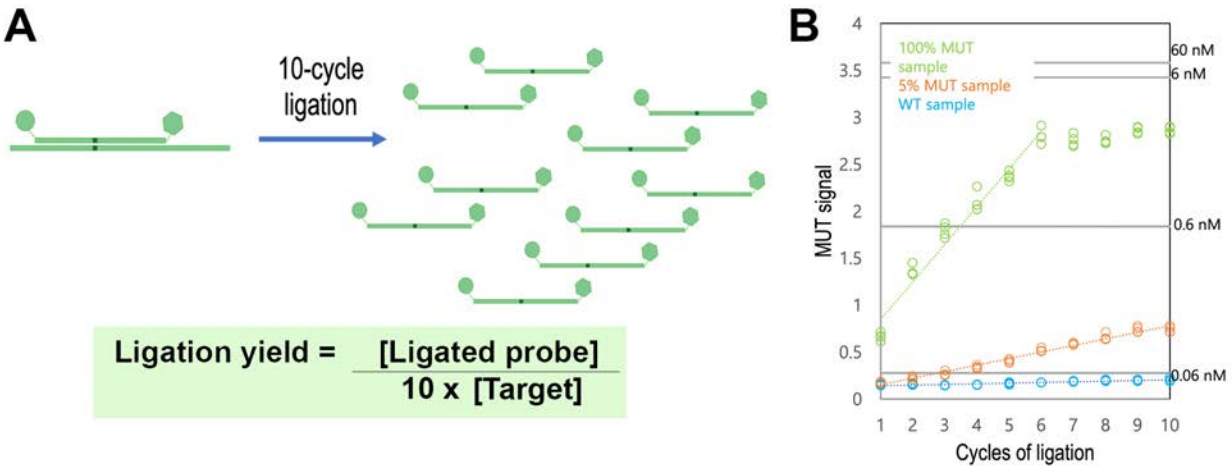

Figure 6.9 | Ligation yield of Y181C mutation assay.

We further investigated the rationale for such a low ligation yield. Successful ligation depends on (i) two matched probes hybridize at the SNP, and (ii) ligase enzyme covalently links the two matched probes (**Figure 6.10**). In step (i), two side reactions could occur in which mismatched probes hybridize at the SNP (competitive side reaction 1) or the ligated probes of the previous run with higher affinity re-anneal to the template (competitive side reaction 2). A separation of WT and MUT probe into two ligation reactions would avoid the competitive side reaction of the mismatched probe. The re-annealing of the ligated probes is not dominant in early cycles of ligation since the unligated probes are present at a much higher concentration. However, as the ligation reaction progresses, the ligated probes have a higher concentration and could outcompete the unligated probes. In step (ii), the complementary strand of the DNA template can displace the unligated probes via toehold-mediated strand displacement (competitive side reaction 2). To overcome this issue, we must ensure that the ligation occurs fast to avoid probe displacement by the

© Copyright 2021 | N Panpradist

complementary strand of the target. Importantly, if we could generate an ssDNA template for the probe to anneal without competing with its complementary strand, this should drive the overall ligation yield since we increase the target without promoting the competitive side reaction 3.

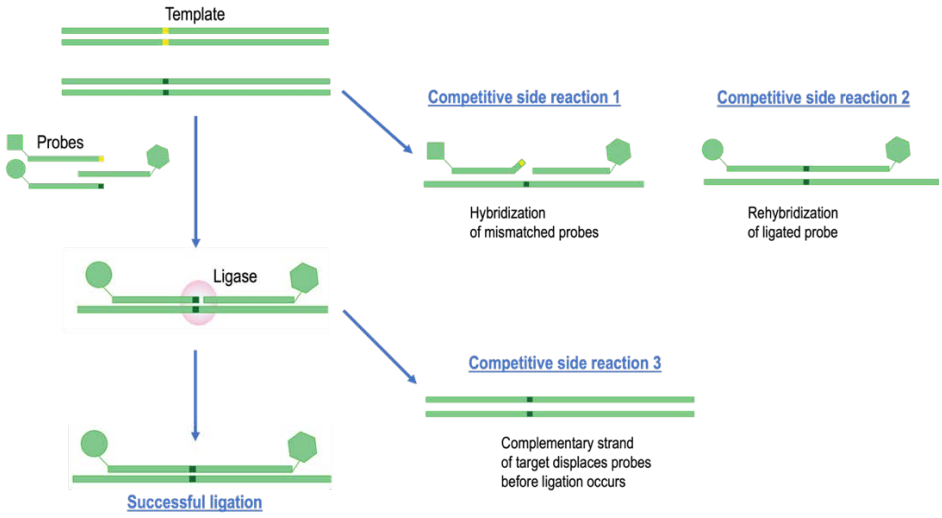

Figure 6.10 | Ligation reaction and its competitive side reactions.

6.3.2 VARIABLE LIGATION YIELD ACROSS MUTATIONS

In addition to ligation yield, we also observed a variable ligation yield across 6 mutations despite starting with the same concentration of ligase, probe, and target. K103N and V106M are strong reacting codons, but if adding too much ligase enzyme, we observed non-specific ligation. G190A yielded strong and specific ligation, while Y181C and M184V have lower yields, with K65R the weakest ligation signal. Ingrid Beck (Frenkel lab) overcame this problem via an iteration of empirical optimization varying ligation probe concentrations and enzyme ligase to achieve. Addressing high polymorphism in the HIV genome in the probe region, Ingrid added up to 2 mixed bases in the other regions of the probe to minimize the T_m reduction due to additional mismatches in the

© Copyright 2021 | N Panpradist

probe region. This probe design was used in conjunction with a low ligation temperature (37 °C) to ensure the hybridization of these mismatched probes.

6.3.3 FACTORS IMPACTING THE LIGATION YIELD, SENSITIVITY, AND SPECIFICITY.

Effect of probe melting temperatures

We noticed that the T_m of both MUT and COM probes are nearly 30 °C higher than the ligation reaction for the codons that have strong ligation reaction but tend to generate false ligation signal (**Table 6.4A**), while the T_m of one or both of the probes are 5 °C lower in the codon with strong but specific ligation (**Table 6.4B**) and weak ligation (**Table 6.4C**). During the ligation reaction, the probes with higher T_m will anneal to the template firs,t and giving a longer period for the ligase to interact at the probe juncture would be longer. However, we are unsure about this effect since the cooling rate of a thermal cycler is ~4°C/s.

Table 6.4 | Probe melting temperature (predicted by IDT OligoAnalyzer), categorized by the assay sensitivity and specificity

A. Strong ligation signal codon with low-specificity mutation:

K103N probes (version 2018):

/56-FAM/CATCCAGC**R**GGG**Y**TAAAAAAGAA**Y** |

/5Phos/AAATCAGT**R**ACAGTACT**R**GATGTGGG/3Bio/

(Tm: 66.4 – 69.6°C | 66.2 – 69.6 °C)

V106M probes (version 2018):

© Copyright 2021 | N Panpradist

/56-FAM/CCAGCAGGGTTAAAAAAGAAAAAATCAA |

/5Phos/TRACAGTACTRGATGTGGGGGATGCATAT/3Bio/

(Tm: 66.5 °C | 68.5 – 71.6 °C)

B. **Strong ligation signal codon with high-specificity mutation**

G190A probe (version 2018):

/56-FAM/CATGGATGA**Y**TTGTATGT**R**GC |/5Phos/ATCTGA**Y**TTAGAAATAGGGCAGCA/3Bio/

Tm: 61.6– 65.3°C | 66.6– 67.8 °C)

C. Low signal codons

Y181C probes (version 2018):

/56-FAM/AAAAAATCCAGAAATA**R**TTAT**Y**TG |/5Phos/**Y**CAATACATGGATGA**Y**TTGTATGTA/3Bio/

(Tm: 58.2– 60°C | 62.5– 63.9 °C)

M184V probes (version 2018):

/56-FAM/ATCCAGAAATA**R**TTATCTATCAATA**Y**G|/5Phos/TGGATGA**Y**TTGTATGTAGGATCTGA

/3Bio/

(Tm: 61.1– 63.5°C | 65.9 - 66.9 °C)

Melting temperature prediction of the ligation probe

Melting temperature (T_m) is the temperature at which 50% of DNA template is bound to the probe. Typically, the reaction is run at 5°C lower than the Tm of the probe to achieve 100% hybridization of the template. The Frenkel lab uses the IDT Oligoanalyzer to predict the melting temperature of the ligation probe, while this program is mainly used to predict the melting temperature of the primers in PCR. In this section, I investigated the Tm of the probe and the temperature range in which the probability of DNA bound to the probe in the context of our OLA assay.

The stability of the probe-template duplex at each temperature can be estimated using the nearest neighbor's method[27, 28]. The Tm can be defined

© Copyright 2021 | N Panpradist

based on the thermodynamic relationship of a bimolecular reaction of probe hybridized to a template with two-state assumption, the Tm is:

$$T_m = \frac{dH}{dS - R*\ln\left(\frac{1}{([Pr]_0 - 0.5[DNA]_0)}\right)}$$

Tm = melting temperature in Kelvin.

R = the gas constant (1.987 $cal.K^{-1}.mole^{-1}$).

dS = entropy of the DNA probe

dH = enthalpy of the DNA probe.

Standard values of dS and dH are estimated at 1M NaCl.

$[Pr]_0$ = the initial concentration of primer DNA.

$[DNA]_0$ = the initial concentration of primer DNA template.

dS and dH values are dependent on salts and can be corrected based on the concentration of monovalent and bivalent salts [29,30]

IDT Oligo Analyzer assumes the concentration of primer is much higher than the target, and thus the term $[Pr]_0 - 0.5[DNA]_0$ can be approximated as $[Pr]_0$. However, in the ligation reaction, the difference of probe and primer concentrations is within an order of magnitude, so the approximation would not apply. To facility the calculation, I wrote a MATLAB algorithm with a GUI that takes an input of the concentrations of probe ($[Pr]_0$), target ($[DNA]_0$), salts and dNTP, and probe sequence accommodating mix bases (**Figure 6.11**). The output provides the dS and dH at the specific salt and dNTP concentrations along with the melting temperature of the bimolecular and unimolecular reaction. In this example of sequence, we predicted 62°C for the Tm of

© Copyright 2021 | N Panpradist

bimolecular reaction for probe-template duplex, which is very close to 60°C for the Tm predicted by the IDT Oligoanalyzer (**Figure 6.12**). However, our prediction for the unimolecular reaction did not include the impact of secondary structure and stress in the loop and overestimated the Tm by 8°C. See **Supplementary Information Chapter 6** for the MATLAB code.

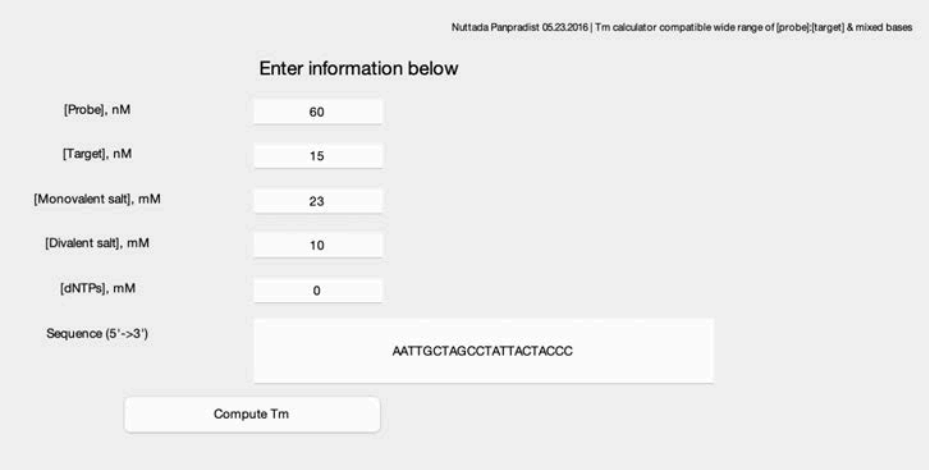

Figure 6.11 | Example of input MATLAB GUI for ligation probe Tm calculation.

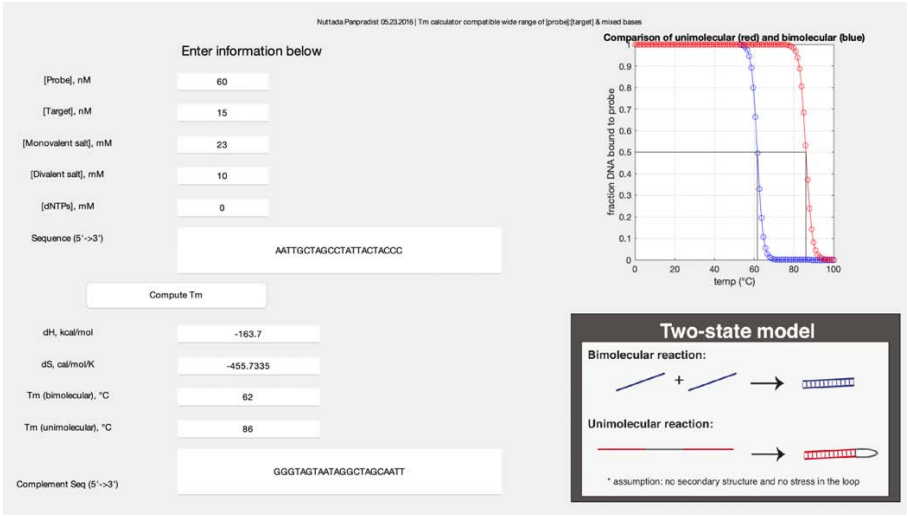

Figure 6.12 | Example of output MATLAB GUI for ligation probe Tm calculation.

Additionally, my current MATLAB melting temperature prediction does not account for the effect of the excipients used in the lyophilized ligation

© Copyright 2021 | N Panpradist

mixture. To obtain the precise Tm, we could measure it empirically by measuring the melt profile that can be visualized by an intercalating dye Evagreen preferably binds the DNA duplex. To run melt analysis, Evagreen is mixed with the probe and its complementary sequence to mimic the DNA template in the actual buffer context.

Effect of probe secondary structure

The analysis of the secondary structure of these ligation probes revealed a possible cause of ligation variation. For the K103N codon(one of strong ligation reaction codons, **Table 6.4A**), the MUT probe (**Figure 6.13A**) and Common probe (**Figure 6.13B**) have very minimal secondary structure with 3' end MUT probe and 5' end COM probe available to anneal to the template. On the other hand, the MUT probe (**Figure 6.13C**) and COM probe (**Figure 6.13D**) of the Y181C codon (weak ligation reaction, **Table 6.4C**) have a lot of secondary structure. The 5' end of MUT probe is self-folded and is not available to anneal to the template. Similarly, most bases in the 3' end of COM probe is also self-folded. These secondary structures would likely impact the ligation yield, as bimolecular reaction of template: probe hybridization is outcompeted by a more thermodynamically stable unimolecular secondary structures within the probes.

© Copyright 2021 | N Panpradist

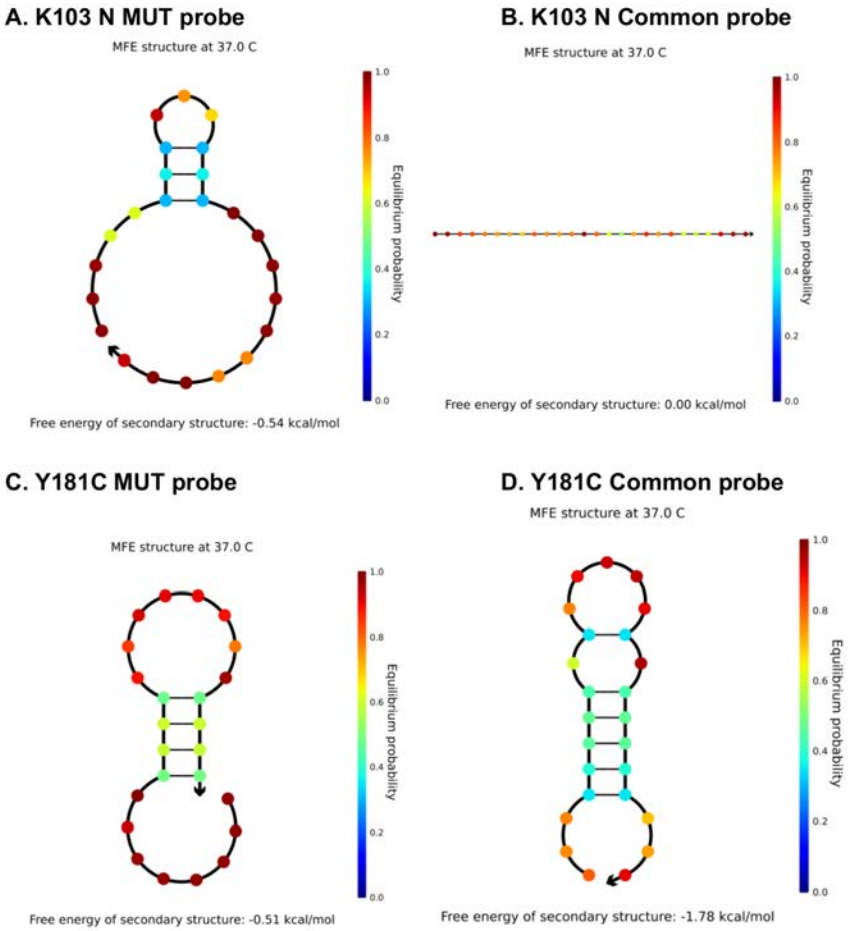

Figure 6.13 | Example of secondary structures in the ligation probes predicted by NuPack.

In **Chapter 11**, we applied an approach to intentionally introduce the mutation in the bases far from the SNP target to eliminate the secondary structure in the native HIV sequence probe. Alternative, a high concentration of 3’ blocked short DNA sequences (complementary to the probe except the region of the SNP) can be used to block the probe and later displaced via toehold mediated strand displacement by the template.

Effect of reaction temperatures on both probe and ligase

© Copyright 2021 | N Panpradist

Table 6.5 shows the summary of the anticipated impact of temperature on probes and ligase. DNA-dependent ligase (TTh) has optimal activity at 68 °C, while the Tm of the probes is ~60 °C for the Y181C codon.

Table 6.5 | Predicted ligation behaviors based on the reaction temperatures.

Reaction Temperature	Probe (Tm = 60C)	Ligase (T optimal = 68C)	Expected outcome
55C	**Optimal** annealing	**Fast** pace	**High true** ligation Low false ligation
37C	Suboptimal annealing (non-specific hybridization)	Slow pace	Low true ligation Low false ligation

Next, we measured the ligation specificity and sensitivity in the ligation mixture in the presence of ssDNA (0%, 10%, 100% Y181C MUT/WT templates). After a 5-minute incubation at 37°C (current ligation temperature) to 55°C (optimal annealing temperature of probes with faster ligase activity). Indeed, we found that the sensitivity of MUT detection increases as the temperature increases (**Figure 6.14**). A 5-minute ligation at a higher temperature showed the MUT signal in 10% and 100% MUT ssDNA target, near or comparable to the traditional 10-cycle ligation using dsDNA 100% MUT template. This promotes the idea that ligation can be isothermal when ssDNA is used. Interestingly, in terms of specificity, we observed a trend of non-specific ligation (0% MUT) peaked at 43-45°C, where the probe annealed non-specifically (15°C lower than their T_m) and ligase enzyme is more active than 37°C.

© Copyright 2021 | N Panpradist

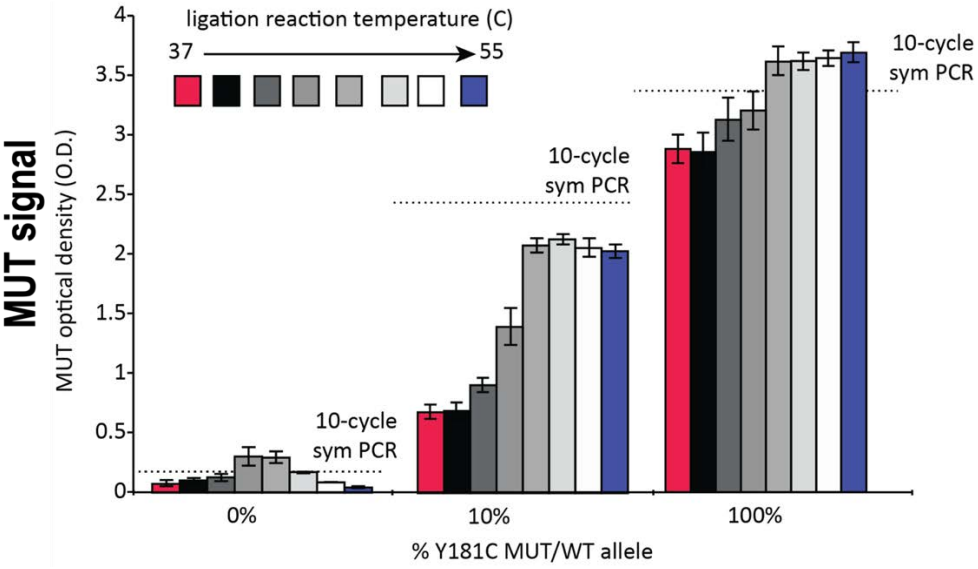

Figure 6.14 | Effect of temperature on the ligation sensitivity and specificity.

Preferentially promiscuous behavior of ligases.

The false positives were found in early-developed ligase-mediated based assays. These assays used a mesophilic ligase enzyme that catalyzes non-template-dependent ligation[31]. The specificity of the ligase-mediated reaction was later improved using a thermostable NAD-dependent ligase that only ligates the base juncture at the nick of the DNA duplex, which results in a 100-fold sensitivity improvement over the mesophilic T4 DNA ligases[32]. Thermostable ligase (*Tth DNA* ligase) is among the first discovered thermostable ligases. It is less specific at discriminating the 5’ end than ehd 3’ end. Thus, this warrants the current design of WT and MUT probes to include the discriminating SNP in the 3’ base. The initial study of wild-type *Tth* ligase enzyme reported

© Copyright 2021 | N Panpradist

non-specific ligation occurred for G3'/5'T and T3'/5'G mismatch (**Figure 6.15**)[33]. Agreeably, the WT and MUT probes of the low-specificity codons (**Table 6.4A**) have these G3'/5'T and T3'/5'G mismatches at the discriminated SNPs.

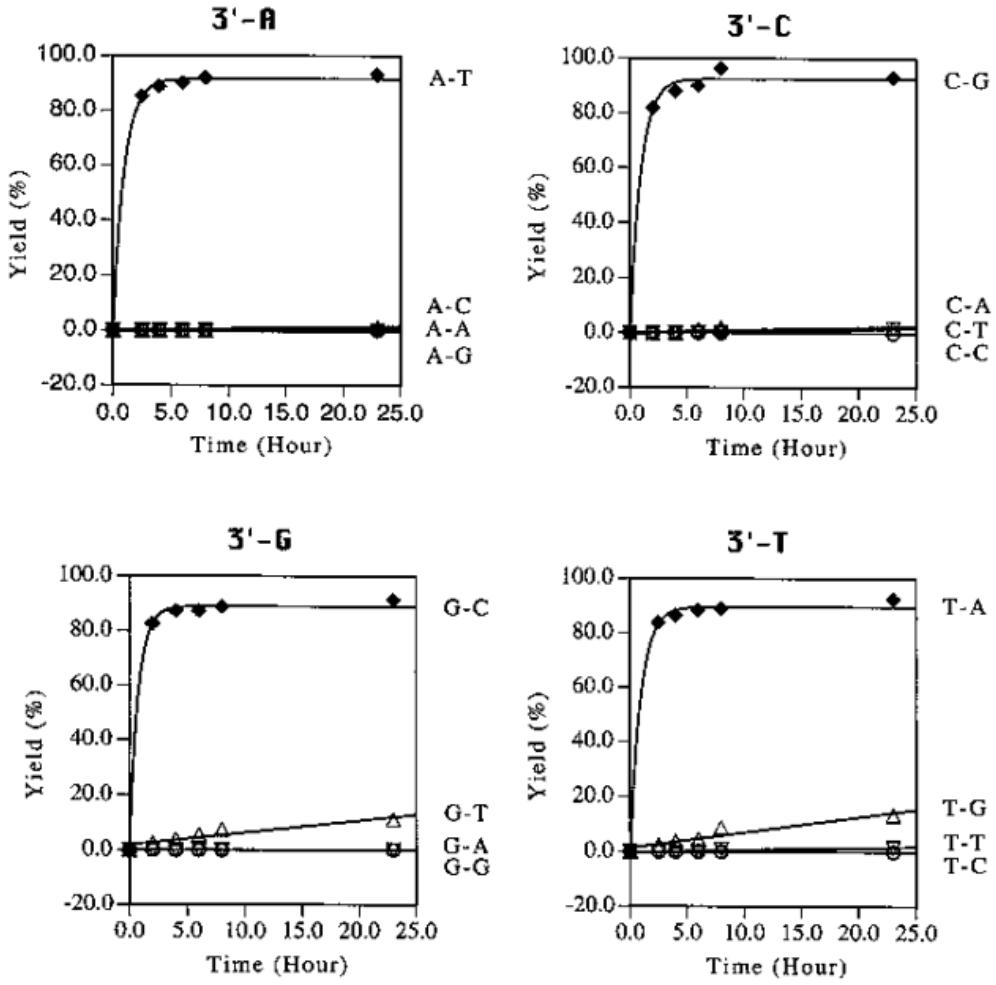

Figure 6.15 | Fidelity of wild-type *Tth* DNA ligase activity

The reaction containing 1mM NAD, 12.5nM nicked DNA duplex substrate, and 0.125nM Tth DNA ligase was incubated at 65°C for 25 hours[33].

© Copyright 2021 | N Panpradist

We used the Ampligase ligase, a proprietary blend of the two thermostable ligases (according to my personal conversation with the manufacturer). It was reportedly more promiscuous than the other two DNA ligases (**Figure 6.16**)[34]. Switching to HIFI Taq DNA ligase would likely lead to a more specific ligation reaction. That said, the company stated that the reaction would be most specific when using a combination of this HiFi Taq DNA ligase enzyme with its proprietary buffer. This would complicate our probe design since we would not be able to straightforwardly predict the melting temperatures and secondary structures without knowing salt concentrations in the buffer. Alternatively, two mutations on the wild-type Tth DNA ligases, K294R and K294P, reportedly could improve the fidelity, and we could generate these ligases in-house instead[33].

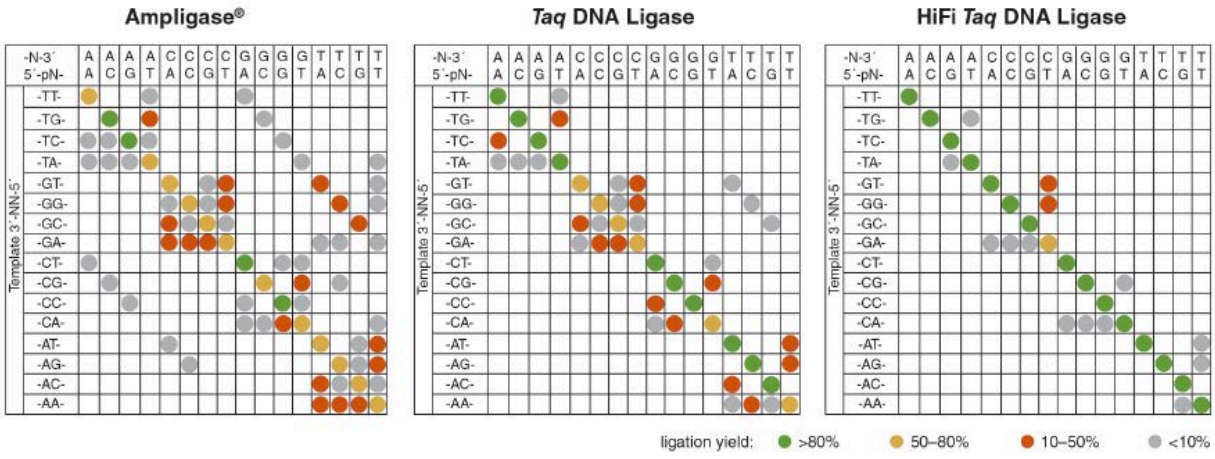

Figure 6.16 | Comparison of ligase fidelity of commercially available ligases [34].

Reaction yield was measured after 3a 0-minute incubation at 55 °C.

© Copyright 2021 | N Panpradist

6.4 STRATEGIES FOR ISOTHERMAL LIGATION (iLDR)

6.4.1 EXONUCLEASE DIGESTION OF THE TEMPLATE AFTER AMPLIFICATION

Lambda exonucleases digest any ssDNA with 5′ phosphorylation. **Figure 6.17** shows the experimental setup where the HIV DNA plasmid containing the M13 primer sites was first amplified using the M13 primers with the 5′phosphorylated forward primers. The 5′ phosphorylated forward strand can then be digested using exonuclease prior to ligation. Gel electrophoreses results showed successful digestion specific to the phosphorylated amplicon (**Figure S6.27** and **Figure S6.28**).

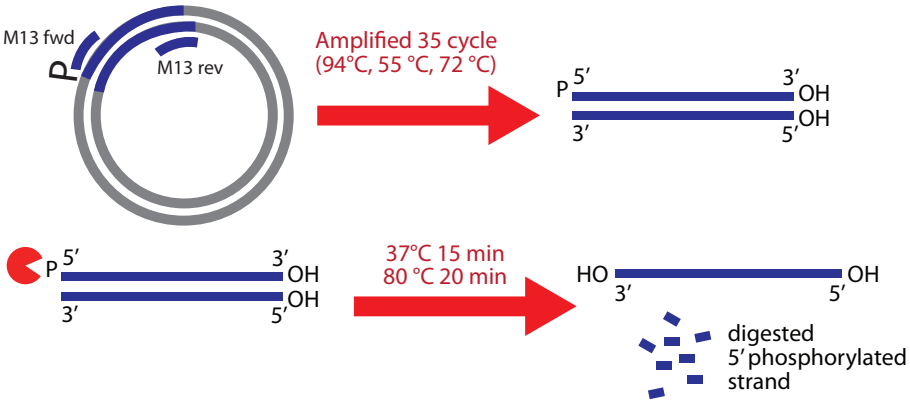

Figure 6.17 | Schematic of lambda exonuclease digestion on phosphorylated amplicon.

6.4.2 ASYMMETRIC PRIMER RATIO IN AMPLIFICATION

Reverse primers can be used in excess to preferentially generate the reverse template that can be readily available to anneal to the ligation step in the downstream iLDR. We found a 1:4 ratio of forward to reverse primers increased the amplification yields in both PCR assay in OLA-Simple 1.0 (**Figure 6.18A**) and tHDA (**Figure 6.18B**). However, the same ratio of primers when applied to RPA RT assay (531 bp) led to weak and failed amplification.

© Copyright 2021 | N Panpradist

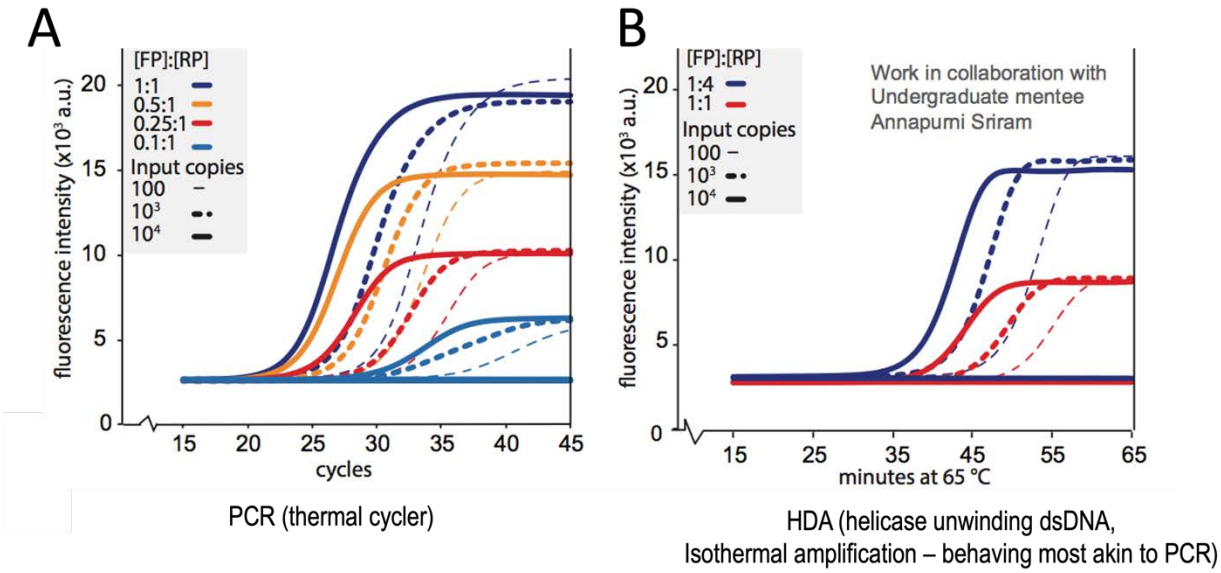

Figure 6.18 | Asymmetric primer ratio in PCR and tHDA.

6.4.3 HELICASE DEPENDENT LIGATION

We envision the use of enzyme helicase to create "isothermal cycling" for ligation. However, the salts required in both reactions are quite different. The ATP-dependent helicase (Thermoanaerobacter tengcongensis) in tHDA uses 4mM $MgCl_2$ while the NAD-dependent DNA Ampligase ligase and *Tth* ligase require 10mM $MgCl_2$. We found that the addition of 6mM $MgCl_2$ to the tHDA reaction to match the 10mM $MgCl_2$ completely inhibits the amplification of HIV DNA. For future investigation, we could investigate alternative helicases from other organisms that are more salt-tolerant could be considered in the future. Regardless, we applied this finding to generate a single-tube amplification and ligation, which will be discussed in **section 6.6 V-OLA 2.0**.

© Copyright 2021 | N Panpradist

6.5 V-OLA 1.0 (FAST SEMI-QUANTITATIVE PCR, iLDR)

V-OLA 1.0 (**Figure 6.19**) shows the vision of the integrated VL and reflexed HIVDR test. First, HIV RNA is analyzed via RT-PCR. The product of RT-PCR can then be visualized through the binding of an intercalating dye Evagreen to duplexed DNA, provide a semi-quantitative signal to differentiate 1000 copies of HIV RNA from 100 copies of HIV RNA. RT-PCR tubes with ≥1000 copies of HIV RNA have then been subjected to the downstream 15-minute isothermal ligation and 15-min detection.

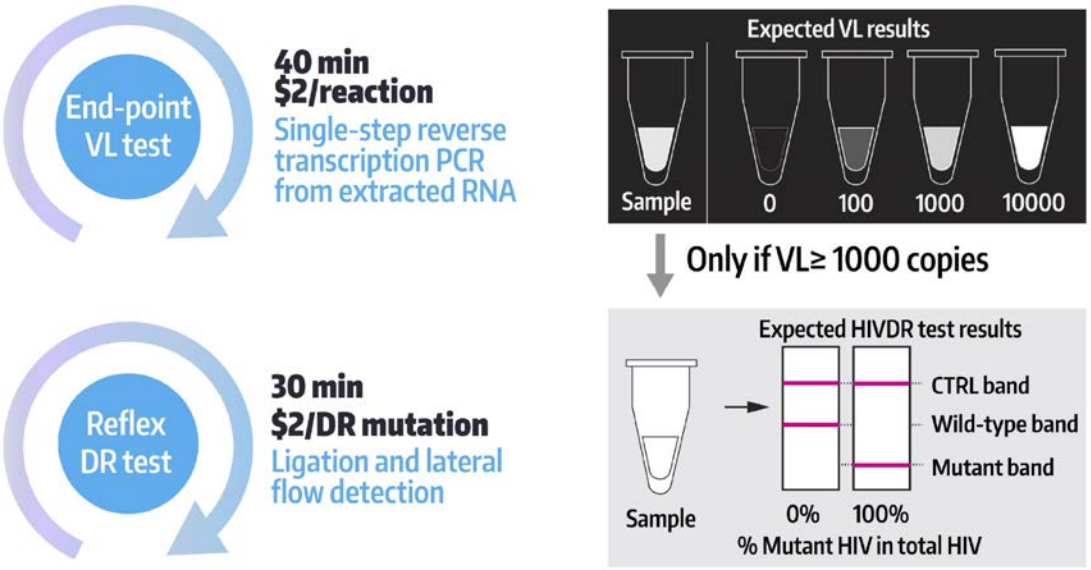

Figure 6.19 | Schema of V-OLA 1.0 workflow.

Here we exploited the combination of the above-described features: asymmetric PCR (**section 6.3.2**) and fast PCR (**section 6.1.1**) to both generate a semi-quantitative VL assay and product for downstream OLA-Simple (bypassing sample collection,

© Copyright 2021 | N Panpradist

extraction, and amplification). **Figure 6.20** shows preliminary results from the amplification of HIV DNA, followed by the detection of HIVDR.

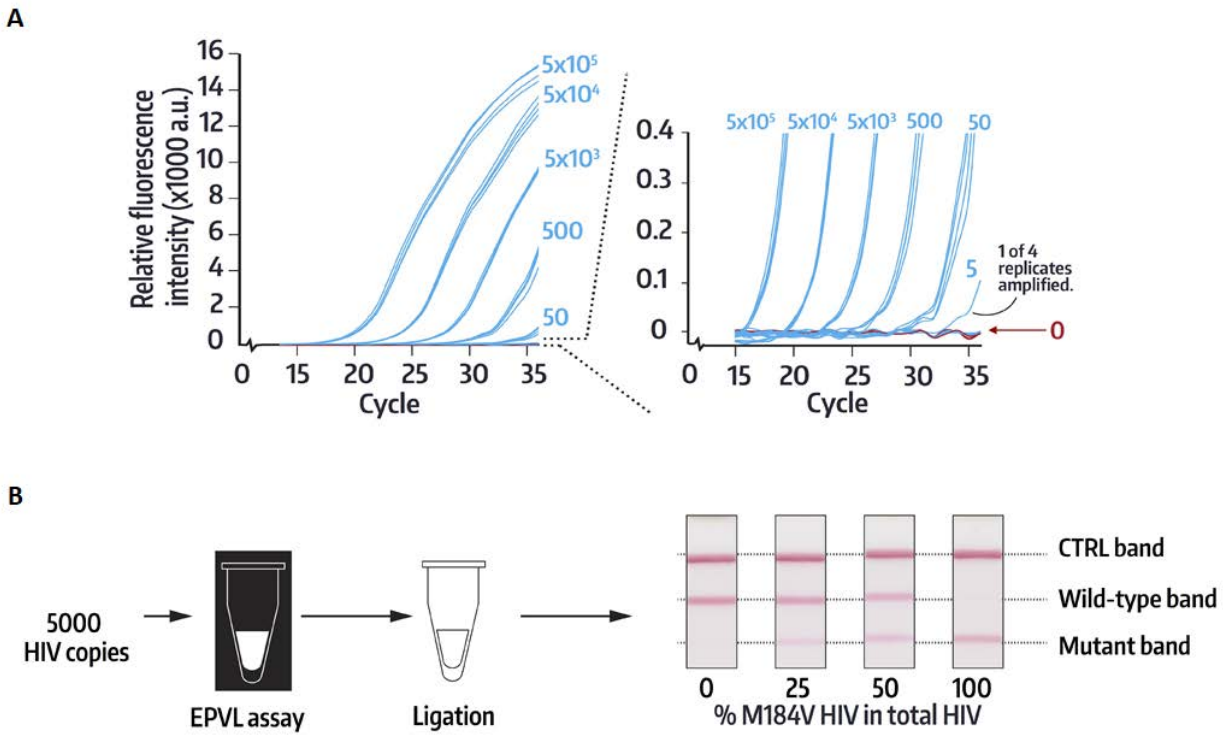

Figure 6.20 | Examples of results of HIV DNA using fast RT-PCR and downstream ligation and detection.

(**A**) Real-time amplification curves of endpoint VL (epVL) RT-PCR assay to amplify HIV DNA of 0 to $5x10^5$ copies/reaction. (**B**) Example of HIVDR analysis directly from the product of the EPVL assay.

The cDNA from patient RNA samples (n=13) were analyzed using our fast epVL PCR assay (compared to the other LTR assay as an extraction control and the RNA analyzed by Abbott m2000, **Figure 6.21**). Our epVL assay accurately estimated 10/13 VL. Two samples fell out of an acceptable variation of measured VL, and one 10-copy sample by Abbott was estimated as <50 copies by epVL assay.

© Copyright 2021 | N Panpradist

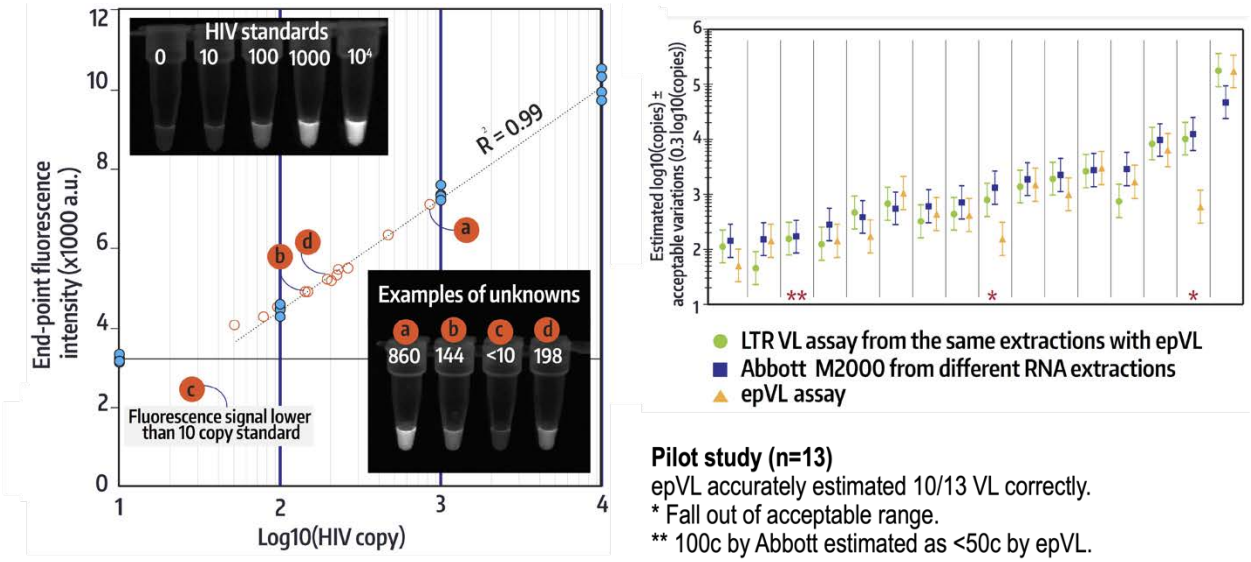

Figure 6.21 | Preliminary results of our endpoint VL fast PCR assay on clinical specimens.

Next, we adapted this fast PCR approach for full-length pol to cover all HIVDR. We switched to another fast polymerase (SpeedStar Hot Start enzyme that can extend at 1 kb/10-the 20s). The preliminary results show we can discriminate 200 copies of HIV DNA/reaction from the no-template control (NTC, **Figure 6.22**), both for real-time and endpoint signals. Our next step is to incorporate the asymmetric primer ratio to partially generate the ssDNA for isothermal ligation.

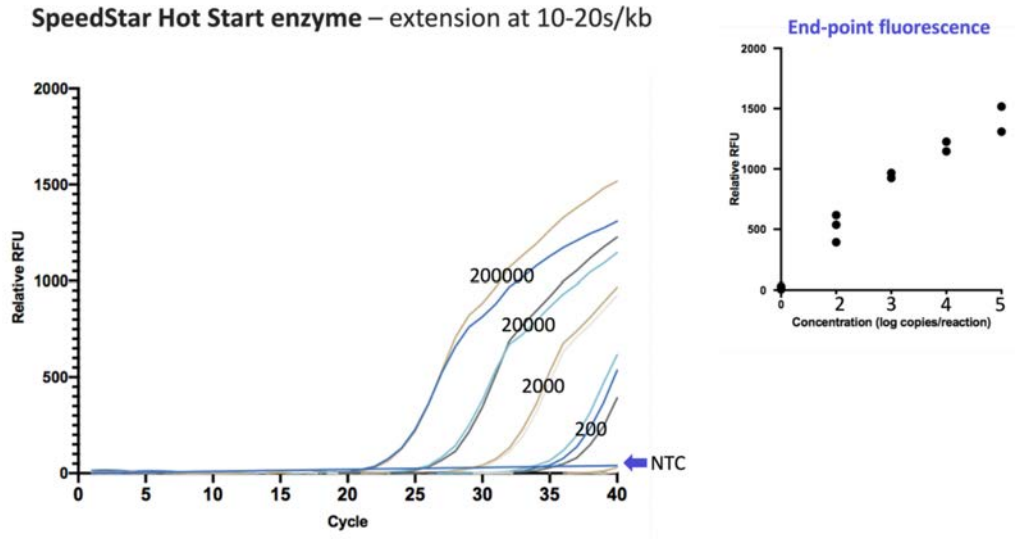

Figure 6.22 | Whole pol endpoint VL fast PCR assay.

© Copyright 2021 | N Panpradist

6.6 V-OLA 2.0 (single-tube quantitative tHDA and iLDR)

In V-OLA 1.0, PCR and ligation cannot be conducted in a single tube because thermostable polymerase can extend the 3’ hydroxyl end of the probes, which inhibits ligation. To avoid this issue, only a small amount of PCR product (1:10 dilution) is added to the ligation reaction. This process, in turn, exposes a high concentration of amplicon and necessitates pre/post PCR space isolation to avoid amplicon carryover contamination.

6.6.1 COMPATIBILITY OF LDR COMPONENT WITH HDA

First, we tested whether it was possible to combine the buffer of the two reactions. We have identified the key components in the LDR: ligase enzyme, NAD enzyme cofactor, and the ligation salt buffer (10mM $MgCl_2$ and 20mM Tris-HCl). One or more component(s) of the LDR was spiked in the HDA reaction to test for compatibility. HDA in the presence of NAD and ligase enzyme showed no inhibition, whereas the ligation salt completely inhibited the HDA at 400 copies HIV/reaction.

6.6.2 COMPATIBILITY OF HDA BUFFER WITH DOWNSTREAM LDR

Buffer incompatibility could result in reduced specificity and sensitivity of LDR. To our knowledge, tHDA amplification products have not been used as the templates for subsequent LDR for SNP testing. To test the HDA buffer compatibility with downstream LDR, the dried ligation mixture (5T1.5PEG1.5PVA) was reconstituted in 1:10 diluted HDA amplicon in water or undiluted HDA amplicon and subjected to the standard ligation protocol. The yield of ligation product from the tHDA amplicon was compared to the standard

© Copyright 2021 | N Panpradist

case where dried ligation mixture was reconstituted with 1:10 diluted PCR amplicon in water. We went on with using the entire reaction of tHDA to rehydrate the ligation reaction. Undiluted HDA amplicon yielded comparable ligated products to the standard case without noticeable non-specificity when 13mM KCl ligation salt was removed.

6.6.3 LIGASE AND NAD ACTIVITY IS MAINTAINED AFTER THDA

NAD, ligase, and tHDA enzymes are the components that require lyophilization, and we first must ensure that ligase and NAD activity remains after being in the presence of the HDA reaction for 90 minutes (**Figure 6.23A**). Either no HIV template (NTC) or 100 copies of wild-type K103N HIV template was added to the HDA reaction in the presence of NAD and ligase. The reaction was incubated for amplification at 65 °C. Subsequently, the tube was inverted, and the dried ligation probe and salt on the lid were dissolved. The reaction was subjected to a 15-minute incubation at 37 °C for isothermal ligation. To eliminate false signal, the solution of competing oligos was added prior to denaturing at 95°C for 30 seconds. The product was detected using lateral flow detection (as described in **Chapter 3**). The strip furthest right showed successful amplification and ligation. Ligase and NAD activity is maintained after 90 minutes of 65 °C incubation (**Figure 6.23B**).

© Copyright 2021 | N Panpradist

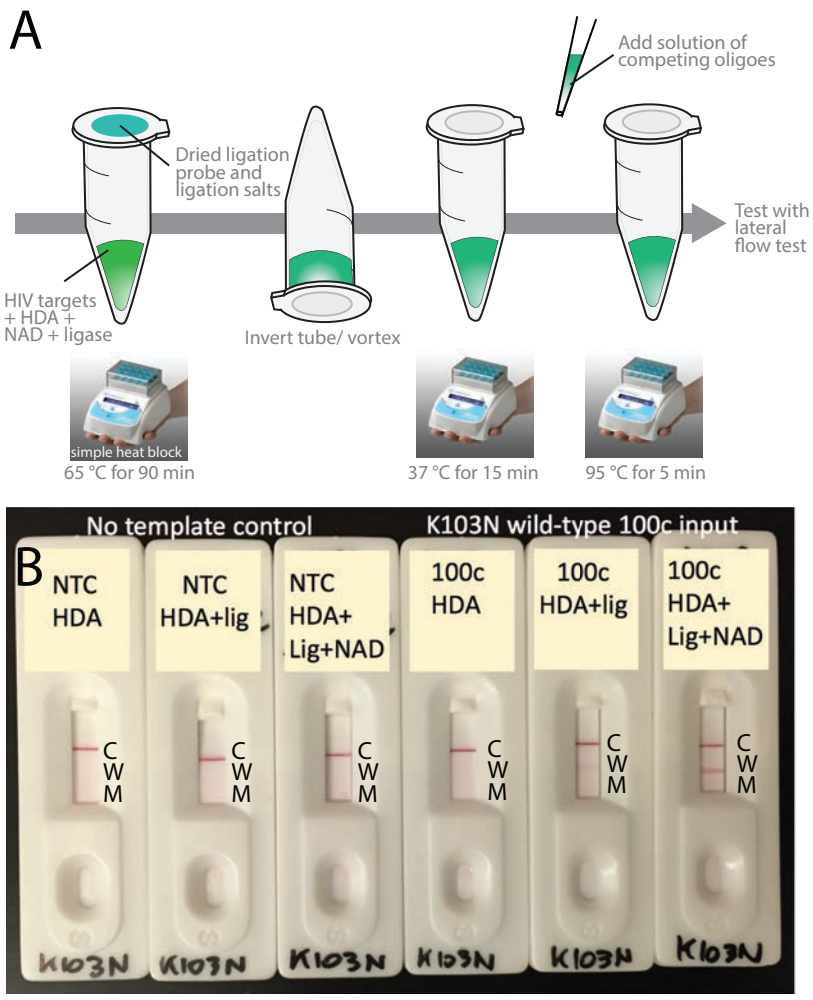

Figure 6.23 | Stability of ligase and NAD during the tHDA.

(**A**) Workflow of single-tube amplification and ligation (**B**) Detection of ligation after product using the proposed workflow with all NAD and ligase added as part of the tHDA reaction and subsequently initiated the ligation via tube inversion.

6.6.4 THE FINAL VERSION OF V-OLA 2.0: SINGLE-TUBE AMPLIFICATION AND ISOTHERMAL LIGATION

The final version contained lyophilized tHDA reaction with ligase, NAD, and ligation probe. Since ligation probes have a lower melting temperature than the HAD reaction, the polymerase cannot extend the 3’ end of the ligation probe. The asymmetric tHDA isothermally amplifies the HIV *pol* gene at 65°C

© Copyright 2021 | N Panpradist

for 50 minutes. After the amplification stage is completed, the tube is inverted to dissolve the salt mixture. The mixture is then incubated at 37 °C for 10 minutes. This step kicks off ligation and simultaneously kills HAD enzymes because ligation salts inhibit the tHDA reaction. Here the competing oligo was added after the completion of the iLDR step and require tube opening. Since then, we have addressed this issue of tube opening in several ways. In Chapter 3.4, we discussed how to integrate the competing oligo as part of the 3rd-generation lateral flow detection without having to open the reaction tube. In Chapter 10, we discussed how to use another approach to put competing oligo in the reaction tube via wax-coated bead.

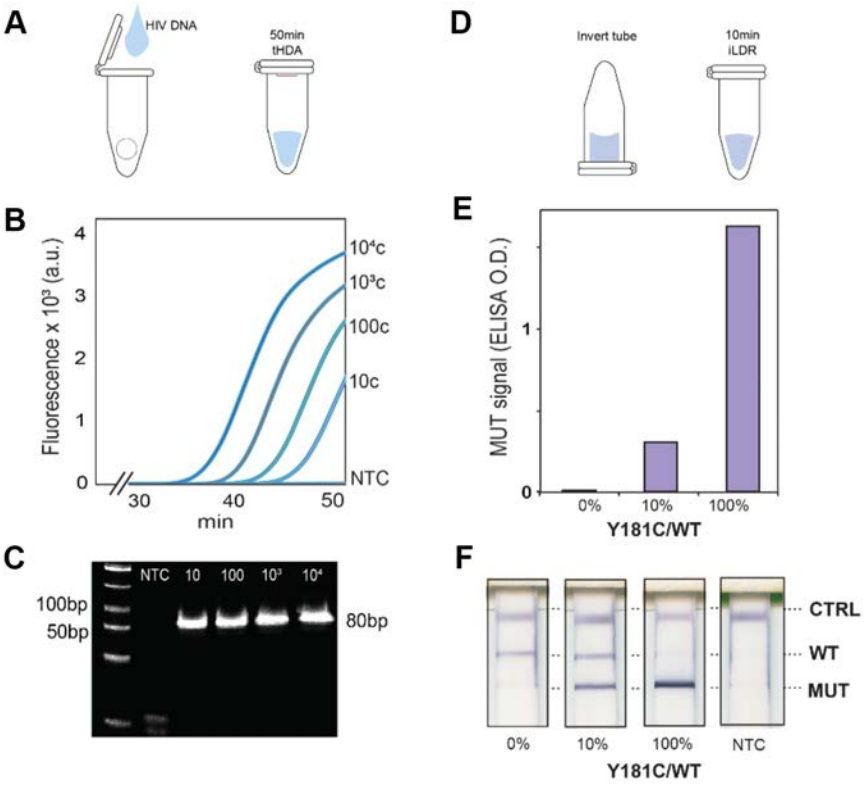

Figure 6.24 | V-OLA 2.0 with completed lyophilized reaction.

(**A)** Schema of the setup of the amplification reaction. HIV DNA is added to rehydrate the tHDA reaction. (**B**) The real-time amplification curves and (**C**) the fragment analysis of the product from tHDA reaction in the presence of NAD,

© Copyright 2021 | N Panpradist

ligase, and ligation probes. (**D**) Schema of the second step to initiate the isothermal ligation. (**E**) Detection of ligation product via ELISA. (**F**) Detection of ligation product via 2nd-generation paper-based detection version AP/purple substrate.

6.7 OLA-Simple 2.0 | Fast RT-RPA and 5-cycle ligation

Here we combined the fast RT-RPA reaction (**section 6.2.3**), 6-cycle ligation (**section 6.3.1**), and 2nd generation of lateral flow detection (**section 3.3**) to achieve a sensitive and specific 1-h OLA-Simple 2.0 from purified RNA (**Figure 6.25**).

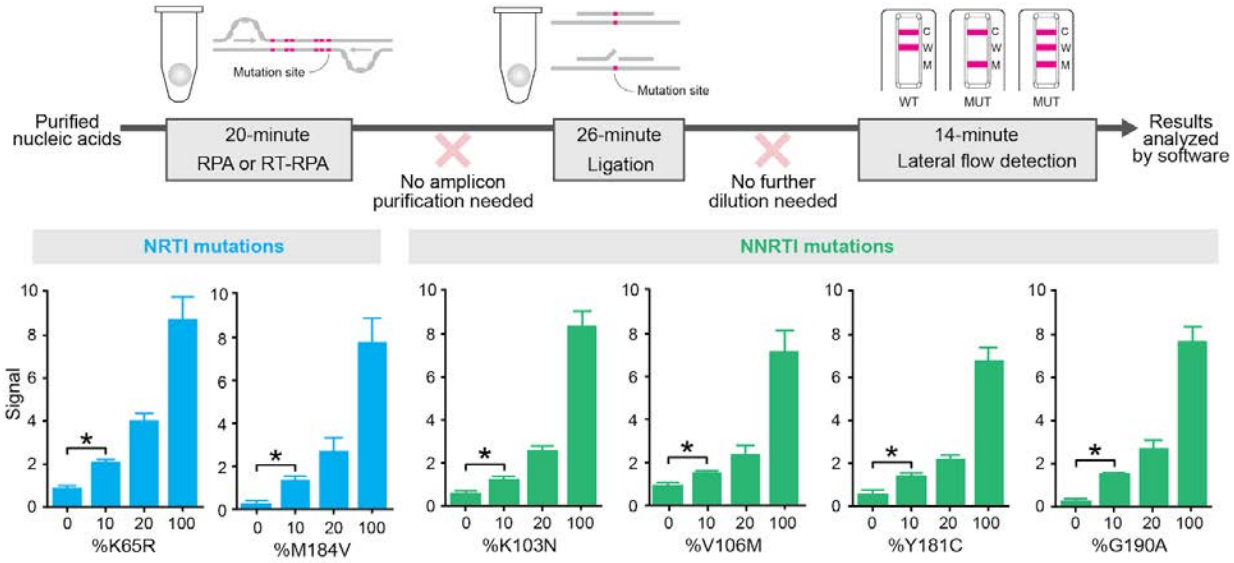

Figure 6.25 | Schema of OLA-Simple 2.0 and its analytical performance.

We validated this workflow on 78 samples derived from patient DNA across subtypes. OLA-Simple 2.0 had 99.0±0.6% concordance to sensitive assays (NGS 1% cutoff or CLIA OLA 2% cutoff) with 98.6±0.8% sensitivity and100% specificity. OLA-Simple 2.0 had 2.98% IND (5 IND matched CLIA-OLA with 1 IND by only OLA-Simple 2.0).

© Copyright 2021 | N Panpradist

As an alternative to the 5-cycle ligation,the RT-RPA assay can be modified to use 5’ phosphorylated forward primers to enable downstream exonuclease digestion and create an ssDNA template for iLDR.

6.8 VL test with low-cost equipment and analysis

HIV RNA was amplified by the RT-LAMP assay (described in **6.2.4**) using the in-house customed heater/reader device. The cell phone application was used to analyze results in real-time. Samples with higher copies of HIV RNA are called positive sooner (**Figure 6.26**).

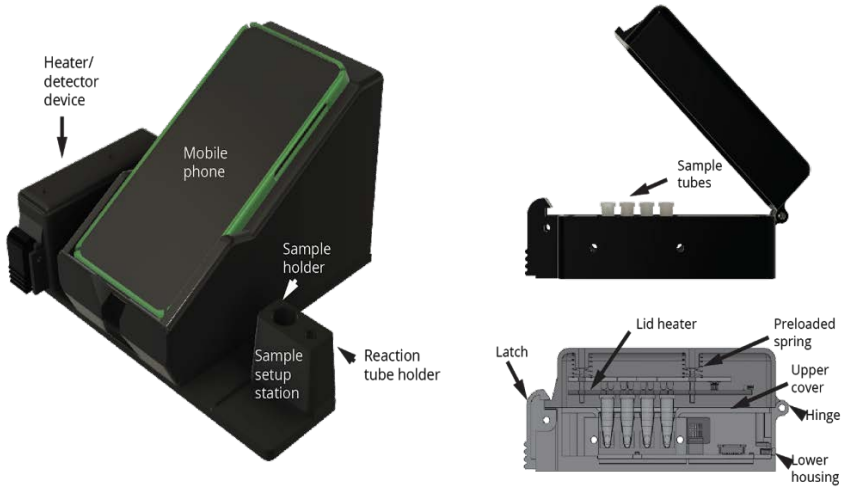

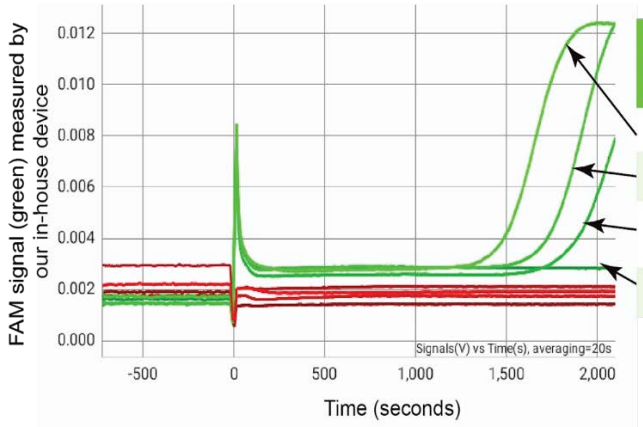

HIV RNA copies/ reaction	Software classification in real-time
18,000	Positive at 22 min
1,800	Positive at 25 min
180	Positive at 29 min
0	Negative at 35 min

Figure 6.26 | Detection of HIV RNA using low-cost heater/reader and cell phone analysis.

© Copyright 2021 | N Panpradist

The mobile phone app (developed by Robert Atkinson) guided the user to load the samples and provided the analysis of positive and negative based on when the signal raised above the baseline. The heater/reader device (developed by Michael Roller) enabled the operation of the RT-LAMP assay. The cell phone and device were originally used in the COVID-19 RNA detection assay (see **Chapter 10** for more details).

© Copyright 2021 | N Panpradist

CHAPTER 6 REFERENCES

1. New England Biolabs One-Step tHDA (thermostable HDA). https://www.neb.com/protocols/0001/01/01/one-step-thda-thermostable-hda.
2. Hosaka, N.; Ndembi, N.; Ishizaki, A.; Kageyama, S.; Numazaki, K.; Ichimura, H., Rapid detection of human immunodeficiency virus type 1 group M by a reverse transcription-loop-mediated isothermal amplification assay. *Journal of virological methods* **2009,** *157* (2), 195-9.
3. Seitz, V.; Schaper, S.; Dröge, A.; Lenze, D.; Hummel, M.; Hennig, S., A new method to prevent carry-over contaminations in two-step PCR NGS library preparations. *Nucleic Acids Research* **2015,** *43* (20), e135-e135.
4. Zanoli, L. M.; Spoto, G., Isothermal amplification methods for the detection of nucleic acids in microfluidic devices. *Biosensors (Basel)* **2013,** *3* (1), 18-43.
5. Craw, P.; Balachandran, W., Isothermal nucleic acid amplification technologies for point-of-care diagnostics: a critical review. *Lab Chip* **2012,** *12* (14), 2469-86.
6. Andresen, D.; von Nickisch-Rosenegk, M.; Bier, F. F., Helicase dependent OnChip-amplification and its use in multiplex pathogen detection. *Clin Chim Acta* **2009,** *403* (1-2), 244-8.
7. Huang, S.; Do, J.; Mahalanabis, M.; Fan, A.; Zhao, L.; Jepeal, L.; Singh, S. K.; Klapperich, C. M., Low cost extraction and isothermal amplification of DNA for infectious diarrhea diagnosis. *PLoS One* **2013,** *8* (3), e60059.

© Copyright 2021 | N Panpradist

8. Chow, W. H.; McCloskey, C.; Tong, Y.; Hu, L.; You, Q.; Kelly, C. P.; Kong, H.; Tang, Y. W.; Tang, W., Application of isothermal helicase-dependent amplification with a disposable detection device in a simple sensitive stool test for toxigenic Clostridium difficile. *J Mol Diagn* **2008,** *10* (5), 452-8.

9. Doseeva, V.; Forbes, T.; Wolff, J.; Khripin, Y.; O'Neil, D.; Rothmann, T.; Nazarenko, I., Multiplex isothermal helicase-dependent amplification assay for detection of Chlamydia trachomatis and Neisseria gonorrhoeae. *Diagn Microbiol Infect Dis* **2011,** *71* (4), 354-65.

10. Walker, G. T.; Fraiser, M. S.; Schram, J. L.; Little, M. C.; Nadeau, J. G.; Malinowski, D. P., Strand displacement amplification--an isothermal, in vitro DNA amplification technique. *Nucleic Acids Res* **1992,** *20* (7), 1691-6.

11. Edwards, T.; Burke, P. A.; Smalley, H. B.; Gillies, L.; Hobbs, G., Loop-mediated isothermal amplification test for detection of Neisseria gonorrhoeae in urine samples and tolerance of the assay to the presence of urea. *J Clin Microbiol* **2014,** *52* (6), 2163-5.

12. Ali, M. M.; Li, F.; Zhang, Z.; Zhang, K.; Kang, D. K.; Ankrum, J. A.; Le, X. C.; Zhao, W., Rolling circle amplification: a versatile tool for chemical biology, materials science and medicine. *Chem Soc Rev* **2014,** *43* (10), 3324-41.

13. Curtis, K. A.; Niedzwiedz, P. L.; Youngpairoj, A. S.; Rudolph, D. L.; Owen, S. M., Real-Time Detection of HIV-2 by Reverse Transcription-Loop-Mediated Isothermal Amplification. *J Clin Microbiol* **2014,** *52* (7), 2674-6.

© Copyright 2021 | N Panpradist

14. Curtis, K. A.; Rudolph, D. L.; Nejad, I.; Singleton, J.; Beddoe, A.; Weigl, B.; LaBarre, P.; Owen, S. M., Isothermal amplification using a chemical heating device for point-of-care detection of HIV-1. *PLoS One* **2012,** *7* (2), e31432.

15. Natoli, M. E.; Rohrman, B. A.; De Santiago, C.; van Zyl, G. U.; Richards-Kortum, R. R., Paper-based detection of HIV-1 drug resistance using isothermal amplification and an oligonucleotide ligation assay. *Analytical biochemistry* **2018,** *544*, 64-71.

16. Lobato, I. M.; O'Sullivan, C. K., Recombinase polymerase amplification: Basics, applications and recent advances. *Trends Analyt Chem* **2018,** *98*, 19-35.

17. TwistDx TwistAmp® DNA Amplification Kits | Assay Design Manual. https://www.twistdx.co.uk/docs/default-source/RPA-assay-design/twistamp-assay-design-manual-v2-5.pdf.

18. Kiefer, J. R.; Mao, C.; Hansen, C. J.; Basehore, S. L.; Hogrefe, H. H.; Braman, J. C.; Beese, L. S., Crystal structure of a thermostable Bacillus DNA polymerase I large fragment at 2.1 A resolution. *Structure* **1997,** *5* (1), 95-108.

19. Toley, B. J.; Covelli, I.; Belousov, Y.; Ramachandran, S.; Kline, E.; Scarr, N.; Vermeulen, N.; Mahoney, W.; Lutz, B. R.; Yager, P., Isothermal strand displacement amplification (iSDA): a rapid and sensitive method of nucleic acid amplification for point-of-care diagnosis. *Analyst* **2015,** *140* (22), 7540-9.

© Copyright 2021 | N Panpradist

20. Vincent, M.; Xu, Y.; Kong, H., Helicase-dependent isothermal DNA amplification. *EMBO Rep* **2004,** *5* (8), 795-800.

21. Motré, A.; Li, Y.; Kong, H., Enhancing helicase-dependent amplification by fusing the helicase with the DNA polymerase. *Gene* **2008,** *420* (1), 17-22.

22. Piepenburg, O.; Williams, C. H.; Stemple, D. L.; Armes, N. A., DNA detection using recombination proteins. *PLoS Biol* **2006,** *4* (7), e204.

23. Li, J.; Macdonald, J.; von Stetten, F., Review: a comprehensive summary of a decade development of the recombinase polymerase amplification. *Analyst* **2019,** *144* (1), 31-67.

24. Boyle, D. S.; Lehman, D. A.; Lillis, L.; Peterson, D.; Singhal, M.; Armes, N.; Parker, M.; Piepenburg, O.; Overbaugh, J., Rapid detection of HIV-1 proviral DNA for early infant diagnosis using recombinase polymerase amplification. *mBio* **2013,** *4* (2).

25. Notomi, T.; Okayama, H.; Masubuchi, H.; Yonekawa, T.; Watanabe, K.; Amino, N.; Hase, T., Loop-mediated isothermal amplification of DNA. *Nucleic Acids Res* **2000,** *28* (12), E63.

26. Rockweiler, T. Loop-Mediated Isothermal Amplification (LAMP) | Primer Design and Assay Optimization. https://www.lucigen.com/docs/slide-decks/Loop-Mediated-Isothermal-Amplification-Design-Primers-Webinar-March-2018.pdf.

27. Breslauer, K. J.; Frank, R.; Blöcker, H.; Marky, L. A., Predicting DNA duplex stability from the base sequence. *Proc Natl Acad Sci U S A* **1986,** *83* (11), 3746-3750.

© Copyright 2021 | N Panpradist

28. SantaLucia, J., Jr., A unified view of polymer, dumbbell, and oligonucleotide DNA nearest-neighbor thermodynamics. *Proc Natl Acad Sci U S A* **1998,** *95* (4), 1460-5.

29. Owczarzy, R.; You, Y.; Moreira, B. G.; Manthey, J. A.; Huang, L.; Behlke, M. A.; Walder, J. A., Effects of sodium ions on DNA duplex oligomers: improved predictions of melting temperatures. *Biochemistry* **2004,** *43* (12), 3537-54.

30. Owczarzy, R.; Moreira, B. G.; You, Y.; Behlke, M. A.; Walder, J. A., Predicting Stability of DNA Duplexes in Solutions Containing Magnesium and Monovalent Cations. *Biochemistry* **2008,** *47* (19), 5336-5353.

31. Barany, F., Genetic disease detection and DNA amplification using cloned thermostable ligase. *Proceedings of the National Academy of Sciences* **1991,** *88* (1), 189-193.

32. Tong, J.; Barany, F.; Cao, W., Ligation reaction specificities of an NAD+-dependent DNA ligase from the hyperthermophile Aquifex aeolicus. *Nucleic Acids Research* **2000,** *28* (6), 1447-1454.

33. Luo, J.; Bergstrom, D. E.; Barany, F., Improving the fidelity of Thermus thermophilus DNA ligase. *Nucleic Acids Res* **1996,** *24* (15), 3071-8.

34. Lohman, G. Substrate specificity and mismatch discrimination in DNA ligases. https://www.neb.com/tools-and-resources/feature-articles/substrate-specificity-and-mismatch--discrimination-in-dna-ligases.

© Copyright 2021 | N Panpradist

6.9 SUPPLEMENTARY INFORMATION FOR CHAPTER 6

Table S6.6 | Primer sequences fast PCR amplification

Underscored bases are the engineered adapters

Primer name	Primer sequences
Fast RT PCR forward 1.0	CCGCAGCCATTGACAGAAGARAAAATAAAAGCA
Fast RT PCR reverse 1.0	CGCCACTGTCCATTTGTCAGGATGGAGTTCATA

Primer design for tHDA (version 2016)

Note: HIVDR SNPs are highlighted in blue. The forward primer is highlighted in purple, and the reverse primer is highlighted in yellow. Underscored bases are the region of ligation probes.

Table S6.7 | tHDA primers for the HIV RT region

Primer region	Primer name	Sequence (5' to 3')
Region 1 containing K65R mutation (114 bp)	Region 1Forward	GGCCTGAAAATCCATACAATA**CTCCAG**
	Region 1 Reverse	CCCAGAAGTCTTGAGTTCTCTTATTAAGTTC
Region 2 containing K103N and V106M	Region 2.1 Forward	
	Region 2.1 Reverse	
	Region 2.2 Forward	
	Region 2.2 Reverse	
Region 3 containing Y181C, M184V, and G190A	Region 3 Forward	GAGCCTTTTAGAAA**ACAAAATCCAGAC**
	Region 3 Reverse	CCTCTATTTTTGTTCTA**TGCTGCCCTA**

Detailed primer design using Primer3 software

Primer set 1 | Amplification of p8E5 region containing codon 65

P8E5 sequence

© Copyright 2021 | N Panpradist

Primer design for tHDA (version 2016)

Note: HIVDR SNPs are highlighted in blue. The forward primer is highlighted in purple, and the reverse primer is highlighted in yellow. Underscored bases are the region of ligation probes.

Table S6.8 | tHDA primers for the HIV RT region

Primer region	Primer name	Sequence (5' to 3')
Region 1 containing K65R mutation (114 bp)	Region 1Forward	GGCCTGAAAATCCATACAATA**CTCCAG**
	Region 1 Reverse	CCCAGAAGTCTTGAGTTCTCTTATTAAGTTC
Region 2 containing K103N and V106M	Region 2.1 Forward	
	Region 2.1 Reverse	
	Region 2.2 Forward	
	Region 2.2 Reverse	
Region 3 containing Y181C, M184V, and G190A	Region 3 Forward	GAGCCTTTTAGAAA**ACAAAATCCAGAC**
	Region 3 Reverse	CCTCTATTTTTGTTCTA**TGCTGCCCTA**

Detailed primer design using Primer3 software

Primer set 1 | Amplification of p8E5 region containing codon 65

P8E5 sequence

5'

TGGCCATTGACAGAAGAAAAAATAAAAGCATTAGTAGAAATTTGTACAGAAATGGAAAA

GGAAGGGAAAATTTCAAAAATTG(GGCCTGAAAATCCATACAATA**CTCCAG**TATTTGCC

ATAAAGAAAAAAGACAGTACTAAATGGAGAAAATTAGTAGATTTCAGAGAACTTAA

TAAGAGAACTCAAGACTTCTGGGAA)GTTCAATTAGGAATACCA**CATCCCGCAGGGTT**

AAAAAAGAAAAAATCAG**TAACAGTACTGGATGTGGGTGATGCATAT**TTTTCAGTCC

CCTTAGATGAAGACTTCAGGAAGTATACTGCATTTACCATACCTAGTATAAACAATGAGA

CACCAGGGATTAGATATCAGTACAATGTGCTTCCACAGGGATGGAAAGGATCACCAGC

AATATTCCAAAGTAGCATGACAAAAATCTTAGAGCCTTTTAGAAAACAAAATCCAGACAT

AGTTATCTATCAATACATGGATGATTTGTGTGTAGGATCTGACTTAGAAATAGGGCAGC

© Copyright 2021 | N Panpradist

ATAGAACAAAAATAGAGGAGCTGAGACAACATCTGTTGAGGTGGGGATTTACCACACCA

GACAAAAAAACACAGAAAGAACCTCCA 3’

Primer3Plus design criteria:

Product size: 80 - 120 bp**

Product T_m: Min. 68; Opt. 71; Max. 75

Primer size: Min. 24; Opt. 27; Max. 33

Primer T_m: Min. 60; Opt. 68; Max. 74

Primer GC%: Min. 35; Opt. 44; Max. 60

Concentration of monovalent cations: 30

Concentration of divalent cations: 3.5

Annealing oligo concentration: 0.05

Concentration of dNTPs: 0.8

Included region: (83, 116)

First primer pair (product length 114 bp)

Primer 1 F: 5’ GGCCTGAAAATCCATACAATACTCCAG 3’ [strand 1]

- Primer 3 T_m: 68.2 °C
- IDT T_m: 63.6 °C
- Self-dimer: ΔG = -9.28 kcal/mole *(Note: no 3’ extensions achievable)*

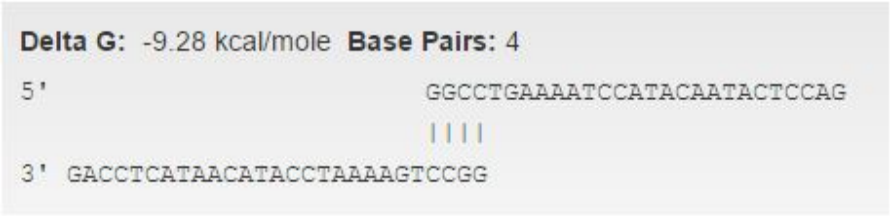

Primer 1 R: 5’ CCCAGAAGTCTTGAGTTCTCTTATTAAGTTC 3’ [strand 2[

© Copyright 2021 | N Panpradist

- Primer 3 T_m: 66.5 °C
- IDT T_m: 63.7 °C
- Self-dimer: ΔG = -5.12 kcal/mole

Delta G: -5.12 kcal/mole **Base Pairs:** 4

```
5'          CCCAGAAGTCTTGAGTTCTCTTATTAAGTTC
               |||| ::   :: ::::
3' CTTGAATTATTCTCTTGAGTTCTGAAGACCC
```

Heterodimer (1R and 1F): ΔG = -4.52 kcal/mole

Delta G: -4.52 kcal/mole **Base Pairs**4

```
5' GGCCTGAAAATCCATACAATACTCCAG
        :::   :     : :   |||| ::
3'      CTTGAATTATTCTCTTGAGTTCTGAAGACCC
```

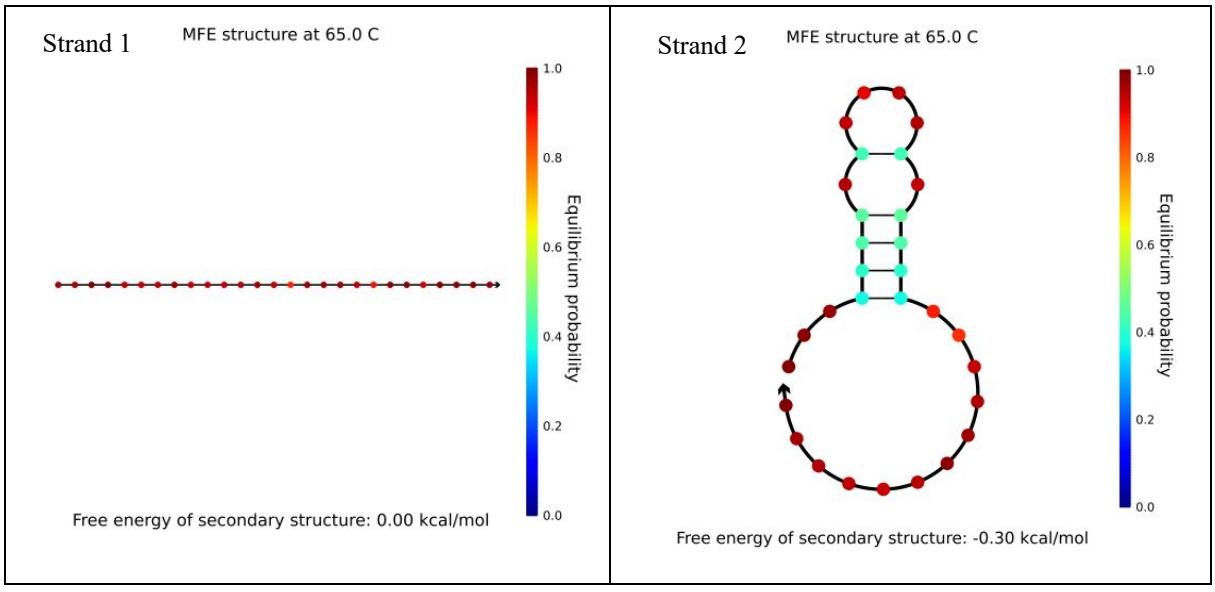

© Copyright 2021 | N Panpradist

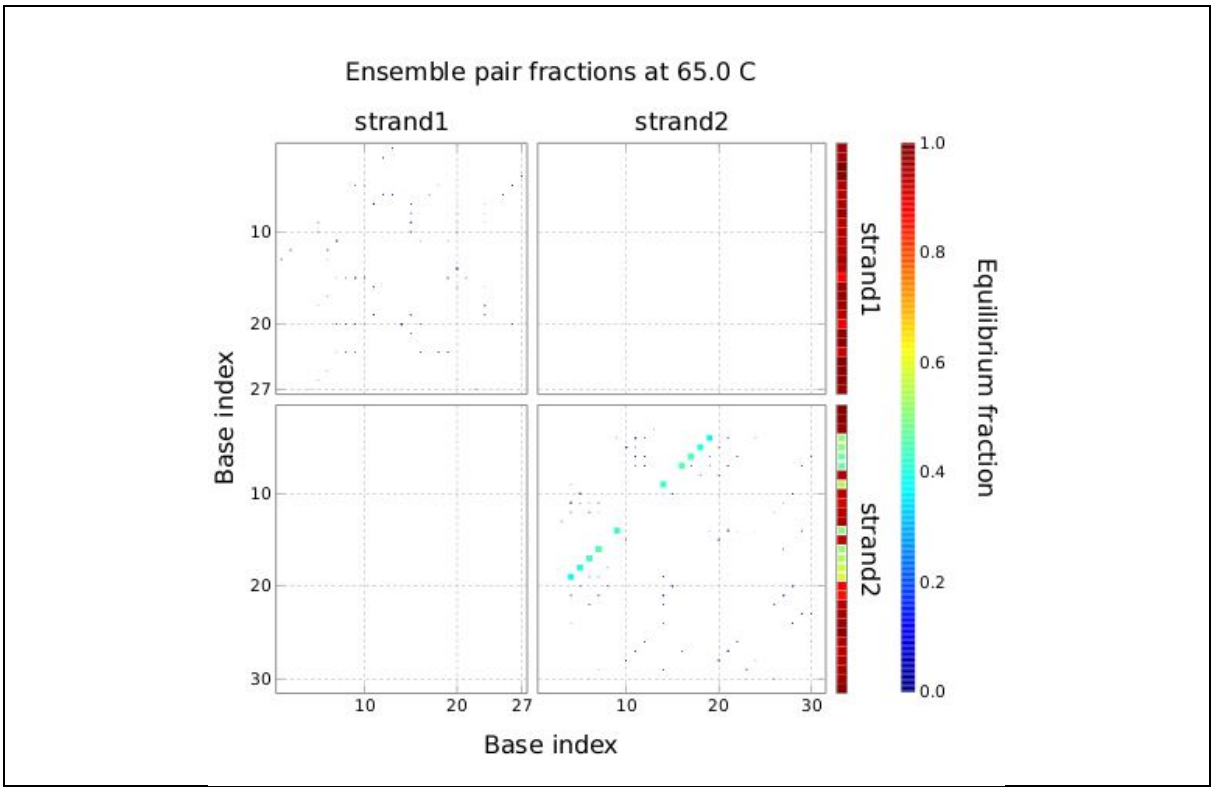

Note: The primers with the fewest number of bases in their final product were chosen. This is because the upper limit of the HDA product size given by the HDA kit used is 120 bases.

Primer set 2 | Amplification of p8E5 region containing codons 103 and 106

P8E5 sequence

5′

TGGCCATTGACAGAAGAAAAAATAAAAGCATTAGTAGAAATTTGTACAGAAATGGAAAA

GGAAGGGAAAATTTCAAAAATTGGGCCTGAAAATCCATACAATA**CTCCAGTATTTGCC**

ATAAAGAAAAAAGACAGTACTAAATGGAGAAAATTAGTAGATTTCAGAGAACTTAATAA

GAGAACTCAAGACTTCTGGGAAGTTCAATTAGGAA[TACCA**CATCCCGCAGGGTTAAA**

© Copyright 2021 | N Panpradist

AAAGAAAAAATCAG**TAA]CAGTACTGGATGTGGGTGATGCATAT**TTTTCAGTCCCC

TTAGATGAAGACTTCAGG]AAGTATACTGCATTTACCATACCTAGTATAAACAATGAGAC

ACCAGGGATTAGATATCAGTACAATGTGCTTCCACAGGGATGGAAAGGATCACCAGCA

ATATTCCAAAGTAGCATGACAAAAATCTTAGAGCCTTTTAGAAAACAAAATCCAGACATA

GTTATCTATCAATACATGGATGATTTGTGTGTAGGATCTGACTTAGAAATAGGGCAGCA

TAGAACAAAAATAGAGGAGCTGAGACAACATCTGTTGAGGTGGGGATTTACCACACCA

GACAAAAAAACACAGAAAGAACCTCCA 3′

Primer3Plus design criteria:

Product size: 80 - 120 bp**

Product T_m: Min. 68; Opt. 71; Max. 75

Primer size: Min. 24; Opt. 27; Max. 33

Primer T_m: Min. 60; Opt. 68; Max. 74

Primer GC%: Min. 35; Opt. 44; Max. 60

Concentration of monovalent cations: 30

Concentration of divalent cations: 3.5

Annealing oligo concentration: 0.05

Concentration of dNTPs: 0.8

Included region: (212, 95)

First primer pair (product length 86 bp)

Primer 1 F: 5′ TACCACATCCCGCAGGGTTAAAAA 3′ [strand 1]

- Primer 3 T_m: 69.1 °C

© Copyright 2021 | N Panpradist

- IDT T_m: 64.6 °C
- Self-dimer: ΔG = -6.14 kcal/mole

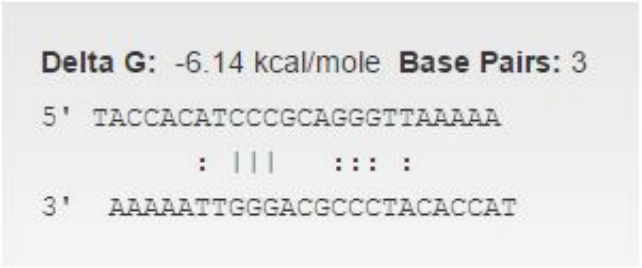

Primer 1 R: 5′ TTCATCTAAGGGGACTGAAAAATATGC 3′ [strand 2]

- Primer 3 T_m: 66.2 °C
- IDT T_m: 62.1 °C
- Self-dimer: ΔG = -5.47 kcal/mole

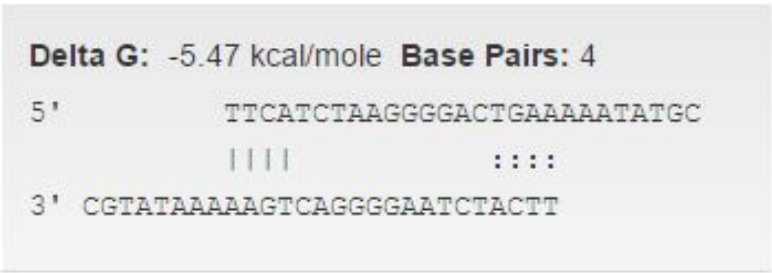

Heterodimer (1R and 1F): ΔG = -7.71 kcal/mole

© Copyright 2021 | N Panpradist

Delta G: -7.71 kcal/mole **Base Pairs**4

```
5'    TTCATCTAAGGGGACTGAAAAATATGC
      :: : :    ||||      :
3' AAAAATTGGGACGCCCTACACCAT
```

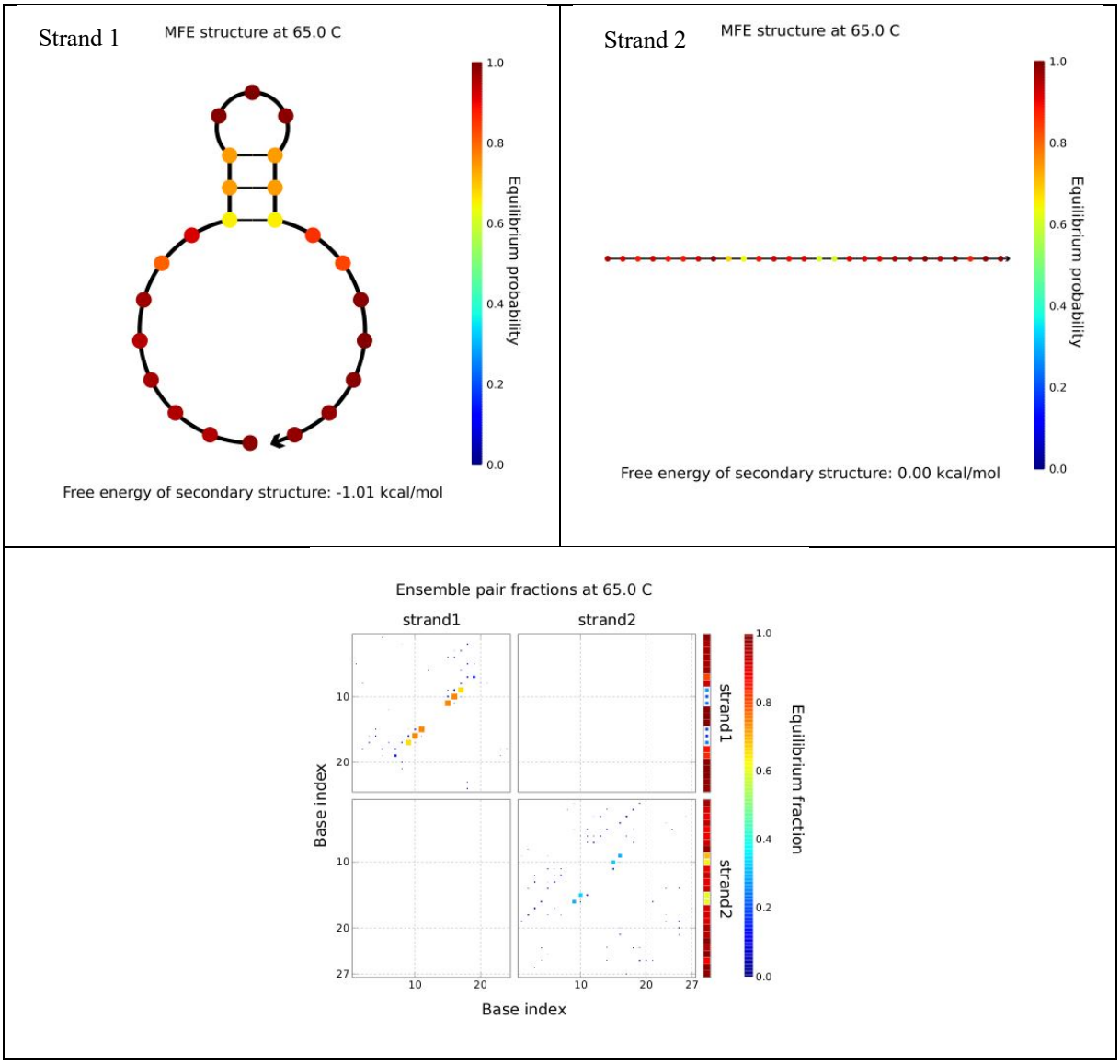

© Copyright 2021 | N Panpradist

Second primer pair (product length 87 bp)

Primer 2 F: 5' TACCACATCCCGCAGGGTTAAAAA 3' [strand 1]

- Primer 3 T_m: 69.1 °C
- IDT T_m: 64.6 °C
- Self-dimer: ΔG = -6.14 kcal/mole

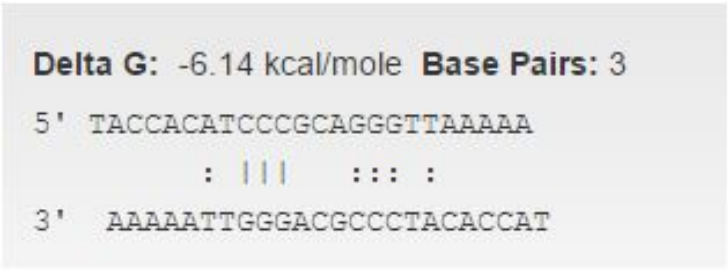

Primer 2 R: 5' CTTCATCTAAGGGGACTGAAAAATATGC 3' [strand 2]

- Primer 3 T_m: 67.1 °C
- IDT T_m: 62.5 °C
- Self-dimer: ΔG = -5.47 kcal/mole

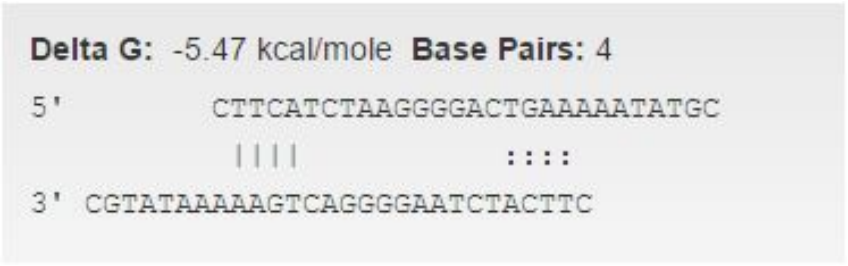

Heterodimer (1R and 1F): ΔG = -7.71 kcal/mole

© Copyright 2021 | N Panpradist

```
Delta G: -7.71 kcal/mole  Base Pairs4
5'        TACCACATCCCGCAGGGTTAAAAA
          :      ||||    : : ::
3' CGTATAAAAAGTCAGGGGAATCTACTTC
```

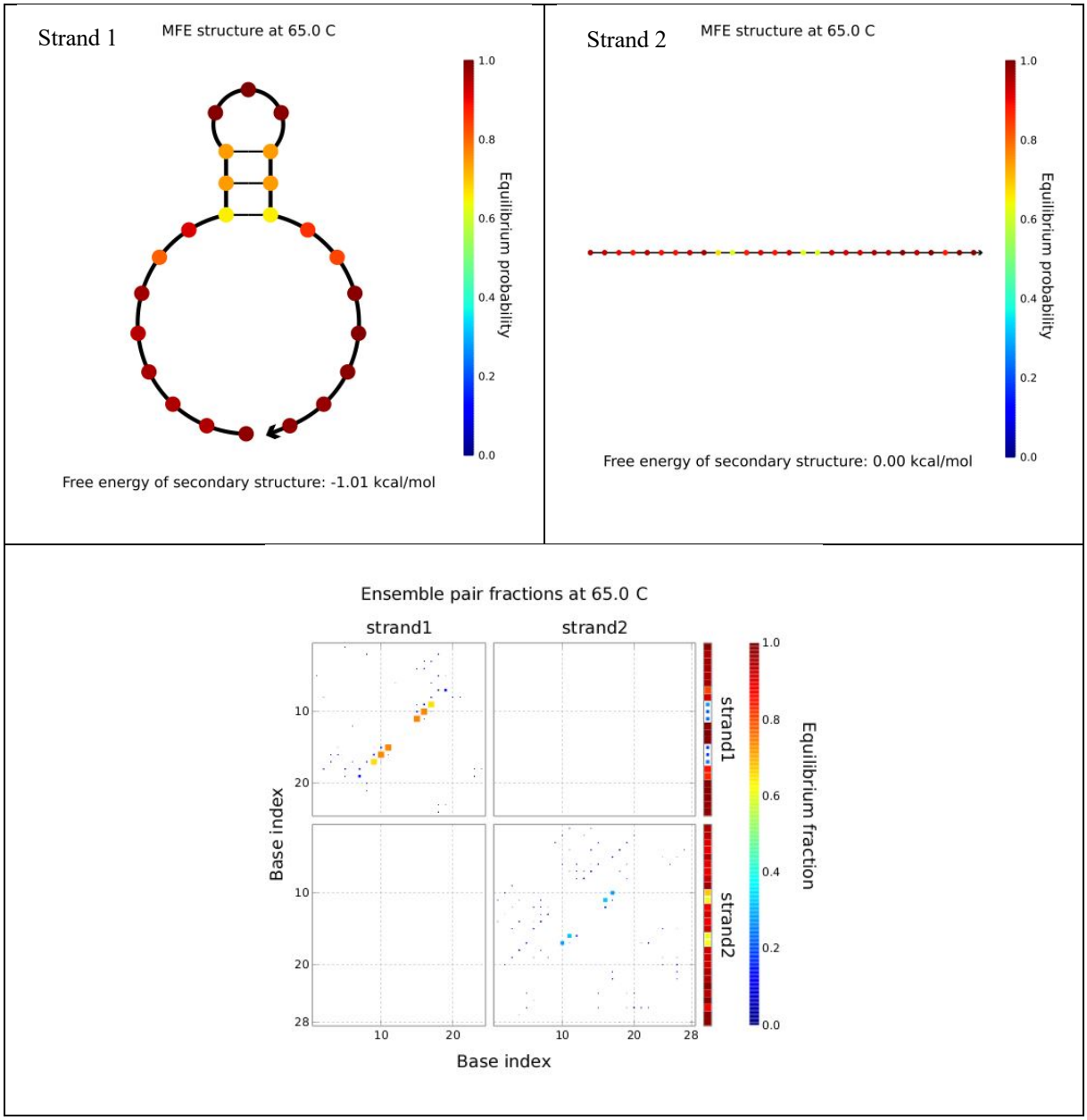

© Copyright 2021 | N Panpradist

Primer set 3 | amplification of p8E5 region containing codons 181, 184 and 190

P8E5 sequence

5’
TGGCCATTGACAGAAGAAAAAATAAAAGCATTAGTAGAAATTTGTACAGAAATGGAAAA
GGAAGGGAAAATTTCAAAAATTGGGCCTGAAAATCCATACAATACTCCAGTATTTGCCA
TAAAGAAAAAAGACAGTACTAAATGGAGAAAATTAGTAGATTTCAGAGAACTTAATAAG
AGAACTCAAGACTTCTGGGAAGTTCAATTAGGAATACCACATCCCGCAGGGTTAAAAAA
GAAAAAATCAGTAACAGTACTGGATGTGGGTGATGCATATTTTTCAGTCCCCTTAGATG
AAGACTTCAGGAAGTATACTGCATTTACCATACCTAGTATAAACAATGAGACACCAGGG
ATTAGATATCAGTACAATGTGCTTCCACAGGGATGGAAAGGATCACCAGCAATATTCCA
AAGTAGCATGACAAAAATCTTAGAGCCTTTTAGAAA**ACAAAATCCAGAC**ATAGTTATC
TATCAATACATGGATGATTTGTGTGTAG**GATCTGACTTAGAAATAGGGCAGC**ATAGA
ACAAAAATAGAGGAGCTGAGACAACATCTGTTGAGGTGGGGATTTACCACACCAGACA
AAAAAACACAGAAAGAACCTCCA 3’

Primer3Plus design criteria:

Product size: 80 - 120 bp**

Product T_m: Min. 68; Opt. 71; Max. 75

Primer size: Min. 24; Opt. 27; Max. 33

Primer T_m: Min. 60; Opt. 68; Max. 74

Primer GC%: Min. 35; Opt. 44; Max. 60

Concentration of monovalent cations: 30

Concentration of divalent cations: 3.5

Annealing oligo concentration: 0.05

Concentration of dNTPs: 0.8

Included region: (447, 81)

First primer pair (product length 106 bp)

Primer 1 F: 5’ GAGCCTTTTAGAAAACAAAATCCAGAC 3’ [strand 1]

© Copyright 2021 | N Panpradist

- Primer 3 T_m: 65.4 °C
- IDT T_m: 61.8 °C
- Self-dimer: ΔG = -5.83 kcal/mole

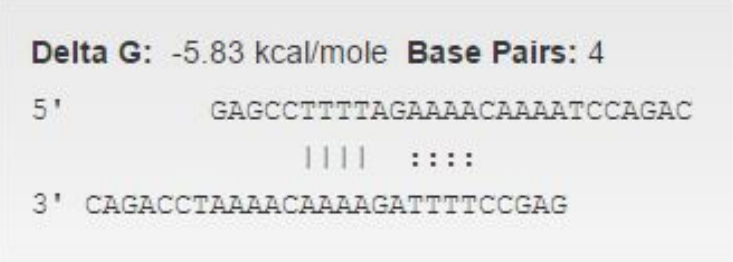

Primer 1 R: 5’ CCTCTATTTTTGTTCTATGCTGCCCTA 3’ [strand 2]

- Primer 3 T_m: 66.5 °C
- IDT T_m: 63.2 °C
- Self-dimer: ΔG = -3.14 kcal/mole

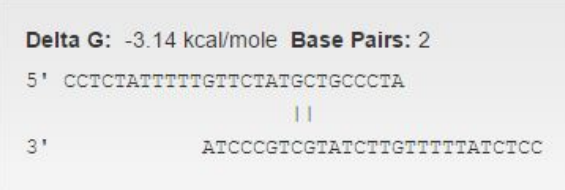

Heterodimer (1R and 1F): ΔG = -11.07 kcal/mole

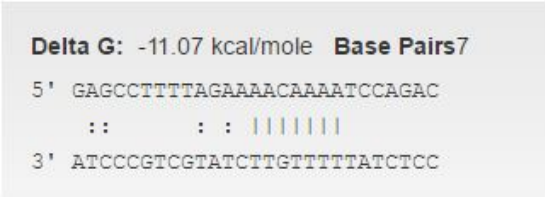

© Copyright 2021 | N Panpradist

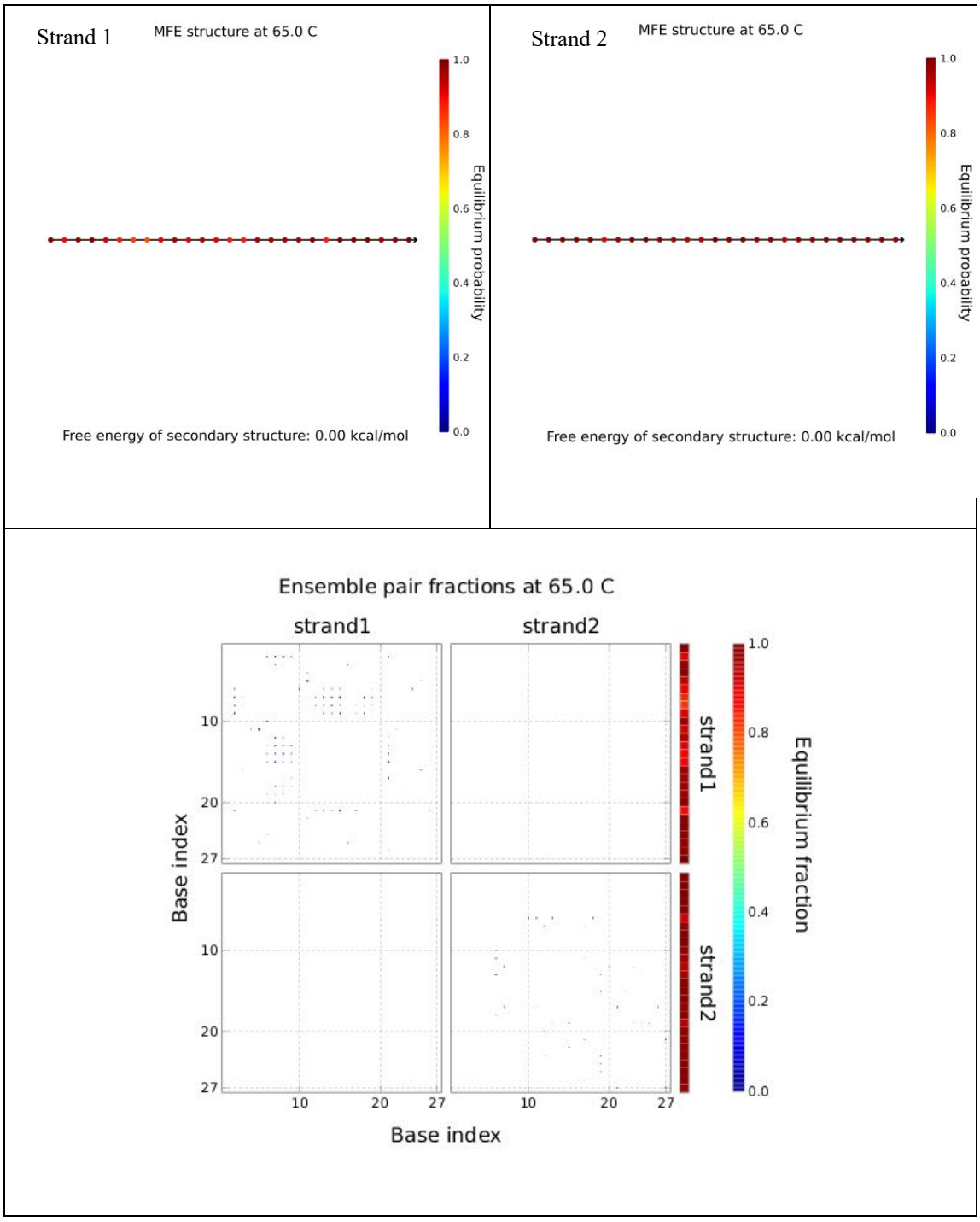

© Copyright 2021 | N Panpradist

Primer design for RPA assay for RT, PI, and INT regions.

Table S6.9 | HIV primers for RPA assays designed by Enos Kline (2017)

Assay	Primer name	Sequence (5' to 3')
RPA RT region (inner primers)	FPv5.2 (inner forward)	GRGGTTCTTTCTGATGYTTYTTRTCTGGTGT
	RPv6 (inner reverse)	AAATTGGGCCTGAAAATC
RPA RT region (outer primers)	FPv3.1 (outer forward)	CCAGCCATTGACAGAAGARAAAATAAAAGCA
	RPv2 (outer reverse)	TCTACTGTCCATTTRTCAGGATGGAGTTCATA

Primer design for HIV RT

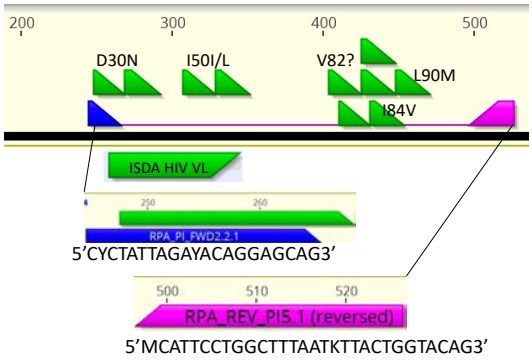

- **90% homology to consensus (5,086 sequences from Los Alamos database 2018)**
- **Amplicon size – 281 bp**
- **Several iterations of design to minim**

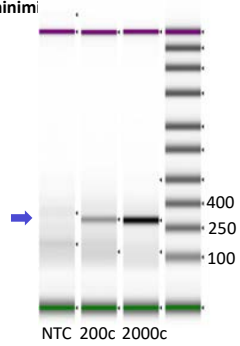

© Copyright 2021 | N Panpradist

Primer design for HIV INT

Omitting 66 and 92 DRMs

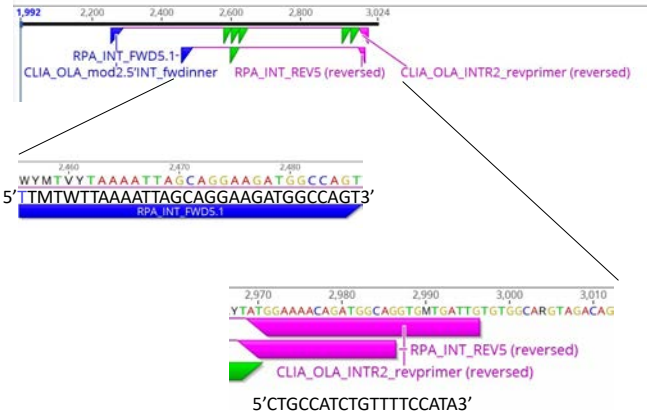

- 90% homology to consensus **(5,086 sequences from Los Alamos database 2018)Amplicon size** – 531 bp
- Several iterations of design to minimize primer dimers

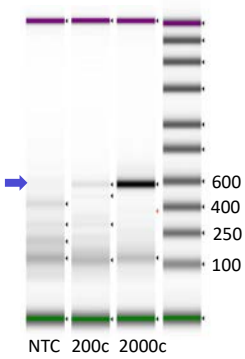

RPA for OLA - INT

Omitting 66 and 92 DRMs

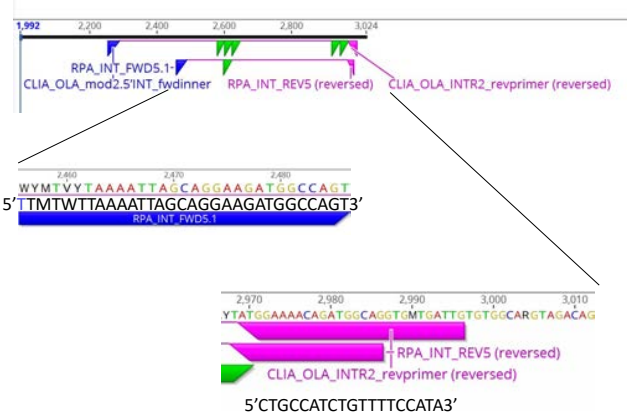

- 90% homology to consensus **(5,086 sequences from Los Alamos database 2018)Amplicon size** – 531 bp
- Several iterations of design to minimize primer dimers

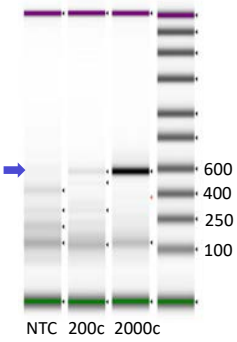

© Copyright 2021 | N Panpradist

MATLAB algorithm to predict the melting temperature of the ligation probe based on nearest neighbor's rule with salt correction.

```
% Nuttada Panpradist 05.22.2016 - 05.23.2016
% Function MyTmCal is a three-layered nested function
% After the user pushes the Tm to compute button, mycallbackfn will be called
% the sequence will be tested if the strands contain wobbles or not to
% select the nested functions (no wobbles vs. wobbles) within the
% mycallbackfn

function MyTmCal
clear all
close all
FigHandle = figure('Position', [100, 100, 1049, 895]);
I = imread('model.tiff');
clf
gl.handles = []; % Setting up a vector of graphical object handles that we can use to
delete them.
% gl.handles is defined in MyTmCal so it should be visible to any nested
% function (e.g. MyCallback).

%axes('position',[0.50,0.56,0.55,0.35])
 %       imshow(I);

% make static text boxes (t = title)
t0 = uicontrol('Style', 'text',...
            'String', 'Nuttada Panpradist 05.23.2016 | Tm calculator compatible wide
range of [probe]:[target] & mixed bases',...
            'Units','normalized',...
            'Position', [0.25 0.95 0.55 0.02], 'FontSize',8);

t = uicontrol('Style', 'text',...
      'String', 'Enter information below',...
      'Units','normalized',...
      'Position', [0.005 0.9 0.55 0.03], 'FontSize',15);
t2 = uicontrol('Style', 'text',...
      'String', '[Probe], nM',...
      'Units','normalized',...
      'Position', [0.005 0.85 0.155 0.03]);
t3 = uicontrol('Style', 'text',...
      'String', '[Target], nM',...
      'Units','normalized',...
      'Position', [0.005 0.80 0.155 0.03]);
t3 = uicontrol('Style', 'text',...
```

© Copyright 2021 | N Panpradist

```
      'String', '[Monovalent salt], mM',...
      'Units','normalized',...
      'Position', [0.005 0.75 0.155 0.03]);
t4 = uicontrol('Style', 'text',...
      'String', '[Divalent salt], mM',...
      'Units','normalized',...
      'Position', [0.005 0.70 0.155 0.03]);
t5 = uicontrol('Style', 'text',...
      'String', '[dNTPs], mM',...
      'Units','normalized',...
      'Position', [0.005 0.65 0.155 0.03]);
t6 = uicontrol('Style', 'text',...
      'String', 'Sequence (5''->3'')',...
      'Units','normalized',...
      'Position', [0.005 0.60 0.155 0.03]);

% make edit text boxes (e = editable text boxes)
ePr = uicontrol('Style', 'edit',...
      'String', '60',...
      'Units','normalized',...
      'Position', [0.2 0.85 0.10 0.03],'BackgroundColor',[1 1 1]);
eTg = uicontrol('Style', 'edit',...
      'String', '15',...
      'Units','normalized',...
      'Position', [0.2 0.80 0.10 0.03],'BackgroundColor',[1 1 1]);
emono_salt = uicontrol('Style', 'edit',...
      'String', '23',...
      'Units','normalized',...
      'Position', [0.2 0.75 0.10 0.03],'BackgroundColor',[1 1 1]);
edivalent_salt = uicontrol('Style', 'edit',...
      'String', '10',...
      'Units','normalized',...
      'Position', [0.2 0.70 0.10 0.03],'BackgroundColor',[1 1 1]);
edNTP = uicontrol('Style', 'edit',...
      'String', '0',...
      'Units','normalized',...
      'Position', [0.2 0.65 0.10 0.03],'BackgroundColor',[1 1 1]);
eSeq = uicontrol('Style', 'edit',...
      'String', 'AATTGCTAGCCTATTACTACCC',...
      'Units','normalized',...
      'Position', [0.2 0.56 0.35 0.075],'BackgroundColor',[1 1 1]);

% add push botton (p)
p = uicontrol('Style','pushbutton','Units','normalized',...
   'position',[0.1 0.50 0.20 0.05],'string','Compute Tm','callback',@MyCallbackFn);


function MyCallbackFn(~,~)
seq = get(eSeq,'String');
lseq = length(seq);
```

© Copyright 2021 | N Panpradist

```
nN1 = findstr(seq,'A'); nN2 = findstr(seq,'C'); nN3 = findstr(seq,'G'); nN4 =
findstr(seq,'T');
n_nwobbles = length(nN1)+length(nN2)+length(nN3) + length(nN4);
if n_nwobbles == lseq Nowobble()
else Wobble()
end
   function Nowobble(~,~)
      delete(gl.handles); % Eliminate plots from previous callbacks

      seq = get(eSeq,'String');
      Pr = 10^-9*str2num(get(ePr,'String'));
      Tg = 10^-9*str2num(get(eTg,'String'));
      mono_salt = str2num(get(emono_salt,'String'));
      divalent_salt = str2num(get(edivalent_salt,'String'));
      dNTP = str2num(get(edNTP,'String'));
      % add more text boxes
t(1) = uicontrol('Style', 'text',...
      'String', 'Complement Seq (5''->3'')',...
      'Units','normalized',...
      'Position', [0.005 0.21 0.155 0.03]);
t(2) = uicontrol('Style', 'text',...
      'String', 'dH, kcal/mol',...
       'Units','normalized',...
      'Position', [0.005 0.45 0.155 0.03]);
t(3) = uicontrol('Style', 'text',...
      'String', 'dS, cal/mol/K',...
       'Units','normalized',...
      'Position', [0.005 0.40 0.155 0.03]);
t(4) = uicontrol('Style', 'text',...
      'String', 'Tm (bimolecular), ¬∞C',...
      'Units','normalized',...
      'Position', [0.005 0.35 0.155 0.03]);
t(5) = uicontrol('Style', 'text',...
      'String', 'Tm (unimolecular), ¬∞C',...
      'Units','normalized',...
      'Position', [0.005 0.30 0.155 0.03]);

% add output textbox (o for output)

odH_salt = uicontrol('Style', 'edit',...
      'String', '',...
       'Units','normalized',...
      'Position', [0.2 0.45 0.155 0.03],...
      'BackgroundColor',[1 1 1]);
odS_salt = uicontrol('Style', 'edit',...
      'String', '',...
       'Units','normalized',...
      'Position', [0.2 0.40 0.155 0.03],...
      'BackgroundColor',[1 1 1]);
oTm = uicontrol('Style', 'edit',...
      'String', '',...
```

© Copyright 2021 | N Panpradist

```
        'Units','normalized',...
        'Position', [0.2 0.35 0.155 0.03],...
        'BackgroundColor',[1 1 1]);
oTm2 = uicontrol('Style', 'edit',...
        'String', '',...
        'Units','normalized',...
        'Position', [0.2 0.30 0.155 0.03],...
        'BackgroundColor',[1 1 1]);
ocom = uicontrol('Style', 'edit',...
        'String', '',...
        'Units','normalized',...
        'Position', [0.2 0.21 0.35 0.075],...
        'BackgroundColor',[1 1 1]);
         % below we is the section we can convert a specific strand (seq variable)...
         % to the reverse complement strand (rev_com) and complement strand (com)

                nA = findstr(seq,'A');
                rev_com = seq;
                for i = 1:size(nA,2);
                rev_com(nA(i)) = 'T';
                end
                nT = findstr(seq,'T');
                for i = 1:size(nT,2);
                rev_com(nT(i)) = 'A';
                end
                nG = findstr(seq,'G');
                for i = 1:size(nG,2);
                rev_com(nG(i)) = 'C';
                end
                nC = findstr(seq,'C');
                for i = 1:size(nC,2);
                rev_com(nC(i)) = 'G';
                end
                rev_com;
                com = fliplr(rev_com);
                set(ocom,'String',com);

         % matrix for Santalucia 2004 dH and dS at 37C
         % from AA, AG, AC, AT, GA, GG, GC, GT, CA, CG, CC, CT, TA, TG, TC, TT)
                NN = [  -7.6    -21.3
                        -8.4    -22.4
                        -7.8    -21
                        -7.2    -20.4
                        -8.5    -22.7
                        -8      -19.9
                        -10.6   -27.2
                        -7.8    -21
                        -8.2    -22.2
                        -9.8    -24.4
                        -8      -19.9
                        -8.4    -22.4
```

© Copyright 2021 | N Panpradist

```
            -7.2   -21.3
            -8.2   -22.2
            -8.5   -22.7
            -7.6   -21.3];

% find # pair neighbor in seq;
      nAA = findstr(seq,'AA');
      nAC = findstr(seq,'AC');
      nAG = findstr(seq,'AG');
      nAT = findstr(seq,'AT');
      nCA = findstr(seq,'CA');
      nCC = findstr(seq,'CC');
      nCG = findstr(seq,'CG');
      nCT = findstr(seq,'CT');
      nGA = findstr(seq,'GA');
      nGC = findstr(seq,'GC');
      nGG = findstr(seq,'GG');
      nGT = findstr(seq,'GT');
      nTA = findstr(seq,'TA');
      nTC = findstr(seq,'TC');
      nTG = findstr(seq,'TG');
      nTT = findstr(seq,'TT');
      nNN = [size(nAA,2) size(nAC,2) size(nAG,2) size(nAT,2)...
         size(nCA,2) size(nCC,2) size(nCG,2) size(nCT,2)...
         size(nGA,2) size(nGC,2) size(nGG,2) size(nGT,2)...
         size(nTA,2) size(nTC,2) size(nTG,2) size(nTT,2)];
      dHS = nNN*NN;
      dH37 = dHS(1)*10^3;
      dS37 = dHS(2);

      % correct dH37 and dS37 with the end base
         if seq(1) =='A'
         dH37 = dH37+2200;
         elseif seq(1) =='T'
         dH37 = dH37+2200;
         elseif seq(end) =='A'
         dH37 = dH37+2200;
         elseif seq(end) =='T'
         dH37 = dH37+2200;
         end

         dH = dH37+200; %initiation

         if seq(1) =='A'
         dS37 = dS37+6.9;
         elseif seq(1) =='T'
         dS37 = dS37+6.9;
         elseif seq(end) =='A'
         dS37 = dS37+6.9;
         elseif seq(end) =='T'
         dS37 = dS37+6.9;
```

© Copyright 2021 | N Panpradist

```
        end
        dS = dS37-5.7; %initiation


        % Apply salt correction since the dH, dS, dG37 is the value at 1M NaCl
        % nP = number of phosphates in duplex = 2*(length of
        % seq-1) since 3prime of engineered primer has OH
        nP = (size(seq,2)-1)*2;

        sum_salt = mono_salt + 120*(divalent_salt-dNTP)^0.5;
        dS_salt = dS + 0.368*nP/2*log(sum_salt/1000);
        % if sum_salt is between 50mM to 1100 mM
        dH_salt = dH;
        sum_salt;
set(odH_salt,'String',num2str(dH_salt/1000));
set(odS_salt,'String',num2str(dS_salt));
dG55 = dH_salt-(273.15+55)*dS_salt


% solve for f by varying T
Tp = linspace(0+273.15,100+273.15,100)';
T = linspace(0,100,100);

f1 = zeros(length(T),1);
b = zeros(length(T),1);

for j = 1:length(T)
a = Tg;
b(i) = -Tg - Pr-1./(exp((Tp(j)*dS_salt-dH_salt)./(1.987*Tp(j))));
c = Pr;

f1(j)= (-b(i)-sqrt(b(i)^2-4*a*c))./(2*a);
end

Tm = dH_salt/(dS_salt-1.987*log(0.5/((0.5)*Pr-0.5*0.5*Tg)))-273.15;
set(oTm,'String',num2str(round(Tm)));

f2 = zeros(length(T),1);
for k = 1:length(T)
f2(k) = 1./(1+1./exp(-(dH_salt-Tp(k)*dS_salt)./(1.987*Tp(k))));
end

Tm2 = dH_salt/(dS_salt-1.987*log(0.5/(1-0.5)))-273.15;
set(oTm2,'String',num2str(round(Tm2)));


melt = [T(:) f1(:) f2(:)]
```

© Copyright 2021 | N Panpradist

```
    hax2 = subplot(2,3,3);
    cla;
    plot(T,f1,'o-','color','b')
    hold on
    plot(T,f2,'o-','color','r')
    grid on
    title('Comparison of unimolecular (red) and bimolecular (blue)')
    ylabel('fraction DNA bound to probe')
    xlabel('temp (¬∞C)')


    line = [0.5 0.5];
    tmline = [T(1) Tm];
    plot(tmline,line,'-','color','k')
    linev = [Tm Tm];
    tmlinev = [0 0.5];
    plot(linev,tmlinev,'-','color','k')
    line2 = [0.5 0.5];
    tmline2 = [T(1) Tm2];
    plot(tmline2,line2,'-','color','k')
    linev2 = [Tm2 Tm2];
    tmlinev2 = [0 0.5];
    plot(linev2,tmlinev2,'-','color','k')
    xlim([T(1) T(end)]);
    hax = axes('position',[0.55,0.2,0.5,0.3]);
    imshow(I);
    gl.handles = [hax hax2 t odH_salt odS_salt oTm oTm2 ocom ];

end




function Wobble(~,~)

  delete(gl.handles); % Eliminate plots from previous callbacks
      inputseq = get(eSeq,'String');
      Pr = 10^-9*str2num(get(ePr,'String'));
      Tg = 10^-9*str2num(get(eTg,'String'));
      mono_salt = str2num(get(emono_salt,'String'));
      divalent_salt = str2num(get(edivalent_salt,'String'));
      dNTP = str2num(get(edNTP,'String'));
   t13 = uicontrol('Style', 'text',...
  'String', 'dH, (mean¬±SD)/ median, kcal/mol',...
   'Units','normalized',...
  'Position', [0.6 0.80 0.2 0.03]);
   t14 = uicontrol('Style', 'text',...
         'String', 'dS, (mean¬±SD)/ median, cal/mol/K',...
```

© Copyright 2021 | N Panpradist

```
       'Units','normalized',...
      'Position', [0.6 0.70 0.2 0.03]);
t15 = uicontrol('Style', 'text',...
      'String', 'Tm (mean¬±SD)/ median, ¬∞C',...
      'Units','normalized',...
      'Position', [0.6 0.60 0.2 0.03]);


% add output textbox (o for output)

odH_salt2 = uicontrol('Style', 'edit',...
      'String', '',...
       'Units','normalized',...
      'Position', [0.65 0.75 0.3 0.03],...
      'BackgroundColor',[1 1 1]);
odS_salt2 = uicontrol('Style', 'edit',...
      'String', '',...
       'Units','normalized',...
      'Position', [0.65 0.65 0.3 0.03],...
      'BackgroundColor',[1 1 1]);
oTm2 = uicontrol('Style', 'edit',...
      'String', '',...
      'Units','normalized',...
      'Position', [0.65 0.55 0.3 0.03],...
      'BackgroundColor',[1 1 1]);
       seq = inputseq;
% create the matrix containing only mix bases
          for i = 1: length(seq)
             if seq(i) == 'A'|...
                   seq(i) == 'C'|...
                   seq(i) == 'G'|...
                   seq(i) == 'T'
                seq(i) = '0';
             end
          end
      seq(seq=='0') = nan;
% nX = number of each wobbles
   nR = findstr(seq,'R');  oR = length(nR);
   nY = findstr(seq,'Y');  oY = length(nY);
   nM = findstr(seq,'M');  oM = length(nM);
   nK = findstr(seq,'K');  oK = length(nK);
   nS = findstr(seq,'S');  oS = length(nS);
   nW = findstr(seq,'W');  oW = length(nW);
   nH = findstr(seq,'H');  oH = length(nH);
   nB = findstr(seq,'B');  oB = length(nB);
   nV = findstr(seq,'V');  oV = length(nV);
   nD = findstr(seq,'D');  oD = length(nD);
   nN = findstr(seq,'N');  oN = length(nN);
   % define the number of outcomes from each wobble letter
   R = ['AG'];     lR = length(R);
   Y = ['CT'];     lY = length(Y);
```

© Copyright 2021 | N Panpradist

```
        M = ['AC'];     lM = length(M);
        K = ['GT'];     lK = length(K);
        S = ['CG'];     lS = length(S);
        W = ['AT'];     lW = length(W);
        H = ['ACT'];    lH = length(H);
        B = ['CGT'];    lB = length(B);
        V = ['ACG'];    lV = length(V);
        D = ['AGT'];    lD = length(D);
        N = ['ACGT'];   lN = length(N);

    % count is the total number of combinations
        count =
lR^oR*lY^oY*lM^oM*lK^oK*lS^oS*lW^oW*lH^oH*lB^oB*lV^oV*lD^oD*lN^oN;
        nseq = seq;
        nseq(nseq=='R') = num2str(lR);
        nseq(nseq=='Y') = num2str(lY);
        nseq(nseq=='M') = num2str(lM);
        nseq(nseq=='K') = num2str(lK);
        nseq(nseq=='S') = num2str(lS);
        nseq(nseq=='W') = num2str(lW);
        nseq(nseq=='H') = num2str(lH);
        nseq(nseq=='B') = num2str(lB);
        nseq(nseq=='V') = num2str(lV);
        nseq(nseq=='D') = num2str(lD);
        nseq(nseq=='N') = num2str(lN);

    % create the table of combinations
        head = seq(seq~=0);
        head2 = num2str(head);
        cseq = fullfact(str2num(nseq));
        cseq2 = cseq(cseq~=0);
        cseq3 = num2str(cseq2);
        cseq4 = reshape(cseq3,count,length(head));
        table = [head2; cseq4];

    for m = 1:length(head)

        if table(1,m) == 'R'
            for i = 2:size(table,1)
                if table(i,m)=='1' table(i,m)=R(1);
                else table(i,m) = R(2);
                end
            end

        elseif table(1,m) == 'Y'...
            for i = 2:size(table,1)
                if table(i,m)=='1' table(i,m)=Y(1);
                else table(i,m) =Y(2);
                end
            end
```

© Copyright 2021 | N Panpradist

```
elseif table(1,m) == 'M'...
   for i = 2:size(table,1)
      if table(i,m)=='1' table(i,m)=M(1);
      else table(i,m) =M(2);
      end
   end
elseif table(1,m) == 'K'...
   for i = 2:size(table,1)
      if table(i,m)=='1' table(i,m)=K(1);
      else table(i,m) =K(2);
      end
   end
elseif table(1,m) == 'S'...
   for i = 2:size(table,1)
      if table(i,m)=='1' table(i,m)=S(1);
      else table(i,m) =S(2);
      end
   end
elseif table(1,m) == 'W'...
   for i = 2:size(table,1)
      if table(i,m)=='1' table(i)=W(1);
      else table(i,m) =W(2);
      end
   end
elseif table(1,m) == 'H'...
   for i = 2:size(table,1)
      if table(i,m)=='1' table(i)=H(1);
      elseif table(i,m)=='2' table(i,m)=H(2);
      else  table(i,m) =H(3);
      end
   end
elseif table(1,m) == 'B'...
   for i = 2:size(table,1)
      if table(i,m)=='1' table(i)=B(1);
      elseif table(i,m)=='2' table(i,m)=B(2);
      else  table(i,m) =B(3);
      end
   end
elseif table(1,m) == 'V'...
   for i = 2:size(table,1)
      if table(i,m)==1 table(i,m)=V(1);
      elseif table(i,m)==2 table(i,m)=V(2);
      else  table(i,m) =V(3);
      end
   end
elseif table(1,m) == 'D'...
   for i = 2:size(table,1)
      if table(i,m)=='1' table(i,m)=D(1);
      elseif table(i,m)=='2' table(i,m)=D(2);
      else  table(i,m) =D(3);
      end
   end
```

© Copyright 2021 | N Panpradist

```
    elseif table(1,m) == 'N'...
        for i = 2:size(table,1)
            if table(i,m)=='1' table(i,m)=N(1);
            elseif table(i,m)=='2' table(i,m)=N(2);
            elseif table(i,m)=='3' table(i,m)=N(3);
            else  table(i,m) =N(4);
            end
        end

    end
end

% xseq will be the full set of all combinations from all the mix bases
% xseq is first made from the input seq
% xseq2 contains the wobbles only
% the position of wobbles are contained in pos variable
% the pos variable is then used as the index to insert the matrix table
% containing all the possible combinations

xseq = repmat(inputseq,count,1);
xseq2 = inputseq;
% create the matrix containing only mix bases
    for i = 1: length(seq)
        if xseq2(i) ~= 'A'&...
                xseq2(i) ~= 'C'&...
                xseq2(i) ~= 'G'&...
                xseq2(i) ~= 'T'
            xseq2(i) = '0';
        end
    end
xseq2(xseq2=='0') = nan;
pos = findstr(xseq2,0);

for i = 1:count
    for j=1:length(pos)
        xseq(i,pos(j)) = table(i+1,j);
    end
end



T = linspace(0,100,100);
table2 = zeros(length(T),(size(xseq,1)+1));
tm_table = zeros(1,size(xseq,1));
H_table = zeros(1,size(xseq,1));
S_table = zeros(1,size(xseq,1));

for i = 1:size(xseq,1)
        % matrix for St lucia 2004 dH and dS at 37C
        % from AA, AG, AC, AT, GA, GG, GC, GT, CA, CG, CC, CT, TA, TG, TC, TT)
```

© Copyright 2021 | N Panpradist

```
        NN = [-7.6  -21.3
        -8.4   -22.4
        -7.8   -21
        -7.2   -20.4
        -8.5   -22.7
        -8  -19.9
        -10.6   -27.2
        -7.8   -21
        -8.2   -22.2
        -9.8   -24.4
        -8  -19.9
        -8.4   -22.4
        -7.2   -21.3
        -8.2   -22.2
        -8.5   -22.7
        -7.6   -21.3];
    % find # pair neighbor in seq;
        nAA = findstr(xseq(i,:),'AA');
        nAC = findstr(xseq(i,:),'AC');
        nAG = findstr(xseq(i,:),'AG');
        nAT = findstr(xseq(i,:),'AT');
        nCA = findstr(xseq(i,:),'CA');
        nCC = findstr(xseq(i,:),'CC');
        nCG = findstr(xseq(i,:),'CG');
        nCT = findstr(xseq(i,:),'CT');
        nGA = findstr(xseq(i,:),'GA');
        nGC = findstr(xseq(i,:),'GC');
        nGG = findstr(xseq(i,:),'GG');
        nGT = findstr(xseq(i,:),'GT');
        nTA = findstr(xseq(i,:),'TA');
        nTC = findstr(xseq(i,:),'TC');
        nTG = findstr(xseq(i,:),'TG');
        nTT = findstr(xseq(i,:),'TT');
        nNN = [size(nAA,2) size(nAC,2) size(nAG,2) size(nAT,2)...
           size(nCA,2) size(nCC,2) size(nCG,2) size(nCT,2)...
           size(nGA,2) size(nGC,2) size(nGG,2) size(nGT,2)...
           size(nTA,2) size(nTC,2) size(nTG,2) size(nTT,2)];
        dHS = nNN*NN;
        dH37 = dHS(1)*10^3;
        dS37 = dHS(2);

        % correct dH37 and dS37 with the end base
           if xseq(i,1) =='A'
           dH37 = dH37+2200;
           elseif xseq(i,1) =='T'
           dH37 = dH37+2200;
           elseif xseq(i,end) =='A'
           dH37 = dH37+2200;
           elseif xseq(i,end) =='T'
           dH37 = dH37+2200;
           end
```

© Copyright 2021 | N Panpradist

```
dH = dH37+200; %initiation

if xseq(i,1) =='A'
dS37 = dS37+6.9;
elseif xseq(i,1) =='T'
dS37 = dS37+6.9;
elseif xseq(i,end) =='A'
dS37 = dS37+6.9;
elseif xseq(i,end) =='T'
dS37 = dS37+6.9;

end
dS = dS37-5.7; %initiation


% Apply salt correction since the dH, dS, dG37 is the value at 1M
NaCl

% nP = number of phosphates in duplex = 2*(length of
% seq-1) since 3prime of engineered primer has OH
nP = (size(xseq,2)-1)*2;

sum_salt = mono_salt + 120*(divalent_salt-dNTP)^0.5;
dS_salt = dS + 0.368*nP/2*log(sum_salt/1000);
% if sum_salt is between 50mM to 1100 mM
dH_salt = dH;
sum_salt;



Tp = linspace(0+273.15,100+273.15,100)';


f1 = zeros(length(T),1);
b = zeros(length(T),1);

for j = 1:length(T)
a = Tg;
b(i) = -Tg - Pr-1./(exp((Tp(j)*dS_salt-dH_salt)./(1.987*Tp(j))));
c = Pr;

f1(j)= (-b(i)-sqrt(b(i)^2-4*a*c))./(2*a);
end

Tm = dH_salt/(dS_salt-1.987*log(0.5/((0.5)*Pr-0.5*0.5*Tg)))-273.15;


table2(:,1) = T(:);
table2(:,1+i) = f1(:);
```

© Copyright 2021 | N Panpradist

```
            H_table(1,i) = dH_salt;
            S_table(1,i) = dS_salt;
            tm_table(1,i) = Tm;


        end
        table2
        H_table;
        S_table;
        mean_tm = mean(tm_table);
        std_tm = std(tm_table);
        med_tm = median(tm_table);
        mean_dH = mean(H_table);
        std_dH = std(H_table);
        med_dH = median(H_table);
        mean_dS = mean(S_table);
        std_dS = std(S_table);
        med_dS = median(S_table);
        dG55 = mean_dH-(55+273.15)*mean_dS
        set(odH_salt2,'String',[num2str(round(mean_dH./1000)),' ¬± 
',num2str(std_dH./1000),' / ',num2str(round(med_dH./1000))]);
        set(odS_salt2,'String',[num2str(mean_dS),' ¬± ',num2str(std_dS),' / 
',num2str(med_dS)]);
        set(oTm2,'String',[num2str(mean_tm),' ¬± ',num2str(std_tm),' / 
',num2str(med_tm)]);

            for i = 1:size(xseq,1)
               hax2 = subplot(2,2,3);
               grid on
               hold on
               plot(table2(:,1),table2(:,i+1),'o-','color',[i*2./256 i./256 i*2./256])
               title('Fraction bound for all probe combinations')
            end

            ylim([0 1])
            ylabel('fraction DNA bound to probe')
            xlabel('temp (¬∞C)')



        hax3 = subplot(2,2,4);
        hist(tm_table')
        title('Tm distribution of all probe combinations')
        xlabel('Tm of probes ¬∞C')
        ylabel('counts')
            % add more text boxes

        gl.handles = [hax2 hax3 t13 t14 t15 odH_salt2 odS_salt2 oTm2 ];

    end
```

© Copyright 2021 | N Panpradist

```
end

end
```

Fragment analysis of exonuclease-treated product using gel electrophoresis (non-denaturing 1% agarose gel). Treatment of exonuclease is specific to the phosphorylated amplicon, generating the ssDNA as shown in **Figure S6.27C**

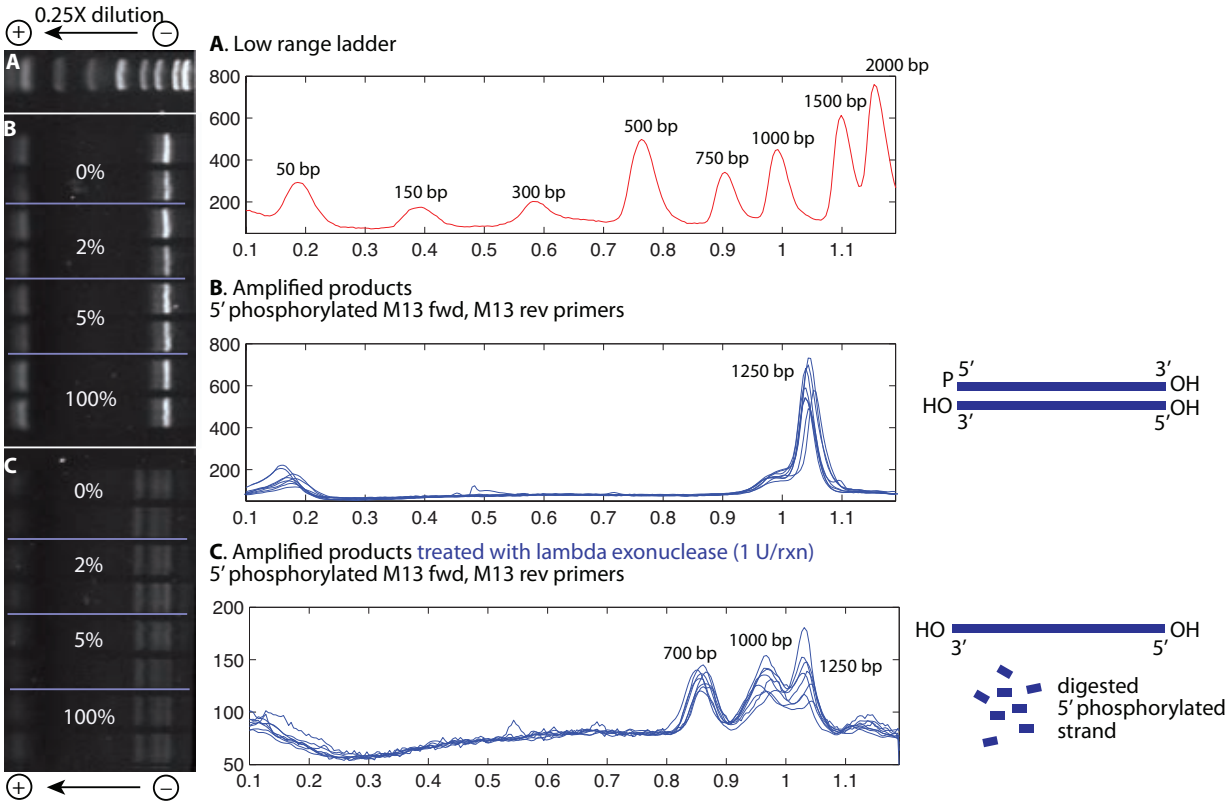

Figure S6.27 | Fragment analyses of amplicon generated by 5'phosphorylated forward primer were treated or not treated with exonuclease.

(A) Ladder (B) Amplicon without treatment with exonuclease (C) Amplicon treated with exonuclease.

© Copyright 2021 | N Panpradist

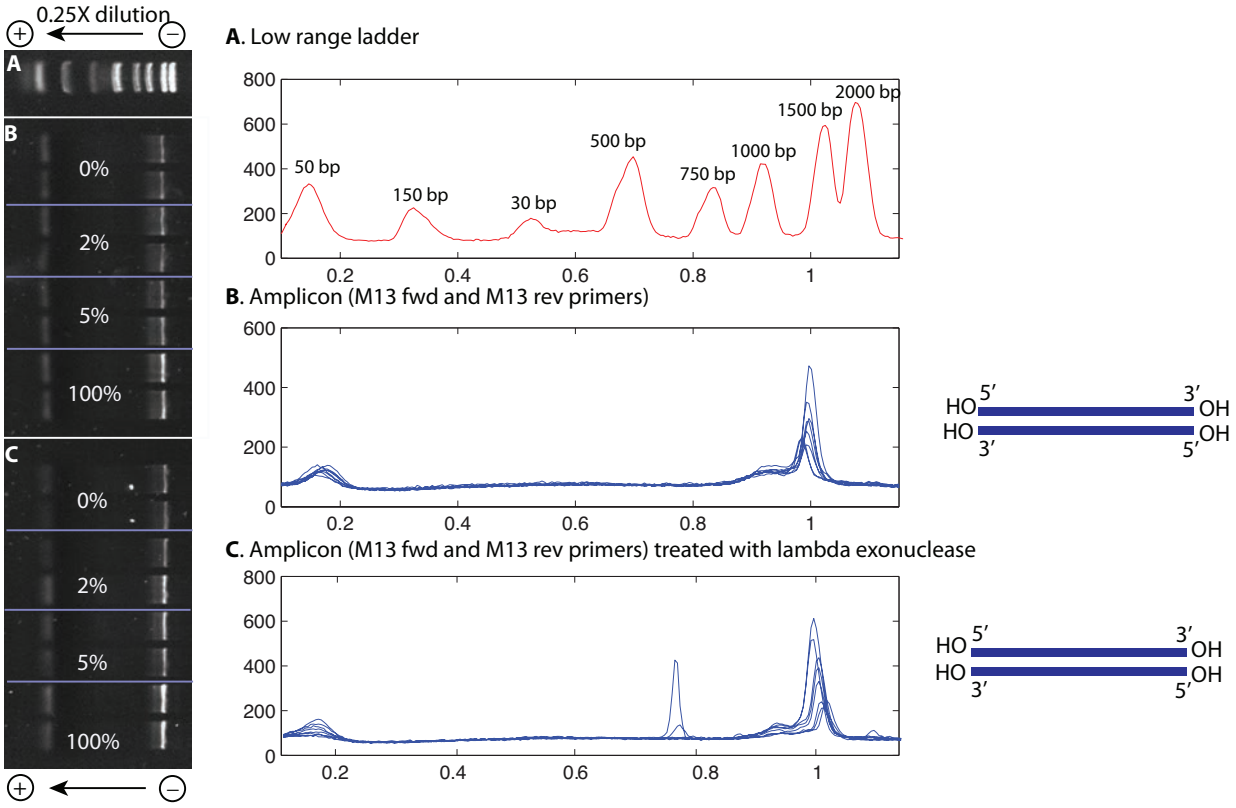

Figure S6.28 | Fragment analyses of amplicon generated by 5'hydroxyl forward primer was treated or not treated with exonuclease.

(A) Ladder (B) Amplicon without treatment with exonuclease (C) Amplicon treated with exonuclease. The peak was due to the artifacts of the white dots in 0%.

© Copyright 2021 | N Panpradist

CHAPTER 7: FLUORESCENCE-BASED DETECTION OF LDR PRODUCTS

Significance: This chapter describes fluorescence-based detection methods that can be used to detect LDR or iLDR products as an alternative to lateral flow detection. The fluorescence-based detection is directly seen from the reaction tube. Thus this approach can achieve resSults faster than the later flow detection method. Moreover, combining this detection method and single-tube amplification/ligation (described in **Chapter 6.6**) could lead to a complete single-tube analysis from sample amplification to results, eliminating the opportunities for amplicon-carryover contamination and requirements for an isolated pre/post-amplification space.

Contributors: Nuttada Panpradist (conception, design, and assay development), Annie Wong-On-Wing (assay development), and Michael Roller (device development).

7.1 MOLECULAR BEACONS AND THEIR USE IN SNP DETECTION

7.1.1 THERMODYNAMICS OF MOLECULAR BEACON

Molecular beacon (**MB**) is a 25-35 nt ssDNA that contains an 18-30nt loop region that connects the two ends complementary 5-7nt stem regions. MB is typically conjugated with a fluorophore and a quencher. A fluorophore emits light at a specific wavelength range when excited by another light with a

© Copyright 2021 | N Panpradist

shorter wavelength. On the other hand, the quencher absorbs light at a specific range of wavelengths when excited. Typically, a pair of fluorophore and quencher is selected so that the excitation wavelength of fluorophore can be entirely or mainly absorbed by the quencher when they are in proximity. The loop region of MB can be designed to specifically hybridize to a nucleic acid target (**Figure 7.1**) and form a rigid double helix more stable than the double helix of the shorter stem region, forcing the MB to undergo a conformational change. The de-hybridized stem region causes the quencher to be apart from the fluorophore, and a fluorophore signal is detected.

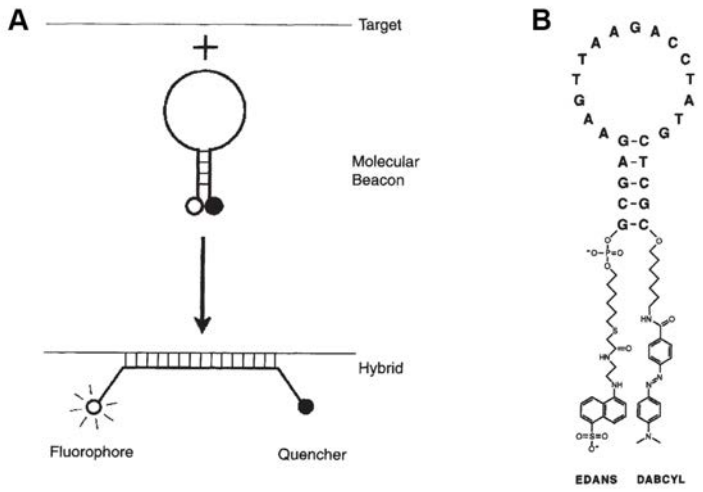

Figure 7.1 | First demonstration of the molecular beacon (MB).

(**A**) Schematic of MB interaction with the target and emission of signal upon linearization. (**B**) An example of the first reported MB. Here the fluorophore is EDANS (5- (2' -aminoethyl) aminonaphthalene-1- sulfonic acid), and the quencher is DABCYL (4-(4' -dimethylaminophenylazo) benzoic acid). The image was merged from the two figures of the original publication[1].

© Copyright 2021 | N Panpradist

MB in the solution has three configurations (**Figure 7.2A**)[2]. In the absence of the target, the MB stem remains hybridized (**Figure 7.2A**, phase 2) generates no/low signal at the temperature well below the melting temperature of the can stem region (**Figure 7.2B**, trace a). As the temperature increases, the stem region rehybridizes and enters a random coil configuration (**Figure 7.2A**, phase 3). In the presence of target (**Figure 7.2B**, trace b and c). and the temperature below the melting temperature of the MB loop: target duplex, the loop region of MB hybridizes to the target and dissociates the MB stem region, which generates a signal (**Figure 7.2A**, phase 1). As the temperature is increased well above the melting temperature of the MB loop: target duplex but below the melting temperature of the MB stem region, target dehybridizes from the MB loop and MB stem reanneal and switches to its closed conformation (**Figure 7.2A**, phase 2).

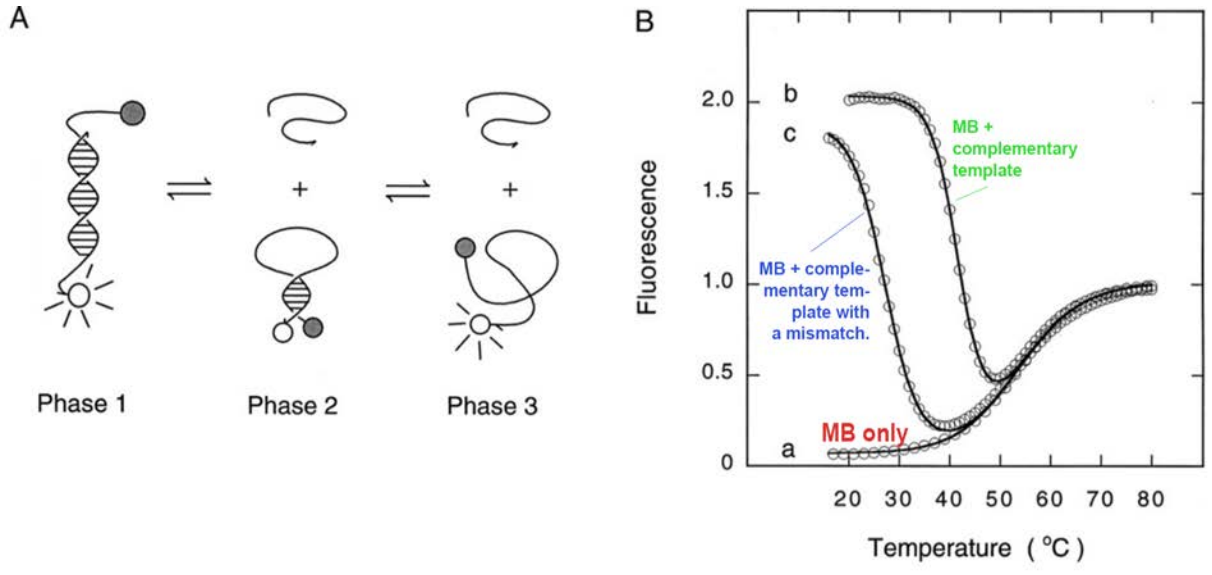

Figure 7.2 | Phase transition of MB.

(**A**) Schematic representation of the 3 phases of MB. (**B**) Melt analysis of solutions containing MB only, MB with a 6-fold excess of perfectly complementary targets, and MB with a 6-fold excess of

© Copyright 2021 | N Panpradist

mismatched targets. The image was modified from the original publication to include colored text labels[2].

7.1.2 USE OF MB TO DETECT SNP

The affinity of the MB loop and target depends on the complementarity of the target and the MB. Thus, MB can be used to discriminate the SNP present in the target (**Figure 7.2B**, trace b and c). In this example, the signal can be measured at 45°C, at which the loop stays hybridized to the perfectly complementary template but already de-hybridized from the template with an SNP (notated as a mismatch).

In the context of OLA, the WT and MUT ligated product could be differentiated by the MB (**Figure 7.3A**), but this technique would likely fail when applied to the highly polymorphemic HIV (**Figure 7.3B**) , especially when only one reaction temperature was pre-decided. Instead of reading the signal at a specific temperature, a high-resolution thermal analysis would likely be needed to differentiate an SNP in HIV, as demonstrated by the Shafer group[3].

© Copyright 2021 | N Panpradist

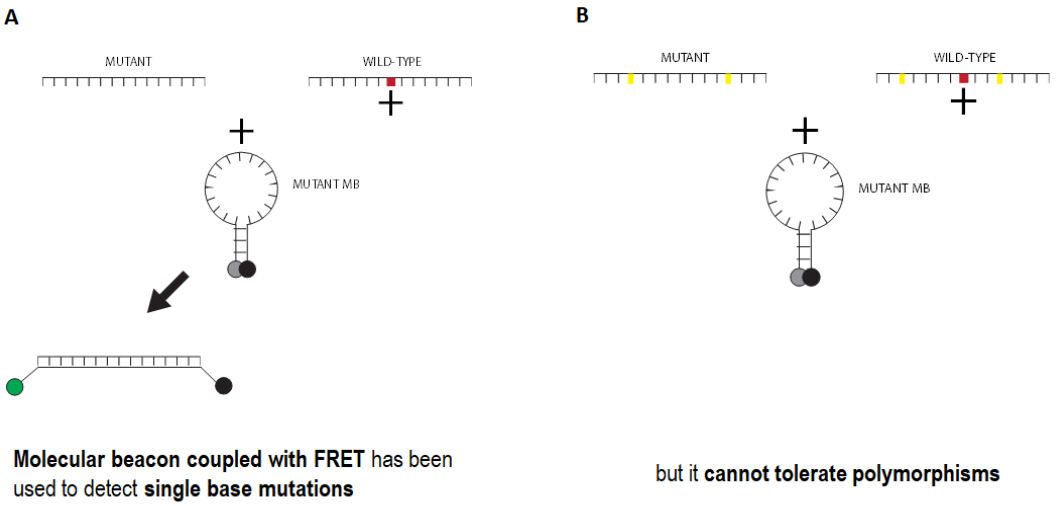

Figure 7.3 | Mismatch discrimination of the MUT and WT ligated probes by MB.

(A) Discrimination of an SNP by MB at a fixed temperature can be effective when the sequence is conserved. (B) Discrimination of an SNP in highly polymorphemic HIV at a fixed temperature would be expectedly less effective.

7.2 OVERCOMING POLYMORPHISM USING REVERSE MB

7.2.1 USE OF rMB TO DETECT LDR PRODUCTS

The current probes can be modified to have regions complementary (like the stem of disconnected MB). This stem region will have a lower Tm than the LDR reaction temperature, allowing the probe regions to anneal to the template. After the template is ligated, the ligated probes turn into a molecular beacon. This reverse-molecular beacon (rMB) approach is advantageous in multiple ways. First, the signal measured is independent of whether polymorphisms are present in the ligation probe. Major Tm distinction between ligated and non-ligated products due to the differences between the thermodynamics of bimolecular and unimolecular reactions of the stem adapter region, which is

© Copyright 2021 | N Panpradist

entirely engineered. **Figure 7.4** derives the thermodynamic equations based on the simplified two-state model. These rMB probes are more inexpensive than traditional MB (short and either have a fluorophore or a quencher).

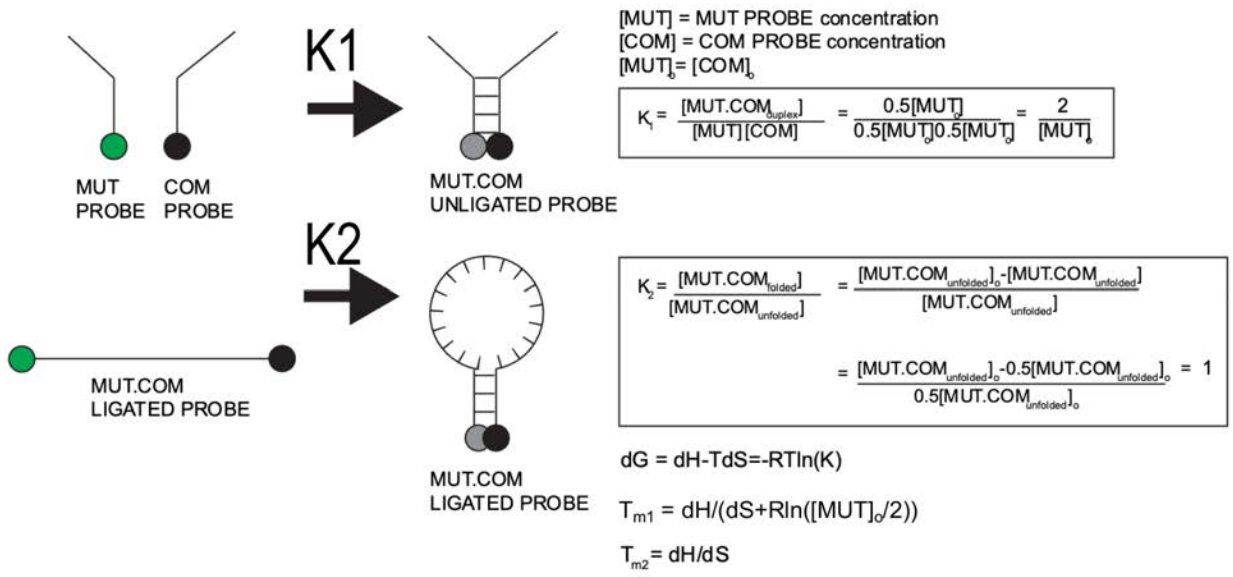

Figure 7.4 | Melting temperature of the stem region in the MB and corresponding linear probe using the two-state model. M-fold by Zuker et al. [4] can provide a more accurate prediction of the MB stem region since it includes the effect of the loop region, etc.

rMB was demonstrated by several groups to detect mostly synthetic and relatively conserved sequences with no polymorphisms around the target SNP [5-8], so its power to address polymorphisms has not yet been investigated.

7.2.2 rMB WITH A "TURN-OFF" SIGNAL SYSTEM

The "turn-off" signal (i.e., drop of fluorophore signal) can be observed in the presence of ligated product (rMB) when measured at the temperature well

© Copyright 2021 | N Panpradist

above the melting temperature of the target:rMB but lower than the melting temperature of the rMB region (**Figure 7.5A**). Multiplexed detection of SNPs using rMB has also been demonstrated[6]. rMB products from each SNP were differentiated by using different stem lengths and different fluorophores.

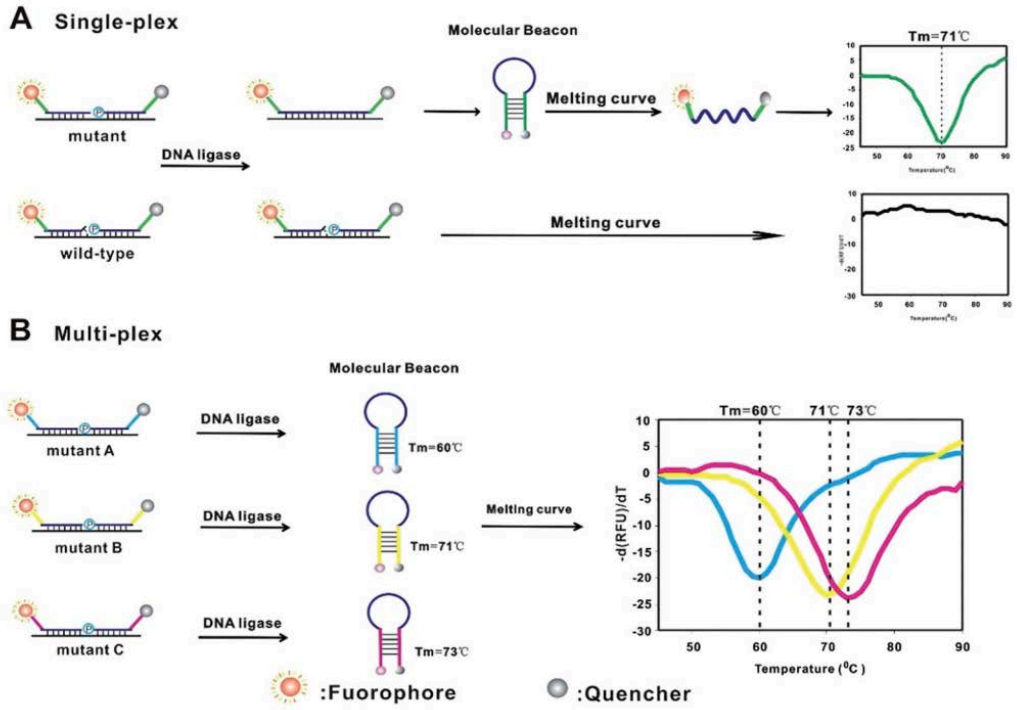

Figure 7.5 | Examples of reverse-molecular beacons to detect LDR products[6]

(A) Single-plex SNP detection (B) Multi-plex SNP detection.

7.2.3 rMB WITH A "TURN-ON" SIGNAL SYSTEM

In this context of HIVDR, we would like to sensitively detect the presence of MUT in WT sequences down to 10% frequency. Based on the previous work[6], the noise level of baseline -dRFU/dT is 5-10 a.u., and the maximum detection of 100% MUT is 15-20 a.u. Thus, observing the signal from the drop in10% MUT sample may be infeasible. A turn-on system where rMB causes the signal to increase would likely

© Copyright 2021 | N Panpradist

be an appropriate candidate for sensitive HIVDR detection. A group has demonstrated a turn-on rMB system using another fluorescence-resource energy transfer (**FRET**) system (Cy5, Cy5'5) [8]. When rMB stem hybridizes, excited photon donor (Cy5) can emit the photon that can be transferred to Cy5'5 molecule when Cy5/Cy5.5 molecules are within the range of 10-100 Å[9]. The SNP a *Kras* cancer gene was sensitivity detected down to a single-molecule level when coupled with diode laser-based fluorescence system[8].

7.2.4 FRET rMB TO DETECT HIVDR

We used traditional FRET (Cy3/Cy5/Cy7) in our system to detect WT and MUT HIVDR. The common probe is labeled with Cy5 so that it can be used as an acceptor for Cy3 labeled MUT probe and a donor for Cy7 labeled WT probe (**Figure 7.6**). Based on the temperature of our assay, we ensured that the Tm of the stem-loop region before ligation is <37°C but > Tm of the template: rMB duplex (**Figure 7.7**). Thermodynamic prediction of the rMB most stable structure based on designed sequences revealed a stable stem at 64°C, at which we plan to measure the signal of rMB.

© Copyright 2021 | N Panpradist

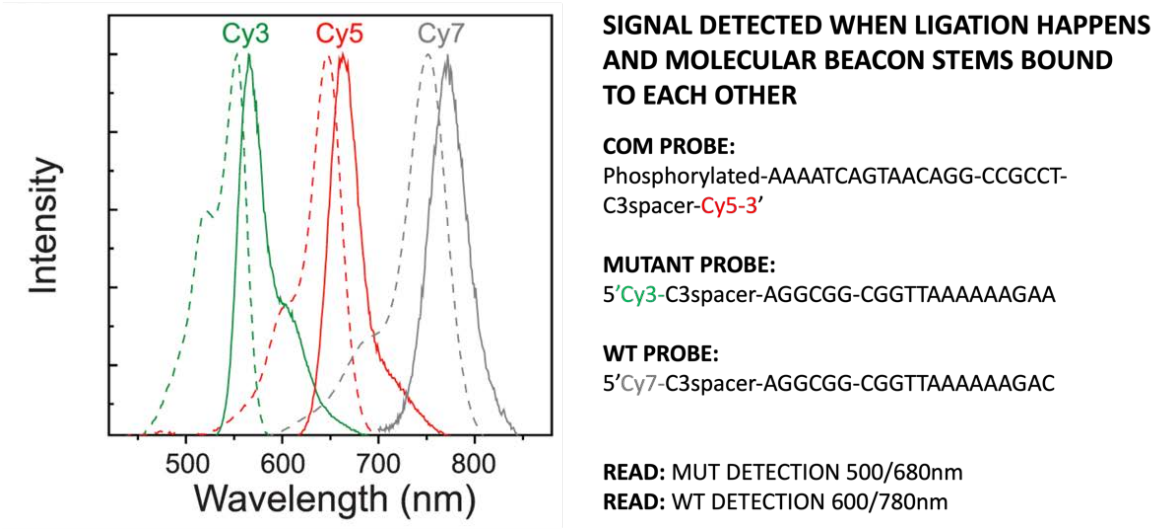

Figure 7.6 | FRET system used in detecting HIVDR and probe sequence.

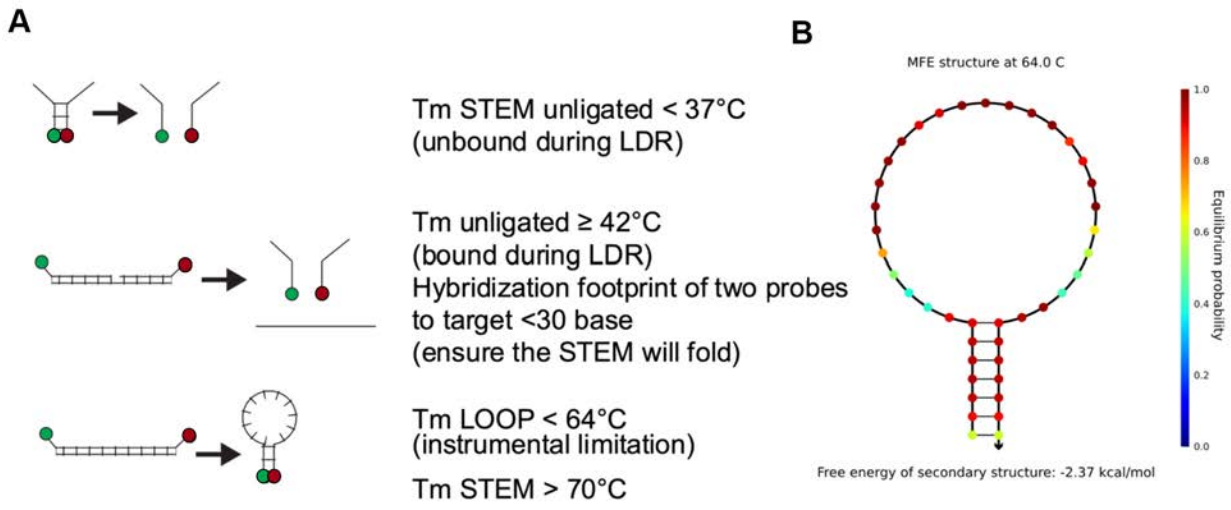

Figure 7.7 | The melting temperature of loop and stem and secondary structure of rMB.

Evaluation of iLDR reaction with FRET-based probes designed in **Figure 7.6** on DNA samples containing 0 – 100% G190A mutation revealed highly sensitive detection down to 5%MUT (**Figure 7.8**).

© Copyright 2021 | N Panpradist

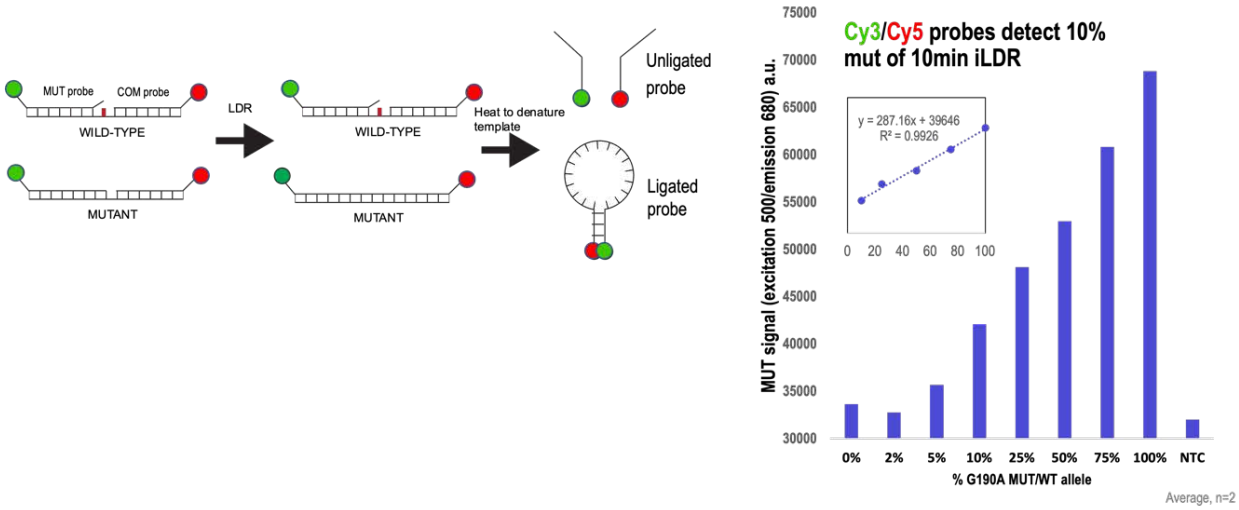

Figure 7.8 | Performance of reverse MB to overcome high polymorphisms.

10-min rMB LDR assay was tested on a DNA template containing 0 – 100%. The signal is read at 64°C by the plate reader (BioTek) with the excitation at 500nm, and emission read at 680nm. The average of two replicates was plotted.

Here we used excitation at 500nm and emission at 680nm to avoid the overlapping spectrum of the Cy3/Cy5 dye. At these wavelengths, we only achieved 20% of maximum excitation and around 30% of the maximum emission (**Figure 7.6**). Moreover, the electron transfer efficiency can drop significantly with a minimal increase in the distance between the two dyes; the efficiency of energy transfer is reciprocal of the sixth power of this distance[10]. Altogether we found that the FRET signal is much weaker than the fluorophore/quencher signal. Michael Roller investigated approaches to build a reader/heater device for the FRET Cy3/Cy5 system and could not achieve highly sensitive detection compared to the commercial plate reader.

7.3 FUTURE WORK

© Copyright 2021 | N Panpradist

NOVEL THAI ELEPHANT PROBE – AN EFFICIENT TURN-ON rMB

The Thai elephant probe is designed to improve the efficiency of FRET rMB (**Figure 7.9**). The probe has a hairpin structure and within the stem adapter region to force the quencher and fluorophore to be in proximity, so there would be no signal before the LDR step. After the LDR, the ligated probe turns into an rMB similar to the previous case. However, the probe on the right side has a longer complementarity to the hairpin region of the probe on the left and can displace via the toehold mediated strand displacement, making emitted fluorophore detectable. For unligated probes, this displacement will not happen because the hybridization of the hairpin region itself will be more thermodynamically stable. We have done extensive characterization of strand displacement (**Chapter 3.4**), and we could identify a range of parameters to support the feasibility of this approach.

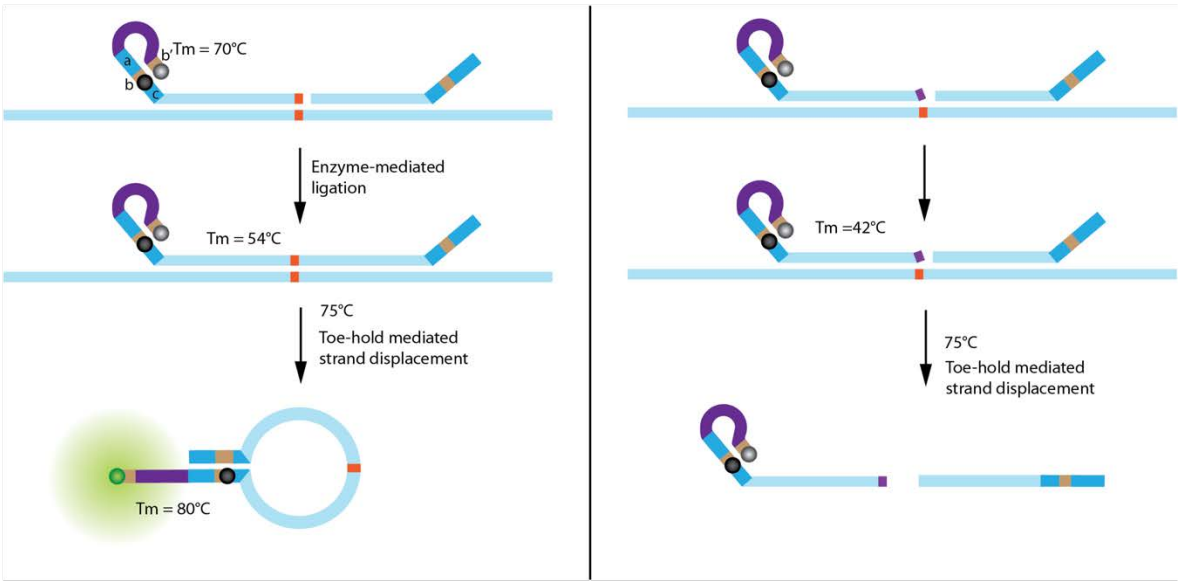

Thai elephant probe: idea conceived on my flight to Thailand March 20; How the probe unfolded looks like how elephant's trunk projects water

Figure 7.9 | Thai elephant probe to overcome the issues of low-level FRET-based rMB.

© Copyright 2021 | N Panpradist

CHAPTER 7 REFERENCES

1. Tyagi, S.; Kramer, F. R., Molecular Beacons: Probes that Fluoresce upon Hybridization. *Nature Biotechnology* **1996,** *14* (3), 303-308.
2. Bonnet, G.; Tyagi, S.; Libchaber, A.; Kramer, F. R., Thermodynamic basis of the enhanced specificity of structured DNA probes. *Proceedings of the National Academy of Sciences* **1999,** *96* (11), 6171-6176.
3. Clutter, D. S.; Mazarei, G.; Sinha, R.; Manasa, J.; Nouhin, J.; LaPrade, E.; Bolouki, S.; Tzou, P. L.; Hannita-Hui, J.; Sahoo, M. K.; Kuimelis, P.; Kuimelis, R. G.; Pinsky, B. A.; Schoolnik, G. K.; Hassibi, A.; Shafer, R. W., Multiplex Solid-Phase Melt Curve Analysis for the Point-of-Care Detection of HIV-1 Drug Resistance. *J Mol Diagn* **2019,** *21* (4), 580-592.
4. Zuker, M., Mfold web server for nucleic acid folding and hybridization prediction. *Nucleic Acids Res* **2003,** *31* (13), 3406-15.
5. Luo, W.; Zhou, D.; Luo, D.; Jiang, J.; Xu, X., Melting temperature of molecular beacons as an indicator of the ligase detection reaction for multiplex detection of point mutations. *Analytical Methods* **2015,** *7* (10), 4225-4230.
6. Peng, Z.; Soper, S. A.; Pingle, M. R.; Barany, F.; Davis, L. M., Ligase detection reaction generation of reverse molecular beacons for near real-time analysis of bacterial pathogens using single-pair fluorescence resonance energy transfer and a cyclic olefin copolymer microfluidic chip. *Anal Chem* **2010,** *82* (23), 9727-35.

© Copyright 2021 | N Panpradist

7. Tang, H.; Yang, X.; Wang, K.; Tan, W.; Li, H.; He, L.; Liu, B., RNA-templated single-base mutation detection based on T4 DNA ligase and reverse molecular beacon. *Talanta* **2008,** *75* (5), 1388-93.

8. Wabuyele, M. B.; Farquar, H.; Stryjewski, W.; Hammer, R. P.; Soper, S. A.; Cheng, Y.-W.; Barany, F., Approaching Real-Time Molecular Diagnostics: Single-Pair Fluorescence Resonance Energy Transfer (spFRET) Detection for the Analysis of Low Abundant Point Mutations in K-ras Oncogenes. *Journal of the American Chemical Society* **2003,** *125* (23), 6937-6945.

9. Held, P. An Introduction to Fluorescence Resonance Energy Transfer (FRET) Technology and its Application in Bioscience. https://www.biotek.com/resources/white-papers/an-introduction-to-fluorescence-resonance-energy-transfer-fret-technology-and-its-application-in-bioscience/.

10. Energy Transfer. In *Principles of Fluorescence Spectroscopy*, Lakowicz, J. R., Ed. Springer US: Boston, MA, 2006; pp 443-475.

© Copyright 2021 | N Panpradist

CHAPTER 8: INTEGRATION OF HIVDR OLA INTO A MORE SIMPLIFIED DEVICE

CONTRIBUTORS: David McIntyre (Pull tab device developer), Michael Roller (developer of the μfluidic chip and the heat-activated valve), Collin Eckhoff (initial heater developer), Dr. Barry Lutz (supervision), Nuttada Panpradist (conception and the rest of the work).

8.1 WAX-BASED BARRIERS

8.1.1 ENCAPSULATION OF COMPETING OLIGOS

Competing oligo (see **Chapter 3.3**) used in the 2nd generation paper-based detection requires heat denaturation. In **Chapter 3.4**, we designed the new competing oligo to avoid the need for heat denaturing. Here we developed an alternative approach that encapsulated the competing oligo and released it upon denaturation. This design helped prevent amplicon exposure after the single tube tHDA/iLDR step (**Chapter 6.6**).

A temperature-sensitive wax valve was used to control and release of dried competing oligos to knock out false-positive signals from duplexes forming from unligated probes and templates**.** Several types of wax were previously used to create physical barriers to molecular reactions. However, a kind of wax used in this application must have a melting temperature above 65°C (i.e., tHDA reaction temperature). Candelilla wax with a melting temperature of 75 – 80°C was considered. We tested the chemical compatibility of candelilla wax in tHDA. 100 HIV copies were amplified in the presence of candelilla, and its

© Copyright 2021 | N Panpradist

amplified products were visualized using PAGE gel electrophoresis. The band intensities were compared to the case without candelilla wax (**Figure 8.1A**). For LDR, 10^{10} copies of HIV containing 0% and 10% K103N mutant strands were subjected to LDR in the presence of candelilla wax. The ligated products were quantified using plate-based ELISA, and their O.D. values were compared to the case without candelilla wax (**Figure 8.1B**). Moderate reduction of the signal was observed in both HDA and LDR when candelilla wax was introduced. However, even with the reduced band intensity in the gel, the amplification reaction should contain sufficient amplified targets, especially when all the amplification products will enter ligation without further dilution.

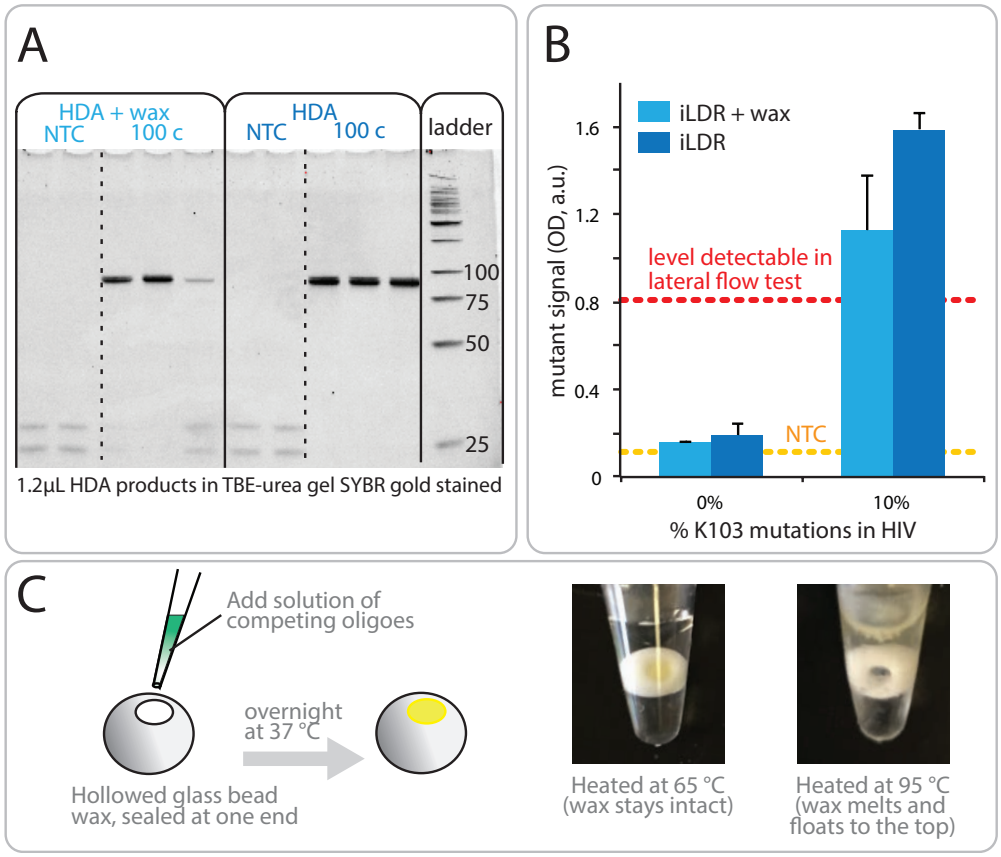

Figure 8.1. | Development of wax encapsulation method for dried competing oligos.

© Copyright 2021 | N Panpradist

(A) Test the effect of candelilla wax on tHDA **(B)** Effect of wax on iLDR **(C)** Preparation and characterization of wax encapsulated glass bead.

ENCAPSULATED COMPETING OLIGO IN THE WAX COATED GLASS BEAD.

We have developed and tested different approaches for the control and release of dried reagents. For example, we have developed wax-encapsulated dried reagent beads; and wax-encapsulated dried reagents in a pipette tip. However, we had ongoing issues with the release. Wax beads and the surface of the pipette tips are both hydrophobic, and even though wax was melted, it would remain wet around itself (in bead format) or on the surface of the pipette tip rather than diffuse and interact with the water phase. Realizing this, we have recently developed a new approach (**Figure 8.1C**). A hollowed glass bead, sealed on both ends with wax, contained the dried competing oligos. This wax encapsulation is stable at 65 °C. However, after the wax melts at 95 °C, it reduces its interaction with both the water and hydrophilic glass surface by floating to the top surface of the reaction fluid, effectively releasing the competing oligos.

8.1.2 WAX PATTERNING ON GLASS FIBER TO CREATE A REAGENT RESERVOIR.

Wax patterning on paper-based microfluidic devices has been used extensively[1, 2]. Cellulose is the most used substrate for this application. However, we are interested in using this method to mass-produce the 3rd generation paper-based detection (**Chapter 3.4**). Instead of placing different

© Copyright 2021 | N Panpradist

glass fiber pads onto the plastic card as previously described[3-5], we envisioned patterning the wax onto the glass fiber to create barriers to separate reagent reservoirs (**Figure 8.2A**). We learned that glass fiber is not a suitable substrate for this method. During the heating step to melt the wax powder into the layer of the glass fiber, we lost the definitions of the pattern (**Figure 8.2B**). The heated wax barriers with 4pt and 5pt sizes protected the fluid in the reservoirs from leakage. Still, the volume capacity was much lower than expected from the size of the starting pattern (**Figure 8.2, C&D**). Future fine-tuning will be required to achieve the optimal condition if we want to pursue this approach.

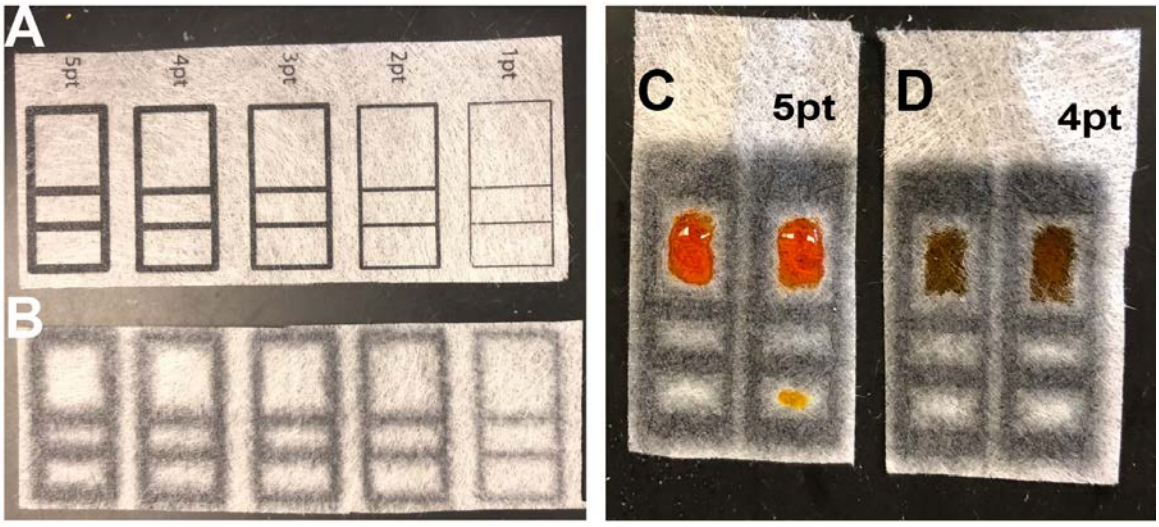

Figure 8.2 | Wax patterning onto glass fiber before and after the heat treatment.

© Copyright 2021 | N Panpradist

8.2 SELF-CONTAINED SYSTEM FOR PAPER-BASED DETECTION

Several amplicon-containing transfer systems have been developed[6, 7,] but we required a customized system for the OLA detection chemistry. I collaborate with David McIntyre (an undergraduate student mentee) to develop a proof-of-concept, self-contained, 3D-printed device. The iLDR product (**V-OLA 2.0**) can be transferred to the lateral flow test without tube opening (**Figure 7.3A**). Instead, the reagent tube was pressed into the wells containing a puncturing spike, which cracks the tube open from the bottom to release sample fluid onto the lateral flow tests. The system has been tested with standard ligation products that were treated with heat-activated encapsulated competing oligos. The system was able to detect the ligated products as expected (**Figure 7.3B**).

© Copyright 2021 | N Panpradist

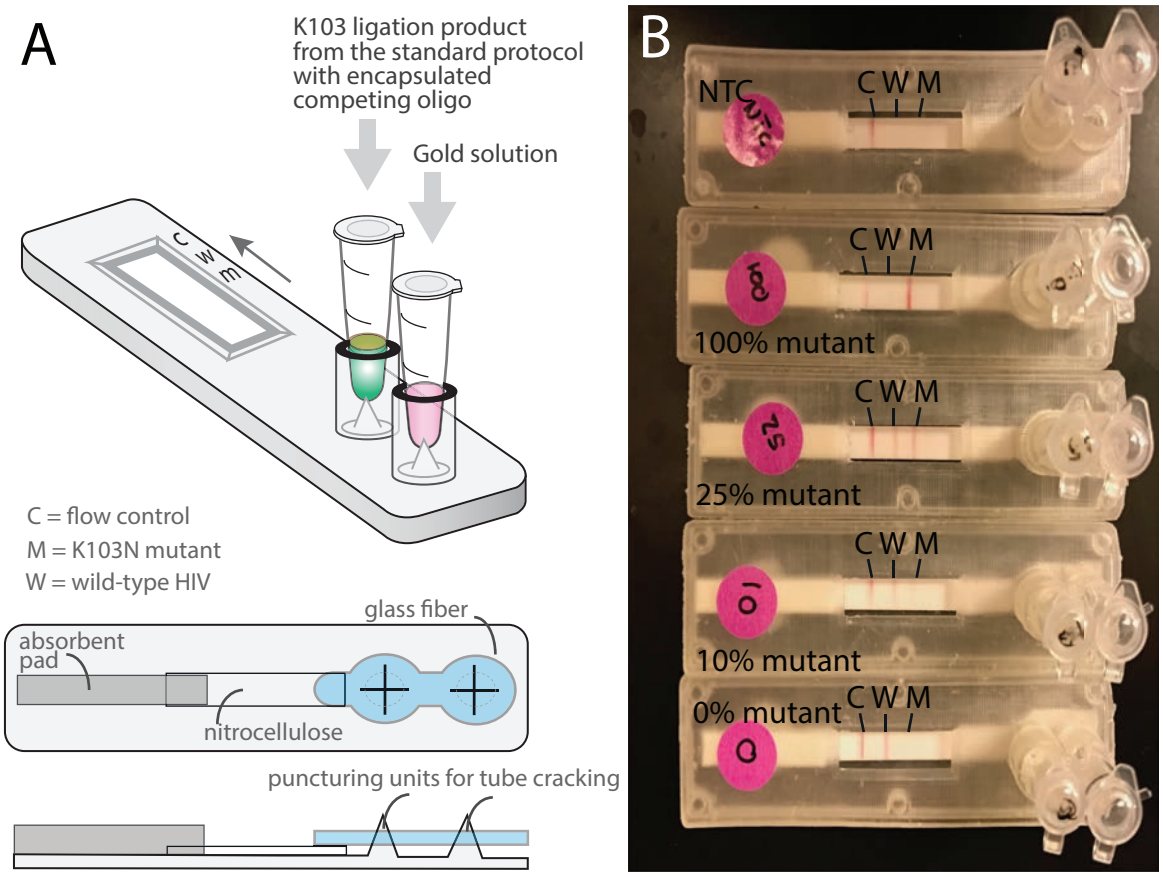

Figure 8.3 | Self-contained lateral flow device version 1.

(**A**) Layout of self-contained lateral flow devices **(B)** The results from testing the ligated products**.** David McIntyre collected data.

We had a few concerns about the above design. (1) loading the tubes requires a strong push to crack the tube down into the device, which may be difficult for the users. (2) Improper discard of the devices could lead to injury. Instead, we have come up with the safety pin and tube seal design below. The tube bottoms are modified with a foil seal that could be easily pierced by the "safe" (less sharp) pins within the device (**Figure 8.4**).

© Copyright 2021 | N Panpradist

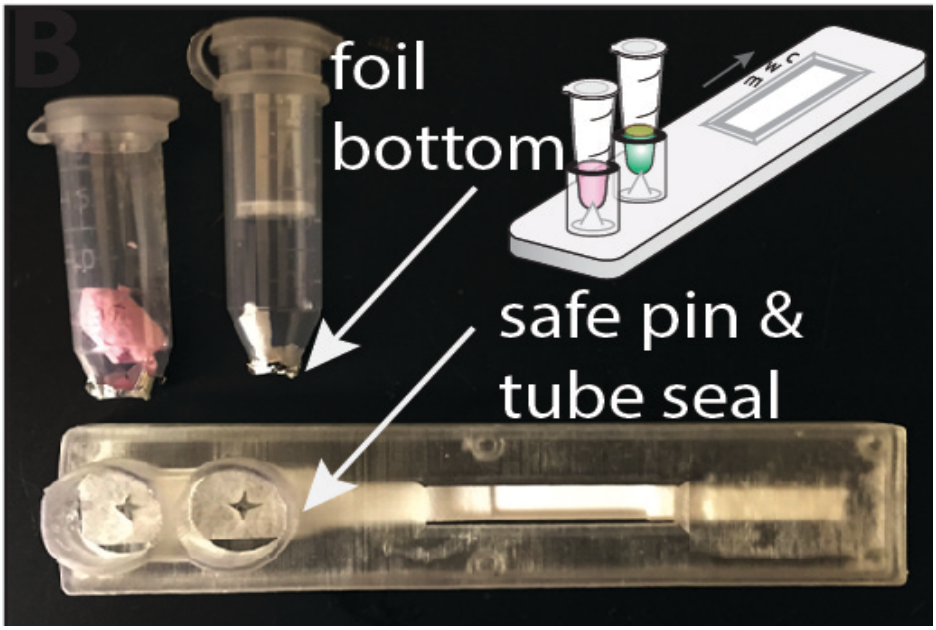

Figure 8.4 | Self-contained lateral flow device version 2.

Nuttada came up with the concept. David McIntyre designed the device.

8.3 PULL-TAB AS A CONTROL TOOL FOR SEQUENTIAL DELIVERY

During the 2nd generation paper-based detection development, we learned that the limited-diffusion premixing of the LDR product, and the gold nanoparticles could lead to false detection. We envision the use of sequential delivery to limit mixing between the two fluids. I worked with David McIntyre to develop the pull-tab system to separate and connect two paper networks initially. This permits the user to easily control the sequential delivery of fluids to maximize the sensitivity and specificity of the assay (see **Chapter 3.3**). **Figure 8.5** shows the schematic of the pull tab and the chemistry involved with each detection step. We also demonstrated the operation of the prototype using colored fluid in **Figure 8.6**.

© Copyright 2021 | N Panpradist

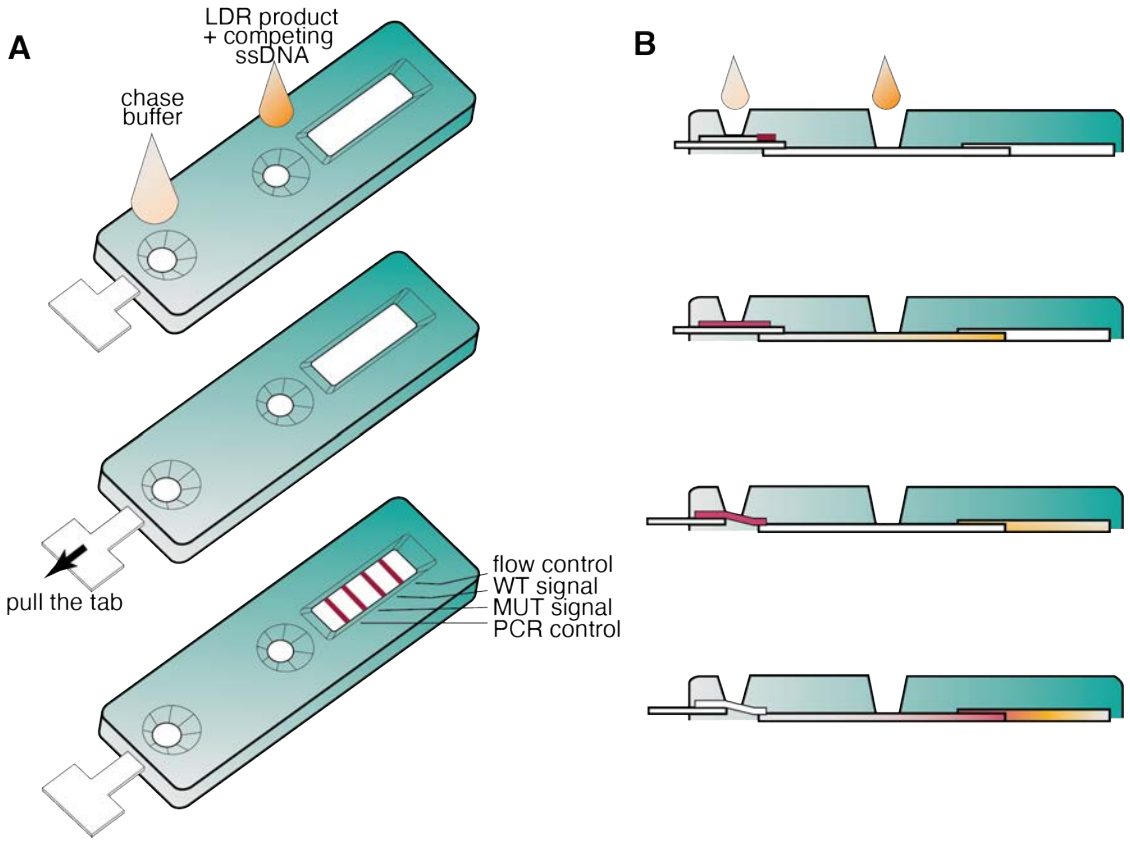

Figure 8.5 | Pull-tab device to enable sequential delivery in OLA detection.

(**A**) Demonstration of user steps. First, users add the LDR product that has been mixed with the dried engineered ssDNA and load the sample into the port closer to the detection window. Immediately after then, the user loads the chase buffer into the well closer to the tab. After 5 minutes, the user pulls the tab, and the visual readouts will show up after 20 minutes. (**B**) Schematic of the fluid flow after each step. After the LDR product and ssDNA mixture are added into the well, the fluid is wicked towards the absorbent pad. The added chase buffer reconstituted the dried gold nanoparticles but is not wicked into the nitrocellulose. After the pad is pulled, the gold nanoparticles flow into the nitrocellulose and bind to the biotin-containing moieties.

© Copyright 2021 | N Panpradist

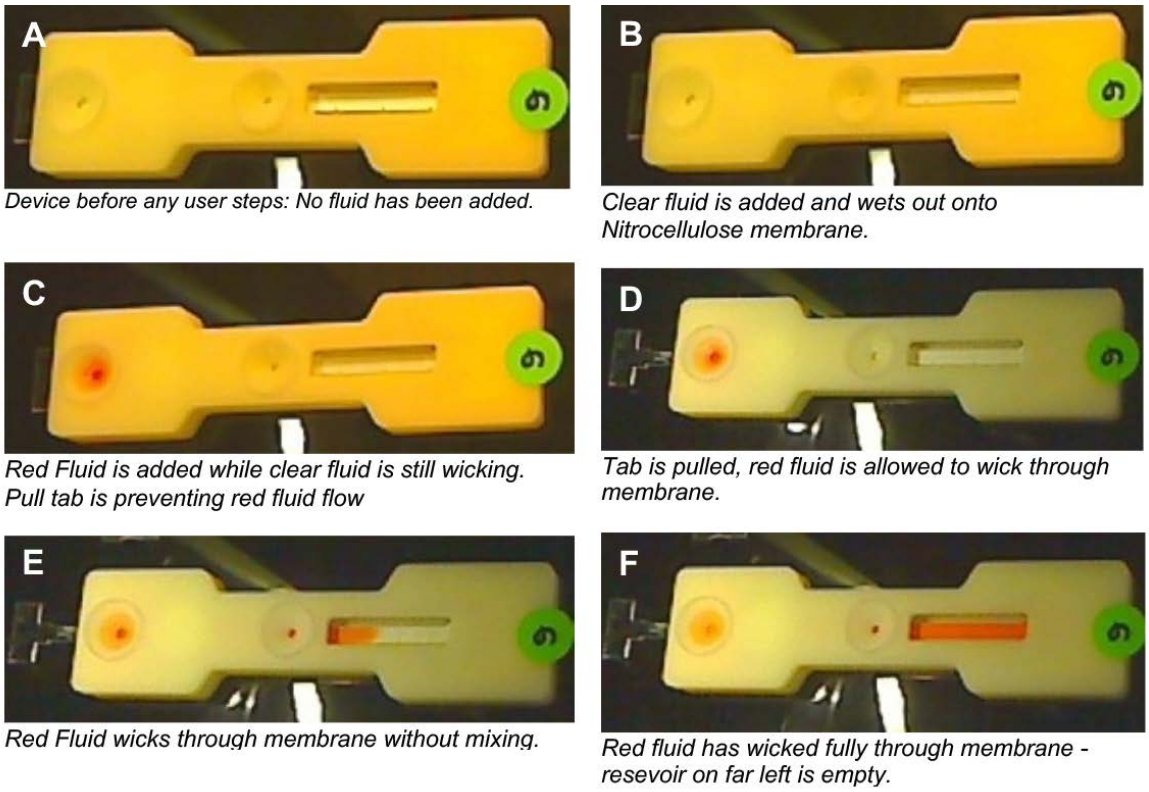

Figure 8.6 | Demonstration of a simple pull tab detection device design using colored fluid

8.4 INTEGRATED OLA DEVICE (VERSION 1)

We envisioned the integrated OLA-Simple device version 1 (**Figure 8.7**). The OLA device will contain fluid release ports, which are connected to the paper network. The paper network will have three zones for different steps in the OLA. ZONE 1 is connected to the sample port, reagent sources, and ZONE 2. This is where HIV RNA extraction will occur, followed by in-situ isothermal amplification. After isothermal amplification completes, the second fluid source will be released to push all the amplified HIV targets to be captured in ZONE 2. The third fluid containing ligation reagents will be released into ZONE 2 and held until the completion of the ligation step. Subsequently, the fourth fluid will contain labeling enzyme conjugates and competing oligos to free the

© Copyright 2021 | N Panpradist

ligated and un-ligated probes to be captured downstream in ZONEs 3 & 4. The final fluid will contain enzyme-substrate and will label both ligated products of HIV viral load control and internal amplification control and drug-resistant ligated probes captured in ZONEs 3 & 4.

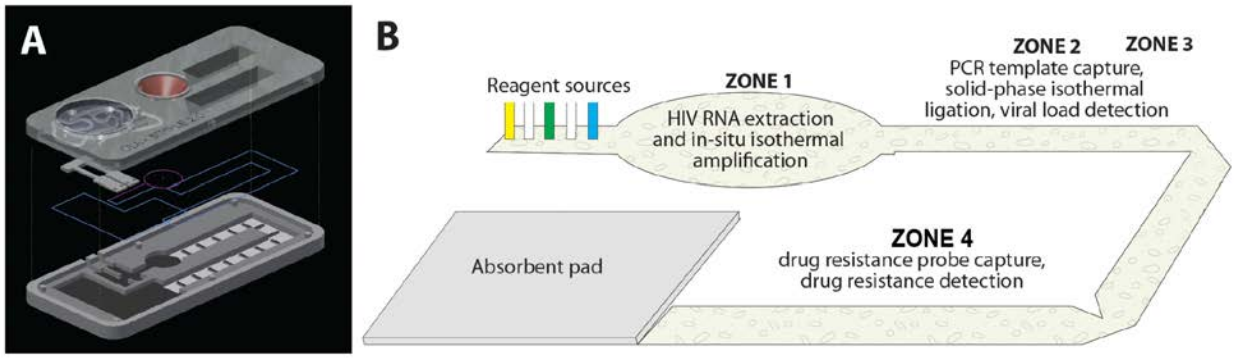

Figure 8.7 | Blueprint of integrated device version 1.

(A) 3D drawing of the integrated device containing two main ports: sample and common buffer ports. The common buffer port will then split into five mini ports to rehydrate the pre-dried reagents. **(B)** Paper network of our OLA device. ZONE 1 is connected to the sample port, reagent sources, and ZONE 2. This is where HIV RNA extraction will occur, followed by in-situ isothermal amplification. After isothermal amplification completes, the second fluid source will be released to push all the amplified HIV targets to be captured in ZONE 2. The third fluid containing ligation reagents will be released into ZONE 2 and held until the completion of the ligation step. Subsequently, the fourth fluid will contain labeling enzyme conjugates and competing oligos to chase the ligated and un-ligated probes downstream and get captured in ZONE 3. The final fluid will be the enzyme substrate and will label both amplified target in ZONE 3 to report viral load and ligated probes captured in ZONE 4 to report HIVDR, respectively. Detailed chemistries are shown in **Figure 8.9**

To use a paper network to control the release of fluids at a precise time to activate and deactivate a series of steps in the OLA, David McIntyre prepared the 3D printed device and demonstrated the sequentially delivery of all the key fluids in the envisioned integrated OLA-Simple v.1 (**Figure 8.8**).

© Copyright 2021 | N Panpradist

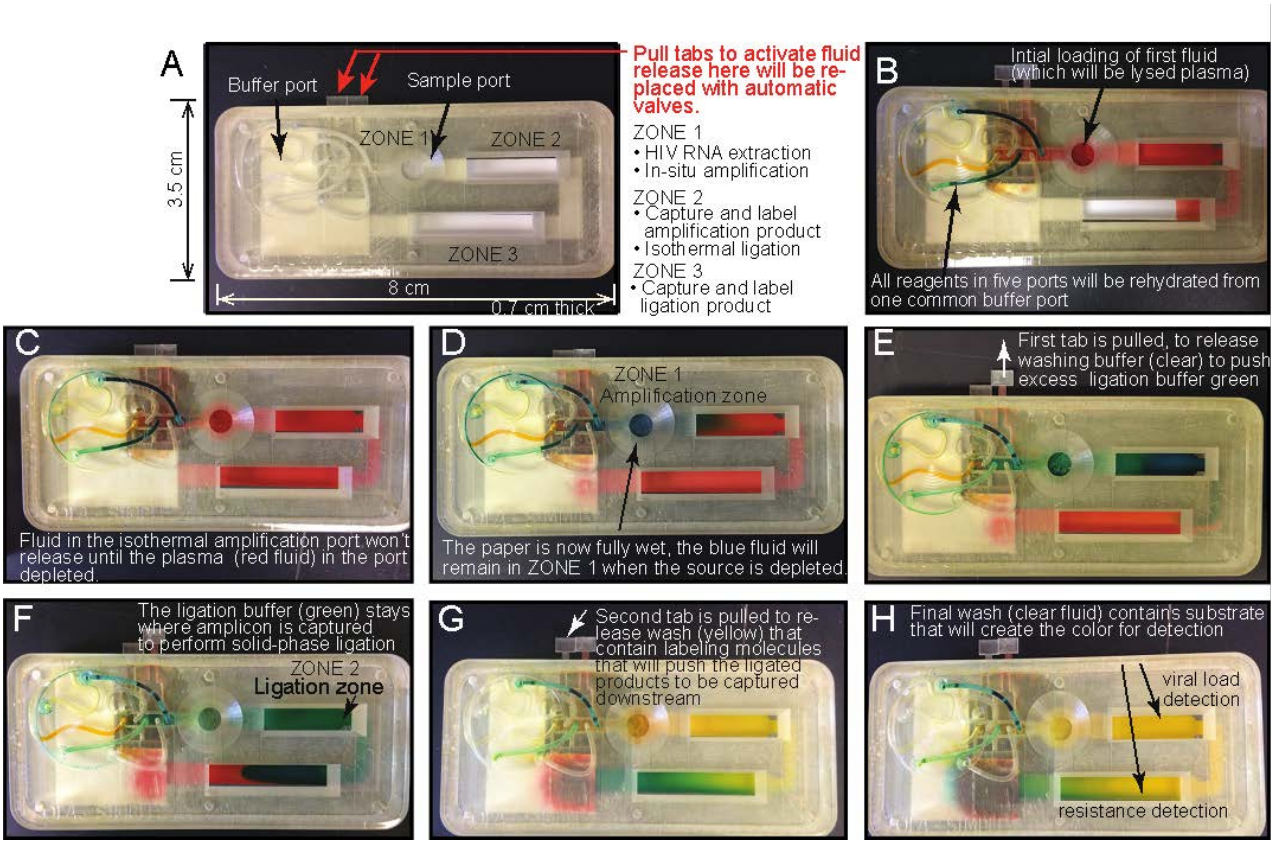

Figure 8.8 | Demonstration of two pull-tab systems with time delays using colored fluid.

Re-engineered chemistry of the OLA (**Figure 8.9**) combined with sequential fluid delivery above could lead to the successful integrated OLA-Simple 1.0. Our next step is to house all heaters, sensors, and electronics in a module (**Figure 8.10A**) to allow for the cartridge to enter. A recess in the DR cartridge exposes the paper to the module's heater element (paper strips are fabricated with conventional cover tape to prevent evaporation and escape of amplicons) (**Figure 8.10B**, left). Collin Eckhoff (student in the Lutz lab) developed a prototype that showed excellent temperature control at the paper surface (via cutout window in **Figure 8.10B**, right). Temperature changes can be programmed; transition time is reasonably fast (**Figure 8.10C**).

© Copyright 2021 | N Panpradist

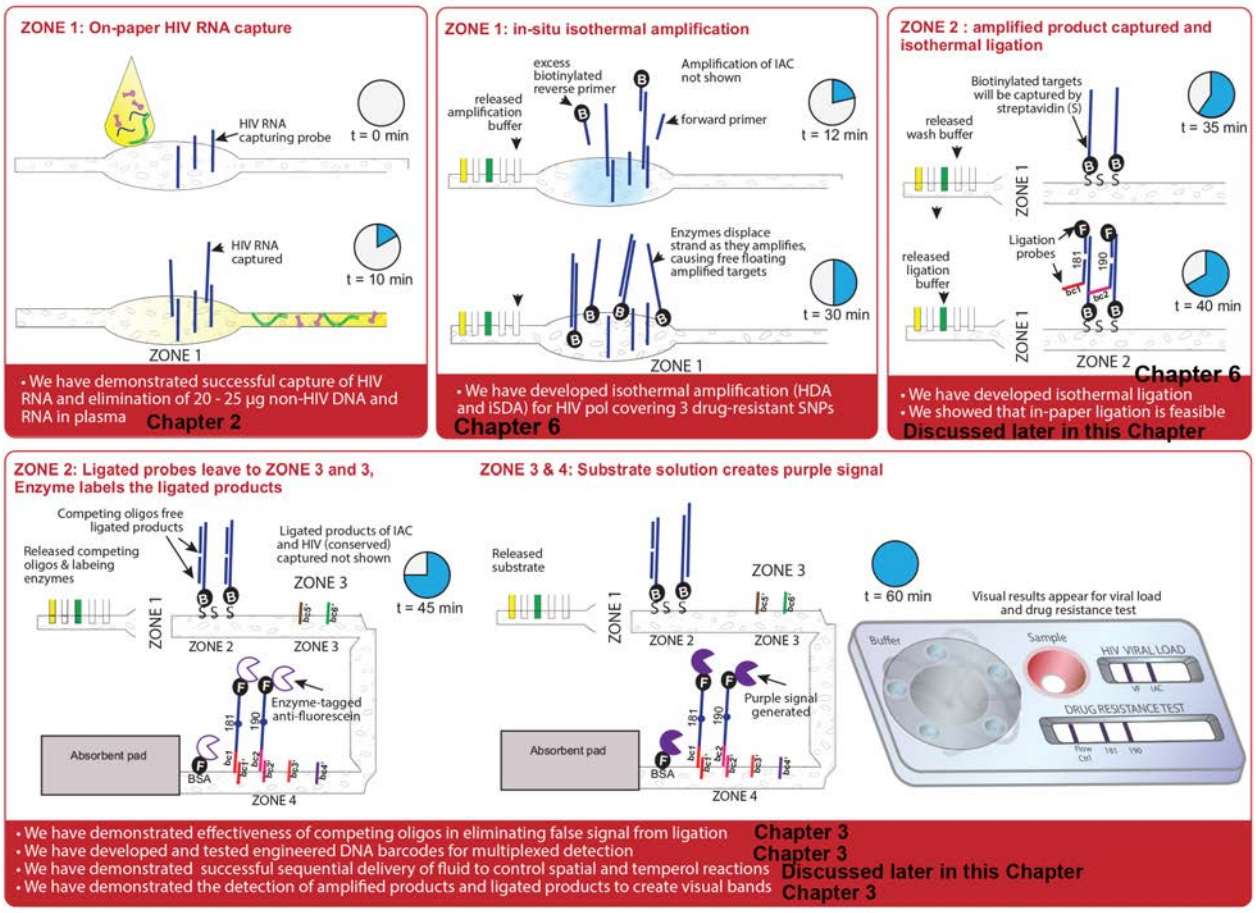

Figure 8.9 | Demonstration of re-engineered physics and chemistries in integrated OLA-Simple device 1.0

All steps in OLA have been re-engineered and demonstrated their feasibility: HIV RNA extraction, solid-phase isothermal amplification, dried reagents, and release of ligated and un-ligated to be captured and detected downstream. We envision our OLA-Simple device to provide the user a very similar experience to using a simple pregnancy test, but our device can detect a single base change HIV RNA in an hour.

© Copyright 2021 | N Panpradist

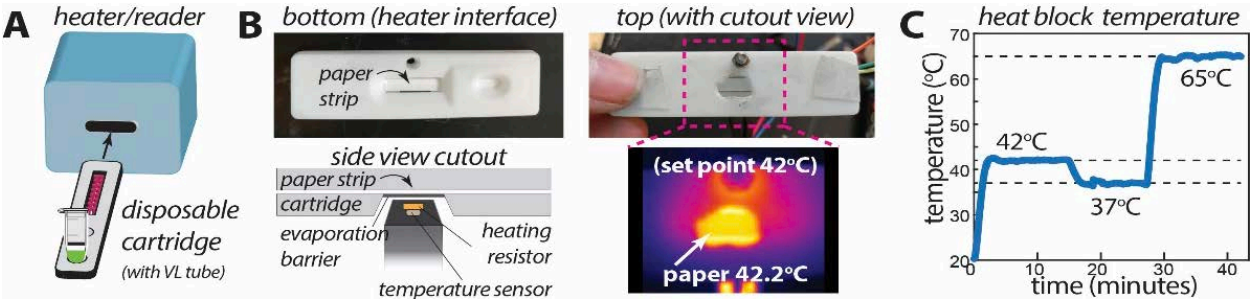

Figure 8.10 | Vision and demonstration for the proof of concept.

The image was obtained from Dr. Lutz's V-OLA R01 application.

FUTURE WORK:

Our housing will be heated during the molecular reactions (49 °C for iSDA or 65 °C for rHDA; and 37 °C for RPA or 55 °C for iLDR), so we will need to test the effect of these temperatures on the microfluidic physics. Different colored fluids will be loaded onto the buffer port on the prototype with only one pull-tab for simplicity. 100µL of 1xPBS (mimicking the extracted RNA sample) will be added into the sample ports, followed by the activation of a pull-tab. The whole prototype will be incubated at 37°C and 65°C in a heated-lid heat block for 1 hour in comparison to the control, which will be run at room temperature. We anticipate minimal difference in microfluidic physics since evaporation is limited from the heated-lid heat block. The first pre-wetting step of the membrane with a 100µL 1xPBS will create an equal pressure across the nitrocellulose. However, if fluid sources deplete prematurely, an additional pull-tab between ZONE 1 and ZONE 2 may be required.

© Copyright 2021 | N Panpradist

8.5 SOLID-PHASE IiNAATS AND iLDR.

Nitrocellulose successfully captured the HIV RNA and HIV DNA in-flow (**Chapter 2**). For the solid-phase reactions, we showed that a glass fiber pad could hold the fluid during the reaction and yielded successful reactions for tHDA, RPA, and shown here iLDR (**Figure 8.11**) can be performed successfully on glass fiber, and others reported RPA on a Whatman cellulose paper pad[8] and iSDA on a glass fiber pad[9].

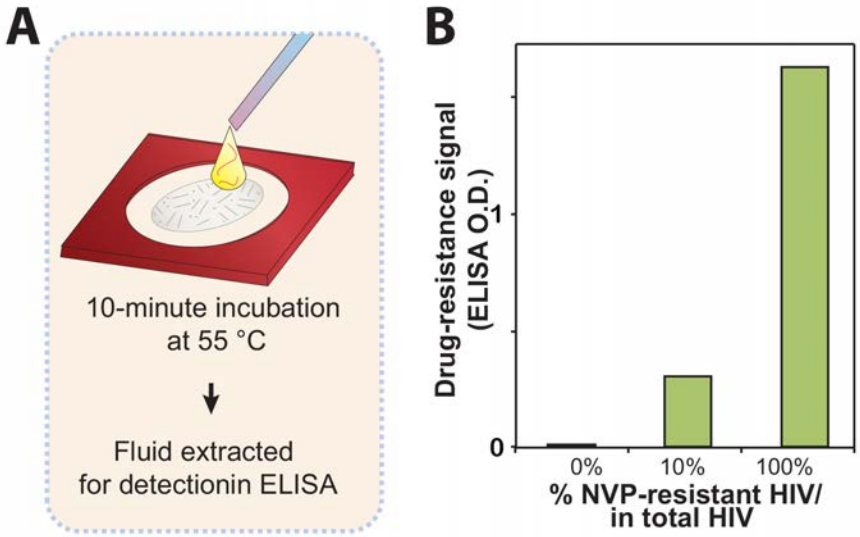

Figure 8.11 | Solid-phase ligation reaction.

(A) Experimental setup. The ligation mixture is added to the glass fiber pad and incubated in a sealed hybridization chamber for 5 minutes at 55 °C. **(B)** Quantitation of drug-resistance signal detected by ELISA. Even for an initial experiment, we could detect 10% MUT HIV.

Here we will need to select one material that satisfies both applications: nucleic acid capture and solid-phase reactions. Porous material should have a sufficiently high surface-to-volume ratio for effective capture of capture nucleic

© Copyright 2021 | N Panpradist

acids as they flow; and have sufficient volume capacity to hold the reaction volume of solid-phase molecular reaction. Nitrocellulose has a high surface-to-volume ratio but binds to all proteins. Nitrocellulose would require additional and pre-blocking steps with casein or BSA for on-paper molecular reactions. Glass fiber has been used as the substrate on which the capturing molecules (e.g., positively charged polymer) are immobilized[6] but its hydrophilic property will require additional treatment prior to protein immobilization. Fusion 5 is a hybrid material that has been used for both holding the reaction volume and for capturing nucleic acid[10]. Based on these considerations, Fusion 5 was used to immobilize streptavidin. A sample containing biotinylated HIV templates (integrated device version 1) or amplicon (integrated device version 2 in **section 8.6**) would be wicked through the capture ZONE containing immobilized streptavidin, followed by wash buffer(s) to remove the non-captured templates (version 1) or remove forward strands of amplicon (version 2). The rehydrated ligation buffer will then be wicked through the capture line, where the template is expected to be captured and subjected to 10 minutes of 55° C incubation. The ligated products will be extracted and subsequently analyzed using the 3rd generation paper-based detection.

8.6 INTEGRATED OLA-SIMPLE VERSION 2 (CROSSROAD DESIGN)

This design is aimed to be used with RT-RPA, which is a faster amplification method, but it is unable to generate excess reverse strands of amplicon via asymmetric amplification like tHDA. To generate an ssDNA template for

© Copyright 2021 | N Panpradist

downstream iLDR, we could use the lambda exonuclease enzyme and conjunction with the 5’ phosphorylated forward primer (**Chapter 6.4**); however,r this step requires additional heat denaturing to deactivate the lambda exonuclease enzyme as it is incompatible with iLDR. To avoid the need for this heat denaturing step, we chose to use a 5’ biotinylated reverse primer to generate the RPA amplicon. The biotin moieties can be captured by streptavidin immobilized on the paper (**Figure 8.12A**), followed by alkaline dissociation of the forward strands (**Figure 8.12B**), neutralization (**Figure 8.12C**), and iLDR reaction (**Figure 8.12D**). The iLDR product was then detected using the 3rd-generation paper-based detection integrated into as part of the device.

We came up with a crossroad design (**Figure 8.13**), in which we have two linear paper circuits. The 1st circuit contained the reagents required for amplification, dissociation, neutralization, and ligation. The 2nd circuit contained the reagents required for the detection (strand displacement competing oligo and gold labeling molecules). After the first series of fluids pass through the streptavidin immobilized pad. The pad was then switched to the second series to be detected.

© Copyright 2021 | N Panpradist

A. Streptavidin captures biotinylated reverse ssDNA hybridized to its forward strand after the RPA step.

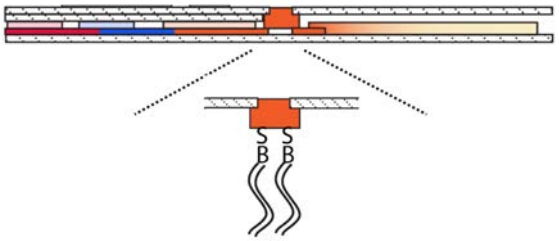

B. NaOH dissociates and washes away the forward strand of the amplicon.

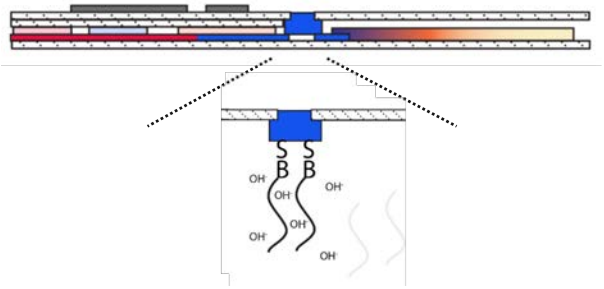

C. Tris-HCl is used to neutralize the remint NaOH residues in the reaction zone.

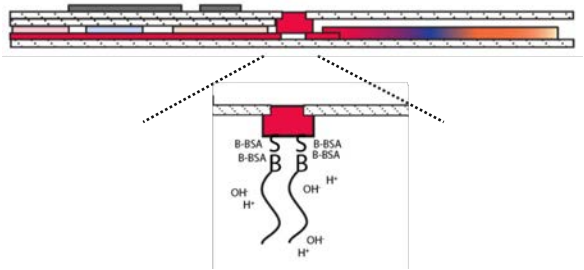

D. Ligation reaction flows to the zone to interact with exposed ssDNA reverse strand.

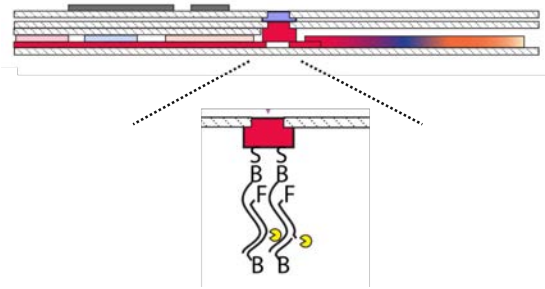

Figure 8.12 | Schematic of on-paper ligation process starting from RPA product.

© Copyright 2021 | N Panpradist

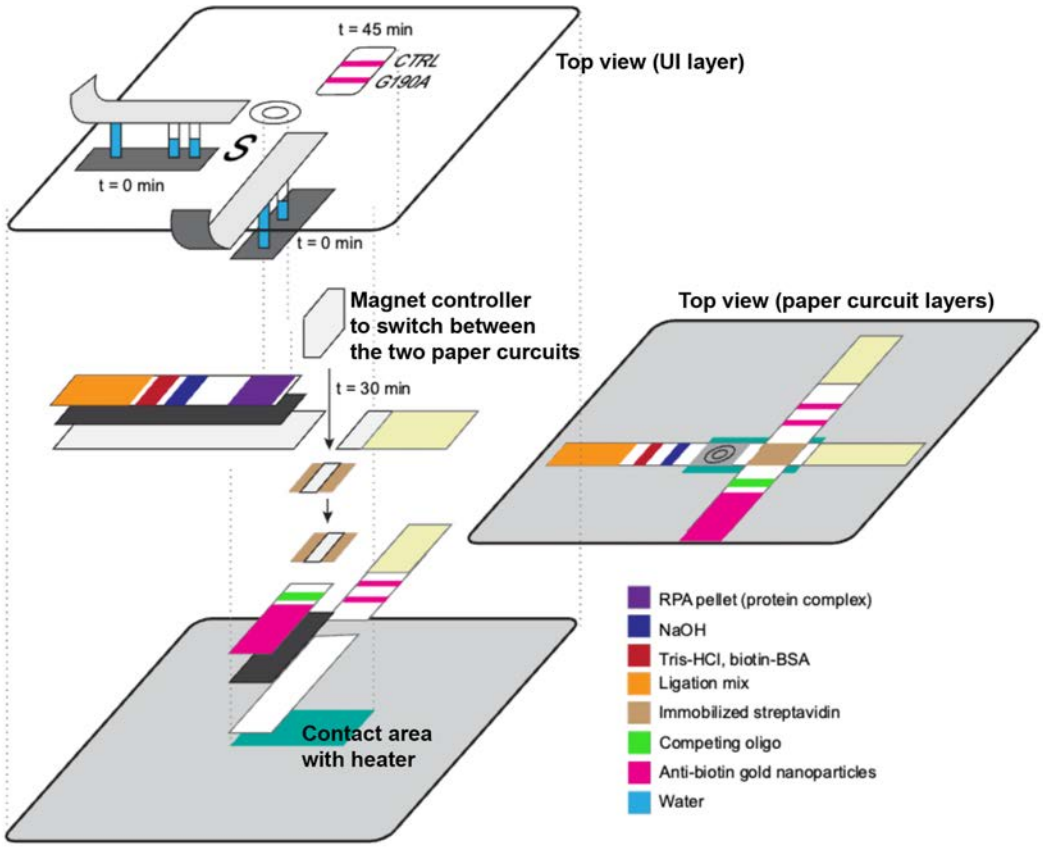

Figure 8.13 | Blueprint of integrated OLA-Simple version 2 (crossroad design).

The yellow paper is the absorbent pad. White is the nitrocellulose. Colored squares represent glass fiber pads containing corresponding reagents.

We planned to use the magnet switch, controlled by the same circuit board for the heating element, to connect and disconnect between the two paper circuits. As a demonstration, I used a weak magnetic to hold the ferrous oxide coated membrane (mimicking the streptavidin pad) to hold them in place (as we would do for the first paper circuit, **Figure 8.14A**). To switch to 2nd circuit, I applied a stronger magnet (**Figure 8.14B**) , and immediately the membrane moved to connect to the other paper circuit (as we would do for the second paper circuit, **Figure 8.14C**).

© Copyright 2021 | N Panpradist

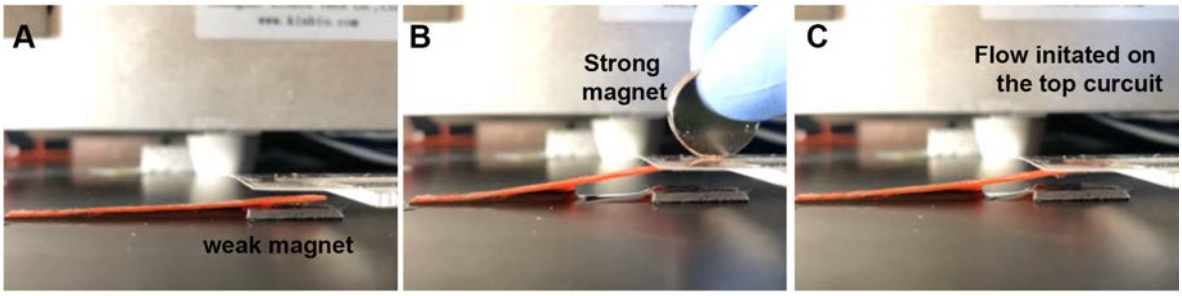

Figure 8.14 | Magnet activated valve enables spontaneous paper circuit switching.

I tested the chemistry compatibility independent of the magnet switch. I assembled the device into two circuits, and the streptavidin pad would be switched manually to start or stop a circuit. **Table 8.1** and **Table 8.2** **show the schema of the assembly for circuits 1 and 2, respectively.**

© Copyright 2021 | N Panpradist

Table 8.1 | Schema of circuit 1 for amplification, dissociation, neutralization, and ligation.

A. Required components

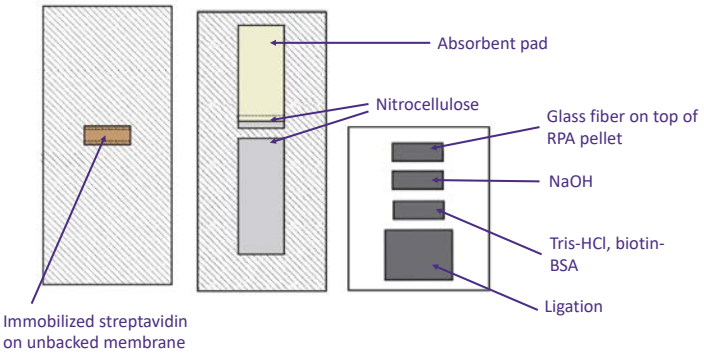

B. Loading reagents on pads

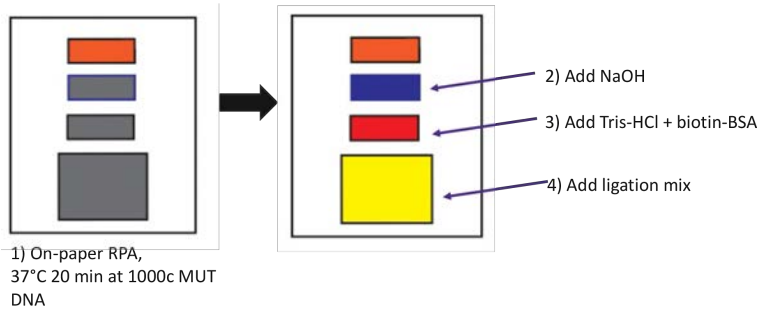

C. Load the above over the bottom nitrocellulose sheet (leaving the gap area)

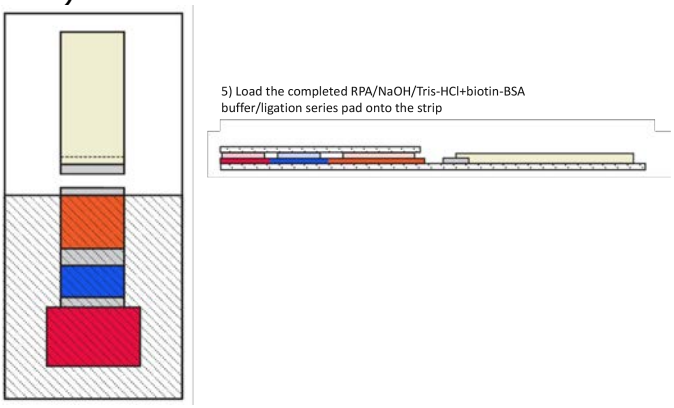

D. Initiate the flow with the other pad series (all dried). Place the pad immobilized with streptavidin on the gap.

© Copyright 2021 | N Panpradist

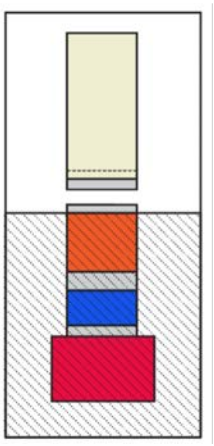

6) Load immobilized streptavidin pad to initiate the flow

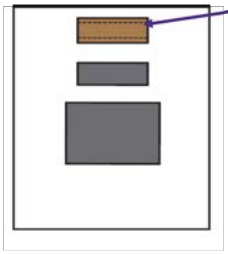

© Copyright 2021 | N Panpradist

Table 8.2 | Assembly of Part 2 device (strand displacement by competing oligo and detection)

Streptavidin pad is disconnected from circuit 1. Load the competing oligo and detection gold on the pads. Place the pad series down on the gap of the other lateral flow detection (with the control and MUT band).

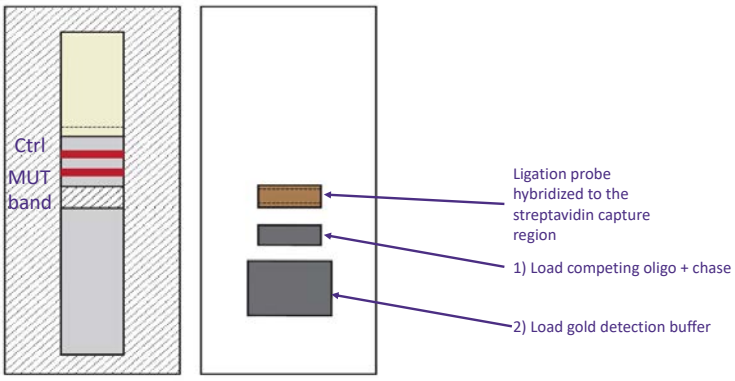

In the actual setup, we had to introduce the hole to allow the streptavidin pad to be removed from the first circuit more easily. As we already knew that RPA amplified on the glass fiber pad, here we aimed to establish the proof-of-concept for the post-amplification steps. RPA amplicon was pre-run and loaded reagents onto the pads according to **Figure 8.15A** and assembled with the streptavidin layer as described the **Table 8.1**. After incubation of the whole device in the heat block at 37 °C. The streptavidin pad was removed and assembled as described in

© Copyright 2021 | N Panpradist

Table 8.2 for detection. The Signal was visualized by a cell phone camera after 15 minutes (**Figure 8.15B**). We observed proper detection of 100% MUT as expected, but future proper experiments will be required to conclude that this experiment is truly successful.

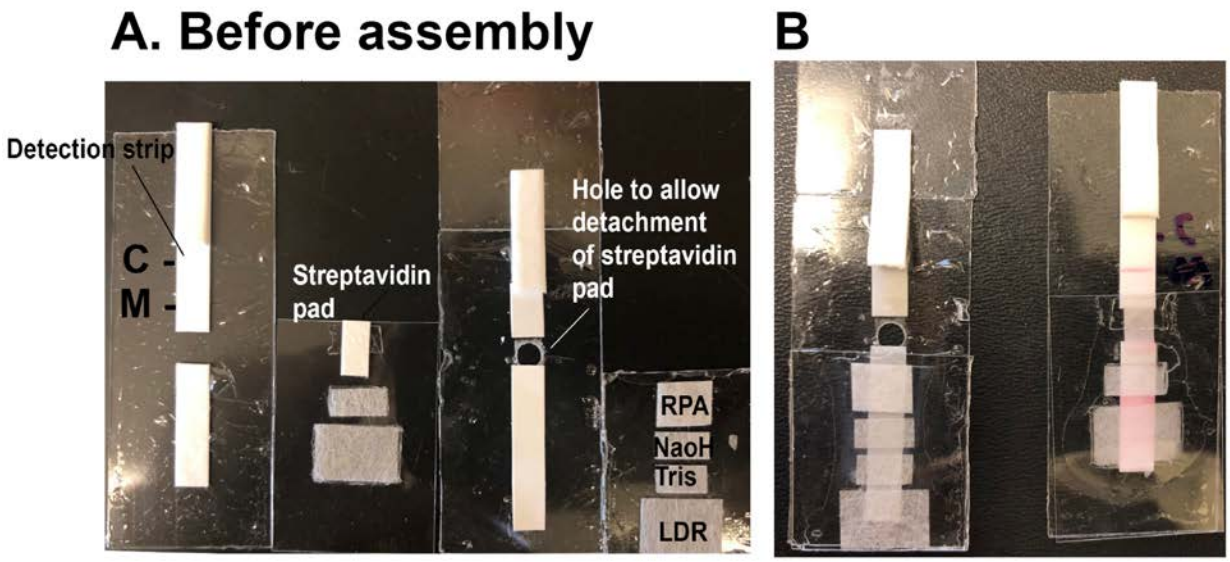

Figure 8.15 | Preliminary results for the chemistry of the crossroad design (Integrated OLA version 2)

© Copyright 2021 | N Panpradist

CHAPTER 8 REFERENCES

1. Altundemir, S.; Uguz, A. K.; Ulgen, K., A review on wax printed microfluidic paper-based devices for international health. *Biomicrofluidics* **2017,** *11* (4), 041501.
2. Carrilho, E.; Martinez, A. W.; Whitesides, G. M., Understanding Wax Printing: A Simple Micropatterning Process for Paper-Based Microfluidics. *Analytical Chemistry* **2009,** *81* (16), 7091-7095.
3. Byers, K. M.; Bird, A. R.; Cho, H. D.; Linnes, J. C., Fully Dried Two-Dimensional Paper Network for Enzymatically Enhanced Detection of Nucleic Acid Amplicons. *ACS Omega* **2020,** *5* (9), 4673-4681.
4. Fu, E.; Liang, T.; Spicar-Mihalic, P.; Houghtaling, J.; Ramachandran, S.; Yager, P., Two-dimensional paper network format that enables simple multistep assays for use in low-resource settings in the context of malaria antigen detection. *Anal Chem* **2012,** *84* (10), 4574-9.
5. Lutz, B. R.; Trinh, P.; Ball, C.; Fu, E.; Yager, P., Two-dimensional paper networks: programmable fluidic disconnects for multi-step processes in shaped paper. *Lab Chip* **2011,** *11* (24), 4274-8.
6. Joung, J.; Ladha, A.; Saito, M.; Segel, M.; Bruneau, R.; Huang, M. W.; Kim, N. G.; Yu, X.; Li, J.; Walker, B. D.; Greninger, A. L.; Jerome, K. R.; Gootenberg, J. S.; Abudayyeh, O. O.; Zhang, F., Point-of-care testing for COVID-19 using SHERLOCK diagnostics. *medRxiv* **2020**.
7. Roskos, K.; Hickerson, A. I.; Lu, H. W.; Ferguson, T. M.; Shinde, D. N.; Klaue, Y.; Niemz, A., Simple system for isothermal DNA amplification coupled to lateral flow detection. *PLoS One* **2013,** *8* (7), e69355.

© Copyright 2021 | N Panpradist

8. Cordray, M. S.; Richards-Kortum, R. R., A paper and plastic device for the combined isothermal amplification and lateral flow detection of Plasmodium DNA. *Malaria journal* **2015,** *14*, 472.

9. Lafleur, L. K.; Bishop, J. D.; Heiniger, E. K.; Gallagher, R. P.; Wheeler, M. D.; Kauffman, P.; Zhang, X.; Kline, E. C.; Buser, J. R.; Kumar, S.; Byrnes, S. A.; Vermeulen, N. M.; Scarr, N. K.; Belousov, Y.; Mahoney, W.; Toley, B. J.; Ladd, P. D.; Lutz, B. R.; Yager, P., A rapid, instrument-free, sample-to-result nucleic acid amplification test. *Lab Chip* **2016,** *16* (19), 3777-87.

10. Gan, W.; Zhuang, B.; Zhang, P.; Han, J.; Li, C. X.; Liu, P., A filter paper-based microdevice for low-cost, rapid, and automated DNA extraction and amplification from diverse sample types. *Lab Chip* **2014,** *14* (19), 3719-28.

© Copyright 2021 | N Panpradist

CHAPTER 9: HOLA: OLA TO DETECT A HUMAN ALLELE (HLA-B*57:01)

SIGNIFICANCE: Abacavir (**ABC**) is a nucleoside reverse transcriptase inhibitor commonly used to treat young children with HIV infection[1-4]. Abacavir can trigger a severe hypersensitivity reaction in people who are homozygous or heterozygous for HLA-B*57:01. Peptide binding groove on the surface of the HLA-B*57-01 antigen-representing cell binds to ABC and peptide PEP-V. The receptors on the T-Cell recognize the complex and tricker cascading immune response leading to adverse drug reactions (**Figure 9.1**).

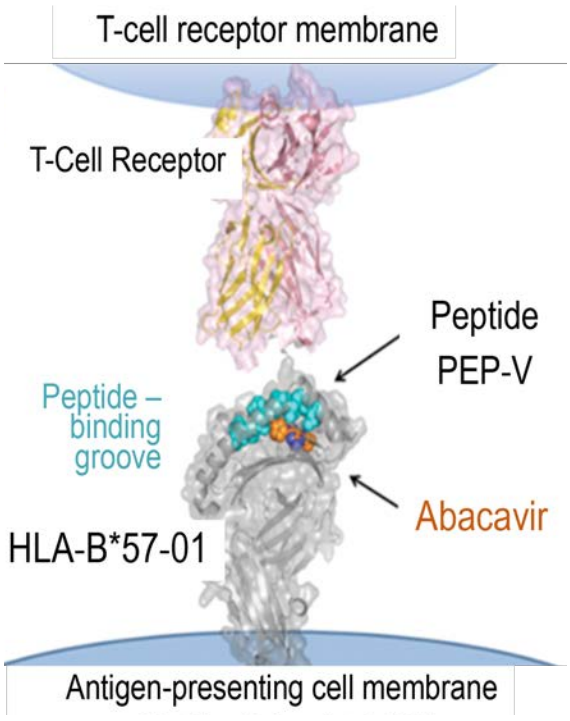

Figure 9.1 | Interaction of HLA-B*57:01 antigen-presenting cell with ABC & peptide PEP-V.

The image was simplified from the original source[5].

© Copyright 2021 | N Panpradist

Despite high tolerability in most patients, ABC triggers a hypersensitivity reaction in 5-8% of people within six weeks of treatment initiation, characterized by fever, rash, nausea, and respiratory distress. Treatment continuation or drug re-initiation can be fatal[6]. The risk of developing a hypersensitivity reaction to ABC is strongly associated with the *HLA-B*57:01* allele[7]. The allele frequency of *HLA-B*57:01* varies by ethnicity, ranging from 0-3% in African and South American populations, 6-10% in Caucasian people, and up to 19% in Southwest Asian populations[8]. Testing for HLA-B*57:01 before abacavir initiation is standard-of-care in high-resource settings [2].

Current tests for ABC hypersensitivity detect the *HLA-B*57:01* subtype by allele-specific PCR or sequencing. Allele-specific PCR uses primers[9, 10] to specifically amplify the *HLA-B*57:01* allele, requiring a standard thermocycler and electrophoresis equipment[9] (cost estimated at US$ 1,500), or real-time fluorescence instruments[11] (cost estimated at US$ 15,000-50,000). Sanger sequencing or next-generation sequencing[9, 12] require even more expensive equipment (>US$ 100,000). Due to high-cost instruments, most *HLA-B*57:01* testing is performed at centralized laboratories, which involves shipping specimens. Slow turn-around-times of 3 days to weeks can delay treatment initiation. Tests that could be performed inexpensively without the need for sequencing technology could increase the safe use of ABC in settings where screening for *HLA-B*57:01* is otherwise cost-prohibitive.

> **DELIVERABLES:** To address this gap, we developed a series of inexpensive, simple-to-use rapid OLA-Simple-based assay "**HOLA-Simple**" to detect HLA-B*57:01. HOLA-Simple version 1 is discussed in **section 9.1** was based on PCR and ligation assay, mainly developed by the Frenkel lab. I contributed to the development of paper-based detection. **Section 9.2** and **Section 9.3**

© Copyright 2021 | N Panpradist

discussed the improvements over the PCR-based HOLA-Simple assay by RPA and LAMP, respectively.

KEY STAKEHOLDER: Through my conversations with drug companies and clinical researchers, I learned that this test might interest the Abacavir manufacturer. For example, ViiV (a large US-based HIV drug company and manufacturer of the formulations containing ABC) paid for the cost of the ABC hypersensitivity test (≥$100/trial).

PREVIOUS PUBLICATIONS

Texts and images in **section 9.1** were obtained from the publication (https://doi.org/10.1101/2021.05.26.21257187).

9.1 HOLA FOR HLA-B 57:01 DETECTION

CONTRIBUTORS AND CONTRIBUTIONS: Jackson J Willer developed and optimized the assay and performed blinded sample testing. Ingrid A Beck and Nuttada Panpradist developed the assay platform and provided writing and project guidance. Nuttada Panpradist and Parker S Ruth manufactured the tests and performed software analysis for the project. H.V-P., M.S-N., S.A-R. Collected and provided samples for blinded testing and sequencing data. B.R.L., S.A-R, and L.M.F. oversaw the project and provided guidance and feedback.

© Copyright 2021 | N Panpradist

MATERIALS AND METHODS

Study design and population. PCR primers were chosen to amplify the region of chromosomal DNA encoding *HLA-B*57* subtypes[9]. OLA probes were designed to detect *HLA-B*57:01* but not other *HLA-B*57* subtypes. The PCR for *HLA-B*57* was multiplexed with primers for human beta-globin as a positive control for DNA extraction, amplification, and ligation. Assay optimization used DNA from five cell lines (LADA, MYE 2004, FH18, 32/32, DBB; from the Fred Hutchinson International Histocompatibility Working Group, Seattle, WA), including *HLA-B*57:01, B*57:02, B*57:03* and a *B*57* negative control. Clinical validation used 60 banked specimens, including 52 Mexican [12] and 8 Seattle Primary Infection Cohort [13] DNA specimens. The Mexican specimens were enriched for *HLA-B*57:01* and other common *B*57* subtypes (i.e., *B*57:02/03*) compared to the Mexican population and were previously typed using next-generation sequencing (Trusight HLA v2 Sequencing Panel on MiniSeq platform [Illumina, San Diego, CA], and Assign v2.0 software was used to assign HLA subtypes) at the Centre for Research in Infectious Diseases (CIENI) of the National Institute of Respiratory Diseases (INER) in Mexico City. Studies collecting these samples and those from the Seattle Primary Infection Cohort were approved by respective Ethics Committees. De-identified DNA from Mexican specimens was sent to Seattle for testing. Following blinded testing by the *HLA-B*57:01* OLA assay, the results were compared to the genotypes determined by sequencing.

Sample preparation. DNA was extracted from the buffy coat (200µL) or PBMCs (peripheral blood mononuclear cells, ~6 million cells) using the QIAmp DNA

© Copyright 2021 | N Panpradist

Blood Mini Kit (Qiagen, Valencia; CA) according to the manufacturer's specifications.

Primers and PCR. The primer sets coamplify a fragment comprising 161 nucleotides of the human beta-globin gene (forward primer: 5'-GGGATCTGTCCACTCCTGATGCTGT; reverse primer: 5'-ATCCACGTGCAGCTTGTCACAGTG) and a region (179bp) specific to *B*57* subtypes using a modification of primers previously published [9] (forward primer: 5'-CCAGGGTCTCACATCATCCAGGT; reverse primer: 5'-CGCCTCCCACTTGCGCTGGG) (Integrated DNA Technology, Coralville, Iowa). The PCR was performed in a 25 µL reaction containing 0.625 U Terra PCR Direct Polymerase (Takara Bio Inc., Shiga, Japan), 0.4 µM of each primer, 12.5 µL Terra buffer, and 2.5 µL of extracted DNA (5-10 ng total DNA). Two-step PCR conditions are as follows: 30 seconds at 95°C, 35 cycles with denaturation for 15 seconds at 95°C followed by annealing for 30 seconds at 68°C, with a final extension at 68°C for 5 minutes.

Ligation. Oligonucleotide probes for *HLA-B*57:01* target a cytosine nucleotide at position 1094 of the *B*57:01* allele (reference sequence *HLA-B*57:01:01*, GenBank Accession number AJ458991), but not other *B*57* types [Z]: *B*57*-probe-1: 5'-FAM-TCCTCC GCGGGCATGACCAGTC; *B*57*-probe-2: 5'-Phosphorylation-YGCCTACGACGGCAAGGATTACA–Biotin. Beta-globin probes ligate when annealed to the beta-globin amplicon and serve as an amplification and ligation control: beta-globin-probe-1: 5'-Digoxigenin-CTCGGTGCCTTTAGTGATGGC CTG; beta-globin-probe-2: 5'-Phosphorylation-GCTCACCTGGACAACCTCAAGGG–Biotin. 2µL amplicon from the

© Copyright 2021 | N Panpradist

multiplex PCR are added directly into 20µL ligation mix containing 1.33U Ampligase DNA Ligase (Lucigen, Middleton, WI), 12.5mM KCl, 1mM NAD, 1x ligase buffer (20mM Tris-HCl, 10mM $MgCl_2$, 1mM DDT), 0.08% TritonX-100, 16.7nM *B*57* probes, 4.2nM beta-globin-probe-1 and 16.7nM beta-globin-probe-2. The ligation reaction conditions are ten cycles with denaturation at 94°C for 30 seconds followed by ligation for 30 seconds at 50°C.

Plate-based OLA detection: Ligated products are captured on a streptavidin-coated 96-well plate (Sigma-Aldrich, St Louis, USA) for one h at room temperature and then denatured by washing with dilute NaOH (0.01 N NaOH and 0.05% Tween®20), followed by incubation with anti-fluorescein and anti-digoxigenin antibodies (Sigma, St. Louis, MO). Secondary reporters are added sequentially for *B*57:01* and beta-globin, and the OD was measured using a Spectramax i3x plate reader (Molecular Devices, San Jose, CA) at 405 and 450 nm, respectively. Samples with high signal (OD > 1.0) at both wavelengths were considered *B*57:01* positive. Samples with low (OD < 0.15) signal at 405nm and high signal at 450 nm were considered negative.

2nd generation paper-based OLA detection for HLA: Unlabeled oligonucleotides with identical sequences to the ligation probes were added at 40-fold higher concentrations than the ligation probes and denatured at 90°C for 30 seconds. The 26.8µL ligation reaction is then added onto lateral flow detection strips and, after 5 minutes, is chased by 43µL buffer containing anti-biotin antibodies conjugated gold nanoparticles (OD=0.7 at 520 nm). Ten minutes after the addition of the gold buffer, the strips were visually inspected for the

© Copyright 2021 | N Panpradist

appearance of precipitated bands to determine genotype or by the scanner and in-house software.

RESULTS

9.1.1 DEVELOPMENT OF THE HLA-B*57:01 OLA ASSAY

We developed an assay that co-amplifies the beta-globin gene and the *B*57* allele from 100% of specimens previously typed as *B*57* positive using supplies costing <US$ 6/specimen. *B*57:01* probe concentrations and ligation conditions were optimized to maximize signal to noise ratio in a 96-well ELISA-based OLA using cell lines with known *B*57:01/02/03* subtypes or no *B*57* variants. The OLA was then adapted to a lateral flow strip format with visual detection. In addition, in-house software was used to quantify band signal intensities from scanned images (**Figure 9.2**).

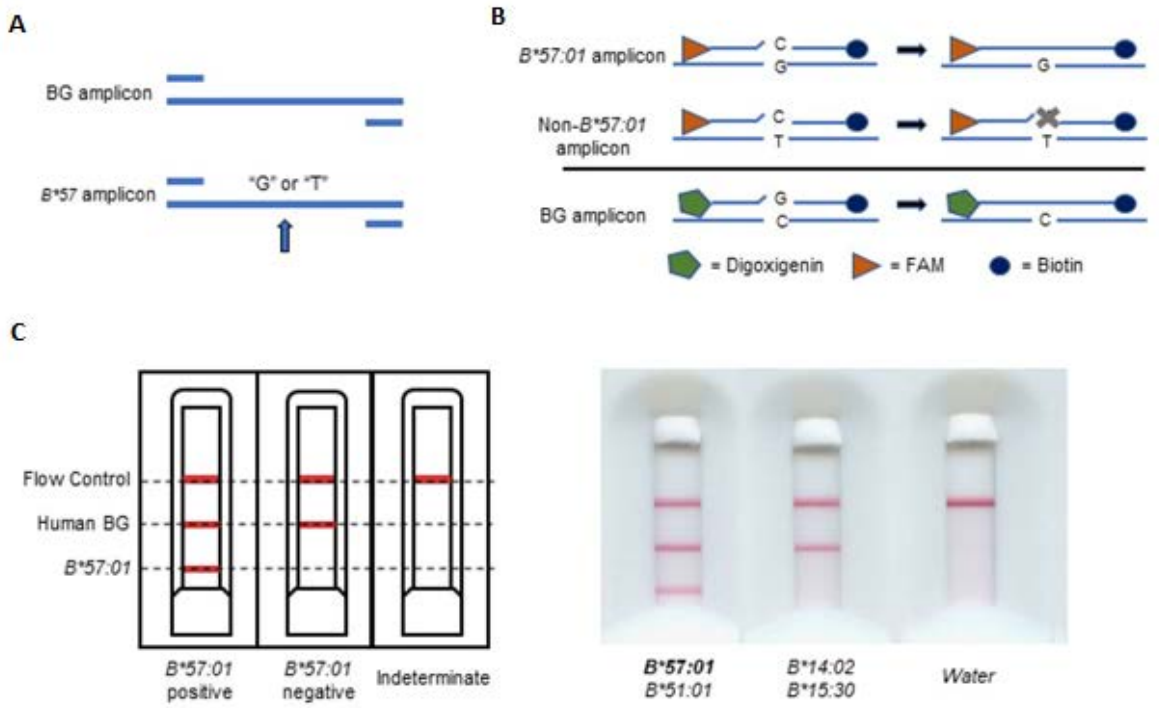

Figure 9.2 | Schematic of OLA-Simple 1.0 for detection of HLA-B*57:01.

© Copyright 2021 | N Panpradist

(**A**) Amplification: Extracted DNA is added to the PCR reaction mixture for multiplexed amplification of human beta-globin (BG) and B*57 gene fragments. (B) Ligation: Labeled B*57:01 probes are selectively ligated together in the presence of amplicons with the B*57:01 allele. BG probes ligate in the presence of the amplified BG region of the somatic genome and serve as a (+) control. (**C**) Lateral flow detection: Chip layout and scanned images of participant sample assays. The appearance of a red line at "Flow Control" indicates the adequate flow of reagents on the single-use cartridge; a red line at "Human BG" indicates the presence of human BG amplicon and confirms adequate DNA extraction, PCR amplification, and ligation; a red line at "B*57:01" indicates detection of B*57:01, either a specimen that is homozygous or heterozygous for the B*57:01 subtype. HLA-B* types determined by Illumina sequencing are shown for two participants' samples tested by OLA.

9.1.2 CLINICAL VALIDATION OF OLA FOR DETECTION OF HLA-B*57:01 SUBTYPES

DNA extracted from 60 clinical samples were tested for *B*57:01* by the lateral flow-based assay and classified as positive or negative for both beta-globin and *B*57:01* bands by visual assessment. Compared to HLA typing by sequencing, visual inspection of the OLA classified as positive all 27 specimens heterozygous for *B*57:01* (100% sensitivity [95% confidence interval: 87.2-100%]) (**Table 9.1**). The remaining 33 specimens were correctly classified as *B*57:01* negative (100% specificity [95% confidence interval: 89.4-100%]). All samples were classified as positive for the human beta-globin control.

© Copyright 2021 | N Panpradist

Table 9.1 | Comparisons of HLA-B-57:01 OLA-Simple visual classifications by human and by software.

HLA-B Typing Results			
***HLA-B* type by Illumina Sequencing**	**Number of specimens**	**Expected outcome by OLA**	**Correct outcome by OLA**
*B*57:01*	27	+	27/27
*B*57:02*	1	-	1/1
*B*57:03*	9	-	9/9
*Non-B*57*	24	-	24/24

Note: *Non-B*57* types tested included - *B*07, 08, 13, 14, 15, 18, 35, 38, 39, 40, 41, 42, 44, 45, 48, 49, 51, 52*

Sensitivity:
27/27 positive for HLA- *B*57:01* = 100%
Specificity:
34/34 negative for HLA- *B*57:01* = 100%

9.1.3 VALIDATION OF OLA BY IN-HOUSE SOFTWARE

To avoid human error, the lateral flow strips can be analyzed using in-house Python software, based on an algorithm previously described[14]. The software automatically detected bands in the paper strips and quantified signal intensity by subtracting brightness within the band and adjacent background regions. By the in-house software, all 60 specimens were correctly classified as *B*57:01* positive or negative (100% sensitivity and specificity).

DISCUSSION

We developed and evaluated an inexpensive and relatively rapid assay that accurately detects the *HLA-B*57:01* subtype, associated with a

© Copyright 2021 | N Panpradist

hypersensitivity reaction to ABC, and discriminates it from similar common *B*57* subtypes (i.e., *B*57:02* and *B*57:03*). Assay operation requires minimal supplies and relatively inexpensive equipment and delivers results in less than 2 hours (i.e., [15]30-minute DNA extraction, 40-minute PCR, 20-minute ligation, and 15-minute detection). Results are simple to analyze by the unaided eye or using a scanner and our in-house software. This assay showed high sensitivity and specificity for detection of *HLA-B*57:01* in clinical samples compared to HLA typing by sequencing. Performance of the OLA was similar to other non-sequencing methods such as allele-specific PCR[9, 11, 16].

This study was limited by a relatively low number of clinical samples tested; however, it was enriched to include all with the *B*57:01* subtype from an HIV cohort of ~1,800 individuals in Mexico City. A sample panel from more diverse populations would allow a more comprehensive validation of primers and probes and discrimination of *B*57:01* from other HLA subtypes. The primers and probes used in this assay are complementary at the site of ligation to sequences described for two other alleles (*B*57:08* and *B*55:14*)[9], which would likely result in a false-positive result for a non-*B*57:01* specimen. However, the frequencies of these two HLA subtypes across most of the world's populations are much lower than that of *HLA-B*57:01*[17-19].

To increase ease of use, test reagents can be lyophilized for single-use aliquots (see **Chapter 4**).

© Copyright 2021 | N Panpradist

9.2 RPA ASSAY AND FAST LIGATION TO SPEED UP ASSAY TIME.

The buccal swab is an excellent sample source for human genomic DNA in place of. They are non-invasive and do not require collection by trained personnel. DNA extractions from buccal swab samples reported yielded a wide range from 360ng to 450µg from the 150-200µL swab eluate[20, 21].

RPA could process complex lysates without DNA purification [22] [23], but detergents reportedly cause false negatives in the RPA assay[24] (and we confirmed this finding in-house). We hypothesize that detergents interfere with the crowding agents required to promote the binding of the recombinases to primers. Thus, we plan to use proteinase K followed by heat treatment to extract the DNA from the swab eluate followed by RPA, ligation, and detection, as shown in **Figure 9.3**.

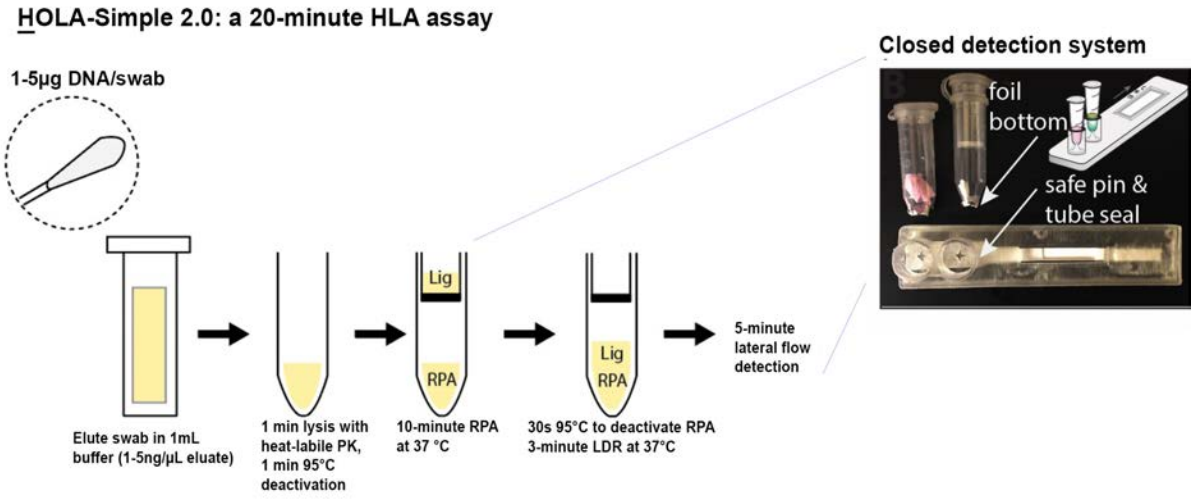

Figure 9.3 | Vision of HOLA 2.0.

© Copyright 2021 | N Panpradist

Swab eluate is lysed by proteinase K (**PK**). After the PK heat-deactivation step, the lysate is added to the RPA reaction tube to rehydrate and covered with the nested closed tube, which contains rehydrated ligation buffer. After 10 minutes at 37C, the ligation mix is spin down via a low-cost minicentrifuge. Followed by 30s at 95°C to deactivate the RPA reaction and denature the template, LDR reaction occurs at 37°C for 3 minutes. The LDR products are then detected using a closed detection system.

I designed RPA primers for both the HLA*B57:01 and human beta-globin control assays (**Table S9.3**). I used the footprints (**Figure 9.4A**) nearly identical to those used in the PCR assay in HOLA-Simple version 1 and modified the primer design to meet RPA requirements. Next, we tested the single-plex and bi-plex RPA assay at the clinically relevant concentrations of the human DNA. Supposing we added 1µL lysed swab eluate into the RPA reaction, we would expect 1-3 ng/reaction. Both single-plex and bi-plex RPA assays detected down to 1ng/reaction, as indicated generated amplicon detectable by fragment analyses (180 bp for the HLA-B*57:01 RPA and 300 bp for Beta globin assay, **Figure 9.4B**). For the bi-place RPA assay, we used a 50% primer concentration of each assay to maintain a total primer concentration and avoid overwhelming the recombinases. Even at a reduced primer concentration, we still observed ~50bp side products, especially for the negative samples in the bi-plexed assay. The amplicon from the bi-plexed assay analyzed by the combination of fast ligation and detection yielded detectable HLA-B*57:01 positive bands within 10 minutes after the RPA step (**Figure 9.5**).

© Copyright 2021 | N Panpradist

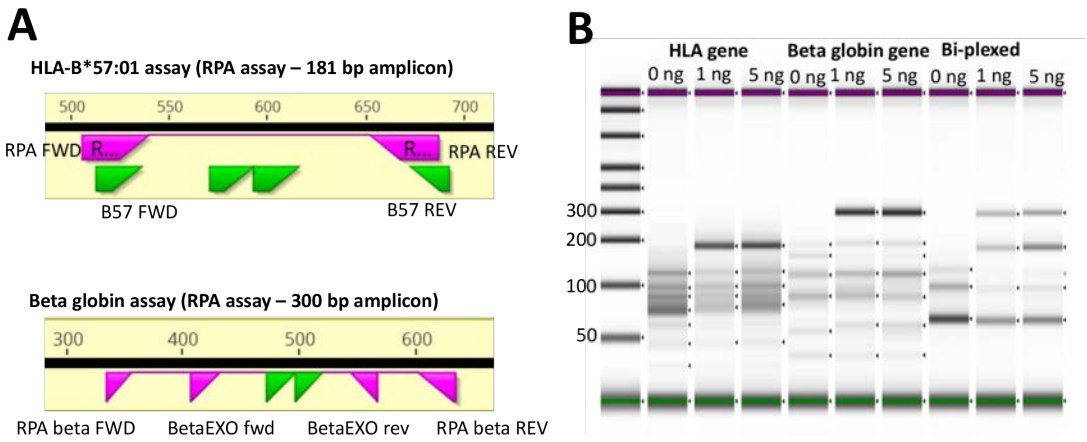

Figure 9.4 | RPA assay for HOLA 2.0.

(**A**) RPA primer footprints compared to PCR. (**B**) Fragment analysis of RPA products. 1µL from 60µL purified amplicon eluate was visualized on TapeStation.

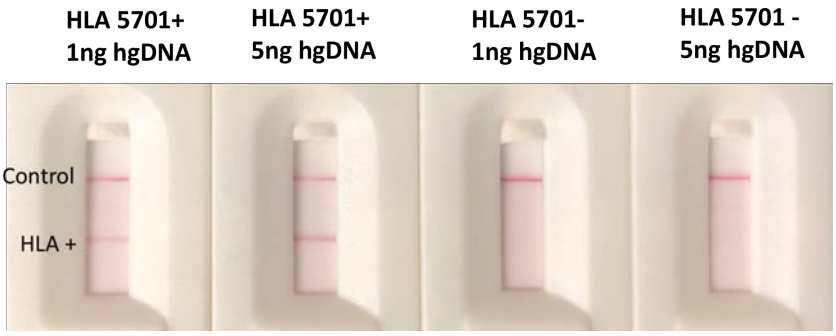

Figure 9.5 | Preliminary results from HOLA-Simple version 2 (excluding extraction).

HLA-B*57:01 DNA template (10^5 copies) or water were spiked in 1ng or 5ng human genomic DNA and amplified using the bi-plexed RPA assay for 10 minutes, followed by 4-minute ligation (95 °C for 30 seconds, 37 °C for 3 minutes) and 5-minute of the3rd generation paper-based detection.

SUMMARY OF THE RPA ASSAY TO IMPROVE HOLA-SIMPLE

We achieved 10-minute RPA amplification down to 1ng/reaction (~300 copy). Sample prep requires initial heat lysis in a separate tube with optional PK de-activation before RPA initiation. We were unable to generate meaningful asymmetric amplification as RPA is sensitive to primer concentration. Buffer

© Copyright 2021 | N Panpradist

exchange or dilution was required for subsequent ligation. Here we used a dilution of 1:6 RPA: ligation buffer to avoid amplicon purification.

9.3 SWAB DIRECT TO AMPLIFICATION VIA LAMP

LAMP has been known for its ability to tolerate sample complexities [25-27], and by far the most often used isothermal assays for direct to amplification applications. In **Chapter 6**, we discussed RT-LAMP for HIV VL test that uses in-house DNA polymerase to enable highly specific isothermal amplification and enable *in-situ* lysis and RT-LAMP in a single temperature. Using LAMP as an amplification method would further improve the speed of HOLA-Simple version 3.

Building on this concept, I designed the primers (**Table S9.4**) for the LAMP assay to amplify the HLA-B*57:01 amplicon. Secondary structure analyses showed stable loop structures (**Figure 9.6**) for the expected amplicon after the initial incorporation of FIP and BIP primers.

© Copyright 2021 | N Panpradist

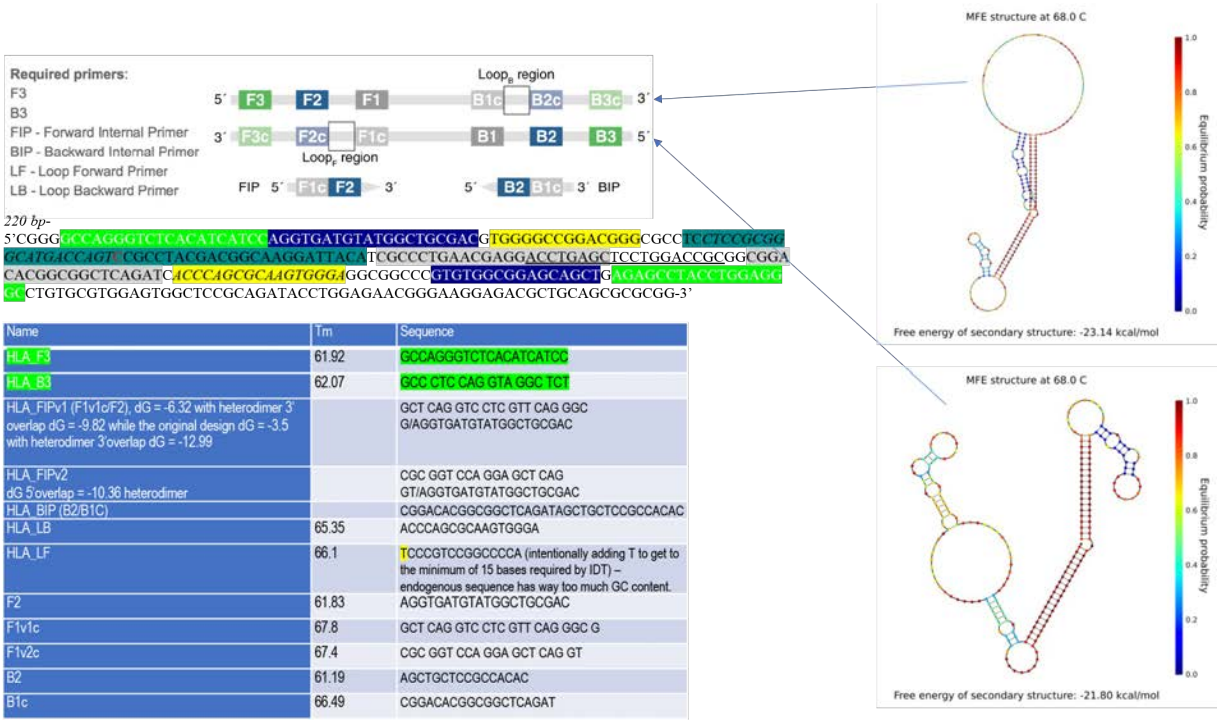

Name	Tm	Sequence
HLA_F3	61.92	GCCAGGGTCTCACATCATCC
HLA_B3	62.07	GCC CTC CAG GTA GGC TCT
HLA_FIPv1 (F1v1c/F2), dG = -6.32 with heterodimer 3' overlap dG = -9.82 while the original design dG = -3.5 with heterodimer 3'overlap dG = -12.99		GCT CAG GTC CTC GTT CAG GGC G/AGGTGATGTATGGCTGCGAC
HLA_FIPv2 dG 5'overlap = -10.36 heterodimer		CGC GGT CCA GGA GCT CAG GT/AGGTGATGTATGGCTGCGAC
HLA_BIP (B2/B1C)		CGGACACGGCGGCTCAGATAGCTGCTCCGCCACAC
HLA_LB	65.35	ACCCAGCGCAAGTGGGA
HLA_LF	66.1	TCCCGTCCGGCCCCA (intentionally adding T to get to the minimum of 15 bases required by IDT) – endogenous sequence has way too much GC content.
F2	61.83	AGGTGATGTATGGCTGCGAC
F1v1c	67.8	GCT CAG GTC CTC GTT CAG GGC G
F1v2c	67.4	CGC GGT CCA GGA GCT CAG GT
B2	61.19	AGCTGCTCCGCCACAC
B1c	66.49	CGGACACGGCGGCTCAGAT

Figure 9.6 | Secondary structure analysis of LAMP amplicon in HOLA-Simple version 3.

Teal-colored bases are the probe region for the LDR step, which are between the F1 and B1 regions.

The HLA-B*57:01 LAMP assay performed the fastest at 68 °C and reliably detected down to 29 copies of purified human genomic DNA/reaction (**Figure 9.7A**). Testing the purified DNA extracted from the patient samples and controls, our assay successfully amplified 100% (8/8) CIENI patient samples and 87% (7/8) Seattle's positive controls (7/8). We are pending confirmation from our collaborators on the identity and concentration of the one control missed by this LAMP assay since we were informed that these control from Seattle were intentionally diluted to test the assay sensitivity and may be lower than what we would expect in clinical specimens. Regardless, all patient and control samples amplified had a liftoff time as early as 15 minutes (30 cycles of the 30s) and reached saturation after 30 minutes (60 cycles of 30s).

© Copyright 2021 | N Panpradist

A. Amplification of purified human DNA

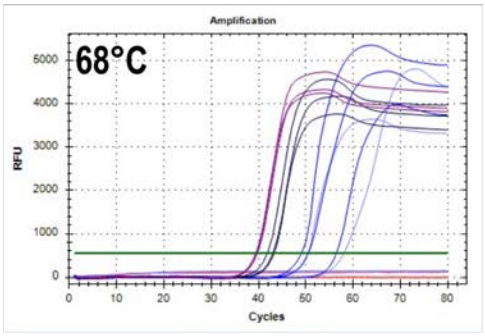

Target concentration	# of detectable replicates	Time to detection (min)
0	0/3	N/A
0.01ng(2.9c)	2/4	25.24; 29.07
0.1ng(29c)	3/3	24.55; 28.24; 25.26
1ng(290c)	3/3	20.94; 21.65; 21.53
10ng (2900c)	3/3	19.89; 19.73; 19.74

B. DNA from patient and control samples

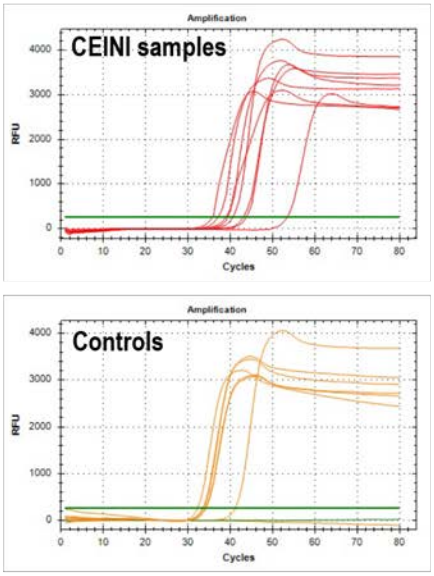

Figure 9.7 | Analysis of LAMP assay in HOLA-OLA-Simple 3.0 in purified human DNA.

Next, I investigated the feasibility of in-situ lysis and amplification from human buccal swabs (self-collected by WhatmanOmnii swab and large tip buccal foam swab). We also spiked in 100mM GuSCN in the LAMP reaction to test whether it could help improve the amplification yield from the buccal swab. Additionally, our in-house TFv1 polymerase is thermostable, so we introduced the initial 5-minute 95°C incubation before standard LAMP at 68°C protocol and compared the amplification yield to the standard protocol. Amplification curves are shown in **Figure 9.8** and summarized in **Table 9.2.**

© Copyright 2021 | N Panpradist

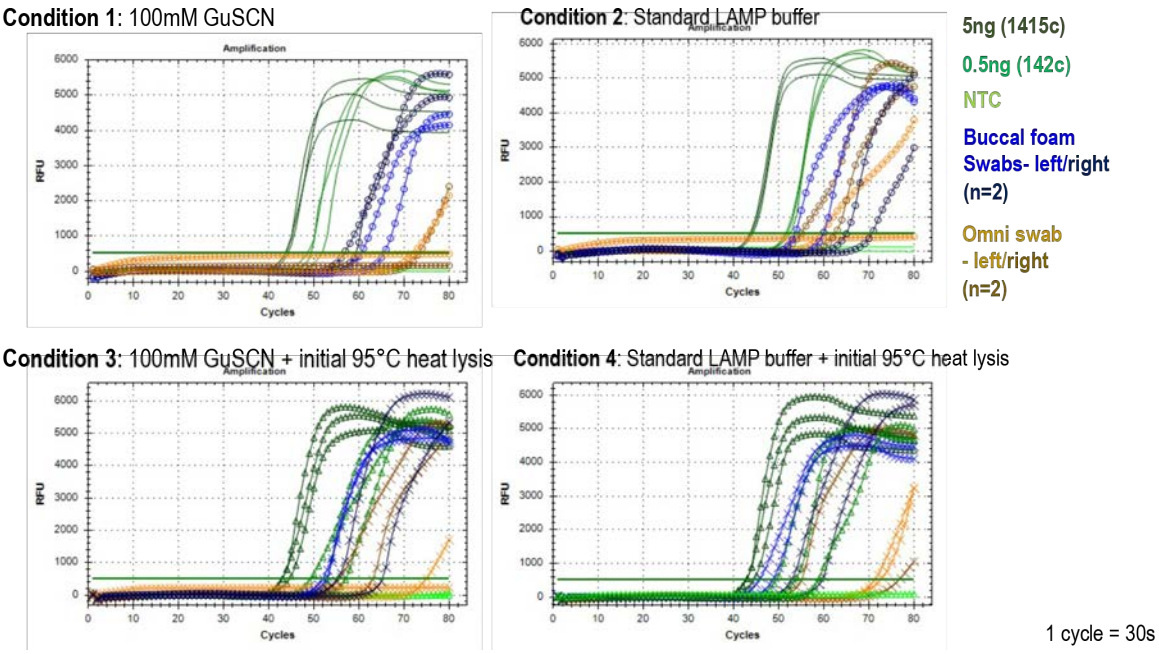

Figure 9.8 | In-situ lysis and amplification in HOLA-Simple 3.0.

Dark green line samples are the amplification of purified human genomic DNA. Light green line samples are the amplification of negative controls. Blue line samples are the amplification from buccal swabs. Brown line samples are the amplification from Omni swabs. Swabs were mixed in 1mL 1xTLE buffer for 30 seconds, and 5µL eluate was added to the 20µL LAMP reaction.

Table 9.2 | Summary of in-situ lysis and amplification in different reaction conditions and swab types.

Condition	Lysis method	Number of detectable samples Omni swab (time to detect, minutes)	Number of detectable samples Foam swab (time to detect, minutes)
1	100mM GuSCN	2/4 (mean±SD: 36.4±0.4)	4/4 (30.24±1.9)
2	Standard LAMP	3/4 (29.6±1.9)	4/4 (31.15±3.6)
3	100mM GuSCN + initial 95°C for 5 minutes	3/4 (32±4.9)	4/4 (28.2±3.0)
4	Standard LAMP + initial 95°C for 5 minutes	4/4 (34±4.8)	4/4 (25±3.0)

© Copyright 2021 | N Panpradist

100mM GuSCN and heat denaturing did not significantly impact the speed of purified DNA amplification. Large tip foam swabs outperformed the Omni swabs in terms of reproducibility. For foam swab samples, GuSCN/heat minimally increased the reaction speed by 2.5-5 minutes. Thus, we concluded that direct amplification by standard LAMP buffer is feasible.

Next, we tested the impact of elution buffer volume in buccal swabs collected from two individuals (1 male and 1 female adult). We found that the time to detection and plausibility of the RT-LAMP assay from the samples eluted 400µL TLE buffer is faster than samples eluted in 800µL. This is likely due to higher target concentrations are present when a less elution volume is used, and the inhibitors from samples were diluted enough to not interfere with the amplification. Thus, we would use this elution volume as the standard protocol moving forward.

- Sample 1-2: Foam buccal swab eluted in 800uL 1xTLE buffer (5uL elution in 20uL PCR)
- Sample 3-4: Foam baccal swab eluted in 400uL 1xTLE buffer (5uL elution in 20uL PCR)

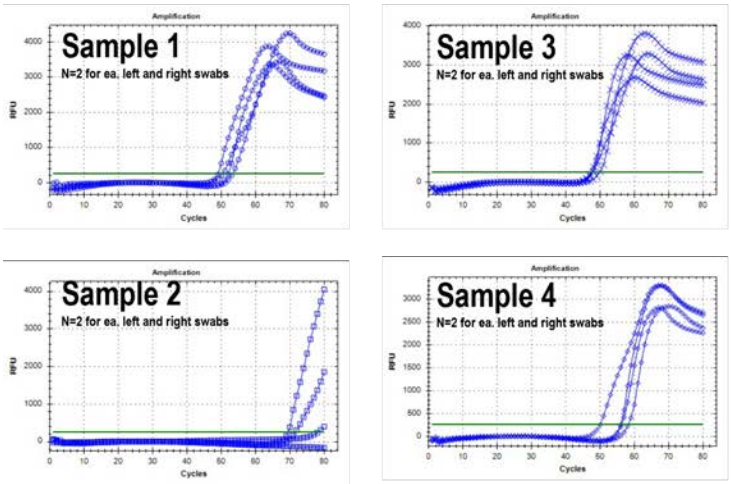

Sample	Number of detectable samples	Time to detection (minutes)
1	4/4	25.6±0.9
2	3/4	36.6±2.3
3	4/4	24.1±0.6
4	4/4	27.6±1.7

Figure 9.9 | Effect of elution buffer volume on in-situ amplification.

© Copyright 2021 | N Panpradist

Next, we will test the compatibility of these LAMP amplicons on LDR and detection, possibly since LAMP has 8mM $MgSO_4$, very similar to the LDR salt concentration (10mM $MgCl_2$). A single-tube LAMP/LDR in one reaction might be feasible. The product of LDR, if detected via fluorescence detection (**Chapter 7**), would lead to a single-tube ABC detection assay.

© Copyright 2021 | N Panpradist

9.4 SUPPLEMENTARY INFORMATION CHAPTER 9

Table S9.3 | HLA B57:01 primer sequences for RPA

Category	Sequence name	Sequence (5' to 3')
HLA-B*57:01 positive template	MUT_HLA_DNA	CTGACCGCGGGGCCGGGGCCAGGGTCTCAC ATCATCCAGGTGATGTATGGCTGCGACGTGG GGCCGGACGGGCGCCTCCTCCGCGGGCATG ACCAGTCCGCCTACGACGGCAAGGATTACAT CGCCCTGAACGTGGACCTGAGCTCCTGGACC GCGGCGGACACGGCGGCTCAGATCACCCAG CGCAAGTGGGAGGCGGC
RPA primers for HLA assay	RPA_57_FWD	GCCGGGGCCAGGGTCTCACATCATCCAGGT
	RPA_57_REV	CCACTTGCGCTGGGTGATCTGAGCCGCCGTG TCC
RPA primers for Beta globin assay	RPA_Beta_FWD	ACCCTTAGGCTGCTGGTGGTCTACCCTTGGA CCCA
	RPA_Beta_REV	CGCCTCCCCTCCTTTTGACATGAATTCACCCC ACGA
Ligation probes with tags	MUTB57_tag	/56-FAM/AGTAATCATCCTCCGCGGGCATGACCAG TC
	COM_B57_tag	/5Phos/YGCCTACGACGGCAAGGATTACAAGT AATCA/3Bio/
Competing oligos with tags	Compt_MUT_B57	GACTGGTCATGCCCGCGGAGGATGATTACT
	Compt_COM_B57	TGATTACTTGTAATCCTTGCCGTCGTAGGCR

HLA B57:01 primer LAMP

Template:

5’ -GCTCCCACTCCATGAGGTATTTCTACACCGCCATGTCCCGGCCCGGCCGCGGG-
GAGCCCCGCTTCATCGCAGTGGGCTACGTGGACGACACCCAGTTCGTGAGGTTCGACAGCGACGCCG
CGAGTCCGAGGATGGCGCCCCGGGCGCCATGGATAGAGCAGGAGGGGCCGGAGTATTGGGAC-
GGGGAGACACGGAACATGAAGGCCTCCGCGCAGACTTACCGAGAGAACCTGCGGATCGCGCTCCGCT
ACTACAACCAGAGCGAGGCCGGTGAGTGACCCCGGCCCGGGGCGCAGGTCAC-
GACTCCCCATCCCCCACGTACGGCCCGGGTCGCCCCGAGTCTCCGGGTCCGAGATCCACCCCCCTGAG
GCCGCGGGACCCGCCCAGACCCTCGACCGGCGA-
GAGCCCCAGGCGCGTTTACCCGGTTTCATTTTCAGTTGAGGCCAAAATCCCCGCGGGTTGGTCAGGGC
GGGGCGGGGTTTTTTTTTTCGGGGCTGAC-
CGCGGGGCCGGGGCCAGGGTCTCACATCATCCAGGTGATGTATGGCTGCGACGTGGGGCCGGACGGG
GCGCCTCCTCCGCGGGCATGACCAGTCCGCCTACGACGGCAAGGATTACATCGCCCTGAAC-
GAGGACCTGAGCTCCTGGACCGCGGCGGACACGGCGGCTCAGATCACCCAGCGCAAGTGGGAGGCG
GCCCGTGTGGCGGAGCAGCTGAGAGCCTACCTGGAGGGCCTGTGCGTGGAGTGGCTCCG-
CAGATACCTGGAGAACGGGAAGGAGACGCTGCAGCGCGCGG - 3’

© Copyright 2021 | N Panpradist

Table S9.4 | Sequence for HLA LAMP primers.

Name	5'pos	3'pos	Len	Tm	Sequence
HLA_F3	512	531	20	61.92	GCCAGGGTCTCACATCATCC
HLA_B3	714	731	18	62.07	GCC CTC CAG GTA GGC TCT
HLA_FIPv1 (F1v1c/F2), dG = -6.32 with heterodimer 3' overlap dG = -9.82 while the original design dG = -3.5 with heterodimer 3'overlap dG = -12.99					GCT CAG GTC CTC GTT CAG GGC G/AGGTGATGTATGGCTGCGAC
HLA_FIPv2 dG both homo/heterodimer 5'overlap = -10.36 heterodimer					CGC GGT CCA GGA GCT CAG GT/AGGTGATGTATGGCTGCGAC
HLA_BIP (B2/B1C)					CGGACACGGCGGCTCAGATAGCTGCTC CGCCACAC
HLA_LB	672	688	17	65.35	ACCCAGCGCAAGTGGGA
HLA_LF	553	566	14	66.1	TCCCGTCCGGCCCCA (intentionally adding T to get to the minimum of 15 bases required by IDT) – endogenous sequence has way too much GC content.
F2	532	551	20	61.83	AGGTGATGTATGGCTGCGAC
F1v1c	617	638	22	67.8	GCT CAG GTC CTC GTT CAG GGC G
F1v2c	631	649	20	67.4	CGC GGT CCA GGA GCT CAG GT
B2	697	712	16	61.19	AGCTGCTCCGCCACAC
B1c	652	670	19	66.49	CGGACACGGCGGCTCAGAT

© Copyright 2021 | N Panpradist

Chapter 9 References

1. Staszewski, S.; Katlama, C.; Harrer, T.; Massip, P.; Yeni, P.; Cutrell, A.; Tortell, S. M.; Harrigan, R. P.; Steel, H.; Lanier, R. E.; Pearce, G., A dose-ranging study to evaluate the safety and efficacy of abacavir alone or in combination with zidovudine and lamivudine in antiretroviral treatment-naive subjects. *AIDS (London, England)* **1998,** *12* (16).
2. World Health Organization Update of recommendations on first-and second-line antiretroviral regimens. . https://apps.who.int/iris/bitstream/handle/10665/325892/WHO-CDS-HIV-19.15-eng.pdf.
3. Moyle, G. J.; DeJesus, E.; Cahn, P.; Castillo, S. A.; Zhao, H.; Gordon, D. N.; Craig, C.; Scott, T. R., Abacavir once or twice daily combined with once-daily lamivudine and efavirenz for the treatment of antiretroviral-naive HIV-infected adults: results of the Ziagen Once Daily in Antiretroviral Combination Study. *Journal of acquired immune deficiency syndromes (1999)* **2005,** *38* (4), 417-25.
4. Panel on Antiretroviral Therapy and Medical Management of Children Living with HIV Guidelines for the Use of Antiretroviral Agents in Pediatric HIV Infection. https://clinicalinfo.hiv.gov/en/guidelines/pediatric-arv/whats-new-guidelines.
5. Redwood, A. J.; Pavlos, R. K.; White, K. D.; Phillips, E. J., HLAs: Key regulators of T-cell-mediated drug hypersensitivity. *Hla* **2018,** *91* (1), 3-16.

© Copyright 2021 | N Panpradist

6. Hetherington, S.; McGuirk, S.; Powell, G.; Cutrell, A.; Naderer, O.; Spreen, B.; Lafon, S.; Pearce, G.; Steel, H., Hypersensitivity reactions during therapy with the nucleoside reverse transcriptase inhibitor abacavir. *Clin Ther* **2001,** *23* (10), 1603-14.
7. Mallal, S.; Nolan, D.; Witt, C.; Masel, G.; Martin, A. M.; Moore, C.; Sayer, D.; Castley, A.; Mamotte, C.; Maxwell, D.; James, I.; Christiansen, F. T., Association between the presence of HLA-B*5701, HLA-DR7, and HLA-DQ3 and hypersensitivity to HIV-1 reverse-transcriptase inhibitor abacavir. *Lancet* **2002,** *359* (9308), 727-32.
8. Martin, M. A.; Klein, T. E.; Dong, B. J.; Pirmohamed, M.; Haas, D. W.; Kroetz, D. L., Clinical pharmacogenetics implementation consortium guidelines for HLA-B genotype and abacavir dosing. *Clin Pharmacol Ther* **2012,** *91* (4), 734-8.
9. Martin, A. M.; Nolan, D.; Mallal, S., HLA-B*5701 typing by sequence-specific amplification: validation and comparison with sequence-based typing. *Tissue Antigens* **2005,** *65* (6), 571-4.
10. Stocchi, L.; Cascella, R.; Zampatti, S.; Pirazzoli, A.; Novelli, G.; Giardina, E., The Pharmacogenomic HLA Biomarker Associated to Adverse Abacavir Reactions: Comparative Analysis of Different Genotyping Methods. *Curr Genomics* **2012,** *13* (4), 314-20.
11. Cesbron-Gautier, A.; Simon, P.; Achard, L.; Cury, S.; Follea, G.; Bignon, J. D., [Luminex technology for HLA typing by PCR-SSO and identification of HLA antibody specificities]. *Ann Biol Clin (Paris)* **2004,** *62* (1), 93-8.

© Copyright 2021 | N Panpradist

12. Soto-Nava, M.; Avila-Ríos, S.; Valenzuela-Ponce, H.; García-Morales, C.; Carlson, J. M.; Tapia-Trejo, D.; Garrido-Rodriguez, D.; Alva-Hernández, S. N.; García-Tellez, T. A.; Murakami-Ogasawara, A.; Mallal, S. A.; John, M.; Brockman, M. A.; Brumme, C. J.; Brumme, Z. L.; Reyes-Teran, G., Weaker HLA Footprints on HIV in the Unique and Highly Genetically Admixed Host Population of Mexico. *J Virol* **2018,** *92* (2).

13. Schacker, T.; Collier, A. C.; Hughes, J.; Shea, T.; Corey, L., Clinical and epidemiologic features of primary HIV infection. *Annals of internal medicine* **1996,** *125* (4), 257-64.

14. Panpradist, N.; Beck, I. A.; Vrana, J.; Higa, N.; McIntyre, D.; Ruth, P. S.; So, I.; Kline, E. C.; Kanthula, R.; Wong-On-Wing, A.; Lim, J.; Ko, D.; Milne, R.; Rossouw, T.; Ute D. Feucht, M. C., Gonzague Jourdain, Nicole Ngo-Giang-Huong, Laddawan Laomanit, Jaime Soria, James Lai, Eric E. Klavins, Lisa M. Frenkel, Barry R. Lutz OLA-Simple: a software-guided HIV-1 drug resistance test for low-resource laboratories. *EBiomedicine* **2019,** *In press*.

15. Panpradist, N.; Beck, I. A.; Ruth, P. S.; Avila-Rios, S.; Garcia-Morales, C.; Soto-Nava, M.; Tapia-Trejo, D.; Matias-Florentino, M.; Paz-Juarez, H. E.; Del Arenal-Sanchez, S.; Reyes-Teran, G.; Lutz, B. R.; Frenkel, L. M., Near point-of-care, point-mutation test to detect drug resistance in HIV-1: a validation study in a Mexican cohort. *AIDS* **2020**.

16. Darke, C.; Corbin, S. A., External quality assessment of patient HLA-B*57:01 testing prior to abacavir prescription. *Int J Immunogenet* **2014,** *41* (4), 277-80.

© Copyright 2021 | N Panpradist

17. Gonzalez-Galarza, F. F.; McCabe, A.; Santos, E.; Jones, J.; Takeshita, L.; Ortega-Rivera, N. D.; Cid-Pavon, G. M. D.; Ramsbottom, K.; Ghattaoraya, G.; Alfirevic, A.; Middleton, D.; Jones, A. R., Allele frequency net database (AFND) 2020 update: gold-standard data classification, open access genotype data and new query tools. *Nucleic Acids Res* **2020,** *48* (D1), D783-d788.

18. Gragert, L.; Madbouly, A.; Freeman, J.; Maiers, M., Six-locus high-resolution HLA haplotype frequencies derived from mixed-resolution DNA typing for the entire US donor registry. *Hum Immunol* **2013,** *74* (10), 1313-20.

19. Hurley, C. K.; Kempenich, J.; Wadsworth, K.; Sauter, J.; Hofmann, J. A.; Schefzyk, D.; Schmidt, A. H.; Galarza, P.; Cardozo, M. B. R.; Dudkiewicz, M.; Houdova, L.; Jindra, P.; Sorensen, B. S.; Jagannathan, L.; Mathur, A.; Linjama, T.; Torosian, T.; Freudenberger, R.; Manolis, A.; Mavrommatis, J.; Cereb, N.; Manor, S.; Shriki, N.; Sacchi, N.; Ameen, R.; Fisher, R.; Dunckley, H.; Andersen, I.; Alaskar, A.; Alzahrani, M.; Hajeer, A.; Jawdat, D.; Nicoloso, G.; Kupatawintu, P.; Cho, L.; Kaur, A.; Bengtsson, M.; Dehn, J., Common, intermediate and well-documented HLA alleles in world populations: CIWD version 3.0.0. *Hla* **2020,** *95* (6), 516-531.

20. Ghatak, S.; Muthukumaran, R. B.; Nachimuthu, S. K., A simple method of genomic DNA extraction from human samples for PCR-RFLP analysis. *J Biomol Tech* **2013,** *24* (4), 224-31.

21. ThermoFisher Scientific DNA Extraction from Buccal Swabs. https://www.thermofisher.com/us/en/home/references/protocols/nucleic-

© Copyright 2021 | N Panpradist

acid-purification-and-analysis/dna-extraction-protocols/dna-extraction-from-buccal-swabs.html.

22. Qian, J.; Boswell, S. A.; Chidley, C.; Lu, Z.-x.; Pettit, M. E.; Gaudio, B. L.; Fajnzylber, J. M.; Ingram, R. T.; Ward, R. H.; Li, J. Z.; Springer, M., An enhanced isothermal amplification assay for viral detection. *Nature Communications* **2020,** *11* (1), 5920.
23. TwistDx Recombinase Polymerase Amplification, or RPA, is the breakthrough, isothermal replacement to PCR. https://www.twistdx.co.uk/en/rpa.
24. Raja, B.; Goux, H. J.; Marapadaga, A.; Rajagopalan, S.; Kourentzi, K.; Willson, R. C., Development of a panel of recombinase polymerase amplification assays for detection of common bacterial urinary tract infection pathogens. *J Appl Microbiol* **2017,** *123* (2), 544-555.
25. Francois, P.; Tangomo, M.; Hibbs, J.; Bonetti, E.-J.; Boehme, C. C.; Notomi, T.; Perkins, M. D.; Schrenzel, J., Robustness of a loop-mediated isothermal amplification reaction for diagnostic applications. *FEMS Immunology & Medical Microbiology* **2011,** *62* (1), 41-48.
26. Thompson, D.; Lei, Y., Mini review: Recent progress in RT-LAMP enabled COVID-19 detection. *Sensors and Actuators Reports* **2020,** *2* (1), 100017.
27. Walker, F. M.; Hsieh, K., Advances in Directly Amplifying Nucleic Acids from Complex Samples. *Biosensors (Basel)* **2019,** *9* (4).

© Copyright 2021 | N Panpradist

CHAPTER 10: TECHNOLOGIES IN RESPONSE TO SARS-COV-2 PANDEMIC

PREFACE

Technologies described in Chapter 2 – 4 and 6 were adapted to generate new protocols and devices for detection SARS-CoV-2 and SARS-CoV-2 variants. **Section 10.1** describes the characterization of swab transfer methods at the point-of-care, based on my original as part of the rotation project. **Section 10.2** discusses the use of lyophilized RT-PCR reagents and a direct to amplification protocol to develop a simpler and faster RT-qPCR workflows for SARS-CoV-2 detection in the labs or at the point-of-care. This lab protocol and in-house kits were used for evaluation in the conjunction with Aquarium guide at Duke University and two labs at the UW as well as shipped to the innovation lab at the University of Zimbabwe to operator with video and manual instructions. The point-of-care RT-PCR test kits were shipped to Georgetown University Pediatric clinic for feasibility testing by healthcare workers. **Section 10.3** describes the development of LAMP-based SARS-CoV-2 assay kits accompanied with the cell phone app and a low-cost heater/reader (used in **Chapter 6**). Last, Section 10.4 discusses ongoing work on SARS-CoV-2 typing.

PREVIOUS PUBLICATIONS. Part of the contents in this section were published in:

1) N Panpradist et al 2014 (https://doi.org/10.1371/journal.pone.0105786)
2) N Panpradist et al 2021 (https://doi.org/10.1101/2021.08.12.21261875).
3) N Panpradist et al 2021 (https://pubmed.ncbi.nlm.nih.gov/33582488/).
4) E Kline et al 2021 (https://pubmed.ncbi.nlm.nih.gov/34462755/).

© Copyright 2021 | N Panpradist

10.1 SAMPLE CHARACTERIZATION & ENGINEERING OF SWAB TRANSFER METHODS

> In 2014 I led a study that quantitatively characterize swabs and methods for swab transfer at the point of care. Then we used the bacteria as a model organism. As for SARS-CoV-2, we have applied similar knowledge to characterize swabs and recruited health care workers to evaluate of the two swab transfer methods.

10.1.1 SWAB SAMPLE TRANSFER FOR POINT-OF-CARE DIAGNOSTICS

> **CONTRIBUTORS**: Nuttada Panpradist, Bhushan J. Toley, Xiaohong Zhang, Samantha Byrnes, Joshua R. Buser, Janet A. Englund, Barry R. Lutz **SIGNIFICANCE**: In many POC tests, sample collection involves swabbing the site (e.g., nose, skin), agitating the swab in a fluid to release the sample, and transferring the fluid to a device for analysis. Poor performance in sample transfer can reduce sensitivity and reproducibility. Here we characterized swabs and proposed different approaches to improve swab transfer step.

MATERIALS AND METHODS

Model organism (Staphylococcus aureus). A single colony of *S. aureus* (ATCC 25923) was inoculated in tryptic soy broth (TSB) (Fisher B11768) and shaken overnight (250 rpm, 37°C). The overnight culture was

© Copyright 2021 | N Panpradist

further diluted 1:100 in TSB and incubated (250, 37°C) for 3 hours until the OD_{600} reached 2±0.2, corresponding to a concentration of ~10^9 CFU/mL. *S. aureus* bacteria were then harvested and resuspended in one of two buffers: 1X Tris-EDTA buffer at pH 8.0 (TE: 10 mM Tris-HCl +1 mM EDTA) or TE buffer with in-house human simulated nasal matrix (SNM: 110 mM NaCl, 1% w/v mucin from porcine stomach Type III (Sigma, M1778-10G) and 10 µg/mL w/v human genomic DNA (Promega G3041)) at 90% v/v of TE/SNM.

Swabs and agitation methods. Seven different commercially-available swabs were tested: rayon (Copan Diagnostics Inc., 170KS0, Murrieta, CA), cotton (Puritan Medical Products Co., LLC, 25–806, Guilford, ME), mid-turbinate (MT) flocked nylon (Copan Diagnostics Inc., 56380CS01, Murrieta, CA), regular-tip flocked nylon (Copan Diagnostics Inc., 502CS01, Murrieta, CA), polyester (PES) (Contec Inc., 19059209, Spartanburg, SC), polyurethane (PUR) (Foamtec International, 19304613, Oceanside, CA), and calcium alginate (Puritan Medical Products Co., LLC, 25-806-2PA, Guilford, ME). Vortexing is commonly used in the laboratory to maximize release of organisms from swabs, but it is likely not available in low resource settings. Agitation methods for POC tests are normally specified in units of time, without definition of the method. For consistency across experiments, we defined a base case method for translating the submerged swab along a circular path against the side of the tube at a rate of 1 cycle per second (1 Hz) for a specified time (e.g., "10 second 1 Hz side twirl"). The swab agitation was done by hand but using the timer as a reference for manual control of the twirling rate. The potential errors introduced by the users were not excluded in the data. The

© Copyright 2021 | N Panpradist

impact of these variations was tested (below in the section titled "*Robustness to user variations in manual agitation").* After the sample was applied to swabs, swabs were agitated in 128 µL of transfer fluid. This volume was chosen to be compatible with the fluid capacity of typical POC devices (~100 µL for LFT) to enable complete utilization of the sample fluid.

Volume recovery experiments. To quantify fluid release volume, 15 µL TE buffer was pipetted onto the tip of a dry swab. The swab was then dipped into pre-weighed 128 µL TE buffer (or 1% w/v sodium citrate solution for calcium alginate swab) and agitated (10 second 1 Hz side twirl). The swab was removed, and the fluid left in the tube was weighed. The volume left in tube was calculated (**Equation 10.1**) and compared to a control (**Equation 10.2**). As the control, 15 µL TE buffer was pipetted into 128 µL of pre-weighed TE buffer, and the fluid in the tube was weighed. The % Volume Recovery was calculated using **Equation 10.3**.

$$\text{Volume available for analysis (test)} = V_{initial} - V_{lost\ to\ swab} = V_{initial} - \frac{(W_{1,test} - W_{2,test})}{\text{density of fluid}} \quad \textbf{(Eq.10.1)}$$

$$\text{Volume available for analysis (control)} = V_{initial} + V_{added} \quad \textbf{(Eq.10.2)}$$

$$\%\text{Volume available for analysis (\% Volume Recovery)} = \frac{\text{Volume available for analysis (test)}}{\text{Volume available for analysis (control)}} \quad \textbf{(Eq.10.3)}$$

Where $W_{1,test}$ = initial weight of test tube containing 128 µL TE buffer

$W_{2,test}$ = weight of test tube after swab transfer and removal

$W_{1,control}$ = initial weight of control tube containing 128 µL TE buffer

© Copyright 2021 | N Panpradist

$W_{2,\,control}$ = weight of control tube after 15 µL TE buffer was added

V_{added} = added volume of TE (either onto swab or onto control tube), 15 µL

$V_{initial}$ = initial volume of TE in test or control tube, 128 µL

$\frac{(W_{2,\,control} - W_{1,\,control})}{V_{added}} = \text{density of fluid}$, used to convert weight change of fluid in the test tube $(W_{2,test} - W_{1,test})$ into volume change. $(W_{2,test} - W_{1,test})$ is negative when the swab absorbed more fluid from the tube than it released. Adding $\frac{(W_{2,\,test} - W_{1,\,test}) \times V_{added}}{(W_{2,\,control} - W_{1,\,control})}$ to $V_{initial}$ would provide the recovered volume in the test tube (Volume available for analysis (test)). A transfer volume of 128 µL was selected because this volume allowed at least 20 µL to be recovered after the swab transfer step for all swab types for further testing by qPCR (as described in the next section); it also represents an appropriate volume for LFTs.

Organism recovery experiments. Bacteria from swabs and control samples were lysed using a method modified from Patel *et al*[1], and lysed samples were analyzed by quantitative PCR (qPCR). Regular-tip nylon, MT nylon, and rayon swabs were obtained in sterile packaging, and PES and PUR swabs and other materials were autoclaved prior to use. All

© Copyright 2021 | N Panpradist

swabs and materials were tested for bacteria and DNA bacteria contamination. In all experiments, bacteria were transferred from the swab to 128 µL of 3 U/µL achromopeptidase (ACP) (Sigma #A3547) in TE to lyse the bacteria. Lysis continued for 2 minutes at room temperature. Following lysis, ACP was deactivated by heating (10 minutes, 95°C), and the sample tube was placed in ice immediately. Bacterial lysate was filtered through a centrifuge tube filter (0.2 µm pore size) to remove debris. 9 µL of the filtered lysate was analyzed by a MRSA/SA ELITe MGB qPCR assay (Elitech Group Molecular Diagnostics, formerly Epoch Biosciences, #M800346). This assay detects a single open reading frame encoding *S. aureus*-specific lactate-dehydrogenase-1 (*ldh1*). The concentration of *ldh1* copies in each sample (copies/µL) was estimated based on a standard curve (80 to 8×10^8 *ldh1* copies). To verify that swabs were not contaminated during experiments, negative control samples (15 µL of TE buffer (N = 3) and swabs with no added bacteria (N = 3)) were transferred to 128 µL of lysis buffer and analyzed by the same procedures as other samples. *S. aureus* was applied to swab tips using one of the three methods described in the following sections and eluted into 128 µL of pre-weighed lysis buffer. In the control case, *S. aureus* was introduced directly to 128 µL of pre-weighed lysis buffer. Both test and control tubes were weighed and set aside to allow for the lysis to complete. Filtered lysate then underwent qPCR for quantitation of *ldh1* concentration (copies/µL). The limit of detection (LoD) of qPCR was less than 5 *ldh1* copies per reaction, corresponding to about 1 CFU per reaction (**Figure S10.38**). Weights of test and control tubes were used to calculate volumes left in the

© Copyright 2021 | N Panpradist

tubes (**Equation 10.1** and **Equation 10.2**, respectively). The number of *ldh1* copies left in tube in each case was calculated using **Equation 10.4**, and the % Organism Recovery was calculated using **Equation 10.5**.

$$ldh1 \text{ copies(control or test)} = ldh1 \text{ concentration (copies/µL)} \times \text{Volume (µL)(control or test)} \quad \textbf{(Eq.10.4)}$$

$$\%\text{Organism Recovery} = \frac{ldh1 \text{ copies (test)}}{ldh1 \text{ copies (control)}} \text{x}100 \quad \textbf{(Eq. 10.5)}$$

Further details on how *S. aureus* was introduced to swabs in each method are described below.

Low-volume fluid sample (less than swab saturation). 15 µL *S. aureus*/TE (100, 10^4, and 10^6 CFU) was pipetted onto a swab tip. The amount of bacteria input exceeded the LoD of the qPCR assay (**Figure S10.38**). The swab was then dipped into lysis buffer, manually agitated (as described above or 10 second 1 Hz side twirl) and removed. The number of *ldh1* copies was measured and compared to a control case in which *S. aureus*/TE solution was directly pipetted into pre-weighed lysis buffer (with no submergence of pipette tip to avoid introducing bacteria from the outside surface of the tip). A fresh pipette tip was then used for mixing.

Excess-volume fluid sample (beyond swab saturation). A dry or a pre-wet (by dipping into TE) swab was dipped into 1 mL of *S. aureus*/TE solution (10^6 CFU/mL) and manually agitated (10 second 1 Hz side twirl) to load sample into the swab. Swabs were transferred into pre-weighed lysis buffer, manually

© Copyright 2021 | N Panpradist

agitated, and removed. The number of *ldh1* copies in the lysis tube was measured and reported.

Sample dried on a surface. Dried bacterial samples were prepared by pipetting 15 µL of *S. aureus*/TSB (10^4 CFU) onto sterilized 25/46-inch diameter polydimethylsiloxane (PDMS) punches and left in a desiccator for 30 minutes. PDMS was chosen as the surface since it is known to not adhere to *S. aureus* organisms [2], and we attempted to remove effects of collection efficiency by using a very vigorous swabbing procedure (goal of 100% collection). A dry or a pre-wet swab was rubbed across the PDMS surface 10 times to pick up organisms (**Figure S10.39**), transferred into the pre-weighed lysis buffer (128 µl), manually agitated, and removed. The number of *ldh1* copies in the lysis tube was measured and compared to a control. In the control, the eluate was derived from placing the PDMS punch with dried bacteria directly in lysis buffer and vortexing for 10 seconds.

Bacterial sample was spotted on the PDMS punch and dried. Starting at step 1, the swab was rubbed on the surface, from left to right. Then, the shaft was rotated 45 degrees clockwise in step 2. After that, the swab was moved to the left position to complete the cycle in step 3. In each test case, 10 cycles of 3 steps were conducted

Robustness to user variations in manual agitation. 15 µL of *S. aureus*/TE solution (10^4 CFU) was pipetted onto a dry swab, and the swab was dipped into lysis buffer. Different manual-twirling methods were used to release bacteria. "Side twirl" refers moving the swab tip around the interior side of the

© Copyright 2021 | N Panpradist

tube in a circular motion. "Bottom twirl" refers to placing the swab tip at the bottom of the tube and rotating the shaft.

Engineering for improved recovery. A forced-flow method using a syringe was developed as an alternative to manual agitation to improve organism recovery. In the test case, 15 µL of *S. aureus*/TE (10^4 CFU) was introduced onto a dry swab, and the swab was dipped into the lysis buffer tube, the bottom of which was connected to a syringe. The plunger of the syringe was then pushed and pulled 5 times. At the end, the swab remained in the tube whereas the eluate was contained within the syringe piston and could be purged through an opening in the side of the syringe.

Bench-top gold standard method. Swabs (N = 5) were tested for organism recovery using a laboratory protocol: vortexing for 10 seconds at the maximum speed. In the test case, 15 µL of *S. aureus*/TE (10^4 CFU) was introduced onto a dry swab, and the swab was dipped into lysis buffer prior to vortexing.

Data Analysis. Statistical analysis was performed using MATLAB (MathWorks, Natick, MA). Analysis of variance (ANOVA) was used to test for significant differences among means. In the case that ANOVA indicated significant differences ($p<0.05$), post-hoc comparisons (Tukey-Kramer procedure, adjusted for multiple comparisons) were used to determine which means were significantly different from one another. The data and analysis underlying the findings are fully available on request.

RESULTS

A variety of swab types were evaluated under different conditions, as illustrated in **Figure 10.1**. We selected a set of commercially-available swabs

© Copyright 2021 | N Panpradist

representing a range of materials, microstructure, and size: low absorbent foam (reticulated polyurethane swab – PUR and knitted-pattern PES swabs – PES), low absorbent fiber (MT nylon flocked swabs – MT nylon, and regular-tip nylon flocked swabs), high absorbent fiber (tightly wound cotton and rayon swabs), and dissolvable swabs (calcium alginate swabs).

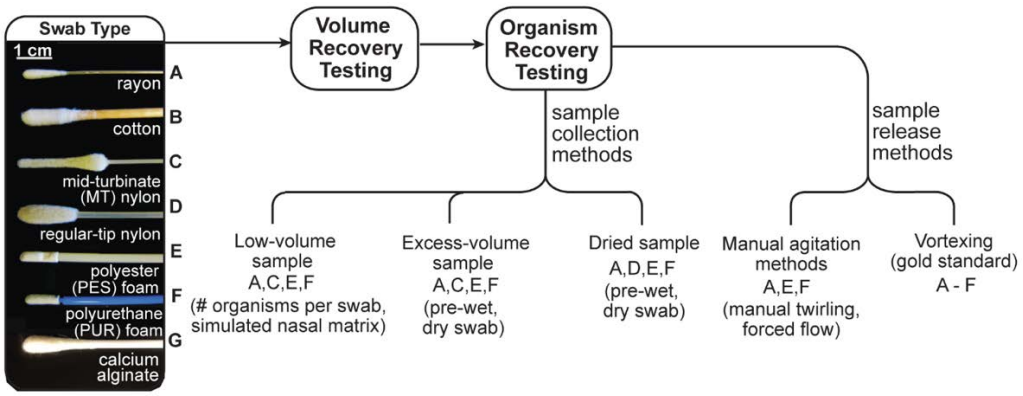

Figure 10.1 | Schematic of swab transfer experiments.

Seven commercially available clinical swabs (labeled A, B, C, D, E, F, and G) were tested for volume recovery and organism recovery. Organisms were applied to swabs in three ways: pipetting a low-volume sample onto the swab, dipping the swab into excess-volume sample, or rubbing the swab across dried sample on a surface. Selected cases included variation in sample concentration, addition of simulated nasal matrix, and comparison of dry and pre-wet swabs. Different manual swab agitation methods, manual twirling and forced flow, were tested for their effects on swab transfer efficiency compared to vortexing (gold standard method).

https://doi.org/10.1371/journal.pone.0105786.g001

Figure S10.40 shows scanning electron microscopy images of the nylon (flocked), PUR (reticulated), PES (knitted), and rayon (wound) swab tips; this set exhibits a wide variety of material structures and pore sizes. We focused on the manual "insert and twirl" agitation method common for LFTs and used a reduced fluid transfer volume (~100 µL) appropriate for typical LFTs. Swabs

© Copyright 2021 | N Panpradist

were evaluated in a series of tests, with subsets of swabs chosen for each test to illustrate key differences and analysis methods. Swabs were first tested for fluid retention (loss of fluid sample to the swab), and swabs with low retention volume were carried forward to test organism recovery. We used *Staphylococcus aureus* as a model system, with recovery quantified by quantitative polymerase chain reaction (qPCR). Organisms were applied to swabs under various conditions to represent a range of sampling conditions from dry to wet: a) low-volume fluid sample (less than swab saturation), b) high-volume fluid sample (beyond swab saturation), and c) sample dried on a surface. For the low-volume sample condition, recovery was tested for a wide range of concentrations (100 to 10^6 organisms)[3], and a simulated human nasal matrix was used as an example of a complex sample. Pre-wet swabs were compared to dry swabs for the cases of excess sample volume and dry sample collection. We also tested variations on manual agitation to identify sensitivity to user operation and demonstrated an engineered manual agitation method to improve recovery for swab-sample combinations that performed poorly.

VOLUME RECOVERY

Fluid volume retention for seven commercially-available swabs is shown in **Figure 10.2**. Swabs with 15 µL of added fluid were inserted into tubes containing 128 µL of fluid and removed, and the fluid remaining in the tube was used to calculate fluid volume lost to the swab (**Figure 10.2A**). **Figure 10.2B** shows the fluid volume lost to each swab, and **Figure 10.2C** shows the percent volume available for analysis (% volume recovery) for a starting volume of 128 µL. PUR and PES yielded the highest volume recovery (PUR:

© Copyright 2021 | N Panpradist

mean ± SE =89±0.4%; PES: 81%±0.3%). Conversely, cotton and regular-tip nylon swabs retained more fluid resulting in the poorest volume recovery (cotton: 8±0.6%; regular-tip nylon: 30±3.4%). The remaining swabs, rayon and MT nylon, had intermediate volume recovery (rayon: 56±2.5%; MT nylon: 70±0.8%). All data points in **Figure 10.2B** and **Figure 10.2C** have 5 replicates. A one-way ANOVA indicated that volume recovery differed significantly across swab types ($p<0.0001$). Post-hoc comparisons indicated that PUR had a significantly higher volume recovery than other swab types ($p<0.05$). Additionally, we tested dissolvable calcium alginate swabs in the recommended dissolution buffer (sodium citrate). The recommended procedure uses a buffer volume that is too large for LFTs (15 mL) and using the small volume (128 µL) resulted in a glue-like gel that would not flow through an LFT.

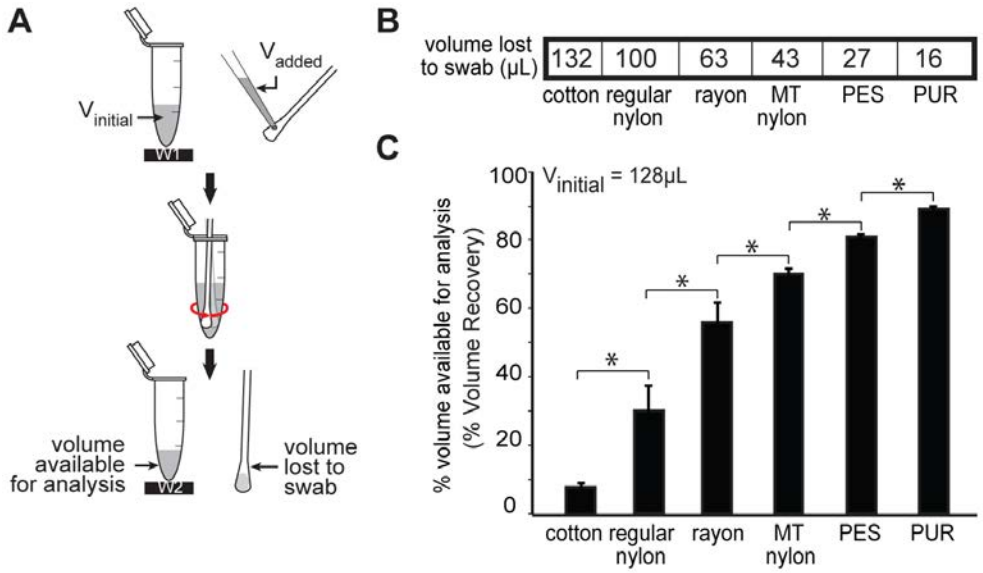

Figure 10.2 | Volume recovery testing.

(**A**) Schematic of the experimental setup. The tube containing 128 µL TE was weighed (W1), and 15 µL TE was pipetted onto the swab, which was then transferred into the tube using 10 second 1 Hz side

© Copyright 2021 | N Panpradist

twirl, and removed. The tube containing the leftover buffer (eluate) was weighed (W2). The % volume available for analysis (% Volume Recovery) was calculated using Eq 10.3 in the text. (**B**) Mean TE volume (μL) absorbed by each type of swab (N = 5). (**C**) Comparison of the % Volume Recovery (mean ± SE; N = 5) from each swab. Calcium alginate swabs were resuspended in 1% w/v sodium citrate buffer to dissolve fibrous tip materials, the % Volume Recovery was not reported here due to density change of the buffer during (**A**). * indicates significant differences (Tukey-Kramer, α = 0.05). https://doi.org/10.1371/journal.pone.0105786.g002

ORGANISM RECOVERY

We determined that our modified ACP lysis method gave the same amount of amplifiable DNA as the original method by Patel *et al* (**Figure 10.3**)[1]. Eluate recovered from swabs was devoid of bacteria or bacterial DNA (**Figure S10.41**) and did not interfere with qPCR or ACP lysis (**Figure S10.42**). The qPCR assay reported 3–6 genomic copies per CFU across all experiments; along with each experiment result we report the sample CFU for reference, but recovery values reported in this paper are based on copies measured by qPCR. Results are reported as absolute organisms recovered **Equation 10.4** or as % organism recovery based on a control sample analyzed by the same method (**Equation 10.5**).

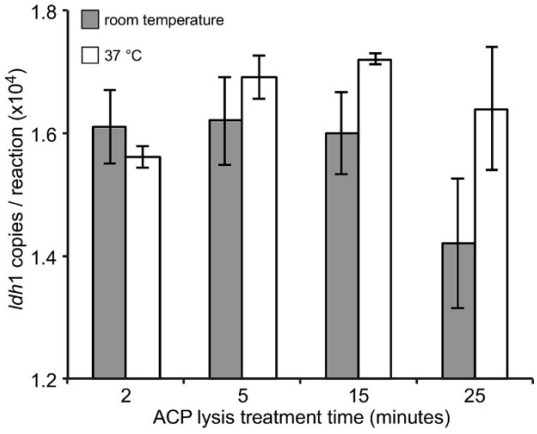

© Copyright 2021 | N Panpradist

Figure 10.3 | ACP lysis efficiency at various treatment times and temperatures.

Our ACP lysis method was adapted from the method previously reported by Patel et al [1]. The lysis time and temperature were changed from 15 minutes at 37°C to 2 minutes at room temperature to be more appropriate for low-resource settings. We observed no growth when plating the bacterial lysate on a tryptic soy agar (data not shown), which confirmed 100% killing efficiency. Furthermore, we compared the amount of amplifiable DNA for different times and temperatures. 2.5×105 CFU in 100 µL S.aureus/TE solution with an addition of 17.6 µL ACP (20 U/µL) underwent ACP lysis for 2, 5, 15, 25 minutes at room temperature and 37°C (N = 3). Then, the ACP was deactivated for 10 minutes at 95°C. 82.4 µL of TE was added to bring up the final volume of lysate to 200 µL. 2 µL lysate was amplified using ldh1 qPCR assay (one S.aureus organism has one copy of the ldh1 gene) to estimate amplifiable DNA (copies/reaction). All tested conditions yielded relatively high ldh1 copies/reaction and there was no significance difference among cases (two-way ANOVA, $p = 0.1912$ for time variables and $p = 0.0943$ for temperature variables). Based on the ACP lysis (2 minutes at room temperature), estimated number of ldh1 copies/CFU = 6.4, (16000 copies/2 µL lysate):(2.5×105 CFU/200 µL lysate). Note that the vertical axis does not span to zero, which makes error bars appear artificially large.

LOW-VOLUME FLUID SAMPLES

Swabs were tested with a sample volume that was less than the fluid capacity for all swabs (15 µL). Four dry swab types (PUR foam, knitted PES, rayon, and MT flocked nylon swabs (N = 5)) were tested for organism recovery using low-volume samples (**Figure 10.4**). When bacterial solution was pipetted onto the swab tip, fluid absorption behaved differently among swab types. For PUR swabs, the fluid beaded up on the surface without absorbing. For PES and nylon swabs, the bacterial fluid formed a thin film around swab tip but did not bead up. For rayon swabs, fluid was completely absorbed into swab tips.

© Copyright 2021 | N Panpradist

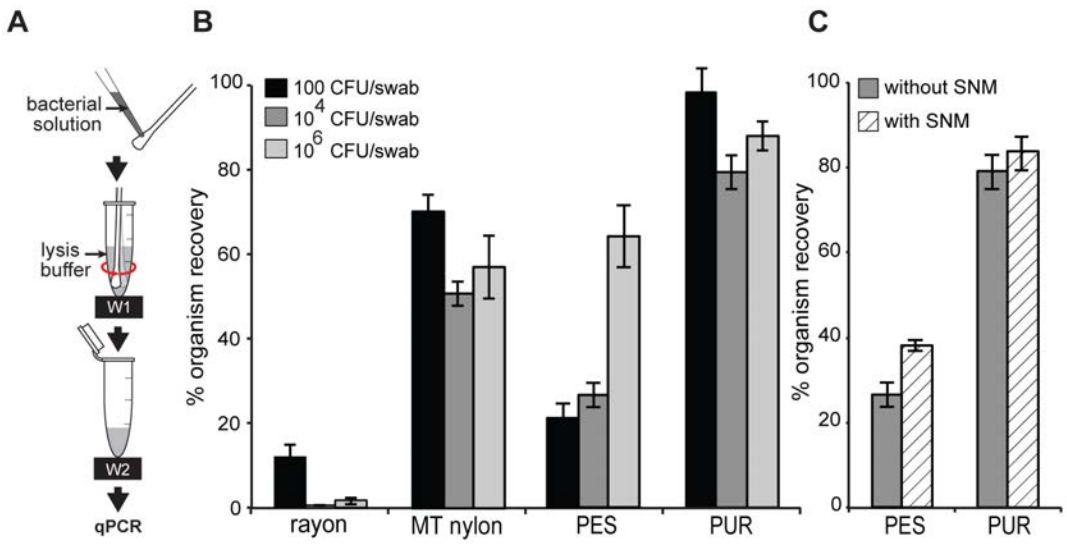

Figure 10.4 | Organism recovery for low-volume samples.

(**A**) Schematic of the experimental set up. 15 µL *S. aureus*/TE (~100, ~10^4, or ~10^6 CFU, equivalent to 500, 6×10^4, or 4×10^6 *ldh1* copies, respectively, as measured by qPCR) was spiked onto the swab, which was then agitated in 128 µL lysis buffer using 10 second 1 Hz side twirl and removed. (**B**) Comparison of the % Organism Recovery in four swabs at three different organism input numbers (mean ± SE, N = 5), which was calculated using Equation 5 in the text. (**C**) Comparison of the % Organism Recovery (mean ± SE; N = 5) using ~10^4 CFU/swab of *S. aureus* in the presence and absence of simulated nasal matrix (SNM). **https://doi.org/10.1371/journal.pone.0105786.g003**

The percent organism recovery of each swab using low-volume samples is shown in **Figure 10.4B**. Regardless of the number of organisms added, PUR foam yielded the highest organism recovery of 79%–98%. MT nylon and PES had intermediate organism recovery of 51–70% and 21–65%, respectively. Rayon provided the lowest organism recovery of 1–12%. A two-way ANOVA indicated significant effects of swab type and numbers of organisms applied to swab, and a significant interaction (every $p<0.05$). Post-hoc comparisons showed that organism recovery of PUR was significantly higher than other swabs (followed by MT nylon, PES, and rayon). **Figure 10.4C** compares %

© Copyright 2021 | N Panpradist

organism recovery of PES (N = 5) and PUR (N = 5) for bacterial samples in the presence and absence of simulated nasal matrix (SNM). We verified that SNM did not interfere with qPCR and ACP lysis (**Figure S10.43**). Despite the presence of SNM, PUR swabs still yielded significantly higher organism recovery than PES swabs; mean ± SE was 84±4% for PUR and 38±2% for PES (two-way ANOVA, effect of swab type, $p<0.0001$). SNM significantly increased % organism recovery ($p = 0.03$).

EXCESS-VOLUME FLUID SAMPLE (BEYOND SWAB SATURATION).

Four swabs (rayon, PES, PUR, and MT nylon (N = 5)) were tested using excess-volume samples (1 mL). As the swab was submerged into 1 mL bacterial solution and twirled (**Figure 10.5**), dry rayon, PUR and PES swabs released air bubbles and allowed solution to flow into the interior of the swab tip. **Figure 10.5B** reports the number of organisms released from the swab into lysis buffer. A two-way ANOVA showed a significant effect of swab type on the number of organisms recovered ($p = 0.0001$) and pre-wetting the swab ($p = 0.001$). No significant interaction was found ($p = 0.63$). Post-hoc analysis indicated that PES swabs yielded significantly fewer organisms recovered than rayon, MT nylon and PUR. Wetting the swab reduced number of organisms recovered. The number of organisms recovered from each swab was then normalized by the product of its volume capacity and the concentration of organisms in the bacterial sample solution (**Figure 10.5C**). Two-way ANOVA indicated significant effect of swab type ($p<0.0001$) and pre-wetting the swab ($p = 0.009$). Post-hoc analysis reported that PUR swabs had significantly higher normalized organism recovery than other swabs.

© Copyright 2021 | N Panpradist

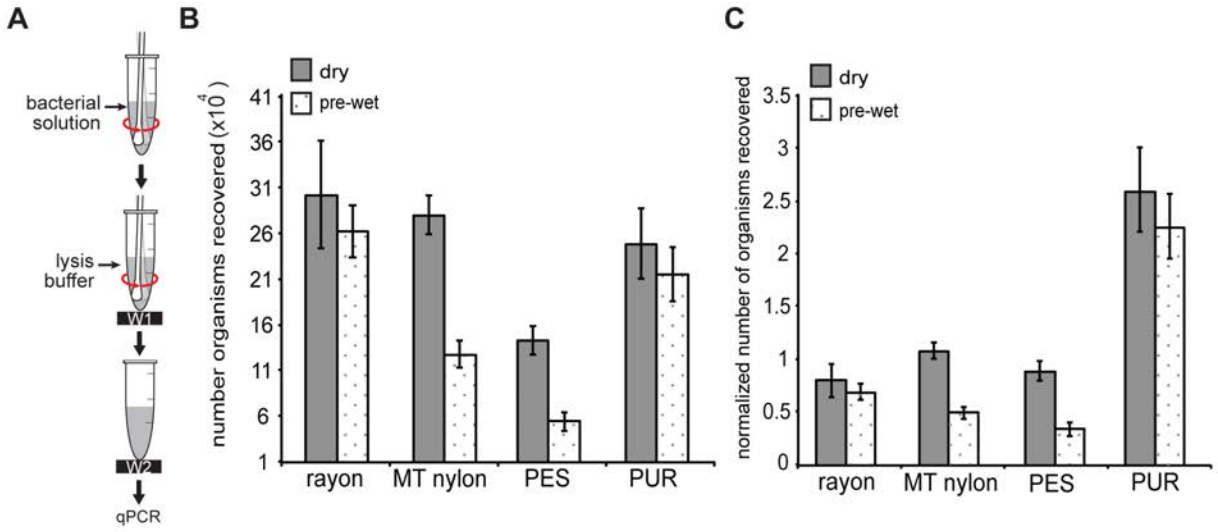

Figure 10.5 | Organism recovery for high-volume samples.

(**A**) Schematic of the experimental set up. Either a dry or pre-wet swab was dipped into 1 mL ~10^6 CFU/mL *S. aureus* solution (equivalent to 6×10^6 *ldh1* copies/mL, as measured by qPCR) and agitated by 10 second 1 Hz side twirl. The swab was then inserted into 128 µL lysis buffer, agitated by 10 second 1 Hz side twirl, and removed. (**B**) Comparison of the absolute number of organisms recovered for dry and pre-wet swabs. Absolute organism recovery was reported (rather than %) since the uptake of sample volume was different for each swab; absolute recovery was calculated using **Equation 10.4** in the text. In all cases, recovery was larger than would be expected based on swab volume and sample concentration by colony counts due to presence of multiple target copies per CFU. (**C**) The number of organisms recovered from each swab from panel (**B**) normalized by the number of organisms expected based solely on the sample concentration and volume capacity of the swab (estimated number of organisms collected by the swab =swab volume capacity (µL) x bacterial stock concentration (copies/µL from qPCR)). **https://doi.org/10.1371/journal.pone.0105786.g004**

SAMPLE DRIED ON A SURFACE.

Four swabs (PUR, PES, rayon, and regular-tip flocked nylon swabs (N=5)) were tested for organism recovery using a dried bacterial sample (**Figure 10.6A**). Swabs were dry or pre-wet (by dipping into TE buffer). To ensure that a swab was able to pick up the dried sample effectively, the swab was rubbed

© Copyright 2021 | N Panpradist

vigorously on the surface of PDMS (**Figure S10.39**). **Figure 10.6B** shows % organism recovery for dried samples. A two-way ANOVA indicated % organism recovery was affected by swab type ($p = 0.0004$) and wet/dry swab pre-conditions ($p = 0.02$) with no significant interaction ($p = 0.4$). Post-hoc comparisons showed rayon had significantly lower % organism recovery than other swabs.

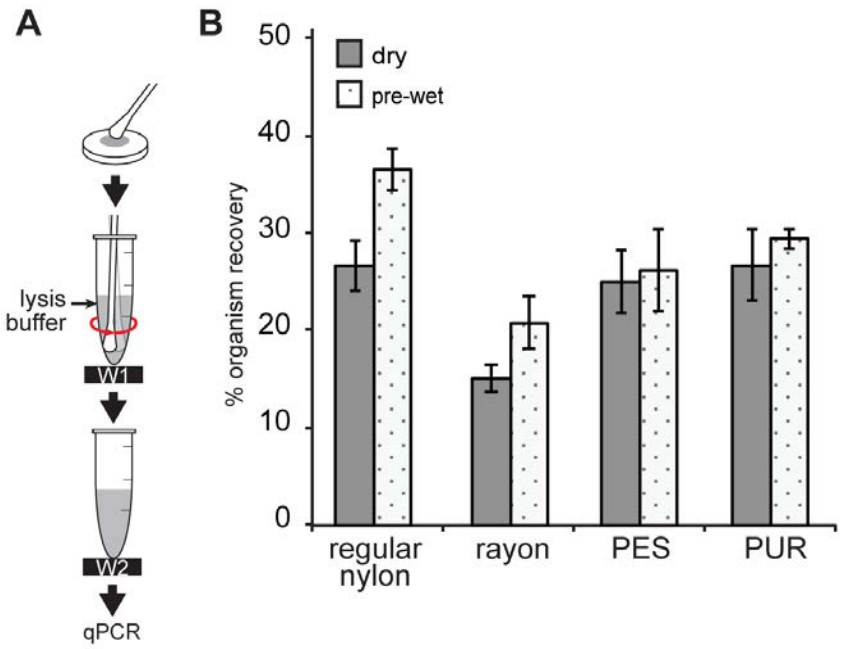

Figure 10.6 | Organism recovery for dried samples.

(**A**) Schematic of the experimental set up. 15 µL of *S. aureus* solution (~10^4 CFU, equivalent to 6×10^4 *ldh1* copies, as measured by qPCR) was spotted on a 25/64-inch diameter PDMS punch and left to dry. A dry or pre-wet swab was rubbed on the PDMS surface (10 times), agitated in 128 µL lysis buffer using 10 second 1 Hz side twirl, and removed. (**B**) Comparison of % organism recovery for pre-wet and dry swabs based on a control sample and an assumption of 100% collection efficiency. **https://doi.org/10.1371/journal.pone.0105786.g005**

© Copyright 2021 | N Panpradist

ROBUSTNESS TO USER VARIATIONS IN MANUAL AGITATION.

Three dry swab types (PUR, PES, and rayon (N = 5)) were tested for variations in manual agitation to release organisms into the lysis buffer (**Figure 10.7A**). All manual twirl methods yielded comparable % organism recovery from PUR swabs (**Figure 10.7B**); the low variation in PUR swabs was likely due to lack of sample absorption into the hydrophobic swab tip, which allowed sample release without agitation. Greater variation was observed in PES and rayon swabs, which represented more realistic sampling conditions. Coefficients of variation of organism recovery of all manual twirling methods were 7% for PUR, 23% for PES and 40% for rayon swabs.

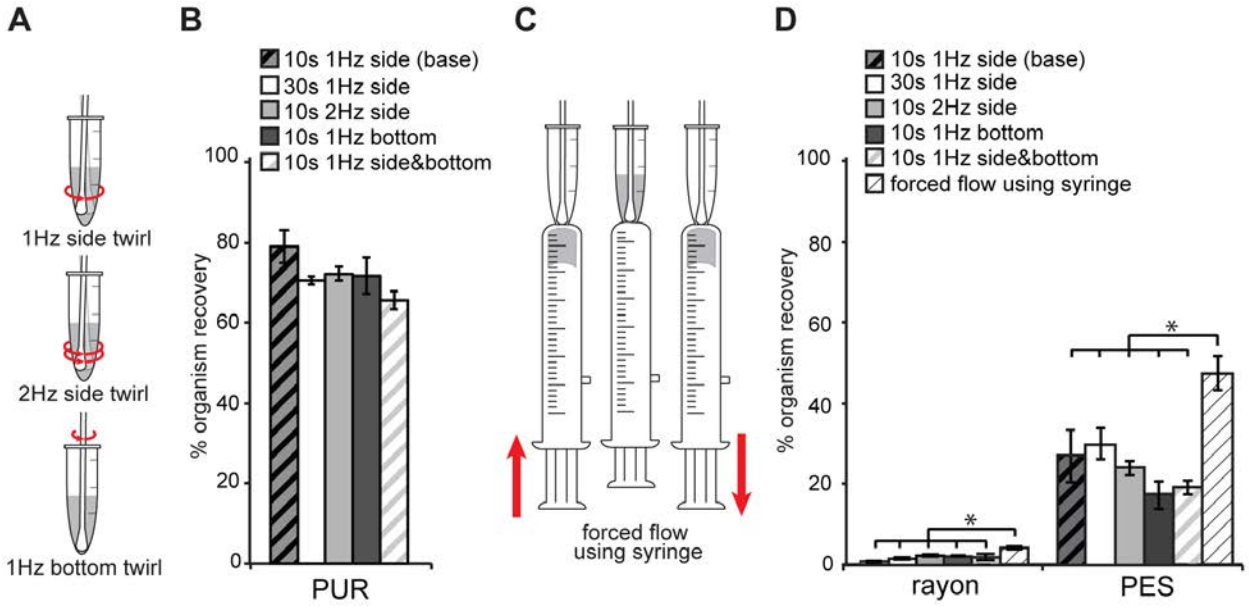

Figure 10.7 | Comparison of manual agitation methods for swab transfer.

(**A**) Schematic of action performed over a period of 1 second for different manual twirling methods. (**B**) Comparison of % organism recovery of PUR swabs using different twirling methods, which was calculated using Equation 10.5 in the text. (**C**) Schematic of the new forced flow syringe method. (**D**) Comparison of % organism recovery for PES and rayon swabs, using different twirling methods and the forced flow

© Copyright 2021 | N Panpradist

syringe method. *indicates statistically significant differences (Tukey-Kramer, α = 0.05). https://doi.org/10.1371/journal.pone.0105786.g006

ENGINEERING FOR IMPROVED RECOVERY.

A new manual agitation method, forced fluid flow using a syringe, was developed to increase organism recovery (**Figure 10.7C**). To test effectiveness of this method in improving organism recovery, intermediate-performing swabs (rayon and PES; **Figure 10.7D**) were selected. We compared % organism recovery derived from the forced flow using the syringe method to other agitation methods (**Figure 10.7D**). A one-way ANOVA rejected the hypothesis that there was no difference among the six agitation methods. Post-hoc comparison (Tukey-Kramer, α = 0.05) indicated that the forced flow using the syringe method yielded significantly higher organism recovery than the other five methods. This was true for both swab types.

BENCH-TOP GOLD STANDARD METHOD.

Six swabs (PUR, PES, MT nylon, regular-tip nylon, cotton, and rayon) were tested for their organism recovery when 10 seconds of vortexing was applied. Organism recovery of cotton swabs could not be reported, since they absorbed all the sample fluid. For the rest of swab types, a one-way ANOVA rejected the hypothesis that there was no difference among swab types. Post-hoc comparison (Tukey-Kramer, α = 0.05) indicated that PUR, PES, and MT nylon yielded significantly higher organism recovery than rayon and regular-tip nylon (**Figure S10.44**). In comparing the efficiency of vortexing and 1 Hz side twirl,

© Copyright 2021 | N Panpradist

vortexing offered a significant improvement over 1 Hz side twirl methods for PES, MT nylon, and rayon ($p<0.001$ in all cases). However, vortexing did not significantly increase organism recovery in PUR ($p>0.05$). Additionally, vortexing yielded a significantly higher organism recovery for PES and rayon compared to forced flow using syringe method ($p>001$ in both cases). Data from all experiments are summarized in

© Copyright 2021 | N Panpradist

Table S10.4 and **Table S10.5**.

DISCUSSION

In this study, we characterized several important properties of swabs currently utilized world-wide in many POC diagnostic tests. The experimental design had three overall aims: 1) to provide quantitative analysis and definitions of swab transfer efficiency that can be used to evaluate swabs and transfer methods, 2) to identify differences in swab transfer efficiency for a selection of common swabs and sample conditions, and 3) to identify commercially available swabs that perform well for sample conditions and manual agitation methods typical of POC testing. The results demonstrate that the choice of swab type for POC testing may be critical to achieving a sensitive and reliable test.

We built on previous work to develop analysis methods and definitions for quantitative evaluation of swab transfer efficiency. Some studies have assumed that the volume absorbed is an accurate representation of organisms picked up by the swab[4-6]. This assumption applies only when organism densities are the same inside and outside the swab; it will be inaccurate if organisms accumulate in the swab during agitation or if organisms do not flow freely into the swab. Our results show that swab transfer efficiency cannot be predicted based on fluid volume recovery alone, rather it requires analysis of organism recovery. The method for measuring the number of organisms in a sample also varies across studies. For bacteria, common measures include optical density at 600 nm (OD_{600}), colony counts (as colony forming units, CFU) [4, 7-9], and quantitative polymerase chain reaction (qPCR). However, OD is only

© Copyright 2021 | N Panpradist

applicable to high organism density. In colony counting, the transfer procedure itself can affect organism vitality (e.g., due to fluid composition, physical damage by vortexing or agitation)[10]. For clustering or biofilm-forming organisms[11], such as *S. aureus*, fragmentation during the transfer procedure can artificially increase the apparent recovery[10]. Thus, colony counting can bias results when comparing transfer methods or using a control to calculate percent organism recovery since each sample experiences different conditions. In contrast, qPCR provides consistent results independent of cell viability or clustering[12, 13], and it allows calculation of transfer efficiency by normalizing organism recovery to an input control sample analyzed by the same method. Our results demonstrate that qPCR and input controls allow quantitative measurement of swab transfer efficiency that can be applied across studies.

The scenario of low-volume samples showed the largest difference between swab types. For example, the sample beaded on the hydrophobic tip of the PUR foam swab and was promptly released into the lysis buffer; this scenario is not a realistic sampling case since the swab resists collection of the small fluid volume, and the high recovery should be interpreted with caution (although we note that PUR swabs also gave high recovery for high-volume samples and dry samples). In less hydrophobic materials such as PES and MT nylon, a thin film coating of bacterial solution was created surrounding the swab tip resulting in intermediate recovery. The hydrophilic tip of the rayon swab[4] fully absorbed the small sample solution, and absorption of transfer fluid may have further driven sample into the swab interior resulting in poor

© Copyright 2021 | N Panpradist

recovery during agitation. Thus, the wettability of the swab itself may impact specimen recovery.

Intuitively, swabs with larger volume capacity will collect more organisms when excess fluid sample is available. We hypothesized that, in addition to the swab volume capacity, swab chemical composition and structure can impact organism pick up and release. To investigate this, we normalized the number of organisms recovered by the estimated number of organisms that would have been picked up if there were no impact of material composition and structure. The nylon, PES, and rayon swabs all transferred near the expected number of organisms based on their volume capacity, but the normalized organism recovery for the PUR swab was more than 2.5-fold higher than the other swabs. This result suggests that swabs may accumulate organisms during agitation. Surprisingly, the PUR and rayon swabs maintained their recovery under pre-wet conditions. For the PUR swab, the large open pore structure may have allowed effective exchange of pre-wetting fluid with sample during collection. For the rayon swab, the large tip and dense structure may have prevented access to sample in the swab interior for both dry and pre-wet conditions; the good recovery would then imply that rayon also accumulated organisms on its outer surfaces during collection. The results suggest that swab composition and structure can have a significant impact on collection and release efficiency and should be evaluated for the specific organism and sample type.

© Copyright 2021 | N Panpradist

Swabs can be used to collect samples from dry surfaces, such as for environmental testing and sampling from skin or dry nasal passages, and pre-wet swabs are sometimes used to increase collection efficiency for dry samples[8]. The improved performance of rayon swabs with dry samples compared to the low-volume case suggests that organisms collected from a dry surface were more accessible to manual agitation. This would be expected since dry collection deposits sample on the exterior surface of the swab, whereas liquid samples wick into the swab interior where they may be inaccessible by manual agitation. Similarly, the effect of pre-wetting was more pronounced for rayon and regular nylon, which have relatively high-volume absorption compared to PES and PUR. The pre-wetting step filled the interior volume of swabs prior to sampling, and presumably this allowed dried sample to remain on the exterior surface of swabs where they were more effectively released during manual agitation.

Biological fluids found in clinical specimens can affect organism recovery. Complex matrices can affect physical properties (e.g., viscosity) or chemical properties (e.g., binding to swab materials or passivating swab surfaces). For example, mucin has been found to reduce non-specific binding of protein and has been used to coat biomaterials to create non-fouling surfaces[14] and repel other negatively charged molecules[15] (e.g., DNA). However, the increased viscosity of complex matrices may reduce the effectiveness of agitation. As an example of a sample matrix, we measured recovery in the presence of simulated nasal matrix (SNM) and found that it had little effect on organism recovery. The effect of sample matrix will be highly dependent on the sample

© Copyright 2021 | N Panpradist

type and should be evaluated for each application; the experimental design used here for SNM can be applied to quantitatively measure the effects of sample matrix on swab transfer efficiency.

User variations in swab transfer procedure could affect test sensitivity and reproducibility. Commercial LFTs typically include instructions to agitate the swab for a given time but do not specify the method. Our results with selected swabs showed that variations in agitation method and time had modest impact on organism recovery for the case of low-volume samples. Robustness to user variation will be especially important to maintain sensitivity and reproducibility for POC tests performed by untrained users and should be tested for all applications.

We demonstrated that an engineered swab transfer method can increase recovery from poorly performing swabs. However, the improved organism recovery was still significantly lower compared to vortexing (gold standard). Other engineered methods could include buffer-filled swab shafts that push fluid from the swab interior or methods that compress the swab to remove absorbed fluid. This finding has direct application to future developments in POC testing.

The PUR swab was the best performing swab across all sample conditions. This may be of clinical interest as similar PUR swabs have been found to be sensitive for the detection of respiratory viruses in immunocompetent and immunocompromised human subjects[16]. In addition, smaller swab size may be applicable to clinical use in subjects of diverse size and in sampling of diverse

© Copyright 2021 | N Panpradist

structure. The small volume of the PUR swab and reproducible recovery for variations in agitation methods also make it well-suited for application in POC devices.

Limitations of this work included the use of analytical samples instead of clinical samples, and the use of a single organism, *Staphyloccocus aureus*, as a model due to its relevance as a human pathogen. However, these choices allowed us to create replicable cultured samples with known numbers of organisms and to create various sample types, representative of swab collection sites (from dry to wet samples, in the presence or absence of other biological components). Other limitations of this work include the evaluation of a limited number of swab types, although they represent some of the most common commercially available swab types used in clinical testing today. Finally, although the number of organisms transferred from swabs involves both collection and release, swab collection efficiency is highly dependent on the target pathogen and details of the sampling site; our work only focused on swab transfer release efficiency.

CONCLUSIONS. We have built on previous work to develop a quantitative method to evaluate and compare swab transfer performance. We evaluated a variety of swabs under manual agitation conditions appropriate for POC testing. By selecting a set of commercially available swabs representing a variety of tip sizes, shapes, and materials, and utilizing qPCR as a direct measure of target quantity, we were able to quantitatively measure the transfer efficiency of a model organism. Our data show that swab size,

© Copyright 2021 | N Panpradist

structure, or composition affects swab release performance under different sampling conditions (low-volume, excess volume, or dry samples). Variations in manual agitation method and time had modest impact on swab transfer efficiency for three swabs tested, which is encouraging considering the likelihood of user variation in POC tests. For cases when a test is constrained to a swab with poor transfer efficiency, we demonstrated how forced-flow transfer methods could be used to improve transfer efficiency. The results and discussion presented here highlight key factors that should be considered in selecting swabs for POC applications. The quantitative evaluation methods developed here can be applied to other swab types in the future, both for POC applications or laboratory tests.

10.1.2. SWAB CHARACTERIZATION AND TRANSFER METHOD IN SARS-COV-2 SAMPLES

> **CONTRIBUTORS:** Nuttada Panpradist, Enos Kline, Barry R Lutz
>
> **SIGNIFICANCE**: Rapid and sensitive point-of-care diagnostics are crucial to slash the transmission of SARS-CoV-2, a pathogen that causes novel coronavirus (COVID-19). Most point-of-care SARS-COV-2 tests rely on non-trained individuals to self-swab nasal samples and subsequently release the virus from the swab into a buffer manually, without vortexing as commonly conducted in laboratories. Here we have analytically compared nasal swab performance in capturing and releasing SARS-CoV-2 using several manual agitation methods.

© Copyright 2021 | N Panpradist

METHODS

Heat-inactivated SARS-CoV-2 viral particles in simulated nasal specimens were used as a model specimen to test the ability of swabs to capture and release the virus in the resuspension buffer by simply soaking swabs, manually twirling swabs, or utilizing the novel Hygiena swab dispensers. Swab eluates were quantified using an inhibitor-tolerant RT-PCR assay that bypasses the RNA extraction step. % Recovery was compared to the control, which specimen directly added to the resuspension buffer.

RESULTS

Across swab types, 30-second manual twirling significantly increased swab recovery compared to 1-minute soaking of swabs alone. When applying the same agitation method, polyurethane swabs had the highest recovery. We observed drastic differences in recovery among tested Nylon flocked swabs. The Hygiena swab dispenser vastly improved the recovery in Rayon swabs and in the best scenario yielded recovery comparable to manually released polyurethane swabs.

Figure 10.8A shows the images of the tips of swabs used in this study. **Figure 10.8B** (top and middle) shows how mock swabs was prepared. Swab after being loaded with samples were either releases in a tube containing buffer (**Figure 10.8B**, bottom) or in the novel self-contained Hygiena buffer dispenser system (**Figure 10.8C**). Across combinations of sample collection and release, polyurethane (**PUR**) foam swabs showed highest recovery compared to other swab tip materials. Hydrophobic swabs such as swab made

© Copyright 2021 | N Panpradist

from Verciflex® elastomer did not absorb samples well, resulting in relatively low recovery (**Figure 10.8D**). Whereas Rayon and polyester (**PES**) swabs with tightly wounded fiber tips absorbed sample fluid well but did not result in high recovery. Across swab types, we found that the recovery was more insistent and higher when additional 30s manual agitation was applied in addition to (**Figure 10.8E**). Human DNA control recovery shows similar results as SARS-CoV-2 recovery (**Figure 10.8F** and **G**).

USE OF NOVEL HYGIENA SYSTEM TO RELEASE THE FLUID

We compare the performance of Rayon swabs in releasing the viruses in the buffer tube (**Figure 10.8B**) and using the hygiene system (**Figure 10.8C**). Swab shaft of the Hygiena system is hollow and fluid can be released upon snapping of the valve to rinse the swab. Swab eluate was then transferred out via the dropper at the bottom. The suggested protocol by the company involves swinging the swab sheath left and right for a few times before releasing the fluid through the tips. We found that this agitation process can the recovery yield by 10% but the use of hygiene to release the fluid from the swab soaking in the sheath significantly contribute to the recovery by at least 20% regardless of whether the swab was agitated prior to dispensing of fluid from the device tip (**Figure 10.8D vs Figure 10.8BE**)

© Copyright 2021 | N Panpradist

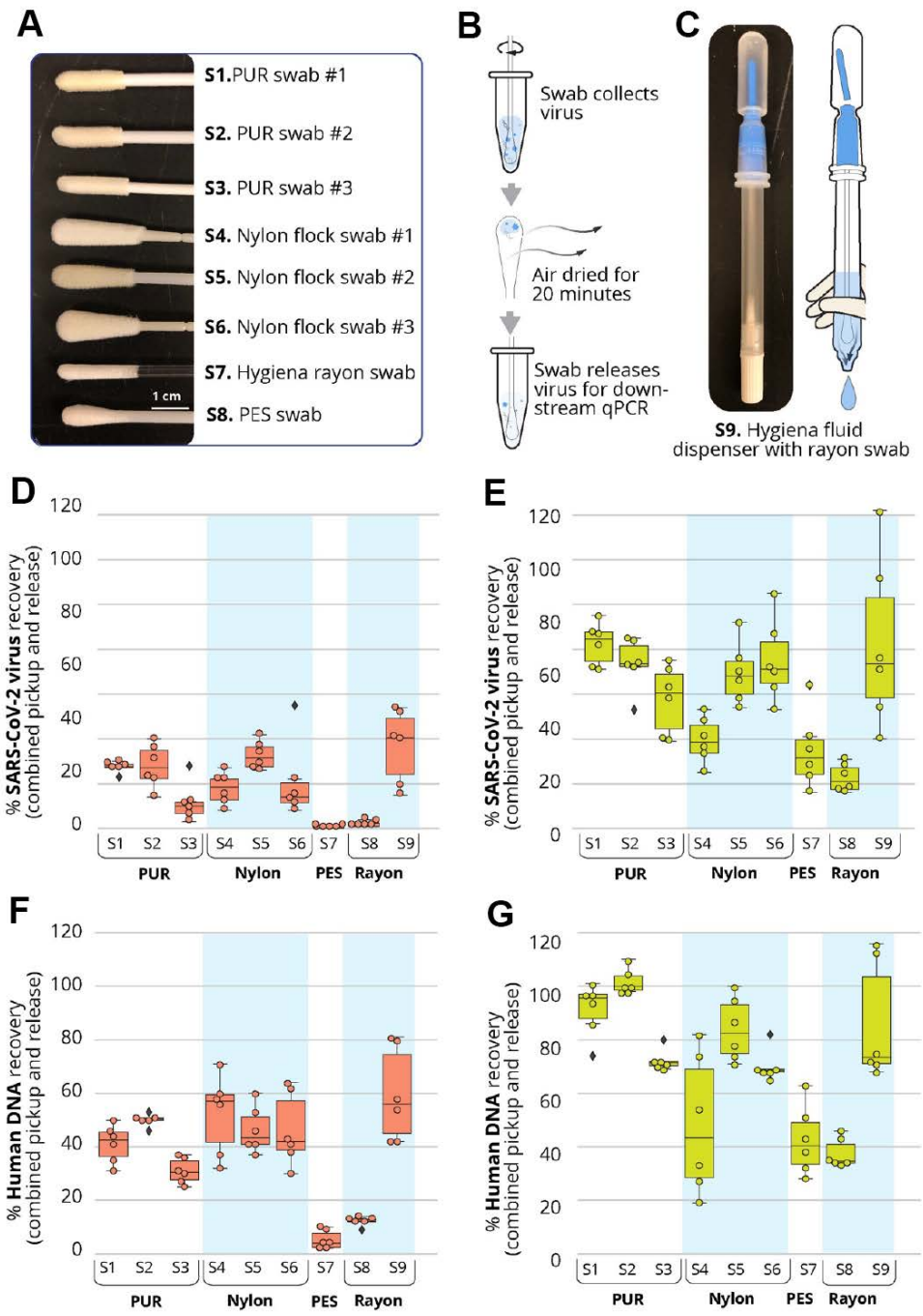

Figure 10.8 | Analytical comparisons of swabs in pick-up and release of SARS-CoV-2

(**A**) Photo of swabs used in this study. (**B**) Schema of experimental design. (**C**) Hygiena device and schema on how it was used to dispense the fluid. % Recovery of SARS-CoV-2 virus (**D**) with and (**E**) without 30s agitation. % Recovery of human DNA in sample (**F**) with and (**G**) without 30s agitation.

© Copyright 2021 | N Panpradist

DISCUSSION

We Characterized commercially available swab tip materials including traditional swabs such as nylon, polyurethane, polyester, and rayon, as well as injection-molded swabs made from elastomer. The key factors that we would like to recommend for swabs at POC, is shown in **Table 10.1**.

Table 10.1 | Recommendations on swabs for use at POC.

Characteristics for swab	Preferences
Swab tip material	Pickup and release viral particles effectively
Swab tip size	Not too small that users can accidentally insert swabs too deeply
Shaft length	Shorter shafts provide a better control for manual agitation in the buffer tube. Long shafts are bulky and prone to accidental spillage of the buffer tubes if soaking step is used.
Shaft thickness	Rigid swab shaft enables better control of manual agitation

Swab evaluation using target solution spiked onto the tips and released could potentially lead to overestimated yields for the swabs with hydrophobic tips, as virus may or may not captured by the swab tip materials but sit loosely within the droplet of fluid and readily released into the buffer. Some swab studies only allow swab to dry for 30 seconds or shorter, which may not necessarily reflect use of swabs at the POC. In this study, we intended to overcome the issue by allowing the swab tips to collect the viral particles in a simulated nasal matrix solution. Some swab materials that are hydrophobic may not absorb a large amount of fluid and yet they should pick up the viruses during the collection step.

© Copyright 2021 | N Panpradist

Here we tested the ability for the swab to pick up and release the SARS-CoV-2 viral particles. Swabs were soaked in simulated nasal matrix by rotating five times for a duration of 15-30 seconds similarly to how they are used in to collect samples from anterior nares[17] but performed in a reaction tube instead. To measure the release only, swabs tips are also loaded with samples directly. After air dry, swabs are released in buffer containing detergents to assist in elution of SARS-CoV-2 from swab tips.

This approach had some limitations because analyte contains simulated nasal matrix in the liquid form and some swab types may not pick up fluid as well, but we hope it will pick up virus during the 15 seconds absorption. Additionally, data was only collected by one person to limit variations across swabs using manual agitation. Results may not reflect actual capture of virus from the human anterior nares.

CONCLUSIONS

Swab types and models could significantly impact the recovery of SARs-CoV-2. Agitation of swabs increased recovery. As used in the Hygiena dispenser, devices that can force the fluid flow near swab tips can improve the release at the point-of-care.

© Copyright 2021 | N Panpradist

10.1.3. SWAB TRANSFER METHODS OPERATED BY TRAINED PERSONNEL VS. HEALTH CARE WORKERS

CONTRIBUTORS: Nuttada Panpradist, Enos Kline, Jack H Kotnik, Victoria Lyon, Qin Wang, Ian T Hull, Amy K Oreskovic, Crissa Bennett, Matthew J Thompson, Barry R Lutz

MATERIALS AND METHODS

We compared the accuracy and reproducibility of two methods for transferring the eluate to the reaction tube when operated by LPs *(n = 5*) and HCWs (such as nurses, medical students, and dental students; *n = 10*). The first method (**Figure 10.9A**) used a unified sampler-dispenser. The second method (**Figure 10.9B**) used a transfer pipette to transfer a fixed volume of fluid to the reaction tube.

© Copyright 2021 | N Panpradist

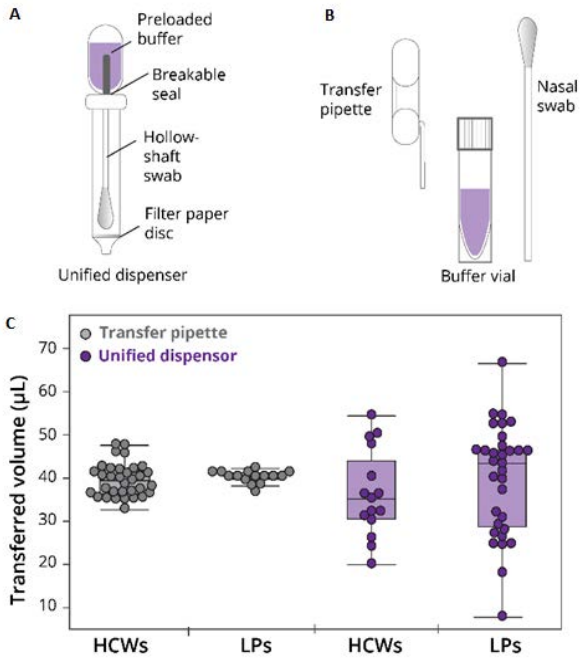

Figure 10.9 | Volume accuracy of two sample transfer methods.

(**A**) Illustration of the first sample transfer method option using a unified dispenser, which integrates a swab, buffer container, and a dropper in a single device. The contained buffer is released to elute the swab sample by cracking a conduit, the user agitates the fluid by shaking the tube, and a dropper tip allows the use to transfer two drops of fluid to the reaction tube by squeezing the body of the device. (**B**) Illustration of the second sample transfer method including a volumetric transfer pipette (40µL), a nasal swab, and a pre-loaded buffer vial. (**C**) Volume transferred by each method performed by healthcare workers (**HCWs**) or laboratory personnel (**LPs**). Individual volume measurements are plotted along with medians (middle lines of the boxes), interquartile ranges (edges of the boxes), and ranges (the ends of whiskers). Image was published in https://doi.org/10.1101/2021.08.12.21261875.

RESULTS

Regardless of the baseline skill of operators, transfer pipettes yielded more reproducible recovered volumes than the unified dispenser (F-test, $p < 0.001$).

© Copyright 2021 | N Panpradist

Recovered volumes of the two methods were not significantly different between HCWs and LPs (student's t-test, two-sided, p = 0.90; **Figure 10.9C**). User feedback on the transfer methods and preferences on tube sizes are summarized in **Table 10.2**.

Among HCWs, 30% (3/10) reported problems dispensing the fluid using the unified system. However, 20% (2/10) of HCWs agreed that the unified dispenser offered an advantage in its similarity to other tools used in healthcare settings, and 30% (3/10) HCWs were concerned about contaminating the sample or the environment with the transfer pipette compared to the unified dispenser system. Only 1/10 (10%) HCW preferred the smallest tube (0.2mL) for either method, and 5/10 (50%) reported that larger (1.5mL) tubes were helpful for the unified system, while 40% (4/10) of HCWs said receptacle size did not make a difference when using the transfer pipette, and none reported preference for tube size when using the unified dispenser system. HCWs reported higher confidence in correctly completing the second kit compared to the first kit of each method, indicating a similar learning curve.

Table 10.2 | Feedback from the HCWs.
(A) User preference for reaction tube size
Note: Cells with 0% response were left empty to aid data visualization

Question	User response, n (%)				
	0.2 mL	0.5 mL	1.5 mL	0.5mL or 1.5mL	no difference
Which tube size were you most confident using with the unified dispenser swab?		4 (**40%**)	5 (**50%**)	1 (**10%**)	
Which tube size were you most confident using with the transfer pipette?	1 (**10%**)	4 (**40%**)	1 (**10%**)		4 (**40%**)

(B) User responses to survey questions during sample transfer usability testing.
Users were asked to provide their response on a Likert scale: (1) Not at all, (2) Slightly, (3) Somewhat, (4) Fairly, (5) Completely. Note: Phrasing of the questions below was slightly modified to be clear outside

© Copyright 2021 | N Panpradist

of the context of the written protocol/survey (original survey here). Cells with 0% response were left empty to aid data visualization.

Question	User response, n (%)				
	(1)	(2)	(3)	(4)	(5)
How confident were you that you added the **correct amount of liquid** to each reaction tube using the **unified dispenser system?**			3 (**30%**)	3 (**30%**)	4 (**40%**)
How confident were you that you completed the protocol correctly using the **unified dispenser system** with the **first kit**?		2 (**20%**)	1 (**10%**)	4 (**40%**)	3 (**30%**)
How confident were you that you completed the protocol correctly using the unified dispenser system with the second kit?				5(**50%**)	5 (**50%**)
How confident were you that you added the correct amount of liquid to each reaction tube using the **transfer pipette**?			2 (**20%**)	2(**20%**)	6 (**60%**)
How confident were you that you completed the protocol correctly using the **transfer pipette** with the **first kit**?			3 (**30%**)	4 (**40%**)	3 (**30%**)
How confident were you that you completed the protocol correctly using the **transfer pipette** with the **second kit**?				5 (**50%**)	5 (**50%**)
How confident were you that you completed the **on-screen instructions correctly**?			1 (**10%**)	4 (**40%**)	5 (**50%**)

(C) User reported errors/challenges between two sample transfer methods. Cells with no response were left empty to aid data visualization.

Reported error	Sample transfer method	
	Number of occurrences for the **unified dispensing system**	Number of occurrences for the **transfer pipette**
The transfer method was hard to aim at the receiving reaction tube.	1	
Transfer method dripped/leaked before dispensing to the reaction tube.	2	
The materials were too small or difficult to handle.		3
It was hard to execute specific instructions due to unfamiliarity with the sample transfer device.	2	1
Challenging to dispense a consistent amount of fluid.	3	
Not confident liquid was dispensed to the tube.		2
Concerned about contaminating samples or the environment.		3

© Copyright 2021 | N Panpradist

DISCUSSION

Volumetric transfer pipettes are used in POC tests, but we have not identified a unified dispenser used in commercial pathogen tests. A unified dispenser integrating the swab and the buffer container in a single unit could reduce opportunities for sample mix-up when multiple samples are processed simultaneously. A simple workflow is crucial, especially in busy settings like clinics. However, in our hands, the in-house built dispenser led to variable dispensed fluid volumes and had a higher failure rate than those of the transfer pipette method. While the unified dispenser has many attractive features, we would not recommend using this in-house assembled dispenser unit until the method has been optimized to achieve a more accurately dispensed volume.

10.2 SIMPLER & FASTER RT-QPCR FOR SARS-COV-2 DETECTION

In early 2020, the World Health Organization and US Centers for Disease Control and Prevention (**CDC**) recommend use of molecular tests to detect acute infection of severe acute respiratory syndrome coronavirus 2 (**SARS-CoV-2**), the pathogen that causes coronavirus disease 2019 (**Covid-19**). We have conducted an in-depth analysis of commercially available RT-PCR tests for **SARS-CoV-2** detection up to April 23rd, 2020. Out of 41 molecular tests that received the US FDA Emergency Use Authorization, 37 are RT-PCR based assays. Due to their complexity, most RT-PCR assays are only approved for operations in Clinical Laboratory Improvement Amendments (**CLIA**)-certified laboratories. A new point-of-care test, Abbott IDNow®, relies on novel

© Copyright 2021 | N Panpradist

isothermal amplification chemistry and can provide positive results as fast as 13 min (1 patient specimen/machine run). Although RT-RPA is fast, high false negative rates were observed in several studies

SIGNIFICANCE. Instead of looking towards new amplification chemistry, we developed and adapted techniques, hardware, and software to simplify existing RT-PCR assays. The result is an easy-to-use platform which enables assay operators to set up an RT-PCR assay in minutes, with results available after 90 min. Keeping in mind that most resource-limited settings do not have access to expensive real-time thermal cyclers or consistent electrical power, we also developed an RT-PCR workflow that requires only battery-powered, low-cost instruments and reagents. A newly developed software algorithm can accurately classify positive and negative tube images taken by different cell phone models, including some commonly used in Asia and Africa.

IMPLICATIONS. We presented RT-PCR assay workflows that are simpler, faster and lower-cost compared to the CDC assay, and successfully amplify SARS-CoV-2 RNA directly from human nasal swab eluates. The simplest workflow we present may allow SARS-CoV-2 RT-PCR testing at point-of-care settings. This test could become an important clinical tool for Covid-19 diagnosis and management in a time when the world desperately needs fast, reliable, low-cost, and rapidly deployable SARS-CoV-2 diagnostic capabilities.

CONTRIBUTORS: Nuttada Panpradist, Qin Wang, Parker S. Ruth, Jack H. Kotnik, Amy K. Oreskovic, Abraham Miller, Samuel W.A. Stewart, Justin Vrana, Peter D. Han, Ingrid A. Beck, Lea M. Starita, Lisa M. Frenkel, Barry R. Lutz.

CONTRIBUTIONS: NP conceived the idea of the assay workflows. NP, QW,

© Copyright 2021 | N Panpradist

and AKO designed, conducted, and analyzed RT-qPCR experiments. QW captured cell phone images of fluorescent tubes. PSR wrote the Python code for automating image fluorescence extraction from tube images. IB tested nasal swab specimens using CDC EUA assay in the CLIA-certified SCRI lab and provided left-over eluate for clinical validation study. JHK arranged the cell phone loan from Michael Maruchek from Audere that we used to study software. JHK and SWAS researched and summarized the information from the EUA-approved kits, and developed the list of open-sourced, commercial equipment. AM and JV discussed the Aquarium software design for assay workflows. PDH and LMS designed and characterized a panel of clinical samples for assay evaluation. LMF and BRL oversaw the study design. All authors provided feedback on data analysis and interpretation, contributed to writing this manuscript and approved the final version of this manuscript.

MATERIALS AND METHODS

Preparation of analytical specimen panel. In this study, we used mid-turbinate nylon swabs (Copan Diagnostics Inc., 56380CS01). Each swab was loaded with 15 µL of simulated nasal matrix (1% *(w/v)* mucin porcine stomach type III, 10 mg/mL human genomic DNA, and 110 mM sodium chloride) [18] and dried for 30 min. Swabs were resuspended in 1x lysis/rehydration buffer containing 2 mM MgSO4, 0.5% *(v/v)* Triton X-100, and 1x buffer (New England Biolab B9023SVIAL). 18 µL or a droplet from a dropper of swab elution was used to rehydrate a lyophilized RT-PCR reaction using micropipettes (Ranin XLS L8–20) or dropper (Nalgene 69047). Rehydrated RT-PCR reactions

© Copyright 2021 | N Panpradist

without or with SARS-CoV-2 RNA at different concentrations were subjected to RT-PCR.

***Preparation of clinical specimen panel*.** Human nasal swabs (*n = 41*) were collected on Puritan™ Polyester-Tipped Applicators (Fisher) by health care workers and tested in the Frenkel CLIA-certified laboratory at Seattle Children's Research Institute. The swabs were resuspended in 1 mL 1xPBS and stored at 4 °C until testing. These swabs were tested for SARS-CoV-2 and shown to be negative. Additionally, we obtained remnant human respiratory specimens that were collected from individuals (*n* = 110) presenting respiratory symptoms, by observed or unobserved collection using mid-turbinate swabs (Copan) or nasopharyngeal swabs collected by healthcare workers. Swabs were stored in 3 mL viral transport medium (Becton Dickinson 220220), aliquoted, and stored at −80 °C until testing.

Preparation of in-vitro SARS-CoV-2 RNA transcript. Synthetic SARS-CoV-2 gBlock (Integrated DNA Technology) containing the consensus sequence (NCBI up to January 2020) was used as the template to generate RNA via in-vitro RNA transcription by Hi-T7 RNA polymerase (New England Biolabs, M0658S), following the protocol from the manufacturer. The RNA was quantified using Qubit RNA HS Assay Kit (Invitrogen, Q32852). Fragment size and integrity of the in-house RNA was confirmed using Tapestation High Sensitivity RNA ScreenTape (Agilent 5067-5579). The in-house RNA showed expected size with no sign of degradation and its concentration was quantified using digital droplet PCR (Stilla, Naica® system workflow) according to the manufacturer's protocol[19].

© Copyright 2021 | N Panpradist

Preparation of lyophilized RT-PCR reagents. 10 µL of magnesium-free RT-PCR mixture contained 2x primer/probe (IDT 10-006-770, sequences are accessible from CDC website[20]), 10 mM DTT, 16.881.6% *(w/v)* trehalose, 400 µM ea. dNTPs, 2 units of OneTaq® Hot-start polymerase (NEB M0481X), 6 units of RTx WarmStart™ (NEB M0380L), and 0.025x RNasIn Plus (NEB N2115). The mixture was submerged into liquid nitrogen for 2 min and dried at 0.018 mbar, −55 °C. Lyophilized reagents were stored with desiccant packets in sealed foil pouches until use.

Setting up RT-PCR reactions. RT-PCR reactions were rehydrated in 1x lysis/rehydration buffer in water for purified RNA experiment and swab eluates in the rest of the experiments. The rehydrated RT-PCR reaction either without (no template control) or with SARS-CoV-2 RNA was then subjected to a cycle run either in a real-time thermal cycler (CFX96 Touch, BioRad), standard thermal cycler (T100, BioRad), and a battery-powered thermal cycler (Mini-16, MiniPCR) of 8 min at 55 °C, 2 min at 94 °C and 50 cycles of 1 second 94 °C and 30 s at 57 °C. In the RT-qPCR experiment, the plate read step via FAM dye channel was performed at the end of each extension cycle. For nasal swabs eluted in 1xPBS, either 1:2, 1:4, or undiluted swab eluates mixed with the lysis buffer were added to lyophilized RT-PCR reagents with or without SARS-CoV-2 RNA at different concentrations before undergoing RT-PCR. For nasal viral transport medium (**VTM**) samples, 1:4 diluted swab eluate was added to lyophilized RT-PCR before undergoing RT-PCR. For the standard protocol, 5 µL of extracted RNA was added to 15 µL RT-PCR mix according to the CDC guideline[20].

© Copyright 2021 | N Panpradist

***Analysis of RT-QPCR results*.** The CFX96 Touch instrument (BioRad) was used to operate RT-qPCR runs. Biorad CFX Maestro software was used to determine the quantification cycle (Cq) of the samples.

Analysis of images from transilluminator and glow box. Images of reaction tubes after completion of the RT-PCR were obtained using a transilluminator or a glow-box and the default Android cell phone camera application without any assisted applications. The fluid-filled tips of the vials were segmented by applying a manually set threshold to the norm of the distance in Red-Green-Blue (**RGB**) space; the distance metric was computed relative to the average RGB pixel value of a positive control sample. Binary opening and closing was applied to the thresholded image to fill holes and remove noise. The tube regions were then selected with a heuristic algorithm. After segmenting tube regions, the mean RGB value for each tube was computed inside the region of interest. For the glow box images, the specular reflections were eliminated by performing k-means clustering on the region of interest pixel values. The mean RGB pixel values for each scenario and phone model were converted to intensity values using a support vector machine (**SVM**) with a linear kernel. P-values and confidence intervals were numerically computed.

Analytical sensitivity assessment. Single-used purified RNA transcript aliquots were stored at −80 °C at a concentration of 2×10^8 copies/μL and diluted fresh for each experiment to 2.5, 3.5, 5, 10, 100, 10^3, 10^4, and 10^5 copies/μL. 2 μL of RNA sample or water (for no template control) were added to 18 μL RT-PCR mix to achieve the final volume of 20 μL.

© Copyright 2021 | N Panpradist

Validation testing in clinical specimens. To test assay accuracy in human nasal matrices, 41 nasal swab eluates (collected in May 2020 from non-symptomatic individuals and tested negative for SARS-CoV-2 RNA) were used to generate contrived specimens for accuracy testing: 41 negative, 21 positive at 100 copies RNA/reaction, 10 positives at 40 copies RNA/reaction, and 10 positives at 20 copies RNA/reaction (1x LoD). For the Scenario 3 workflow, we tested 30 negative, 6 positive at 100 copies RNA/reaction, 16 positives at 40 copies RNA/reaction, and 8 positives at 20 copies RNA/reaction. In addition to contrived nasal specimens, we analysed remnant upper respiratory specimens, collected from November 2019 – April 2020. These specimens were positive (n = 40) and negative (n = 70) for SARS-CoV-2 RNA, as determined by the protocol previously described[21]. Presence of adenovirus, seasonal coronavirus, influenza, respiratory syncytial virus, parainfluenza virus, metapneumovirus, enterovirus, parechovirus, bocavirus, and pneumoniae were also tested in these specimens using TaqMan® OpenArray™ Respiratory Tract Microbiota Plate (Thermo Fisher A41237). We performed both standard and modified protocols on these specimens. For the standard protocol, 100µL each sample was extracted (Qiagen 52-906) following the CDC protocol, except the purified RNA was eluted in 70µL (instead of 100µL). 5 µL purified RNA was subsequently added to 15µL RT-PCR mixture according to the standard CDC protocol. For the modified workflow, 5µL each sample was directly added to each 15µL rehydrated, lyophilized RT-PCR. Cq values of the paired samples were compared. Discordant results from the standard and modified protocols were verified using previous analysis by the University of Washington Virology

© Copyright 2021 | N Panpradist

lab. Additionally, end-point fluorescence of each N1, N2, and RP assays was plotted to determine its feasibility to classify positive from negative samples.

Ethics. All specimens were left-over from previous studies at the Frenkel lab at Seattle Children's Research Institute and the Starita lab at the University of Washington. Nasal swabs were collected and tested for SARS-CoV-2 infection as part of the Seattle Children's SARS2 Prospective Cohort, as approved by the Seattle Children's Institutional Review Board (IRB#: STUDY00002434) and as part of the Seattle Flu Study, as approved by the Institutional Review Board at the University of Washington (IRB#: STUDY0006181). Informed consent was obtained for all participant samples, including for use of de-identified, remnant specimens.

Statistical analysis. Number of specimens tested in each experiment are reported in the method section or at the legends. To assess the accuracy of our tests, we performed a power calculation using binomial cumulative distribution function. A minimum sample size of 30 was required to achieve the confidence interval (**CI**) of 90–100% should all results be accurate. We selected a sample size, n, such that a 95% confidence interval for p included 0.9–1 which, based on our previous work, was likely to be the proportion of accurate tests. The upper bound of this confidence interval was 1. The lower bound was the largest value of p for which the P ($X < 0.05$), where X~binomial (n, 0.9). Mean, CI, and standard deviations (**SD**) were provided along with individual data points in each experiment. To evaluate the statistical significance of the SVM classifier outputs, we developed a nonparametric numerical p-value. For each dataset, we randomly shuffled the positive and

© Copyright 2021 | N Panpradist

negative class labels 1000 times, retraining the SVM and computing ROC AUC values for each; the p-value was the number of AUC values greater than or equal to the observed AUC value. We chose this method because it avoids assumptions of large dataset size or normality. To quantify the uncertainty of the AUC values for dataset, we computed confidence intervals using a parametric numeric simulation. For each dataset, we added gaussian noise to the RGB pixel values extracted from the tubes. The covariance of the gaussian noise was estimated from the covariance of the observed RGB data. To account for the effect of different copy numbers on the tube color variance, the noise covariance was estimated after subtracting the means from each set of tube replicates. An SVM was retrained for 10,000 independent gaussian noise additions, and the resulting distribution of AUC values gave bounds for the confidence intervals.

RESULTS

10.2.1 DEVELOPMENT OF LYOPHILIZED RT-PCR REAGENTS FOR SARS-COV-2 RNA DETECTION AND ANALYTICAL SENSITIVITY OF OUR PROTOCOL COMPARED TO THE CDC PROTOCOL

Instead of using RT-PCR mix listed on the US CDC protocol[22], we chose to develop a new RT-PCR formulation that *(i)* is compatible with detergent-based lysis buffer and other contaminants from simulated nasal matrix containing mucin, human genomic DNA, and salts; *(ii)* contains cryoprotectant to stabilize RT-PCR reactions during lyophilization and *(iii)* maintains sensitivity comparable to the CDC RT-PCR assay. The assay uses the same primers and probes as the CDC protocol, but for the master mix we chose the combination

© Copyright 2021 | N Panpradist

of the warm-start reverse transcriptase, RTx WarmStart®, and the hot-start OneTaq® DNA polymerase. We found that the two enzymes are compatible, and both are resistant to mild detergents present in the lysis buffer (**Figure S10.45**). Trehalose, a universal cryoprotectant and protein thermal stabilizer[23], was used for lyophilization. We optimized the annealing/extension temperature in the presence of different trehalose concentrations to achieve the highest analytical sensitivity (**Figure S10.46**). We selected 8.4% w/v trehalose coupled with 57 °C annealing temperature for the base assay.

Analytical sensitivity (*i.e.,* Limit of Detection (**LoD**)) of lyophilized RT-PCR with human genomic DNA background is 10 and 5 SARS-CoV-2 RNA copies/reaction for N1 (**Figure 10.10A**) and N2 (**Figure 10.10B**) assay, respectively. In some cases, we were able to detect 7 copies/reaction for N1. **Figure 10.10C** shows an overview comparison of our modified protocol and the CDC protocol. In the CDC protocol, 5 µL RNA sample was added to 20 µL RT-PCR reaction. In contrast, our lyophilized reaction can be entirely rehydrated with 20 µL RNA sample. Thus, the analytical sensitivity of 10 copies/reaction is equivalent to a 0.5 ($10^{-0.3}$) RNA copies/µL sample. For direct comparison, we analyzed spiked-in SARS-CoV-2 RNA in viral transport medium according to the CDC protocol. We observed the analytical sensitivity of 5 copies/reaction, equivalent to 1 (10°) RNA copy/µL sample, matching the reported analytical sensitivity by CDC (**Figure 10.10D**).

© Copyright 2021 | N Panpradist

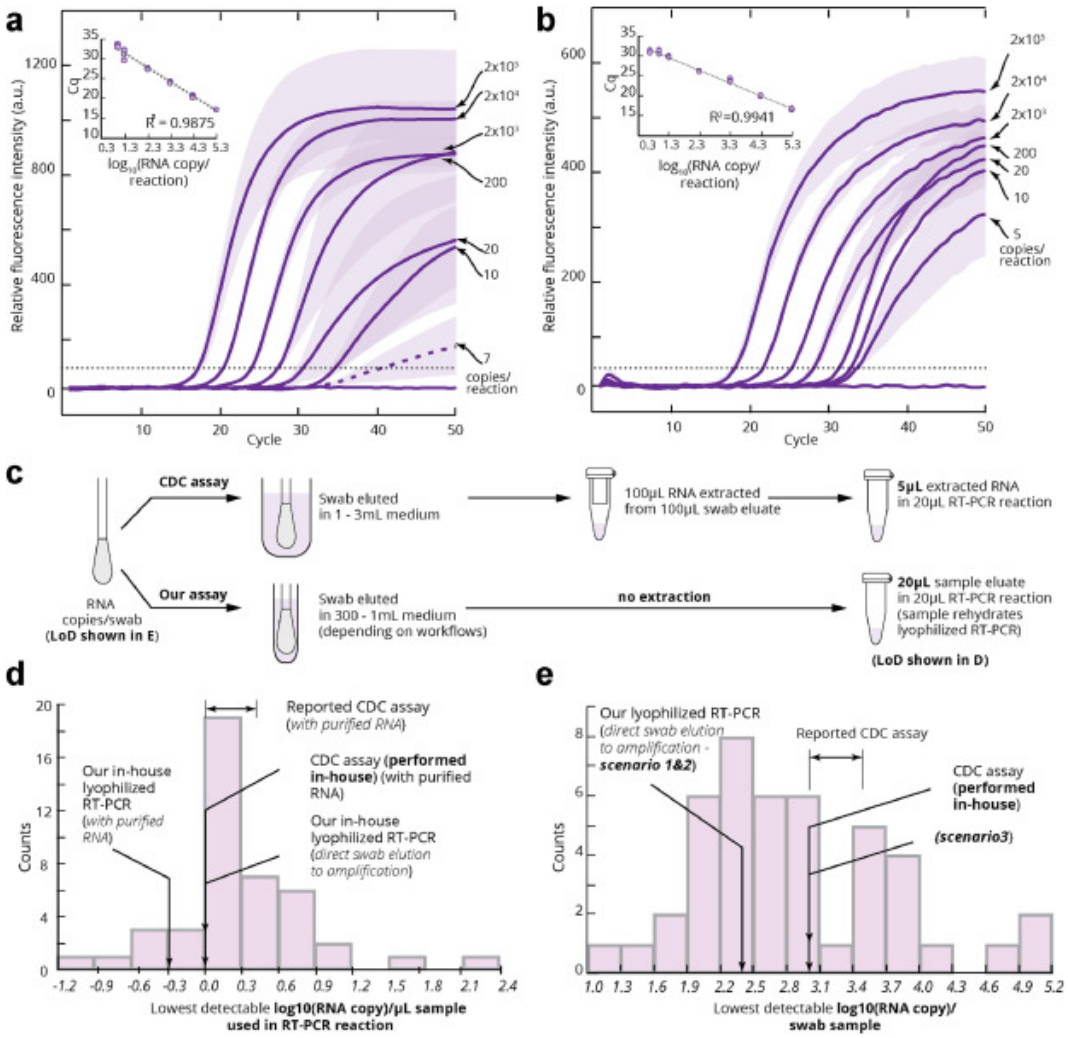

Figure 10.10 | *Analytical sensitivity of a newly developed lyophilized RT-qPCR formulation using CDC primers/probes.*

(**A**) N1 and (**B**) N2 assay amplification curves of SARS-CoV-2 RNA at 0, 5 or 7, 10, 20, 200, 2 × 10^3, or 2 × 10^4 copies in the presence of 1 ng human genomic DNA (3 technical replicates, mean ± SD). Dashed amplification curve shows average of the 2/3 replicates of 7 copies/reaction for N1 assay. Dotted horizontal lines in (A) and (B) indicate the detection threshold that defines the quantification cycle (Cq). The insets of each plot show RT-PCR efficiency plot. (**C**) Workflow comparison between the CDC protocol and our assay (**D**) Histogram of the reported LoD (log_{10}P of RNA copy**/µL eluate**) from the existing EUA molecular assays, CDC protocol performed in-house, and our lyophilized RT-PCR assay. Note that extraction efficiencies were not reported, and 100% extraction efficiency was assumed to calculate the log_{10} (RNA copy/µL eluate). CDC assay reported two LoDs from the two recommended RNA extraction

© Copyright 2021 | N Panpradist

kits, so we indicated the range of LoD in the histogram (i.e., 10^0 – $10^{0.4}$ copies/µL) of the CDC assay. (**E**) Histogram of the reported LoD (log_{10} of RNA copy**/swab**) in existing EUA approved molecular assays, CDC protocol performed in-house, and our lyophilized RT-qPCR assay. Note that in the CDC protocol, swabs were eluted in at least 1 mL medium while our protocols used 300 µL - 1 mL depending on the scenario, which will be discussed (3.2, 3.4). For (C) and (D), only tests that provided sufficient information in their EUA IFU to calculate the necessary values were included. Additionally, for tests that reported multiple analytical sensitivities depending on extraction methods, both were included. Refer to supplementary table 1 for a complete summary.

Next, we demonstrated direct amplification of swab eluate without an RNA extraction step. The swab elution buffer used in our workflow is multipurpose. It is used to directly rehydrate the lyophilized reagents to run the assay. The detergent present in the buffer will also lyse the virus in conjunction with the mild heating at the 55 °C reverse transcription step. We tested the lysing efficiency by using our lyophilized N2 assay to directly amplify the intact AccuPlex™ virus control – a SARS-CoV-2 RNA control that is packaged within a viral protein envelope. Our RT-PCR assay detected 25 copies of the control virus, and the mixture of enveloped RNA and swab elution buffer stored for 2h at 4 °C had similar results to the fresh lysate (**Figure S10.48**). We also assessed the effects of potential inhibitors that may be present in human nasal samples. We first used human DNA spiked in porcine simulated nasal matrices and salts, similar to formulations used to evaluate US FDA-cleared influenza tests (e.g. Xpert® Flu[24]). We amplified SARS-CoV-2 naked RNA in the presence of the simulated nasal matrix and lysis buffer showing analytical sensitivity of 20 copies/reaction, equivalent to 1 (10^0) RNA copy/µL (**Figure 10.10D**).

© Copyright 2021 | N Panpradist

For comparison, we compiled the reported sensitivities on existing EUA authorized approved molecular assays (up to April 23rd, 2020) and created a frequency distribution plots of the LoD based on the copy number of purified RNA (**Figure 10.10D,** purified RNA copy/µL eluates after extraction) and the copy number in original swabs prior to extraction (**Figure 10.10E**, RNA copies/swab sample). The LoD of our lyophilized RT-qPCR is in the middle range of the LoD from the available tests and lower than or comparable to that of the CDC assay.

10.2.2 SCENARIO 1 – HIGH-THROUGHPUT RT-QPCR WORKFLOW FOR LABORATORIES

Figure 10.11A shows a diagnostic testing workflow designed for a high-throughput lab that first screens for infection using a more sensitive SARS-CoV-2 assay (i.e., N2 primer set) and the human control (*i.e.,* RP primer set). Only samples positive for N2 would then be confirmed with primers for N1. This Scenario 1 workflow requires a single-channel real-time thermal cycler (see example models and listed prices in **Table S10.7**), and optional multichannel micropipettes to allow faster parallel processing of samples. The streamlined workflow (**Figure 10.11B**) begins with the elution of dry swabs in barcoded racked tubes containing 300 µL elution/rehydration buffer. Each barcode would be associated with both a patient ID and its designated location on the 96-well rack. We chose 300 µL because it is the lowest volume that can provide sufficient dilutions of inhibitors from the sample as well as enough volume to run three RT-PCR reactions. 20 µL eluate from each swab is directly transferred to the lyophilized RT-PCR plate. The plate with the rehydrated RT-

© Copyright 2021 | N Panpradist

PCR mixtures is then sealed and run in a real-time thermal cycler using the RT-PCR protocol. The analytical sensitivity of this assay using SARS-CoV-2 RNA in background eluate from simulated nasal matrix is 20 copies/reaction, corresponding to a starting RNA concentration of 1 (10^0) copy/µL eluate (**Figure 10.11C**) and 300 ($10^{2.48}$) copies/swab sample (**Figure 10.11D**).

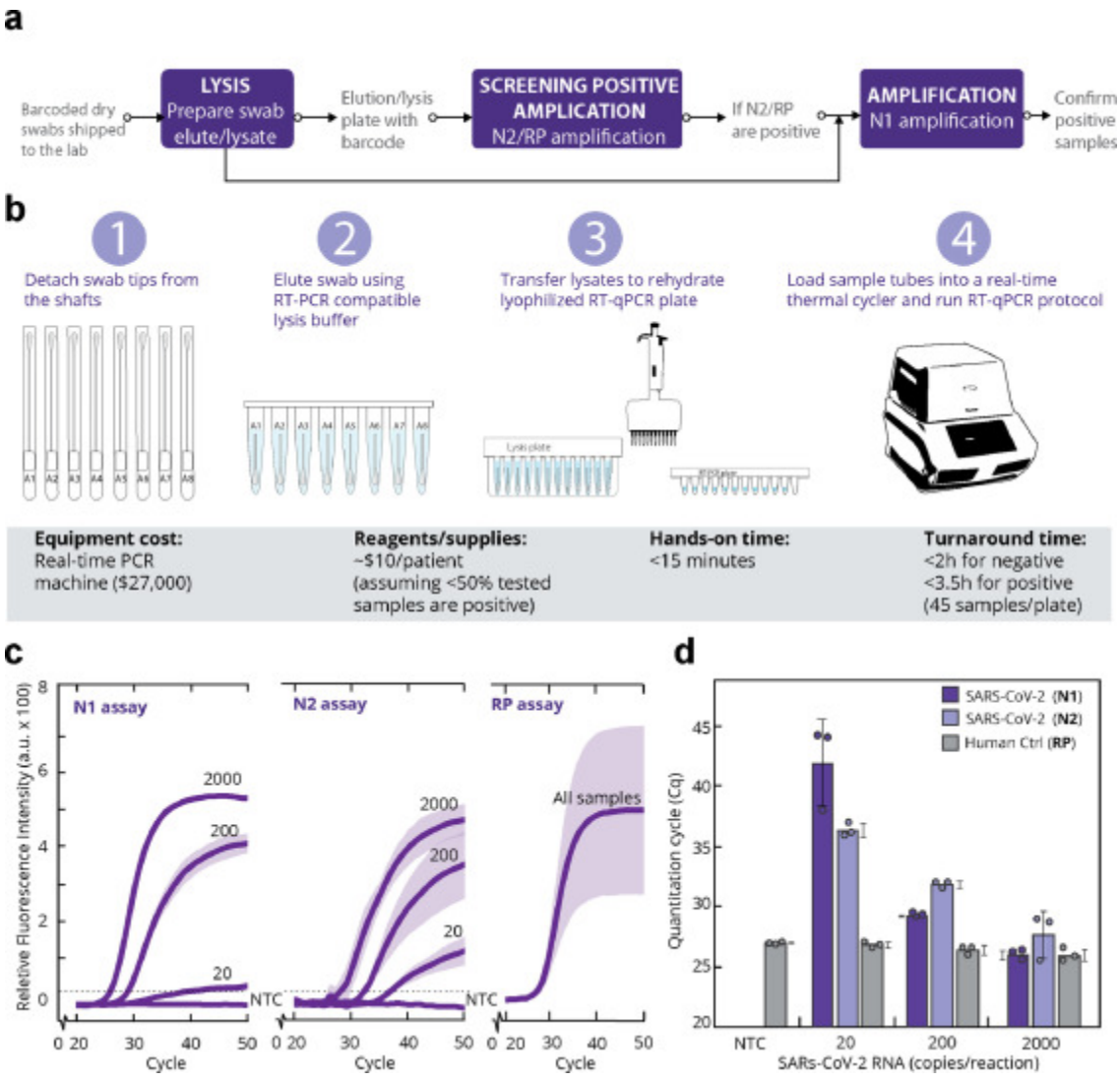

Figure 10.11 | High-throughput laboratories with access to a real-time thermal cycler.

(**A**) Diagnostic algorithm modified from the original CDC protocol to increase speed and cost-effectiveness. (**B**) Demonstration of high-throughput RT-qPCR workflow. Swab eluates are lysed and used directly in RT-qPCR. (**C**) Amplification curves of lyophilized RT-qPCR using N1, N2, and RP primers.

© Copyright 2021 | N Panpradist

15 µL of simulated nasal matrix (1% w/v mucin, 110 mM NaCl, and 10 ng/µL human genomic DNA) were spiked on swabs and eluted in 300 µL lysis buffer (0.5% Triton-X 100, 2 mM $MgSO_4$ in water). 18 µL of lysate with 2 µL of SARS-CoV-2 RNA at 0 (no template control), 20, 200, 2000 copies/reaction were then subjected to RT-PCR. Relative fluorescence signal of each sample (3 technical replicates, mean ± SD) at the end of each amplification cycle were plotted. (**D**) Quantification cycles (Cq) of the samples tested using lyophilized RT-qPCR reactions with N1, N2 primers (SARS-CoV-2) or RP primers (positive human control) with 3 technical replicates, mean ± SD. Water control (no simulated nasal matrix) did not generate signals detectable by N2 primers. Equipment costs listed are based on the models we used in this study.

10.2.3 SCENARIO 2 – HIGH THROUGHPUT LABORATORY END-POINT RT-PCR WORKFLOW

For laboratories without access to a real time thermal cycler, we propose the Scenario 2 workflow where a standard 96-well thermal cycler (**Table S10.8**) and a low-cost fluorescence reader can be employed (**Table S10.9**), together with a phone-based image processing software. Like Scenario 1, the lyophilized RT-PCR can be rehydrated directly by swab eluates and tested using the same diagnostic algorithm presented in **Figure 10.11A**. However, in this Scenario 2 workflow (**Figure 10.12A**), laboratories can reduce the cost of required equipment whilst maintaining high assay throughput. As in Scenario 1, during the annealing/extension step in RT-PCR, the polymerase enzyme hydrolyses the 5’ TaqMan™ probe and releases FAM signal proportionally to the amplified targets. The product of the RT-PCR step is temperature stable, and this end-point product can be read at ambient temperature under a transilluminator (**Figure 10.12B**) or a battery-powered glow box (**Figure 10.12C**). To the unaided eye, the no template control signals from the glow box image were

© Copyright 2021 | N Panpradist

not distinguishable from 20 copies/reaction. However, with software image processing, the analytical sensitivity of this assay is the same as the Scenario 1 workflow (20 copies/reaction) regardless of visualization tools used. Classification of negative and positive SARS-CoV-2 samples using software-analyzed relative fluorescence intensities was excellent. Receiver operating characteristic area under the curve (**ROC AUC**) computed from the relative fluorescence intensities is 0.999 and 1, respectively, for transilluminator and glow box.

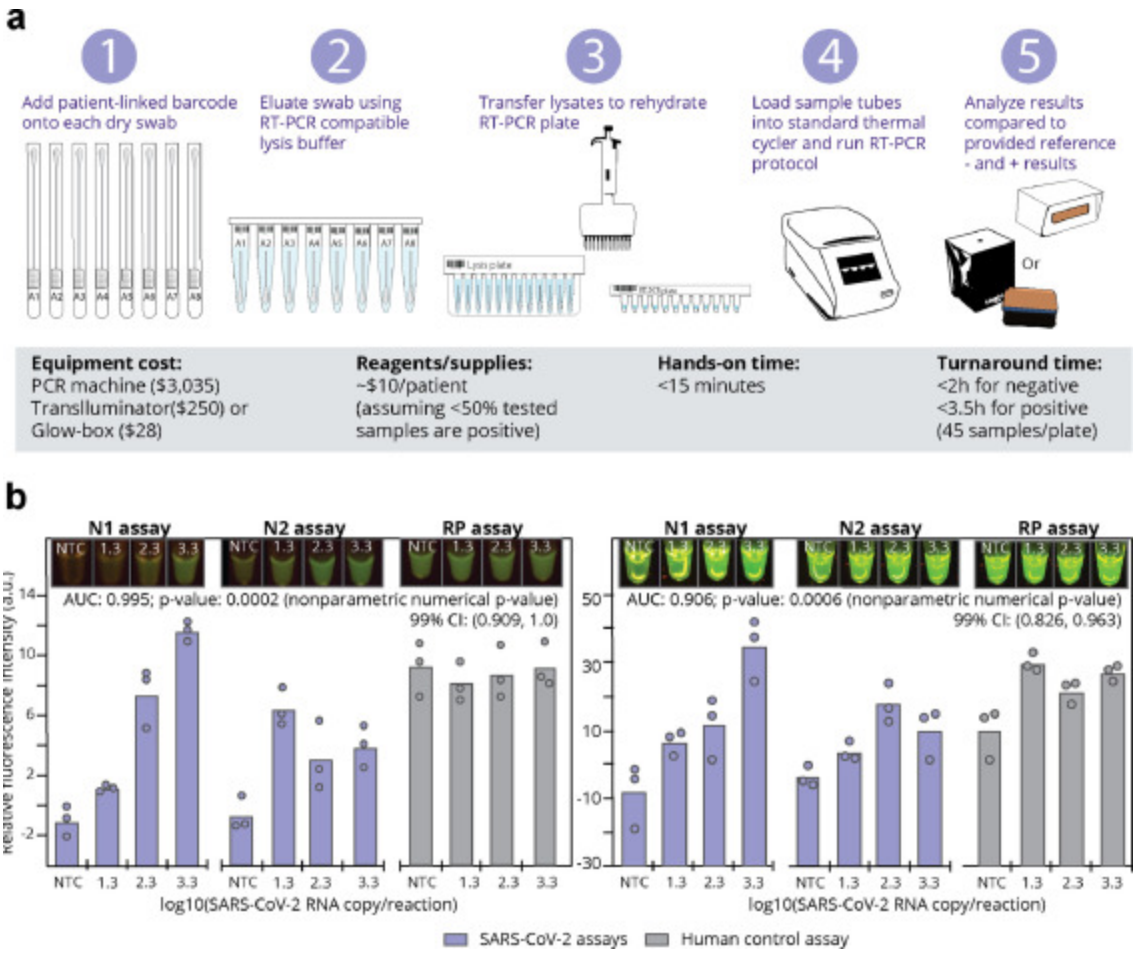

Figure 10.12 | Workflow *for high-throughput end-point RT-PCR Covid-19 assay for laboratories with access to a 96-well thermal cycler and a fluorescence visualizer.*

© Copyright 2021 | N Panpradist

(**A**) Step-wised protocol from the steps 1–3 is similar to Scenario 1, but the RT-PCR step takes place in a standard thermal cycler. Results are visualized after the completion of RT-PCR step by either a transilluminator *(left)* or battery-powered fluorescence box with an orange filter *(right).* Equipment costs listed are based on the models we used in this study. (**B**) Analytical sensitivity of the Scenario 2 workflow visualized under a transilluminator. A serial dilution of SARS-CoV-2 RNA spiked in simulated nasal mix at 0 (no template control), 20, 200, or 200 copies/reaction was carried through the Scenario 2 workflow. After the RT-PCR step, images of the tubes visualized under a transilluminator were taken by a cell phone (one replica shown). (**C**) Analytical sensitivity of Scenario 2 workflow visualized under a battery-powered fluorescence box from the same set of RT-PCR products. Each group of data had 3 triplicates. Mean values were reported along with individual data points. P-values and confidence intervals were numerically computed.

10.2.4 SCENARIO 3 – LOW THROUGHPUT CLINICS WITH ACCESS TO A BATTERY-POWERED THERMAL CYCLER AND FLUORESCENCE READER

In this scenario (**Figure 10.13A**), users do not need access to micropipettes. Instead, a dropper container is used to dispense the lysate. The dry swab is resuspended in the bottle containing 1 mL of lysis/rehydration buffer. 1 mL of buffer is used in this scenario instead of 300 µL because the dropper has some dead volume. The dropper tip is then loaded onto the top of the bottle and used to dispense 20 µL of the lysate into each lyophilized RT-PCR reaction (N1 or N2 primer set to target SARS-CoV-2; and RP human control primer set). We chose a battery-powered thermal cycler to eliminate interruptions due to power outage, a common issue in low-resource settings. The analytical sensitivity of this assay is the same as the Scenario 1 workflow (20 copies/reaction) regardless of visualization tools used (**Figure 10.13B** and

© Copyright 2021 | N Panpradist

Figure 10.13C). Differentiation of negative from positive SARS-CoV-2 samples using software-analyzed relative fluorescence intensities remained excellent. ROC AUC computed from the relative fluorescence intensities was 1 and 0.967, respectively, for transilluminator and glow box.

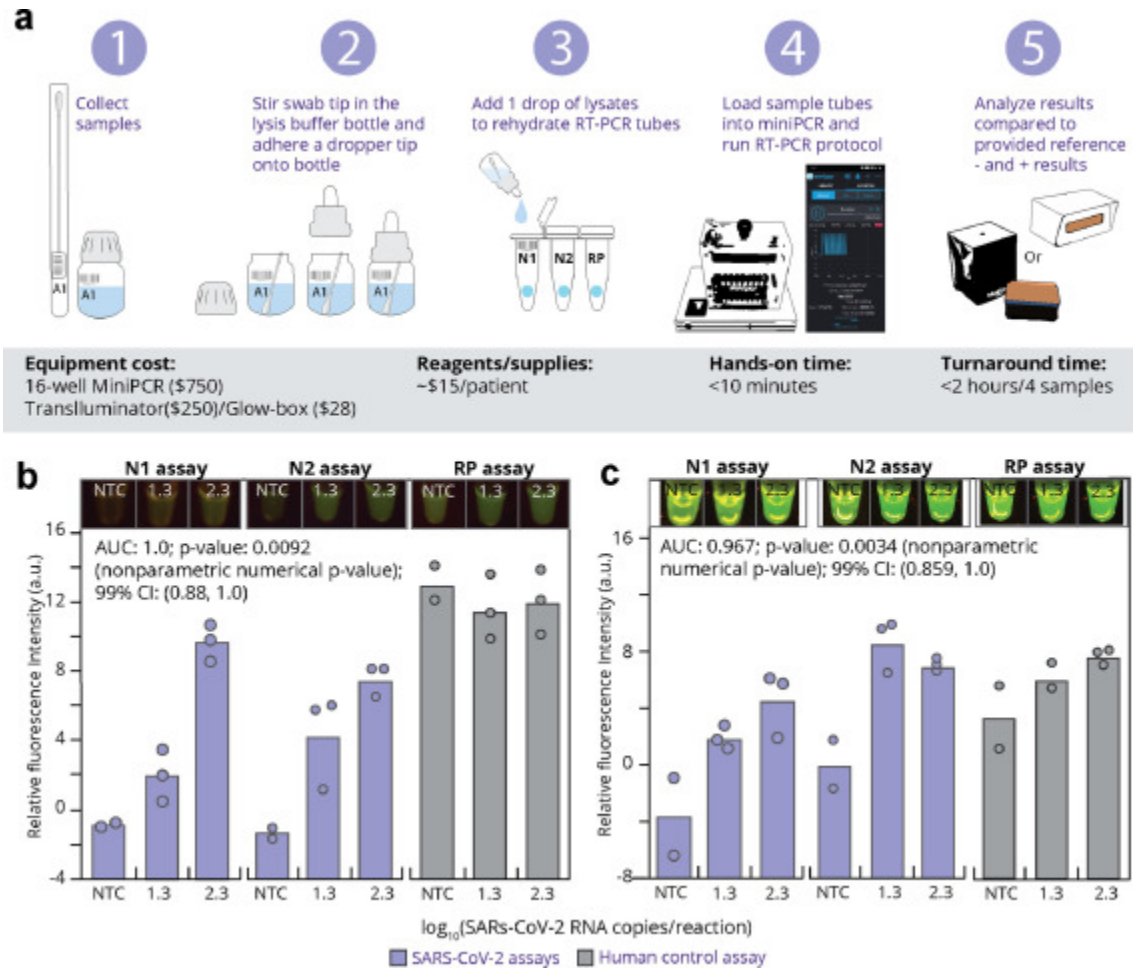

Figure 10.13 | Workflow and performance for low throughput for point-of-care settings such as small hospitals or clinics.

(**A**) Stepwise protocol for the Scenario 3 workflow eliminates the need for micropipettes and consistent electricity. Equipment costs listed are based on the models we used in this study. (**B**) Analytical sensitivity of the Scenario 3 workflow visualized under a transilluminator. A serial dilution of SARS-CoV-2 RNA spiked in simulated nasal mix at 0 (no template control), 20, 200, or 2000 copies/reaction was carried through the Scenario 3 workflow. After the RT-PCR step, images of the tubes visualized under a transilluminator were taken by a cell phone (one replica shown). (**C**) Analytical sensitivity of Scenario 3

© Copyright 2021 | N Panpradist

workflow visualized under a battery-powered fluorescence box from the same set of RT-PCR products. Two replicates for no template control. Three replicates for 20 and 200 copies/reaction. Mean values are plotted with individual data points. Equipment costs listed are based on the models we used in this study. P-values and confidence intervals were numerically computed.

10.2.4 SOFTWARE ANALYSIS OF FLUORESCENCE TUBE IMAGES

All images in the previous experiments in the Scenario 2 and Scenario 3 workflows were captured using a single cell phone (i.e., OnePlus 7 Pro) to maintain consistency across experiments. The fluorescence of each image (**Figure S10.49 - Figure S10.52**) was quantified using a newly-developed image processing Python algorithm (**Figure 10.14A**). We observed strong linear correlation of the end-point fluorescence signal measured by the real-time qPCR machine and the processed relative fluorescence signal from both the transilluminator (**Figure 10.14B,** R^2=0.77, 95% CI: 0.67–0.87 Olkin and Kinn's approximation) and the glow box (**Figure 10.14C,** R^2=0.84, 95% CI: 0.76–0.91). Additionally, we performed two-fold cross validation of the algorithm across four independent datasets and observed excellent classification performance (**Figure S10.53**) with the ROC AUC of 0.978 – 1.0 (mean ± SD: 0.991±0.009). Next, we investigated whether this software would be robust across images taken by different models of cell phones, including models used in the US and models commonly used in Asia and Africa (**Table S10.10**). We observed dramatic differences in the quality of images taken by the cell phones, but software-processed images successfully distinguished between the no SARS-CoV-2 RNA template plate control (**NTC**) and 20 copies/reaction. Example images are shown in **Figure 10.14, D-F** show the software analyzed signals from cell phone images under the

© Copyright 2021 | N Panpradist

transilluminator and the glow box, respectively. Classification of the negative from the positive reaction tube images from Scenario 2 taken by all cell phones were excellent (p-value <0.05, nonparametric numerical p-value), except for TecnoB1F (**Figure 10.14F,** p-value = 0.079, nonparametric numerical p-value).

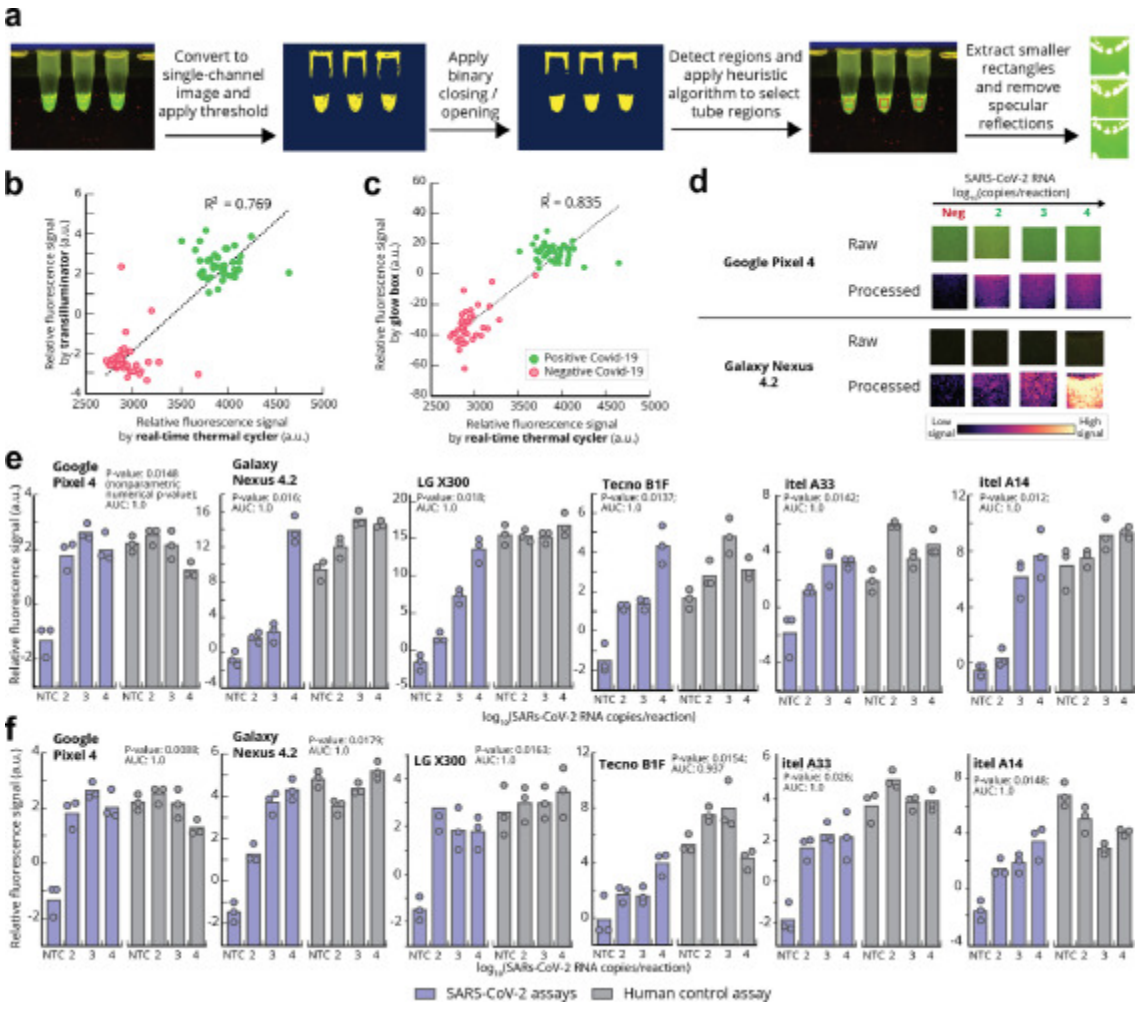

Figure 10.14 | Software analysis of fluorescence tube images.

(**A**) Image processing algorithm workflow for an example image from the glow box at 2000 copies/reaction. Details of the algorithm are in the method section. (**B**) Correlation plot of end-point fluorescence intensity read by the real-time thermal cycler and the signal from the transilluminator and (**C**) from the glow box. (**D**) Comparison of processed image examples (support-vector machine projected pixels) and their original images under the transilluminator. (**E**) Comparison of software analysis of images by different models of cell phones under transilluminator and (**F**) under the glow box. These images were taken from RT-PCR products that underwent the Scenario 2 workflow. Samples were SARs-

© Copyright 2021 | N Panpradist

CoV-2 RNA spiked in the simulated nasal swab lysate at 0 (NTC: no template control), 20, 200, or 2000 copies/reaction in the N2 and RP assay (3 technical replicates with mean). Each circle represents individual data points. All processed ROI of images from each cell phone model are available in **Figure S10.53**.

10.2.5 ACCURACY VALIDATION OF ASSAY WORKFLOWS IN CONTRIVED RNA SPIKE-IN NEGATIVE HUMAN NASAL SPECIMENS IN PBS – SCENARIOS 1–3

We validated analytical performance of this assay using leftover human nasal specimens that tested negative for SARS-CoV-2. These swabs were previously eluted in 1xPBS buffer. 1x PBS significantly interferes with RT-PCR (**Figure S10.47**), where the amplification of spiked SARS-CoV2 RNA at up to 100 copies/reaction was completely inhibited. To ensure successful amplification in less ideal buffer (PBS with nasal matrix), we proceeded with assay validation with samples diluted 4-fold in water, and tested at RNA concentrations of 0, 20, 40, and 100 copies/reaction.

When testing these contrived positive samples at ≥20 copies SARS-CoV-2 RNA using Scenario 1 o 1 (**Figure 10.15A**), the N2 assay had 100% sensitivity (41/41, 95% CI: 94.1–100%) and 100% (40/40, 95% CI: 91.2–100%) specificity. One negative sample was classified as inconclusive, **INC** (*i.e.,* false positive (**FP**) by the N2 assay, true negative by N1 assay, positive by RP assay). We re-ran this sample and did not detect a signal (ID 41) in either of two replicates, suggesting the false positive signal was likely caused by cross-contamination of samples rather than the primer/probe cross-reactivity. All the true positive (**TP**) samples by the N2 assay were successfully detected by the

© Copyright 2021 | N Panpradist

N1 assay. RP assay also successfully amplified all samples with Cq values in our Scenario 1 workflow of 28.2 ± 2.6 (mean ± SD).

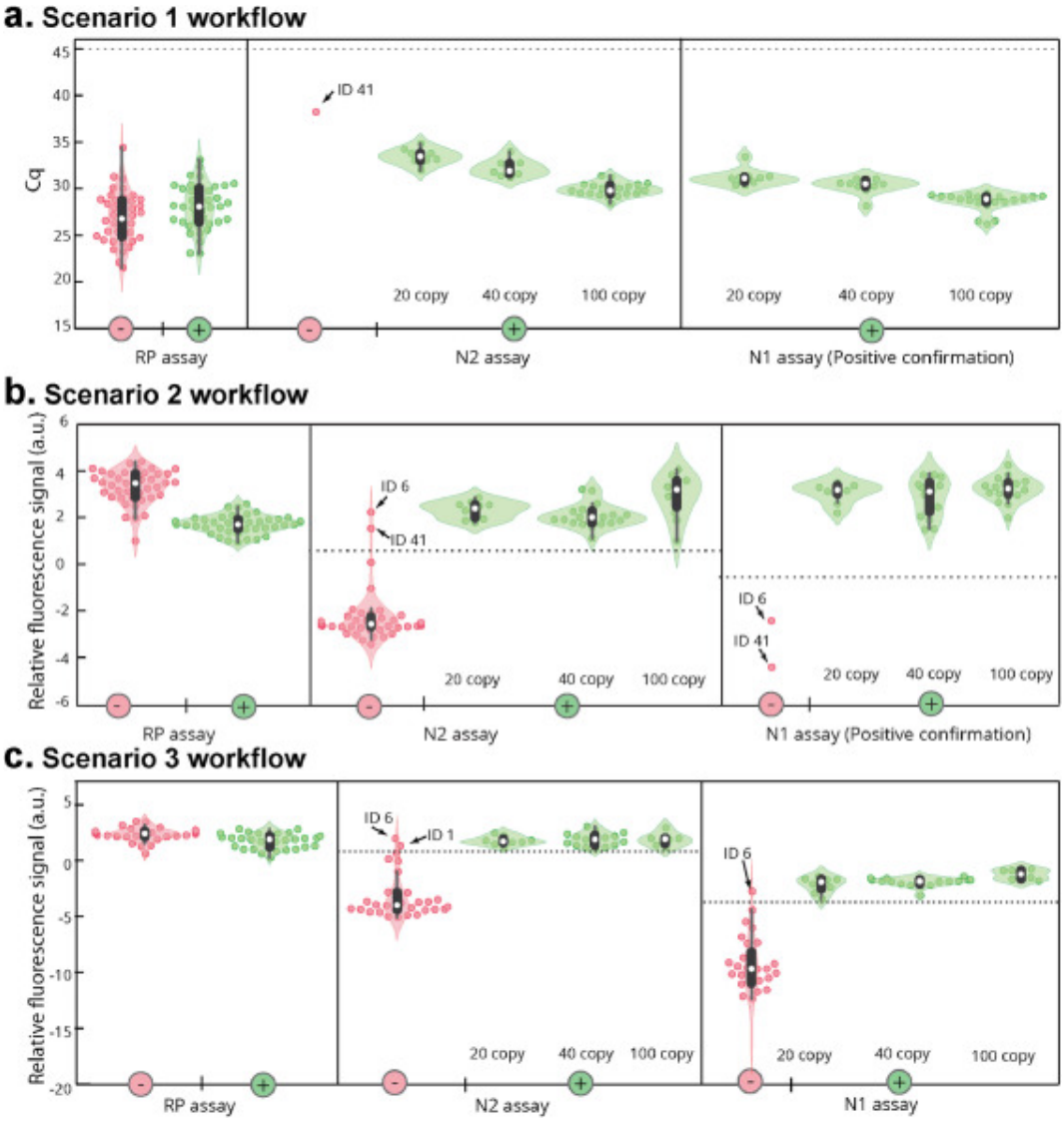

Figure 10.15 | *Validation of contrived clinical specimens in 0.25x PBS.*

Each of 41 human nasal swab eluates were used to generate a pair of negative and positive samples. Positive samples were spiked with purified SARS-CoV-2 RNA at 20, 40, and 100 copies/reaction. Both positives and negatives were run on both N2 and N1 (SARS-CoV-2 detection) and RP (human control) RT-PCR assays. (**A**) Scenario 1 workflow was used to process this panel of specimens. Cq (quantification thresholds) of each sample from N2, N1 and RP assays were plotted. (**B**) Images of the RT-PCR products generated in (**A**) were captured under the transilluminator to mimic the outcome of the Scenario 2

© Copyright 2021 | N Panpradist

workflow. Dotted lines show the positive thresholds for N2 and N1 primer assays. (**C**) Due to a low-throughput capacity of the Scenario 3 workflow, we tested 30 samples. Images of the reaction tubes were captured under the glow box. Dotted line is the positive threshold for N1 and N2 assays. The mean of each group is presented as the white circle with interquartile range box as well as range. The density distribution is also shown.

For the Scenario 2 workflow, we analyzed the end-point fluorescence signal from the images visualized in the transilluminator and captured by the cell phone on the successfully amplified contrived clinical samples, using the software developed for this project (**Figure 10.15B**). The end-point results reported analytical sensitivity and specificity of 100% with two (ID 41 from cross-contamination and ID 6) INC results. All samples previously determined as positive in the Scenario 1 workflow were positive, including the N2 assay for the FP sample (ID 41). One additional sample (ID 6) was classified as positive for the N2 assay only. This sample also had high end-point fluorescence in Scenario 1 but was classified as negative by the Bio-Rad software because it was a non-sigmoidal curve.

For the Scenario 3 workflow (**Figure 10.15C**), we tested 30 of the 0.25x diluted specimens (30 negative and 30 positives with SARS-CoV-2 RNA spiked in at 20, 40, or 100 copies). N1 and N2 assays had 100% sensitivity (30/30, 95% CI: 88.4–100%) when testing contrived positive samples at ≥20 copies of SARS-CoV-2 RNA and 96.7% (29/30, 95% CI: 82.8–99.9%) specificity when testing contrived negative samples. The one FP sample (ID 6) previously showed non-specific amplification with N2 primers in the Scenario 1 and 2 workflows. **Figure S10.54** shows images of these reaction tubes.

© Copyright 2021 | N Panpradist

10.2.6 CLINICAL VALIDATION OF ASSAY WORKFLOWS IN VTM SPECIMENS COLLECTED FROM INDIVIDUALS WITH RESPIRATORY SYMPTOMS

We validated our modified protocol in 110 VTM specimens. This number of specimens is suitable for high throughput assays; thus, we chose to use the Scenario 1 workflow. **Table S10.11** shows a comparison of Cq values from N1, N2, and RP primers using the standard protocol versus the Scenario 1 workflow. We observed strong correlations (**Figure 10.16A** - **Figure 10.16C**) of Cq values for N1 (R^2 = 0.90, 95% CI: 0.84–0.96, Olkin and Kinn's Approximation) and N2 (R^2 = 0.89, 95% CI: 0.82–0.96) primers using the two protocols. However, we observed less correlation of Cq values (R^2 = 0.29, 95% CI: 0.15–0.42) for RP human control primers. The Scenario 1 workflow detected 35/40 positive specimens, of which one was FN and three were INC by the standard CDC protocol. The five positives misclassified by our modified assay were two FN and three INC, of which one tested INC and four tested positive by the standard protocol. Of 70 negatives, our protocol reported 67 TN and 4 indeterminate (**IND**, i.e., samples tested negative by all primers) whereas the standard protocol reported 61 TN and 9 IND (3 were concordant between the two methods). Excluding IND and INC results, clinical sensitivity and sensitivity of Scenario 1 workflow was 94.6% (35/37, CI: 81.8 – 99.3%) and 100% (67/67, 95% CI: 94.6 – 100%). The indeterminate rate of 3.64% (4/110, 95% CI: 1.00 – 9.05%) for the modified protocol is much lower than 8.1% (9/110, 95% CI: 3.8 – 15%) for the standard protocol.

© Copyright 2021 | N Panpradist

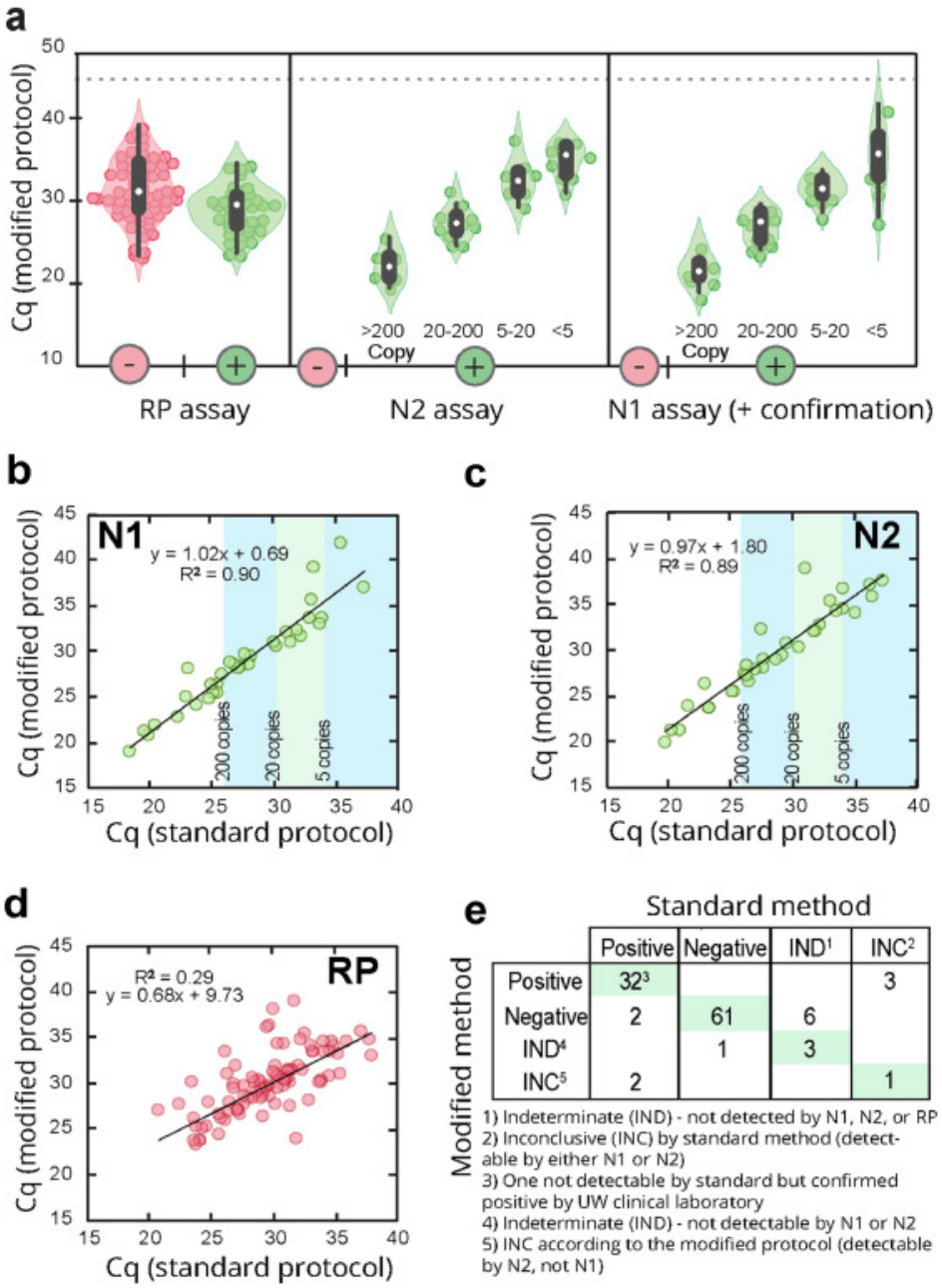

Modified method \ Standard method	Positive	Negative	IND[1]	INC[2]
Positive	32[3]			3
Negative	2	61	6	
IND[4]		1	3	
INC[5]	2			1

Figure 10.16 | Validation of our modified protocol (*Scenario 1 workflow*) on clinical VTM specimens.

(**A**) C_q values of N1, N2, and RP modified protocol. Dotted lines show the positive thresholds for N2 and N1 primer assays. The mean of each group is presented as the white circle with interquartile range box as well as range. The density distribution is also shown. C_q values of the (**B**) N1, (**C**) N2 assay, and (**D**) RP assay was compared to those obtained by the CDC standard protocol. (**E**) Qualitative comparison of

© Copyright 2021 | N Panpradist

positive, negative, indeterminate (**IND**), inconclusive (**INC**) results from our modified protocol vs standard protocol.

We showed that signal from cellphone images obtained from glow box or transilluminator (**Figure 10.14B,C**) used in the Scenario 2 and Scenario 3 workflows were highly correlated with the end-point signal from the real-time PCR machine. Building from this finding, we recorded end-point fluorescence signal by the real-time PCR machine to represent the Scenario 2 workflow. End-point fluorescence results (**Figure S10.55, A-C**) from N1, N2, and RP assays revealed lower sensitivity and specificity than the Scenario 1 workflow. **Figure S10.55,D** summarizes the qualitative comparison to the standard protocol. Of 40 positive samples 31 were TP, 5 were FN, and 3 were inconclusive (i.e., only detectable by N2). Of 70 negative samples, our assay classified 60 TN, 2 FP; 3 INC, and 5 IND. Overall sensitivity and specificity of the modified protocol using end-point fluorescence was 83.8% (31/37, 95% CI: 68.0 – 93.8%) and 96.8% (60/62, 95% CI: 88.8 – 99.6%), respectively.

DISCUSSION

We simplified an existing SARS-CoV-2 RT-PCR through several key innovations. We leveraged lyophilized reagents to bypass the need for manual preparation of master mix and distribution of the master mix into each sample reaction tube at the testing laboratories. We bypassed the RNA extraction step, which is the bottleneck of many laboratories that do not have access to an automatic extraction robot. Finally, we adapted these innovations to equipment appropriate for both high complexity labs and low resource

© Copyright 2021 | N Panpradist

environments. Our simplified methods could benefit laboratories, clinics, and hospitals interested in scaling up and decentralizing SARS-CoV-2 molecular testing or aid commercial assay developers in designing point-of-care tests where results are useful for clinical care or public health management.

Lyophilization of molecular reactions is essential to enable assay setup by non-trained personnel at the point-of-care; Abbott IDNow®, Cephied Xpert®, and BioFire® FilmArray also take advantage of this technique. We believe the main bottleneck for lyophilization of RT-PCR is the lack of expertise to develop excipient formulations for molecular assays that can maintain high sensitivity and specificity. To eliminate this bottleneck, we have developed and disclosed the excipient formulation compatible with an established US CDC RT-PCR assay. Moreover, lyophilized reagents that have no liquid volume allow for greater sample input and could even further boost sensitivity of this assay.

Our assay bypasses an RNA extraction step by using swab eluate to directly amplify samples. Not only does removing this RNA extraction step reduce turnaround and cost, it also avoids use of toxic reagent, guanidinium thiocyanate (**GuSCN**), a common component of lysis buffer used with all the silica column based kits listed on the CDC protocol and in many point-of-care assays. In the standard CDC protocol, the RNA extraction step is crucial to remove any RT-PCR inhibitors, namely fetal bovine serum and antibiotics present in VTM. In this study, we suggest transport of dry swabs that are introduced into mild lysis buffer to enable extraction-free, direct amplification. Use of dry swabs can eliminate the need for VTM, which has seen supply shortage due to high demand of SARS-CoV-2 testing. Detection of SARS-CoV-

© Copyright 2021 | N Panpradist

2 directly from dry swabs has been used in some EUA tests including the Abbott IDNow®[25]. We used a relatively high concentration of RNAse inhibitors that can deactivate endogenous RNAses during the mild heating step at 55 °C for reverse transcription. Moderate heat in conjunction with mild detergents (i.e. Triton X-100, NP-20, and Tween-20) have been shown to lyse virus and human cells[26-28]. Here, we show that ≤1% of these detergents do not negatively impact our RT-PCR, and 0.5% triton-X100 and 55 °C during reverse transcription were sufficient to open the viral envelope of the control virus and release RNA, with detection of 25 SARS-CoV-2 RNA copies/reaction. The volume of swab elution buffer required will depend on the absorbency of swabs[29], geometry of the buffer containers, and the level of inhibitors that may be present in the patient specimens. The first two factors can be determined by the assay developers, but the interference levels may vary across individual clinical samples. For the mid-turbinate swab used in our study, we determined an elution volume of 300 µL-1000 µL based on the lysis buffer container used in our workflow. We successfully detected 20 copies of RNA/reaction in the presence of simulated nasal matrix, which corresponds to 300–1000 RNA copies/swab sample. This level of sensitivity may already be sufficient to detect SARS-CoV-2 in the early days after the onset of symptoms (peaked at 10^4 RNA copies/nasopharyngeal swab and 10^7 RNA copies/throat swab[30]).

Direct amplification of contrived nasal swab PBS eluates by this test showed 100% sensitivity at ≥20 copies/reaction and 96.7%−100% specificity using all three workflows. Overall sensitivity and specificity of this test are similar to

© Copyright 2021 | N Panpradist

other RT-PCR tests that received US FDA EUA[31] when processing similar types of contrived samples. In this study, we were limited by the swab elution buffer used in these leftover specimens (i.e., PBS). We found that salt (137 mM NaCl) in the PBS in combination with clinical nasal matrices caused RT-PCR inhibition, and dilution factors of 0.25x or 0.5x were needed to rescue amplification of the human RP control. Whilst further dilution of PBS is not ideal, the results served as promising strategies for direct amplification. Both N1 and N2 assays in 0.25x PBS sensitively detected down to 20 copies/reaction.

For direct comparison with the CDC protocol using clinical nasal specimens stored in VTM, we used a 0.25x dilution factor to directly amplify VTM samples in lyophilized RT-PCR. This 0.25x concentration of VTM is higher than the 0.07x– 0.1x VTM concentrations used in other studies for direct amplification[28, 32], suggesting that our RT-PCR may tolerate inhibitory substances better than other RT-PCR assays. The Scenario 1 workflow compared well to the CDC standard protocol with 94.6% sensitivity and 100% specificity. Of the four positive samples not detected by the modified protocol, three had low target concentrations (<5 copies/reaction): two were INC (Cq: 37.7, 37.3; not detected, 40.8 by N1 and N2 standard protocol, respectively) and one was FN (Cq: 41.9, 38.3). One FN had a high copy (>200 copies/reaction; Cq: 20.7, 21.9) but was not detectable, likely due to high concentration of PCR inhibitors in this sample. Surprisingly, IND occurred much less in our protocol than in the standard protocol (3.6% vs 8.2%), while INC results were comparable (2.7% vs 3.6%). Technically RNA extraction removed any inhibitors from the nasal samples, and we expected a higher amplification yield. However, the

© Copyright 2021 | N Panpradist

Scenario 1 workflow showed that only 1/110 samples were likely to have benefitted by this step.

In addition to developing the assay chemistry for lyophilization and direct amplification, we developed three workflows aimed at three different equipment sets and designed to cover most common laboratory setups that could run the assay. The Scenario 1 workflow is most analogous to what is currently done in medium to high complexity laboratories with access to real-time thermal cyclers. A 96-well plate can screen up to 45 samples (if 6 wells are used for negative and positive controls). This screening approach would reduce the overall assay cost compared to the CDC protocol. The Scenario 2 workflow drops the equipment cost around 10-fold by removing the need for a real-time thermal cycler, making it less cost-prohibitive to perform a high-throughput assay, in exchange for an additional step of end-point fluorescence signal analysis. End-point detection of RT-PCR may lead to false positive results. For analysis of contrived specimens in human matrix using end-point fluorescence results in the Scenario 3 workflow, 1/30 samples had false positive due to non-specific amplification in a sample with high amount of mucus, which cannot be differentiated from the true positive, whereas manual inspections of real-time RT-qPCR curves can help rule out non-specific amplification because true positives have a characteristic sigmoidal amplification curve. We also observed similar non-sigmoidal signals in 3/70 negatives when analyzing the clinical nasal specimens in VTM.

© Copyright 2021 | N Panpradist

The Scenario 3 workflow was designed for the lowest resource environment and may be useful as a point-of-care, low-throughput RT-PCR testing. The use of a battery-powered, low-cost thermal cycler enables reliable Covid-19 testing in low-resource settings where power outage is common. We observed that the battery-powered thermal cycler performed 10-minutes slower than the traditional 96-well thermal cycler, but this additional time delay may not significantly impact the clinical management of patient care. The battery-powered, low-cost glow box also improves resilience to power outages, but with the tradeoff of poorer signal to the unaided eye compared to the transilluminator. However, with the help of software image processing, negative samples can be differentiated from 20 copies/reaction, providing similar results to those from transilluminator images. To further explore the limitations of our fluorescence classification software and the robustness of the approach across different phone models, we tested the software using images captured by six additional cell phone models commonly used in low-resource settings. The images had varied quality for capturing the fluorescence signal. Some phone models also have incorporated features in the camera that may affect the image analysis. In addition to the phone models, it is also noteworthy to mention that the room light conditions could add artifacts to the pictures taken. In this study, we kept the image-taking process consistent, but further testing using different phone models under various conditions should be performed to ensure robustness of data collection and analysis.

Besides the thermal cycler and fluorescence reader, micropipettes are impractical for point-of-care settings. Instead, our Scenario 3 workflow uses

© Copyright 2021 | N Panpradist

an inexpensive bottle with a dropper adapter to dispense lysates to the dry reagents and requires no specialized training. This bottle has a larger dead volume than the swab elution tubes used in Scenario 1 and 2 workflows, causing us to adjust the swab elution volume to 1000 µL instead of 300 µL. The dead volume could be reduced with a narrower bottle. Whilst there are still changes that can be made to optimize this workflow, its simplicity makes it a promising platform for RT-PCR at the point-of-care. The relatively economical list of required materials makes it a low cost and highly scalable alternative to other point-of-care products. A single Abbott IDNow® machine costs as much as ~20 battery-powered thermal cyclers that can test 80 clinical samples in two hours, compared to 8 samples for Abbott IDNOW® (one specimen/15 min). Moreover, we have gathered the information for commercial equipment that could be used for the three workflows presented (**Table S10.6 – Table S10.10**), but without access we did not validate our assays on all of the equipment. However, we showed that the assay chemistry is sufficiently robust across a battery powered thermal cycler, a standard thermal cycler, and a real-time thermal cycler. This is a promising indicator that this assay should be suitable for use in other commercially available thermal cyclers.

At the time that we wrote this manuscript, we were working to develop interactive software to guide technicians in performing these three laboratory workflows. A collaboration is set to begin demonstration of these workflows in comparison to the standard CDC protocols at several sites in the USA. Previously, we have used the software guidance at sites in Kenya and the US

© Copyright 2021 | N Panpradist

to operate a more complicated workflow successfully. We used Aquarium, which is a web-based human-in-the-loop laboratory automation application that integrates inventory tracking, data collection, experimental protocols, and workflow management[33]. We are transforming our SARS-CoV-2 RNA detection lab procedures into guided Aquarium protocols to gain the advantages of laboratory automation, data collection, and protocol distribution. We envision that our high-performance SARS-CoV-2 diagnostic workflows encoded as Aquarium protocols will facilitate the rapid deployment of low-cost and efficient Covid-19 testing sites.

10.3 HARMONY POINT-OF-CARE SARS-COV-2 DETECTION

CONTRIBUTORS. Nuttada Panpradist, Enos C Kline, Robert G Atkinson, Michael Roller, Qin Wang, Ian T Hull, Jack H Kotnik, Amy K Oreskovic, Crissa Bennett, Daniel Leon, Victoria Lyon, Shane D Gilligan-Steinberg, Peter D Han, Paul K Drain, Lea M Starita, Matthew J Thompson, Barry R Lutz. **CONTRIBUTIONS.** NP developed lyophilized RT-LAMP and outlined the overall plan for experiments and data visualization presented in this manuscript. RGA developed a mobile software application for operating the device and analyzing results in real-time. MR developed the heater and fluorescent reader device. ECK designed the RT-LAMP assay primers and probes and engineered polymerase. ECK, ITH and QW synthesized polymerase and provided usability feedback during the development of the Harmony COVID-19 system. ITH and

© Copyright 2021 | N Panpradist

QW prepared *in vitro* RNA transcripts. JHK and VL led the usability study. NP, AKO, and CB tested clinical and contrived specimens. RGA, NP, AKO, SDG, and JHK analyzed the data. ITH and QW prepared the kits and blinded mock samples for usability testing. DL developed housing units to integrate the cell phone, sample preparation station, and the device. LMS and PDH designed and characterized the clinical specimen panel used in this study. PKD provided technical insights. MT oversaw the usability study. BRL oversaw the development and evaluation of the Harmony COVID-19 system. All authors contributed to writing this manuscript and approved the final version.

SUMMARY. We report the development of Harmony COVID-19 — a complete moderate-throughput sample-to-result system for sensitive POC detection of SARS-CoV-2 RNA. Harmony simplifies testing with ready-to-use assay reagents, an easy-to-use dedicated smartphone interface, and an inexpensive isothermal heater/detector device to enable POC testing. The assay includes three redundant SARS-CoV-2 targets to avoid false negatives due to viral mutation and an internal amplification control (**IAC**) in each test to avoid false negatives in case of assay failure. The heater/detector detects two-color real-time fluorescence for the SARS-CoV-2 redundant targets and IAC, and results are automatically reported on the smartphone. We evaluated the system using two panels of specimens - a panel of extracted nasal specimens from individuals with respiratory symptoms, and a panel of contrived specimens from the XPRIZE Rapid COVID Testing competition – and we conducted usability testing of Harmony by healthcare workers (**HCWs**). These evaluations have demonstrated that Harmony is a complete system for sample-to-result

© Copyright 2021 | N Panpradist

testing that is highly accurate in moderate complexity laboratories and clinic-based patient care settings.

Materials and Methods

Preparation of synthetic RNA standards. MERS and SARS-CoV-1 plasmid standards (10006623 and 10006624, Integrated DNA Technologies, Coralville, IA) were amplified using M13 PCR primers to generate DNA templates tagged with T7 promoter sequences. DNA templates containing T7 promoter sequences were transcribed using Hi-T7 RNA polymerase (M0658, New England Biolabs, Lawley, MA) following the manufacturer's protocol, with 1 U/μL RNase inhibitor (N2611, Promega, Madison, WI) added. Following transcription, 0.01U/μL DNase I (EN0521, ThermoFisher Scientific, Waltham, MA) was added to each reaction, and incubated at 37°C for 15 min. RNA transcripts were purified with Monarch RNA Cleanup Kits (T2040, New England Biolabs). RNA was quantified on a Qubit 4 fluorometer (Q32852, RNA HS Assay Kit, ThermoFisher Scientific, Waltham, MA), and checked for length and integrity by electrophoresis on a 2200 TapeStation (5067 RNA ScreenTape, Agilent Technologies, Santa Clara, CA). RNA at 10^{10} copies/μL was stored in nuclease-free water in single-use aliquots. SARS-CoV-2 RNA was prepared and quantified as previously described[19, 34].

In-house TFv1 polymerase production

Plasmid preparation. The chimeric polymerase (TFv1) was generated by assembly PCR using genomic material from *Thermus thermophilus* (*T. th*) HB27 (ATCC BAA-163D-5™, Gaithersburg, MD) and a synthetic gene fragment

© Copyright 2021 | N Panpradist

derived from *Thermodesulfatator indicus* (*T. in*), (Integrated DNA Technologies, Coralville, IA), similar to the method previously described (*37*). Briefly, a 3' terminal fragment of the *T. th* HB27 *polA* gene downstream of the finger domain was amplified by PCR using Phusion® Hot Start Flex DNA Polymerase (M0535L, New England Biolabs) with a modified forward primer containing sequence overlap with the *T. in polA* gene fragment *(AA734-795,* codon optimized for *E. coli)*. A chimeric sequence was then generated by assembly PCR. A second *T. th* polymerase fragment, upstream of the finger domain and lacking the 3' to 5' exonuclease domains, was similarly amplified and appended to the 5' end of the chimeric fragment. The resultant sequence corresponds to a *T. th* DNA polymerase I fragment, orthologous to the Stoffel fragment of *T. aq* polymerase, with a replacement in the finger domain derived from *T. in*. This gene was then cloned into the expression vector pET His6 TEV LIC cloning vector (2B-T) (a gift from Scott Gradia, Plasmid # 29666, Addgene, Watertown, MA) by ligation independent cloning[35]. The annealed vector and insert were transformed into T7 Express lysY/Iq Competent *E. coli* (C2987H, New England Biolabs) per the manufacturer's protocol and plated on LB 100µg/mL carbenicillin plates. Colony plasmid inserts were verified by Sanger sequencing.

***Protein expression and purification*.** 50mL starter culture in LB broth with 100µg/mL carbenicillin was inoculated with a sequence-verified colony and incubated at 30°C overnight in a shaking incubator at 200rpm. The culture was centrifuged at 5,000 RCF for 15 min and resuspended in an equivalent volume fresh LB carbenicillin media. Flasks of 500mL LB broth with 100µg/mL

© Copyright 2021 | N Panpradist

carbenicillin were inoculated with 5mL each of resuspended starter culture and incubated at 37°C in a shaking incubator at 200rpm until OD_{600} of 0.4-0.6 had been achieved. Cultures were induced with 0.4mg/mL of IPTG and incubated for two hours then harvested by centrifugation at 5,000 RCF for 15 min, decanted, and stored as cell pellets at –80°C until needed. Prior to purification, cell pellets were resuspended in lysis buffer (20mM sodium phosphate pH 7.4, 80mM NaCl, 1% *(v/v)* Triton (648466 Sigma, St. Louis, MO), and 1mg/mL lysozyme from chicken egg white (Millipore Sigma, Burlington, MA)). Suspensions were heated at 37°C for 20 min, then lysed by ultrasonic disruption using a Fisherbrand™ Model 120 Sonic Dismembrator (Fisher Scientific, Waltham, MA) with two cycles of two-second pulses at 50% amplitude for 2 min, while on ice. Lysates were heat-clarified at 65°C for 20 min, followed by centrifugation at 20,000 RCF. The supernatant was collected and diluted with sample diluent buffer (20mM sodium phosphate, 1.8M NaCI, pH 7.4 for 6x stock; 5 parts supernatant to 1 part diluent buffer) and filtered with a 0.22 µm syringe filter (25-342 Olympus, Genesee Scientific, San Diego, CA). The purified clarified lysate was applied to a 1mL Hitrap Talon Crude column (Cytiva, Marlborough, MA) and enriched per manufacturer's default recommended specifications using an ÄKTA start system with the Frac30 fraction collector (Cytiva). Elution fractions were evaluated by A_{280} on a spectrophotometer (2200 Nanodrop, Fisher Scientific) using the protein's expected molecular weight (63.062 kDa) and extinction coefficient (60,850 m^2/mol) of the His-tagged polymerase. Elution fractions containing protein were diluted 1:10 with 10mM sodium phosphate and applied to a 1mL HiTrap®

© Copyright 2021 | N Panpradist

Heparin HP column and purified per the manufacturer's recommended specifications except for a modified binding buffer (10mM sodium phosphate and 30mM NaCl at pH 7). Fractions containing protein were concentrated and buffer exchanged into storage buffer (17mM Tris-HCI, 167mM KCI, 17% glycerol, pH 7.5) using an Amicon® Ultra-2 30K centrifugal filter (Millipore Sigma), as recommended by the manufacturer. The recovered polymerase solution was then adjusted to 10mM Tris-HCI, 100mM KCI, 2mM DTT, 0.1% Triton X-100, 50% glycerol, pH 7.5. Polymerase purity was evaluated by SDS-PAGE and spectrophotometry throughout purification.

RT-LAMP assay design. Alignment of SARS-CoV-2 sequences (available on NCBI up to January 2020) were performed using Geneious (Auckland, New Zealand). Three sets of LAMP primers (Harmony NC1, Harmony NC2, and Harmony NC3) were developed targeting the 22,285 – 28,517 (232 bases), 28,528 – 28,471 (213 bases), and 29,135 – 29,416 (281 bases) regions of the SARS-CoV-2 nucleocapsid phosphoprotein gene. *In silico* analysis showed that this primer design matched 100% of SARS-CoV-2 sequences and did not have cross-reactivity to MERS and SARS-CoV-1. We used two detection probes, each comprised of a fluorescent probe and its complementary quencher probe. For detection of SARS-CoV-2 RNA amplification, we used FAM labeled detection probe and Iowa Black™ quencher probe. For detection of IAC amplification, we used TEX 615 labeled detection probe and BHQ2 labeled quencher probe. The primer and probe sequences are listed in **Table S10.13**.

Wet RT-LAMP reactions. Characterization of polymerases was conducted in the wet reaction format. 2µL water or SARS-CoV-2 RNA at 200 or 2000

© Copyright 2021 | N Panpradist

copies/μL was added to 38μL master mix to achieve a 40μL RT-LAMP reaction. 20x Harmony NC1, NC2, and NC3 primer mix for SARS-CoV-2 amplification each contained 20μM each FIP/BIP primer, 10μM each loop primer, and 4μM each F3/B3 primer. 20x IAC primer stock contained 10μM loop primer. 20x probe/quencher mix for SARS-CoV-2 or IAC amplification contained 4μM fluorophore probes and 6μM quencher probes). Depending on the experimental design, each RT-LAMP reaction contained 1x each primer mix or only 1x NC1 primer mix, 1x each probe or only 1x FAM probe, 2.5% (*v/v*) mannitol (OPS Diagnostics EXMN 500-01), 5mM DTT, 0.6U/μL WarmStart RTx, 0.7μg TFv1 DNA polymerase or 0.32U/μL Warmstart DNA polymerase 2.0 (M 0538, New England Biolabs), 1.4mM each dNTP, 1U/μL RNase inhibitor (N2615, Promega), 25mU/μL thermostable inorganic pyrophosphatase (M0296L, New England Biolabs), 250 copies/μL IAC DNA, 6mM magnesium sulfate, 1x ThermoPol buffer (B9004S, New England Biolabs) in nuclease-free water. RT-LAMP reactions were incubated at 63.3°C and FAM and/or Texas Red signal was read every 13s for 1h using a CFX96 thermal cycler (Bio-Rad).

Lyophilization of RT-LAMP reagents. Reactions containing 2x primers (2μM each FIP/BIP primer, 1μM each loop primer, and 0.4μM each F3/B3 primer) and probes (0.4μM fluorophore probes and 0.6μM quencher probes) in the presence of 5% *(v/v)* mannitol, 10mM DTT, 1.4μg TFv1 DNA polymerase, 1.2U/μL WarmStart RTx, 2.8mM each dNTP in 10mM Tris-HCl, pH 7.4, 2U/μL RNase inhibitor, 50mU/μL thermostable inorganic pyrophosphatase, and 500 copies/μL IAC DNA were prepared in 20μL aliquots of 0.2mL reagent tubes and lyophilized. Packages were stored in desiccant packets at -20°C until use.

© Copyright 2021 | N Panpradist

Harmony RT-LAMP reaction setup. Lyophilized reagents were resuspended in a final volume of 40µL containing 1x rehydration buffer (1x ThermoPol buffer (B9004S, New England Biolabs), 6mM supplemental $MgSO_4$, and 0.5% *(v/v)* Triton X-100). For analytical sensitivity experiments, 2µL SARS-CoV-2 RNA in water was added. For clinical testing, 10µL extracted RNA was added to each RT-LAMP reaction. For testing the XPRIZE contrived specimens or VTM in direct-to-amplification experiments, 10µL sample (not extracted) was added to each RT-LAMP reaction. For usability testing, 40µL swab eluate was added directly to the RT-LAMP reaction using transfer pipettes or the in-house unified dispensers.

Analytical sensitivity of RT-LAMP assay. Analytical sensitivity of lyophilized RT-LAMP was tested using purified RNA (0-2x10^6 copies/40µL reaction). We also tested the effect of salt, human DNA, and mucin on amplification of SARS-CoV-2 RNA and IAC DNA using simulated nasal matrix as previously described[18].

***Preparation of contrived swab samples and kits for usability testing*.** For the transfer pipette workflow, each kit contained one swab (either positive or negative), a vial (10-500-25, Fisher Scientific, Waltham, MA) containing 400µL of 1x rehydration buffer (see section RT-LAMP reaction setup), and one lyophilized RT-LAMP reagent tube. For positive swabs, 10µL of 100 copies/µL SARS-CoV-2 DNA in 0.05% Triton X-100 was pipetted onto the swab (1804-PF, Puritan Medical) and dried at room temperature in an air-clean chamber (825-PCR/HEPA, Plas-Labs, Lansing, NI) for 4 hours before packaging in a sealed foil pouch with desiccant (S-8032, ULINE). The unified sampler was

© Copyright 2021 | N Panpradist

built from parts using an assembly jig (custom order from Hygiena, LLC, Camarillo, CA). The unified dispenser contained a hollow-shaft polyurethane swab attached to a bulb preloaded with 400µL 1x rehydration buffer and a separate tube with a filter and drip dispenser friction fit inside the tube. Each custom sampler kit contained an in-house assembled dispenser unit and one lyophilized RT-LAMP reagent tube.

***Usability study*.** The Harmony usability study was approved by the Institutional Review Board at the University of Washington (IRB#: STUDY00010884), and informed consent was provided by participants. HCWs (*n = 10*), including registered nurses, medical students, and dental students were enrolled in this study over the course of 1 month. All data was collected without identifiers. The primary objective of this study was to determine the accuracy and precision of the two sample transfer methods and test if variation in reproducibility impacted assay performance, and the secondary objective was to gather user input on the feasibility of each protocol. Participants first received an explanation of the test and its intended use, then watched an instructional video narrated by the facilitator to become familiar with the Harmony workflow. After watching the video, participants were given a packet with a unique identifier that contained comprehensive instructions for the study procedures and survey questions. Study procedures were modeled on a coaching methodology[36] to allow natural progression of the procedures and to identify blocking steps in the instructions. The facilitator sat 10 feet from the participant and kept a record of verbal questions and comments from

© Copyright 2021 | N Panpradist

participants but did not provide answers to procedural questions unless the participant could not proceed.

For part 1, data related to user preference on sample preparation, tube sizes, and their level of confidence in performing each task were collected anonymously as prompts within their study packet. Open-ended questions were extracted for themes in errors or issues and supplemented with comments and observations recorded by the facilitator. Samples were saved with de-identified labels, and after all participants had completed the study facilitators measured volumes in each receiving tube from part 1. The variances of the volume recovered by each method were tested for their equality using F-Test, and the P-value was reported. The means of the recovered volumes transferred by LPs or HCWs were compared using Student's *t*-test (two-sided), and the *p*-value was reported.

For part 2, each participant followed instructions in the packet and on the integrated mobile phone to complete the entire Harmony workflow on four total contrived samples (two samples using the transfer pipette protocol and two using the unified sampler system). Kits were prepared as specified above.

The lab personnel ($n = 5$) portion of the user testing aimed to compare performance of the Harmony device by HCW to that of an "experienced" population, by replicating this process with four students and a researcher from the Lutz Lab. Survey questions were omitted for this group because these volunteers provided feedback throughout the development of Harmony and their views are included in the discussion of this manuscript. The accuracies of

© Copyright 2021 | N Panpradist

tests performed by LPs and HCWs using each method were tested for their equality using *Z*-test (two-sided), and the *p*-value was reported.

Clinical nasal swab specimens from individuals presenting respiratory symptoms. A minimum sample size of 30 (each negative and positive) was required to achieve the confidence interval (**CI**) of 90 -100% (binomial cumulative distribution function) should all results be accurate. Our clinical specimen panel (*n = 110*) was previously used to evaluate other SARS-CoV-2 assays (*35*), but 9 specimens had insufficient volume for RNA extraction and were thus excluded from the study. These specimens were collected with informed consent as part of the Seattle Flu Study, approved by the Institutional Review Board at the University of Washington (IRB#: STUDY0006181). Thermo Fisher's OpenArray is an arrayed RT-qPCR system capable of detecting up to 26 pathogens simultaneously in a semi-quantitative manner. Specimens from the Seattle Flu Study that had other respiratory pathogens detected using the OpenArray platform were used to determine cross reactivity with Harmony. All participant specimens were de-identified prior to the transfer to the Lutz Lab at the University of Washington for analysis. The remaining 101 specimens were evaluated using the newly extracted RNA for analysis by RT-qPCR and Harmony system, to avoid variations introduced from different batches of extraction. RNA was extracted from clinical nasal swab specimens stored in viral transport media using the QIAamp Viral RNA Mini Kit (52906; Qiagen, Hilden, Germany). Prior to extraction, 100µL of each specimen was mixed with 40µL negative VTM to reach the suggested 140µL sample volume. RNA was extracted according to the manufacturer's protocol, eluted into 70µL of EB

© Copyright 2021 | N Panpradist

buffer, and stored at -80°C in single-use aliquots until amplification. 5µL of RNA was used for analysis in 20µL RT-qPCR using U.S. CDC N1, N2, or RP human control assays[37]. 10µL of RNA was used for analysis in 40µL lyophilized RT-LAMP in the Harmony workflow. Each sample was run in duplicate. Only samples with positive results from both Harmony replicates were reported as positive for SARS-CoV-2. Sensitivity (TP/(TP + FN)), specificity (TN/(TN+FP)), and concordance ((TP+TN)/(TP+TN+FP+FN)) were calculated and reported with 95% CI using binomial exact proportions.

XPRIZE contrived sample panel. The blinded panel was assembled and distributed by HudsonAlpha Discovery (Huntsville, AL) for the COVID-19 XPRIZE competition, and information on the samples was revealed to the authors only after results were submitted to XPRIZE. Samples were shipped to the Lutz Lab at the University of Washington. We reported results for contrived samples of chemically inactivated SARS-CoV-2 viral particle (ZeptoMetrix Corporation, Buffalo, NY) spiked in phosphate-buffered saline (**1x PBS**) (*n = 29*), nasal specimens (*n = 20*), or saliva (*n = 20*) at 0 to 1000 copies/reaction. All samples came in liquid form. We added 10µL sample and 30µL Harmony rehydration buffer to rehydrate each lyophilized reagents and tested across 7 different Harmony devices. Each sample was originally tested once for each sample. To affirm the identity of these specimens, we also performed RT-qPCR using CDC primer/probes after the samples had been tested using the Harmony system. To improve our confidence in reporting sensitivity and specificity, we tested two additional replicates for each sample to achieve a total of triplicates.

© Copyright 2021 | N Panpradist

Housing . The housing combines the heater/reader assembly with the cell phone, while concealing the connector cables and presenting a sturdy and easy-to-use platform. The 3D CAD program, Fusion 360 (AutoDesk), was used for the design of housing. Prototypes were printed in PLA plastic (Overture™ Filament, OVPLA175) using a Prusa i3 MK3s at 0.3mm layer height. Power was supplied to both the heater/reader assembly and the phone simultaneously using a Charge-Plus USB-C (LAVA Computer Manufacturing Inc.) connector device and a standard fast-charging American cellphone charger. The LAVA device also facilitates the transfer of data between the devices.

Reader/heater device. The aluminum block to house the reagent tubes was custom-made by Bryan Willman according to the specifications in **Figure S10.57**. The circuit boards were designed using Autodesk Eagle (San Rafael, CA), and the assembly of the circuit boards are shown in **Figure S10.58** and **Figure S10.59**. The lid, latch, and upper and lower housing of the device were drawn using SolidWorks (Dassault Systèmes, Waltham, MA) and printed by Xometry - HP MultiJet Fusion 3D (Gaithersburg, MD). All parts were assembled as shown in **Figure S10.60**.

Real-time fluorescence signal analysis. After the user inserts the reaction tube into the device, the software adjusts the temperature to re-equilibrate the temperature of heat block back to the reaction temperature. During this initial period, the signals from the photo diodes (the blue LED (FAM signal for target amplification) and the yellow LED (TEX 615 signal for the IAC amplification)) are collected but not used in analyses. Once the initial period is

© Copyright 2021 | N Panpradist

over, signal analysis commences. Each signal is analyzed in real time by comparing the current mean of the signal over the most recent 60s interval to the signal's behavior some 360s in the past. Specifically, the current mean is compared to a bound consisting of the signal's mean over the period from 420s to 360s in the past plus a multiple (1.9x for target, 1.5x for IAC) of the signal's sample standard deviation over that same period. If the current mean exceeds the bound, and maintains that condition for at least 15s, the signal is said to have "indicated". If the signal from the target emission indicates, the presence of SARS-CoV-2 has been detected, and the software immediately reports "positive COVID-19". If the signal from the IAC emission indicates, successful amplification of the IAC has been detected. Then, if the target emission does not also indicate before the end of the run, then a "negative COVID-19" result is reported; this delay in reporting negative results provides the maximum opportunity to detect low concentrations of SARS-CoV-2 that may be present in samples. If neither the target emission nor the IAC emission is detected, "test failed" is reported.

© Copyright 2021 | N Panpradist

RESULTS

10.3.1 WORKFLOW AND OPERATION OF COVID-19 HARMONY

The Harmony test kit and detector were engineered for low-cost and simplicity of use to enable POC testing (**Figure 10.17A**). The test involves taking a nasal swab, eluting the swab in a non-toxic buffer, and transferring the buffer to a reaction tube containing ready-to-use reagents. The reagent tube is inserted into the custom-designed heater/reader operated by a cell phone that provides instructions and displays the result. For samples with no target (**Figure 10.17B**, left; NTC), detection of the IAC confirms that the reaction was functional; the absence of both target and IAC amplification indicates a failed reaction. For samples with SARS-CoV-2 RNA (**Figure 10.17B**, middle; 200 copies/reaction, corresponding to 5 copies/μL), the green signal indicates a positive test, regardless of whether IAC is detected. Harmony using dry reagents detects down to 200 copies of SARS-CoV-2 RNA on a swab (**Figure 10.17B**, right; 20 copies/reaction, corresponding to 0.5 copies/μL). Real-time detection reports a positive sample as soon as the target signal appears, allowing detection in <30 min for samples ≥2000 copies per swab (**Figure 10.17C**), with earlier results for higher viral load.

© Copyright 2021 | N Panpradist

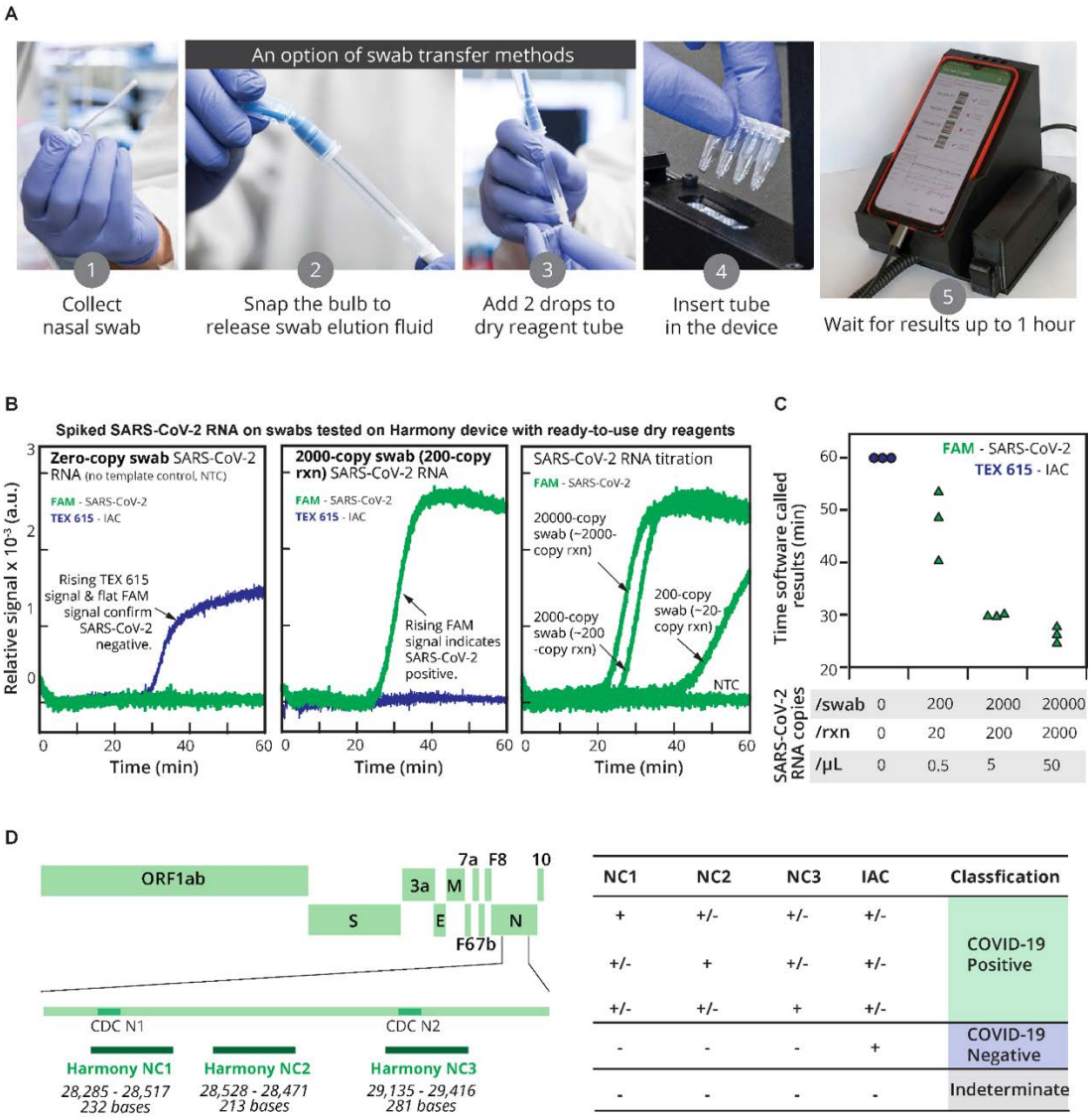

Figure 10.17 | Harmony COVID-19 workflow, analytical performance, and interpretation.

(**A**) User workflow. A nasal swab is collected and eluted in the rehydration buffer using either a unified sampler-dispenser (shown) or a tube-and-bulb method (**Fig. 8**). The swab eluate is then transferred into the reaction tube to rehydrate lyophilized, pre-loaded RT-LAMP reagents. Users follow the instructions on the cell phone app to record the sample identity, insert the tube in the test slot, and close the device. Four samples can be analyzed in parallel. (Photo credits: (**A**)1-(**A**)4, Mark Stone at the University of Washington and (A)5, Christopher Snyder at North Seattle College). (**B**) Examples of on-device analysis. Lyophilized reagents were rehydrated with the eluate from swabs spiked with 0, 200, 2000, or 20,000 copies of SARS-CoV-2 RNA, run on the device, and analyzed in real-time. The samples with SARS-CoV-2 RNA at 2000, 200, and 20 copies/reaction (**rxn**) were reported as positive by software

© Copyright 2021 | N Panpradist

at 27 min, 30 min, and 41 min, respectively; after 60 min the NTC reaction was classified as negative. (**C**) Time-to-result. Individual detection time points (*n = 3*) are plotted. Variation in detection time increases as samples approach the detection limit. (**D**) Diagnostic algorithm. Harmony COVID-19 software calls samples as positive, negative, or indeterminate based on detection of the three regions in the nucleocapsid gene (Harmony NC1 overlapping with the CDC N1 region, Harmony NC2 (overlapping with CDC N3 region excluded from the current kit), and Harmony NC3 overlapping with the CDC N2 region) and the engineered IAC sequence.

10.3.2 NOVEL MODIFICATIONS OF RT-LAMP CORE ASSAY CHEMISTRY

The Harmony assay uses a unique variation of reverse transcription loop-mediated isothermal amplification (**RT-LAMP**) that allows fluorescence detection of multiple targets in the same reaction. The four-plexed assay amplifies three non-overlapping genomic regions (**Figure 10.17D**) of the SARS-CoV-2 nucleocapsid phosphoprotein (**N gene**) reported by a green fluorescence signal (**FAM**) and an engineered **IAC** reported by a red fluorescence signal (TEX 615 or Texas Red® - used interchangeably). A positive test result is reported when any of the three SARS-CoV-2 targets are present. Presence of IAC amplification is not necessary in a positive test. A negative test result is reported if SARS-CoV-2 RNA is undetected, and the IAC is detected. If neither target nor IAC is detected, it indicates a test failure, and the result is reported as indeterminate (**IND**).

Harmony primers target the SARS-CoV-2 N gene. Based on the initial design process in early 2020, alignments of related coronaviruses (e.g., SARS-COV-1, MERS, bat coronaviruses) confirmed that the N gene was likely to be a well-conserved target (not the most conserved region) but was sufficiently

© Copyright 2021 | N Panpradist

divergent from related species to be organism specific. At the time the sequence diversity of the virus was very low, thus further SARS-CoV-2 specific analysis of the N gene by sequence analysis was not possible. Therefore, primer design decisions were based on performance-driven parameters such as computational estimates of primer properties (e.g., homodimers, hairpin structures, Tm, %GC). Our recent *in-silico* analysis revealed that our primers still have high coverage across new variants[38]. The specific overlap with the U.S. CDC primers (**Figure 10.17D**) was semi-coincidental and possibly a consequence of shared primer design requirements as suitable regions evaluated by analysis software, and the small size of the N gene (1,275bp) relative to the footprint of our LAMP assays (213-281bp). The proximity of our LAMP amplification targets on the same contiguous DNA fragment may have an extra advantage to enable a synergistic initiation effect. Amplification events could occur closely enough such that they could bump each other. Other RT-LAMP technologies (**Table S10.12**) that amplify different genes would not benefit from this effect. For the IAC amplification, we used a single LAMP loop primer to intentionally impair the IAC amplification (**Table S10.12**) so that it would not outcompete SARS-CoV-2 amplification.

Harmony also uses novel universal probes containing entirely engineered sequences [38]. The 5’ FAM or 5’TEX 615 signal probes each have a 5’ sequence region hybridized to the complementary sequence region of its quencher probe that has 3’ Iowa Black FQ or 3’ BHQ-2, respectively. In the absence of target or IAC amplification, these quencher molecules remain proximal to their fluorophore pairs and absorb the fluorophore’s emission wavelengths. The

© Copyright 2021 | N Panpradist

signal probes each have a 3' overhang with a sequence region identical to the 5' overhang of the loop primer for target or IAC. In the presence of target or IAC amplification, quencher probes are displaced, enabling signal detection.

To facilitate Harmony's multiplexed RT-LAMP, we employed newly developed, strand displacing TFv1 chimeric DNA polymerase. Compared to the WarmStart Bst DNA polymerase 2.0 commonly used in RT-LAMP SARS-CoV-2 assays (**Figure 10.8B**)[39], TFv1 chimeric DNA polymerase has a comparable amplification rate in a single-plex RT-LAMP (**Figure 10.18A**) but a drastically faster amplification of SARS-CoV-2 (**Figure 10.18B**) and IAC targets in our four-plexed RT-LAMP (**Figure 10.18C**).

10.3.3 READY-TO-USE REAGENTS

Our lyophilized RT-LAMP mixture contains primers, sequence-specific fluorescence probes, IAC DNA template, polymerases, supporting proteins, and co-factors (**Figure 10.19A**) and is activated by adding the nasal swab eluate containing additional buffer, salts, and detergent. We initially screened excipient formulations that can preserve enzymatic activity and do not significantly interfere with the primer or probe behaviors. We selected trehalose and mannitol since they have been used as excipients for PCR[40-44] and LAMP[45]. We found that mannitol did not drastically impact the Harmony's sensitivity compared to trehalose at the same concentration (**Figure S10.56**) and did not require adjusting the reaction temperature to maintain the assay speed. Possibly, this is because of trehalose altering primer and probe melting temperatures[46].

© Copyright 2021 | N Panpradist

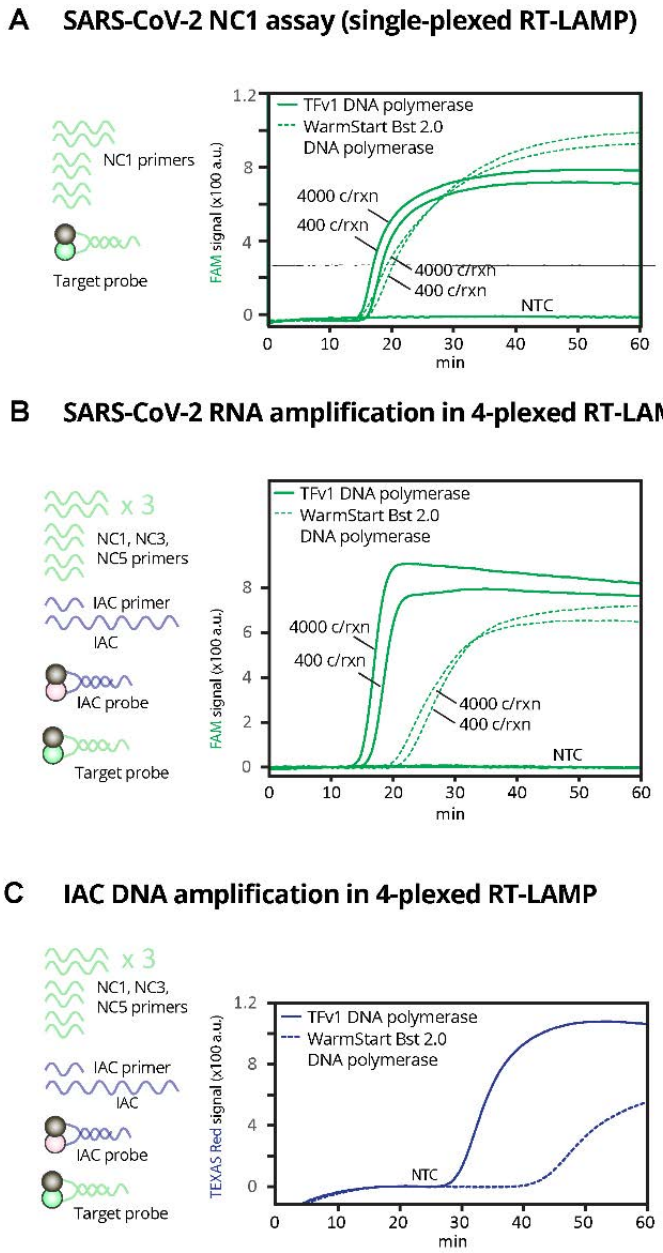

Figure 10.18 | Comparison of RT-LAMP using TFv1 polymerase vs commercial Bst polymerase using conventional RT-qPCR machine.

(**A**) FAM signal of the RT-LAMP assay using fresh reagents (not lyophilized) containing only NC1 primer set (6 primers total) and SARS-CoV-2 detection probe and quencher with 0, 400, or 4000 SARS-CoV-2 RNA copies/reaction (corresponding to 0, 100, or 1,000 SARS-CoV-2 RNA copies/µL, respectively). (**B**) FAM signal and (**C**) IAC signal of the 4-plexed RT-LAMP assay using fresh reagents containing all primers

© Copyright 2021 | N Panpradist

(18 SARS-CoV-2 primers and 1 IAC primer), SARS-CoV-2 detection probe and quencher, and IAC detection probe and quencher with 0, 400, or 4000 SARS-CoV-2 RNA copies/reaction (corresponding to 0, 100, or 1,000 SARS-CoV-2 RNA copies/µL, respectively). For (C) only NTC is shown to indicate true negative. All reactions were incubated at 63.3 °C for 1 hour and read every 13s in commercial thermal cycler. Image was obtained from https://doi.org/10.1101/2021.08.12.21261875

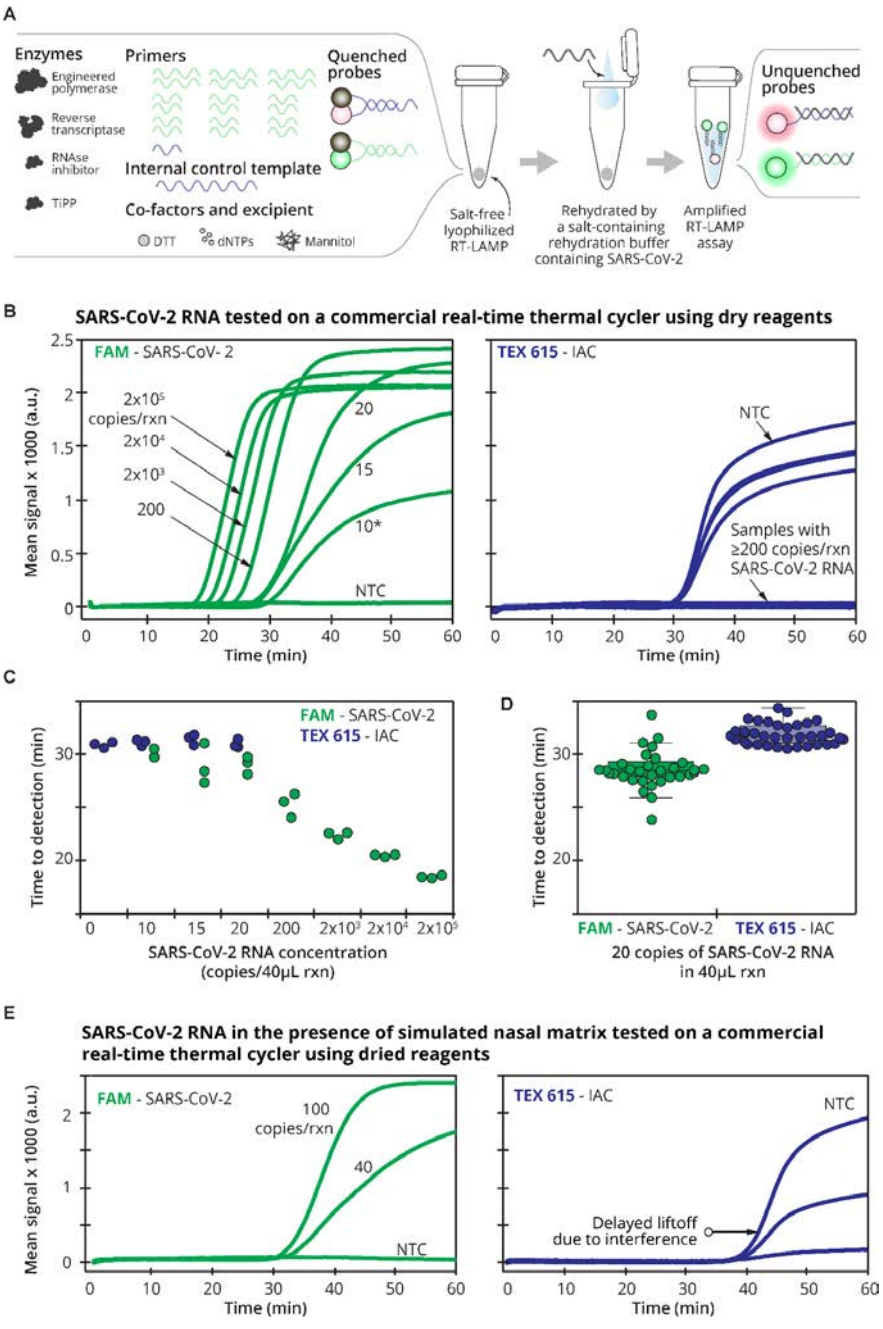

Figure 10.19 | Lyophilized RT-LAMP and its analytical sensitivity.

© Copyright 2021 | N Panpradist

(**A**) To set up the assay, a sample in elution/rehydration buffer containing magnesium, Thermopol buffer, and detergents is added to rehydrate the lyophilized RT-LAMP reagents in a single step. (**B**) Real-time amplification signal of RT-LAMP reactions containing SARS-CoV-2 RNA (**NTC**; no template control), 10, 15, 20, 200, 2000, $2x10^4$, or $2x10^5$ copies/40µL reaction (**rxn**). The left panel shows the average (*n = 3*) FAM signal detecting SARS-CoV-2. *Only 2/3 replicates of 10 copies/rxn amplified so the average was from duplicate reactions. The right panel shows TEX 615 signal detecting the internal amplification control (IAC). The IAC was detected in the NTC (*n* = 3) and in the single 10 copies/reaction that did not detect SARS-CoV-2. (**C**) Time to detection of SARS-CoV-2 and IAC targets reported by the real-time thermal cycler. Individual data points are plotted. Note that only 2/3 replicates of 10 copies/reaction amplified. IAC signals were properly detected in NTC (*n = 3*) and 1 of the 3 replicates of 10 copies/reaction undetected for SARS-CoV-2. (**D**) Evaluation of analytical sensitivity at 20 copies/reaction of SARS-CoV-2 RNA (*n = 40*), performed in two different runs (*n = 20* each) with two different serially diluted RNA samples. Time-to-result of individual samples are plotted along with medians (middle lines of the boxes), interquartile ranges (edges of the boxes), ranges (the ends of whiskers), and outliers (data points outside the whiskers). (**E**) Impact of nasal matrix. SARS-CoV-2 RNA at 0, 40, or 100 copies/reaction (corresponding to 0, 1, or 2.5 copies/µL) was amplified in lyophilized RT-LAMP in the presence of simulated nasal matrix (*n = 3*). All data was measured every 13s using FAM and TEX 615 channels, by a real-time thermal cycler in 1h reactions at 63.3°C, and (**C**). Image was obtained from https://doi.org/10.1101/2021.08.12.21261875.

Using a commercial real-time thermal cycler, lyophilized RT-LAMP detected 3/3 replicates of 15 RNA copies/reaction (0.38 copies/µL), and IAC was detected in all negative samples (**Figure 10.19B**). RT-LAMP amplification of 2 x 10^5 RNA copies/reaction using the dry reagents generated detectable signal in 17 min (**Figure 10.19C**). We subsequently tested our in-house lyophilized reagents on a larger number of technical replicates of SARS-CoV-2 RNA at 20 copies/reaction (0.5 copies/µL) using multiple batches, and 90% (36/40, 95% confidence interval (**CI**): 76 - 97%) were amplified (**Figure 10.19D**). Medians

© Copyright 2021 | N Panpradist

of time to detection for FAM and TEX 615 signals were 28.6 min (range: 28.0 - 29.4) and 31.7 min (range: 31.1 - 32.7), respectively. Based on these preliminary experiments, our limit of detection (**LOD**) is 15-20 copies/reaction (0.38 - 0.5 copies/µL) when analyzing purified, synthetic SARS-CoV-2 RNA. Next, we tested our lyophilized RT-LAMP reactions with simulated nasal matrix (salt, mucin, human DNA) to mimic human nasal samples. We observed a 10-min delay in amplification of both SARS-CoV-2 RNA and IAC DNA (**Figure 10.19E**), but all targets were detected correctly. Greater interference or other harm to the reaction will further delay IAC amplification; thus, the IAC serves as an indicator of the reaction's function and can prevent reporting false negatives due to interference or damaged reagents. By setting a 60-min reaction time, the assay can suffer some delay while still correctly identifying positive samples. Specificity testing against closely related pathogens MERS and SARS-CoV-1 showed no cross-reactivity (**Figure 10.20**).

non-SARS-CoV-2 RNA (copies/reaction)	**SARS-CoV-2 RNA** (copies/reaction)	**min to detection** SARS-CoV-2	IAC
4000 copies SARS-CoV-1	0	N/A	29.0, 30
4000 copies SARS-CoV-1	100	23.5, 24.1	N/A
4000 copies MERS	0	N/A	29.8, 30.1
4000 copies MERS	100	24.7, 24.7	N/A

Figure 10.20 | Cross-reactivity of MERS and SARS in lyophilized RT-LAMP.

Detection time (min) of SARS-CoV-2 RNA and IAC targets in the presence of 4000 copies of either SARS-CoV-1 RNA or MERS RNA in 40µL RT-LAMP reactions at 63°C. Two technical replicates were conducted in each condition. In the reactions without SARS-CoV-2 RNA, we did not observe amplification of FAM signal but observed IAC amplification indicating the amplification reaction was functioning properly in each replicate. 100 copies of SARS-CoV-2 RNA were amplified in each positive control replicate,

© Copyright 2021 | N Panpradist

indicating proper function of SARS-CoV-2 amplification in this master mix. Table was obtained from https://doi.org/10.1101/2021.08.12.21261875.

10.3.4 HARDWARE: HOUSING AND REAL-TIME FLUORESCENCE READER DEVICE

The Harmony system includes a heater/detector device controlled by a dedicated cell phone and plastic housing with a sample setup station (**Figure 10.21A**). The heater/detector device (**Figure 10.21B**) includes an aluminum heater block with four wells and a spring-loaded heated lid to prevent condensation. A proportional integral derivative (**PID**) feedback loop running on a microcontroller allows recovery of the temperature setpoint within 3-4 min after disturbance from opening the lid (**Figure 10.21C**). Two LEDs (**Figure 10.21D**) provide the excitation light by shining down through the top of each sample tube. Fluorescence emission passes through holes drilled on the side of the heater block. Each sample well has an emission filter/photodiode set on each side to detect two emission wavelengths (**Figure 10.21E**). A blue LED (dominant wavelength 470nm) is used to excite FAM, and the emission photodiode sits behind a dielectric 550nm longpass filter. A yellow LED (dominant wavelength 587nm) is used to excite TEX 615, and a second emission photodiode sits behind a 630nm longpass dielectric filter.

© Copyright 2021 | N Panpradist

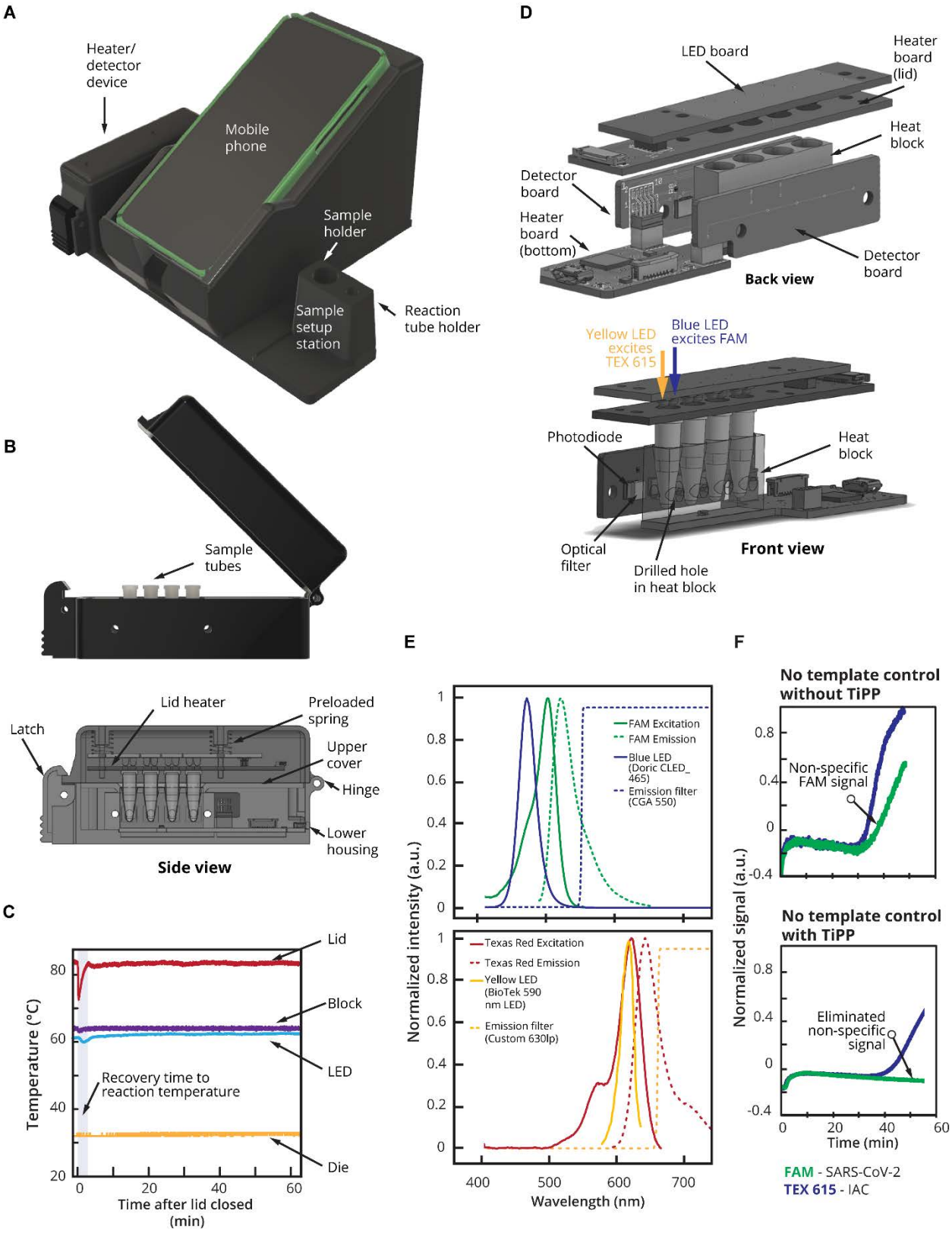

Figure 10.21 | Overview of Harmony COVID-19 hardware.

© Copyright 2021 | N Panpradist

(**A**) Plastic case cradles the cell phone (removable and connected by a spring cable), mounts the heater/reader device, and houses a Charge-Plus USB-C connector hub (not shown). A sample station holds the sample and reaction tube during processing and is detachable to allow cleaning. Weight: 266g housing, 104g heater/reader device (total <0.5kg). Dimensions: 205mm x 167.5mm x 125mm housing, 30mm x 120mm x 50mm heater/reader device. (**B**) The heater/reader device contains an aluminum block with wells for four samples (0.2mL reagent tubes) and is heated from the bottom by a resistive heater made from serpentine conductive traces on a printed circuit board. In the middle of the heater, a temperature sensor (Class B Platinum RTD) is used to measure the heat block temperature. Power to the heater is supplied by a MOSFET and modulated by varying the PWM duty cycle of the MOSFET. (**C**) Temperature profile after the lid opening throughout a 60-min assay run. The microcontroller (die) is measured to ensure the electronics are not overheated. (**D**) Lid heater, LED, and detector. A heater (85°C) on top of the tube prevents condensation on the tube lid. The lid heater is spring loaded to apply a preload force to the tubes to ensure good thermal contact and contains pass-through holes for excitation LEDs. (**E**) Spectral characteristics of the detection system. Blue and yellow LEDs provide excitation for FAM and TEX 615, respectively, and photodetectors on each side detect light passing through emission filters (spectral information from manufacturers[47-49]. The LEDs are operated independently (only one LED is illuminated at a given time). (**F**) Effect of thermostable inorganic pyrophosphatase (**TiPP**) on RT-LAMP signal in the Harmony device. Normalized signal of negative control samples using the RT-LAMP formulation with and without TiPP (*n = 1* each) at 64°C. Michael Roller developed the heater/reader. Daniel Leon developed the housing. Image was obtained from https://doi.org/10.1101/2021.08.12.21261875.

10.3.5 THERMOSTABLE INORGANIC PYROPHOSPHATASE ENABLES REAL-TIME LAMP DETECTION IN THE HARMONY COVID-19 DEVICE

RT-LAMP generates inorganic pyrophosphates (**PPi**) that precipitate from the solution. The cloudiness created by precipitates has been used as a visual readout signal for LAMP[50], but here the cloudiness scattered light and caused non-specific signals in NTC samples (**Figure 10.21F,** top) when tested on

© Copyright 2021 | N Panpradist

device. Inorganic pyrophosphatase (**TiPP**) can be added to the LAMP reaction to hydrolyze built-up pyrophosphate, and this combination has been used in other contexts to improve differentiation of LAMP products in melt analysis[51] and indirectly detect LAMP via phosphate ions hydrolyzed by the TiPP[52]. In fact, TiPP was advertised for its use for the enhancement of DNA replication[53], mitigating pyrophosphorolysis during DNA synthesis for sequencing[54]. In our context, we added TiPP in the RT-LAMP reaction to eliminate scattered signal from pyrophosphate to prevent non-specific signal in negative reactions (**Figure 10.21F,** bottom). Interestingly, this effect was not observed when the reaction was tested in the commercial thermal cycler (BioRad CFX96). This is potentially because the commercial thermal cycler uses bandpass filters for both excitation and emission wavelengths, while our device does not have excitation filters.

In addition to the physical effects, we have postulated that PPi accumulation may inhibit LAMP; as PPi forms, magnesium phosphate precipitate, Mg^{2+}, will be sequestered from the reaction, potentially impairing polymerase activity and primer hybridization. TiPP addition reduces the turbidity that is indicative of magnesium phosphate precipitate, so it may limit the depletion of reaction components. This has implications for multiplexed LAMP reactions, where concurrent amplification of multiple targets is a desired outcome. This possibility or the specific capability of TiPP to "enhance" LAMP has not yet been evaluated.

© Copyright 2021 | N Panpradist

10.3.6 MULTI-PURPOSE ANDROID MOBILE APP: INSTRUCTION, TEMPERATURE CONTROL, AND REAL-TIME ANALYSIS OF RESULTS

The phone software provides interactive guidance for setting up the test. It prompts the user to input a sample ID by scanning a barcode, capturing a photo, or typing a sample ID (**Figure 10.22, A-D**). The software also carries out the closed-loop temperature control for the heater block and lid heater, and it displays the status of the heater block to prompt the user to insert the reaction tubes only after the heater reaches the reaction temperature (**Figure 10.22E)**. During the test run, the screen displays the test status ("analysis in progress") and elapsed time, or it reports any detected errors ("failed run") (**Figure 10.22F**). Importantly, the software performs real-time data analysis that detects fluorescence intensity rise above a dynamically and automatically computed background level. Signals from SARS-CoV-2 can appear early in the test, especially for high viral loads, and the real-time analysis allows reporting of positive tests immediately after they are detected (**Figure 10.22G**). Negative results and IND results are reported at the end of the test run time (**Figure 10.22H**). Software analysis is described in the Methods section.

© Copyright 2021 | N Panpradist

Figure 10.22 | Cell phone user interface and result reporting.

The Android Harmony application guides the user through steps to set up and run the test. (**A**) Intended use of the device. (**B**) Instructions for the user to prepare samples. (**B**) Selection of the number of samples. (**D**) Collection of sample identifiers by barcode, photo capture, or manual typing. (**E**) Instruction to insert the tube when the temperature of the device reaches the reaction

© Copyright 2021 | N Panpradist

temperature. (**F**) Real-time analysis during the test run. (**G**) Positive results are reported as soon as they are detected. (**H**) Negative and IND results are reported at the end of the run time. Robert Atkinson developed this software app guide and analysis. Image was obtained from https://doi.org/10.1101/2021.08.12.21261875.

10.3.6 EVALUATION HARMONY COVID-19 SYSTEM ON CONTRIVED SARS-COV-2 SAMPLES (XPRIZE PANEL) WITHOUT EXTRACTION

A panel of contrived samples from the COVID-19 XPRIZE competition were tested on the Harmony system. For SARS-CoV-2 virus in 1xPBS (**Figure 10.23A**), Harmony detected all positive samples containing ≥50 SARS-CoV-2 viral particles/rxn, and 96% of samples containing ≥20 viral particles/rxn. In human nasal matrix (**Figure 10.23B**) and human saliva (**Figure 10.23C**), Harmony detected 97% and 83%, respectively, of samples containing ≥20 viral particles/rxn. Harmony had zero false positives across all sample types. Interestingly, unlike the case of simulated nasal matrix (**Figure 10.23E**), we did not observe delayed detection time of IAC in human nasal or saliva samples. Detection times (mean ± SD) for IAC amplification in negative samples were 32.9 ± 3.8 min for PBS, 35.8 ± 4.8 min for human nasal matrix, and 34.3 ± 11 min for human saliva, respectively ($p>0.05$; t-test, two-tailed). It is worth noting that in this experiment RT-LAMP reactions were either set up at room temperature (intended protocol for our assay, hollow symbols) or on ice (protocol used by most EUA RT-LAMP assays as summarized in **Table S10.12**, solid symbols). Even with a small sample size, we observed relatively delayed reaction and more false negative results when the reaction was set up on ice, especially those near the LoD (*i.e.*, 20 copies/rxn).

© Copyright 2021 | N Panpradist

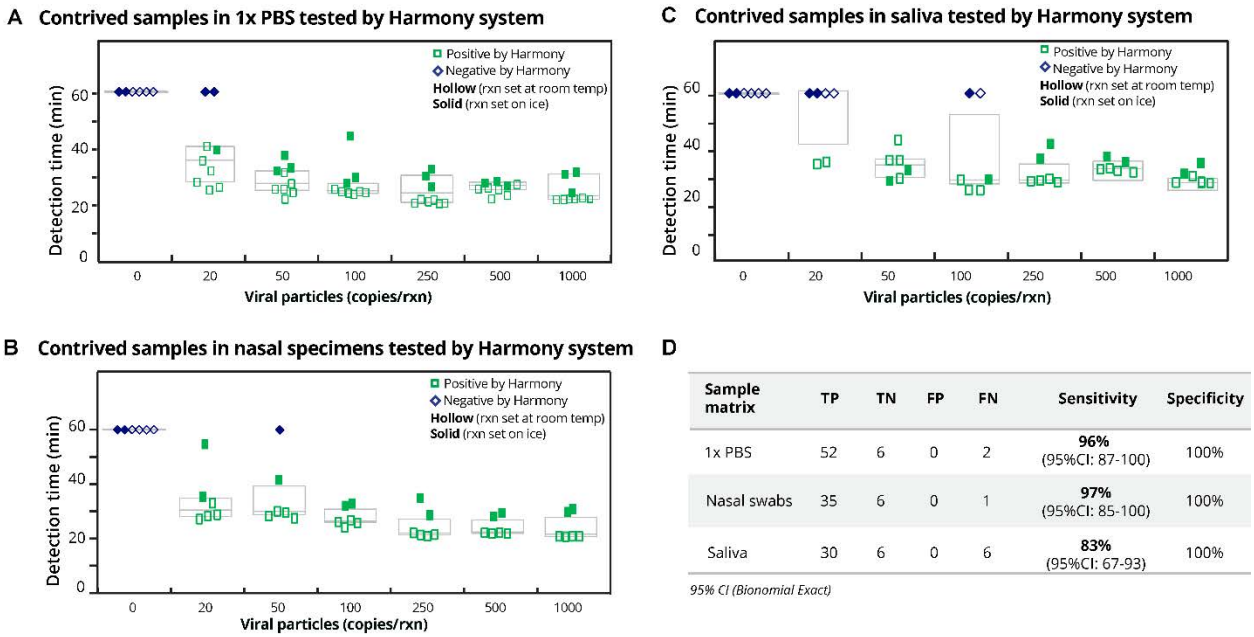

Sample matrix	TP	TN	FP	FN	Sensitivity	Specificity
1x PBS	52	6	0	2	**96%** (95%CI: 87-100)	100%
Nasal swabs	35	6	0	1	**97%** (95%CI: 85-100)	100%
Saliva	30	6	0	6	**83%** (95%CI: 67-93)	100%

95% CI (Bionomial Exact)

Figure 10.23 | Analysis of XPRIZE contrived sample panel without RNA extraction.

(**A**) Viral particles spiked in 1xPBS were tested in triplicate for each sample (n = 9 total for positive sample concentrations and n = 6 total for negative samples). (**B**) Viral particles spiked in human nasal matrix were tested in triplicate (n = 6 total for each concentration). (**C**) Viral particles spiked in saliva (n = 6 total for each concentration). (D) Summary table for the sensitivity and specificity of the Harmony COVID-19 system on the XPRIZE contrived samples. Concentrations of viral particles are the final concentrations in each 40uL reaction. Threshold concentration for positive is at 20 viral particle copies/reaction (0.5 copies/µL). Contrived samples below the positive threshold were also tested (**Figure S10.64**). Real-time amplification curves of these data are in Fig. S8. Reactions were set up either at room temperature (*hollow*) or on ice (*solid*).

10.3.7 EVALUATION OF CLINICAL SPECIMENS USING THE HARMONY COVID-19 SYSTEM

We first tested the assay for reactivity with SARS-CoV-2 and cross-reactivity with other respiratory pathogens using RNA extracted from infected patient specimens. The retrospective clinical samples had been collected in viral transport medium (VTM), which is not the intended sample type for Harmony,

© Copyright 2021 | N Panpradist

since a POC test uses fresh samples and does not require sample transport. Subsequently, we tested a smaller panel enriched with positive specimens to assess the feasibility of detecting SARS-CoV-2 RNA in VTM specimens without extraction.

Clinical VTM specimens were collected from individuals positive for SARS-CoV-2 (*n = 33*) or for other pathogenic respiratory infections (*n = 68*) and were re-tested by RT-qPCR using CDC primer and probe sequences[55] to measure the SARS-CoV-2 viral load and provide the reference test result. Using RT-qPCR with CDC primers/probes, 68 specimens were confirmed to be SARS-CoV-2 negative (**Figure 10.24A,** left), 30 specimens were confirmed to be SARS-CoV-2 positive (**Figure 10.24A**, right), and three previously positive specimens were only detected by one RT-qPCR assay (either N1 or N2) and classified as inconclusive (**INC**, **Figure 10.24A**, middle).

© Copyright 2021 | N Panpradist

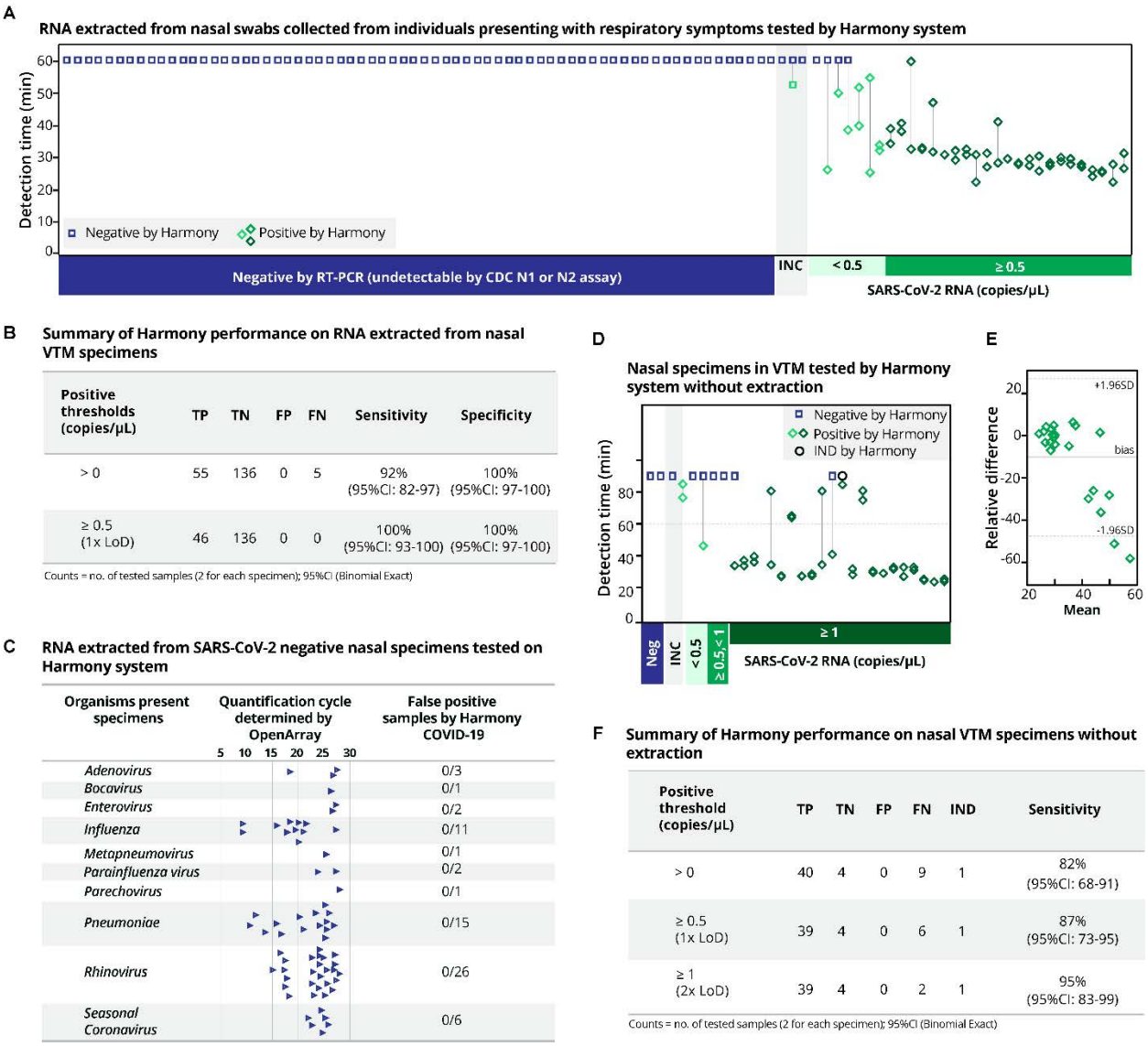

Positive thresholds (copies/µL)	TP	TN	FP	FN	Sensitivity	Specificity
> 0	55	136	0	5	92% (95%CI: 82-97)	100% (95%CI: 97-100)
≥ 0.5 (1x LoD)	46	136	0	0	100% (95%CI: 93-100)	100% (95%CI: 97-100)

Counts = no. of tested samples (2 for each specimen); 95%CI (Binomial Exact)

Positive threshold (copies/µL)	TP	TN	FP	FN	IND	Sensitivity
> 0	40	4	0	9	1	82% (95%CI: 68-91)
≥ 0.5 (1x LoD)	39	4	0	6	1	87% (95%CI: 73-95)
≥ 1 (2x LoD)	39	4	0	2	1	95% (95%CI: 83-99)

Counts = no. of tested samples (2 for each specimen); 95%CI (Binomial Exact)

Figure 10.24 | Harmony COVID-19 performance on clinical specimens.

(**A**) Detection time by Harmony software for the analysis of RNA extracted from human nasal specimens from 101 patients presenting respiratory symptoms. Stored specimens were re-tested by RT-qPCR using N1,N2 CDC primers; results matched previous results in 30 previous positive specimens (positive for N1, N2) and 68 previous negative specimens, with three previous positive specimens classified as inconclusive (**INC**) because they were negative for either CDC N1 or N2 by RT-qPCR. Samples are ranked from left to right by increasing SARS-CoV-2 concentrations quantified by RT-qPCR. Extracted RNA from specimens was analyzed by Harmony (10µL RNA in 40µL dry RT-LAMP, *n = 2*). The classification results by Harmony were compared to RT-qPCR using CDC primers and probes (5µL RNA in 20µL RT-qPCR). (**B**) Organisms in clinical nasal specimens were quantified using OpenArray, as

© Copyright 2021 | N Panpradist

described (*35*). High quantification cycle values indicate low concentrations. All these specimens were correctly identified as SARS-CoV-2 negative by Harmony. (**C**) Summary table for the sensitivity and specificity of the Harmony using extracted RNA from clinical specimens (RT-qPCR INC samples excluded). (**D**) Detection time by Harmony software for the analysis on 27 VTM specimens previously tested in (**A**). Without the RNA extraction step, 10µL VTM was added in the final 40µL RT-LAMP rxn, (*n = 2*). Dashed line indicates the detection time at 60 min. (**E**) Bland-Altman plot of the detection time of SARS-CoV-2 positive specimens of the direct VTM group compared to the extracted RNA group. Dashed lines indicate the acceptable bound of the difference of the detection time (mean ± 1.96SD). (**F**) Summary table for the sensitivity of the Harmony using VTM specimens without extraction.

Specimens were tested in duplicate on Harmony using the ready-to-use reagents (**Figure 10.24A**), amplification curves are arranged from low to high virus concentration as quantified by RT-qPCR assay (**Figure S10.62** and **Figure S10.63**). Out of 30 RT-qPCR-positive specimens, Harmony detected 26 specimens in both technical replicates and 3 specimens in one of the two replicates. In the three RT-qPCR INC results, one sample was detected by Harmony in one of the two replicates. Excluding the RT-qPCR INC specimens and applying a stringent requirement for both Harmony replicates to be detected to report a positive test, Harmony achieved 96% accuracy (94/98, 95%CI: 88-98%), 87% sensitivity (26/30, 95%CI: 69-96%), and 100% specificity (68/68, 95%CI: 94-100%). If replicates are treated independently (**Figure 10.24B**), Harmony detected 55/60 positive specimens (92% sensitivity, 95%CI: 82-97%). Harmony detected all positive specimens with ≥20 copies/reaction (0.5 copies/µL). The clinical panel (**Figure 10.24A**) included 68 specimens that were SARS-CoV-2 negative but contained other respiratory pathogens including influenza, rhinovirus, and seasonal

© Copyright 2021 | N Panpradist

coronavirus (**Figure 10.24C**), as determined using OpenArray (a laboratory PCR test with microarray detection)[56]. Harmony correctly identified all SARS-CoV-2 negative specimens (**Figure 10.24A**, left). **Figure 10.24B** summarizes the performance of Harmony on detecting extracted RNA from clinical VTM specimens.

Next, we used Harmony to detect SARS-CoV-2 in VTM specimens without RNA extraction. We expected the presence of microbial agents in the VTM to delay amplification and thus we ran the reaction for additional 30 min. Compared to RT-qPCR, Harmony with 90-min run time detected 18/24 positive specimens in both replicates and 3/24 in one of the replicates. Considering each replicate independently, Harmony detected 78% (32/41) and 95% (39/41) SARS-CoV-2 RNA positive specimens within 60- and 90-min detection time, respectively. Detection time (mean ± SD) of IAC in the negative samples with direct VTM amplification (43.9 ± 6.4 min) was significantly slower than the detection time with extracted RNA (38.5 ± 1.6 min; p=0.03, t-test, two-tailed). Pair-wise comparison among positive SARS-CoV-2 specimens (**Figure 10.24E**) showed two specimens with significantly different detection time. Even though VTM is not the intended sample type, Harmony detected 95% of SARS-CoV-2 VTM specimens that contained at least 1 copy/μL (**Figure 10.24F**).

10.3.8 FEASIBILITY TESTING: SAMPLE-TO-RESULT SYSTEM TESTED BY HEALTHCARE WORKERS AND LABORATORY PERSONNEL

To complete the system, we developed a test kit that included all components needed for running a test, including the swab, elution buffer, a fluid transfer

© Copyright 2021 | N Panpradist

device, and a ready-to-use reagent tube. Swabs were pre-loaded with SARS-CoV-2 DNA to serve as a control sample to evaluate performance by HCWs and laboratory personnel (**LPs**).

Next, HCWs and LPs executed the full Harmony workflow on contrived SARS-CoV-2 DNA swab samples (**Figure 10.25**). Using the transfer pipette workflow (**Figure 10.25A**), the test accuracy was 100% (10/10) for LPs and 95% (19/20) for HCWs. Surprisingly, we found that the HCWs performed better than the LPs when using the unified dispenser system (**Figure 10.25B**) when considering both accuracy and IND rates. HCWs had significantly lower (Z-test, two-tailed, $p<0.05$) IND results (1/20) than LPs (3/10) when using the unified dispenser system. Excluding IND results, the HCWs had 89% accuracy, higher than LPs with 71% accuracy (Z-test, two-tailed, $p<0.05$), when using the unified dispenser system.

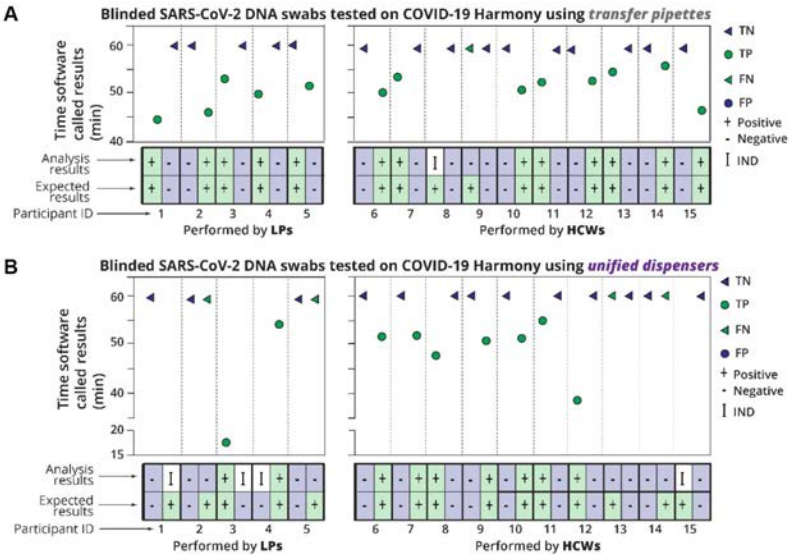

C

Performance with *transfer pipettes*

	TP	TN	FP	FN	IND	% Accuracy	% IND
LPs	5	5	0	0	0	100	0
HCWs	9	9	0	1	1	95	5

D

Performance with *unified dispenser*

	TP	TN	FP	FN	IND	% Accuracy	% IND
	2	3	0	2	3	71	30
	7	10	0	2	1	89	5

© Copyright 2021 | N Panpradist

Figure 10.25 | Usability study of Harmony COVID-19 workflow including two sample transfer methods at the POC.

(**A**) and **(B),** Assay performance on blinded contrived swabs (one negative swab and one positive swab with SARS-CoV-2 DNA at 1,000 copies/swab, corresponding to 100 copies/reaction) by LPs (*n = 5*) and untrained HCWs (*n = 10*) using transfer pipettes, (**A**) or unified dispensers, (**B**) The usability experiment written protocol is available on protocol.io (https://dx.doi.org/10.17504/protocols.io.bkvskw6e).(**C**) Performance summary for the transfer pipette method. (**D**) Performance summary for the unified dispenser method.

DISCUSSION

This work presents a combination of multi-disciplinary engineering (molecular, mechanical, electrical, software, human interface design) to develop a complete system for SARS-CoV-2 detection at the POC. The system is inexpensive and simple yet has features comparable to laboratory-based tests (

© Copyright 2021 | N Panpradist

Table 10.3**A**). The assay has high sensitivity and specificity in clinical and contrived specimens, and HCWs successfully performed the workflow with high accuracy.

© Copyright 2021 | N Panpradist

Table 10.3 | Feature comparison between the Harmony COVID-19 system and other assays.

(**A**) Comparison to the U.S. CDC assay. Full cost calculations for reagents and devices are enclosed in **Table S10.14** and **Table S10.15.**

Item	Standard RT-PCR assay (based on the U.S. CDC protocol)	Covid-19 Harmony
SARS-CoV-2 primer detection	Separate reactions for N1 and N2	Multi-target redundancy amplifying three regions of the N gene in a single reaction tube
Process control	Human RP gene	Engineered internal control
LoD	1-3.2 copies/µL from extracted RNA	0.5 copies/µL (20 copies/40µL reaction) from synthetic RNA; 1 copies/µL (40 copies/40µL reaction) from extracted RNA from VTM; 2.5 copies/µL (100 copies/40µL reaction) from contrived nasal samples
Consumable cost	$12.94 / sample ($6 extraction kit and $6.94 for three RT-PCR Taq Path/IDT probes)	$8.00 / sample
Easy to use reagents	No	Yes
Batch size	24 specimens	Not required, run up to 4 samples
Equipment cost	> $5000 qPCR machine	$247 customized heater/reader
Time for sample-to-result	260 min Hands-on: 120 min Wait-time: 120 min Interpretation: 20 min	21-91 min Hands-on: 1 min for direct amplification Wait-time: 20-45 min for positive samples, but 90 min is required to confirm true negative

(B) Comparison of Harmony COVID-19 to other isothermal assays for SARS-CoV-2.

Published assays	Amplification chemistry	Multi-target redundancy in a single tube	Reported LoD	User-friendly device with ready-to-use reagents and a closed system	Demonstration of use by HCWs
Harmony COVID-19 (This study)	RT-LAMP	Yes	0.5-2.5 copies/µL	Yes	Yes
A Alekseenko *et. al.* 2021[57]	RT-LAMP	No	10 copies/µL	No	No
BA Rabe and C Cepko[58].	RT-LAMP	No	50 copies/µL	No	No
S Wei, *et. al*[59].	RT-LAMP	No	2.5 copies/µL	No	No
D Thi, *et. a*[39]*l.*	RT-LAMP	No	5 copies/µL	No	No
L Bokelmann *et. al*[60]*l.*	RT-LAMP	No	5-20 copies/µL	No	No
W Yamazaki *et. al*[61].	RT-LAMP	Yes	25 copies/µL	No	No
J Qian *et. al*[62].	RPA	Yes	0.5 copies/µL	No	No
M Patchsung *et. al*[63].	SHERLOCK	No	2.1 copies/µL	No	No

© Copyright 2021 | N Panpradist

J Joung *et. a*[64]*l.*	SHERLOCK	No	2 copies/μL	No	No
J Broughton *et.al*[65]*.*	CRISPR cas12	No	10 copy/μL	No	No

Harmony uses ready-to-use reagents that enables fast and accurate assay setup compared to lab PCR while maintaining high assay sensitivity and specificity. The lyophilized Harmony assay detected as low as 15 copies/reaction of synthetic SARS-CoV-2 RNA and detected all extracted RNA from clinical specimens at ≥20 copies/reaction with no false positives across all sample types. Harmony chemistry is also robust, enabling detection of contrived samples in human nasal matrix (intended sample type) and saliva without RNA extraction. We found excellent sensitivity when testing samples with ≥20 viral particles in nasal matrix (estimated 500 copies/swab for 1mL elution buffer and 40μL reaction). In saliva samples at the same concentrations (not the intended sample type), Harmony showed moderate sensitivity. Heat treatment of saliva shown to enable detection by RT-PCR[66] would likely improve the sensitivity of Harmony with saliva samples. Regardless, our current level of assay sensitivity would be sufficient to detect SARS-CoV-2 in most nasal specimens (~10^3 to ~10^9 copies/swab) [67] or saliva (~10^4 to ~10^8 copies/mL)[68] from infected individuals during the first week after the onset.

Harmony's high assay sensitivity and specificity despite its high multiplexity was made possible by multiple modifications to traditional RT-LAMP. We used novel polymerase and probe design that can specifically discriminate between the SARS-CoV-2 from IAC amplification while most RT-LAMP analysis in tube relies on detection of total amplification and split each RT-LAMP reaction to

© Copyright 2021 | N Panpradist

detect only one target/reaction (**Table S10.14**). Multi-target amplification is essential to reduce false negatives in SARS-CoV-2 nucleic acid tests as the new variants continue to emerge.

In addition to the core assay, our lyophilization process also involves non-traditional modifications. Unlike other lyophilized RT-LAMP[69], our lyophilized reagents are magnesium-free, which prohibits any enzymatic activity that may occur before assay initiation. Our lyophilized RT-LAMP is activated upon the addition of sample which contains magnesium and detergent. Thus, it should be less prone to moisture degradation than magnesium-containing lyophilized RT-LAMP. Secondly, RT-WarmStart enzyme in Harmony assay is inactive at room-temperature and thus prevented activities during the reaction set up and eliminated the need for setting up the reaction on ice as performed in other SARS-CoV-2 LAMP assays (**Table S10.12**). Cold temperature can promote dimer and/or secondary structures of LAMP primers, which we observed as a negative impact on the assay sensitivity and speed. In fact, while setting up Harmony assay for lyophilization, RT-LAMP primers and probes were heated and cooled down passively at room temperature to minimize secondary structures prior to mixing with the other components. Last, we removed water to reduce the final volume of lyophilized reaction to 20µL. This enabled doubling the excipient concentrations in the lyophilized pellet and shortens the lyophilization drying time. When testing samples, the excipients are then diluted by half to 40µL reaction, thus reducing any impact of excipients on the core assay function. We anticipate that these components will be stable up to

© Copyright 2021 | N Panpradist

30 °C but future experiments will be conducted in the final form of the product for future commercialization efforts.

Isothermal amplification, like RT-LAMP in Harmony, is often promoted as ideal for POC testing because it can be carried out using a constant temperature heat source, such as a water bath, heat block, or even more novel sources (chemical heat source, sunlight, body temperature) [70]. However, reported tests often have other limitations that may prevent their use in POC testing (

© Copyright 2021 | N Panpradist

Table 10.3**B**). Common limitations include use of frozen reagent stocks that must be thawed and then formulated using laboratory pipettes, manual steps for sample processing that require laboratory skill, or detection steps that rely heavily on user interpretation or analysis by a user's cell phone. Harmony is a complete sample-to-result system that uses ready-to-use reagents for simple 1-minute setup and a dedicated device that reports results without extra post-amplification steps or reliance on user interpretation.

Some RT-LAMP tests use end-point lateral flow strips for detection (**Table S10.12**), which adds a user step, but more importantly, should not be done at the POC because it exposes the testing site to amplicons that will give false positive results in subsequent tests. Others use in-tube detection by eye[71] or a cell phone[72] which increases the user burden and could introduce additional sources of error. Real-time detection used in Harmony COVID-19 removes the need for extra detection steps or user interpretation. Real-time detection also allows Harmony to report positive results as soon as the SARS-CoV-2 signal appears rather than waiting for an end-point detection method. High viral load samples could be detected in as little as 20 min, which could enable more timely infection control measures to limit viral spread. Harmony real-time detection allows testing without opening tubes after amplification, requires no extra steps or interpretation by the user, and allows reporting a positive sample earlier than end-point detection methods.

The Harmony device automates heating, multiplexed detection, and data interpretation. We integrated a simple heater with low-cost LEDs and sensors

© Copyright 2021 | N Panpradist

to enable real-time two-color detection of RT-LAMP fluorescence in four independent sample wells. The device costs <US$300 in parts for prototypes, while the lowest cost of a commercial RT-PCR machine on the market is >US$5000[73]. Moreover, the Harmony device is portable and energy-efficient, requiring <15 watts and operable by USB power sources. These features are attractive for use at the POC in the U.S. and resource-limited settings.

Lastly, the simple workflow and analysis of Harmony is appropriate for POC testing. Test operation involves a few simple steps that take ~1 minute, and there are no further user steps after starting the test. Here, HCWs were able to operate the tests with simple written instructions and a video showing the procedures. The simplicity of the Harmony procedure and completeness of the stand-alone system can be a significant advantage for onboarding to ambulatory care settings and potentially community testing locations. Compared to existing US FDA EUA RT-LAMP tests (**Table S10.12**), Harmony is very competitive. Most RT-LAMP technologies are not designed for use in CLIA-waived settings. Lucira™ is the only product approved for use at the POC, but it is custom-designed to be battery-powered and completely disposable. This strategy, while is convenient for users, can contribute to electronic waste and relatively high cost for producing a unit. In contrast, Harmony relies on low-cost consumables and generates no electronic waste after each run.

In this study, we evaluated the system using contrived specimens in nasal and saliva matrix (XPRIZE) and clinical specimens stored in VTM, which may not reflect the performance in fresh clinical samples. These samples were used due

© Copyright 2021 | N Panpradist

to the difficulty of obtaining fresh dry swabs intended for this POC test. Because VTM is irrelevant for immediate testing at the POC, we tested RNA extracted from clinical samples to assess the overall assay performance on clinical RNA and subsequently tested feasibility of direct amplification of VTM samples. Nevertheless, this testing shows excellent analytical reactivity to clinical specimens, no cross-reactivity with other respiratory pathogens, analytical sensitivity comparable to the CDC RT-PCR, and resilience in the presence of nasal matrix. While our assay is relatively fast and sensitive, there is potential to further improve the performance. We ran RT-LAMP at 64°C, which is 9°C above the optimal temperature for the RT enzyme. We hypothesize that cooling of the heat block when the lid is open, followed by a few minutes to ramp back up to 64°C, provided an opportunity for the RT enzyme to operate. In contrast, the reaction speed of the temperature stable TFv1 DNA polymerase in this assay is optimal at higher temperature. Thus, operating the device with an initial 55°C step for optimal RT activity followed by a higher temperature step for fast DNA amplification could increase sensitivity and/or speed.

The current design of RT-LAMP assay can be improved to include an IAC that is more representative of the SARS-CoV-2 virus. We currently use a DNA IAC, which has been used in several EUA assays, but the DNA control does not capture the potential failure of the lysis and cDNA conversion processes. We are developing a new IAC that uses RNA that can be packaged in a viral envelope. This modification may require re-development of excipients that preserve the RT-LAMP enzymes and the enveloped RNA.

© Copyright 2021 | N Panpradist

POC tests like Harmony could provide rapid testing to enable the re-opening of businesses, schools, and borders; but the need for POC testing extends beyond the current emergency. As natural immunity and vaccination take hold, COVID-19 is likely to become endemic with seasonal outbreaks. Tests such as Harmony will be necessary not only to help identify individuals with SARS-CoV-2, but other respiratory pathogens such as influenza and RSV, as the symptoms of these are similar. Prior to the current SARS-CoV-2 pandemic, the yearly influenza infections caused nearly 30 million cases in the U.S. alone, with 400,000 hospital admission and 35,000 deaths[74, 75]. Indeed, particularly when more typical patterns of respiratory infections occur, there will be a need for tests that can perform multiplex testing for individuals presenting respiratory symptoms. Tests such as Harmony will become a common practice for confirming presence of viral infections that can be treated with antiviral therapies or that demand infection control, as well as helping to reduce inappropriate use of antibiotics. Further, test platforms developed for this pandemic could be more readily adapted to detect new diseases to increase readiness for future pandemics. The advances in awareness and acceptance of testing for infections at scale, and the technology platforms developed will have an ongoing benefit for COVID-19 control, reducing harm from other endemic diseases, and fighting future pandemics.

ACKNOWLEDGMENTS. We thank Bryan Willman for his support in fabricating customized heat blocks, Jan Gray for his help with firmware development, Tom Blank for sharing the PCB fabrication resources, and Dr. Liz Sanocki for the useful feedback on the software user interface. We thank Shawna Cooper for

© Copyright 2021 | N Panpradist

sharing the graphics and content used in Audere's mobile app's flu@home, which influenced the design of the first few screens of the Harmony COVID-19 software. We thank Dr. Paul Yager and Steven Bennett for use of their optical filters during the initial stage of device development. We thank Jason Tauscher at the Washington Nanofabrication Facility for his assistance in cutting the plastic sheet filters. The Washington Nanofabrication Facility is a National Nanotechnology Coordinated Infrastructure (NNCI) site at the University of Washington with partial support from the National Science Foundation via awards NNCI-2025489 and NNCI-1542101. We thank Seattle Flu Study researchers Dr. Jay Shendure and Dr. Jase Gehring for their helpful technical discussion. We thank Dr. Syamal Raychaudhuri, Dr. Frances Chu from Inbios International, and Dr. Gwong-Jen J. Chang for the stimulating discussion. We thank the Seattle Flu Study and the Seattle Coronavirus Assessment Network (SCAN) teams led by Principal Investigators: Helen Y. Chu, MD, MPH, Michael Boeckh, MD, PhD, Janet A. Englund, MD, Michael Famulare, PhD, Barry R. Lutz, PhD, Deborah A. Nickerson, PhD, Mark J. Rieder, PhD, Lea M. Starita, PhD, Matthew Thompson, MD, MPH, DPhil, Jay Shendure, MD, PhD and Trevor Bedford, PhD for providing specimens for testing.

10.4 ONGOING WORK

10.4.1 A FEASIBILITY STUDY OF SIMPLIFIED, LOW-COST COVID-19 ASSAY IN ZIMBABWE

© Copyright 2021 | N Panpradist

CONTRIBUTORS: Nuttada Panpradist, Qin Wang,Lisa M Frenkel, Jack Henry Kotnik, Vinie Kouamou, Barry R Lutz, Justen Manasa, Abraham Miller, Parker S Ruth, Chunjong Park

INTRODUCTION: In response to the first case of the coronavirus disease 2019 (**COVID-19**) on 20th March 2020, the Zimbabwean government put in place measures to curb the spread of severe acute respiratory syndrome coronavirus 2 (**SARS-CoV-2**), the virus that causes COVID-19. One of these measures included multiple national lockdowns (stay-at-home) for periods of 21 days since the 30th March [76]. This strategy successfully helped contain community spread; as of 13th June 2020, 356 Zimbabweans have been confirmed positive for COVID-19; Of which 298 are active cases, 54 recovered and only 4 deaths were recorded. However, the lockdown in the past few months, in turn, unleashes economic and social devastation. With respect to the World Health Organization's criteria, Zimbabwe is now considering step-by-step strategies to lift the lockdown particularly issues surrounding diagnostic testing. To safely reopen the country, high throughput, and low-cost molecular diagnostics of SARS-COV-2 is critically needed for routine case management and to contain disease transmission. Rapid diagnostic tests (**RDTs**) have been used as the mainstay approach in the country and started at the National Microbiology Reference Laboratory (**NMRL**) in Harare and were then expanded to the National Tuberculosis Reference Laboratory (**NTBRL**) in Bulawayo. The RDTs have now been decentralized throughout the country with both public and private facilities taking up. However, the antibody-based RDTs only detect human immune response to the SARS-CoV-2 that may be

© Copyright 2021 | N Panpradist

present a week to 12 days after initial infection. Zimbabwean doctors are concerned that RDTs are not able to sensitively detect SARS-CoV-2 during acute infection. Molecular assays (i.e. reverse-transcription polymerase chain reaction, RT-PCR) at present are the fastest and most reliable method for screening early infection of COVID-19 and are being used in the country. However, the current RT-PCR reference assay requires extensive material resources and involves collection steps that can increase the exposure risk of healthcare personnel to contract COVID-19. First, nasopharyngeal swab samples involve potentially symptomatic individuals to travel to the clinics or hospitals for sample collection by the trained personnel. This sample collection step can increase the exposure risk for frontline healthcare workers, especially when personal protective equipment is reportedly unavailable. Next, to ensure the stability of samples, swabs are submerged in the viral transport media (which has sometimes been lacking/insufficient or again not provided with the kits) and stored under the cold chain during specimen shipping to the reference laboratories. Furthermore, the laboratory protocol of the reference lab protocol itself requires 2 hours of extensive hands-on to extract the ribonucleic acid (RNA) of 24 samples and 8 hours for an RT-PCR batch 96 samples/RT-PCR run. Moreover, setting up the reference RT-PCR requires preparation and aliquoting of master mix across samples at the testing laboratories. Thus, the assay operators require extensive training before performing the test. The total assay turnaround time from sample collection to results is multiple days to weeks. As a result, less time consuming, safer and simpler SARS-COV-2 diagnostic assays are needed. This will help in augmenting the number of diagnostic testings done per day so as to better

© Copyright 2021 | N Panpradist

understand the COVID-19 transmission in the country. The goal of this collaborative project 'Hanya' (i.e. 'care' in Shona) is to validate an assay to enable simpler and faster high-throughput SARS-COV-2 in Zimbabwe using contrived spiked-in RNA in self-collected dry swabs. We present our initial promising results, validating the two high-throughput workflows that rely on *(i)* real-time fluorescence-based detection and *(ii)* end-point fluorescence based detection.

Nasopharyngeal swabs have been used as the standard sample in Zimbabwe, but this sample collection causes discomfort for patients and posts contraction risks to doctors or other front-line health workers required to collect these samples. To address this issue, we chose to use nasal swabs (anterior nare) which have been approved for self-collection in the United States. The swab tips are large and cannot be pushed too deep inside the nasal cavity. Volunteers participating in this study reported the average level of pain of (0 for painless and 10 for extremely painful). This finding is similar to other previous studies. Additionally, a study comparing the level of viral loads from different sample sources showed that nasal swabs had a higher number of viruses than nasopharyngeal swabs. Self-collection swabs open more opportunities for individuals suspected of having COVID-19 to request a collection kit from local clinics or pharmacies and ship the samples to the laboratory sites for processing. A similar model for shipping dry samples has been routinely used for dry blood spot samples for routine HIV testing, and this approach may work well for settings where getting to the hospitals may be a challenge. To do this successfully, we must ensure the stability of RNA in these swabs during shipping at ambient temperature. Only some VTM are stable at ambient temperature, and often are not available due to the high demand for

© Copyright 2021 | N Panpradist

COVID-19 testing. The WHO recommends alternative VTM recipes but swab samples in these VTM still require cold chain storage during shipping. Dry swabs (without submerging in VTM) are recommended by some point-of-care tests and have been shown to give similar results to swabs in VTM.

The traditional RT-PCR assay currently used in Zimbabwe by the NMRL and specific private and public laboratories (BRTI, Aibst, Lancet, Cimax and PSMI) required trained personnel and have only been carried out in the two main cities in the countries. Furthermore, this assay is time consuming, and the collection of samples put doctors and frontline health workers at risk. The country has been facing some challenges particularly with the acquisition of swabs and transport media which often lack in the supplier/donation kits. In this study, we have successfully validated a RT-PCR assay which bypasses all these challenges. The lyophilized assay is much simpler, safer, and less time consuming and can be easily decentralized to increase the testing in various parts of the country.

METHODS

Ethical statement

This study was approved by the Medical Research Council of Zimbabwe. Specimens used in this study were self-collected dry swabs from healthy volunteers. Those specimens were de-identified prior to being used in the validation experiment using the novel modified US CDC protocol. Indeterminates, false positives, and false negatives were confirmed using the reference assay. The confirmed positive results were handled according to the COVID-19 Zimbabwe national guideline for public health.

© Copyright 2021 | N Panpradist

Clinical specimens and collection

A minimum of 30 specimens is required to achieve at least 90% accuracy if a test has a diagnostic accuracy of 100% (binomial cumulative distribution function). In this study, 40 participants negative in symptom-based screening (no new fever, cough, shortness of breath, sore throat, muscle aches, respiratory symptoms, chills or repeated shaking with chills, or loss of taste or smell) were given swabs (Puritan) for self-collection (**Figure 10.26**). These swabs were intended to stay in the anterior nares. The large tips cannot be pushed too deeply inside the nasal cavity. Nasal swabs will be stored dried in 15mL barcoded tubes and transported to the University of Zimbabwe laboratory within 1-2 hours and stored at -20°C or lower until testing.

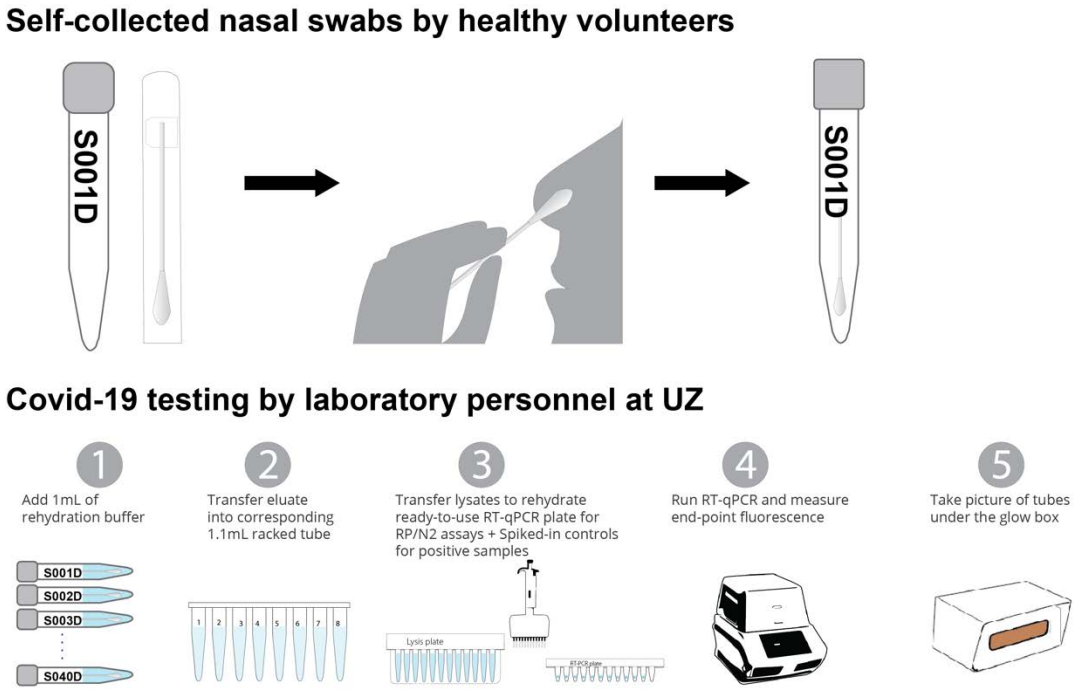

Figure 10.26 | Workflow of SARS-CoV-2 RT-PCR assay using lyophilized reagents at University of Zimbabwe.

© Copyright 2021 | N Panpradist

Modified US CDC protocol using real-time thermal cycler

Each dried swab was rehydrated using 1mL of buffer containing 0.5% TritonX-100 and 2mM MgSO4. Eighteen µL of swab eluates were used to rehydrate the lyophilized RT-PCR reagents for N2 or RP assays prepared as previously described. Negative specimens (n=40) were added with 2µL of nuclease-free water while positive specimens were added with 2µL of 100 (n=30) or 250 (n=10) copies/µL genome equivalent made from RNA target packed in the pseudo virus (DAAN Gene Co., Ltd of Sun Yat Sen University). The RT-PCR reactions were run using the ABI 7500 Real Time PCR System (Applied Biosystems, California, USA) at 55°C for 5 minutes, 94°C for 2 minutes and 50 cycles of 94°C for 1 second and 57 °C for 30 seconds. The FAM channel fluorescence was read at the end of 30 seconds at 57°C for each cycle. At the end of the run, the classifications of negative and positive were automatically analyzed using the designed ABI 7500 software version 2.0. Samples classified as positive by N2 assay were re-tested using N1 assay. The RT-PCR reactions were rehydrated using 18µL of swab elutes spiked with 2µL of 100 (n=30) or 250 (n=10) copies/µL genome equivalent.

Modified US CDC protocol using an end-point fluorescence reader

All the reaction tubes previously processed on the ABI 7500 were analyzed for their end-point fluorescence intensities. The cell phone was used to capture the image of the RT-PCR tubes under the glow box. Images of human samples along with negative and positive samples were de-identified before sending for the blind analysis by the software team in Seattle. The analyzed images were

© Copyright 2021 | N Panpradist

sent to Zimbabwe with the blinded nasal swab results and disclosed the identity of the control tubes. The Zimbabwe team then determined the signal threshold based on the NTC and low template signal to classify the negative from the positive groups.

Cell phone application for SARS-CoV-2 classification

The images of the tubes taken in above sections were used to train the classification software. The standalone Android application was developed to automatically analyze the captured image in real-time and reported results as positive and negatives. The application was downloaded by the Zimbabwean team and used to re-analyze the newly captured images of the tubes involved in this study. False positives are to be confirmed using the reference assay (**Figure 10.27).**

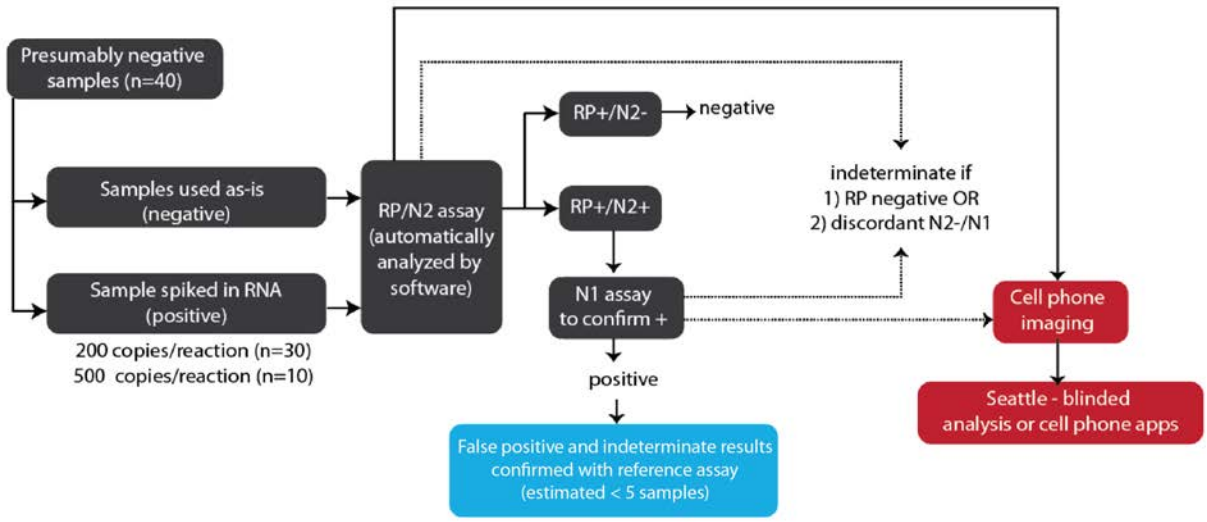

Figure 10.27 | Study design of SARS-CoV-2 RT-PCR assay using lyophilized reagents at University of Zimbabwe.

© Copyright 2021 | N Panpradist

PROGRESS TO DATE: Early April 2020, the recruitment of samples was completed at the UZ, and samples were stored at -80C until tested. Kits were manufactured in the Lutz lab and shipped using cold pack via DHL in June 2020. A package containing a cell phone was lost, so we had to re-ship it. Unfortunately, the lab at UZ had issues with their qPCR machine broken and the unit was sent for maintained for 3 months in South Africa. After the machine was returned in August 2021, the reagent quality of our assay was QCed using the pooled negative samples, showing all 100% RP amplification (**Figure 10.28**). Currently, the lab at UZ is in the process of securing positive virus control to complete the remaining of the data collection.

© Copyright 2021 | N Panpradist

Figure 10.28 | Dr. Vinie Kouamou tested the workflow at the laboratory in the University of Zimbabwe.

10.4.2 IN-CLINIC FEASIBILITY TESTING OF A POINT-OF-CARE LOW-COST COVID-19 RT-PCR TEST: A CASE STUDY AT MEDSTAR GEORGETOWN UNIVERSITY HOSPITAL PEDIATRIC CLINICS

CONTRIBUTORS: Nuttada Panpradist, Jack Henry Kotnik, Qin Wang, Ian Hull, Parker S Ruth, Chunjong Park, Samuel Stewart, David Nelson, Sejal Bavishi, Ami Patel, Barry R Lutz, Ruth Kanthula

INTRODUCTION

The delay in results can impact care providers' decisions in providing access to care in an individual. For the symptomatic group, the delay in test results causes diagnostic delays, a lot of anxiety for families, delays in schools/daycares determining next steps for other peers. For the asymptomatic, delay in test results affects children's return to school/daycare as well as disrupts parent's ability to

© Copyright 2021 | N Panpradist

work due to childcare issues. Point-of-care molecular testing is a promising intervention that allows fast on-site testing and provides much faster turnaround results. To date, there are several commercially available point-of-care molecular tests for COVID-19. The wide adoption of these point-of-care molecular tests in all communities still presents significant economic challenges, especially in vulnerable communities that may not have insurance coverage. We are still in need of a low-cost point-of-care platform for COVID-19 testing that is more accessible to the general US population and beyond. Due to cost constraints, many practices and testing sites opt to use antigen testing as their rapid test, which are less sensitive and more prone to false negative results, creating additional challenges to provider clinical decision making.

The Lutz laboratory at the University of Washington developed a modified US CDC SARS-CoV-2 assay to expand its use from high-complexity labs to the point-of-care. The workflow uses direct samples, bypassing cumbersome extraction steps as illustrated by other groups. Moreover, the modified RT-PCR test kit utilizes lyophilized reagents to simplify the workflow and to allow for a greater volume of extracted samples to be added directly to the assay. The UW work developed multiple configurations of test kit components based on commercially available materials, and the point of care configuration uses low-cost, commercially available, off-the-shelf consumables and equipment that makes it more affordable than other point-of-care options on the market. This test is currently being evaluated on different clinical specimens. In this study, we report a new case study to test the feasibility of this point-of-care test outside laboratories. Testing

© Copyright 2021 | N Panpradist

patients in clinics or hospitals may help contribute to the urgent need for routine COVID-19 testing around the US and the world.

METHODS

The feasibility testing of an alternative point-of-care RT-PCR test kit modified from the US CDC protocol was conducted at the Pediatric clinics at Georgetown University (**Figure 10.29**). Healthcare workers with no experience running the COVID-19. RT-PCR were each tested three swabs: negative, low positive, and high positive (**Figure 10.30**).

Figure 10.29 | Setup at the Georgetown University Pediatric clinic

(**A**) 60 kits were stored in a minifridge ($60). (**B**) The set up at the beginning of the PCR run. The operator received a notebook instruction, and the space is cleaned with bleach to avoid contamination. (**C**) the setup after the PCR run for visualization of the results via cell phone.

SMARTPHONE IMAGE CAPTURE APPS

Smartphones have been used for accurately capturing images of rapid diagnostic tests for various infectious diseases. Similar to the previous work, we built a dedicated mobile application to accurately capture fluid-filled fluorescent tubes. To link the tube image with a unique identifier, the application first asks to scan its QRCode, using a 3rd party open source QRCode reader that returns the unique identifier from the QRcode to the application via Android Intent. Then, the

© Copyright 2021 | N Panpradist

application configures the smartphone camera with manual exposure time and white balance setting that is optimized to yield best quality images of the tube in the UV illuminated box. The image is captured with the user's touch input and is uploaded to a secure server for image processing.

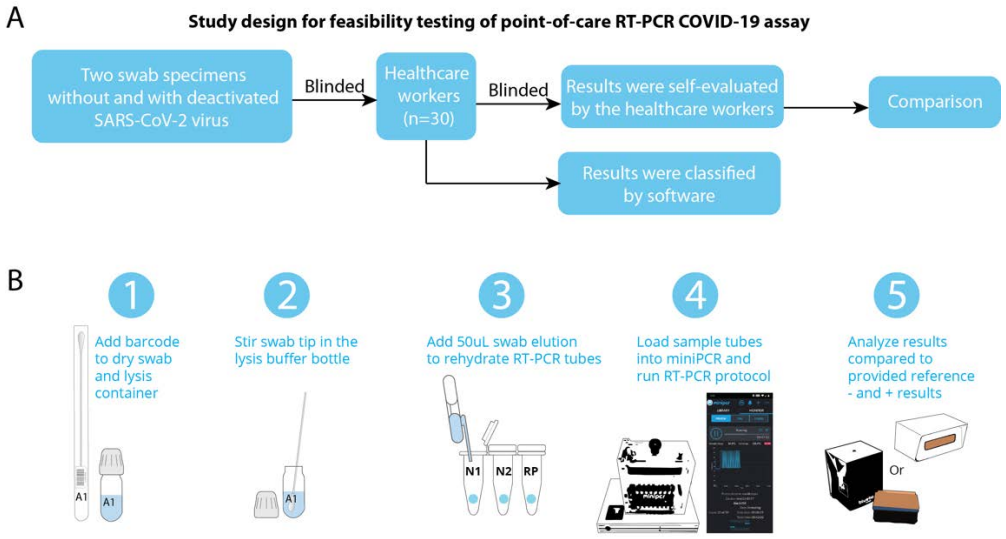

Figure 10.30 | Study design and workflow for POC testing of SARS-CoV-2 by clinic HCWs

(**A**) Study design (**B**) Workflow for point-of-care RT-PCR and analytical sensitivity performed by trained personnel

RESULTS

Preliminary results (n=11) showed a high rate of failure. First, the users did could not see the fluid in the transfer pipette well and the buffer volume was insufficient for most users who squeezed the bulbs so strongly, causing excess fluid to get trapped in the overflow chamber of the transfer pipette. We thus decided to adjust the study design to include two phases, where the second phase was designed to address the issues in the first phase (**Figure 10.31**). The new kits were made to adjust the volume of the buffer to 1mL. The buffer also included the Allura red dye

© Copyright 2021 | N Panpradist

at 0.01%, which gave the visible color without inhibiting the results. Additionally, we found that adding the red color dye improved the contrast between the negative and positive samples (**Figure 10.32**). The updated kits were sent in July and the study in the second phase is ongoing.

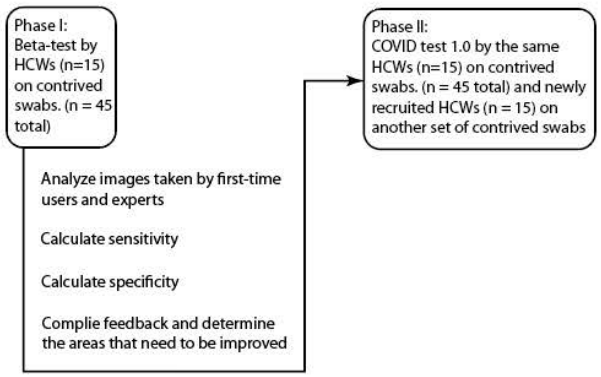

Figure 10.31 | Adjusted study design

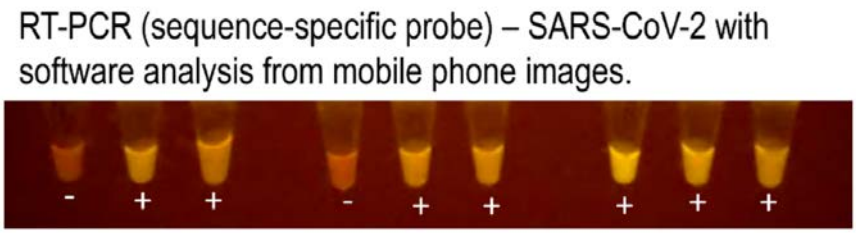

Figure 10.32 | Examples of the end-point results

10.4.3 USE OF HUMAN-IN-THE-LOOP AUTOMATION TO ENABLE RAPIDLY DEPLOYABLE COVID-19 MOLECULAR TESTING IN MULTIPLE ACADEMIC LABORATORIES.

CONTRIBUTORS: Cannon Mallory, Nuttada Panpradist, Anastasia Deckard,Samuel W A Stewart, Qin Wang, Jack Henry Kotnik, Robert Moseley,Sophia Campione, Barry R Lutz, Steve Haase, Eric Klavins, Benjamin J Keller, Devin Strickland

© Copyright 2021 | N Panpradist

CONTRIBUTIONS: CM, BJK, DS, and EK developed the Aquarium-based COVID-19 qPCR protocol. NP, SW, QW, JH developed and designed the contrived sample panels to evaluate Aquarium. NP and AD performed data analyses. CM, NP, QW, SWAS, JHK, SC, RM performed experiments and contributed to planning of the study. BRL, SH, DS, and EK oversaw study design.

STUDY DESIGN:

We designed four separated experiments (**Figure 10.33**) to capture the possible sources of variables (Figure 10.34) from sample preparation to qPCR methods.

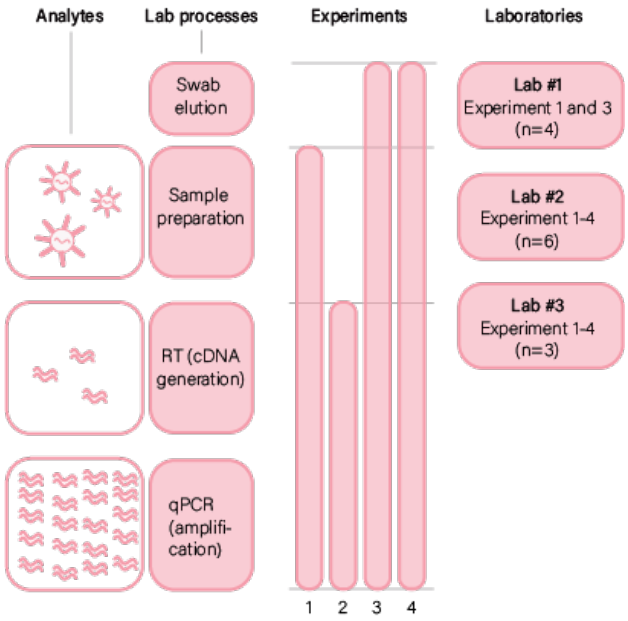

Figure 10.33 | Study design for detection of SARS-CoV-2 analytes enabled by Aquarium. Different analytes (SARS-CoV-2 RNA, DNA, or intact viral particles) were analyzed using multiple laboratory processes: swab elution, sample preparation (i.e. viral lysis and/or nucleic acid extraction), cDNA generation through reverse transcription, and quantitation using qPCR amplification. Four different experiments were used to capture failure of each process. In experiment 1 and 3, analytes were added directly to the RT-PCR reaction mixture using CDC modified and CDC protocols, respectively. In

© Copyright 2021 | N Panpradist

experiment 2 and 4, analytes loaded onto swab were first eluted prior to other remaining steps in the CDC modified and CDC protocols, respectively. To capture variables from operators and settings, different experiments were performed in three different laboratories involving a total number of 13 operators across sites.

Experiment Design: Variables

Lab	Experiment	target
Klavins	1, 2, 3, 4	DNA, RNA
Haase	1, 2, 3, 4	DNA, RNA, Virus
Lutz	1, 2	DNA, RNA, Virus
Duke Genome	1, 2	DNA, RNA, Virus

Exp.	protocol	sample type
1	cdc_mod	rxn
2	cdc_mod	swab
3	cdc_std	rxn
4	cdc_std	swab

sample type	concentrations
rxn	0, 50, 100, 1000
swab	0, 3000, 7500

probe
N1
N2

operators
performed experiments in lab

Figure 10.34 | Design variables included in the study.

RESULTS:

Based on the data collected by the personnel in the Klavins Lab, across Experiments 1-4 using both target (DNA or RNA) and Probe (N1 or N2). Initial analysis showed good separation between Cq of positive and negative samples (**Figure 10.35**). Further analysis is in progress.

© Copyright 2021 | N Panpradist

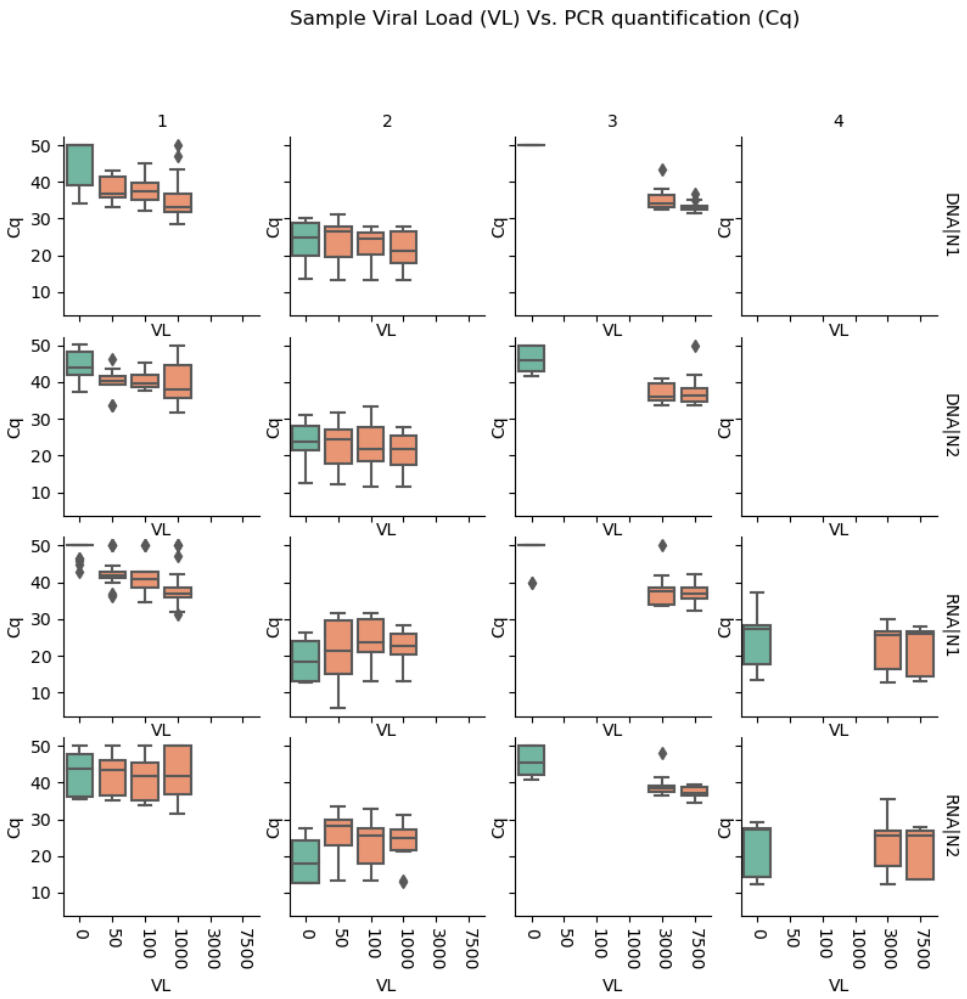

Figure 10.35 | Correlation of the VL and Cq across experiments.

VL (Viral Load in the Sample) and Cq is the PCR quantification of the viral load in cycles (50 is max and indicates lowest viral load.

10.4.4 SARS-CoV-2 TYPING ASSAY

CONTRIBUTORS: Nuttada Panpradist, Michael Roller, Qin Wang, Benjamin Chimukangara, Parker S Ruth, Beatrix Kele, Kathryn Harris, Maria-Teresa Cutino-Moguel, Anton Pozniak, Santiago Ávila-Ríos, Celia Boukadida, Margarita Matías Florentino, Malaya Kumar Sahoo, Daniel Solis, Mamdouh

© Copyright 2021 | N Panpradist

Sibai, ChunHong Huang, Benjamin Pinsky, Pavitra Roychoudhury, Keith Jerome, Nathalia Mantovani, Ricardo S Diaz, Paul Yager, Barry R Lutz

INTRODUCTION: It has been nearly two years since the World Health Organization (WHO) declared severe acute respiratory syndrome coronavirus 2 (SARS-CoV-2) a global public health emergency, on 30 January 2020[77]. The United States has the largest number of SARS-CoV-2 cases, accounting for almost 1 in every 4 confirmed SARS-CoV-2 cases globally (~29.1 million) and almost 1 in every 5 deaths globally (~0.53 million), by mid-March 2021[78]. In as much as global cases of SARS-CoV-2 are reducing, there is an ever growing concern over the emergence of new SARS-CoV-2 variants[79]. Mutations in functional regions of the spike protein are a cause of concern as they could increase the ability of the virus to spread faster, i.e. higher transmissibility[80]. More importantly, emerging variants have the potential to increase the ability of the virus to escape natural or vaccine-induced immunity, as has been shown with the three most reported variants, 501Y.V1, 501Y.V2 and 501Y.V3[81-83].

The 501Y.V1 variant (classified under lineage B.1.1.7) which emerged with several mutations was first identified in the United Kingdom (UK), and has since been detected in different parts of the world including the United States (US)[84]. In addition to D614G mutation, 501Y.V1 was initially identified with two deletions (69-70del and 144del) in the N-terminal domain (NTD), one mutation (N501Y) in the receptor binding domain (RBD), and one mutation (P681H) near the furin cleavage site,[85] as well as A222V in the NTD[86]. Recently, the E484K mutation has been reported in this variant[87]. The 501Y.V2 variant (classified under lineage

© Copyright 2021 | N Panpradist

B.1.351) was first identified in South Africa, and has since been detected in the United States (US)[84]. Again, in addition to D614G, the variant has several spike gene mutations which include 242-244del and R246I in NTD, A701V near the furin cleavage site, as well as key mutations K417N, E484K and N501Y in RBD[88]. The 501Y.V3 variant (classified under lineage B1.1.28/ P1) was first identified in Brazil, where it rapidly spread with three main spike mutations K417T, E484K, and N501Y in RBD[89]. This variant has also since been detected in the US[88]. In addition to these 3 common variants, a CAL.20C variant (spanning lineages B.1.427/ B.1.427) has been identified as originating in the US, in California, and is characteristic of a L452R mutation in the viral RBD[90].However, it does not seem to be spreading as quickly as the 501Y.V1 – V3 variants, being more localised to California[90].

At this rate, new variants of the SARS-CoV-2 will continue to emerge and will require continued efforts in vaccine development and SARS-CoV-2 detection. Based on current knowledge of these ever-expanding SARS-CoV-2 variants, we selected six specific spike gene mutations from and across the different lineages, that are potentially associated with higher transmissibility, severe disease, and evasion of natural and vaccine-induced immunity. These include A222V, K417N, K417T, L452R, E484K, and N501Y. The A222V mutation in NTD was first identified in Spain and spread rapidly across Europe[91]. It has been suggested to have an evasive immunological advantage to avoid B-cell response[86]. A combination of K417N/T, E484K and N501Y has been shown to cause a larger decrease in antibody neutralization than any of these mutations alone,[92, 93] and may further

© Copyright 2021 | N Panpradist

increase and stabilize ACE2 binding[94]. L452R has also been shown to enhance escape from neutralization by monoclonal antibodies and some convalescent sera,[95, 96] and to cause modest increase in infectivity[90, 95].

Currently these mutations are detected mainly *via* sequencing approaches to detect any new mutations and screen for existing notable mutations associated with variants. For the latter, different PCR-based approaches such as allele-specific PCR or hybridization probes have been used to detect these SNPs. From our years of experience working with highly mutating HIV, primers or probes may fail when there are many polymorphisms. To maximize sensitivity and specificity, we have developed an oligonucleotide ligation assay to discriminate these SARS-CoV-2 variants (**Figure 10.36**). We used a novel assay chemistry architecture that would enable fast iteration of assay development in response to the pandemic and marry it with simple lateral flow detection that can provide visual results and easy interpretation.

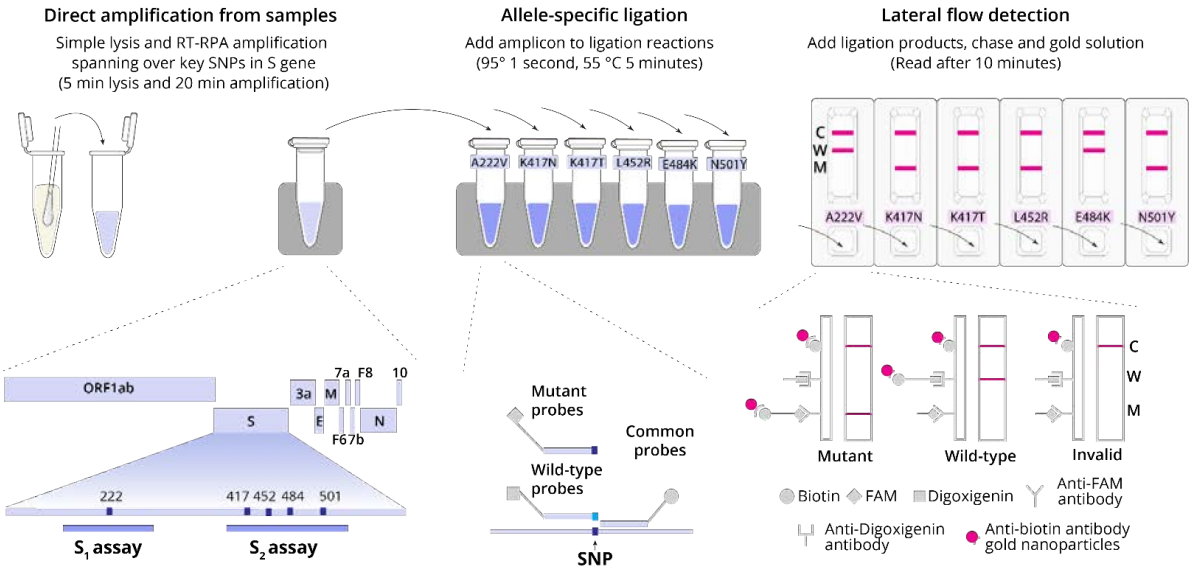

Figure 10.36 | Assay workflow and analytical performance.

© Copyright 2021 | N Panpradist

A simplified workflow from sample to results for detection of key SARS-CoV-2 mutations. Virus is lysed and RNA was released. The lysate was reverse-transcribed and amplified via two sets of the primers targeting the two regions spanning over the mutations of interest in the S gene of SARS-CoV-

RESULTS.

We designed an OLA-based workflow for SARS-CoV-2 detection have successfully developed RPA assay S1 and S2 with a sensitivity of 10 copies/reaction (**Figure 10.37**). We will next test these with the ligation reaction using the probes we already designed (**Table S10.16**)

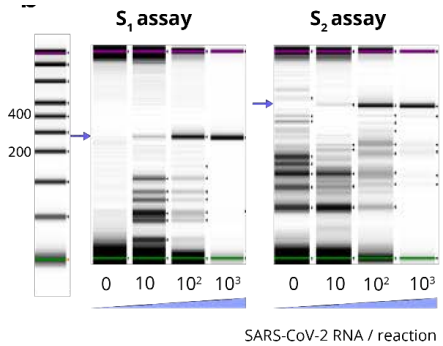

Figure 10.37 | RT-RPA assay for SARS-CoV-2 RNA transcript covering the regions of interest

© Copyright 2021 | N Panpradist

10.5 SUPPLEMENTARY INFORMATION FOR CHAPTER 10

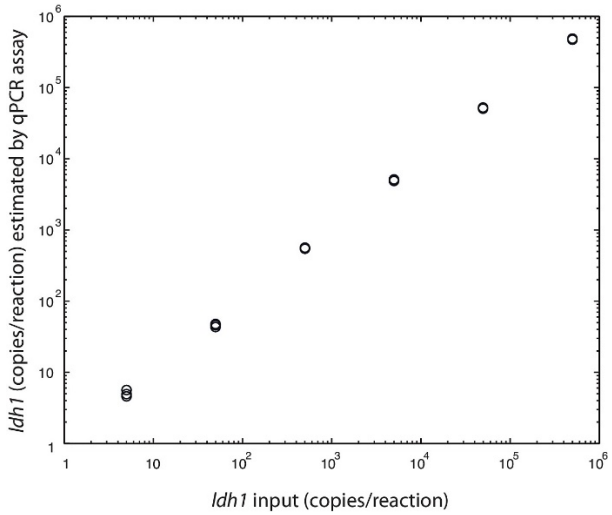

Figure S10.38 | Sensitivity of the MRSA/SA ELITe MGB qPCR assay.

10-fold serial dilutions of ldh1 copies (5 to 5×10^5 copies/reaction) and in negative TE control (N=3) were analyzed by the qPCR assay. The result shows the linearity across the concentration range. Five copies/reaction (~1 CFU/reaction) was detected reproducibly (mean ± SE = 5.08±0.314, CV = 0.107) while none of the negative TE controls was falsely detected.

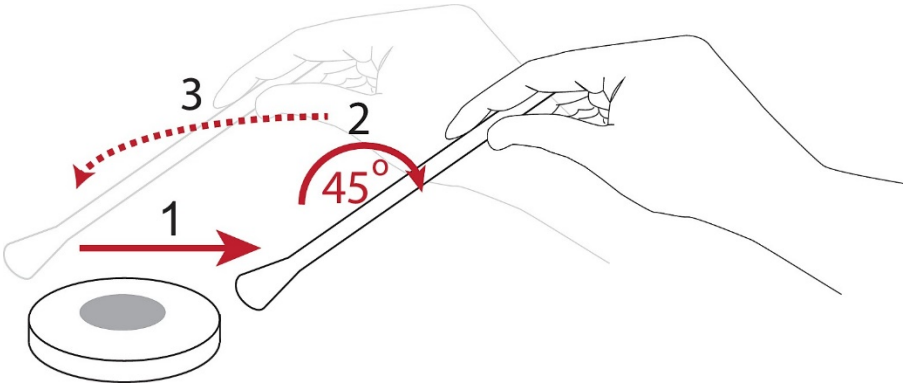

Figure S10.39 | Schematic of how swab was rubbed on PDMS surface.

© Copyright 2021 | N Panpradist

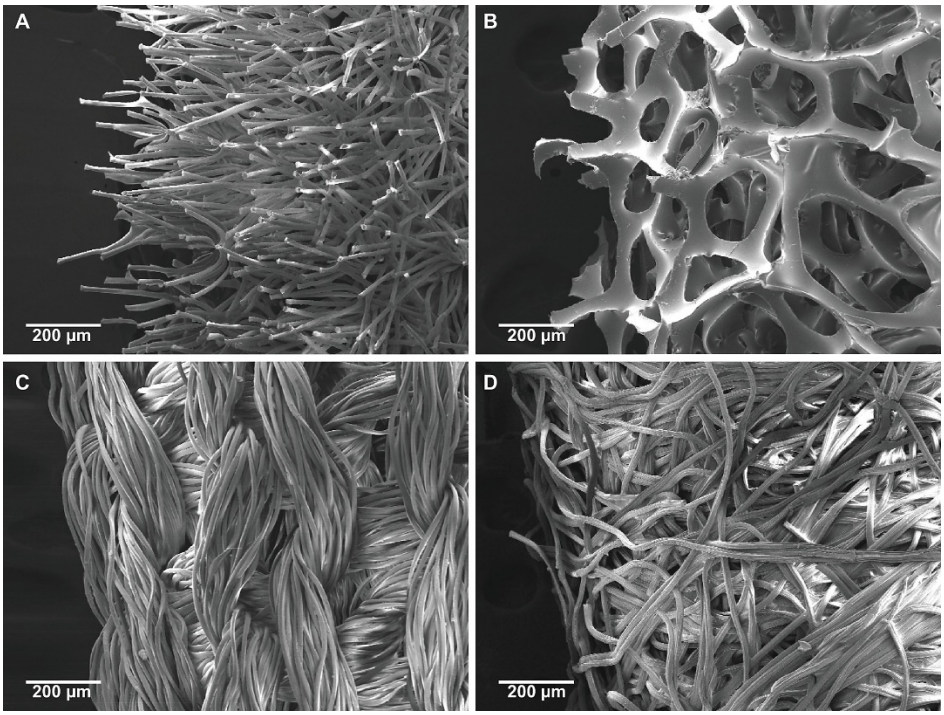

Figure S10.40 | Scanning electron micrographs of swab tips.

(**A**) mid-turbinate nylon (**B**) polyurethane (**C**) polyester (**D**) rayon. Scanning electron micrographs were obtained using an FEI Sirion scanning electron microscope. Samples were sputtered with an 11 nm Au/Pd coating prior to imaging (SPI Module Control, Structure Probe, Inc., West Chester, PA, USA.) SEM imaging and sputter coating work was performed at the University of Washington Nanotech User Facility (NTUF), a member of the NSF-sponsored National Nanotechnology Infrastructure Network (NNIN).

© Copyright 2021 | N Panpradist

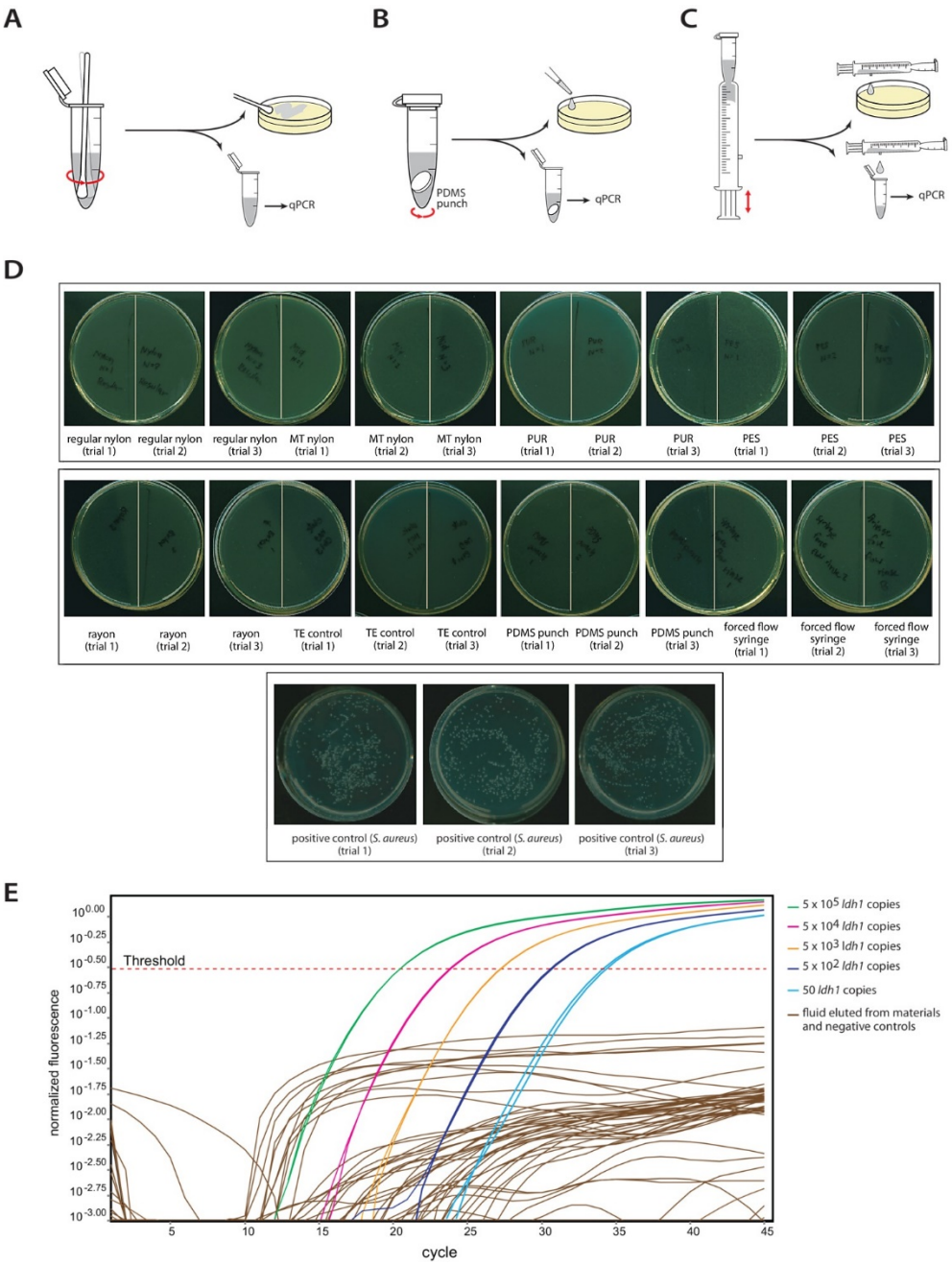

Figure S10.41 | Testing bacteria and bacterial DNA contamination in swabs and other materials.

The eluate from different dry swabs, PDMS punches, and forced-flow syringes was tested for bacteria and bacterial DNA contamination. (**A**) Swabs (PES, PUR, MT Nylon, Regular Nylon, Rayon (N = 3)) were dipped into 128 µL TE buffer and agitated (10 seconds, 1 Hz twirl) to generate eluate. (**B**) PDMS punches (N = 3) were added to 128 µL of TE buffer and vortexed for 10 seconds to generate eluate. (**C**) Forced-flow syringes (N = 3) were used to draw 128 µL TE buffer; the fluid was introduced to the

© Copyright 2021 | N Panpradist

tube adhered on the top of the syringe and purged via the side outlet to generate eluate. (**D**) Swabs were wiped onto the TSA plate. 30 µL of the eluate from PDMS punches and forced-flow syringe were spread onto the TSA plate. The plates were cultured overnight at 37°C to observe the growth of bacteria. None of plates with the eluates from swabs and other materials was devoid of bacterial colonies, except the positive control (30 µL of 10^5 CFU/mL *S.aureus*). This demonstrated that the swabs and all materials were not contaminated with bacteria. (**E**) Positive controls (10-fold serial dilution of 50 to 5×10^5 ldh1 copies) and negative controls (9 µL of eluate from swabs, punches, and syringes) were analyzed by the qPCR assay. The qPCR did not detect any ldh1 copies in eluate. This confirmed the absence of bacterial DNA contamination.

© Copyright 2021 | N Panpradist

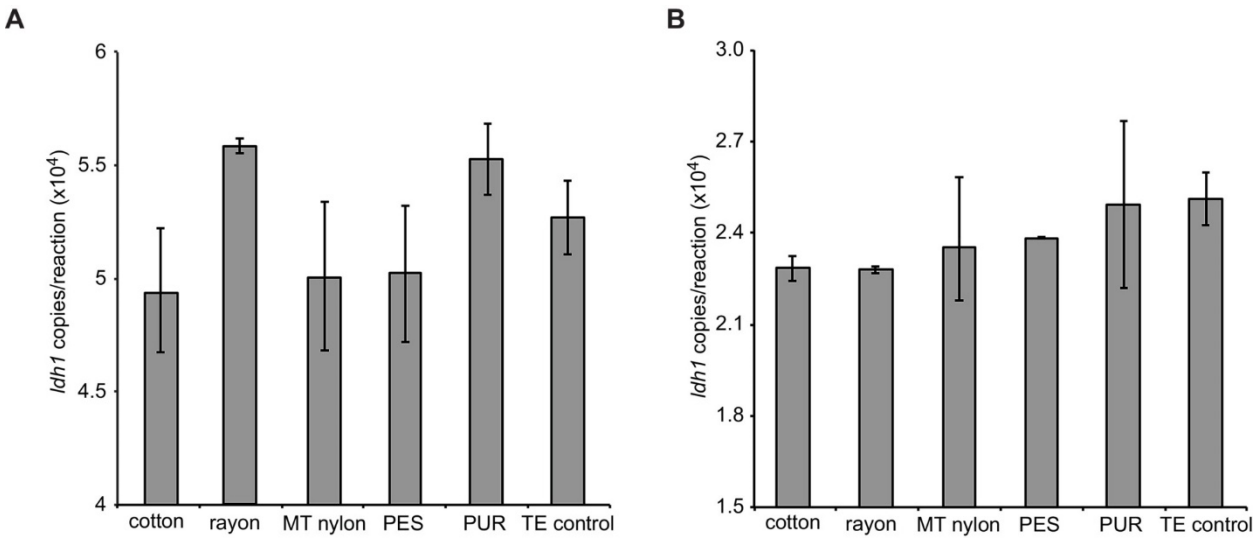

Figure S10.42 | Testing effect of swab components on ACP lysis and qPCR.

The eluate from different dry swabs was added to the qPCR reaction or ACP lysis mixture to test for chemical interference by components leached from the swabs. Swabs (PES, PUR, MT Nylon, Rayon, Cotton (N = 3)) were dipped into 128 µL TE buffer and agitated by 10 second 1 Hz twirl to generate swab eluate. Lysis and qPCR efficiency in presence and absence of swab eluate from each swab type were compared. (**A**) For qPCR experiments, each reaction contained the mixture of 5 µL of 10,000 S. aureus genomic copies with 4 µL of different swab eluate or 4 µL of TE alone. ldh1 copies (mean ± SE) estimated by qPCR were plotted. (**B**) For lysis experiments, the mixture of 50 µL of 5×104 CFU of S. aureus/TE and 50 µL of different swab eluate or TE alone were mixed with 17.6 ACP (20 U/µL) and underwent lysis at room temperature for 2 minutes. The ACP was then deactivated by heating at 95°C for 10 minutes. 9 µL of lysate was analyzed by qPCR. ldh1 copies/reaction in the lysate (mean ± SE) of each sample was plotted. Based on the ACP lysis (in TE case) the estimated number of ldh1 copies/CFU was 6.5: (25,000 copies/9 µL lysate) :(5×10^4 CFU/117.6 µL lysate). No significant difference among samples was found in A and B (One-way ANOVA, p = 0.4211 and 0.7073 respectively). Note that the vertical axis does not span to zero, which makes error bars appear artificially large.

© Copyright 2021 | N Panpradist

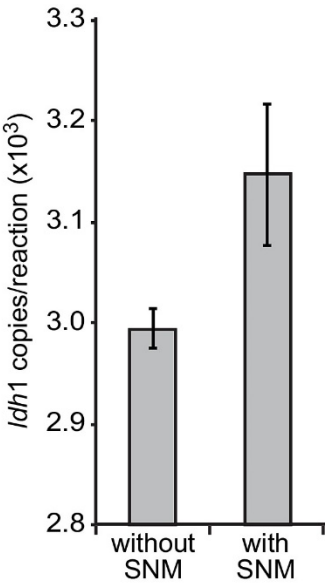

Figure S10.43 | Effect of simulated nasal matrix (SNM) on qPCR and ACP lysis efficiency.

100 µL of 105 CFU S. aureus solution/TE, either with or without the addition of 15 µL of SNM, was mixed with 17.6 µL of ACP (20 U/µL) and then kept at room temperature for 2 minutes. The lysis was then deactivated by heating at 95°C for 10 minutes and each tube was added with TE to bring up the final volume to 200 µL. 2 µL of final lysate was added in each qPCR reaction. The graph compares the number of ldh1 copies/reaction (mean ± SE; N = 4) from lysate in both cases (with and without SNM). Based on the lysate without SNM, the number of ldh1 copies/CFU was 3; (3,000 copies/2 µL lysate):(10^5 CFU/200 µL lysate). One-way ANOVA did not indicate the significant difference ($p = 0.08$). Note that the vertical axis does not span to zero, which makes error bars appear artificially large.

© Copyright 2021 | N Panpradist

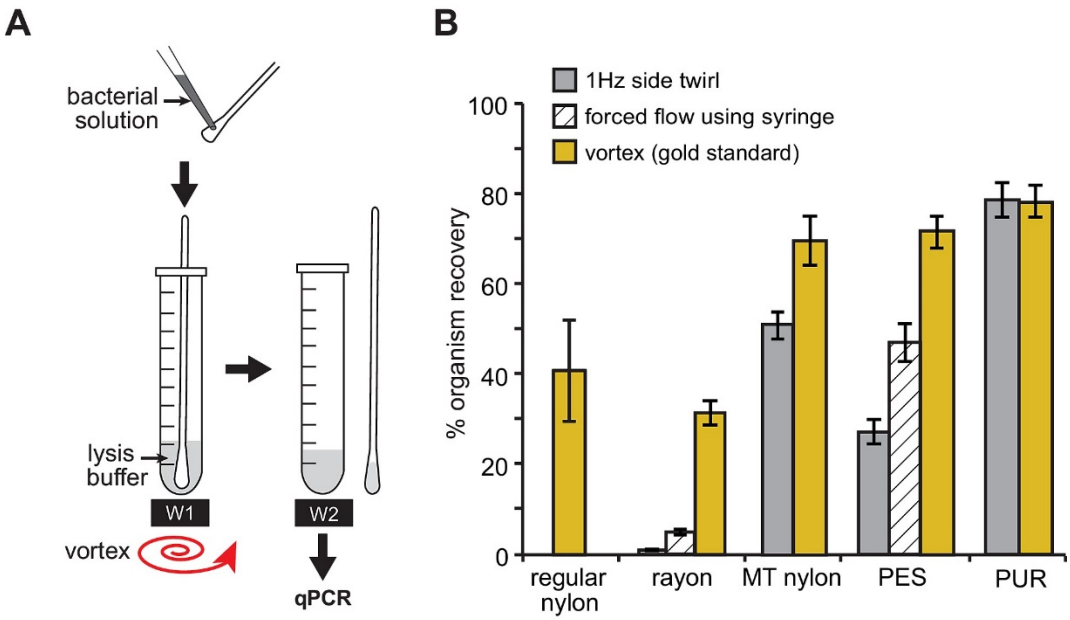

Figure S10.44 | Vortexing (gold standard) swab transfer.

(**A**) Schematic of experimental set up. 15 µL S. aureus/TE (104 CFU equivalent to 6×104ldh1 copies) was spiked onto the swab, which was then agitated in 128 µL lysis buffer using 10-second vortexing and removed. (**B**) Comparison of the % Organism Recovery in five swabs (mean ± SE, N=5), which was calculated using Equation 5 in the text. (**C**) Comparison of the % Organism Recovery of four swabs (mean ± SE; N=5) using vortexing and manual 10 second, 1 Hz side twirl. (**D**) Comparison of the % Organism Recovery of two swabs (mean ± SE; N=5) using vortexing and forced flow using syringe method.

© Copyright 2021 | N Panpradist

Table S10.4 Summary of experimental data (mean ± SE, N = 5).

volume recovery						
	Cotton	MT Nylon	PES	PUR	Rayon	Regular Nylon
	8 ± 0.6 %	70 ± 0.8%	81 ± 0.3%	89 ± 0.4%	56 ± 2.5%	30 ± 3.4%
organism recovery						
low-volume sample						
S.aureus (CFU/swab) without SNM		MT Nylon	PES	PUR	Rayon	
10^6		57 ± 7.4 %	65 ± 7.4 %	87 ± 3.5 %	2 ± 0.9 %	
10^4		51 ± 3.0 %	27 ± 2.9 %	79 ± 3.9 %	1 ± 0.1 %	
100		70 ± 4.0 %	21 ± 3.6 %	98 ± 5.8 %	12 ± 2.9 %	
S.aureus (CFU/swab) with SNM			PES	PUR		
10^6			54 ± 9.9 %	101 ± 12.6 %		
10^4			38 ± 2.3 %	84 ± 4.1 %		
100			62 ± 5.2 %	93 ± 5.6 %		
Agitation methods		MT Nylon	PES	PUR	Rayon	Regular Nylon
1Hz-side 10s			27 ± 2.9 %	79 ± 4.0 %	1 ± 0.1%	
1Hz side 30s			31 ± 3.8 %	70 ± 1.0 %	2 ± 0.2 %	
2Hz-side 10s			25 ± 1.8 %	72 ± 1.7 %	2 ± 0.3 %	
1Hz-bottom 10s			18 ± 3.6 %	71 ± 4.7 %	2 ± 0.2%	
1Hz-random 10s			19 ± 1.7 %	66 ± 2.2 %	3 ± 0.2 %	
forced-flow using syringe			47 ± 4.3 %		5 ± 0.7 %	
vortex 10 s		69 ± 5.4%	72 ± 3.6 %	78 ± 3.6 %	31 ± 2.9 %	41 ± 11.3%
excess-volume sample						
swab pre-condition		MT Nylon	PES	PUR	Rayon	
dry		1.1 ± 0.08	0.9 ± 0.10	2.6 ± 0.40	0.8 ± 0.15	
wet		0.5 ± 0.06	0.3 ± 0.07	2.3 ± 0.31	0.7 ± 0.80	
dried sample						
swab pre-condition			PES	PUR	Rayon	Regular Nylon
dry			25 ± 3.3 %	27 ± 3.6 %	15 ± 1.4 %	27 ± 2.5%
wet			26 ± 4.2 %	30 ± 1.0 %	21 + 2.7 %	37 ± 2.1%

© Copyright 2021 | N Panpradist

Table S10.5 | Coefficient of variation (CV) of experimental data (N=5).

volume recovery						
	Cotton	MT Nylon	PES	PUR	Rayon	Regular Nylon
	0.170	0.025	0.008	0.011	0.100	0.250
organism recovery						
low-volume sample						
S.aureus (CFU/swab) without SNM		MT Nylon	PES	PUR	Rayon	
10^6		0.292	0.252	0.090	1.105	
10^4		0.132	0.240	0.110	1.311	
100		0.127	0.374	0.132	0.532	
S.aureus (CFU/swab) without SNM			PES	PUR		
10^6			0.409	0.280		
10^4			0.136	0.110		
100			0.189	0.135		
Agitation methods		MT Nylon	PES	PUR	Rayon	Regular Nylon
1Hz-side 10s			0.240	0.110	1.311	
1Hz side 30s			0.274	0.031	0.299	
2Hz-side 10s			0.165	0.051	0.300	
1Hz-bottom 10s			0.448	0.148	0.263	
1Hz-random 10s			0.198	0.074	0.190	
Forced-flow using syringe			0.202		0.299	
Vortex 10s		0.174	0.114	0.104	0.203	0.618
saturated-volume sample						
swab pre-condition		MT Nylon	PES	PUR	Rayon	
dry		0.170	0.240	0.344	0.431	
wet		0.253	0.443	1.305	0.244	
dried sample						
swab pre-condition			PES	PUR	Rayon	Regular Nylon
dry			0.293	0.302	0.208	0.213
wet			0.361	0.078	0.285	0.130
Effect of swab component on analysis						
	Cotton	MT Nylon	PES	PUR	Rayon	
lysis	0.032	0.150	0.002	0.190	0.009	
qPCR	0.095	0.113	0.103	0.060	0.010	

© Copyright 2021 | N Panpradist

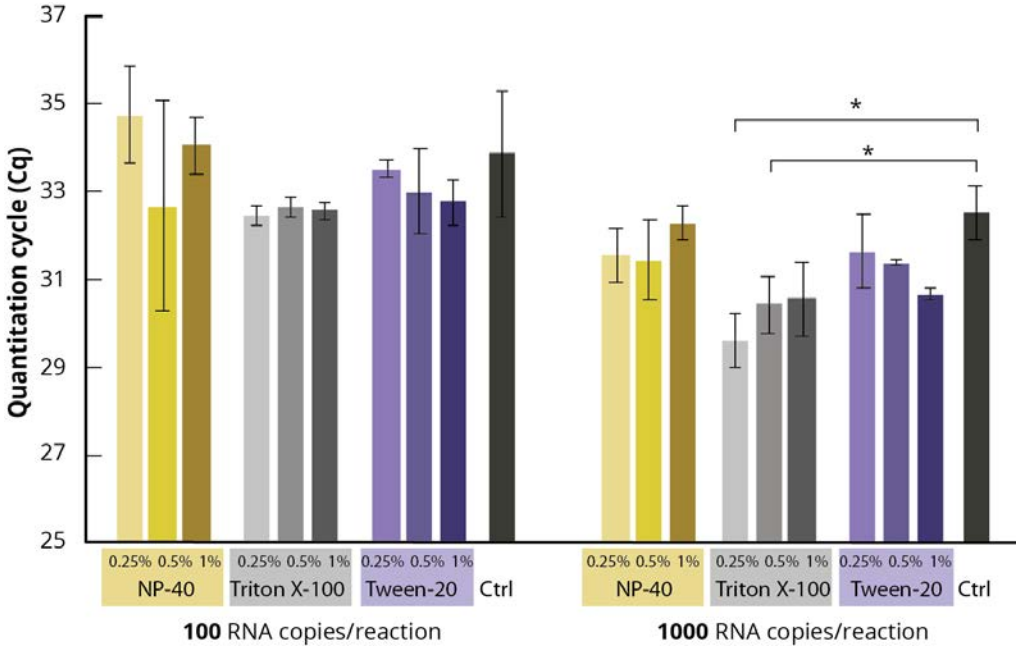

Figure S10.45 | Effect of detergents on RT-PCR formulations.

Tween-20, NP-40, or TritonX-100 was added to the RT-qPCR reactions at 0.25%, 0.5%, and 1% v/v. The quantitation cycles, Cq, (mean±SD, n=3) from reactions containing 100 or 1000 RNA copies/reaction were compared to a no-detergent control (Ctrl). In each condition, we also included no template controls (*n=3*) and none of these reactions had detected Cq. * p-value <0.05 (Student's t-test with Holm-Bonferroni correction).

© Copyright 2021 | N Panpradist

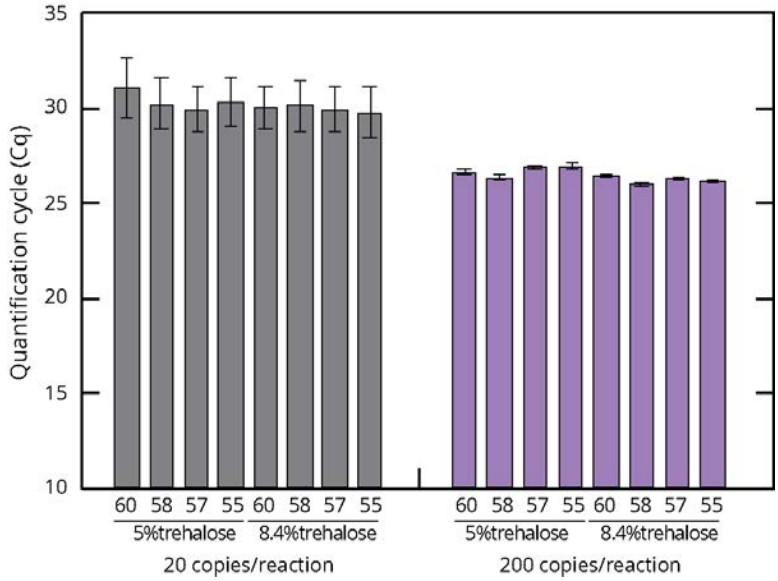

Figure S10.46 | Optimization of RT-PCR protocol.

Different trehalose concentrations and annealing/extension temperatures in two-stage RT-PCR were tested. RT-PCR reactions in the presence of either 5% or 8.4% w/v trehalose were run using different annealing temperatures (55 – 60°C) at 0, 20, or 200 copies/reaction.

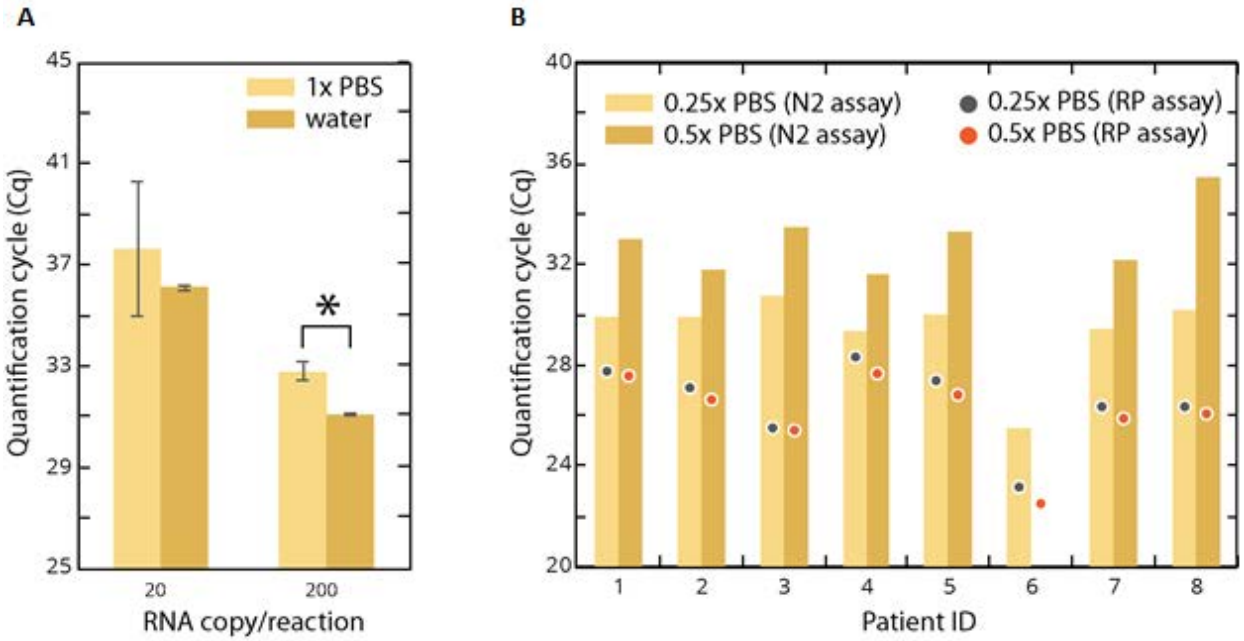

Figure S10.47 | Effect of PBS and human nasal matrix on lyophilized RT-PCR.

(A) Effect of PBS on RT-qPCR. Purified SARS-CoV-2 RNA (0, 20 or 200 copies/reaction) were amplified in lyophilized RT-qPCR reactions rehydrated by the buffer containing 1xPBS or water. (**B**) Effect of PBS and human nasal matrixes. 8 human swab elutes either undiluted (1x PBS), 1:2 diluted (0.5x PBS),

© Copyright 2021 | N Panpradist

and 1:4 diluted (0.25x PBS) were used to rehydrate lyophilized RT-qPCR reactions in the presence of 0 or 500 SARS-CoV-2 RNA copies.

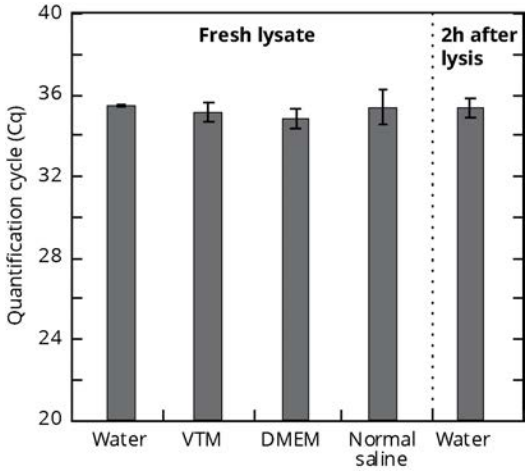

Figure S10.48 | Direct amplification of Accuplex™ packaged RNA in viral envelope.

To study the feasibility of lysis, we used the Accuplex™ (Seracare), and control to evaluate the full process (from virus to amplification) as it was previously used by commercial assay developers (e.g., Cepheid) to evaluate SARS-CoV-2 assay to obtain US EUA. Lyophilized RT-PCR rehydrated with 0.5% Triton-X100, 2mM MgSO, and 0.25x challenging media or water was spiked with 25 copies of enveloped RNA. Media used were viral transport medium (VTM, BD 220531), Dulbecco's modified eagle's medium (Sigma, D5796), Normal saline (0.9% NaCl). Water control (i.e. no challenging media) was either amplified immediately or amplified after 2h storage at 4°C. The quantitation threshold (Cq) was automatically reported by the CFX software.

© Copyright 2021 | N Panpradist

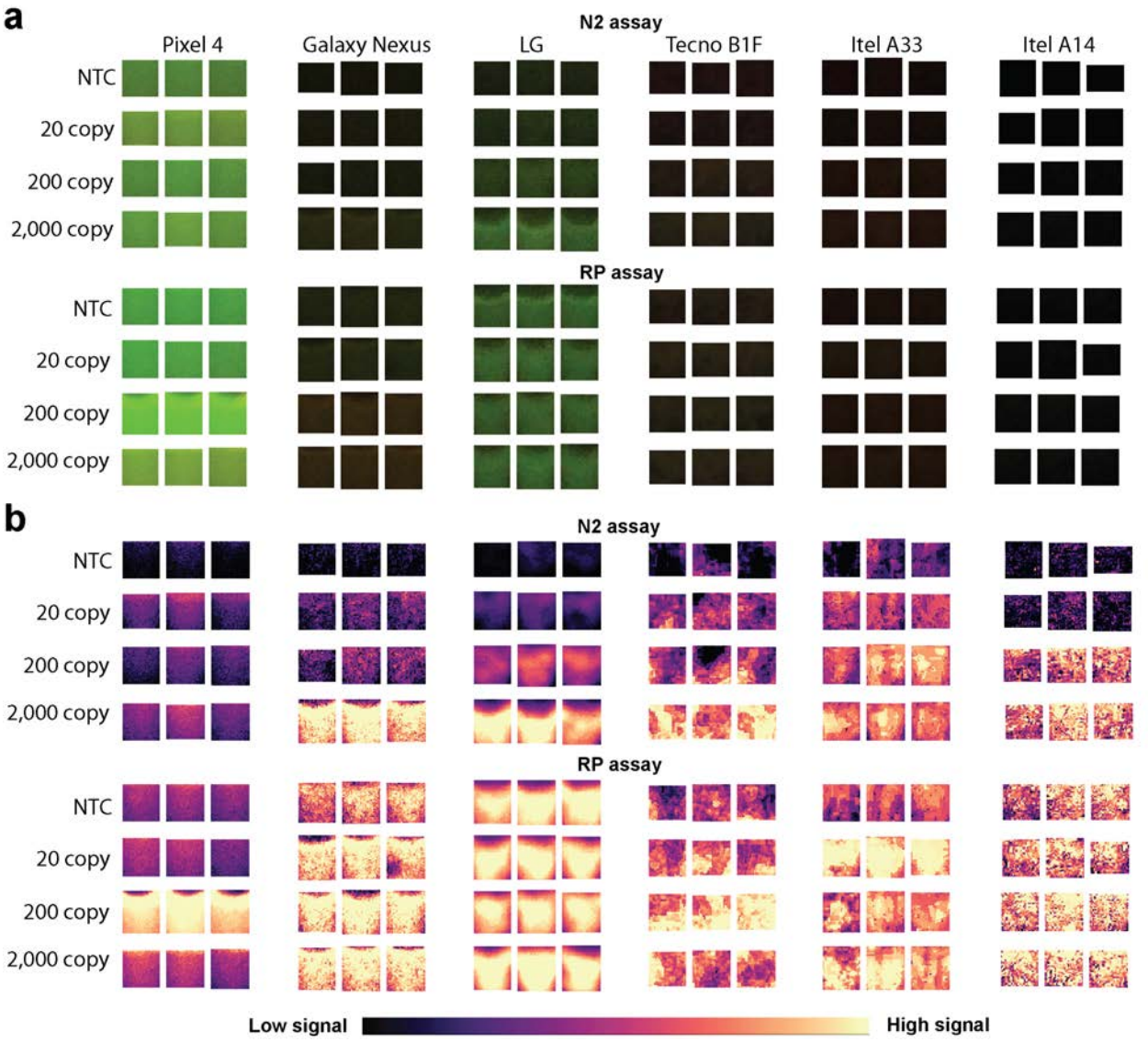

Figure S10.49 | Cell phone raw and processed images of workflow-2 under a transiluminator.

Side-by-side comparison of **(A)** raw and **(B)** processed images of the reaction tubes from the scenario-2 workflow under a transilluminator captured by different cell phones.

© Copyright 2021 | N Panpradist

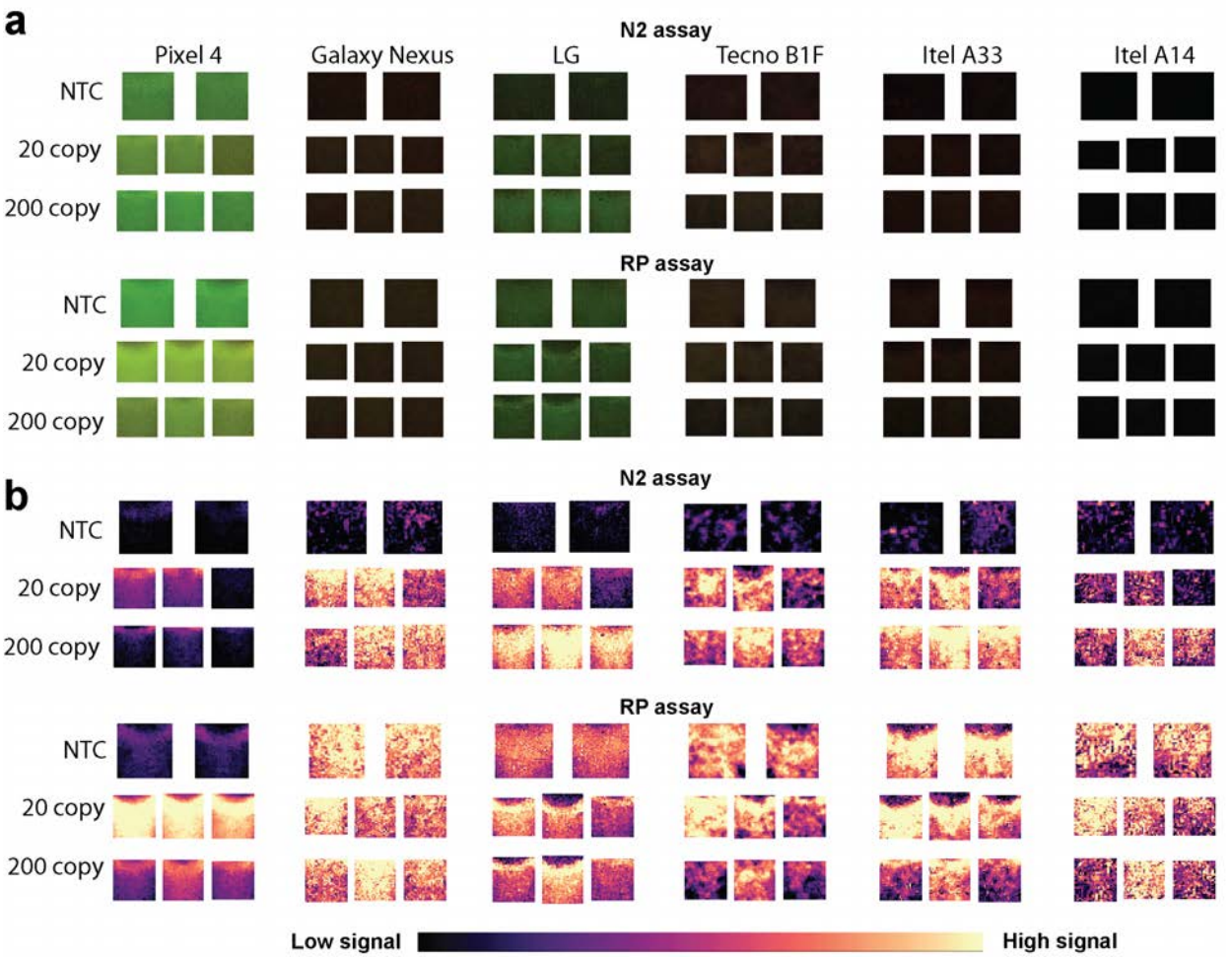

Figure S10.50 | Cell phone raw and processed images of workflow-3 under a transilluminator.

Side-by-side comparison of (**A**) raw and (**B**) processed images of the reaction tubes from the scenario-3 workflow under a transilluminator captured by different cell phones.

© Copyright 2021 | N Panpradist

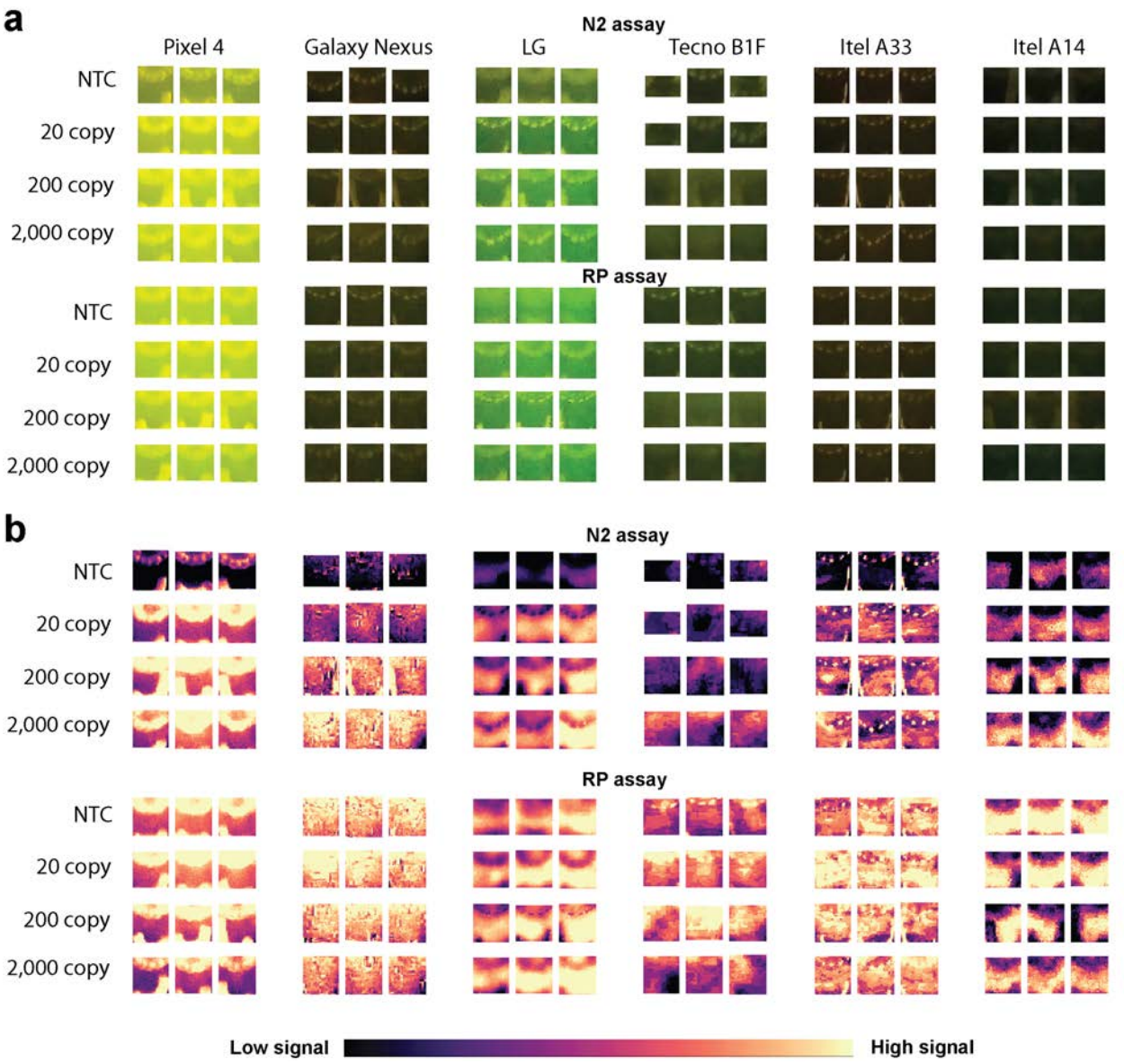

Figure S10.51 | Cell phone raw and processed images of workflow-2 under glow box. Side-by-side comparison of (**A**) raw and (**B**) processed images of the reaction tubes from the scenario-2 workflow under the glow box captured by different cell phones.

© Copyright 2021 | N Panpradist

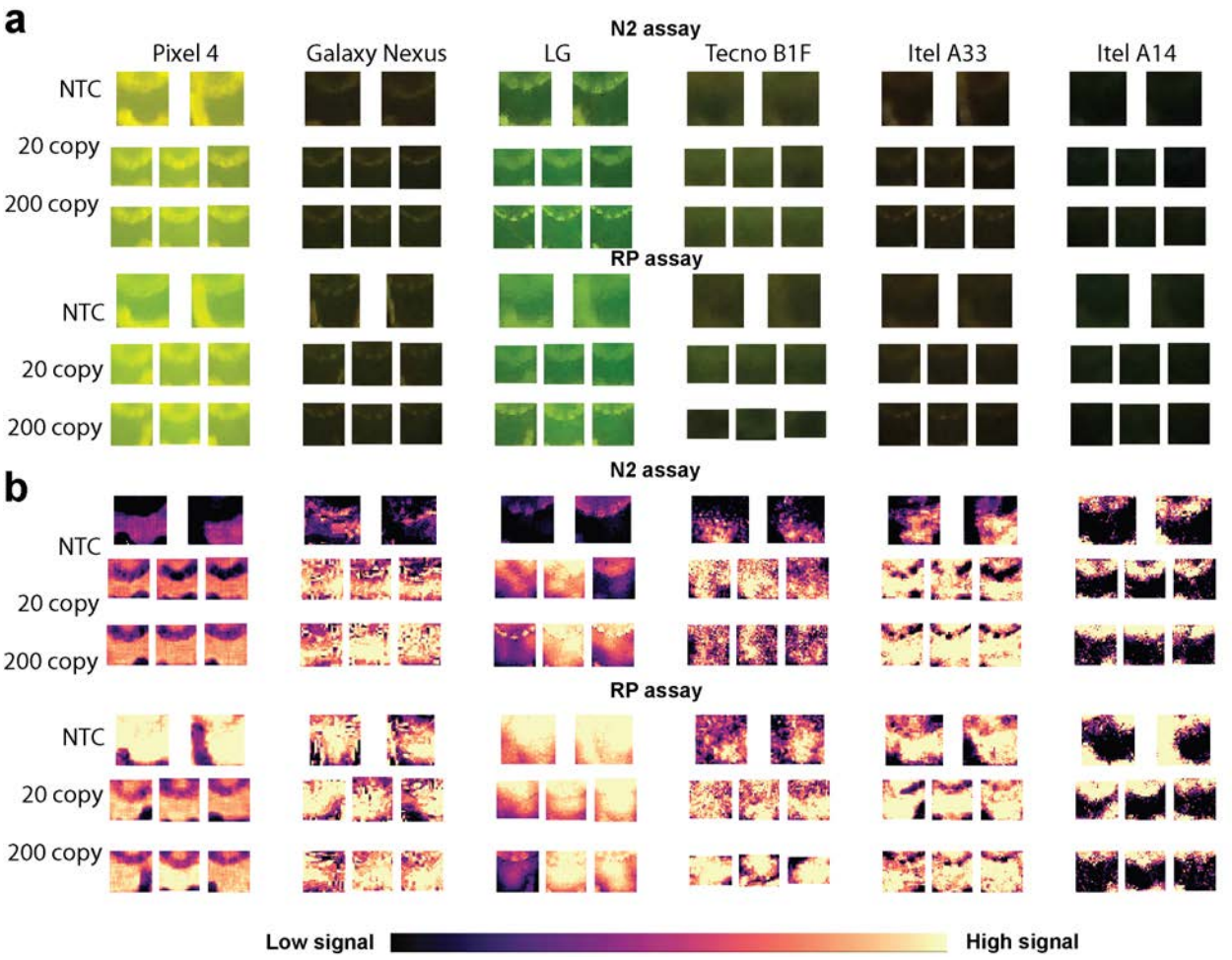

Figure S10.52 | Cell phone raw and processed images of workflow-3 under glow box.

(**A**) raw and (**B**) processed images of the reaction tubes from the scenario-3 workflow under the glow box captured by different cell phones.

© Copyright 2021 | N Panpradist

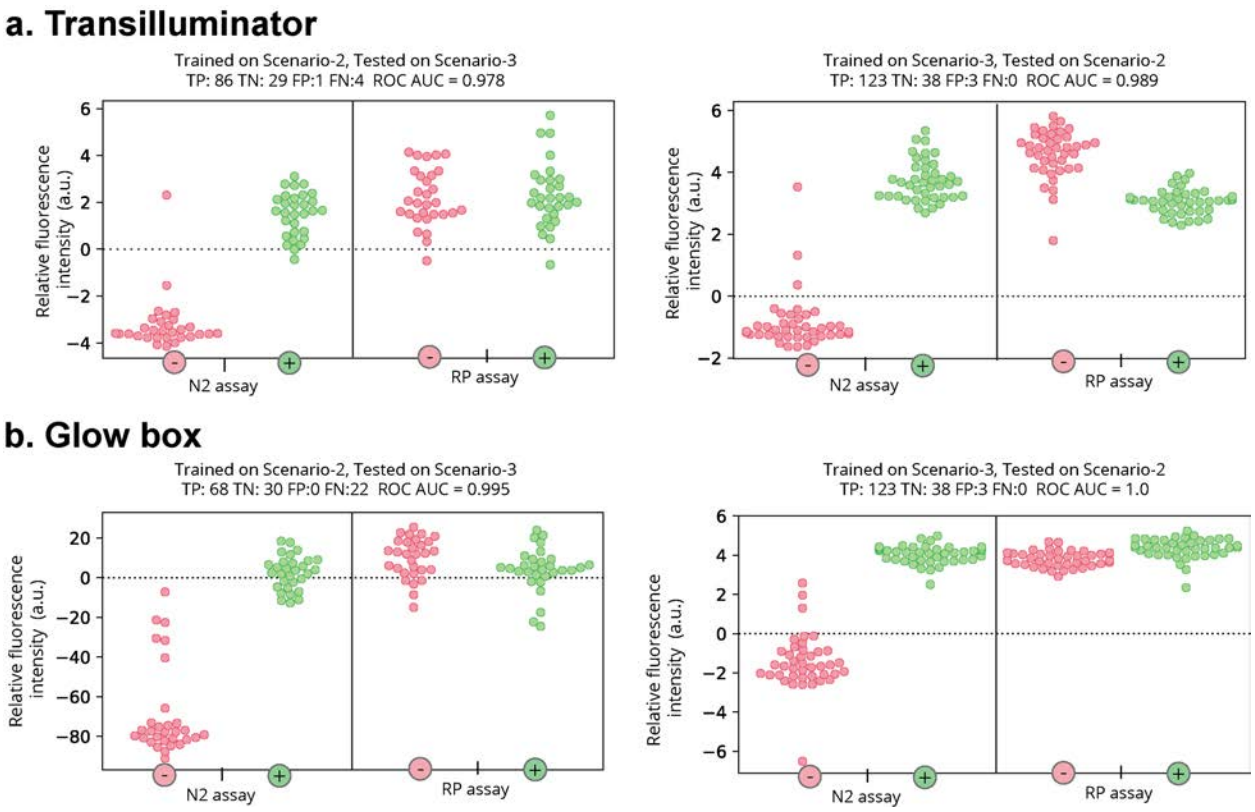

Figure S10.53 | Two-fold cross validation of using patient sample data.

Images from scenarios 2 and 3 are used as separate folds to train linear SVMs from RGB pixel space to fluorescence intensity data for (A) transilluminator and (B) glow box. The number of true positive (TP), true negative (TN), false positive (FP), and false negative (FN) predictions are shown, alongside receiver operating characteristic area under the curve (ROC AUC). The high ROC AUC values show that the transformation from RGB pixels to fluorescence values generalizes across datasets, while errors are mainly due to differences in fluorescence thresholds, which are attributed.to the differences in chemistries in scenarios 2 and 3.

© Copyright 2021 | N Panpradist

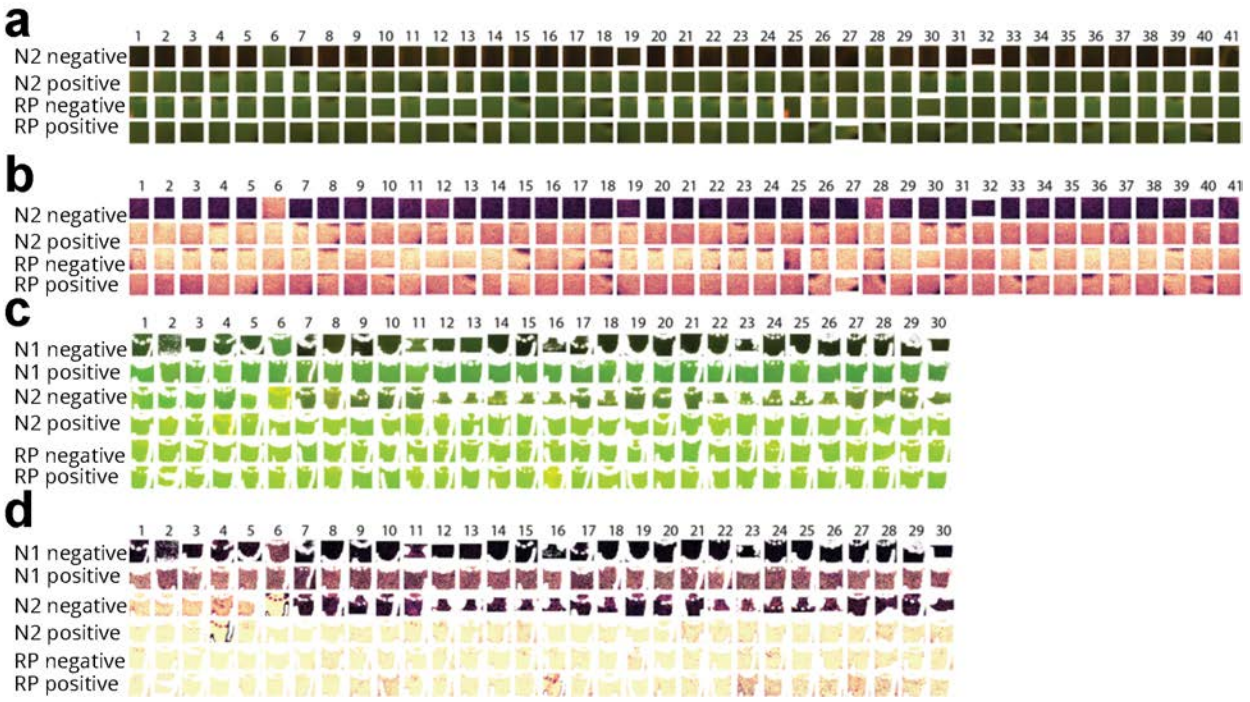

Figure S10.54| Raw and processed images of patient specimens.

(A) Raw and (B) Processed images of tube reactions in scenario-2 workflow. (C) Raw and (D) Processed images of tube reactions in scenario-3 workflow.

© Copyright 2021 | N Panpradist

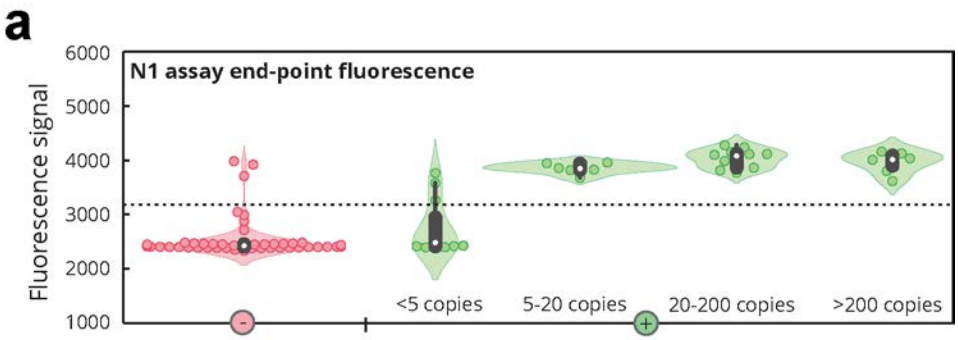

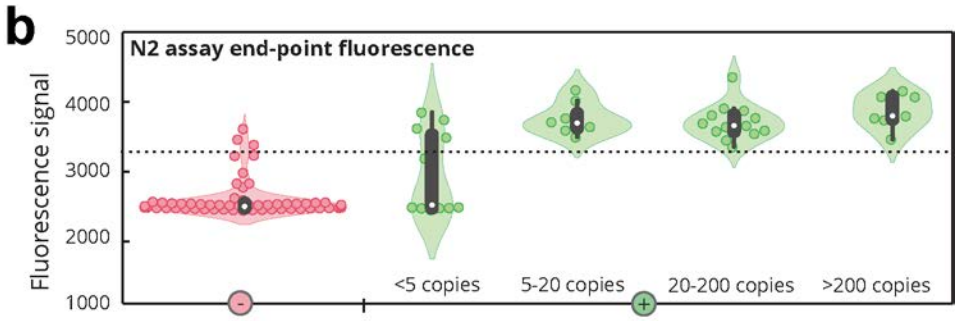

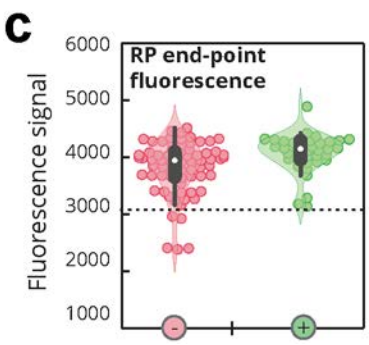

d

Modified method \ Standard method	Positive	Negative	IND[1]	INC[2]
Positive	31	2		
Negative	6	47	8	5
IND[3]		4	1	
INC[4]	3	3		

1) Indeterminate (IND) - not detected by N1, N2, or RP
2) Inconclusive (INC) by standard method (detectable by either N1 or N2)
3) Indeterminate (IND) - not detectable by N1 or N2
4) INC according to the modified protocol (detectable by N2, not N1)

Figure S10.55 | Validation of our modified protocol on clinical VTM specimens using end-point fluorescence values measured by a real-time PCR machine at room temperature.

(**A**) for N1 primers, (**B**) N2 primers, and (**C**) RP primers, grouped by negative and positive samples at different concentrations. Dotted lines show the positive thresholds for N2 and N1 primer assays. The mean of each group is presented as the white circle with interquartile range box as well as range. The density distribution is also shown. (D) Qualitative comparison of positive, negative, indeterminate (IND), inconclusive (INC) results from the modified protocol vs standard protocol.

Table S10.6 | Comparison of the analytical sensitivity of EUA-approved nucleic acid tests.

© Copyright 2021 | N Panpradist

Manufacturer	Name of Test	Stated LoD (c/μL)	Estimated copies in human sample /1 mL VTM	Concen-tration of eluate (copies/μL)	Volume eluate added to RT-PCR master mix (μL)	Copies/ Reaction
SD Biosensor, Inc.	STANDARD M nCoV Real-Time Detection Kit*	0.13	125	0.417	10	4.17
SD Biosensor, Inc.	STANDARD M nCoV Real-Time Detection Kit*	0.5	500	9.091	10	16.67
Seegene, Inc.	Allplex 2019-nCoV Assay	1.25	1250	3.75	8	30
Trax Management Services Inc.	PhoenixDx 2019-CoV	0.1	100	`n/a	5	n/a
OSANG Healthcare	GeneFinder COVID-19 Plus RealAmp Kit	0.5	500	1.4	5	7
Fosun Pharma USA Inc.	Fosun COVID-19 RT-PCR Detection Kit	0.3	300	1	10	10
GenoSensor, LLC	GS COVID-19 RT-PCR KIT	1	1000	2.333	13	30.33
KorvaLabs Inc.	Curative-Korva SARS-Cov-2 Assay	0.2	200	1	5	5
Maccura Biotechnology (USA) LLC	SARS-CoV-2 Fluorescent PCR Kit*	0.2	200	4	20	80
Maccura Biotechnology (USA) LLC	SARS-CoV-2 Fluorescent PCR Kit*	1	1000	5.71	20	114.29
Atila BioSystems, Inc.	iAMP COVID-19 Detection Kit***	4	4000	4	15	60
Becton, Dickinson & Company	BD SARS-CoV-2Reagents for BD MAX System^	0.04	40	1.92	n/a	n/a
DiaCarta, Inc.	QuantiVirus SARS-CoV-2 Test kit*	0.2	200	1	5.5	5.5
DiaCarta, Inc.	QuantiVirus SARS-CoV-2 Test kit*	0.1	100	0.5	5.5	2.75
InBios International, Inc.	InBios Int. Smart Detect	1.1	1100	2.567	5	12.83
Gnomegen LLC	Gnomegen COVID-19 RT-Digital PCR Detection Kit**	0.86	860	2.007	4	8.03
Co-Diagnostics, Inc.	Logix Smart Coronavirus Disease 2019 (COVID-19) Kit	4.29	4290	6.006	5	30.03
ScienCell Research Laboratories	ScienCell SARS-CoV-2 Coronavirus Real-time RT-PCR (RT-qPCR) Detection Kit	3.16	3162.28	7.379	5	36.89
Luminex Corporation	ARIES SARS-CoV-2 Assay^	75	75000	n/a	n/a	n/a
Becton, Dickinson & Company (BD)	BioGX SARS-CoV-2 Reagents for BD MAX System^	0.04	40	n/a	n/a	n/a
Ipsum Diagnostics, LLC	COV-19 IDx assay	8.5	8500	n/a	n/a	n/a
QIAGEN GmbH	QIAstat-Dx Respiratory SARS-CoV-2 Panel^	0.5	500	n/a	n/a	n/a
NeuMoDx Molecular, Inc	NeuMoDx SARS-CoV-2 Assay^	0.15	150	n/a	n/a	n/a
Luminex Molecular Diagnostics, Inc.	NxTAG CoV Extended Panel Assay 5		5000	9.091	35	318.18
Abbott Diagnostics Scarborough, Inc.	ID NOW COVID-19^	0.13	125		n/a	n/a
BGI Genomics Co. Ltd	Real-Time Fluorescent RT-PCR Kit for Detecting SARS-CoV-2	0.15	150	0.35	10	3.5
Avellino Lab USA, Inc.	AvellinoCoV2 test	55	55000	128.333	2.15	275.92
PerkinElmer, Inc.	PerkinElmer New Coronavirus Nucleic Acid Detection Kit*	0.01	9.31	0.062	40	2.48
PerkinElmer, Inc.	PerkinElmer New Coronavirus Nucleic Acid Detection Kit*	0.02	24.88	0.166	40	6.63
Mesa Biotech Inc.	Accula SARS-Cov-2 Test^***	3.33	3330	n/a	n/a	n/a
BioFire Defense, LLC	BioFire COVID-19 Test^	0.33	330	n/a	n/a	n/a
Cepheid	Xpert Xpress SARS-CoV-2 test^	0.25	250	n/a	n/a	n/a
Primerdesign Ltd	Primerdesign Ltd COVID-19 genesig Real-Time PCR assay	0.33	330	0.77	9	6.93
GenMark Diagnostics, Inc.	ePlex SARS-CoV-2 Test^	100	100000	n/a	n/a	n/a

n/a = not available.
Tests approved after 4/23/2020 were excluded; unless explicitly stated otherwise, all LoDs were assumed to be the concentration of the primary sample prior to extraction/purification; tests that reported LoD in PFU or TCID50 were excluded; for multiple sample types but the same extraction/amplification protocol, worst performing sample was included. All values are estimates and do not account for loss of viral RNA during the extraction/purification step. (Centre for Devices and Radiological H...)
^Test processes are contained to a single cartridge and no specific reaction volumes were included
*Multiple LoDs reported in IFU, high and low LoDs reported here.
***Protocol does not include an extraction/purification step

© Copyright 2021 | N Panpradist

Table S10.7 | Commercially available quantitative RT PCR machine

Model	Vendor	Cost
LightCycler 480	Roche	$39,990
CFX Connect Real Time	Bio-Rad	$27,000
7500 Real Time	Applied Biosystems	$53,000
Rotor-Gene Q	Qiagen	$25,390
Open PCR	ChaiBio	$4,999
Quanti Studio 3.0	ThermoFisher	$22,000

Table S10.8 | Commercially available thermal cycler and the listed price

Model	Vendor	Cost
T100	Biorad T100	$3,035
MiniAmp Thermocycler	Thermofisher	$2,500
Surecycler 8800	Agilent	$2,000
Biometra TONE	Analytik Jena	$6,700
16-well PCR	MiniPCR	$775

Table S10.9 | Commercially available fluorescence reader

Model	Vendor	Cost
Transilluminator	MiniPCR	$250-$350
P51	MiniPCR	$28

Table S10.10 | List prices for the mobile phones used in this study

Model	Vendor	Cost
OnePlus 7 Pro	OnePlus	$499
Google Pixel4	Google Store	$799
Galaxy Nexus 4.2	Amazon	$130
LG X300	Gadgets Now	$195
Galaxy S4	Amazon	$129
Itel A33, Transsion	Jumia	$51
Itel A14, Transsion	Jumia	$37
Tecno B1fcell phones	Simba Telecom	$81

© Copyright 2021 | N Panpradist

Table S10.11 | Comparison of Quantification Cycle (Cq) values from N1, N2, and RP primers using the standard vs modified protocol.

Negative COVID-19 samples were also tested for other respiratory pathogens using the microarray. MTB and NP are mid-turbinate and nasopharyngeal swabs, respectively.

ID	Date	Swab type	Modified protocol			Standard CDC			Adenovirus	Seasonal Coronavirus	Influenza	RSV	Parainfluenza virus	Meta pneumovirus	Enterovirus	Parechovirus	Bocavirus	Rhinovirus	Pneumoniae	RnaseP	Xeno (Spike-control)
			N1	N2	RP	N1	N2	RP													
1	11/27/19	MTB																17.2		19.6	18.4
2	N/A	N/A											23.6							26.9	18.7
3	3/31/20	MTB																	25.8		18.4
4	11/27/19	MTB			38.5															25.8	17.8
5	3/2/20	N/A			38.0										27.3			26.6	23.3	22.0	18.1
6	11/19/19	MTB			37.1				27.5		18.3							24.3			17.4
7	N/A	N/A			35.7																17.7
8	11/17/19	MTB			34.7													17.2		19.6	18.4
9	11/21/19	MTB			27.9													15.1	11.6	12.3	16.8
10	3/5/20	NP						27.4											25.5	24.0	17.8
11	4/1/20	MTB			39.1			31.7											26.7	20.1	18.4
12	N/A	MTB			38.0			30.0											10.5		18.4
13	4/1/20	N/A			36.3			29.7			14.4							22.7		19.9	17.4
14	11/17/19	MTB			38.1			29.6											25.5	21.9	17.2
15	11/20/19	MTB			35.7			44.1												24.4	17.8
16	3/6/20	NP			35.6			37.1			16.3							26.5		19.0	18.5
17	2/24/20	MTB			35.4			42.5													17.4
18	N/A	MTB			35.4			32.5	27.0						23.8			25.1	20.2	19.2	17.1
19	12/2/19	MTB			34.9			32.2											20.9	23.1	17.7
20	11/19/19	MTB			34.8			37.8											26.7		18.3
21	2/27/20	MTB			34.6			35.9									20.2			16.7	17.1
22	3/31/20	MTB			34.6			34.7	18.4	21.9									15.8	18.6	17.8
23	2/20/20	N/A			34.4			30.3										24.1	13.5	16.5	16.8
24	3/4/20	MTB			34.2			35.0									20.3			21.0	16.6
25	11/18/19	N/A			33.6			34.1										18.8	18.3	16.3	16.8
26	11/9/19	MTB			33.5			33.2									26.7			19.5	17.4
27	12/11/19	MTB			33.5			26.2												26.2	18.3
28	11/29/19	MTB			33.5			34.6			9.3										17.5
29	N/A	N/A			33.3			50.0			13.3							18.0		19.1	17.8
30	2/26/20	MTB			33.3			35.2			22.4							21.7		18.2	17.7
31	11/20/19	MTB			33.0			37.9												27.3	17.3
32	11/27/19	MTB			32.4			41.0		25.2										18.5	17.5
33	11/17/19	MTB			32.0			27.1										26.1		14.5	17.6
34	11/17/19	MTB			31.5			31.2												22.1	17.1
35	11/19/19	MTB			31.5			32.4			19.9								15.8	12.8	16.8
36	3/29/20	N/A			31.4			31.3											27.0	23.6	17.9
37	11/19/19	MTB			31.3			31.2	26.3										25.2	23.4	17.7
38	N/A	MTB			31.1			30.2			20.9							24.0	25.1	17.5	16.9
39	4/3/20	N/A			31.1			26.3			15.6							22.5	27.0	20.1	17.8
40	11/17/19	MTB			30.8			30.3	26.8	26.0							26.3		24.1	22.4	17.8
41	N/A	MTB			30.7			34.6												N/A	N/A
42	N/A	MTB			30.7			28.4						25.5						13.9	17.7
43	2/27/20	MTB			30.6			31.1			27.3									18.8	17.2
44	12/2/19	MTB			30.5			31.0					27.3							16.1	16.9
45	11/19/19	MTB			30.4			33.9			21.5							26.9		17.0	17.2
46	3/23/20	MTB			30.3			30.8										27.1		21.7	18.3
47	4/4/20	MTB			30.3			31.0			19.5							22.5		21.0	17.7
48	4/1/20	MTB			30.3			28.48*											20.3	21.5	18.5
49	11/19/19	MTB			30.2			33.9										26.0		17.3	17.7
50	4/1/20	MTB			30.2			33.6			15.8									25.7	17.0
51	11/9/19	MTB			29.5			29.0											25.6	17.1	17.8
52	11/20/19	MTB			29.5			30.4												18.7	18.4
53	3/31/20	MTB			29.4			29.3		22.7										19.6	17.5
54	4/1/20	MTB			29.1			29.1										27.2		18.7	17.4
55	11/20/19	MTB			29.1			28.7										27.8		22.4	17.4
56	4/4/20	MTB			28.9			40.7			17.9									18.4	17.2
57	12/2/19	MTB			28.6			27.6										14.9	14.0	16.8	16.8
58	3/2/20	MTB			28.6			29.8												N/A	N/A
59	2/20/20	MTB			28.5			29.2											25.5	24.0	17.8
60	N/A	N/A			28.5			29.0										22.4		16.5	17.7
61	3/7/20	MTB			28.2			32.9		24.4								17.0		17.1	16.9
62	3/25/20	MTB			27.5			31.3										16.5	16.8		16.5
63	12/2/19	MTB			27.1			27.2								27.9				14.7	18.4
64	3/23/20	MTB			27.0			20.74*												N/A	N/A
65	11/20/19	MTB			26.3			29.1										19.9	15.6	17.1	16.8
66	11/19/19	MTB			26.0			26.2		24.4	20.2									21.6	17.4
67	3/8/20	MTB			24.4			25.6												24.9	18.1
68	12/2/19	MTB			24.1			31.9												15.2	17.7
69	11/19/19	MTB			23.8			23.6			23.4								16.8	17.2	17.2
70	11/20/19	MTB			23.4			23.9												14.2	17.8

© Copyright 2021 | N Panpradist

ID	Date	Swab type	Modified protocol			Standard CDC			Adenovirus	Seasonal Coronavirus	Influenza	RSV	Parainfluenza virus	Meta pneumovirus	Enterovirus	Parechovirus	Bocavirus	Rhinovirus	Pneumoniae	RnaseP	Xeno (Spike-control)	
			N1	N2	RP	N1	N2	RP														
71	3/23/20	MTB	37.8	38.6	29.7			30.9												18.6	17.5	
72	N/A	N/A		38.5	32.0	40.8		30.2												23.9	16.6	
73	3/23/20	MTB	36.9	38.1	31.5	37.3		31.6												16.9	17.8	
74	3/23/20	MTB	31.6	34.0	26.3	32.2*		23.7*												16.6	17.6	
75	3/23/20	MTB	28.1	32.0	23.7	23.2*		24.2*												N/A	N/A	
76	N/A	MTB			28.1	41.9	38.3	26.5												12.6	24.6	<5 copies/ reaction
77	11/20/19	MTB		37.5	25.2	37.7	37.3	24.7												11.7	16.6	
78	3/3/20	N/A	33.6	35.7	26.9		36.4	26.4												12.9	19.4	
79	N/A	MTB	39.1	37.0	30.2	33.3	36.3	29.0										26.8		14.0	23.1	
80	3/31/20	MTB	41.7		26.6	35.4	35.5	25.7												12.0	16.5	
81	4/2/20	MTB	33.0	34.0	26.7	33.7	35.1	27.3												15.7	18.3	
82	3/10/20	MTB	35.7	36.7	28.4	33.1	34.1	28.3											22.9	16.9	18.7	
83	3/10/20	N/A	33.7	34.4	25.1	32.8	34.0	24.3												19.1	18.5	
84	12/2/19	MTB	33.6	34.3	29.8	33.8	33.6	29.5												14.8	18.8	
85	11/27/19	MTB	32.3	35.4	30.0	31.8	33.1	26.9												10.6	18.2	
86	11/17/19	MTB	32.0	32.7	34.5	31.1	32.3	34.0												21.6	23.4	≥5-20 copies/ reaction
87	11/21/19	MTB	30.6	32.1	28.0	30.2*	31.9*	24.8*										25.5		15.9	17.7	
88	11/19/19	MTB	31.0	32.1	30.2	31.4	31.8	31.4												17.6	18.0	
89	3/29/20	MTB	30.9	38.9	26.2	30.0	31.0	25.8												14.1	18.1	
90	11/20/19	MTB	28.7	30.2	25.3	26.5	30.6	23.8												N/A	N/A	
91	3/5/20	NP	29.3	30.6	29.6	28.3	29.5	27.6												13.6	18.5	
92	11/19/19	MTB	28.3	29.3	29.5	27.4*	29.2*	26.9*												N/A	N/A	
93	2/23/20	MTB	28.0	28.8	28.4	27.2	28.6	28.1							26.7			17.4		15.6	18.3	
94	4/2/20	MTB	28.6	29.0	34.2	28.0	27.7	33.1												19.1	23.8	
95	N/A	N/A	28.6	28.1	31.9	26.9	27.7	32.1	20.7											22.1	19.2	
96	1/30/20	MTB	29.6	32.3	27.8	27.7	27.6	30.2													18.4	>20-200 copies/ reaction
97	4/2/20	MTB	26.3	27.7	27.8	25.6	27.0	27.6												16.6	19.1	
98	11/16/19	N/A	25.4	26.6	27.2	25.5	26.4	27.1												15.9	18.1	
99	11/20/19	MTB	26.2	27.4	27.8	25.0*	26.1*	22.5*												13.5	17.6	
100	11/23/19	MTB	27.5	28.3	34.3	25.9	26.4	30.8												16.6	23.8	
101	11/17/19	MTB	25.4	27.1	23.8	25.2	26.3	24.2											20.8	14.7	18.8	
102	12/11/19	MTB	24.8	25.3	30.8	24.8	25.4	30.3												18.5	19.0	
103	11/17/19	MTB	24.2	25.3	27.2	23.8	25.1	27.2												12.2	24.0	
104	4/1/20	MTB	22.8	23.7	29.8	22.3	23.3	29.7			8.8									13.3	18.5	
105	3/9/20	MTB	25.1	26.3	31.1	23.0	23.0	35.4												14.4	18.5	
106	11/27/19	MTB			30.2	20.7	21.9	23.6												14.2	18.7	>200 copies/ reaction
107	3/31/20	MTB	21.8	23.8	30.4	20.4	21.7	28.9												13.7	17.1	
108	12/3/19	MTB	20.8	21.3	31.2	20.0	20.9	30.0											19.3	19.8	18.6	
109	3/10/20	N/A	21.2	21.1	33.5	19.7	20.3	33.2												19.7	16.7	
110	N/A	MTB	19.0	19.8	29.5	18.4	19.8	29.1										19.8		17.1	18.8	

© Copyright 2021 | N Panpradist

A

Target (copies/ reaction)	min to detection							
	65 °C		63 °C		59 °C		55 °C	
	SARS-CoV-2	IAC	SARS-CoV-2	IAC	SARS-CoV-2	IAC	SARS-CoV-2	IAC
0	N/A	27.3, 27.7	N/A	31.8, 30.7	N/A	44.7, 42.6	N/A	N/A
20	N/A	29.8, 27.5	N/A, 31.63	30.6, 32.1	N/A, 43.0	42.0, 42.8	N/A	N/A, 60.4
200	N/A	27.3, 27.4	N/A, 27.86	29.4, 39.5	N/A, 43.2	47.9, 40.4	N/A	N/A, 62.0
2000	24.7, 28.6	N/A	28.0, 28.2	30.3, 32.8	N/A, 51.0	43.3, 41.8	N/A	N/A, 60.3

B

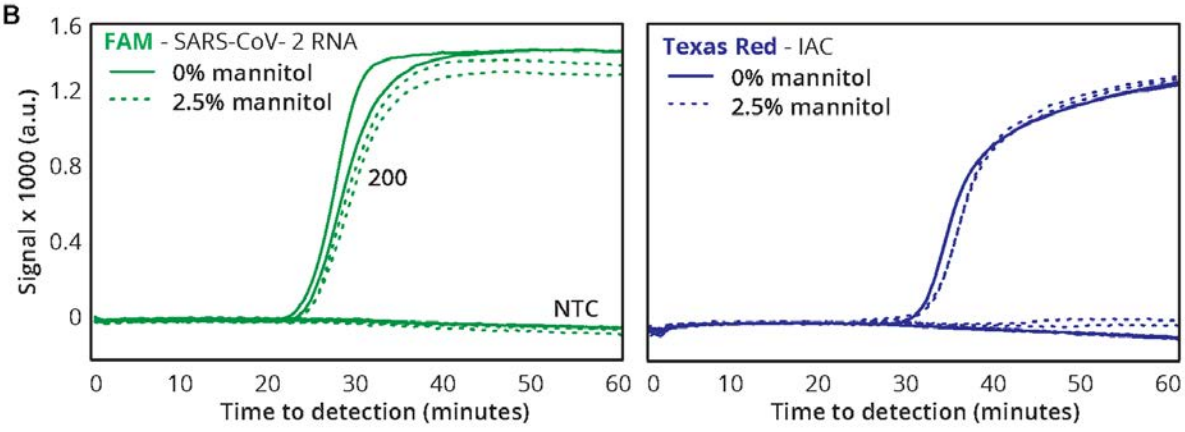

% mannitol	Target (copies/reaction)	SARS-CoV-2 (min to detection)	IAC (min to detection)
0	0	N/A	33.0, 33.0
	20	25.0, 25.7	N/A
2.5	0	N/A	33.9, 34.0
	20	26.3, 26.3	N/A

Figure S10.56 | Effects of excipients on fresh RT-LAMP reactions tested on a commercial real-time thermal cycler.

(**A**) Time to detection of SARS-CoV-2 RNA and IAC targets in the RT-LAMP containing 2.5% *(w/v)* trehalose and 0-2000 copies of SARS-CoV-2 RNA/40µL reaction. N/A means undetectable. For each condition, two technical replicates were run at 4 different reaction temperatures (i.e., 55°C, 59°C, 63°C, and 65°C). (**B**) Time to detection of SARS-CoV-2 RNA and IAC targets in the RT-LAMP reactions containing 0 or 20 copies of SARS-CoV-2 RNA/reaction, with and without 2.5% (*w/v*) mannitol, at 63°C.

© Copyright 2021 | N Panpradist

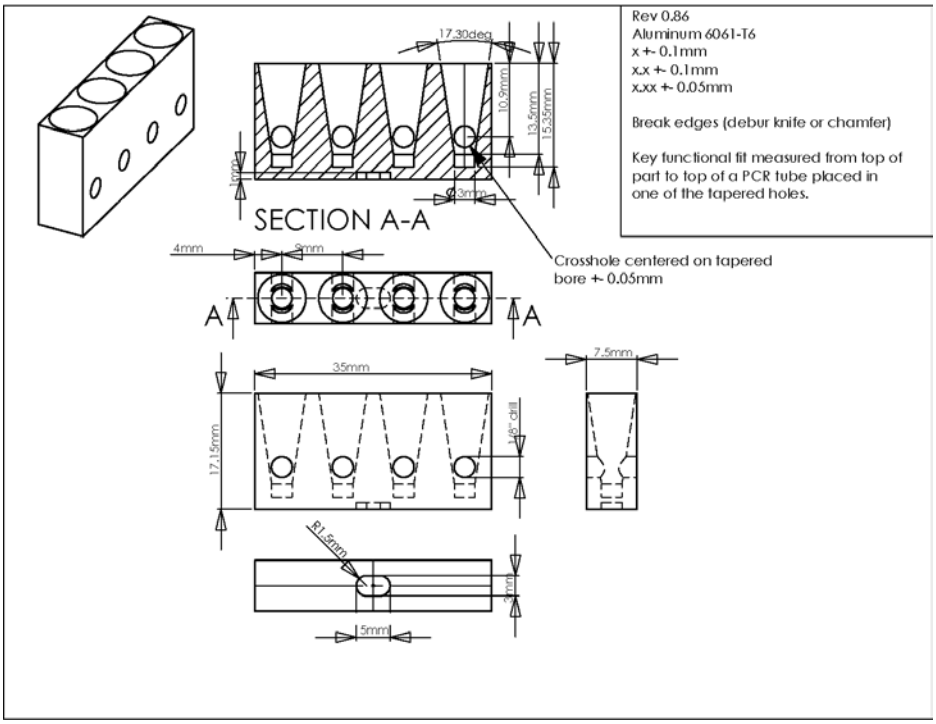

Figure S10.57 | Heat block used in Harmony COVID-19 device.

Drawing credit: Bryan Willman.

© Copyright 2021 | N Panpradist

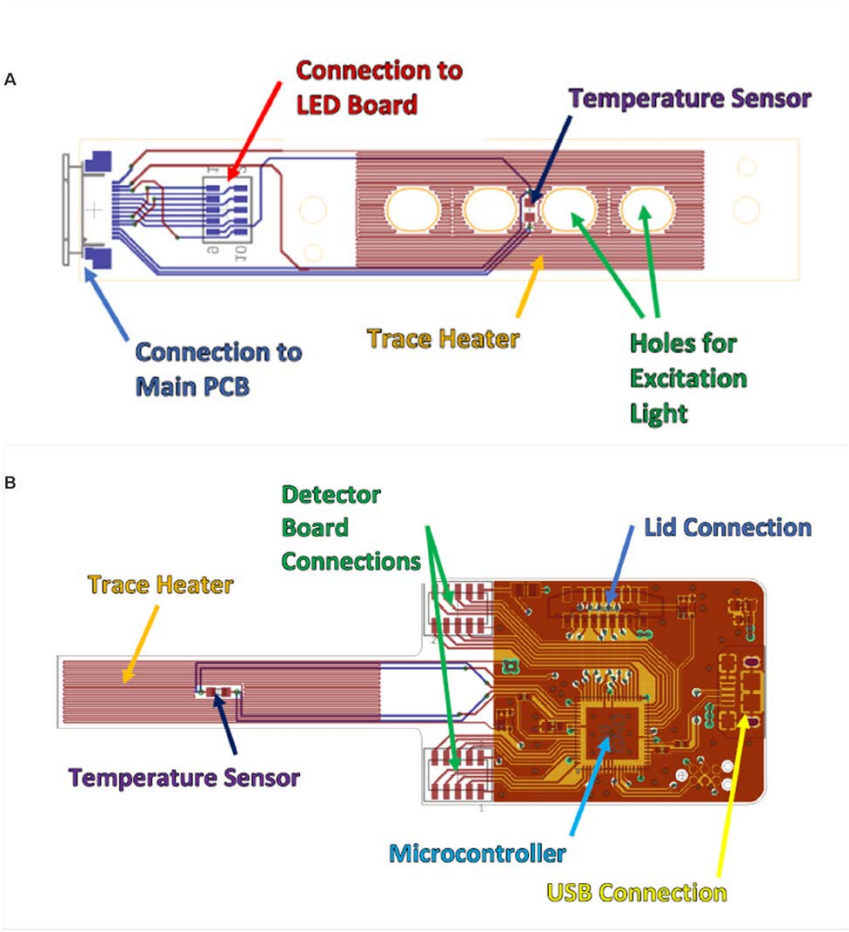

Figure S10.58 | The design of optical and heater circuit boards for the Harmony COVID-19 device.

(A) LED board (B) the detector board

© Copyright 2021 | N Panpradist

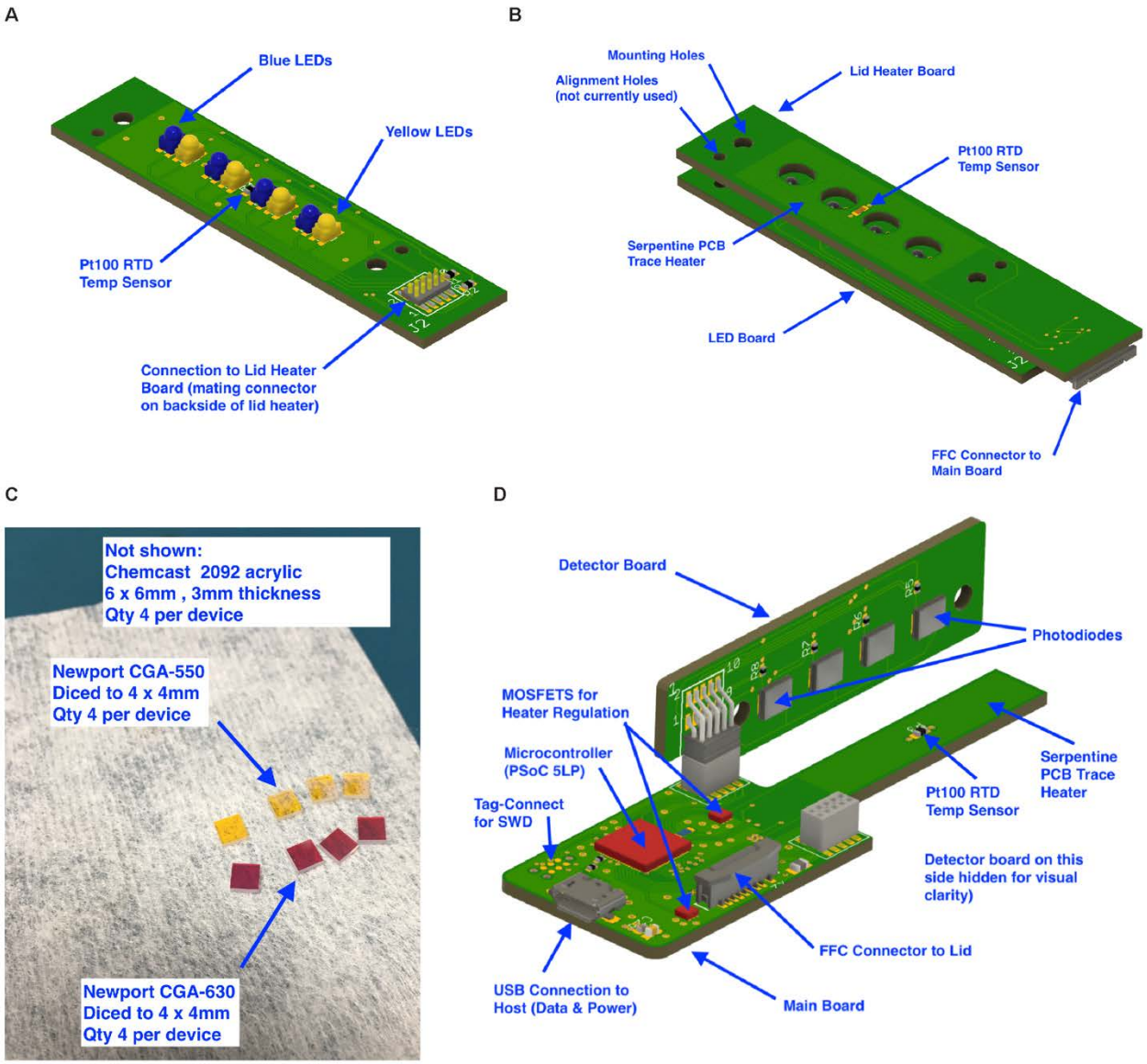

Figure S10.59 | Circuit board assembly and required parts.

(**A)** LED board. (**B**) LED board assembled to the lid heater board. (**C**) Custom-cut filter pieces. (**D**) Detector board and the main board. Each device require the following parts: thick film resistors (RCL12251R20FKEG, RCL12252R20FKEG, CRCW08050000Z0EBC and RCL12254R70FKEG from Vishey; RN73C1J75RBTDF from TE Connectivity; FTS-105-03-F-DV from Samtec; CR0402AJW-472GAS from Bourns), thin film resistors (RN73H1ETTP3003B25 from KOA Speer; ERJ-2RKF22R0X from Panasonic), multilayer ceramic capacitors (C0402C104M4RACAUTO, KEMET; 0603YC105KAT2A, AVX),

© Copyright 2021 | N Panpradist

multilayer ceramic capacitor (GRM188R60J226MEA0D, Murata), USB connectors (10118193-0001LF and 10118192-0001LF, FCI / Amphenol), FFC & FPC connector (52745-1497, Molex), standard yellow LEDs (LY E63B-CBEA-26-1-Z, Osram Opto Semiconductor), standard blue LEDs (150141BS63140, Wurth Elektronik), board-to-board & mezzanine connector (CLP-105-02-F-D and FLE-105-01-G-DV-K-TR, Samtec), FFC/FPC jumper cables (15166-0143, Molex), FFC & FFC connector (52559-1452, Molex), 2 headers & wire Housings (FTSH-105-01-F-DH, Samtec), MOSFET (FDMA410NZ, ON Semiconductor), 2 board-mount temperature sensors (PTS060301B100RP100 from Vishay), ARM Microcontrollers (CY8C5888LTI-LP097, Cypress Semiconductor), Photodiodes (SFH 2201, Opto Semiconductor).

A **B**

Fig. S8.

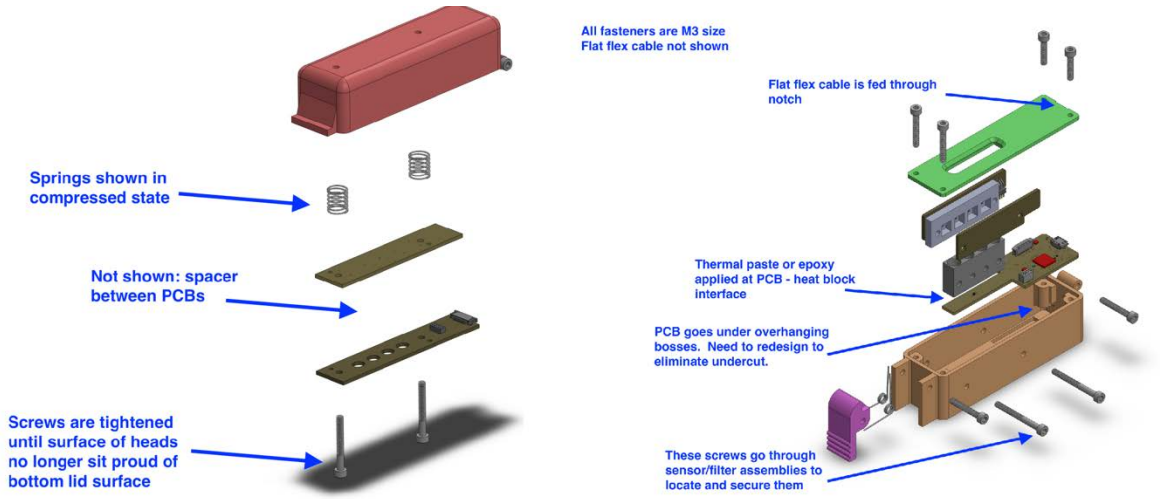

Figure S10.60 | Device assembly.

(**A**), Top part (**B**), Bottom part of the device are assembled using 10 screws, 2 compression springs, and 2 torsion springs (McMaster-Carr, Elmhurst, IL) including: Torsion Spring 90 Degree Angle, Left-Hand Wound, 0.204" OD (9271K109), Torsion Spring 90 Degree Angle, Right-Hand Wound, 0.204" OD (9271K143),Black-Oxide Alloy Steel Socket Head Screw M3 x 0.5 mm Thread, 5 mm Long (91290A110), Black-Oxide Alloy Steel Socket Head Screw M3 x 0.5 mm Thread, 10 mm Long (91290A115), Black-Oxide Alloy Steel Socket Head Screw M3 x 0.5 mm Thread, 15 mm Long (91290A572), Black-Oxide Alloy Steel Socket Head Screw M3 x 0.5 mm Thread, 20 mm Long (91290A123), Black-Oxide Alloy Steel Socket Head Screw M3 x 0.5 mm Thread, 25 mm Long

© Copyright 2021 | N Panpradist

(91290A125), Black-Oxide Alloy Steel Socket Head Screw M3 x 0.5 mm Thread, 30 mm Long, Partially Threaded (91290A130), Music-Wire Steel Compression Springs 0.875" Long, 0.36" OD, 0.296" ID (9434K73).

A

© Copyright 2021 | N Panpradist

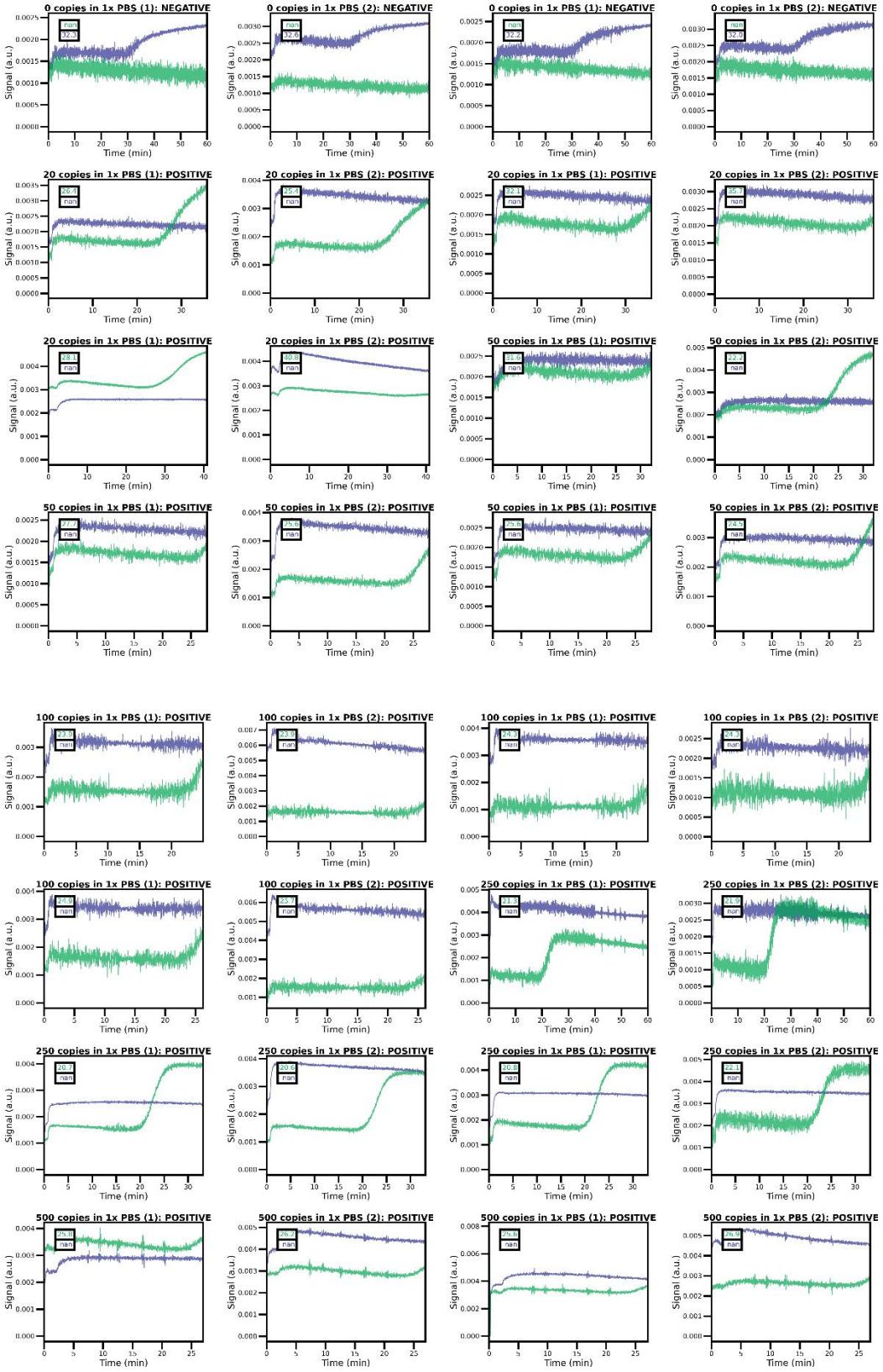

© Copyright 2021 | N Panpradist

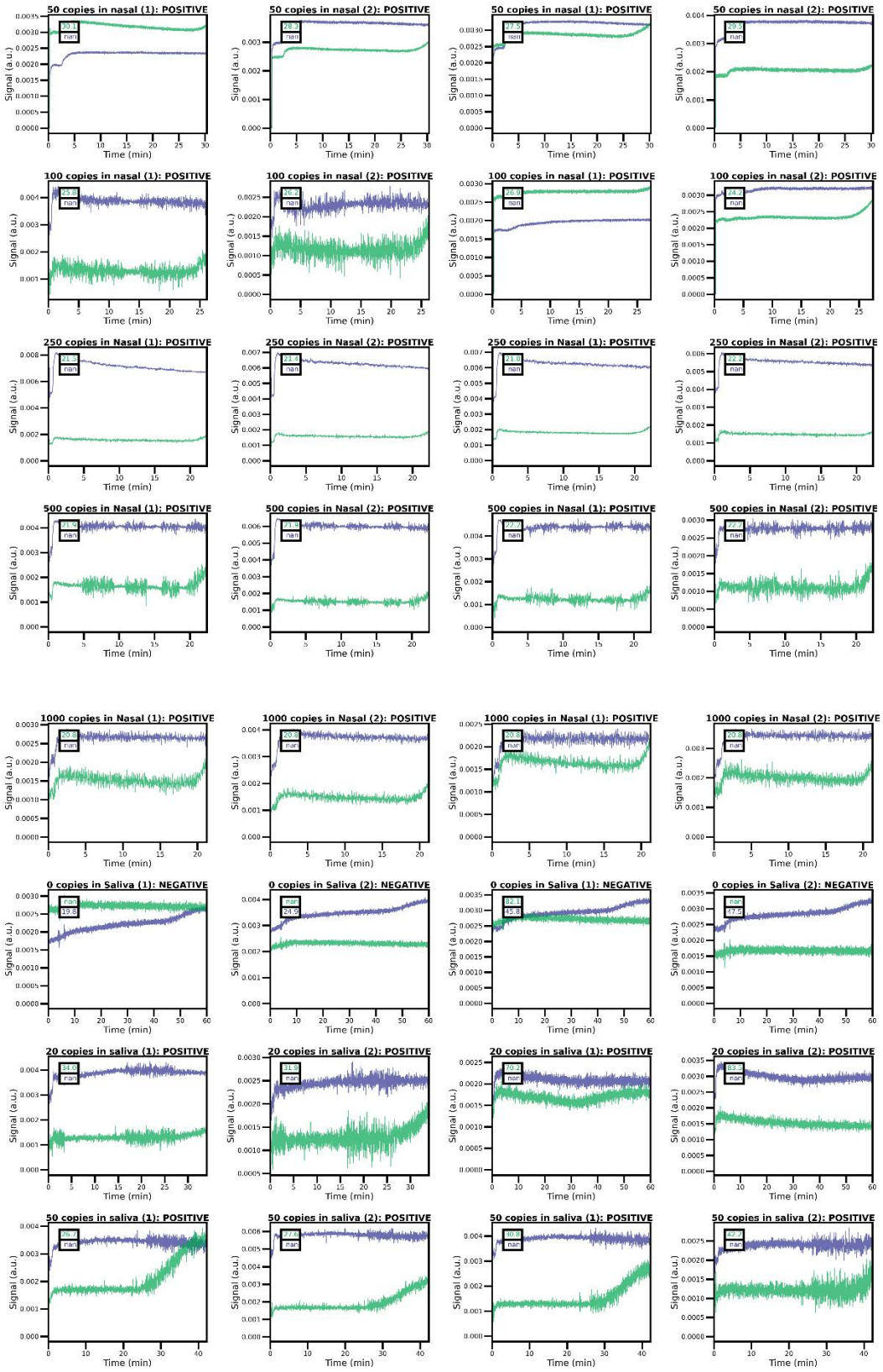

© Copyright 2021 | N Panpradist

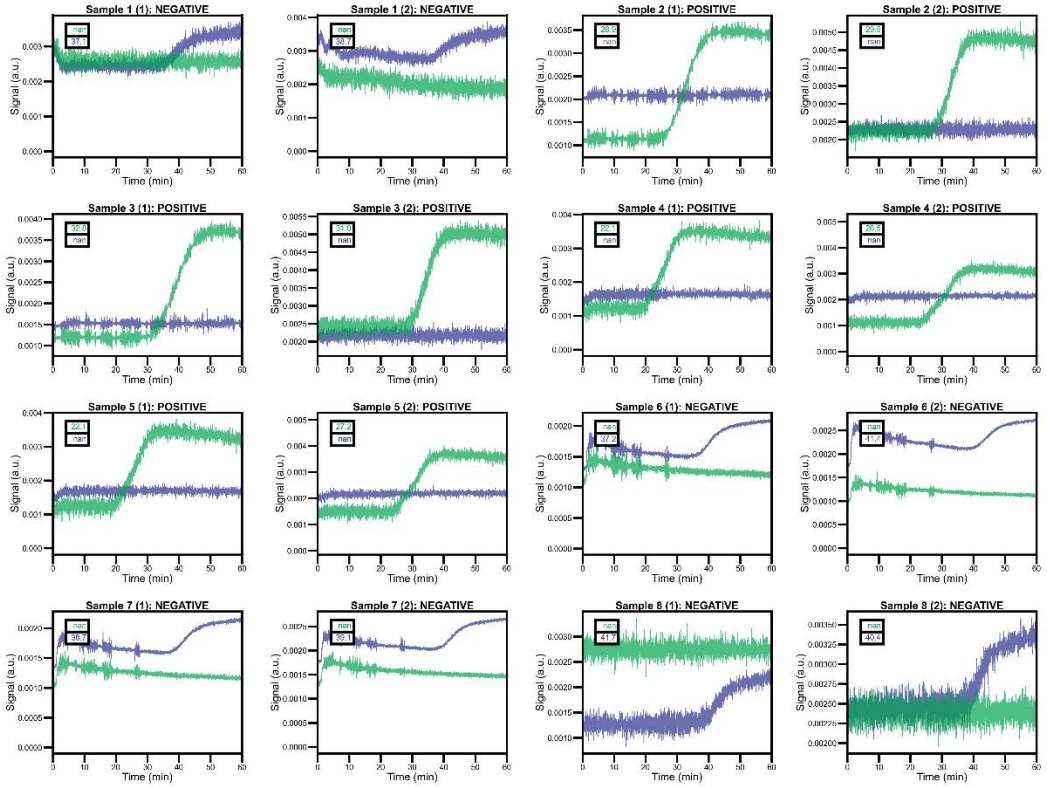

B

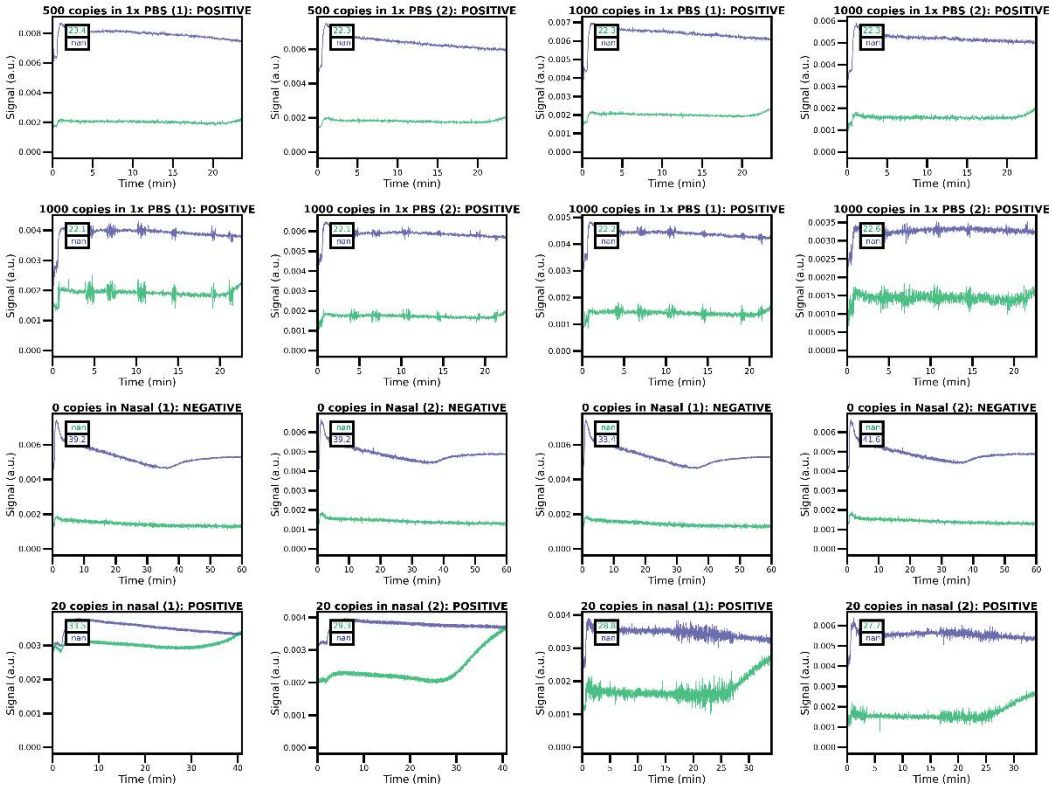

© Copyright 2021 | N Panpradist

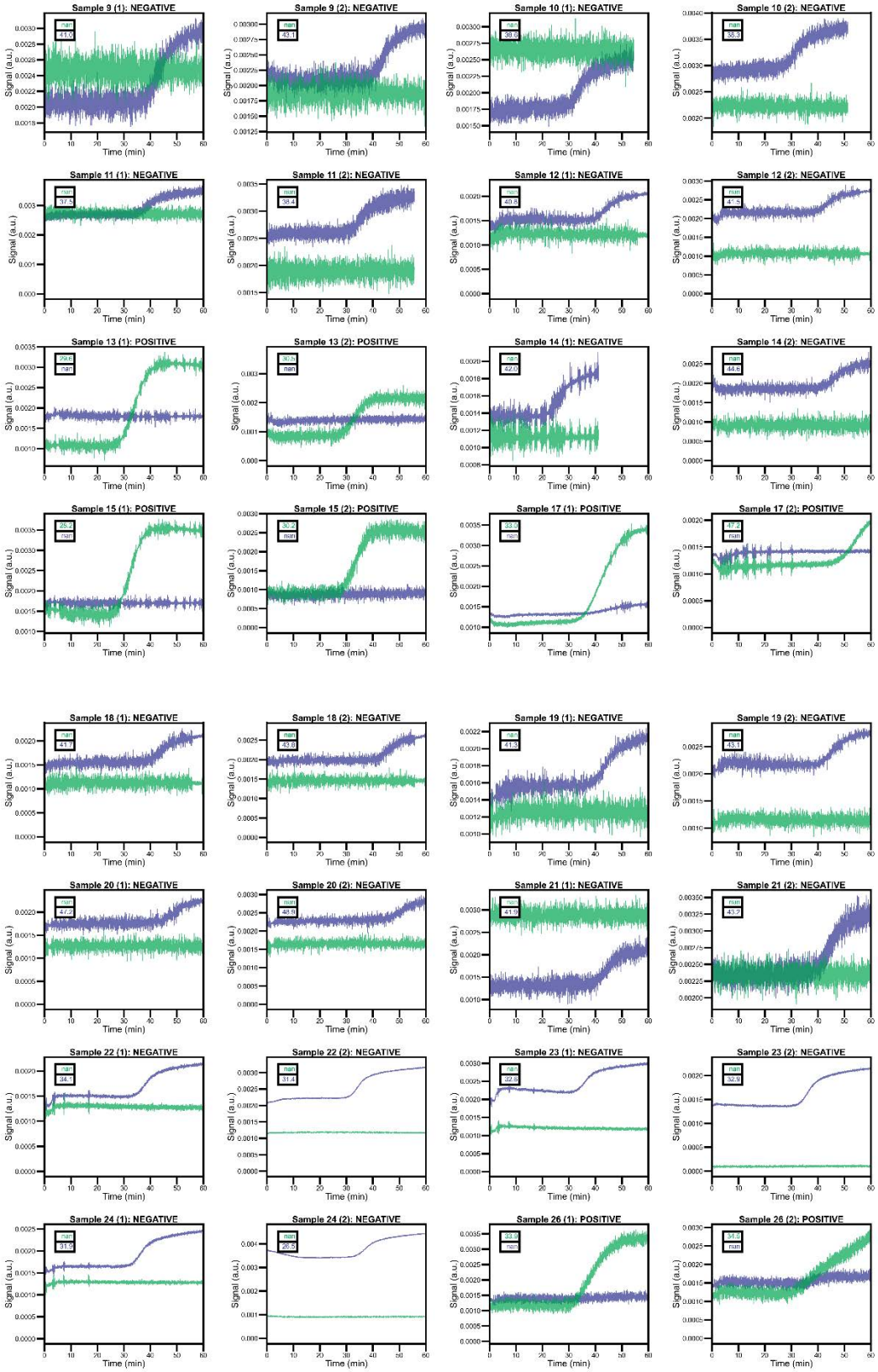

© Copyright 2021 | N Panpradist

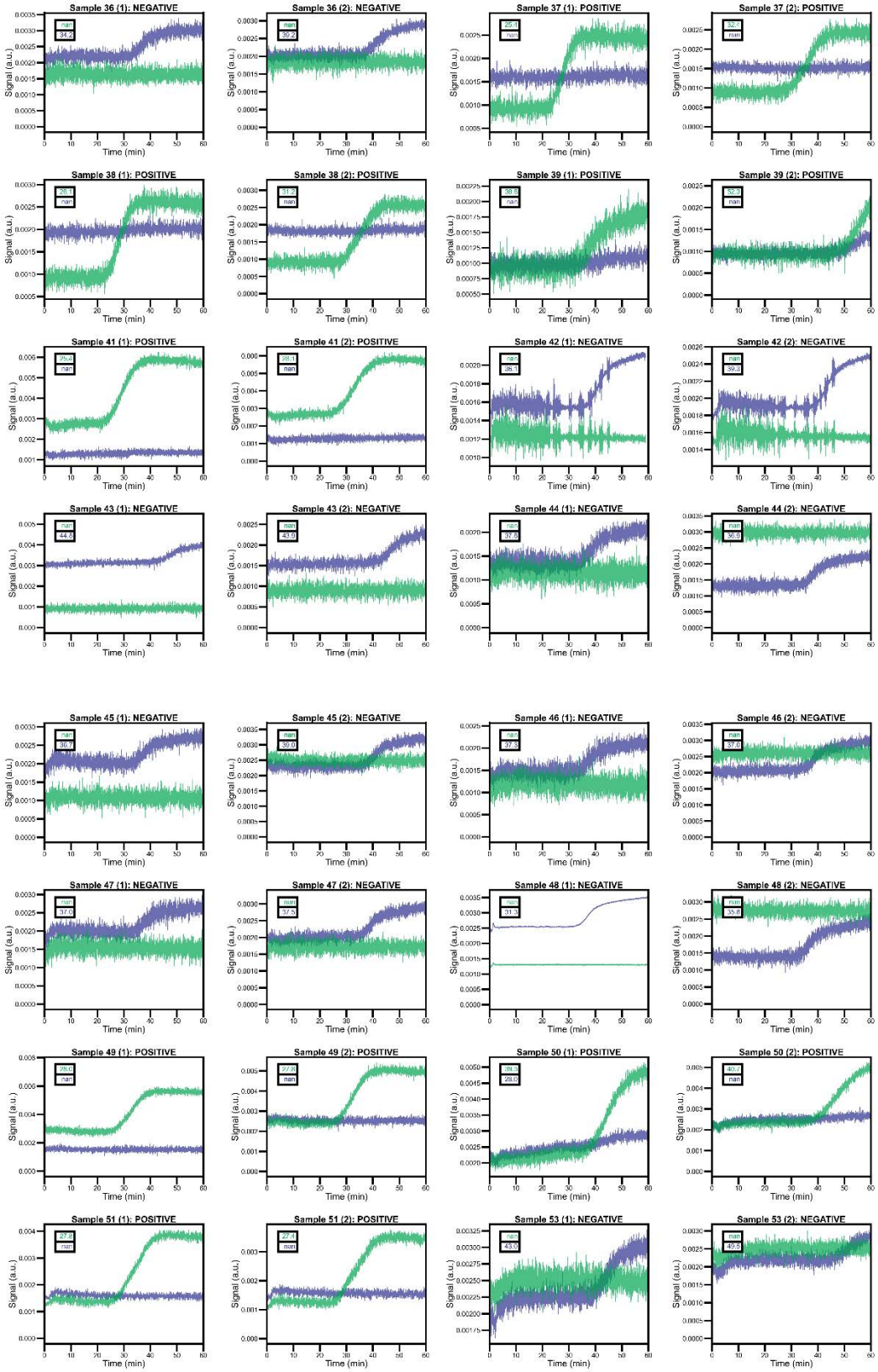

© Copyright 2021 | N Panpradist

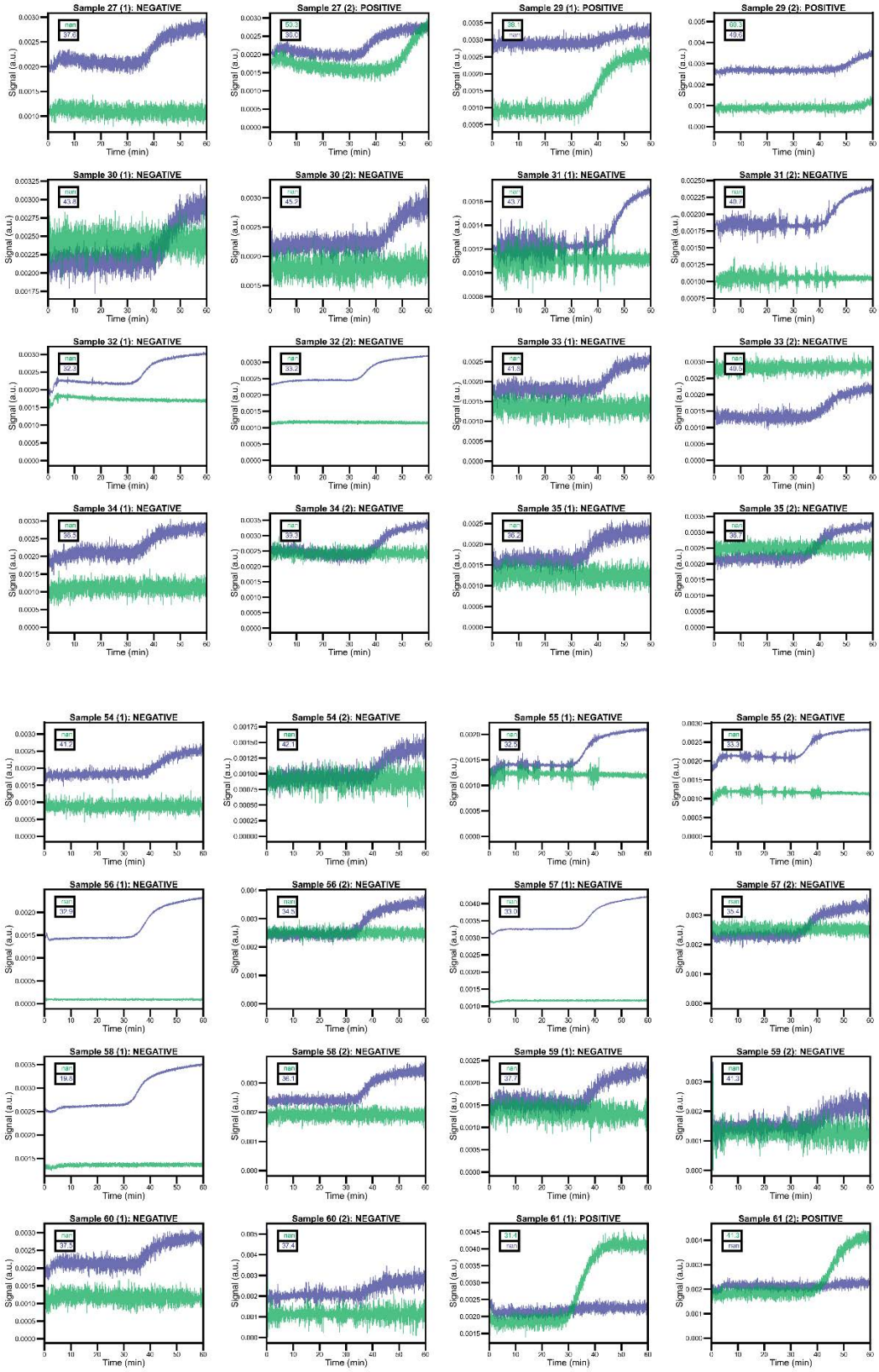

© Copyright 2021 | N Panpradist

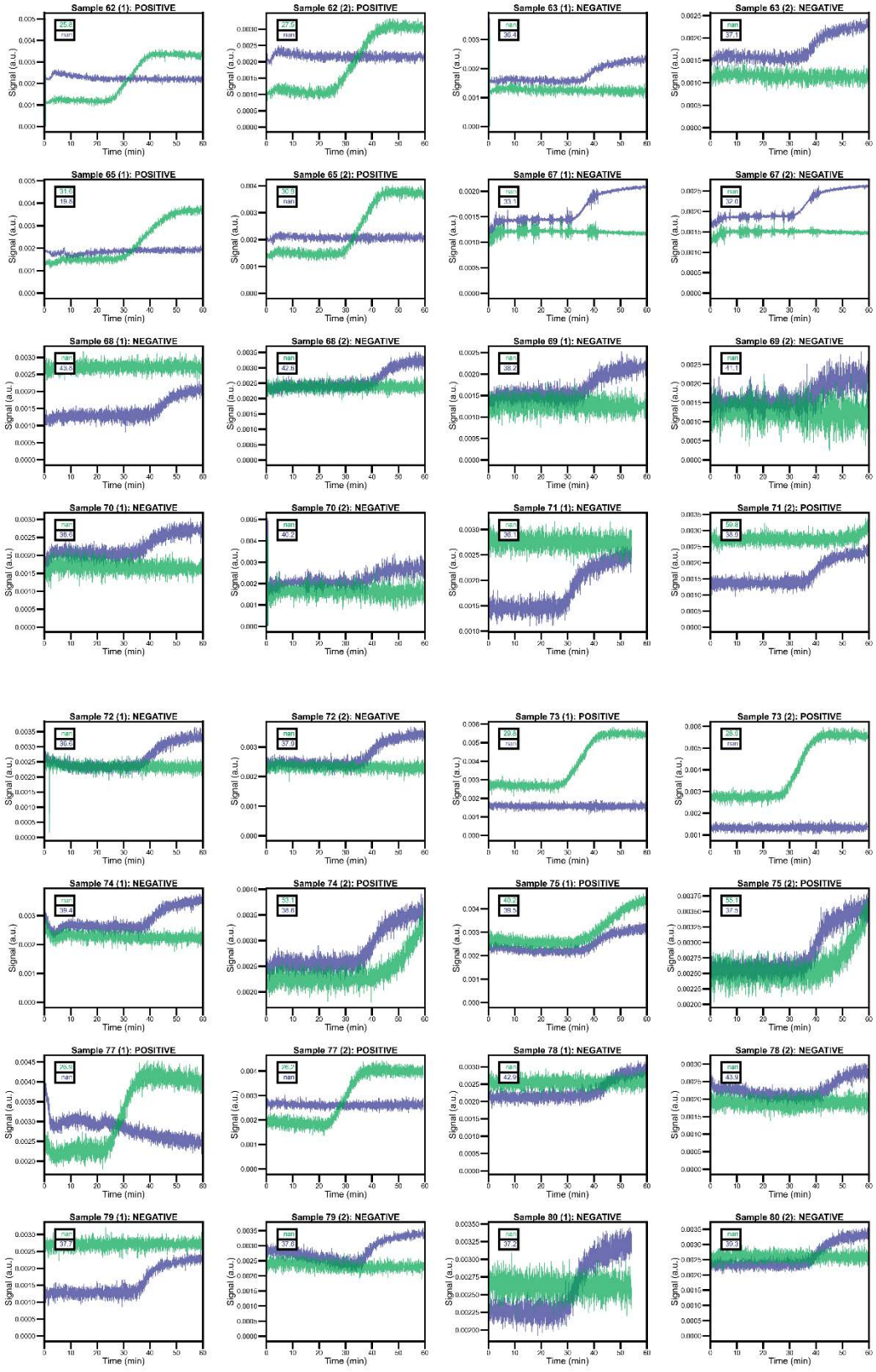

© Copyright 2021 | N Panpradist

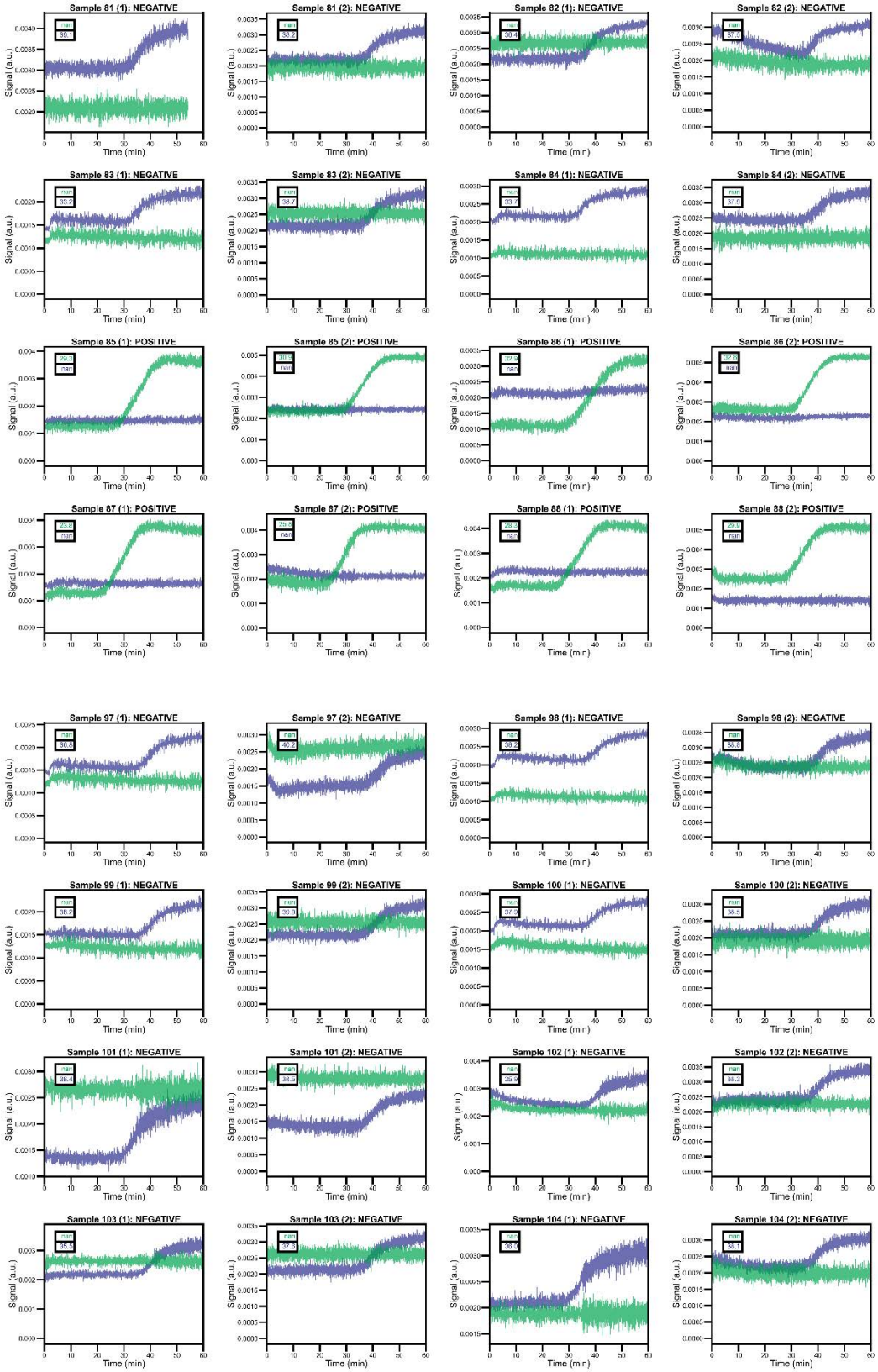

© Copyright 2021 | N Panpradist

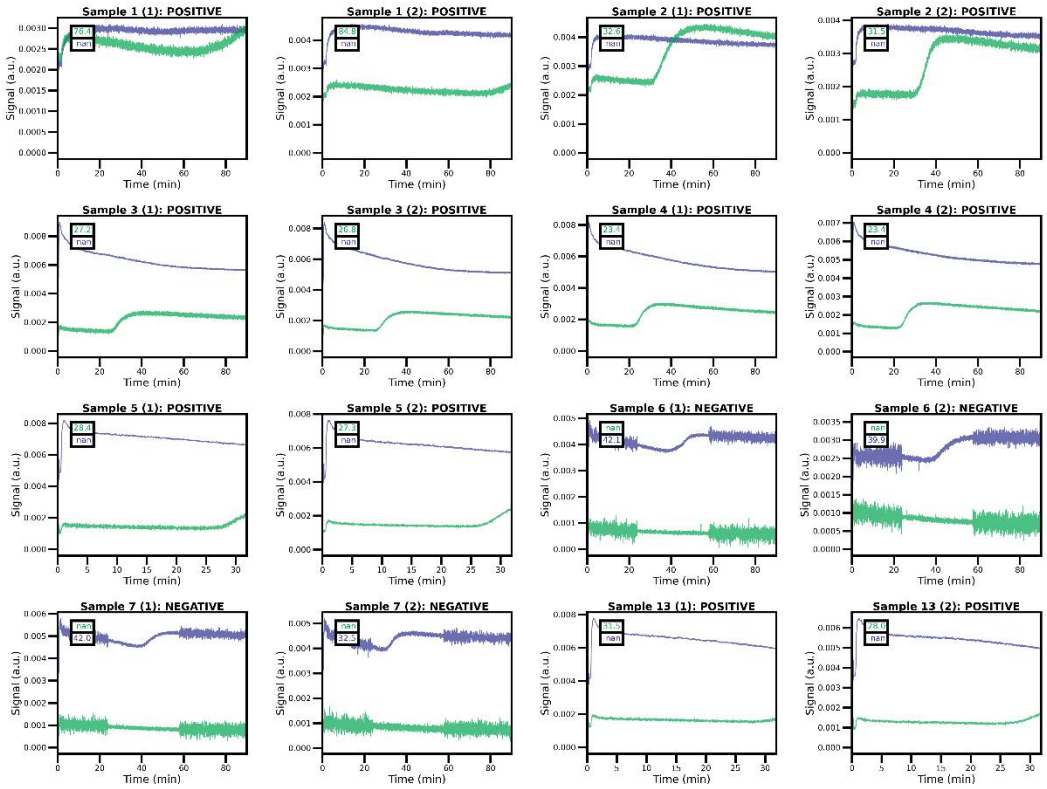

C

© Copyright 2021 | N Panpradist

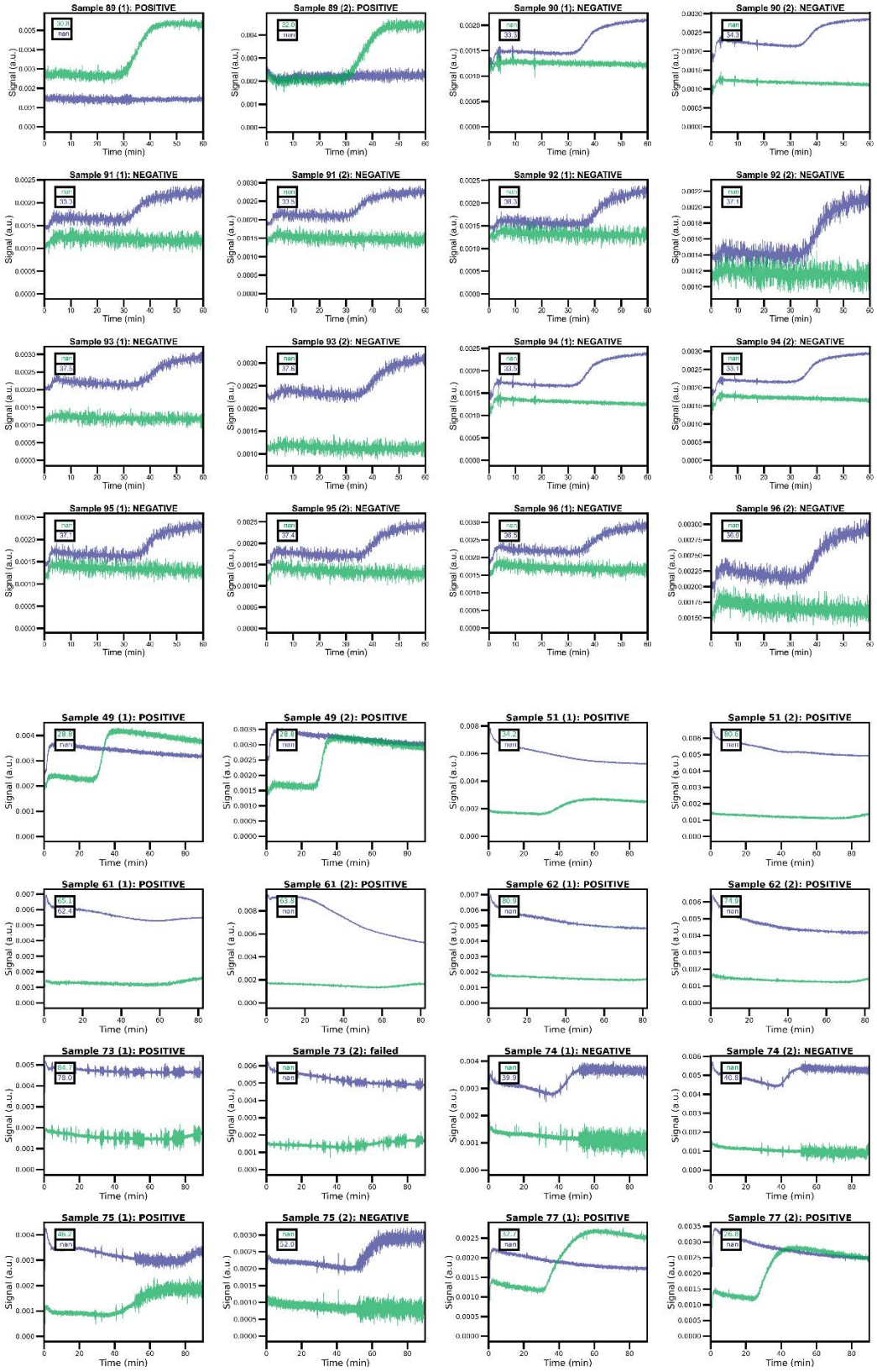

© Copyright 2021 | N Panpradist

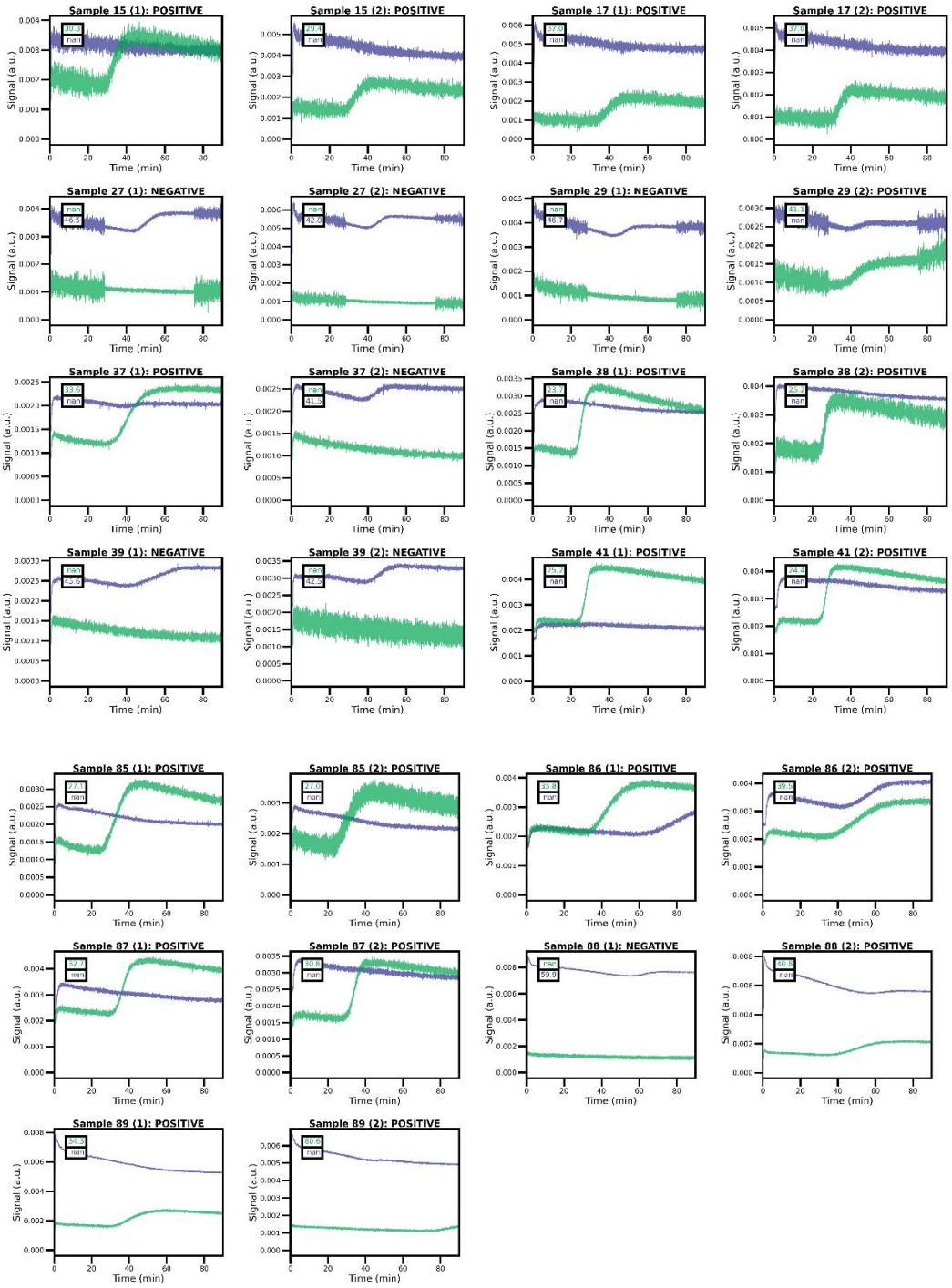

Figure S10.61 | Real-time amplification curves of samples analyzed by HARMONY Covid-19. **(A**) XPRIZE panel of contrived specimens (**B**) Extracted RNA from VTM specimens (**C**) VTM specimens without extraction. Data were exported from the software as .txt file and plotted using in-house Python code available at https://github.com/sgillig1/COVID_Data_Analysis.

© Copyright 2021 | N Panpradist

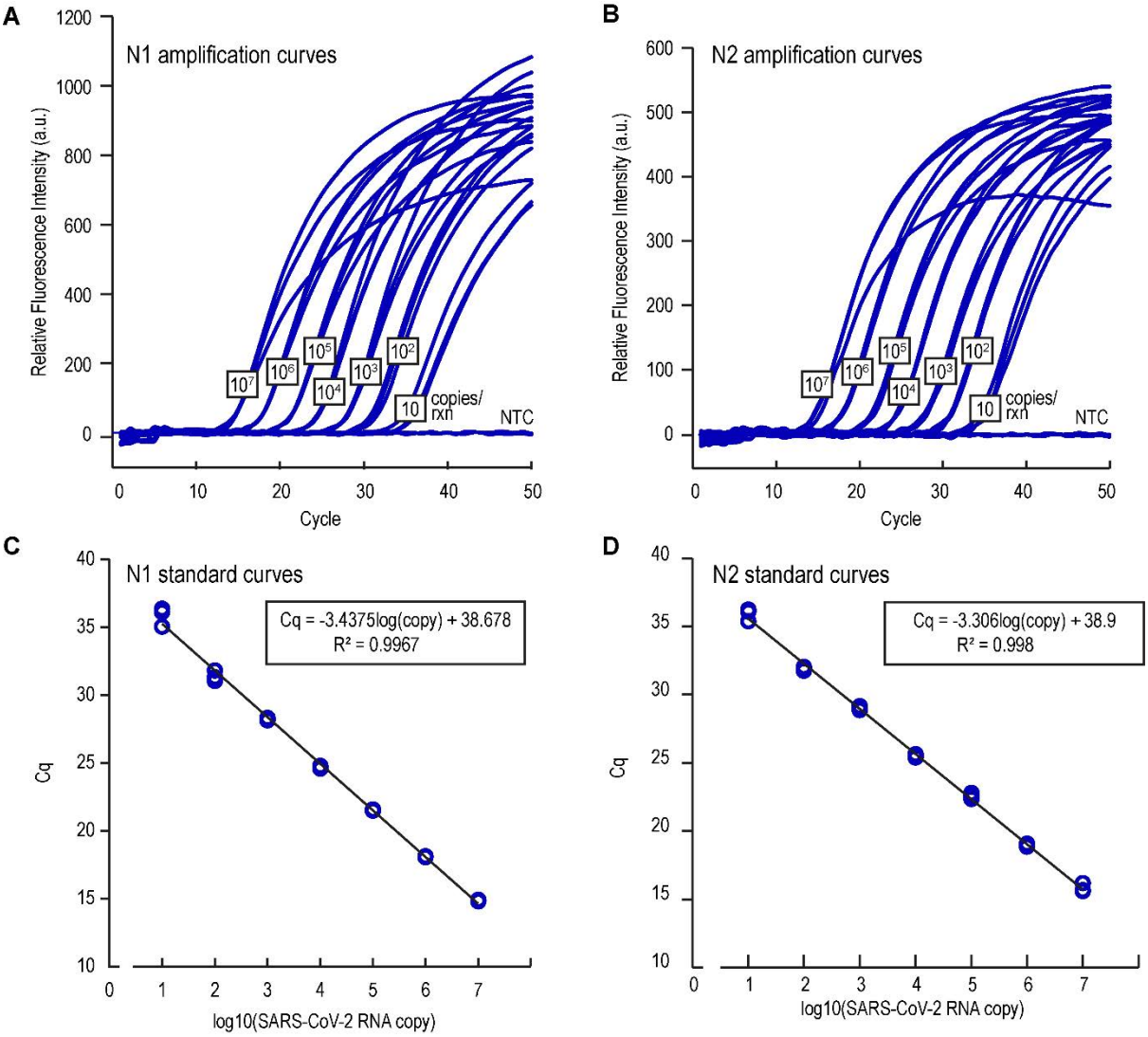

Figure S10.62 | Standard curves of RT-qPCR using CDC N1 and N2 primers.

(A) Amplification curves of N1 assay and (B) N2 assay ranging from 0 to 10^7 copies/reaction (rxn) of SARS-CoV-2 synthetic RNA. Calibration curves for (C) N1 and (D) N2 assays.

© Copyright 2021 | N Panpradist

A

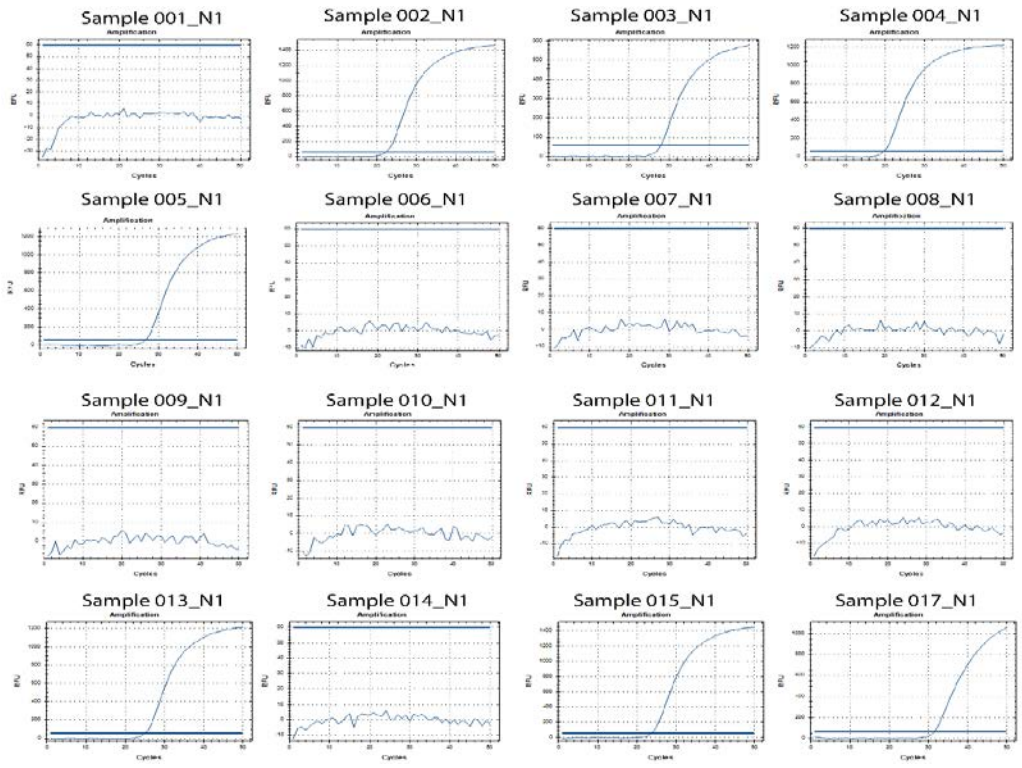

© Copyright 2021 | N Panpradist

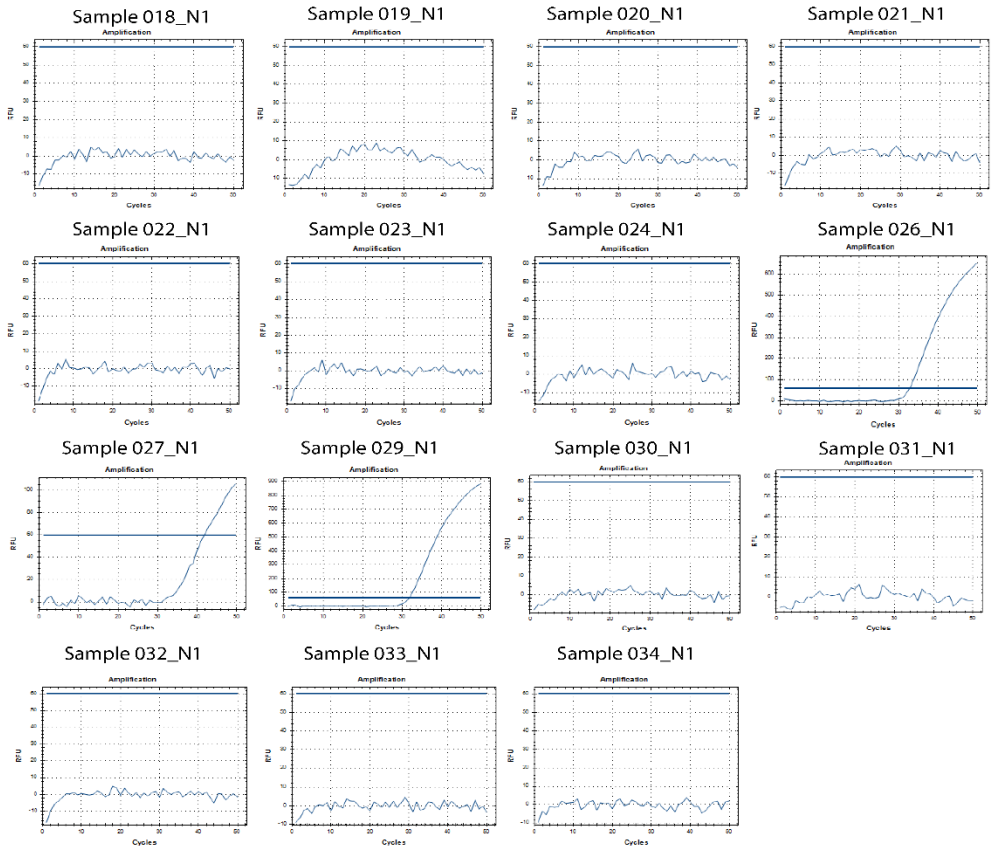

© Copyright 2021 | N Panpradist

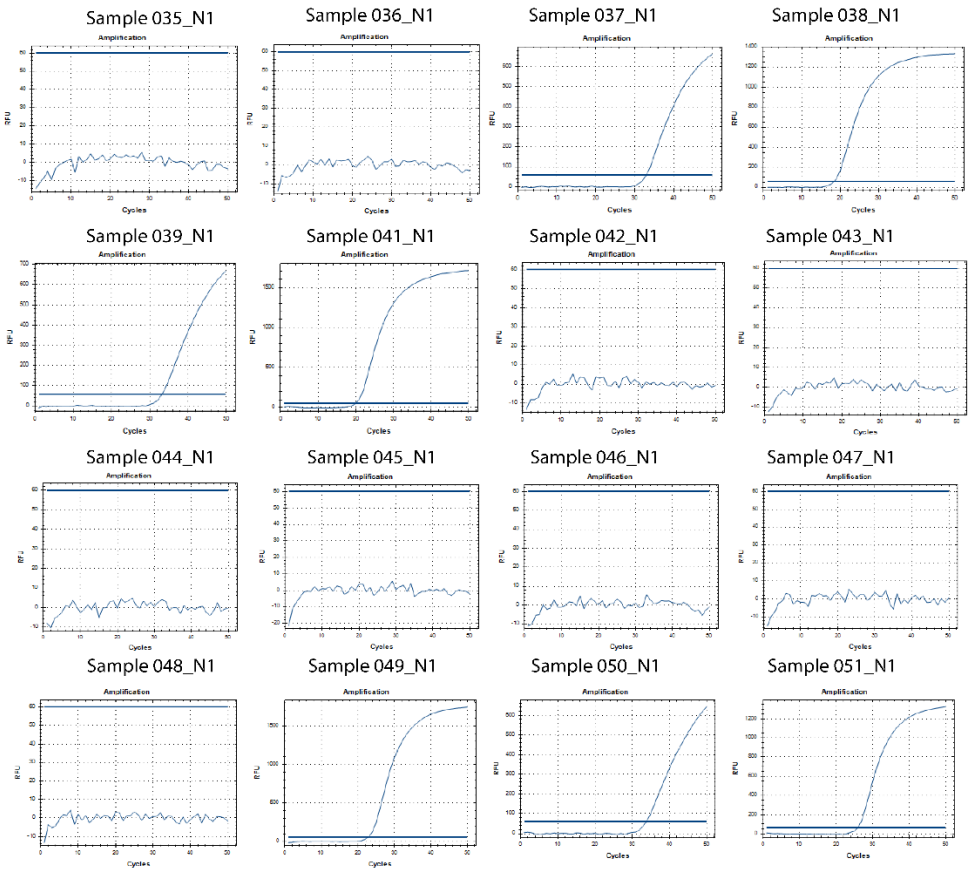

© Copyright 2021 | N Panpradist

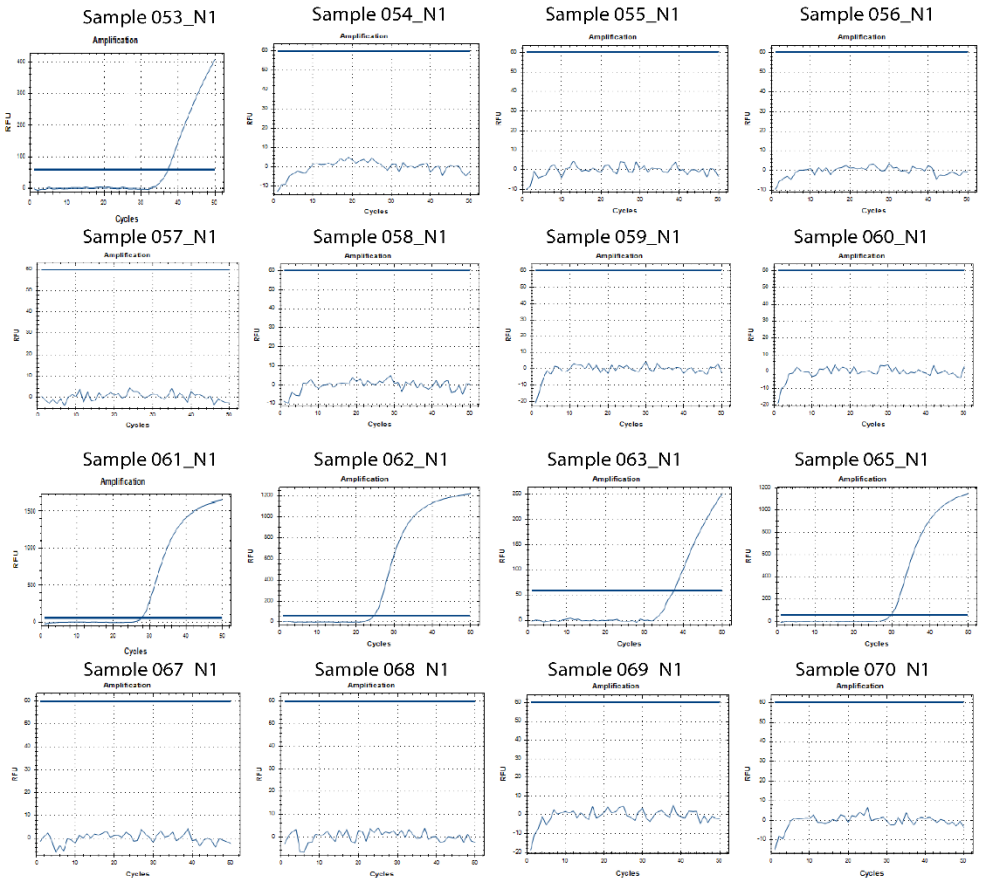

© Copyright 2021 | N Panpradist

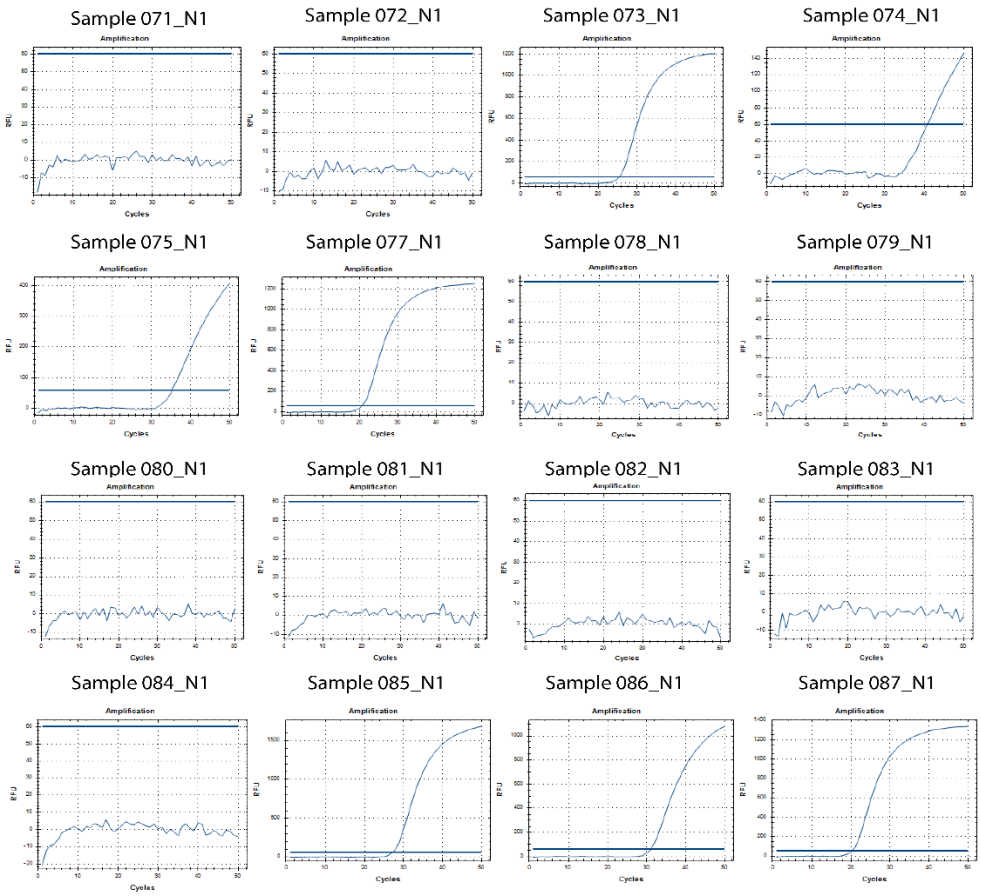

© Copyright 2021 | N Panpradist

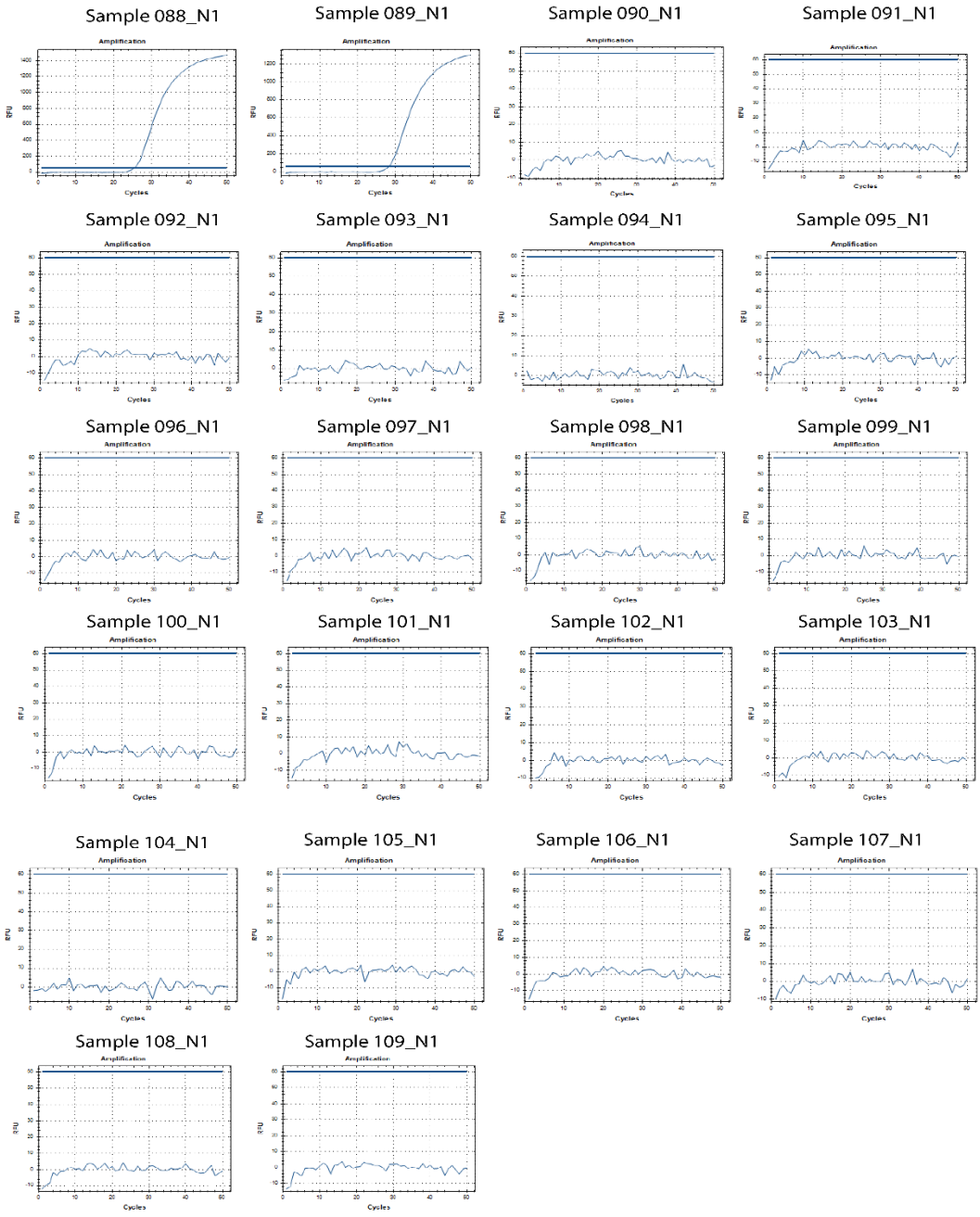

B

© Copyright 2021 | N Panpradist

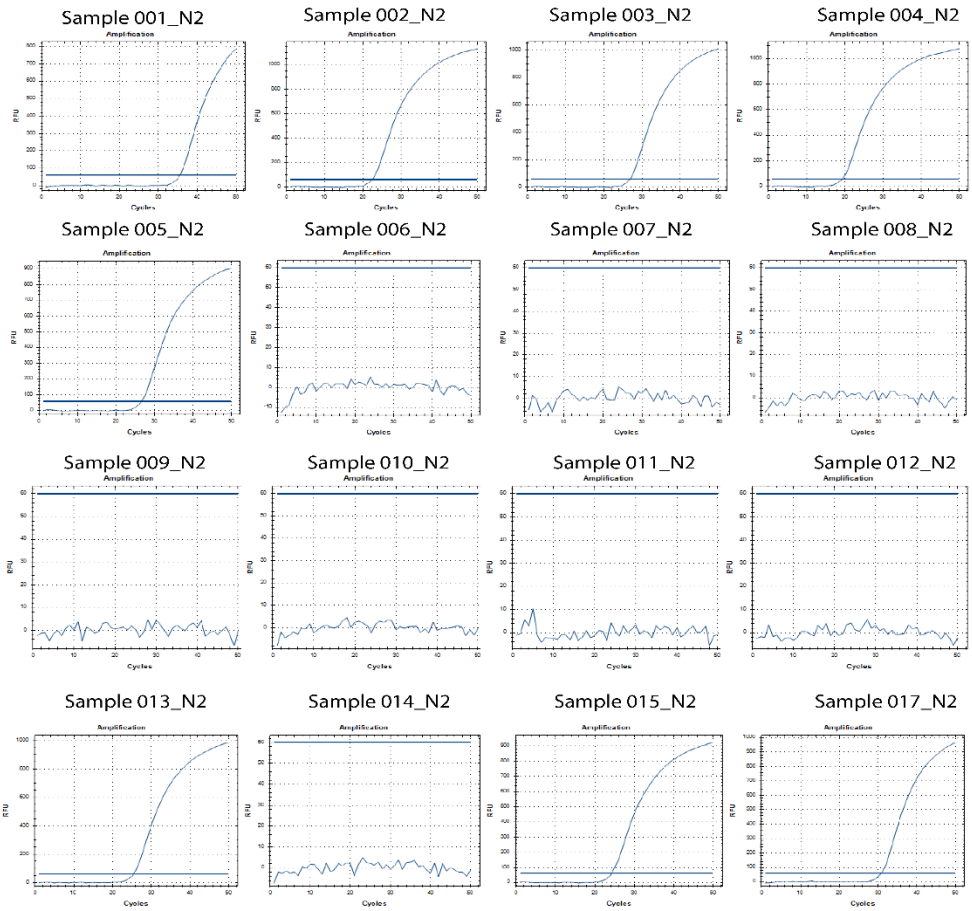

© Copyright 2021 | N Panpradist

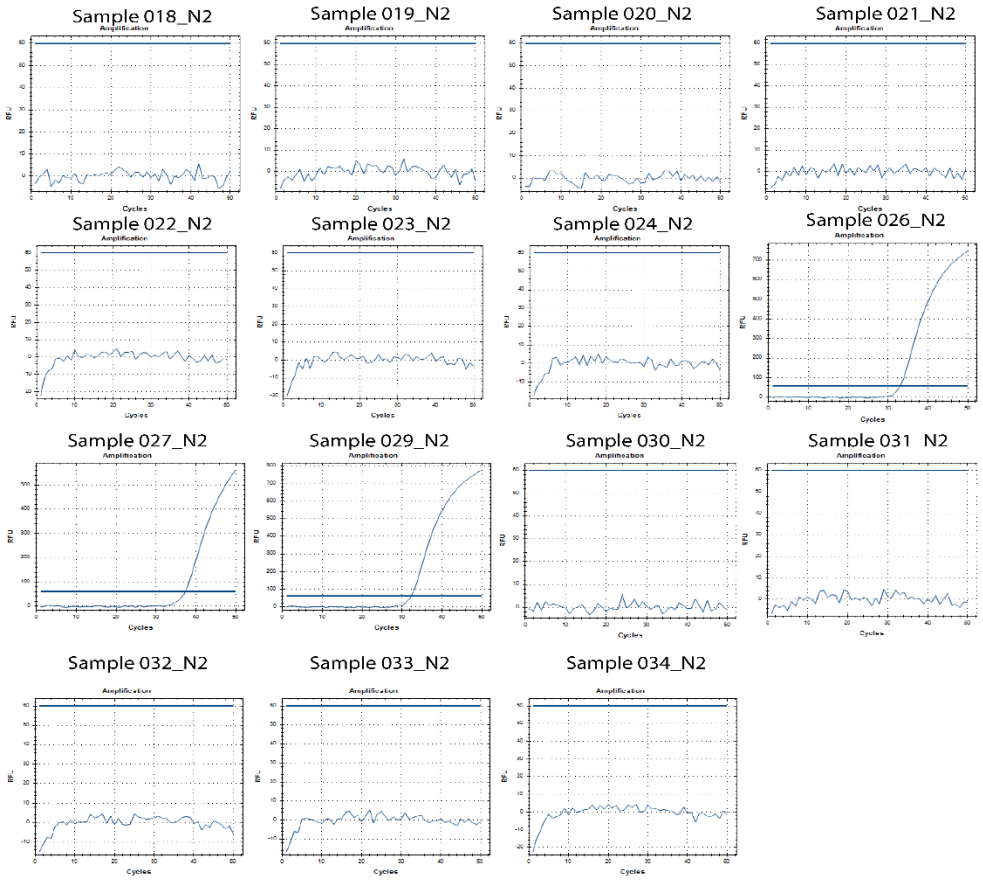

© Copyright 2021 | N Panpradist

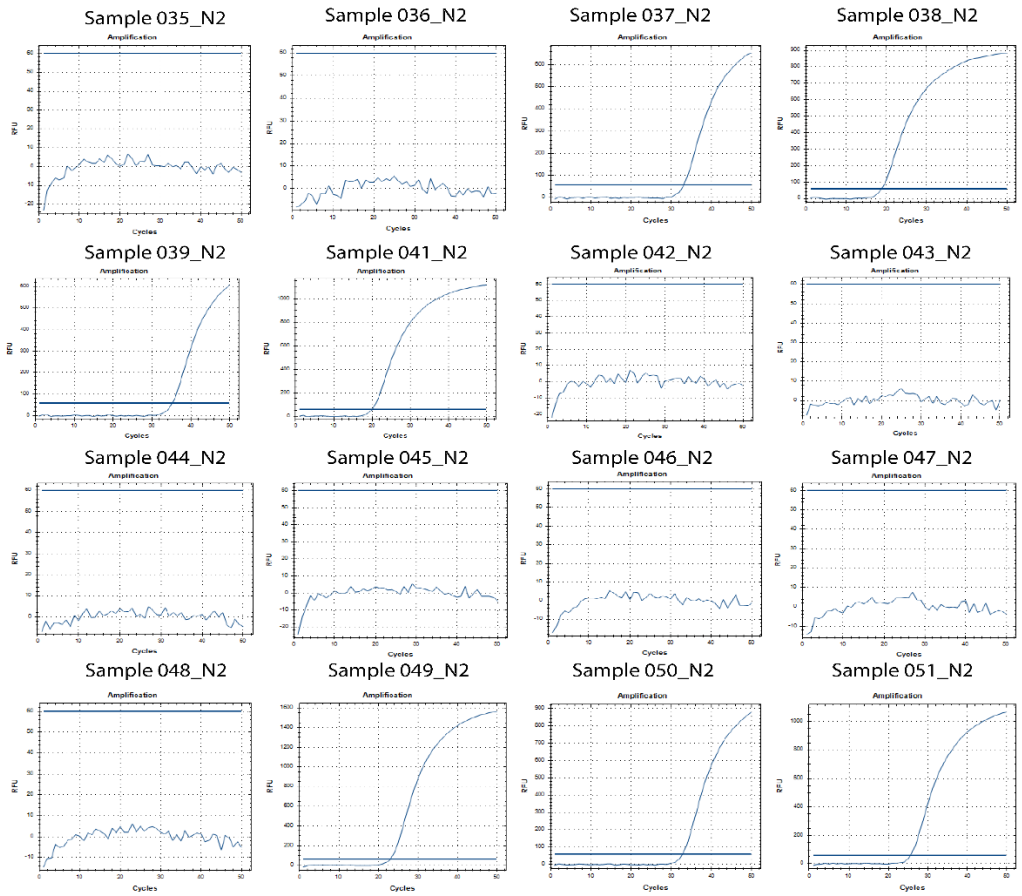

© Copyright 2021 | N Panpradist

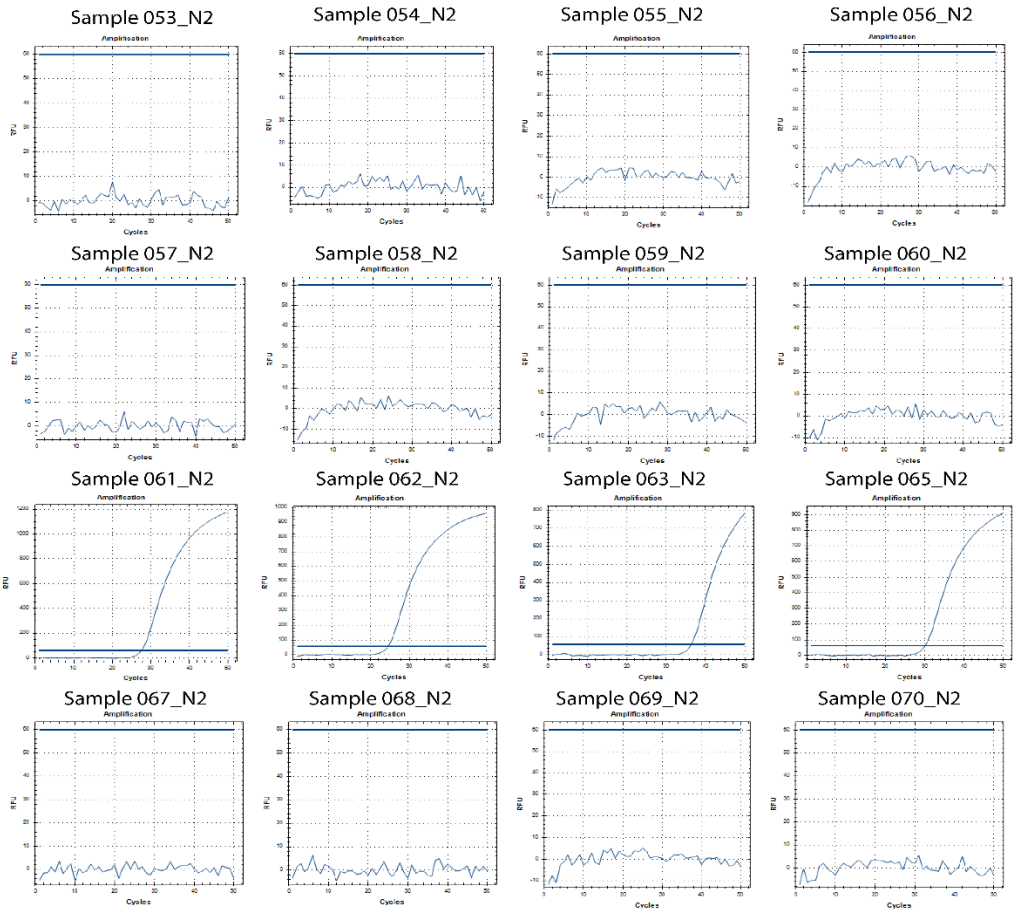

© Copyright 2021 | N Panpradist

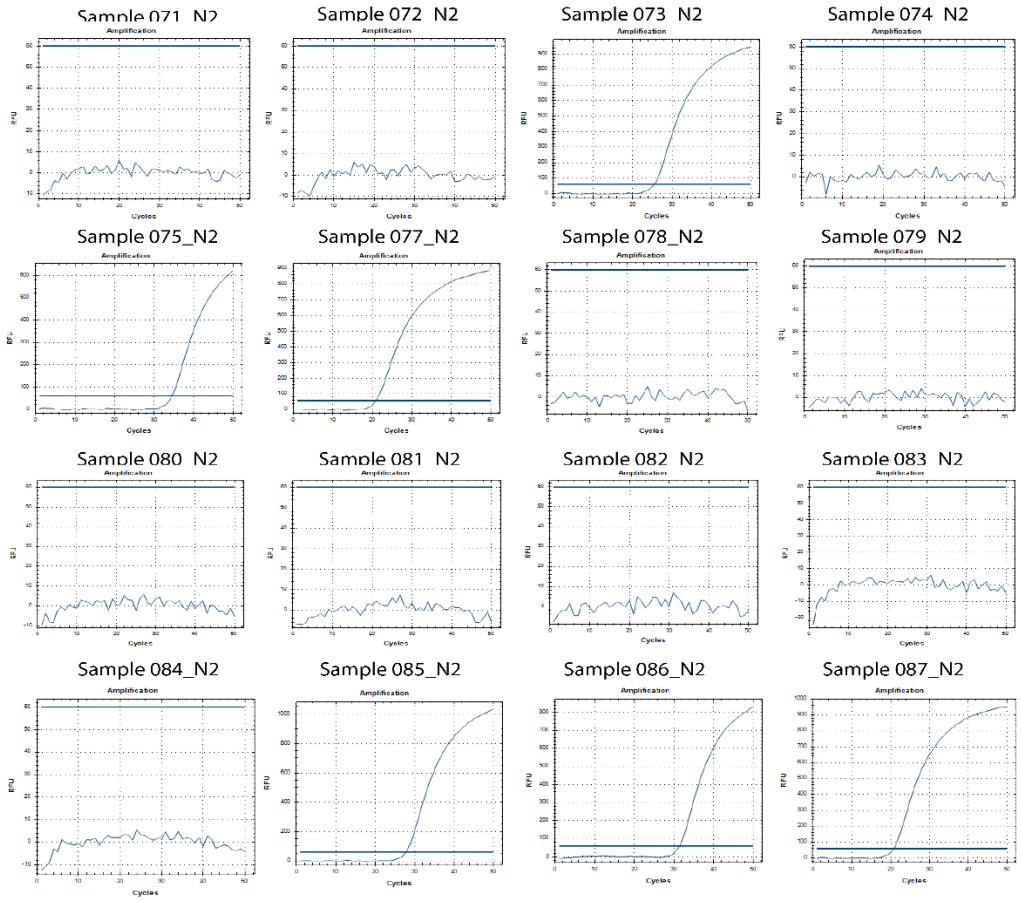

© Copyright 2021 | N Panpradist

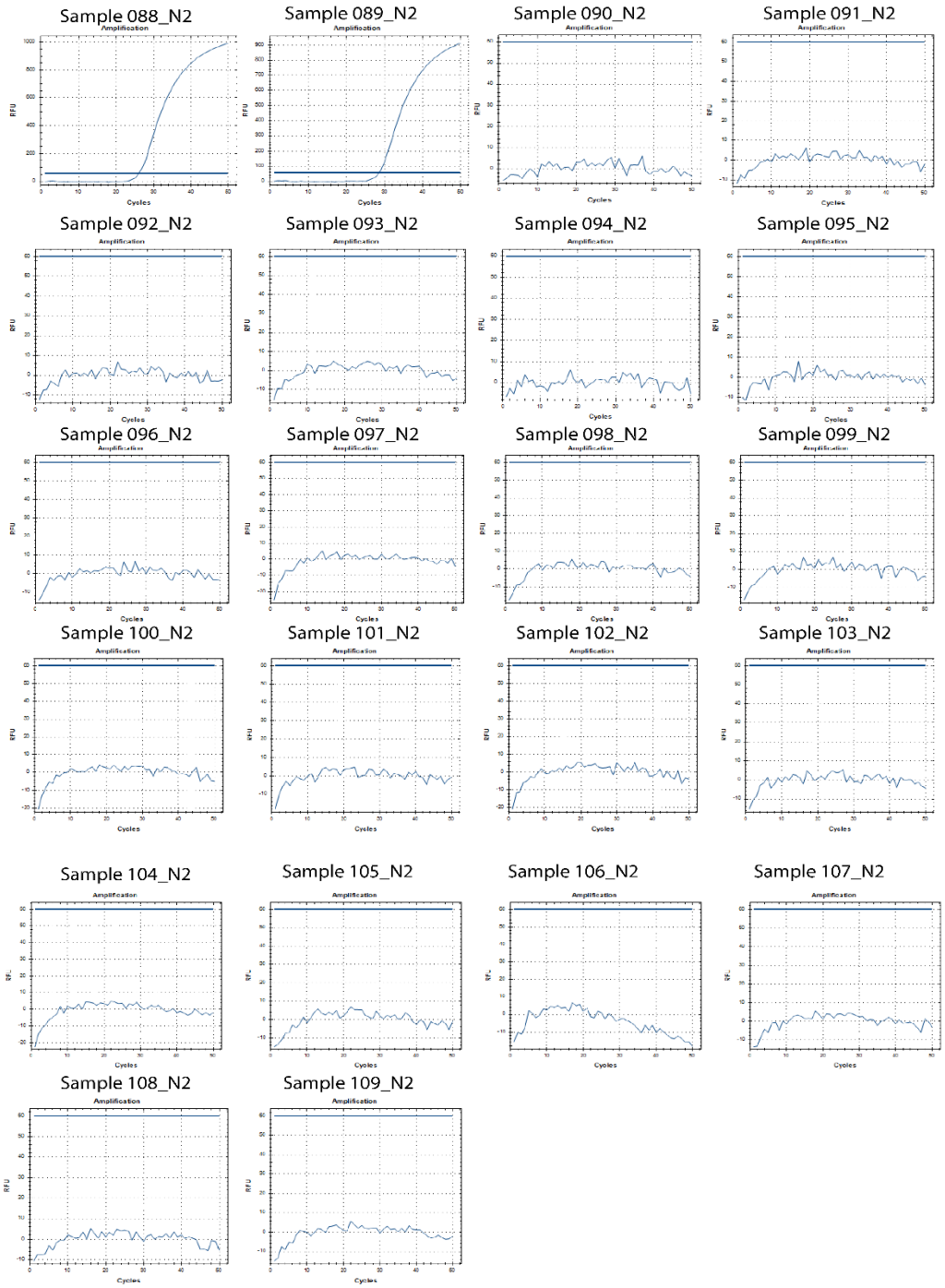

c

© Copyright 2021 | N Panpradist

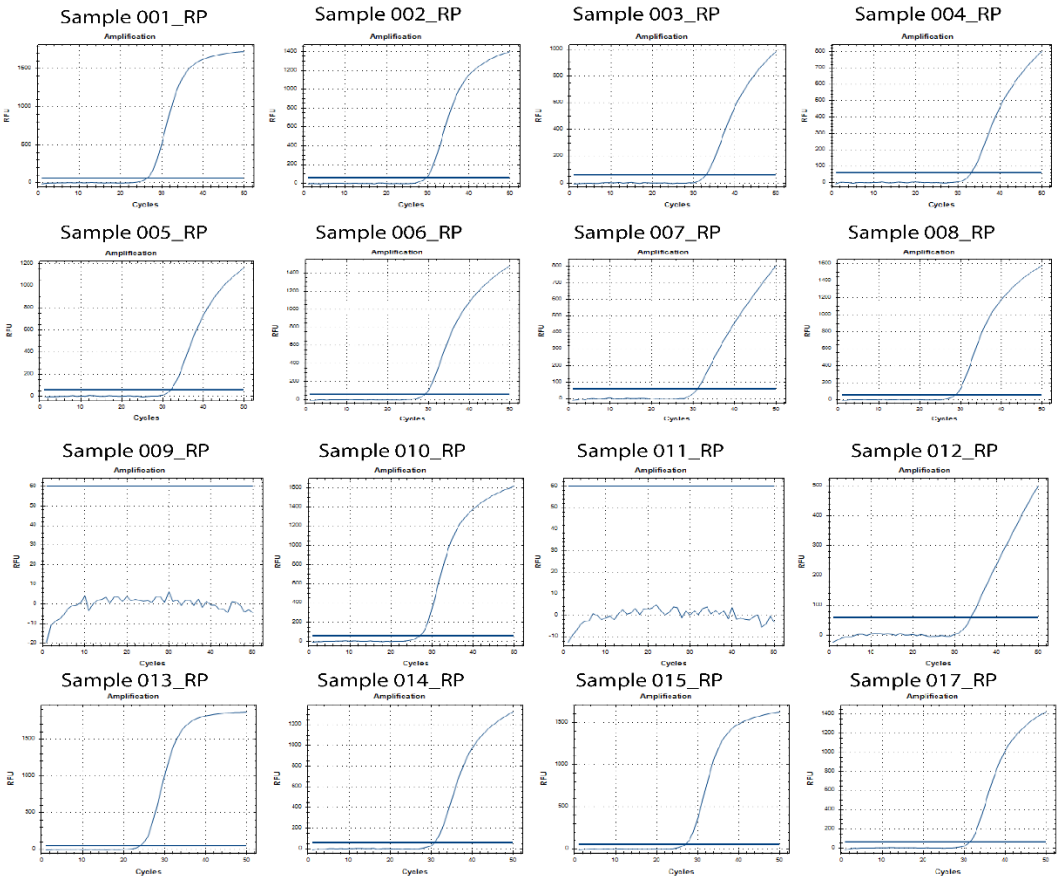

© Copyright 2021 | N Panpradist

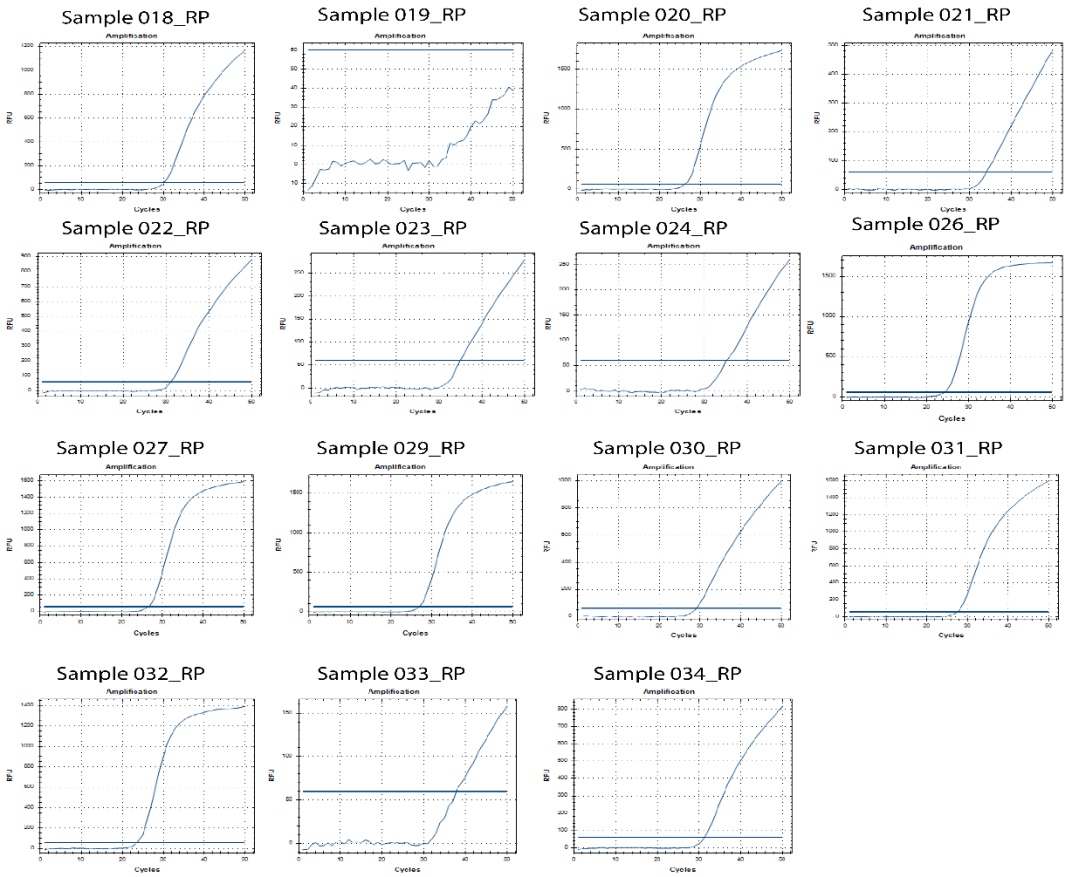

© Copyright 2021 | N Panpradist

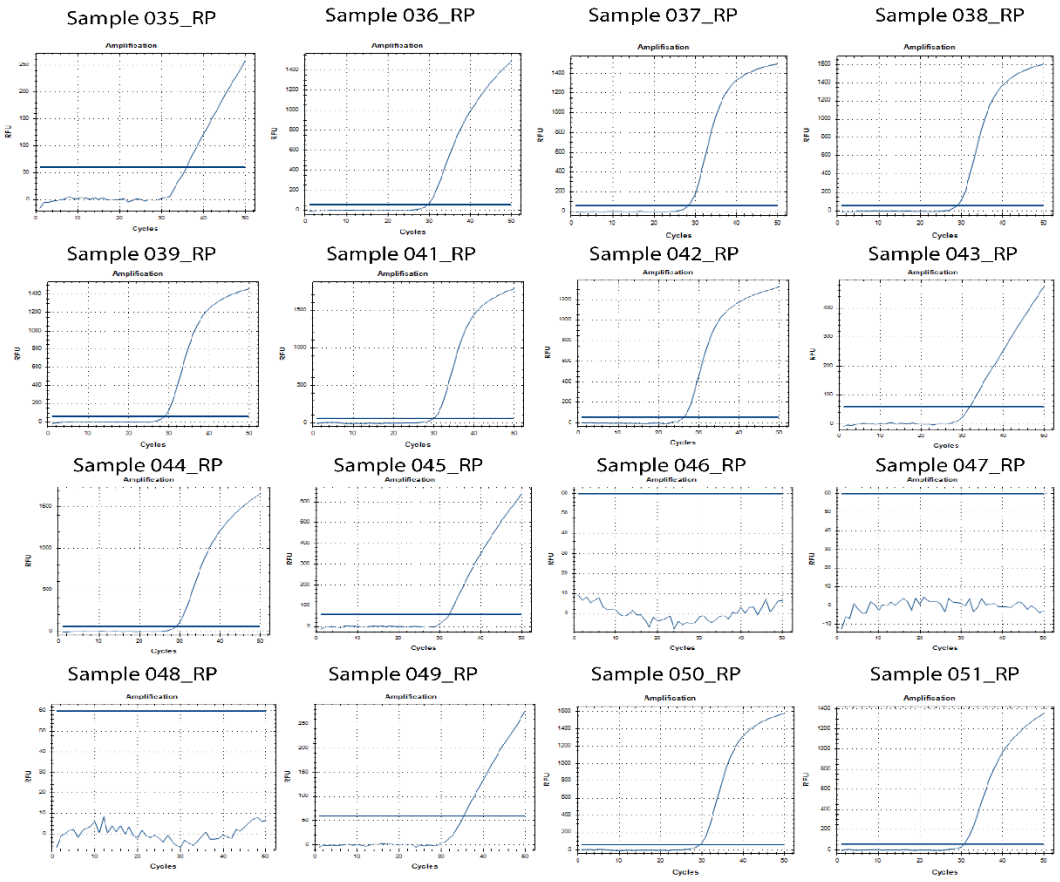

© Copyright 2021 | N Panpradist

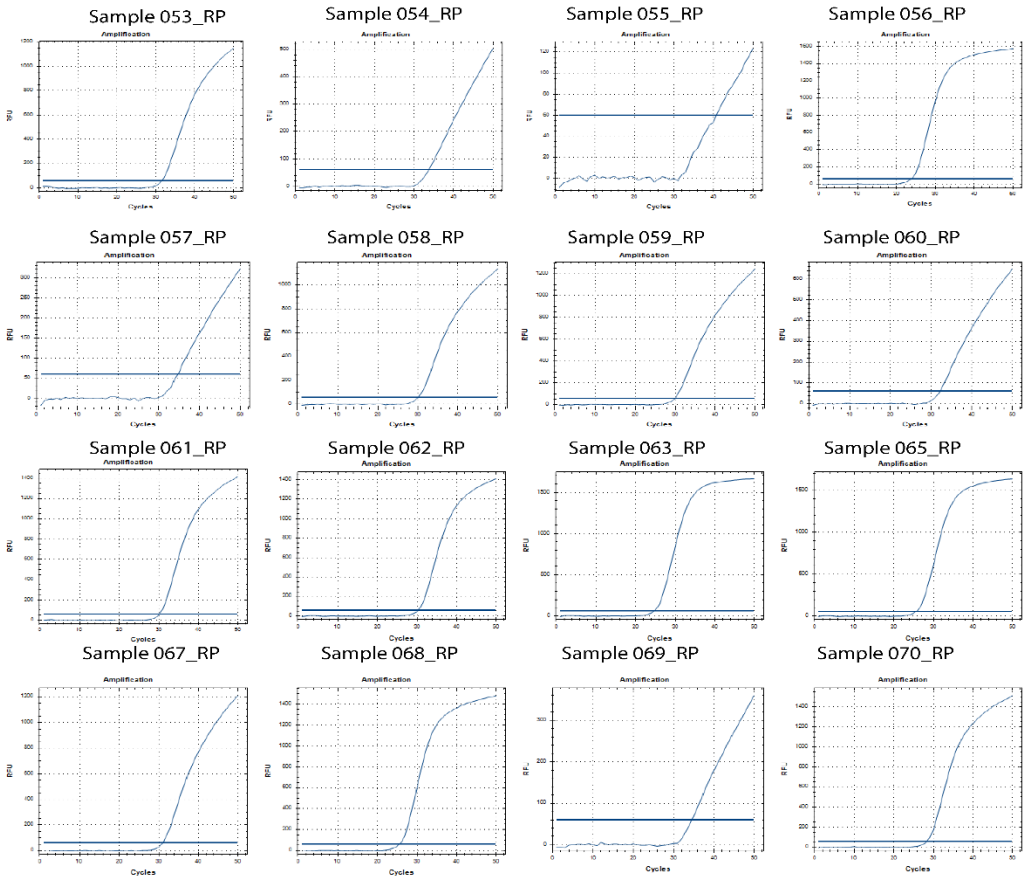

© Copyright 2021 | N Panpradist

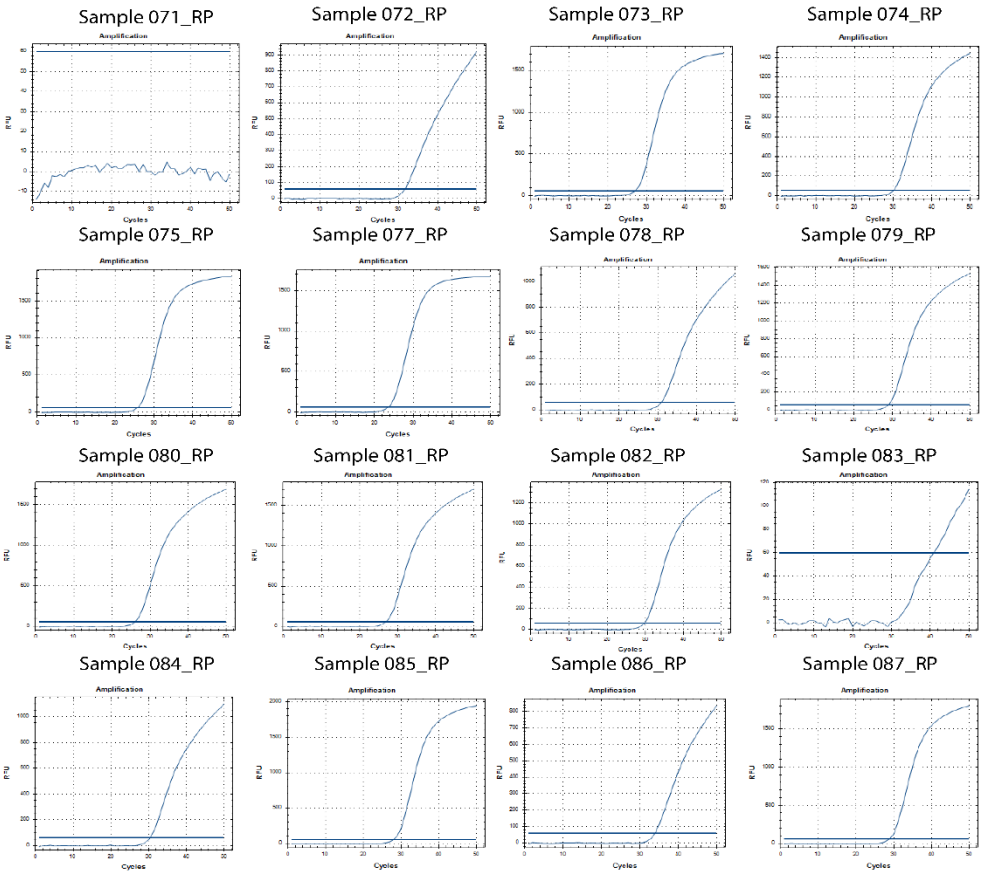

© Copyright 2021 | N Panpradist

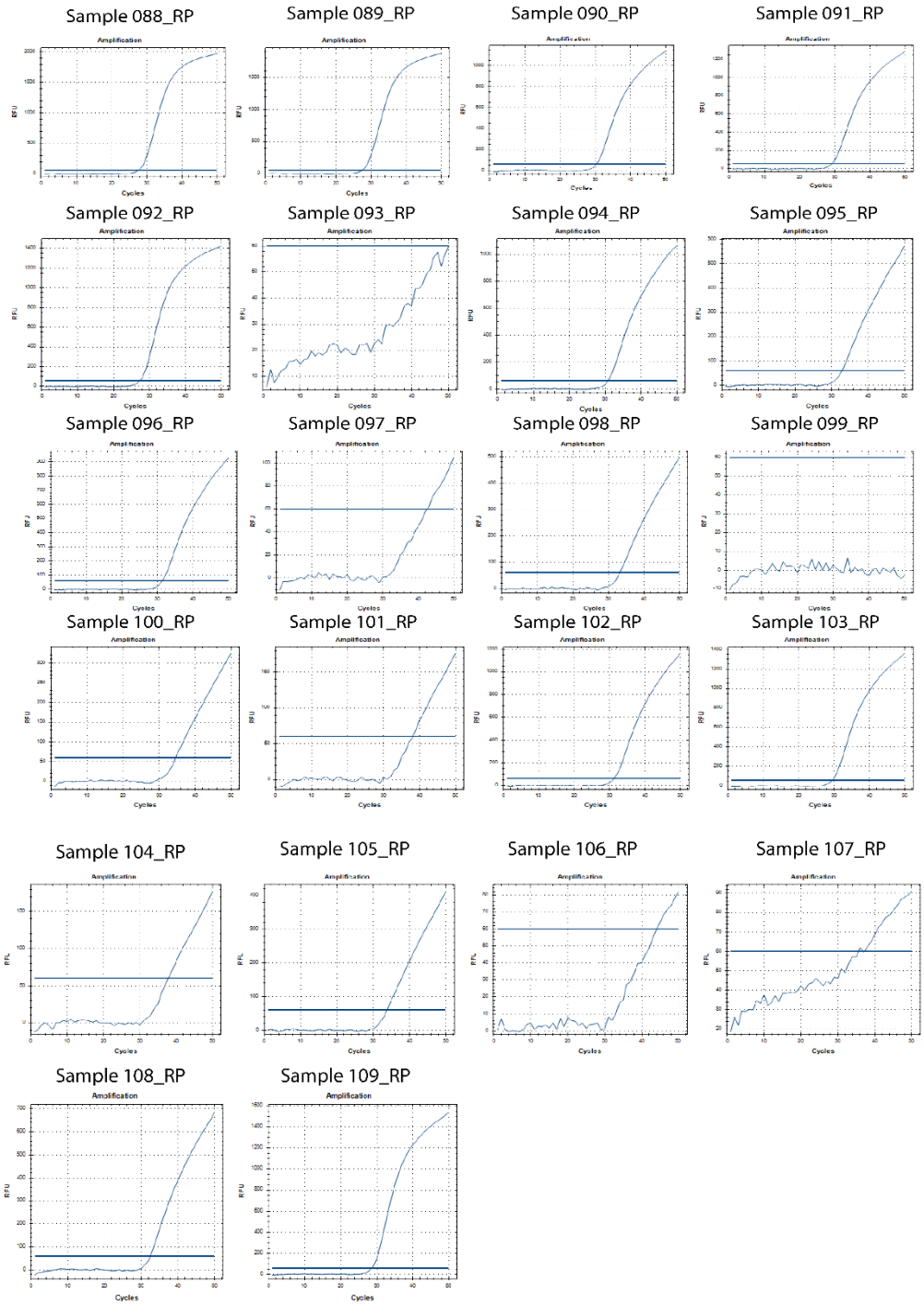

Figure S10.63 | Real-time amplification curves of RT-qPCR using CDC primers/probes.

(**A**) N1 assay. (**B**) N2 assay. (**C**) RP assay. Data were exported from the CFX Maestro (Biorad).

© Copyright 2021 | N Panpradist

Table S10.12 |Summary of RT-LAMP based technologies that have received the US FDA emergency use authorization as of July 15th, 2021.

Note that multiple tests were previously approved but recently removed from the list. Information was gathered from the package inserts and patents. Some aspects of the tests are not available, so listed as not available (N/A).

Developer	Intended use[1]	Product name	Core technology	DNA polymerase	SARS-CoV-2 target(s)	Control	# reaction/ sample tested	LAMP multiplexity	Reported LoD				Samples require nucleic acid extraction prior to RT-LAMP	Reagent set up from wet reaction (no lyophilized reaction)	Additional reaction setup after RT-LAMP	Post-reaction analysis
									Copies/uL of unpurified sample	Copies/uL of extracted RNA	Copies/reaction	Copies/uL of reaction				
Mammoth Biosciences, Inc OR University of California, San Francisco (UCSF) and Mammoth Biosciences	H	SARS-CoV-2 DETECTR™ Reagent Kit	RT-LAMP, CRISPR	Bst	N	Human RP	2	Single-target LAMP	12	20	100	4	Yes, EZ1 Virus Mini Kit v2.0 with automated extraction	Yes, reagents are thawed at room temperature but kept on ice throughout setting up.	Yes, CRISPR	Yes, based on the difference of end-point fluorescence signal from baseline signal
MobileDetect Bio Inc.	H, M	MobileDetect Bio BCC19 (MD-Bio BCC19) Test Kit	RT-LAMP	Not provided	N,E	N/A	1	Two-target, single readout	75	N/A	75	3	No, 1uL VTM sample directly amplified in 25uL reaction.	Yes, reagents must be thawed on ice 30 min prior to set up.	No	Yes, cell phone analysis based on color difference of positive and negative.
SEASUN BIOMATERIALS, Inc.	H	AQ-TOP™ COVID-19 Rapid Detection Kit PLUS	RT-LAMP	Bst	N, ORF	Human RP	2	Biplexed FAM/HEX-VIC-JOE with amp control	1	5	50	1.67	Yes, multiple authorized kits	Yes, reagents are thawed at room temperature but kept on ice throughout setting up.	No	Yes, based on automatic CT call by RT-qPCR machine
Sherlock BioSciences, Inc.	H	Sherlock™ CRISPR SARS-CoV-2 Kit	RT-LAMP, CRISPR	Not provided	N, ORF	Human RP	3	Single-target LAMP	6.75	45	360	18	Yes, PureLink™ Viral RNA/DNA Mini Kit	Yes, 2 components for RT-LAMP master mix, 8 components for CRISPR reaction	Yes, CRISPR	Yes, manual calculation of signal ratio
Color Health, Inc.	H	Color SARS-CoV-2 RT-LAMP Diagnostic Assay	RT-LAMP	Not provided	N, E[2]	Human RP	3	Single-target LAMP	0.75	N/A	N/A	N/A	Yes, Viral DNA/RNA 300 Kit H96 (Perkin Elmer, CMG-1033)	Yes	No	Yes, manual calculation of signal ratio

© Copyright 2021 | N Panpradist

Lucira Health, Inc.	Home, H, M, W	Lucira™ CHECK-IT COVID-19 Test Kit	RT-LAMP	Bst or GspM	N (2 regions)	Multiple chambers detecting the sample, a positive internal control (PIC), and a lysis internal control (LIC).	5	Biplexed LAMP without internal control	0.9	N/A	N/A	N/A	No	No	No	No, real-time analysis based on on the color change of halochromic agent(s) due to pH change as an outcome from amplification

© Copyright 2021 | N Panpradist

Continued

Developer	Intended use	Product name	Amplicon exposure after LAMP	Estimated operating time	Test batch size (reaction, samples)	Cost	Equipment involved
Mammoth Biosciences, Inc OR University of California, San Francisco (UCSF) and Mammoth Biosciences	H	SARS-CoV-2 DETECTR™ Reagent Kit	Yes	**85 min excluding analysis step** 20-min automatic extraction; 30-min RT-LAMP; 15-min CRISPR (anticipated minimal 20-min hands on from thawing, mixing, and aliquoting reactions for both steps)	96 (reaction), 48 (samples)	N/A	• Qiagen EZ1 Advanced benchtop automated extraction (48 samples) • ABI 7500 Fast Dx Real-Time PCR system (Thermo Scientific) with software • Mini Centrifuges • Multichannel or single channel pipette and barrier tips (10 µL – 200 µL); • PCR plate/tube strip support frame/racks • PCR cooler rack
MobileDetect Bio Inc.	H, M	MobileDetect Bio BCC19 (MD-Bio BCC19) Test Kit	No	60 min excluding post-analysis step 30-min thawing reagents, 30-min RT-LAMP; (anticipated 10-min hands-on from mixing and aliquoting reagents)	8 or 96	N/A	• Custom heater or thermal cycler • Cell phone with software • Minivortex • Reaction set up station • Reaction analysis station • Micropipettes • Filtered tips
SEASUN BIOMATERIALS, Inc.	H	AQ-TOP™ COVID-19 Rapid Detection Kit PLUS	No	**70 min excluding analysis step** 30-min manual extraction; 30 min RT-LAMP (anticipated minimal 10-min hands-on from thawing, mixing, and aliquoting reactions)	96 (reaction), 48 (samples)	N/A	• Real-time PCR system (CFX 96 real-time PCR detection system with software CFX manager V3.1 or Applied Biosystems real-time PCR system 7500 with Software 2.0.6) • Centrifuge • Micropipettes • Filtered tips • Vortex
Sherlock BioSciences, Inc.	H	Sherlock™ CRISPR SARS-CoV-2 Kit	Yes	110 min excluding analysis step 30-min manual extraction; 40 min RT-LAMP; 10-min CRISPR (anticipated minimal 30 -min hands-on from thawing, mixing, and aliquoting reactions)	383(reaction), 30 (samples)	N/A	• Heat block with a heated lid capable of maintaining 61°C or PCR instrument with a heated lid • Vortex • Microcentrifuge • Cold blocks • Micropipettes • Filtered tips
Color Health, Inc.	H	Color SARS-CoV-2 RT-LAMP Diagnostic Assay	No	110 min excluding analysis step 20-min bead-based RNA extraction; 70 min RT-LAMP; (anticipated minimal 20-min hands-on from thawing, mixing, and aliquoting reactions with robots)	384 (reaction), 128(samples)	N/A	• Hamilton STAR/STARlet automated liquid handler with Venus 4 software • Agilent Bravo automated liquid handling platform with software • Perkin Elmer Chemagic 360 extraction instrument platform and Chemagic software v6.3.0.3 • Biotek Synergy NEO2 multi-mode microplate reader with Gen5 software v3.9

© Copyright 2021 | N Panpradist

Lucira Health, Inc.	Home, H, M, W	Lucira™ CHECK-IT COVID-19 Test Kit	No	30-min sample run time (with anticipated 2-min handson). Positive samples are called as soon as finished	1	$50/test	• Single-use, disposable, customed heater, reader and sample collecter/transfer with 2 AA batteries

SARS-CoV-2 DETECTR Reagent Kits [1, 2]
MobileDetect Bio BCC19 (MD-Bio BCC19) Test Kit [3, 4]
Sherlock CRISPR SARS-CoV-2 Kit [5]
Color SARS-CoV-2 RT-LAMP Diagnostic Assay [6]
Lucira CHECK-IT COVID-19 Test Kit [7, 8]

1 H (High complexity CLIA labs), M (Moderate complexity CLIA labs), W (CLIA-waived, patient care settings), Home (used at home)
2 ORF assay is available but removed from the current kit

1. Mammoth Biosciences, I. INSTRUCTIONS FOR USE SARS-CoV-2 DETECTRTM Reagent Kit 2020. https://www.fda.gov/media/141765/download.
2. UCSF Health Clinical Laboratories, U. C. L. a. C. B. SARS-CoV-2 RNA DETECTR Assay. https://www.fda.gov/media/139937/download.
3. MobileDetect Bio, I. MobileDetectBIO - COVID-19 (SARS-CoV-2) Detection. https://mobiledetectbio.com/.
4. MobileDetect Bio, I. MobileDetect-BIO BCC19 Test Kit for SARS-CoV-2 Detection 2020. https://www.fda.gov/media/141791/download.
5. Sherlock Biosciences, I. INSTRUCTIONS FOR USE SherlockTM CRISPR SARS-CoV-2 kit 2021. https://www.fda.gov/media/137746/download.
6. Color Health, I. Color SARS-CoV-2 RT-LAMP Diagnostic Assay EUA Summary. https://www.fda.gov/media/138249/download.
7. Lucira Health. Lucira™ CHECK-IT COVID-19 Test Kit 2021. https://www.fda.gov/media/147494/download.
8. Mitra, D.; Dimov, I. K.; Waldeisen, J. R. Colorimetric Detection of Nucleic Acid Amplification. **https://patents.google.com/patent/US20170044599A1/pt-pt**.

© Copyright 2021 | N Panpradist

Table S10.13 | Primers, probes, and control sequences.

For primers and probes F2/B2 sequences are underlined, non-template linker sequences are italicized, and adapter sequences are in bold.

SARS-CoV-2 NC1 Primers	Sequence (5' to 3')
NC1 FIP	**CCACTGCGTTCTCCATTC*TTTT*CCCCGCATTACGTTTGGT**
NC1 BIP	GCGATCAAAACAACGTCGG*TTAT*TGCCATGTTGAGTGAGAGCG
NC1 LF	TGGTTACTGCCAGTTGAATCT
NC1 LB + T Adapter	**ACCAACACCTCACATCACACATAATA**GGTTTACCCAATAATACTGCGTCTTG
NC1 F3	TGGACCCCAAAATCAGCG
NC1 B3	ATCTGGACTGCTATTGGTGTTA
SARS-CoV-2 NC2 Primer	Sequence
NC2 FIP	**CAGCTTCTGGCCCAGTTCCTGTGGTGGTGACGGTAAAATG**
NC2 BIP	CTTCCCTATGGTGCTAACAAAG*T*CCAATGTGATCTTTTGGTGTATTCA
NC2 LF	GTAGTAGAAATACCATCTTGGACT
NC2 LB + T Adapter	**ACCAACACCTCACATCACACATAATA**ATATGGGTTGCAACTGAGGGAG
NC2 F3	CTACTACCGAAGAGCTACCAG
NC2 B3	GCAGCATTGTTAGCAGGATTG
SARS-CoV-2 NC3 Primers	Sequence
NC3 FIP	**TGTGTAGGTCAACCACGTTC*T*GCTTCAGCGTTCTTCGGA**
NC3 BIP	GTGCCATCAAATTGGATGACAAAGGTTTTGTATGCGTCAATATGCTTATTCAG
NC3 LF + T Adapter	**ACCAACACCTCACATCACACATAATA**TCCATGCCAATGCGCGACA
NC3 LB	CCAAATTTCAAAGATCAAGTCAT
NC3 F3	GACCAGGAACTAATCAGACAAG
NC3 B3	GCTTGAGTTTCATCAGCCTTC
IAC (NC1) primer	Sequence
IAC FL + C Adapter	**ACCACACCTACCACCACTAATAACTAACTCCAGCCATCCTCACCATC**
Target UDP	Sequence
CoV UDP Probe	**FITC – CCATCAGCACCAAGACTACCCACCTCGCCACCAAACCAACACCTCACATCACACATAATA**
CoV UDP Quencher	TTGGTGGCGAGGTGGGTAGTCTTGGTGCTGATGG– Iowa Black® FQ
Control UDP	Sequence
IAC UDP Probe	**Tex615 – CCTGACCACTTCCGAACCCAACCACCTACGACAGACCACACCTACCACCACTAATAACTAA**
IAC UDP Quencher	CTGTCGTAGGTGGTTGGGTTCGGAAGTGGTCAGG – BHQ2
IAC Template	Sequence
IAC (NC1) ssDNA	**AAT GGA CCC CAA AAT CAG CGA AAT GCA CCC CGC ATT ACG TTT GGT GGA CCC TCT GGA GTC AAT GGG TGG TGC CAG AAT GGA GAA CGC AGT GGG GCG CGA TCA AAA CAA CGT CGG CCC CAA GTT GAT CTC CAG CCA TCC TCA CCA TCG TTC ACC GCT CTC ACT CAA CAT GGC AAG AAT TAA CAC CAA TAG CAG TCC AGA TG**

© Copyright 2021 | N Panpradist

Table S10.14 | Detailed reagent and device cost at a production scale of 10,000 units

Item	Supplier	Cost/device (US$)
Detector boards	Macrofab	$7 each x 2 ($14 total)
Main board	Macrofab	$25 each
LED board	Macrofab	$9 each
Lid Heater	Oshpark	$7 each
Heat block	Bryan Willman	$12 each
Housing	Xometry – HP MultiJet Fusion 3D printing, no volume discount	$50 (costs here should be reduced for scale-up production)
Red filters	Newport	$10 each, $40 in total
Green filters	Newport	$20 each, $80 in total
Assembly	N/A	$30 (half an hour assembly time at $60/hour cost)
	Total	**$267 per unit**
Item	Supplier	Cost/device (US$)
Detector boards	Macrofab	$7 each x 2 ($14 total)
Main board	Macrofab	$25 each
LED board	Macrofab	$9 each
Lid Heater	Oshpark	$7 each
Heat block	Bryan Willman	$12 each
Housing	Xometry – HP MultiJet Fusion 3D printing, no volume discount	$50 (costs here should be reduced for scale-up production)
Red filters	Newport	$10 each, $40 in total
Green filters	Newport	$20 each, $80 in total
Assembly	N/A	$30 (half an hour assembly time at $60/hour cost)
	Total	**$267 per unit**

© Copyright 2021 | N Panpradist

Table S10.15 | Consumable costs per test

Item	Supplier	Costs per kit (US$)
Sampling components ($2 maximum)	Multiple sources	$2
Desiccant	Multiple sources	$0.5
PCR tube	Multiple sources	Negligible
DNA polymerase	Produced in-house	Negligible
Reverse transcriptase	New England Biolabs	$3.5
ThermosTable S10.inorganic pyrophosphatase	New England Biolabs	$0.23
Primers	Integrated DNA Technologies	$0.03
Fluorescent probe/quenchers	Integrated DNA Technologies	$0.24
Triton-X100	Sigma-Aldrich	Negligible
dNTPs	New England Biolabs	$0.38
Mannitol	OPS Diagnostics	Negligible
DL-Dithiothreitol (DTT)	Promega	Negligible
Nuclease-free water	VWR	Negligible
1X Tris low-EDTA buffer	VWR	Negligible
Rnasin ribonuclease inhibitor	Promega	$0.71
DNA internal amplification control	Integrated DNA Technologies	$0.01
Cost of goods		**$8.00**

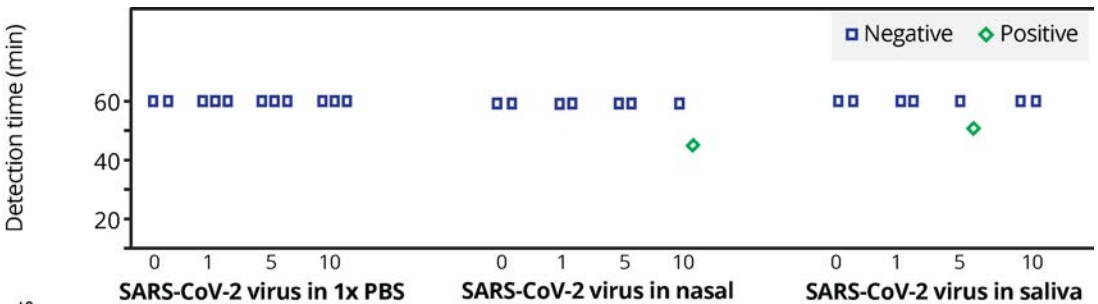

SARS-CoV-2 virus (copies/reaction)

0	0/2	0/2	0/2
1	0/3	0/2	0/2
5	0/3	0/2	1/2
10	0/3	1/2	0/2

Figure S10.64 | Analysis of XPRIZE panel of contrived samples containing less than 20 copies/reaction.

© Copyright 2021 | N Panpradist

Table S10.16 | Primer and probe sequences for SARS-CoV-2 typing assay.

Category	Name	Sequence
RT-LAMP S gene section 1	S1F3v1	GGACCTTGAAGGAAAACAGGG
RT-LAMP S gene section 1	S1LFv1	GGTAGGTAGAGAAGGGACTGG
RT-LAMP S gene section 1	S1FIPv1	CACACGCCTATTAATTTA+GT+GCCCAGTCCCTTCTCTACCTACCACACGCCTATTAATTTAGTGCGT
RT-LAMP S gene section 1	S1B3v1	AGCTGTCCAACCTGAAGAAGA
RT-LAMP S gene section 1	S1BIPv1	TGCCAATAGGTATTAACATCACTAGGTTCACTGCCAATACTCCACTCAGGAGTCAAATAACTTCTATGTAAAGC
RT-LAMP S gene section 1	S1LBv1	TCACTGCCAATACTCCACTC
Adapter for ligation	SPECIFIC_FAMv1	/56-FAM/ACTGACTACTCACTACACAACCCATTAGTAGCTTC
Adapter for ligation	SPECIFIC_DIGv1	/5DiGN/ATTGATTTTGAGAGGGTGGTAGATTTAGTTGGG
Adapter for ligation	COM_Biotinv1	/5Phos/TATAAACAATTTCCTTAACCACCCTAACATAAACGAC/3Bio/
Seed for ligation	SEED_FAMv1	GGTTTAAGATTAAGTGAAGCTTGGATAGGAAGCTACTAATGGGTTGTGTAGTGAG
ligation probe	MUT_222v1	/5Phos/CTATCCAAGCTTCACTTAATCTTAAACACTGACTAGTGATCTCCCTCAGGGTTTTTCGGT
ligation probe	WT_222v1	/5Phos/CATAGGAGGTAAGTGGTATAAGTGTAGAGTGTGTTAGTGATCTCCCTCAGGGTTTTTCGGC
Seed for ligation	SEED_DIGv1	GATCTACACTTATACCACTTACCTCCTATGCCCAACTAAATCTACCACCCTCTCA
Seed for ligation	SEED_Biotinv1	TGTTAGGGTGGTTAAGGAAATTGTTTATAAGCCGTGTGTGAGTAATGTGTAGTGT
ligation probe	Com_222	/5Phos/TTTAGAACCATTGGTAGATTTGCCAATAAAAAGTGCACTACACATTACTCACACACGGCT
Seed for ligation	SEED DIGv2	GATCTACACTTATACCACTTACCTCCTATGTTCTTTTTTARCCCYGCTGGATG
Seed for ligation	SEED BioV2	TGTTAGGGTGGTTAAGGAAATTGTTTATATGCTGCCCTATTTCTAARTCAGAT

© Copyright 2021 | N Panpradist

Seed for ligation	SEED FAMV2	GTTTAAGATTAAGTGAAGCTTGGATAGCRTATTGATAGATAAYTATTTCTGGAT
ligation probe	MUT_510v1	/5Phos/CTATCCAAGCTTCACTTAATCTTAAACACTGACTAATATGGTTTCCAACCCACTT
ligation probe	WT_510v1	/5Phos/CATAGGAGGTAAGTGGTATAAGTGTAGAGTGTGTTAATATGGTTTCCAACCCACTA
ligation probe	COM_510v1	/5Phos/ATGGTGTTGGTTACCAACCATACAAAAAGTGCACTACACATTACTCACACACGGCT
ligation probe	MUT_222v1	/5Phos/CTATCCAAGCTTCACTTAATCTTAAACGGATTCAAGTGATCTCCCTCAGGGTTTTTCGGT
ligation probe	WT_222v1	/5Phos/CATAGGAGGTAAGTGGTATAAGTGTAGGGATTCAAGTGATCTCCCTCAGGGTTTTTCGGC
ligation probe	COM_222v1	/5Phos/TTTAGAACCATTGGTAGATTTGCCAATAAAAAGTGCACTACACATTACTCACACACGGC
ligation probe	MUT_417Nv1	/5Phos/CTATCCAAGCTTCACTTAATCTTAAACACTGACTACGCTCCAGGGCAAACTGGAAMT
ligation probe	WT_417Nv1	/5Phos/CATAGGAGGTAAGTGGTATAAGTGTAGAGTGTGTTACGCTCCAGGGCAAACTGGAAMG
ligation probe	Com_417Nv1	/5Phos/ATTGCTGATTATAATTATAAATTAAAAAGTGCACTACACATTACTCACACACGGC
ligation probe	Com_417Tv1	/5Phos/KTTGCTGATTATAATTATAAATTACAAAAGTGCACTACACATTACTCACACACGGC
ligation probe	MUT_417Tv1	/5Phos/CTATCCAAGCTTCACTTAATCTTAAACACTGACTAATCGCTCCAGGGCAAACTGGAAC
ligation probe	WT_417Tv1	/5Phos/CATAGGAGGTAAGTGGTATAAGTGTAGAGTGTGTTAATCGCTCCAGGGCAAACTGGAAA
ligation probe	WT_484v1	/5Phos/CATAGGAGGTAAGTGGTATAAGTGTAGAGTGTGTTATAGCACACCTTGTAATGGTGTTG
ligation probe	Com_484	/5Phos/AAGGTTTTAATTGTTACTTTCCTTTAAAAGTGCACTACACATTACTCACACACGGCT
ligation probe	MUT_484v1	/5Phos/CTATCCAAGCTTCACTTAATCTTAAACACTGACTATAGCACACCTTGTAATGGTGTTA

© Copyright 2021 | N Panpradist

competing oligo	Compt222_v1	ACCGAAAAACCCTGAGGGAGATCACTTGAATCC
competing oligo	Compt222_v2	CACTTTTTATTGGCAAATCTACCAATGGTTCTAAA
Competing oligo	Compt417N_v1	AKTTCCAGTTTGCCCTGGAGCGTAGTCAGT
Competing oligo	Compt417N_v2	CACTTTTTAATTTATAATTATAATCAGCAAT
Competing oligo	Compt417T_v1	GTTCCAGTTTGCCCTGGAGCGATTAGTCAGT
Competing oligo	Compt417T_v2	CACTTTTGTAATTTATAATTATAATCAGCAAM
Competing oligo	Compt484_v1	TAACACCATTACAAGGTGTGCTATAGTCAGT
Competing oligo	Compt484_v2	CACTTTTAAAGGAAAGTAACAATTAAAACCTT
Competing oligo	Compt510_v1	AAGTGGGTTGGAAACCATATTAGTCAGT
Competing oligo	Compt510_v2	CACTTTTTGTATGGTTGGTAACCAACACCAT
RT-LAMP S2 gene section 2	S2BIPv1	CTATCAGGCCGGTAGCACACTCACTGCCAATACTCCACTCGTGCATGTAGAAGTTCAAAAGAAAGT
RT-LAMP S2 gene section 2	S2B3v1	GTGTGCTACCGGCCTGATAG
RT-LAMP S2 gene section 2	S2F3v1	GTGATGAAGTCAGACAAATCGCT
RT-LAMP S2 gene section 2	S2FIPv1	TGGTGGTTGGAATCTTAGTTCTACCAGTCCCTTCTCTACCTACCCAGGCTGCGTTATAGCTTGGA

© Copyright 2021 | N Panpradist

INTRUCTION BOOKLETS FOR THE POINT-OF-CARE RT-PCR TEST

COVID-19 RT-PCR assay
Collaboration between University of Washington and Georgetown University

PART 1

COVID-19 RT-PCR assay
Collaboration between University of Washington and Georgetown University

Is this your first time operating this COVID-19 test?

- Yes (if answer Yes, you can skip to 1.2)

© Copyright 2021 | N Panpradist

- No

Part 1 | Reaction Setup

⚠ Before starting, ensure the space has been wiped clean with 10% bleach, and the bleach residue is removed using 70% ethanol.

1. Use clean gloves to handle samples
2. Change gloves after handing each sample.
3. Tube racks should be washed with soap water and dried after each run.

Failure to do the above steps can lead to false positive COVID-19 detection results.

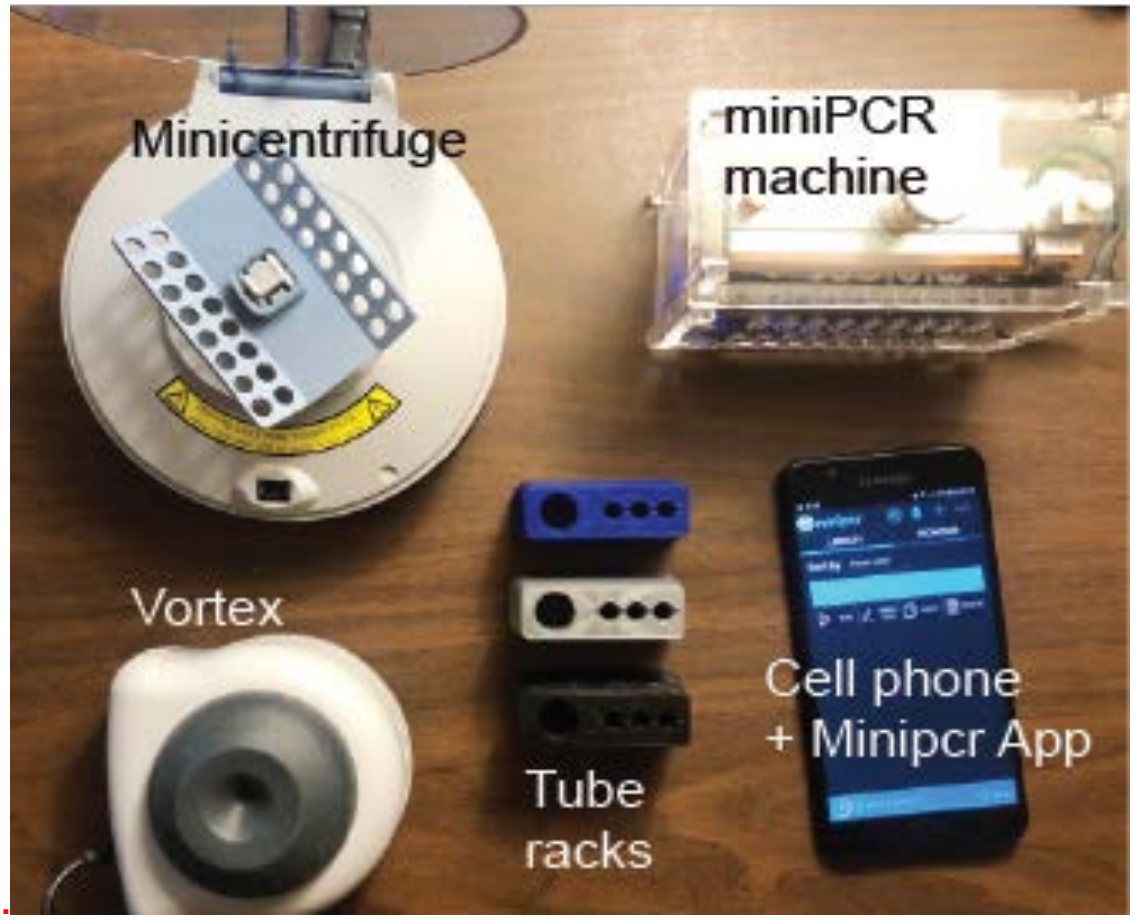

1.1 Review of tools

- Vortex (fluid mixer)
- Minicentrifuge

⚠ **Warning:** Failure to follow below instructions can lead to injury.

1.**Always balance** the tubes.

© Copyright 2021 | N Panpradist

2.**Wait until the spin completely stops** before accessing the tubes.

- Tube rack (three colors: blue, grey, and black for three different samples)
- Cell phone with miniPCR app
- MiniPCR machine

1.2 Check the components for your kit

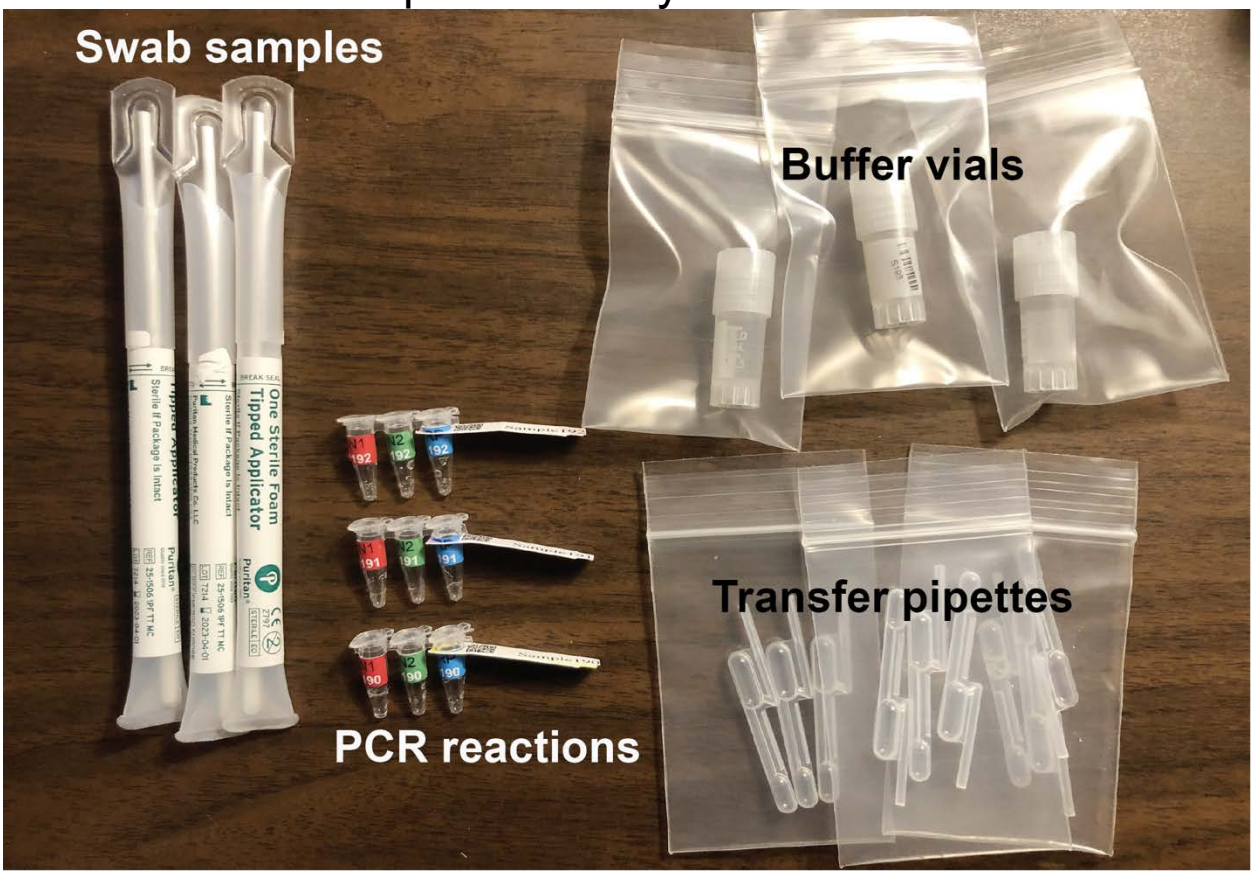

Record the kit number: _____

1. Control swabs
    1. Swab # _____
    2. Swab # _____
    3. Swab # _____
2. PCR tube reactions (3 tubes for each sample) are in the foil pouches
    1. Sample # _____
    2. Sample # _____
    3. Sample # _____
3. Buffer vials (1 tube for each sample)

- Check if any buffer tube leaks. Notify supervisor if tube leaks.

a. Buffer vial # _____
b. Buffer vial # _____
c. Buffer vial # _____

4. Transfer pipettes (1 bag for each sample; each bag contains 3 transfer pipette)

© Copyright 2021 | N Panpradist

- Check if each bag contains 3 transfer pipettes. If you don't have three bags each containing 3 transfer pipettes, notify your supervisor.

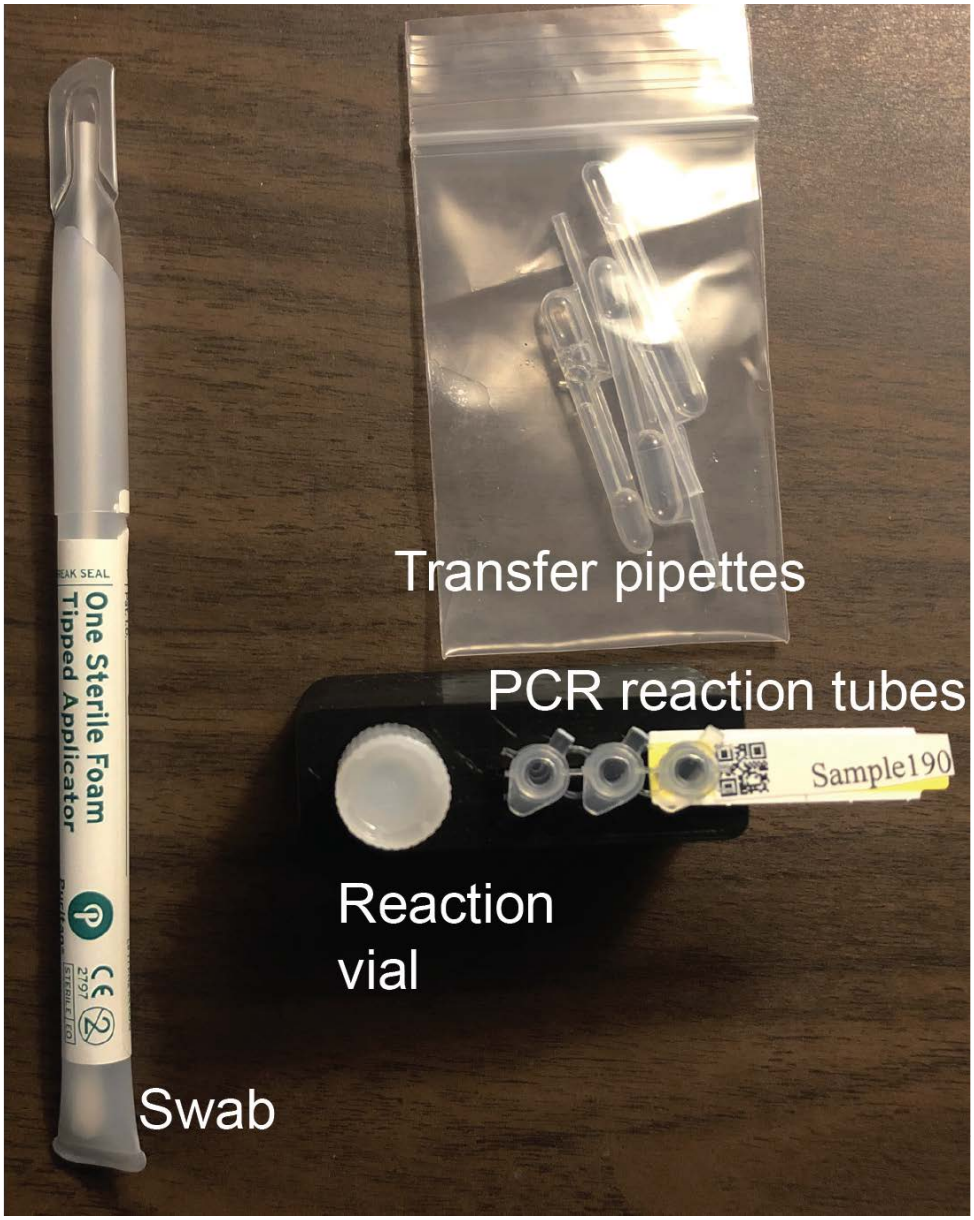

1.3 Set up reaction for each sample sequentially

1. Set aside the following:
    1. 1 swab
    2. 1 buffer vial (matching with swab number)
    3. 1 PCR reaction set (3 tubes) - matching with swab number
    4. 1 bag of transfer pipettes

© Copyright 2021 | N Panpradist

2. If you find swab, buffer tube, and PCR reaction numbers **do not match, record the pairing below:**

a. Swab # _____

b. Paired with Buffer vial # _____

c. PCR reaction sample # _____

3. Place PCR reaction tubes on the rack.

4. Place buffer vial on the rack

5. Remove swab from the sleeve tube. **Avoid touching the swab tip**.

6. Place the swab in the buffer vial and let sit for one minute.

WAIT FOR 1 MINUTE.

7. Press the swab tip against the side of the buffer 5 times while stirring the swab to release materials from the swab.

8. Before discarding the swab, press the swab against the side of the tube above the fluid level to remove fluid from the swab tip as much as possible.

9. Discard the swab in **the biohazard bag**.

10. Open three of the PCR reaction tubes.

11. Use transfer pipette to transfer the buffer from the vial to each PCR reaction tube.

© Copyright 2021 | N Panpradist

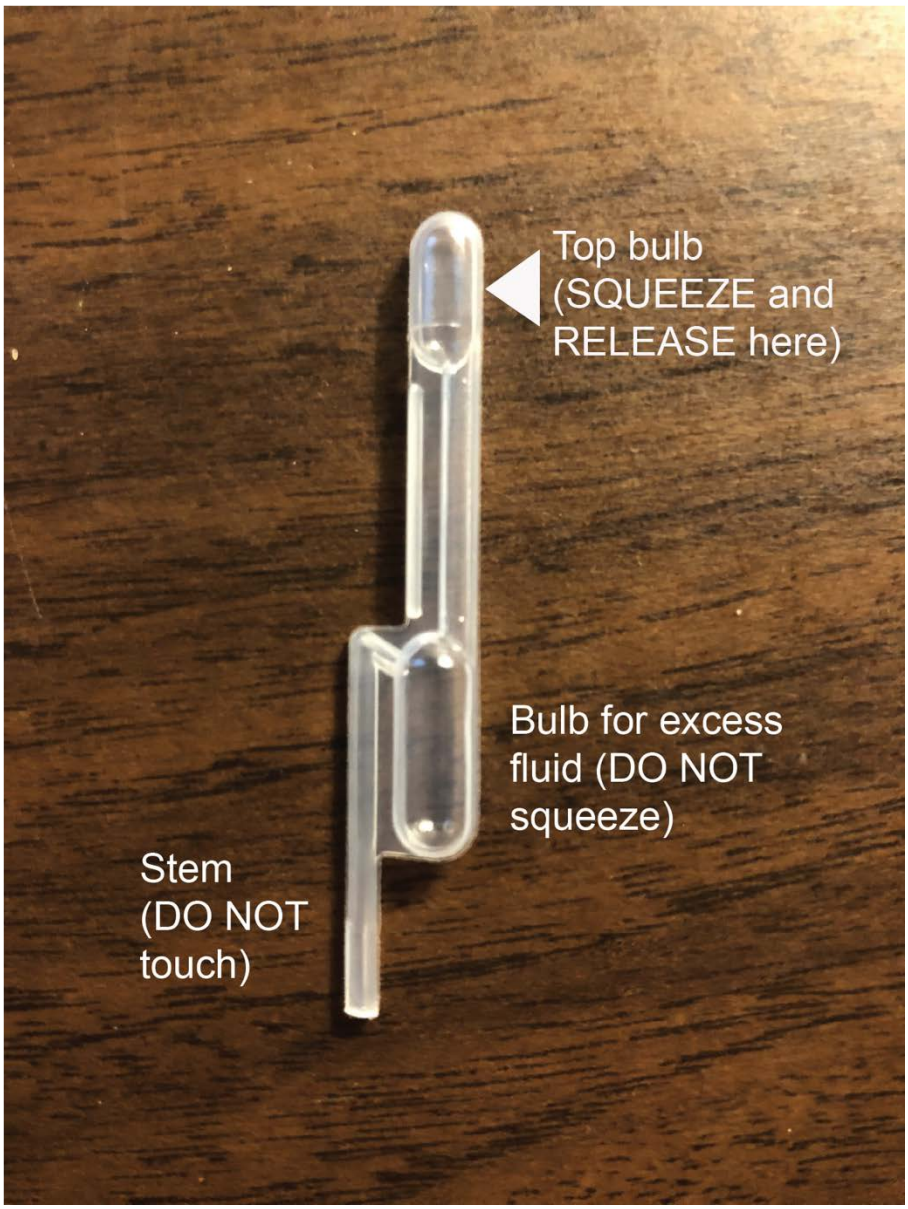

a. Remove the transfer pipette from the bag. **Avoid touching the stem part**.
b. Squeeze the top bulb and hold.
c. Submerge the pipette stem down to the bottom of the buffer vial.
d. Release the bulb to let the fluid flow inside the stem. Check if you get fluid inside the stem with no bubbles. (Repeat **b-d** if you have bubbles.)
e. Place the stem in the first PCR tube. Squeeze the bulb to release the fluid. It is okay if you have extra fluid in the bottom bulb.
f. Discard the transfer pipette in the biohazard bag.
g. Close the lid of the first tube.
h. Repeat step **a-g** for the second and third PCR tubes using new transfer pipette.

12. Change gloves

© Copyright 2021 | N Panpradist

13. Set aside the **second set**: buffer vial, swab, PCR reaction tubes, and transfer pipette.
a. Use a new tube rack for each sample.
b. Repeat step 1
c. Record the pairing for step 2:
If you find swab, buffer tube, and PCR reaction numbers do not match, record the pairing below:
1. Swab # _____
2. Paired with Buffer vial # _____
3. PCR reaction sample # _____
d. Repeat steps 3-11.
14. Set aside the **third set**: buffer vial, swab, PCR reaction tubes, and transfer pipette.
a. Use a new tube rack.
b. Repeat step 1
c. Record the pairing for step 2:
If you find swab, buffer tube, and PCR reaction numbers do not match, record the pairing below:
1. Swab # _____
2. Paired with Buffer vial # _____
3. PCR reaction sample # _____
d. Repeat steps 3-11.
15. Vortex the PCR reaction tubes for 5 seconds twice.
16. Use microcentrifuge to pull down the fluid to the bottom of the tube. Load PCR reaction tubes set 1 and set 2 on the opposite side of centrifuge racks to balance the weight of the two PCR tube sets (see the position of tubes in the picture below. Avoid tags getting caught on the side of the minicentrifuge).

⚠ Failure to balance the tubes or touching the tubes during the spinning can lead to injury.

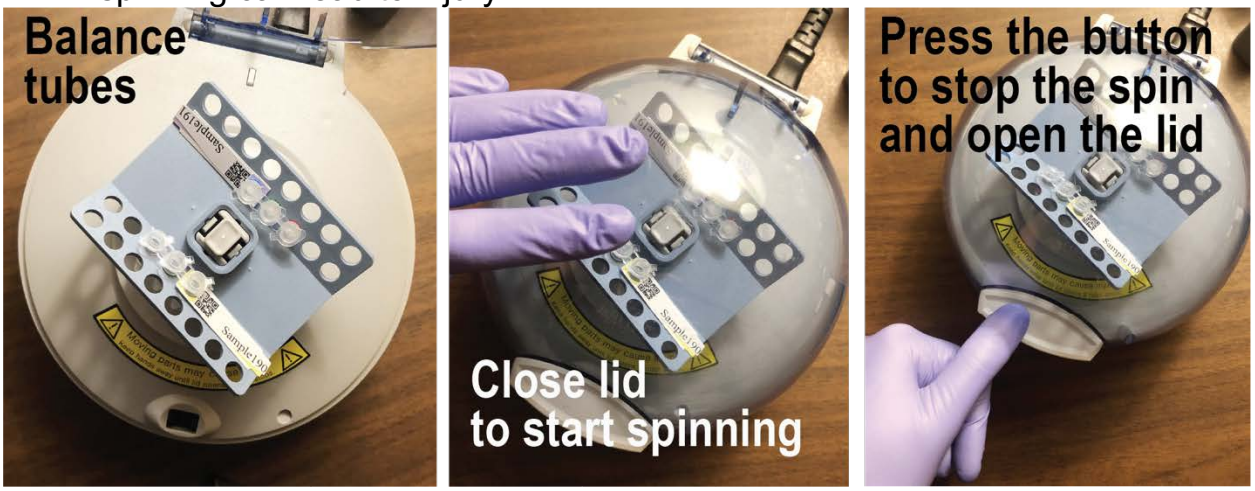

© Copyright 2021 | N Panpradist

17. Close the lid to start spinning. Let the tubes spin for 5 seconds.
18. Press the button at the front of minicentrifuge to stop the spin. Wait until the microcentrifuge comes to a complete stop before opening the lid.
19. Remove the PCR reaction tubes set 1 and replace with the PCR reaction tubes set 3.
20. Repeat steps 16-17.
21. Unload the PCR reaction tubes while making sure that the **fluid stays at the bottom of the tube** (avoid additional shaking).
22. Load sample to miniPCR machine and start the run

a. Supervisor - ensure connection between the miniPCR and the miniPCR app. Check device serial number and ensure it matches.

a. Squeeze the lock with one hand. Use the other hand to lift open the latch.

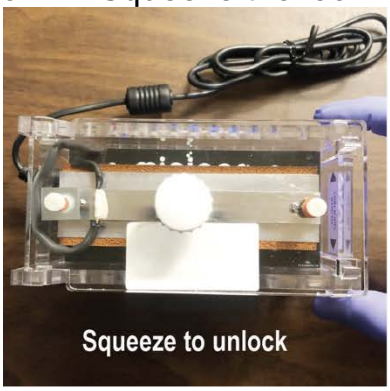

b. Load PCR reaction tubes as shown in the picture below. **Press down the tubes to make sure** they are securely in place.

c. Close the latch. Press down until you hear the “click” sound.

d. Adjust the **knob clockwise** until you feel resistance.

e. Open the miniPCR app on the phone. Select the COVID-19 PCR protocol and start the run.

f. Return after 1.5h.

COVID-19 RT-PCR assay **Record Kit # _____**

Collaboration between University of Washington and Georgetown University

© Copyright 2021 | N Panpradist

Part 2 | Signal analysis using cell phone application.

2.1 Review the tools:

1. **Transilluminator** ⚠ This has a very bright blue light source. **Do not look directly at ligh**t without the orange filter cover. Failure to do so can lead to eye injury.
2. **Black box** to cover transilluminator and serve as the phone image station.
3. **Cell phone** with the COVIDcapture App.
4. **Minicentrifuge** to pull down the liquid to the bottom of the PCR tubes.

2.2 Remove tubes from the miniPCR machine and centrifuge the tubes to pull down all the fluid to the bottom of the tubes.

1. Remove the PCR tubes from the PCR machine.

a. Turn the knob counterclockwise.

b. Squeeze the lock on the right side with one hand. Use the other hand to lift open the latch.

c. Spin down the PCR reaction tubes.

d. Load PCR reaction tubes set 1 and set 2 on the opposite side of centrifuge racks to balance the weight of the two PCR tube sets (See the position in the picture below).

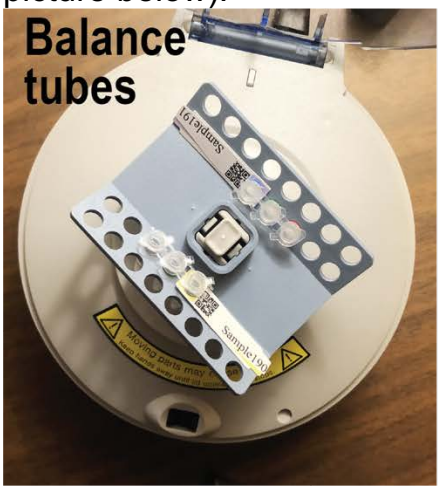

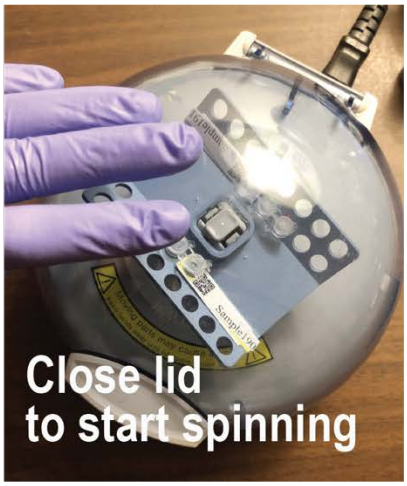

e. Close the lid to start spinning. Let the spin continue for 5 seconds (count 1 to 5).

f. Press the button to stop the centrifuge from spinning. Wait until the centrifuge comes to complete stop before opening the lid

g. Remove the PCR reaction tubes set 1 and replace with the PCR reaction tubes set 3.

h. Repeat steps 16-17.

© Copyright 2021 | N Panpradist

i. Remove the PCR reaction tubes while making sure that the fluid stays at the bottom of the tube (avoid additional shaking).

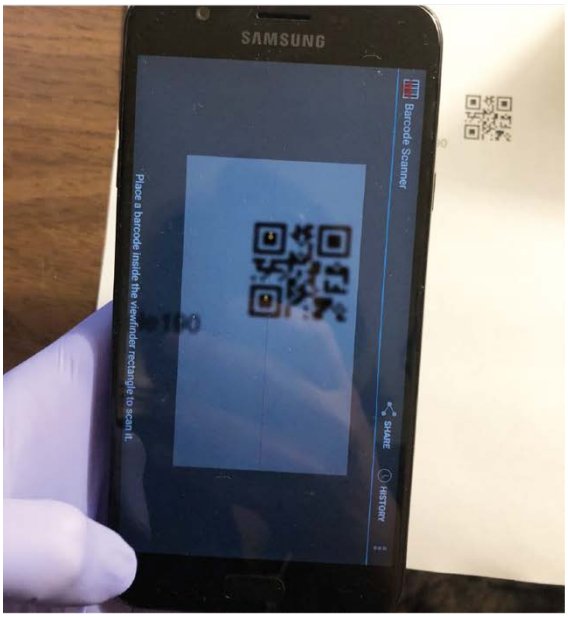

2.3 Taking picture using the transilluminator

1. Take an image of **one set of the PCR tubes at the time**.

2. Use the **the paper QR code matching the sample #** of the PCR tube reactions. Notify the supervisor if the number does not match.

3. Open the COVID19Capture App.

a. Select QRCODE button.

© Copyright 2021 | N Panpradist

b. Move the phone camera over the paper QR code until the App scans the barcode and shows the sample number on the screen. Put the cellphone aside. **Do not press CAPTURE until advised**.
c. If you accidentally press CAPTURE ahead of time, repeat step 3a-3b.

4. Prepare tubes for imaging on transilluminator
a. Ensure the **blue light is off** (switch is on the left side) before loading the sample tube for imaging.

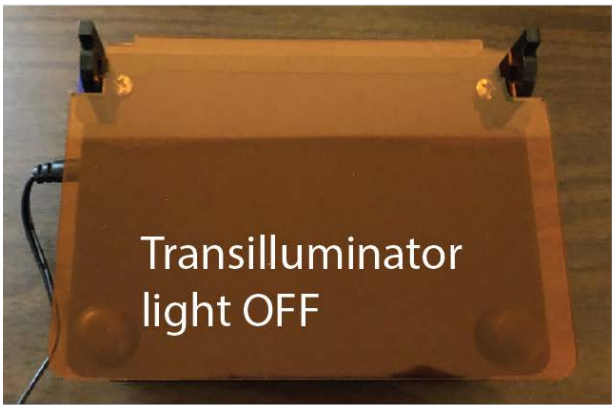

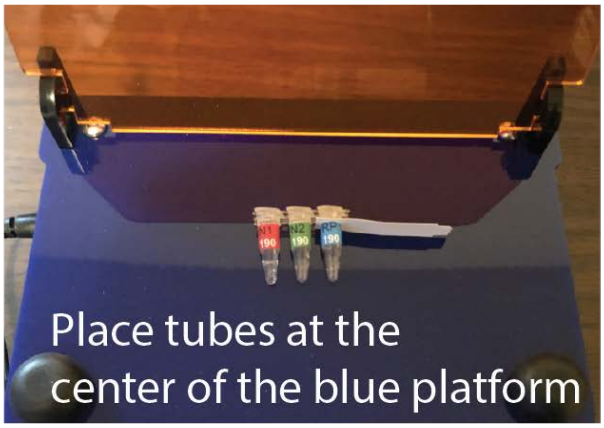

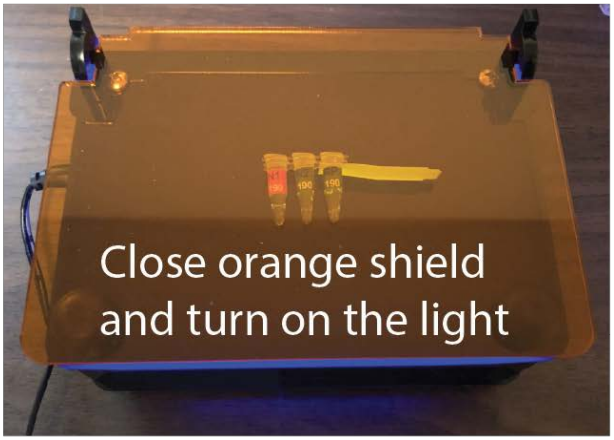

b. Lift the orange shield and place the PCR tube in the middle of the plate.
c. Close the orange shield.
d. Turn on the blue light (switch on the side).
e. Cover the transilluminator with the black box. The gap at the bottom of the box should cover the plug area on the left side.
f. Rest the cell phone on top of the black box. Put the camera lens over the hole on top. Adjust the position until you observe the image of the tubes on the phone.

© Copyright 2021 | N Panpradist

g. Press CAPTURE. If you can see the image of the tube on the cell phone, click UPLOAD. If not, please repeat steps **a-f**.

5. Repeat step 1-4 for the remaining two sets of the PCR reaction tubes.

© Copyright 2021 | N Panpradist

CHAPTER 10 REFERENCES

1. Patel, P. A.; Ledeboer, N. A.; Ginocchio, C. C.; Condon, S.; Bouchard, S.; Qin, P.; Karchmer, T.; Peterson, L. R., Performance of the BD GeneOhm MRSA achromopeptidase assay for real-time PCR detection of methicillin-resistant Staphylococcus aureus in nasal specimens. *J Clin Microbiol* **2011,** *49* (6), 2266-8.
2. Andras, K.; Reinhard, I. B.; Hailong, Z.; Milton, T. W. H.; Dan, V. N. In *Effect of various artificial surfaces on the colonization and viability of E. coli and S. aureus*, Proc.SPIE, 2008.
3. Verhoeven, P.; Grattard, F.; Carricajo, A.; Pozzetto, B.; Berthelot, P., Better detection of Staphylococcus aureus nasal carriage by use of nylon flocked swabs. *Journal of clinical microbiology* **2010,** *48* (11), 4242-4244.
4. Turner, J. C.; Harry, K.; Lofland, D.; Kunapuli; Madhusudhan, T. The Characterization of the Absorption and Release Properties of Various Clinical Swabs. https://www.puritanmedproducts.com/media/studies/CET_CVS_ASM_10_4_7_10_FINAL_poster_Absorb_Release_Various_Swabs_Comparison.pdf.
5. Rossney, A. S.; Herra, C. M.; Brennan, G. I.; Morgan, P. M.; O'Connell, B., Evaluation of the Xpert methicillin-resistant Staphylococcus aureus (MRSA) assay using the GeneXpert real-time PCR platform for rapid detection of MRSA from screening specimens. *J Clin Microbiol* **2008,** *46* (10), 3285-90.
6. Harry, K. H.; Turner, J. C.; Madhusudhan, K. T., Comparison of physical characteristics and collection and elution performance of clinical swabs. *African Journal of Microbiology Research* **2013,** *7*, 4039-4048.

© Copyright 2021 | N Panpradist

7. Rubin, L. G.; Rizvi, A.; Baer, A., Effect of swab composition and use of swabs versus swab-containing skim milk-tryptone-glucose-glycerol (STGG) on culture- or PCR-based detection of Streptococcus pneumoniae in simulated and clinical respiratory specimens in STGG transport medium. *J Clin Microbiol* **2008,** *46* (8), 2635-40.
8. Landers, T. F.; Hoet, A.; Wittum, T. E., Swab type, moistening, and preenrichment for Staphylococcus aureus on environmental surfaces. *J Clin Microbiol* **2010,** *48* (6), 2235-6.
9. Matheson, A.; Christie, P.; Stari, T.; Kavanagh, K.; Gould, I. M.; Masterton, R.; Reilly, J. S., Nasal swab screening for methicillin-resistant Staphylococcus aureus--how well does it perform? A cross-sectional study. *Infect Control Hosp Epidemiol* **2012,** *33* (8), 803-8.
10. Sparham, P. D.; Lobban, D. I.; Speller, D. C., Isolation of Staphylococcus aureus from sputum in cystic fibrosis. *J Clin Pathol* **1978,** *31* (10), 913-8.
11. Freitas, A. I.; Vasconcelos, C.; Vilanova, M.; Cerca, N., Optimization of an automatic counting system for the quantification of Staphylococcus epidermidis cells in biofilms. *J Basic Microbiol* **2014,** *54* (7), 750-7.
12. Jonas, D.; Speck, M.; Daschner, F. D.; Grundmann, H., Rapid PCR-based identification of methicillin-resistant Staphylococcus aureus from screening swabs. *J Clin Microbiol* **2002,** *40* (5), 1821-3.
13. Paule, S. M.; Mehta, M.; Hacek, D. M.; Gonzalzles, T. M.; Robicsek, A.; Peterson, L. R., Chromogenic media vs real-time PCR for nasal surveillance of methicillin-resistant Staphylococcus aureus: impact on detection of MRSA-positive persons. *Am J Clin Pathol* **2009,** *131* (4), 532-9.

© Copyright 2021 | N Panpradist

14. Ratner, B.; Dyro, J.; Kyle, R.; Preim, B.; Grimnes, S.; Schoen, F.; Vallero, D.; Martinsen, O.; Hoffman, A.; Lemons, J.; Semmlow, J.; Murray, W.; Perez, R.; Bankman, I.; Dunn, S.; Ikada, Y.; Moghe, P.; Constantinides, A., *Biomedical Engineering e-Mega Reference 1st Edition*. Academic Press, 2009.

15. Hollingsworth, M. A.; Swanson, B. J., Mucins in cancer: protection and control of the cell surface. *Nat Rev Cancer* **2004,** *4* (1), 45-60.

16. Campbell, A. P.; Kuypers, J.; Englund, J. A.; Guthrie, K. A.; Corey, L.; Boeckh, M., Self-collection of foam nasal swabs for respiratory virus detection by PCR among immunocompetent subjects and hematopoietic cell transplant recipients. *J Clin Microbiol* **2013,** *51* (1), 324-7.

17. U.S. Centers for Disease Control and Prevention Interim Guidelines for Collecting and Handling of Clinical Specimens for COVID-19 Testin. https://www.cdc.gov/coronavirus/2019-ncov/lab/guidelines-clinical-specimens.html#:~:text=Using%20a%20flocked%20or%20spun%20polyester%20swab%2C%20insert%20the%20entire,seconds%20to%20collect%20the%20specimen.

18. Panpradist, N.; Toley, B. J.; Zhang, X.; Byrnes, S.; Buser, J. R.; Englund, J. A.; Lutz, B. R., Swab sample transfer for point-of-care diagnostics: characterization of swab types and manual agitation methods. *PLoS One* **2014,** *9* (9), e105786.

19. Gulati, G. K.; Panpradist, N.; Stewart, S. W. A.; Beck, I. A.; Boyce, C.; Oreskovic, A. K.; Avila-Ríos, S.; Han, P. D.; Reyes-Terán, G.; Starita, L.; Frenkel, L. M.; Lutz, B. R.; Lai, J. J., Inexpensive workflow to enable

© Copyright 2021 | N Panpradist

simultaneous monitoring HIV viral load and detection of SARS-CoV-2 infection. *medRxiv* **2021**.

20. U.S. Centers for Disease Control and Prevention Research Use Only 2019-Novel Coronavirus (2019-nCoV) Real-time RT-PCR Primers and Probes. https://www.cdc.gov/coronavirus/2019-ncov/lab/rt-pcr-panel-primer-probes.html.
21. Rogers, J. H.; Link, A. C.; McCulloch, D.; Brandstetter, E.; Newman, K. L.; Jackson, M. L.; Hughes, J. P.; Englund, J. A.; Boeckh, M.; Sugg, N.; Ilcisin, M.; Sibley, T. R.; Fay, K.; Lee, J.; Han, P.; Truong, M.; Richardson, M.; Nickerson, D. A.; Starita, L. M.; Bedford, T.; Chu, H. Y., Characteristics of COVID-19 in Homeless Shelters : A Community-Based Surveillance Study. *Ann Intern Med* **2020**.
22. US Centers for Disease Control and Prevention CDC 2019-Novel Coronavirus (2019-nCoV) Real-Time RT-PCR Diagnostic Panel. https://www.fda.gov/media/134922/download.
23. Olsson, C.; Jansson, H.; Swenson, J., The Role of Trehalose for the Stabilization of Proteins. *J. Phys. Chem. B* **2016,** *120* (20), 4723-4731.
24. Cepheid *510(k) Substantial Equivalence Determination Decision* K180218; U.S. Food & Drug Adminstration.
25. Abbott ID NOW COVID-19 Quick Reference Instructions. https://www.alere.com/en/home/product-details/id-now-covid-19.html.
26. Li, L.; He, J.-A.; Wang, W.; Xia, Y.; Song, L.; Chen, Z.-H.; Zuo, H.-Z.; Tan, X.-P.; Ho, A. H.-P.; Kong, S.-K.; Loo, J. F.-C.; Li, H.-W.; Gu, D.,

© Copyright 2021 | N Panpradist

Development of a direct reverse-transcription quantitative PCR (dirRT-qPCR) assay for clinical Zika diagnosis. *Int. J. Infect. Dis.* **2019,** *85*, 167-174.

27. Srivatsan, S.; Han, P. D.; van Raay, K.; Wolf, C. R.; McCulloch, D. J.; Kim, A. E.; Brandstetter, E.; Martin, B.; Gehring, J.; Chen, W.; Kosuri, S.; Konnick, E. Q.; Lockwood, C. M.; Rieder, M. J.; Nickerson, D. A.; Chu, H. Y.; Shendure, J.; Starita, L. M.; Seattle Flu Study, I., Preliminary support for a "dry swab, extraction free" protocol for SARS-CoV-2 testing via RT-qPCR.
28. Smyrlaki, I.; Ekman, M.; Lentini, A.; Rufino de Sousa, N.; Papanicolaou, N.; Vondracek, M.; Aarum, J.; Safari, H.; Muradrasoli, S.; Rothfuchs, A. G.; Albert, J.; Hogberg, B.; Reinius, B., Massive and rapid COVID-19 testing is feasible by extraction-free SARS-CoV-2 RT-PCR. *Nat Commun* **2020,** *11* (1), 4812.
29. Panpradist, N.; Beck, I. A.; Ruth, P. S.; Ávila-Ríos, S.; García-Morales, C.; Soto-Nava, M.; Tapia-Trejo, D.; Matías-Florentino, M.; Paz-Juarez, H. E.; Del Arenal-Sanchez, S.; Reyes-Terán, G.; Lutz, B. R.; Frenkel, L. M., Near point-of-care, point-mutation test to detect drug resistance in HIV-1: a validation study in a Mexican cohort. *AIDS* **2020,** *34* (9), 1331-1338.
30. Woelfel, R.; Corman, V. M.; Guggemos, W.; Seilmaier, M.; Zange, S.; Mueller, M. A.; Niemeyer, D.; Vollmar, P.; Rothe, C.; Hoelscher, M.; Bleicker, T.; Bruenink, S.; Schneider, J.; Ehmann, R.; Zwirglmaier, K.; Drosten, C.; Wendtner, C., Clinical presentation and virological assessment of hospitalized cases of coronavirus disease 2019 in a travel-associated transmission cluster.

© Copyright 2021 | N Panpradist

31. Inbios International Smart Detect™ SARS-CoV-2 rRT-PCR Kit 2020. https://inbios.com/smart-detecttm-sars-cov-2-rrt-pcr-kit/.

32. Bruce, E. A.; Huang, M. L.; Perchetti, G. A.; Tighe, S.; Laaguiby, P.; Hoffman, J. J.; Gerrard, D. L.; Nalla, A. K.; Wei, Y.; Greninger, A. L.; Diehl, S. A.; Shirley, D. J.; Leonard, D. G. B.; Huston, C. D.; Kirkpatrick, B. D.; Dragon, J. A.; Crothers, J. W.; Jerome, K. R.; Botten, J. W., DIRECT RT-qPCR DETECTION OF SARS-CoV-2 RNA FROM PATIENT NASOPHARYNGEAL SWABS WITHOUT AN RNA EXTRACTION STEP. *bioRxiv* **2020**.

33. Keller, B.; Vrana, J.; Miller, A.; Newman, G.; Klavins, E., Aquarium: The Laboratory Operating System (Version v2.5.0). *Zenodo.* *http://doi.org/10.5281/zenodo.2535715* **2019**.

34. Panpradist, N.; Beck, I. A.; Chung, M. H.; Kiarie, J. N.; Frenkel, L. M.; Lutz, B. R., Simplified Paper Format for Detecting HIV Drug Resistance in Clinical Specimens by Oligonucleotide Ligation. *PLoS One* **2016,** *11* (1), e0145962.

35. Addgene Ligation Independent Cloning. https://www.addgene.org/protocols/lic/ (accessed April 8th).

36. Mack, R.; Robinson, J. B., When Novices Elicit Knowledge: Question Asking in Designing, Evaluating, and Learning to Use Software. In *The Psychology of Expertise*, R.R., H., Ed. Springer: New York, NY, 1992; pp 245-268.

37. U.S. Centers for Disease Control and Prevention *CDC 2019-Novel Coronavirus (2019-nCoV) Real-Time RT-PCR Diagnostic Panel For Emergency Use Only*; December 1st, 2020, 2020.

© Copyright 2021 | N Panpradist

38. Kline, E.; Panpradist, N.; Hull, I. T.; Wang, Q.; Oreskovic, A. K.; Han, P. D.; Starita, L. M.; Lutz, B. R., Multiplex target-redundant RT-LAMP for robust detection of SARS-CoV-2 using novel Fluorescent Universal Displacement Probes. *medRxiv* **2021**.

39. Dao Thi, V. L.; Herbst, K.; Boerner, K.; Meurer, M.; Kremer, L. P.; Kirrmaier, D.; Freistaedter, A.; Papagiannidis, D.; Galmozzi, C.; Stanifer, M. L.; Boulant, S.; Klein, S.; Chlanda, P.; Khalid, D.; Barreto Miranda, I.; Schnitzler, P.; Krausslich, H. G.; Knop, M.; Anders, S., A colorimetric RT-LAMP assay and LAMP-sequencing for detecting SARS-CoV-2 RNA in clinical samples. *Sci Transl Med* **2020,** *12* (556).

40. Xu, J.; Wang, J.; Zhong, Z.; Su, X.; Yang, K.; Chen, Z.; Zhang, D.; Li, T.; Wang, Y.; Zhang, S.; Ge, S.; Zhang, J.; Xia, N., Room-temperature-storable PCR mixes for SARS-CoV-2 detection. *Clin Biochem* **2020,** *84*, 73-78.

41. Panpradist, N.; Beck, I. A.; Vrana, J.; Higa, N.; McIntyre, D.; Ruth, P. S.; So, I.; Kline, E. C.; Kanthula, R.; Wong-On-Wing, A.; Lim, J.; Ko, D.; Milne, R.; Rossouw, T.; Ute D. Feucht, M. C., Gonzague Jourdain, Nicole Ngo-Giang-Huong, Laddawan Laomanit, Jaime Soria, James Lai, Eric E. Klavins, Lisa M. Frenkel, Barry R. Lutz OLA-Simple: a software-guided HIV-1 drug resistance test for low-resource laboratories. *EBiomedicine* **2019,** *In press*.

42. Panpradist, N.; Beck, I. A.; Ruth, P. S.; Avila-Rios, S.; Garcia-Morales, C.; Soto-Nava, M.; Tapia-Trejo, D.; Matias-Florentino, M.; Paz-Juarez, H. E.; Del Arenal-Sanchez, S.; Reyes-Teran, G.; Lutz, B. R.; Frenkel, L. M., Near

© Copyright 2021 | N Panpradist

point-of-care, point-mutation test to detect drug resistance in HIV-1: a validation study in a Mexican cohort. *AIDS* **2020**.

43. Vrana, J.; Chohan, B.; Chung, M.; Higa, N.; Kanthula, R.; Lutz, B.; Panpradist, N.; Ruth, P.; Frenkel, L., OLA Simple v 1.0: observational study of an app-guided HIV drug resistance test at the Coptic Hope Center in Kenya. *medRxiv* **2021**.
44. Moon, B.; Jones, M.; Valdez, J. Lyophilized beads containing mannitol 2003. https://patents.google.com/patent/US20050069898A1/en.
45. Nyan, D.-C.; Ulitzky, L. E.; Cehan, N.; Williamson, P.; Winkelman, V.; Rios, M.; Taylor, D. R., Rapid Detection of Hepatitis B Virus in Blood Plasma by a Specific and Sensitive Loop-Mediated Isothermal Amplification Assay. *Clinical Infectious Diseases* **2014,** *59* (1), 16-23.
46. Spiess, A. N.; Mueller, N.; Ivell, R., Trehalose is a potent PCR enhancer: lowering of DNA melting temperature and thermal stabilization of taq polymerase by the disaccharide trehalose. *Clin Chem* **2004,** *50* (7), 1256-9.
47. FPbase. Spectra viewer 2021. https://www.fpbase.org/spectra/.
48. Newport. Optical Filters 2021. https://www.newport.com/c/optical-filters.
49. Mousers Electronics. LED lighting 2021. https://www.mouser.com/Optoelectronics/LED-Lighting/_/N-74g9t.
50. Mori, Y.; Nagamine, K.; Tomita, N.; Notomi, T., Detection of loop-mediated isothermal amplification reaction by turbidity derived from magnesium pyrophosphate formation. *Biochem Biophys Res Commun* **2001,** *289* (1), 150-4.

© Copyright 2021 | N Panpradist

51. Tone, K.; Fujisaki, R.; Yamazaki, T.; Makimura, K., Enhancing melting curve analysis for the discrimination of loop-mediated isothermal amplification products from four pathogenic molds: Use of inorganic pyrophosphatase and its effect in reducing the variance in melting temperature values. *J Microbiol Methods* **2017,** *132*, 41-45.

52. Xie, S.; Yuan, Y.; Chai, Y.; Yuan, R., Tracing Phosphate Ions Generated during Loop-Mediated Isothermal Amplification for Electrochemical Detection of Nosema bombycis Genomic DNA PTP1. *Anal Chem* **2015,** *87* (20), 10268-74.

53. New England Biolabs, I. Thermostable Inorganic Pyrophosphatase 2021. https://www.neb.com/products/m0296-thermostable-inorganic-pyrophosphatase#Product%20Information.

54. Lennox, T.; Slatko, B. E.; Sears, L. E. Purified thermostable inorganic pyprophosphatase obtainable from thermococcus litoralis 1995. https://patents.google.com/patent/US5861296A/en.

55. U.S. Centers for Disease Control and Prevention. CDC 2019-Novel Coronavirus (2019-nCoV) Real-Time RT-PCR Diagnostic Panel For Emergency Use Only 2020. https://www.fda.gov/media/134922/download (accessed December 1st, 2020).

56. Thermo Fisher Scientific, C. OpenArray Technology Overview 2021. https://www.thermofisher.com/us/en/home/life-science/pcr/real-time-pcr/real-time-openarray/open-array-technology.html.

57. Alekseenko, A.; Barrett, D.; Pareja-Sanchez, Y.; Howard, R. J.; Strandback, E.; Ampah-Korsah, H.; Rovsnik, U.; Zuniga-Veliz, S.; Klenov,

© Copyright 2021 | N Panpradist

A.; Malloo, J.; Ye, S.; Liu, X.; Reinius, B.; Elsasser, S. J.; Nyman, T.; Sandh, G.; Yin, X.; Pelechano, V., Direct detection of SARS-CoV-2 using non-commercial RT-LAMP reagents on heat-inactivated samples. *Sci Rep* **2021,** *11* (1), 1820.

58. Rabe, B. A.; Cepko, C., SARS-CoV-2 detection using isothermal amplification and a rapid, inexpensive protocol for sample inactivation and purification. *Proc Natl Acad Sci U S A* **2020,** *117* (39), 24450-24458.

59. Wei, S.; Kohl, E.; Djandji, A.; Morgan, S.; Whittier, S.; Mansukhani, M.; Hod, E.; D'Alton, M.; Suh, Y.; Williams, Z., Direct diagnostic testing of SARS-CoV-2 without the need for prior RNA extraction. *Sci Rep* **2021,** *11* (1), 2402.

60. Bokelmann, L.; Nickel, O.; Maricic, T.; Paabo, S.; Meyer, M.; Borte, S.; Riesenberg, S., Point-of-care bulk testing for SARS-CoV-2 by combining hybridization capture with improved colorimetric LAMP. *Nat Commun* **2021,** *12* (1), 1467.

61. Yamazaki, W.; Matsumura, Y.; Thongchankaew-Seo, U.; Yamazaki, Y.; Nagao, M., Development of a point-of-care test to detect SARS-CoV-2 from saliva which combines a simple RNA extraction method with colorimetric reverse transcription loop-mediated isothermal amplification detection. *J Clin Virol* **2021,** *136*, 104760.

62. Qian, J.; Boswell, S. A.; Chidley, C.; Lu, Z. X.; Pettit, M. E.; Gaudio, B. L.; Fajnzylber, J. M.; Ingram, R. T.; Ward, R. H.; Li, J. Z.; Springer, M., An enhanced isothermal amplification assay for viral detection. *Nat Commun* **2020,** *11* (1), 5920.

© Copyright 2021 | N Panpradist

63. Patchsung, M.; Jantarug, K.; Pattama, A.; Aphicho, K.; Suraritdechachai, S.; Meesawat, P.; Sappakhaw, K.; Leelahakorn, N.; Ruenkam, T.; Wongsatit, T.; Athipanyasilp, N.; Eiamthong, B.; Lakkanasirorat, B.; Phoodokmai, T.; Niljianskul, N.; Pakotiprapha, D.; Chanarat, S.; Homchan, A.; Tinikul, R.; Kamutira, P.; Phiwkaow, K.; Soithongcharoen, S.; Kantiwiriyawanitch, C.; Pongsupasa, V.; Trisrivirat, D.; Jaroensuk, J.; Wongnate, T.; Maenpuen, S.; Chaiyen, P.; Kamnerdnakta, S.; Swangsri, J.; Chuthapisith, S.; Sirivatanauksorn, Y.; Chaimayo, C.; Sutthent, R.; Kantakamalakul, W.; Joung, J.; Ladha, A.; Jin, X.; Gootenberg, J. S.; Abudayyeh, O. O.; Zhang, F.; Horthongkham, N.; Uttamapinant, C., Clinical validation of a Cas13-based assay for the detection of SARS-CoV-2 RNA. *Nat Biomed Eng* **2020,** *4* (12), 1140-1149.

64. Joung, J.; Ladha, A.; Saito, M.; Segel, M.; Bruneau, R.; Huang, M. W.; Kim, N. G.; Yu, X.; Li, J.; Walker, B. D.; Greninger, A. L.; Jerome, K. R.; Gootenberg, J. S.; Abudayyeh, O. O.; Zhang, F., Point-of-care testing for COVID-19 using SHERLOCK diagnostics. *medRxiv* **2020**.

65. Broughton, J. P.; Deng, X.; Yu, G.; Fasching, C. L.; Servellita, V.; Singh, J.; Miao, X.; Streithorst, J. A.; Granados, A.; Sotomayor-Gonzalez, A.; Zorn, K.; Gopez, A.; Hsu, E.; Gu, W.; Miller, S.; Pan, C. Y.; Guevara, H.; Wadford, D. A.; Chen, J. S.; Chiu, C. Y., CRISPR-Cas12-based detection of SARS-CoV-2. *Nat Biotechnol* **2020,** *38* (7), 870-874.

66. Vogels, C. B. F.; Watkins, A. E.; Harden, C. A.; Brackney, D. E.; Shafer, J.; Wang, J.; Caraballo, C.; Kalinich, C. C.; Ott, I. M.; Fauver, J. R.; Kudo, E.; Lu, P.; Venkataraman, A.; Tokuyama, M.; Moore, A. J.;

© Copyright 2021 | N Panpradist

Muenker, M. C.; Casanovas-Massana, A.; Fournier, J.; Bermejo, S.; Campbell, M.; Datta, R.; Nelson, A.; Dela Cruz, C. S.; Ko, A. I.; Iwasaki, A.; Krumholz, H. M.; Matheus, J. D.; Hui, P.; Liu, C.; Farhadian, S. F.; Sikka, R.; Wyllie, A. L.; Grubaugh, N. D., SalivaDirect: A simplified and flexible platform to enhance SARS-CoV-2 testing capacity. *Med (N Y)* **2021,** *2* (3), 263-280.e6.

67. Wolfel, R.; Corman, V. M.; Guggemos, W.; Seilmaier, M.; Zange, S.; Muller, M. A.; Niemeyer, D.; Jones, T. C.; Vollmar, P.; Rothe, C.; Hoelscher, M.; Bleicker, T.; Brunink, S.; Schneider, J.; Ehmann, R.; Zwirglmaier, K.; Drosten, C.; Wendtner, C., Virological assessment of hospitalized patients with COVID-2019. *Nature* **2020,** *581* (7809), 465-469.

68. Zhu, J.; Guo, J.; Xu, Y.; Chen, X., Viral dynamics of SARS-CoV-2 in saliva from infected patients. *J Infect* **2020,** *81* (3), e48-e50.

69. Pang, B.; Xu, J.; Liu, Y.; Peng, H.; Feng, W.; Cao, Y.; Wu, J.; Xiao, H.; Pabbaraju, K.; Tipples, G.; Joyce, M. A.; Saffran, H. A.; Tyrrell, D. L.; Zhang, H.; Le, X. C., Isothermal Amplification and Ambient Visualization in a Single Tube for the Detection of SARS-CoV-2 Using Loop-Mediated Amplification and CRISPR Technology. *Analytical Chemistry* **2020,** *92* (24), 16204-16212.

70. Craw, P.; Balachandran, W., Isothermal nucleic acid amplification technologies for point-of-care diagnostics: a critical review. *Lab Chip* **2012,** *12* (14), 2469-86.

71. Gonzalez-Gonzalez, E.; Lara-Mayorga, I. M.; Rodriguez-Sanchez, I. P.; Zhang, Y. S.; Martinez-Chapa, S. O.; Santiago, G. T.; Alvarez, M. M.,

© Copyright 2021 | N Panpradist

Colorimetric loop-mediated isothermal amplification (LAMP) for cost-effective and quantitative detection of SARS-CoV-2: the change in color in LAMP-based assays quantitatively correlates with viral copy number. *Anal Methods* **2021,** *13* (2), 169-178.

72. Rodriguez-Manzano, J.; Malpartida-Cardenas, K.; Moser, N.; Pennisi, I.; Cavuto, M.; Miglietta, L.; Moniri, A.; Penn, R.; Satta, G.; Randell, P.; Davies, F.; Bolt, F.; Barclay, W.; Holmes, A.; Georgiou, P., Handheld Point-of-Care System for Rapid Detection of SARS-CoV-2 Extracted RNA in under 20 min. *ACS Cent Sci* **2021,** *7* (2), 307-317.

73. Chai Bio. A FAST, ACCURATE, AND PORTABLE REAL-TIME PCR MACHINE 2019. https://www.chaibio.com/openqpcr?utm_campaign=1043261491&utm_source=google&utm_medium=cpc&utm_content=305077454122&utm_term=&adgroupid=60556126477&gclid=Cj0KCQiA4aXiBRCRARIsAMBZGz--Gam63rloCoY2BrlcIhJlfk8U8tsxTgYkEPsN9iaAJR5L9_itX0YaAu6MEALw_wcB.

74. Putri, W.; Muscatello, D. J.; Stockwell, M. S.; Newall, A. T., Economic burden of seasonal influenza in the United States. *Vaccine* **2018,** *36* (27), 3960-3966.

75. Centers for Diseases Control and Prevention Influenza Updates. https://www.cdc.gov/flu/index.htm (accessed Febrary 19th).

76. VoA News Zimbabwe Begins Lockdown to Fight COVID19. https://www.voanews.com/a/science-health_coronavirus-outbreak_zimbabwe-begins-lockdown-fight-covid19/6186637.html.

© Copyright 2021 | N Panpradist

77. Sohrabi, C.; Alsafi, Z.; O'Neill, N.; Khan, M.; Kerwan, A.; Al-Jabir, A.; Iosifidis, C.; Agha, R., World Health Organization declares global emergency: A review of the 2019 novel coronavirus (COVID-19). *Int J Surg* **2020,** *76*, 71-76.

78. World Health Organization Coronavirus disease (COVID-19) Weekly Epidemiological Update and Weekly Operational Update. https://www.who.int/emergencies/diseases/novel-coronavirus-2019/situation-reports.

79. Moore, J. P.; Offit, P. A., SARS-CoV-2 Vaccines and the Growing Threat of Viral Variants. *Jama* **2021,** *325* (9), 821-822.

80. Arora, P.; Pöhlmann, S.; Hoffmann, M., Mutation D614G increases SARS-CoV-2 transmission. *Signal Transduct Target Ther* **2021,** *6* (1), 101.

81. Volz, E.; Mishra, S.; Chand, M.; Barrett, J. C.; Johnson, R.; Geidelberg, L.; Hinsley, W. R.; Laydon, D. J.; Dabrera, G.; O'Toole, Á.; Amato, R.; Ragonnet-Cronin, M.; Harrison, I.; Jackson, B.; Ariani, C. V.; Boyd, O.; Loman, N. J.; McCrone, J. T.; Gonçalves, S.; Jorgensen, D.; Myers, R.; Hill, V.; Jackson, D. K.; Gaythorpe, K.; Groves, N.; Sillitoe, J.; Kwiatkowski, D. P.; consortium, T. C.-G. U.; Flaxman, S.; Ratmann, O.; Bhatt, S.; Hopkins, S.; Gandy, A.; Rambaut, A.; Ferguson, N. M., Transmission of SARS-CoV-2 Lineage B.1.1.7 in England: Insights from linking epidemiological and genetic data. *medRxiv* **2021**, 2020.12.30.20249034.

82. ChAdOx1 nCoV-19 Vaccine Efficacy against the B.1.351 Variant. *New England Journal of Medicine* **2021,** *385* (6), 571-572.

© Copyright 2021 | N Panpradist

83. Greaney, A. J.; Loes, A. N.; Crawford, K. H. D.; Starr, T. N.; Malone, K. D.; Chu, H. Y.; Bloom, J. D., Comprehensive mapping of mutations in the SARS-CoV-2 receptor-binding domain that affect recognition by polyclonal human plasma antibodies. *Cell Host Microbe* **2021,** *29* (3), 463-476.e6.

84. Corum, J.; Zimmer, C. Coronavirus Variants and Mutations. . https://www.nytimes.com/interactive/2021/health/coronavirus-variant-tracker.html.

85. Ho, D.; Wang, P.; Liu, L.; Iketani, S.; Luo, Y.; Guo, Y.; Wang, M.; Yu, J.; Zhang, B.; Kwong, P.; Graham, B.; Mascola, J.; Chang, J.; Yin, M.; Sobieszczyk, M.; Kyratsous, C.; Shapiro, L.; Sheng, Z.; Nair, M.; Huang, Y., Increased Resistance of SARS-CoV-2 Variants B.1.351 and B.1.1.7 to Antibody Neutralization. *Res Sq* **2021**.

86. Vilar, S.; Isom, D. G., One Year of SARS-CoV-2: How Much Has the Virus Changed? *Biology (Basel)* **2021,** *10* (2).

87. Wise, J., Covid-19: The E484K mutation and the risks it poses. *Bmj* **2021,** *372*, n359.

88. Tegally, H.; Wilkinson, E.; Giovanetti, M.; Iranzadeh, A.; Fonseca, V.; Giandhari, J.; Doolabh, D.; Pillay, S.; San, E. J.; Msomi, N.; Mlisana, K.; von Gottberg, A.; Walaza, S.; Allam, M.; Ismail, A.; Mohale, T.; Glass, A. J.; Engelbrecht, S.; Van Zyl, G.; Preiser, W.; Petruccione, F.; Sigal, A.; Hardie, D.; Marais, G.; Hsiao, N.-y.; Korsman, S.; Davies, M.-A.; Tyers, L.; Mudau, I.; York, D.; Maslo, C.; Goedhals, D.; Abrahams, S.; Laguda-Akingba, O.; Alisoltani-Dehkordi, A.; Godzik, A.; Wibmer, C. K.; Sewell, B. T.; Lourenço, J.; Alcantara, L. C. J.; Kosakovsky Pond, S. L.; Weaver, S.;

© Copyright 2021 | N Panpradist

Martin, D.; Lessells, R. J.; Bhiman, J. N.; Williamson, C.; de Oliveira, T., Detection of a SARS-CoV-2 variant of concern in South Africa. *Nature* **2021,** *592* (7854), 438-443.

89. Faria, N. R.; Claro, I. M.; Candido, D.; Franco, L. A. M.; Andrade, P. S.; Coletti, T. M.; Silva, C. A. M.; Sales, F. C.; Manuli, E. R.; Aguiar, R. S.; Gaburo, N.; Camilo, C. d. C.; Fraiji, N. A.; Crispim, M. A. E.; Carvalho, M. d. P. S. S.; Rambaut, A.; Loman, N.; Pybus, O. G.; Sabino, E. C.; Network1, o. b. o. C. G. Genomic characterisation of an emergent SARS-CoV-2 lineage in Manaus: preliminary findings. https://virological.org/t/genomic-characterisation-of-an-emergent-sars-cov-2-lineage-in-manaus-preliminary-findings/586.

90. Tchesnokova, V.; Kulakesara, H.; Larson, L.; Bowers, V.; Rechkina, E.; Kisiela, D.; Sledneva, Y.; Choudhury, D.; Maslova, I.; Deng, K.; Kutumbaka, K.; Geng, H.; Fowler, C.; Greene, D.; Ralston, J.; Samadpour, M.; Sokurenko, E., Acquisition of the L452R mutation in the ACE2-binding interface of Spike protein triggers recent massive expansion of SARS-Cov-2 variants. *bioRxiv* **2021**.

91. Bartolini, B.; Rueca, M.; Gruber, C. E. M.; Messina, F.; Giombini, E.; Ippolito, G.; Capobianchi, M. R.; Di Caro, A., The newly introduced SARS-CoV-2 variant A222V is rapidly spreading in Lazio region, Italy. *medRxiv* **2020**, 2020.11.28.20237016.

92. Cele, S.; Gazy, I.; Jackson, L.; Hwa, S.-H.; Tegally, H.; Lustig, G.; Giandhari, J.; Pillay, S.; Wilkinson, E.; Naidoo, Y.; Karim, F.; Ganga, Y.; Khan, K.; Bernstein, M.; Balazs, A. B.; Gosnell, B. I.; Hanekom, W.;

© Copyright 2021 | N Panpradist

Moosa, M.-Y. S.; NGS-SA; Team, C.-K.; Lessells, R. J.; Oliveira, T. d.; Sigal, A., Escape of SARS-CoV-2 501Y.V2 from neutralization by convalescent plasma. *medRxiv* **2021**, 2021.01.26.21250224.

93. Wibmer, C. K.; Ayres, F.; Hermanus, T.; Madzivhandila, M.; Kgagudi, P.; Oosthuysen, B.; Lambson, B. E.; de Oliveira, T.; Vermeulen, M.; van der Berg, K.; Rossouw, T.; Boswell, M.; Ueckermann, V.; Meiring, S.; von Gottberg, A.; Cohen, C.; Morris, L.; Bhiman, J. N.; Moore, P. L., SARS-CoV-2 501Y.V2 escapes neutralization by South African COVID-19 donor plasma. *Nat Med* **2021,** *27* (4), 622-625.

94. Nelson, G.; Buzko, O.; Spilman, P.; Niazi, K.; Rabizadeh, S.; Soon-Shiong, P., Molecular dynamic simulation reveals E484K mutation enhances spike RBD-ACE2 affinity and the combination of E484K, K417N and N501Y mutations (501Y.V2 variant) induces conformational change greater than N501Y mutant alone, potentially resulting in an escape mutant. *bioRxiv* **2021**, 2021.01.13.426558.

95. Liu, Z.; VanBlargan, L. A.; Rothlauf, P. W.; Bloyet, L.-M.; Chen, R. E.; Stumpf, S.; Zhao, H.; Errico, J. M.; Theel, E. S.; Ellebedy, A. H.; Fremont, D. H.; Diamond, M. S.; Whelan, S. P. J., Landscape analysis of escape variants identifies SARS-CoV-2 spike mutations that attenuate monoclonal and serum antibody neutralization. *bioRxiv* **2020**, 2020.11.06.372037.

96. Li, Q.; Wu, J.; Nie, J.; Zhang, L.; Hao, H.; Liu, S.; Zhao, C.; Zhang, Q.; Liu, H.; Nie, L.; Qin, H.; Wang, M.; Lu, Q.; Li, X.; Sun, Q.; Liu, J.; Zhang, L.; Li, X.; Huang, W.; Wang, Y., The Impact of Mutations in SARS-

© Copyright 2021 | N Panpradist

CoV-2 Spike on Viral Infectivity and Antigenicity. *Cell* **2020,** *182* (5), 1284-1294.e9.

© Copyright 2021 | N Panpradist

CHAPTER 11: Fish-OLA - SPECIES IDENTIFICATION TOOL TO REGULATE IUU

CONTRIBUTORS: Nuttada Panpradist, Carolyn Tarpey, Anita Wray, Parker S Ruth, Ingrid Spies, Barry R Lutz, Karl F Bohringer, Lorenz Hauser. **CONTRIBUTIONS**: NP designed the primer and probe sequences, developed, and manufactured the kits, and outlined the study presented in this manuscript. BRL conceived the idea for a three-probe detection system. CT, AW, and NP conducted experiments. All authors contributed to data analysis. IS, LH, BRL, and KFB provided feedback on the study design and discussion.

SIGNIFICANCE. Pacific cod (*Gadus macrocephalus*) has been identified as particularly vulnerable to Illegal, Unreported, Unregulated (**IUU**) and seafood fraud, primarily because of uncertain provenance of import[1]. A proportion of the catch is exported to China for local consumption and reportedly mislabeled as Alaska pollock[2] or others[3, 4]. Wild-caught cods are processed and re-imported to the US [5]. Consequently, the US imported over 41,000 tons of cod products in the value of over $ 217M from China alone. Given the uncertain naming of these cod products, with mislabeling exceeding 60%[3], the identification of species origin and trading networks is, therefore, a primary goal of the U.S. National Oceanographic Atmospheric Administration (**NOAA**) Seafood Import Program. A method to allow easy, fast, and cheap identification not only to species but also to the population of origin at the point of contact may be invaluable in these efforts.

© Copyright 2021 | N Panpradist

Moreover, recent changes in the distribution of Pacific cod and consequent disruption in the fishery may add further urgency to such population identification. The biomass of Pacific cod at the northern end of the distribution in the northern Bering Sea has increased almost ten-fold since 2010[6]. On the other hand, following the 'blob,' a heatwave in the Gulf of Alaska (**GoA**) in 2014-2016, the spawning habitat of Pacific cod was significantly reduced[7]. The catch in the GOA was reduced in 2019 (13,372t) due to the observed stock decline. In comparison, catch in the GOA 85,412t in 2011[8]. In 2019, NOAA declared a fishery disaster for the GoA Pacific cod fishery, and in 2020, there was no federal quota in the area. Further south, Pacific cod in the Salish Sea in Washington State have declined to sufficiently low levels to be declared a Species of Concern by NOAA. A genetic identification tool that can distinguish between declining and increasing populations of Pacific cod would be useful in ascertaining the sustainability of fish and fish products.

Ingrid Spies et al. previously reported fixed genetic differences at the *zona pellucida 3* (ZP3) gene between cod from the Bering Sea and those from the Gulf of Alaska and further South [9]. Here, we used this gene to develop a cod population assignment assay that can quickly, easily, and cheaply screen these signature polymorphisms. We aimed to *(i)* develop a sample preparation kit to quickly obtain DNA from whole fish and fillets, *(ii)* develop an oligonucleotide ligation assay (**OLA**) containing lyophilized PCR and ligation reactions and that can be detected in a lateral flow detection system, and *(iii)* evaluate the complete "**Fish-OLA**" system using blinded samples and compare the original fish assignment.

© Copyright 2021 | N Panpradist

MATERIALS AND METHODS

Sample collection. Three types of fish samples were tested: fin clip, swab collection from fish fillets, and manually groundfish fillets. Fish fin clip samples were collected from four sites, including two on the Eastern Bering Sea shelf (Pervenets Canyon collected in 2016), Zhemchug Canyon (collected in 2017), and two sites in the southern Gulf of Alaska (Washington Coast collected in 2005) and Puget Sound. Fin clips were stored in 95% ethanol until extraction. In addition, frozen cod fillets were purchased from two Seattle stores. After thawing, a polyurethane swab (PF-1804, Puritan Medical, Guilford, ME) was inserted into the fish fillets, and the swab shaft was rotated five times to obtain samples. The swab was then eluted in 0.4 mL 1x TLE buffer (10mM Tris-HCl, pH 8.0, 0.1mM EDTA). Alternatively, the cod fillet was also cut into the size of 1 cm x 0.5 cm and transferred in a 1.5mL DNA LoBind tube (Eppendorf, Hamburg, Germany).

Extraction-free DNA preparation approaches

Alkaline lysis. Each of the fish fin clip samples or ground tissues (using a manual plastic grinder) were mixed 100µL alkaline lysis solution (100mM freshly prepared sodium hydroxide, 2%*(v/v)* Tween-20 in water), followed by incubation at 95 °C for 2 minutes, 5 minutes, or 10 minutes. The lysate was mixed with 100µL Tris-HCl pH 2 to neutralize the lysate. Sample tubes were spun down for 10 seconds using a mini centrifuge. 2-10µL supernatant was directly added to the PCR reaction without purification. ***Enzymatic lysis***. Manually ground tissues were mixed with 200µL enzymatic lysis solution -

© Copyright 2021 | N Panpradist

containing 0.5 units/µL of Acromopeptidase, **ACP** (A3547-100KU, Sigma Aldrich, St. Louis, MI) in 1x TLE - and incubated at room temperature for 2 minutes, 5 minutes, or 10 minutes. The ACP lysis buffer was then inactivated at 95 °C for 2 minutes, as described [10]. ***Heat lysis*.** Ground tissues or swab eluate from fish fillets were added to PCR reactions directly and "lysed" through the initial denaturation step at 95 °C for 5 minutes, introduced as part of the PCR cycle.

Analytical sensitivity and specificity of OLA-Fish. Gene sequences (GenBlock, Integrated DNA Technology, Coralville, IA) spanning over the region of Gadus morhua chromosome 9, gadMor3.0, whole genome shotgun sequence (Accession number: NC_044056) containing different mutations at the two polymorphisms were used as the DNA standards. The dilutions of DNA standards (0 to 10^4 copies/reaction) were run to determine the analytical sensitivity of the qPCR assay. Samples detectable by qPCR with confirmed expected melt peaks at 79.5 - 80°C are classified as positive. To assess the specificity of the Fish-OLA, 2000 copies of standards containing different polymorphisms were amplified and tested with downstream ligation and lateral flow detection.

Validation of OLA-Fish on a panel of specimens. Fish-OLA was evaluated using the DNA from Pacific cod of the Bering Sea and non-Bering Sea origin (n=200; 100 from non-Bering Sea cods and 100 from Bering Sea cods) and direct lysate prepared from the fin clip using the Alkaline lysis method (n=35; 16 from non-Bering Sea cods and 19 from Bering Sea cods). These DNA

© Copyright 2021 | N Panpradist

samples were extracted from fish fins using the Qiagen DNEasy Blood and Tissue extraction kit according to the manufacturer's specifications.

Preparation of Fish-OLA DNA analysis kit

Lyophilized PCR reactions. 10µL 2x PCR reactions — containing 16.8%*(w/v)* trehalose, 2.5U OneTaq polymerase (M0480, New England Biolab, Ipswich, MA), 0.4mM each dNTPs, 40x Evagreen dye (31000, Biotium, Fremont, CA), 0.4mM each forward fish primerV4 and reverse fish primerV4 — were flashed frozen in liquid nitrogen bath for 2 minutes and lyophilized at 130 mbar and -55 °C for at least two hours, as previously described[11, 12].

Lyophilized ligation reactions. 24µL ligation reactions — containing 5%*(w/v)* trehalose, 0.1%*(v/v)* Triton X-100, 1.5%*(w/v)* poly(ethylene glycol), 1mM NAD, 0.07U ligase (A3210K, Lugicen, Middleton, WI), 1mM Tris-HCl at pH 7.4, 13mM KCl, 0.3µM first-sectionV2 probe and 0.1µM each Middle_Section probe, Last_Section probe, Control_leftV2, and Control_rightV2 oligonucleotide probes — were lyophilized in the similar to above PCR reactions.

Lyophilized stop solution. 1µM each Compt Left, Compt Right, Compt first_sectionV2, and Compt Last_section oligonucleotides were lyophilized in the presence of 5% *(v/v)* trehalose. All nucleotide sequences are listed in **Table 11.1**.

Lateral strip flow strip preparation. 0.5ug anti-fluorescein, anti-digoxigenin, and biotinylated BSA were immobilized onto the nitrocellulose and visualized for its presence using Ponceau staining[13]. The nitrocellulose sheet

© Copyright 2021 | N Panpradist

was then assembled with an absorbent pad and glass fiber before being sliced into a 0.5 x 5 cm strip and packaged in a lateral flow cassette as previously described (**Chapter 3.3**). The gold solution was lyophilized. Kit components are stored in foil pouches with desiccant packets at 4 °C until use.

Table 11.1 | Primer and probe sequences used in development and the final DNA analysis kits
Yellow highlighted bases are engineered sequences.

Sequence Name	Sequence (5' to 3')
Fwd primer V1	CTG TAG ATG ATT GCA ACT CCA GTT GC
Fwd primer V2	CTG TAG ATG ATT GCA ACT CCA
Fwd primer V3	ACCCCCAAGCCACTGGATC
Fwd primer V4	GTACACCCCCAAGCCACTGGATC
Rev primer V1	GCT CCT CGG ACA CTT TGA TGG C
Rev primer V2	CTC CTC GGA CAC TTT GAT G
Rev primer V3	TGCAAAAGCTCCTCGGACACT
Rev primer V4	TACCTGCAAAAGCTCCTCGGACACT
First section V1	/56FAM/
First section V2	/56-FAM/TATTA*ACTTGATGTTCAAATTCTGCAGGAT*
Middle section	/5Phos/GCATAACGTGAGCAGTCTGGCCCTGA
Last section	/5Phos/ACCCGATCTTCACCCCGTTCTCGG/3Bio/
Control left V1	/5Biosg/GA ATT TTA ATT AAA ATT AAT TCA TT
Control right V1	TTG AAG AGT GCA AAG /3Dig_N/
Control left V2	/5DigN/TAACCATACAAAGAAAATGGCAGGGTTAAA
Control right V2	/5Phos/CTGTAGATGATTGCAACTCCAGTT GCTTG/3Bio/
Compt detect V1	CCG CGC GCT ATT AAC TTG ATG TTC AAA TCC TGC AGG AT
Compt detect V1	AC CCG ATC TTC ACC CCG TTC TCG GGC GCG CGG

FISH-OLA procedures

Setting up PCR reactions. Lyophilized PCR pellets were rehydrated with 18 µL of 1.1x rehydration buffer (0.5x Evagreen, 80mM Tris-SO_4, 20mM $(NH_4)_2SO_4$, 4mM $MgSO_4$, 5% glycerol, 5% DMSO, 0.06% IGEPAL CA-630,

© Copyright 2021 | N Panpradist

0.05% Tween-20, pH 9.2). 2µL extracted DNA was added to each and vortexed briefly. Samples were run on a CFX Connect qPCR machine (CFX-96, BioRad, Hercules, CA). PCR Protocol consisted of an initial denaturation step at 94°C (5 min) followed by two cycles of 94 °C for 3 seconds, 55 °C for 30 seconds, and 68 °C 10 seconds and a plate read (SYBR channel). This was followed by 37 cycles of 94 °C for 3 seconds, 64 °C for 10 seconds, 68 °C for 10 seconds, and a plate read. A melt curve analysis was run to ensure the successful amplification of the target. Samples with melt peaks in the range of 79.5 - 80 °C are classified positive. ***Setting up Ligation***. Lyophilized ligation pellets were rehydrated with 24µL water and 2.4µL of the PCR amplicon and vortexed to mix. Ligation samples were run on the standard thermal cycler (T100, Biorad) using five cycles of 95 °C for 1 second and 45 °C for 3 minutes. ***Setting up detection***. The ligation reaction mixed with 2.4µL of stop solution (5µM of Comptv1 and Comptv2 in 1x TE) was subjected to 95°C for 1 second and 45 °C for 3 minutes to stop the reaction. 24µL of the stopped reaction was added to the sample port of each lateral flow strip. After 5 minutes, the rehydrated lyophilized gold solution was added to the sample port to label the ligated products. The lateral flow strips were scanned after 15 minutes of gold solution addition.

Data analysis

The results from Fish-OLA (i.e., scanned lateral flow images) were blindly classified as individuals and by an in-house Python software [14]. Human calls (mode calls from seven individuals) and software calls were compared to the fish assignment by the locations. Discordant results are tie-broken by the

© Copyright 2021 | N Panpradist

Sanger sequencing. The sensitivity and specificity were calculated and reported with a 95% confidence interval (**CI**).

RESULTS

Overview and analytical performance of Fish-OLA

Principles of Fish-OLA to assign individual cod to either Bering Sea/Aleutian Islands or populations further south (**Figure 11.1A**) relied on **OLA**, containing four main steps: sample preparation, PCR amplification, ligation, and lateral flow detection. A three-probe ligation system was designed to detect the presence of the two polymorphisms unique to the BSAI cod (**Figure 11.1B**), reporting as a visible band on the lateral flow strip (**Figure 11.1C**). A traditional two-probe ligation system was designed to target the other conserved regions within the same amplified region to serve as a cod positive control band. The sensitivity of the Fish-OLA assay depended on the PCR amplification step, which detected down to 10 copies of synthetic cod DNA, while most extracted cod samples tested had a concentration range of 10^3 - 10^4 copies/reaction (**Figure 11.1D**). The ligation and detection of the Fish-OLA can specifically differentiate BSAI cod DNA from other cod DNA (**Figure 11.1E**) both via human calls and signal analysis.

© Copyright 2021 | N Panpradist

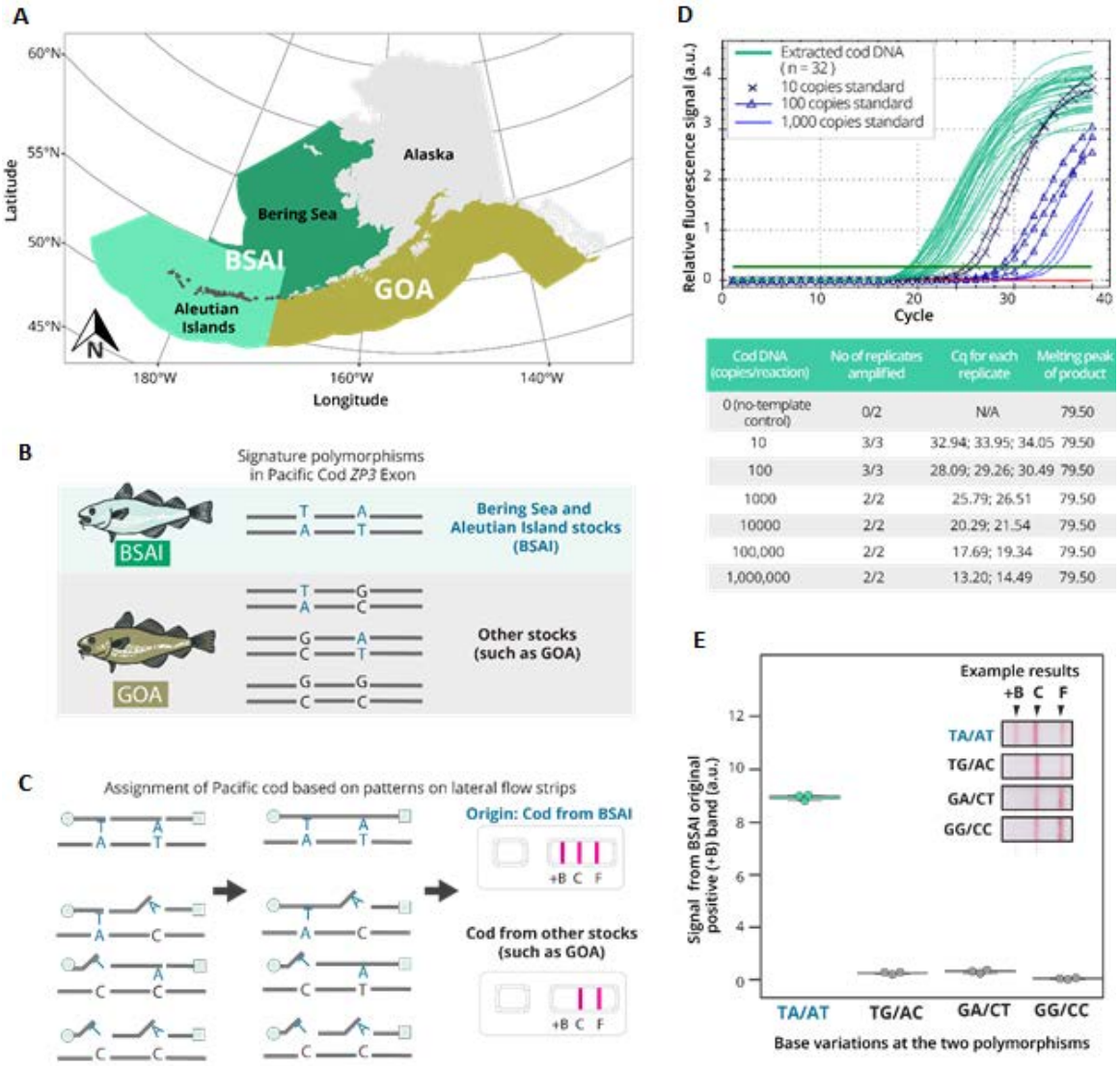

Cod DNA (copies/reaction)	No of replicates amplified	Cq for each replicate	Melting peak of product
0 (no-template control)	0/2	N/A	79.50
10	3/3	32.94; 33.95; 34.05	79.50
100	3/3	28.09; 29.26; 30.49	79.50
1000	2/2	25.79; 26.51	79.50
10000	2/2	20.29; 21.54	79.50
100,000	2/2	17.69; 19.34	79.50
1,000,000	2/2	13.20; 14.49	79.50

Figure 11.1 | Fish-OLA assignment of cod populations.

The Gulf of Alaska (GOA) management region is managed separately from the Bering Sea and Aleutian Islands (BSAI) management regions. Pacific cod are also managed separately in the Aleutian from the remainder of the Bering Sea (**A**). Our previous study shows codfish from BSAI have two signature single nucleotide polymorphisms (SNPs) different from codfish from the other stocks such as GOA (**B**). The new DNA analysis tool relies on the three probes covalently linked (i.e., ligation) upon perfect complementarity at the two signature SNPs. These probes are (i) the sequences complementary to the sequence upstream of the first SNP with 5' tagged with FAM (circle symbol) and 3'complementary to the first SNP sequence "A"; (ii) the sequences complementary to the sequences in between the two SNPs with 5' phosphorylation and 3' complementary to the second SNP sequence "T"; and (iii) the

© Copyright 2021 | N Panpradist

sequences complementary to the sequences downstream of the second SNP with 5’ phosphorylation and 3’ biotin (square symbol). In the presence of a template-dependent ligase, Probe/template complement results in ligated probes (end-joined probes). Only when the DNA target has both signature SNPs, the ligated products from the three probes will be formed. The ligated products from the three probes with 5’ tagged with FAM and 3’ biotin can then be detected on lateral flow test and visualized as two lines (SNP detection and control line) (**C**). Analytical sensitivity of the PCR component of the Fish-OLA is the new method to detect the signature SNP from different DNA template input (**D**). Specificity of the Fish-OLA to discriminate the sequence containing SNP in different concentrations of other codfish DNA species (**E**).

PCR PRIMER DESIGN

Four different primers were designed (**Table 11.1**) and tested in PCR reaction in the presence of an excipient to preserve the reagents during the lyophilization. Different annealing temperatures were used to determine the condition that achieved the most robust and rapid PCR. Final primer sets (**Figure 11.2A**) included both Pacific Cod endogenous sequence and engineered sequence adapter. After the first two cycles, these two segments of the primers were incorporated in amplicon and can be amplified at an escalated annealing temperature which increases PCR specificity and shortens ramping and cooling time. Initial testing of the final lyophilized qPCR formulations in 32 cod DNA samples showed high correlations with theoretical copies estimated by mass conversion (**Figure 11.2B**), proving that this non-traditional PCR assay yielded an expected outcome like a typical qPCR.

© Copyright 2021 | N Panpradist

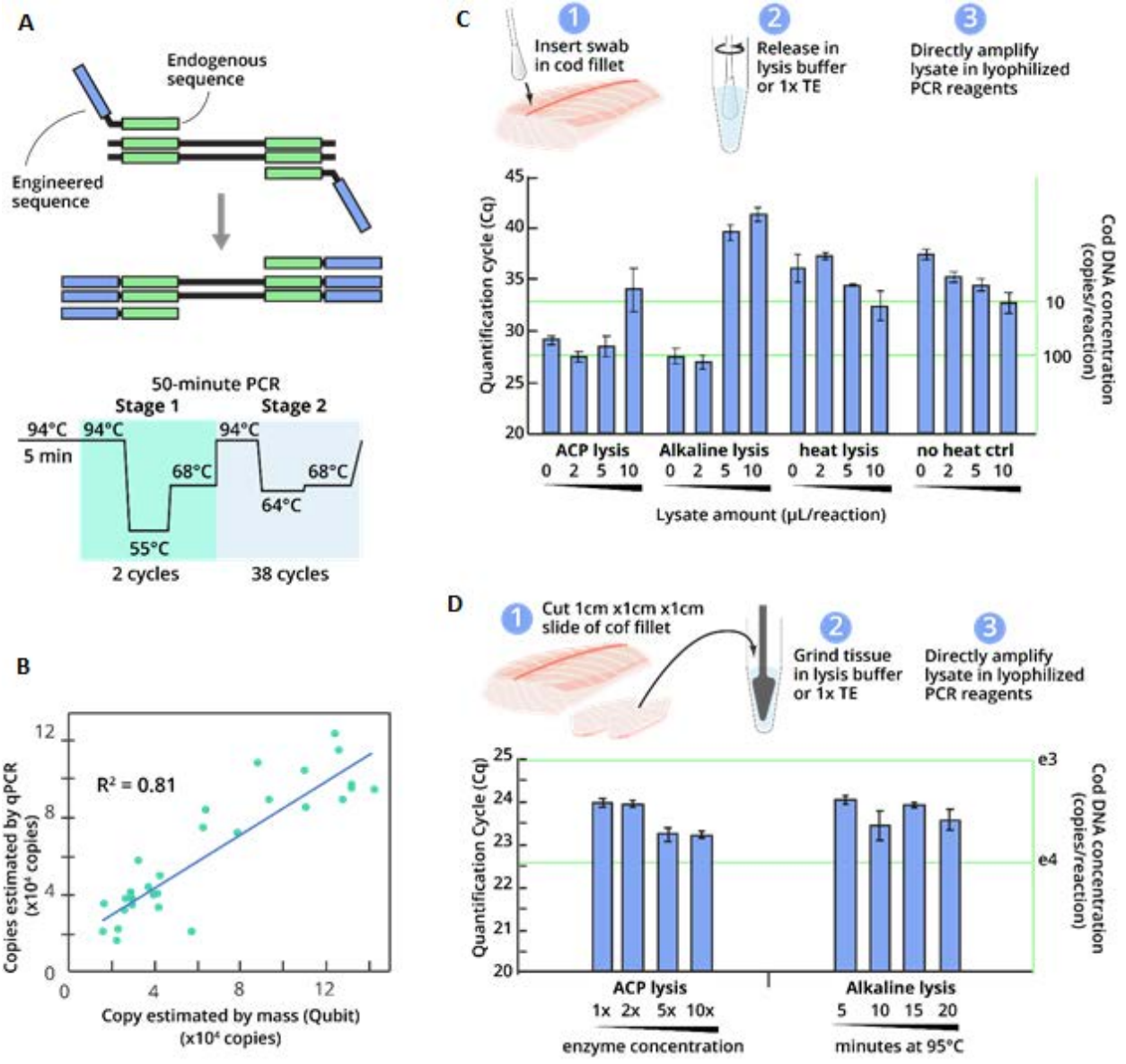

Figure 11.2 | Fish-OLA PCR design and integration with direct amplification from fish filet lysates.

(**A**) Primer design and temperature cycling to enable rapid PCR within 1 hour while typical PCR runs take 1.5 - 2 hours in our previous iterations. (**B**) Correlation of cod DNA copies estimated by our qPCR vs. theoretical number calculated from mass measured by Qubit assay. (**C**) Comparison of amplification yield from different sample preparation on the swab collection of cod fillets. Cq values (mean + SE, *n=4*) were plotted. (**D**) Comparison of amplification yields from different sample preparation on manually ground cod tissues. Cq values (mean + SE, n=4) were plotted.

© Copyright 2021 | N Panpradist

EXTRACTION-FREE DNA SAMPLE PREPARATION

We tested different methods for lysis: heat lysis, alkaline lysis, and enzymatic lysis. First, we used the swab method (see method for details) on the cod fillet. The yields were in the range of 10 - 100 copies/reaction (**Figure 11.2C**). Enzymatic lysis and alkaline lysis seemed to show the highest yield among the four methods. We hypothesized that this could be due to the limited amount of the cells picked up by the swab itself and using higher amounts of fish tissue might have resulted in a larger yield. Manually ground fish fillet indeed increased the amplification yields, with the amount comparable to the yield obtained from the DNA extracted by the standard methods (**Figure 11.2D**). We also used alkaline lysis on the archived fish fin (n=35) and found 100% successful PCR amplification.

LIGATION PROBE DESIGN

For ligation, the region near the upstream allele has a high secondary structure, where the 3’ end forms a palindrome to its own strand (**Figure 11.3A**). To resolve this secondary structure, we intentionally mutate the base at position 1tenand resolve this palindromic structure (**Figure 11.3B**). Further, several combinations of enzyme concentrations, annealing temperatures and annealing time were tested to achieve the highest sensitivity and specificity for ligation (**Figure 11.3C**). We had to account for the reduced melting temperature introduced by the mismatch; 45 °C annealing temperature (i.e., ten0 °C lower than the melting temperature of the non-mismatched probe) with 3 minutes of annealing time yielded high specificity

© Copyright 2021 | N Panpradist

and sensitivity for discrimination of the two polymorphisms in synthetic cod DNA variants.

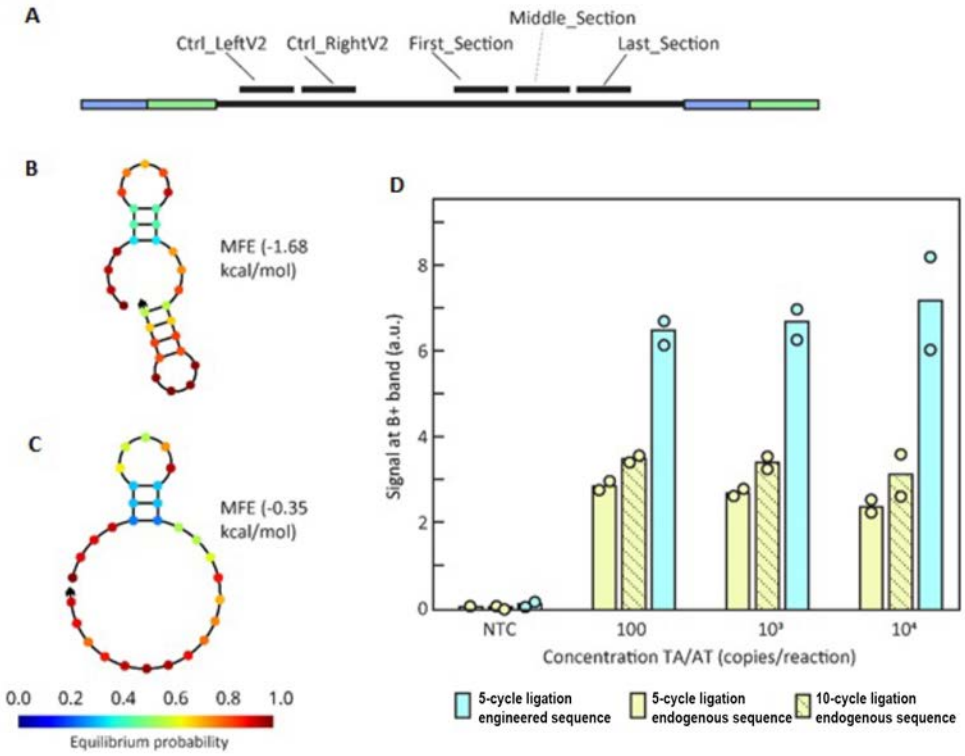

Figure 11.3 | Ligation probes and optimization.

(**A**) Schema of the relative location of ligation probes. (**B**) Most stable secondary structures of the endogenous First_Section probe. (**C**) Most stable secondary structures of the intentionally mutated "engineered" First_Section probe to reduce secondary structure at the 3'end of the probe. (**D**) Comparison of the signal generated by the engineered and the endogenous probes.

BLINDED EVALUATION OF FISH-OLA PERFORMANCE

Ligation, detection, and interpretation of Fish-OLA results were blinded (**Figure 11.4A**). Fish-OLA classification was compared to the Sanger sequencing and primary assignment of the Codfish (**Figure 11.4B**). The signals of the +B and C bands analyzed by our in-house software were used to classify the results into fish from BSAI or GOA **Figure 11.4C**. Signals from the +B and C bands above 3SD of

© Copyright 2021 | N Panpradist

the average band signal of the negative controls (grey group on the right of **Figure 11.4C**) are used as the thresholds for positive. Across all samples, human visual classification had at least 80% agreement to the call by software. We are awaiting the answer keys from the collaborators to confirm the true identities of these blinded samples.

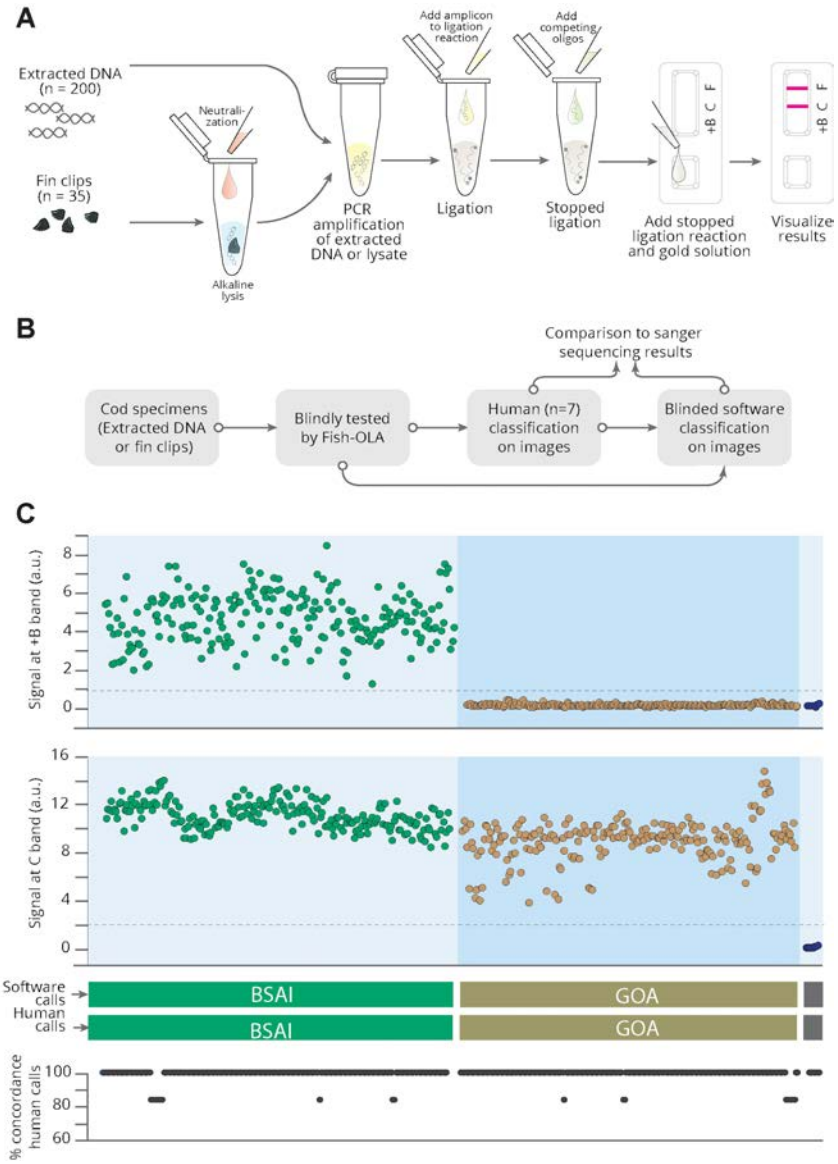

Figure 11.4 | Analysis of cod DNA and fin samples using Fish-OLA.

© Copyright 2021 | N Panpradist

(**A**) Workflow (**B**) Study design (**C**) Signal intensity of the Bering Sea (+B) cod positive bands and (C) cod control bands across all samples as well as classifications by software and human calls along with % concordance among human calls.

DISCUSSION

Here, we describe the development and evaluation of an assay to differentiate the population of Pacific cod (*Gadus macrocephalus*). Although the population structure in this species is subtle [6, 15, 16], we identified a signature gene involved in gamete recognition (Zona Pellucida 3) that shows almost fixed differences between the Bering Sea and more southern populations in the east and west Pacific (Spies et al. et al.) Our group previously determined a specific set of SNPs that are only found in the Cod from the Bering Sea and Aleutian Island stocks but differ east and south of Kodiak Island. Building upon this knowledge, we have developed and validated a novel DNA kit to classify the origins of the codfish.

The Fish-OLA kit uses the lyophilized reagents to enable easy assay to set up and a lateral flow test that allows visualization of the results by an unaided eye or software. Fish-OLA sensitively detected down to 10 copies/reaction of purified DNA and successfully amplified crude lysates from cod tissues or fin clips that were prepared by alkaline, heat, or enzymatic approaches. The amplified DNA was predictive of fish origins. Downstream ligation and detection also include the positive control for cod that serves as the process control from the beginning of sample preparation to detection. The flow control was useful to detect detection failure.

© Copyright 2021 | N Panpradist

The estimated cost for reagents and supplies for Fish-OLA is $US 10 per test. Although the real-time qPCR machine was used during the development to confirm the success of the amplification steps, a standard thermal cycler (the US $500) can be used to generate robust PCR products for downstream ligation, as previously shown [17]. Altogether, the cost of required equipment (i.e., vortex mixer, minicentrifuge, small heat block, and optional scanner) can be less than $1000. In contrast, satellite tags currently being used to understand the movement of cod from their feeding to spawning grounds cost $4000/tag. Sanger sequencing was criticized for low throughputs (leading to slow turnaround time) and high costs[18].

Here we present a newly developed DNA analysis tool that can differentiate the origin of the codfish in real-time that could be implemented at sea to identify the type of cod during feeding migrations in the Gulf of Alaska. This method can be used in conjunction with tagging to identify the ZP3 type of cod prior to tag release to implement an informed study of movement patterns of the two ZP3 types. DNA-analysis tools can be used to objectively identify the fish species and the origin of the fish. Such a marker would be a powerful tool in the management of the species, which supports the fourth largest commercial fishery in Alaska. Pacific cod are caught in roughly equal proportions during the winter (January-April) spawning season when they aggregate to spawn and their feeding migrations during the remainder of the year. Like Atlantic cod, Pacific cod aggregate to spawn at their native spawning sites (Drinan et al. 2018) but may disperse for the rest of the year - fisheries targeting feeding cod, therefore, exploit different populations that mix in

© Copyright 2021 | N Panpradist

unknown proportions. As widely recognized in Pacific salmonids, the accurate quantification of these proportions is a crucial component in the sustainable management of the species.

ACKNOWLEDGMENTS

We thank our collaborators Dr. Lisa Frenkel and Ingrid A Beck from Seattle Children's Research Institute, who have contributed to the development of the OLA-Simple HIVDR test, which we adapted to genotype these cod species. We thank other Lutz lab members: Samuel Stewart and Leila Ahmadinia, for the technical support. NP was partially funded by NIH AI145486 (BRL). The reagents and supplies used in this study were funded by National Science Foundation ECCS-1835847 (KFB). The funding organizations do not have an influence on the study design, interpretation, and writing of this manuscript.

© Copyright 2021 | N Panpradist

CHAPTER 11 REFERENCES

1. NOAA Fisheries Seafood Import Monitoring Program. https://www.fisheries.noaa.gov/international/seafood-import-monitoring-program (accessed 17th March).
2. Clarke, S. *Understanding China's Fish Trade and Tracibility*; Hong Kong, China, 2009.
3. Xiong, X.; D'Amico, P.; Guardone, L.; Castigliego, L.; Guidi, A.; Gianfaldoni, D.; Armani, A., The uncertainty of seafood labeling in China: A case study on Cod, Salmon and Tuna. *Marine Policy* **2016,** *68*, 123-135.
4. Xiong, X.; Guardone, L.; Giusti, A.; Castigliego, L.; Gianfaldoni, D.; Guidi, A.; Andrea, A., DNA barcoding reveals chaotic labeling and misrepresentation of cod (鳕, Xue) products sold on the Chinese market. *Food Control* **2016,** *60*, 519-532.
5. Hadden, H.; Newman, J., Fish Caught in America, Processed in China Get Trapped by Trade Dispute *The Wall Street Journal* 9th August, 2018, 2018.
6. Spies, I.; Gruenthal, K. M.; Drinan, D. P.; Hollowed, A. B.; Stevenson, D. E.; Tarpey, C. M.; Hauser, L., Genetic evidence of a northward range expansion in the eastern Bering Sea stock of Pacific cod. *Evol Appl* **2020,** *13* (2), 362-375.
7. Barbeaux, S. J.; Holsman, K.; Zador, S., Marine Heatwave Stress Test of Ecosystem-Based Fisheries Management in the Gulf of Alaska Pacific Cod Fishery. *Frontiers in Marine Science* **2020,** *7*.

© Copyright 2021 | N Panpradist

8. Barbeaux, S.; Aydin, K.; Fissel, B.; Holsman, K.; Laurel, B.; Palsson, W.; Rogers, L.; Shotwell, K.; Yang, Q.; Zador, S. *Chapter 2: Assessment of the Pacific cod stock in the Gulf of Alaska*; NOAA Fisheries: 2019.

9. Spies, I.; Spurr, R.; Hartinger, T.; Drinan, D.; Tarpey, C.; Hauser, L., Diversifying selection and spatial patterns in the zona pellucida gene suggest local adaptation in Pacific cod. 2021.

10. Panpradist, N.; Toley, B. J.; Zhang, X.; Byrnes, S.; Buser, J. R.; Englund, J. A.; Lutz, B. R., Swab sample transfer for point-of-care diagnostics: characterization of swab types and manual agitation methods. *PLoS One* **2014,** *9* (9), e105786.

11. Panpradist, N.; Beck, I. A.; Ruth, P. S.; Avila-Rios, S.; Garcia-Morales, C.; Soto-Nava, M.; Tapia-Trejo, D.; Matias-Florentino, M.; Paz-Juarez, H. E.; Del Arenal-Sanchez, S.; Reyes-Teran, G.; Lutz, B. R.; Frenkel, L. M., Near point-of-care, point-mutation test to detect drug resistance in HIV-1: a validation study in a Mexican cohort. *AIDS* **2020,** *34* (9), 1331-1338.

12. Panpradist, N.; Beck, I. A.; Vrana, J.; Higa, N.; McIntyre, D.; Ruth, P. S.; So, I.; Kline, E. C.; Kanthula, R.; Wong-On-Wing, A.; Lim, J.; Ko, D.; Milne, R.; Rossouw, T.; Feucht, U. D.; Chung, M.; Jourdain, G.; Ngo-Giang-Huong, N.; Laomanit, L.; Soria, J.; Lai, J.; Klavins, E. D.; Frenkel, L. M.; Lutz, B. R., OLA-Simple: A software-guided HIV-1 drug resistance test for low-resource laboratories. *EBioMedicine* **2019,** *50*, 34-44.

13. Panpradist, N.; Beck, I. A.; Chung, M. H.; Kiarie, J. N.; Frenkel, L. M.; Lutz, B. R., Simplified Paper Format for Detecting HIV Drug Resistance in Clinical Specimens by Oligonucleotide Ligation. *PLoS One* **2016,** *11* (1), e0145962.

© Copyright 2021 | N Panpradist

14. Vrana, J.; Chohan, B.; Chung, M.; Higa, N.; Kanthula, R.; Lutz, B.; Panpradist, N.; Ruth, P.; Frenkel, L., OLA Simple v 1.0: observational study of an app-guided HIV drug resistance test at the Coptic Hope Center in Kenya. *medRxiv* **2021**.

15. Cunningham, K. M.; Canino, M. F.; Spies, I. B.; Hauser, L., Genetic isolation by distance and localized fjord population structure in Pacific cod (Gadus macrocephalus): limited effective dispersal in the northeastern Pacific Ocean. *Canadian Journal of Fisheries and Aquatic Sciences* **2009,** *66* (1), 153-166.

16. Drinan, D. P.; Gruenthal, K. M.; Canino, M. F.; Lowry, D.; Fisher, M. C.; Hauser, L., Population assignment and local adaptation along an isolation-by-distance gradient in Pacific cod (Gadus macrocephalus). *Evol Appl* **2018,** *11* (8), 1448-1464.

17. Panpradist, N.; Wang, Q.; Ruth, P. S.; Kotnik, J. H.; Oreskovic, A. K.; Miller, A.; Stewart, S. W. A.; Vrana, J.; Han, P. D.; Beck, I. A.; Starita, L. M.; Frenkel, L. M.; Lutz, B. R., Simpler and faster Covid-19 testing: Strategies to streamline SARS-CoV-2 molecular assays. *EBioMedicine* **2021,** *64*, 103236.

18. Lu, G.; Luo, M., Genomes of major fishes in world fisheries and aquaculture: Status, application and perspective. *Aquaculture and Fisheries* **2020,** *5* (4), 163-173.

© Copyright 2021 | N Panpradist

CHAPTER 12: SUMMARY OF CONTRIBUTIONS AND IMPACT

People living with HIV can live almost normal lives if they have access to effective antiretroviral drugs. HIV drug resistance (**HIVDR**) testing, in conjunction with viral load (**VL**) monitoring, provides the most useful information for doctors to select the drugs that work for an individual. Since 2002, Dr. Frenkel and her team have expanded access to HIVDR by using a more simplified assay that does not need a million-dollar Sanger sequencer. The 2002 OLA protocol costs only $5/SNP, but the implementation of the OLA widely was ultimately prohibited by workflow complexity.

This thesis summarizes nearly a decade worth of work through the collaboration between the Lutz lab and the Frenkel and Lai labs to make OLA more accessible. We first addressed crucial areas that are most complex and time-consuming. Improved sample preparation methods (**Chapter 2**), simplified paper-based detection (**Chap-ter 3**), ready-to-use reagents (**Chapter 4**) were crucial developments that led to the first OLA-Simple kit 1.0. Our initial evaluation of OLA-Simple 1.0 on South African infant dry blood spots was selected for an oral presentation at the 2017 international WHO HIV Drug Resistance meeting. The OLA-Simple prototype was brought up on the stage, and after the talk, we received copious feedback from global clinicians and potential users that changed my way of thinking.

© Copyright 2021 | N Panpradist

Dr. Frenkel (left) and Dr. Lutz (Right) carrying the 2017 OLA-Simple demo at the 2017 WHO HIV Drug Resistance Meeting.

Vongani VM. Muthambi and Nonhlanhla Mbenenge of the University of the Witwatersrand/National Health Laboratory Service, and Nuttada Panpradist with OLA-Simple demo.

Three questions were raised: ***Would this test work for patients in my country? Where can I buy this? Would this test require a lot of training?*** In response to these questions, we sought to expand the validation of OLA-Simple in multiple HIV subtypes. ~1000 OLA-Simple kits prototypes were produced; dry reagents were manufactured in-house, and lateral flow tests were manufactured with support from Dr. Syamal Raychaudhuri of InBios International, Inc. These kits were used to test clinical specimens from globally representative subtypes (A, B, C, AE, and D) and showed nearly perfect results compared to Sanger sequencing and the 2002 OLA. Through a new collaboration with the Klavins lab I initiated, we launched the inter-active guide for non-trained users to evaluate OLA-Simple at the UW and in Kenya, showing 97% assay accuracy. A manuscript describing our development, evaluation in archived clinical samples through a multi-continent collaboration, and usability in the US was published in 2019. This work was highlighted in a commentary (M Nogu-era-Julian EbioMedicine, 2019).

> *"Importantly, in the work of Panpradist et al., PoC testing is conceptually described as a whole, comprising technology and context. Not only the complex molecular biology machinery is craftfully embedded and tested within a single-*

© Copyright 2021 | N Panpradist

> *use, low cost device, but also assayed and validated in a close-to-real context, putting it to use by inexperienced users that are guided by ad hoc created companion tools in carefully designed feasibility tests. Of note, ad hoc mobile software not only increases test robustness and usability but may also be an entry point to controlled data collection for surveillance. While such PoC technology deployment into a real-world setting faces challenges such as materials, continued supply, and cold chain maintenance that demand operational research and cost-benefit studies, work by Panpradist et al. represents an important step forward for HIV drug resistance testing."*

Simultaneously, we began working with UW CoMotion. I participated in competitions (Holloman Health Innovation Challenge, Business Plan Competitions, I-Corps, and WE-REACH boot camp), interviewed stakeholders, and en-gaged partners to manufacture and use kits at scale. The landscape for the demand of HIVDR tests for nucleoside-based regimens began to change in early 2018 as low-income countries, through the sponsorship of the WHO and other international entities, began to switch to the new dolutegravir-based regimen.

In 2018, Mexico, a medium-income country, was unable to afford the new DTG-based regimens. We thought the country would benefit from OLA-Simple. It could also be an excellent opportunity to reach a broad audience because the 2019 International AIDS Society meeting was to be hosted in Mexico City. I wrote an email to Dr. San-tiago Ávila-Ríos, the Head Scientist at the WHO-certified HIV lab in Mexico, to discuss potential collaboration.

© Copyright 2021 | N Panpradist

1-minute pitch at the HIC won 2nd place $10k award

Business plan competition event

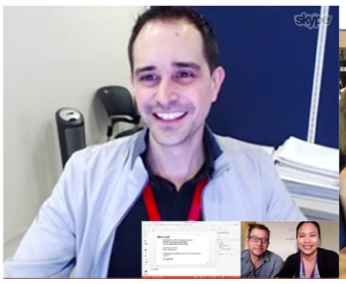

Meeting with Dr. Santiago Avila-Rios, the lead scientist at the WHO-certified HIV lab in Mexico

Our follow-up visit in Mexico (partially supported by the monetary prize from business competitions) left to a new collaboration.

Our meetings led to a new collaboration to develop a subtype-B-specific OLA-Simple kit for the Mexican population. Despite being able to do work only on weekends because I was doing my fellowship at Stanford University, our team completed the study showing 90% accuracy compared to NGS, presented at the 2020 International AIDS Society as planned, and published in the AIDS journal later in the year. The study sparked an interest in the HIV community. An interview related to our publication was published on the Reuters Health news blog (https://www.medscape.com/viewarticle/928372). However, the landscape for the demand for HIVDR tests in Mexico also changed later in 2019, as Mexico was able to negotiate the price for the DTG-based regimen and switched its first-line treatment. It made the use of our OLA-Simple kit for NNRTI resistance less relevant to Mexico's majority HIV population.

Our team switched the focus to pediatric and pregnant mother populations. Not until mid-2020 did the WHO recommend the use of dolutegravir-based regimens in infants and pregnant women. Dr. Rena Patel (UW Global Health) secured funding to support

© Copyright 2021 | N Panpradist

the study to validate the OLA-Simple in this population in 2020. I connected our team to Dr. Mansour Samadpour, the President of IEH Laboratory and Consulting Group, whom I met at the 2018 UW business plan competition. This company manufactured most OLA-Simple kit components for this study. Due to the COVID-19 pandemic, our study was significantly delayed.

Later in 2020, Drs. Phyllis Kanki and Holly Rawizza, with whom I pitched the OLA-Simple kit at the 2017 International AIDS Society, pursued a collaboration to develop OLA-Simple for subtype G/AG in Nigerian pediatric populations. The proposal was funded. I designed the probes for this subtype and am in the process of evaluating the patient samples and preparing the manuscript. This subtype G/AG-specific OLA-Simple kit will be used as part of a study in 2022.

To address the need for HIVDR in the adult population, the Frenkel lab continues to validate the new probe sequences to detect HIVDR in other drug classes. We were contacted by the national laboratories in Uganda and Zimbabwe, but we did not have the capacity to collaborate with all these partners in the past. Given that now we have established the pipeline for development to production, we hope that this would allow us to collaborate with other researchers more widely.

Currently, VL monitoring and HIVDR testing are disconnected. Once a patient is found to have unsuppressed VL, samples are re-collected and shipped out for the HIVDR

© Copyright 2021 | N Panpradist

test. This long wait time could lead to patient loss-to-follow-up and worse treatment outcomes. **Chapter 6** – **Chapter 8** discuss different strategies that could be used to improve the performance of OLA-Simple and the potential to upgrade to "V-OLA," an integrated VL and reflexed HIVDR test. V-OLA would be beneficial not just for the HIV population starting or failing treatment but the remaining 40M people living with HIV who need to be tested for HIV VL twice a year. Existing collaborations both on the side of clinicians and manufacturers put us in a strong position to contribute to the still-unmet need for accessible HIVDR and VL tests. Moreover, our team remains engaged with the WHO by participating in annual meetings in which the WHO seeks advice from experts to prepare for HIVDR issues.

In addition to HIVDR applications, this thesis showcases the adaptation of OLA-Simple kits to other applications to detect SNPs in human allele HLA-B*57:01 associated with abacavir hypersensitivity (**Chapter 8**), SARS-CoV-2 (**Chapter 9**), and codfish (**Chapter 10**). This is just a start since hundreds of SNPs are proven to be biomarkers for other disease conditions, unique variants of pathogens such as SARS-CoV-2 or hepatitis C. The applications are limitless, but OLA-Simple would be particularly useful in applications that require fast turnaround time and are constrained by costs and access to expensive equipment.

The development of healthcare technologies is challenging, and it is even more challenging to transfer the technology in the lab to make an impact. Technology developers, besides having intelligence and a strong work ethic, need to seek advice from the key stakeholders and end-users during the development process. Engaging international audiences at academic conferences would open the door to future

© Copyright 2021 | N Panpradist

collaborations. Technology developers can share their vision and provoke potential users to think outside the normal practice on how such technologies could improve effectiveness in healthcare and save more lives. If users and developers share the same vision, we could increase the chance for a technology to be successfully implemented in user settings. Moreover, technology developers also need to establish an understanding of industrial productions so that the designed devices can be readily scalable by the manufacturers. Such insights can be obtained via Summer Internships or on-site visit activities arranged by BioEngage or other UW organizations. Business competitions are very useful venues that connect technology developers to potential manufacturers or investors.

The success of the OLA-Simple project relies on the collaboration of researchers and scientists across disciplines and regions. Indeed, back in 2013, the OLA-Simple project began from a Global-WACh seminar series in which Dr. James Lai and Dr. Lisa Frenkel were invited to lecture on HIVDR. Motivated by this, I participated as a student in this class in 2014. As part of a classroom assignment, I was paired with Dr. Diana Marangu, and we developed a proposal idea for tuberculosis diagnostics from urine samples. This idea led to a 2014 Global WACh Seed grant award (PI: Dr. Barry Lutz, Dr. James Lai, and Dr. David Horne) and an R21. In the following years, I was subsequently invited to co-lecture with other professors from the Department of Global Health on HIV, tuberculosis, and pathogens causing

© Copyright 2021 | N Panpradist

diarrhea (see **Appendix 5**). Being a part of the research environment in the OLA-Simple project, I have developed a collaborative mindset, and I witnessed its impact on discovery first-hand. I did not stop at the UW. I passed on this thinking through my research talks (see **Appendix 9**) in Thailand, Zimbabwe, Switzerland, and South Africa. Recently, I contributed to the development of a proposal to establish a program in Thailand similar to Global WACh with the hope of cultivating a culture for collaborations across disciplines.

While developing OLA-Simple technologies, we also built a team of talented, motivated, creative, and productive undergraduate student researchers. These students were trained and challenged to grow and become future independent researchers. Recently, our team has contributed to significant work in the field of HIVDR, as evidenced by the invitation to present our progress on the OLA-Simple kits at the 2015-2016 international HIVDR workshops, exclusive events for only 200 delegates. The meeting includes key stakeholders: the representatives from the WHO, the CDC, and other international entities – who stressed the urgent need for a point-of-care HIVDR test in low-resource settings. Below are a few sentences from each undergraduate student researcher noting how this project impacts their professional and personal life. They wrote this when we competed for the national APF Student Prize in 2017, and our team won the third prize of a total of $60,000.

Left to Right: Annie Wong-On-Wing, Betty Yohannes, Nikki Higa, Dr. Barry Lutz, Nuttada Panpradist, David McIntyre, and Jonathan Lim

© Copyright 2021 | N Panpradist

"*As a student researcher, I was originally drawn to the OLA project because I would have the opportunity to address a critical challenge in global health through developing novel innovations in molecular diagnostics, all while improving my own skills as a scientist and engineer. Indeed, my work on this project as an undergraduate student was integral in my decision to pursue a Ph.D. in Biological Engineering at MIT, with a focus on global health infectious disease work, following my undergraduate studies."* - Ian Andrews, 2016 B.S. UW Bioengineering

"*The OLA project has allowed me the opportunity to engage in meaningful research that will soon benefit areas with some of the highest rates of HIV in the world. As an aspiring Ph.D. student and research scientist, this experience has also helped me develop crucial skills that I will need to be successful in the future. Working at the crossroads of molecular diagnostics and global health can be challenging at times. However, I am grateful to be a part of this amazing research team, and I look forward to being a part of the exciting developments ahead.*" - Nikki Higa, 2017 B.S. UW Bioengineering.

"*Since I joined the OLA team in 2014, the OLA project has been a valuable opportunity for me to extend my skills as a biochemistry major in a biomedical engineering setting, collaborate with clinicians and scientists across the globe, grow as a researcher, and be a part of a motivated and dedicated team. It is amazing how rapidly we have made progress*

© Copyright 2021 | N Panpradist

over the past few years, consistently fueled by the desire to lessen the burden of HIV drug resistance, which affects countless individuals around the globe today. This award will provide our team with resources essential to engineer the OLA HIV drug resistance test to full automation in a single device fully capable of addressing the urgent need for point-of-care testing of drug-resistant HIV." – Annie Wong-On-Wing, 2017 B.S. Biochemistry and Chemistry.

"*When I started researching as an undergraduate, my main goal was to find work that would directly help people that do not have access to healthcare. On the OLA project, I am able to try and make some impact and hopefully see the hours I spend in the lab prove its value in the clinic around the world. In the nine months that I have been part of the group, I have worked on every stage of lateral flow diagnostic development, from 3-D printed prototyping of device designs to optimization of a novel detection technique, giving me a breadth of knowledge that I would not think to be attainable in such a short amount of time."* – David McIntyre, 2018 B.S. Bioengineering.

"*Being a part of the OLA-Simple team has been an opportunity for me to embark on an independent yet interdependent research topic in the sphere of Global Health. My experience with my team members has taught me the importance of effective research planning and information delivery in working towards congruent research goals. Receiving this*

© Copyright 2021 | N Panpradist

> *award to fund the further progress of this research will definitely validate our team's effort and boost our morale in working towards this device which I believe has great potential to benefit lives on a global scale*." – Jonathan Lim, 2018 B.S. Bioengineering.

> "*Growing up in Ethiopia where HIV and AIDS is one of the leading causes of death, to me this project holds special importance. To be able to take part in creating a technology that will aid in the process of effective care for HIV-infected individuals is a fulfilling and motivational experience and one that I am truly excited to be a part of*." - Betelhem Yohannes, 2018 B.S. Bioengineering.

Over the past eight years, I have developed expertise in the field of HIV diagnostics and molecular diagnostics in general. These skills became highly relevant when the COVID-19 pandemic started. I have contributed to multiple ongoing projects ranging from SARS-CoV-2 detection in Seattle Metro buses to the evaluation of our SARS-CoV-2 assay in Zimbabwe. I worked with other lab members to develop and validate a point-of-care Harmony COVID-19 device that is being licensed to a company. The complete project list is in **Appendix 6**.

© Copyright 2021 | N Panpradist

APPENDIX 1: FIGURE LIST

CHAPTER 1: INTRODUCTION

Figure 1.2 | Schema of HIV integration into human genomic DNA 3
Figure 1.3 | Different HIV antiretroviral treatments disrupt different steps of HIV replication 4
Figure 1.4 | Amino acid residues near the binding pockets of RT inhibitors 7
Figure 1.5 | Comparison of HIV treatment strategies 9
Figure 1.6 | SNPs associated with ART failures 13
Figure 1.7 | Hybridization-based SNP detection 15
Figure 1.8 | Hybridization-based SNP detection in a highly-polymorphemic genome 16
Figure 1.9 | Nucleotide-incorporating SNP detection 18
Figure 1.10 | Nucleotide-cleave assay to detect SNPs 19
Figure 1.11 | Ligation-based SNP detection 22
Figure 1.12 | Schematic of enzyme-mediated ligation in OLA for HIVDR test 23
Figure 1.13 | Workflow of CLIA-OLA (Frenkel lab 2002) 24

CHAPTER 2: NUCLEIC ACID PREPARATION

Figure 2.1 | Schema of in-house CD4+ cell enrichment chemistry 45
Figure 2.2 | Impact of carryover inhibitors from different blood specimen types 47
Figure 2.3 | Protocol for CD4 cell enrichment protocol from fresh whole blood 48
Figure 2.4 | Workflows for SARS-CoV-2 screening and HIV VL testing 60
Figure 2.5 | Effect of DTT concentrations in in-house lysis buffer 63
Figure 2.6 | Effect of carrier RNA in in-house lysis buffer 64
Figure 2.7 | Impact of carrier tRNA concentration on RT-qPCR 65
Figure 2.8 | Quantitation and classification of HIV and SARS-CoV-2 68
Figure 2.9 | Quantitation and classification of HIV RNA in clinical plasma specimens 70
Figure 2.10 | Quantification and detection of SARS-CoV-2 RNA in clinical NS 72
Figure 2.11 | HIV LTR and SARS-CoV-2 Cq values from RNA co-extracted from NS/plasma specimens 74
Figure 2.12 | Non-target DNA harms sensitivity and specificity of amplification 80
Figure 2.13 | HIV DNA was captured specifically in the presence of non-HIV DNA and/or plasma 81
Figure 2.14 | Sequence-specific capture of synthetic HIV DNA & genomic clinical HIV RNA 83
Figure 2.15 | Vision of our novel simple and fast sample preparation method 85
Figure 2.16 | Schema of HIV RNA capture in large volume specimens 87
Figure S2.17 | Characterization of in vitro transcribed RNA standards using Crystal digital PCR (cdPCR) 95

Figure S2.18 | Standard curves of RT-qPCR assays 96
Figure S2.19 | Correlation plots of measured VL from co-extraction of contrived plasma/NS 97
Figure S2.20 | Levels of RP gene of clinical specimens 98

CHAPTER 3: PAPER-BASED DETECTION FOR HIVDR OLA

Figure 3.1 | Comparison of the plate and 1st-generation paper OLA detection 103
Figure 3.2 | Different assembly for the 1st-generation paper dipstick 108
Figure 3.3 | Species present in the reaction at the end of the ligation step 110
Figure 3.4 | Schema of detection mechanisms in the 1st-generation paper dipstick 110
Figure 3.5 | Comparison of plate vs. 1st-generation paper detection for analysis of Y181C plasmid standards 113
Figure 3.6 | Analysis of clinical specimens by 1st-generation paper detection for K103A & Y181C 115
Figure 3.7 | Analysis of clinical specimens by 1st-generation paper detection for M184V & G190A 116
Figure 3.8 | Correlation plots of the signal ratio by plate vs.. 1st-generation paper detection 117
Figure 3.9 | Denaturing of non-ligated probes to remove the background using NaOH 118
Figure 3.10 | On-paper oligonucleotide capture by immobilized streptavidin 119
Figure 3.11 | Traditional plate-based ELISA versus Generation 1 dipstick paper-based detection (CDD) 124
Figure 3.12 | Comparison of 1st and 2nd generation paper detection 125
Figure 3.13 | Detection of single-base mutations in 2nd generation paper detection 127
Figure 3.14 | Characterization of antibody capture cross-reactivity 129
Figure 3.15 | Use of Fab fragment tagged AP antibodies as capture molecules 130
Figure 3.16 | Effect of buffer pH and salts on immobilized IgG 131
Figure 3.17 | Effect of different denaturation methods on the immobilized antibody 133
Figure 3.18 | Detection of HIVDR on a single strip using AP/Purple substrate system 133
Figure 3.19 | Detection of HIVDR on a single strip using POD/DAB system. 134
Figure 3.20 | Effect of buffer on lateral flow detection with streptavidin polystyrene beads 135
Figure 3.21 | Specific antibody pairs tested on the lateral flow detection. 136
Figure 3.22 | Streptavidin-limited detection can cause false results. 137
Figure 3.23 | Effect of streptavidin: biotin ratio on false MUT detection. 138
Figure 3.24 | Partially filled streptavidin reduced the effect of diffusion limit during the pre-mixing step. 139
Figure 3.25 | Detection of ligation products with 1µg-BSA prefilled streptavidin microsphere beads. 140
Figure 3.26 | Paper-based detection for amplification products. 142
Figure 3.27 | Experimental design to investigate toehold-mediated strand displacement in OLA buffer. 144
Figure 3.28 | Effect of toehold length on strand displacement in OLA buffer 145
Figure 3.29 | Effect of competing oligo concentrations on toehold-mediated strand displacement. 146
Figure 3.30 | Effect of polymorphisms on toehold-mediated strand displacement 147

Figure 3.31 | Effect of modified bases (SuperT and SuperG) on improving polymorphisms 148
Figure 3.32 | Effect of displaced length on toehold-mediated strand displacement 149
Figure 3.33 | Secondary structures of single-stranded HIV DNA near and within the probe regions 150
Figure 3.34 | Novel design of the ligation probe adapter to overcome issues with endogenous HIV sequence 152
Figure 3.35 | Effect of human genomic DNA on engineered toehold-mediated strand displacement 153
Figure 3.36 | Schematic of the fluorescence measurement system 154
Figure 3.37 | Toehold-mediated strand displacement on paper 158
Figure 3.38 | Autonomous pseudo 1DPN sequential fluid delivery 159
Figure 3.39 | Set up for sequential delivery for 3rd generation paper-based detection 160
Figure 3.40 | 3rd-generation paper detection of HIVDR ligation reaction 160
Figure 3.41 | Our high specific computationally designed DNA barcodes 162
Figure 3.42 | Sensitivity of DNA derivative barcodes 163
Figure 3.43 | Our on-paper multiplexed detection using DNA barcodes 165
Figure 3.44 | Effect of UV-crosslinking on barcode sequences 165
Figure 3.45 | Analysis of OLA-Simple by human visual calls from scanned images 167
Figure 3.46 | Intensity and RGB values 168
Figure 3.47 | Linear Discriminant Analysis (LDA) unit vector 170
Figure 3.48 | Justification for a method to determine the best differentiation 173
Figure 3.49 | Discriminations of blue bead signal by different unit vectors 174
Figure 3.50 | Discriminations of DAB/HRP signal by different unit vectors 174
Figure 3.51 | Software Image Processing using t-statistics 177
Figure 3.S52 | Correlation plots of OD and MUT OD ratios by plate CLIA-OLA vs. intensities and MUT intensity ratio by 1st generation paper-based detection 179
Figure S3.53 | Correlation plots of MUT ratio by 1st-generation paper detection vs. CLIA-OLA 180
Figure S3.54 | Schematic of Chemistry of Ligation and Detection System in OLA on Membrane 187

CHAPTER 4: READY-TO-USE DRY REAGENTS

Figure 4.1 | Concept of lyophilization and critical temperatures 215
Figure 4.2 | Commonly used excipients for lyophilization of small molecules. 216
Figure 4.3 | Excipient formulations for OLA. 219
Figure 4.4 | Effect of polymerase concentrations on PCR. 221
Figure 4.5 | Effect of ligase concentration on OLA. 222
Figure 4.6 | Physical appearance of dried ligation mix in the presence of excipients. 223
Figure 4.7 | X-ray Diffraction of matrices. 224

Figure 4.8 | Platforms for dried reagents. 226
Figure 4.9 | Dry reagents in the bead format using 5% trehalose, 1.5% PEG, and 1.5% PVA. 227
Figure 4.10 | Novel, high-throughput fabrication of dried reagent pellets. 228
Figure 4.11 | Evaluation of in-tip dried reagent in OLA workflow. 229
Figure 4.12 | Long-term stability of lyophilized LDR mixtures. 231
Figure 4.13 | Performance of OLA-Simple components after long-term storage. 232
Figure 4.14 | Functionality of immobilized anti-digoxigenin IgG after 1 and 90 days. 234
Figure 4.15 | Lyophilized reactions with 10% glycerol. 236
Figure 4.16 | Set up of reagent rehydration and buffer loading. 240
Figure S4.17 | Estimated amplicon concentration with quantitative gel electrophoresis. 241
Figure S4.18 | Estimation of amplicon concentration based on purified DNA kit and mass measurement. 242

CHAPTER 5: OLA-SIMPLE 1.0 KIT FOR HIVDR

Figure 5.1 | Workflow and analytical performance of the OLA-Simple HIV genotyping assay. 250
Figure 5.2 | Validations of the OLA-Simple on clinical specimens, compared to other comparator assays. 253
Figure 5.3 | Nucleotide sequences in the regions of the OLA-Simple's ligation probes for indeterminates identified by OLA-Simple and/or CLIA-OLA. 256
Figure 5.4 | Receiver Operating Characteristic (ROC) curves of OLA-Simple and Sanger sequencing. 259
Figure 5.5 | The vision of the OLA Automation. 261
Figure 5.6 | Feasibility testing of OLA-Simple by inexperienced users guided by Aquarium software. 263
Figure 5.7 | OLA-Simple laboratory setup and workflow. 269
Figure 5.8 | OLA-Simple HIVDR results and interpretations. 272
Figure 5.9 | Workflow and analytical sensitivity of the OLA-Simple kit using plasma. 282
Figure 5.10 Receiver-operating characteristic (ROC) curves. 285
Figure 5.11 | Transition of technical knowledge and skills for OLA-Simple 1.0 to InBios International, Inc. 308
Figure S5.12 | Commercial and alternative PCR chamber. 309
Figure S5.13 | Overall workflow of implementation study in Kenya 309
Figure S5.14 | HIVDR CD4 extraction module in Aquarium 2018. 310
Figure S5.15 | HIVDR lysis module in Aquarium 2018. 310
Figure S5.16 | HIVDR PCR module in Aquarium 2018. 311
Figure S5.17 | HIVDR ligation module in Aquarium 2018. 311
Figure S5.18 | HIVDR detection module in Aquarium 2018. 312
Figure S5.19 | HIVDR ligation module in Aquarium 2018. 312

Figure S5.20 | HIVDR visual call module in Aquarium 2018. 313
Figure S5.21 | HIVDR Interpretation module in Aquarium 2018 313

CHAPTER 6: STRATEGIES TO IMPROVE AMPLIFICATION AND LIGATION FOR HIVDR OLA

Figure 6.1. | Traditional VL and HIVDR workflow versus V-OLA (HIV VL with reflexed OLA-Simple). 337
Figure 6.2. HIV isothermal strand displacement (iSDA) assay for HIV RT. 343
Figure 6.3 | An example of tHDA real-time amplification and fragment analysis (denaturing gel) 345
Figure 6.4 | OLA analysis of the product from tHDA to confirm the sequence accuracy. 345
Figure 6.5 | Mechanisms of RPA[22] 347
Figure 6.6 | RPA amplification of the whole HIVDR region in HIV RT. 351
Figure 6.7 | Examples of the sequences of patient specimens in the RPA primer regions. 352
Figure 6.8 Schematic of LAMP mechanisms 353
Figure 6.9 | Ligation yield of Y181C mutation assay. 356
Figure 6.10 | Ligation reaction and its competitive side reactions. 357
Figure 6.11 | Example of input MATLAB GUI for ligation probe Tm calculation. 361
Figure 6.12 | Example of output MATLAB GUI for ligation probe Tm calculation. 361
Figure 6.13 | Example of secondary structures in the ligation probes predicted by NuPack. 363
Figure 6.14 | Effect of temperature on the ligation sensitivity and specificity. 365
Figure 6.15 | Fidelity of wild-type Tth DNA ligase activity 366
Figure 6.16 | Comparison of ligase fidelity of commercially available ligases [34]. 367
Figure 6.17 | Schematic of lambda exonuclease digestion on phosphorylated amplicon. 368
Figure 6.18 | Asymmetric primer ratio in PCR and tHDA. 369
Figure 6.19 | Schema of V-OLA 1.0 workflow. 370
Figure 6.20 | Examples of results of HIV DNA using fast RT-PCR and downstream ligation and detection. 371
Figure 6.21 | Preliminary results of our endpoint VL fast PCR assay on clinical specimens. 372
Figure 6.22 | Whole pol endpoint VL fast PCR assay. 372
Figure 6.23 | Stability of ligase and NAD during the tHDA. 375
Figure 6.25 | V-OLA 2.0 with completed lyophilized reaction. 376
Figure 6.26 | Schema of OLA-Simple 2.0 and its analytical performance. 377
Figure 6.27 | Detection of HIV RNA using low-cost heater/reader and cell phone analysis. 378
Figure S6.28 | Fragment analyses of amplicon generated by 5'phosphorylated forward primer were treated or not treated with exonuclease. 414
Figure S6.29 | Fragment analyses of amplicon generated by 5'hydroxyl forward primer was treated or not treated with exonuclease. 415

CHAPTER 7: FLUORESCENCE-BASED DETECTION OF LDR PRODUCTS

Figure 7.1 | First demonstration of the molecular beacon (MB). 417
Figure 7.2 | Phase transition of MB. 418
Figure 7.3 | Mismatch discrimination of the MUT and WT ligated probes by MB. 420
Figure 7.4 | Melting temperature of the stem region in the MB and corresponding linear probe using the two-state model. M-fold by Zuker et al. [4] can provide a more accurate prediction of the MB stem region since it includes the effect of the loop region, etc. 421
Figure 7.5 | Examples of reverse-molecular beacons to detect LDR products[6] 422
Figure 7.6 | FRET system used in detecting HIVDR and probe sequence. 424
Figure 7.7 | The melting temperature of loop and stem and secondary structure of rMB. 424
Figure 7.8 | Performance of reverse MB to overcome high polymorphisms. 425
Figure 7.9 | Thai elephant probe to overcome the issues of low-level signal on FRET-based rMB. 426

CHAPTER 8: INTEGRATION OF HIVDR OLA INTO A MORE SIMPLIFIED DEVICE

Figure 8.1. | Development of wax encapsulation method for dried competing oligos. 430
Figure 8.2 | Wax patterning onto glass fiber before and after the heat treatment. 433
Figure 8.3 | Self-contained lateral flow device version 1. 434
Figure 8.4 | Self-contained lateral flow device version 2. 435
Figure 8.5 | Pull-tab device to enable sequential delivery in OLA detection. 436
Figure 8.6 | Demonstration of a simple pull tab detection device design using colored fluid 437
Figure 8.7 | Blueprint of integrated device version 1. 438
Figure 8.8 | Demonstration of two pull-tab systems with time delays using colored fluid. 439
Figure 8.9 | Demonstration of re-engineered physics and chemistries in integrated OLA-Simple device 1.0 440
Figure 8.10 | Vision and demonstration for the proof of concept. 441
Figure 8.11 | Solid-phase ligation reaction. 442
Figure 8.12 | Schematic of on-paper ligation process starting from RPA product. 445
Figure 8.13 | Blueprint of integrated OLA-Simple version 2 (crossroad design). 446
Figure 8.14 | Magnet activated valve enables spontaneous paper circuit switching. 447
Figure 8.15 | Preliminary results for the chemistry of the crossroad design (Integrated OLA version 2) 451

CHAPTER 9: HOLA: OLA TO DETECT A HUMAN ALLELE (HLA-B*57:01)

Figure 9.1 | Interaction of HLA-B*57:01 antigen-presenting cell with ABC and peptide PEP-V. 455
Figure 9.2 | Schematic of OLA-Simple 1.0 for detection of HLA-B*57:01. 461
Figure 9.3 | Vision of HOLA 2.0. 465

Figure 9.4 | RPA assay for HOLA 2.0. 467
Figure 9.5 | Preliminary results from HOLA-Simple version 2 (excluding extraction). 467
Figure 9.6 | Secondary structure analysis of LAMP amplicon in HOLA-Simple version 3. 469
Figure 9.7 | Analysis of LAMP assay in HOLA-OLA-Simple 3.0 in purified human DNA. 470
Figure 9.8 | In-situ lysis and amplification in HOLA-Simple 3.0. 471
Figure 9.9 | Effect of elution buffer volume on in-situ amplification. 472

CHAPTER 10: TECHNOLOGIES IN RESPONSE TO SARS-COV-2 PANDEMIC

Figure 10.1 | Schematic of swab transfer experiments. 489
Figure 10.2 | Volume recovery testing. 491
Figure 10.3 | ACP lysis efficiency at various treatment times and temperatures. 493
Figure 10.4 | Organism recovery for low-volume samples. 494
Figure 10.5 | Organism recovery for high-volume samples. 496
Figure 10.6 | Organism recovery for dried samples. 497
Figure 10.7 | Comparison of manual agitation methods for swab transfer. 498
Figure 10.8 | Analytical comparisons of swabs in pick-up and release of SARS-CoV-2 510
Figure 10.9 | Volume accuracy of two sample transfer methods. 514
Figure 10.10 | Analytical sensitivity of a newly developed lyophilized RT-qPCR formulation using CDC primers/probes. 527
Figure 10.11 | High-throughput laboratories with access to a real-time thermal cycler. 530
Figure 10.12 | Workflow for high-throughput end-point RT-PCR Covid-19 assay for laboratories with access to a 96-well thermal cycler and a fluorescence visualizer. 532
Figure 10.13 | Workflow and performance for low throughput for point-of-care settings such as small hospitals or clinics. 534
Figure 10.14 | Software analysis of fluorescence tube images. 536
Figure 10.15 | Validation of contrived clinical specimens in 0.25x PBS. 538
Figure 10.16 | Validation of our modified protocol (Scenario 1 workflow) on clinical VTM specimens. 541
Figure 10.17 | Harmony COVID-19 workflow, analytical performance, and interpretation. 564
Figure 10.18 | Comparison of RT-LAMP using TFv1 polymerase vs commercial Bst polymerase using conventional RT-qPCR machine. 568
Figure 10.19 | Lyophilized RT-LAMP and its analytical sensitivity. 569
Figure 10.20 | Cross-reactivity of MERS and SARS in lyophilized RT-LAMP. 571
Figure 10.21 | Overview of Harmony COVID-19 hardware. 573
Figure 10.22 | Cell phone user interface and result reporting. 577
Figure 10.23 | Analysis of XPRIZE contrived sample panel without RNA extraction. 579
Figure 10.24 | Harmony COVID-19 performance on clinical specimens. 581
Figure 10.25 | Usability study of Harmony COVID-19 workflow including two sample transfer

methods at the POC. 585
Figure 10.26 | Workflow of SARS-CoV-2 RT-PCR assay using lyophilized reagents at University of Zimbabwe. 600
Figure 10.27 | Study design of SARS-CoV-2 RT-PCR assay using lyophilized reagents at University of Zimbabwe. 602
Figure 10.28 | Dr. Vinie Kouamou tested the workflow at the laboratory in the University of Zimbabwe. 604
Figure 10.29 | Setup at the Georgetown University Pediatric clinic 606
Figure 10.30 | Study design and workflow for POC testing of SARS-CoV-2 by clinic HCWs 607
Figure 10.31 | Adjusted study design 608
Figure 10.32 | Examples of the end-point results 608
Figure 10.33 | Study design for detection of SARS-CoV-2 analytes enabled by Aquarium. 609
Figure 10.34 | Design variable included in the study. 610
Figure 10.35 | Correlation of the VL and Cq across experiments. 611
Figure 10.36 | Assay workflow and analytical performance. 614
Figure 10.37 | RT-RPA assay for SARS-CoV-2 RNA transcript covering the regions of interest 616
Figure S10.38 | Sensitivity of the MRSA/SA ELITe MGB qPCR assay. 617
Figure S10.39 | Schematic of how swab was rubbed on PDMS surface. 617
Figure S10.40 | Scanning electron micrographs of swab tips. 618
Figure S10.41 | Testing bacteria and bacterial DNA contamination in swabs and other materials. 619
Figure S10.42 | Testing effect of swab components on ACP lysis and qPCR. 620
Figure S10.43 | Effect of simulated nasal matrix (SNM) on qPCR and ACP lysis efficiency. 621
Figure S10.44 | Vortexing (gold standard) swab transfer. 622
Figure S10.45 | Effect of detergents on RT-PCR formulations. 625
Figure S10.46 | Optimization of RT-PCR protocol. 626
Figure S10.47 | Effect of PBS and human nasal matrix on lyophilized RT-PCR. 626
Figure S10.48 | Direct amplification of Accuplex™ packaged RNA in viral envelope. 627
Figure S10.49 | Cell phone raw and processed images of workflow-2 under a transilluminator. 628
Figure S10.50 | Cell phone raw and processed images of workflow-3 under a transilluminator. 629
Figure S10.51 | Cell phone raw and processed images of workflow-2 under glow box. 630
Figure S10.52 | Cell phone raw and processed images of workflow-3 under glow box. 631
Figure S10.53 | Two-fold cross validation of using patient sample data. 632
Figure S10.54| Raw and processed images of patient specimens. 633
Figure S10.55 | Validation of our modified protocol on clinical VTM specimens using end-point fluorescence values measured by a real-time PCR machine at room temperature. 634
Figure S10.56 | Effects of excipients on fresh RT-LAMP reactions tested on a commercial real-time thermal cycler. 639
Figure S10.57 | Heat block used in Harmony COVID-19 device. 640

Figure S10.58 | The design of optical and heater circuit boards for the Harmony COVID-19 device. 641
Figure S10.59 | Circuit board assembly and required parts. 642
Figure S10.60 | Device assembly. 643
Figure S10.61 | Real-time amplification curves of samples analyzed by HARMONY Covid-19. 655
Figure S10.62 | Standard curves of RT-qPCR using CDC N1 and N2 primers. 656
Figure S10.63 | Real-time amplification curves of RT-qPCR using CDC primers/probes. 674
Figure S10.64 | Analysis of XPRIZE panel of contrived samples containing less than 20 copies/reaction. 681

CHAPTER 11: FISH-OLA - SPECIES IDENTIFICATION TOOL TO REGULATE IUU

Figure 11.1 | Fish-OLA assignment of cod populations. 723
Figure 11.2 | Fish-OLA PCR design and integration with direct amplification from fish filet lysates. 725
Figure 11.3 | Ligation probes and optimization. 727
Figure 11.4 Analysis of cod DNA and fin samples using Fish-OLA. 728

APPENDIX 2: TABLE LIST

CHAPTER 1: INTRODUCTION

Table 1.1 | Landscape of adult global HIV treatment over the past 10 years. 5
Table 1.2 | WHO 2019 Pediatric ART recommendations 5
Table 1.3 | Properties of CRISPR/Cas systems commonly used in diagnostics61. 21

CHAPTER 2: NUCLEIC ACID PREPARATION

Table 2.1 | Quantification of human DNA yield from the sample preparation steps. 49
Table S2.2 | List of items used in non-proprietary RNA extraction kit. 99
Table S2.3 | Primers and probe sequences. 100
Table S2.4 | Probe sequences for HIV RNA capture. 101

CHAPTER 3: PAPER-BASED DETECTION FOR HIVDR OLA

Table 3.1 | Examples of unit vectors that can be used to discriminate two distributions. 169
Table S3.2 | Oligonucleotide probe sequences and concentration in OLA ligation (version 2016) 178
Table S3.3 | Signal ratios of samples evaluated by CLIA-OLA. 181
Table S3.4 | Signal ratios of samples evaluated by 1st-generation paper detection. 182
Table S3.6 | Comparison of 1st-generation paper-based detection and CLIA-OLA. 183
Table S3.7 | Compositions and anticipated functions in candidate buffers. 183

CHAPTER 4: READY-TO-USE DRY REAGENTS

Table 4.1 | Critical temperatures of excipient candidates (°C) 217

CHAPTER 5: OLA-SIMPLE 1.0 KIT FOR HIVDR

Table 5.1. Demographics of participants 267
Table 5.2 | Response to the OLA-Simple user questionnaire 275
Table 5.3 | Summary of responses from OLA-Simple users 275
Table 5.4 | Genotyping results by OLA-Simple adapted for a Mexican cohort. 284
Table 5.5 | Summary improvement of OLA-Simple 1.0 from OLA 2002. 294
Table S5.6 | Sequences of OLA-Simple probes (2017). 295
Table S5.7 | Comparison of genotyping results by OLA-Simple to other comparator assays. 296
Table S5.8 | Probe sequences for Mexican cohort (subtype B, 2020). 304
Table S5.9 | Genotyping results by OLA-Simple and MiSeq. 305
Table S5.10 | Specificity and sensitivity of the updated OLA-Simple kit at different diagnostic thresholds. 306
Table S5.11 | Comparison of the workflows of OLA-Simple and MiSeq assays performed in this

study. 307
Table S5.12 | Comparison of reagent costs, equipment costs, and assay times required in OLA-Simple and MiSeq. 308

CHAPTER 6: STRATEGIES TO IMPROVE AMPLIFICATION AND LIGATION FOR HIVDR OLA

Table 6.1 | Key HIVDR mutations associated with NNRTI and NRTI resistance. 341
Table 6.2 | Summary of RPA reaction components and their typical concentrations and functions[23] 347
Table 6.3 | Summary of improvement in the OLA amplification step 354
Table 6.4 | Probe melting temperature (predicted by IDT OligoAnalyzer), categorized by the assay sensitivity and specificity 358
Table 6.5 | Predicted ligation behaviors based on the reaction temperatures. 364
Table S6.6 | Primer sequences fast PCR amplification 385
Table S6.7 | tHDA primers for the HIV RT region 385
Table S6.7 | tHDA primers for the HIV RT region 386
Table S6.8 | HIV primers for RPA assays designed by Enos Kline (2017) 398

CHAPTER 8: INTEGRATION OF HIVDR OLA INTO A MORE SIMPLIFIED DEVICE

Table 8.1 | Schema of circuit 1 for amplification, dissociation, neutralization, and ligation. 448
Table 8.2 | Assembly of Part 2 device (strand displacement by competing oligo and detection) 450

CHAPTER 9: HOLA: OLA TO DETECT A HUMAN ALLELE (HLA-B*57:01)

Table 9.1 | Comparisons of HLA-B-57:01 OLA-Simple visual classifications by human and by software. 463
Table 9.2 | Summary of in-situ lysis and amplification in different reaction conditions and swab types. 471
Table S9.3 | HLA B57:01 primer sequences for RPA 474
Table S9.4 | Sequence for HLA LAMP primers. 475

CHAPTER 10: TECHNOLOGIES IN RESPONSE TO SARS-COV-2 PANDEMIC

Table 10.2 | Feedback from the HCWs. 515
Table 10.3 | Feature comparison between the Harmony COVID-19 system and other assays. 587
Table S10.4 Summary of experimental data (mean ± SE, N=5). 623

Table S10.5 | Coefficient of variation (CV) of experimental data (N=5). 624
Table S10.6 | Comparison of the analytical sensitivity of EUA-approved nucleic acid tests. 634
Table S10.7 | Commercially available quantitative RT PCR machine 636
Table S10.8 | Commercially available thermal cycler and the listed price 636
Table S10.9 | Commercially available fluorescence reader 636
Table S10.10 | List prices for the mobile phones used in this study 636
Table S10.11 | Comparison of Quantification Cycle (Cq) values from N1, N2, and RP primers using the standard vs modified protocol. 637
Table S10.12 |Summary of RT-LAMP based technologies that have received the US FDA emergency use authorization as of July 15th, 2021. 675
Table S10.13 | Primers, probes, and control sequences. 679
Table S10.14 | Detailed reagent and device cost at a production scale of 10,000 units 680
Table S10.15 | Consumable costs per test 681
Table S10.16 | Primer and probe sequences for SARS-CoV-2 typing assay. 682

CHAPTER 11: FISH-OLA - SPECIES IDENTIFICATION TOOL TO REGULATE IUU

Table 10.1 Primer and probe sequences used in development and the final DNA analysis kits 720

APPENDIX 3: LIST OF ACRONYMS

AP	Alkaline phosphatase
ART	Antiretroviral therapy
ART	Antiretroviral therapy
ARV	Antiretroviral
AS-LAMP	Allele specific LAMP
AS-PCR	Allele specific PCR
asHDA	Asymmetric HDA
asPCR	Asymmetric PCR
AU	Arbitrary unit
cas	CRISPR-associated proteins
CCR5	Chemokine receptor 5
CD4	Cluster of differentiation 4
CDC	Centers for Disease Control and Prevention
CDD	Capture, Denaturation, and Detection
cDNA	complementary DNA
CLIA	Clinical laboratory improvement amendment
CRISPR	Clustered regularly interspaced short palindromic repeats
CRISPR	Clustered regularly interspaced short palindromic repeats
DBS	Dry blood spot
dsDNA	doublestranded DNA
DTG	Dolutegavir
ELISA	Enzyme linked immunosorbent assay
ELISA	Enzyme-linked immunoassay
FEN	Flap endonuclease
FEN	Structure-specific flap endonuclease
FI	Fusion inhibitors
FIs	Fusion inhibitor
HDA	Helicase Dependent Amplification
HIV	Human Immunodeficiency Virus

HIVDR	HIV drug resistance
HIVDR	HIV Drug Resistance
INSTI	Integrase inhibitors
INSTIs	Integrase strand transfer inhibitor
KE	Kenya
LCR	Ligase chain reaction
LDR	Ligase detection reaction
LRA	Ligation RNA amplification
LRA	Ligation RNA Amplification
MIPA	Molecular inversion probe assay
MIPA	Molecular Inversion Probe Assay
mL	Milliliter
MLPA	molecular inversion probe assay
MTCT	Mother-to-child transmission
NGS	Next-generation sequencing
NNRTI	Non-nucleoside reverse transcriptase inhibitor
NNRTIs	Non-nucleoside reverse transcriptase inhibitor
NRTI	Nucleoside reverse transcriptase inhibitor
NRTIs	Nucleoside reverse transcriptase inhibitor
NS	Nasal secretions
NTC	No template control (negative control)
OD	Optical density
OLA	Oligonucleotide ligation assay
OLA	Oligonucleotide Ligation Assay
OLA-Simple	Simplified OLA
PAM	Protospacer adjacent motifs
PAM	Protospacer adjacent motifs
PANDAA	Pan Degenerate Adaptation and Amplification
PANDAA	Pan Degenerate Adaptation and Amplification
PBMC	Peripheral blood mononuclear cell
PBS	Phosphate Buffered Saline

PCR	Polymerase chain reaction
PCR	Polymerase Chain Reaction
PDR	Pretherapy drug resistance
PEG	Poly (ethylene glycol)
PI	Protease inhibitor
PI	Protease inhibitor
PIH	People Living with HIV
POD	Peroxidase
PVA	Poly (vinyl alcohol)
ROI	Region of interest
RPA	Recombinase Polymerase Amplification
RT-RPA	reverse transcription, recombinase polymerase amplification
SNP	Single nucleotide polymorphisms
tHDA	Thermophilic HDA
TMB	Tetramethylbenzidine
UK	United Kingdom
US	United States of America
V-OLA	VL test with a reflexed HIVDR test
VF	Virologic failure
VL	Viral load
VL	Viral Load
VL	Viral load
VLS	Virologic suppressed
VTM	Viral transport medium
WHO	World Health Organization
µL	Microliter

APPENDIX 4: AWARDS & RECOGNITIONS

4.1 AWARDS

2021 College of Engineering, University of Washington
Student Research Award

2020 Semi-Finalist X-Prize Rapid Covid Testing Competition
Other team members are Dr. Barry Lutz, Robert Atkinson, Enos Kline, Michael Roller, Amy Oreskovic, Daniel Leon, and Jack Henry Kotnik

2019 $2.5k from the UW NSF I-Corp Program to support customer discovery for OLA-Simple Technology

2018 $2.5k Best Idea for Global Reach + 16 Finalists BUSINESS PLAN COMPETITION
Worked with the team of students: Blythe Anderson, Rahil Jain, Richard Lee, Justin Vrana, David McIntyre, Annapurni Sriram, presenting a business model of OLA SIMPLE

2018 $10k USD 2nd PLACE (+ $2.9k USD PROTOTYPE FUNDING) HOLLAMAN HEALTH INNOVATION CHALLENGE
Worked with the team of students: Rahil Jain, Josh Buser, and Qin Wang, presenting a business model of OLA SIMPLE

2017 6.8k ZAR YOUNG SCIENTIST SCHOLARSHIP & SHOW-AND-TELL AWARD
26th International Workshop for HIV Drug Resistance and Treatment Strategies, Johannesburg, South Africa

2017 50k USD BUD TRIBBLE AND SUSAN BARNES GRADUATE DISCOVERY FELLOWSHIP
UW School of Medicine funded 3 graduate students to explore a new area of research that is independent of their researchers. I received a six-month fellowship to conduct research at Stanford University under Dr. Shirit Einav.

2017 BIOMEDICAL ENGINEERING SOCIETY (BMES) EARLY CAREER AWARD
Invited to give an oral presentation at the national BMES annual conference with complimentary registration & $600 USD

2017 UW GRADUATE SCHOOL'S FUNDING FOR EXCELLENCE AND INNOVATION
$500 USD travel fund to attend 2017 HIV Transmission Workshop in Paris, France

2016 50k USD 3rd PRIZE (+ 10k USD FINALIST) APF STUDENT TECHNOLOGY PRIZE FROM

MASSACHUSETTS GENERAL HOSPITAL
I led the team of undergraduate student mentees and researchers to develop a proposal titled "OLA–Simple: Point-of-care HIV Drug Resistance Test for Future of Individualized Medicine"

2015 UW GRADUATE SCHOOL'S FUNDING FOR EXCELLENCE AND INNOVATION
$300 USD travel fund to attend 2015 International HIV Drug Resistance Workshop, Boston, United States

2014 30k USD GLOBAL WACH - COULTER FOUNDATION SEED GRANT AWARD
Technical inventor and grant initiator for a proposal titled "Point-of-care Diagnostics of TB from Urine Samples". This proposal was originated from a class project and submitted under Profs. Barry Lutz, James Lai, and David Horne.

2013 3k USD NORTH SEATTLE COLLEGE'S MERIT SCHOLARSHIP
One of the three international students who received the tuition waiver based on academic achievement

2005 -06 1k THB ACADEMIC ACHIEVEMENT SCHOLARSHIPS
One of the five students with the highest GPAs in Petrochemicals and Polymeric Materials Program at Silpakorn University received this award.

4.2 RECOGNITIONS AND NOMINATIONS

2018 GRADUATE SCHOOL MEDAL AWARD
Nominated by the Department of Bioengineering, University of Washington.

2018 HUSKY 100
Recognition of 100 UW students in all areas of studies who were making the most of their time at the UW (Tri-campus student competition).

2017 ACKNOWLEDGED AS A CONTRIBUTING RESEARCHER BY THE WORLD HEALTH ORGANIZATION |Global Action Plan on HIV Drug Resistance (2017 - 2021), Paris, France.

2016 UW UNDERGRADUATE RESEARCH MENTOR AWARD
One of the seven awardees selected from graduate students and faculty members from tri-campus nominations. This award recognizes excellent mentorship as indicated by the accomplishments of mentees.

2015-16 HHMI INTERNATIONAL STUDENT RESEARCH FELLOWSHIP NOMINEE
One of the ten students in biological sciences and engineering fields, selected to represent the University of Washington to compete in the 2015 and 2016 national competitions.

2015 OUTSTANDING GRADUATE STUDENT MENTOR AWARD
Department of Bioengineering, University of Washington selected one graduate student nominee based on his/her recognition of excellent research mentorship.

2010 HIGHEST ACHIEVEMENT AWARD FOR THE PHARMACY TECHNICIAN PROGRAM
Pima Medical Institute recognized students with highest academic achievement in each program.

4.3 INTERVIEWS AND MEDIA

08.2021 Jocelyn Solis-Moreira, Study suggests Harmony COVID-19 assay is superior to laboratory-based tests. <https://www.news-medical.net/news/20210818/Study-suggests-Harmony-COVID-19-assay-is-superior-to-laboratory-based-tests.aspx>

11.2020 Chelsea Yates, A Culture of collaboration: Bioengineering Faculty Pivot Diagnostics Research to Support the Need for COVID-19 Testing <https://www.engr.washington.edu/news/article/2020-11-16/engineering-covid19-testing>

06.2020 UW Bioengineering. Meeting the need for COVID-19 test kits: pivoting from Seattle Flu Study and developing new rapid tests <https://bioe.uw.edu/meeting-the-need-for-covid-19-test-kits-pivoting-from-seattle-flu-study-and-developing-new-rapid-tests/>

06.2020 Why I-Corp? Interview participants for the UW CoMotion NSF I-Corps Program <https://www.youtube.com/watch?v=RYWm6Zy5vo&list=PLgY5Ho7zWk2OdddvkMzeqwcQQqIhKqe_K&index=3>

09.2019 Bus and postage campaign in Seattle area advertising by North Seattle College. "Nuttada changes the world, and she started at North."

04.2019 North Seattle College
"GRADUATE SPOTLIGHT"
<https://www.youtube.com/watch?v=ZOKWam3I3uY>

03.2017 School of Public Health, University of Washington

"CLOSE UP MARCH 2017: NUTTADA PANPRADIST" By Ashlie Chandler <http://sph.washington.edu/news/closeup/profile.asp?content_ID=8363>

02.2017 SEATTLE KING 5 NEWS "UW student wins coveted grant to develop HIV rapid test" By Lily Tan <http://www.king5.com/article/news/local/uw-student-wins-coveted-grant-to-develop-hiv-rapid-test/ 415096016>

02.2017 Department of Bioengineering, University of Washington "NUTTADA PANPRADIST WINS $50,000 THIRD PLACE APF STUDENT TECHNOLOGY PRIZE FOR PRIMARY HEALTHCARE" By Laura Wright <http://bioe.uw.edu/nuttada-panpradist-wins-50000-third-place-apf-student-technology-prize/>

12.2017 Department of Bioengineering, University of Washington "NUTTADA PANPRADIST PRESENTS OLA-SIMPLE HIV DRUG RESISTANCE TEST IN SOUTH AFRICA" By Laura Wright <http://bioe.uw.edu/nuttada-panpradist-ola-simple- south-africa-2017/>

06.2017 Department of Bioengineering, University of Washington "NUTTADA PANPRADIST RECEIVES GRADUATE DISCOVERY FELLOWSHIP" By Laura Wright <http://bioe.uw.edu/nuttada-panpradist-receives-graduate-discovery-fellowship/>

02.2017 College of Engineering, University of Washington "Global research impact: BioE grad student seeks to develop instrument-free diagnostic device to detect HIV infection and drug resistance" By Chelsea Yates <http://www.engr.washington.edu/news/panpradist>

09.2017 Biomedical Engineering Society (BMES) "BMES ANNOUNCES TRAVEL AWARD WINNERS"<http://www.bmes.org/blog_home.asp?display=57>

09.2016 Massachusetts General Hospital Press Release "$400,000 Awarded to Three Students for Primary Healthcare Technology." <http://www.massgeneral.org/apf/assets/pdf/APF-2016-PressRelease.pdf>

12.2014 Department of Bioengineering, University of Washington "PH.D. STUDENT AND HHMI NOMINEE NUTTADA PANPRADIST BRINGS GLOBAL PERSPECTIVE TO CONFRONTING HIV, TB" By Laura Wright <http://bioe.uw.edu/nuttada-panpradist-global-perspective-hiv-tb/>

09.2014 Department of Bioengineering, University of Washington
"PH.D. STUDENT'S IDEA FOR DEVICE THAT DIAGNOSES TUBERCULOSIS FROM URINE LEADS TO GLOBAL WACH/W.H. COULTER FOUNDATION SEED GRANT" By Laura Wright <http://bioe.uw.edu/coulter-seed-grant-tb- diagnosis-urine-2/>

05.2016 Department of Bioengineering, University of Washington
"WENDY THOMAS AND NUTTADA PANPRADIST RECEIVE 2016 UW UNDERGRADUATE RESEARCH MENTOR AWARDS" By Laura Wright <http://bioe.uw.edu/wendy-thomas-and-nuttada-panpradist-receive-uw-undergraduate-research-mentor-awards/>

06.2015 Department of Bioengineering, University of Washington "2015 BIOE AWARDS RECIPIENT PROFILES: SUZIE PUN, NUTTADA PANPRADIST, TED CHEN AND COLLEEN IRVIN" By Laura Wright <http://bioe.uw.edu/2015-bioe-awards-profiles-suzie-pun-nuttada-panpradist-ted-chen-colleen-irvin/>

10.2014 Department of Bioengineering, University of Washington "PH.D. STUDENT'S QUANTITATIVE ANALYSIS OF SWAB PERFORMANCE PUBLISHED IN PLOS ONE, MAY INFORM FUTURE DIAGNOSTIC TEST DEVELOPMENT" By Laura Wright <http://bioe.uw.edu/swab-performance-plos-one/>

08.2014 Global Center for Integrated Health of Women, Adolescents and Children, University of Washington "Global WACh & Coulter Foundation 2014 Pilot Award" By Jennifer Spragg <http://depts.washington.edu/gwach/global-wach-coulter-foundation-2014-pilot-award/

APPENDIX 5: TEACHING & MENTORING

5.1 TEACHING EXPERIENCE

03.26.18	INVITED LECTURER GH403/503 Multidisciplinary Perspectives in Global Health (Dr. Patricia Pavlinac) "Engineering, Bioengineering Interventions and Global Health" (class of 120 students, Department of Global Health, University of Washington).
02.14.18	INVITED LECTURER GH499/599 Bioengineering Solutions to Improve the Health of Women, Children, and Adolescents (Dr. Brandon Guthrie) "Challenges and Opportunities to Improve Health of Women, Adolescents and Children in Resource-Poor Settings" (class of 30 students, Department of Global Health, University of Washington)
11.20.17	INVITED LECTURER BIOEN215 Introduction to Bioengineering (Dr. Dianne Hendricks) "Development of Point-of-care Technologies for HIV Drug Resistance Testing" (class of 200 students, Department of Bioengineering, University of Washington)
03.30.17	INVITED LECTURER GH403/503 Multidisciplinary Perspectives in Global Health (Dr. Patricia Pavlinac) "Engineering, Bioengineering Interventions and Global Health" (class of 150 students, Department of Global Health, University of Washington)
01.25.17	INVITED LECTURER GH499/599 Bioengineering Solutions to Improve the Health of Women, Children, and Adolescents (Dr. Brandon Guthrie) "Etiology Diagnosis of Pediatric Diarrhea" co-lectured with Asst. Prof. Patricia Pavlinac, co-director of the Health Growth & Development Core, Global WACh (class of 30 students, Department of Global Health, University of Washington)
01.20.16	INVITED LECTURER GH499/599 Bioengineering Solutions to Improve the Health of Women, Children, and Adolescents (Dr. Brandon Guthrie) "Opportunities for Point-of-Care Tuberculosis Diagnostics from a Urine Sample" co- lectured with Dr. Silvia

LaCourse, a clinician, research, and tuberculosis expert. (class of 30 students, Department of Global Health, University of Washington)

01.2016 — 03.2016 TEACHING ASSISTANT
BIOEN531 Proposal Writing (Dr. Martha Scatena)
This is one of the three graduate-level core classes (class of 27 students, the Department of Bioengineering, University of Washington)

09.2014 —12.2014 GRADER
BIOEN499 Biomaterials (Dr. James Bryers and Dr. Buddy Ratner)
(class of 40 students, the Department of Bioengineering, University of Washington)

01.2012 — 06.2012 CHEMISTRY TUTOR

- Math Learning Center at North Seattle Community College
- Assisted one-on-one or small groups of undergraduate students with problem sets for General Chemistry, Organic Chemistry, and Biochemistry classes.
- Assisted undergraduate students in designing experiments, interpreting results, drawing conclusions using statistical tools, and writing technical reports.

5.2 RESEARCH MENTORING EXPERIENCE

02.2017 — 06.2018 BETELHEM YOHANNES
(2018 B.S. Bioengineering, co-mentor with Dr. James Lai)
2015 Mary Gates Research Scholar, 2016 William P. and Ruth Gerberding/Early Identification Program Scholar

10.2016 —06.2018 ANNAPURNI SRIRAM (2018 B.S. Bioengineering)
2017 Mary Gates Research Scholar, 2017 President of UW Biomedical Engineering Society

01.2016 —06.2018 JONATHAN LIM (2018 B.S. Bioengineering, co-mentor with Amy Oreskovic)
2017 Mary Gates Research Scholar

12.2015 — 06.2018 DAVID MCINTYRE (2018 B.S. Bioengineering)

	2016 Mary Gates Research Scholar, 2016 President of UW Engineering Without Border, 2017 Husky 100, 2017 Member of UW Engineering Without Border
10.2016 — 07.2017	ISAAC SO (Researcher from Seattle Children's Research Institute, 2015 B.S. Molecular Biology) Current student in Dental School, University of Washington
10.2015 —12.2015	SURASAK KASETSIRIKUL (Intern from M.S. Mechanical Engineering Program at Chulalongkorn University, Thailand) Current researcher at Singapore National Laboratory
11.2016 — 06.2017	ANNIE WONG-ON-WING (2017 B.S. Chemistry and Biochemistry) 2016 Mary Gates Research Scholar, ACS Certified, Current researcher at Seattle's Children Research Institute
12.2013 — 06.2017	NIKKI HIGA (2017 B.S. Bioengineering) 2015 Mary Gates Research Scholar, Current researcher at Seattle's Children Research Institute
01.2014 — 06.2016	IAN ANDREWS (2016 B.S. Bioengineering) 2014 Mary Gates Research Scholar, 2015 President of UW Biomedical Engineering Society, 2016 Husky 100 Current Ph.D. student in Biological Engineering Program at Massachusetts Institute of Technology

APPENDIX 6: COLLABORATORS & PROJECTS

6.1 PROJECTS BASED ON SINGLE NUCLEOTIDE POLYMORPHISM DETECTION

(MY ROLE: TECHNICAL LEAD)

OLA SIMPLE | HIV Drug Resistance test 01.2014 – 01.2019

Main PI: Dr. Lisa Frenkel; Co-PI: Dr. Barry Lutz and Dr. James Lai
Collaborators: Dr. Ruth Kanthula (Georgetown University), Dr. Rena Patel (Kenya), Dr. Santiago Avila-Rios (Mexico), Dr. Nicole Ngo-Giang-Huong (Thailand), Dr. Gonzague Jourdain (Thailand), Dr. Michael Chung (Kenya), Dr. Holly Rawizza, Dr. Kanki Phyllis (Harvard University), Dr. Theresa Rossouw (South Africa), Dr. Jaime Soria (Peru); Industrial collaborators: (Elitech; InBios International).

V-OLA – an HIV viral load test with a reflexed drug resistance test. 04.2019 – Present

PI: Dr. Barry Lutz; Co-PIs: Dr. Lisa Frenkel, Dr. James Lai, and Dr. Eric Klavins
Collaborators: Dr. Gaurav Gulati, Amy Oreskovic, Ian Hull, Enos Kline, Michael Roller

SARS-CoV-2 typing: Fast and simple assay to differentiate COVID-19 variants. 02.2021 – Present

I was the Project Initiator. I received the funding support from Dr. Barry Lutz to pivot the work from HIV application to address the need for SARS-CoV-2 typing in low-resource settings.
Collaborators: Dr. Anton Pozniak (UK), Dr. Jose Luis Blanco (Spain), Dr. Santiago Avila-Rios (Mexico), Dr. Ricardo Diaz (Brazil), Dr. Michael Gale (UW Department of Immunology), Dr. Benjamin (Stanford); Dr. Benjamin (US NIH and South Africa)

Development of novel methods to classify and assign cod fish in Bering Sea and Aleutian Island. 06.2020 – Present

PI: Dr. Karl Bohringer (UW Electrical Engineering); Co-PIs: Dr. Barry Lutz and Dr. Lorenz Hauser (UW Fishery); Collaborators: Ingrid Spies (NOAA), Anita Wray, Carolyn Tarpey

6.2 PROJECTS BASED ON LYOPHILIZED REAGENTS

(MY ROLE: ASSAY DEVELOPER)

Human-in-the-loop Aquarium enabled COVID-19 testing. 03.2020 – 08.2020

I was the Project Initiator and led the study design as a consultant of a DARPA-funded project to develop an Aquarium-based software to enable deployment of SARS-CoV-2 RT-PCR detection workflows. PI: Dr. Eric Klavins (UW EE); Co-PI: Dr. Steve Hasse - Professor of Biology at Duke University; Dr. Anastasia Deckard, a scientist at Geometrix Data;
Collaborators: Dr. Barry Lutz, Samuel Stewart, Qin Wang, Jack Henry, and Cannon Mallory

Feasibility testing of SARS-CoV-2 detection using lyophilized RT-PCR reagents in a laboratory in Zimbabwe. 06.2020 – Present

I was the Project Initiator, co-leading the study design with Vinnie Kouama.
PI: Dr. Justen Manasa (Medicine, University of Zimbabwe)
Co-PI: Dr. Barry Lutz; Lead researcher on Zimbabwe side: Vinie Kouamou
Collaborators: Qin Wang, Samuel Stewart, Jack Henry Kotnik, Parker S Ruth and Chunjong Park (UW CSE)

Feasibility testing of SARS-CoV-2 lyophilized RT-PCR reagents at a pediatric clinic at Georgetown University. 06.2020 – Present

I was the Project Initiator, co-leading the study design with Dr. Ruth Kanthula
PI: Dr. Ruth Kanthula and Dr. Barry Lutz; Collaborators: Qin Wang, Samuel Stewart, Jack Henry Kotnik, Parker S Ruth and Chunjong Park (UW CSE)

Harmony COVID-19 – Point-of-care nucleic acid amplification 03.2020 – 01.2021

PI: Dr. Barry Lutz
Collaborators: Dr. Lea Starita (UW Genome Sciences), Dr. Matthew Thompson (UW Family Medicine), Dr. Jay Shendure (UW Genome Sciences), and other members in the Lutz lab (Enos Kline, Ian Hull, Qin Wang, Jack Henry Kotnik, Daniel Leon, Amy Oreskovic, and Crissa Bennett)

6.3 PROJECTS BASED ON PAPER-BASED MICROFLUIDIC DEVICES (MY ROLE: ASSAY DEVELOPER)

Paper-based detection of SARS-CoV-2 surface antigens 01.2021 – Present

PI: Dr. David Baker (UW Institute of Protein Design); Lead Researcher: Dr. Andy Yeh

6.4 PROJECT BASED ON MY EXPERIENCE IN TECHNOLOGY TRANSFER AND COMMERCIALIZATION TRAINING (MY ROLE: CONTRIBUTOR)

COVID-UP – Outwitting the next COVID-19 testing bottleneck: User adoption of home-based testing. 07.2020 – 12.2020

PIs: Dr. Matthew Thompson and Dr. Barry Lutz

6.5 DISCOVERY FELLOWSHIP PROJECT FUNDED BY UW MEDICINE (MY ROLE: CONTRIBUTOR)

I received the Graduate Discovery Fellowship from the UW School of Medicine to spend 6 months to learn new skills and knowledge that will help establish an independent research program. 06.2018 - 12.2018

Project: Improvement of viral-inclusive, single-cell analysis pipeline to study host dynamic responses in dengue, zika, and Venezuelan equine encephalitis.

PIs: Dr. Shirit Einav, Dr. Stephen Quake at Stanford University

Lead researchers: Dr. Fabio Zazini, Dr. Zhiyuan Yao

Scientific contributions

- Designed and evaluated the NGS and PCR primers for Dengue, Zika, and Venezuelan equine encephalitis viruses.
- Analyzed the NGS MiSeq results and visualized data using Python packages.
- Wrote the method section of the manuscript.

6.6 ROTATION PROJECT: MAD NAAT - MULTIPLEXABLE AUTONOMOUS DISPOSABLE NUCLEIC ACID AMPLIFICATION TEST

(MY ROLE: CONTRIBUTOR)

Main PI: Dr. Paul Yager; Collaborators: PATH, GE Global Research, Seattle Children's Hospital, and Elitech, Co., Ltd. 06.2013-09.2013

Scientific contributions

- Led the development of a quantitative method for characterizing the effects of clinical swab types and agitation methods on swab sample transfer efficiency for use in low resource settings.
- Engineered a novel forced-flow device for enhanced swab sample transfer efficiency,
- Analyzed multi-factorial data by linear discriminant analysis, principal component analysis, and ANOVA.

6.7 LUTZ LAB PROJECTS I SERVED AS A TECHNICAL CONSULTANT.

Development of tuberculosis (TB) diagnostics in urine samples 09.2014 – 12.2019

I was the Project Initiator. PI: Dr. Barry Lutz, Dr. James Lai, and Dr. David Horne

Lead student: Amy Oreskovic

TB drug adherence test from urine samples

This project was initiated from my conversation with Dr. Sylvia LaCourse (co-lecturer in Global WACh class), who sought collaborators that can create low-cost lateral flow strips for the detection of INH metabolites as a drug adherence test in patients infected with tuberculosis.

PI: Dr. Grace John-Stewart; Lead researcher: Daniel Leon

6.8 PROJECT I SERVED AS A TECHNICAL CONSULTANT INDEPENDENT FROM THE LUTZ LAB.

SARS-CoV-2 Screening in Public Transportation Air Filtration 06.2020 – Present

PI: Dr. Shwetak Patel (UW CSE)

Lead student: Jason Hoffman; Collaborators: Matthew Hirano, Joe Breda, Ellen Xu, Parker Ruth, Antony Tang, Dr. Igor Novosselov (Environmental Science at UW)

APPENDIX 7: PUBLICATIONS AND MANUSCRIPTS

To access a real-time update list, please visit my Google Scholar page.

7.1 PEER-REVIEWED PUBLICATIONS

7.1.1. **Nuttada Panpradist**, Robert Atkinson, Michael Roller, Enos Kline, Ian Hull, Qin Wang, Jack Henry Kotnik, Amy K Oreskovic, Crissa Bennett, Daniel Leon, Victoria Lyon, Peter D Han, Lea M Starita, Matthew Thompson, Barry R Lutz. "Harmony Covid-19: development and evaluation of ready-to-use reagents, hardware, and software package for point-of-care SARS-CoV-2 nucleic acid amplification test" Accepted to Science Advances. (https://doi.org/10.1101/2021.08.12.21261875).

7.1.2. Zhiyuan Yao, Fabio Zanini, Sathish Kumar, Marwah Karim, Sirle Saul, Nishank Bhalla, **Nuttada Panpradist**, Avery Muniz, Aarthi Narayanan, Stephen R Quake, Shirit Einav. "The transcriptional landscape of Venezuelan equine encephalitis virus infection" 2021. PLoS Neglected Diseases, DOI: 10.1371/journal.pntd.0009306

7.1.3. Amy Oreskovic, **Nuttada Panpradist,** Diana Marangu, M William Ngwane, Zanele P Magcaba, Sindiswa Ngcobo, Zinhle Ngcobo, David J Horne, Douglas PK Wilson, Adrienne E Shapiro, Paul K Drain, Barry R Lutz. "Diagnosing pulmonary tuberculosis using sequence-specific purification of urine cell-free DNA."2021. JCM. PMID: 33789959; DOI: 10.1128/JCM.00074-21

7.1.4. **Nuttada Panpradist**, Qin Wang, Parker S Ruth, Jack H Kotnik, Amy K Oreskovic, Abraham Miller, Samuel WA Stewart, Justin Vrana, Peter D Han, Ingrid A Beck, Lea M Starita, Lisa M Frenkel, Barry R Lutz. "Simpler and faster Covid-19 testing: Strategies to streamline SARS-CoV-2 molecular assays." EBiomedicine. 2021. PMID: 33582488. DOI: 10.1016/j.ebiom.2021.103236

7.1.5. Sylvia M LaCourse, Daniel Leon, **Nuttada Panpradist**, Barbra A Richardson, Elizabeth Maleche-Obimbo, Jerphason Mecha, Daniel Matemo, Jaclyn N Escudero, John Kinuthia, Barry Lutz, Grace John-Stewart. "Urine Biomarker Assessment of Infant Adherence to

Isoniazid Prophylaxis" Pediatr Infect Dis J. 2021 Jan;40(1):e43-e45. DOI: 10.1097/INF.0000000000002936

7.1.6. **Nuttada* Panpradist**, Ingrid A* Beck, Parker S Ruth, Santiago Avila-Rios, Claudia Garcia-Morales, Maribel Soto-Nava, Daniela Tapia-Trejo, Margarita Matias-Florentino, Hector E Paz-Juarez, Silvia Del Arenal-Sanchez, Gustovo Reyes-Teran, Barry R Lutz, Lisa M Frenkel. "Near point-of-care, point-mutation test to detect drug resistance in HIV-1: A validation study in a Mexican cohort." AIDS PMID:32205723 DOI: 10.1097/QAD.0000000000002524 * Authors with equal contributions.

An interview related to this study was published on the Reuters news blog: (https://www.medscape.com/viewarticle/928372).

"*NEW YORK (Reuters Health) - A new, near-point-of-care test detects drug-resistance mutations in HIV-1 with greater than 90% accuracy across mutant frequency thresholds, according to a validation study in Mexico."*

7.1.7. **Nuttada Panpradist**, Ingrid A Beck, Justin Vrana, Nikki Higa, David McIntyre, Parker S Ruth, Isaac So, Enos C Kline, Ruth Kanthula, Annie Wong-On-Wing, Jonathan Lim, Daisy Ko, Ross Milne, Theresa Rossouw, Ute D Feucht, Michael Chung, Gonzague Jourdain, Nicole Ngo-Giang-Huong, Laddawan Laomanit, Jaime Soria, James Lai, Eric D Klavins, Lisa M Frenkel, Barry R Lutz. "OLA-Simple: A software-guided HIV-1 drug resistance test for low-resource laboratories". EBiomedicine. 2019. DOI: 10.1016/j.ebiom.2019.11.002

The journal Editor wrote a commentary to highlight this work. Marc Noguera-Julian. "HIV drug resistance testing - The quest for Point-of-Care" EBiomedicine. DOI: 10.1016/j.ebiom.2019.11.040

"Importantly, in the work of Panpradist et al., PoC testing is conceptually described as a whole, comprising technology and context. Not only the complex molecular biology machinery is craftfully embedded and tested within a single use, low cost device, but also assayed and validated in a close-to-real context, putting it to use inexperienced users that are guided by ad hoc created companion tools in carefully designed feasibility tests. Of note, ad hoc mobile software not only increases test robustness and usability but may also be an entry point to

controlled data collection for surveillance. While such PoC technology deployment into a real-world setting faces challenges such as materials, continued supply, and cold chain maintenance that demand operational research and cost-benefit studies [10], work by Panpradist et al. represents an important step forward for HIV drug resistance testing."

7.1.8. Amy Oreskovic, Norman D Brault, **Nuttada Panpradist**, James J Lai, Barry R Lutz. "Analytical comparison of methods for extraction of short cell-free DNA from urine" The Journal of Molecular Diagnostics. 2019. PMID: 31442674. DOI: 10.1016/j.jmoldx.2019.07.002

7.1.9. Horacio A Duarte, **Nuttada Panpradist**, Ingrid A Beck, Barry Lutz, James Lai, Ruth M Kanthula, Rami Kantor, Anubhav Tripathi, Shanmugam Saravanan, Iain J MacLeod, Michael H Chung, Guoqing Zhang, Chunfu Yang, Lisa M Frenkel. "Current status of point-of-care testing for human immunodeficiency virus drug resistance" J Infect Dis. 2017 ;216(suppl_9):S824-S828. PMID: 29040621. DOI: 10.1093/infdis/jix413.

7.1.10. **Nuttada Panpradist**, Ingrid A Beck, Michael H Chung, James N Kiarie, Lisa M Frenkel, Barry R Lutz. "Simplified paper format for detecting HIV drug resistance in clinical specimens by oligonucleotide ligation". PLoS One. 2016. DOI: 10.1371/journal.pone.0145962

7.1.11. **Nuttada Panpradist**, James J Lai. "Point-of-care diagnostics" 2016. Biomaterials Nanoarchitectonics. 2016. DOI: 10.1016/B978-0-323-37127-8.00009-1

7.1.12. **Nuttada Panpradist**, Bhushan J Toley, Xiaohong Zhang, Samantha Byrnes, Joshua R Buser, Janet A Englund, Barry R Lutz. "Swab sample transfer for point-of-care diagnostics: characterization of swab types and manual agitation methods" 2014. PLos One. PMID: 25181250. DOI: 10.1371/journal.pone.0105786

Nuttada's work establishes "some of the first objective, quantitative analysis of swab performance, which can be critically important when health care providers want to test patients for infectious disease," explained collaborator and co-author Dr. Janet A. Englund, M.D., professor and clinician of pediatric infectious disease at UW and Seattle Children's Hospital. "The results of this paper have implications for future development of point-of-care testing for

important infections in developing countries as well as here at home," she said.

7.2. MANUSCRIPTS UNDER REVIEW / MEDRXIV PREPRINTS

7.2.1. Justin D Vrana*, **Nuttada Panpradist***, Nikki Higa, Daisy Ko, Parker Ruth, Ruth Kanthula, James J Lai, Yaoyu Yang, Samar Rafie Sakr, Bhavna Chohan, Michael H Chung, Lisa M Frenkel, Barry R Lutz, Eric Klavins, Ingrid A Beck. "Implementation of an interactive mobile application to pilot a rapid assay to detect HIV drug resistance mutations in Kenya". * **Authors with equal contributions**. (https://doi.org/10.1101/2021.05.06.21256654)

7.2.2. Jackson J Wallner, Ingrid A Beck, **Nuttada Panpradist**, Santiago Avila-Ríos, Humberto Valenzuela-Ponce, Maribel Soto-Nava, Barry R Lutz, Lisa M Frenkel. "Rapid, Near Point-of-Care Assay for HLA-B*57:01 Genotype Associated with Severe Hypersensitivity to Abacavir". (Manuscript draft was approved for submission by all authors. Submitted to AIDS; (https://doi.org/10.1101/2021.05.26.21257187).

7.2.3. Gaurav Gulati*, **Nuttada Panpradist***, Samuel W A Stewart, Amy K Oreskovic, Santiago Avila, Gustavo Reyes-Terán, Peter D Han, Lea M Starita, Ingrid Beck, Lisa M Frenkel, Barry R Lutz, James J Lai. **"**Inexpensive workflow to enable simultaneous screening for Covid-19 and monitoring HIV viral load" * **Authors with equal contributions.** (medRxiv)

7.2.4. Enos Kline, **Nuttada Panpradist**, Ian Hull, Qin Wang, Amy K Oreskovic, Peter D Han, Lea M Starita, Barry R Lutz. "Development of novel engineered polymerase and universal probe design to enable robust RT-LAMP for SARS-CoV-2 detection." (doi: 10.1101/2021.08.13.2126199)

7.2.5. Jason Hoffman, Matthew Hirano, **Nuttada Panpradist**, Joseph Breda, Parker Ruth, Yuan yi Xu, Jonathan Lester, Bichlien Nguyen, Luis Ceze, Shwetak N. Patel. "Passively Sensing SARS-CoV-2 RNA in Public Transit Buses" https://doi.org/10.1101/2021.06.02.21258184

7.2.6. Andrew C. Hunt, James Brett Case, Young-Jun Park, Longxing Cao, Kejia Wu, Alexandra C. Walls, Zhuoming Liu, John E. Bowen, Hsien-Wei Yeh, Shally Saini, Louisa Helms, Yan Ting Zhao, Tien-Ying Hsiang, Tyler, N. Starr, Inna Goreshnik, Lisa Kozodoy, Lauren

Carter, Rashmi Ravichandran, Lydia B. Green, Wadim L. Matochko, Christy A. Thomson, Bastain Vögeli, Antje Krüger-Gericke, Laura A. VanBlargan, Rita E. Chen, Baoling Ying, Adam L. Bailey, Natasha M. Kafai, Scott Boyken, Ajasja Ljubetič, Natasha Edman, George Ueda, Cameron Chow, Amin Addetia, **Nuttada Panpradist**, Michael Gale Jr, Benjamin S. Freedman, Barry R. Lutz, Jesse D. Bloom, Hannele Ruohola-Baker, Sean P. J. Whelan, Lance Stewart, Michael S. Diamond, David Veesler, Michael C. Jewett, David Baker. "Multivalent designed proteins protect against SARS-CoV-2 variants of concern" https://doi.org/10.1101/2021.07.07.451375

7.2.7. Ross S. Milne, Ingrid A. Beck, Molly Levine, Isaac So, Nina Anderson, Wenjie Deng, Thomas R. Sibley, **Nuttada Panpradist**, James Kingoo, Catherine Kiptinness, Nelly Yatich, James N Kiarie, Samah R Sakr, Michael H Chung, Lisa M Frenkel. "Low-frequency pretreatment HIV drug-resistance effects on 2-year outcome of first-line efavirenz-based antiretroviral therapy" submitted to AIDS.

7.2.8. Ian T. Hull, Enos C. Kline, Gaurav K. Gulati, Jack Henry Kotnik**, Nuttada Panpradist**, Kamal G. Shah, Qin Wang, Lisa Frenkel, James Lai, Joanne Stekler, and Barry R. Lutz. "Isothermal Amplification with a Target-Mimicking Internal Control and Quantitative Lateral Flow Readout for Rapid HIV Viral Load Testing in Low-Resource Settings" submitted to Analytical Chemistry.

7.3. MANUSCRIPTS IN PREPARATION (SELECTED)

7.3.1. **Nuttada Panpradist**, Carolyn M Tarpey, Anita Wray, Parker S Ruth, Ingrid Spies, Barry R Lutz, Karl F Bohringer, Lorenz Hauser. "Fish-OLA: rapid and inexpensive population assignment for Pacific Cod (Gadus macrocephalus)"

7.3.2. **Nuttada Panpradist***, Amy Oreskovic*, Enos Kline, Ian Hull, Parker Ruth, Ingrid A Beck, Santiago Avila-Rios, Michael Chung, Ute Feucht, Lisa Frenkel, Gonzhang Jourdain, Enos Kline, Jonathan Lim, Nicole Ngo-Niang-Ngo, Theresa Rossouw, Lisa M Frenkel, Barry R Lutz. "Hour-long assay for detection of drug resistance in HIV-1 cross subtypes using recombinase polymerase amplification integrated into paper-based oligonucleotide ligation" * **Authors with equal contributions.**

PRIMARY REVIEWER FOR SCIENTIFIC MANUSCRIPTS

Journal of BMC Infectious Disease (2019)

Journal of Acquired Immune Deficiency Syndromes (2021)

APPENDIX 8: PATENT APPLICATIONS

8.1. Provisional Patent Application 63/165,029 filed 3/23/2021 Entitled: "SYSTEMS AND METHODS FOR DETECTING SARS-COV-2 RNA."

8.2. Provisional Patent Application 63/049,941 filed 7/9/2020 Entitled: "Kit for Sample Collection and Preparation for Amplification."

8.3. Provisional Patent Application 63/049,758 filed 7/9/2020 Entitled: "Amplification Device."

8.4. PCT Application WO 2019/222716 filed on 05/17/2019 Entitled: "Systems and

APPENDIX 9: PRESENTATIONS

8.1 CONFERENCE PRESENTATIONS

8.1.1. S LaCourse, D Leon, **N Panpradist**, B Richardson, E Maleche-Obimbo, J Mecha, D Matemo, J Escudero, J Kinuthia, B Lutz, G John-Stewart. "Biomarker assessment of infant adherence to isoniazid prophylaxis in a primary TB infection prevention trial in Kenya." 2020 International AIDS Society Meeting, San Francisco, USA (Oral Presentation)

8.1.2. A Oreskovic, **N Panpradist**, D Marangu, N Brault, J Lai, D Horne, B Lutz. "Sensitive Hybridization Capture and Detection of Urine Cell-free DNA for Tuberculosis Diagnosis." 2019 Association of Molecular Pathology meeting, Baltimore, Maryland (Poster Presentation)

8.1.3. **N Panpradist**, EC Kline, IA Beck, AK Oreskovic, I Hull, M Purfield, S Avila-Ríos, C García-Morales, G Reyes- Terán, LM Frenkel, BR Lutz. "Rapid semi-quantitative viral load assay and reflex drug resistance test for management of HIV antiretroviral therapy". 28th International Workshop on HIV Drug Resistance & Treatment Strategies. 2019. Johannesburg, South Africa. (Poster Presentation)

8.1.4. JJ Wallner, IA Beck, **N Panpradist**, S Avila-Ríos, H Valenzuela-Ponce, BR Lutz, LM Frenkel. "Rapid, Near Point- of-Care Assay for HLA-B*57:01 Genotype Associated with Severe Hypersensitivity to Abacavir". 28th International Workshop on HIV Drug Resistance & Treatment Strategies. 2019. Johannesburg, South Africa. (Poster Presentation)

8.1.5. **N Panpradist***, IA Beck*, PS Ruth, S Avila-Rios, C García-Morales, M Soto-Nava, D Tapia-Trejo, M Matias- Florentino, HE Paz-Juarez, S del Arenal-Sanchez, G Reyes-Teran, BR Lutz, LM Frenkel. "Development and evaluation

of a low-cost drug resistance test "OLA-Simple" for non-nucleoside-based ART for Mexico's HIV population." International AIDs Society Conference. 2019. Mexico City, Mexico. * Authors with equal contribution. (Poster presentation)

8.1.6. JD Vrana, IA Beck, **N Panpradist**, N Higa, D Ko, R Kanthula, B Chohan, J Lai, M Chung, LM Frenkel, BR Lutz, E Klavins. "Implementation of an interactive mobile application to pilot a same-day HIV drug resistance assay from whole-blood in Kenya". International Aids Society Conference. 2019. Mexico City, Mexico.

8.1.7. **N Panpradist**, F Zanini, S Quake, S Einav. "Identification of Molecular Biomarkers for Severe Dengue". 2019 UW Global WACh End of the Year Event, Seattle, Washington (Poster Presentation)

8.1.8. N Panpradist, IA Beck, J Vrana, N Higa, D McIntyre, P Ruth, I So, E Kline, R Milne, R Kanthula, A Wong-On- Wing, J Lim, D Ko, T Rossouw, U Feucht, M Chung, G Jourdain, N Ngo-Giang-Huong, L Laomanit, J Soria, J Lai, E Klavins, LM Frenkel, BR Lutz. "OLA Simple": a deployable, software-guided assay for detection of drug resistance in HIV-1 DNA and RNA from multiple patient cohorts". XXVI International Workshop on HIV Drug Resistance and Treatment Strategies. Johannesburg, South Africa. (Poster Presentation)

8.1.9. **N Panpradist**, I So, I Beck, D McIntyre, N Higa, A Wong-On-Wing, J Lim, D Ko, R Kanthula, T Russouw, UD Feucht, L Frenkel, B Lutz. "Evaluation of Low-Cost OLA Simple 1.0 Lab Kit for Detection of HIV Drug Resistance in Dried Blood Spot Specimens from South African Infants". XXVI International Workshop on HIV Drug Resistance and Treatment Strategies. Johannesburg, South Africa. 2017 (Oral and Poster Presentations)

8.1.10. **N Panpradist**, D McIntyre, A Wong-On-Wing, A Sriram, I Beck, L Frenkel, B Lutz. "Development of a Near Equipment-free, Self-Contained HIV Drug

Resistance Test". Biomedical Engineering Society Conference, Phoenix, Arizona, USA. 2017 (Oral Presentation)

8.1.11. A Oreskovic, **N Panpradist**, D Horne, and Barry Lutz, "Sequence-Specific Purification of Urine Cell-Free DNA for Tuberculosis Diagnosis." Biomedical Engineering Society Conference, Phoenix, Arizona, USA. 2017 (Oral Presentation)

8.1.12. **N Panpradist**, D McIntyre, N Higa, I So, D Ko, A Wong-On-Wing, I Andrews, I Beck, L Frenkel, B Lutz. "OLA Simple 1.0: Laboratory Kit for HIV Drug Resistance Testing in Low-Resource Settings". 12th HIV Transmission Workshop, Paris, France. 2017 (Poster Presentation)

8.1.13. **N Panpradist**, A Wong-On-Wing, I Beck, J Lai, L Frenkel, B Lutz. "Progress towards Development of a Novel Isothermal Ligation Reaction for HIV Drug Resistance Testing". XXV International Workshop on HIV Drug Resistance. Boston, MA. 2016 (Poster Presentation)

8.1.14. **N Panpradist**, N Higa, A Wong-On-Wing, I Andrews, B Atkinson, I Beck, L Frenkel, B Lutz. "Novel Platform for Simple Lab-based Oligonucleotide Ligation Assay for Detection of HIV Drug Resistance in sub-Saharan Africans". XXV International Workshop on HIV Drug Resistance. Boston, MA. 2016 (Poster Presentation)

8.1.15. **N Panpradist**, I Beck, J Lai, L Frenkel, B Lutz. "Engineering a Paper-based Microfluidic Device for Genotyping HIV Drug Resistance at Point-of-Treatment". XXV International Workshop on HIV Drug Resistance. Seattle, WA. 2015 (Poster Presentation)

8.1.16. **N Panpradist**, I Beck, M Chung, J Kiarie, L Frenkel, B Lutz. "Simplified Paper Format for Detecting HIV Drug Resistance in Clinical Specimens by Oligonucleotide Ligation Assay (OLA)". XXV International Workshop on HIV Drug Resistance. Seattle, WA. 2015 (Poster Presentation)

8.1.17. **N Panpradist**, I Beck, J Lai, L Frenkel, B Lutz. "Point-of-Treatment HIV Drug Resistance Test," Biomedical Engineering Society Conference, Seattle, WA. 2013 (Poster Presentation)

8.2 INVITED ORAL PRESENTATIONS.

8.2.1. PHPT Thailand, Chiang Mai University, Thailand, "Development of tests for HIV drug resistance and diagnosis of other infections" on 2nd March 2020.

8.2.2. Department of Medicine, University of Zimbabwe, "Development of OLA-Simple – HIV drug resistance test" on 24th October 2019.

8.2.3. KwaZulu-Natal Research Innovation and Sequencing Platform (KRISP), UKZN, Durban, South Africa, "Development of OLA-Simple – HIV drug resistance test" on October 22nd, 2020.

8.2.4. Michael Mayer Lab, University of Fribourg, Switzerland. "Development of OLA-Simple Technology Series for Detection of HIV Infection and Resistance in Low Resource Settings" on 26th July 2017.

8.2.5. Bioengineering Journal Club, University of Washington, USA. "Development of OLA Simple Technology Series for Detection of HIV Infection and Resistance in Low Resource Settings" on 14th May 2017.

8.2.6. BioEngage Symposium, Department of Bioengineering, University of Washington, USA. "Engineered Advances Nucleic Acid Tests for Resource-limited Settings" Co-presented with Dr. Barry Lutz and Amy Oreskovic on 10th December 2016.

8.2.7. Seattle Area Tuberculosis Diagnostics Symposium - Mycobacterial Interest Group MIG II, South Lake Union, Washington, USA. "Point-of-Care Tuberculosis Diagnostics from a Urine Sample." Co-presented with Dr. Barry Lutz on 20th November 2015.

8.2.8. MEMS Research Unit, University of Mechanical Engineering, Chulalongkorn University, Bangkok, Thailand. "Special Talk on Point-of-Care HIV/TB Diagnostics: My Journey from Waitress to Bioengineer" on 10th September 2015.

8.2.9. IRD-PHPT - a non-profit, non-governmental, collaborative program between the Institut de recherche pour le développement and Department of Medical Technology, Faculty of Associated Medical Sciences at Chiang Mai University, Chiang Mai, Thailand "Special Talk on Point-of-Care HIV/TB Diagnostics: My Journey from Waitress to Bioengineer" on 14th September 2015.

8.2.10. Department of Material Sciences, Silpakorn University, Nakhon Pathom, Thailand "Special Talk on Point-of-Care HIV/TB Diagnostics: My Journey from Waitress to Bioengineer" on 22nd September 2015.

8.2.11. UW Bioengineering / Global WACh Event - Seed Grant Progress Report "Point-of-Care Tuberculosis Diagnostics from a Urine Sample." University of Washington, Seattle, Washington, USA on 27th May 2015.

8.2.12. UW Bioengineering / Global WACh Event - Seed Grant Progress Report "1st-Step Towards Point-of-Care HIV Drug Resistance." University of Washington, Seattle, Washington, USA on 10th June 2012.

8.3 NON-ABSTRACT DRIVEN POSTER PRESENTATIONS

8.3.1. Achievement Rewards for College Scientist (ARCS) Visit, "Point-of-treatment HIV drug resistance test: re- engineering the oligonucleotide ligation assay (OLA) for simplicity and speed" University of Washington, Seattle, Washington, USA on 21st April 2014.

8.3.2. UW Bioengineering / Global Heath Exposition "OLA-Simple: HIV drug resistance screening" University of Washington, USA on 26th February 2014.

8.3.3. UW Center for AIDS Research's Annual STD/HIV Research Symposium. "1st Step towards a point-of-care HIV drug resistance test" South Lake Union, Washington, USA on 29th October 2013.

© Copyright 2021 | N Panpradist